MOLECULES OF THE EXTRACELLULAR MATRIX AS CANCER TARGETS

EDITED BY: Nikos Karamanos, Martin Götte and Alberto Passi
PUBLISHED IN: Frontiers in Oncology and
Frontiers in Cell and Developmental Biology

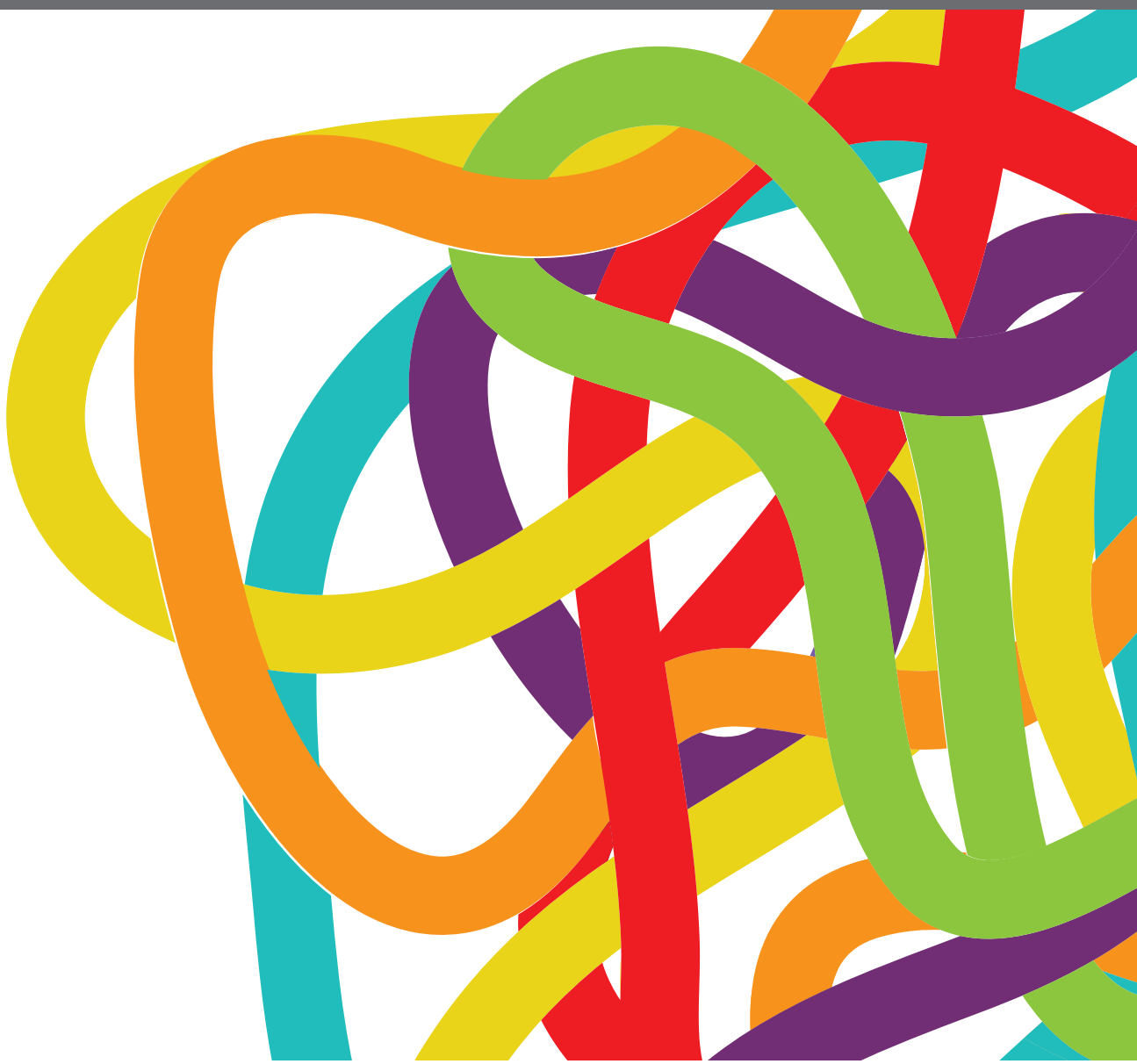

frontiers Research Topics

Frontiers eBook Copyright Statement

The copyright in the text of individual articles in this eBook is the property of their respective authors or their respective institutions or funders. The copyright in graphics and images within each article may be subject to copyright of other parties. In both cases this is subject to a license granted to Frontiers.

The compilation of articles constituting this eBook is the property of Frontiers.

Each article within this eBook, and the eBook itself, are published under the most recent version of the Creative Commons CC-BY licence. The version current at the date of publication of this eBook is CC-BY 4.0. If the CC-BY licence is updated, the licence granted by Frontiers is automatically updated to the new version.

When exercising any right under the CC-BY licence, Frontiers must be attributed as the original publisher of the article or eBook, as applicable.

Authors have the responsibility of ensuring that any graphics or other materials which are the property of others may be included in the CC-BY licence, but this should be checked before relying on the CC-BY licence to reproduce those materials. Any copyright notices relating to those materials must be complied with.

Copyright and source acknowledgement notices may not be removed and must be displayed in any copy, derivative work or partial copy which includes the elements in question.

All copyright, and all rights therein, are protected by national and international copyright laws. The above represents a summary only. For further information please read Frontiers' Conditions for Website Use and Copyright Statement, and the applicable CC-BY licence.

ISSN 1664-8714
ISBN 978-2-83250-389-8
DOI 10.3389/978-2-83250-389-8

About Frontiers

Frontiers is more than just an open-access publisher of scholarly articles: it is a pioneering approach to the world of academia, radically improving the way scholarly research is managed. The grand vision of Frontiers is a world where all people have an equal opportunity to seek, share and generate knowledge. Frontiers provides immediate and permanent online open access to all its publications, but this alone is not enough to realize our grand goals.

Frontiers Journal Series

The Frontiers Journal Series is a multi-tier and interdisciplinary set of open-access, online journals, promising a paradigm shift from the current review, selection and dissemination processes in academic publishing. All Frontiers journals are driven by researchers for researchers; therefore, they constitute a service to the scholarly community. At the same time, the Frontiers Journal Series operates on a revolutionary invention, the tiered publishing system, initially addressing specific communities of scholars, and gradually climbing up to broader public understanding, thus serving the interests of the lay society, too.

Dedication to Quality

Each Frontiers article is a landmark of the highest quality, thanks to genuinely collaborative interactions between authors and review editors, who include some of the world's best academicians. Research must be certified by peers before entering a stream of knowledge that may eventually reach the public - and shape society; therefore, Frontiers only applies the most rigorous and unbiased reviews.
Frontiers revolutionizes research publishing by freely delivering the most outstanding research, evaluated with no bias from both the academic and social point of view. By applying the most advanced information technologies, Frontiers is catapulting scholarly publishing into a new generation.

What are Frontiers Research Topics?

Frontiers Research Topics are very popular trademarks of the Frontiers Journals Series: they are collections of at least ten articles, all centered on a particular subject. With their unique mix of varied contributions from Original Research to Review Articles, Frontiers Research Topics unify the most influential researchers, the latest key findings and historical advances in a hot research area! Find out more on how to host your own Frontiers Research Topic or contribute to one as an author by contacting the Frontiers Editorial Office: frontiersin.org/about/contact

MOLECULES OF THE EXTRACELLULAR MATRIX AS CANCER TARGETS

Topic Editors:
Nikos Karamanos, University of Patras, Greece
Martin Götte, University of Münster, Germany
Alberto Passi, University of Insubria, Italy

Citation: Karamanos, N., Götte, M., Passi, A., eds. (2022). Molecules of the Extracellular Matrix as Cancer Targets. Lausanne: Frontiers Media SA.
doi: 10.3389/978-2-83250-389-8

Table of Contents

06 ***Editorial: Molecules of the Extracellular Matrix as Cancer Targets***
Nikos K. Karamanos, Martin Götte and Alberto Passi

12 ***Chemotherapy-Induced Degradation of Glycosylated Components of the Brain Extracellular Matrix Promotes Glioblastoma Relapse Development in an Animal Model***
Alexandra Y. Tsidulko, Oleg B. Shevelev, Anna S. Khotskina, Mariia A. Kolpakova, Anastasia V. Suhovskih, Galina M. Kazanskaya, Alexander M. Volkov, Svetlana V. Aidagulova, Evgenii L. Zavyalov and Elvira V. Grigorieva

26 ***The Heparan Sulfate Binding Peptide in Tumor Progression of Triple-Negative Breast Cancer***
Carina Mucciolo Melo, Huawei Wang, Ken Fujimura, Jan Strnadel, Maria Cecília Zorél Meneghetti, Helena Bonciani Nader, Richard L. Klemke and Maria Aparecida Silva Pinhal

40 ***LncRNA RP11-499E18.1 Inhibits Proliferation, Migration, and Epithelial–Mesenchymal Transition Process of Ovarian Cancer Cells by Dissociating PAK2–SOX2 Interaction***
Juan Yang, Shuping Peng and Keqiang Zhang

56 ***Syndecans and Their Synstatins: Targeting an Organizer of Receptor Tyrosine Kinase Signaling at the Cell-Matrix Interface***
Alan C. Rapraeger

68 ***Heparan Sulfate Biosynthesis and Sulfation Profiles as Modulators of Cancer Signalling and Progression***
Catarina Marques, Celso A. Reis, Romain R. Vivès and Ana Magalhães

85 ***The Role of Decorin and Biglycan Signaling in Tumorigenesis***
Valentina Diehl, Lisa Sophie Huber, Jonel Trebicka, Malgorzata Wygrecka, Renato V. Iozzo and Liliana Schaefer

102 ***Cold Atmospheric Plasma Attenuates Breast Cancer Cell Growth Through Regulation of Cell Microenvironment Effectors***
Christos A. Aggelopoulos, Anna-Maria Christodoulou, Myrsini Tachliabouri, Stauros Meropoulis, Maria-Elpida Christopoulou, Theodoros T. Karalis, Athanasios Chatzopoulos and Spyros S. Skandalis

118 ***The Impact of Hyaluronan on Tumor Progression in Cutaneous Melanoma***
Piia Takabe, Hanna Siiskonen, Aino Rönkä, Kirsi Kainulainen and Sanna Pasonen-Seppäne

136 ***Differential Impact of Membrane-Bound and Soluble Forms of the Prognostic Marker Syndecan-1 on the Invasiveness, Migration, Apoptosis, and Proliferation of Cervical Cancer Cells***
Katharina Hilgers, Sherif Abdelaziz Ibrahim, Ludwig Kiesel, Burkhard Greve, Nancy A. Espinoza-Sánchez and Martin Götte

149 ***SPOCK1 Promotes the Development of Hepatocellular Carcinoma***
Lóránd Váncza, Katalin Karászi, Bálint Péterfia, Lilla Turiák, Katalin Dezső, Anna Sebestyén, Andrea Reszegi, Gábor Petővári, András Kiss, Zsuzsanna Schaff, Kornélia Baghy and Ilona Kovalszky

167 ***Comprehensive Analysis of the Expression and Prognosis for ITGBs: Identification of ITGB5 as a Biomarker of Poor Prognosis and Correlated with Immune Infiltrates in Gastric Cancer***
Dongliang Liu, Shaojun Liu, Yu Fang, Liu Liu and Kongwang Hu

182 ***Serglycin Is Involved in TGF-β Induced Epithelial-Mesenchymal Transition and Is Highly Expressed by Immune Cells in Breast Cancer Tissue***
Marta Tellez-Gabriel, Xavier Tekpli, Trine M. Reine, Beate Hegge, Stephanie R. Nielsen, Meng Chen, Line Moi, Lisa Svartdal Normann, Lill-Tove R. Busund, George A. Calin, Gunhild M. Mælandsmo, Maria Perander, Achilleas D. Theocharis, Svein O. Kolset and Erik Knutsen

195 ***MCF10CA Breast Cancer Cells Utilize Hyaluronan-Coated EV-Rich Trails for Coordinated Migration***
Niina Aaltonen, Heikki Kyykallio, Sylvain Tollis, Janne Capra, Jaana M. Hartikainen, Johanna Matilainen, Sanna Oikari and Kirsi Rilla

208 ***Chondroitin Sulfates Control Invasiveness of the Basal-Like Breast Cancer Cell Line MDA-MB-231 Through ROR1***
Satomi Nadanaka, Jun-ichi Tamura and Hiroshi Kitagawa

220 **ESR2** ***Drives Mesenchymal-to-Epithelial Transition in Triple-Negative Breast Cancer and Tumorigenesis*** **In Vivo**
Zoi Piperigkou, Anastasios Koutsandreas, Marco Franchi, Vasiliki Zolota, Dimitrios Kletsas, Alberto Passi and Nikos K. Karamanos

234 ***Revisiting the Tenascins: Exploitable as Cancer Targets?***
Richard P. Tucker and Martin Degen

256 ***CD44 In Sarcomas: A Comprehensive Review and Future Perspectives***
Enrique Fernández-Tabanera, Raquel M. Melero-Fernández de Mera and Javier Alonso

278 ***New Functions of DDR1 Collagen Receptor in Tumor Dormancy, Immune Exclusion and Therapeutic Resistance***
Audrey Sirvent, Kevin Espie, Evangelia Papadopoulou, Dana Naim and Serge Roche

284 ***Heparanase Regulates EMT and Cancer Stem Cell Properties in Prostate Tumors***
Valentina Masola, Marco Franchi, Gianluigi Zaza, Francesca Mansa Atsina, Giovanni Gambaro and Maurizio Onisto

295 ***Interplay Between Chemotherapy-Activated Cancer Associated Fibroblasts and Cancer Initiating Cells Expressing CD44v6 Promotes Colon Cancer Resistance***
Shibnath Ghatak, Vincent C. Hascall, Nikos Karamanos, Roger R. Markwald and Suniti Misra

325 ***Upregulated Integrin α11 in the Stroma of Cutaneous Squamous Cell Carcinoma Promotes Skin Carcinogenesis***
Guillermo A. Martínez-Nieto, Hanna-Riikka Teppo, Noora Petrelius, Valerio Izzi, Raman Devarajan, Tiina Petäistö, Hengshuo Liu, Kris S. Kim, Sanna-Maria Karppinen, Heli Ruotsalainen, Jarkko Koivunen, Joni M. Mäki, Gilbert C. Walker, Taina Pihlajaniemi, Donald Gullberg and Ritva Heljasvaara

342 ***LRP-1-dependent Control of Calpain Expression and Activity: A New Mechanism Regulating Thyroid Carcinoma Cell Adhesion***
Benoit Langlois, Julie Martin, Christophe Schneider, Cathy Hachet, Christine Terryn, Damien Rioult, Laurent Martiny, Louis Théret, Stéphanie Salesse and Stéphane Dedieu

360 ***Adhesion Strength and Anti-Tumor Agents Regulate Vinculin of Breast Cancer Cells***
Despoina Nektaria Metsiou, Despina Deligianni, Efstathia Giannopoulou, Haralabos Kalofonos, Angelos Koutras and George Athanassiou

375 ***Decellularization of Xenografted Tumors Provides Cell-Specific* in vitro *3D Environment***
Gaia Iazzolino, Unai Mendibil, Blanca Arnaiz, Ane Ruiz-de-Angulo, Mikel Azkargorta, Kepa B. Uribe, Neda Khatami, Felix Elortza, Beatriz Olalde, Vanessa Gomez-Vallejo, Jordi Llop and Ander Abarrategi

390 ***Proteolytic Modulation of Tumor Microenvironment Signals During Cancer Progression***
Yoshifumi Itoh

406 ***Chemotherapy Induces Feedback Up-Regulation of CD44v6 in Colorectal Cancer Initiating Cells Through β-Catenin/Mdr1 Signaling to Sustain Chemoresistance***
Shibnath Ghatak, Vincent C. Hascall, Nikos Karamanos, Roger R. Markwald and Suniti Misra

frontiers | Frontiers in Oncology

TYPE Editorial
PUBLISHED 20 September 2022
DOI 10.3389/fonc.2022.1034646

Check for updates

OPEN ACCESS

EDITED AND REVIEWED BY
Tao Liu,
University of New South Wales,
Australia

*CORRESPONDENCE
Nikos K. Karamanos
n.k.karamanos@upatras.gr

SPECIALTY SECTION
This article was submitted to Molecular and Cellular Oncology, a section of the journal Frontiers in Oncology

RECEIVED 01 September 2022
ACCEPTED 09 September 2022
PUBLISHED 20 September 2022

CITATION
Karamanos NK, Götte M and Passi A (2022) Editorial: Molecules of the extracellular matrix as cancer targets. *Front. Oncol.* 12:1034646. doi: 10.3389/fonc.2022.1034646

COPYRIGHT
© 2022 Karamanos, Götte and Passi. This is an open-access article distributed under the terms of the Creative Commons Attribution License (CC BY). The use, distribution or reproduction in other forums is permitted, provided the original author(s) and the copyright owner(s) are credited and that the original publication in this journal is cited, in accordance with accepted academic practice. No use, distribution or reproduction is permitted which does not comply with these terms.

Editorial: Molecules of the extracellular matrix as cancer targets

Nikos K. Karamanos[1]*, Martin Götte[2] and Alberto Passi[3]

[1]Biochemistry, Biochemical Analysis & Matrix Pathobiology Res. Group, Laboratory of Biochemistry, Department of Chemistry, University of Patras, Patras, Greece, [2]Department of Gynecology and Obstetrics, Münster University Hospital, Münster, Germany, [3]Department of Medicine and Surgery, University of Insubria, Varese, Italy

KEYWORDS

extracellular matrix, cancer, proteoglycans, glycosaminoglycans, metalloproteinases, heparanase, tenascins, molecular targets

Editorial on the Research Topic
Molecules of the extracellular matrix as cancer targets

Extracellular Matrices (ECMs) are potent 3D-milieux contributing to the structural integrity of tissues and organs (1). The complex interactions between cells and the surrounding matrix but also within ECM are pivotal for normal development and tissue homeostasis (2). ECM networks, formed by cooperating macromolecules and active effectors, also modulate cell–matrix interactions, cell morphology, growth and function. The ECMs building blocks comprise proteoglycans (PGs) and glycosaminoglycans (GAGs), collagens, fibronectin, tenascins, elastin as well as cell-surface receptors such as integrins, CD44, discoidin domain receptors (DDRs), and receptor tyrosine kinases (RTKs) (3). ECMs function as intermediates between the cells in organs and tissues by regulating multiple inside-out or outside-in signals.

ECM macromolecules play key regulatory roles in gene expression, cell signaling and functions in tissue properties affecting human pathophysiology. Cell-matrix interactions and matrix remodeling are crucial for development, tissue regeneration, as well as disease development and progression. Interactions within the ECMs are quite convoluted and responsible for producing commands to determine vital cellular properties, such as proliferation, motility, autophagy, adhesion, and differentiation (4–7). Building biomolecular networks allows for the conjecture of individual cell properties through association of matrix components, and assists the discovery of targeted therapeutics and their use in drug design (8). It is worth noticing that ECM assembly and organization is constantly adapted based on distinct biomechanical signals.

ECM as a regulatory partner in tissue homeostasis, cancer development and progression, is an emerging field of research, and expression of matrix macromolecules and ECM structural integrity are significantly altered in cancer. Research in the field is focused not only to the extracellularly secreted macromolecules, but also key intracellular, pericellular and basement membrane

molecules. Considering its relevance for disease development, the ECM-related field, although emerging, has been underestimated in terms of studies on the mechanistic links behind matrix and several diseases, its prognostic value, and the designing of novel comprehensive treatment strategies.

Recent advances in ECM research have shown that several ECM effectors could be useful potential markers for diagnostic purposes and pharmacological targeting of cancer. Accumulative knowledge has also demonstrated that apart from their action at a cellular level, ECM effectors within their interaction networks could be useful modern biotechnological tools for drug delivery and targeted therapies. Recent research in this area will improve our understanding on the underlying mechanisms involved in cancer development and progression. Advancement in knowledge around ECM has the possibility to guide the development of novel diagnostic tools, innovative therapies, and biomarkers, improving disease management.

This Research Topic collection consists of 26 papers, 18 original research and 8 review articles, co-authored by 166 researchers in the field, and aims to provide the latest advances and insights in the field of ECM in cancer with focus on the ECM roles in cell signaling and cellular functions (proliferation, differentiation, migration, morphology, epithelial-to-mesenchymal transition, angiogenesis, autophagy, etc), pharmacological targeting/treatment and bioengineering approaches.

PGs significantly contribute to the cell signaling and immune responses. The extracellular small leucine-rich proteoglycans, decorin and biglycan, affect tumor growth and progression. Diehl et al. present and critically discuss the complex roles of decorin and biglycan signaling in tumor biology and their potential novel therapeutic implications. Soluble decorin and biglycan modulate key processes vital for tumor initiation and progression, such as autophagy, inflammation, cell-cycle, apoptosis, and angiogenesis. The adaptive nature of a malignant neoplasm is also a major challenge for the development of effective anti-oncogenic therapies.

The RTKs-mediated cell signaling, and integrin matrix receptors have well-established roles in tumor growth and propagation. Rapraeger discussed the syndecans as key molecules in this context. The syndecans, a family of cell membrane heparan sulfate proteoglycans (HSPGs), acting as matrix receptors, organize RTKs and integrins into functional units. Synstatins, peptide mimetics of the docking motifs in the syndecans, prevent assembly of these receptor complexes, block signaling activities and are highly effective against tumor cell invasion, survival and angiogenesis. Syndecan-1, on the other hand, has also been correlated with the development of cervical carcinoma. Syndecan-1 serves as a matrix receptor and coreceptor for receptor tyrosine kinases and additional signaling pathways. The loss of syndecan-1 expression is associated with low differentiation of cervical carcinoma and with an increased rate of lymph node metastases. Hilgers et al. analysed the clinical impact of syndecan-1 expression by analysis of public gene expression datasets and studied the effect of an overexpression of syndecan-1 in the human cervical carcinoma HeLa cells. High syndecan-1 expression correlated with a poor prognosis, suggesting its important role in cervical cancer progression. The reduced syndecans-1-dependent cell motility was linked to the Rho-GTPase signaling pathway. Conclusively, in cervical cancer syndecan-1 modulates pathogenetically relevant processes, which depend on the membrane-association of syndecan-1.

Serglycin, a well-known intracellular PG, is highly expressed by immune cells., It has been recently demonstrated that serglycin is also expressed by several other cell types, such as endothelial cells, muscle cells, and multiple types of cancer cells. Tellez-Gabriel et al. demonstrated that serglycin expression is upregulated in TGF-β induced epithelial-mesenchymal transition (EMT) and provided evidence that is a significant EMT marker gene. Notably, serglycin is more expressed by breast cancer cell lines with a mesenchymal phenotype as well as the basal-like subtype of breast cancers. Authors also found that serglycin is highly expressed by infiltrating immune cells in breast tumor tissue.

The extracellular matrix proteoglycan SPOCK1 contributes to the development and progression of cancers. SPOCK1 present in non-tumorous hepatocytes at low concentrations, promotes the development and progression of malignant hepatocellular tumors. It is worth noticing that syndecan-1, the major proteoglycan of the liver, and SPOCK1 are in inverse correlation. Váncza et al. showed that SPOCK1 downregulation of hepatoma cell lines upregulated p21 and p27 and interfered with pAkt and CDK4 expression. SPOCK1 in the liver cancer cells altered MAPK signaling and downregulated several members of the Src family, all related with the aggressive potential of the hepatoma cells. Therefore, SPOCK1 enhancement in the liver is an active contributor to hepatocarcinogenesis and cancer progression.

The fine structural features of heparan sulfate (HS) chains, including length and sulfation patterns, are crucial for the biological roles displayed by HSPGs, as these features determine binding affinities and selectivity. Marques et al. address in their review the regulatory mechanisms underlying HS biosynthesis and provide insights on the impact of different HS structural epitopes as well as on the effects of deregulated expression of HS modifying enzymes in the development and progression of cancer. The clinical potential of HS biosynthetic enzymes as novel targets for cancer therapy are also presented and discussed. HS chains of endothelial cell PGs interact with the major angiogenic factors, regulating blood vessels´ formation. Melo et al. investigated the effect of a selected HS-binding peptide in angiogenesis and tumor progression. The HS-binding peptide showed a higher affinity for N-sulfated heparin. The HS-binding peptide inhibits the proliferation of human endothelial umbilical cord cells by modulation of FGF-2

and significantly decreases the tube formation of endothelial cells and capillary formation of aorta, the formation of sub-intestinal blood vessels and the tumor size in zebrafish embryos.

Another type of sulfated GAGs, chondroitin sulfate (CS) differs from HS in structural unit hexosamine component and the fine sulfation features. CS chains may also regulate cancer cell properties. CS enhances the invasive activity of the human triple-negative breast cancer (TNBC) cell line MDA-MB-231, but its molecular mechanism remains unclear. Nadanaka et al. demonstrated that CSs bind to ROR1 in the presence of WNT5A. The invasive activity of MDA-MB-231 cells enhanced by CSs was completely suppressed by ROR1 knockdown and knockdown of the CS biosynthesis inhibited invasive activity, even in the presence of ROR1, suggesting that CS is required to induce an ROR1-dependent, aggressive phenotype. Taking into consideration that CS promotes cancer aggressiveness through the ROR1–JNK axis, this study opens a new area of research to help pharmaceutical targeting in TNBC. Tsidulko et al. investigated off-target negative effects of the systemic chemotherapy on glycosylated components of the brain ECM. Using an elaborated glioblastoma multiforme (GBM) relapse animal model, authors demonstrated that healthy brain tissue resists GBM cell proliferation and invasion, thereby restricting tumor development. Adjuvant chemotherapy with temozolomide induced changes in composition and content of brain PGs resulted in the accelerated adhesion, proliferation, and invasion of GBM cells into brain organotypic slices *ex vivo* and more active growth and invasion of experimental xenograft GBM tumors in SCID mouse brain *in vivo*. Notably, degradation of CS chains was identified as a key event responsible for the observed functional effects. As a future perspective, authors suggest that ECM-targeted supportive therapy might mitigate the negative off-target effects of the adjuvant GBM treatment and increase the relapse-free survival of GBM patients.

The well-known high molecular weight non-sulfated GAG, hyaluronan (HA), plays pivotal roles in tissue homeostasis, regeneration, several cell functional properties, but also has been related to various pathological conditions including inflammation and cancer. We are delighted that Takabe et al. reviewed the role of HA in the progression of cutaneous melanoma, an aggressive type of skin cancer. The expansion of melanoma is affected by the ECM surrounding the tumor together with immune cells. In early disease stages, HA is the major matrix component in cutaneous melanoma microenvironment. In advanced melanoma, HA content decreases due to altered synthesis and degradation, correlating with poor prognosis. This review focuses on HA matrix in cutaneous melanoma and how the changes in HA metabolism affect the progression of melanoma. HA, as one of the most abundant molecules in the TME, is also often found to coat extracellular vesicles (EVs). EVs derived from plasma membrane tentacles of cancer cells are crucial for migration, such as filopodia, and are abundant in tumor niches. Thus, it is possible that HA and HA-coated EVs have a cooperative role in promoting migration. Aaltonen et al. compared the HA synthesis, EV secretion and migratory behavior of normal and aggressive MCF10 series breast cell lines. Authors demonstrated that EVs left behind by tumor cells during migration are strongly positive for CD9. A leader-follower behavior was significantly decreased upon removal of pericellular HA, indicating that HA promotes the pathfinding behavior of follower cells. The results suggest the orchestrated role of HA, EVs and other extracellular cues in coordinated migration and pathfinding behavior of follower cells.

It is widely accepted that the TME, particularly the ECM, plays an essential role in tumor development through the interaction with specific protein-membrane receptors. One of the most relevant proteins in this context is the transmembrane protein CD44. The role of CD44 in tumor progression, invasion, and metastasis has been well established in many cancers. Fernández-Tabanera et al. summarize its role in sarcomas. CD44 is overexpressed in most sarcomas and exhibits a direct effect on tumor progression, dissemination, and drug resistance. CD44 is a useful prognostic and diagnostic marker (CD44v6 isoform) in osteosarcoma. HA-functionalized liposomes therapy has become an excellent CD44-mediated intracellular delivery system for osteosarcoma. Further research involving the specific role of CD44 in different sarcoma subgroups could provide a more innovative perspective for novel therapies and future clinical trials. Cancer-initiating cells (CICs) drive colorectal tumor growth and interact with multiple cell types within TME, including cancer-associated fibroblasts (CAFs). Chemoresistance in colorectal CICs involves the sustained activation of multiple drug resistance and WNT/β-catenin signaling pathways, as well as of alternatively spliced-isoforms of CD44 containing variable exon-6 (CD44v6). However, the mechanisms underlying sustained WNT/β-catenin signaling have remained elusive. Ghatak et al. investigated the interplay between the CICs and the chemotherapeutic FOLFOX that creates the persistent tumorigenic properties of colorectal CICs and stimulates the microenvironmental factors derived from the CAFs. Using biochemical, molecular and cell biology approaches, cell signaling pathways evaluation and *in vivo* mouse authors demonstrated that the interplay between chemotherapy-activated CAFs and CICs expressing cd44v6 promotes colon cancer resistance. These findings have crucial clinical implications suggesting that more specific therapeutic approaches required to block a chemotherapy induced remodeling of a TME that acts as a paracrine regulator to enrich CD44v6 (+) in colorectal CICs. In the subsequent study Misra et al. provide evidence that targeting CD44v6-mediated LRP6/β-catenin-signaling and drug efflux may represent a novel approach to overcome FOLFOX resistance and inhibit tumor progression in colorectal CICs. Sustained drug resistance in colorectal CICs is mediated by overexpression of CD44v6,

which is both a functional biomarker and a therapeutic target in colorectal cancer. Cold atmospheric plasma (CAP) has been proposed as an emerging anti-cancer treatment modality. Aggelopoulos et al. investigated the effects of direct and indirect CAP treatment on breast cancer cells of different estrogen receptor (ER) status. CAP treatment induced intense phenotypic changes and apoptosis in both ER+ and ER- cells. Interestingly, CAP significantly reduced CD44 protein expression, while differentially affected the expression of proteases and inflammatory mediators. Collectively, the findings of the present study suggest that CAP suppresses breast cancer cell growth and regulates several effectors of the TME and thus it could represent an efficient therapeutic approach for distinct breast cancer subtypes.

DDR1, a collagen receptor and tyrosine kinase, has emerged as an important player in cancer. Sirvent et al. review new DDR1 functions in tumor dormancy following dissemination, immune exclusion and therapeutic resistance induced by stromal collagens deposition. The signaling mechanisms behind these tumor activities and the therapeutic strategies aiming at targeting these collagens-dependent tumor responses as well as future perspectives are also presented and discussed.

Integrin β superfamily members (ITGBs) play important roles in various biological processes and are associated with carcinogenic effects in several malignancies. However, the expression and prognostic values of ITGBs and potential mechanism in gastric cancer (GC), a highly complex and heterogeneous disease, remain largely unclear. Liu et al. evaluated the ITGBs expression profiles in GC using various bioinformatic databases. Authors found that ITGB1-2 and ITGB4-8 are significantly higher in GC, high ITGB5 expression contributes to a poor prognosis and its expression is significantly associated with the ECM organization, cell-substrate adhesion, and ossification. Conclusively, ITGB5 may function as a valid biomarker of prognosis, and high expression of ITGB5 predicts poor prognosis for in GC and might be a potential target of precision therapy. Integrin α11β1 is a collagen-binding integrin. The expression of the α11 is upregulated in CAFs in various human neoplasms. Martínez-Nieto et al. investigated α11 expression in human cutaneous squamous cell carcinoma (cSCC) and in benign and premalignant human skin lesions and monitored its effects on cSCC development. Integrin α11 expression was significantly upregulated in the desmoplastic tumor stroma of human and mouse cSCCs, and the highest α11 expression was detected in high-grade tumors. Authors suggest that α11β1 operates in a complex interactive TME to regulate ECM synthesis and collagen organization and thus foster cSCC growth. Advanced experimental models will help to define the exact roles and molecular mechanisms of stromal α11β1 in skin tumorigenesis.

Targeting tumor-specific ECM molecules and stromal cells or disrupting aberrant mesenchyme-cancer communications might normalize the TME and improve cancer treatment outcome. The tenascins are a family of large, multifunctional extracellular glycoproteins consisting of four members. Tenascin-C and -W are currently the most promising candidates for exploitability and clinical use as they are highly expressed in various tumor stroma with relatively low abundance in healthy tissues. Tucker and Degen review the expression of all four tenascins in tumors, followed by a more thorough discussion on tenascin-C and tenascin-W focusing on their oncogenic functions and their potential as diagnostic and/or targetable molecules for anti-cancer treatment purposes.

Cells recognize and communicate with the surrounding cells and ECM to maintain homeostasis. ECM remodeling is critical for the maintenance of normal functionality. The cellular microenvironment is optimized for the proper functioning of the tissues and organs. Nevertheless, under pathological conditions like cancer, ECM remodeling ceases to be subject to control resulting in disease initiation and progression (9, 10). The actions of proteolytic enzymes such as matrix metalloproteinases (MMPs) as well as non-proteolytic ones such as heparanase (HPSE) alter the ECM composition, can modify the stability and functions of the ECM and drive disease initiation and progression. When cancer arises, the cellular microenvironment is modified to optimize its malignant growth, evading the host immune system and finding ways to invade and metastasize to other organs. Indeed, cancer progression relies on not only the performance of cancer cells but also the surrounding microenvironment. Itoh in his mini review discusses the current understanding of proteolytic modification of the TME signals during cancer progression.

Among glycosidic enzymes, HPSE, the mammalian endoglycosidase degrading HS, has been extensively studied the last decade. It regulates EMT and cancer stem cell properties and involved in prostate cancer progression. Cancer stem cells (CSCs) or cancer-initiating cells contribute to the initiation and tumor growth, the metastatic potential and drug resistance. Masola et al. evaluated two prostate cancer cell lines (DU145 and PC3) following HPSE silencing and overexpression. Expression of EMT and stemness markers was evaluated. The novel findings support a new mechanism of HPSE action in sustaining prostate cancer growth and diffusion and highlight the importance of HPSE as a potential pharmacological target.

Interactions among cancer cells and TME are orchestrated by the ECM contributing to fundamental processes of breast cancer progression. Estrogen receptors (ERs) have pivotal roles in the development and progression of TNBC. Early studies have correlated ERβ expression in tumor sites with a more aggressive clinical outcome (11). Piperigkou et al introduced the functional role of ERβ suppression following isolation of monoclonal cell populations of MDA-MB-231 breast cancer and demonstrated that clone selection results in suppression of the aggressive cell functional properties by transforming their morphological characteristics, eliminating the mesenchymal-like traits. shERβ MDA-MB-231 cells undergo universal matrix reorganization,

pass on a MET transition state and prevent tumorigenesis *in vivo*. These novel findings highlight the promising role of ERβ targeting in future pharmaceutical approaches for managing the high metastatic potential of TNBC.

A major and urgent issue is to identify diagnostic biomarkers of ovarian cancer (OC) to understand the underlying mechanism. Yang et al. studied cell functional properties and EMT using bioinformatic tools, biochemical and cell molecular biology approaches. LncRNA RP11-499E18.1 coexists in the nucleus and cytoplasm of OC cells. Its overexpression suppressed OC cell proliferation, migration, and colony formation, as well as SOX2 nuclear translocation. Interestingly, RP11-499E18.1 downregulated, while PAK2 and SOX2 was upregulated in OC tissues and cells. The new concept of this study indicates that RP11-499E18.1 might be a valuable diagnostic biomarker in OC and might play its tumor suppressor roles *via* regulation of the RP11-499E18.1–PAK2–SOX2 axis.

The low-density lipoprotein receptor-related protein 1 (LRP1), an endocytic receptor, mediates the clearance of ECM and regulates the expression of matrix receptors. However, the underlying mechanisms remains partial in the frame of cancer cells interaction with matricellular substrates. Langlois et al. identified that LRP1 downregulates calpain activity and calpain 2 transcriptional expression in an invasive thyroid carcinoma cell model, limiting cell-matrix attachment strength. Authors found that LRP-1 exerts a dual mode of control of calpain activity fine-tunes carcinoma cell spreading and suggest an additional and innovative intracellular mechanism which demonstrates LRP-1 pro-motile action in thyroid cancer cells.

Vinculin as a focal adhesion protein play critical role in cell attachment and detachment during migration. Metsiou et al. evaluated the spreading rate and the adhesion strength between breast cancer cells and ECM prior to and post-treatment with anti-tumor agents using tamoxifen treatment for ER+ breast cancer cells, and trastuzumab and pertuzumab for HER2+ cells. Post-treatment spreading rate was significantly decreased in both types of breast cancer, suggesting a lower metastatic potential. Treated cells required greater adhesion forces to detach from the ECM. Post-detachment and post-treatment vinculin levels were increased, indicating tighter cell–ECM junctions, limiting the probability of cell motility and migration.

Although 2D *in vitro* cell culture studies are common in the cancer research, reliable biomimetic 3D models are needed to ensure physiological relevance. Iazzolino et al. hypothesized that decellularized xenograft tumors can serve as an optimal 3D substrate to generate a top-down approach for *in vitro* tumor modeling. Authors found that samples decellularized from TNBC basal-like subtype xenograft models had different ECM compositions compared to the rest of the xenograft tumors tested. The *in vitro* recellularization of decellularized ECM (dECM) yields tumor-type–specific cell behavior in the TNBC context. Authors suggest that dECM is a feasible substrate for reseeding purposes, thereby promoting tumor-type–specific cell behavior, a proof-of-concept for further potential generation of patient-specific *in vitro* research models.

Author contributions

All authors listed have made a substantial, direct, and intellectual contribution to the work and approved it for publication.

Acknowledgments

Guest editors appreciate the kind participation of scientists contributed in this Research Topic with their research and review articles. We also thank the valuable help of Dr. K. Kyriakopoulou for the initial drafting of the editorial.

Conflict of interest

The authors declare that the research was conducted in the absence of any commercial or financial relationships that could be construed as a potential conflict of interest.

Publisher's note

All claims expressed in this article are solely those of the authors and do not necessarily represent those of their affiliated organizations, or those of the publisher, the editors and the reviewers. Any product that may be evaluated in this article, or claim that may be made by its manufacturer, is not guaranteed or endorsed by the publisher.

References

1. Karamanos NK, Theocharis AD, Piperigkou Z, Manou D, Passi A, Skandalis SS, et al. A guide to the composition and functions of the extracellular matrix. *FEBS J* (2021) 288(24):6850–912. doi: 10.1111/febs.15776

2. Manou D, Caon I, Bouris P, Triantaphyllidou I-E, Giaroni C, Passi A, et al. The complex interplay between extracellular matrix and cells in tissues. *Methods Mol Biol* (2019) 1952:1–20. doi: 10.1007/978-1-4939-9133-4_1

3. Hu M, Ling Z, Ren X. Extracellular matrix dynamics: tracking in biological systems and their implications. *J Biol Eng* (2022) 16(1):13. doi: 10.1186/s13036-022-00292-x

4. Vitale D, Kumar Katakam S, Greve B, Jang B, Oh E, Alaniz L, et al. Proteoglycans and glycosaminoglycans as regulators of cancer stem cell function and therapeutic resistance. *FEBS J* (2019) 286(15):2870–82. doi: 10.1111/febs.14967

5. Karousou E, Misra S, Ghatak S, Dobra K, Götte M, Vigetti D, et al. Roles and targeting of the HAS/hyaluronan/CD44 molecular system in cancer. *Matrix Biol* (2017) 59:3–22. doi: 10.1016/j.matbio.2016.10.001

6. Schaefer L, Dikic I. Autophagy: Instructions from the extracellular matrix. *Matrix Biol* (2021) 100–101:1–8. doi: 10.1016/j.matbio.2021.06.002

7. Chen CG, Iozzo RV. Extracellular matrix guidance of autophagy: a mechanism regulating cancer growth. *Open Biol* (2022) 12(1):210304. doi: 10.1098/rsob.210304

8. Karamanos NK, Piperigkou Z, Passi A, Götte M, Rousselle P, Vlodavsky I. Extracellular matrix-based cancer targeting. *Trends Mol Med* (2021) 27 (10):1000–13. doi: 10.1016/j.molmed.2021.07.009

9. Piperigkou Z, Kyriakopoulou K, Koutsakis C, Mastronikolis S, Karamanos NK. Key matrix remodeling enzymes: Functions and targeting in cancer. *Cancers (Basel)* (2021) 13(6):1441. doi: 10.3390/cancers13061441

10. Passi A, Vigetti D, Buraschi S, Iozzo RV. Dissecting the role of hyaluronan synthases in the tumor microenvironment. *FEBS J* (2019) 286(15):2937–49. doi: 10.1111/febs.14847

11. Piperigkou Z, Tzaferi K, Makrokanis G, Cheli K, Karamanos NK. The microRNA-cell surface proteoglycan axis in cancer progression. *Am J Physiol Physiol* (2022) 322(5):C825–32. doi: 10.1152/ajpcell.00041.2022

frontiers in Oncology

ORIGINAL RESEARCH
published: 19 July 2021
doi: 10.3389/fonc.2021.713139

Chemotherapy-Induced Degradation of Glycosylated Components of the Brain Extracellular Matrix Promotes Glioblastoma Relapse Development in an Animal Model

*Alexandra Y. Tsidulko[1], Oleg B. Shevelev[2], Anna S. Khotskina[2], Mariia A. Kolpakova[1], Anastasia V. Suhovskih[1,3], Galina M. Kazanskaya[1], Alexander M. Volkov[4], Svetlana V. Aidagulova[5], Evgenii L. Zavyalov[2] and Elvira V. Grigorieva[1,3]**

[1] Institute of Molecular Biology and Biophysics, Federal Research Center of Fundamental and Translational Medicine, Novosibirsk, Russia, [2] Institute of Cytology and Genetics, Siberian Branch of the Russian Academy of Sciences, Novosibirsk, Russia, [3] V. Zelman Institute for Medicine and Psychology, Novosibirsk State University, Novosibirsk, Russia, [4] Meshalkin National Medical Research Center, Ministry of Healthcare of the Russian Federation, Novosibirsk, Russia, [5] Novosibirsk State Medical University, Ministry of Healthcare of the Russian Federation, Novosibirsk, Russia

OPEN ACCESS

Edited by:
Nikos Karamanos, University of Patras, Greece

Reviewed by:
Davide Vigetti, University of Insubria, Italy
Marilena Formato, University of Sassari, Italy
Mauro Sergio Pavao, Federal University of Rio de Janeiro, Brazil

***Correspondence:**
Elvira V. Grigorieva
elv_grig@yahoo.com

Specialty section:
This article was submitted to Molecular and Cellular Oncology, a section of the journal Frontiers in Oncology

Received: *21 May 2021*
Accepted: *29 June 2021*
Published: *19 July 2021*

Citation:
Tsidulko AY, Shevelev OB, Khotskina AS, Kolpakova MA, Suhovskih AV, Kazanskaya GM, Volkov AM, Aidagulova SV, Zavyalov EL and Grigorieva EV (2021) Chemotherapy-Induced Degradation of Glycosylated Components of the Brain Extracellular Matrix Promotes Glioblastoma Relapse Development in an Animal Model. Front. Oncol. 11:713139. doi: 10.3389/fonc.2021.713139

Adjuvant chemotherapy with temozolomide (TMZ) is an intrinsic part of glioblastoma multiforme (GBM) therapy targeted to eliminate residual GBM cells. Despite the intensive treatment, a GBM relapse develops in the majority of cases resulting in poor outcome of the disease. Here, we investigated off-target negative effects of the systemic chemotherapy on glycosylated components of the brain extracellular matrix (ECM) and their functional significance. Using an elaborated GBM relapse animal model, we demonstrated that healthy brain tissue resists GBM cell proliferation and invasion, thereby restricting tumor development. TMZ-induced [especially in combination with dexamethasone (DXM)] changes in composition and content of brain ECM proteoglycans (PGs) resulted in the accelerated adhesion, proliferation, and invasion of GBM cells into brain organotypic slices *ex vivo* and more active growth and invasion of experimental xenograft GBM tumors in SCID mouse brain *in vivo*. These changes occurred both at core proteins and polysaccharide chain levels, and degradation of chondroitin sulfate (CS) was identified as a key event responsible for the observed functional effects. Collectively, our findings demonstrate that chemotherapy-induced changes in glycosylated components of brain ECM can impact the fate of residual GBM cells and GBM relapse development. ECM-targeted supportive therapy might be a useful strategy to mitigate the negative off-target effects of the adjuvant GBM treatment and increase the relapse-free survival of GBM patients.

Keywords: glioblastoma multiforme, chemotherapy, extracellular matrix, proteoglycan, glycosaminoglycan, chondroitin sulfate, temozolomide, dexamethasone

INTRODUCTION

GBM is an aggressive malignant brain tumor with a very poor prognosis. The conventional treatment protocol includes surgery followed by concurrent radiotherapy (30 fractions*2 Gy) and chemotherapy with TMZ, with subsequent TMZ courses (1, 2). This adjuvant treatment targets the eliminiation of residual GBM cells and, in the most cases, accompanied by DXM as a basic anti-edema drug (3, 4). During the last decade, substantial efforts have been made to develop new anti-GBM drugs and different treatment strategies; however, they did not lead to significant improvement in survival rates of GBM patients yet (5, 6). Unfortunately, despite the temporal improvement in the disease course, a GBM relapse can develop at 6 to 8 months after surgery resulting in a lethal outcome. At recurrence, there is no standard of care, and there is a clear need for better therapeutic options (7, 8).

The known molecular mechanisms of adverse TMZ effects on the residual GBM cells are presented in detail in the comprehensive reviews (9, 10) and include largely induced resistance of GBM cells to the drug(s) due to DNA repair (11, 12) and contribution of cancer stem-like cells (13–16). For the last years, the tumor microenvironment (TME) also appeared on this scene as an important regulator of phenotypic GBM cells heterogeneity and tumorigenic potential rather than multipotency of cancer stem-cell cells (17).

The role of the microenvironment in brain cancer has been extensively studied during last decades, but that is related, initially, to the role of cellular components of the brain tissue, like the astrocytes (18, 19). ECM components remain less investigated, although their importance to GBM development is not in doubt (20). Brain tissue ECM represents a unique structure, mainly composed of proteoglycans (PGs) and glycosaminoglycans (GAGs), which involvement in normal physiology and carcinogenesis is extensively studied for different cancers (21, 22). The important role of PGs in brain carcinogenesis is comprehensively discussed in the recent reviews (23–25), with special attention to chondroitin sulfate proteoglycans (CSPGs) (26, 27) and CSPG4 (28), heparan sulfate proteoglycans (HSPGs) (29), and polysaccharide molecules of heparan sulfate (HS) (30–32) and keratan sulfates (KS) (33). As for GAGs, one of the most abundant GAGs in brain ECM is hyaluronan (HA), which has a functional role in the GBM development and is comprehensively described in the recent review by Pibuel et al. (34).

During GBM chemotherapy, TMZ affects PGs expression in both the residual cancer cells and surrounding normal brain tissue. More data are available for TMZ effects on PGs in GBM tumor/cells because of the possibility of using experimental cancer cell culture systems *in vitro* and *in vivo* as well as clinical data. Important results are obtained from the experiments with TMZ-resistant GBM cells, which allow us to identify potential resistance-related PGs: glypican-1–silenced U-251 cells were much more susceptible to TMZ than intact U-251 MG cells (35); high expression of decorin and lumican in GBM and neuroblastoma stem cells are associated with TMZ resistance (36); CSPG4 is related in molecular mechanisms of TMZ resistance of GBM cells (37); experimental degradation of CS by chondroitinase ABC sensitizes glioblastoma cells to TMZ (38). The observed changes in the PGs expression in TMZ-resistant GBM cells seem to be induced by the systemic long-term TMZ treatment during the selection of the resistant cell clones. Overall, although the use of TMZ in the experimental models does not reflect the clinical situation of GBM development completely (39, 40), the experiments allow for the revealing of important molecular mechanisms of GBM development and identifying PGs as markers for GBM cells transformation.

Effects of systemic long-term TMZ on the extracellular components of normal brain tissue (PGs, GAGs) remain much less investigated due to restricted set of the research methods, which include mainly GBM animal models *in vivo* (41–44) and brain organotypic culture *ex vivo* (45–47). In our previous study, we demonstrated for the first time the ability of TMZ and DXM to affect PG/GAG expression and composition in normal rat brain tissue in the experimental system *in vivo*. TMZ treatment affects mainly GAG chains of the intact PG molecules, while DXM increases overall transcriptional activity and expression patterns of the PGs (changes in syndecan-1 (+4-fold), glypican-1 (+3-fold), brevican (+7-fold), CSPG4/NG2 (+2-fold), decorin (−2-fold), and lumican (+3-fold) expression) in brain zone-dependent manner (48). Combination of TMZ with DXM results in the most profound deterioration in PGs composition and content in the brain tissue both at core protein and glycosaminoglycan levels. In this study, we aimed to investigate the functional role of the TMZ-induced changes in the expression of PGs and content of their polysaccharide GAG chains in GBM relapse development using a novel GBM relapse model.

MATERIALS AND METHODS

Animals

For *in vivo* studies, male SCID mice (n=64) aged 10 weeks and weighing 23 to 30 g were used. Animals were housed in groups of two to five mice in individually ventilated polycarbonate cages OptiMice (Animal Care Systems, USA) in special clean rooms with HEPA13-filtered incoming air, with free access to food and water, 12/12-h light/dark cycle, air temperature of 22 ± 2°C, and relative humidity of 45 ± 10%. All *in vivo* experiments were conducted at SPF Animal Facility at the Institute of Cytology and Genetics SB RAS (Novosibirsk, Russia). For *ex vivo* organotypic hippocampal slice culture, Wistar rat pups aged 8 to 9 days were used. All procedures were conducted in accordance with the European Communities Council Directive 2010/63/EU and were approved by the Animal Care and Use Committees of the Institute of Cytology and Genetics SB RAS and FRC FTM. All efforts were made to minimize animal suffering and to reduce the number of animals used.

Cells

The human glioblastoma U87 cell line was obtained from the Karolinska Institute (Stockholm, Sweden). The U87-RFP cell line

was purchased from Creative Biogene (Shirley, NY, USA). Cells were maintained in IMDM medium supplemented with 2 mM L-glutamine, 100 units/ml penicillin, 100 µg/ml streptomycin, and 10% fetal bovine serum at 37°C in a humidified 5% CO_2 incubator. For analysis, cells were harvested using trypsin/EDTA.

Primary Mixed Glial Culture

Primary mixed glia was obtained using gentleMACS™ Octo Dissociator with Heaters and Adult Brain Dissociation Kit (Miltenyi Biotec, Germany) according to the manufacturer's protocol. Briefly, two 10-week-old C57BL/6J mice were sacrificed by cervical dislocation; brains were removed and washed in cold PBS. Brains were cut into 0.5-cm slices and transferred to C Tubes (Miltenyi Biotec, Germany), containing enzyme mix 1. Enzyme mix 2 was added, and the brains were dissociated using the gentleMACS program 37C_ABDK_01. After the termination of the program, the suspension was filtered through a 70-µm strainer and centrifuged at 300*g* for 10 min. Debris was removed using centrifugation with Debris Removal Solution at 3000*g* for 10 min. Cells were washed with cold PBS, incubated with 1× Red Blood Cell Removal Solution for 10 min at 4°C and centrifuged at 300*g* for 10 min. The remaining cells were resuspended in IMDM (Gibco, USA) medium supplemented with 2 mM L-glutamine, 100 units/ml penicillin, 100 µg/ml streptomycin, and 10% fetal bovine serum. Cells were seeded onto poly-D-lysine-covered flasks and incubated at 37°C in a humidified 5% CO_2 incubator. The medium was changed completely after 24 h, and ½ of the medium was changed every 3 days. At day 11, cells reached 85% to 90% of confluency and were used for further experiments.

Cell Viability and Proliferation Assay

Cell viability and proliferation were detected by Hoechst 33342/PI staining. Primary mixed glial cells were seeded on 96-well plates at 10^4 cells per well and allowed to attach and grow for 24 h. After 24 h medium was changed to the medium containing TMZ (250 µM), DXM (1 µM), TMZ+DXM (250 and 1 µM, respectively) or DMSO (0.25%) as control, ½ medium was replaced with fresh medium containing corresponding drugs every 3 days. Cells viability and proliferation were analyzed at 24, 48, 72, 144, 168, and 192 h of incubation with the drugs. Cells were stained with Hoechst 33342 (Sigma-Aldrich) for 30 min at 37°C and PI (Sigma-Aldrich, USA) for 10 min at 37°C. An IN Cell Analyzer 2200 (GE Healthcare, UK) was used to perform automatic imaging of six fields per well under 200× magnification, in bright field and fluorescence channels. The images produced were used to analyze live and dead cells using the IN Cell Investigator software (GE Healthcare, UK).

RT-PCR Analysis

Total RNA was extracted from the brain samples and organotypic hippocampal slices using the TRIzol Reagent (Thermo Fisher Scientific, USA) and RNeasy Plus Mini kit (Qiagen, USA) according to the manufacturer's instructions. cDNA was synthesized from 1 µg of total RNA using a first strand cDNA Synthesis kit (Fermentas, USA). Quantitative real-time RT-PCR was performed using the CFX96 Real-Time PCR Detection System (Bio-Rad, USA) and the PCR iTaq Universal SYBR Green Supermix (Bio-Rad, USA) under the following conditions: 95°C for 2 min, followed by 40 cycles at 95 °C for 10 s and 60°C for 30 s. The total reaction volume was 25 µl. The relative amount of mRNA was normalized against Gapdh mRNA, and the fold change for each mRNA was calculated by the $2^{-\Delta Ct}$ method. Primer sequences for rat and mouse genes are presented in **Table 1**.

Immunostaining

For immunohistochemistry, 3-µm sections of formalin-fixed, paraffin-embedded tissue samples were used. Deparaffinization and antigen retrieval were performed in PT Module with Dewax and HIER Buffer L (Thermo Scientific, USA). Tissue sections were stained using Lab Vision™ Autostainer 720-2D according to the UltraVisionQuanto HRP DAB Protocol (Thermo Scientific, USA). Briefly, sections were incubated with UltraVision Hydrogen Peroxide Block buffer for 10 min RT and then UltraVision Protein Block solution for 5 min RT before being incubated with primary mouse monoclonal antibody to CS-AC (1:100, CS-56, C8035, Sigma-Aldrich, USA) for 1 h RT. The signal was visualized by incubations with Primary Antibody Amplifier Quanto (10 min, RT), HRP Polymer Quanto (10 min, RT), and DAB Quanto solutions (5 min, RT). All washing steps were performed with Tris-buffered saline and Tween-20 buffer (Thermo Scientific, USA). Staining patterns were counterstained with hematoxylin and photographed by light microscopy with magnification ×400 (AxioScope.A1 with AxioCamMRc5 (Carl Zeiss, Germany).

Dot-Blots for Chondroitin Sulfate Content

Brain tissue samples were lysed with RIPA-buffer (Thermo Scientific, USA), containing "Complete" Protease Inhibitor Cocktail (Roche, USA), sonicated, and centrifuged for 15 min at 14,000*g*. The protein concentration was quantified using Pierce™ BCA Protein Assay Kit (Thermo Scientific, USA). 1 µg of total proteins were dot-blotted onto PVDF membranes in a volume of 1 µl. The membranes were blocked with 5% non-fat milk for 1 h and incubated with mouse anti-CS primary antibody (1:500, CS-56, C8035, Sigma-Aldrich, USA) overnight at 4°C followed by secondary peroxidase-conjugated antibodies goat anti-Mouse IgG (Abcam, UK) for 1 h at RT. GAGs were detected with an Optiblot ECL Detection Kit (Abcam, UK) according to the manufacturer's instructions. Blots were imaged using ChemiDoc (BioRad, USA) and analyzed semi-quantitatively using ImageJ 1.52 software.

Organotypic Hippocampal Slice Culture *Ex Vivo*

Organotypic hippocampal slice cultures (OHSCs) were prepared according to the previously described protocol (49). Briefly, neonatal Wistar rat pups (postnatal days 8–9) were decapitated, and the brains were rapidly removed under aseptic conditions and placed into ice-cold Hank's balanced solution with 0.9% glucose. The hippocampi were removed and cut rapidly into 400-µm transversal slices with a manual McIlwain tissue chopper (Stoelting Co., USA). The slices were transferred to Millicell

TABLE 1 | Sequences of primers used in PCR analysis.

Description	GeneBank	Gene	Organism	Sequence
Syndecan-1	NM_013026.2	Sdc1	*Rattus norvegicus*	F 5'-GAACCCACCAGCAGGGATAC-3'
				R 5'-CACACTTGGAGGCTGATGGT-3'
	NM_011519.2	Sdc1	*Mus musculus*	F 5'-GGTCTGGGCAGCATGAGAC-3'
				R 5'-GGAGGAACATTTACAGCCACA-3'
Glypican-1	NM_030828.1	Gpc1	*Rattus norvegicus*	F 5'-GCCAGATCTACGGGGCTAAG-3'
				R 5'-AGACGCAGCTCAGCATACAG-3'
	NM_016696.5	Gpc1	*Mus musculus*	F 5'-CTTTAGCCTGAGCGATGTGC-3'
				R 5'-GGCCAAATTCTCCTCCATCT-3'
Perlecan	XM_017593851.1	Hspg2	*Rattus norvegicus*	F 5'-TGATGACGAGGACTTGCTGG-3'
				R 5'-ACACCACACTGACAACCTGG-3'
	NM_008305.3	Hspg2	*Mus musculus*	F 5'-CCGTGCTATGGACTTCAACG-3'
				R 5'-TGAGCTGTGGAGGGTGTATG-3'
Versican	NM_001170558.1	Vcan	*Rattus norvegicus*	F 5'-ATGTGGATCATCTGGACGGC-3'
				R 5'-GTTTCGATGGTGGTTGCCTC-3'
	NM_001081249.1	Vcan	*Mus musculus*	F 5'-GGAGGTCTACTTGGGGTGAG-3'
				R 5'-GGGTGATGAAGTTTCTGCGAG-3'
Brevican	NM_012916.2	Bcan	*Rattus norvegicus*	F 5'-AGGGGACCTCACAAGTTCTTC-3'
				R 5'-ATTTGACTCGGGGAAAGCCC-3'
	NM_012916.2	Bcan	*Mus musculus*	F 5'-GTGGAGTGGCTGTGGCTC-3'
				R 5'-AACATAGGCAGCGGAAACC-3'
CSPG4/NG2	NM_031022.1	Cspg4	*Rattus norvegicus*	F 5'-ATCTGGGAGGGGGCTATTGT-3'
				R 5'-GTACGCCATCAGAGAGGTCG-3'
	NM_139001.2	Cspg4	*Mus musculus*	F 5'-TCTTACCTTGGCCCTGTTGG-3'
				R 5'-ACTCTGGTCAGAGCTGAGGG-3'
CD44	NM_009851.2	Cd44	*Mus musculus*	F 5'-CAAGTTTTGGTGGCACACAG-3'
				R 5'-AGCGGCAGGTTACATTCAAA-3'
Decorin	NM_024129.1	Dcn	*Rattus norvegicus*	F 5'-AATGCCATCTCCGAGTGGTG-3'
				R 5'-TTGTCGTGGAGTCGAAGCTC-3'
	NM_007833.6	Dcn	*Mus musculus*	F 5'-CCCCTGATATCTATGTGCCC-3'
				R 5'-GTTGTGTCGGGTGGAAAATC-3'
Biglycan	NM_017087.1	Bgn	*Rattus norvegicus*	F 5'-GAACAGTGGCTTTGAACCCG-3'
				R 5'-CCTCCAACTCGATAGCCTGG-3'
	NM_007542.5	Bgn	*Mus musculus*	F 5'-GCCTGACAACCTAGTCCACC-3'
				R 5'-CAGCAAGGTGAGTAGCCACA-3'
Lumican	NM_031050.1	Lum	*Rattus norvegicus*	F 5'-AATTTGACCGAGTCCGTGGG-3'
				R 5'-GCCTTTCAGAGAAGCCGAGA-3'
Neurocan	NM_007789.3	Ncan	*Mus musculus*	F 5'-CCAGCGACATGGGAGTAGAT-3'
				R 5'-GGGACACTGGGTGAGATCAA-3'
Gapdh	NM_017008.4	Gapdh	*Rattus norvegicus*	F 5'-ATGGCCTTCCGTGTTCCTAC-3'
				R 5'-TCCAGGGTTTCTTACTCCTTGG-3'
	NM_008084.3	Gapdh	*Mus musculus*	F 5'-CGTCCCGTAGACAAAATGGT-3'
				R 5'-TTGATGGCAACAATCTCCAC-3'

culture inserts (Millipore, PICM0RG50) placed into six-well plate containing 1.2 ml of culture medium, consisting of 30% Hank's balanced solution, 60% IMDM and 10% fetal bovine serum. The organotypic hippocampal slices were cultivated in a 90% humidified atmosphere with 5% CO_2 at 37°C. The medium was changed the next day. At the day 4 of the experiment, ½ of the medium was replaced with neurobasal medium supplemented with B27 (Gibco, USA), at day 7, medium was completely replaced with Neurobasal+B27 medium and changed twice a week.

TMZ and/or DXM were added to the culture medium to final concentrations 250 and 1 μM, respectively, at day 7 of the experiment, the treatment conditions were taken from our previous work (48). The organotypic hippocampal slices were incubated with drugs for 24 h, washed with fresh medium and used for co-culture with glioma cells or collected into RNA*Later* solution for RT-PCR analysis.

GAG Content Manipulation in Rat Brain Organotypic Slices

To degrade endogenous GAGs in the organotypic slices, enzymes chondroitinase AC (EC 4.2.2.5, Sigma-Aldrich, USA), and chondroitinase B (EC 4.2.2.19, Sigma-Aldrich, USA) were used. Chondroitinase AC (0.5 U/ml) or chondroitinase B (30 U/ml) were resuspended in the reaction buffer (150 mM NaCl, 25 mM K_2PO_4, pH 6.5) and applied to brain organotypic slices on the day 8 of the experiment in a volume of 10 μl/slice. The slices were incubated for 1 h at 37°C and 5% CO_2, washed with fresh culture medium and used to co-culture with glioblastoma U87-RFP cells.

To increase the amount of GAGs in the organotypic culture, endogenous CS-A/C (Sigma-Aldrich, USA) or CS-B (Sigma-Aldrich, USA) were added to the culture medium on the 8th day of the experiment to a final concentration 0.5 mg/ml. The

content of exogenous GAGs in the medium was maintained during subsequent cultivation with GBM U87-RFP cells.

Validation of the used reagents' specificity is provided on the technical specification inserts.

Co-Culture of Organotypic Hippocampal Slices With U87 GBM Cells

U87-RFP cells were harvested using trypsin/EDTA, pelleted by centrifugation, and resuspended in Neurobasal medium.

To analyze the adhesion of tumor cells to the surface of organotypic slices, 12500 cells in 10 µl were applied onto each slice, incubated for 2 h at 37°C and 5% CO_2, washed in PBS, and fixed in 10% neutral buffered formalin at 4°C for 16 h. To assess the proliferation of tumor cells and their invasion into organotypic slices, 2,500 cells in 5 µl were applied onto each slice, incubated for 7 days at 37°C and 5% CO_2, then washed with PBS and fixed in 10% neutral buffered formalin at 4°C for 16 h. After fixation, organotypic slices-U87-RFP co-cultures were washed three times in PBS, transferred onto microscope slides, and covered with a coverslip using SlowFade Gold medium with DAPI (Thermo Scientific, USA). These co-cultures were visualized using an LSM 710 laser confocal microscope (Carl Zeiss, Germany). Images were acquired in z-stack and tile-scan modes to visualize the signal over the entire volume of the slice. The acquisition, processing, and analysis of images were performed using the ZEN Black 2012 software (Carl Zeiss, Germany). Tumor cell adhesion was determined as the percentage of the slice surface area occupied by tumor cells (summarized signal from 20 µm deep slice volume); the proliferation of tumor cells was determined as a percentage of the area occupied by tumor cells in the maximum intensity projection mode (summarized signal from the whole slice volume); the invasion of tumor cells was determined as a percentage of the area occupied by tumor cells at a depth of 25 µm from the slice surface.

Drug Administration to Healthy SCID Mice *In Vivo*

In total, 64 male SCID mice were randomly divided into four experimental groups. TMZ-group (n = 16) received TMZ (MSD, Finland) intragastric as a water suspension in a dose of 30 mg/kg; DXM-group (n=16) received intraperitoneal injection of 1 mg/kg DXM (KRKA, Slovenia), TMZ-DXM-group (n=16) received both TMZ and DXM; control group received water intragastric in the same volume as the TMZ-group. The drugs were administered according to the scheme: three cycles of 5 consecutive days of administration with a 9-day break between cycles (a total of 15 drug injections). The animals were weighed once a week. On the 39th day of the experiment, six animals from each group were sacrificed by cervical dislocation; the brains were removed, one hemisphere was divided into cerebral cortex and subcortex and collected in RNA*Later* solution (Invitrogen, USA) for RT-PCR analysis, the second hemisphere was incubated in 10% neutral buffered formalin for 24 h at room temperature and used to prepare paraffin blocks.

The remaining animals received an orthotopic injection of human GBM U87 cells.

Orthotopic Experimental Tumors Development in the Pre-Treated SCID Mice Brain

The experimental human GBM tumors were induced in the brain of the pre-treated SCID mice by a stereotactic inoculation of U87 cells into the subcortical brain structures (50). Briefly, mice were placed into a chamber with 1.5% isoflurane and airflow of 450 to 500 ml/min for 3 min, and then transferred onto a 37°C heated operating table and placed under an anesthesia mask with 1.5% isoflurane. A 3- to 4-mm incision on the head skin was made in the caudal-cranial direction in the bregma area, and 5 µl of U87 cells suspension in serum-free DMEM/F12 medium (5×10^5 cells per animal) was injected into the subcortical brain structures with a Hamilton syringe through a hole in the skull. The experimental tumor growth was monitored by magnetic resonance imaging (MRI) every 5 days starting at day 10 after tumor cells inoculation using a BioSpec 117/16 USR horizontal tomograph (Bruker, Germany) at 11.7 T using a TurboRARE (Rapid Imaging with Refocused Echoes) T2 scanning sequence (TR=2500 ms, TE_{eff}=24 ms, NA=5, Rare factor = 8, matrix 256×256 dots, field of view 2.0 cm × 2.0 cm). All manipulations were performed on anesthetized animals (1.5% isoflurane in a gas mixture with oxygen and a flow rate of 350–450 ml/min). Tumor size was calculated using the Paravision 5.1 (Bruker) and ImageJ software and expressed in µl. Mice were sacrificed upon 20% weight loss by decapitation using guillotine according AVMA Guidelines for the Euthanasia of Animals (American Veterinary Medical Association, 2013); no hunching, rough coat, ataxia, head tilt, and paralysis were detected. Brains were removed, one hemisphere was divided into the cerebral cortex, subcortex, and tumor and collected into RNA*Later* for RT-PCR analysis, the other hemisphere was fixed in 10% neutral buffered formalin and used to prepare paraffin blocks.

Statistical Analysis

ANOVA analysis with Fisher's least significant difference (LSD) *post hoc* test was performed to determine statistical significance between the studied groups. A value of $p<0.05$ was considered to indicate a statistically significant difference. Data are expressed as means ± SD. Survival analysis was performed by the Kaplan-Meier method. Pearson correlation coefficient was determined to analyze the correlation between PGs expression and tumor volume. All statistical analyses were performed using OriginPro 8.5 software.

RESULTS

Because our previous data indicated that TMZ and DXM change PGs structure and composition in normal rat brain tissue (48), we performed a number of functional tests to investigate whether the structural ECM changes affect a fate of GBM cells in pre-treated

brain microenvironment and contribute to experimental tumor development mimicking a GBM relapse. Two complementary approaches were combined in a GMB relapse mouse model—xenograft tumor growth in immunocompromised mice *in vivo* and co-culture of GBM cells with brain slice cultures *ex vivo* that closely mimic tumor cell invasion into the brain *in vivo* (46).

TMZ and DXM Facilitates Adhesion, Proliferation, and Invasion of GBM Cells Into Rat Brain Organotypic Slices *Ex Vivo*

First, we performed the experiment on co-culture of organotypic brain slices with U87-RFP cells (**Figure 1A**). The hippocampal slices were treated with TMZ and/or DXM, and the drugs were removed from the culture medium before addition of U87 cells. TMZ/DXM-induced changes in PGs expression were verified by real-time RT-PCR analysis (**Supplementary Figure 1**). Adhesion, proliferation, and invasion of the fluorescent-labeled cells on the pre-treated brain tissue were assessed as shown (**Figure 1B**), representative pictures are presented (**Figure 1C**), and staining signal was quantified using ImageJ 1.52 software (51) (**Figure 1D**). It was shown that TMZ and DXM possess different effects on brain ECM structure. Although DXM-induced changes facilitated adhesion of GBM cells to the pre-treated hippocampus slices (4- to 5-fold, $p<0.05$), TMZ-induced changes favored the proliferation of the cells (7-fold, $p<0.001$) (**Figures 1C, D**). The most drastic deterioration of brain ECM occurred upon combined TMZ/DXM treatment that resulted in significant activation of U87 adhesion (4- to 5-fold $p< 0.01$), proliferation (9- to 10-fold, $p< 0.001$), and invasion (9- to 10-fold, $p< 0.001$) to the pre-treated brain organotypic culture. These data demonstrate that healthy brain tissue is capable of suppressing adhesion and proliferation of cancer cells, but the systemic use of TMZ (especially in combination with DXM) attenuates this ability and contributes to the transformation of brain microenvironment into a pro-invasive niche. Together, these results reveal the overall toxic effects of systemic use of TMZ (especially in combination with DXM) to brain tissue structure in terms of PGs/GAGs pattern and content, and their impaired ability to resist cancer cells adhesion and proliferation in experimental system *ex vivo*.

Pre-Treatment of SCID Mice With TMZ and DXM Increases Growth and Invasive Potential of Xenograft U87 Tumors *In Vivo*

To investigate the effects of TMZ chemotherapy *in vivo*, we elaborated a mouse model of GBM relapse, where healthy animals were first treated with TMZ and/or DXM, and then the glioma U87 cells were inoculated into the brain pre-exposed to chemotherapeutic drug(s) (**Figure 2**). This model mimics a clinical situation where post-surgery residual GBM cells have to survive and proliferate in the microenvironment compromised by a long-term TMZ pressure. Indeed, we observed a significant (2.5- to 3-fold) increase in the growth rate and final volume of xenograft U87 tumors in the animals that have undergone

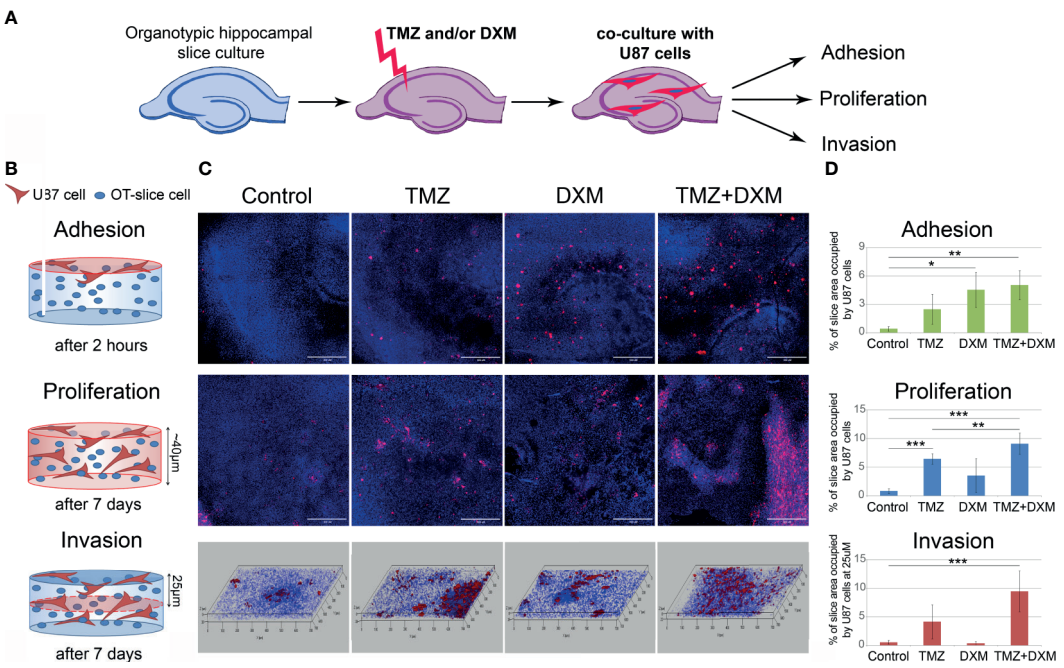

FIGURE 1 | Effects of TMZ and/or DXM-induced changes in brain organotypic slices on adhesion, proliferation and invasion of GBM cells *ex vivo*. **(A)** Scheme of the experiment. **(B)** Methodology for detection of the studied parameters. **(C)** Confocal microscopy of U87-RFP cells seeded on the control and TMZ/DXM-treated organotypic brain slices. Cells nuclei are stained with DAPI. Magnification, ×200, scale bar 500 μm. **(D)** Quantitative analysis of the U87-RFP cells on the control and treated rat brain tissues. ANOVA and post-hoc Fisher's LSD test, *$p < 0.05$, **$p < 0.01$, ***$p < 0.001$. TMZ, temozolomide; DXM, dexamethasone.

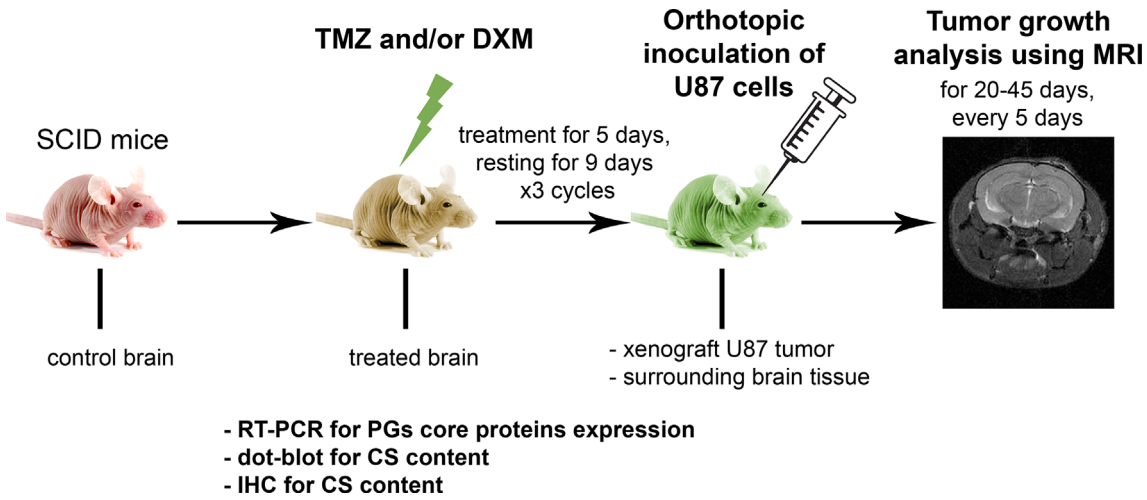

FIGURE 2 | Experimental GBM relapse animal model. Scheme of the experiment to study the effects of pre-treatment of SCID mice with chemotherapeutic drugs on the growth of xenograft U87 tumors. PG, proteoglycan; CS, chondroitin sulfate; TMZ, temozolomide; DXM, dexamethasone.

TMZ or DXM treatments compared with control animals (**Figures 3A–C**). Other things being equal, normal brain tissue possessed a restraining effect on tumor growth *in vivo*, being similar to the results obtained in the *ex vivo* model system.

Interestingly, the xenograft tumors grown in the animals that received TMZ or combined TMZ-DXM treatment demonstrated not only the bigger tumor size but also more invasive phenotype as well, seen on MRI images, unlike those with DXM-treatment (**Figure 3A**). They developed extracranial tumors at significantly higher rates (**Figure 3D**), supporting further the conclusion about an accelerated invasion of GBM cells into the TMZ-compromised brain tissue. The calculated odds ratio showed a 3.8- to 4.5-fold higher probability of extracranial tumor formation in the brain of TMZ-treated animals (**Figure 3E**). At the same time, the final body weight of the mice from different experimental groups did not differ (although some fluctuations following the TMZ/DXM treatments occurred), and overall survival rates were similar (**Figures 3F, G**).

These *in vivo* results match to the data obtained in brain organotypic slices *ex vivo* and demonstrate different effects of TMZ and DXM on healthy brain tissue, where TMZ pre-treatment (especially in combination with DXM) facilitates adhesion, proliferation, and invasion of GBM cells into the surrounding brain tissue and active growth of the experimental tumors.

TMZ and/or DXM Affect PGs Expression in Normal Mouse Brain Tissue

To analyze the effect of TMZ or DXM on cellular components of normal mouse brain tissue, the viability of primary mixed glial cells from mouse brain and their proliferation rate upon TMZ/DXM treatment were analyzed using InCell Analyzer 2000 System (**Figure 4**). None of the treatments had a significant effect on the amount of dead cells in the culture (**Figure 4A**), although their proliferative activity was inhibited (**Figures 4B, C**).

TMZ/DXM treatment significantly affected the expression of some PG core proteins in the brain of healthy SCID mice in brain zone-specific manner (**Figure 4D**), whereas U87 xenograft tumor growth did not significantly change PGs' expression in the brain of the SCID mice (**Figure 4E**). The most significant changes were observed after combined treatment with TMZ/DXM (**Figure 4F**). DXM increased mRNA levels of biglycan (2.7-fold, $p<0.05$) in the cortex, and glypican-1 (3.5-fold, $p<0.01$), syndecan-1 (4.3-fold, $p<0.05$), and versican (3.1-fold, $p<0.001$) in the subcortex. TMZ alone did not significantly affect the transcriptional activity of PG-coding genes in the brain tissue, but in combination with DXM resulted in a completely different pattern of PG expression: up-regulation of biglycan (4.3-fold, $p<0.05$), CD44 (6.3-fold, $p<0.01$), and decorin (3.6-fold, $p<0.01$) in cortex and increased expression of glypican-1 (3.2-fold, $p<0.01$) and versican (3.7-fold, $p<0.001$) in subcortex. The obtained results demonstrate that TMZ/DXM selectively affect the expression of some PGs at the mRNA levels, resulting in the specific PGs expression patterns and deteriorated brain ECM composition.

TMZ and/or DXM Decrease CS Content in Normal Mouse Brain Tissue

Because the functional properties of complex PG molecules to a large extent depend on their GAG chains, and decorin and brevican are the most expressed PGs in mouse brain tissue responding to TMZ/DXM treatment, we next analyzed the content of CS-AC in the TMZ/DXM-treated brain tissues. According immunohistochemical analysis (IHC) of brain tissue samples (include cerebral cortex and subcortex structures), CS is abundant in healthy SCID mice brain tissue, but combined TMZ/DXM treatment significantly decreased total CS-AC content (−2.3-fold, $p<0.05$) (**Figure 5A**, upper line). Inoculation of U87 GBM cells into the mouse brain resulted in the decrease of CS-AC

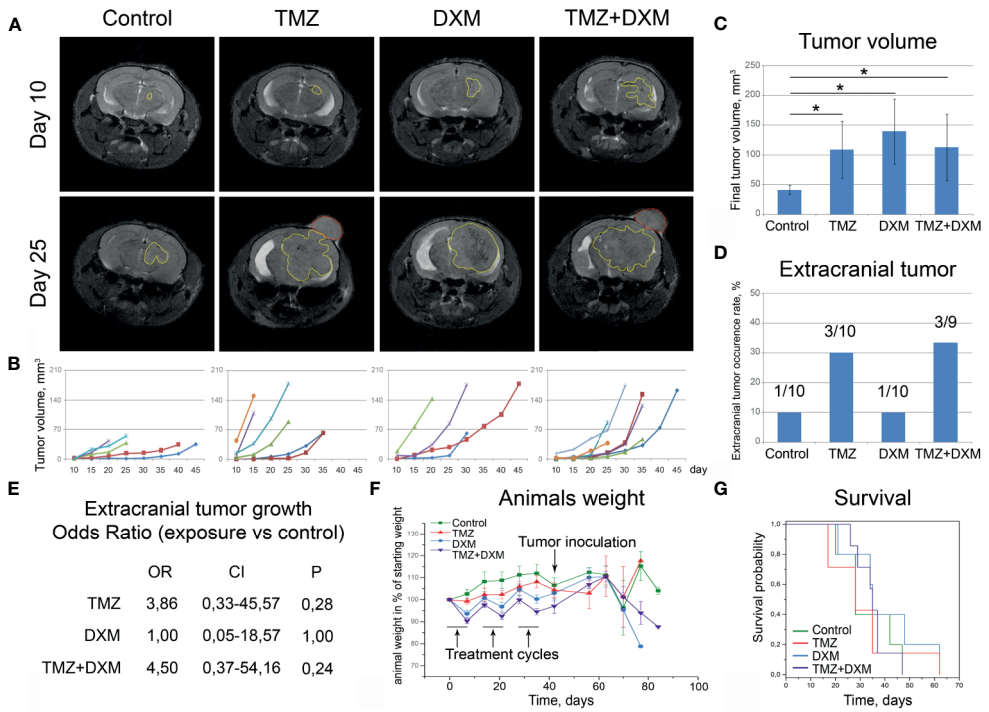

FIGURE 3 | Functional effects of TMZ and/or DXM-induced changes in brain tissue on the development of experimental U87 xenograft tumors. **(A)** MRT-images of the representative U87 xenografts. Intracranial tumors marked with a yellow outline, extracranial—red outline. **(B)** Growth curves for the xenografts in control and treated brains. **(C)** Final volume of the xenografts. ANOVA and post-hoc Fisher's LSD test, *p < 0.05. **(D)** Frequency of the extracranial tumors in all experimental groups. **(E)** Odds ratio of extracranial tumors development (OriginPro 8.5). **(F)** Weight of the animals during the experiment. **(G)** Survival of the animals (Kaplan-Meier curve). TMZ, temozolomide; DXM, dexamethasone.

content in paratumorous tissue to approximately the same level as that in TMZ/DXM-treated brain tissue, and this effect was even more pronounced when U87 xenografts were developed in TMZ/DXM pre-treated animals (**Figure 5A**, middle line). The U87 xenograft tumors themselves retained a high level of CS-AC content, mainly in the GBM cells (**Figure 5A**, lower line).

Quantitative analysis of the changes in CS-AC content was performed using dot-blot analysis with CS-AC–specific antibody (clone CS-56) for cerebral cortex and subcortex tissues separately (**Figures 5B–E**, respectively). Cerebral cortex was relatively resistive to the manipulations and showed significant decrease of CS content only after combined TMZ/DXM treatment (−2-fold, $p<0.05$) or U87 inoculation (−2-fold, $p<0.05$) (**Figures 5B, C**). Subcortex was more sensitive to any influence (TMZ, DXM, U87 inoculation with/without drug pre-treatments) demonstrating −2- −4-, 5-fold decrease in CS-AC content ($p<0.01$) (**Figures 5D, E**).

Together, these data support a hypothesis that both GBM cells and TMZ treatment contribute to the reorganization of brain ECM towards a pro-tumorigenic and pro-invasive microenvironmental niche, being more susceptible to GBM relapse development, through the attenuation of CS-AC content in brain ECM.

The obtained results for the first time indicate PGs/GAGs as potential targets for chemotherapeutic drug(s) in brain tissue, possibly involved in its transformation to a pro-tumorigenic niche.

Xenograft U87 Tumors Growth Is Associated With PGs Expression in Mouse Brain Tissue

To investigate whether these TMZ/DXM-induced changes in PGs expression are associated with the increased proliferation and invasion of U87 cells, we used two complementary approaches.

First, all the mice bearing U87 xenografts were allocated to three groups with relatively small (<30 μl), medium (30–70 μl), or big (>70 μl) tumors, and PG expression in the brain tissue surrounding these xenografts was analyzed separately in each of the cohorts (**Figure 6A**). Indeed, the normal tissue surrounding bigger-sized U87 tumors possessed significantly higher mRNA levels for multiple PGs, such as decorin (+3.2-fold, $p<0.01$), biglycan (+2.7-fold, $p<0.05$), glypican-1 (+4.7-fold, $p<0.01$), syndecan-1 (+3.4-fold, $p<0.05$), brevican (+3.8-fold, $p<0.01$), NG2/CSPG4 (+4.9-fold, $p<0.01$), neurocan (+4.7-fold, $p<0.05$), compared with the normal tissue surrounding small tumors.

Then, the whole experimental cohort was analyzed according to the high or low expression level of each individual PG and

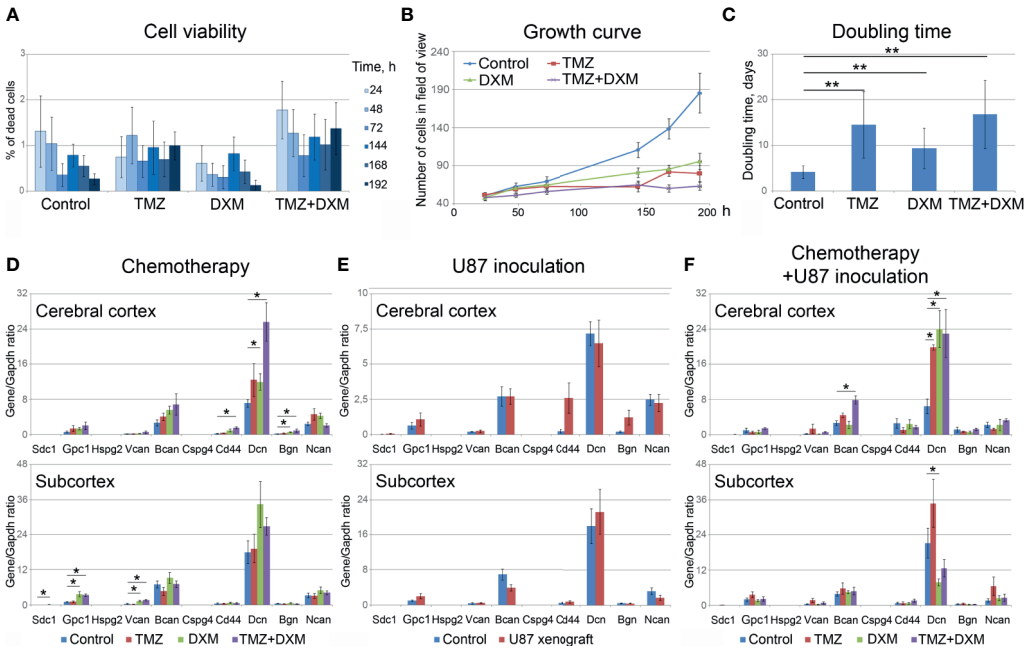

FIGURE 4 | Effects of TMZ and/or DXM on normal glial cells and proteoglycans expression in brain tissue. **(A)** Viability of primary glial cells during the treatments (as a percentage of dead cells in the culture). **(B)** Growth curves of the control and TMZ/DXM-treated cells. **(C)** Doubling time for the control and treated cells. **(D, E)** PG core proteins mRNA levels in cortex and subcortex before and after treatments with TMZ and/or DXM **(D)** or U87 cells inoculation **(E)** or combination of TMZ/DXM treatments and inoculation of U87 cells **(F)**. Real-time RT–PCR analysis, intensity of the amplified DNA fragments normalized to that of *Gapdh*. Bars represent the mean ± SD from triplicate experiments (OriginPro 8.5). ANOVA + Fisher's LSD test, *p < 0.05, **p < 0.01. TMZ, temozolomide; DXM, dexamethasone.

xenograft size in these animals. The transcriptional activity of three of the studied PGs (decorin, glypican-1, brevican) demonstrated a clear tendency to be correlated with the size of the experimental xenograft tumors (**Figure 6B**). To verify this observation, correlation analysis was performed for these best candidate PGs and confirmed a high correlation between the U87 xenograft volumes and the expression levels of the PGs surrounding the normal mouse brain tissue: decorin (Pearson's correlation coefficient r=0.69), brevican (Pearson's r=0.77), and glypican-1 (Pearson's r=0.80) (**Figure 6C**).

These data suggest that TMZ-induced changes in the PGs expression in brain tissue contribute to the increased proliferative and invasive capacity of GBM cells in TMZ-compromised microenvironment.

Degradation of Chondroitin Sulfate but Not Dermatan Sulfate Results in the Accelerated Adhesion and Invasion of GBM Cells Into Brain Tissue

To study a functional role of CS in GBM cells fate in the pre-treated microenvironment further, we used two approaches, consisting of the removal of different CS sub-types (CS-A/C or CS-B, called also dermatan sulfate, DS) by chondroitinase AC or chondroitinase B treatments (**Figure 7A**) and addition of exogenous CS-AC or CS-B (**Figure 7B**). The enzymes (chondroitinase AC and chondroitinase B) have been reported to be specific for the native CS polysaccharide molecules. They degrade specifically CS sub-types A/C and B, respectively, and may be used for identification of these CS sub-types in tissues and cells.

It was shown that enzymatic degradation of CS-AC in the organotypic brain slices before their co-culture with U87 cells increased adhesion and invasion but not proliferation of U87 cells on these pre-treated slices, whereas addition of exogenous CS-AC to the intact co-cultures of brain slices with U87 cells did not affect any of the studied functional characteristics of the GBM cells (adhesion, proliferation, migration) (**Figures 7C, D**). Pre-treatment of the brain slices with chondroitinase B did not affect the interaction of U87 cells with the brain tissue, although the exogenous CS-B significantly increased adhesion, proliferation, and migration of U87 cells (**Figures 7C, D**). The results suggest that CS-AC is a vital component, and an optimal balance of CS-AC and CS-B is required for the ability of healthy brain tissue to resist glioblastoma cells proliferation and invasion.

Taken together, the obtained results for the first time demonstrate that the TMZ-induced changes of PGs expression and CS-AC/CS-B content directly contribute to the accelerated proliferation and invasion of GBM cells into the compromised brain tissue and xenograft tumor growth in the used GBM relapse model.

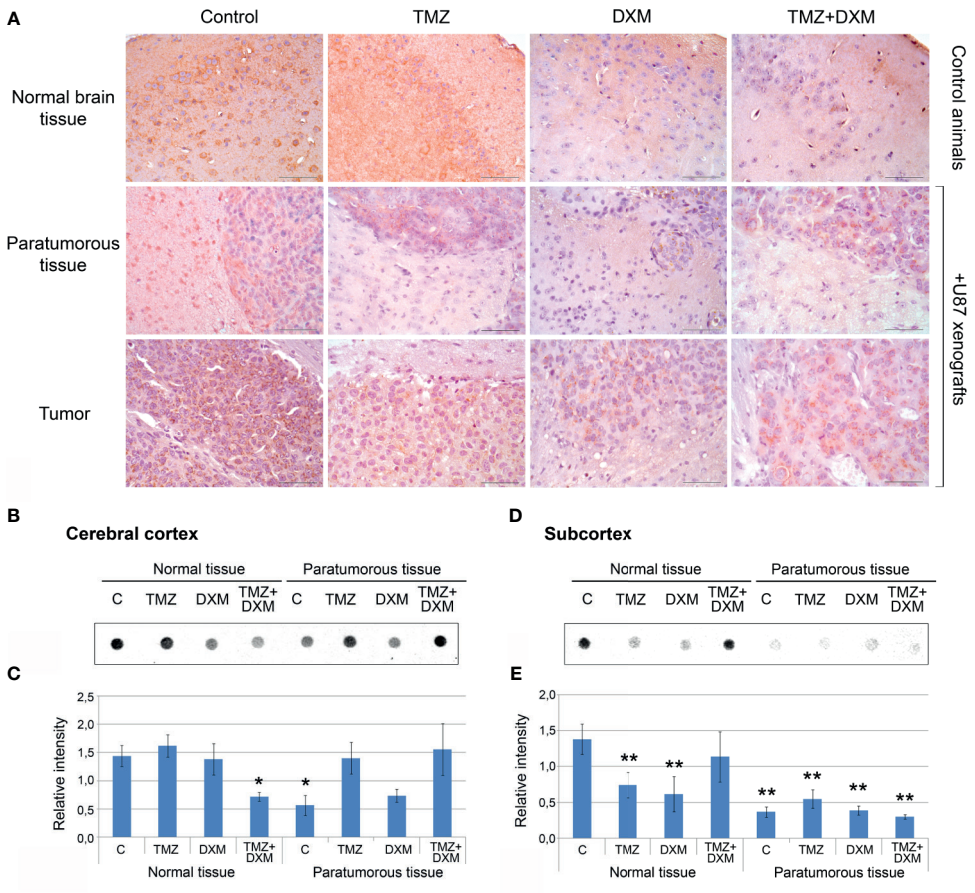

FIGURE 5 | Chondroitin sulfate content in SCID mice brain tissues before and after treatments with TMZ and/or DXM. **(A)** Immunohistochemical analysis of CS content before and after TMZ/DXM treatments in normal SCID mouse brain tissue, paratumorous tissue and U87 xenografts. Magnification *400. Scale bars 50 μm. **(B–E)** Dot-blot analysis of the total CS content using anti-CS antibody in cortex and subcortex structures. **(B, D)** Original representative dot blots. **(C, E)** Semi-quantitative analysis of the dot-blots (ImageJ 1.52 software). Bars represent the mean ± SD from triplicate experiments (OriginPro 8.5). ANOVA + Fisher's LSD test, *$p < 0.05$, **$p < 0.01$. Control, non-treated mouse brain tissue; TMZ, temozolomide; DXM, dexamethasone.

DISCUSSION

It is known that after adjuvant chemoradiotherapy, GBM commonly recurs around the tumor removal site. It was suggested by Hide and Komohara that the microenvironment at the tumor border ("border niche") provides therapeutic resistance to residual GBM cells that allows them to survive and recur at the tumor border, and its understanding is critical to prevent GBM relapse (52). Investigation of GBM TME, especially its extracellular components, demands specific approach related to the preservation of brain tissue ECM.

Currently, multiple glioma models were developed to investigate molecular mechanisms of GBM development, drug resistance of GBM cells, and role of cancer-initiating cells in these processes (41, 42). However, the number of models for studying GBM microenvironment is much smaller (44), and this is also the case for the number of models that investigate molecular mechanisms of GBM relapse development (43). In common, these parameters were investigated separately like studying cellular components (astrocytes) in the recurrent tumors grown after the resection of the primary glioma xenografts (43) or investigation of glioma cells invasion into normal brain slice cultures (45–47). In this study, we suggested a novel GBM relapse model combining mouse experiments *in vivo* and organotypic brain culture *ex vivo*, where normal brain tissue was pre-modified by TMZ and/or DXM before the inoculation of GBM cells to mimic GBM relapse development after extensive adjuvant chemotherapy (in contrast to conventional glioma models in which drug treatments are usually performed after the inoculation of cancer cells). Compared with other approaches, a specificity of this model is in the joining GBM relapse study and investigation of the role of glycosylated extracellular components of brain tissue in organotypic brain culture *ex vivo* pre-treated with TMZ/DXM. This approach allows obtaining original data on the involvement of brain TME in the GBM relapse development and can be useful for further research in this field.

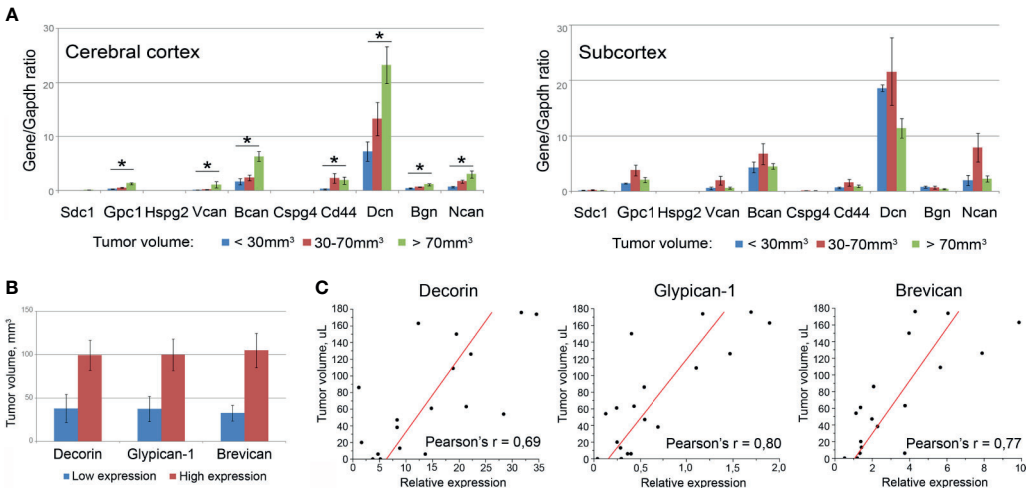

FIGURE 6 | Association of the PGs expression levels in surrounding tumor normal tissue with the total volume of U87 xenografts. **(A)** PG expression levels in brain tissue of animals grouped according to the xenograft tumors size (small <30 µl; medium 30-70 µl; big >70 µl). Bars represent the mean ± SD from triplicate experiments (OriginPro 8.5). ANOVA + Fisher's LSD test, *p < 0.05. **(B)** Tumor volumes in animals with relatively high or low expression of selected PGs (decorin, brevican, glypican-1). **(C)** Pearson's linear correlation of the xenograft volumes with the expression levels of the PGs in surrounding normal brain tissue (OriginPro 8.5).

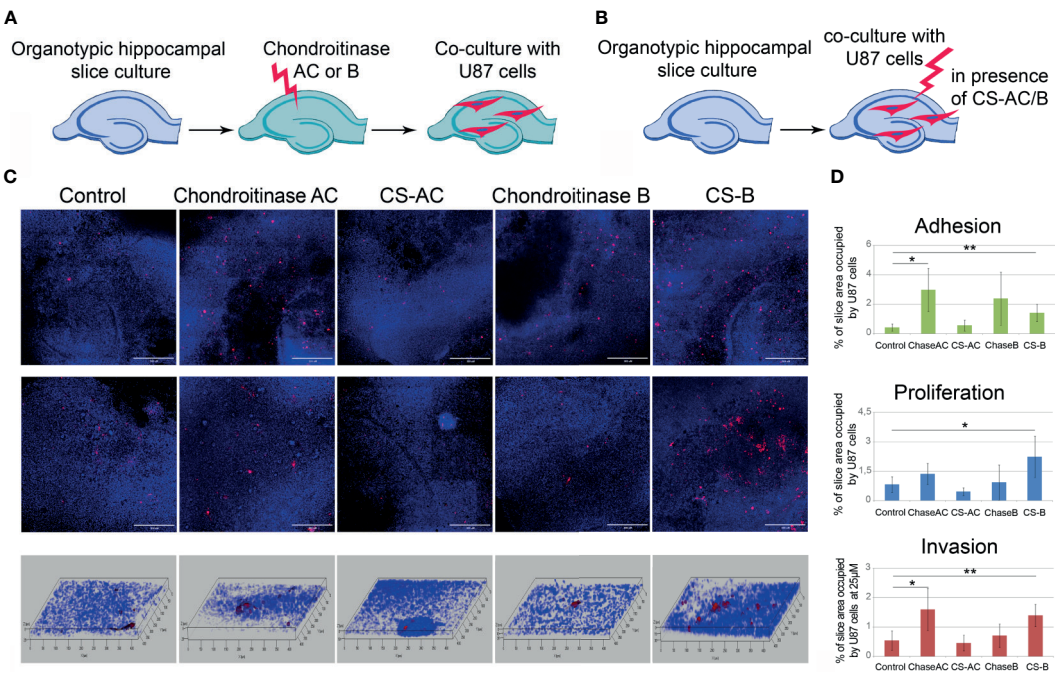

FIGURE 7 | Effects of experimental modulation of CS content on adhesion, proliferation and invasion of GBM cells *ex vivo*. **(A, B)** Schemes of the experiment. **(C)** Confocal microscopy of U87-RFP cells seeded on the control organotypic brain slices and slices treated with chondroitinase AC or exogenous chondroitin sulfate AC (CSAC), chondroitinase B or chondroitin sulfate B (CSB). Cells nuclei are stained with DAPI. Scale bar 500 µm. **(D)** Quantitative analysis of the U87-RFP cells on the control and treated rat brain tissues (ImageJ 1.52 software). ANOVA and post-hoc Fisher's LSD test, *p < 0.05, **p < 0.01. TMZ, temozolomide; DXM, dexamethasone.

Our results for the first time demonstrate that TMZ-induced deterioration of PGs expression and degradation of polysaccharide molecules CA-AC (but not CS-B) in normal brain tissue may represent a molecular mechanism for survival of the GBM cells and their active proliferation and invasion in the surrounding pre-treated brain tissue resulting in the relapse tumor development. These results add a piece of knowledge to the scarce published data on this issue and stay in line with the findings that CSPGs-rich brain ECM is associated with a noninvasive phenotype of GBM tumors, whereas low CSPGs content is more common for infiltrating tumors (26, 27). The effects are realized through activation of tumor-associated microglia and tumor encapsulation (26) and regulation of the dynamics of the CSPG binding with its receptor LAR (27) and are attributed to the complex CSPG proteoglycan molecules. At first glance, contradictory results were shown by Logun et al., showing that blockade of sulfated polysaccharide CS chains by the sulfated GAG antagonist surfen reduces adhesion and invasion of GBM cells in 3D composite highly sulfated CSA/E matrices. However, this effect was much weaker for low- or non-sulfated matrices and suggested that the functional effects of CSPGs to GBM cells invasion depend on CS sub-types and their sulfation (53). Together with different functional effects of CS-AC or CS-B (dermatan sulfate) degradation on the proliferation and invasion GBM cells shown in this study, these data perfectly correspond to the known differential functional properties of CS/DS molecules with different sulfation level (54, 55) and underline a necessity of careful consideration of CS/DS sub-types in further research on glioma cells behavior and GBM relapse development.

Overall, our findings indicate that long-term TMZ treatment affects the polysaccharide components of brain tissue ECM, transforming that into the pro-carcinogenic niche and creating a favorable microenvironment for GBM relapse development. A balance between the targeted effects and negative side effects of the systemic TMZ treatment toward brain ECM might have a principal mean for GBM relapse development and needs further investigation.

DATA AVAILABILITY STATEMENT

The original contributions presented in the study are included in the article/**Supplementary Material**. Further inquiries can be directed to the corresponding author.

ETHICS STATEMENT

The animal study was reviewed and approved by Animal Care and Use Committees of the Institute of Cytology and Genetics SB RAS and FRC FTM.

AUTHOR CONTRIBUTIONS

Conceptualization was performed by AT and EG. Investigation was performed by AT, OS, AK, MK, AS, GK, and AV. Data curation and analysis were performed by AT, SA, EZ, and EG. The writing and editing were performed by AT, SA, and EG. All authors contributed to the article and approved the submitted version.

FUNDING

This study was supported by the Russian Science Foundation (grant 16-15-10243) in part of SCID mice *in vivo* experiments and Russian Foundation for Basic Research (grant 18-29-01036) in part of molecular effects of therapy on CS pathway. AT was supported by scholarship of Russian Federation President for young scientists (SP-5435.2018.4). AS was supported by a scholarship of Russian Federation President for young scientists (SP-1816.2019.4).

ACKNOWLEDGMENTS

Authors thank Dr. Sergey Baiborodin for help with confocal microscopy and Mr. Anton Grigoriev for providing language help and proofreading the article; the "Proteomic analysis" Center and the Multi-Access Center "Modern Optical Systems" (Federal Research Center of Fundamental and Translational Medicine, Novosibirsk, Russia), "Center for Genetic Resources of Laboratory Animals" (RFMEFI62119X0023), and the "Microscopy Center" (Institute of Cytology and Genetics SB RAS, Novosibirsk, Russia) for granting access to the equipment.

SUPPLEMENTARY MATERIAL

The Supplementary Material for this article can be found online at: https://www.frontiersin.org/articles/10.3389/fonc.2021.713139/full#supplementary-material

REFERENCES

1. Stupp R, Mason W, van den Bent MJ, Weller M, Fisher BM, Taphoorn MJB, et al. Radiotherapy Plus Concomitant and Adjuvant Temozolomide for Glioblastoma. *N Engl J Med* (2005) 352:987–96. doi: 10.1056/NEJMoa043330
2. Ortiz R, Perazzoli G, Cabeza L, Jiménez-Luna C, Luque R, Prados J, et al. Temozolomide: An Updated Overview of Resistance Mechanisms, Nanotechnology Advances and Clinical Applications. *Curr Neuropharmacol* (2021) 19(4):513–37. doi: 10.2174/1570159X18666200626204005
3. Cenciarini M, Valentino M, Belia S, Sforna L, Rosa P, Ronchetti S, et al. Dexamethasone in Glioblastoma Multiforme Therapy: Mechanisms and Controversies. *Front Mol Neurosci* (2019) 12:65. doi: 10.3389/fnmol.2019.00065
4. Dubinski D, Hattingen E, Senft C, Seifert V, Peters KG, Reiss Y, et al. Controversial Roles for Dexamethasone in Glioblastoma - Opportunities for Novel Vascular Targeting Therapies. *J Cereb Blood Flow Metab* (2019) 39:1460–8. doi: 10.1177/0271678X19859847
5. Mohtashami E, Shafaei-Bajestani N, Mollazadeh H, Mousavi SH, Jalili-Nik M, Sahebkar A, et al. The Current State of Potential Therapeutic Modalities for Glioblastoma Multiforme: A Clinical Review. *Curr Drug Metab* (2020) 21(8):564–78. doi: 10.2174/1389200221666200714101038
6. Lucifero AG, Luzzi S, Brambilla I, Trabatti C, Mosconi M, Savasta S, et al. Innovative Therapies for Malignant Brain Tumors: The Road to a Tailored Cure. *Acta BioMed* (2020) 91:5–17. doi: 10.23750/abm.v91i7-S.9951
7. Tan AC, Ashley DM, López GY, Malinzak M, Friedman HS, Khasraw M. Management of Glioblastoma: State of the Art and Future Directions. *CA Cancer J Clin* (2020) 70(4):299–312. doi: 10.3322/caac.21613

8. Kamiya-Matsuoka C, Gilbert MR. Treating Recurrent Glioblastoma: An Update. *CNS Oncol* (2015) 4:91–104. doi: 10.2217/cns.14.55
9. Johannessen TA, Bjerkvig R. Molecular Mechanisms of Temozolomide Resistance in Glioblastoma Multiforme. *Expert Rev Anticancer Ther* (2012) 12:635–42. doi: 10.1586/era.12.37
10. Safari M, Khoshnevisan A. Cancer Stem Cells and Chemoresistance in Glioblastoma Multiform: A Review Article. *J Stem Cells* (2015) 10:271–85.
11. Erasimus H, Gobin M, Niclou S, Van Dyck E. DNA Repair Mechanisms and Their Clinical Impact in Glioblastoma. *Mutat Res Rev Mutat Res* (2016) 769:19–35. doi: 10.1016/j.mrrev.2016.05.005
12. Atkins RJ, Ng W, Stylli SS, Hovens CM, Kaye AH. Repair Mechanisms Help Glioblastoma Resist Treatment. *J Clin Neurosci* (2015) 22:14–20. doi: 10.1016/j.jocn.2014.09.003
13. Sørensen MD, Fosmark S, Hellwege S, Beier D, Kristensen BW, Beier CP. Chemoresistance and Chemotherapy Targeting Stem-Like Cells in Malignant Glioma. *Adv Exp Med Biol* (2015) 853:111–38. doi: 10.1007/978-3-319-16537-0_7
14. Beier D, Schulz JB, Beier CP. Chemoresistance of Glioblastoma Cancer Stem Cells–Much More Complex Than Expected. *Mol Cancer* (2011) 10:128. doi: 10.1186/1476-4598-10-128
15. Happold C, Roth P, Wick W, Schmidt N, Florea A, Silginer, et al. Distinct Molecular Mechanisms of Acquired Resistance to Temozolomide in Glioblastoma Cells. *J Neurochem* (2012) 122:444–55. doi: 10.1111/j.1471-4159.2012.07781.x
16. Jackson M, Hassiotou F, Nowak A. Glioblastoma Stem-Like Cells: At the Root of Tumor Recurrence and a Therapeutic Target. *Carcinogenesis* (2015) 36:177–85. doi: 10.1093/carcin/bgu243
17. Dirkse A, Golebiewska A, Buder T, Nazarov PV, Muller A, Poovathingal S, et al. Stem Cell-Associated Heterogeneity in Glioblastoma Results From Intrinsic Tumor Plasticity Shaped by the Microenvironment. *Nat Commun* (2019) 10:1787. doi: 10.1038/s41467-019-09853-z
18. Placone AL, Quiñones-Hinojosa A, Searson PC. The Role of Astrocytes in the Progression of Brain Cancer: Complicating the Picture of the Tumor Microenvironment. *Tumour Biol* (2016) 37:61–9. doi: 10.1007/s13277-015-4242-0
19. Brandao M, Simon T, Critchley G, Giamas G. Astrocytes, the Rising Stars of the Glioblastoma Microenvironment. *Glia* (2019) 67:779–90. doi: 10.1002/glia.23520
20. Hatoum A, Mohammed R, Zakieh O. The Unique Invasiveness of Glioblastoma and Possible Drug Targets on Extracellular Matrix. *Cancer Manag Res* (2019) 11:1843–55. doi: 10.2147/CMAR.S186142
21. Theocharis AD, Karamanos NK. Proteoglycans Remodeling in Cancer: Underlying Molecular Mechanisms. *Matrix Biol* (2019) 75-76:220–59. doi: 10.1016/j.matbio.2017.10.008
22. Iozzo RV, Gubbiotti MA. Extracellular Matrix: The Driving Force of Mammalian Diseases. *Matrix Biol* (2018) 71-72:1–9. doi: 10.1016/j.matbio.2018.03.023
23. Yan Z, Wang S. Proteoglycans as Therapeutic Targets in Brain Cancer. *Front Oncol* (2020) 10:1358. doi: 10.3389/fonc.2020.01358
24. Schwartz NB, Domowicz MS. Proteoglycans in Brain Development and Pathogenesis. *FEBS Lett* (2018) 592:3791–805. doi: 10.1002/1873-3468.13026
25. Wade A, Robinson AE, Engler JR, Petritsch C, James CD, Phillips JJ. Proteoglycans and Their Roles in Brain Cancer. *FEBS J* (2013) 280:2399–417. doi: 10.1111/febs.12109
26. Silver DJ, Siebzehnrubl FA, Schildts MJ, Yachnis AT, Smith GM, Smith AA, et al. Chondroitin Sulfate Proteoglycans Potently Inhibit Invasion and Serve as a Central Organizer of the Brain Tumor Microenvironment. *J Neurosci* (2013) 33:15603–17. doi: 10.1523/JNEUROSCI.3004-12.2013
27. Kim Y, Kang H, Powathil G, Kim H, Trucu D, Lee W, et al. Role of Extracellular Matrix and Microenvironment in Regulation of Tumor Growth and LAR-Mediated Invasion In Glioblastoma. *PloS One* (2018) 13 (10):e0204865. doi: 10.1371/journal.pone.0204865
28. Mellai M, Casalone C, Corona C, Crociara P, Favole A, Cassoni P, et al. Chondroitin Sulphate Proteoglycans in the Tumour Microenvironment. *Adv Exp Med Biol* (2020) 1272:73–92. doi: 10.1007/978-3-030-48457-6_5
29. De Pasquale V, Pavone LM. Heparan Sulfate Proteoglycan Signaling in Tumor Microenvironment. *Int J Mol Sci* (2020) 21(18):6588. doi: 10.3390/ijms21186588
30. Xiong A, Spyrou A, Forsberg-Nilsson K. Involvement of Heparan Sulfate and Heparanase in Neural Development and Pathogenesis of Brain Tumors. *Adv Exp Med Biol* (2020) 1221:365–403. doi: 10.1007/978-3-030-34521-1_14
31. Tran VM, Wade A, McKinney A, Chen K, Lindberg OR, Engler JR, et al. Heparan Sulfate Glycosaminoglycans in Glioblastoma Promote Tumor Invasion. *Mol Cancer Res* (2017) 15:1623–33. doi: 10.1158/1541-7786.MCR-17-0352
32. Bartolini B, Caravà E, Caon I, Parnigoni A, Moretto P, Passi A, et al. Heparan Sulfate in the Tumor Microenvironment. *Adv Exp Med Biol* (2020) 1245:147–61. doi: 10.1007/978-3-030-40146-7_7
33. Hayes AJ, Melrose J. Keratan Sulphate in the Tumour Environment. *Adv Exp Med Biol* (2020) 1245:39–66. doi: 10.1007/978-3-030-40146-7_2
34. Pibuel MA, Poodts D, Díaz M, Hajos SE, Lompardía SL. The Scrambled Story Between Hyaluronan and Glioblastoma. *J Biol Chem* (2021) 296:100549. doi: 10.1016/j.jbc.2021.100549
35. Listik E, Toma L. Glypican-1 in Human Glioblastoma: Implications in Tumorigenesis and Chemotherapy. *Oncotarget* (2020) 11:828–45. doi: 10.18632/oncotarget.27492
36. Farace C, Oliver JA, Melguizo C, Alvarez P, Bandiera P, Rama AR, et al. Microenvironmental Modulation of Decorin and Lumican in Temozolomide-Resistant Glioblastoma and Neuroblastoma Cancer Stem-Like Cells. *PloS One* (2015) 10(7):e0134111. doi: 10.1371/journal.pone.0134111
37. Chen L, Liu Y-C, Zheng Y-Y, Xu J, Zhang Y, Liu W-L, et al. Furanodienone Overcomes Temozolomide Resistance in Glioblastoma Through the Downregulation of CSPG4-Akt-ERK Signalling by Inhibiting EGR1-Dependent Transcription. *Phytother Res* (2019) 33:1736–47. doi: 10.1002/ptr.6363
38. Jaime-Ramirez AC, Dmitrieva N, Yoo JY, Banasavadi-Siddegowda Y, Zhang J, Relation T, et al. Humanized Chondroitinase ABC Sensitizes Glioblastoma Cells to Temozolomide. *J Gene Med* (2017) 19(3):10.1002/jgm.2942. doi: 10.1002/jgm.2942
39. Herbener VJ, Burster T, Goreth A, Pruss M, von Bandemer H, Baisch T, et al. Considering the Experimental Use of Temozolomide in Glioblastoma Research. *Biomedicines* (2020) 8:151. doi: 10.3390/biomedicines8060151
40. Stepanenko AA, Chekhonin VP. On the Critical Issues in Temozolomide Research in Glioblastoma: Clinically Relevant Concentrations and MGMT-Independent Resistance. *Biomedicines* (2019) 7:92. doi: 10.3390/biomedicines7040092
41. Kegelman TP, Hu B, Emdad L, Das SK, Sarkar D, Fisher PB. In Vivo Modeling of Malignant Glioma: The Road to Effective Therapy. *Adv Cancer Res Rev* (2014) 121:261–330. doi: 10.1016/B978-0-12-800249-0.00007-X
42. Stylli SS, Luwor RB, Ware TMB, Tan F, Kaye AH. Mouse Models of Glioma. *J Clin Neurosci* (2015) 22:619–26. doi: 10.1016/j.jocn.2014.10.013
43. Okolie O, Bago JR, Schmid RS, Irvin DM, Bash RE, Miller CR, et al. Reactive Astrocytes Potentiate Tumor Aggressiveness in a Murine Glioma Resection and Recurrence Model. *Neuro Oncol* (2016) 18:1622–33. doi: 10.1093/neuonc/now117
44. Nakod PS, Kim Y, Rao SS. Biomimetic Models to Examine Microenvironmental Regulation of Glioblastoma Stem Cells. *Cancer Lett* (2018) 429:41–53. doi: 10.1016/j.canlet.2018.05.007
45. Aaberg-Jessen C, Nørregaard A, Christensen K, Pedersen CB, Andersen C, Kristensen BW. Invasion of Primary Glioma- and Cell Line-Derived Spheroids Implanted Into Corticostriatal Slice Cultures. *Int J Clin Exp Pathol* (2013) 6:546–60.
46. Jensen SS, Meyer M, Petterson SA, Halle B, Rosager AM, Aaberg-Jessen C, et al. Establishment and Characterization of a Tumor Stem Cell-Based Glioblastoma Invasion Model. *PloS One* (2016) 11(7):e0159746. doi: 10.1371/journal.pone.0159746
47. Marques-Torrejon MA, Gangoso E, Pollard SM. Modelling Glioblastoma Tumour-Host Cell Interactions Using Adult Brain Organotypic Slice Co-Culture. *Dis Model Mech* (2018) 11(2):dmm031435. doi: 10.1242/dmm.031435
48. Tsidulko AY, Bezier C, de la Bourdonnaye G, Suhovskih AV, Pankova TM, Kazanskaya GM, et al. Conventional Anti-Glioblastoma Chemotherapy Affects Proteoglycan Composition of Brain Extracellular Matrix in Rat Experimental Model in Vivo. *Front Pharmacol* (2018) 9:1104. doi: 10.3389/fphar.2018.01104
49. Gogolla N, Galimberti I, DePaola V, Caroni P. Preparation of Organotypic Hippocampal Slice Cultures for Long-Term Live Imaging. *Nat Protoc* (2006) 1:1165–71. doi: 10.1038/nprot.2006.168

50. Zavjalov EL, Razumov IA, Gerlinskaya LA, Romashchenko AV. In Vivo MRI Visualization of U87 Glioblastoma Development Dynamics in the Model of Orthotopic Xenotransplantation to the Scid Mouse. *Russ J Genet Appl Res* (2016) 6:448–53. doi: 10.1134/S2079059716040225
51. Schneider CA, Rasband WS, Eliceiri KW. NIH Image to ImageJ: 25 Years of Image Analysis. *Nat Methods* (2012) 9:671–5. doi: 10.1038/nmeth.2089
52. Hide T, Komohara Y. Oligodendrocyte Progenitor Cells in the Tumor Microenvironment. *Adv Exp Med Biol* (2020) 1234:107–22. doi: 10.1007/978-3-030-37184-5_8
53. Logun M, Wynens KE, Simchick G, Karumbaiah L. Surfen-Mediated Blockade of Extratumoral Chondroitin Sulfate Glycosaminoglycans Inhibits Glioblastoma Invasion. *FASEB J* (2019) 33(11):fj.201802610RR. doi: 10.1096/fj.201802610RR
54. Malavaki C, Mizumoto S, Karamanos N, Sugahara K. Recent Advances in the Structural Study of Fuctional Chondroitin Sulfate and Dermatan Sulfate in Health and Disease. *Connect Tissue Res* (2008) 49:133–9. doi: 10.1080/03008200802148546
55. Pudełko A, Wisowski G, Olczyk K, Koźma EM. The Dual Role of the Glycosaminoglycan Chondroitin-6-Sulfate in the Development, Progression and Metastasis of Cancer. *FEBS J* (2019) 286:1815–37. doi: 10.1111/febs.14748

Conflict of Interest: The authors declare that the research was conducted in the absence of any commercial or financial relationships that could be construed as a potential conflict of interest.

Copyright © 2021 Tsidulko, Shevelev, Khotskina, Kolpakova, Suhovskih, Kazanskaya, Volkov, Aidagulova, Zavyalov and Grigorieva. This is an open-access article distributed under the terms of the Creative Commons Attribution License (CC BY). The use, distribution or reproduction in other forums is permitted, provided the original author(s) and the copyright owner(s) are credited and that the original publication in this journal is cited, in accordance with accepted academic practice. No use, distribution or reproduction is permitted which does not comply with these terms.

frontiers in Oncology

ORIGINAL RESEARCH
published: 04 August 2021
doi: 10.3389/fonc.2021.697626

The Heparan Sulfate Binding Peptide in Tumor Progression of Triple-Negative Breast Cancer

Carina Mucciolo Melo[1,2], *Huawei Wang*[3], *Ken Fujimura*[3], *Jan Strnadel*[4], *Maria Cecília Zorél Meneghetti*[1], *Helena Bonciani Nader*[1], *Richard L. Klemke*[3] *and Maria Aparecida Silva Pinhal*[1,2*]

[1] Department of Biochemistry/Molecular Biology, Universidade Federal de São Paulo, São Paulo, Brazil, [2] Department of Biochemistry, Faculdade de Medicina do ABC, Santo André, Brazil, [3] Department of Pathology, School of Medicine, University of California San Diego, La Jolla, CA, United States, [4] Department of Molecular Medicine, Biomedical Center Martin, Jessenius Faculty of Medicine in Martin, Comenius University in Bratislava, Martin, Slovakia

OPEN ACCESS

Edited by:
Nikos Karamanos,
University of Patras, Greece

Reviewed by:
Lorenzo Depau,
University of Siena, Italy
Teresa Gagliano,
University of Udine, Italy

***Correspondence:**
Maria Aparecida Silva Pinhal
maspinhal@yahoo.com.br

Specialty section:
This article was submitted to Molecular and Cellular Oncology, a section of the journal Frontiers in Oncology

Received: 20 April 2021
Accepted: 29 June 2021
Published: 04 August 2021

Citation:
Melo CM, Wang H, Fujimura K, Strnadel J, Meneghetti MCZ, Nader HB, Klemke RL and Pinhal MAS (2021) The Heparan Sulfate Binding Peptide in Tumor Progression of Triple-Negative Breast Cancer. Front. Oncol. 11:697626. doi: 10.3389/fonc.2021.697626

Angiogenesis is the formation of new vessels from pre-existing vasculature. The heparan sulfate chains from endothelial cell proteoglycans interact with the major angiogenic factors, regulating blood vessels´ formation. Since the FDA´s first approval, anti-angiogenic therapy has shown tumor progression inhibition and increased patient survival. Previous work in our group has selected an HS-binding peptide using a phage display system. Therefore, we investigated the effect of the selected peptide in angiogenesis and tumor progression. The HS-binding peptide showed a higher affinity for heparin N-sulfated. The HS-binding peptide was able to inhibit the proliferation of human endothelial umbilical cord cells (HUVEC) by modulation of FGF-2. It was verified a significant decrease in the tube formation of human endothelial cells and capillary formation of mice aorta treated with HS-binding peptide. HS-binding peptide also inhibited the formation of sub-intestinal blood vessels in zebrafish embryos. Additionally, in zebrafish embryos, the tumor size decreased after treatment with HS-binding peptide.

Keywords: anti-angiogenic, breast neoplasia, glycosaminoglycans, phage display, breast cancer (BC)

INTRODUCTION

Angiogenesis is forming new vessels from pre-existing vasculature during embryonic development and adult life (1).

Among the angiogenic factors that participate in neovascularization, we highlight the vascular endothelial growth factor (VEGF), hypoxia-induced factor (HIF), placental growth factor (PGF),

fibroblast growth factor (FGF), angiopoietin-1 (Angp), platelet-derived growth factor (PDGF), tumor necrosis factor (TNF), interleukins (IL), epidermal growth factor (EGF), insulin-like growth factor (IGF), angiogenin (Ang), stromal cell-derived factor (SDF) and transforming growth factor (TGF) (2).

The heparan sulfate (HS) chains from endothelial cell proteoglycans interact with the major angiogenic factors, regulating blood vessels´ formation (3). In general, HS stabilizes the complex formation between angiogenic factors and the respective receptors (4). Furthermore, HS can also modulate the release of such angiogenic factors after the action of the enzyme heparanase or proteoglycan cleavage by proteases, forming a concentration gradient that may direct angiogenesis (5–7).

Heparin and HS exhibit structural similarities and share the same biosynthetic pathway. Both HS and heparin are formed by repeated disaccharide units of glucosamine and uronic acid (D-glucuronic acid or L-iduronic acid) residues linked by glycosidic α-intradisaccharide and β-interdisaccharide bonds (5, 7, 8).

Angiogenesis plays an essential role in physiological events such as placenta formation, cicatrization, and the menstrual cycle but is also essential in pathological processes, such as neoplasia (9). In addition, during tumorigenesis, the formation of neovascularization supplies nutrients and oxygen to tumor cells, allowing intense cell proliferation and enabling tumor metastases (9).

In 1971, it was hypothesized that the molecules involved in the angiogenic process could be a good target for antitumor therapy (10). Since then, several treatments have been investigated and developed (10).

In 2004, the US Food and Drug Administration approved using the first anti-VEGF-A monoclonal antibody, called bevacizumab, to treat colorectal cancer. Since then, anti-angiogenic therapy has shown temporary inhibition of tumor progression and increased patient survival. Moreover, the anti-angiogenic treatment combined with chemotherapeutic treatments proved to be more efficient, with a significant increase in survival rate than isolated chemotherapy (4, 10).

Previous work in our group has selected an HS-binding peptide using a phage display system. The biopanning assay was performed using the random peptide library expressed in the bacteriophage system to target the recombinant enzyme N-deacetylase N-sulfotransferase-1 (NDST1) involved in HS/heparin synthesis. The NDST1 enzyme removes the N-linked acetyl group at carbon 2 from glucosamine residue and adds a sulfate group at such a position (SO3-). In addition to selecting a peptide that binds to NDST, an HS ligand peptide was also selected since that HS is present at the catalytic domain of such recombinant enzyme (11).

Peptides have been used as a potential treatment in cancer. Arap and colleagues selected specific peptides that target to tumor vasculature of breast cancer, melanoma, and Kaposi's sarcoma (12). The selection of specific peptides can be performed by screening using a phage display peptide library. George Smith first described filamentous phage as a random peptide library by fusing the peptide into capsid proteins.

This phage peptide library could be used to select a peptide that binds towards a specific target after rounds of binding assays. These peptides have lower production costs, good affinity, good tissue penetration, and little immune response (13).

Therefore, we were interested in evaluating the ligation specificity and the possible effect of the selected peptide in angiogenesis and tumor progression.

MATERIALS AND METHODS

Animals

According to the University of California San Diego animal welfare guidelines, all animals were treated as described and approved by the UCSD Institutional Animal Care and Use Committee and comply with the ARRIVE guidelines (S12005 and S06008). Transgenic Tg[(Fli1: eGFP)] zebrafish were kindly provided by Dr. David Traver (UCSD). Zebrafish were maintained as previously described. C57BL/6 J mice were purchased from Jackson Laboratory, and mice were euthanized with CO_2. All mice were maintained in a specific pathogen-free vivarium.

Analysis of Tryptophan Emission

Tryptophan can be excited at wavelengths between 280-290 nm and emission at 350 nm. It is important to note that the emission spectrum of tryptophan can be altered depending on its conformation. Therefore, changes in the emission spectrum of tryptophan during the titration of some glycosaminoglycans (heparin, dermatan sulfate, and chondroitin sulfate) suggest an interaction between the glycosaminoglycan and the peptide. The synthetic peptide SADGARGWRGEKIGNGAAG (3 μM, Peptide 2.0, Chantilly, Virginia, USA) or the scramble peptide SADGAIENKWRGGRGGAAG (used as specificity control; 3 μM Peptide 2.0, Chantilly, Virginia, USA) was dissolved in phosphate-buffered saline, PBS (137 mM NaCl, 2.7 mM KCl, 10 mM Na_2HPO_4, 1.8 mM KH_2PO_4, pH 7.4). The peptide solution was filtered through a 0.22 μM sterilizing filter (Millipore, Billerica, Mass., USA), followed by collecting of the emission spectrum in a cuvette of quartz. Under constant stirring, each of the glycosaminoglycans were titrated separately, and the emission spectrum was collected by Fluorimeter (Shimadzu, Kyoto, Kyoto, Japan). Chondroitin sulfate from cartilage, and dermatan sulfate from bovine intestinal mucosa were obtained from Seikagaku (Seikagaku Kogyo Co, Tokyo, Japan) and was obtained from Sigma-Aldrich, St. Louis, Missouri, USA.

Circular Dichroism (CD)

Circular Dichroism spectra were recorded by Chirascan Plus (AppliedPhotophysics) using a quartz cuvette with a 0.1-mm optical path. The CD spectra (185-250nm) were collected with

12μM of peptide and 6.7 μg/mL of porcine heparin in sodium phosphate solution (10 mM). All spectra obtained represent the average of eight independent repetitions. Chemically modified heparins were used in the CD assays Heparin N-sulfated (HepNS); Heparin 2-O-Sulfated (Hep2S); Heparin 6-O-sulfated (Hep6S); Heparin 2-O-sulfated and 6-O-sulfated (Hep2S6S); Heparin 6-O-Sulfated and N-sulfated (Hep6SNS); Heparin 2-O-Sulfated and N-sulfated (Hep2SNS). The chemically modified heparins were graciously provided by Dr. Marcelo Lima (Universidade Federal de São Paulo). The modification was performed as described by Yates and co-workers (14). BestSel Software predicted the secondary structure and fold recognition.

Cell Proliferation

Five thousand (5,000) human umbilical vein endothelial cells (HUVEC, ATCC) were plated in a 96-well plate with F-12 medium (ThermoFisher Scientific, Waltham, Mass., USA) containing 10% FBS, penicillin (100 U/ml), and streptomycin (100 μg/ml), 37°C, 5% CO_2. HUVEC cells were treated with the selected HS-binding peptide at different concentrations (1 μM, 5 μM, 10 μM and 50 μM) for 18 hours. Proliferation analysis was performed using Cell Proliferation ELISA Kit, BrdU (Roche, Basel, Switzerland), following the manufacturer's instructions. This assay was performed in triplicate.

Capillary Formation

Matrigel (Becton, Dickinson-BD, Franklin Lakes, New Jersey, USA) was thawed at 4°C, and aliquots of 100 μl (10 mg/ml) applied to 96 well-plate (Corning, New York, New York, USA), which were maintained at 37°C in a humidified atmosphere with 2.5% CO_2 for 16 h for gelation. Seven thousand (7,000) endothelial cells from human umbilical vein endothelial cells (HUVEC, ATCC) were plated in the 96-well plate coated with Matrigel (Becton, Dickinson-BD, Franklin Lakes, New Jersey, USA) in the presence of F-12 medium (Thermo Fisher Scientific, Waltham, Mass, USA), containing 10% fetal bovine serum, penicillin (100 U/ml) and streptomycin (100 μg/ml), 37°C, 5% CO_2. The cells were treated in the presence or absence of HS-binding peptide (10 μM) for 18 hours. This assay was performed in quadruplicate. The tube formation was analyzed by microscopy (Zeiss, Oberkochen, Germany) 20x magnification. Three images were randomly taken in different areas and quantified by two different observers. The total length tubular structures on the Matrigel was measured and determined using image analysis software (AxioVision software, Carl Zeiss). The results are expressed as lumen length.

Angiogenesis Assay Using Zebrafish Model

For analysis of angiogenesis zebrafish mutant Tg[(Fli1: eGFP)], embryos were cultured in E3 medium containing 1-phenyl 2-thiourea (PTU 0.003%) (Sigma-Aldrich, St. Louis, MO, USA) at 28°C. Different doses of HS-binding peptide or scrambled peptide were microinjected into the heart of 2-day post-fertilization (2 dpf) embryos. On the third day post-fertilization (3 dpf), the formation of subintestinal vessels was analyzed by confocal microscopy. The analysis was performed by confocal images (Nikon C1Si, Minato, Tokyo, Japan). For quantification, it was measured to the size of the subintestinal vessels using ImageJ software. Ten embryos were used in each experimental group, 10x magnification.

Mouse Aortic Ring Assay

Two female C57BL mice (age 6 to 8 weeks) were euthanized with CO_2 at the University of California San Diego; the experiments were approved and performed by relevant named guidelines and regulations. The aortas were removed with tweezers' aid, adipose tissue, and other tissues detached to the aorta. Next, aortas were cut into 0.5 mm rings. The *ex vivo* aorta rings were incubated for 18 hours in an Opti-MEM culture medium (ThermoFisher Scientific, Waltham, Mass., USA) at 37°C, 5% CO_2. Next, 60 μl of Matrigel (10 mg/mL) (Corning, New York, New York, USA) was added to the center of the 24-well plate, and the plate was incubated for 10 minutes at 37°C, 5% CO_2. The aortic ring was placed on top of the Matrigel and incubated for 15 minutes at 37°C. Additionally, 50 μl of Matrigel (10 mg/mL) and incubated for an additional 30 minutes at 37°C. The culture of the aortas was maintained into Opti-MEM medium supplemented with 2.5% FBS, penicillin (100 U/mL), streptomycin (100 μg/mL), 50 ng/mL VEGF-A and 20 ng/mL FGF-2. The aortas were incubated for 7 days, 37°C, 5% CO_2, with the treatment of the HS-binding peptide (10 μM and 100 μM) or scramble peptide (10 μM). Approximately 50% of the culture medium was changed every 4 days. The peptides and growth factors (VEGF-A, FGF-2) were replenished every 2 days. The aortic rings were analyzed by microscopy (Zeiss). This assay was performed in quadruplicate using 10x magnification.

Cell Index of HUVEC Cells in the Presence of VEGF-A and FGF-2

HUVEC (ATCC) cells (1,500 cells) were cultured in a 96-well plate containing type 1 collagen from rat tail (Sigma-Aldrich, St. Louis, Missouri, USA). First, the culture plates were pretreated with type 1 collagen (10 μg/ml, 1-hour incubation, 37°C). Then, cells were plated in Opti-MEM culture medium (ThermoFisher Scientific, Waltham, Massachusetts, USA), containing 2% FBS, penicillin (100 U/ml), streptomycin (100 μg/ml), 50 ng/ml VEGF-A or 20 ng/ml FGF-2, in the presence of 10 μM of the HS-binding peptide. During 50 hours, the cell index number was determined using xCELLigence (ACEA Bioscience, San Diego, California, USA). The cell index is directly related to the rate of cell proliferation and cell viability. The experiment was performed in triplicate.

3D Culture

PDX (patient-derived tumor xenograft) cells from a patient with a triple-negative breast tumor were used. PDX cells were kindly provided by CROWN Bioscience (San Diego, California, USA). Briefly, the tumor was collected from the patient and injected into a NOD/SCID mouse. After 21 days, the tumor was resected and digested with collagenase for tissue dissociation. Approximately 2,500 PDX cells in 50 µl DMEM/F-12 medium (ThermoFisher Scientific, Waltham, Mass., USA) were supplemented with 10% fetal bovine serum, 100 U/ml penicillin, 100 µg/mL streptomycin, and glutamine/gentamicin solution (Sigma-Aldrich, St. Louis, Missouri, USA). The cells were plated on a 96-well plate (Corning, New York, New York, USA) coated with 50 µl of Matrigel (10 mg/mL) (Corning, New York, New York, USA). Next, culture medium DMEM/F12 containing 5% of Matrigel was added on top of cell culture. The cells were treated with 10 µM or 100 µM of the HS-binding peptide and cultured for 14 days, 37°C, 5% CO_2 to obtain the spheres (3D cultures). Exchange of the culture medium and replacement of HS-binding peptide was performed every three days. Cell proliferation and viability analysis were determined by the size of the colonies (area). Measurements were obtained using a Nikon microscope using 10X magnification (Nikon, Minato, Tokyo, Japan). The assay was performed in triplicate.

Effect of HS-Binding Peptide on Tumor Progression

The chorion of the zebrafish embryos Tg[(Fli1: eGFP)], with 1-day post-fertilization (1 dpf), were manually removed with tweezers, the was anesthetized with tricaine, and immobilized. The experiments were performed following relevant named guidelines and regulations in the University of California San Diego. After immobilization, the embryos were microinjected with 150 cells. The same PDX cells (triple-negative breast cancer) obtained in the 3D culture described previously were used for the xenograft assay in zebrafish. Embryos were incubated at 35.5°C for 18 hours and then treated with the injection of 10 µM of the HS-binding peptide. Treatment analysis was completed at 3 dpf. Microinjection was performed in the yolk sac of the animal. PDX cells were first transduced with lentivirus to express a red fluorescent protein (RFP) for fluorescent labeling of tumor cells. The translucent lentivirus cells were selected using 2 µg/ml puromycin for 5 days. The cells exhibiting the greatest expression of the red fluorescent protein were selected by cell sorting BD Influx (Becton, Dickinson-BD). Analysis of the HS-binding peptide effect on tumor progression was performed by 10X magnification confocal microscopy (Nikon C1Si, Minato, Tokyo, Japan), and the amount of red tumor fluorescence was measured by ImageJ software. Also, the survival of the animals was analyzed. The tests were performed with ten zebrafish embryos per group.

RESULTS

The HS binding peptide RGWRGEKIGN was selected by the phage display system published by our group. The synthetic HS-binding peptide used for the experimental assays presents flanked amino acid residues displayed at the pIII capsid protein, where the peptide was expressed in the bacteriophage library. The HS-binding peptide's affinity was previously analyzed by HS/heparin interaction assays, as described in the article already published by Gesteira et al. (11).

Characterization of the HS-Binding Peptide

The HS-binding peptide interaction with heparin was performed by the emission spectrum of tryptophan (W), showing that HS-binding peptide interacted exclusively with heparin, while the scrambled peptide (SADGAIENKWRGGRGGAAG) interacted with heparin, dermatan sulfate (DS), and chondroitin sulfate (CS). The results showed that the scrambled peptide has lower specificity since it binds with other glycosaminoglycans and presents a higher affinity to heparin than the HS-binding peptide. Such results show that the amino acid sequence is important for the HS/heparin-binding specificity (**Figure 1**).

Considering heparin as an analog of heparan sulfate, we used chemically modified heparins to evaluate the HS-binding peptide´s affinity by dichroism analysis. In addition, nuclear magnetic resonance (NMR) was used to characterize each modified heparin (data are not shown). It is noteworthy that the sulfation profile at the C3 position of glucosamine residues was not analyzed; therefore, we cannot determine whether or not there is sulfation at such position in the different modified heparin molecules used in the present study.

The synthetic peptide SADGARGWRGEKIGNGAAG was analyzed by circular dichroism. The peptide presents 41.7% of β-sheet antiparallel conformation, 14.3% turn, 44.1% other conformation. Additionally, 25.9% of β-sheet antiparallel conformation is right-twisted.

The dichroism analysis shows that the HS-binding peptide has a higher affinity for heparin N-sulfated (HepNS) Heparin 2-O-sulfated and N-sulfated (Hep2SNS); heparin 6-O-sulfated and N-sulfated (Hep6SNS) and heparin N-sulfated (HepNS) and lower affinity for N-acetylated heparins, suggesting specific interaction with the N-sulfation pattern (**Figure 2A**).

The HS-binding peptide interaction with modified heparins decreased the right-twisted conformation percentage since the interaction with heparin replaced the right-twisted conformation with left-twisted or relaxed β-sheet antiparallel. (**Figure 2B**).

Furthermore, the secondary structure analysis predicted by Best Software detected a similarity between HS binding peptide with Taiwan snake cardiotoxin A3 named PDB 2BHI, which is a polypeptide containing a heparin-binding domain corroborating our results (15).

Effect of HS-Binding Peptide in Angiogenesis

The *in vitro* proliferating assay using BrdU shows HS-binding peptide could inhibit the proliferation of human endothelial

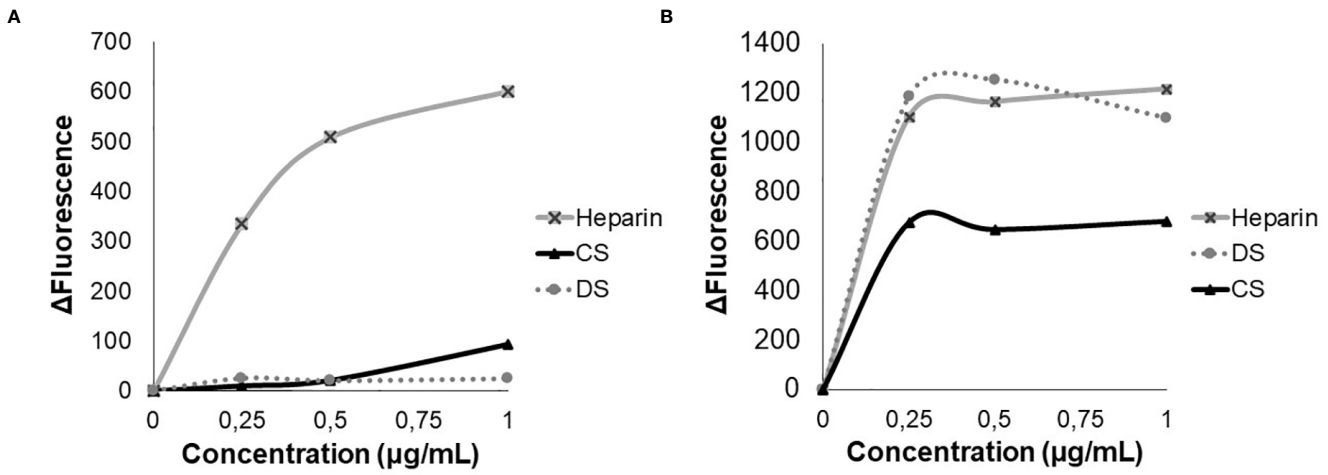

FIGURE 1 | Analysis of tryptophan emission. Heparin, dermatan sulfate (DS) and chondroitin sulfate (CS), were titrated in the presence of 3 μM of HS-binding peptide **(A)** or in the presence of 3 μM of scrambled peptide **(B)**. Excitation 280 nm, emission 350 nm. The HS- binding peptide interacts only with heparin.

umbilical cord cells (HUVEC) at doses from 1 to 100 μM of the, reaching the maximum inhibition the concentration of 5 μM (**Figure 3**).

Also, there was a significant alteration in the tube formation when HUVEC cells were treated with 10 μM of HS-binding peptide for 18 hours. The capillaries had a higher diameter, or the lumen formation was abrogated formed compared to non-treated cells, as shown in **Figure 3**.

The assay using such peptide was performed with transgenic zebrafish embryos Tg (Fli1:eGFP), that express a green fluorescent protein (GFP) in blood vessels, which allowed us to investigate some effect of the HS-binding peptide *in vivo*. **Figure 4** demonstrates that HS-binding peptide (10 μM) inhibits the formation of sub-intestinal blood vessels in zebrafish embryos Tg(Fli1:eGFP), confirming the anti-angiogenic activity of such peptide obtained by *in vitro* assays using HUVEC cell line. However, there was no benefit for using a higher dose of the HS-binding peptide (50-100 μM), confirming *in vitro* experiments described previously.

Aortas were collected from two C57BL/6 mice, sectioned in rings, and cultured in Matrigel for seven days to evaluate new blood vessel formation. HS-binding peptide decreased the number and the size of blood vessels in sectioned aorta rings (**Figure 5**). Thus, this *ex vivo* experimental model reinforces the inhibitory effect of the HS-binding peptide. Furthermore, the ex vivo assay also confirmed that increasing the HS-binding peptide doses did not intensify the anti-angiogenic effect.

Possible Mechanisms Involved With Angiogenesis Inhibition

Cell index analysis of HUVEC cells in the presence of VEGF-A or FGF-2 was performed using xCELLigence equipment (ACEA Bioscience, San Diego, California, USA). The results showed that the HS-binding peptide inhibited the rate of endothelial cells´ proliferation and viability in the presence of FGF-2 (**Figure 6A**). However, the proliferation and viability of HUVEC cells were not significant altered by the HS-binding peptide in the presence of VEGF-A (**Figure 6B**).

A control assay was performed exclusively in the presence of fetal bovine serum (FBS) to confirm that the enhancement in the proliferation and viability of HUVEC cells was related to FGF-2 and had not been affected by growth factors that were present in the culture medium, which was supplemented by FBS (**Figure 6C**).

The data suggest that decreased HUVEC cell proliferation after treatment of the HS-binding peptide may be mediated by inhibiting the interaction between HS and FGF-2.

Effect of HS-Binding Peptide on Tumor Progression

Finally, we sought to determine whether the HS-binding peptide could block tumor growth. A tissue biopsy collected from resection of a triple-negative breast cancer patient was cultured in Matrigel to obtain a 3D culture. Patient-derived xenotransplant cells (PDX cells) were maintained for 14 days in a culture medium in the presence or absence of the HS-binding peptide. There was no change in the growth of the 3D culture of PDX colonies after HS binding-peptide treatment, as shown in **Figure 7**.

However, when triple-negative PDX cells were injected in zebrafish embryos Tg (Fli1: eGFP) and subsequently treated with HS-binding peptide, the tumor size decreased, and there was also an increase in the survival rate of the zebrafish embryos (**Figure 8**), suggesting an antitumor efficacy of HS-binding peptide.

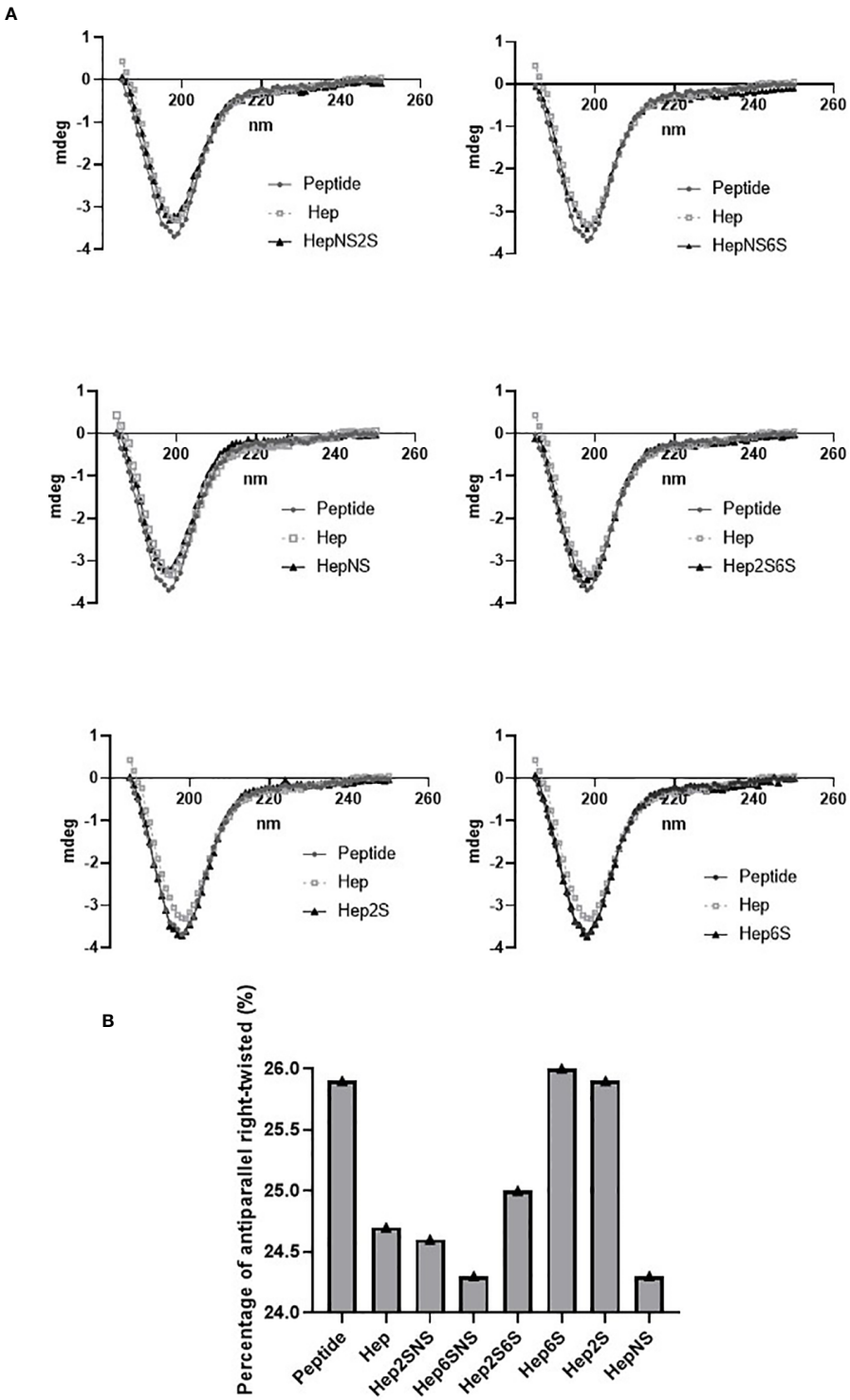

FIGURE 2 | A spectrum obtained by circular dichroism. Circular dichroism was performed to determine the peptide interaction with chemically modified heparins, demonstrating an alteration in the secondary structure of this peptide. Porcine heparin (Hep), Heparin 2-O-sulfated and N-sulfated heparin (Hep2SNS), Heparin 6-O-sulfated and N-sulfated (Hep6SNS), Heparin 2-O-sulfated and 6-O-sulfated (Hep2S6S), Heparin 6-sulfated (Hep6S), Heparin 2-sulfated (Hep2S), and Heparin N-sulfated (HepNS). The heparins that showed the greatest interaction with the peptide were the molecules containing N-sulfation. The assay was performed in the presence of 12 μM of the HS binding peptide and 6.7 μg/ml of each heparin in a 10 mM sodium phosphate solution. Control, 12μM of peptide in 10mM sodium phosphate solution. **(A)** The lines represent the repeat averages of eight different experimental readings. **(B)** The percentage of right-twisted antiparallel beta-sheet was analyzed. A reduction from the right-twisted shape to the left-twisted or relaxed shape was observed specifically with N-sulfated heparins.

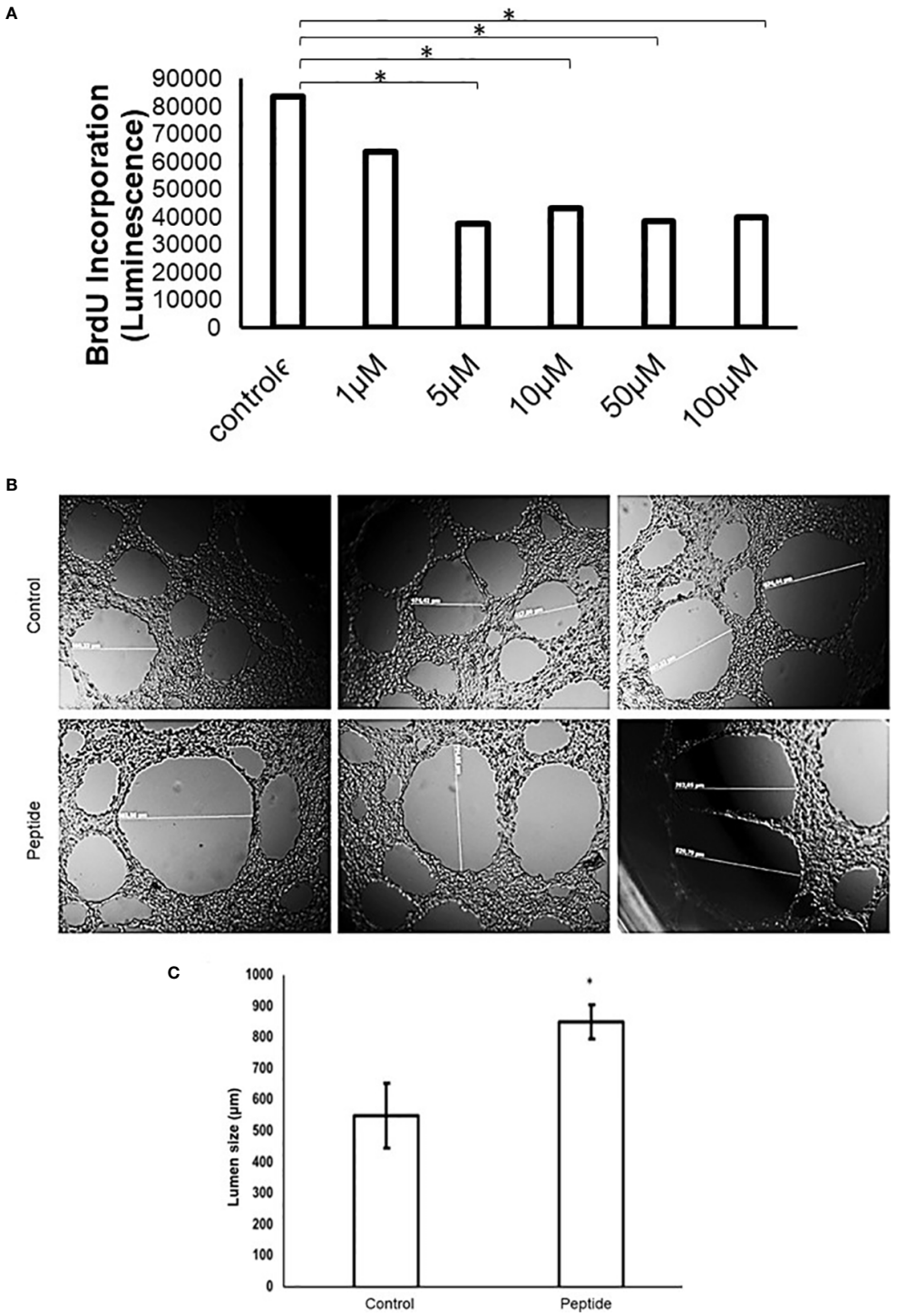

FIGURE 3 | Angiogenesis *in vitro* analysis. **(A)** Cell proliferation assay in the presence of HS-binding peptide. Proliferation assays were performed using BrdU as described in Methods. HUVEC cells were treated with the HS-binding peptide at different doses for 18 hours. After treatment, BrdU was added into the cell culture and luminescence was analyzed. Assay performed in triplicate, the bar represents average and lines represent standard deviation. The proliferation is inhibited from 1 μM of HS-binding peptide and reaches maximum inhibition at 5 μM. *$p < 0.05$ (Kruskall-Wallis). **(B)** Tubular formation with endothelial cells. Control, Cells remain in the absence of treatment. Peptide, Cells were treated with the HS-binding peptide (10 μM) for 18 hours. The tubular formation was analyzed by microscopy 20x magnification. **(C)** Lumen size was measured, the bar represents average and lines represent standard deviation, *$p < 0.05$ (Kruskall-Wallis). Control, cells remain in the absence of treatment. Peptide, cells were treated with HS-binding peptide (10μM) for 18hours. It was verified that peptide was capable to inhibit the tubular formation of endothelial cells.

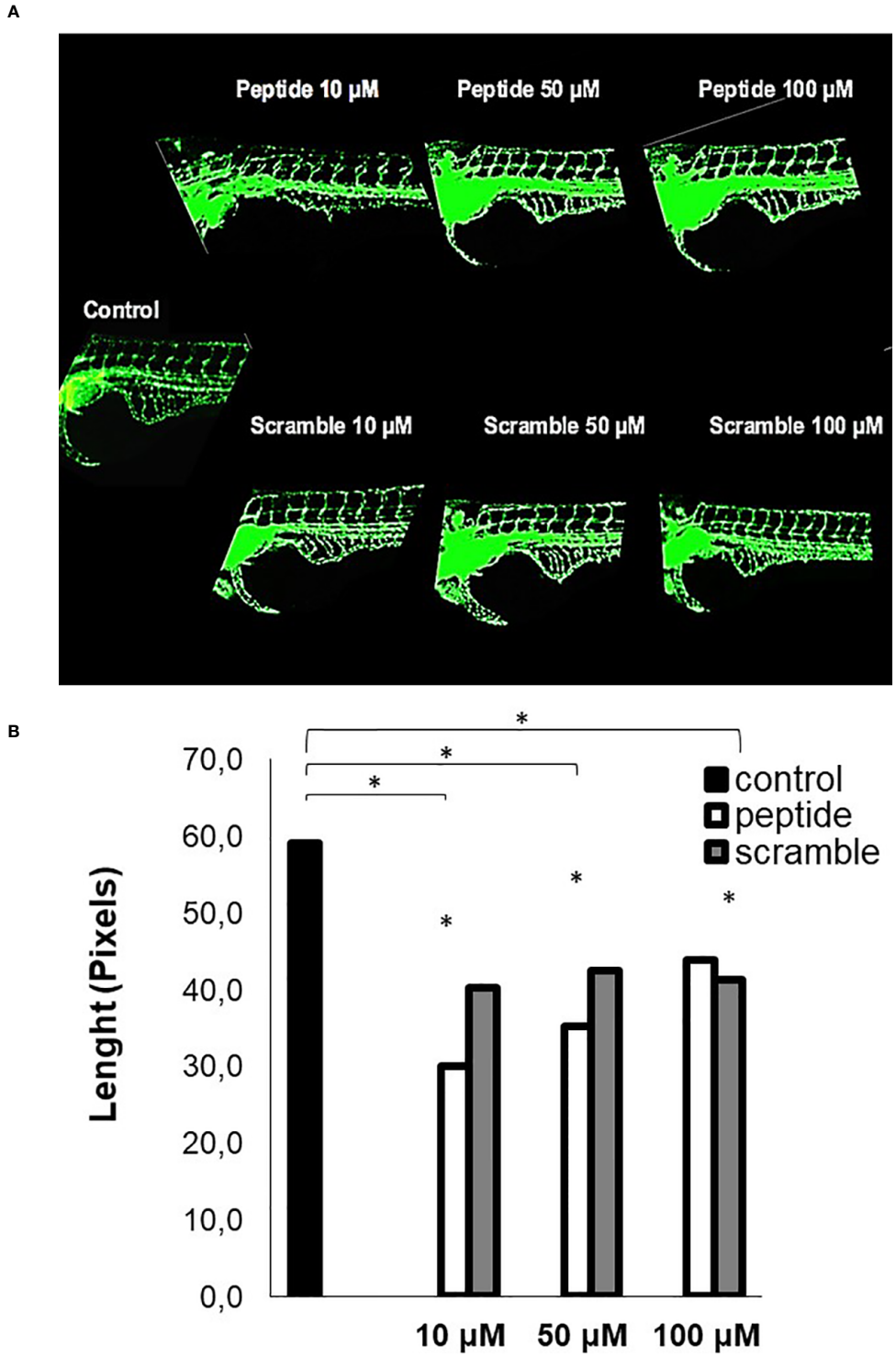

FIGURE 4 | Analysis of angiogenesis in *vivo*. This assay was performed with Tg [Fli1: eGFP] embryos (10 embryos per group). **(A)** the image of zebrafish embryos. Control, untreated embryos. Peptide, embryos treated with the HS-binding peptide. Scramble, embryos treated with scrambled peptide. Assays were performed with zebrafish embryos 2 days after fertilization (2 dpf). After 24 hours of treatment, the animals were analyzed by confocal microscopy and the images obtained in 10X magnification. Subintestinal vessels were analyzed. **(B)** the quantification of the subintestinal vessels was evaluated using ImageJ software. The values express the mean and standard deviation in each group. *$p < 0.05$ (ANOVA). The HS-binding peptide was capable of inhibiting angiogenesis of sub intestinal vessels.

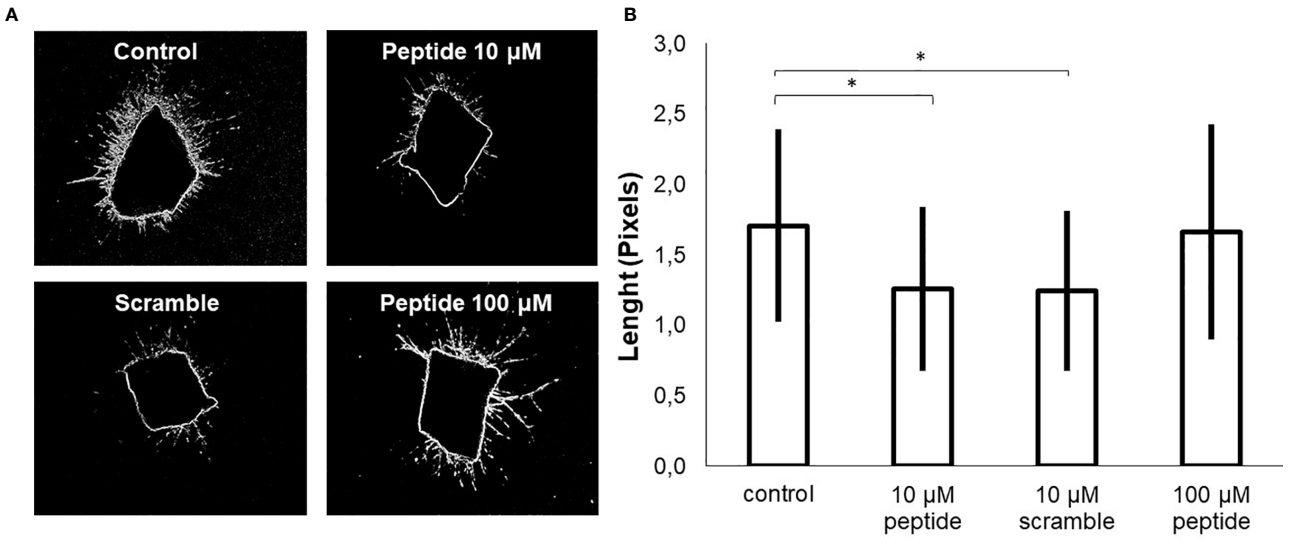

FIGURE 5 | *Ex vivo* angiogenesis assay. Sixteen rings of mouse aortas were collected and cultured in culture plates containing Matrigel for seven days, **(A)** aorta ring cultured in the absence of peptide (control); aorta ring cultured in the presence of HS-binding peptide (10 µM or 100 µM) and aorta ring cultured in the presence of scrambled peptide (10 µM). **(B)** The area of the formed blood vessels was analyzed using ImageJ software. The values represent means and standard deviations the area reached by the blood vessels formed from the aorta. *$p < 0.05$ (ANOVA). The HS-binding peptide decreased blood formation from the aorta.

We hypothesize that the decrease in tumor growth promoted by the HS-binding peptide in the *in vivo* assay is possibly due to inhibition of angiogenesis since the peptide does not appear to alter the viability or the proliferation of triple-negative breast tumor cells.

DISCUSSION

Breast tumors are classified according to the presence of some plasma membrane receptors, such as estrogen receptors (ER), progesterone receptors (PR), and human epidermal growth factor type 2 receptor (HER-2). Triple-negative breast cancer has low or absent ER, PR, and HER-2 expression. Consequently, hormone treatment or treatment with the anti-HER-2 monoclonal antibody does not have efficacy in these patients (16). Also, triple-negative breast tumor has a higher growth rate compared to the other types of breast tumors. Therefore, new treatment alternatives are important for tumors such as triple-negative breast cancer.

Tumor progression steps include tumor cells´ proliferation, the formation of new blood vessels, and metastasis. The proliferation of the tumor cells and metastatic events is dependent on the neovascularization that nourishes and carries oxygen to the tumor, besides allowing the extravasation of tumor cells. Thus, angiogenesis favors tumor progression and the invasion of tumor cells (16).

The angiogenic process involves cross-talk between tumor cells, stromal cells, and endothelial cells. Tumor and stromal cells appear to activate proliferation, migration and modify endothelial cell phenotype due to the release of soluble factors, mainly VEGF and FGF-2 (4, 9).

The heparan sulfate proteoglycans present in the plasma membrane modulate various cellular responses, including cell proliferation, migration and adhesion, apoptosis, inflammatory response, and angiogenesis (7). It is known that the structural modifications of HS and heparin molecules promote significant changes in the interactions of a variety of compounds. The degree of sulfation and the distribution and conformation of D-glucuronic acid and L-iduronic acid residues interfere with HS/heparin molecule conformation, affecting the interaction of HS with other molecules (5).

It is important to emphasize that the HS-binding peptide was selected by Phage Display using as target endogenous heparan sulfate present at the active site of the recombinant purified enzyme N-deacetylase-N-sulfotransferase-1 (NDST-1) (11).

Moreover, HS-binding peptide has structural similarity with the polypeptide Taiwan snake cardiotoxin A3 (PDB 2BHI), which presents a heparin-binding domain results (15).

The HS-binding peptide has a majority antiparallel beta-sheet conformation that is characteristic of peptides with a heparin-binding site (15, 17).

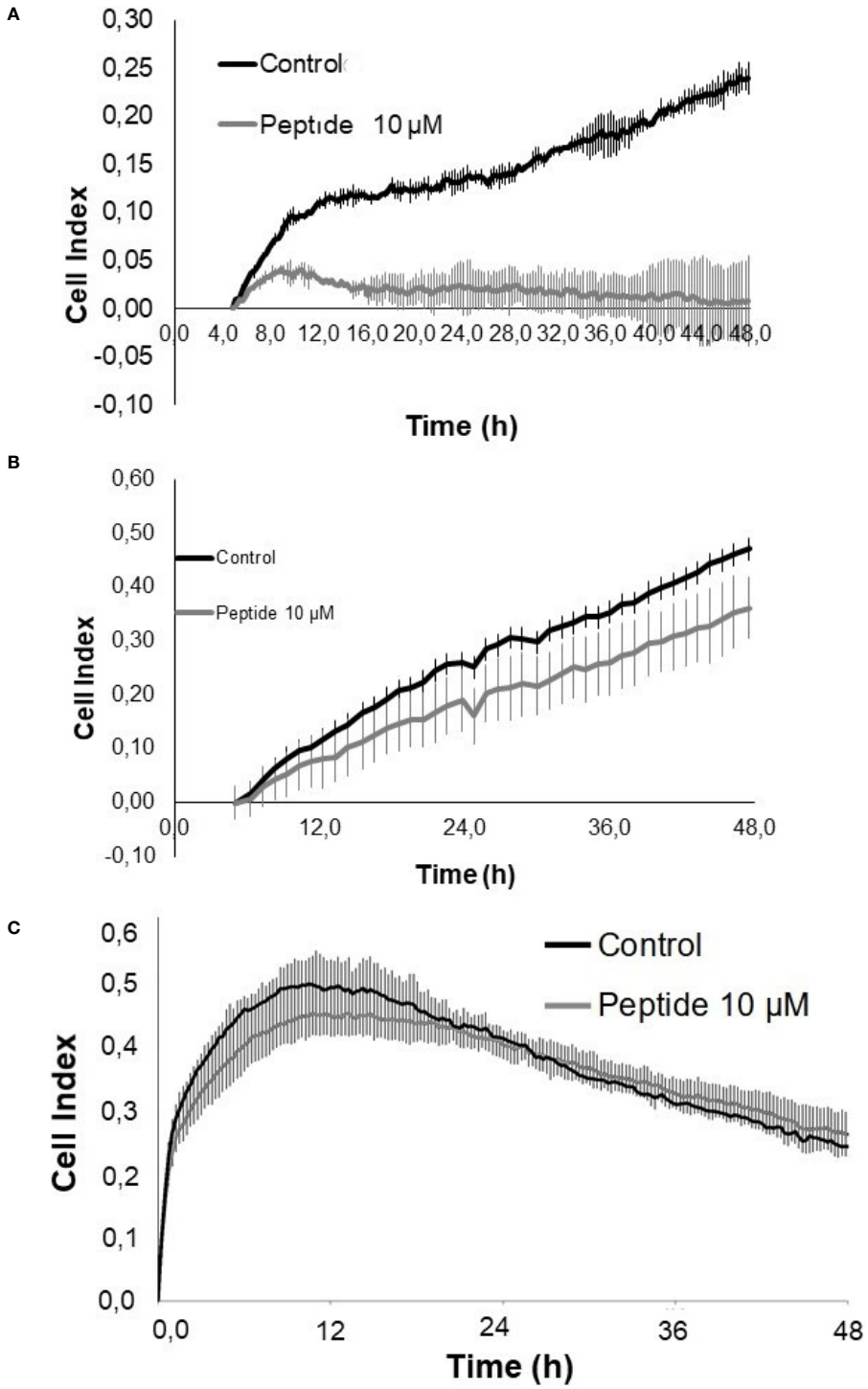

FIGURE 6 | Cell proliferation/viability assay in the presence of growth factors. HUVEC cells were cultured for 50 hours on collagen type 1 in medium containing 2% fetal bovine serum (FBS) and 20 ng/mL FGF-2 or 50 ng/mL VEGF-A, in the presence or absence of the HS-binding peptide. **(A)** VEGF-A + 2% SFB. **(B)** FGF-2 + 2% SFB. **(C)** 2% SFB. Control, HUVEC cells in the absence of treatment. Peptide, HUVEC cells with HS-binding peptide treatment (10 µM). Assay performed in triplicate. The values indicate the mean and standard deviation of the cell index (index proportional to the number of cells adhered to the plate). Peptide inhibited FGF-2 proliferation. Each point of FGF-2 assay was statically significant $p<0.05$ (Kruskall-Wallis) while the decrease of proliferation/viability with VEGF-A was not significant.

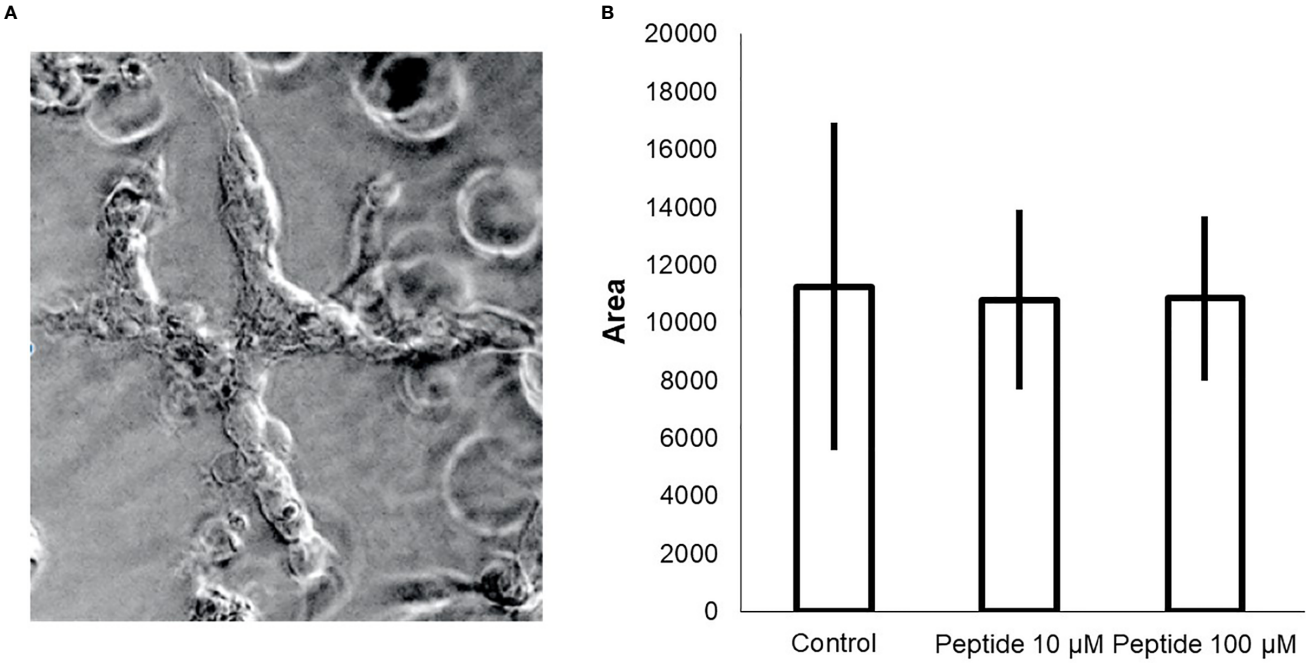

FIGURE 7 | Effect of HS-binding peptide in the 3D culture (spheroid) triple-negative breast cancer. Patient-derived xenotransplant cells (PDX cells) were obtained from tissue collected of a triple negative breast cancer patient. **(A)** The cells cultured for 14 days. The exchange of culture medium was performed every three days. **(B)** Cell proliferation and viability analysis were determined by the size of the colonies (area). Measurements were obtained using a Nikon microscope using 10X magnification (Nikon, Minato, Tokyo, Japan). The assay was performed in triplicate. Peptide did not affect triple-negative cells, $p>0.05$ (Kruskall-Wallis).

The present results demonstrate that HS-binding peptide interacts preferentially with N-sulfated heparin. It is well known that N-sulfation and 2-O-sulfation are required for HS binding with FGF-2, while sulfation at the carbon 6 of glucosamine residues is specifically important for FGFR-1 binding (18–24). Our results corroborate these previous studies confirming that HS-binding peptide interacts with N-sulfated and 2-O-sulfated heparin, representing FGF-specific binding domains in the HS molecule, indicating that such an anti-angiogenic effect peptide might be controlled by the specific interaction between FGF-2 and such HS domains.

The involvement of HS proteoglycans (HSPG) in the formation of new blood vessels is well-known. Studies with zebrafish have shown that the decrease of HSPG, syndecan-2, reduces the migration of endothelial cells during the formation of new capillaries during embryonic development and indicates that such inhibition is modulated by VEGF (25). Moreover, some data in the literature demonstrate that a VEGF analogous peptide interacts with HS chains, promotes inhibition of endothelial cell migration, and decreases tumor size in the mouse model (26). Consequently, HS involvement in forming new blood vessels is obvious, which is essential for carcinogenesis.

In this context, the HS-binding peptide indicates a therapeutic potential to inhibit angiogenesis. Moreover, the data showed that HS-binding peptide was able to decrease tumor growth and increase survival of zebrafish embryos, likely by promoting the formation of fewer new blood vessels and not by the direct effect on the tumor cell, since *in vitro* assays showed that HS-binding peptide did not alter the viability and the proliferation of triple-negative breast tumor cells. Therefore, HS-binding peptide may represent a potential adjuvant treatment for triple-negative breast tumors, known to be poorly responsive to conventional therapy such as chemotherapy.

The selected HS-binding peptide interacts with a specific structure of heparan sulfate and inhibits tumor growth of triple-negative breast cancer cells, possibly interfering with the proliferation signaling modulated by FGF-2 and consequently decreasing angiogenesis.

Despite molecular mechanisms that need to be further investigated, the set of results obtained in the present study highlights the potential use of the HS-binding peptide as an angiogenesis inhibitor and might be useful in combination with other antitumor drugs in cancer therapy.

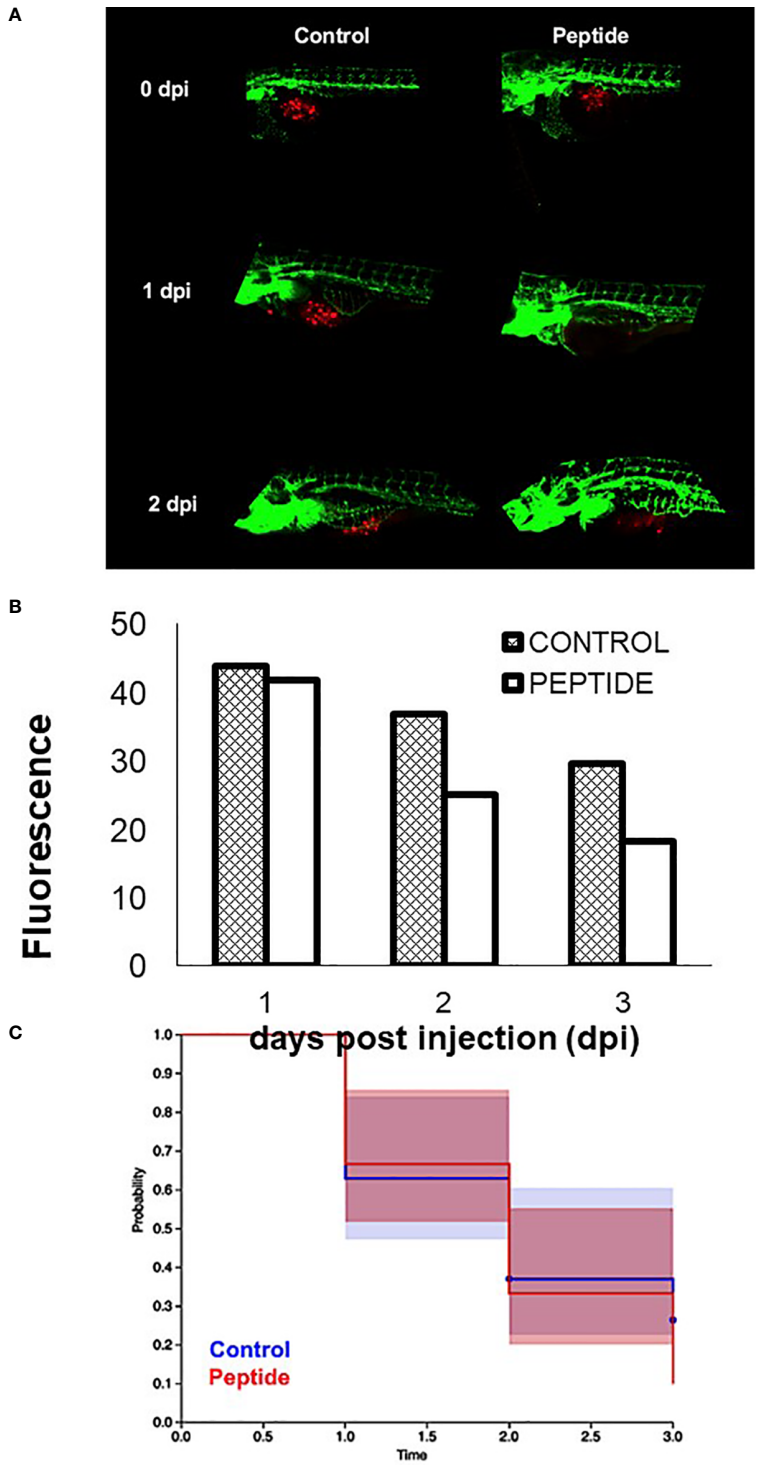

FIGURE 8 | Effect of HS-binding peptide on tumor progression. Approximately 150 PDX cells obtained by surgical resection of a patient with triple-negative breast cancer were labeled with red fluorescent protein (RFP) and injected into the zebrafish embryo yolk sac after 1 day of fertilization (1 dpf). Embryos were incubated for 18 hours, 35.5°C. Peptide, animals were treated with 10 μM HS-binding peptide. Control, animals were not treated. Green; green fluorescent protein (GFP) labeled blood vessels. Red; red fluorescent protein (RFP) labeled tumor cells. **(A)** Representative images of the control group and the treated group. **(B)** Quantification of tumor fluorescence (tumor size). The bar represent the average of red fluorescence in zebrafish embryos. **(C)** Values express percent survival of animals; red line (10 μM of peptide treatment); blue line (animals in the absence of treatment). Each group contains 10 zebrafish embryos. Peptide decreased the number of tumoral cells and increased survival.

DATA AVAILABILITY STATEMENT

The raw data supporting the conclusions of this article will be made available by the authors, without undue reservation.

ETHICS STATEMENT

According to the University of California San Diego animal welfare guidelines, all animals were treated as described and approved by the UCSD Institutional Animal Care and Use Committee and in compliance with the ARRIVE guidelines (S12005 and S06008). Transgenic Tg[(Fli1: eGFP)] zebrafish were kindly provided by Dr. David Traver (UCSD). Zebrafish were maintained as previously described. C57BL/6 J mice were purchased from Jackson Laboratory, and mice were euthanized with CO2. All mice were maintained in a specific pathogen-free vivarium.

AUTHOR CONTRIBUTIONS

CM, contributions to the conception; the acquisition and analysis; interpretation of data; have drafted the work or substantively revised it. HW, contributions to the conception; acquisition and analysis; FK, the acquisition and analysis; SJ, the acquisition and analysis; MMCZ, the acquisition and analysis; NHB, have drafted the work or substantively revised; KRL, have drafted the work or substantively revised; PMAS, contribution to the conception, interpretation of data, have drafted the work or substantively revised. All authors contributed to the article and approved the submitted version.

FUNDING

This work was supported by FAPESP (process number 2016/01357-8 and 2019/03024-4), CNPQ and CAPES.

ACKNOWLEDGMENTS

We thank Dr. Marcelo Lima for providing modified heparins, Crowbio for providing PDX cells and Dr. David Traver for providing zebrafish line. This work was supported by FAPESP, CNPQ and CAPES.

REFERENCES

1. Herbert SP, Stainier DY. Molecular Control of Endothelial Cell Behaviour During Blood Vessel Morphogenesis. *Nat Rev Mol Cell Biol* (2011) 12:551–64. doi: 10.1038/nrm3176
2. Gacche RN, Meshram RJ. Targeting Tumor Micro-Environment for Design and Development of Novel Anti-Angiogenic Agents Arresting Tumor Growth. *Prog Biophys Mol Biol* (2013) 2:333–54. doi: 10.1016/j.pbiomolbio.2013.10.001
3. Weiss RJ, Esko JD, Tor Y. Targeting Heparin and Heparan Sulfate Protein Interactions. *Org Biomol Chem* (2017) 15:5656–68. doi: 10.1039/c7ob01058c
4. van Wijk XM, van Kuppevelt TH. Heparan Sulfate in Angiogenesis: A Target for Therapy. *Angiogenesis* (2014) 17:443–62. doi: 10.1007/s10456-013-9401-6
5. Dreyfuss JL, Regatieri CV, Jarrouge TR, Cavalheiro RP, Sampaio LO, Nader HB. Heparan Sulfate Proteoglycans: Structure, Protein Interactions and Cell Signaling. *Acad Bras Cienc* (2009) 81:409–29. doi: 10.1590/S0001-37652009000300007
6. Sarrazin S, Lamanna WC, Esko JD. Heparan Sulfate Proteoglycans. *Cold Spring Harb Perspect Biol* (2011) 3:a004952. doi: 10.1101/cshperspect.a004952
7. Bishop JR, Schuksz M, Esko JD. Heparan Sulphate Proteoglycans Fine-Tune Mammalian Physiology. *Nature* (2007) 446:1030–7. doi: 10.1038/nature05817
8. Dietrich CP, Nader HB, Straus AH. Structural Differences of Heparan Sulfates According to the Tissue and Species of Origin. *Biochem Biophys Res Commun* (1983) 111:865–71. doi: 10.1016/0006-291X(83)91379-7
9. Gacche RN, Meshram RJ. Targeting Tumor Micro-Environment for Design and Development of Novel Anti-Angiogenic Agents Arresting Tumor Growth. *Prog Biophys Mol Biol* (2013) 113:333–54. doi: 10.1016/j.pbiomolbio.2013.10.001
10. Ferrara N, Kerbel RS. Angiogenesis as a Therapeutic Target. *Nature* (2005) 438:967–74. doi: 10.1038/nature04483
11. Gesteira TF, Coulson-Thomas VJ, Taunay-Rodrigues A, Oliveira V, Thacker VE, Juliano MA, et al. Inhibitory Peptides of the Sulfotransferase Domain of the Heparan Sulfate Enzyme, N-Deacetylase-N-Sulfotransferase-1. *J Biol Chem* (2011) 286:5338–46. doi: 10.1074/jbc.M110.100719
12. Arap W, Pasqualini R, Ruoslahti E. Cancer Treatment by Targeted Drug Delivery to Tumor Vasculature in a Mouse Model. *Science* (1998) 279:377–80. doi: 10.1126/science.279.5349.377
13. Saw PE, Song EW. Phage Display Screening of Therapeutic Peptide for Cancer Targeting and Therapy. *Protein Cell* (2019) 10:787–807. doi: 10.1007/s13238-019-0639-7
14. Yates EA, Santini F, Guerrini M, Naggi A, Torri G, Casu B. 1H and 13C NMR Spectral Assignments of the Major Sequences of Twelve Systematically Modified Heparin Derivatives. *Carbohydr Res* (1996) 294:15–27. doi: 10.1016/S0008-6215(96)90611-4
15. Wang CH, Liu JH, Lee SC, Hsiao CD, Wu WG. Glycosphingolipid-Facilitated Membrane Insertion and Internalization of Cobra Cardiotoxin. The Sulfatide.Cardiotoxin Complex Structure in a Membrane-Like Environment Suggests a Lipid-Dependent Cell-Penetrating Mechanism for Membrane Binding Polypeptides. *J Biol Chem* (2006) 281:656–67. doi: 10.1074/jbc.M507880200
16. Giussani M, Merlino G, Cappelletti V, Tagliabue E, Daidone MG. Tumor-Extracellular Matrix Interactions: Identification of Tools Associated With Breast Cancer Progression. *Semin Cancer Biol* (2015) 35:3–10. doi: 10.1016/j.semcancer.2015.09.012
17. Kilpelainen I, Kaksonen M, Kinnunen T, Avikainen H, Fath M, Linhardt RJ, et al. Heparin-Binding Growth-Associated Molecule Contains Two Heparin-Binding Beta -Sheet Domains That Are Homologous to the Thrombospondin Type I Repeat. *J Biol Chem* (2000) 275:13564–70. doi: 10.1074/jbc.275.18.13564
18. Schlessinger J, Plotnikov AN, Ibrahimi OA, Eliseenkova AV, Yeh BK, Yayon A, et al. Crystal Structure of a Ternary FGF-FGFR-Heparin Complex Reveals a Dual Role for Heparin in FGFR Binding and Dimerization. *Mol Cell* (2000) 6:743–50. doi: 10.1016/S1097-2765(00)00073-3
19. Roy S, Lai H, Zouaoui R, Duffner J, Zhou H, Jayaraman LP, et al. Bioactivity Screening of Partially Desulfated Low-Molecular-Weight Heparins: A Structure/Activity Relationship Study. *Glycobiology* (2011) 21:1194–205. doi: 10.1093/glycob/cwr053
20. Robinson CJ, Mulloy B, Gallagher JT, Stringer SE. VEGF165-Binding Sites Within Heparan Sulfate Encompass Two Highly Sulfated Domains and Can Be Liberated by K5 Lyase. *J Biol Chem* (2006) 281:1731–40. doi: 10.1074/jbc.M510760200
21. Ferrara N, Gerber HP, LeCouter J. The Biology of VEGF and Its Receptors. *Nat Med* (2003) 9:669–76. doi: 10.1038/nm0603-669
22. Olsson AK, Dimberg A, Kreuger J, Claesson-Welsh L. VEGF Receptor Signalling - in Control of Vascular Function. *Nat Rev Mol Cell Biol* (2006) 7:359–71. doi: 10.1038/nrm1911
23. Ornitz DM, Itoh N. The Fibroblast Growth Factor Signaling Pathway. *Wiley Interdiscip Rev Dev Biol* (2015) 4:215–66. doi: 10.1002/wdev.176
24. Turner N, Grose R. Fibroblast Growth Factor Signalling: From Development to Cancer. *Nat Rev Cancer* (2010) 10:116–29. doi: 10.1038/nrc2780
25. Arrington CB, Yost HJ. Extra-Embryonic Syndecan 2 Regulates Organ Primordia Migration and Fibrillogenesis Throughout the Zebrafish Embryo. *Development* (2009) 136:3143–52. doi: 10.1242/dev.031492

26. Lee TY, Folkman J, Javaherian K. HSPG-Binding Peptide Corresponding to the Exon 6a-Encoded Domain of VEGF Inhibits Tumor Growth by Blocking Angiogenesis in Murine Model. *PLoS One* (2010) 5:e9945. doi: 10.1371/journal.pone.0009945

Conflict of Interest: The authors declare that the research was conducted in the absence of any commercial or financial relationships that could be construed as a potential conflict of interest.

Publisher's Note: All claims expressed in this article are solely those of the authors and do not necessarily represent those of their affiliated organizations, or those of the publisher, the editors and the reviewers. Any product that may be evaluated in this article, or claim that may be made by its manufacturer, is not guaranteed or endorsed by the publisher.

Copyright © 2021 Melo, Wang, Fujimura, Strnadel, Meneghetti, Nader, Klemke and Pinhal. This is an open-access article distributed under the terms of the Creative Commons Attribution License (CC BY). The use, distribution or reproduction in other forums is permitted, provided the original author(s) and the copyright owner(s) are credited and that the original publication in this journal is cited, in accordance with accepted academic practice. No use, distribution or reproduction is permitted which does not comply with these terms.

frontiers in Cell and Developmental Biology

ORIGINAL RESEARCH
published: 21 September 2021
doi: 10.3389/fcell.2021.697831

LncRNA RP11-499E18.1 Inhibits Proliferation, Migration, and Epithelial–Mesenchymal Transition Process of Ovarian Cancer Cells by Dissociating PAK2–SOX2 Interaction

Juan Yang[1], Shuping Peng[2,3] and Keqiang Zhang[1]**

[1] Department of Gynecologic Oncology Ward 5, Hunan Cancer Hospital, The Affiliated Cancer Hospital of Xiangya School of Medicine, Central South University, Changsha, China, [2] NHC Key Laboratory of Carcinogenesis of Hunan Cancer Hospital, The Affiliated Cancer Hospital of Xiangya School of Medicine, Central South University, Changsha, China, [3] The Key Laboratory of Carcinogenesis and Cancer Invasion of the Chinese Ministry of Education, Cancer Research Institute, Central South University, Changsha, China

OPEN ACCESS

Edited by:
Nikos Karamanos, University of Patras, Greece

Reviewed by:
Andreas Scorilas, National and Kapodistrian University of Athens, Greece
Julio Morales, The University of Oklahoma, United States

***Correspondence:**
Shuping Peng
shuping@csu.cn
Keqiang Zhang
keqiangzhang985@163.com

Specialty section:
This article was submitted to Molecular and Cellular Oncology, a section of the journal Frontiers in Cell and Developmental Biology

Received: *20 April 2021*
Accepted: *23 August 2021*
Published: *21 September 2021*

Citation:
Yang J, Peng S and Zhang K (2021) LncRNA RP11-499E18.1 Inhibits Proliferation, Migration, and Epithelial–Mesenchymal Transition Process of Ovarian Cancer Cells by Dissociating PAK2–SOX2 Interaction. Front. Cell Dev. Biol. 9:697831. doi: 10.3389/fcell.2021.697831

Background: Ovarian cancer (OC)is a deadly gynecological malignancy worldwide. It is urgent to identify diagnostic biomarkers of OC to disclose the underlying mechanism.

Methods and Materials: Bioinformatics analysis was used to identify target genes. Gene expression was detected and altered by qRT-PCR and cell transfection, respectively. The interaction between RP11-499E18.1 and PAK2, as well as that between PAK2 and SOX2, was determined using RNA pulldown, RNA immunoprecipitation (RIP), and co-immunoprecipitation (co-IP) assay, respectively. Localizations of RP11-499E18.1, PAK2, and SOX2 were respectively determined employing immunohistochemical (IHC), IF, and FISH. The regulatory effects of RP11-499E18.1, PAK2, and SOX2 on OC cell proliferation, migration, colony formation, epithelial–mesenchymal transition (EMT)-related factor expression, and SOX2 nuclear translocation were determined. Finally, the effects of RP11-499E18.1 and PAK2 expression on the tumor growth in nude mice were determined.

Results: RP11-499E18.1, PAK2, and SOX2 were selected in our study. RP11-499E18.1 was downregulated, while PAK2 and SOX2 was upregulated in OC tissues and cells. RP11-499E18.1 coexists in the nucleus and cytoplasm of OC cells. There is an interaction between RP11-499E18.1 and PAK2, as well as PAK2 and SOX2 in OC cells. Alteration of RP11-499E18.1 and PAK2 expression both had no influence on PAK2 and SOX2 levels, but PAK2 upregulation notably augmented p-SOX2 level. RP11-499E18.1 overexpression suppressed OC cell proliferation, migration, and colony formation, as well as SOX2 nuclear translocation. Besides, it inhibited tumor growth in nude mice. However, these effects were notably reversed by PAK2 upregulation and eventually offset by SOX2 knockdown. Additionally, RP11-499E18.1 overexpression reduced PAK2–SOX2 interaction and SOX phosphorylation, and increased the binding of RP11-499E18.1 by PAK2.

Conclusion: These lines of evidence demonstrated that RP11-499E18.1 might play its tumor suppressor roles in OC *via* regulation of the RP11-499E18.1–PAK2–SOX2 axis. This research indicated that RP11-499E18.1 might be used as a diagnostic biomarker for OC in the future.

Keywords: ovarian cancer, RP11-499E18.1, PAK2, SOX2, EMT

INTRODUCTION

Ovarian cancer (OC) is one of the most common and deadly gynecological malignancies in the world, which is characterized by high incidence and poor prognosis (Allemani et al., 2018; Kossaï et al., 2018). The overall 5-year survival rate of OC patients is merely 30–50%, because approximately 80% of the patients were in advanced stages at the time of diagnosis (Sundar et al., 2015; Allemani et al., 2018). The major reasons for such poor survival rate mainly lie in the inconspicuous early symptoms and limited screening approaches (Au et al., 2015; Menon et al., 2018). Considering that the outcomes of OC patients diagnosed at the early stage of OC is more satisfactory (Cress et al., 2015), identifying new clinical diagnostic biomarkers of OC with high sensitivity and accuracy and thereby obtaining a further understanding of the potential molecular regulating mechanism will be of great significance for future OC treatment.

Long non-coding RNAs (lncRNAs) are a set of ncRNAs composed of more than 200 nucleotides transcribed by RNA polymerase II (Nagano and Fraser, 2011; Huarte, 2015). In recent years, accumulating investigations have recorded that it functions as a key regulator in tumor development and progression (Hosono et al., 2017; Bill et al., 2019; Wang et al., 2020). It was disclosed that lncRNAs can exert its regulating roles in various biological functions of tumors, such as proliferation, apoptosis, and metastasis, by post-transcriptional regulation, ceRNA regulation mechanism, genomic stability, and epigenetics (Gutschner and Diederichs, 2012; Arnes et al., 2019; Tang et al., 2019). Besides, an earlier literature demonstrated that lncRNAs participated in the regulation of cellular processes depending on their location: cytoplasmic lncRNAs can affect cellular signaling cascades and regulate mRNA translation or stability, while nuclear lnRNAs are capable of transcriptional regulation, RNA processing, and chromatin interactions (Schmitt and Chang, 2016). In the last few years, the functions of many lncRNAs in OC have been investigated. For instance, it was reported that lncRNA NORAD knockdown markedly repressed the proliferation, epithelial–mesenchymal transition (EMT), migration, and invasion of OC cells (Xu et al., 2020). Similar results were also recorded in another investigation that demonstrated the tumor-suppressing roles of LINC-PINT in OC (Hao et al., 2020). Therefore, investigation of the efficacies of lncRNAs in OC may be of great significance for future treatments.

As an emerging biomedical auxiliary research technology, bioinformatics analysis has been widely used in various aspects of basic and clinical medical researches in recent years. At present, numbers of previous investigations have been performed based on the ovarian gene expression profiles available on NCBI Gene Expression Omnibus (GEO) database, and screened out a great many of differentially expressed genes (DEGs) that correlated with the development and progression of OC. For instance, Chen et al. (2020) screened out four hub genes as promising prognostic biomarkers for OC, followed by characterization of gene functions and mutual interactions employing bioinformatic analysis. Besides, Zhang et al. (2019) identified the potential prognostic and early detection biomarkers for OC by use of integrated bioinformatics approaches. Additionally, a previous study conducted utilizing bioinformatic analysis combined with experimental analysis proved that lncRNA FLJ33360 participated in the progression of OC through regulating miR-30b-3p (Yang et al., 2019). These lines of evidence testified that integrated bioinformatical approaches could make great contribution to the exploration for biomarkers and understanding of potential mechanism of the occurrence and development of OC.

In this research, DEGs were firstly screened out based on three OC-related microarray datasets (GSE14407, GSE18520, and GSE26712) obtained from the GEO database. Then, Gene Ontology (GO) analysis, protein–protein interaction (PPI) construction, and identification of hub genes were respectively conducted, followed by survival analysis. Finally, RP11-499E18.1, PAK2, and SOX2 were screened out as the target gene to carry out further investigation based on the results of bioinformatic analysis and previous published literatures. Thereafter, experimental analysis was further performed to reveal the underlying regulating mechanisms.

MATERIALS AND METHODS

Microarray Data Analysis

In this study, three OC-related microarray datasets [GSE14407, GSE18520 (GPL570 platform), and GSE26712 (GPL96 platform)] were obtained from the GEO database[1]. The GSE14407 dataset contained 12 ovarian serous papillary carcinoma (OSPC) samples and 12 normal human ovarian surface epithelial (OSE) samples, while the GSE18520 had 53 advanced OC samples and 10 normal OSE samples. In addition, 185 primary OC samples and 10 normal OSE samples were included in the GSE26712 dataset (**Table 1**). Identification of the DEGs was performed with the help of an interactive online tool GEO2R[2]. The threshold for the DEGs was set as $p < 0.05$. Then, Venn analysis was conducted to identify the overlapping DEGs, and survival analysis was performed to screen the potential tumor suppressor genes.

[1]https://www.ncbi.nlm.nih.gov/geo/

[2]https://www.ncbi.nlm.nih.gov/geo/geo2r/

TABLE 1 | The information about the GEO datasets analyzed in this study.

GEO accession	Platform	Sample size
GSE14407	GPL570	24, OSE (n = 12), PSOC (n = 12)
GSE18520	GPL570	63, OSE (n = 10), advanced OC (n = 53)
GSE26712	GPL96	195, OSE (n = 10), primary OC (n = 185)

GEO, Gene Expression Omnibus; OSE, ovarian surface epithelial; PSOC, papillary serous ovarian cancer; OC, ovarian cancer.

Gene Ontology Analysis

Gene ontology (GO) enrichment analysis of the commonly upregulated mRNAs was performed with the help of the Database for Annotation, Visualization, and Integrated Discovery (DAVID[3]). The top 10 pathways were selected to draw the bubble charts. $p < 0.05$ indicates a significant difference.

catRAPID Database Analysis

catRAPID database[4] is a tool for predicting the binding area of RNA and protein. In this study, catRAPID database was used to identify the interaction between the identified mRNA and proteins.

Cell Lines, Ovarian Cancer Tissues, and Nude Mice

The OC cell lines (CaOV3, OVCAR3, SKOV3, A2780, HO-8910, and IOSE80) used in this study were obtained from the American Type Culture Collection (ATCC, Rockville, United States). CaOV3 and SKOV3 cells were respectively cultured in Dulbecco's Modified Eagle's Medium (DMEM, ATCC) and modified McCoy's 5a Medium (ATCC), replenished with 10% fetal bovine serum (FBS, Gibco, Australia). OVCAR3, A2780, HO-8910, and IOSE80 cells were maintained in RPMI-1640 medium (ATCC) supplemented with 10% FBS. Cell cultivation was performed in a humidified, 5% CO_2 and 37°C incubator, and the culture medium was replaced three times each week.

A total of eight pairs of OC tissues and its corresponding pericarcinomatous tissues were obtained from Hunan Cancer Hospital and the Affiliated Cancer Hospital of Xiangya School of Medicine (Changsha, China). One part was stored in a −80°C refrigerator (Harier, Qingdao, China), while another part was fixed in formalin (Aladdin, Shanghai, China) and then embedded in paraffin for subsequent immunohistochemical (IHC) staining. All patients who participated in this research were diagnosed as ovarian serous adenocarcinoma by two pathologists, and none of them received any radiotherapy or chemotherapy prior to surgery. Signed informed consent was obtained from each patient.

A total of 18 female BALB/c nude mice (aged 4–6 weeks) were acquired from the Experimental Animal Center of Hunan Cancer Hospital and the Affiliated Cancer Hospital of Xiangya School of Medicine (Changsha, China) and were divided into three groups (six mice/each group) in the following experiments. The animals were reared in a pathogen-free room under 45–50% humidity and 25–27°C temperature conditions. All procedures involved in this study had obtained the approval from the Animal Ethic Committee of the Hunan Cancer Hospital and the Affiliated Cancer Hospital of Xiangya School of Medicine Hospital.

CaOV3 cells were harvested in the exponential phase and then were digested into single-cell suspensions. After that, the nude mice, which had been reared under standard conditions for 1 week, were inoculated subcutaneously with 1×10^6 cells in 0.2 ml of phosphate-buffered saline (PBS) at the right dorsal proximal upper limbs. The tumor size (width and length) was measured every 3 days for a total of six times after the tumor was visible to the naked eye. Tumor volume calculation was performed according to the formula listed below: tumor volume (V, mm^3) = 0.5 × length × width. Additionally, the tumor tissues were collected, fixed in formalin, and embedded in paraffin for subsequent IHC staining to detect the expression of proliferation-related Ki67 and apoptosis-associated caspase-3.

Quantitative Reverse-Transcription Polymerase Chain Reaction

RNA isolation was carried out from the collected tissues and cells utilizing TRIZOL reagent (TAKARA, Beijing, China). Genomic DNA was removed using RiboLock RNase Inhibitor and DNase I (Sangon Biotech, Shanghai, China). Quality control and concentration determination of the isolated RNA was fulfilled with the help of the spectrophotometer (HACH, Shanghai, China). RNA integrity was examined with 1% agarose gel electrophoresis. Then, reverse transcription was conducted with oligo(dT) primers utilizing Revertaid M Mulv Reverse Transcriptase (Thermo Fisher Scientific). Thereafter, qRT-PCR was carried out with the help of 2 × SYBR Green PCR Master mix (Thermo Fisher Scientific). Relative expression of target genes was calculated with the $2^{-\Delta\Delta Ct}$ method (Livak and Schmittgen, 2001). β-actin was set as the internal control. The primers used in this study were synthesized by Sangon Biotech and are listed in **Table 2**.

Cell Transfection

The full-length complementary cDNA of human RP11-499E18.1 and PAK2 were synthesized by Sangon Biotech and cloned into pcDNA3.1 vector (TAKARA) to construct overexpression plasmids pcDNA-RP11-499E18.1 and pcDNA-PAK2. DNA Midiprep Kits (Thermo Fisher Scientific) were used for preparation of the overexpression plasmids. Meanwhile, the small interfering (si)RNA of RP11-499E18.1 (si-RP11-310-332, si-RP11-454-476 and si-RP11-589-611) and short harpin (sh)RNA of SOX2, as well as their corresponding negative control (NC) were synthesized to perform RNA knockdown. CaOV3 and SKOV3 cells were respectively plated in six-well plates (2×10^5/well) and grown in a 37°C incubator overnight. Thereafter, the overexpression plasmids, pcDNA-RP11-499E18.1 and pcDNA-PAK2, were respectively transfected or co-transfected into the prepared cells. The knockdown sequences si-RP11-499E18.1 and shSOX2 were respectively transfected into cells. Besides, co-transfection of pcDNA-PAK2

[3]https://david.ncifcrf.gov/

[4]http://service.tartaglialab.com/page/catrapid_group

TABLE 2 | The sequences of the primers used in qRT-PCR.

Gene name	Primer sequences
EGOT-F	5′-ACCGACTGTCCAACTAGCAA-3′
EGOT-R	5′-TTGTGTTTCCCTGTGCAGTG-3′
RP11-499E18.1-F	5′-AGCGTTGGGATTACAGGAGT-3′
RP11-499E18.1-R	5′-AGGACAGAAGCCAGAAGTTGA-3′
WT1-AS-F	5′-ACTCGTCTGTTCTGATGCCA-3′
WT1-AS-R	5′-ATGGGCCTACGTATCTGCTC-3′
HAND2-AS1-F	5′-TCCCCGAATCTGTAGTGTGG-3′
HAND2-AS1-R	5′-GAGTCACAGGCAGTCGTAGA-3′
PAK2-F	5′-TGAGCACACCATCCATGTTGG-3′
PAK2-R	5′-AGGTCTGTAGTAATCGAGCCC-3′
SOX2-F	5′-TACAGCATGTCCTACTCGCAG-3′
SOX2-R	5′-GAGGAAGAGGTAACCACAGGG-3′
β-actin-F	5′-ACCCTGAAGTACCCCATCGAG-3′
β-actin-R	5′-AGCACAGCCTGGATAGCAAC-3′
Primers U1-F	5′-GGGAGATACCATGATCACGAAGGT-3′
Primers U1-R	5′-CCACAAATTATGCAGTCGAGTTTCCC-3′

TABLE 3 | The sequences of siRNAs and shRNAs used in cell transfection.

Name	Sequences
si-RP11-310-332	5′-UCCAUAUCCUCUUAACCAGGA CUGGUUAAGAGGAUAUGGAUA-3′
si-RP11-454-476	5′-UCCUUUUAUCUUUGUCUUCAU GAAGACAAAGAUAAAAGGAAC-3′
si-RP11-589-611	5′-UAGGAUAUGGUAAACACUGUU CAGUGUUUACCAUAUCCUAAU-3′
si-PAK2	5′-AGAAGGAACUGAUCAUUAA-3′
si′-PAK2	5′-GAAACUGGCCAAACCGUUAUU-3′
shSOX2-1	5′-CGAGATAAACATGGCAATCAA-3′
shSOX2-2	5′-GTACAGTATTTATCGAGATAA-3′

TABLE 4 | The oligonucleotide sequences used for RNA pulldown assay.

Name	Sequences
RP11-499E18.1-sense-F	5′-TAATACGACTCACTATAGGGAGACCTCAGCGTCCGGAG TAGCTA-3′
RP11-499E18.1-sense-R	5′-TTGCAAGTTAGAGCACTATATT-3′
RP11-499E18.1-antisense-F	5′-CCTCAGCGTCCGGAGTAGCTA-3′
RP11-499E18.1-antisense-R	5′-TAATACGACTCACTATAGGGAGATTGCAAGTTAGAGCAC TATATT-3′

and shSOX2 were also performed. Cell transfections were performed with the help of Lipofectamine 3000 (Invitrogen, California, United States). Cells were harvested 48 h post transfection to conduct further experiments. The sequences of the plasmids, siRNAs, and shRNAs are detailed in **Table 3**.

Cell Proliferation

After transfection, (3-(4,5-Dimethylthiazol-2-yl)-2,5-diphenyltetrazoliumbromide) MTT assay was carried out to assess cell proliferation. Briefly, 100 μl of the transfected CaOV3 and SKOV3 cells was resuspended and seeded into 96-well plates at a concentration of 1×10^4 cells per well. Then, 50 μl of MTT reagent that was dissolved in PBS was respectively provided into each well at 0, 12, 24, 48, and 72 h after transfection, and the mixtures were maintained in a 37°C incubator for another 4 h. Thereafter, 150 μl of dimethyl sulfoxide (DMSO) was supplied into each well to dissolve the formazan. The optical density (OD) at 570 nm was measured utilizing a microplate reader (Bio-Rad, Hercules, CA, United States). Cell proliferation ratio (%) was calculated according to the formula listed below: Cell proliferation ratio (%) = $OD_{experimentalgroup}/OD_{NC} \times 100\%$.

After transfection, CaOV3 and SKOV3 cells were resuspended and plated into 6-well plates at a concentration of 1,000 cells per well. Then, the plates were maintained in a humidified incubator under 5% CO_2 and 37°C conditions for 2–3 weeks. Colony fixation and staining were respectively conducted utilizing methanol and 0.1% crystal violet (Sangon Biotech). Finally, the images of the colonies were photographed with a microscope (Olympus, Tokyo, Japan).

Transwell Assay

After transfection, the invasive capacity of CaOV3 and SKOV3 cells was determined using transwell assay. Briefly, the Matrigel chamber (Corning, New York, United States) used in this study was coated with 50 μl Matrigel (1:8) in advance. CaOV3 and SKOV3 cells were suspended in serum-free medium at a concentration of 5×10^4/ml. Then, 200 μl of the suspended cells was added to the upper chamber, and 600 μl of complete medium was provided to the lower chamber. After maintaining for 48 h in a 5% CO_2 and 37°C incubator, the uninvaded cells on the upper chamber were wiped off, while the successfully invaded cells on the lower chamber were fixed with 95% ethanol (Aladdin) for 20 min and stained with hematoxylin (Sangon Biotech) for 10 min. Finally, the images of the invaded cells were photographed with a microscope (Olympus).

Immunohistochemical

The prepared tissues were respectively sliced into 3-μm-thick sections, and baked in a 60–65°C incubator for 4 h. Then, the slices were dewaxed in xylene, rehydrated in grade ethanol, and rinsed with 1× PBS for three times. Afterward, the slices were put into the citrate buffer (10 mmol/L, pH 6.0) and heated to 121°C in an autoclave for 20 min. The endogenous peroxidase was blocked in 50 μl of 5% H_2O_2 for 10 min at room temperature (RT). Subsequently, incubation of primary antibodies, including anti-PAK2 (ab76293, Abcam, Cambridge, United Kingdom), anti-SOX2 (#2748, Cell Signal Technology, Boston, United States), anti-Caspase3 (ab4051, Abcam), and anti-Ki67 (ab15580, Abcam), was performed at 4°C overnight. After rinsing, each slice was incubated with 50 μl of HRP-labeled secondary antibody (ab6721, Abcam) for 10 min at RT. Then, 50 μl of streptomyces anti-biotin-peroxidase solution was provided to each slice and reacted for 10 min. After rinsing, the slices were incubated with 3,39-diaminobenzidine tetrahydrochloride (DAB) reagent for approximately 10 min to develop color. Then, the reaction was terminated, and hematoxylin re-staining was performed, followed by dehydration

and transparency, and neutral resin mounting. For the NC group, the slices were incubated with PBS instead of primary antibodies. Each slice was respectively photographed at 200 and 400× magnification with the help of a microscope (Olympus).

Immunofluorescence

CaOV3 and SKOV3 cells were respectively seeded into six-well plates with the autoclaved cover glasses placed at the bottom of the wells. After cells grown to 50% confluence on the coverslips, PBS rinsing was performed, followed by 4% paraformaldehyde (PFA) fixation at RT for 10 min. After washing, cells were permeated with PBS, which contains 0.5% Triton X-100 for 20 min and blocked with 3% bovine serum albumin (BSA, Thermo Fisher Scientific) for 1 h at RT. After rinsing with PBS, primary antibody anti-SOX2 (#92186, Cell Signal Technology) incubation was carried out with

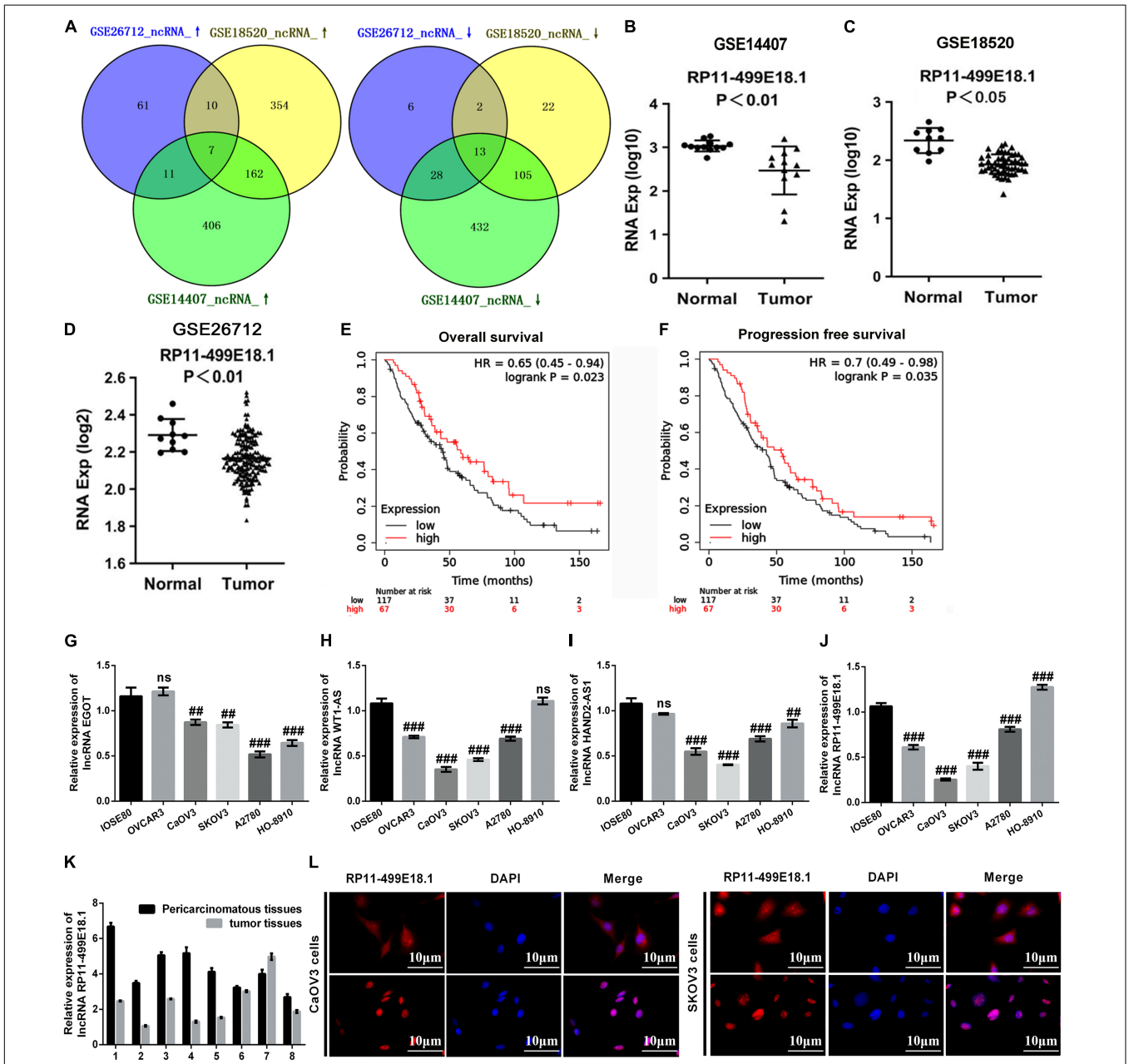

FIGURE 1 | RP11-49E18.1 was verified to be a potential tumor suppressor gene of OC. **(A)** Venn diagram analysis respectively identified 7 upregulated and 13 downregulated DEGs. **(B–D)** RP11-499E18.1 was distinctly downregulated in OC tissues. **(E,F)** Low expression of RP11-499E18.1 was closely associated with poor prognosis of OC patients. **(G–J)** RP11-499E18.1 was the lowest expressed gene in a series of OC cells, especially in CaOV3 and SKOV3 cells. **(K)** RP11-499E18.1 expression in OC tissues was notably lower than in pericarcinomatous tissues. **(L)** RP11-499E18.1 exists in cells in the form of plasma–nucleus coexistence. DEGs, differentially expressed genes; OC, ovarian cancer. $^{\#\#}p < 0.01$, $^{\#\#\#}p < 0.001$, ns, no significance.

the cells attached on the coverslips at 4°C overnight. Alexa Fluor® 488-conjugated secondary antibody (ab150077, Abcam) incubation was conducted at RT for 1 h. Then, the cell nuclei were counterstained with 4-6-diamidino-2-phenylindole (DAPI) reagent (Sangon Biotech) for 10 min and the slices were mounted. Finally, images were observed and photographed using a confocal microscope (Zeiss, Jena, Germany).

Fluorescence *in situ* Hybridization

The RP11-499E18.1 and U6 probes were both purchased from RiboBio (Guangzhou, China). CaOV3 and SKOV3 cells were respectively seeded into 24-well plates (approximately 6×10^4/well) with the autoclaved cover glasses placed at the bottom of the wells. After the cells were grown to 60–70% confluence on the coverslips, 4% PFA fixation was performed at RT for 10 min, followed by PBS rinsing. Afterward, cells were permeabilized with 1 ml of pre-cooled PBS containing 0.5% Triton X-100 at 4°C for 5 min. Then, the supernatant was discarded. After that, 200 μl of pre-hybridization reagent was provided and reacted for 30 min at 4°C. Thereafter, the pre-hybridization reagent was removed. The hybridization solution containing RP11-499E18.1 or U6 probes were respectively added under dark conditions, and the solution was maintained at 37°C overnight. Then, 4 × SSC (containing 0.1% Tween-20) rinsing was performed to reduce the background signal, followed by 2 × SSC, 1 × SSC, and PBS rinsing under dark conditions. Subsequently, DAPI reagent was added and reacted for 10 min to counterstain cell nuclei. After rinsing, the slices were mounted and subjected to fluorescent signal detection employing a confocal microscopy (Zeiss).

Western Blot

Protein extraction was performed by use of RIPA lysis buffer (Beyotime, Shanghai, China), in the presence of protease inhibitors (Thermo Fisher Scientific). Quantification of the extracted proteins was fulfilled employing a Nanodrop 2000 system (Thermo Scientific). Afterward, protein separation was carried out utilizing SDS-PAGE. Subsequently, the target proteins were transferred onto the nitrocellulose (NC) membrane, and blocked in 5% BSA. Thereafter, incubation of primary antibodies, including anti-PAK2 (ab76293, Abcam), anti-SOX2 (#2748, Cell Signal Technology), anti-p-SOX2 (#92186, Cell Signal Technology), anti-E-cadherin (ab40772, Abcam), anti-Vimentin (ab137321, Abcam), and anti-β-actin (66009-1-Ig, Ptgcn, IL, United States), was conducted at 4°C overnight. After that, the target proteins were incubated with HRP-labeled secondary antibody (ab6721, Abcam) at RT for 1 h. Finally, the signals were developed using ECL reagent and detected with the help of a LAS-3000 (FUJIFILM, Tokyo, Japan) system.

RNA Pulldown Assay

The biotin-labeled full-length RP11-499E18.1 and antisense RP11-499E18.1 were synthesized using Biotin RNA Labeling Mix (Roche, Basel, Switzerland) and T7 RNA polymerase (Promega, Wisconsin, United States), in the presence of RNase-free DNase I (Thermo Fisher Scientific). Then, the products were purified with the help of RNeasy Mini Kit (Qiagen, MD, United States). Afterward, the proteins exacted from CaOV3 and SKOV3 cells were respectively incubated with the biotinylated RNA at RT for 4 h. Thereafter, the streptavidin magnetic beads (Thermo Fisher Scientific) were provided and

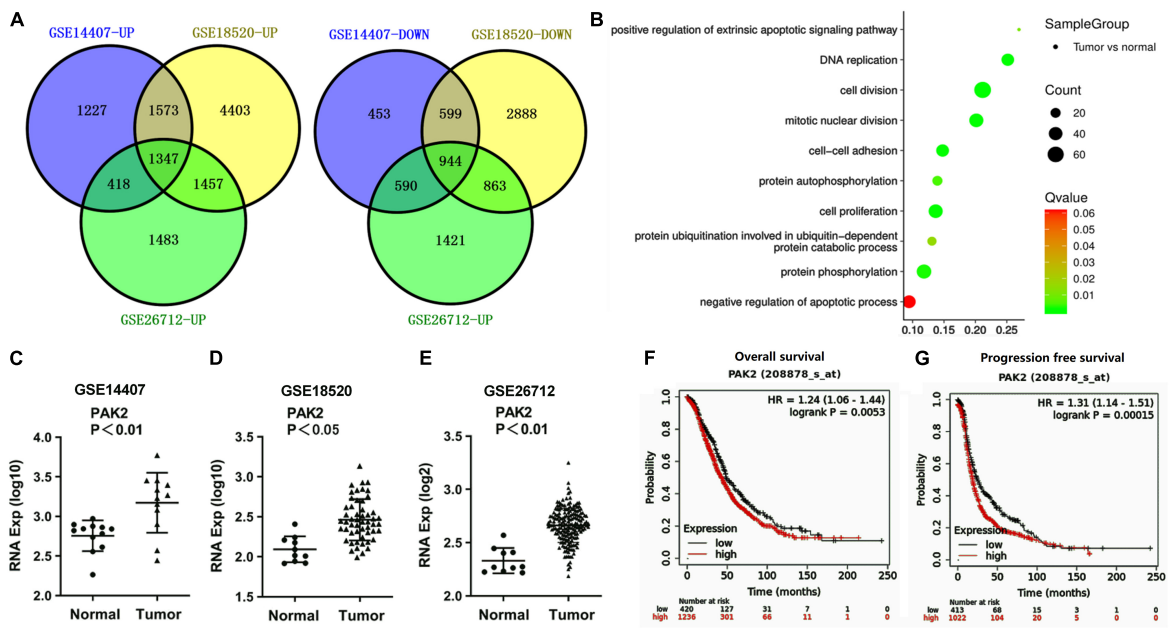

FIGURE 2 | PAK2 was predicted to be an oncogene of OC. **(A)** Venn diagram analysis respectively identified 1,347 upregulated and 944 downregulated differentially expressed mRNAs. **(B)** The top 10 pathways obtained by GO term analysis. **(C–E)** PAK2 expression was distinctly upregulated in OC tissues. **(F,G)** High expression of PAK2 was closely associated with poor prognosis of OC patients. OC, ovarian cancer; GO, Gene Ontology; PAK2, P21 (RAC1) Activated Kinase 2.

the mixtures were maintained at 4°C overnight. After that, the unbounded proteins were removed, while the bounded proteins were eluted and further analyzed by electrophoresis, silver staining, mass spectrometry (MS), and Western blot. The oligonucleotide sequences used for RNA pulldown are listed in **Table 4**.

RNA Immunoprecipitation Assay

RNA immunoprecipitation (RIP) was carried out utilizing EZ-Magna RIP Kit (Millipore, United States) following the manufacturer's instructions. Briefly, CaOV3 and SKOV3 cells were lysed in RIP lysis buffer, and then the cell lysates were incubated with RIP buffer, with magnetic beads conjugated with AGO2 antibody or NC mouse IgG with rotation at 4°C overnight. After centrifugation, the beads were collected and rinsed by RIP Wash Buffer. Thereafter, the complexes were incubated with proteinase K buffer to remove proteins. After that, isolation and purification of the immunoprecipitated RNA was performed. Further analysis was conducted utilizing qRT-PCR.

Co-immunoprecipitation

For co-immunoprecipitation (co-IP), both of the untransfected and transfected CaOV3 and SKOV3 cells were incubated with RIPA lysis buffer (Beyotime), in the presence of protease inhibitors (Thermo Fisher Scientific). Afterward, the supernatants of cell lysates were collected by centrifugation and then were respectively incubated with primary antibodies, including PAK2 antibody and SOX2 antibody, or control IgG at 4°C overnight. After that, the Protein A/G PLUS-Agarose beads (Santa Cruz Biotechnology) were provided and the mixtures were maintained at 4°C for 2 h. Thereafter, the beads were isolated and rinsed with lysis buffer, and finally analyzed by Western blot.

Statistical Analysis

Each experiment possesses three replications. Data analysis was completed employing GraphPad Prism (GraphPad software, CA, United States). Data were expressed as mean ± standard deviation (SD). The association between RP11-499E18.1, PAK2, and SOX2 expression with the overall survival (OS) was determined with the Kaplan–Meier survival analysis using the log-rank test. Comparison between two groups and among multi-groups was respectively conducted utilizing Student's *t*-test and one-way ANOVA followed by Tukey's *post hoc* test. $p < 0.05$ represents statistically significant.

RESULTS

RP11-49E18.1 Was Verified to Be a Potential Tumor Suppressor Gene of Ovarian Cancer

In this study, a variety of bioinformatics approaches were employed to identify the genes that played crucial roles in the regulation of OC. Analysis of GSE14407, GSE18520, and GSE26712 respectively identified 1,164 (586 upregulated, 578 downregulated), 675 (533 upregulated, 142 downregulated), and 138 (89 upregulated, 49 downregulated) DEGs. Venn analysis discovered that there were a total of 20 consistently expressed genes, of which 7 were upregulated, while 13 were downregulated (**Figure 1A**). Based on these results, survival analysis was further performed to evaluate the relationship between these genes and survival prognosis. Outcomes showed that the four downregulated lncRNAs, including EGOT, WT1-AS, HAND2-AS1, and RP11-499E18.1, exerted typical low expression and poor prognosis, which indicates that these four lncRNAs might be the potential tumor suppressor genes of OC. As shown in **Figures 1B–D**, RP11-499E18.1 was significantly downregulated in different types of OC ($p < 0.01$ or $p < 0.05$). Besides, survival analysis results showed that low expression of RP11-499E18.1 was closely associated with poor prognosis of OC patients (**Figures 1E,F**, $p < 0.05$), in which the RP11-499E18.1 high expression group accounts for 40% according to the cutoff values. Afterward, we detected the expression of EGOT, WT1-AS, HAND2-AS1, and RP11-499E18.1 in a series of OC cells. Result shown in **Figures 1G–J** showed that RP11-499E18.1 was the lowest expressed gene, especially in CaOV3 and SKOV3 cells ($p < 0.01$ or $p < 0.001$). Subsequently, the expression of RP11-499E18.1 in eight pairs of clinical OC tissues was also detected. Results showed that its expression in OC tissues was notably lower than in pericarcinomatous tissues (**Figure 1K**). In addition, the location of RP11-499E18.1 in OC cells was further

TABLE 5 | Gene ontology (GO) analysis of five typical pathways associated with ovarian cancer (OC).

Term/gene function	Genes
GO:0006468 ~protein phosphorylation	NUAK2, FASTK, PASK, PKMYT1, RPS6KB2, AURKA, AURKB, PRKY, CCNE1, ACVR1B, ADCK2, CSNK2A1, PAK2, TLK1, CDK16, CSK, LIMK1, PHKG2, PRKCI, PKN1, MINK1, PBK, SRPK1, GAK, CCND1, MAST2, HIPK2, BUB1B, WNT11, EIF2AK2, LRRK1, KALRN, NEK2, MAP4K1, MAPKAPK2, BUB1, CAMK2B, DYRK2, STK19, RUNX3, AATK, CSNK1A1, TAF1, TRIO, BIRC5, ILF3, IKBKE, CSNK1E, GSK3A, GRK6, TSSK2, JAK3, CIT, IKBKB
GO:0098609 ~cell–cell adhesion	ALDOA, YWHAZ, SEPT2, ZC3HAV1, RANGAP1, SFN, TAGLN2, PKM, EPCAM, PAK6, BZW2, PAK2, DDX3X, CC2D1A, CLINT1, TES, GOLGA2, HIST1H3J, STX5, MYO6, BAIAP2, TRIM29, CBL, DOCK9, PFKP, LYPLA2, MICALL1, CORO1B, EPB41L1, CCNB2, HIST1H3B, HIST1H3E, ERC1, HIST1H3F, DBN1, HIST1H3G, HIST1H3H, PUF60, HIST1H3I, SEPT9
GO:0046777 ~protein autophosphorylation	FGFR2, TAF1, FLT1, NEK2, PASK, MAP4K1, TTK, MINK1, AURKA, CAD, MAPKAPK2, AURKB, EPHB3, PRKX, ACVR1B, DDR1, PTK2, PAK2, MAP3K10, TSSK2, CAMK2B, EIF2AK2, CSK, MELK
GO:2001238 ~positive regulation of extrinsic apoptotic signaling pathway	BID, LTBR, PAK2, TNFRSF12A, PML, RBCK1, WWOX
GO:0043066 ~negative regulation of apoptotic process	STIL, CLDN7, PPARD, YWHAZ, HTATIP2, MCL1, NUAK2, AURKA, BCL2L1, SOX9, ADORA1, EPCAM, PTK2, PAK2, DDX3X, ITCH, ARHGDIA, DHCR24, KIF14, CDK1, PRAME, SOCS3, SMAD6, CBL, TP53, PRKCI, BIRC5, HMGA2, PPIF, ATF5, PA2G4, HSP90B1, MSX1, MAD2L1, UCP2, VEGFA, TFAP2A, WNT11, IKBKB, EIF2AK2, CLEC5A, GSTP1, BARD1

$p \leq 0.01$

determined by FISH, and outcomes demonstrated that RP11-499E18.1 exists in cells in the form of plasma–nucleus coexistence (**Figure 1L**). Therefore, RP11-499E18.1 was chosen to conduct further research in this study.

PAK2 Was Predicted to Be an Oncogene of Ovarian Cancer

In order to explore how RP11-499E18.1 exerts its regulatory roles in OC, we further analyzed these datasets to figure out the crucial mRNAs participated in the regulation of OC. There were respectively 7,132 (4,546 upregulated, 2,586 downregulated), 14,074 (8,780 upregulated, 5,294 downregulated), and 8,523 (4,705 upregulated, 3,818 downregulated) differentially expressed mRNAs screened out. Venn diagram exhibited that there were a total of 2,291 consistently expressed mRNAs, namely, 1,347 upregulated and 944 downregulated genes (**Figure 2A**). Considering that the upregulated mRNAs were much more than downregulated mRNAs in OC, GO enrichment analysis was performed among the upregulated mRNAs. Results showed that 2 of the top 10 pathways were related to protein phosphorylation (**Figure 2B**). Besides, PAK2 was found to exist in several typical GO pathways mentioned above (**Table 5**), indicating that PAK2 might be the functional protein of RP11-499E18.1. Thereafter, PAK2 expression in OC tissues and the association between PAK2 expression and prognosis of OC patients were further analyzed. Results shown in **Figures 2C–E** demonstrated that PAK2 was notably upregulated in different types of OC ($p < 0.01$ or $p < 0.05$). Besides, survival analysis revealed that there was a close association between high expression of PAK2 and poor prognosis of OC patients (**Figures 2F,G**, $p < 0.01$), among which PAK2 high expression groups account for 75% according to the cutoff values. These results indicated that PAK2 might exert a pro-cancer efficacy in OC.

Validation of the Interactions Among RP11-499E18.1, PAK2, and SOX2

Numbers of previous investigations have clarified the interaction between PAK2 and SOX2 in various human diseases (Huttlin et al., 2015, 2017). Therefore, relative expression of SOX2 in OC tissues and the correlation between SOX2 expression and the prognosis of OC patients were also analyzed. Outcomes displayed in **Figures 3A–C** showed that there was no significant change of SOX2 expression between OC tissues and normal tissues. Besides, survival analysis revealed that SOX2 was a poor prognostic

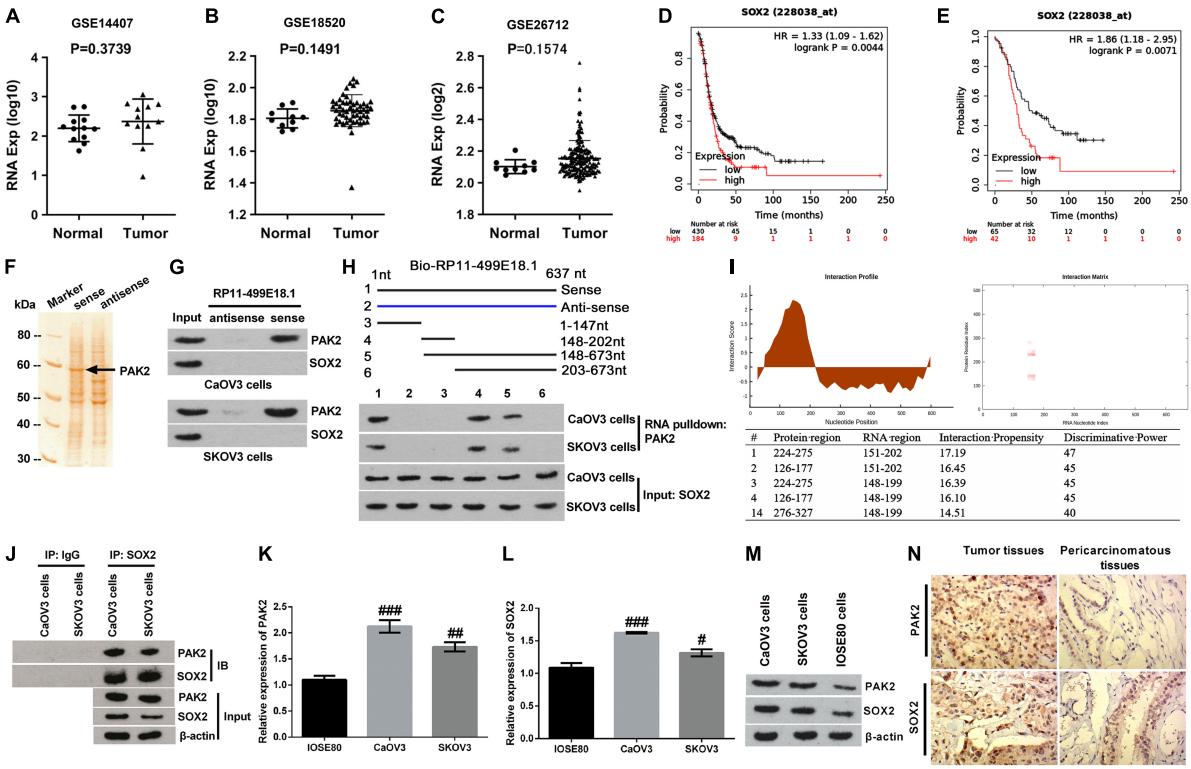

FIGURE 3 | Validation of the interactions among RP11-499E18.1, PAK2, and SOX2. **(A–C)** There was no significant difference of SOX2 expression between normal tissues and OC tissues. **(D,E)** High expression of SOX2 was closely associated with poor prognosis of OC patients. **(F)** The band located at 60 kDa was identified as PAK2. **(G)** RNA pulldown assay affirmed that there was an interaction between RP11-499E18.1 and PAK2. **(H,I)** Domain mapping assay and catRAPID database analysis confirmed that there was a strong binding effect between the 150–200 bp region of lncRNA RP11-49E18.1 and the 126–177/245–275 amino acid region of PAK2. **(J)** There was an interaction between PAK2 and SOX2 in CaOV3 and SKOV3 cells. **(K–M)** The expression of PAK2 and SOX2 in CaOV3 and SKOV3 cells was notably higher than in IOSE80 cells. **(N)** The expression of PAK2 and SOX2 in OC tissues was much higher than in pericarcinomatous tissues. OC, ovarian cancer; PAK2, P21 (RAC1) activated kinase 2; SOX2, SRY-box transcription factor 2. $^{\#}p < 0.05$, $^{\#\#}p < 0.01$, $^{\#\#\#}p < 0.001$.

factor (**Figures 3D,E**), in which the SOX2 high expression group accounts for 30% according to cutoff values. Combined with the results of PAK2 GO enrichment analysis, these results indicated that PAK2 might function through regulating the phosphorylation level of SOX2, which could further influence gene transcription.

Based on the aforementioned results, we deduced that RP11-499E18.1 might exert its anti-cancer efficacy in OC *via* regulation of the RP11-499E18.1–PAK2–SOX2 axis. Therefore, RNA pulldown assay was carried out to explore whether there exist an association among RP11-499E18.1, PAK2, and SOX2. MS analysis revealed that the protein with a molecular weight close to 60 kDa in the electrophoresis was PAK2 (**Figure 3F**). In addition, results displayed in **Figure 3G** confirmed that RP11-499E18.1 could directly bind to PAK2 in both CaOV3 and SKOV3 cells, while there was no interaction between RP11-499E18.1 and SOX2. After that, a series of biotin-labeled RP11-499E18.1 fragments were constructed to

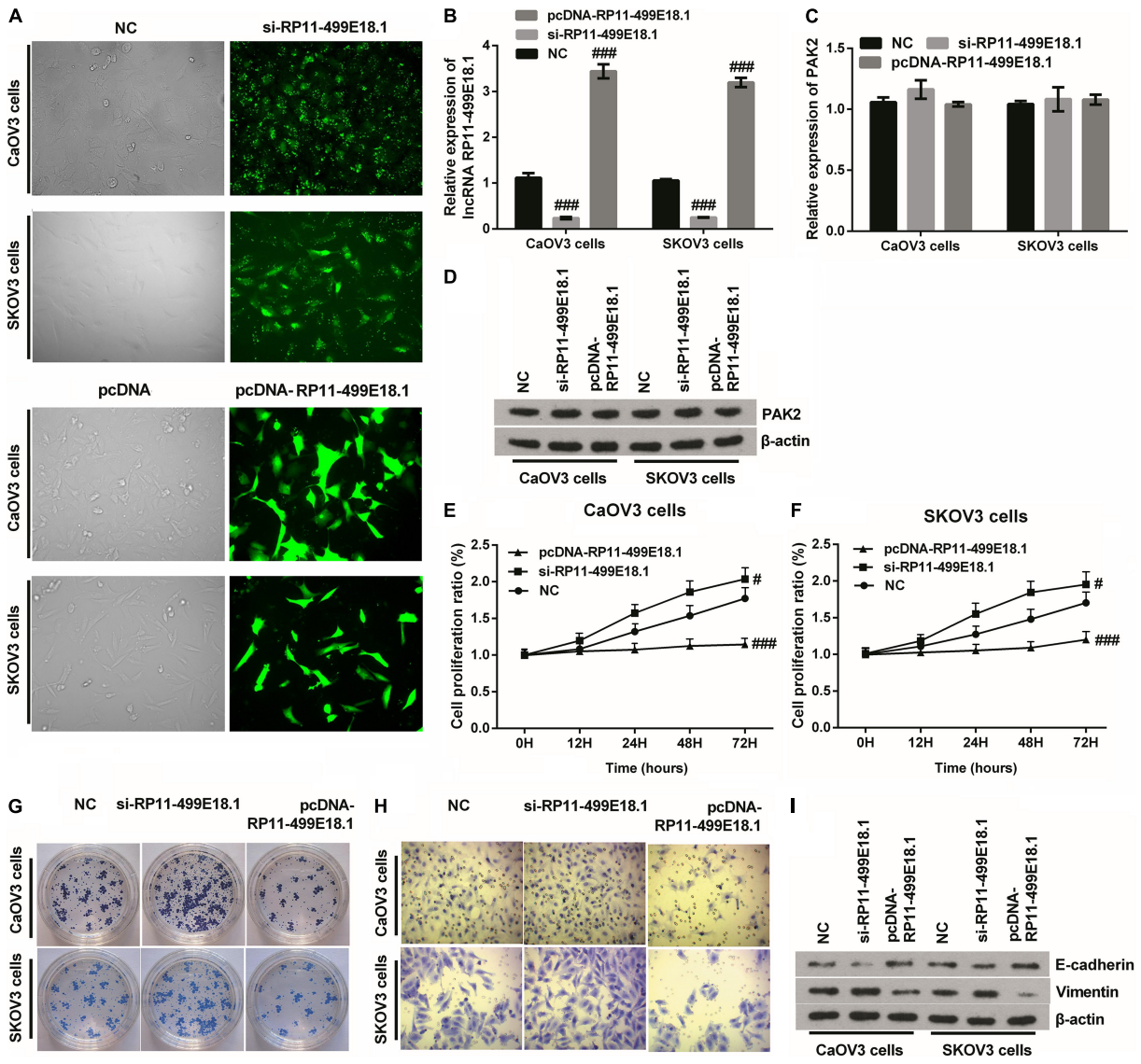

FIGURE 4 | RP11-499E18.1 overexpression obviously suppressed cell proliferation, migration, colony formation, and EMT transformation. The sequences of NC and si-RP11-499E18.1 were respectively transfected into CaOV3 and SKOV3 cells to silence RP11-499E18.1 expression. The plasmids pcDNA 3.1 and pcDNA-RP11-499E18.1 were respectively transfected into CaOV3 and SKOV3 cells to overexpress RP11-499E18.1. **(A,B)** The transfection efficiency was high, and RP11-499E18.1 was successfully silenced and overexpressed in CaOV3 and SKOV3 cells. **(C,D)** There was no obvious influence of RP11-499E18.1 knockdown or overexpression on the expression of PAK2. **(E–H)** The proliferation, colony formation, and migration of CaOV3 and SKOV3 cells were distinctly repressed by RP11-499E18.1 overexpression, while notably promoted by RP11-499E18.1 knockdown. **(I)** The expression of EMT-related E-cadherin was distinctly increased, while Vimentin was notably decreased by RP11-499E18.1 overexpression. RP11-499E18.1 knockdown performed the opposite effects. NC, negative control; si, small interfering; PAK2, P21 (RAC1) activated kinase 2; EMT, epithelial–mesenchymal transition. $^{\#}p < 0.05$, $^{\#\#\#}p < 0.001$.

determine the specific and effective binding region of RP11-499E18.1 when binding to PAK2. Results showed that the 148–202 bp region of RP11-499E18.1 is the possible binding region of PAK2 (**Figure 3H**). Meanwhile, catRAPID database analysis revealed that there was a strong binding effect between the 150–200 bp region of lncRNA RP11-49E18.1 and the 126–177/245–275 amino acid region of PAK2 (**Figure 3I**). Thereafter, Co-IP assay was conducted to confirm whether there exists an interaction between PAK2 and SOX2. Results verified that there was an association between PAK2 and SOX2 in CaOV3 and SKOV3 cells (**Figure 3J**). Then, the expression of PAK2 and SOX2 in OC cells and tissues was respectively testified. qRT-PCR and Western blot results displayed that both PAK2 and SOX2 in CaOV3 and SKOV3 cells was notably higher than their expression in IOSE80 cells (**Figures 3K–M**, $p < 0.05$ or $p < 0.01$ or $p < 0.001$). IHC results demonstrated that the expression of PAK2 and SOX2 in OC tissues was much higher than in pericarcinomatous tissues (**Figure 3N**). These results indicated that RP11-49E18.1 might perform its tumor-suppressive roles through influencing its interaction with PAK2 and the interaction between PAK2 and SOX2.

RP11-499E18.1 Overexpression Obviously Suppressed Cell Proliferation, Migration, Colony Formation, and Epithelial–Mesenchymal Transition Transformation

After transfection, the transfection efficiency was respectively testified employing qRT-PCR and fluorescence microscope. Outcomes verified that the expression of RP11-499E18.1

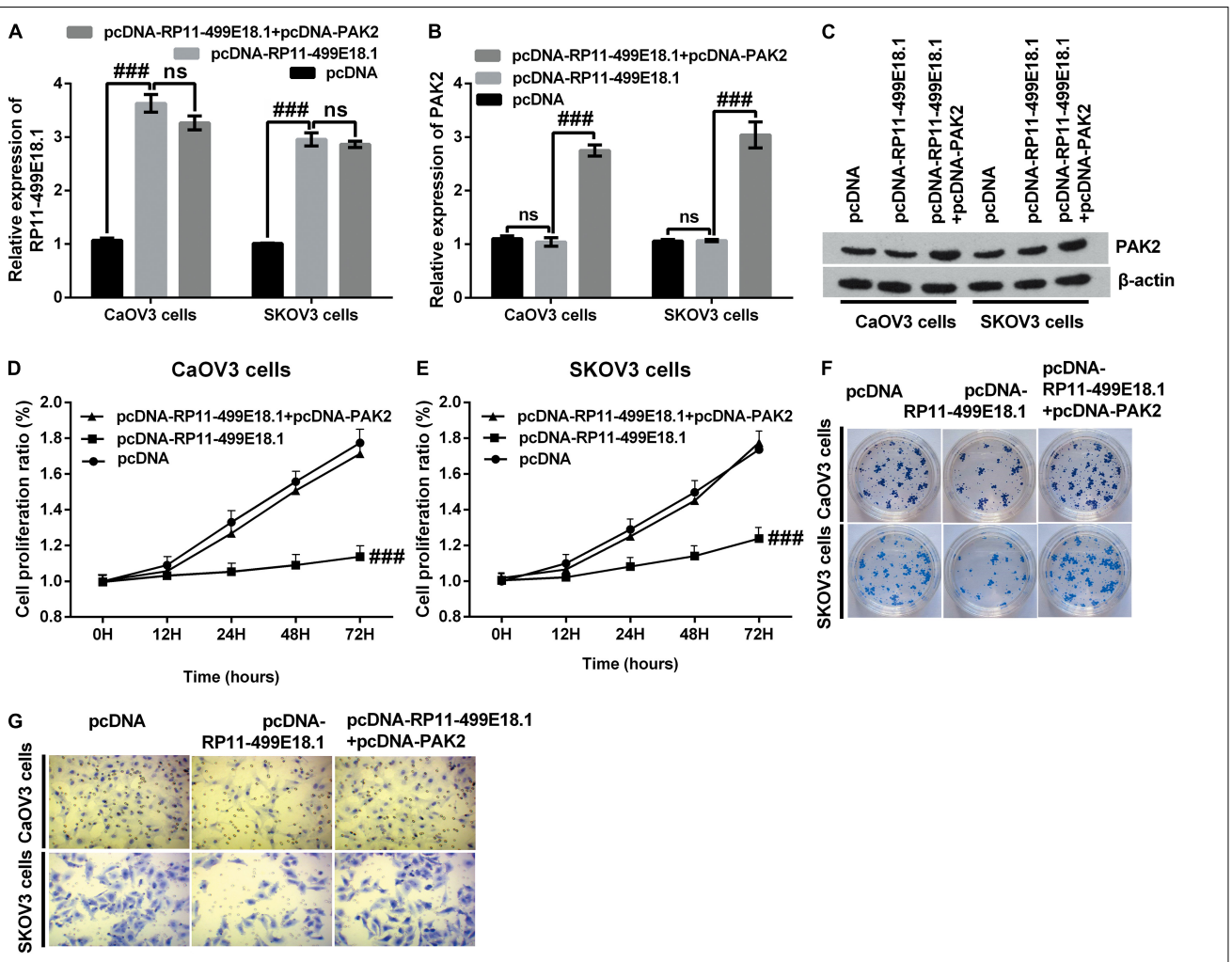

FIGURE 5 | PAK2 upregulation notably counteracted RP11-499E18.1 overexpression-triggered tumor-suppressing effects. The plasmids pcDNA3.1, pcDNA-RP11-499E18.1, and pcDNA-RP11-499E18.1 + pcDNA-PAK2 were respectively transfected into CaOV3 and SKOV3 cells. **(A)** RP11-499E18.1 was successfully overexpressed in CaOV3 and SKOV3 cells. **(B,C)** PAK2 was successfully overexpressed in CaOV3 and SKOV3 cells. **(D–G)** PAK2 overexpression distinctly counteracted RP11-499E18.1 overexpression-triggered suppressing effects on the proliferation, colony formation, and migration of CaOV3 and SKOV3 cells. PAK2, P21 (RAC1) activated kinase 2. $^{###}p < 0.001$, ns, no significance.

was successfully knocked down or overexpressed after cell transfection (**Figures 4A,B** and **Supplementary Figure 1**, $p < 0.01$ or $p < 0.001$), and the knockdown efficiency was especially high when cells were transfected with si-RP11-454-476. Afterward, the expression of PAK2 was detected, and outcomes demonstrated that overexpression or knockdown of RP11-499E18.1 had no significant influence on the expression of PAK2 on both mRNA and protein levels (**Figures 4C,D**). Thereafter, cell proliferation, migration, and colony formation, as well as the expression of EMT transformation-related factors (E-cadherin and Vimentin) were tested in the transfected cells. Outcomes demonstrated that overexpression of RP11-499E18.1 obviously suppressed the proliferation, migration, and colony formation of both CaOV3 and SKOV3 cells (**Figures 4E–H**, $p < 0.01$ or $p < 0.001$). Besides, the expression of EMT transformation-related E-cadherin was notably augmented, while the expression of Vimentin was obviously decreased by RP11-499E18.1 overexpression in both CaOV3 and SKOV3 cells (**Figure 4I**). However, RP11-499E18.1 knockdown exerted the opposite effects as RP11-499E18.1 overexpression is performed (**Figures 4E–I**).

PAK2 Upregulation Notably Counteracted RP11-499E18.1 Overexpression-Triggered Tumor-Suppressing Effects

Previous RNA pulldown assay verified that there was an interaction between RP11-49E18.1 and PAK2. Based on this result, we speculated that RP11-49E18.1 might perform its tumor-suppressive roles through interacting with PAK2. Therefore, we respectively co-overexpressed RP11-49E18.1 and PAK2 in CaOV3, SKOV3, and OVCAR3 cells. Results displayed that co-transfection with pcDNA-RP11-49E18.1 and pcDNA-PAK2 had no significant influence on the expression of RP11-49E18.1 (**Figure 5A** and **Supplementary Figure 2**), while it had distinctly increased the expression of PAK2 compared with pcDNA-RP11-49E18.1 transfected cells (**Figures 5B,C**,

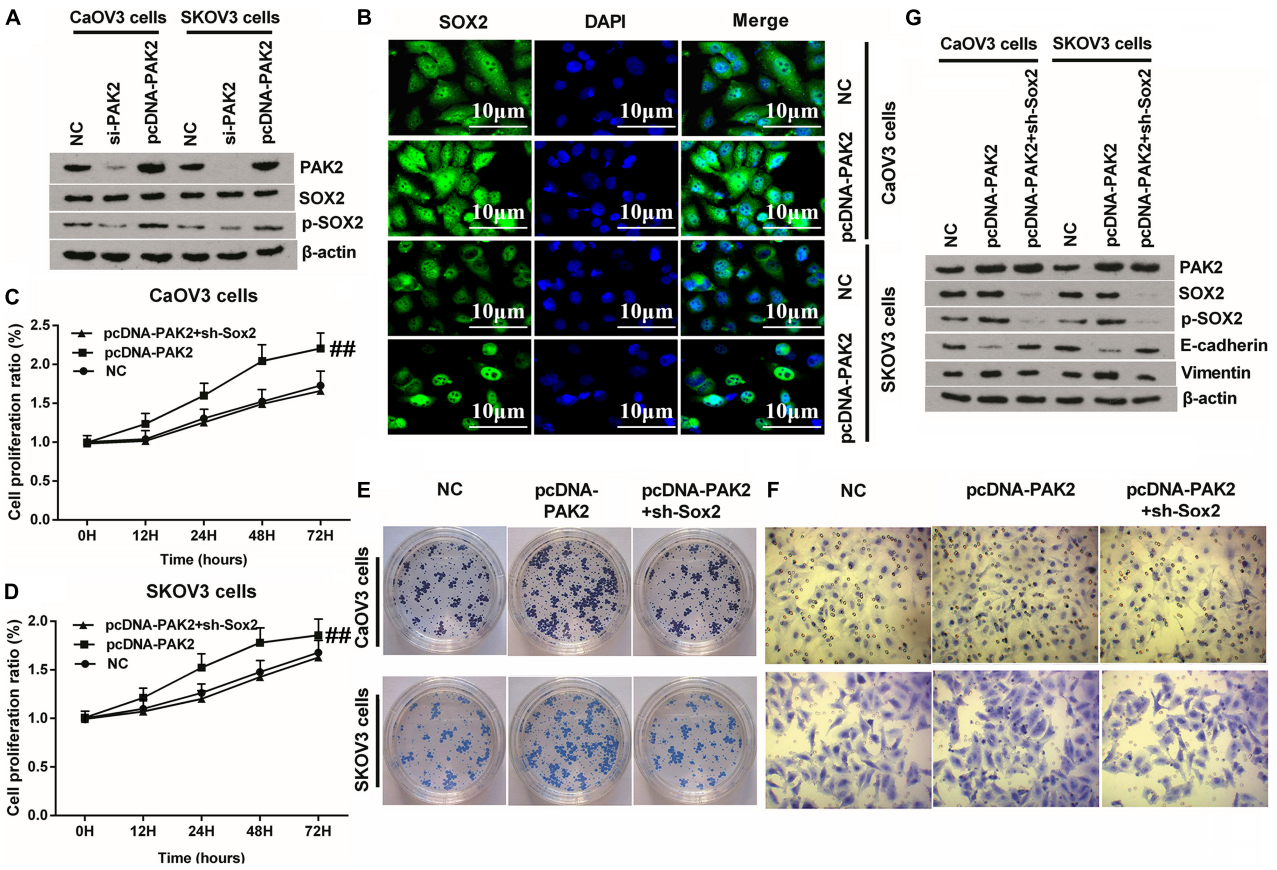

FIGURE 6 | Knockdown of SOX2 notably reversed PAK2 overexpression-triggered tumor-promoting effects. **(A)** PAK2 overexpression notably have no notable influence on the expression of SOX2, but obviously increased the expression of p-SOX2. **(B)** PAK2 overexpression promoted the nuclear translocation of SOX2. **(C–F)** Knockdown of SOX2 obviously reversed PAK2 overexpression-induced augmenting effects on the proliferation, colony formation, and migration of CaOV3 and SKOV3 cells. **(G)** PAK2 overexpression obviously decreased the expression of EMT-associated E-cadherin, and increased the expression of Vimentin. Knockdown of SOX2 notably counteracted PAK2 overexpression-induced effects. PAK2, P21 (RAC1) activated kinase 2; SOX2, SRY-box transcription factor 2; EMT, epithelial–mesenchymal transition. $^{\#\#}p < 0.01$.

both $p < 0.01$). Following experiments further verified that co-overexpression of RP11-49E18.1 and PAK2 notably counteracted RP11-499E18.1 overexpression-triggered suppressing effects on the proliferation, migration, and colony formation of CaOV3 and SKOV3 cells (**Figures 5D–G**, $p < 0.01$ or $p < 0.001$). These outcomes indicated that PAK2 might perform a tumor-promoting efficacy in OC, which is consistent with the prognosis analysis results.

Knockdown of SOX2 Notably Reversed PAK2 Overexpression-Triggered Tumor-Promoting Effects

Considering that PAK2 is a member of the serine/threonine kinases family, bioinformatic analysis revealed that there were two pathways related to protein phosphorylation. Besides, previous investigation verified that the phosphorylated SOX2 could be transferred into the nucleus and promote gene transcription (Ravindran Menon et al., 2018; Wang Z. et al., 2019). Therefore, we detected the expression of p-SOX2 in OC cells. Western blot results displayed that there was no obvious change between the expression of SOX2 in both PAK2 knockdown or overexpressed cells. However, p-SOX2 expression was distinctly decreased by PAK2 knockdown, while notably upregulated by PAK2 overexpression (**Figure 6A** and **Supplementary Figure 3**). Therefore, we deduced that PAK2 overexpression might have promoted the nuclear translocation of SOX2, and this speculation was subsequently testified by the IF assay results (**Figure 6B**). Afterward, NC, pcDNA-PAK2, and pcDNA-PAK2 plus sh-SOX2 transfection was respectively conducted in CaOV3 and SKOV3 cells to explore the underlying regulating mechanism. Detection of cell phenotype confirmed that PAK2 overexpression obviously promoted the proliferation, migration, and colony formation of CaOV3 and SKOV3 cells (**Figures 6C–F**, $p < 0.01$ or $p < 0.001$). Besides, the expression of p-SOX2 and EMT-related Vimentin was both notably augmented, while E-cadherin expression was significantly reduced by PAK2 overexpression. Meanwhile, no significant change of SOX2 expression was observed (**Figure 6G**). More importantly, these tumor-promoting effects triggered by PAK2 overexpression were distinctly reversed by SOX2 knockdown (**Figures 6C–G**). Combination

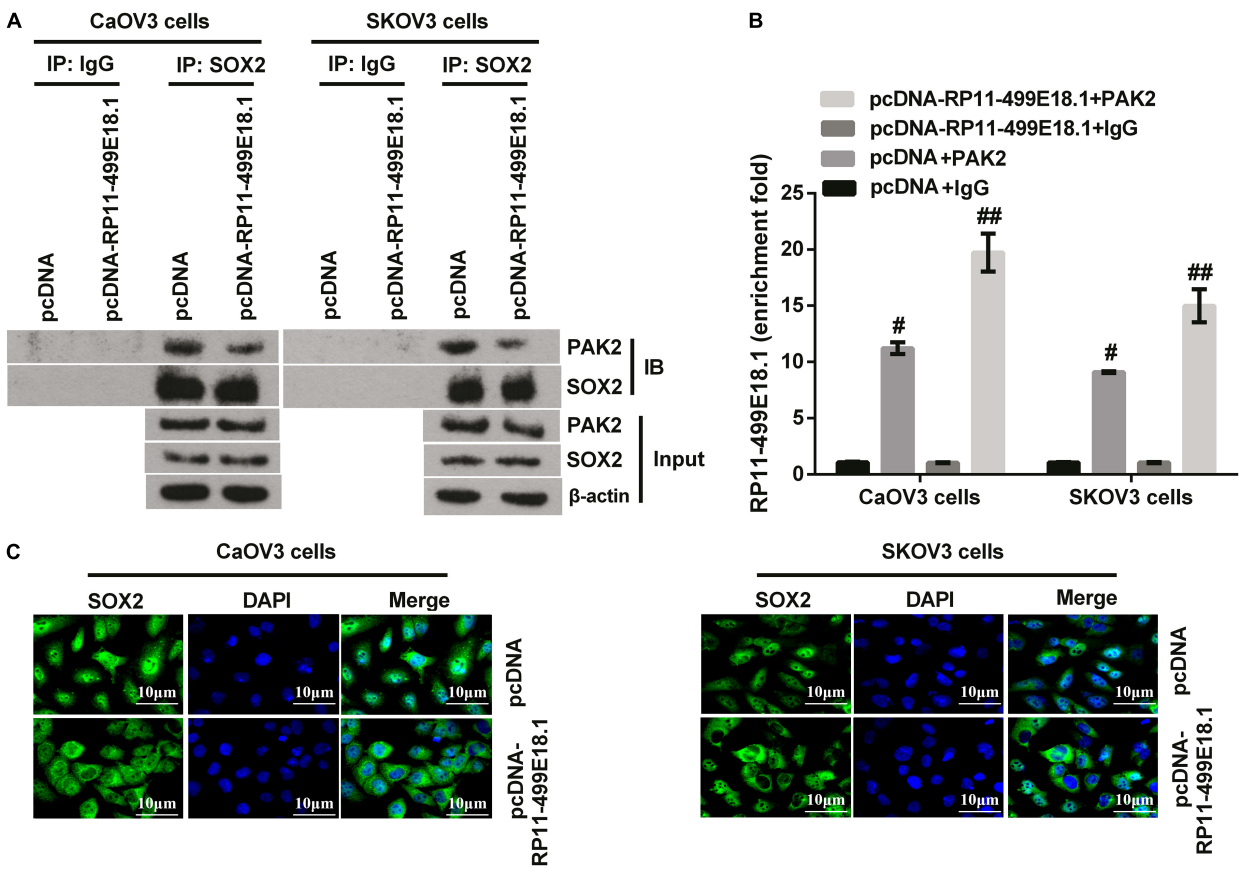

FIGURE 7 | RP11-499E18.1 overexpression reduced the interaction between PAK2 and SOX2, and increased the binding of RP11-499E18.1 by PAK2. **(A)** Co-IP assay confirmed that RP11-499E18.1 overexpression remarkably reduced the interaction between PAK2 and SOX2. **(B)** RIP assay affirmed that RP11-499E18.1 overexpression notably increased the binding of RP11-499E18.1 by PAK2. **(C)** Overexpression of RP11-499E18.1 remarkably decreased the nuclear translocation of SOX2 in CaOV3 and SKOV3 cells. Co-IP, co-immunoprecipitation; RIP, RNA immunoprecipitation; PAK2, P21 (RAC1) activated kinase 2; SOX2, SRY-box transcription factor 2. $^{\#}p < 0.05$, $^{\#\#}p < 0.01$.

of these results indicated that PAK2 overexpression might perform its tumor-promoting efficacy through increasing the phosphorylation of SOX2.

RP11-499E18.1 Overexpression Reduced the Interaction Between PAK2 and SOX2 and Increased the Binding of RP11-499E18.1 by PAK2

For further disclosing the regulating mechanism among RP11-499E18.1, PAK2, and SOX2, co-IP and RIP assay were performed in RP11-499E18.1-overexpressing cells. Results of co-IP assay revealed that RP11-499E18.1 overexpression markedly reduced the interaction between PAK2 and SOX2 compared with the NC group (**Figure 7A**). Besides, outcomes of RIP assay disclosed that RP11-499E18.1 overexpression distinctly increased the binding of RP11-499E18.1 by PAK2 (**Figure 7B**, $p < 0.05$ or $p < 0.01$). In addition, detection of the location of SOX2 in RP11-499E18.1-overexpressed CaOV3 and SKOV3 cells was carried out. Outcomes displayed that RP11-499E18.1 overexpression obviously reduced the nuclear translocation of SOX2, and SOX2 is more localized in the cytoplasm compared with pcDNA transfected cells (**Figure 7C**). These outcomes manifested that RP11-499E18.1 overexpression might carry out its tumor-suppressing efficacy through decreasing the interaction between PAK2 and SOX2, and thereby lessen the nuclear translocation of SOX2.

PAK2 Upregulation Reversed RP11-499E18.1 Overexpression-Induced Facilitating Effects on Tumor Formation

To verify the effect of RP11-499E18.1 and PAK2 overexpression on tumor development, we implanted pcDNA-RP11-499E18.1 or pcDNA-RP11-499E18.1 plus pcDNA-PAK2 transfected CaOV3 cells into the nude mice. Tumor volume measurement results demonstrated that RP11-499E18.1 overexpression distinctly inhibited tumor development of CaOV3 cells as time prolongs, while PAK2 upregulation notably reversed this effect (**Figure 8A**, both $p < 0.001$). These effects could be obviously observed from the final tumor volume formatted in nude mice (**Figure 8B**). In addition, expression of proliferation-related Ki67 and apoptosis-associated Caspase 3 was determined employing IHC assay. Outcomes showed

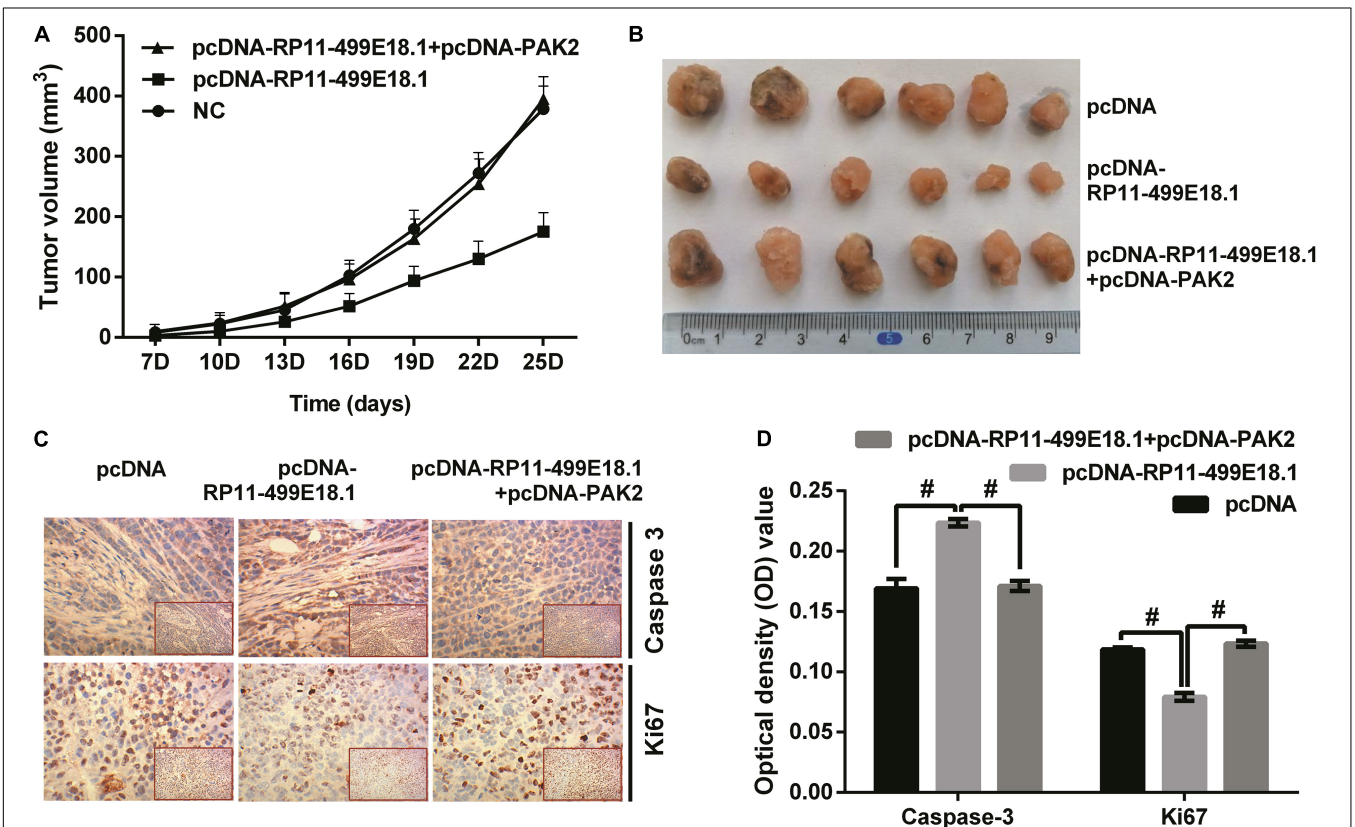

FIGURE 8 | PAK2 upregulation reversed RP11-499E18.1 overexpression-induced facilitating effects on tumor formation. The plasmids pcDNA3.1, pcDNA-RP11-499E18.1, and pcDNA-RP11-499E18.1 + pcDNA-PAK2 were respectively, transfected into CaOV3 cells. Then, the transfected cells were respectively inoculated at the right dorsal proximal upper limbs of nude mice. **(A,B)** RP11-499E18.1 overexpression remarkably inhibited tumor growth as time prolongs, while PAK2 upregulation notably reversed this effect. **(C,D)** RP11-499E18.1 overexpression remarkably increased the expression of apoptosis-related Caspase 3, while notably decreased the expression of proliferation-associated Ki67. These effects were notably counteracted by PAK2 upregulation. PAK2, P21 (RAC1) activated kinase 2. $^{\#}p < 0.05$.

that the expression of Ki67 was notably reduced, while Caspase 3 expression was remarkably augmented by RP11-499E18.1 overexpression compared with the pcDNA transfected group. Whereas PAK2 upregulation remarkably decreased Caspase 3 expression, it notably increased Ki67 expression compared to the pcDNA-RP11-499E18.1 plus pcDNA-PAK2 transfected group (**Figures 8C,D**, all $p < 0.05$). These results further validated the tumor volume outcomes, indicating that RP11-499E18.1 overexpression might carry out its tumor-suppressing effects by increasing the expression of apoptosis-related gene expression and decreasing the expression of proliferation-associated gene expression.

DISCUSSION

Ovarian cancer is a deadly gynecological malignancy in the world. In recent years, a number of former investigations have discovered the participation of lncRNAs in the regulation of OC progression with the help of bioinformatic analysis (Wu et al., 2017; Li et al., 2018). In this research, we identified lncRNA RP11-499E18.1, which was downregulated in OC tissues, as a potential biomarker of OC *via* GEO database screening and prognostic analysis. Then, GEO database analysis combined with GO term analysis discovered that PAK2 might be the critical mRNA that participated in the regulation of RP11-499E18.1, while literature analysis found that SOX2 could be the target protein of PAK2. After that, experimental analysis verified that there was an interaction between RP11-499E18.1 and PAK2, as well as PAK2 and SOX2. Therefore, we speculated that RP11-499E18.1 might play its tumor suppressor roles in OC *via* regulation of the RP11-499E18.1–PAK2–SOX2 axis.

Obviously, we discovered that RP11-499E18.1 functions as a tumor suppressor in OC exhibiting as RP11-499E18.1 overexpression, which notably suppressed the proliferation, migration, and EMT process of OC cells. These outcomes were consistent with former researches. For instance, it was demonstrated that overexpression of Titin-antisense RNA1 (TTN-AS1) repressed colony formation and proliferation, while facilitating apoptosis of OC cells (Miao et al., 2020). Besides, Ma et al. (2018) reported that decreased expression of growth arrest-specific transcript 5 (GAS5) was correlated with advanced clinical stage, and overexpression of GAS5 obviously suppressed the proliferation of OC cells. Moreover, Tao et al. (2020) clarified that maternally expressed 3 gene (MEG3) overexpression notably promoted apoptosis, while restraining the viability and invasion of OC cells.

LncRNAs have been widely proved to be the controller of their downstream targets in OC (Liang et al., 2018; Chen X. et al., 2019; Sun et al., 2019; Yang et al., 2019). For example, Kong et al. (2019) clarified that lncRNA PCAT6 facilitated the initiation and development of OC through repressing the expression of PTEN. Another research demonstrated that lncRNA LINC00702 accelerated the development of OC by interacting with EZH2 and thereby repressing the transcription of KLF2 (Wang L. et al., 2019). Herein, this research identified PAK2 as a target of RP11-499E18.1 and proved that there was an interaction between RP11-499E18.1 and PAK2. Besides, PAK2 upregulation partially reversed RP11-499E18.1 overexpression-triggered tumor-suppressing effects on OC cells. However, RP11-499E18.1 overexpression did not alter the expression of PAK2, so we deduced that RP11-499E18.1 might function in OC through affecting the interaction between PAK2 and its target and thereby influencing the downstream gene transcription.

Considering that PAK2 is a member of the serine/threonine kinases family, this study subsequently focused on the target effect of PAK2 kinase and further searched for the potential PAK2 kinase target proteins. Former investigations pointed out that SOX2 was an interacting protein of PAK2 (Huttlin et al., 2015, 2017). Besides, SOX2 was reported to be associated with early tumor initiation (Robinson et al., 2021), and its level in high-grade serous carcinoma (HGSC) effusions was demonstrated to be markers of clinically aggressive disease (Sherman-Samis et al., 2019). Additionally, SOX2 expression was found to be positively correlated with the proliferation and migration capacities of tumor cells (Chen B. et al., 2019; Meng et al., 2020), and its high expression is a poor prognostic marker for OC. Furthermore, it was clarified that the interaction between SOX2 and UBR5 was inhibited after phosphorylation of SOX2, and thereby stabilized SOX2 in esophageal cancer (Wang Z. et al., 2019). Moreover, CDK1 knockdown decreased the phosphorylation, transcription activity, and nuclear distribution of SOX2, while knockout of SOX2 significantly reduced CDK1 overexpression-induced tumor-initiating capacity (Ravindran Menon et al., 2018). Based on these evidences, we speculated that PAK2 upregulation might perform its tumor-promoting

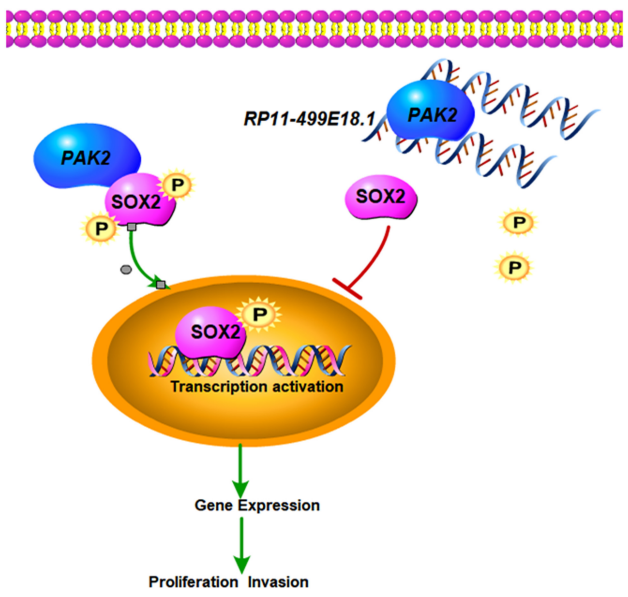

FIGURE 9 | The putative regulation network of this study. Upregulated RP11-499E18.1 inhibits the proliferation, migration, colony formation, and EMT process of OC cells through dissociating the interaction between PAK2 and SOX2 and reducing the nuclear translocation of p-SOX2.

efficacy through increasing the phosphorylation and nuclear distribution of SOX2 in OC cells. Following results confirmed this speculation. Additionally, knockdown of SOX2 notably counteracted PAK2 upregulation-induced tumor-promoting effects on cell proliferation, migration, and expression of EMT-related factors.

Previous investigation demonstrated that the core of personalized medicine for cancer lies in the discovery and development of biomarkers, which reveal information that leads to the diagnosis, prognosis, and therapy of the disease (Dlamini et al., 2021). Besides, a previous research pointed out that uncertainty of prognosis is the main reason that patients with hematologic malignancies receive aggressive therapy near end of life (Iizuka-Honma et al., 2021). In OC, patients are generally diagnosed at an advanced stage primarily because there are few early symptoms and limited screening approaches. Therefore, we hold the opinion that identification of novel effective diagnostic biomarkers, like RP11-499E18.1, will be of great significance for better management of OC in the future.

CONCLUSION

Our results demonstrated that RP11-499E18.1 overexpression might have inhibited proliferation, migration, colony formation, and EMT process of OC cells through dissociating the interaction between PAK2 and SOX2 and reducing the nuclear translocation of p-SOX2. This research mainly explored the potential regulating mechanisms of RP11-499E18.1 on OC progression *in vitro*, but whether it functions through the same pattern *in vivo* still needs further investigation. The putative regulation network is displayed in **Figure 9**.

DATA AVAILABILITY STATEMENT

The original contributions presented in the study are included in the article/**Supplementary Material**, further inquiries can be directed to the corresponding authors.

ETHICS STATEMENT

The studies involving human participants were reviewed and approved by Ethics Committee of Medical ethics committee of Hunan Cancer Hospital. The patients/participants provided their written informed consent to participate in this study. The animal study was reviewed and approved by Medical ethics committee of Hunan Cancer Hospital. Written informed consent was obtained from the owners for the participation of their animals in this study.

AUTHOR CONTRIBUTIONS

JY and SP conceived and designed the study. JY, KZ, and SP performed the experiments and interpreted the data. JY collected the data. KZ and SP analyzed the data and wrote the manuscript. All authors reviewed the results and approved the final version of the manuscript.

SUPPLEMENTARY MATERIAL

The Supplementary Material for this article can be found online at: https://www.frontiersin.org/articles/10.3389/fcell.2021.697831/full#supplementary-material

REFERENCES

Allemani, C., Matsuda, T., Di Carlo, V., Harewood, R., Matz, M., Nikšić, M., et al. (2018). Global surveillance of trends in cancer survival 2000–14 (CONCORD-3): analysis of individual records for 37 513 025 patients diagnosed with one of 18 cancers from 322 population-based registries in 71 countries. *Lancet* 391, 1023–1075.

Arnes, L., Liu, Z., Wang, J., Maurer, C., Sagalovskiy, I., Sanchez-Martin, M., et al. (2019). Comprehensive characterisation of compartment-specific long non-coding RNAs associated with pancreatic ductal adenocarcinoma. *Gut* 68, 499–511. doi: 10.1136/gutjnl-2017-314353

Au, K. K., Josahkian, J. A., Francis, J. A., Squire, J. A., and Koti, M. (2015). Current state of biomarkers in ovarian cancer prognosis. *Future Oncol.* 11, 3187–3195. doi: 10.2217/fon.15.251

Bill, M., Papaioannou, D., Karunasiri, M., Kohlschmidt, J., Pepe, F., Walker, C. J., et al. (2019). Expression and functional relevance of long non-coding RNAs in acute myeloid leukemia stem cells. *Leukemia* 33, 2169–2182. doi: 10.1038/s41375-019-0429-5

Chen, B., Zhu, Z., Li, L., Ye, W., Zeng, J., Gao, J., et al. (2019). Effect of overexpression of Oct4 and Sox2 genes on the biological and oncological characteristics of gastric cancer cells. *Onco Targets Ther.* 12, 4667–4682. doi: 10.2147/ott.s209734

Chen, J., Cai, Y., Zhou, J., and Mei, J. (2020). Identification of four hub genes as promising biomarkers to evaluate the prognosis of ovarian cancer in silico. *Cancer Cell Int.* 20, 1–11.

Chen, X., Wu, W., Cao, X., Zhao, X., Li, W., Deng, C., et al. (2019). lncRNA mortal obligate RNA transcript was downregulated in ovarian carcinoma and inhibits cancer cell proliferation by downregulating miRNA-21. *J. Cell. Biochem.* 120, 11949–11954. doi: 10.1002/jcb.28478

Cress, R. D., Chen, Y. S., Morris, C. R., Petersen, M., and Leiserowitz, G. S. (2015). Characteristics of long-term survivors of epithelial ovarian cancer. *Obstetr. Gynecol.* 126:491. doi: 10.1097/aog.0000000000000981

Dlamini, Z., Mbele, M., Makhafola, T. J., Hull, R., and Marima, R. (2021). HIV-Associated Cancer Biomarkers: A Requirement for Early Diagnosis. *Int. J. Mol. Sci.* 22:8127. doi: 10.3390/ijms22158127

Gutschner, T., and Diederichs, S. (2012). The hallmarks of cancer: a long non-coding RNA point of view. *RNA Biol.* 9, 703–719. doi: 10.4161/rna.20481

Hao, T., Huang, S., and Han, F. (2020). LINC-PINT suppresses tumour cell proliferation, migration and invasion through targeting miR-374a-5p in ovarian cancer. *Cell Biochem. Funct.* 38, 1089–1099. doi: 10.1002/cbf.3565

Hosono, Y., Niknafs, Y. S., Prensner, J. R., Iyer, M. K., Dhanasekaran, S. M., Mehra, R., et al. (2017). Oncogenic Role of THOR, a Conserved Cancer/Testis Long Non-coding RNA. *Cell* 171, 1559.e–1572.e.

Huarte, M. (2015). The emerging role of lncRNAs in cancer. *Nat. Med.* 21, 1253–1261. doi: 10.1038/nm.3981

Huttlin, E. L., Bruckner, R. J., Paulo, J. A., Cannon, J. R., Ting, L., Baltier, K., et al. (2017). Architecture of the human interactome defines protein communities and disease networks. *Nature* 545, 505–509. doi: 10.1038/nature22366

Huttlin, E. L., Ting, L., Bruckner, R. J., Gebreab, F., Gygi, M. P., Szpyt, J., et al. (2015). The BioPlex network: a systematic exploration of the human interactome. *Cell* 162, 425–440. doi: 10.1016/j.cell.2015.06.043

Iizuka-Honma, H., Mitsumori, T., Yoshikawa, S., Takizawa, H., and Noguchi, M. (2021). Prognostic Value of Palliative Prognostic Index for Hospitalized Patients

With End-of-Life Hematologic Malignancies in a Japanese University Hospital. *JCO Oncol. Pract.* 2021:O2100243.

Kong, F. R., Lv, Y. H., Yao, H. M., Zhang, H. Y., Zhou, Y., and Liu, S. E. (2019). LncRNA PCAT6 promotes occurrence and development of ovarian cancer by inhibiting PTEN. *Eur. Rev. Med. Pharmacol. Sci.* 23, 8230–8238.

Kossaï, M., Leary, A., Scoazec, J. Y., and Genestie, C. (2018). Ovarian cancer: a heterogeneous disease. *Pathobiology* 85, 41–49.

Li, N., Zhan, X., and Zhan, X. (2018). The lncRNA SNHG3 regulates energy metabolism of ovarian cancer by an analysis of mitochondrial proteomes. *Gynecol. Oncol.* 150, 343–354. doi: 10.1016/j.ygyno.2018.06.013

Liang, H., Yu, T., Han, Y., Jiang, H., Wang, C., You, T., et al. (2018). LncRNA PTAR promotes EMT and invasion-metastasis in serous ovarian cancer by competitively binding miR-101-3p to regulate ZEB1 expression. *Mol. Cancer* 17, 1–13.

Livak, K. J., and Schmittgen, T. D. (2001). Analysis of relative gene expression data using real-time quantitative PCR and the 2- ΔΔCT method. *Methods* 25, 402–408. doi: 10.1006/meth.2001.1262

Ma, N., Li, S., Zhang, Q., Wang, H., Qin, H., and Wang, S. (2018). Long non-coding RNA GAS5 inhibits ovarian cancer cell proliferation via the control of microRNA-21 and SPRY2 expression. *Exp. Therapeut. Med.* 16, 73–82.

Meng, Y., Xu, Q., Chen, L., Wang, L., and Hu, X. (2020). The function of SOX2 in breast cancer and relevant signaling pathway. *Pathol. Res. Pract.* 216:153023. doi: 10.1016/j.prp.2020.153023

Menon, U., Karpinskyj, C., and Gentry-Maharaj, A. (2018). Ovarian cancer prevention and screening. *Obstetr. Gynecol.* 131, 909–927.

Miao, S., Wang, J., Xuan, L., Liu, X., and LncRNA, T. T. N. (2020). AS1 acts as sponge for miR-15b-5p to regulate FBXW7 expression in ovarian cancer. *BioFactors* 46, 600–607. doi: 10.1002/biof.1622

Nagano, T., and Fraser, P. (2011). No-nonsense functions for long noncoding RNAs. *Cell* 145, 178–181. doi: 10.1016/j.cell.2011.03.014

Ravindran Menon, D., Luo, Y., Arcaroli, J. J., Liu, S., KrishnanKutty, L. N., Osborne, D. G., et al. (2018). CDK1 interacts with Sox2 and promotes tumor initiation in human melanoma. *Cancer Res.* 78, 6561–6574. doi: 10.1158/0008-5472.can-18-0330

Robinson, M., Gilbert, S. F., Waters, J. A., Lujano-Olazaba, O., Lara, J., Alexander, L. J., et al. (2021). Characterization of SOX2, OCT4 and NANOG in Ovarian Cancer Tumor-Initiating Cells. *Cancers* 13:262. doi: 10.3390/cancers13020262

Schmitt, A. M., and Chang, H. Y. (2016). Long Noncoding RNAs in Cancer Pathways. *Cancer Cell* 29, 452–463. doi: 10.1016/j.ccell.2016.03.010

Sherman-Samis, M., Onallah, H., Holth, A., Reich, R., and Davidson, B. (2019). SOX2 and SOX9 are markers of clinically aggressive disease in metastatic high-grade serous carcinoma. *Gynecol. Oncol.* 153, 651–660. doi: 10.1016/j.ygyno.2019.03.099

Sun, Q., Li, Q., and Xie, F. (2019). LncRNA-MALAT1 regulates proliferation and apoptosis of ovarian cancer cells by targeting miR-503-5p. *OncoTargets Therapy* 12:6297. doi: 10.2147/ott.s214689

Sundar, S., Neal, R. D., and Kehoe, S. (2015). Diagnosis of ovarian cancer. *BMJ* 2015:351.

Tang, X. J., Wang, W., and Hann, S. S. (2019). Interactions among lncRNAs, miRNAs and mRNA in colorectal cancer. *Biochimie* 163, 58–72. doi: 10.1016/j.biochi.2019.05.010

Tao, P., Yang, B., Zhang, H., Sun, L., Wang, Y., and Zheng, W. (2020). The overexpression of lncRNA MEG3 inhibits cell viability and invasion and promotes apoptosis in ovarian cancer by sponging miR-205-5p. *Int. J. Clin. Exp. Pathol.* 13:869.

Wang, L., Ye, T. Y., Wu, H., Chen, S. Y., Weng, J. R., and Xi, X. W. (2019). LINC00702 accelerates the progression of ovarian cancer through interacting with EZH2 to inhibit the transcription of KLF2. *Eur. Rev. Med. Pharmacol. Sci.* 23(3 Suppl.), 201–208.

Wang, Y., Zhang, M., and Zhou, F. (2020). Biological functions and clinical applications of exosomal long non-coding RNAs in cancer. *J. Cell Mol. Med.* 24, 11656–11666. doi: 10.1111/jcmm.15873

Wang, Z., Kang, L., Zhang, H., Huang, Y., Fang, L., Li, M., et al. (2019). AKT drives SOX2 overexpression and cancer cell stemness in esophageal cancer by protecting SOX2 from UBR5-mediated degradation. *Oncogene* 38, 5250–5264. doi: 10.1038/s41388-019-0790-x

Wu, D. D., Chen, X., Sun, K. X., Wang, L. L., Chen, S., and Zhao, Y. (2017). Role of the lncRNA ABHD11-AS(1) in the tumorigenesis and progression of epithelial ovarian cancer through targeted regulation of RhoC. *Mol. Cancer* 16:138.

Xu, C., Zhu, L. X., Sun, D. M., Yao, H., and Han, D. X. (2020). Regulatory mechanism of lncRNA NORAD on proliferation and invasion of ovarian cancer cells through miR-199a-3p. *Eur. Rev. Med. Pharmacol. Sci.* 24, 1672–1681.

Yang, M., Zhai, Z., Guo, S., Li, X., Zhu, Y., and Wang, Y. (2019). Long non-coding RNA FLJ33360 participates in ovarian cancer progression by sponging miR-30b-3p. *OncoTargets Therapy* 12:4469. doi: 10.2147/ott.s205622

Zhang, Y. B., Jiang, Y., Wang, J., Ma, J., and Han, S. (2019). Evaluation of core serous epithelial ovarian cancer genes as potential prognostic markers and indicators of the underlying molecular mechanisms using an integrated bioinformatics analysis. *Oncol. Lett.* 18, 5508–5522.

Conflict of Interest: The authors declare that the research was conducted in the absence of any commercial or financial relationships that could be construed as a potential conflict of interest.

Publisher's Note: All claims expressed in this article are solely those of the authors and do not necessarily represent those of their affiliated organizations, or those of the publisher, the editors and the reviewers. Any product that may be evaluated in this article, or claim that may be made by its manufacturer, is not guaranteed or endorsed by the publisher.

Copyright © 2021 Yang, Peng and Zhang. This is an open-access article distributed under the terms of the Creative Commons Attribution License (CC BY). The use, distribution or reproduction in other forums is permitted, provided the original author(s) and the copyright owner(s) are credited and that the original publication in this journal is cited, in accordance with accepted academic practice. No use, distribution or reproduction is permitted which does not comply with these terms.

frontiers in Oncology

REVIEW
published: 27 October 2021
doi: 10.3389/fonc.2021.775349

Syndecans and Their Synstatins: Targeting an Organizer of Receptor Tyrosine Kinase Signaling at the Cell-Matrix Interface

Alan C. Rapraeger *

Department of Human Oncology, School of Medicine and Public Health, University of Wisconsin-Madison, Madison, WI, United States

Receptor tyrosine kinases (RTKs) and integrin matrix receptors have well-established roles in tumor cell proliferation, invasion and survival, often functioning in a coordinated fashion at sites of cell-matrix adhesion. Central to this coordination are syndecans, another class of matrix receptor, that organize RTKs and integrins into functional units, relying on docking motifs in the syndecan extracellular domains to capture and localize RTKs (e.g., EGFR, IGF-1R, VEGFR2, HER2) and integrins (e.g., αvβ3, αvβ5, α4β1, α3β1, α6β4) to sites of adhesion. Peptide mimetics of the docking motifs in the syndecans, called "synstatins", prevent assembly of these receptor complexes, block their signaling activities and are highly effective against tumor cell invasion and survival and angiogenesis. This review describes our current understanding of these four syndecan-coupled mechanisms and their inhibitory synstatins ($SSTN_{IGF1R}$, $SSTN_{VEGFR2}$, $SSTN_{VLA-4}$, $SSTN_{EGFR}$ and $SSTN_{HER2}$).

Keywords: EGFR, IGF-1R, CXCR4, VEGFR2, synstatin, integrin signaling, ASK-1

OPEN ACCESS

Edited by:
Nikos Karamanos, University of Patras, Greece

Reviewed by:
Nikolaos A. Afratis, Weizmann Institute of Science, Israel
Mauro Sergio Pavao, Federal University of Rio de Janeiro, Brazil

***Correspondence:**
Alan C. Rapraeger
rapraeger@humonc.wisc.edu

Specialty section:
This article was submitted to Molecular and Cellular Oncology, a section of the journal Frontiers in Oncology

Received: *13 September 2021*
Accepted: *27 September 2021*
Published: *27 October 2021*

Citation:
Rapraeger AC (2021) Syndecans and Their Synstatins: Targeting an Organizer of Receptor Tyrosine Kinase Signaling at the Cell-Matrix Interface. Front. Oncol. 11:775349. doi: 10.3389/fonc.2021.775349

INTRODUCTION

The growth and progression of tumors is influenced by the tumor microenvironment, including growth factors, cytokines, and components of the extracellular matrix produced by the tumor stroma and the tumors themselves. Receptors on the surface of the tumor cells, of which growth factor receptor tyrosine kinases (RTKs) and integrins are prominent, mediate the response of the tumor to these factors, including enhanced proliferation, survival, metastasis, and resistance to therapeutic drugs. Effective RTK signaling often requires coordination with integrins and RTK activation in turn serves to potentiate integrin signaling (1–4). Integrins are cell-cell and cell-matrix receptors composed of α and β subunits that assemble into 22 distinct receptors with individual signaling and ligand specificity. Their activation is promoted by signaling from inside the cell (e.g., inside-out signaling), often from RTKs, leading to stable adhesion. In addition, they respond to ligands in the tumor microenvironment to activate signaling (outside-in signaling) through cytoplasmic effectors such as FAK, paxillin, Src kinases, and others, often coordinated with RTK signaling (1). It is well established, for example, that integrin-mediated matrix adhesion is required for growth factor-stimulated cell cycle progression [reviewed in (5, 6)]. This extends to the tumor

microenvironment as well, where RTKs and integrins function on endothelial cells, stromal cells and immune cells participating in vascular angiogenesis, lymphangiogenesis, and inflammation in support of tumor growth (7). A number of examples have now emerged to suggest that this coordinated signaling requires the RTK and integrin to be assembled into a functional unit [see (8, 9)]. A well-described example involves the α6β4 integrin. Usually found in resting epithelia and endothelia as the central adhesion receptor in highly stable hemidesmosomes, the α6β4 integrin is converted to a signaling scaffold during wound healing or tumorigenesis when phosphorylated by serine-threonine kinases activated downstream of RTKs (10). The free integrin associates with RTKs (e.g., EGFR, HER2, c-Met, Ron kinase), resulting in phosphorylation of tyrosines in the β4 integrin cytoplasmic domain and activation of signaling effectors that drive proliferation, survival and invasion of the tumor cells (11–15). Another example is the interdependence of the αvβ3 integrin and VEGFR2, an example in which upregulated expression and activation of the αvβ3 integrin is observed on endothelial cells in response to the induction of angiogenesis by VEGF (16–18). When activated, these two receptors co-immunoprecipitate as a functional complex from the endothelial cells, and loss or prevention of activation of either receptor negatively impacts the activation of the other (16–18). The αvβ3 integrin also engages in coordinated signaling with the type 1 insulin-like growth factor receptor (IGF-1R) in smooth muscle cells where IGF-1R is recruited to active αvβ3 integrin, which attenuates the IGF-1R signal *via* SHP2 phosphatase localized to the integrin (19, 20). Despite these and other examples, however, the means by which the RTKs and integrins interact and whether or not these interactions are regulated, often remains unknown. Work over the past decade has identified the syndecans as potential organizers of these signaling units. This review will summarize several examples in which docking sites in the extracellular domains of syndecans serve to organize and regulate the signaling of RTKs and integrins.

AN ORGANIZER ROLE FOR SYNDECANS

The syndecans are a family of four cell surface heparan sulfate (HS) proteoglycans, united by their highly homologous transmembrane and cytoplasmic domains, and their display of 2-3 HS glycosaminoglycan chains at the distal tips of their extracellular domains. These conserved features have attracted the attention of investigators attempting to understand syndecan functions [see reviews (21–30)]. In brief, the HS chains endow the syndecans with modulatory roles in numerous processes by engaging "heparin binding domains" in a variety of ligands, including growth factors (FGFs, VEGFs, PDGFs, HGF, EGFs, etc.), proteases and protease inhibitors, and essentially all extracellular matrix (ECM) ligands. Conserved alanine and glycine repeats interrupt their bulky hydrophobic membrane-spanning domains to promote syndecan homo- and heterodimerization, suggesting potential interactions with other membrane receptors as well. Exactly conserved C1 and C2 motifs found in their cytoplasmic domains bind to FERM- and PDZ-domain proteins and work in conjunction with syndecan-type-specific variable (V) domains to promote cytoplasmic activities; these range from chaperoning integrins and other receptors during endocytic and intracellular trafficking to signaling within focal adhesions. Less attention, however, has focused on their extracellular protein domains, which, apart from the conserved motifs that encode HS attachment, share little or no homology across the syndecan family. Emerging work now shows that these domains may be key to a central syndecan function, namely, acting as a "signaling organizer" at the cell surface by providing docking sites for other plasma membrane receptors, especially integrins and RTKs with well-known roles in cancer, that are highly dependent on the syndecan for their activation and signaling.

COUPLING OF IGF-1R TO THE αvβ3 OR αvβ5 INTEGRIN

The αvβ3 and αvβ5 integrins have been shown in now classical studies from the Cheresh group to play essential roles in vascular angiogenesis stimulated by fibroblast growth factor-2 (FGF-2) and vascular endothelial growth factor (VEGF) (31). These integrins also have other tumor-promoting activities, including displaying upregulated expression in a variety of tumor cells, having a role in the differentiation of tumor progenitor cells and being essential for the differentiation and bone-eroding activity of osteoclasts triggered by tumors homing to the bone marrow (7). The type 1 insulin like growth factor receptor (IGF-1R) is widely expressed in normal tissues and has important roles in prenatal and postnatal organ growth, with key roles in cell cycle progression and cell survival signaling (32). Pups of IGF-1R null mice are born with severe organ hypoplasia and are less than half of normal size (33). These roles are equally, if not more, striking in cancer. Fibroblasts derived from IGF-1R null mice resist transformation by most oncogenes, and tumor growth in mice is blocked by IGF-1R siRNAs that otherwise have little or no effect on normal tissues (34, 35).

An involvement of IGF-1R in cell-matrix adhesion came to light when the Clemmons group demonstrated an important co-regulatory interaction between the αvβ3 integrin, the integrin-associated protein (IAP) and IGF-1R in smooth muscle cells, in which IGF1 stimulates activation of the integrin and the integrin attenuates IGF-1R signaling by recruitment of the phosphatase SHP-2 (19, 20, 36–38). Subsequent studies focusing largely on cancer mechanisms have shown that the activities of the αvβ3 and αvβ5 integrins and IGF-1R are linked and regulated by syndecan-1 (Sdc1). The αvβ3 and αvβ5 integrins are well-studied integrins that are upregulated in the tumor microvasculature and in many tumors as well, where they are likely to engage provisional matrix consisting of vitronectin, fibronectin, osteopontin, fibrinogen and von Willebrand factor in the tumor microenvironment (7). A pre-assembled complex consisting of Sdc1, inactive αvβ3 or αvβ5 integrin and inactive IGF-1R is found in fibroblasts, breast cancer and other carcinomas, multiple myeloma and activated vascular

endothelial cells undergoing pathological angiogenesis (39–42) (**Figure 1**) and is likely found in many cancers. Clustering of this ternary receptor complex, occurring when Sdc1 in adherent cells engages the vast polyvalent array of heparin-binding domains presented by proteins in the basement membrane and stromal ECM, or mimicked by plating cells on Sdc1-specific antibody, leads to ligand-independent activation of the IGF-1R, which initiates inside-out signaling through talin to activate the integrin (41) (**Figure 1B**). Syndecan mutagenesis studies, together with competitive inhibition of IGF-1R or integrin activation by recombinant Sdc1 ectodomain or peptides derived from the Sdc1 ectodomain, localizes the integrin/IGF-1R docking site to amino acids 93-120 in the extracellular domain of the membrane-anchored human Sdc1 (27, 39) (**Figure 1A**). A peptide mimetic of this site, originally called "synstatin" (SSTN) and now referred to as "$SSTN_{IGF1R}$" to distinguish it from other synstatins subsequently identified against other RTKs, directly binds the integrins and IGF-1R and prevents their interaction with the syndecan (**Figure 1A**). This blocks the autophosphorylation of IGF-1R, even in the presence of IGF-1 (40), and prevents activation of the integrin. *In vitro* binding experiments using purified IGF-1R, integrin and recombinant Sdc1 extracellular domain show that the ternary complex can be formed *in vitro* from these three components alone; but, whereas the integrin alone is readily captured by Sdc1, IGF-1R binds only after the integrin is engaged by the syndecan, suggesting that IGF-1R docks to an interface comprised of Sdc1 together with the integrin (41). This feature of the capture mechanism serves to restrict this unique regulation of IGF-1R signaling to select cell types that express all three receptors, typically tumor cells and

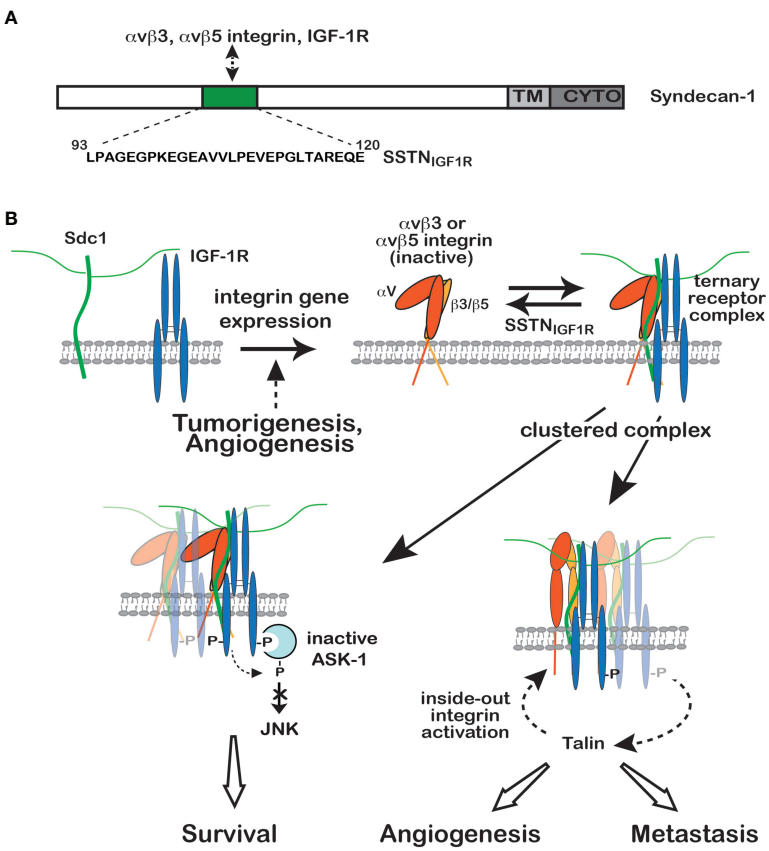

FIGURE 1 | Regulation of IGF-1R signaling by Sdc1. **(A)** Model depicting site of IGF-1R capture, along with either the αvβ3 or αvβ5 integrin, in the extracellular domain of human Sdc1. A peptide mimetic of this site, $SSTN_{IGF1R}$, competitively blocks receptor binding. **(B)** IGF-1R is not engaged with Sdc1 in nontransformed cells, typically because they lack the αvβ3 and αvβ5 integrins (top left). But integrin expression, usually in response to malignant transformation or activation of endothelial cells during angiogenesis, results in integrin docking to the extracellular domain of Sdc1, which is followed by IGF-1R capture at the same docking site (top right). Once formed, constitutive or matrix-induced clustering of the ternary receptor complex activates IGF-1R by autophosphorylation that does not require IGF-1. Activated endothelial cells or tumor cells bearing the ternary receptor complex rely on the syndecan-activated IGF-1R to phosphorylate and suppress the activity of Apoptosis-Signal regulating Kinase-1 (ASK-1) engaged with the IGF-1R cytoplasmic domain (bottom left), preventing ASK-1-mediated activation of Jun-N-terminal Kinase (JNK) and blocking entry into apoptosis, thus promoting tumor cell survival. In a second activity (bottom right), downstream signaling from IGF-1R activates the αvβ3 or αvβ5 integrin *via* an inside-out signaling pathway that targets the integrin-activating protein Talin, resulting in endothelial or tumor cell motility during the onset of angiogenesis or tumor cell invasion. $SSTN_{IGF1R}$ competitively disrupts the ternary receptor complex, preventing integrin activation and removing the constitutive suppression of ASK-1. Neither activity can be rescued by IGF-1 when the receptor complex is disrupted by $SSTN_{IGF1R}$, emphasizing the singular role played by the syndecan in this IGF-1R signaling mechanism (see discussion in text, references (27, 39–41) and references therein.

endothelial cells undergoing pathological angiogenesis. Whether there are additional membrane components expressed in tumor cells that stimulate the assembly of this receptor complex ranging from protein partners such as tetraspannins to specialized lipid rafts has not been explored.

Immunoprecipitation studies suggest that the majority, if not all, of the IGF-1R in tumor cells is associated with Sdc1, potentially making $SSTN_{IGF1R}$ a highly specific cancer therapy. It resists proteolytic degradation in plasma that usually leads to the rapid demise of most peptides *in vivo*, and is cleared only slowly from the circulation, displaying a t½ of 27 hr in mice (40). It is highly effective against tumor xenografts, which are reduced in size over 10-fold in mice treated with 0.365 mg/kg/day of the peptide, sufficient to reach a concentration of 3 μM in the blood (39, 40). Restriction of the mechanism to tumors and pathological angiogenesis and its apparent absence in normal tissues suggests that $SSTN_{IGF1R}$ may have little impact, if any, on normal metabolism and low toxicity to normal organs. Conventional therapeutic approaches such as IGF-1R kinase inhibitors also target the insulin receptor and the IGF-1R-feedback loop in the hypothalmus, leading to increased insulin and IGF1 levels in the plasma that are thought to stimulate rather than disrupt tumorigenesis (43). IGF-1R-blocking antibodies developed as potential therapeutics also disrupt the feedback loop and fail to disrupt IGF1R-coupled to Sdc1, which is IGF1-independent (43).

Examination of SSTN-treated tumors demonstrates that not only are they reduced in size, but they display a 10-fold reduction in vascularization as well. This is due to $SSTN_{IGF1R}$'s activity against both the tumor cell, in which it not only blocks migration but also activates apoptosis, and against activated endothelial cells engaged in tumor-induced angiogenesis. The peptide blocks αvβ3-mediated migration of vascular endothelial cells *in vitro* with an IC_{50} of ca. 300 nM and displays similar activity against FGF-induced corneal angiogenesis *in vivo* when delivered systemically *via* Alzet pump (39). This traces to the dependence of VEGF signaling on the αvβ3 integrin. A clear example of this dependence is the defective VEGFR2 activation and blocked angiogenesis observed in genetically-engineered mice expressing the $\beta3^{Y747F/Y757F}$ integrin mutant, which prevents αvβ3 integrin activation and signaling (16, 17). In similar fashion, treatment of endothelial cells with $SSTN_{IGF1R}$ not only blocks αvβ3 activation, but also prevents VEGFR2 activation by VEGF (44). The Sdc1-, IGF-1R- and integrin-dependent regulation of VEGFR2 activation depends on cell-cell contact mediated by VE-cadherin, long known to be a regulator of VEGFR2 activation and angiogenesis (45, 46), linking these disparate mechanisms. This linkage appears to be complex and remains largely unknown, but depends in some manner on the clustering of VE-cadherin (44) and activation of Src (17), ostensibly to phosphorylate tyrosines Y747 and Y757 in the β3 integrin cytoplasmic domain (17). The activation of VEGFR2 by VEGF is blocked by VE-cadherin blocking antibodies, but VEGFR2 activation is restored if the blocking antibodies engaged with the cadherin are artificially clustered, mimicking VE-cadherin clustering that occurs during cell-cell adhesion (44). In step-wise fashion, this causes IGF-1R autophosphorylation that is nonetheless dependent on Src and is prevented by $SSTN_{IGF1R}$, followed by downstream activation of VEGFR2 (44).

SDC1-COUPLED IGF-1R IN TUMOR CELL SURVIVAL

Perhaps the greatest impact of Sdc1-coupled IGF-1R on tumorigenesis is its role in tumor survival, revealed in myeloma cells that express high levels of Sdc1 (CD138) and constitutively active Sdc1-coupled IGF-1R. $SSTN_{IGF1R}$ induces the rapid activation of Jun-N-terminal kinase (JNK)/stress-activated protein kinase (SAPK) in myeloma cells, and p38MAPK as well in activated endothelial cells and carcinoma cells, two stress-activated MAPKs capable of initiating apoptosis in response to genotoxic and metabolic stressors common in cancer (40). A key upstream activator in myeloma appears to be Apoptosis-signal Regulating Kinase-1 (ASK-1), a MAP3K with critical roles in plasma cell and myeloma cell survival (47). ASK-1 binds the cytoplasmic domain of IGF-1R and is maintained in an inactive state by IGF-1R-mediated tyrosine phosphorylation, as well as by serine-threonine phosphorylation carried out by other enzymes activated downstream of IGF-1R (48, 49). However, inhibition of IGF-1R by $SSTN_{IGF1R}$ prevents these inhibitory phosphorylation events, allowing ASK-1 autoactivation, its subsequent activation of JNK/SAPK, and entry of myeloma cells into apoptosis (40) (**Figure 1B**). It is of interest to note that although $SSTN_{IGF1R}$ inhibits both IGF-1R and its downstream activation of the αvβ3 or αvβ5 integrin in endothelial and carcinoma cells, the integrin is not active in the myeloma cells, suggesting that it is IGF-1R alone that is required for the survival signaling (40). The signaling pathway downstream of IGF-1R that activates talin and thus the αvβ3 or αvβ5 integrin remains to be identified and the question remains as to whether it is present but inactive in myeloma cells, or if a critical component of the pathway is lacking altogether. Also unique to the myeloma cells compared to carcinoma or endothelial cells is that IGF-1R in the pre-assembled Sdc1-coupled ternary receptor complex is constitutively active (40); it is not dependent on cell adhesion or IGF-1, although exogenous IGF1 stimulates increased levels of IGF-1R activation. But even the IGF1-mediated activation is strictly dependent on the interaction of IGF-1R with the syndecan and is blocked by $SSTN_{IGF1R}$ (40).

Several key questions about this activation mechanism remain unanswered, including how clustering of Sdc1 activates IGF1-R independent of IGF1 ligand, how $SSTN_{IGF1R}$ blocks IGF1 stimulation of IGF-1R in myeloma and whether $SSTN_{IGF1R}$ blocks IGF1-induced IGF-1R activation in tumors other than myeloma. IGF-1R is a dimeric receptor composed of α and β subunits that relies on tyrosine kinase phosphorylation to recruit adaptor proteins (e.g., IRS-1, IRS-2, Shc) that mediate signaling leading to cell proliferation, cell migration and apoptosis (7). High resolution structural modeling suggests that the receptor is auto-inhibited due to wide separation of its

cytoplasmic kinase domains (50). Binding of a single IGF1 monomer relieves these constraints and fosters a pseudoligand interaction between the two extracellular domains that re-positions the cytoplasmic kinase domains to undergo transphosphorylation (50). In the case of IGF-1R activation by Sdc1, it is clear that clustering of the syndecan must in some manner reproduce this positioning of the kinase domains. One scenario suggests that IGF-1R is optimally oriented when complexed with Sdc1 and αvβ3 or αvβ5 integrin to favor autophosphorylation in *trans* between the kinase domains of distinct IGF-1Rs when clustered by the syndecan. A less likely scenario envisions interactions between the IGF-1R extracellular domains promoted by clustering that mimic ligand binding and thus re-orient and activate the kinase domains in a single receptor similar to IGF1 binding.

SDC1 AS AN ORGANIZER OF VLA-4/ VEGFR2-MEDIATED CELL POLARITY AND INVASION

The α4β1 integrin, known as VLA-4 (very late antigen-4) on leukocytes, modulates the recruitment of leukocytes during immunity and autoimmune diseases, the dissemination of stem cell precursors into the blood, and the invasive phenotype of blood cell cancers (51). The integrin recognizes several ligands, but most prominently vascular cell adhesion molecule-1 (VCAM-1), which is largely expressed on vascular endothelial cells and stromal cells in the bone marrow, and the stromal matrix macromolecule fibronectin, in which it recognizes a VLA-4-specific PVD binding motif in the CS-1 domain (52). Engagement of these ligands regulates the extravasation of leukocytes through the blood vessel wall and their migration within the interstitial matrix and has been shown to have a similar role on some tumor cells (reviewed in (51). VLA-4 is also expressed on vascular and lymphatic endothelial cells where it plays a role during angiogenesis and polarized re-orientation of endothelial cells in response to blood flow (53, 54). A critical step in these activities is the binding of the scaffolding protein paxillin to the cytoplasmic domain of the α4 integrin subunit, which localizes paxillin-bound signaling effectors to the integrin, including focal adhesion kinase (FAK), proline-rich tyrosine kinase-2 (Pyk2) and G-protein coupled receptor kinase interacting protein-1 (GIT1), an Arf-6 GAP (55–58). GIT1 prevents the local activation of Arf6 and its downstream target Rac-1, the latter necessary for lamellipodium formation in response to VLA-4-mediated adhesion. In contrast, FAK and Pyk2 provide downstream transregulatory signaling leading to activation of leucocyte functional antigen-1 (LFA-1, also known as the αLβ2 integrin), a second integrin important in leukocyte extravasation, shifting the cell invasion behavior to this integrin (57). However, phosphorylation of the α4 cytoplasmic domain on S988 by PKA, which occurs only at the site destined to be the leading edge of the cell, releases the block to Rac1 activation by displacing paxillin from the integrin, and induces VLA-4-mediated, rather than LFA-1-mediated, generation of an active lamellipodium and polarized migration of the cell (54, 59). But how PKA is activated, and how it is localized to the integrin in order to carry out this phosphorylation, has remained unknown.

A recent clue to the activation mechanism comes from the study of multiple myeloma, a disease in which malignant plasma cells extravasate throughout the bone marrow of affected patients, and a unique response of the cells when CD138 (syndecan-1) is targeted by heparanase (HPSE), an HS-degrading endoglucuronidase (60). Although circulating B lymphocytes reportedly express low levels of syndecans, if any, the expression of Sdc1 is greatly upregulated in plasma cells and their malignant counterparts. Poor prognosis in the disease accompanies those tumors that express high levels of HPSE, which trims the HS chains of Sdc1 and causes shedding of high levels of Sdc1 into the bone marrow microenvironment (61–63). Using human CAG myeloma cells expressing low versus high levels of HPSE as a test system, it is observed that high HPSE expression promotes an invasive phenotype that depends on VLA-4; VLA-4 is localized to the leading edge when the cells are plated on fibronectin or VCAM-1, and is responsible for cell invasion through filters coated with these VLA-4 ligands (60). Several lines of evidence trace the polarization mechanism to Sdc1 ectodomain that has been shed from the cell surface. First, polarization is blocked by MMP-9 inhibitors that prevent shedding of the syndecan. Second, polarization can be rescued when shedding is blocked if conditioned medium containing shed Sdc1 is added to the cells, but not if Sdc1 is immunodepleted from the medium. Third, the invasive phenotype on VLA-4 ligands can be stimulated by exogenous recombinant human Sdc1 ectodomain alone in the absence of HPSE, or a peptide representing a putative active site contained within amino acids 210-236 of the recombinant protein (**Figure 2A**). An asp-phe-thr-phe (DFTF) motif at the N-terminus of this peptide represents a site in the Sdc1 ectodomain that is essential for binding VLA-4 and a pro-val-asp (PVD) sequence at its C-terminus mimics a motif in Sdc1 that captures vascular endothelial cell growth factor receptor-2 (VEGFR2) (60) (**Figures 2A, B**).

The proposed mechanism that emerges from these studies is as follows. Engagement of VLA-4 with its ligands causes its rapid activation and clustering (avidity modulation), an initial first step designed to rapidly strengthen its affinity for VCAM-1 on the blood vessel wall during leukocyte activation and extravasation from the blood stream (58). In myeloma, this initial step requires association of VLA-4 with membrane-bound Sdc1 *via* its DFTF motif (60) (**Figure 2B**), although whether this docking plays a role in the integrin's conformational change that promotes ligand engagement, or in strengthening the adhesion by avidity modulation, or in some other step, is not yet clear. This step is prevented by a syndecan-derived peptide containing the DFTF motif ($SSTN_{VLA4}$) but lacking the PVD motif necessary for capturing VEGFR2 (60) (**Figure 2C**). Next, shedding of Sdc1, induced by HPSE-mediated trimming of its HS chains and carried out by MMP-9, releases Sdc1 from its membrane domain and allows it to engage VEGFR2, which requires the PVD motif in the syndecan (**Figure 2C**). The result is coupling of VEGFR2 to the

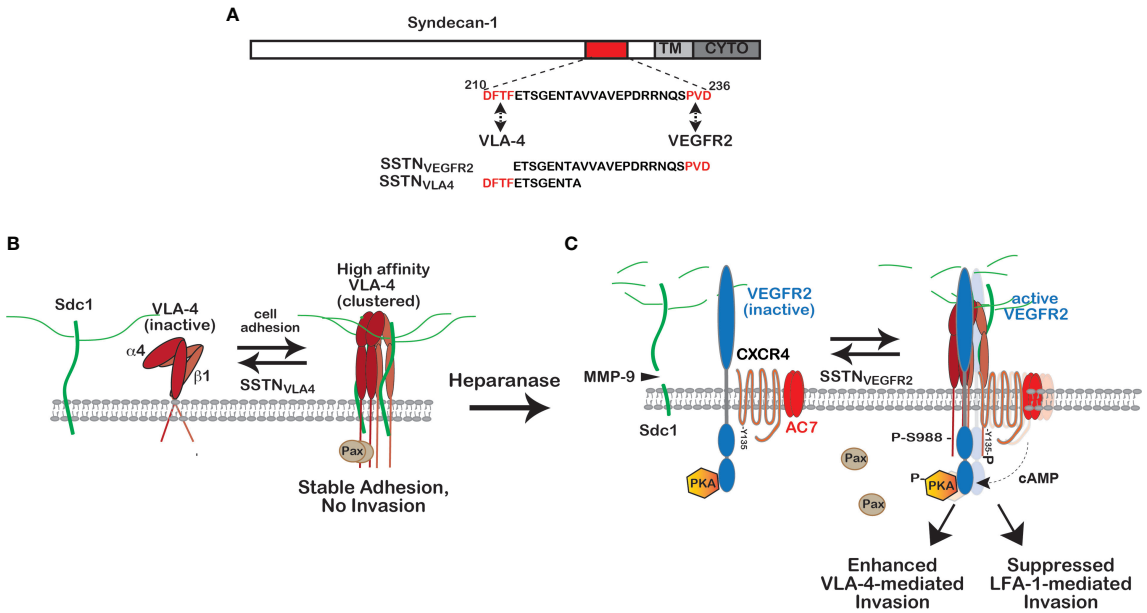

FIGURE 2 | Regulation of VLA-4 activation and polarized cell invasion by Sdc1. **(A)** *VLA-4 and VEGFR2 docking sites in Sdc1.* Juxtamembrane sites in the extracellular domain of human Sdc1 (DFTF and PVD) responsible for engaging very late antigen-4 (VLA-4, α4β1 integrin) and vascular endothelial growth factor receptor-2 (VEGFR2), respectively. Synstatin peptides containing one, but not both of these sites (e.g., $SSTN_{VLA-4}$ or $SSTN_{VEGFR2}$), prevent VLA-4 or VEGFR2 capture by the syndecan and disrupt signaling that relies on the co-capture of both receptors. **(B)** *Regulation of high affinity VLA-4 adhesion by Sdc1.* VLA-4 undergoes rapid activation when engaging ligand, involving a conformation change and clustering (avidity modulation) to increase binding affinity. On cells expressing Sdc1 (e.g., myeloma cells, vascular endothelial cells, melanoma, Jurkat-T cells), this activation is blocked by preventing VLA-4 docking with Sdc1 using $SSTN_{VLA-4}$ or mutating the DFTF motif in the syndecan. The mechanism underlying this dependence on the syndecan remains under investigation. **(C)** *Role of heparanase and shed Sdc1 in polarized cell invasion*. The heparan-sulfate-degrading enzyme heparanase is a known tumor promoter and enhancer of leukocyte recruitment during inflammation. Trimming of the HS chains on Sdc1 exposes its core protein to cleavage by matrix-metalloproteinase-9 (MMP-9), releasing the syndecan ectodomain. The shed syndecan couples an inactive receptor complex consisting of VEGFR2 with inactive protein kinase A (PKA) attached to its cytoplasmic domain, the cytokine receptor CXCR4 and adenylate cyclase 7 (AC7) to the clustered integrin, causing VEGF-independent activation of VEGFR2; VEGFR2 phosphorylates CXCR4 on Y135, activating its $G\alpha_i\beta\gamma$ GTPase and the $G\alpha_i$-dependent AC7. Local generation of cAMP leads to activation of protein kinase-A (PKA) engaged with the VEGFR2 cytoplasmic domain and phosphorylation of the α4-integrin cytoplasmic domain on serine 988. This displaces the Rac-inhibitory paxillin from the integrin, causing polarized invasion of VLA-4-dependent immune cells, typically tumor supporting cells such a macrophages, MDSCs and others, as well as myeloma cells. Displacement of paxillin also inhibits the cross-talk between VLA-4 and LFA-1 necessary for LFA-1-mediated migration that characterizes tumor suppressor cells, such as NK and cytotoxic T cells. Either prevention of integrin activation by $SSTN_{VLA-4}$ or VEGFR2-coupling to the integrin by $SSTN_{VEGFR2}$ serves to block these processes [see discussion in text, references (60, 64) and references therein].

clustered VLA-4 by shed Sdc1, which in turn clusters and activates VEGFR2 *via* autophosphorylation, and induces the polarized invasion of the cells. No VEGF is required and VEGFR2 blocking antibodies fail to disrupt this mechanism (60).

The next important step in the understanding of this mechanism is the target of VEGFR2 phosphorylation that activates and localizes PKA to the integrin, where it carries out the phosphorylation of S988 on the α4 subunit. Cell staining demonstrates that shed Sdc1 causes VLA-4 to re-localize from the lagging edge to the leading edge of myeloma cells where it localizes with the shed Sdc1 and VEGFR2 when cells are plated on VLA-4 ligands (60). Recent work now shows that VEGFR2 is preassembled into a complex with PKA, the cytokine receptor CXCR4, and adenylate cyclase 7 (AC7) (64) (**Figure 2C**). The target of the VEGFR2 kinase that is activated by clustering when engaged with the shed Sdc1 is tyrosine 135 (Y135) within an asparagine-arginine-tyrosine (DRY) microswitch in cytoplasmic loop 2 of CXCR4, part of an activation switch present throughout the broad superfamily of G-coupled protein receptors (65). Although this tyrosine is highly conserved in the superfamily, there was little prior evidence to support a direct role in G-protein activation until to this demonstration of CXCR4 activation by VEGFR2 phosphorylation. Activation of VLA-4 can also occur if CXCR4 in this complex is activated by its ligand, CXCL12, but this still requires linkage of the complex to VLA-4 by shed Sdc1 (64). Activation of CXCR4 and its $G\alpha_i\beta\gamma$ heterotrimeric G-protein activates AC7, one of a small number of adenylate cyclases that are activated by $G\alpha_i$-containing G-proteins, resulting in increased cAMP levels that locally activate PKA-mediated phosphorylation of Y988 in VLA-4 (64).

This VLA-4 activation mechanism is blocked by syndecan-derived peptides that contain the PVD motif ($SSTN_{VEGFR2}$) and lack the DFTF motif, thus binding VEGFR2 and competitively preventing it from engaging shed Sdc1 and docking with the integrin (60). These two SSTN peptides provide new tools to either block VLA4-mediated adhesion altogether ($SSTN_{VLA4}$) or to specifically target VLA-4 actively engaged in cell invasion ($SSTN_{VEGFR2}$). It is envisioned that in myeloma this mechanism

plays a major role in the extravasation of myeloma throughout the bone marrow by engaging VCAM-1 expressed by the vascular endothelium of bone marrow capillaries and VCAM-1 and fibronectin that are richly expressed in the bone marrow stroma. Although initially discovered in HPSE-overexpressing myeloma cells, this mechanism is also operative on vascular endothelial cells, in which VEGFR2 and the α4β1 integrin are commonly expressed (60). VEGFR2 has been shown previously to associate with Sdc1 in myeloma-derived vascular endothelial cells (66). In addition, the short-chain (scFv) recombinant human antibody OC-46F2, which binds to a juxtamembrane site in the Sdc1 ectodomain that overlaps with the VEGFR2 binding motif, disrupts angiogenesis and melanoma xenograft growth in NOD-SCID mice (67).

Further insight into this mechanism and its role in tumorigenesis emerges from an understanding of the role played by α4-S988 phosphorylation during the transregulation that occurs between VLA-4 and LFA-1 (the αLβ2 integrin), the latter utilized for invasion by tumor suppressing cells such as natural killer cells and cytotoxic T-cells (57, 68, 69). LFA-1 activity requires co-signaling from VLA-4 that depends on paxillin, PyK2 and FAK engagement with VLA-4 (57, 58, 70). Thus, phosphorylation of Y988 that displaces paxillin and enhances VLA-4-mediated invasion serves to suppress LFA-1-mediated invasion. This is elegantly shown by the increased LFA-1 activity of cytotoxic leukocytes bearing phosphorylation-resistant α4-S988A integrin; these cells appear to invade the tumor microenvironment more readily, leading to enhanced destruction of melanoma xenografts (71). It has been shown more recently that mouse NK and cytotoxic T-cells rely on Sdc1 as a regulator of this mechanism. NK and T-cells express Sdc1, VEGFR2, CXCR4, AC7 and HPSE and their LFA-1-mediated migration in *in vitro* invasion assays is dramatically increased by $SSTN_{VEGFR2}$ while at the same time the peptide inhibits the VLA-4-mediated invasion of myeloma cells (64). This brings into focus the protumorigenic role of heparanase in myeloma and other tumors (72, 73). Myeloma patients with advanced disease are known to express high levels of heparanase and to have high levels of shed Sdc1 in the tumor microenviroment and the blood (74–76). By engaging VLA-4 and VEGFR2 on the myeloma cells and tumor suppressor cells in the tumor microenvironment, the shed syndecan is likely to promote VLA-4-mediated extravasation of myeloma cells in and out of the bone marrow and to extramedullary organs. At the same time, the LFA-1-mediated invasion of NK and cytotoxic T cells is suppressed by the Sdc1 shed into the tumor microenvironment, providing a protected environment for growth of the tumor (71, 77).

COUPLING OF EGFR AND HER2 TO THE α3β1 AND α6β4 INTEGRINS BY SYNDECANS

Work from multiple laboratories has shown that the α6β4 integrin has a signaling role during epithelial wound healing, carcinoma invasion and survival (10). This contrasts with its role on quiescent cells, where it functions as the central adhesion receptor in hemidesmosomes found in epithelial and endothelial cell layers (78–80) (**Figure 3A**). Here, its uniquely long cytoplasmic domain (over 1,000 amino acids) is linked by plectin to the keratin cytoskeleton, and its extracellular domain engages laminin 332 (LN332, also known as laminin 5) in the basement membrane (84, 85). But activation of RTKs, of which EGFR, HER2, and HGFR (c-Met) have been clearly implicated, causes hemidesmosome breakdown, freeing the integrin to associate with these kinases and resulting in phosphorylation of tyrosines in its "signaling domain" that acts as a scaffold for binding Shc, IRS-1/2 and other mediators in order to activate cell proliferation, invasion and survival (11, 13, 86–92). Cell migration utilizing this integrin occurs on a polarized substratum of LN332 that the cells deposit as they migrate through cooperative signaling from the α6β4 and α3β1 integrin (93). LN332 expression is upregulated along with the β4 integrin in epidermal squamous cell carcinomas (94) and these and other carcinomas depend on it and the α3β1 and α6β4 integrins for their invasion and survival (reviewed by Marinkovich (95). Mouse tumor models expressing a β4 mutant lacking its "signaling domain" ($\beta4^{1355T}$) have been instrumental in demonstrating its critical role in tumorigenesis and tumor-induced angiogenesis that depends on EGFR, HER2 or c-MET (12, 96, 97). Importantly for this review, two of these RTKs (EGFR and HER2) rely on syndecans to pair them with the α6β4 and α3β1 integrins to carry out these important signaling roles (81, 82).

Immunoprecipitation studies show that Sdc1 is assembled into a quaternary receptor complex with HER2, the α6β4 integrin and the laminin-binding α3β1 integrin (81–83) (**Figure 3C**). A homologous receptor complex containing α3β1 and α6β4 integrins, along with EGFR rather than HER2, assembles with Sdc4 rather than Sdc1 (**Figure 3C**) (81, 83). The fact that homologous, but clearly distinct, receptor complexes are organized by these two syndecans is explained by the finding that they depend on the two domains of the syndecans that set them apart as family members: their extracellular domain and the V region of their cytoplasmic domains. Sdc1 captures HER2 and the α3β1 integrin *via* a juxtamembrane "co-receptor" binding site in its extracellular domain (amino acids 210-240) that is unique to Sdc1 (**Figure 3B**). A peptide mimetic of this extracellular docking site (called $SSTN_{HER2}$) prevents capture of HER2 and the integrin and blocks epithelial cell motility on LN332 in wound healing assays (**Figure 3C**) (83). Binding studies using recombinant HER2 and Sdc1 extracellular domain show that the binding is direct and is competed by the $SSTN_{HER2}$ peptide. Interestingly, the juxtamembrane site in Sdc1 required for the assembly of this receptor complex overlaps extensively with the site required for Sdc1 to capture VLA-4 and VEGFR2. Indeed, the DFTF motif necessary for VLA-4 capture plays a role in HER2 binding as well. In contrast, however, the PVD motif required to bind VEGFR2 appears to have no role in binding either HER2 or α3β1 integrin; instead, a QGAT motif (amino acids 237-240) must be present (83).

In addition to this extracellular docking site, a five-amino acid motif (QEExYx-c) at the C-terminus of the short Sdc1 cytoplasmic domain, comprised partly of its syndecan-specific V region (.QE.) and the C2 region shared by all four syndecans

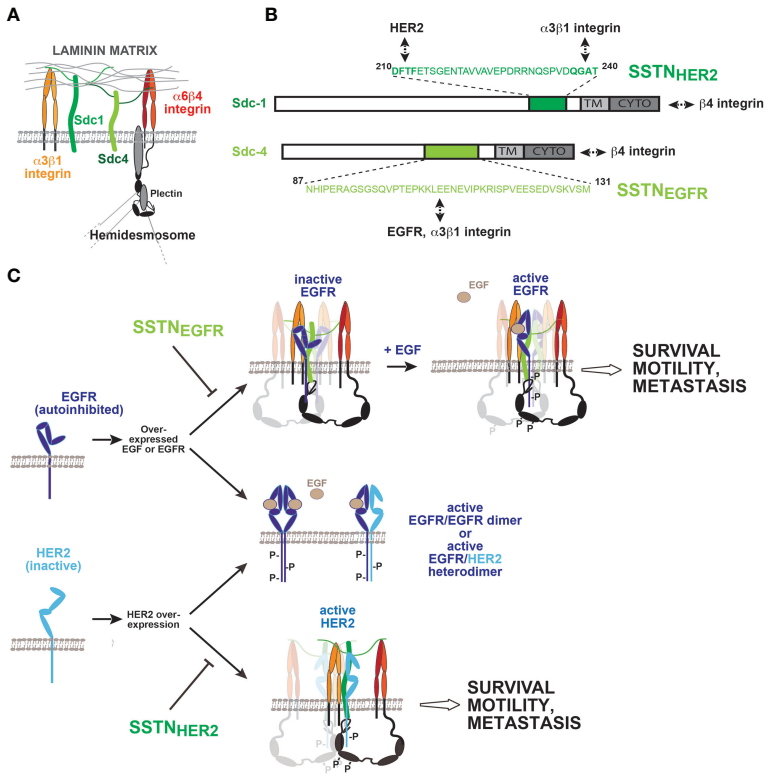

FIGURE 3 | Coupling of EGFR family members to integrins by Sdc1 and Sdc4 regulates wound healing, tumor cell invasion and survival. **(A)** *Syndecans and integrins on quiescent epithelial or endothelial cells.* The laminin-332 (LN332) binding α3β1 and α6β4 integrin, along with Sdc1 and Sdc4 *via* their heparan sulfate chains, mediate binding to LN332-rich basement membrane. The long (>1,000 amino acids) cytoplasmic domain of the β4 integrin subunit engages the plectrin and BP180 scaffolding proteins, which engage the intermediate filament network and help stabilize the incorporation of the α6β4 integrin into hemidesmosomes. **(B)** *Sites of EGFR, HER2 and integrin capture in Sdc1 and Sdc4.* The multifunctional juxtamembrane site in Sdc1 captures HER2 and the α3β1 integrin. Multiple binding interactions occur throughout the sequence; nonetheless, the DFTF motif that is also essential for binding VLA-4 plays a prominent role in HER2 binding, whereas α3β1 integrin capture is highly dependent on the QGAT motif. An analogous juxtamembrane site in Sdc4, which bears no homology to the site in Sdc1, captures EGFR and the α3β1 integrin, relying on multiple binding interactions throughout the sequence. Synstatin peptides based on these sites are highly selective for EGFR ($SSTN_{EGFR}$) or HER2 ($SSTN_{HER2}$) and displace α3β1 integrin only when coupled with the EGFR family member for which they are specific. In addition to these interactions, the C-termini of the syndecans engage the cytoplasmic C-terminus of the β4 integrin, which comprises the α6β4 integrin. This is also syndecan-type specific; mutations that disrupt Sdc1 binding having no effect on Sdc4 and *vice versa*. **(C)** *Formation and activation of syndecan-organized quaternary receptor complexes containing EGFR or HER2.* EGFR and HER2 are overexpressed in squamous cell carcinomas, along with EGF. EGFR depends on EGF for dimerization, and to relieve constraints in its extracellular domain that prevent dimerization. HER2 lacks these extracellular constraints but lacks a ligand to promote its dimerization. Relief of the inhibitory constraints in EGFR allows it to form active homodimers or active heterodimers with HER2. Activation of receptor tyrosine kinases causes the breakdown of hemidesmosomes, freeing the cytoplasmic domain of the β4 integrin to engage Sdc1 and Sdc4. Quaternary receptor complex is formed when EGFR and the α3β1 integrin, or HER2 and the α3β1 integrin assemble with their respective docking site on the syndecans as well. The kinases appear to be captured as monomers and rely on clustering of the complexes to sites of matrix adhesion to be activated. Simple clustering of the syndecan is sufficient to activate HER2, but EGFR also requires EGF, ostensibly to relieve the dimerization constraints in its extracellular domain. Several tyrosines in the β4 cytoplasmic domain become phosphorylated, and support signaling that leads to epithelial cell migration during wound healing, or invasion and survival signaling in tumor cells and endothelial cells engaged in pathological angiogenesis. Synstatin peptides specific for HER2 capture by Sdc1 ($SSTN_{HER2}$) or EGFR capture by Sdc4 ($SSTN_{EGFR}$) are highly specific inhibitors of these processes. [See discussion in text, references (81–83) and references therein].

(…EFYA-c) engages the extreme C-terminus of the β4 integrin cytoplasmic domain, presumably positioning the integrin tail at the plasma membrane and in close proximity to HER2, where it's signaling domain is phosphorylated by Fyn downstream of activated HER2 (81, 82). Deletion of the C2 region of Sdc1 or the last 28 amino acids in the β4 integrin tail (Δ1728-1752), or mutation of R1733 within this sequence, abolishes the interaction, prevents tyrosine phosphorylation of the integrin and blocks epithelial cell migration on LN332 and breast carcinoma cell survival.

The functional assembly of the Sdc4-coupled receptor complex occurs in a similar manner, but utilizing Sdc4-specific protein sequences. Sdc4 also binds the extreme C-terminus of the β4 integrin but requires E1729 rather than the R1733 required by Sdc1; introducing an E1729A mutation into the β4 cytoplasmic domain prevents its association with Sdc4 but has no effect on its ability to engage Sdc1 (81). Similarly, the R1733A mutant that fails to bind Sdc1 maintains its interaction with Sdc4. These β4 integrin mutants act as dominant negative receptors in cultured cells by outcompeting the wt β4 subunit for a limiting supply of

α6 integrin subunit when overexpressed. Integrin subunits containing the R1733A mutation fail to activate HER2-dependent cell migration that depends on Sdc1 yet trigger migration in response to EGF. The E1729A mutant integrin sustains HER2-dependent migration, but cells expressing this mutant fail to migrate when stimulated with EGF.

Analogous to Sdc1, an extracellular, juxtamembrane site in Sdc4 consisting of amino acids 87-131 is responsible for capturing the α3β1 integrin and EGFR (**Figure 3A**) (83). A peptide mimetic of this site ($SSTN_{EGFR}$) competes for the interaction and displaces EGFR and α3β1 integrin from the remaining Sdc4-α6β4 integrin duplex. As observed for Sdc1 and HER2, the interaction between Sdc4 and EGFR is direct, as purified recombinant ectodomains interact and are displaced from one another by $SSTN_{EGFR}$. This peptide also blocks EGF-stimulated epithelial cell migration on LN332 that depends on α3β1 integrin but has no effect on HER2-stimulated migration. Like the juxtamembrane site in Sdc1, there are strong hints that the site in Sdc4 is also multifunctional. It was first described by McFall and Rapraeger as a site in Sdc4 that promoted the adhesion of fibroblasts and endothelial cells, although binding partners were not identified (98, 99). Further work from Couchman and Whiteford has shown that conserved amino acids within this site (I^{89} and the C-terminal GAT motif) regulate β1 integrin function in zebrafish, although potential interacting partners remain uncertain in those studies as well (100).

As with the other syndecan-organized signaling complexes, questions remain on how association with the syndecan and matrix-mediated clustering may serve to activate HER2 or EGFR and whether this occurs independent of classical growth factor binding. It is clear that stimulation of cell migration by EGFR paired with Sdc4 and the laminin-binding integrins still requires EGF (81, 83). This requirement for an RTK ligand contrasts with each of the other syndecan-organized complexes that have been described, including the HER2 mechanism, where clustering mediated by the adhesion receptors in the receptor complex appears to be sufficient to activate the associated RTK (IGF1R, HER2, VEGFR2) (41, 60, 81). It is possible that this traces to the specific mechanisms that regulate activation of the EGFR family of kinases. Activation of EGFR and HER2 kinases is known be caused by receptor dimerization, leading to head-to tail interactions of their cytoplasmic kinase domains that convert them to the active conformation (101). For EGFR, receptor dimerization is highly regulated by interactions in extracellular domains II and IV that are dependent on growth factor binding (102–104). EGF binding alters the conformation of domain IV, allowing the receptor to transition from a "closed" to an "open" conformation, relieving steric hindrance that otherwise prevents the adjacent receptors from dimerizing. In addition, EGF binding exposes a dimerization arm in domain II that interacts with a corresponding arm in the adjacent partner, stabilizes the receptor pair, and causes kinase activation through "head to tail" interactions of the two kinase domains (102–105) (**Figure 3C**). It is intriguing to note that HER2 is an orphan receptor that does not depend on ligand binding and is not inhibited by these regulatory sequences in domains II and IV (102–104). In its native state it favors the "open" conformation with exposed dimerization arm and as such does not depend on ligand binding in order to dock with other ligand-activated EGFR family members, such as EGF-bound EGFR (**Figure 3C**). This may be key to the mechanisms for HER2 and EGFR activation when assembled with the syndecan and integrins. HER2 is autoactivated when the quaternary Sdc1-HER2-integrin complex becomes clustered, either by integrin or syndecan-mediated binding to LN332, or when cells are plated solely on an artificial substratum consisting of β4-integrin-specific antibodies, suggesting that HER2 is captured by Sdc1 as a monomer, and becomes activated when the syndecan with which it is associated is clustered (81, 82). On the same cells, EGFR engaged with Sdc4, α3β1 integrin and α6β4 integrin is not activated when exposed to the same native LN332 or artificial β4-integrin antibody substrata unless EGF is provided. This suggests that matrix-driven clustering is sufficient to activate the kinases, as observed with HER2, but cannot act alone if impediments to dimerization require the additional action of a growth factor.

SUMMARY AND PERSPECTIVES

The lack of amino acid conservation and recognizable structural motifs in syndecan extracellular domains across each of the four syndecan family members, in sharp contrast to shared motifs in their transmembrane and cytoplasmic domains, belies an important organizer role for these domains in which each syndecan functions as a highly specific organizer of RTKs and integrins at the cell-matrix interface. Each of the RTKs identified to date, EGFR, HER2, VEGFR2 and IGF-1R, have been well-studied and structurally characterized. Yet, their interactions with syndecans have only recently come to light, suggesting that further work may identify a similar dependence for other RTKs. The general picture that emerges is one where RTK signaling can be triggered either by the binding of soluble cytokines or growth factors to exert paracrine growth control over a population of cells, or by syndecans engaged with the ECM that directly pair the RTK with integrins, leading to autocrine, growth factor-independent RTK activation, cell migration and survival. These local mechanisms are likely to play a role in wound healing, where cells depend on the activation of a migratory apparatus and anti-apoptosis signaling as they migrate out of their normal niche and are likely to be co-opted by tumor cells that rely on the same mechanisms for metastasis and survival. Whereas organizer roles for Sdc1 and Sdc4 have now been described, similar roles for Sdc2 and Sdc3 remain unknown but seem likely to exist as well. The examples discovered to date show that a single syndecan may have multiple organizer activities, as revealed by three distinct organizer activities for Sdc1 alone. Sdc4 also appears to be multifunctional, although the full extent of its repertoire remains to be defined. The lack of structural data for any of the four syndecan extracellular domains hampers a full analysis of how these multifunctional sites work to assemble distinct sets of receptors but lead to the speculation that certain amino acids provide a docking structure or motif while others are critical for specific protein-protein interactions with their target receptors. SSTN peptides derived from these sites benefit from this high

degree of specificity, which, together with the targets being extracellular, provide promising approaches to target tumor cells and tumor-induced angiogenesis. To date, such studies have relied on cell culture and animal models of tumorigenesis and angiogenesis ($SSTN_{IGF1R}$). Further work involving all synstatins in animal models is ongoing and will hopefully be extended to human cancer in future clinical trials.

AUTHOR CONTRIBUTIONS

The author confirms being the sole contributor of this work and has approved it for publication.

FUNDING

The work summarized in this review was supported by funds from the National Institutes of Health to the author's laboratory (R01-CA139872, R01-CA118839, R01-CA163662, R01-DE028341), and to the University of Wisconsin Carbone Cancer Center (P30-CA014520).

ACKNOWLEDGMENTS

The author thanks the members of the Rapraeger research lab and collaborators, past and present, whose ideas and novel discoveries made this review possible.

REFERENCES

1. Ivaska J, Heino J. Cooperation Between Integrins and Growth Factor Receptors in Signaling and Endocytosis. *Annu Rev Cell Dev Biol* (2011) 27:291–320. doi: 10.1146/annurev-cellbio-092910-154017
2. Miranti CK, Brugge JS. Sensing the Environment: A Historical Perspective on Integrin Signal Transduction. *Nat Cell Biol* (2002) 4:E83–90. doi: 10.1038/ncb0402-e83
3. Miyamoto S, Teramoto H, Gutkind JS, Yamada KM. Integrins can Collaborate With Growth Factors for Phosphorylation of Receptor Tyrosine Kinases and MAP Kinase Activation: Roles of Integrin Aggregation and Occupancy of Receptors. *J Cell Biol* (1996) 135:1633–42. doi: 10.1083/jcb.135.6.1633
4. Schwartz MA, Ginsberg MH. Networks and Crosstalk: Integrin Signalling Spreads. *Nat Cell Biol* (2002) 4:E65–8. doi: 10.1038/ncb0402-e65
5. Assoian RK, Klein EA. Growth Control by Intracellular Tension and Extracellular Stiffness. *Trends Cell Biol* (2008) 18:347–52. doi: 10.1016/j.tcb.2008.05.002
6. Lee JW, Juliano R. Mitogenic Signal Transduction by Integrin- and Growth Factor Receptor-Mediated Pathways. *Mol Cells* (2004) 17:188–202.
7. Desgrosellier JS, Cheresh DA. Integrins in Cancer: Biological Implications and Therapeutic Opportunities. *Nat Rev Cancer* (2010) 10:9–22. doi: 10.1038/nrc2748
8. Guo W, Giancotti FG. Integrin Signalling During Tumour Progression. *Nat Rev Mol Cell Biol* (2004) 5:816–26. doi: 10.1038/nrm1490
9. Streuli CH, Akhtar N. Signal Co-Operation Between Integrins and Other Receptor Systems. *Biochem J* (2009) 418:491–506. doi: 10.1042/BJ20081948
10. Wilhelmsen K, Litjens SH, Sonnenberg A. Multiple Functions of the Integrin Alpha6beta4 in Epidermal Homeostasis and Tumorigenesis. *Mol Cell Biol* (2006) 26:2877–86. doi: 10.1128/MCB.26.8.2877-2886.2006
11. Bertotti A, Comoglio PM, Trusolino L. Beta4 Integrin Activates a Shp2-Src Signaling Pathway That Sustains HGF-Induced Anchorage-Independent Growth. *J Cell Biol* (2006) 175:993–1003. doi: 10.1083/jcb.200605114
12. Guo W, Pylayeva Y, Pepe A, Yoshioka T, Muller WJ, Inghirami G, et al. Beta 4 Integrin Amplifies ErbB2 Signaling to Promote Mammary Tumorigenesis. *Cell* (2006) 126:489–502. doi: 10.1016/j.cell.2006.05.047
13. Mariotti A, Kedeshian PA, Dans M, Curatola AM, Gagnoux-Palacios L, Giancotti FG. EGF-R Signaling Through Fyn Kinase Disrupts the Function of Integrin Alpha6beta4 at Hemidesmosomes: Role in Epithelial Cell Migration and Carcinoma Invasion. *J Cell Biol* (2001) 155:447–58. doi: 10.1083/jcb.200105017
14. Santoro MM, Gaudino G, Marchisio PC. The MSP Receptor Regulates Alpha6beta4 and Alpha3beta1 Integrins via 14-3-3 Proteins in Keratinocyte Migration. *Dev Cell* (2003) 5:257–71. doi: 10.1016/S1534-5807(03)00201-6
15. Yu PT, Babicky M, Jaquish D, French R, Marayuma K, Mose E, et al. The RON-Receptor Regulates Pancreatic Cancer Cell Migration Through Phosphorylation-Dependent Breakdown of the Hemidesmosome. *Int J Cancer* (2012) 131:1744–54. doi: 10.1002/ijc.27447
16. Mahabeleshwar GH, Feng W, Phillips DR, Byzova TV. Integrin Signaling is Critical for Pathological Angiogenesis. *J Exp Med* (2006) 203:2495–507. doi: 10.1084/jem.20060807
17. Mahabeleshwar GH, Feng W, Reddy K, Plow EF, Byzova TV. Mechanisms of Integrin-Vascular Endothelial Growth Factor Receptor Cross-Activation in Angiogenesis. *Circ Res* (2007) 101:570–80. doi: 10.1161/CIRCRESAHA.107.155655
18. Soldi R, Mitola S, Strasly M, Defilippi P, Tarone G, Bussolino F. Role of Alphavbeta3 Integrin in the Activation of Vascular Endothelial Growth Factor Receptor-2. *EMBO J* (1999) 18:882–92. doi: 10.1093/emboj/18.4.882
19. Maile LA, Clemmons DR. Regulation of Insulin-Like Growth Factor I Receptor Dephosphorylation by SHPS-1 and the Tyrosine Phosphatase SHP-2. *J Biol Chem* (2002) 277:8955–60. doi: 10.1074/jbc.M109258200
20. Maile LA, Clemmons DR. The Alphavbeta3 Integrin Regulates Insulin-Like Growth Factor I (IGF-I) Receptor Phosphorylation by Altering the Rate of Recruitment of the Src-Homology 2-Containing Phosphotyrosine Phosphatase-2 to the Activated IGF-I Receptor. *Endocrinology* (2002) 143:4259–64. doi: 10.1210/en.2002-220395
21. Cheng B, Montmasson M, Terradot L, Rousselle P. Syndecans as Cell Surface Receptors in Cancer Biology. A Focus on Their Interaction With PDZ Domain Proteins. *Front Pharmacol* (2016) 7:10. doi: 10.3389/fphar.2016.00010
22. Couchman JR. Transmembrane Signaling Proteoglycans. *Annu Rev Cell Dev Biol* (2010) 26:89–114. doi: 10.1146/annurev-cellbio-100109-104126
23. Elfenbein A, Simons M. Syndecan-4 Signaling at a Glance. *J Cell Sci* (2013) 126:3799–804. doi: 10.1242/jcs.124636
24. Friand V, David G, Zimmermann P. Syntenin and Syndecan in the Biogenesis of Exosomes. *Biol Cell* (2015) 107:331–41. doi: 10.1111/boc.201500010
25. Gopal S, Multhaupt HA, Pocock R, Couchman JR. Cell-Extracellular Matrix and Cell-Cell Adhesion Are Linked by Syndecan-4. *Matrix Biol* (2016) 60-61:57–69. doi: 10.1016/j.matbio.2016.10.006
26. Lambaerts K, Wilcox-Adelman SA, Zimmermann P. The Signaling Mechanisms of Syndecan Heparan Sulfate Proteoglycans. *Curr Opin Cell Biol* (2009) 21:662–9. doi: 10.1016/j.ceb.2009.05.002
27. Rapraeger AC. Synstatin: A Selective Inhibitor of the Syndecan-1-Coupled IGF1R-Alphavbeta3 Integrin Complex in Tumorigenesis and Angiogenesis. *FEBS J* (2013) 280:2207–15. doi: 10.1111/febs.12160
28. Roper JA, Williamson RC, Bass MD. Syndecan and Integrin Interactomes: Large Complexes in Small Spaces. *Curr Opin Struct Biol* (2012) 22:583–90. doi: 10.1016/j.sbi.2012.07.003
29. Stepp MA, Pal-Ghosh S, Tadvalkar G, Pajoohesh-Ganji A. Syndecan-1 and Its Expanding List of Contacts. *Adv Wound Care (New Rochelle)* (2015) 4:235–49. doi: 10.1089/wound.2014.0555
30. Teng YH, Aquino RS, Park PW. Molecular Functions of Syndecan-1 in Disease. *Matrix Biol* (2012) 31:3–16. doi: 10.1016/j.matbio.2011.10.001
31. Friedlander M, Brooks PC, Shaffer RW, Kincaid CM, Varner JA, Cheresh DA. Definition of Two Angiogenic Pathways by Distinct Alpha V Integrins. *Science* (1995) 270:1500–2. doi: 10.1126/science.270.5241.1500
32. Adams TE, Epa VC, Garrett TP, Ward CW. Structure and Function of the Type 1 Insulin-Like Growth Factor Receptor. *Cell Mol Life Sci* (2000) 57:1050–93. doi: 10.1007/PL00000744
33. Liu JP, Baker J, Perkins AS, Robertson EJ, Efstratiadis A. Mice Carrying Null Mutations of the Genes Encoding Insulin-Like Growth Factor I (Igf-1) and Type 1 IGF Receptor (Igf1r). *Cell* (1993) 75:59–72. doi: 10.1016/S0092-8674(05)80084-4

34. Baserga R, Peruzzi F, Reiss K. The IGF-1 Receptor in Cancer Biology. *Int J Cancer* (2003) 107:873–7. doi: 10.1002/ijc.11487
35. Chitnis MM, Yuen JS, Protheroe AS, Pollak M, Macaulay VM. The Type 1 Insulin-Like Growth Factor Receptor Pathway. *Clin Cancer Res* (2008) 14:6364–70. doi: 10.1158/1078-0432.CCR-07-4879
36. Clemmons DR, Maile LA. Minireview: Integral Membrane Proteins That Function Coordinately With the Insulin-Like Growth Factor I Receptor to Regulate Intracellular Signaling. *Endocrinology* (2003) 144:1664–70. doi: 10.1210/en.2002-221102
37. Ling Y, Maile LA, Badley-Clarke J, Clemmons DR. DOK1 Mediates SHP-2 Binding to the Alphavbeta3 Integrin and Thereby Regulates Insulin-Like Growth Factor I Signaling in Cultured Vascular Smooth Muscle Cells. *J Biol Chem* (2005) 280:3151–8. doi: 10.1074/jbc.M411035200
38. Maile LA, Clemmons DR. Integrin-Associated Protein Binding Domain of Thrombospondin-1 Enhances Insulin-Like Growth Factor-I Receptor Signaling in Vascular Smooth Muscle Cells. *Circ Res* (2003) 93:925–31. doi: 10.1161/01.RES.0000101754.33652.B7
39. Beauvais DM, Ell BJ, McWhorter AR, Rapraeger AC. Syndecan-1 Regulates Alphavbeta3 and Alphavbeta5 Integrin Activation During Angiogenesis and is Blocked by Synstatin, a Novel Peptide Inhibitor. *J Exp Med* (2009) 206:691–705. doi: 10.1084/jem.20081278
40. Beauvais DM, Jung O, Yang Y, Sanderson RD, Rapraeger AC. Syndecan-1 (CD138) Suppresses Apoptosis in Multiple Myeloma by Activating IGF1 Receptor: Prevention by SynstatinIGF1R Inhibits Tumor Growth. *Cancer Res* (2016) 76:4981–93. doi: 10.1158/0008-5472.CAN-16-0232
41. Beauvais DM, Rapraeger AC. Syndecan-1 Couples the Insulin-Like Growth Factor-1 Receptor to Inside-Out Integrin Activation. *J Cell Sci* (2010) 123:3796–807. doi: 10.1242/jcs.067645
42. McQuade KJ, Beauvais DM, Burbach BJ, Rapraeger AC. Syndecan-1 Regulates Alphavbeta5 Integrin Activity in B82L Fibroblasts. *J Cell Sci* (2006) 119:2445–56. doi: 10.1242/jcs.02970
43. Yee D. A Tale of Two Receptors: Insulin and Insulin-Like Growth Factor Signaling in Cancer. *Clin Cancer Res* (2015) 21:667–9. doi: 10.1158/1078-0432.CCR-14-2056
44. Rapraeger AC, Ell BJ, Roy M, Li X, Morrison OR, Thomas GM, et al. Vascular Endothelial-Cadherin Stimulates Syndecan-1-Coupled Insulin-Like Growth Factor-1 Receptor and Cross-Talk Between Alphavbeta3 Integrin and Vascular Endothelial Growth Factor Receptor 2 at the Onset of Endothelial Cell Dissemination During Angiogenesis. *FEBS J* (2013) 280:2194–206. doi: 10.1111/febs.12134
45. Carmeliet P, Lampugnani MG, Moons L, Breviario F, Compernolle V, Bono F, et al. Targeted Deficiency or Cytosolic Truncation of the VE-Cadherin Gene in Mice Impairs VEGF-Mediated Endothelial Survival and Angiogenesis. *Cell* (1999) 98:147–57. doi: 10.1016/S0092-8674(00)81010-7
46. Liao F, Li Y, O'Connor W, Zanetta L, Bassi R, Santiago A, et al. Monoclonal Antibody to Vascular Endothelial-Cadherin Is a Potent Inhibitor of Angiogenesis, Tumor Growth, and Metastasis. *Cancer Res* (2000) 60:6805–10.
47. Lin FR, Huang SY, Hung KH, Su ST, Chung CH, Matsuzawa A, et al. ASK1 Promotes Apoptosis of Normal and Malignant Plasma Cells. *Blood* (2012) 120:1039–47. doi: 10.1182/blood-2011-12-399808
48. Galvan V, Logvinova A, Sperandio S, Ichijo H, Bredesen DE. Type 1 Insulin-Like Growth Factor Receptor (IGF-IR) Signaling Inhibits Apoptosis Signal-Regulating Kinase 1 (ASK1). *J Biol Chem* (2003) 278:13325–32. doi: 10.1074/jbc.M211398200
49. Hattori K, Naguro I, Runchel C, Ichijo H. The Roles of ASK Family Proteins in Stress Responses and Diseases. *Cell commun Signaling CCS* (2009) 7:9. doi: 10.1186/1478-811X-7-9
50. Li J, Choi E, Yu H, Bai XC. Structural Basis of the Activation of Type 1 Insulin-Like Growth Factor Receptor. *Nat Commun* (2019) 10:4567. doi: 10.1038/s41467-019-12564-0
51. Schlesinger M, Bendas G. Contribution of Very Late Antigen-4 (VLA-4) Integrin to Cancer Progression and Metastasis. *Cancer Metastasis Rev* (2015) 34:575–91. doi: 10.1007/s10555-014-9545-x
52. Humphries JD, Byron A, Humphries MJ. Integrin Ligands at a Glance. *J Cell Sci* (2006) 119:3901–3. doi: 10.1242/jcs.03098
53. Garmy-Susini B, Avraamides CJ, Schmid MC, Foubert P, Ellies LG, Barnes L, et al. Integrin Alpha4beta1 Signaling is Required for Lymphangiogenesis and Tumor Metastasis. *Cancer Res* (2010) 70:3042–51. doi: 10.1158/0008-5472.CAN-09-3761
54. Goldfinger LE, Tzima E, Stockton R, Kiosses WB, Kinbara K, Tkachenko E, et al. Localized Alpha4 Integrin Phosphorylation Directs Shear Stress-Induced Endothelial Cell Alignment. *Circ Res* (2008) 103:177–85. doi: 10.1161/CIRCRESAHA.108.176354
55. Han J, Liu S, Rose DM, Schlaepfer DD, McDonald H, Ginsberg MH. Phosphorylation of the Integrin Alpha 4 Cytoplasmic Domain Regulates Paxillin Binding. *J Biol Chem* (2001) 276:40903–9. doi: 10.1074/jbc.M102665200
56. Nishiya N, Kiosses WB, Han J, Ginsberg MH. An Alpha4 Integrin-Paxillin-Arf-GAP Complex Restricts Rac Activation to the Leading Edge of Migrating Cells. *Nat Cell Biol* (2005) 7:343–52. doi: 10.1038/ncb1234
57. Rose DM, Liu S, Woodside DG, Han J, Schlaepfer DD, Ginsberg MH. Paxillin Binding to the Alpha 4 Integrin Subunit Stimulates LFA-1 (Integrin Alpha L Beta 2)-Dependent T Cell Migration by Augmenting the Activation of Focal Adhesion Kinase/Proline-Rich Tyrosine Kinase-2. *J Immunol* (2003) 170:5912–8. doi: 10.4049/jimmunol.170.12.5912
58. Rose DM, Alon R, Ginsberg MH. Integrin Modulation and Signaling in Leukocyte Adhesion and Migration. *Immunol Rev* (2007) 218:126–34. doi: 10.1111/j.1600-065X.2007.00536.x
59. Goldfinger LE, Han J, Kiosses WB, Howe AK, Ginsberg MH. Spatial Restriction of Alpha4 Integrin Phosphorylation Regulates Lamellipodial Stability and Alpha4beta1-Dependent Cell Migration. *J Cell Biol* (2003) 162:731–41. doi: 10.1083/jcb.200304031
60. Jung O, Trapp-Stamborski V, Purushothaman A, Jin H, Wang H, Sanderson RD, et al. Heparanase-Induced Shedding of Syndecan-1/CD138 in Myeloma and Endothelial Cells Activates VEGFR2 and an Invasive Phenotype: Prevention by Novel Synstatins. *Oncogenesis* (2016) 5:e202. doi: 10.1038/oncsis.2016.5
61. Fux L, Ilan N, Sanderson RD, Vlodavsky I. Heparanase: Busy at the Cell Surface. *Trends Biochem Sci* (2009) 34:511–9. doi: 10.1016/j.tibs.2009.06.005
62. Ramani VC, Purushothaman A, Stewart MD, Thompson CA, Vlodavsky I, Au JL, et al. The Heparanase/Syndecan-1 Axis in Cancer: Mechanisms and Therapies. *FEBS J* (2013) 280:2294–306. doi: 10.1111/febs.12168
63. Sanderson RD, Yang Y. Syndecan-1: A Dynamic Regulator of the Myeloma Microenvironment. *Clin Exp metastasis* (2008) 25:149–59. doi: 10.1007/s10585-007-9125-3
64. Jung O, Beauvais DM, Adams KM, Rapraeger AC. VLA-4 Phosphorylation During Tumor and Immune Cell Migration Relies on its Coupling to VEGFR2 and CXCR4 by Syndecan-1. *J Cell Sci* (2019) 132:1–14. doi: 10.1242/jcs.232645
65. Fredriksson R, Lagerstrom MC, Lundin LG, Schioth HB. The G-Protein-Coupled Receptors in the Human Genome Form Five Main Families. Phylogenetic Analysis, Paralogon Groups, and Fingerprints. *Mol Pharmacol* (2003) 63:1256–72. doi: 10.1124/mol.63.6.1256
66. Lamorte S, Ferrero S, Aschero S, Monitillo L, Bussolati B, Omede P, et al. Syndecan-1 Promotes the Angiogenic Phenotype of Multiple Myeloma Endothelial Cells. *Leukemia* (2012) 26:1081–90. doi: 10.1038/leu.2011.290
67. Orecchia P, Conte R, Balza E, Petretto A, Mauri P, Mingari MC, et al. A Novel Human Anti-Syndecan-1 Antibody Inhibits Vascular Maturation and Tumour Growth in Melanoma. *Eur J Cancer* (2013) 49:2022–33. doi: 10.1016/j.ejca.2012.12.019
68. Chan JR, Hyduk SJ, Cybulsky MI. Alpha 4 Beta 1 Integrin/VCAM-1 Interaction Activates Alpha L Beta 2 Integrin-Mediated Adhesion to ICAM-1 in Human T Cells. *J Immunol* (2000) 164:746–53. doi: 10.4049/jimmunol.164.2.746
69. May AE, Neumann FJ, Schomig A, Preissner KT. VLA-4 (Alpha(4)Beta(1)) Engagement Defines a Novel Activation Pathway for Beta(2) Integrin-Dependent Leukocyte Adhesion Involving the Urokinase Receptor. *Blood* (2000) 96:506–13. doi: 10.1182/blood.V96.2.506.014k41_506_513
70. Alon R, Kassner PD, Carr MW, Finger EB, Hemler ME, Springer TA. The Integrin VLA-4 Supports Tethering and Rolling in Flow on VCAM-1. *J Cell Biol* (1995) 128:1243–53. doi: 10.1083/jcb.128.6.1243
71. Cantor JM, Rose DM, Slepak M, Ginsberg MH. Fine-Tuning Tumor Immunity With Integrin Trans-Regulation. *Cancer Immunol Res* (2015) 3:661–7. doi: 10.1158/2326-6066.CIR-13-0226

72. Sanderson RD, Elkin M, Rapraeger AC, Ilan N, Vlodavsky I. Heparanase Regulation of Cancer, Autophagy and Inflammation: New Mechanisms and Targets for Therapy. *FEBS J* (2017) 284:42–55. doi: 10.1111/febs.13932
73. Teixeira F, Gotte M. Involvement of Syndecan-1 and Heparanase in Cancer and Inflammation. *Adv Exp Med Biol* (2020) 1221:97–135. doi: 10.1007/978-3-030-34521-1_4
74. Seidel C, Sundan A, Hjorth M, Turesson I, Dahl IM, Abildgaard N, et al. Serum Syndecan-1: A New Independent Prognostic Marker in Multiple Myeloma. *Blood* (2000) 95:388–92. doi: 10.1182/blood.V95.2.388
75. Dhodapkar MV, Kelly T, Theus A, Athota AB, Barlogie B, Sanderson RD. Elevated Levels of Shed Syndecan-1 Correlate With Tumour Mass and Decreased Matrix Metalloproteinase-9 Activity in the Serum of Patients With Multiple Myeloma. *Br J Haematol* (1997) 99:368–71. doi: 10.1046/j.1365-2141.1997.3893203.x
76. Rangarajan S, Richter JR, Richter RP, Bandari SK, Tripathi K, Vlodavsky I, et al. Heparanase-Enhanced Shedding of Syndecan-1 and Its Role in Driving Disease Pathogenesis and Progression. *J Histochem Cytochem* (2020) 68:823–40. doi: 10.1369/0022155420937087
77. Feral CC, Rose DM, Han J, Fox N, Silverman GJ, Kaushansky K, et al. Blocking the Alpha 4 Integrin-Paxillin Interaction Selectively Impairs Mononuclear Leukocyte Recruitment to an Inflammatory Site. *J Clin Invest* (2006) 116:715–23. doi: 10.1172/JCI26091
78. Koster J, Geerts D, Favre B, Borradori L, Sonnenberg A. Analysis of the Interactions Between BP180, BP230, Plectin and the Integrin Alpha6beta4 Important for Hemidesmosome Assembly. *J Cell Sci* (2003) 116:387–99. doi: 10.1242/jcs.00241
79. Jones JC, Hopkinson SB, Goldfinger LE. Structure and Assembly of Hemidesmosomes. *Bioessays* (1998) 20:488–94. doi: 10.1002/(SICI)1521-1878(199806)20:6<488::AID-BIES7>3.0.CO;2-I
80. Stepp MA, Spurr-Michaud S, Tisdale A, Elwell J, Gipson IK. Alpha 6 Beta 4 Integrin Heterodimer is a Component of Hemidesmosomes. *Proc Natl Acad Sci USA* (1990) 87:8970–4. doi: 10.1073/pnas.87.22.8970
81. Wang H, Jin H, Beauvais DM, Rapraeger AC. Cytoplasmic Domain Interactions of Syndecan-1 and Syndecan-4 With Alpha6beta4 Integrin Mediate Human Epidermal Growth Factor Receptor (HER1 and HER2)-Dependent Motility and Survival. *J Biol Chem* (2014) 289:30318–32. doi: 10.1074/jbc.M114.586438
82. Wang H, Leavitt L, Ramaswamy R, Rapraeger AC. Interaction of Syndecan and Alpha6beta4 Integrin Cytoplasmic Domains: Regulation of ErbB2-Mediated Integrin Activation. *J Biol Chem* (2010) 285:13569–79. doi: 10.1074/jbc.M110.102137
83. Wang H, Jin H, Rapraeger AC. Syndecan-1 and Syndecan-4 Capture Epidermal Growth Factor Receptor Family Members and the Alpha3beta1 Integrin Via Binding Sites in Their Ectodomains: Novel Synstatins Prevent Kinase Capture and Inhibit Alpha6beta4-Integrin-Dependent Epithelial Cell Motility. *J Biol Chem* (2015) 290:26103–13. doi: 10.1074/jbc.M115.679084
84. Rezniczek GA, de Pereda JM, Reipert S, Wiche G. Linking Integrin Alpha6beta4-Based Cell Adhesion to the Intermediate Filament Cytoskeleton: Direct Interaction Between the Beta4 Subunit and Plectin at Multiple Molecular Sites. *J Cell Biol* (1998) 141:209–25. doi: 10.1083/jcb.141.1.209
85. Geerts D, Fontao L, Nievers MG, Schaapveld RQ, Purkis PE, Wheeler GN, et al. Binding of Integrin Alpha6beta4 to Plectin Prevents Plectin Association With F-Actin But Does Not Interfere With Intermediate Filament Binding. *J Cell Biol* (1999) 147:417–34. doi: 10.1083/jcb.147.2.417
86. Margadant C, Frijns E, Wilhelmsen K, Sonnenberg A. Regulation of Hemidesmosome Disassembly by Growth Factor Receptors. *Curr Opin Cell Biol* (2008) 20:589–96. doi: 10.1016/j.ceb.2008.05.001
87. Wilhelmsen K, Litjens SH, Kuikman I, Margadant C, van Rheenen J, Sonnenberg A. Serine Phosphorylation of the Integrin Beta4 Subunit Is Necessary for Epidermal Growth Factor Receptor Induced Hemidesmosome Disruption. *Mol Biol Cell* (2007) 18:3512–22. doi: 10.1091/mbc.e07-04-0306
88. Dans M, Gagnoux-Palacios L, Blaikie P, Klein S, Mariotti A, Giancotti FG. Tyrosine Phosphorylation of the Beta 4 Integrin Cytoplasmic Domain Mediates Shc Signaling to Extracellular Signal-Regulated Kinase and Antagonizes Formation of Hemidesmosomes. *J Biol Chem* (2001) 276:1494–502. doi: 10.1074/jbc.M008663200
89. Dutta U, Shaw LM. A Key Tyrosine (Y1494) in the Beta4 Integrin Regulates Multiple Signaling Pathways Important for Tumor Development and Progression. *Cancer Res* (2008) 68:8779–87. doi: 10.1158/0008-5472.CAN-08-2125
90. Merdek KD, Yang X, Taglienti CA, Shaw LM, Mercurio AM. Intrinsic Signaling Functions of the Beta4 Integrin Intracellular Domain. *J Biol Chem* (2007) 282:30322–30. doi: 10.1074/jbc.M703156200
91. Shaw LM. Identification of Insulin Receptor Substrate 1 (IRS-1) and IRS-2 as Signaling Intermediates in the Alpha6beta4 Integrin-Dependent Activation of Phosphoinositide 3-OH Kinase and Promotion of Invasion. *Mol Cell Biol* (2001) 21:5082–93. doi: 10.1128/MCB.21.15.5082-5093.2001
92. Yang X, Dutta U, Shaw LM. SHP2 Mediates the Localized Activation of Fyn Downstream of the Alpha6beta4 Integrin to Promote Carcinoma Invasion. *Mol Cell Biol* (2010) 30:5306–17. doi: 10.1128/MCB.00326-10
93. Sehgal BU, DeBiase PJ, Matzno S, Chew TL, Claiborne JN, Hopkinson SB, et al. Integrin Beta4 Regulates Migratory Behavior of Keratinocytes by Determining Laminin-332 Organization. *J Biol Chem* (2006) 281:35487–98. doi: 10.1074/jbc.M606317200
94. Dajee M, Lazarov M, Zhang JY, Cai T, Green CL, Russell AJ, et al. NF-kappaB Blockade and Oncogenic Ras Trigger Invasive Human Epidermal Neoplasia. *Nature* (2003) 421:639–43. doi: 10.1038/nature01283
95. Marinkovich MP. Tumour Microenvironment: Laminin 332 in Squamous-Cell Carcinoma. *Nat Rev Cancer* (2007) 7:370–80. doi: 10.1038/nrc2089
96. Nikolopoulos SN, Blaikie P, Yoshioka T, Guo W, Giancotti FG. Integrin Beta4 Signaling Promotes Tumor Angiogenesis. *Cancer Cell* (2004) 6:471–83. doi: 10.1016/j.ccr.2004.09.029
97. Yoshioka T, Otero J, Chen Y, Kim YM, Koutcher JA, Satagopan J, et al. Beta4 Integrin Signaling Induces Expansion of Prostate Tumor Progenitors. *J Clin Invest* (2013) 123:682–99. doi: 10.1172/JCI60720
98. McFall AJ, Rapraeger AC. Identification of an Adhesion Site Within the Syndecan-4 Extracellular Protein Domain. *J Biol Chem* (1997) 272:12901–4. doi: 10.1074/jbc.272.20.12901
99. McFall AJ, Rapraeger AC. Characterization of the High Affinity Cell-Binding Domain in the Cell Surface Proteoglycan Syndecan-4. *J Biol Chem* (1998) 273:28270–6. doi: 10.1074/jbc.273.43.28270
100. Whiteford JR, Couchman JR. A Conserved NXIP Motif is Required for Cell Adhesion Properties of the Syndecan-4 Ectodomain. *J Biol Chem* (2006) 281:32156–63. doi: 10.1074/jbc.M605553200
101. Zhang X, Gureasko J, Shen K, Cole PA, Kuriyan J. An Allosteric Mechanism for Activation of the Kinase Domain of Epidermal Growth Factor Receptor. *Cell* (2006) 125:1137–49. doi: 10.1016/j.cell.2006.05.013
102. Garrett TP, McKern NM, Lou M, Elleman TC, Adams TE, Lovrecz GO, et al. Crystal Structure of a Truncated Epidermal Growth Factor Receptor Extracellular Domain Bound to Transforming Growth Factor Alpha. *Cell* (2002) 110:763–73. doi: 10.1016/S0092-8674(02)00940-6
103. Ogiso H, Ishitani R, Nureki O, Fukai S, Yamanaka M, Kim JH, et al. Crystal Structure of the Complex of Human Epidermal Growth Factor and Receptor Extracellular Domains. *Cell* (2002) 110:775–87. doi: 10.1016/S0092-8674(02)00963-7
104. Ferguson KM, Berger MB, Mendrola JM, Cho HS, Leahy DJ, Lemmon MA. EGF Activates its Receptor by Removing Interactions That Autoinhibit Ectodomain Dimerization. *Mol Cell* (2003) 11:507–17. doi: 10.1016/S1097-2765(03)00047-9
105. Cho HS, Mason K, Ramyar KX, Stanley AM, Gabelli SB, Denney DW Jr, et al. Structure of the Extracellular Region of HER2 Alone and in Complex With the Herceptin Fab. *Nature* (2003) 421:756–60. doi: 10.1038/nature01392

Conflict of Interest: The author declares that the research was conducted in the absence of any commercial or financial relationships that could be construed as a potential conflict of interest.

Publisher's Note: All claims expressed in this article are solely those of the authors and do not necessarily represent those of their affiliated organizations, or those of the publisher, the editors and the reviewers. Any product that may be evaluated in this article, or claim that may be made by its manufacturer, is not guaranteed or endorsed by the publisher.

Copyright © 2021 Rapraeger. This is an open-access article distributed under the terms of the Creative Commons Attribution License (CC BY). The use, distribution or reproduction in other forums is permitted, provided the original author(s) and the copyright owner(s) are credited and that the original publication in this journal is cited, in accordance with accepted academic practice. No use, distribution or reproduction is permitted which does not comply with these terms.

frontiers in Oncology

REVIEW
published: 11 November 2021
doi: 10.3389/fonc.2021.778752

Heparan Sulfate Biosynthesis and Sulfation Profiles as Modulators of Cancer Signalling and Progression

Catarina Marques[1,2,3], *Celso A. Reis*[1,2,4,5], *Romain R. Vivès*[6] *and Ana Magalhães*[1,2,4*]

[1] Instituto de Investigação e Inovação em Saúde (i3S), Universidade do Porto, Porto, Portugal, [2] Instituto de Patologia e Imunologia Molecular da Universidade do Porto (IPATIMUP), Porto, Portugal, [3] Programa Doutoral em Biologia Molecular e Celular (MCbiology), Instituto de Ciências Biomédicas Abel Salazar (ICBAS), Universidade do Porto, Porto, Portugal, [4] Instituto de Ciências Biomédicas Abel Salazar (ICBAS), Universidade do Porto, Porto, Portugal, [5] Faculdade de Medicina da Universidade do Porto (FMUP), Porto, Portugal, [6] Univ. Grenoble Alpes, CNRS, CEA, IBS, Grenoble, France

Heparan Sulfate Proteoglycans (HSPGs) are important cell surface and Extracellular Matrix (ECM) maestros involved in the orchestration of multiple cellular events in physiology and pathology. These glycoconjugates bind to various bioactive proteins *via* their Heparan Sulfate (HS) chains, but also through the protein backbone, and function as scaffolds for protein-protein interactions, modulating extracellular ligand gradients, cell signalling networks and cell-cell/cell-ECM interactions. The structural features of HS chains, including length and sulfation patterns, are crucial for the biological roles displayed by HSPGs, as these features determine HS chains binding affinities and selectivity. The large HS structural diversity results from a tightly controlled biosynthetic pathway that is differently regulated in different organs, stages of development and pathologies, including cancer. This review addresses the regulatory mechanisms underlying HS biosynthesis, with a particular focus on the catalytic activity of the enzymes responsible for HS glycan sequences and sulfation motifs, namely D-Glucuronyl C5-Epimerase, N- and O-Sulfotransferases. Moreover, we provide insights on the impact of different HS structural epitopes over HSPG-protein interactions and cell signalling, as well as on the effects of deregulated expression of HS modifying enzymes in the development and progression of cancer. Finally, we discuss the clinical potential of HS biosynthetic enzymes as novel targets for therapy, and highlight the importance of developing new HS-based tools for better patients' stratification and cancer treatment.

Keywords: cancer, cell signalling, glycosyltransferases, glycosaminoglycan, heparan sulfate, heparan sulfate binding epitopes, sulfotransferases

OPEN ACCESS

Edited by:
Nikos Karamanos, University of Patras, Greece

Reviewed by:
Luigi Michele Pavone, University of Naples Federico II, Italy
Dimitrios Moschonas, Royal Surrey County Hospital, United Kingdom

***Correspondence:**
Ana Magalhães
amagalhaes@ipatimup.pt

Specialty section:
This article was submitted to Molecular and Cellular Oncology, a section of the journal Frontiers in Oncology

Received: *17 September 2021*
Accepted: *15 October 2021*
Published: *11 November 2021*

Citation:
Marques C, Reis CA, Vivès RR and Magalhães A (2021) Heparan Sulfate Biosynthesis and Sulfation Profiles as Modulators of Cancer Signalling and Progression. Front. Oncol. 11:778752. doi: 10.3389/fonc.2021.778752

INTRODUCTION

Heparan Sulfate Proteoglycans (HSPGs) are important glycoconjugates ubiquitously expressed on cells glycocalyx and Extracellular Matrix (ECM), as well as in secreted extracellular vesicles (1–3). These macromolecules control several regulatory mechanisms related to the formation of extracellular gradients, cellular growth and proliferation, cell adhesion, migration and invasion, membrane trafficking and angiogenesis (4, 5). By interfering with these cellular events, HSPGs

display important functions both in physiology and pathology, controlling embryonic development, ECM assembly and maintenance, tissue remodelling, metabolism homeostasis, pathogen invasion and inflammation (6–12). Particularly in cancer, HSPGs and HS chains hold very relevant roles in the development and progression of the disease. Their interaction with different ligands and structural proteins, and modulation of several signalling networks, prompts their active participation in cell transformation and proliferation, tumour growth and metastasis, amongst other cell oncogenic events (2, 12, 13), highlighting the fundamental need of further studying HS biosynthesis in the context of cancer.

HSPGs are composed by a core protein to which Heparan Sulfate (HS) polysaccharide chains are covalently attached, and can be differentially classified according to (i) their cellular and subcellular localization; (ii) PGs core protein homology; and (iii) function (14). HS is an anionic, long and linear glycosaminoglycan (GAG) chain consisting of repeating disaccharide units of N-acetyl-glucosamine (GlcNAc) and hexuronic acid residues, that can be either glucuronic acid (GlcA) or its C5 epimer, iduronic acid (IdoA) (1). The biosynthesis of HS chains occurs at the endoplasmic reticulum-Golgi apparatus interface and in the Golgi apparatus, and includes: i) assembly of a GAG-protein linker, which initiates the covalent binding of HS to proteoglycan core proteins; ii) the polymerization of the HS chain; and iii) the structural modification of the elongated chain (8). The first two stages of HS biosynthesis involve the sequential transfer of sugar residues to the growing chain and are catalysed by different glycosyltransferases. The polymerized chain then undergoes maturation by several HS modifying enzymes, including N-Deacetylase/N-Sulfotransferases (NDSTs), D-Glucuronyl C5-Epimerase (GLCE) and different O-Sulfotransferases (2OST, 6OSTs, 3OSTs) (15). Finally, further modifications of HS structure take place post-synthetically, through the action of 6-O-endosulfatases Sulf-1 and Sulf-2, and Heparanase (16, 17). Structural modification reactions catalysed by these enzymes modulate glycan chain length, epimerization and sulfation profiles, resulting in the synthesis of HS chains with extremely high structural variability (8). These features are key for regulating HSPG biological roles, since they dictate HS-protein binding affinity and selectivity. HS sulfation degree and patterns are particularly relevant, giving rise to highly negatively charged regions and further promoting non-covalent ionic bonding between HS and positively charged amino acid residues in multiple protein targets, including transmembrane receptors, ECM structural proteins and soluble molecules (18). These features allow HSPGs to participate in signalling cascades and take over a range of cell regulatory events. However, the molecular mechanisms promoting the synthesis of particular HS structures are still largely unknown. Furthermore, only a few specific HS sequences have been identified as essential motifs for HS-protein interactions. A significant limitation in studies that aim to uncover HS-ligand binding specificities is the frequent use of heparin and/or short oligosaccharides, which only partially mimic HS natural complexity. The structural details of HSPG interactomes remains therefore mostly unexplored.

HS BIOSYNTHESIS AND MODIFICATION

Biosynthetic Pathway

The biosynthesis of GAGs, and HS in particular, is not a template-driven process, meaning that the extent of modification reactions that the glycan chains may undergo, and the consequent HS final structural motifs, are not directly encoded in the genome. The current general view is that HS biosynthesis is regulated by the availability and expression levels of the enzymes involved in this pathway, and by the binding specificities of these enzymes towards the sequences that are formed in HS growing chains (19). Hence, the structural features resulting from each stage of HS biosynthesis determine subsequent modification reactions, contributing to the "step-by-step" fine tuning of HS overall structure. However, not all of the HS substrates are equally modified, thus giving rise to a great HS structural variability.

The majority of the enzymes that intervene and control HS biosynthesis are located in the Golgi apparatus and are classified as type II transmembrane proteins (15). A HS biosynthesis model has proposed that these enzymes are in tight interaction with each other, forming a supramolecular complex called "GAGosome", which ensures quick and concerted reactions towards the formation of the GAG chains (20). However, the regulatory mechanisms underlying the activity of this possible enzymatic machinery complex and its impact in HS high structural variability are not yet fully disclosed.

HS biosynthesis is initiated by the formation of a universal tetrasaccharide linker covalently attached to the core protein of all GAG bearing proteoglycans, including HSPGs. Assembly of this tetrasaccharide linker starts with the transfer of a xylose (Xyl) residue to specific protein serine amino acids by two O-Xylosyltransferases (XYLT1 and XYLT2) (**Figure 1**) (22). This is followed by the sequential transfer of two galactose (Gal) residues, successively added by the Galactosyltransferase-I/β4-Galactosyltransferase 7 (β4Gal-T7) and the Galactosyltransferase-II/β3-Galactosyltransferase 6 (β3Gal-T6), and lastly by the addition of one GlcA residue by the Glucuronyltransferase-I (GlcAT-I), to form the linker GlcAβ1-3Gal-β1-3Gal-β1-4Xyl-β1-O-Ser. During this assembly, transient phosphorylation of the Xyl residue by the kinase FAM20B and dephosphorylation by the 2-Phosphoxylose phosphatase (XYLP) also take place, which enhance the activity of β3Gal-T6, further promoting the maturation of the linker (23, 24). The polymerization of HS chains is then initiated by the transfer of a GlcNAc residue to the tetrasaccharide linker, which is regulated by Exostosin Like 2 (EXTL2) (25) and EXTL3 glycosyltransferases (26), and is followed by further chain elongation promoted by a hetero-oligomeric complex formed by EXT1 and EXT2, which catalyses the alternate transfer of GlcNAc and GlcA residues (**Figure 1**) (27). Polymerized HS chains then undergo extensive processing and modification reactions that give rise to fully mature HS chains, which are the main focus of this review.

Catalytic Activity of HS Modifying Enzymes

N-Deacetylation and *N*-Sulfation

During the HS modification stage, native HS polysaccharides, consisting of unmodified repeating GlcNAc residues linked to

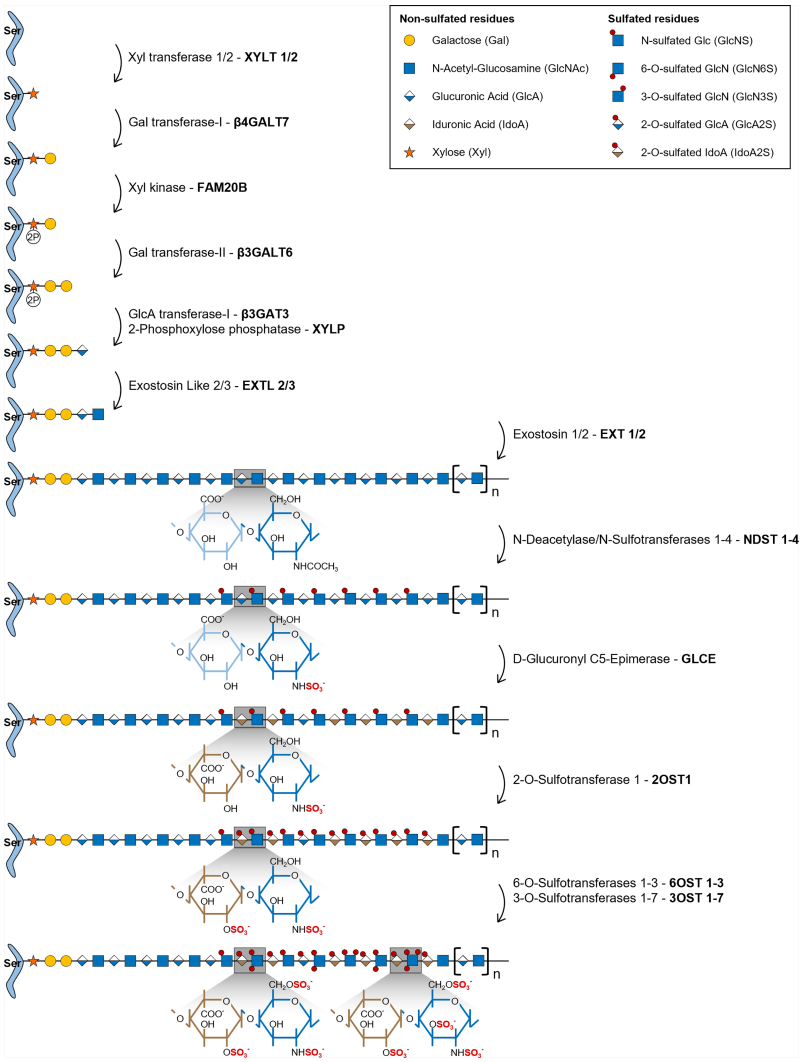

FIGURE 1 | Illustrative representation of the HS biosynthetic pathway and the disaccharide structural changes that occur during each modification reaction. HS biosynthesis comprises the stepwise transfer of different sugar residues that leads to the elongation of HS chains. In the last stage of this biosynthetic pathway, polymerized HS chains undergo multiple modification reactions: i) NDSTs 1-4 catalyse the removal of the acetyl group from GlcNAc residues and the transfer of a sulfate group to free amino groups to form GlcNS; ii) GLCE epimerizes GlcA residues into IdoA; iii) these residues are then targeted by 2OST1, that transfers sulfate groups to the C2-position of IdoA (more rarely GlcA),thereby preventing further epimerization; iv) lastly, 6OSTs 1-3 and 3OSTs 1-7 add sulfate groups to the C6- and C3-positions of GlcN residues, respectively. Chains non-reducing termini are to the right of the saccharide's sequences. Glycan structures are represented according to the Symbol Nomenclature for Glycans (SNFG) (21).

GlcA, are initially targeted by N-Deacetylase/N-Sulfotransferases 1-4 (NDSTs 1-4), that remove *N*-acetyl groups from GlcNAc residues and transfer a sulfate group to the generated free amino groups to form *N*-sulfated glucosamine residues (GlcNS) (**Figure 1**). This first modification is essential to all the remaining reactions that take place in the Golgi, since most of the modifying enzymes act on GlcNS containing motifs (20). Of note, a small subset of *N*-deacetylated residues do not undergo *N*-sulfation, giving rise to unsubstituted glucosamine molecules ($GlcNH_3$), which elicit specific biological functions (1, 19). In vertebrates, NDST1 and NDST2 are the most widely expressed isoforms, occurring in several tissues, while NDST3 and NDST4 are more expressed at the embryonic stage and adult brain (28). The different isoforms also vary in their activity, NDST1 and NDST2 have similar *N*-deacetylase/*N*-sulfotransferase ratio activity, while NDST3 and NDST4 exhibit opposite trends, with NDST3 presenting the lowest sulfotransferase capacity (28) and NDST4 the lowest *N*-deacetylase activity (29) of all four enzymes.

Epimerization and 2-*O*-Sulfation

HS chains are subsequently modified by D-Glucuronyl C5-Epimerase (GLCE), which catalyses the epimerization of D-GlcA residues into L-IdoA (**Figure 1**) (30). This enzyme

targets specifically GlcA residues located at the reducing side of GlcNS residues and catalyses both irreversible and reversible epimerization, since it can also convert IdoA units back to GlcA (31). This "two-way" catalytic activity was observed through *in vitro* enzymatic assays and it was shown to depend upon HS *N*-sulfation patterns (GlcNS vs GlcNAc content) (32).

2OST1 catalyses then the transfer of sulfate groups to the C2-position of both GlcA and IdoA residues, although with significantly increased efficiency towards the later, displaying around five-fold higher affinity to epimerized IdoA units (**Figure 1**) (33). 2-*O*-sulfation of IdoA residues prevents their reverse epimerization into GlcA, since GLCE cannot use IdoA2S as substrate, which promotes accumulation of these residues on HS chains (34). In addition, it has been proposed that 2-*O*-sulfated GlcA residues (GlcA2S), generated at a smaller extent in HS chains, might result from early 2-*O*-sulfation, prior to the epimerization of GlcA, blocking the subsequent activity of GLCE and conversion of those residues into IdoA (35). Moreover, as a prerequisite for 2OST1 efficient activity, the targeted GlcA or IdoA residues must also be flanked by two GlcNS residues, instead of GlcNAc (36).

These structural alterations that ultimately dictate HS GlcA/IdoA ratio are of extreme relevance for HS functional diversity, since GlcA to IdoA epimerization confers higher structural flexibility to HS chains, which is reflected on HS-protein binding properties (30).

6-*O*-Sulfation and 3-*O*-Sulfation

In the later stages of HS biosynthesis, 6-O-Sulfotransferases 1-3 (6OSTs 1-3) and 3-O-Sulfotransferases 1-7 (3OSTs 1-7) add sulfate groups to the C6- and C3-positions of glucosamine (GlcN) residues, respectively, contributing to the formation of more heterogeneous HS structures (**Figure 1**) (37). 6OSTs have broader substrate recognition and 6-*O*-sulfation activity. Enzymatic assays performed with recombinant mouse 6OSTs 1-3 have shown that all isoforms can transfer sulfate groups to both GlcNAc and GlcNS residues attached to either GlcA or IdoA residues, although they target preferably IdoA-containing disaccharides (38). Furthermore, it was demonstrated that 2-*O*-sulfation of IdoA residues did not affect 6OST activity (38). Interestingly, a different study using heparin-based oligosaccharide libraries to assess 6OST preferred substrates, revealed that both 6OST2 and 6OST3 had higher specificity for oligosaccharides with higher content in 2-*O*-sulfation (39). Habuchi H. et al. have also reported that different 6OST isoforms expressed in mice had different specificities towards varied HS polysaccharide samples depending on their hexuronic acid content: 6OST1 targeted preferentially substrates containing IdoA-GlcNS disaccharide units, 6OST2 could act on both IdoA-GlcNS or GlcA-GlcNS motifs depending on substrate concentration, and 6OST3 utilized both substrates independently of substrate abundance (40). 6OST differential expression over different mouse organs was also reported, which supports tissue-dependent expression and consequent varying effects on HS structural motifs (40). 6-*O*-sulfation contributes to fine-tune the sequential biosynthesis of HS chains, since GlcA epimerization by GLCE is precluded by 6-*O*-sulfation of adjacent GlcN residues (34), and 2-*O*-sulfation of IdoA by 2OST1 is inhibited if the adjacent GlcN residue is 6-*O*-sulfated (36, 41). These data are in line with the described stepwise mechanism underlying HS biosynthesis, further supporting that epimerization and 2-*O*-sulfation reactions usually take place prior to 6-*O*-sulfation (**Figure 1**). More recently, it was uncovered that 6-*O*-sulfated HS oligosaccharides were able to bind to 2OST1, with higher affinity than 2OST1 direct substrates, and inhibit its catalytic activity (42). In light of these results, it was hypothesized that enzymes involved in the HS biosynthetic pathway might be temporarily and/or spatially separated from the intermediate substrates produced downstream on the Golgi. This would explain why HS modified structures do not impair the activity of initially acting sulfotransferases towards new native glycans (42).

Although 3OSTs constitute the largest family of HS sulfotransferases, composed by 7 isoforms (3OST-1, -2, -3a, -3b, -4, -5 and -6), GlcN 3-*O*-sulfation is the least frequent modification (8). The different isoforms exhibit specific binding affinity to GlcN residues linked to different hexuronic acid residues contributing to the functional diversity of HS chains. 3OST1 transfers sulfate groups to GlcNS and GlcNS6S bound to unsulfated GlcA and IdoA units (43, 44). *In vitro* enzymatic assays have revealed that murine 3OST1 activity is specifically inhibited by IdoA2S residues linked to the targeted GlcN residues, suggesting an additional layer of regulation, according to which HS 2-*O*-sulfation content impacts 3-*O*-sulfation patterns and overall levels (44). 3OST2 transfers sulfate groups to GlcNS residues attached to either GlcA2S or IdoA2S, while 3OST3A and 3OST3B isoforms act on GlcNS linked to IdoA2S (45). Later, it was also shown that the 3OST3A isoform can utilize substrates on rarer regions of HS motifs, including *N*-unsubstituted glucosamine ($GlcNH_3$) and *N*-unsubstituted 6-*O*-sulfated glucosamine ($GlcNH_26S$) residues linked to IdoA2S at the non-reducing end (46). 3OST4 and 3OST6 catalyse 3-*O*-sulfation on similar disaccharides targeted by 3OST3 isozymes (GlcN residues linked to IdoA2S residues at the non-reducing site) (47, 48). Lastly, 3OST5 was revealed to have a broader substrate specificity when compared with the other isoforms, targeting both $GlcNH_3$ and GlcNS residues at the reducing end of GlcA, IdoA and IdoA2S residues (49).

Post-Synthetic Modifications

Once HS chains are fully synthesized, and mature HSPGs are expressed at the cell surface, additional post-synthesis reactions can take place and further modify HS chains, namely 6-*O*-desulfation catalysed by 6-O-endosulfatases Sulf-1 and Sulf-2, and cleavage of the chains by Heparanase, thus generating additional structural diversity with biological relevance. These HS chain edition steps have been described in detail in (8, 17). Interestingly, there is evidence of an interplay between biosynthetic enzymatic activity and post-synthesis modification mechanisms. Lamanna W. C. et al. showed that Sulf-1 and/or Sulf-2 KO mice displayed HS structural changes that were not dependent directly on the Sulfs enzymatic activity, such as altered *N*- and 2-*O*-sulfation, which may be explained by the different HS sulfotransferase expression profile observed in these *in vivo* models (50).

HS SULFATION EPITOPES AND LIGAND BINDING SPECIFICITIES

HS chains feature two main types of structural domains: sulfated (S)-domains, enriched in highly modified disaccharides, i.e. sulfated hexuronic acid units linked to *O*-sulfated GlcNS residues, that are successively intercalated by *N*-acetylated (NA)-domains bearing mostly non-modified GlcNAc units linked predominantly to GlcA residues (**Figure 2**) (8, 51). HS S-domains are responsible for most of the polysaccharide biological activities, their epimerization level and sulfation patterns providing functional diversity. These features indeed modulate HS binding specificities to protein targets, and vary over different organs (52), developmental stages (53–55) and pathologies (56–58). Although most biomolecules interact with the S domains of HS chains, HSPGs can also bind ligands and transduce signal through their protein core (59, 60).

HS chains bind to multiple biologically active molecules, including growth factors, chemokines, cytokines, morphogens, extracellular structural proteins, enzymes involved in different biochemical pathways and transmembrane signalling receptors (5, 61). This prompts cell surface HSPGs to modulate main cellular events, by acting as co-receptors or scaffolds for protein-protein interactions, triggering receptors activation and subsequent signalling transduction, and as important mechanosignalling transducers of extracellular stimuli (13, 62). HSPGs not only enhance the activity of neighbouring receptors expressed on the same cell, but also participate in the transactivation of receptors, including key Receptor Tyrosine Kinases (RTKs), in adjacent cells, mediating cell-cell crosstalk (63). Recently, HSPGs have been shown to play a regulatory role in the activation of calcium channels, and it has been proposed a mechanism dependent on the cytosolic calcium levels, through which HSPGs modulate cells' cytoskeleton organization and adhesion (64). In the ECM, HSPGs can also function as storage units and contribute to the formation of extracellular gradients of varied soluble molecules, thereby modulating their availability (6).

The impact of HS overall sulfation degree *versus* specific sulfation patterns as determinants for HS-protein binding has been debated over a long time. It has been established that in the majority of cases tissue-dependent HS general sulfation, and sulfation distribution by blocks (S-domains and NA-domains), rather than unique sulfation sequences encoded in HS glycan chains, determine binding affinities (65). The current consensus is that *N*- and 2-*O*-sulfated units are involved in low specificity binding, 6-*O*-sulfated units in intermediate specificity binding and 3-*O*-sulfated and *N*-unsubstituted units are responsible for high specificity binding, which justifies the strong binding overlap of protein ligands towards HS with variable sulfation patterns reported in different HS-binding protein assays.

Low and Intermediate HS-Ligand Binding Specificities

Although unique and distinctive biologically active HS structural motifs have not been disclosed for most protein-HS interactions, distinct roles of the most common types of sulfation (*N*-, 2-*O*- and 6-*O*-sulfation) have been reported for protein binding affinities and biological activities. Basic Fibroblast Growth Factor (FGF2 or bFGF) was the first growth factor reported to depend upon cell surface HS as a co-receptor required for the formation of a biologically active FGFR-FGF2-HS ternary complex (66, 67). FGFs constitute a large family of mitogens involved in the regulation of cellular migration,

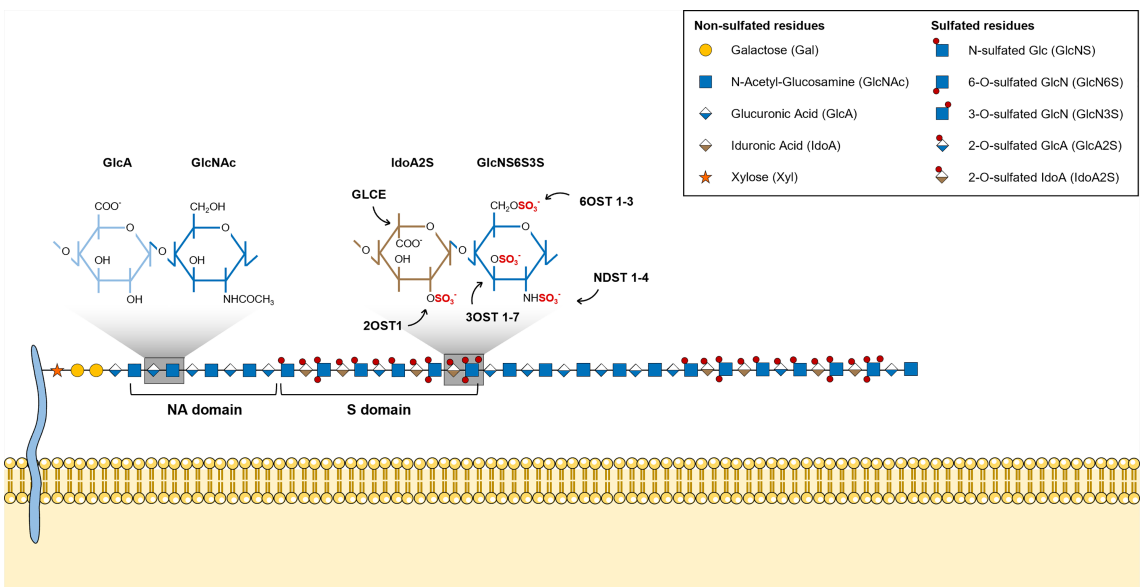

FIGURE 2 | Illustrative representation of a mature HS chain and its structural organization. In mature HS chains, HS disaccharides are organized in two main structural domains: sulfated (S)-domains, enriched in highly modified disaccharides, and *N*-acetylated (NA)-domains, that are mostly composed by non-modified GlcNAc units linked predominantly to GlcA residues. Glycan structures are represented according to the Symbol Nomenclature for Glycans (SNFG) (21).

proliferation, differentiation, and survival (68). FGF2-HS interaction, in particular, is important not only for receptor dimerization and activation, but also for evasion of degradation by FGF2 molecules (69). Maccarana M. et al. showed that IdoA2S and GlcNS were important units for FGF2 binding, whereas the presence of GlcN6S residues was irrelevant for HS-FGF2 interaction (70). It was later reported that 6-*O*-sulfated residues were required to bridge FGF2 and FGFR, promoting the formation of the full ternary complexes and receptor activation (71–73).

Interestingly, a specific trisaccharide that included both IdoA2S and GlcNS6S residues (IdoA2S–GlcNS6S–IdoA2S) was invariably detected in FGF1 binding sites in HS chains (74). It was demonstrated that the presence of this specific motif repeated in HS polysaccharides contributed to higher FGF1 binding affinity, when compared with HS polysaccharides with increased overall sulfation, and that 6-*O*-sulfation was important for FGF1-HS interaction (74). Overall, HS structural requisites for binding of FGF1 and FGF2 illustrate the consensus on the general role of *N*- and 2-*O*-sulfation in ligand binding and the specificity provided by 6-*O*-sulfation.

Another example illustrating the biological impact of 6-*O*-sulfation in HS binding specificities relates to Vascular Endothelial derived-Growth Factors (VEGF) driven-signalling. VEGFs are key molecules in vasculogenesis and angiogenesis, regulating these events during homeostasis and pathology progression (75). In a recent report, it was revealed that HS chains present on the transmembrane HSPG syndecan-2 formed a ternary complex with $VEGFA_{165}$ and its target receptor VEGFR2. $VEGFA_{165}$ is an important growth factor involved in retinal angiogenesis, and the formation of this complex was shown to enhance significantly VEGFR2 signalling in endothelial cells, when compared to the binary complex VEGFA-VEGFR2 (76). GAG disaccharide analyses revealed high 6-*O*-sulfation in HS of syndecan-2 (76), a structural feature that had been previously shown to be specifically related with the increased $VEGFA_{165}$ binding affinity to HS chains (77).

HSPGs also modulate the activity of morphogens, which are key elements in the cellular events that occur during early development, by providing a scaffold for stabilizing extracellular gradients of these signalling molecules, or acting directly as cell surface co-receptors for receptors activation. Noteworthy, signalling pathways of major HS-binding morphogens including Hedgehog, Bone Morphogenic Protein (BMP) and Wnt, were shown to be impaired by aberrant HS biosynthesis, resulting from the loss of *EXT* gene expression and function (78, 79). HS bioactive domains for Wnt and for a member of the BMP family, BMP-2, have also been previously disclosed. Wnt interaction with HS and subsequent activation were associated mainly with the polysaccharide 6-*O*-sulfation content, and its structural remodelling by the Sulfs (80, 81). The most critical components of BMP-2 HS-binding domain were revealed to be GlcNS residues, while 6-*O*- and 2-*O*-sulfation were also important, but to a lesser extent (82).

High HS-Ligand Binding Specificities

The most selective interactions take place in regions of HS chains that contain rare modifications, such as $GlcNH_3$ and 3-*O*-sulfated GlcN residues (83). The first identified and most studied example of a HS specific saccharide sequence required for protein high specificity binding and activity relates to antithrombin, an important inhibitor of blood coagulation, whose inhibitory activity is potentiated upon binding to heparin (84). Since the late 70s, many studies have been dedicated to disclose a specific binding epitope within heparin responsible for antithrombin interactions and activity, and led to the identification of an antithrombin binding pentasaccharide GlcNAc6S-GlcA-GlcNS3S6S-IdoA2S-GlcNS6S (85, 86). Within this sequence, the GlcNS3S residue is highlighted as a fundamental distinctive structural feature as it is an otherwise rare unit within heparin/HS chains (85, 87).

The binding of Herpes simplex virus type 1 glycoprotein D to cell surface HS, that functions as a critical receptor for the virus entry in host cells, was shown to also depend on specific sites within HS chains that include 3-*O*-sulfation (either IdoA2S-$GlcNH_2$3S6S or IdoA2S-$GlcNH_2$3S) (88). In addition to its role in antithrombin activity and cellular viral entry, this less frequent type of HS modification has been associated with a few highly selective interactions with other types of bioactive molecules with impact in cell physiology, including the growth factor FGF7 (89), cyclophilin B (90) and the cell surface receptor Neuropilin-1 (91). Lastly, a recent report showed that 3-*O*-sulfation significantly enhances tau binding to cell surface HS, and subsequent tau cellular uptake, ultimately contributing to the prion-like spread of tau pathology in Alzheimer's Disease (92).

HS SULFATION PROFILES IN CANCER

HSPGs are key players in cancer development and progression, acting as important maestros of cancer cell interaction with the ECM and cancer cell communication, ultimately controlling the tumour microenvironment biochemical and biophysical features (12, 93, 94). The expression of these macromolecules has been shown to be altered in several types of cancer, contributing to the deregulation of different cell events, including proliferation, angiogenesis, adhesion, migration and invasion. The altered cellular levels of HS, resulting from aberrant HSPGs expression and abnormal expression of enzymes involved in HS biosynthesis and editing, are main features heavily involved in cells' malignant transformation (**Table 1**) (12, 13). Comparative studies have demonstrated aberrant expression of several genes encoding HS biosynthesis machinery in cancer. Transcriptomic and immunohistochemical analyses have been performed in breast (58) and colorectal (113, 114) tumour samples and indicated significant variations in the expression and tissue-distribution of several enzymes involved mostly in HS epimerization and sulfation. In fact, most variations in the expression of HS-related genes detected in several cancer pathologies concern enzymes specifically involved in HS modification reactions that change HS sulfation degree and patterns. This is likely justified by the dependence of the numerous biological roles displayed by HSPGs on these structural features, as discussed previously.

TABLE 1 | Aberrant expression of HS modifying enzymes on cancer and its effects on cellular features and patient's prognosis.

Gene/protein deregulation	Cancer	Altered HS sulfation	Effect on tumour cell and patient's prognosis	Refs
↓ *NDST4*	Colorectal cancer (tissue, in higher pathological stages [T3 and T4], and several colorectal cancer cell lines)	■	Patient's poor overall survival.	(95)
Ø *Ndst1*	Lung cancer (LLC cells were injected in *Ndst1$^{f/f}$TekCre^{+}* mice)	Reduced N-sulfation. Reduced 6-*O*- and 2-*O*-sulfation (mice endothelial cells).	Impaired angiogenesis-related signalling pathways: decreased FGF2- and VEGF-dependent Erk1/2 phosphorylation. Decreased tumour vascularization. Reduced tumour growth.	(96)
↓ *GLCE*	Breast cancer (tissue and MCF-7 cells)	■	–	(97, 98)
	Lung cancer (several lung cancer cell lines cells)	■	–	(99)
⊕ *GLCE*	Breast (MCF7 cells) and small-cell lung cancer (U2020 cells)	■	Decreased cell proliferation. Supressed the growth of U2020 xenograft tumours.	(98, 99)
↑ *2OST1*	Prostate cancer (tissue and LNCaP, C4, C4-2, C4-2B cells)	■	Correlated with metastatic potential.	(100)
Ø *2OST1*	Prostate cancer (LNCaP, C4, C4-2, C4-2B cells)	■	Decreased cell proliferation and invasion.	(100)
↓ *2OST1*	Leukaemia (SKM-1 cells under granulocytic differentiation)	■	Cell growth inhibition and less aggressive phenotypes.	(101)
⊕ *2OST1*	Breast cancer (MDA-MB-231 and MCF-7 cells)	■	Acquisition of cancer stem cell-like properties.	(102)
⊕ *2OST1*	Breast cancer (MCF-7 and MDA-MB-231 cells)	Increased 2-*O*-sulfation.	Decreased EGFR expression and activation. Upregulated E-cadherin. Promoted cell-cell and cell-ECM adhesion. Inhibited cell migration and invasion.	(103)
↑ 6OST1	Chondrosarcoma (tissue; correlated with increasing tumour histological grade)	■	–	(104)
↑ 6OST2	Chondrosarcoma (tissue; correlated with increasing tumour histological grade)	■	–	(104)
	Colorectal cancer (tissue and several colorectal cancer cell lines)	■	–	(105)
↑ 6OST3	Chondrosarcoma (tissue)	■	–	(104)
	Breast cancer (T47D, MCF7 and MDA-MB-231 cells)	■	–	(106)
Ø *6OST3*	Breast cancer (T47D, MCF7 cells)	■	Increased cell apoptosis and adhesion. Reduced cell proliferation. Reduced cell migration and invasion (except for T47D cells).	(106)
↓ *3OST2*	Breast, colon, lung and pancreatic cancer (tissue and several breast cancer cell lines)	■	–	(107)
	Non-small cell lung cancer (tissue and several NSCLC cell lines)	■	Poor patient's survival.	(108)
⊕ *3OST2*	Non-small cell lung cancer (H460 and H23 cells)	■	Reduced cell proliferation, migration and invasion.	(108)
	Breast cancer (MDA-MB-231 cells)	Increased 3-*O*-sulfation.	Increased activation of MAPK and Wnt/β-catenin signalling pathways. Increased cell invasiveness, motility and chemoresistance.	(109)

(Continued)

TABLE 1 | Continued

Gene/protein deregulation	Cancer	Altered HS sulfation	Effect on tumour cell and patient's prognosis	Refs
	Breast cancer (MDA-MB-231 and MCF-7 cells)	■	Acquisition of cancer stem cell-like properties.	(102)
↓ *3OST3A*	Breast cancer (luminal-A and triple-negative breast cancer tissues and MCF-7 and MDA-MB-231 cells)	■	Promoted oncogenic features.	(110)
↑ *3OST3A*	Breast cancer HER2+ tumours	■	Decreased disease-free survival.	(110)
⊕ *3OST3B1*	Acute myeloid leukaemia (U937 cells)	■	Induced cell proliferation. Induced expression and shedding of proangiogenic factors. Promoted pro-angiogenic signalling pathways.	(111)
↑ *3OST3B1*	Non-small cell lung cancer (tissue and several NSCLC cell lines)	■	Regulated epithelial-to-mesenchymal transition (EMT).	(112)

↓ *downregulation or loss of expression in cancer.*
↑ *upregulation in cancer.*
Ø *induced silencing or KO in cancer cell models.*
⊕ *induced overexpression in cancer cell models.*
■ *HS sulfation features were not described.*
– *effects on cell behaviour or patient's prognosis were not reported.*

Sulfotransferase Deregulation and Aberrant HS Sulfation Profiles

Regarding NDST isozymes that act in the initial step of HS modification, namely *N*-deacetylation and *N*-sulfation of GlcN, loss of *NDST4* gene expression in colorectal cancer has been associated with higher pathological stages and patient's poor prognosis (95). Additionally, Fuster M. M. et al. studied the impact of another NDST isoform, NDST1, on tumour angiogenesis, and showed that endothelial cells isolated from *Ndst1* KO mice synthesized structurally modified HS chains that impaired angiogenesis-related signalling pathways, leading to decreased vascularization of lung tumours and consequent reduced tumour growth (96). Altered expression of GLCE, the epimerase controlling HS GlcA/IdoA ratio, was also reported in cancer. Studies indicated significant decreased expression of *GLCE* in breast tumours (97), even at premalignant stages of the disease, and in lung cancer cells (99). Furthermore, anti-proliferative effects were reported on both breast (98) and small-cell lung (99) cancer cells after induced re-expression of *GLCE*, highlighting this gene as a potential tumour-suppressor gene.

The sulfotransferases that catalyse the more common HS *O*-sulfation reactions, 2OST1 and 6OSTs, have also been implicated in cancer pathology. Gene expression datasets from the Oncomine database were explored and revealed that *2OST1* expression is upregulated in prostate carcinoma and functional assays showed that it correlates with cell proliferation and invasion capabilities, known to enhance cancer cells metastatic behaviour (100). In the same line, but in a different model, it was demonstrated that downregulation of *2OST1*, and concomitant change in HS structural patterns, accompanied the granulocytic differentiation of SKM-1 leukaemia cells and were associated with cells' growth inhibition and less aggressive phenotypes (101). In breast cancer, *2OST1* expression was shown to promote the acquisition of cancer stem cell-like properties, by activating stemness-associated signalling pathways (102). Additionally, and contradicting the previously reported *2OST1* "tumour promoter gene"-like features, upregulation of *2OST1* in breast cancer cell lines was shown to promote cell-cell and cell-ECM adhesion and to inhibit cell migration and invasion capabilities (103). These effects were associated with increased HS 2-*O*-sulfation and subsequent altered growth factor binding affinities, decreased expression and activation of the Epidermal Growth Factor Receptor (EGFR), which impaired different signalling pathways that modulate cancer cell invasiveness, and increased expression of E-cadherin (103).

Regarding 6OSTs, Waaijer C. et al. reported upregulated expression of 6OST1 and 6OST2 during chondrosarcoma progression, correlated with increasing tumour histological grade, higher levels of 6OST3 in most of the analysed cartilage tumours, and higher levels of 6-*O*-sulfated HS disaccharides in high-grade chondrosarcoma cell lines (104). Similarly, the isoforms *6OST2* and *6OST3* were also found to be overexpressed in colorectal (105) and breast (106) cancer, respectively. *6OST3* expression in particular was shown to influence breast tumour cell growth, invasion and migration (106). HS 6-*O*-sulfation content was also shown to be augmented in the ovarian endothelium of patients with advanced stage ovarian cancer (115). In agreement with this work, it was later disclosed the impact of HS 6-*O*-sulfation content, majorly determined by 6OST isozymes, on ovarian cancer angiogenesis (116). In this work, Cole C. L. et al. showed that HS 6-*O*-sulfation stimulates the heparin-binding EGF-like growth factor (HB-EGF)-dependent activation of cell surface receptor EGFR, which leads to increased expression of angiogenic cytokines (interleukin 6, interleukin 8 and FGF2) by ovarian tumour cells (116). HS post-biosynthesis editing by 6-O-endosulfatases represents an additional regulatory mechanism frequently altered in different tumour models, further emphasizing the role of polysaccharide altered 6-*O*-sulfation in cancer (16, 117).

Lastly, aberrant expression of 3OSTs, which catalyse the rarest HS modification, was also reported in various human cancers, suggesting an important role in cell malignant transformation and tumour cells' functional features. Miyamoto K. et al. described hypermethylation of 5' region of the *3OST2* gene and consequent loss of its expression in human primary breast, colon, lung and pancreatic cancers (107). Later, Kumar A. V. et al. have taken this premise and further investigated the possible functions of *3OST2* in tumorigenesis (109). These authors reported that re-expression of this gene in a highly invasive breast cancer cell line augmented the activation of Mitogen-Activated Protein Kinase (MAPK) and Wnt/β-catenin signalling pathways, which promoted breast cancer cell invasiveness, motility and chemoresistance (109). Additionally, *3OST2* expression in breast cancer cells was shown to be related with acquisition of a cancer stem cell-like phenotype (102). Hypermethylation and silencing of *3OST2* was also reported in non-small cell lung cancer, and it was associated with poor overall patient survival. Hwang J. A. et al. induced exogenous expression of this gene in two lung cancer cell lines and observed reduced cells' migration and invasion capabilities, as well as their lower proliferation rate, supporting that *3OST2* hypermethylation might promote lung tumorigenesis (108). Regarding different isoforms, *3OST3A* was revealed to be epigenetically repressed in breast cancer cell lines representative of distinct molecular subgroups, and it was shown to induce opposite effects, either oncogenic or tumour-suppressive, depending on tumour cell phenotypes (110). Moreover, *3OST3B1* expression was associated to acute myeloid leukaemia progression, by inducing expression and shedding of proangiogenic factors (111), and, more recently, it was found to be upregulated on non-small cell lung cancer and to regulate epithelial-to-mesenchymal transition (112). Interestingly, the telomerase protein TRF2, whose expression is upregulated in tumour cells and associated to suppression of immune response, was shown to regulate *3OST4* expression and to prevent natural killer (NK) cell recruitment and promote cancer immune escape (118, 119).

Together with changes in HS modifying enzymes, altered HS sulfation levels and structural conformations have also been studied and described in different types of cancer, in an attempt to profile specific sulfation patterns as distinctive traits in cancer pathologies that can potentially serve as predictive biomarkers.

GAG disaccharide profiling of cancer patients' tissue samples has revealed decreased HS 6-*O*-sulfation and total *O*-undersulfation in Hepatocellular cancer (120) and overall decreased HS sulfation, both *N* and *O*, in renal cell carcinoma, mainly due to lower levels of mono 6-*O*-sulfated disaccharides, and all disulfated disaccharides (121). HS sulfation was also shown to vary in breast cancer but in a cell dependent manner. As such, it was shown that MCF7 breast cancer cells, expressing oestrogen and progesterone receptors, produce HS with reduced content in 2-*O*-sulfated disaccharides and enriched in 6-*O*-sulfation. In contrast, HS isolated from MDA-MB-231 and HCC38 cells, triple-negative for oestrogen and progesterone receptors, as well as human epidermal growth factor receptor-2 (HER2), were more 2-*O*-sulfated and less 6-*O*-sulfated, both compared with a non-tumorigenic human mammary gland epithelial cell line (122).

On the other hand, data regarding 3-*O*-sulfation levels in tumours is very scarce. This is mainly due to the shortage of commercially available 3-*O*-sulfated disaccharide standards that can be used for comparison in HS disaccharide structural analyses, as well as the low susceptibility of 3-*O*-sulfated disaccharides to the currently used Heparinases (I, II and III) for exhaustive HS depolymerisation, which is a prerequisite for this type of analyses.

TARGETING OF HS AND HS BIOSYNTHETIC ENZYMES

Numerous studies reported abnormal expression of HSPGs and HS biosynthesis enzymes in a myriad of different types of cancers, associated with tumour cell transformation, disease progression and patient outcomes. These may therefore have a significant clinical potential as molecular biomarkers to improve cancer diagnosis and prognosis, and as targets for novel treatment strategies. In addition, and considering the important biological roles displayed by HS chains and how these polysaccharides impact cell malignant features, pharmaceutical strategies that also target HS functions and HS-protein interactions are being developed to tackle cancer pathologies. These strategies include small-molecule inhibitors of HS biosynthesis, HS mimetics, synthetic xylosides and anti-HS/HSPG antibodies (**Figure 3**).

There are also several therapeutical strategies in pre-clinical or clinical studies that target post-biosynthesis editing mechanisms involving the activity of Sulfs and Heparanase, which have been thoroughly reviewed in (16, 17). Still, these are out of the scope of this review, whose primary focus is on the role and activity of HS biosynthesis enzymes, mainly HS sulfotransferases, and on HS-ligand interactions, and therefore have not been further discussed in the following sections.

Small-Molecule Inhibitors of HS Biosynthesis

Despite the known role of HS sulfotransferases in determining HS conformations and interacting partners, which influences cell signalling networks, the targeting of these enzymes has been considerably less explored for innovative therapeutic strategies. Some reports have focused on the use of small molecules to manipulate the binding and/or activity of HS sulfotransferases over the last years (**Figure 3A**). In one of these projects, Byrne D. P. et al. screened several small-molecules from a Public Kinase Inhibitor Set library, and validated cell permeable compounds as probes with inhibitory activity against 2OST, namely three polyanionic compounds - suramin, aurintricarboxylic acid and rottlerin - and one oxindole RAF kinase inhibitor - GW407323A (123). In addition, a new approach for quicker, reproducible and cheaper detection of substrate sulfation was employed. This sulfation detection strategy is based on microfluidics and differential scanning fluorimetry, and in the future it could be

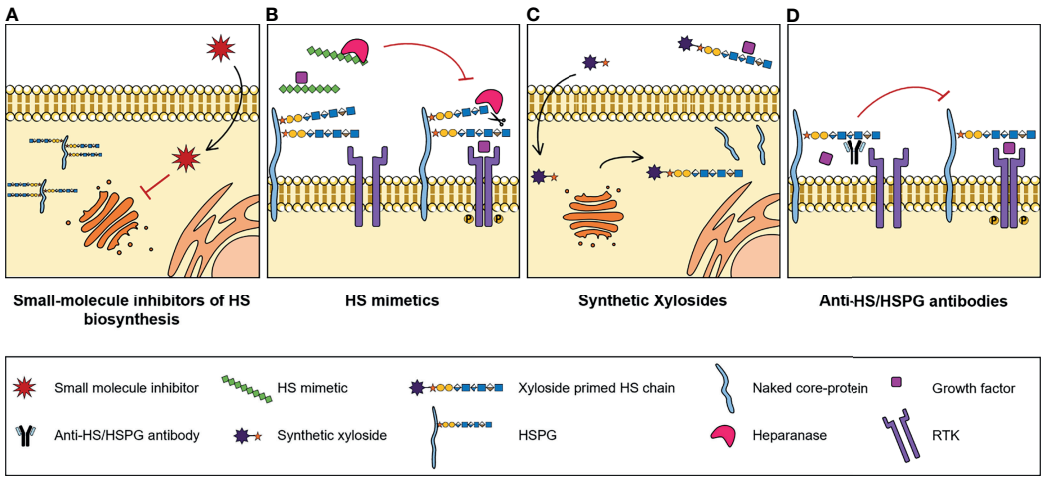

FIGURE 3 | Illustrative representation of the mechanisms of action of four types of molecules developed to target HS biosynthesis and HS-protein interactions, with potential for cancer therapy: **(A)** Small-molecule inhibitors of HS biosynthesis. Cell-permeable, small-molecule compounds with inhibitory activity against GAG biosynthesis enzymes, that impair glycans' biosynthesis and sulfation. **(B)** HS mimetics. HS-like compounds that compete with HS chains for the binding of enzymes, like Heparanase, or HS-binding proteins, like growth factors, blocking HS-protein interactions and inhibiting the formation of important cell signalling complexes. **(C)** Synthetic xylosides. Synthetic primers for protein-free GAG biosynthesis, that interfere with the GAGosylation of native PGs' core protein, and when secreted into de extracellular environment, compete with endogenous GAGosylated PGs for the binding of biologically active ligands. **(D)** Anti-HS/HSPG antibodies. Antibody molecules developed to target HS and HSPGs and to inhibit HS-ligand interactions and downstream signalling cascades.

applied for the discovery of new inhibitory compounds against other sulfotransferases, like 6OSTs and 3OSTs (123).

More recently, it was reported a methodology for transient and reversible inhibition of HS biosynthesis also involving a small cell-permeable compound, the tetra-acetylated N-azidoacetylgalactosamine (Ac_4GalNAz). Maciej-Hulme M. *et al.* have shown that the treatment of Chinese hamster ovary cells with Ac_4GalNAz induces early termination of HS elongation, reducing HS levels and length, potentially by interfering with the activity of NDSTs (124). In a first instance these types of tools will be extremely relevant to further study HS and HS-sulfation dependent cell mechanisms and impact in cancer pathology, and in the long-term these could potentially be applied in cancer research and therapy.

HS Mimetics

HS mimetics are synthetic and homogenous molecules, that can either be saccharide or non-saccharide based, with great potential as anti-cancer agents. These molecules function by competing with HS native chains and blocking HS-protein interactions (**Figure 3B**), and a few of them either have been or are currently under clinical trials, namely CX-01 (ODSH), Roneparstat (SST0001), Necuparanib (M402), Muparfostat (PI-88) and Pixatimod (PG545) (125). A great variety of these HS mimetics inhibit either Heparanase and/or Sulfs activity and directly target HS-growth factor interactions, and their specific features and functions have been recently reviewed in (126). Furthermore, it has been reported that these mimetics may also inhibit the activation of RTKs. For example, Roneparstat was shown to inhibit FGF, Insulin Growth Factor (IGF), EGF and Platelet-Derived Growth Factor (PDGF) receptors expressed in sarcoma cells (127).

In addition to these widely studied HS mimetics, several different HS-like compounds have been developed and/or discovered and studied specifically due to their ability to interfere with HS mediated signalling cascades, that are yet to be further explored in clinical studies.

Sutton A. et al. revealed the anti-tumour effects of two synthetic sulfated polymers HS mimetics, OTR4120 and OTR4131, in hepatoma cells. These compounds interfere with a HS-mediated signalling pathway regulated by the CC-chemokine Regulated upon Activation, Normal T Cell Expressed and Presumably Secreted (RANTES), also referred to as CCL5, which was shown to induce cell migration and invasion in a HS-dependent manner (128). The G2.2, another synthetic sulfated non-saccharide HS mimetic, has also been evaluated in regard to its anti-tumour activity and it was shown to selectively target and reduce colorectal cancer stem cells, by inducing the activation of p38 MAPK and impairing cell self-renewal, ultimately reducing tumour growth (129). In a different study, Shanthamurthy C. D. et al. synthesized a highly sulfated IdoA-based oligosaccharide as a novel HS mimetic to target chemokines and modulate its activity in cancer progression, and reported its high binding affinity towards several homeostatic and inflammatory chemokines. Additionally, they showed that this HS mimetic, potentially by binding to CCL2, inhibits breast cancer CCL2-mediated cell proliferation and CCR2/CCL2-mediated cell migration, and it reduces cell invasiveness (130). More recently, Jain P. et al. have resorted to a library of HS tetrasaccharide ligands with varying sulfation patterns and high-throughput array binding assays to further address HS binding specificities, and validated two HS analogues, HT-2,6S-NAc and HT-6S-NAc, as potential ligands to target $VEGF_{165}$-mediated

cellular events, as these were shown to not only bind with high affinity to the mentioned growth factor but also to inhibit endothelial cells' $VEGF_{165}$-induced proliferation, migration and tube formation, which are known to be relevant tumour related features (131).

Synthetic Xylosides

Another promising tool for cancer therapy pertains to the use of synthetic xylosides. These molecules comprise a xylose residue linked to an aglycone group and serve as primers for protein-free GAG biosynthesis in the Golgi. Synthetic xylosides compete with PGs' core protein for biosynthetic enzymes, impairing the elongation and modification of GAG chains attached to PGs, while on the other hand the xyloside primed GAG chains secreted into the extracellular environment also compete with endogenous PG-linked GAGs for binding of different ligands (**Figure 3C**) (132).

The use of synthetic xylosides with HS priming activity was shown to effectively inhibit several tumour-related cellular events. Raman K. et al. revealed significant reduction of the invasive capabilities of glioma cells treated with click-xylosides (133). It has also been reported the anti-angiogenic efficacy of two different fluoro-xylosides that by inhibiting HS synthesis in endothelial cells, ultimately inhibit tumour cells' angiogenesis (134), which is in agreement with the previously mentioned role of HSPGs as important binding partners and co-receptors of pro-angiogenic factors, including VEGF and FGF. More recently, novel xyloside-derived compounds with potential to be used in therapy for glioblastoma were identified due to their ability of impairing endogenous GAG biosynthesis by binding to XYLT1 and β4GAL T7 active sites, and consequently decreasing glioblastoma cell viability (135). In a different study, Mani K. et al. demonstrated that the use of the synthetic xyloside 2(6-hydroxynaphthyl)-β-D-xylopyranoside inhibited tumour cell growth *in vitro*, in human lung and hepatocellular carcinoma, and SV40-transformed mouse embryonic fibroblasts 3T3 cells, as well as *in vivo*, in human bladder carcinoma cells (136). However, unlike the previously mentioned studies, they hypothesised that this anti-proliferative effect, observed at low xyloside doses, was due to the accumulation of antiproliferative products resulting from degradation of the xyloside-primed HS chains inside the cells, rather than competition with PG core protein or PG-linked GAGs for HS biosynthesis or ligand-binding, respectively (136).

HSPGs expressed at cell glycocalyx also function as internalizing receptors for extracellular vesicles (EVs). EVs are cell-derived vesicles that mediate intercellular communication and display crucial roles in a multitude of physiological and pathophysiological processes. In recent years, it has been suggested that EVs released by tumour cells play an important role in the establishment of premetastatic niches and in metastasis. Christianson H. C. et al. have shown that treatment of glioma cells with xylosides inhibited EV cellular uptake and consequently it reduced cell migratory capabilities (137).

Treatment of cancer cells that feature aberrant expression of HS sulfotransferases with xylosides could potentially lessen the synthesis of endogenous PGs modified with HS chains with altered sulfation patterns, diminishing the effects of PG-linked GAG oversulfation on different cell signalling pathways involved in tumorigenesis. Moreover, a higher impact over HS sulfotransferase activities could be achieved by manipulating the structure of the aglycone portion of the synthetic xylosides (138), which could be employed to further increase enzyme affinity towards these synthetic molecules. This type of xyloside dependent HS structural changes were also reported by Chen Y. et al. when comparing the GAG priming efficiency of two synthetic xylosides, 2-naphthyl-β-D-xylopyranoside and its derivative 2-(6-((3-aminopropyl)oxy)-naphthyl)-β-D-xylopyranoside, particularly in terms of sulfation (139).

Anti-HSPG Antibodies

In addition to the previously mentioned strategies, a different line of investigation has been dedicated to the development and study of molecules that impair HS-ligand interactions by directly targeting HS and HSPGs, namely anti-HSPG antibodies (**Figure 3D**).

Gao W. et al. generated a human monoclonal HS-specific antibody, HS20, targeting HS chains found on glypican-3 (140), a cell surface HSPG known to be highly expressed in hepatocellular carcinoma and associated with patient poor prognosis (141). Treatment of hepatocellular carcinoma cells with HS20 was revealed to block the activation of the HGF/Met pathway, and consequently to inhibit HGF-induced cell migration, motility, and 3D-spheroid formation, as well as *in vivo* liver tumour growth (140).

Syndecan-1 is another cell-surface HSPG that has been revealed to be a potential immunotherapeutic target for cancer therapy, more specifically for multiple myeloma. Jiang H. et al. developed modified NK cells expressing a syndecan-1-specific chimeric antigen receptor (CAR), that showed enhanced *in vitro* and *in vivo* cytotoxicity against syndecan-1 positive multiple myeloma cells, presenting a new possible approach for efficient and specific cancer immunotherapy (142). More recently, it was also developed a new monoclonal anti-syndecan-1 antibody, VIS832, to use in multiple myeloma therapy, and it was shown to induce potent NK cell-mediated antibody-dependent cellular cytotoxicity and macrophage-mediated antibody-dependent cellular phagocytosis against myeloma cells either sensitive or resistant to current therapies (143). In this study it was further demonstrated the efficacy of the VIS832 treatment in a murine model of disseminated human multiple myeloma, both as monotherapy and combined with a proteasome inhibitor (bortezomib) used in therapy (143).

In addition, anti-HSPG antibodies also hold great potential for safer and highly specific drug delivery in cancer immunotherapy. Indatuximab ravtansine (BT062) is an example of such therapeutic approach, as an anti-syndecan-1 monoclonal antibody (nBT062) conjugated with a highly cytotoxic maytansinoid derivative (DM4). This antibody-drug conjugate displayed *in vitro* and *in vivo* anti-tumour activity against multiple myeloma cells expressing syndecan-1, both as monotherapy (144) and in combination with other clinically approved anti-myeloma drugs (145), and more recently it has been under phase I and phase I/IIa clinical trials as monotherapy for relapsed and/or refractory multiple myeloma (146). In a different study, Bosse K. R. et al. have identified glypican-2 as a potential immunotherapeutic target

for neuroblastoma due to its significantly higher expression in high-risk neuroblastomas, which was also associated with patient worse overall survival, and developed a highly cytotoxic antibody-drug conjugate that specifically targets glypican-2-expressing neuroblastoma cells (147).

CONCLUSION AND PERSPECTIVES OF FUTURE RESEARCH

In summary, the roles of HS and HSPGs in physiological events, but most importantly in cancer, highlight these molecules, as well as HS biosynthesis enzymes, as key players during tumorigenic progression. The increasing need for efficient and highly specific biomarkers, and personalized anti-cancer therapies, including new selective drugs, prompts a more in-depth research of these promising tools, inciting further investigation of HS fine structures and their impact in cancer cell behaviour.

Many studies in this field, that have been performed to infer about structural-functional relationships, resorted to artificial *in vitro* models, *via* binding assays and using heavily sulfated heparin molecules and short HS-like oligosaccharides, with the purpose of unravelling bioactive sulfation arrangements and distinctive protein-binding sites within HS chains (70, 148, 149). However, structural differences between these molecules and full-length cellular HS chains might lead to deceitful results, since the use of heavily sulfated heparin might mask specific binding sites and HS oligosaccharides are not presented as embedded in a full-length HS chain. Such assays might thus not accurately represent what occurs in nature (51). Therefore, it has been increasingly important to apply the current knowledge to cell models to assess native GAG biological functions in more complex systems (72, 139), and potentially in disease progression. The great length and high heterogeneity of natural HS chains, whose structures are highly variable, and whose expression is spatially and temporally dependent in organisms, represents a great challenge to this plan (150, 151). Fortunately, the GAG research field is moving at a fast-evolving pace. The development and improvement of robust and sensitive glycoproteomic analytical methodologies combined with computational studies and bioinformatic approaches, such as HS interactome database, will be crucial to assess detailed sequences and conformations adopted by HS glycans implicated in their interactions with proteins in the cell environment (152, 153).

It is also critical to better understand the fine-tuned enzymatic regulatory events that underly HS biosynthesis to elucidate the mechanisms through which endogenous HS modification enzymes regulate tumour cell signalling and disease progression. Overall, the numerous reports describing altered expression of HS sulfotransferases and the abnormal HS sulfation profiles in cancer, further support the clinical potential of these enzymes and structural features as important biomarkers for better diagnosis and prognosis of cancer patients, and as novel targets for improved cancer therapy. However, due to the ubiquitous nature of HSPGs, that exert multiple functions at the physiologic level, it is essential to develop therapeutic approaches targeting specific disease-related modifications, both in terms of HSPG deregulation and GAG conformations. This imposes the challenge of identifying unique cancer Gagosylation signatures to ensure specific targeting and avoid therapy side effects.

AUTHOR CONTRIBUTIONS

CM and AM: conceptualization. CM: original draft writing. RV, CR, and AM: manuscript writing and review. All authors contributed to the article and approved the submitted version.

FUNDING

This work was funded by FEDER funds through the Operational Programme for Competitiveness Factors-COMPETE (POCI-01-0145-FEDER-007274 and POCI-01-0145-FEDER-028489) and National Funds through the Foundation for Science and Technology (FCT), under the project: PTDC/MED-ONC/28489/2017 (to AM); and COST Action CA18103 INNOGLY: INNOvation with Glycans new frontiers from synthesis to new biological targets (ECOST-STSM-Request-CA18103-45514). CM acknowledges the FCT PhD scholarship 2020.06412.BD. This work was also supported by the "Investissements d'avenir" program Glyco@Alps (ANR-15-IDEX-02) and by grants from the Agence Nationale de la Recherche (ANR-17-CE11-0040 and ANR-19-CE13-0031). IBS acknowledges integration into the Interdisciplinary Research Institute of Grenoble (IRIG, CEA).

ACKNOWLEDGMENTS

We would like to apologize to all the authors who have made important contributions in the understanding of HSPG biosynthetic pathways and impact on cancer and which work could not be cited due to space limitation.

REFERENCES

1. Lindahl U, Couchman J, Kimata K, Esko JD. Proteoglycans and Sulfated Glycosaminoglycans. In: A Varki, RD Cummings, JD Esko, P Stanley, GW Hart, et al, editors. *Essentials of Glycobiology*. Cold Spring Harbor (NY: Cold Spring Harbor Laboratory Press (2015). p. 207–21. Copyright 2015-2017 by The Consortium of Glycobiology Editors, La Jolla, California. All rights reserved. doi: 10.1101/glycobiology.3e.017
2. Couchman JR, Multhaupt H, Sanderson RD. Recent Insights Into Cell Surface Heparan Sulphate Proteoglycans and Cancer. *F1000Res* (2016) 5:1541. doi: 10.12688/f1000research.8543.1
3. Theocharis AD, Skandalis SS, Gialeli C, Karamanos NK. Extracellular Matrix Structure. *Adv Drug Delivery Rev* (2016) 97:4–27. doi: 10.1016/j.addr.2015.11.001
4. Sarrazin S, Lamanna WC, Esko JD. Heparan Sulfate Proteoglycans. *Cold Spring Harb Perspect Biol* (2011) 3(7):a004952. doi: 10.1101/cshperspect.a004952

5. Karamanos NK, Piperigkou Z, Theocharis AD, Watanabe H, Franchi M, Baud S, et al. Proteoglycan Chemical Diversity Drives Multifunctional Cell Regulation and Therapeutics. *Chem Rev* (2018) 118(18):9152–232. doi: 10.1021/acs.chemrev.8b00354
6. Matsuo I, Kimura-Yoshida C. Extracellular Distribution of Diffusible Growth Factors Controlled by Heparan Sulfate Proteoglycans During Mammalian Embryogenesis. *Philos Trans R Soc Lond B Biol Sci* (2014) 369(1657):20130545. doi: 10.1098/rstb.2013.0545
7. Hull EE, Montgomery MR, Leyva KJ. Epigenetic Regulation of the Biosynthesis & Enzymatic Modification of Heparan Sulfate Proteoglycans: Implications for Tumorigenesis and Cancer Biomarkers. *Int J Mol Sci* (2017) 18(7):1361. doi: 10.3390/ijms18071361
8. Annaval T, Wild R, Crétinon Y, Sadir R, Vivès RR, Lortat-Jacob H. Heparan Sulfate Proteoglycans Biosynthesis and Post Synthesis Mechanisms Combine Few Enzymes and Few Core Proteins to Generate Extensive Structural and Functional Diversity. *Molecules* (2020) 25(18):4215. doi: 10.3390/molecules25184215
9. Pessentheiner AR, Ducasa GM, Gordts P. Proteoglycans in Obesity-Associated Metabolic Dysfunction and Meta-Inflammation. *Front Immunol* (2020) 11:769. doi: 10.3389/fimmu.2020.00769
10. De Pasquale V, Quiccione MS, Tafuri S, Avallone L, Pavone LM. Heparan Sulfate Proteoglycans in Viral Infection and Treatment: A Special Focus on SARS-CoV-2. *Int J Mol Sci* (2021) 22(12):6574. doi: 10.3390/ijms22126574
11. O'Callaghan P, Zhang X, Li JP. Heparan Sulfate Proteoglycans as Relays of Neuroinflammation. *J Histochem Cytochem* (2018) 66(4):305–19. doi: 10.1369/0022155417742147
12. Faria-Ramos I, Poças J, Marques C, Santos-Antunes J, Macedo G, Reis CA, et al. Heparan Sulfate Glycosaminoglycans: (Un)Expected Allies in Cancer Clinical Management. *Biomolecules* (2021) 11(2):136. doi: 10.3390/biom11020136
13. Hassan N, Greve B, Espinoza-Sánchez NA, Götte M. Cell-Surface Heparan Sulfate Proteoglycans as Multifunctional Integrators of Signaling in Cancer. *Cell Signal* (2021) 77:109822. doi: 10.1016/j.cellsig.2020.109822
14. Iozzo RV, Schaefer L. Proteoglycan Form and Function: A Comprehensive Nomenclature of Proteoglycans. *Matrix Biol* (2015) 42:11–55. doi: 10.1016/j.matbio.2015.02.003
15. Li JP, Kusche-Gullberg M. Heparan Sulfate: Biosynthesis, Structure, and Function. In: KW Jeon, editor. *Int Rev Cell Mol Biol, Vol 325. International Review of Cell and Molecular Biology. 325*. San Diego: Elsevier Academic Press Inc (2016). p. 215–73. doi: 10.1016/bs.ircmb.2016.02.009
16. Vivès RR, Seffouh A, Lortat-Jacob H. Post-Synthetic Regulation of HS Structure: The Yin and Yang of the Sulfs in Cancer. *Front Oncol* (2014) 3:331. doi: 10.3389/fonc.2013.00331
17. Vlodavsky I, Ilan N, Sanderson RD. Forty Years of Basic and Translational Heparanase Research. *Adv Exp Med Biol* (2020) 1221:3–59. doi: 10.1007/978-3-030-34521-1_1
18. Soares da Costa D, Reis RL, Pashkuleva I. Sulfation of Glycosaminoglycans and Its Implications in Human Health and Disorders. *Annu Rev BioMed Eng* (2017) 19:1–26. doi: 10.1146/annurev-bioeng-071516-044610
19. Zhang X, Wang F, Sheng J. "Coding" and "Decoding": Hypothesis for the Regulatory Mechanism Involved in Heparan Sulfate Biosynthesis. *Carbohydr Res* (2016) 428:1–7. doi: 10.1016/j.carres.2016.04.002
20. Esko JD, Selleck SB. Order Out of Chaos: Assembly of Ligand Binding Sites in Heparan Sulfate. *Annu Rev Biochem* (2002) 71:435–71. doi: 10.1146/annurev.biochem.71.110601.135458
21. Neelamegham S, Aoki-Kinoshita K, Bolton E, Frank M, Lisacek F, Lütteke T, et al. Updates to the Symbol Nomenclature for Glycans Guidelines. *Glycobiology* (2019) 29(9):620–4. doi: 10.1093/glycob/cwz045
22. Pönighaus C, Ambrosius M, Casanova JC, Prante C, Kuhn J, Esko JD, et al. Human Xylosyltransferase II Is Involved in the Biosynthesis of the Uniform Tetrasaccharide Linkage Region in Chondroitin Sulfate and Heparan Sulfate Proteoglycans. *J Biol Chem* (2007) 282(8):5201–6. doi: 10.1074/jbc.M611665200
23. Wen J, Xiao J, Rahdar M, Choudhury BP, Cui J, Taylor GS, et al. Xylose Phosphorylation Functions as a Molecular Switch to Regulate Proteoglycan Biosynthesis. *Proc Natl Acad Sci USA* (2014) 111(44):15723–8. doi: 10.1073/pnas.1417993111
24. Koike T, Izumikawa T, Sato B, Kitagawa H. Identification of Phosphatase That Dephosphorylates Xylose in the Glycosaminoglycan-Protein Linkage Region of Proteoglycans. *J Biol Chem* (2014) 289(10):6695–708. doi: 10.1074/jbc.M113.520536
25. Nadanaka S, Zhou S, Kagiyama S, Shoji N, Sugahara K, Sugihara K, et al. EXTL2, a Member of the EXT Family of Tumor Suppressors, Controls Glycosaminoglycan Biosynthesis in a Xylose Kinase-Dependent Manner. *J Biol Chem* (2013) 288(13):9321–33. doi: 10.1074/jbc.M112.416909
26. Kim BT, Kitagawa H, Tamura J, Saito T, Kusche-Gullberg M, Lindahl U, et al. Human Tumor Suppressor EXT Gene Family Members EXTL1 and EXTL3 Encode Alpha 1,4- N-Acetylglucosaminyltransferases That Likely Are Involved in Heparan Sulfate/Heparin Biosynthesis. *Proc Natl Acad Sci USA* (2001) 98(13):7176–81. doi: 10.1073/pnas.131188498
27. McCormick C, Duncan G, Goutsos KT, Tufaro F. The Putative Tumor Suppressors EXT1 and EXT2 Form a Stable Complex That Accumulates in the Golgi Apparatus and Catalyzes the Synthesis of Heparan Sulfate. *Proc Natl Acad Sci USA* (2000) 97(2):668–73. doi: 10.1073/pnas.97.2.668
28. Aikawa J-i, Grobe K, Tsujimoto M, Esko JD. Multiple Isozymes of Heparan Sulfate/Heparin GlcNAcN-Deacetylase/GlcN N-Sulfotransferase: STRUCTURE AND ACTIVITY OF THE FOURTH MEMBER, Ndst4*. *J Biol Chem* (2001) 276(8):5876–82. doi: 10.1074/jbc.M009606200
29. Li YJ, Yin FX, Zhang XK, Yu J, Zheng S, Song XL, et al. Characterization of Heparan Sulfate N-Deacetylase/N-Sulfotransferase Isoform 4 Using Synthetic Oligosaccharide Substrates. *Biochim Biophys Acta Gen Subj* (2018) 1862(3):547–56. doi: 10.1016/j.bbagen.2017.11.016
30. Debarnot C, Monneau YR, Roig-Zamboni V, Delauzun V, Le Narvor C, Richard E, et al. Substrate Binding Mode and Catalytic Mechanism of Human Heparan Sulfate D-Glucuronyl C5 Epimerase. *Proc Natl Acad Sci USA* (2019) 116(14):6760–5. doi: 10.1073/pnas.1818333116
31. Hagner-Mcwhirter A, Lindahl U, Li J. Biosynthesis of Heparin/Heparan Sulphate: Mechanism of Epimerization of Glucuronyl C-5. *Biochem J* (2000) 347 Pt 1(Pt 1):69–75. doi: 10.1042/0264-6021:3470069
32. Sheng J, Xu Y, Dulaney SB, Huang X, Liu J. Uncovering Biphasic Catalytic Mode of C5-Epimerase in Heparan Sulfate Biosynthesis. *J Biol Chem* (2012) 287(25):20996–1002. doi: 10.1074/jbc.M112.359885
33. Rong J, Habuchi H, Kimata K, Lindahl U, Kusche-Gullberg M. Substrate Specificity of the Heparan Sulfate Hexuronic Acid 2-O-Sulfotransferase. *Biochemistry* (2001) 40(18):5548–55. doi: 10.1021/bi002926p
34. Jacobsson I, Lindahl U, Jensen JW, Rodén L, Prihar H, Feingold DS. Biosynthesis of Heparin. Substrate Specificity of Heparosan N-Sulfate D-Glucuronosyl 5-Epimerase. *J Biol Chem* (1984) 259(2):1056–63. doi: 10.1016/S0021-9258(17)43565-4
35. Préchoux A, Halimi C, Simorre JP, Lortat-Jacob H, Laguri C. C5-Epimerase and 2-O-Sulfotransferase Associate *In Vitro* to Generate Contiguous Epimerized and 2-O-Sulfated Heparan Sulfate Domains. *ACS Chem Biol* (2015) 10(4):1064–71. doi: 10.1021/cb501037a
36. Liu C, Sheng J, Krahn JM, Perera L, Xu Y, Hsieh PH, et al. Molecular Mechanism of Substrate Specificity for Heparan Sulfate 2-O-Sulfotransferase. *J Biol Chem* (2014) 289(19):13407–18. doi: 10.1074/jbc.M113.530535
37. El Masri R, Seffouh A, Lortat-Jacob H, Vivès RR. The "In and Out" of Glucosamine 6-O-Sulfation: The 6th Sense of Heparan Sulfate. *Glycoconj J* (2017) 34(3):285–98. doi: 10.1007/s10719-016-9736-5
38. Smeds E, Habuchi H, Do AT, Hjertson E, Grundberg H, Kimata K, et al. Substrate Specificities of Mouse Heparan Sulphate Glucosaminyl 6-O-Sulphotransferases. *Biochem J* (2003) 372(Pt 2):371–80. doi: 10.1042/bj20021666
39. Jemth P, Smeds E, Do AT, Habuchi H, Kimata K, Lindahl U, et al. Oligosaccharide Library-Based Assessment of Heparan Sulfate 6-O-Sulfotransferase Substrate Specificity. *J Biol Chem* (2003) 278(27):24371–6. doi: 10.1074/jbc.M212155200
40. Habuchi H, Tanaka M, Habuchi O, Yoshida K, Suzuki H, Ban K, et al. The Occurrence of Three Isoforms of Heparan Sulfate 6-O-Sulfotransferase Having Different Specificities for Hexuronic Acid Adjacent to the Targeted N-Sulfoglucosamine. *J Biol Chem* (2000) 275(4):2859–68. doi: 10.1074/jbc.275.4.2859
41. Jacobsson I, Lindahl U. Biosynthesis of Heparin. Concerted Action of Late Polymer-Modification Reactions. *J Biol Chem* (1980) 255(11):5094–100. doi: 10.1016/S0021-9258(19)70754-6
42. Thieker DF, Xu Y, Chapla D, Nora C, Qiu H, Felix T, et al. Downstream Products Are Potent Inhibitors of the Heparan Sulfate 2-O-Sulfotransferase. *Sci Rep* (2018) 8(1):11832. doi: 10.1038/s41598-018-29602-4

43. Kusche M, Bäckström G, Riesenfeld J, Petitou M, Choay J, Lindahl U. Biosynthesis of Heparin. O-Sulfation of the Antithrombin-Binding Region. *J Biol Chem* (1988) 263(30):15474–84. doi: 10.1016/S0021-9258(19)37613-6
44. Zhang L, Lawrence R, Schwartz JJ, Bai X, Wei G, Esko JD, et al. The Effect of Precursor Structures on the Action of Glucosaminyl 3-O-Sulfotransferase-1 and the Biosynthesis of Anticoagulant Heparan Sulfate. *J Biol Chem* (2001) 276(31):28806–13. doi: 10.1074/jbc.M100204200
45. Liu J, Shworak NW, Sinaÿ P, Schwartz JJ, Zhang L, Fritze LM, et al. Expression of Heparan Sulfate D-Glucosaminyl 3-O-Sulfotransferase Isoforms Reveals Novel Substrate Specificities. *J Biol Chem* (1999) 274 (8):5185–92. doi: 10.1074/jbc.274.8.5185
46. Liu J, Shriver Z, Blaiklock P, Yoshida K, Sasisekharan R, Rosenberg RD. Heparan Sulfate D-Glucosaminyl 3-O-Sulfotransferase-3A Sulfates N-Unsubstituted Glucosamine Residues. *J Biol Chem* (1999) 274(53):38155–62. doi: 10.1074/jbc.274.53.38155
47. Lawrence R, Yabe T, Hajmohammadi S, Rhodes J, McNeely M, Liu J, et al. The Principal Neuronal gD-Type 3-O-Sulfotransferases and Their Products in Central and Peripheral Nervous System Tissues. *Matrix Biol* (2007) 26 (6):442–55. doi: 10.1016/j.matbio.2007.03.002
48. Xu D, Tiwari V, Xia G, Clement C, Shukla D, Liu J. Characterization of Heparan Sulphate 3-O-Sulphotransferase Isoform 6 and Its Role in Assisting the Entry of Herpes Simplex Virus Type 1. *Biochem J* (2005) 385(Pt 2):451–9. doi: 10.1042/bj20040908
49. Chen J, Duncan MB, Carrick K, Pope RM, Liu J. Biosynthesis of 3-O-Sulfated Heparan Sulfate: Unique Substrate Specificity of Heparan Sulfate 3-O-Sulfotransferase Isoform 5. *Glycobiology* (2003) 13(11):785–94. doi: 10.1093/glycob/cwg101
50. Lamanna WC, Frese MA, Balleininger M, Dierks T. Sulf Loss Influences N-, 2-O-, and 6-O-Sulfation of Multiple Heparan Sulfate Proteoglycans and Modulates Fibroblast Growth Factor Signaling. *J Biol Chem* (2008) 283 (41):27724–35. doi: 10.1074/jbc.M802130200
51. Khan S, Fung KW, Rodriguez E, Patel R, Gor J, Mulloy B, et al. The Solution Structure of Heparan Sulfate Differs From That of Heparin: Implications for Function. *J Biol Chem* (2013) 288(39):27737–51. doi: 10.1074/jbc.M113.492223
52. Warda M, Toida T, Zhang F, Sun P, Munoz E, Xie J, et al. Isolation and Characterization of Heparan Sulfate From Various Murine Tissues. *Glycoconj J* (2006) 23(7-8):555–63. doi: 10.1007/s10719-006-7668-1
53. Garner OB, Bush KT, Nigam KB, Yamaguchi Y, Xu D, Esko JD, et al. Stage-Dependent Regulation of Mammary Ductal Branching by Heparan Sulfate and HGF-Cmet Signaling. *Dev Biol* (2011) 355(2):394–403. doi: 10.1016/j.ydbio.2011.04.035
54. Shah MM, Sakurai H, Gallegos TF, Sweeney DE, Bush KT, Esko JD, et al. Growth Factor-Dependent Branching of the Ureteric Bud Is Modulated by Selective 6-O Sulfation of Heparan Sulfate. *Dev Biol* (2011) 356(1):19–27. doi: 10.1016/j.ydbio.2011.05.004
55. Nigam SK, Bush KT. Growth Factor-Heparan Sulfate "Switches" Regulating Stages of Branching Morphogenesis. *Pediatr Nephrol* (2014) 29(4):727–35. doi: 10.1007/s00467-013-2725-z
56. Jayson GC, Lyon M, Paraskeva C, Turnbull JE, Deakin JA, Gallagher JT. Heparan Sulfate Undergoes Specific Structural Changes During the Progression From Human Colon Adenoma to Carcinoma In Vitro. *J Biol Chem* (1998) 273(1):51–7. doi: 10.1074/jbc.273.1.51
57. Theocharis AD, Vynios DH, Papageorgakopoulou N, Skandalis SS, Theocharis DA. Altered Content Composition and Structure of Glycosaminoglycans and Proteoglycans in Gastric Carcinoma. *Int J Biochem Cell Biol* (2003) 35(3):376–90. doi: 10.1016/s1357-2725(02)00264-9
58. Fernandez-Vega I, Garcia O, Crespo A, Castanon S, Menendez P, Astudillo A, et al. Specific Genes Involved in Synthesis and Editing of Heparan Sulfate Proteoglycans Show Altered Expression Patterns in Breast Cancer. *BMC Cancer* (2013) 13:24. doi: 10.1186/1471-2407-13-24
59. Filmus J, Capurro M. The Role of Glypicans in Hedgehog Signaling. *Matrix Biol* (2014) 35:248–52. doi: 10.1016/j.matbio.2013.12.007
60. Afratis NA, Nikitovic D, Multhaupt HA, Theocharis AD, Couchman JR, Karamanos NK. Syndecans - Key Regulators of Cell Signaling and Biological Functions. *FEBS J* (2017) 284(1):27–41. doi: 10.1111/febs.13940
61. Billings PC, Pacifici M. Interactions of Signaling Proteins, Growth Factors and Other Proteins With Heparan Sulfate: Mechanisms and Mysteries. *Connect Tissue Res* (2015) 56(4):272–80. doi: 10.3109/03008207.2015.1045066
62. Mereiter S, Balmaña M, Campos D, Gomes J, Reis CA. Glycosylation in the Era of Cancer-Targeted Therapy: Where Are We Heading? *Cancer Cell* (2019) 36(1):6–16. doi: 10.1016/j.ccell.2019.06.006
63. Jakobsson L, Kreuger J, Holmborn K, Lundin L, Eriksson I, Kjellén L, et al. Heparan Sulfate in Trans Potentiates VEGFR-Mediated Angiogenesis. *Dev Cell* (2006) 10(5):625–34. doi: 10.1016/j.devcel.2006.03.009
64. Gopal S, Søgaard P, Multhaupt HA, Pataki C, Okina E, Xian X, et al. Transmembrane Proteoglycans Control Stretch-Activated Channels to Set Cytosolic Calcium Levels. *J Cell Biol* (2015) 210(7):1199–211. doi: 10.1083/jcb.201501060
65. Casu B, Naggi A, Torri G. Heparin-Derived Heparan Sulfate Mimics to Modulate Heparan Sulfate-Protein Interaction in Inflammation and Cancer. *Matrix Biol* (2010) 29(6):442–52. doi: 10.1016/j.matbio.2010.04.003
66. Yayon A, Klagsbrun M, Esko JD, Leder P, Ornitz DM. Cell Surface, Heparin-Like Molecules Are Required for Binding of Basic Fibroblast Growth Factor to Its High Affinity Receptor. *Cell* (1991) 64(4):841–8. doi: 10.1016/0092-8674(91)90512-w
67. Rapraeger AC, Krufka A, Olwin BB. Requirement of Heparan Sulfate for bFGF-Mediated Fibroblast Growth and Myoblast Differentiation. *Science* (1991) 252(5013):1705–8. doi: 10.1126/science.1646484
68. Xie Y, Su N, Yang J, Tan Q, Huang S, Jin M, et al. FGF/FGFR Signaling in Health and Disease. *Signal Transduct Target Ther* (2020) 5(1):181. doi: 10.1038/s41392-020-00222-7
69. Saksela O, Moscatelli D, Sommer A, Rifkin DB. Endothelial Cell-Derived Heparan Sulfate Binds Basic Fibroblast Growth Factor and Protects it From Proteolytic Degradation. *J Cell Biol* (1988) 107(2):743–51. doi: 10.1083/jcb.107.2.743
70. Maccarana M, Casu B, Lindahl U. Minimal Sequence in Heparin/Heparan Sulfate Required for Binding of Basic Fibroblast Growth Factor. *J Biol Chem* (1993) 268(32):23898–905. doi: 10.1016/S0021-9258(20)80470-0
71. Sugaya N, Habuchi H, Nagai N, Ashikari-Hada S, Kimata K. 6-O-Sulfation of Heparan Sulfate Differentially Regulates Various Fibroblast Growth Factor-Dependent Signalings in Culture. *J Biol Chem* (2008) 283 (16):10366–76. doi: 10.1074/jbc.M705948200
72. Qiu H, Shi S, Yue J, Xin M, Nairn AV, Lin L, et al. A Mutant-Cell Library for Systematic Analysis of Heparan Sulfate Structure–Function Relationships. *Nat Methods* (2018) 15(11):889–99. doi: 10.1038/s41592-018-0189-6
73. Pye DA, Vives RR, Turnbull JE, Hyde P, Gallagher JT. Heparan Sulfate Oligosaccharides Require 6-O-Sulfation for Promotion of Basic Fibroblast Growth Factor Mitogenic Activity. *J Biol Chem* (1998) 273(36):22936–42. doi: 10.1074/jbc.273.36.22936
74. Kreuger J, Salmivirta M, Sturiale L, Giménez-Gallego G, Lindahl U. Sequence Analysis of Heparan Sulfate Epitopes With Graded Affinities for Fibroblast Growth Factors 1 and 2. *J Biol Chem* (2001) 276(33):30744–52. doi: 10.1074/jbc.M102628200
75. Apte RS, Chen DS, Ferrara N. VEGF in Signaling and Disease: Beyond Discovery and Development. *Cell* (2019) 176(6):1248–64. doi: 10.1016/j.cell.2019.01.021
76. Corti F, Wang Y, Rhodes JM, Atri D, Archer-Hartmann S, Zhang J, et al. N-Terminal Syndecan-2 Domain Selectively Enhances 6-O Heparan Sulfate Chains Sulfation and Promotes VEGFA165-Dependent Neovascularization. *Nat Commun* (2019) 10(1):1562. doi: 10.1038/s41467-019-09605-z
77. Robinson CJ, Mulloy B, Gallagher JT, Stringer SE. VEGF165-Binding Sites Within Heparan Sulfate Encompass Two Highly Sulfated Domains and can be Liberated by K5 Lyase. *J Biol Chem* (2006) 281(3):1731–40. doi: 10.1074/jbc.M510760200
78. Takei Y, Ozawa Y, Sato M, Watanabe A, Tabata T. Three Drosophila EXT Genes Shape Morphogen Gradients Through Synthesis of Heparan Sulfate Proteoglycans. *Development* (2004) 131(1):73–82. doi: 10.1242/dev.00913
79. Han C, Belenkaya TY, Khodoun M, Tauchi M, Lin X, Lin X. Distinct and Collaborative Roles of Drosophila EXT Family Proteins in Morphogen Signalling and Gradient Formation. *Development* (2004) 131(7):1563–75. doi: 10.1242/dev.01051

80. Kleinschmit A, Koyama T, Dejima K, Hayashi Y, Kamimura K, Nakato H. Drosophila Heparan Sulfate 6-O Endosulfatase Regulates Wingless Morphogen Gradient Formation. *Dev Biol* (2010) 345(2):204–14. doi: 10.1016/j.ydbio.2010.07.006
81. Gao W, Xu Y, Liu J, Ho M. Epitope Mapping by a Wnt-Blocking Antibody: Evidence of the Wnt Binding Domain in Heparan Sulfate. *Sci Rep* (2016) 6:26245. doi: 10.1038/srep26245
82. Smith RAA, Murali S, Rai B, Lu X, Lim ZXH, Lee JJL, et al. Minimum Structural Requirements for BMP-2-Binding of Heparin Oligosaccharides. *Biomaterials* (2018) 184:41–55. doi: 10.1016/j.biomaterials.2018.08.056
83. Thacker BE, Xu D, Lawrence R, Esko JD. Heparan Sulfate 3-O-Sulfation: A Rare Modification in Search of a Function. *Matrix Biol* (2014) 35:60–72. doi: 10.1016/j.matbio.2013.12.001
84. Mulloy B, Hogwood J, Gray E, Lever R, Page CP. Pharmacology of Heparin and Related Drugs. *Pharmacol Rev* (2016) 68(1):76–141. doi: 10.1124/pr.115.011247
85. Lindahl U, Bäckström G, Thunberg L, Leder IG. Evidence for a 3-O-Sulfated D-Glucosamine Residue in the Antithrombin-Binding Sequence of Heparin. *Proc Natl Acad Sci USA* (1980) 77(11):6551–5. doi: 10.1073/pnas.77.11.6551
86. Lindahl U, Thunberg L, Bäckström G, Riesenfeld J, Nordling K, Björk I. Extension and Structural Variability of the Antithrombin-Binding Sequence in Heparin. *J Biol Chem* (1984) 259(20):12368–76. doi: 10.1016/S0021-9258(18)90755-6
87. Atha DH, Lormeau JC, Petitou M, Rosenberg RD, Choay J. Contribution of 3-O- and 6-O-Sulfated Glucosamine Residues in the Heparin-Induced Conformational Change in Antithrombin III. *Biochemistry* (1987) 26(20):6454–61. doi: 10.1021/bi00394a024
88. Shukla D, Liu J, Blaiklock P, Shworak NW, Bai X, Esko JD, et al. A Novel Role for 3-O-Sulfated Heparan Sulfate in Herpes Simplex Virus 1 Entry. *Cell* (1999) 99(1):13–22. doi: 10.1016/s0092-8674(00)80058-6
89. Ye S, Luo Y, Lu W, Jones RB, Linhardt RJ, Capila I, et al. Structural Basis for Interaction of FGF-1, FGF-2, and FGF-7 With Different Heparan Sulfate Motifs. *Biochemistry* (2001) 40(48):14429–39. doi: 10.1021/bi011000u
90. Vanpouille C, Deligny A, Delehedde M, Denys A, Melchior A, Liénard X, et al. The Heparin/Heparan Sulfate Sequence That Interacts With Cyclophilin B Contains a 3-O-Sulfated N-Unsubstituted Glucosamine Residue. *J Biol Chem* (2007) 282(33):24416–29. doi: 10.1074/jbc.M701835200
91. Thacker BE, Seamen E, Lawrence R, Parker MW, Xu Y, Liu J, et al. Expanding the 3-O-Sulfate Proteome–Enhanced Binding of Neuropilin-1 to 3-O-Sulfated Heparan Sulfate Modulates Its Activity. *ACS Chem Biol* (2016) 11(4):971–80. doi: 10.1021/acschembio.5b00897
92. Zhao J, Zhu Y, Song X, Xiao Y, Su G, Liu X, et al. 3-O-Sulfation of Heparan Sulfate Enhances Tau Interaction and Cellular Uptake. *Angew Chem Int Ed Engl* (2020) 59(5):1818–27. doi: 10.1002/anie.201913029
93. Piperigkou Z, Mohr B, Karamanos N, Götte M. Shed Proteoglycans in Tumor Stroma. *Cell Tissue Res* (2016) 365(3):643–55. doi: 10.1007/s00441-016-2452-4
94. De Pasquale V, Pavone LM. Heparan Sulfate Proteoglycan Signaling in Tumor Microenvironment. *Int J Mol Sci* (2020) 21(18):6588. doi: 10.3390/ijms21186588
95. Tzeng ST, Tsai MH, Chen CL, Lee JX, Jao TM, Yu SL, et al. NDST4 Is a Novel Candidate Tumor Suppressor Gene at Chromosome 4q26 and Its Genetic Loss Predicts Adverse Prognosis in Colorectal Cancer. *PloS One* (2013) 8(6):e67040. doi: 10.1371/journal.pone.0067040
96. Fuster MM, Wang L, Castagnola J, Sikora L, Reddi K, Lee PH, et al. Genetic Alteration of Endothelial Heparan Sulfate Selectively Inhibits Tumor Angiogenesis. *J Cell Biol* (2007) 177(3):539–49. doi: 10.1083/jcb.200610086
97. Grigorieva E, Eshchenko T, Rykova VI, Chernakov A, Zabarovsky E, Sidorov SV. Decreased Expression of Human D-Glucuronyl C5-Epimerase in Breast Cancer. *Int J Cancer* (2008) 122(5):1172–6. doi: 10.1002/ijc.23203
98. Prudnikova TY, Mostovich LA, Domanitskaya NV, Pavlova TV, Kashuba VI, Zabarovsky ER, et al. Antiproliferative Effect of D-Glucuronyl C5-Epimerase in Human Breast Cancer Cells. *Cancer Cell Int* (2010) 10:27. doi: 10.1186/1475-2867-10-27
99. Grigorieva EV, Prudnikova TY, Domanitskaya NV, Mostovich LA, Pavlova TV, Kashuba VI, et al. D-Glucuronyl C5-Epimerase Suppresses Small-Cell Lung Cancer Cell Proliferation *In Vitro* and Tumour Growth In Vivo. *Br J Cancer* (2011) 105(1):74–82. doi: 10.1038/bjc.2011.170
100. Ferguson BW, Datta S. Role of Heparan Sulfate 2-O-Sulfotransferase in Prostate Cancer Cell Proliferation, Invasion, and Growth Factor Signaling. *Prostate Cancer* (2011) 2011:893208. doi: 10.1155/2011/893208
101. Zhao S, Wang Z. Changes in Heparan Sulfate Sulfotransferases and Cell-Surface Heparan Sulfate During SKM-1 Cells Granulocytic Differentiation and A549 Cells Epithelial-Mesenchymal Transition. *Glycoconj J* (2020) 37(2):151–64. doi: 10.1007/s10719-019-09903-0
102. Teixeira F, Vijaya Kumar A, Kumar Katakam S, Cocola C, Pelucchi P, Graf M, et al. The Heparan Sulfate Sulfotransferases HS2ST1 and HS3ST2 Are Novel Regulators of Breast Cancer Stem-Cell Properties. *Front Cell Dev Biol* (2020) 8:559554. doi: 10.3389/fcell.2020.559554
103. Vijaya Kumar A, Brézillon S, Untereiner V, Sockalingum GD, Kumar Katakam S, Mohamed HT, et al. HS2ST1-Dependent Signaling Pathways Determine Breast Cancer Cell Viability, Matrix Interactions, and Invasive Behavior. *Cancer Sci* (2020) 111(8):2907–22. doi: 10.1111/cas.14539
104. Waaijer CJ, de Andrea CE, Hamilton A, van Oosterwijk JG, Stringer SE, Bovée JV. Cartilage Tumour Progression Is Characterized by an Increased Expression of Heparan Sulphate 6O-Sulphation-Modifying Enzymes. *Virchows Arch* (2012) 461(4):475–81. doi: 10.1007/s00428-012-1300-5
105. Hatabe S, Kimura H, Arao T, Kato H, Hayashi H, Nagai T, et al. Overexpression of Heparan Sulfate 6-O-Sulfotransferase-2 in Colorectal Cancer. *Mol Clin Oncol* (2013) 1(5):845–50. doi: 10.3892/mco.2013.151
106. Iravani O, Bay BH, Yip GW. Silencing HS6ST3 Inhibits Growth and Progression of Breast Cancer Cells Through Suppressing IGF1R and Inducing XAF1. *Exp Cell Res* (2017) 350(2):380–9. doi: 10.1016/j.yexcr.2016.12.019
107. Miyamoto K, Asada K, Fukutomi T, Okochi E, Yagi Y, Hasegawa T, et al. Methylation-Associated Silencing of Heparan Sulfate D-Glucosaminyl 3-O-Sulfotransferase-2 (3-OST-2) in Human Breast, Colon, Lung and Pancreatic Cancers. *Oncogene* (2003) 22(2):274–80. doi: 10.1038/sj.onc.1206146
108. Hwang JA, Kim Y, Hong SH, Lee J, Cho YG, Han JY, et al. Epigenetic Inactivation of Heparan Sulfate (Glucosamine) 3-O-Sulfotransferase 2 in Lung Cancer and Its Role in Tumorigenesis. *PloS One* (2013) 8(11):e79634. doi: 10.1371/journal.pone.0079634
109. Vijaya Kumar A, Salem Gassar E, Spillmann D, Stock C, Sen YP, Zhang T, et al. HS3ST2 Modulates Breast Cancer Cell Invasiveness *via* MAP Kinase- and Tcf4 (Tcf7l2)-Dependent Regulation of Protease and Cadherin Expression. *Int J Cancer* (2014) 135(11):2579–92. doi: 10.1002/ijc.28921
110. Mao X, Gauche C, Coughtrie MW, Bui C, Gulberti S, Merhi-Soussi F, et al. The Heparan Sulfate Sulfotransferase 3-OST3A (HS3ST3A) Is a Novel Tumor Regulator and a Prognostic Marker in Breast Cancer. *Oncogene* (2016) 35(38):5043–55. doi: 10.1038/onc.2016.44
111. Zhang L, Song K, Zhou L, Xie Z, Zhou P, Zhao Y, et al. Heparan Sulfate D-Glucosaminyl 3-O-Sulfotransferase-3B1 (HS3ST3B1) Promotes Angiogenesis and Proliferation by Induction of VEGF in Acute Myeloid Leukemia Cells. *J Cell Biochem* (2015) 116(6):1101–12. doi: 10.1002/jcb.25066
112. Zhang Z, Jiang H, Wang Y, Shi M. Heparan Sulfate D-Glucosamine 3-O-Sulfotransferase 3B1 Is a Novel Regulator of Transforming Growth Factor-Beta-Mediated Epithelial-to-Mesenchymal Transition and Regulated by miR-218 in Nonsmall Cell Lung Cancer. *J Cancer Res Ther* (2018) 14(1):24–9. doi: 10.4103/jcrt.JCRT_659_17
113. Fernandez-Vega I, Garcia-Suarez O, Garcia B, Crespo A, Astudillo A, Quiros LM. Heparan Sulfate Proteoglycans Undergo Differential Expression Alterations in Right Sided Colorectal Cancer, Depending on Their Metastatic Character. *BMC Cancer* (2015) 15:742. doi: 10.1186/s12885-015-1724-9
114. Crespo A, Garcia-Suarez O, Fernandez-Vega I, Solis-Hernandez MP, Garcia B, Castanon S, et al. Heparan Sulfate Proteoglycans Undergo Differential Expression Alterations in Left Sided Colorectal Cancer, Depending on Their Metastatic Character. *BMC Cancer* (2018) 18(1):687. doi: 10.1186/s12885-018-4597-x
115. Ferreras C, Rushton G, Cole CL, Babur M, Telfer BA, van Kuppevelt TH, et al. Endothelial Heparan Sulfate 6-O-Sulfation Levels Regulate Angiogenic Responses of Endothelial Cells to Fibroblast Growth Factor 2 and Vascular

Endothelial Growth Factor. *J Biol Chem* (2012) 287(43):36132–46. doi: 10.1074/jbc.M112.384875
116. Cole CL, Rushton G, Jayson GC, Avizienyte E. Ovarian Cancer Cell Heparan Sulfate 6-O-Sulfotransferases Regulate an Angiogenic Program Induced by Heparin-Binding Epidermal Growth Factor (EGF)-Like Growth Factor/EGF Receptor Signaling. *J Biol Chem* (2014) 289(15):10488–501. doi: 10.1074/jbc.M113.534263
117. Hammond E, Khurana A, Shridhar V, Dredge K. The Role of Heparanase and Sulfatases in the Modification of Heparan Sulfate Proteoglycans Within the Tumor Microenvironment and Opportunities for Novel Cancer Therapeutics. *Front Oncol* (2014) 4:195. doi: 10.3389/fonc.2014.00195
118. Cherfils-Vicini J, Iltis C, Cervera L, Pisano S, Croce O, Sadouni N, et al. Cancer Cells Induce Immune Escape *via* Glycocalyx Changes Controlled by the Telomeric Protein TRF2. *EMBO J* (2019) 38(11):e100012. doi: 10.15252/embj.2018100012
119. Biroccio A, Cherfils-Vicini J, Augereau A, Pinte S, Bauwens S, Ye J, et al. TRF2 Inhibits a Cell-Extrinsic Pathway Through Which Natural Killer Cells Eliminate Cancer Cells. *Nat Cell Biol* (2013) 15(7):818–28. doi: 10.1038/ncb2774
120. Tátrai P, Egedi K, Somorácz A, van Kuppevelt TH, Ten Dam G, Lyon M, et al. Quantitative and Qualitative Alterations of Heparan Sulfate in Fibrogenic Liver Diseases and Hepatocellular Cancer. *J Histochem Cytochem* (2010) 58(5):429–41. doi: 10.1369/jhc.2010.955161
121. Ucakturk E, Akman O, Sun X, Baydar DE, Dolgun A, Zhang F, et al. Changes in Composition and Sulfation Patterns of Glycoaminoglycans in Renal Cell Carcinoma. *Glycoconj J* (2016) 33(1):103–12. doi: 10.1007/s10719-015-9643-1
122. Sembajwe LF, Katta K, Grønning M, Kusche-Gullberg M. The Exostosin Family of Glycosyltransferases: mRNA Expression Profiles and Heparan Sulphate Structure in Human Breast Carcinoma Cell Lines. *Biosci Rep* (2018) 38(4):BSR20180770. doi: 10.1042/bsr20180770
123. Byrne DP, Li Y, Ramakrishnan K, Barsukov IL, Yates EA, Eyers CE, et al. New Tools for Carbohydrate Sulfation Analysis: Heparan Sulfate 2-O-Sulfotransferase (HS2ST) Is a Target for Small-Molecule Protein Kinase Inhibitors. *Biochem J* (2018) 475(15):2417–33. doi: 10.1042/bcj20180265
124. Maciej-Hulme ML, Dubaissi E, Shao C, Zaia J, Amaya E, Flitsch SL, et al. Selective Inhibition of Heparan Sulphate and Not Chondroitin Sulphate Biosynthesis by a Small, Soluble Competitive Inhibitor. *Int J Mol Sci* (2021) 22(13):6988. doi: 10.3390/ijms22136988
125. Morla S. Glycosaminoglycans and Glycosaminoglycan Mimetics in Cancer and Inflammation. *Int J Mol Sci* (2019) 20(8):1963. doi: 10.3390/ijms20081963
126. Lanzi C, Cassinelli G. Heparan Sulfate Mimetics in Cancer Therapy: The Challenge to Define Structural Determinants and the Relevance of Targets for Optimal Activity. *Molecules* (2018) 23(11):36. doi: 10.3390/molecules23112915
127. Cassinelli G, Favini E, Dal Bo L, Tortoreto M, De Maglie M, Dagrada G, et al. Antitumor Efficacy of the Heparan Sulfate Mimic Roneparstat (SST0001) Against Sarcoma Models Involves Multi-Target Inhibition of Receptor Tyrosine Kinases. *Oncotarget* (2016) 7(30):47848–63. doi: 10.18632/oncotarget.10292
128. Sutton A, Friand V, Papy-Garcia D, Dagouassat M, Martin L, Vassy R, et al. Glycosaminoglycans and Their Synthetic Mimetics Inhibit RANTES-Induced Migration and Invasion of Human Hepatoma Cells. *Mol Cancer Ther* (2007) 6(11):2948–58. doi: 10.1158/1535-7163.mct-07-0114
129. Boothello RS, Patel NJ, Sharon C, Abdelfadiel EI, Morla S, Brophy DF, et al. A Unique Nonsaccharide Mimetic of Heparin Hexasaccharide Inhibits Colon Cancer Stem Cells *via* P38 MAP Kinase Activation. *Mol Cancer Ther* (2019) 18(1):51–61. doi: 10.1158/1535-7163.mct-18-0104
130. Shanthamurthy CD, Leviatan Ben-Arye S, Kumar NV, Yehuda S, Amon R, Woods RJ, et al. Heparan Sulfate Mimetics Differentially Affect Homologous Chemokines and Attenuate Cancer Development. *J Med Chem* (2021) 64 (6):3367–80. doi: 10.1021/acs.jmedchem.0c01800
131. Jain P, Shanthamurthy CD, Leviatan Ben-Arye S, Yehuda S, Nandikol SS, Thulasiram HV, et al. Synthetic Heparan Sulfate Ligands for Vascular Endothelial Growth Factor to Modulate Angiogenesis. *Chem Commun (Camb)* (2021) 57(28):3516–9. doi: 10.1039/d1cc00964h
132. Chua JS, Kuberan B. Synthetic Xylosides: Probing the Glycosaminoglycan Biosynthetic Machinery for Biomedical Applications. *Acc Chem Res* (2017) 50(11):2693–705. doi: 10.1021/acs.accounts.7b00289
133. Raman K, Kuberan B. Click-Xylosides Mitigate Glioma Cell Invasion In Vitro. *Mol Biosyst* (2010) 6(10):1800–2. doi: 10.1039/c0mb00020e
134. Raman K, Ninomiya M, Nguyen TKN, Tsuzuki Y, Koketsu M, Kuberan B. Novel Glycosaminoglycan Biosynthetic Inhibitors Affect Tumor-Associated Angiogenesis. *Biochem Biophys Res Commun* (2011) 404(1):86–9. doi: 10.1016/j.bbrc.2010.11.069
135. Kalita M, Villanueva-Meyer J, Ohkawa Y, Kalyanaraman C, Chen K, Mohamed E, et al. Synthesis and Screening of α-Xylosides in Human Glioblastoma Cells. *Mol Pharm* (2021) 18(1):451–60. doi: 10.1021/acs.molpharmaceut.0c00839
136. Mani K, Belting M, Ellervik U, Falk N, Svensson G, Sandgren S, et al. Tumor Attenuation by 2(6-Hydroxynaphthyl)-Beta-D-Xylopyranoside Requires Priming of Heparan Sulfate and Nuclear Targeting of the Products. *Glycobiology* (2004) 14(5):387–97. doi: 10.1093/glycob/cwh035
137. Christianson HC, Svensson KJ, van Kuppevelt TH, Li JP, Belting M. Cancer Cell Exosomes Depend on Cell-Surface Heparan Sulfate Proteoglycans for Their Internalization and Functional Activity. *Proc Natl Acad Sci USA* (2013) 110(43):17380–5. doi: 10.1073/pnas.1304266110
138. Fritz TA, Lugemwa FN, Sarkar AK, Esko JD. Biosynthesis of Heparan Sulfate on Beta-D-Xylosides Depends on Aglycone Structure. *J Biol Chem* (1994) 269(1):300–7. doi: 10.1016/S0021-9258(17)42349-0
139. Chen Y-H, Narimatsu Y, Clausen TM, Gomes C, Karlsson R, Steentoft C, et al. The GAGOme: A Cell-Based Library of Displayed Glycosaminoglycans. *Nat Methods* (2018) 15(11):881–8. doi: 10.1038/s41592-018-0086-z
140. Gao W, Kim H, Ho M. Human Monoclonal Antibody Targeting the Heparan Sulfate Chains of Glypican-3 Inhibits HGF-Mediated Migration and Motility of Hepatocellular Carcinoma Cells. *PloS One* (2015) 10(9): e0137664. doi: 10.1371/journal.pone.0137664
141. Shirakawa H, Suzuki H, Shimomura M, Kojima M, Gotohda N, Takahashi S, et al. Glypican-3 Expression Is Correlated With Poor Prognosis in Hepatocellular Carcinoma. *Cancer Sci* (2009) 100(8):1403–7. doi: 10.1111/j.1349-7006.2009.01206.x
142. Jiang H, Zhang W, Shang P, Zhang H, Fu W, Ye F, et al. Transfection of Chimeric Anti-CD138 Gene Enhances Natural Killer Cell Activation and Killing of Multiple Myeloma Cells. *Mol Oncol* (2014) 8(2):297–310. doi: 10.1016/j.molonc.2013.12.001
143. Yu T, Chaganty B, Lin L, Xing L, Ramakrishnan B, Wen K, et al. VIS832, a Novel CD138-Targeting Monoclonal Antibody, Potently Induces Killing of Human Multiple Myeloma and Further Synergizes With IMiDs or Bortezomib *In Vitro* and *In Vivo*. *Blood Cancer J* (2020) 10(11):110. doi: 10.1038/s41408-020-00378-z
144. Ikeda H, Hideshima T, Fulciniti M, Lutz RJ, Yasui H, Okawa Y, et al. The Monoclonal Antibody Nbt062 Conjugated to Cytotoxic Maytansinoids has Selective Cytotoxicity Against CD138-Positive Multiple Myeloma Cells *In Vitro* and In Vivo. *Clin Cancer Res* (2009) 15(12):4028–37. doi: 10.1158/1078-0432.ccr-08-2867
145. Schönfeld K, Zuber C, Pinkas J, Häder T, Bernöster K, Uherek C. Indatuximab Ravtansine (BT062) Combination Treatment in Multiple Myeloma: Pre-Clinical Studies. *J Hematol Oncol* (2017) 10(1):13. doi: 10.1186/s13045-016-0380-0
146. Jagannath S, Heffner LTJr., Ailawadhi S, Munshi NC, Zimmerman TM, Rosenblatt J, et al. Indatuximab Ravtansine (BT062) Monotherapy in Patients With Relapsed and/or Refractory Multiple Myeloma. *Clin Lymphoma Myeloma Leuk* (2019) 19(6):372–80. doi: 10.1016/j.clml.2019.02.006
147. Bosse KR, Raman P, Zhu Z, Lane M, Martinez D, Heitzeneder S, et al. Identification of GPC2 as an Oncoprotein and Candidate Immunotherapeutic Target in High-Risk Neuroblastoma. *Cancer Cell* (2017) 32(3):295–309.e12. doi: 10.1016/j.ccell.2017.08.003
148. Ashikari-Hada S, Habuchi H, Kariya Y, Itoh N, Reddi AH, Kimata K. Characterization of Growth Factor-Binding Structures in Heparin/Heparan Sulfate Using an Octasaccharide Library. *J Biol Chem* (2004) 279(13):12346–54. doi: 10.1074/jbc.M313523200
149. Sun L, Chopra P, Boons GJ. Modular Synthesis of Heparan Sulfate Oligosaccharides Having N-Acetyl and N-Sulfate Moieties. *J Org Chem* (2020) 85(24):16082–98. doi: 10.1021/acs.joc.0c01881
150. Kjellén L, Lindahl U. Specificity of Glycosaminoglycan-Protein Interactions. *Curr Opin Struct Biol* (2018) 50:101–8. doi: 10.1016/j.sbi.2017.12.011
151. Zaia J. Glycosaminoglycan Glycomics Using Mass Spectrometry. *Mol Cell Proteomics* (2013) 12(4):885–92. doi: 10.1074/mcp.R112.026294
152. Ricard-Blum S, Lisacek F. Glycosaminoglycanomics: Where We Are. *Glycoconj J* (2017) 34(3):339–49. doi: 10.1007/s10719-016-9747-2

153. Vallet SD, Clerc O, Ricard-Blum S. Glycosaminoglycan-Protein Interactions: The First Draft of the Glycosaminoglycan Interactome. *J Histochem Cytochem* (2021) 69(2):93–104. doi: 10.1369/0022155420946403

Conflict of Interest: The authors declare that the research was conducted in the absence of any commercial or financial relationships that could be construed as a potential conflict of interest.

Publisher's Note: All claims expressed in this article are solely those of the authors and do not necessarily represent those of their affiliated organizations, or those of the publisher, the editors and the reviewers. Any product that may be evaluated in this article, or claim that may be made by its manufacturer, is not guaranteed or endorsed by the publisher.

Copyright © 2021 Marques, Reis, Vivès and Magalhães. This is an open-access article distributed under the terms of the Creative Commons Attribution License (CC BY). The use, distribution or reproduction in other forums is permitted, provided the original author(s) and the copyright owner(s) are credited and that the original publication in this journal is cited, in accordance with accepted academic practice. No use, distribution or reproduction is permitted which does not comply with these terms.

frontiers in Oncology

REVIEW
published: 30 November 2021
doi: 10.3389/fonc.2021.801801

The Role of Decorin and Biglycan Signaling in Tumorigenesis

Valentina Diehl[1], *Lisa Sophie Huber*[1], *Jonel Trebicka*[2], *Malgorzata Wygrecka*[3], *Renato V. Iozzo*[4] *and Liliana Schaefer*[1]*

[1] Institute of Pharmacology and Toxicology, Goethe University, Frankfurt, Germany, [2] Department of Internal Medicine I, Goethe University, Frankfurt, Germany, [3] Center for Infection and Genomics of the Lung, Member of the German Center for Lung Research, University of Giessen and Marburg Lung Center, Giessen, Germany, [4] Department of Pathology, Anatomy and Cell Biology and the Translational Cellular Oncology Program, Sidney Kimmel Cancer Center, Sidney Kimmel Medical College at Thomas Jefferson University, Philadelphia, PA, United States

The complex and adaptive nature of malignant neoplasm constitute a major challenge for the development of effective anti-oncogenic therapies. Emerging evidence has uncovered the pivotal functions exerted by the small leucine-rich proteoglycans, decorin and biglycan, in affecting tumor growth and progression. In their soluble forms, decorin and biglycan act as powerful signaling molecules. By receptor-mediated signal transduction, both proteoglycans modulate key processes vital for tumor initiation and progression, such as autophagy, inflammation, cell-cycle, apoptosis, and angiogenesis. Despite of their structural homology, these two proteoglycans interact with distinct cell surface receptors and thus modulate distinct signaling pathways that ultimately affect cancer development. In this review, we summarize growing evidence for the complex roles of decorin and biglycan signaling in tumor biology and address potential novel therapeutic implications.

Keywords: extracellular matrix, proteoglycan, autophagy, inflammation, angiogenesis, cancer, toll-like receptor

OPEN ACCESS

Edited by:
Martin Götte,
University of Münster, Germany

Reviewed by:
Dragana Nikitovic,
University of Crete, Greece
Kornelia Baghy,
Semmelweis University, Hungary

***Correspondence:**
Liliana Schaefer
schaefer@med.uni-frankurt.de

Specialty section:
This article was submitted to Molecular and Cellular Oncology, a section of the journal Frontiers in Oncology

Received: *25 October 2021*
Accepted: *09 November 2021*
Published: *30 November 2021*

Citation:
Diehl V, Huber LS, Trebicka J, Wygrecka M, Iozzo RV and Schaefer L (2021) The Role of Decorin and Biglycan Signaling in Tumorigenesis. Front. Oncol. 11:801801. doi: 10.3389/fonc.2021.801801

1 INTRODUCTION

1.1 Extracellular Matrix Guidance in Tumor Initiation and Progression

Over the past decades, it has become apparent that tumorigenesis is not merely the result of accumulated DNA mutations, but tumor development and progression also depend on the context in which malignant cells subsist (1–3). The tumor microenvironment (TME) is a permissive infrastructure primarily composed of non-malignant resident cells, cancer-associated fibroblasts, macrophages, and a variety of inflammatory and immune cells (4–7), pericytes (8, 9), and cells of the tumor-associated vascular system (10, 11). Moreover, the TME includes the extracellular matrix (ECM), an acellular structure with, as has become evident by now, unique tumor-specific characteristics (12, 13).

The ECM forms an intricate, highly ordered, 3D meshwork of large macromolecules, the components of which have been considered in the past solely as structural scaffolds that enable cellular adhesion and migration. However, a vast body of emerging evidence has led to a paradigmatic shift implicating ECM proteins in various signaling pathways and cellular processes

including autophagy, inflammation, proliferation, survival, cell morphology, and motility (14–22). To date, several ECM components are increasingly appreciated for mediating and modulating cellular signaling (18, 23–26), and presumably even inter-organ cross-talk (27). Importantly, changes in the ECM are known to lead to, or to correlate with several diseases such as cardiovascular and skeletal disorders, fibrosis and importantly cancer (24, 28–30). The observations that link the ECM to cancer are as diverse as the different macromolecules that comprise the ECM. The impact of the biochemical composition of the ECM on tumor progression (12, 31–33), the ECM-dependent development of metastatic niches (34, 35), and the signaling between the tumor-adjacent ECM and the different players of the TME have been reviewed in detail (36, 37). In this review, we will focus on two proteoglycans of the ECM, biglycan and decorin. We will discuss their implications in selected pathways that are linked to the hallmarks of cancer, with special emphasis on autophagy and inflammation, whose contribution to tumorigenesis is increasingly recognized. Lastly, we will critically discuss recent advances and future perspectives in therapeutic targeting of these proteoglycans for cancer therapy.

1.2 Inflammation as an Emerging Hallmark of Cancer

Tumorigenesis is a multi-factorial process that is characterized by specific biological capabilities that are acquired during the development of tumors. These hallmarks of cancer include evading apoptosis, increased angiogenesis, insensitivity to anti-growth signals, and tissue invasion and metastasis (38). In addition to these established hallmarks of cancer, the vital roles of inflammation and the immune response have gained recognition as emerging hallmarks and enabling characteristics of cancer (31, 39, 40). Intricate interactions between cells of the tumor proper, surrounding stromal cells, and inflammatory cells result in an inflammatory TME. Indeed, chronic tissue inflammation has been linked to a heightened risk for malignant transformation, and additionally, sustained inflammation is assumed to cause pre-cancerous lesions (41–43). Moreover, it is well-established that the TME of most tumors is characterized by the presence of highly abundant inflammatory cells and inflammatory mediators, irrespective of the stages of tumor progression (44). Generally, there are two different types of cancer-associated inflammation. One can exert tissue-protective, anti-tumoral functions; the second on the other hand, is linked to pro-tumorigenic effects, presumably in a context and spatiotemporal-dependent manner (45).

Historically, cancer-associated inflammation was attributed to an attempt by the host immune system to eliminate the tumor and provide tissue-protection. Indeed, for some tumor types, there is increasing evidence for an acute immune response against the tumor, and the primary tumor development depends on the ability of tumor cells to escape the immune-mediated destruction (46, 47). This concept has been exploited for the development and application of immuno-therapies that reinstall or enhance the patient's immune response towards recognizing and eradicating cancer cells (48, 49). Conversely, the tumor-associated inflammatory response can also facilitate tumorigenesis by providing an inflammatory milieu. This "cancer-promoting inflammation" relies on secretion of growth factors and enzymes to sustain proliferation, inhibit cell death, promote epithelial-mesenchymal transition (EMT), facilitate angiogenesis, invasion, and metastasis (39, 45, 50). In line with this, chronic inflammation has been linked to cancer-promoting effects in so-called 'hot' tumors, which are densely infiltrated by immune cells and are often unresponsive to immuno-therapy (44, 45, 51).

On a molecular level, constitutively active NF-κB (nuclear factor kappa-light-chain-enhancer of activated B-cells) signaling is considered to be one of many possible factors that promote chronic inflammation in the context of tumorigenesis (52). NF-κB downstream signaling results in expression of inflammatory cytokines, adhesion molecules, the inducible nitric oxide synthase and angiogenic factors. Inducers of NF-κB include cytokines such as tumor necrosis factor alpha (TNF-α) and interleukin 1 beta (IL-1β). The activation of the NF-κB pathway is mediated through Toll-like receptors (TLRs) that act in concert with their adaptor molecules and co-receptors (53–55). Another signaling pathway that links inflammatory signaling to tumorigenesis includes the NOD-like receptor protein 3 (NLRP3) inflammasome, which activates NOD-like receptors or AIM2-like receptors and ultimately promotes the release of the inflammatory cytokines *via* activating Caspase 1, however, its precise function in tumor biology remains controversial (56–58).

In summary, inflammation and immune responses can critically contribute to the cancer onset and determine the outcome of the disease progression. Therefore, inflammation can be considered an enabling characteristic of cancer (39). Investigating the role of proteoglycans in mediating these cancer-associated inflammatory processes may provide novel insights in tumor biology.

1.3 Emerging Implications of Autophagy in Tumorigenesis

Autophagy has an ambivalent role in cancer development and progression. Depending on several factors, such as the tumor progression state, the TME and the genetic context, it can exert opposite outcomes and promote or decrease tumorigenesis (59–61). On one hand, before the onset of malignant transformation and tumorigenesis, the cytoprotective effect of autophagy can promote tumor suppression (62–65). On the other hand, evidence suggest autophagy to promote the survival of cancer cells under certain stress conditions, including therapy-induced stress. Moreover, various cancer types were shown to be linked to a high autophagy (66), such as cancers associated with *RAS* (Ras GTPase, Rat sarcoma) mutations (67, 68), or pancreatic cancer (66, 69), which have been reported to exhibit a high autophagic dependency. Additionally, the upregulation of autophagy is considered to be a frequent side effect of cancer therapies. Therefore, diverse autophagy inhibitors were suggested to increase the efficiency of therapeutics by reducing the tumor cells autophagy-dependent adaptive response mechanisms (70–72). However, increased therapy

efficiencies have has also been reported upon activation of autophagy (73). Furthermore, unconventional secretion, endosomal and exosomal pathways have been shown to link autophagy to affecting cancer metastasis, immune responses and shaping the TME (74). Additionally, cross-talk between autophagy and the EMT was reported (75). In this context, autophagy induction was shown to impair EMT (76, 77), which is a critical contributor to metastasis. Other studies, however, showed that treatment-induced autophagy could exert cyto-protective functions and promote melanoma cell EMT (78). In line with this, knockdown of Beclin-1, which is required for autophagosome formation, reduced EMT of colon cancer cells (79). Notably, autophagy activation was also associated with increased anoikis resistance and enhanced metastasis in several tumor models (80, 81).

Several autophagy inhibitors and inducers are currently being evaluated as treatment options in cancer therapies (82, 83), however, the ambiguous roles of autophagy in tumor biology and the highly context-dependent outcomes of modulating autophagy in different cancer types and progression stages impede the translation to clinical applications. A deeper understanding of how proteoglycans influence autophagy in cancer might allow more precise indications for autophagy inhibitors and inducers, and enable the development of adjuvant therapies.

1.4 Structural Characteristics of Small Leucine-Rich Proteoglycans

Proteoglycans are complex molecules that are embedded in the ECM and comprise a protein core and one or more glycosaminoglycan (GAG) chains, which are covalently tethered to the protein core. The different types of GAG chains can be formed by heparan sulfate, chondroitin sulfate/dermatan sulfate (CS/DS), or keratan sulfate (84–86). In mammalian cells, more than 40 proteoglycans have been described, which are classified according to their localization into extra-, peri-, and intracellular, as well as plasma membrane-associated proteoglycans (85). The divers and manifold biological roles of proteoglycans can be attributed to their variability and modularity, as their protein cores and the heterogeneous GAG chains can be variously modified. Proteoglycans critically provide structure to the ECM, are key receptors to diverse signaling stimuli, such as growth factors, cytokines, chemokines, and important regulators at the intersection of the cell and matrix (87, 88).

The complex and multifaceted regulatory functions of proteoglycans are well exemplified by their largest protein family, the small leucine-rich proteoglycans (SLRPs), which are ubiquitously expressed and highly abundant in the ECM (89). After being secreted into the pericellular space SLRPs are incorporated into the ECM. They are composed of a relatively small protein core of about 40–60 kDa that contains 10–12 motifs of leucine-rich repeats (LRRs) and is flanked by characteristic cysteine-rich clusters with defined spacing. Additionally, the heterogeneous GAG chains are post-translationally attached to the protein core (85, 90–92). To date, there are 18 known SLRPs, which are classified into five distinct classes, based on their N-terminal cysteine-rich clusters, evolutionary conservation, sequence homology, and GAG chains (85). The LRRs of the protein core, which give rise to the characteristic solenoid structure of SLRPs, contain a conserved hydrophobic motif wherein distinct leucines can be substituted by other hydrophobic amino acids (90). Irrespective of their classification, all SLRPs share common biological functions, and most importantly, their capability to interact with various cell surface receptors such as receptor tyrosine kinases (RTKs) and TLRs, thus mediating divers downstream signaling events that regulate vital cellular pathways and processes that are also implicated in cancer, including inflammation and autophagy (17). SLRPs can be released upon tissue stress or injury and can act as damage-associated molecular patterns (DAMPs) (93, 94).

Importantly, an emerging body of evidence points to the vital implications of the SLRPs decorin and biglycan in several hallmarks of cancer and regulating tumor-associated pathways, such apoptosis, proliferation, angiogenesis, inflammation, and autophagy (17, 18, 87, 93–95). In the following sections, we will summarize and discuss the major signaling functions of biglycan and decorin in normal physiology and in the context of cancer.

2 DECORIN FUNCTION IN TUMORIGENESIS

Decorin is a well-characterized, prototypical member of the SLRP family and ubiquitously expressed in most tissues (96). It is mainly known for its vital functions in inflammation, innate immunity, wound healing, fibrotic diseases, angiogenesis, autophagy and cancer, where it is found in the stroma of several cancer types (97–100). Decorin, whose eponym derives from its high affinity for collagen fibrils and thus able to "decorate" collagen fibrils (92, 101, 102), was the first proteoglycan that was associated with regulating the cell cycle by inhibiting transforming growth factor β (TGF-β) signaling (103). This has led to a paradigmatic shift in matrix biology research, since proteoglycans have previously been described only as structural components. Indeed, decorin deficiency in mice leads to a permissive environment favoring tumorigenesis and EMT (104, 105). The diverse functions can be attributed to its ability to interact with numerous components of the ECM and cellular receptors, thereby inducing intracellular signaling cascades. Decorin has the ability to acts as a Pan-RTK inhibitor by engaging numerous RTKs, including the epidermal growth factor receptor (EGFR), the vascular endothelial growth factor receptor 2 (VEGFR2) and the mesenchymal-epithelial transition factor (Met) receptor (**Figure 1**), and can induce caveosomal internalization and degradation of the RTKs, thus restraining angiogenesis. Therefore, and because of its capability to inhibit cancer growth by sequestrating TGF-β, decorin has also been described as "the guardian from the matrix" (99).

2.1 Decorin Acts as a Versatile Tumor Suppressor

One of the most significant RTKs, whose downstream signaling is affected by decorin, is the Met receptor pathway (106–108). Met receptor-mediated signaling is vital for embryonic development and upregulation of the receptor has been linked to tumorigenesis and metastasis (109–112). Direct binding of decorin to the Met receptor results in tumor suppression by

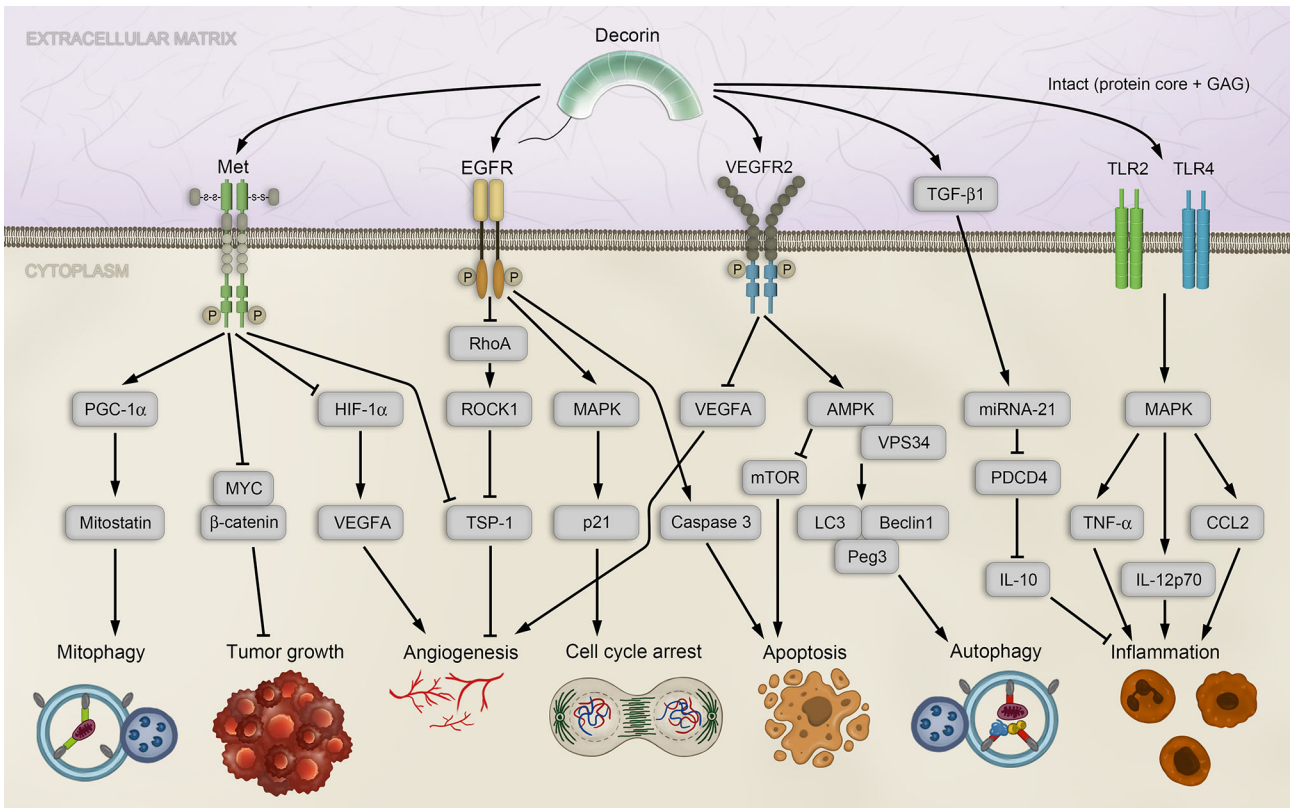

FIGURE 1 | Decorin-mediated signaling affects diverse pathways associated with tumorigenesis. Decorin activates mitophagy in breast carcinoma cells by binding to the Met receptor and activating PGC-1α, leading to accumulation of Mitostatin. Further, *via* Met receptor signaling, decorin inhibits tumor growth by down-regulating β-catenin and MYC, and inhibiting angiogenesis by repressing HIF-1α and VEGFA. Angiogenesis is also modulated by decorin through EGFR in a signaling cascade that employs Rho and ROCK1, leading to upregulation of the anti-angiogenic effector TSP-1. EGFR phosphorylation by decorin induces intracellular MAPK, resulting in enhanced expression of p21 and cell cycle arrest, and in release of Caspase 3 and apoptosis. Decorin-mediated VEGFR2 signaling inhibits angiogenesis and induces autophagy in endothelial cells by inhibiting mTOR, activating VPS34, Beclin-1, LC3 and Peg3. Decorin regulates inflammation in a PDCD4-dependent manner through miRNA-21, or by TLR2/4 signaling. AMPK, AMP-activated protein kinase; CCL, chemokine C–C motif-ligand; EGFR, epidermal growth factor receptor; GAG, glycosaminoglycan; HIF-1α, hypoxia-inducible factor 1α; IL, interleukin; LC3, microtubule-associated protein 1A/1B-light chain 3; MAPK, mitogen-activated protein kinase; Met, mesenchymal-epithelial transition factor; miRNA, microRNA; mTOR, mammalian target of rapamycin; MYC, myelocytomatosis oncogene protein; PDCD4, programmed cell death protein 4; Peg3, paternally expressed 3; PGC-1α, peroxisome proliferator-activated receptor-γ co-activator 1-α; Rho, RAS homolog family member A; ROCK1, Rho-associated coiled-coil kinase 1; TGF-β1, transforming growth factor β isoform 1; TLR, Toll-like receptor; TNF-α, tumor necrosis factor alpha; TSP-1, thrombospondin-1; VEGFA, vascular endothelial growth factor A; VEGFR2, vascular endothelial growth factor receptor 2; VPS34, vacuolar protein sorting 34.

phosphorylation of Met tyrosine sites (106), leading to recruitment of the proto-oncogene CBL (Casitas B-lineage Lymphoma) and subsequent proteosomal degradation of the Met receptor (113). This prevents binding of the natural ligand of the Met receptor, HGF (hepatocyte growth factor), which can contribute to tumor survival, growth, angiogenesis, and metastasis under pathologic conditions (112). The antagonistic effect of decorin on Met signaling results in down-regulation of the major oncogene β-catenin and its downstream effector MYC (myelocytomatosis oncogene protein), both involved in the pathologies of various cancers (107, 114), and thus promotes an anti-tumorigenic activity of decorin (**Figure 1**).

Apart from engaging the Met receptor, decorin can attenuate tumor growth as a monomeric proteoglycan (115). To date, the protein interacting network centered on decorin is vast and expanding (116), with numerous growth factors, receptors, and various matrix molecules. The interaction of decorin with TGF-β causes strong inhibition of proliferation in various cancer cell lines, presumably by decorin-binding activity on TGF-β isoform 1 (TGF-β1), thereby sequestrating it in the ECM and limiting its bioactivity (117). Mechanistically, EGFR phosphorylation by decorin induces intracellular MAPK (mitogen-activated protein kinase) signaling that results in enhanced expression of the cyclin-dependent kinase inhibitor p21, triggering cell cycle arrest, and in release of Caspase 3 to promote apoptosis (99, 108, 118, 119) (**Figure 1**). Moreover, decorin competes with the natural ligand of EGFR, the epidermal growth factor (EGF), and the decorin-EGFR interaction results in internalization and degradation of the receptor *via* caveolar endocytosis (120), thus controlling tumor growth (121–123).

2.2 Decorin Regulates Angiogenesis *via* Receptor Tyrosine Kinase Signaling

A central issue of tumorigenesis is angiogenesis, an intrinsic process required for supplying oxygen and nutrients to the growing tumor through vessels newly formed from preexisting large vessels. The role of decorin in regulating angiogenesis is ambivalent, as decorin promotes angiogenesis by facilitating endothelial cell adhesion and migration in a non-malignant state (108, 124, 125). Likewise, it was shown in healthy, non-tumorigenic models that decorin protects endothelial cells from hypoglycemia and promotes angiogenesis through IGF-1R (insulin-like growth factor type 1 receptor) signaling (126). Conversely, multiple independent studies have clearly demonstrated an angiostatic effect of decorin in the setting of cancer and its down-regulation correlates with the degree of tumor vascularization in various cancer types (99, 100, 108, 127).

The interaction of decorin with VEGFR2 constitutes the most significant contribution to impairing tumor angiogenesis (98, 99) (**Figure 1**). By competing with its canonical¨ ligand VEGFA (vascular endothelial growth factor A), decorin acts as a partial antagonist of VEGFR2 which is specifically located on the surface of endothelial cells to facilitate their angiogenic activity (128–130). Additionally, decorin decreases the proteolytic cleavage of matrix-bound VEGFA in the ECM by inhibiting matrix-metalloprotease activities and expression (99, 107, 131, 132).

Another contributing mechanism of decorin-mediated angiostasis is the recent observation that soluble decorin can reduce VGFA levels by evoking its catabolic degradation *via* autophagy (133) (see below). In parallel to suppressing these pro-angiogenic effectors *via* VEGFR2 signaling, angiogenesis can be modulated by decorin through EGFR. The decorin-EGFR interaction interferes with the signaling cascade that employs Rho (RAS homolog family member A) and the Rho-associated coiled-coil kinase 1 (ROCK1), leading to upregulation of anti-angiogenic effectors, such as thrombospondin-1 (TSP-1) and tissue inhibitor of metalloproteinases-3 (TIMP-3) (108, 131, 132) (**Figure 1**).

Additionally, decorin inhibits angiogenesis by impairing Met signaling, because attenuation of Met signaling causes an induction of TIMP-3. In parallel, hypoxia-inducible factor 1α (HIF-1α) is being repressed and degraded and Met-induced VEGFA expression is inhibited (107, 131). Regulated by a negative feedback loop, loss of HIF-1α in turn inhibits Met expression (131). Collectively, these observations posit the small leucine-rich proteoglycan decorin as an important component of the angiostatic network and the cross-talk between and endothelial and tumor cells.

2.3 Decorin Activates Endothelial Autophagy and Cancer Cell Mitophagy

The anti-tumor activities of decorin additionally include the regulation of the autophagy and mitophagy pathways. In vascular endothelial cells, a decorin-induced indirect induction of autophagy was demonstrated by promoting the formation of autophagic initiation complexes and by down-regulation of autophagy inhibitors (134–136). Decorin interaction with VEGFR2 induces the AMP-activated protein kinase (AMPK) and initiates a signaling cascade to activate VPS34 (vacuolar protein sorting 34) and to inhibit mTOR (mammalian target of rapamycin). Decorin evokes sustained autophagy by transcriptional activation of *Peg3* (Paternally expressed gene 3), an imprinted gene expressed exclusively from the paternal allele (137), and that is often silenced in several tumor types by promoter hypomethylation (138, 139). This leads to accumulation of Beclin-1 and LC3 (microtubule-associated protein 1A/1Blight chain 3), which are required for autophagosome formation (130, 136, 140). As $Peg3^{+}$ progenitor cells participate in vascular remodeling (141), and as Peg3 represents a marker for a subset of vessel-associated endothelial progenitors (142), it is possible that decorin may additionally affect angiogenesis *via* Peg3-endothelial stem cells interactions.

A recently uncovered implication of decorin in regulating mitophagy has been reported, which linked decorin directly to affecting the catabolic process of mitophagy within the tumor proper. In line with this, decorin directly activated mitophagy in breast carcinoma cells trough Met receptor activation and subsequent mobilization of PGC-1α (Peroxisome proliferator-activated receptor-γ co-activator 1-α) (143), accompanied by a decorin-mediated mRNA stabilization accumulation of Mitostatin (143) (**Figure 1**). Thus, decorin can affect the cellular energy production and indirectly cell death/apoptosis by evoking autophagic catabolism of mitochondria.

2.4 Decorin Regulates Inflammation and the Innate Immune Response

Extensive studies using models for tissue stress and injuries have demonstrated the well-established roles of decorin, and likewise biglycan, in regulating inflammatory and immune responses by interaction with TLR2 and TLR4 (144). There are two mechanisms for decorin-dependent control of inflammation and tumor growth that are based on either stimulation of PDCD4 (programmed cell death protein 4) expression, or on it translational repression (145). PDCD4 is known to promote the inflammatory response by activating NF-κB and suppressing the anti-inflammatory mediator interleukin 10 (IL-10) expression (146). PDCD4 expression is increased by decorin acting as an endogenous ligand of TLR2/4 and stimulating production of proinflammatory molecules, including PDCD4 (145). In a second mechanism, decorin down-regulates the pool of bioactive TGF-β1, which, as mentioned before, can be sequestered by decorin in the ECM. TGF-β1 in turn is an inducer of oncogenic microRNA (miRNA)-21 (147), which functions as a translational repressor of PDCD4 (148). Therefore, decorin indirectly regulates the levels of PDCD4 (145) (**Figure 1**).

3 BIGLYCAN IS A MATRIX-DERIVED SIGNALING MOLECULE IN CANCER

Biglycan, another member of class I SLRPs and structurally homologous to decorin, is a ubiquitously expressed ECM protein (23, 85, 149). The 42 kDa protein core consists of 10

LRRs as well as two N-terminal, covalently bound, tissue-specific CS/DS type GAG chains (23, 150). Through its protein core and GAG chains, biglycan interacts with other ECM proteins like collagen types I-IV and elastin, thereby providing stability and organization in tissues, as well as bone composition (151–156). Although biglycan is tightly bound to the ECM under physiological conditions, the proteoglycan is released from its ECM-bound state during tissue stress and injury through cleavage by proteases (87, 157–160). Additionally, biglycan can be synthesized *de novo* in macrophages during inflammation and is released into circulation (161). In its soluble state, biglycan can be found in the bloodstream in many acute or chronic inflammatory disease acting as a DAMP (93, 159). Biglycan holds great potential as biomarker as deregulated levels of soluble biglycan are detected in a variety of inflammatory and chronic disease, such lupus nephritis (144), diabetes (162, 163), fibrosis (164), renal diseases (159), and cancer (165), biglycan holds great potential as biomarker.

Just as decorin, biglycan has proven to be a versatile matrix-derived signaling molecule that can trigger induction of several pathways involved in tumorigenesis *via* its complex and diverse interactions with both growth factors/cytokines and cell surface receptors (18, 23, 157).

3.1 Mechanisms of Biglycan-Induced Inflammation

Under physiological conditions, in its soluble and intact form, biglycan acts as a DAMP and engages in the innate immunity by binding TLR2 and/or TLR4, mimicking gram negative and positive microbial responses and triggering an inflammatory cell response (93, 157). This results in induction of NF-κB and Erk (extracellular signal-regulated kinase) signaling pathways leading to increased levels pro-inflammatory cytokines and chemokines. Most importantly, these include TNF-α and IL-1β, as well as C-C motif ligand (CCL) and C-X-C motif ligand (CXCL) proteins and ultimately result in recruitment of immune cells such as neutrophils, T-cells, B-cells and macrophages into the inflamed regions, infiltrating tissues and organs (23, 161).

The biglycan-induced downstream signaling and its outcome depend on the selective utilization of either TLR2 or TLR4, or both, as well as on the interactions with their distinct co-receptors and adaptor molecules (157, 161). For instance, while TLR4/2 interaction with MyD88 specifically induces TNF-α, IL-1β, CXCL1, CCL2, and CCL20, interaction of biglycan with TLR4 and TRIF (TIR-domain-containing adapter-inducing interferon-β) results in expression of CCL5 and CXCL10 (161) (**Figure 2**). Moreover, biglycan interaction with only TLR2 and MyD88 regulates the expression of HSP70 (heat shock protein 70), which binds to NADPH oxidase (NOX)2, and thereby impairs the inhibitory function of NOX2 on IL-1β expression (166) (**Figure 2**). The repertoire of co-receptors employed by TLR2/4 was extended by the discovery of the co-receptor CD14, a high-affinity ligand of biglycan, whose deficiency resulted in abrogated NF-κB, MAPK and ERK signaling and consequent absence of biglycan-induced increase of cytokine expression in macrophages (167).

Additionally, biglycan mediates clustering of TLR2/4 and the purigenic receptors P2X4/P2X7 (168) (**Figure 2**). This enables a cross-talk signaling between both receptor types and allows biglycan to autonomously activate the NLRP3 inflammasome assembly, which is followed by Caspase 1 activation and processing of pro-IL-1β and pro-IL-18 to their mature forms (168).

Biglycan signaling bridges innate and adaptive immune responses as it is involved not only in recruitment of innate immune cells, most importantly macrophages, but also induces synthesis of chemoattractants of B cells and T helper (Th) cells. Mechanistically, the biglycan/TLR4 interaction mediates signaling to sphingosine kinase-1 to regulate the synthesis of macrophage chemoattractants (169). In macrophages and dendritic cells, biglycan/TLR2/4 signaling evokes the expression of a key chemoattractant of B-cells, namely CXCL13 (144). Additionally, biglycan regulates the expression of CXCL9 and CXCL10 *via* TLR4 and TRIF to drive recruitment of Th1 and Th17 cells into the kidney (170). The signaling axis of biglycan and TLR2/4 also enhances antigen-specific T cell activation, potentially in a MyD88/TRIF-dependent manner, and induces autoimmune perimyocarditis (171).

The above-mentioned roles of biglycan in regulating inflammatory signaling and immune response, and in particular the recruitment of immune cells, posit several key connections between biglycan-mediated signaling and cancer-associated inflammation. For instance, the significant role of NLRP3 inflammasome activation in cancer is indisputable but ambivalent and complex (58). Thus, biglycan-mediated NLRP3 inflammasome activation provides an additional regulatory mechanism contributing to its complex regulation. Moreover, CCL2 and CCL5, whose expression is regulated in a biglycan-dependent manner, are known contributors that promote immune cells infiltration at the tumor site, metastasis, and angiogenesis (172–175). In addition, Th1 cells promote synthesis of pro-inflammatory factors, such as IL-12, IL-2, IFNγ and TNFα, thus driving inflammation. Tumor-infiltrating Th1 and Th17 cells have also been identified in various cancers inducing both, pro-tumoral and anti-tumoral immunity (176–178). In line with this, it is possible that biglycan-driven recruitment of immune cells could promote an inflammatory milieu that facilitates tumorigenesis, but also support immuno-surveillance by enhanced Th1, Th17 and macrophage recruitment in some cases with anti-tumorigenic effects of biglycan. These diverse implications of biglycan in triggering and modulating inflammation and the immune response suggest an important role for this proteoglycan in the development of tumor-associated inflammation.

3.2 Biglycan as a Regulator of Autophagy

In addition to the various biological roles of biglycan in inflammation, this proteoglycan can cause a switch between inflammation and autophagy in macrophages by selectively binding either CD14 or CD44 with equally high affinities causing an opposing biological outcome. While the interaction of biglycan and CD14, in an TLR2/4-dependent manner, results in an increase of pro-inflammatory signaling and the

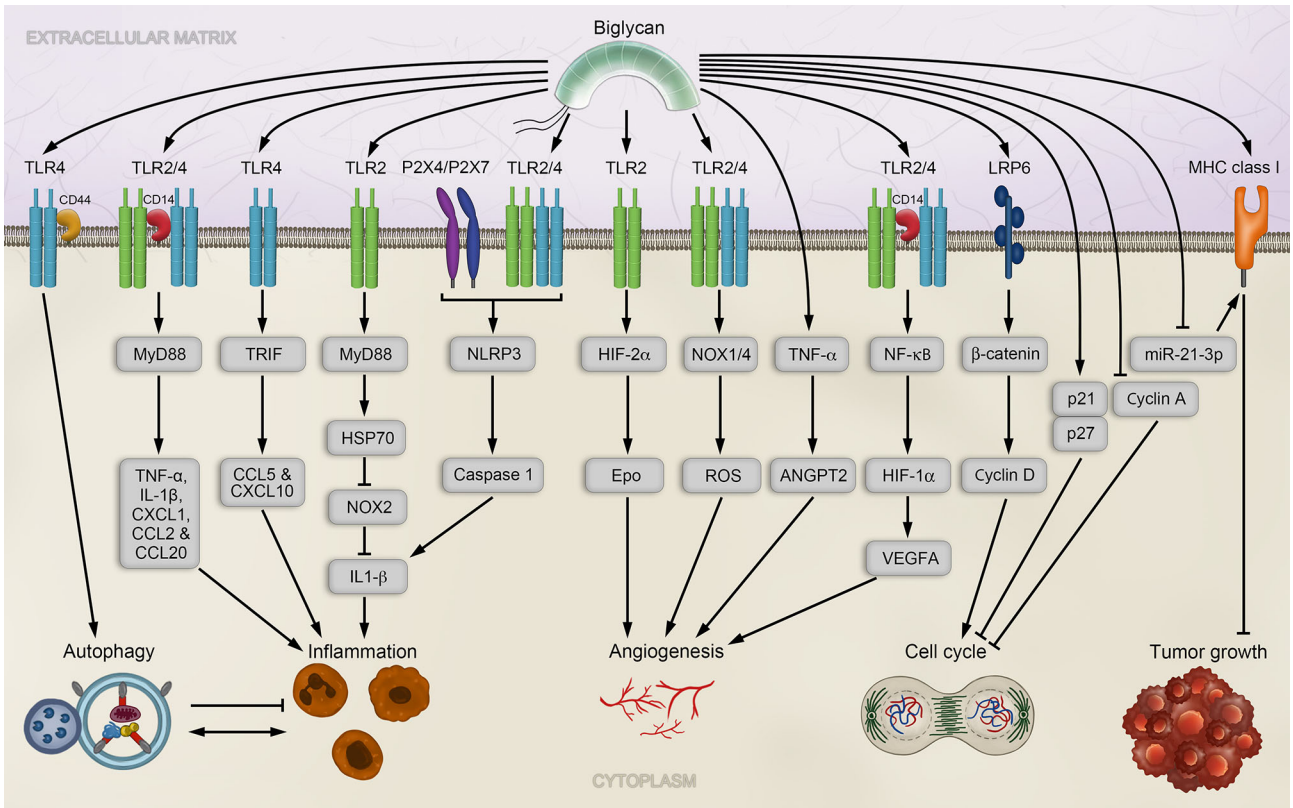

FIGURE 2 | Biglycan signaling and implications in tumorigenesis. Soluble biglycan induces TLR4/CD44mediated autophagy in macrophages and TLR2/4/CD14-mediated inflammation *via* the adaptor molecule MyD88. Inflammation is also trigger by biglycan binding to TLR4 *via* TRIF, or TLR 2 *via* MyD88. Biglycan-mediated clustering of TLR2/4 with the P2X4/P2X7 receptors, which activates the NLRP3 inflammasome, consequently leading to the maturation of IL-1β. In endothelial cells, biglycan promotes angiogenesis in a TLR2/4-dependent manner by enhancing HIF-1α activity and VEGFA expression. Biglycan further affects ROS production *via* TLR2 and TLR4 in a NOX1- and NOX4-dependent manner. Biglycan stabilizes HIF-2α *via* TLR2 interaction and leads to of Epo synthesis. Biglycan knockout impaired tumor by repressing TNF-α and ANGPT2 signaling in a cancer mouse model. Additionally, biglycan can induces a cell cycle arrest by increasing the expression p27 and p21 and decreasing Cyclin A levels. By increasing MHC complex I expression *via* miR-21-3p, biglycan exerts anti-tumoral activities.ANGPT2, angiopoietin 2; CCL, chemokine C–C motif-ligand; CD, cluster of differentiation; CXCL, chemokine C-X-C motif-ligand; Epo, erythropoietin; HIF-1/2α, hypoxia-inducible factor 1/2α; HSP70, heat shock protein 70; IL-1β, interleukin 1 beta; LRP6, low-density lipoprotein receptor-related protein 6; MHC, major histocompatibility complex; miR, microRNA; MyD88, myeloid differentiation primary response 88; NF-κB, nuclear factor kappa-light-chain-enhancer of activated B-cells; NLRP3, NOD-like receptor protein 3; NOX, NADPH oxidase; ROS, reactive oxygen species; TLR2/4, Toll-like receptor 2/4; TNF-α, tumor necrosis factor alpha; TRIF, TIR-domain-containing adapter-inducing interferon-β; VEGFA, vascular endothelial growth factor A.

polarization of M1 macrophages (179), the interaction between biglycan and CD44 counteracts these events and results in the polarization of M2 macrophages as well as in an increase of autophagy-flux and anti-inflammatory effects (180) (**Figure 2**). The unexpected biglycan-induced opposing switch between inflammation and autophagy is solely caused by fluctuations in interaction partners. This process determines whether the downstream signaling will ultimately lead to chronic inflammation, fibrosis and possibly facilitate tumorigenesis, or promote regeneration. These findings underline how tightly those molecular processes, inflammation, and autophagy, are regulated in non-malignant tissues and presumably also in cancer. Accordingly, we presume that a subtle modulation of either one may have major impact on the other, a key factor affecting their therapeutic targeting. The described regulation of immunity responses by biglycan could, for example, affect the resolution of early pre-cancerous lesions, or promote their tumorigenic development. The cause of this switch is yet to be established and future studies will be needed to unravel the precise function of the biglycan-binding epitopes of CD14 and CD44. While these observations were made in non-malignant cells, the fact that biglycan mediates M2 macrophage polarization through autophagy induction suggests that biglycan could be involved in tumor-associated macrophage (TAM) activation during tumor progression at late stages. This is particularly important as sustained biglycan overexpression is linked to enhanced M2 macrophage numbers in ischemia reperfusion injury (180).

Emerging evidence over the past years has demonstrated the crucial role of autophagy in regulating cancer-associated inflammation, and vice versa. For example, autophagy critically affects inflammation by influencing the development,

homeostasis, and survival of immune cells, including macrophages, neutrophils and lymphocytes (181, 182). In the future, it will be vital to investigate the mechanisms that regulate the intricate interplay of autophagy and inflammation. Therefore, this recent discovery of CD44 as an additional co-receptor for TLR4 and a high-affinity ligand for biglycan provide novel and valuable insights of possible cross-talk mechanisms between autophagy and inflammation (179, 180).

3.3 Mechanisms of Biglycan-Mediated Angiogenesis

Angiogenesis is an important hallmark of cancer and vital for tumor growth and metastasis, as it provides vessels for blood supply and allows transformed cells to enter the circulation (39). Despite their structural homology, the roles of decorin and biglycan in neovascularization are rather opposing. The main mechanism of biglycan signaling employs TLR2 and TLR4 receptors and results in pro-tumorigenic effects, including the production of cytokines and growth factors that ultimately promote tumor angiogenesis. For instance, biglycan-induced, upregulated VEGFA expression promotes neovascularization and cancer growth in colon cancer cells (183). Moreover, biglycan stimulation of human umbilical vein endothelial cells results in increased tubular formation capacity (184). On a molecular basis, biglycan stimulation of endothelial cells results in increased interaction between NF-κB and the HIF-1α promoter in a TLR2/4-dependent manner, enhanced HIF-1α levels and activity, and consequently increased VEGFA expression (184) (**Figure 2**). These findings support a promoting role of biglycan in cancer development and progression, likely by promoting and activating tumor angiogenesis (184).

An additional mechanism that links biglycan signaling to angiogenesis regulation is the enhanced production of reactive oxygen species (ROS). ROS can be produced by NOX enzymes and result in enhanced angiogenesis and tumor growth by increased NF-κB and VEGF expression (185). Due to the ability of biglycan to affect ROS production *via* TLR2 and TLR4 in a NOX1- and NOX4-dependent manner (166, 168) (**Figure 2**), it is very likely that biglycan potentially influences tumor angiogenesis *via* ROS level regulation.

Alternatively, angiogenesis in cancer could be affected by biglycan through the stabilization HIF-2α, which is induced by TLR2 interaction with biglycan and results in the induction of erythropoietin (Epo) synthesis and polycythemia (186) (**Figure 2**). Changes in HIF-2α expression levels have been described in a variety of solid tumors and are linked to TAMs and HIF-2α is, similar to biglycan, associated with late tumor progression stages (187).

In a mouse model of breast cancer with tumor-bearing mice, knockout of biglycan in the stroma inhibited metastasis to the lung, impaired tumor angiogenesis and normalized tumor vasculature by repressing TNF-α and angiopoietin 2 (ANGPT2) signaling (188) (**Figure 2**).

Several studies have focused on the role of biglycan in colon cancer (183, 189, 190). For instance, it was shown that, in colon cancer cells, inhibiting biglycan results in increased expression of pro-apoptotic effectors and is linked to suppressed NF-κB pathway activity. On the other hand, biglycan overexpression does the opposite effect (190). Moreover, biglycan-mediated chemotherapy resistance in colon cancer cells occurs by activating NF-κB signaling (190). Considering the well-established, TLR2/4-dependent function of biglycan in NF-κB signaling, the fact that TLRs have been linked to tumorigenesis of multiple tumor types (191, 192), and the known implications of the NF-κB pathway in the development of chemotherapy resistance in cancers (193, 194), it is convincing that biglycan may promote resistance mechanisms by regulating the NF-κB pathway.

3.4 The Role of Biglycan in Promoting Cancer Cell Proliferation, Invasion, and Metastasis

Already a decade ago, a study in osteoprogenitor cells and bone fracture healing models revealed the ability of biglycan to enhance canonical Wnt signaling and to interact with the Wnt co-receptor low-density lipoprotein receptor-related protein 6 (LRP6) (195). Wnt signaling is considered to be a major pathway regulating development and has also been closely linked to carcinogenesis, particularly in the context of colorectal cancer (196, 197). Therefore, these findings suggested a potential function of biglycan in tumorigenesis based on its ability to affect cancer cell proliferation *via* Wnt signaling modulation. More recently, a link between biglycan and Wnt/LRP6 signaling was additionally reported in the context of osteosarcoma. Specifically, biglycan favors MG63 osteosarcoma cell proliferation *via* a LPR6/β-catenin/IGF-1R signaling axis and functions in a positive feedback loop regulating osteosarcoma growth (198). By binding to LRP6, biglycan inhibits the destruction of β-catenin, an inducer of Cyclin D1 expression. Increased Cyclin D1 levels, in turn, activate IGF-1R and ultimately result in enhanced biglycan secretion (198).

Another observation that links biglycan signaling to the regulation of cancer cell proliferation was reported in a study conducted in HCT116 colon cancer cells. In this cellular context, suppression of biglycan expression *via* short hairpin RNA (shRNA) decreases cancer cell proliferation and causes cell cycle arrest at the G0/G1 phase, accompanied by decreased levels of cell cycle associated proteins, including Cyclin A and Cyclin D1 (189). In contrast, expression levels of p21 and p27 are markedly increased in the cancer cells of the control shRNA group (189). Furthermore, the decreased biglycan levels suppressed colon cancer cell migration and invasion, and induced apoptosis in a p38 and MAPK-dependent manner (189).

In the context of gastric cancer, significantly increased tissue biglycan levels have been linked to lymph node metastasis and depth of tumor invasion, both *in vivo* and *in vitro* (199). *In vitro*, investigation of endothelial cell migration, invasion and tube formation ability was positively linked to biglycan levels (199). *In vivo*, biglycan induced focal adhesion kinase (FAK) phosphorylation, suggesting an oncogenic function of biglycan in gastric cancer metastasis in a FAK signaling-dependent manner (199). In line with this, biglycan was recently shown to modulate gastric cancer aggressive features as cell survival, migration, and angiogenesis and biglycan knockout gastric

cancer cells showed increased levels of PARP1 (Poly [ADP-ribose] polymerase 1) and Caspase 3 cleavage (200).

Additional roles of biglycan in cancer cell proliferation, migration and metastasis were reported in tumor endothelial cells, where biglycan mediated tumor cell migration *via* TLR2/TLR4/NF-κB/Erk1/2 (201), in melanoma cells, where biglycan increased invasiveness by enhancing integrin-β1 expression (202), and in endometrial cancer cells, where knockdown of biglycan reduced migration, tubular formation and metastasis (203). Collectively, these studies point to a pro-tumorigenic role of biglycan proteoglycan in both mesenchymal (osteosarcoma) and epithelial (colon and breast carcinomas) malignancies.

3.5 Anti-Tumorigenic Effects Mediated by Biglycan

The vast majority of research on biglycan in cancer indicate its pro-tumorigenic function. However, several studies have also linked anti-tumorigenic effects to higher biglycan expression levels. Tumor suppressive effects have, for instance, been reported in pancreatic cancer cell lines, where treatment with exogenous biglycan leads to an up-regulation of cyclin-dependent kinase inhibitor p27, down-regulation of Cyclin A and PCNA (proliferating cell nuclear antigen), and cell cycle arrest (204) (**Figure 2**).

Similarly, treatment with exogenous biglycan of bladder cancer cells inhibits cell proliferation and high biglycan levels correlate with prolonged survival of bladder cancer patients (205), and superior patient prognosis of patients with diffuse large B-cell lymphoma (206). In this context, $CD40^+$ tumors exhibit increased levels of biglycan that additionally correlate with the number of infiltrating macrophages and $CD4^+$ and $CD8^+$ T-cells. *In vitro* experiments have demonstrated that CD40 signaling can enhance antigen presentation from malignant B-cells, thus inducing an autologous immune response (207, 208). In line with this, higher biglycan levels could be linked to a high intra-tumoral inflammatory reaction that may result in an increased tumor response, and thereby a better prognosis (206).

In an *in vitro* model of oncogenic transformation, the role of biglycan in the initiation and maintenance of neoplastic transformation was investigated (209). In this study, the HER-2-mediated oncogenic transformation caused silencing of biglycan gene expression, while reconstitution of biglycan expression led to an impaired proliferation and migration of oncogenic transformed cells (209). Therefore, HER2-mediated silencing of biglycan expression may promote tumor cell proliferation and migration and provides a putative therapeutic target for the treatment of $HER2^+$ tumor cells (209). Moreover, restoration of biglycan in HER2 fibroblasts decreases their tumorigenic potential when compared to HER2 cells with low biglycan levels (210). Biglycan restoration is linked to an enhanced immune cell responses and increases numbers of immune effector cells in tumors and peripheral blood, possibly resulting from up-regulated major histocompatibility complex (MHC) class I surface antigens, and decreased expression levels of TGF-β and the TGF-β receptor 1 (210). The overexpression of biglycan in HER2 cells additionally mediates an upregulation of decorin, which also elevates MHC class I surface expression in biglycan negative HER2 cells, suggesting a putative synergistic action of both SLRPs (210). Most recently, miR-21-3p mediates down-regulation of MHC class I surface antigens, interferes with the expression of immune-modulating effectors and promotes immune suppression in HER-2/neu cells (211). Induced overexpression of biglycan in HER-2/neu cells increases MHC class I expression and decreases miR-21-3p, highlighting the vital role of biglycan in the MHC class I-driven immune escape in tumor cells (211) (**Figure 2**).

4 THERAPEUTIC IMPLICATIONS AND FUTURE PERSPECTIVES

Cancer development and progression are multifaceted processes that involve an intricate interplay of genetic and environmental factors. Transformed cells continuously interact with their surroundings, mostly constituted by ECM components. Therefore, proteoglycans, key constituents of the tumor stroma, are increasingly recognized as crucial contributors in shaping the cancer microenvironment by regulating inflammatory and immune responses, affecting autophagy, mediating angiogenesis, and modulating cellular signaling pathways to control cell proliferation, migration and metastasis. All these processes can ultimately either promote resolution and regeneration, or lead to tumor development and disease progression. The diverse implications of proteoglycans in these processes highlight their broad potential as therapeutic targets in cancer therapy. Indeed, the characteristic expression patterns of proteoglycans and their interaction partners in diverse tumor types have been exploited as biomarkers for prognosis and indication for therapy efficiencies.

The well-known pan-tyrosine kinase inhibiting capabilities of decorin have made the SLRP an attractive target for cancer therapies. Although the underlying molecular functions of decorin are complex and not yet fully understood, the evidence favor an antitumorigenic role of decorin. This notion holds great potential of clinical relevance and has led to a variety of studies focused on expressing decorin to attenuate tumorigenic growth (17, 212). Delivery of decorin can be mediated *via* adenoviral vectors or by systemic administration of decorin proteoglycan, protein core or fragments (212). Numerous studies have showed that expression of exogenous decorin can suppress tumor growth, in particular for cancer types that depend on RTK signaling, such as EGFR, Met and IGF-1R (212). Delivery of decorin *via* adenoviral vectors into the tumor cells has been demonstrated to inhibit tumor growth of colon, lung, and squamous cell carcinoma (122, 213). Other decorin gene therapy approaches have been successfully tested in various types of cancer including models of breast cancer (214), glioblastoma (215, 216), prostate tumors (213). These studies have largely confirmed the therapeutic capability of decorin in suppressing tumor development and/or growth (212). Despite the promising evidence from *in vivo* and *in vitro* studies, and although decorin is unlikely to exhibit toxic side effects, the translation into a clinical drug has not been finalized. One major

challenge that limits the development of decorin-based clinical drugs are technical limitations in proteoglycan mass production (217). Future improvements in production, delivery and efficiency will improve the rationale for applying decorin in the treatment of cancer.

Over the past few years, our understanding of how biglycan mediated signaling in the state of health and during disease progression has significantly improved. In particular, the recent evidence of the fine-tuned biglycan-mediated regulation of the inflammatory response, which is orchestrated *via* distinct receptor, co-receptor, and adaptor molecules, constitutes an important step towards understanding how biglycan signaling can induce different, and often conflicting, downstream signaling outcomes (218). The biglycan-mediated switch between inflammation and autophagy, depending on the respective co-receptor (167, 180), is of particular interest, but raises several questions that await further investigations. These questions include for example, the identification of the binding stoichiometry of biglycan and its co-receptors CD14 and CD44, of the selection mechanisms that govern the choice of the co-receptors and of the CD14 and CD44 binding motifs. The answers will ultimately enable the translation of the current knowledge of biglycan-mediated signaling into pharmacological interventions, as the ability to precisely modulate the biglycan-induced downstream signaling could be a promising therapeutic approach.

In contrast to decorin, which is associated with mainly anti-tumorigenic effects and where administration of the proteoglycan provides a potent strategy for cancer therapy, biglycan is rather linked to pro-tumorigenic effects. However, TLRs have crucial physiological functions, inhibitory targeting of biglycan-mediated signaling cascades requires further studies to gain precise knowledge on the co-receptors and downstream mechanisms of biglycan/TLR signaling to ensure selective targeting in the context of cancer. In cases where tumor growth is linked to decreased levels of biglycan, delivering biglycan could be beneficial to promote immunogenicity. For example, in the context of HER2 cells, where increased biglycan expression is linked to tumor suppression, the recent discovery of the biglycan/miR-21-3p/MHC class I axis provides an interesting and innovative therapeutic concept for HER2+ cancers by administration of biglycan (211). This could increase immunogenicity mediated by a strong infiltration with effector T cells, macrophages, and support inflammation by the production of pro-inflammatory factors, thus inhibit the escape from immune surveillance. Lastly, it is of note that the regulation of tumorigenesis likely depends on the synergistic and timely action of several components of the ECM and thus it is indispensable to broaden our knowledge on the intricate interplay of these proteoglycans in normal and malignant physiology.

In spite of the rapid progress in this field of research, there are still several outstanding questions. For example, given the cell-dependent context of decorin and biglycan in evoking autophagy in tumorigenesis, at what stage do these proteoglycans play an active role in either suppressing or promoting tumor development? Moreover, do the downstream signaling effects of these autophagic modulators occur independently or are they synergistically coordinated in the tumor stroma? Is decorin vs biglycan more critical in regulating disease-altering autophagy in certain types of malignancies over others? We feel that further investigations into these inquiries are required to better decipher the aberrant matrix remodeling and clarify the disease-driving impact of the ECM in carcinogenesis.

AUTHOR CONTRIBUTIONS

All authors listed have made a substantial, direct, and intellectual contribution to the work and approved it for publication.

FUNDING

The authors' laboratories were supported by the German Research Council (SFB 1039, project B02, SFB 1177, 259130777, project E02, all to LS; and the CardioPulmonary Institute (CPI), EXC 2026, Project ID: 390649896 (to LS and MW); WY119/1-3 (to MW), the Else Kroner-Fresenius-Foundation (to MW), and the German Center for Lung Research (to MW);¨ European Union's Horizon 2020 research and innovation program's MICROBPREDICT study (No 825694), European Union's Horizon 2020 Research and Innovation Program GALAXY (No. 668031) and Societal Challenges LIVERHOPE (Health, demographic change, and well-being, No. 731875) the German Research Council (SFB TRR57, CRC1382), Cellex Foundation (PREDICT) all to JT. The original research in Dr. Iozzo laboratory was supported in part by National Institutes of Health Grants RO1 CA39481 and RO1 CA245311.

ACKNOWLEDGMENTS

The authors apologize to those researchers whose work could not be cited due to space limitation.

REFERENCES

1. DeClerck YA, Pienta KJ, Woodhouse EC, Singer DS, Mohla S. The Tumor Microenvironment at a Turning Point—Knowledge Gained Over the Last Decade, and Challenges and Opportunities Ahead: A White Paper From the NCI TME Network. *Cancer Res* (2017) 77:1051–9. doi: 10.1158/0008-5472.CAN-16-1336
2. Hinshaw DC, Shevde LA. The Tumor Microenvironment Innately Modulates Cancer Progression. *Cancer Res* (2019) 79:4557–66. doi: 10.1158/0008-5472.CAN-18-3962
3. Werb Z, Lu P. The Role of Stroma in Tumor Development. *Cancer J* (2015) 21:250. doi: 10.1097/PPO.0000000000000127
4. Noy R, Pollard JW. Tumor-Associated Macrophages: From Mechanisms to Therapy. *Immunity* (2014) 41:49–61. doi: 10.1016/j.immuni.2014.06.010
5. Lewis CE, Harney AS, Pollard JW. The Multifaceted Role of Perivascular Macrophages in Tumors. *Cancer Cell* (2016) 30:18–25. doi: 10.1016/j.ccell.2016.05.017
6. Santi A, Kugeratski FG, Zanivan S. Cancer Associated Fibroblasts: The Architects of Stroma Remodeling. *Proteomics* (2018) 18:1700167. doi: 10.1002/pmic.201700167

7. Bremnes RM, Dønnem T, Al-Saad S, Al-Shibli K, Andersen S, Sirera R, et al. The Role of Tumor Stroma in Cancer Progression and Prognosis: Emphasis on Carcinoma-Associated Fibroblasts and Non-Small Cell Lung Cancer. *J Thorac Oncol* (2011) 6:209–17. doi: 10.1097/JTO.0b013e3181f8a1bd
8. Palucka AK, Coussens LM. The Basis of Oncoimmunology. *Cell* (2016) 164:1233–47. doi: 10.1016/j.cell.2016.01.049
9. Picoli CC, Gonçalves BÔ, Santos GS, Rocha BG, Costa AC, Resende RR, et al. Pericytes Cross-Talks Within the Tumor Microenvironment. *Biochim Biophys Acta (BBA)-Reviews Cancer* (2021) 41:188608. doi: 10.1016/j.bbcan.2021.188608
10. Fukumura D, Duda DG, Munn LL, Jain RK. Tumor Microvasculature and Microenvironment: Novel Insights Through Intravital Imaging in Pre-Clinical Models. *Microcirculation* (2010) 17:206–25. doi: 10.1111/j.1549-8719.2010.00029.x
11. Forster JC, Harriss-Phillips WM, Douglass MJ, Bezak E. A Review of the Development of Tumor Vasculature and Its Effects on the Tumor Microenvironment. *Hypoxia* (2017) 5:21–32. doi: 10.2147/HP.S133231
12. Cox TR. The Matrix in Cancer. *Nat Rev Cancer* (2021) 21:1–22. doi: 10.1038/s41568-020-00329-7
13. Henke E, Nandigama R, Ergün S. Extracellular Matrix in the Tumor Microenvironment and Its Impact on Cancer Therapy. *Front Mol Biosci* (2020) 6:160. doi: 10.3389/fmolb.2019.00160
14. Neill T, Schaefer L, Iozzo RV. Instructive Roles of Extracellular Matrix on Autophagy. *Am J Pathol* (2014) 184:2146–53. doi: 10.1016/j.ajpath.2014.05.010
15. Schaefer L, Dikic I. Autophagy: Instructions From the Extracellular Matrix. *Matrix Biol* (2021) 101:1–11. doi: 10.1016/j.matbio.2021.06.002
16. Hastings JF, Skhinas JN, Fey D, Croucher DR, Cox TR. The Extracellular Matrix as a Key Regulator of Intracellular Signalling Networks. *Br J Pharmacol* (2019) 176:82–92. doi: 10.1111/bph.14195
17. Schaefer L, Tredup C, Gubbiotti MA, Iozzo RV. Proteoglycan Neofunctions: Regulation of Inflammation and Autophagy in Cancer Biology. *FEBS J* (2017) 284:10–26. doi: 10.1111/febs.13963
18. Moreth K, Iozzo RV, Schaefer L. Small Leucine-Rich Proteoglycans Orchestrate Receptor Crosstalk During Inflammation. *Cell Cycle* (2012) 11:2084–91. doi: 10.4161/cc.20316
19. Miller AE, Hu P, Barker TH. Feeling Things Out: Bidirectional Signaling of the Cell–ECM Interface, Implications in the Mechanobiology of Cell Spreading, Migration, Proliferation, and Differentiation. *Adv Healthcare Mater* (2020) 9:1901445. doi: 10.1002/adhm.201901445
20. Raines EW. The Extracellular Matrix can Regulate Vascular Cell Migration, Proliferation, and Survival: Relationships to Vascular Disease. *Int J Exp Pathol* (2000) 81:173–82. doi: 10.1046/j.1365-2613.2000.00155.x
21. Sorokin L. The Impact of the Extracellular Matrix on Inflammation. *Nat Rev Immunol* (2010) 10:712–23. doi: 10.1038/nri2852
22. Rozario T, DeSimone DW. The Extracellular Matrix in Development and Morphogenesis: A Dynamic View. *Dev Biol* (2010) 341:126–40. doi: 10.1016/j.ydbio.2009.10.026
23. Nastase MV, Young MF, Schaefer L. Biglycan: A Multivalent Proteoglycan Providing Structure and Signals. *J Histochem Cytochem* (2012) 60:963–75. doi: 10.1369/0022155412456380
24. Gullberg D, Paraskevi H, Schaefer L, Tenni R, Theocharis A, Winberg JO. *Extracellular Matrix: Pathobiology and Signaling (Walter De Gruyter)*. Boston/Berlin: Walter de Gruyter (2012).
25. Merline R, Schaefer RM, Schaefer L. The Matricellular Functions of Small Leucine-Rich Proteoglycans (Slrps). *J Cell Commun Signaling* (2009) 3:323–35. doi: 10.1007/s12079-009-0066-2
26. Zeng-Brouwers J, Pandey S, Trebicka J, Wygrecka M, Schaefer L. Communications *via* the Small Leucine-Rich Proteoglycans: Molecular Specificity in Inflammation and Autoimmune Diseases. *J Histochem Cytochem* (2020) 68:887–906. doi: 10.1369/0022155420930303
27. Schulz M, Diehl V, Trebicka J, Wygrecka M, Schaefer L. Biglycan in Hepatorenal Crosstalk Biglycan: A Regulator of Hepatorenal Inflammation and Autophagy. *Matrix Biol* (2021) 100–101:150–61. doi: 10.1016/j.matbio.2021.06.001
28. Ortiz C, Schierwagen R, Schaefer L, Klein S, Trepat X, Trebicka J. Extracellular Matrix Remodeling in Chronic Liver Disease. *Curr Tissue Microenviron Rep* (2021) 2:1–12. doi: 10.1007/s43152-021-00030-3
29. Bonnans C, Chou J, Werb Z. Remodelling the Extracellular Matrix in Development and Disease. *Nat Rev Mol Cell Biol* (2014) 15:786–801. doi: 10.1038/nrm3904
30. Iozzo RV, Gubbiotti MA. Extracellular Matrix: The Driving Force of Mammalian Diseases. *Matrix Biol* (2018) 71:1–9. doi: 10.1016/j.matbio.2018.03.023
31. Pickup MW, Mouw JK, Weaver VM. The Extracellular Matrix Modulates the Hallmarks of Cancer. *EMBO Rep* (2014) 15:1243–53. doi: 10.15252/embr.201439246
32. Paolillo M, Schinelli S. Extracellular Matrix Alterations in Metastatic Processes. *Int J Mol Sci* (2019) 20:4947. doi: 10.3390/ijms20194947
33. Brassart-Pasco S, Brézillon S, Brassart B, Ramont L, Oudart JB, Monboisse JC. Tumor Microenvironment: Extracellular Matrix Alterations Influence Tumor Progression. *Front Oncol* (2020) 10:397. doi: 10.3389/fonc.2020.00397
34. Oskarsson T, Massagué J. Extracellular Matrix Players in Metastatic Niches. *EMBO J* (2012) 31:254–6. doi: 10.1038/emboj.2011.469
35. Zhuyan J, Chen M, Zhu T, Bao X, Zhen T, Xing K, et al. Critical Steps to Tumor Metastasis: Alterations of Tumor Microenvironment and Extracellular Matrix in the Formation of Pre-Metastatic and Metastatic Niche. *Cell Biosci* (2020) 10:1–9. doi: 10.1186/s13578-020-00453-9
36. Yamauchi M, Gibbons DL, Zong C, Fradette JJ, Bota-Rabassedas N, Kurie JM. Fibroblast Heterogeneity and Its Impact on Extracellular Matrix and Immune Landscape Remodeling in Cancer. *Matrix Biol* (2020) 91:8–18. doi: 10.1016/j.matbio.2020.05.001
37. Nazemi M, Rainero E. Cross-Talk Between the Tumor Microenvironment, Extracellular Matrix, and Cell Metabolism in Cancer. *Front Oncol* (2020) 10:239. doi: 10.3389/fonc.2020.00239
38. Hanahan D, Weinberg RA. The Hallmarks of Cancer. *Cell* (2000) 100:57–70. doi: 10.1016/S0092-8674(00)81683-9
39. Hanahan D, Weinberg RA. Hallmarks of Cancer: The Next Generation. *Cell* (2011) 144:646–74. doi: 10.1016/j.cell.2011.02.013
40. Colotta F, Allavena P, Sica A, Garlanda C, Mantovani A. Cancer-Related Inflammation, the Seventh Hallmark of Cancer: Links to Genetic Instability. *Carcinogenesis* (2009) 30:1073–81. doi: 10.1093/carcin/bgp127
41. Dunn GP, Old LJ, Schreiber RD. The Immunobiology of Cancer Immunosurveillance and Immunoediting. *Immunity* (2004) 21:137–48. doi: 10.1016/j.immuni.2004.07.017
42. Hibino S, Kawazoe T, Kasahara H, Itoh S, Ishimoto T, Sakata-Yanagimoto M, et al. Inflammation-Induced Tumorigenesis and Metastasis. *Int J Mol Sci* (2021) 22:5421. doi: 10.3390/ijms22115421
43. Castle PE, Hillier SL, Rabe LK, Hildesheim A, Herrero R, Bratti MC, et al. An Association of Cervical Inflammation With High-Grade Cervical Neoplasia in Women Infected With Oncogenic Human Papillomavirus (HPV). *Cancer Epidemiol Prev Biomarkers* (2001) 10:1021–7.
44. Balkwill F, Charles KA, Mantovani A. Smoldering and Polarized Inflammation in the Initiation and Promotion of Malignant Disease. *Cancer Cell* (2005) 7:211–7. doi: 10.1016/j.ccr.2005.02.013
45. Greten FR, Grivennikov SI. Inflammation and Cancer: Triggers, Mechanisms, and Consequences. *Immunity* (2019) 51:27–41. doi: 10.1016/j.immuni.2019.06.025
46. Dunn GP, Bruce AT, Ikeda H, Old LJ, Schreiber RD. Cancer Immunoediting: From Immunosurveillance to Tumor Escape. *Nat Rev Cancer* (2002) 3:991–8. doi: 10.1038/ni1102-991
47. Dirnhofer S, Zippelius A. Cancer Immunology, Inflammation, and Tolerance: An Introduction. *Eur J Pathol* (2019) 474:405–6. doi: 10.1007/s00428-019-02547-3
48. Binnewies M, Roberts EW, Kersten K, Chan V, Fearon DF, Merad M, et al. Understanding the Tumor Immune Microenvironment (TIME) for Effective Therapy. *Nat Med* (2018) 24:541–50. doi: 10.1038/s41591-018-0014-x
49. Kumar A, Swain CA, Shevde LA. Informing the New Developments and Future of Cancer Immunotherapy. *Cancer Metastasis Rev* (2021) 40:549–62. doi: 10.1007/s10555-021-09967-1
50. Mantovani A, Allavena P, Sica A, Balkwill F. Cancer-Related Inflammation. *Nature* (2008) 454:436–44. doi: 10.1038/nature07205
51. Hou J, Karin M, Sun B. Targeting Cancer-Promoting Inflammation—Have Anti-Inflammatory Therapies Come of Age? *Nat Rev Clin Oncol* (2021) 18:261–79. doi: 10.1038/s41571-020-00459-9

52. Taniguchi K, Karin M. NF-κB, Inflammation, Immunity and Cancer: Coming of Age. *Nat Rev Immunol* (2018) 18:309–24. doi: 10.1038/nri.2017.142
53. Sabroe I, Parker L, Dower S, Whyte M. The Role of TLR Activation in Inflammation. *J Pathol: A J Pathological Soc Great Britain Ireland* (2008) 214:126–35. doi: 10.1002/path.2264
54. Sun SC, Ley SC. New Insights Into NF-κB Regulation and Function. *Trends Immunol* (2008) 29:469–78. doi: 10.1016/j.it.2008.07.003
55. Bryant CE, Gay NJ, Heymans S, Sacre S, Schaefer L, Midwood KS. Advances in Toll-Like Receptor Biology: Modes of Activation by Diverse Stimuli. *Crit Rev Biochem Mol Biol* (2015) 50:359–79. doi: 10.3109/10409238.2015.1033511
56. Moossavi M, Parsamanesh N, Bahrami A, Atkin SL, Sahebkar A. Role of the NLRP3 Inflammasome in Cancer. *Mol Cancer* (2018) 17:1–13. doi: 10.1186/s12943-018-0900-3
57. Sharma BR, Kanneganti TD. NLRP3 Inflammasome in Cancer and Metabolic Diseases. *Nat Immunol* (2021) 22:550–9. doi: 10.1038/s41590-021-00886-5
58. Hamarsheh S, Zeiser R. NLRP3 Inflammasome Activation in Cancer: A Double-Edged Sword. *Front Immunol* (2020) 11:1444. doi: 10.3389/fimmu.2020.01444
59. Li X, He S, Ma B. Autophagy and Autophagy-Related Proteins in Cancer. *Mol Cancer* (2020) 19:1–16. doi: 10.1186/s12943-019-1085-0
60. Nazio F, Bordi M, Cianfanelli V, Locatelli F, Cecconi F. Autophagy and Cancer Stem Cells: Molecular Mechanisms and Therapeutic Applications. *Cell Death Differ* (2019) 26:690–702. doi: 10.1038/s41418-019-0292-y
61. Garg M. Epithelial Plasticity, Autophagy and Metastasis: Potential Modifiers of the Crosstalk to Overcome Therapeutic Resistance. *Stem Cell Rev Rep* (2020) 16:503–10. doi: 10.1007/s12015-019-09945-9
62. Mathew R, Karp CM, Beaudoin B, Vuong N, Chen G, Chen HY, et al. Autophagy Suppresses Tumorigenesis Through Elimination of P62. *Cell* (2009) 137:1062–75. doi: 10.1016/j.cell.2009.03.048
63. Liu W, Meng Y, Zong C, Zhang S, Wei L. Autophagy and Tumorigenesis. In: *Autophagy: Biology and Diseases*. Singapore: Springer (2020). p. 12..
64. Mainz L, Rosenfeldt MT. Autophagy and Cancer–Insights From Mouse Models. *FEBS J* (2018) 285:792–808. doi: 10.1111/febs.14274
65. Cianfanelli V, Fuoco C, Lorente M, Salazar M, Quondamatteo F, Gherardini PF, et al. AMBRA1 Links Autophagy to Cell Proliferation and Tumorigenesis by Promoting C-Myc Dephosphorylation and Degradation. *Nat Cell Biol* (2015) 17:20–30. doi: 10.1038/ncb3072
66. Amaravadi RK, Kimmelman AC, Debnath J. Targeting Autophagy in Cancer: Recent Advances and Future Directions. *Cancer Discov* (2019) 9:1167–81. doi: 10.1158/2159-8290.CD-19-0292
67. Guo JY, Chen HY, Mathew R, Fan J, Strohecker AM, Karsli-Uzunbas G, et al. Activated Ras Requires Autophagy to Maintain Oxidative Metabolism and Tumorigenesis. *Genes Dev* (2011) 25:460–70. doi: 10.1101/gad.2016311
68. Seton-Rogers S. Eliminating Protective Autophagy in KRAS-Mutant Cancers. *Nat Rev Cancer* (2019) 19:247–7. doi: 10.1038/s41568-019-0137-5
69. Bryant KL, Der CJ. Blocking Autophagy to Starve Pancreatic Cancer. *Nat Rev Mol Cell Biol* (2019) 20:265–5. doi: 10.1038/s41580-019-0120-8
70. Apel A, Herr I, Schwarz H, Rodemann HP, Mayer A. Blocked Autophagy Sensitizes Resistant Carcinoma Cells to Radiation Therapy. *Cancer Res* (2008) 68:1485–94. doi: 10.1158/0008-5472.CAN-07-0562
71. Liu D, Yang Y, Liu Q, Wang J. Inhibition of Autophagy by 3-MA Potentiates Cisplatin-Induced Apoptosis in Esophageal Squamous Cell Carcinoma Cells. *Med Oncol* (2011) 28:105–11. doi: 10.1007/s12032-009-9397-3
72. Shingu T, Fujiwara K, Bögler O, Akiyama Y, Moritake K, Shinojima N, et al. Inhibition of Autophagy at a Late Stage Enhances Imatinib-Induced Cytotoxicity in Human Malignant Glioma Cells. *Int J Cancer* (2009) 124:1060–71. doi: 10.1002/ijc.24030
73. Galluzzi L, Bravo-San Pedro JM, Demaria S, Formenti SC, Kroemer G. Activating Autophagy to Potentiate Immunogenic Chemotherapy and Radiation Therapy. *Nat Rev Clin Oncol* (2017) 14:247–58. doi: 10.1038/nrclinonc.2016.183
74. Papandreou ME, Tavernarakis N. Crosstalk Between Endo/Exocytosis and Autophagy in Health and Disease. *Biotechnol J* (2020) 15:1900267. doi: 10.1002/biot.201900267
75. Chen HT, Liu H, Mao MJ, Tan Y, Mo XQ, Meng XJ, et al. Crosstalk Between Autophagy and Epithelial-Mesenchymal Transition and Its Application in Cancer Therapy. *Mol Cancer* (2019) 18:1–19. doi: 10.1186/s12943-018-0930-x
76. Catalano M, D'Alessandro G, Lepore F, Corazzari M, Caldarola S, Valacca C, et al. Autophagy Induction Impairs Migration and Invasion by Reversing EMT in Glioblastoma Cells. *Mol Oncol* (2015) 9:1612–25. doi: 10.1016/j.molonc.2015.04.016
77. Lv Q, Wang W, Xue J, Hua F, Mu R, Lin H, et al. DEDD Interacts With PI3KC3 to Activate Autophagy and Attenuate Epithelial–Mesenchymal Transition in Human Breast Cancer. *Cancer Res* (2012) 72:3238–50. doi: 10.1158/0008-5472.CAN-11-3832
78. Bao Y, Ding Z, Zhao P, Li J, Chen P, Zheng J, et al. Autophagy Inhibition Potentiates the Anti-EMT Effects of Alteronol Through TGF-β/Smad3 Signaling in Melanoma Cells. *Cell Death Dis* (2020) 11:1–10. doi: 10.1038/s41419-020-2419-y
79. Shen H, Yin L, Deng G, Guo C, Han Y, Li Y, et al. Knockdown of Beclin-1 Impairs Epithelial-Mesenchymal Transition of Colon Cancer Cells. *J Cell Biochem* (2018) 119:7022–31. doi: 10.1002/jcb.26912
80. Zhu HD, Liu L, Deng H, Li ZB, Sheng JQ, He XX, et al. Astrocyte Elevated Gene 1 (AEG-1) Promotes Anoikis Resistance and Metastasis by Inducing Autophagy in Hepatocellular Carcinoma. *J Cell Physiol* (2020) 235:5084–95. doi: 10.1002/jcp.29377
81. Peng YF, Shi YH, Ding ZB, Ke AW, Gu CY, Hui B, et al. Autophagy Inhibition Suppresses Pulmonary Metastasis of HCC in Mice *via* Impairing Anoikis Resistance and Colonization of HCC Cells. *Autophagy* (2013) 9:2056–68. doi: 10.4161/auto.26398
82. Liu T, Zhang J, Li K, Deng L, Wang H. Combination of an Autophagy Inducer and an Autophagy Inhibitor: A Smarter Strategy Emerging in Cancer Therapy. *Front Pharmacol* (2020) 11:408. doi: 10.3389/fphar.2020.00408
83. Cordani M, Somoza Á, Tafani M, Dando I, Kumar S. Novel Cancer Treatments Based on Autophagy Modulation. *Front Pharmacol* (2021) 12:650559. doi: 10.3389/fphar.2021.650559
84. Ruoslahti E. Structure and Biology of Proteoglycans. *Annu Rev Cell Biol* (1988) 4:229–55. doi: 10.1146/annurev.cb.04.110188.001305
85. Iozzo RV, Schaefer L. Proteoglycan Form and Function: A Comprehensive Nomenclature of Proteoglycans. *Matrix Biol* (2015) 42:11–55. doi: 10.1016/j.matbio.2015.02.003
86. Esko JD, Kimata K, Lindahl U. Proteoglycans and Sulfated Glycosaminoglycans. In: *Essentials of Glycobiology*, *2nd edition*. La Jolla, California: Cold Spring Harbor Laboratory Press (2009) p. 1–27.
87. Schaefer L, Schaefer RM. Proteoglycans: From Structural Compounds to Signaling Molecules. *Cell Tissue Res* (2010) 339:237–46. doi: 10.1007/s00441-009-0821-y
88. Neill T, Schaefer L, Iozzo RV. Decoding the Matrix: Instructive Roles of Proteoglycan Receptors. *Biochemistry* (2015) 54:4583–98. doi: 10.1021/acs.biochem.5b00653
89. Iozzo RV. The Family of the Small Leucine-Rich Proteoglycans: Key Regulators of Matrix Assembly and Cellular Growth. *Biochem Mol Biol* (1997) 32:141–74. doi: 10.3109/10409239709108551
90. Matsushima N, Miyashita H, Kretsinger RH. Sequence Features, Structure, Ligand Interaction, and Diseases in Small Leucine Rich Repeat Proteoglycans. *J Cell Commun Signaling* (2021) 1:1–13. doi: 10.1007/s12079-021-00616-4
91. Huxley-Jones J, Robertson DL, Boot-Handford RP. On the Origins of the Extracellular Matrix in Vertebrates. *Matrix Biol* (2007) 26:2–11. doi: 10.1016/j.matbio.2006.09.008
92. Hocking AM, Shinomura T, McQuillan DJ. Leucine-Rich Repeat Glycoproteins of the Extracellular Matrix. *Matrix Biol* (1998) 17:1–19. doi: 10.1016/S0945-053X(98)90121-4
93. Schaefer L. Complexity of Danger: The Diverse Nature of Damage-Associated Molecular Patterns. *J Biol Chem* (2014) 289:35237–45. doi: 10.1074/jbc.R114.619304
94. Frey H, Schroeder N, Manon-Jensen T, Iozzo RV, Schaefer L. Biological Interplay Between Proteoglycans and Their Innate Immune Receptors in Inflammation. *FEBS J* (2013) 280:2165–79. doi: 10.1111/febs.12145
95. Iozzo RV, Sanderson RD. Proteoglycans in Cancer Biology, Tumour Microenvironment and Angiogenesis. *J Cell Mol Med* (2011) 15:1013–31. doi: 10.1111/j.1582-4934.2010.01236.x

96. Iozzo RV. The Biology of the Small Leucine-Rich Proteoglycans: Functional Network of Interactive Proteins. *J Biol Chem* (1999) 274:18843–6. doi: 10.1074/jbc.274.27.18843
97. Iozzo RV, Moscatello DK, McQuillan DJ, Eichstetter I. Decorin is a Biological Ligand for the Epidermal Growth Factor Receptor. *J Biol Chem* (1999) 274:4489–92. doi: 10.1074/jbc.274.8.4489
98. Järveläinen H, Sainio A, Wight TN. Pivotal Role for Decorin in Angiogenesis. *Matrix Biol* (2015) 43:15–26. doi: 10.1016/j.matbio.2015.01.023
99. Neill T, Schaefer L, Iozzo RV. Decorin: A Guardian From the Matrix. *Am J Pathol* (2012) 181:380–7. doi: 10.1016/j.ajpath.2012.04.029
100. Salomaki HH, Sainio AO, Söderström M, Pakkanen S, Laine J, Jarvelainen HT. Differential Expression of Decorin by Human Malignant and Benign Vascular Tumors. *J Histochem Cytochem* (2008) 56:639–46. doi: 10.1369/jhc.2008.950287
101. Vogel KG, Paulsson M, Heinegård D. Specific Inhibition of Type I and Type II Collagen Fibrillogenesis by the Small Proteoglycan of Tendon. *Biochem J* (1984) 223:587–97. doi: 10.1042/bj2230587
102. Scott JE. Proteoglycan-Fibrillar Collagen Interactions. *Biochem J* (1988) 252:313–23. doi: 10.1042/bj2520313
103. Yamaguchi Y, Mann DM, Ruoslahti E. Negative Regulation of Transforming Growth Factor-βby the Proteoglycan Decorin. *Nature* (1990) 346:281–4. doi: 10.1038/346281a0
104. Iozzo RV, Chakrani F, Perrotti D, McQuillan DJ, Skorski T, Calabretta B, et al. Cooperative Action of Germ-Line Mutations in Decorin and P53 Accelerates Lymphoma Tumorigenesis. *Proc Natl Acad Sci* (1999) 96:3092–7. doi: 10.1073/pnas.96.6.3092
105. Mao L, Yang J, Yue J, Chen Y, Zhou H, Fan D, et al. Decorin Deficiency Promotes Epithelial-Mesenchymal Transition and Colon Cancer Metastasis. *Matrix Biol* (2021) 95:1–14. doi: 10.1016/j.matbio.2020.10.001
106. Goldoni S, Humphries A, Nyström A, Sattar S, Owens RT, McQuillan DJ, et al. Decorin Is a Novel Antagonistic Ligand of the Met Receptor. *J Cell Biol* (2009) 185:743–54. doi: 10.1083/jcb.200901129
107. Buraschi S, Pal N, Tyler-Rubinstein N, Owens RT, Neill T, Iozzo RV. Decorin Antagonizes Met Receptor Activity and Down-Regulates β-Catenin and Myc Levels. *J Biol Chem* (2010) 285:42075–85. doi: 10.1074/jbc.M110.172841
108. Neill T, Schaefer L, Iozzo RV. Oncosuppressive Functions of Decorin. *Mol Cell Oncol* (2015) 2:e975645. doi: 10.4161/23723556.2014.975645
109. Boccaccio C, Comoglio PM. Invasive Growth: A MET-Driven Genetic Programme for Cancer and Stem Cells. *Nat Rev Cancer* (2006) 6:637–45. doi: 10.1038/nrc1912
110. Chen K, Ma X, Nehme A, Wei J, Cui Y, Cui Y, et al. Time-Delimited Signaling of MET Receptor Tyrosine Kinase Regulates Cortical Circuit Development and Critical Period Plasticity. *Mol Psychiatry* (2020) 26:1–14. doi: 10.1038/s41380-019-0635-6
111. Lai AZ, Abella JV, Park M. Crosstalk in Met Receptor Oncogenesis. *Trends Cell Biol* (2009) 19:542–51. doi: 10.1016/j.tcb.2009.07.002
112. Gao CF, Woude GFV. HGF/SF-Met Signaling in Tumor Progression. *Cell Res* (2005) 15:49–51. doi: 10.1038/sj.cr.7290264
113. Taher TE, Tjin EP, Beuling EA, Borst J, Spaargaren M, Pals ST. C-Cbl Is Involved in Met Signaling in B Cells and Mediates Hepatocyte Growth Factor-Induced Receptor Ubiquitination. *J Immunol* (2002) 169:3793–800. doi: 10.4049/jimmunol.169.7.3793
114. Yeh E, Cunningham M, Arnold H, Chasse D, Monteith T, Ivaldi G, et al. A Signalling Pathway Controlling C-Myc Degradation That Impacts Oncogenic Transformation of Human Cells. *Nat Cell Biol* (2004) 6:308–18. doi: 10.1038/ncb1110
115. Goldoni S, Owens RT, McQuillan DJ, Shriver Z, Sasisekharan R, Birk DE, et al. Biologically Active Decorin Is a Monomer in Solution. *J Biol Chem* (2004) 279:6606–12. doi: 10.1074/jbc.M310342200
116. Gubbiotti MA, Vallet SD, Ricard-Blum S, Iozzo RV. Decorin Interacting Network: A Comprehensive Analysis of Decorin-Binding Partners and Their Versatile Functions. *Matrix Biol* (2016) 55:7–21. doi: 10.1016/j.matbio.2016.09.009
117. Zhang W, Ge Y, Cheng Q, Zhang Q, Fang L, Zheng J. Decorin is a Pivotal Effector in the Extracellular Matrix and Tumour Microenvironment. *Oncotarget* (2018) 9:5480–91. doi: 10.18632/oncotarget.23869
118. Santra M, Reed CC, Iozzo RV. Decorin Binds to a Narrow Region of the Epidermal Growth Factor (EGF) Receptor, Partially Overlapping But Distinct From the EGF-Binding Epitope. *J Biol Chem* (2002) 277:35671–81. doi: 10.1074/jbc.M205317200
119. Seidler DG, Goldoni S, Agnew C, Cardi C, Thakur ML, Owens RT, et al. Decorin Protein Core Inhibits *In Vivo* Cancer Growth and Metabolism by Hindering Epidermal Growth Factor Receptor Function and Triggering Apoptosis *via* Caspase-3 Activation. *J Biol Chem* (2006) 281:26408–18. doi: 10.1074/jbc.M602853200
120. Zhu JX, Goldoni S, Bix G, Owens RT, McQuillan DJ, Reed CC, et al. Decorin Evokes Protracted Internalization and Degradation of the Epidermal Growth Factor Receptor *via* Caveolar Endocytosis. *J Biol Chem* (2005) 280:32468–79. doi: 10.1074/jbc.M503833200
121. Csordas G, Santra M, Reed CC, Eichstetter I, McQuillan DJ, Gross D, et al. Sustained Down-Regulation of the Epidermal Growth Factor Receptor by Decorin: A Mechanism for Controlling Tumor Growth In Vivo. *J Biol Chem* (2000) 275:32879–87. doi: 10.1074/jbc.M005609200
122. Reed CC, Gauldie J, Iozzo RV. Suppression of Tumorigenicity by Adenovirus-Mediated Gene Transfer of Decorin. *Oncogene* (2002) 21:3688–95. doi: 10.1038/sj.onc.1205470
123. Sainio AO, Järveläinen HT. Decorin-Mediated Oncosuppression–a Potential Future Adjuvant Therapy for Human Epithelial Cancers. *Br J Pharmacol* (2019) 176:5–15. doi: 10.1111/bph.14180
124. Schönherr E, Sunderkötter C, Schaefer L, Thanos S, Grässel S, Oldberg Å, et al. Decorin Deficiency Leads to Impaired Angiogenesis in Injured Mouse Cornea. *J Vasc Res* (2004) 41:499–508. doi: 10.1159/000081806
125. Mohan RR, Tovey JC, Sharma A, Schultz GS, Cowden JW, Tandon A. Targeted Decorin Gene Therapy Delivered With Adeno-Associated Virus Effectively Retards Corneal Neovascularization *In Vivo*. *PloS One* (2011) 6:e26432. doi: 10.1371/journal.pone.0026432
126. Lai J, Chen F, Chen J, Ruan G, He M, Chen C, et al. Overexpression of Decorin Promoted Angiogenesis in Diabetic Cardiomyopathy *via* Igf1r-Akt-Vegf Signaling. *Sci Rep* (2017) 7:1–11. doi: 10.1038/srep44473
127. Grant DS, Yenisey C, Rose RW, Tootell M, Santra M, Iozzo RV. Decorin Suppresses Tumor Cell-Mediated Angiogenesis. *Oncogene* (2002) 21:4765–77. doi: 10.1038/sj.onc.1205595
128. Mustonen T, Alitalo K. Endothelial Receptor Tyrosine Kinases Involved in Angiogenesis. *J Cell Biol* (1995) 129:895–8. doi: 10.1083/jcb.129.4.895
129. Khan GA, Girish GV, Lala N, Di Guglielmo GM, Lala PK. Decorin is a Novel Vegfr-2-Binding Antagonist for the Human Extravillous Trophoblast. *Mol Endocrinol* (2011) 25:1431–43. doi: 10.1210/me.2010-0426
130. Goyal A, Neill T, Owens RT, Schaefer L, Iozzo RV. Decorin Activates AMPK, an Energy Sensor Kinase, to Induce Autophagy in Endothelial Cells. *Matrix Biol* (2014) 34:46–54. doi: 10.1016/j.matbio.2013.12.011
131. Neill T, Painter H, Buraschi S, Owens RT, Lisanti MP, Schaefer L, et al. Decorin Antagonizes the Angiogenic Network: Concurrent Inhibition of Met, Hypoxia Inducible Factor 1αVascular Endothelial Growth Factor A, and Induction of Thrombospondin-1 and TIMP3. *J Biol Chem* (2012) 287:5492–506. doi: 10.1074/jbc.M111.283499
132. Neill T, Jones HR, Crane-Smith Z, Owens RT, Schaefer L, Iozzo RV. Decorin Induces Rapid Secretion of Thrombospondin-1 in Basal Breast Carcinoma Cells *via* Inhibition of Ras Homolog Gene Family, Member A/Rho-Associated Coiled-Coil Containing Protein Kinase 1. *FEBS J* (2013) 280:2353–68. doi: 10.1111/febs.12148
133. Neill T, Chen CG, Buraschi S, Iozzo RV. Catabolic Degradation of Endothelial VEGFA *via* Autophagy. *J Biol Chem* (2020) 295:6064–79. doi: 10.1074/jbc.RA120.012593
134. Buraschi S, Neill T, Goyal A, Poluzzi C, Smythies J, Owens RT, et al. Decorin Causes Autophagy in Endothelial Cells *via* Peg3. *Proc Natl Acad Sci* (2013) 110:E2582–91. doi: 10.1073/pnas.1305732110
135. Buraschi S, Neill T, Iozzo RV. Decorin Is a Devouring Proteoglycan: Remodeling of Intracellular Catabolism *via* Autophagy and Mitophagy. *Matrix Biol* (2019) 75:260–70. doi: 10.1016/j.matbio.2017.10.005
136. Torres A, Gubbiotti MA, Iozzo RV. Decorin-Inducible Peg3 Evokes Beclin 1-Mediated Autophagy and Thrombospondin 1-Mediated Angiostasis. *J Biol Chem* (2017) 292:5055–69. doi: 10.1074/jbc.M116.753632

137. Relaix F, Wei XJ, Wu X, Sassoon DA. Peg3/Pw1 Is an Imprinted Gene Involved in the TNF-NFκB Signal Transduction Pathway. *Nat Genet* (1998) 18:287–91. doi: 10.1038/ng0398-287
138. Kohda T, Asai A, Kuroiwa Y, Kobayashi S, Aisaka K, Nagashima G, et al. Tumour Suppressor Activity of Human Imprinted Gene PEG3 in a Glioma Cell Line. *Genes to Cells* (2001) 6:237–47. doi: 10.1046/j.1365-2443.2001.00412.x
139. Dowdy SC, Gostout BS, Shridhar V, Wu X, Smith DI, Podratz KC, et al. Biallelic Methylation and Silencing of Paternally Expressed Gene 3 (PEG3) in Gynecologic Cancer Cell Lines. *Gynecologic Oncol* (2005) 99:126–34. doi: 10.1016/j.ygyno.2005.05.036
140. Neill T, Sharpe C, Owens RT, Iozzo RV. Decorin-Evoked Paternally Expressed Gene 3 (PEG3) is an Upstream Regulator of the Transcription Factor EB (TFEB) in Endothelial Cell Autophagy. *J Biol Chem* (2017) 292:16211–20. doi: 10.1074/jbc.M116.769950
141. Dierick F, Héry T, Hoareau-Coudert B, Mougenot N, Monceau V, Claude C, et al. Resident PW1+ Progenitor Cells Participate in Vascular Remodeling During Pulmonary Arterial Hypertension. *Circ Res* (2016) 118:822–33. doi: 10.1161/CIRCRESAHA.115.307035
142. Malinverno M, Corada M, Ferrarini L, Formicola L, Marazzi G, Sassoon D, et al. Peg3/PW1 Is a Marker of a Subset of Vessel Associated Endothelial Progenitors. *Stem Cells* (2017) 35:1328–40. doi: 10.1002/stem.2566
143. Neill T, Torres A, Buraschi S, Owens RT, Hoek JB, Baffa R, et al. Decorin Induces Mitophagy in Breast Carcinoma Cells *via* Peroxisome Proliferator-Activated Receptor γ Coactivator-1α(PGC-1α) and Mitostatin. *J Biol Chem* (2014) 289:4952–68. doi: 10.1074/jbc.M113.512566
144. Moreth K, Brodbeck R, Babelova A, Gretz N, Spieker T, Zeng-Brouwers J, et al. The Proteoglycan Biglycan Regulates Expression of the B Cell Chemoattractant CXCL13 and Aggravates Murine Lupus Nephritis. *J Clin Invest* (2010) 120:4251–72. doi: 10.1172/JCI42213
145. Merline R, Moreth K, Beckmann J, Nastase MV, Zeng-Brouwers J, Tralhão JG, et al. Signaling by the Matrix Proteoglycan Decorin Controls Inflammation and Cancer Through PDCD4 and MicroRNA-21. *Sci Signaling* (2011) 4:ra75–5. doi: 10.1126/scisignal.2001868
146. Yasuda M, Schmid T, Rübsamen D, Colburn NH, Irie K, Murakami A. Downregulation of Programmed Cell Death 4 by Inflammatory Conditions Contributes to the Generation of the Tumor Promoting Microenvironment. *Mol Carcinog* (2010) 49:837–48. doi: 10.1002/mc.20660
147. Davis BN, Hilyard AC, Lagna G, Hata A. SMAD Proteins Control DROSHA-Mediated microRNA Maturation. *Nature* (2008) 454:56–61. doi: 10.1038/nature07086
148. Asangani IA, Rasheed SA, Nikolova D, Leupold J, Colburn N, Post S, et al. MicroRNA-21 (miR-21) Post-Transcriptionally Downregulates Tumor Suppressor PDCD4 and Stimulates Invasion, Intravasation and Metastasis in Colorectal Cancer. *Oncogene* (2008) 27:2128–36. doi: 10.1038/sj.onc.1210856
149. Bianco P, Fisher LW, Young MF, Termine JD, Robey PG. Expression and Localization of the Two Small Proteoglycans Biglycan and Decorin in Developing Human Skeletal and non-Skeletal Tissues. *J Histochem Cytochem* (1990) 38:1549–63. doi: 10.1177/38.11.2212616
150. Choi H, Johnson T, Pal S, Tang L, Rosenberg L, Neame P. Characterization of the Dermatan Sulfate Proteoglycans, DS-PGI and DS-PGII, From Bovine Articular Cartilage and Skin Isolated by Octyl-Sepharose Chromatography. *J Biol Chem* (1989) 264:2876–84. doi: 10.1016/S0021-9258(19)81694-0
151. Schönherr E, Witsch-Prehm P, Harrach B, Robenek H, Rauterberg J, Kresse H. Interaction of Biglycan With Type I Collagen. *J Biol Chem* (1995) 270:2776–83. doi: 10.1074/jbc.270.6.2776
152. Wiberg C, Hedbom E, Khairullina A, Lamandé SR, Oldberg Å, Timpl R, et al. Biglycan and Decorin Bind Close to the N-Terminal Region of the Collagen VI Triple Helix. *J Biol Chem* (2001) 276:18947–52. doi: 10.1074/jbc.M100625200
153. Wiberg C, Heinegard D, Wenglen C, Timpl R, Moergelin M. Biglycan Organizes Collagen VI Into Hexagonal-Like Networks Resembling Tissue Structures. *J Biol Chem* (2002) 277:49120–6. doi: 10.1074/jbc.M206891200
154. Wiberg C, Klatt AR, Wagener R, Paulsson M, Bateman JF, Heinegard D, et al. Complexes of Matrilin-1 and Biglycan or Decorin Connect Collagen Vi Microfibrils to Both Collagen Ii and Aggrecan. *J Biol Chem* (2003) 278:37698–704. doi: 10.1074/jbc.M304638200
155. Reinboth B, Hanssen E, Cleary EG, Gibson MA. Molecular Interactions of Biglycan and Decorin With Elastic Fiber Components: Biglycan Forms a Ternary Complex With Tropoelastin and Microfibril-Associated Glycoprotein 1. *J Biol Chem* (2002) 277:3950–7. doi: 10.1074/jbc.M109540200
156. Douglas T, Heinemann S, Bierbaum S, Scharnweber D, Worch H. Fibrillogenesis of Collagen Types I, II, and III With Small Leucine-Rich Proteoglycans Decorin and Biglycan. *Biomacromolecules* (2006) 7:2388–93. doi: 10.1021/bm0603746
157. Schaefer L, Babelova A, Kiss E, Hausser HJ, Baliova M, Krzyzankova M, et al. The Matrix Component Biglycan Is Proinflammatory and Signals Through Toll-Like Receptors 4 and 2 in Macrophages. *J Clin Invest* (2005) 115:2223–33. doi: 10.1172/JCI23755
158. Schaefer L, Iozzo RV. Biological Functions of the Small Leucine-Rich Proteoglycans: From Genetics to Signal Transduction. *J Biol Chem* (2008) 283:21305–9. doi: 10.1074/jbc.R800020200
159. Hsieh LTH, Nastase MV, Zeng-Brouwers J, Iozzo RV, Schaefer L. Soluble Biglycan as a Biomarker of Inflammatory Renal Diseases. *Int J Biochem Cell Biol* (2014) 54:223–35. doi: 10.1016/j.biocel.2014.07.020
160. Moreth K, Frey H, Hubo M, Zeng-Brouwers J, Nastase MV, Hsieh LTH, et al. Biglycan-Triggered TLR-2-and TLR-4-Signaling Exacerbates the Pathophysiology of Ischemic Acute Kidney Injury. *Matrix Biol* (2014) 35:143–51. doi: 10.1016/j.matbio.2014.01.010
161. Zeng-Brouwers J, Beckmann J, Nastase MV, Iozzo RV, Schaefer L. *De Novo* Expression of Circulating Biglycan Evokes an Innate Inflammatory Tissue Response *via* MyD88/TRIF Pathways. *Matrix Biol* (2014) 35:132–42. doi: 10.1016/j.matbio.2013.12.003
162. Schaefer L, Raslik I, Gröne HJ, Schönherr E, Macakova K, Ugorcakova J, et al. Small Proteoglycans in Human Diabetic Nephropathy: Discrepancy Between Glomerular Expression and Protein Accumulation of Decorin, Biglycan, Lumican, and Fibromodulin. *FASEB J* (2001) 15:559–61. doi: 10.1096/fj.00-0493fje
163. Bolton K, Segal D, Walder K. The Small Leucine-Rich Proteoglycan, Biglycan, Is Highly Expressed in Adipose Tissue of Psammomys Obesus and Is Associated With Obesity and Type 2 Diabetes. *Biologics: Targets Ther* (2012) 6:67–72. doi: 10.2147/BTT.S27925
164. Ciftciler R, Ozenirler S, Yucel AA, Cengiz M, Erkan G, Buyukdemirci E, et al. The Importance of Serum Biglycan Levels as a Fibrosis Marker in Patients With Chronic Hepatitis B. *J Clin Lab Anal* (2017) 31:e22109. doi: 10.1002/jcla.22109
165. Zhao SF, Yin XJ, Zhao WJ, Liu LC, Wang ZP. Biglycan as a Potential Diagnostic and Prognostic Biomarker in Multiple Human Cancers. *Oncol Lett* (2020) 19:1673–82. doi: 10.3892/ol.2020.11266
166. Hsieh LTH, Frey H, Nastase MV, Tredup C, Hoffmann A, Poluzzi C, et al. Bimodal Role of NADPH Oxidases in the Regulation of Biglycan-Triggered IL-1βSynthesis. *Matrix Biol* (2016) 49:61–81. doi: 10.1016/j.matbio.2015.12.005
167. Roedig H, Nastase MV, Frey H, Moreth K, Zeng-Brouwers J, Poluzzi C, et al. Biglycan is a New High-Affinity Ligand for CD14 in Macrophages. *Matrix Biol* (2019) 77:4–22. doi: 10.1016/j.matbio.2018.05.006
168. Babelova A, Moreth K, Tsalastra-Greul W, Zeng-Brouwers J, Eickelberg O, Young MF, et al. Biglycan, a Danger Signal That Activates the NLRP3 Inflammasome *via* Toll-Like and P2X Receptors. *J Biol Chem* (2009) 284:24035–48. doi: 10.1074/jbc.M109.014266
169. Hsieh LTH, Nastase MV, Roedig H, Zeng-Brouwers J, Poluzzi C, Schwalm S, et al. Biglycan-And Sphingosine Kinase-1 Signaling Crosstalk Regulates the Synthesis of Macrophage Chemoattractants. *Int J Mol Sci* (2017) 18:595. doi: 10.3390/ijms18030595
170. Nastase MV, Zeng-Brouwers J, Beckmann J, Tredup C, Christen U, Radeke HH, et al. Biglycan, a Novel Trigger of Th1 and Th17 Cell Recruitment Into the Kidney. *Matrix Biol* (2018) 68:293–317. doi: 10.1016/j.matbio.2017.12.002
171. Popovic ZV, Wang S, Papatriantafyllou M, Kaya Z, Porubsky S, Meisner M, et al. The Proteoglycan Biglycan Enhances Antigen-Specific T Cell Activation Potentially *via* MyD88 and TRIF Pathways and Triggers Autoimmune Perimyocarditis. *J Immunol* (2011) 187:6217–26. doi: 10.4049/jimmunol.1003478
172. Bonapace L, Coissieux MM, Wyckoff J, Mertz KD, Varga Z, Junt T, et al. Cessation of CCL2 Inhibition Accelerates Breast Cancer Metastasis by

Promoting Angiogenesis. *Nature* (2014) 515:130–3. doi: 10.1038/nature13862
173. Kitamura T, Qian BZ, Soong D, Cassetta L, Noy R, Sugano G, et al. CCL2-Induced Chemokine Cascade Promotes Breast Cancer Metastasis by Enhancing Retention of Metastasis-Associated Macrophages. *J Exp Med* (2015) 212:1043–59. doi: 10.1084/jem.20141836
174. Hao Q, Vadgama JV, Wang P. CCL2/CCR2 Signaling in Cancer Pathogenesis. *Cell Commun Signaling* (2020) 18:1–13. doi: 10.1186/s12964-020-00589-8
175. Aldinucci D, Borghese C, Casagrande N. The CCL5/CCR5 Axis in Cancer Progression. *Cancers* (2020) 12:1765. doi: 10.3390/cancers12071765
176. Gnerlich JL, Mitchem JB, Weir JS, Sankpal NV, Kashiwagi H, Belt BA, et al. Induction of Th17 Cells in the Tumor Microenvironment Improves Survival in a Murine Model of Pancreatic Cancer. *J Immunol* (2010) 185:4063–71. doi: 10.4049/jimmunol.0902609
177. Najafi S, Mirshafiey A. The Role of T Helper 17 and Regulatory T Cells in Tumor Microenvironment. *Immunopharmacol Immunotoxicol* (2019) 41:16–24. doi: 10.1080/08923973.2019.1566925
178. Renaude E, Kroemer M, Loyon R, Binda D, Borg C, Guittaut M, et al. The Fate of Th17 Cells Is Shaped by Epigenetic Modifications and Remodeled by the Tumor Microenvironment. *Int J Mol Sci* (2020) 21:1673. doi: 10.3390/ijms21051673
179. Roedig H, Nastase MV, Wygrecka M, Schaefer L. Breaking Down Chronic Inflammatory Diseases: The Role of Biglycan in Promoting a Switch Between Inflammation and Autophagy. *FEBS J* (2019) 286:2965–79. doi: 10.1111/febs.14791
180. Poluzzi C, Nastase MV, Zeng-Brouwers J, Roedig H, Hsieh LTH, Michaelis JB, et al. Biglycan Evokes Autophagy in Macrophages *via* a Novel CD44/Toll-Like Receptor 4 Signaling Axis in Ischemia/Reperfusion Injury. *Kidney Int* (2019) 95:540–62. doi: 10.1016/j.kint.2018.10.037
181. Deretic V, Levine B. Autophagy Balances Inflammation in Innate Immunity. *Autophagy* (2018) 14:243–51. doi: 10.1080/15548627.2017.1402992
182. Matsuzawa-Ishimoto Y, Hwang S, Cadwell K. Autophagy and Inflammation. *Annu Rev Immunol* (2018) 36:73–101. doi: 10.1146/annurev-immunol-042617-053253
183. Xing X, Gu X, Ma T, Ye H. Biglycan Up-Regulated Vascular Endothelial Growth Factor (VEGF) Expression and Promoted Angiogenesis in Colon Cancer. *Tumor Biol* (2015) 36:1773–80. doi: 10.1007/s13277-014-2779-y
184. Hu L, Hx W, Jf Li, Lp Su, Yan M, Li C, et al. Biglycan Stimulates VEGF Expression in Endothelial Cells by Activating the TLR Signaling Pathway. *Mol Oncol* (2016) 10:1473–84. doi: 10.1016/j.molonc.2016.08.002
185. Xia C, Meng Q, Liu LZ, Rojanasakul Y, Wang XR, Jiang BH. Reactive Oxygen Species Regulate Angiogenesis and Tumor Growth Through Vascular Endothelial Growth Factor. *Cancer Res* (2007) 67:10823–30. doi: 10.1158/0008-5472.CAN-07-0783
186. Frey H, Moreth K, Hsieh LTH, Zeng-Brouwers J, Rathkolb B, Fuchs H, et al. A Novel Biological Function of Soluble Biglycan: Induction of Erythropoietin Production and Polycythemia. *Glycoconjugate J* (2017) 34:393–404. doi: 10.1007/s10719-016-9722-y
187. Talks KL, Turley H, Gatter KC, Maxwell PH, Pugh CW, Ratcliffe PJ, et al. The Expression and Distribution of the Hypoxia-Inducible Factors HIF-1αand HIF-2αin Normal Human Tissues, Cancers, and Tumor-Associated Macrophages. *Am J Pathol* (2000) 157:411–21. doi: 10.1016/S0002-9440(10)64554-3
188. Cong L, Maishi N, Annan DA, Young MF, Morimoto H, Morimoto M, et al. Inhibition of Stromal Biglycan Promotes Normalization of the Tumor Microenvironment and Enhances Chemotherapeutic Efficacy. *Breast Cancer Res* (2021) 23:1–17. doi: 10.1186/s13058-021-01423-w
189. Xing X, Gu X, Ma T. Knockdown of Biglycan Expression by RNA Interference Inhibits the Proliferation and Invasion of, and Induces Apoptosis in, the HCT116 Colon Cancer Cell Line. *Mol Med Rep* (2015) 12:7538–44. doi: 10.3892/mmr.2015.4383
190. Liu B, Xu T, Xu X, Cui Y, Xing X. Biglycan Promotes the Chemotherapy Resistance of Colon Cancer by Activating NF-κB Signal Transduction. *Mol Cell Biochem* (2018) 449:285–94. doi: 10.1007/s11010-018-3365-1
191. Shatz M, Menendez D, Resnick MA. The Human TLR Innate Immune Gene Family is Differentially Influenced by DNA Stress and P53 Status in Cancer Cells. *Cancer Res* (2012) 72:3948–57. doi: 10.1158/0008-5472.CAN-11-4134
192. Korneev KV, Atretkhany KSN, Drutskaya MS, Grivennikov SI, Kuprash DV, Nedospasov SA. TLR-Signaling and Proinflammatory Cytokines as Drivers of Tumorigenesis. *Cytokine* (2017) 89:127–35. doi: 10.1016/j.cyto.2016.01.021
193. Li F, Sethi G. Targeting Transcription Factor Nf-κb to Overcome Chemoresistance and Radioresistance in Cancer Therapy. *Biochim Biophys Acta (BBA)-Reviews Cancer* (2010) 1805:167–80. doi: 10.1016/j.bbcan.2010.01.002
194. Sakamoto K, Maeda S. Targeting NF-κB for Colorectal Cancer. *Expert Opin Ther Targets* (2010) 14:593–601. doi: 10.1517/14728221003769903
195. Berendsen AD, Fisher LW, Kilts TM, Owens RT, Robey PG, Gutkind JS, et al. Modulation of Canonical Wnt Signaling by the Extracellular Matrix Component Biglycan. *Proc Natl Acad Sci* (2011) 108:17022–7. doi: 10.1073/pnas.1110629108
196. Clements WM, Wang J, Sarnaik A, Kim OJ, MacDonald J, Fenoglio-Preiser C, et al. β-Catenin Mutation Is a Frequent Cause of Wnt Pathway Activation in Gastric Cancer. *Cancer Res* (2002) 62:3503–6.
197. Zhan T, Rindtorff N, Boutros M. Wnt Signaling in Cancer. *Oncogene* (2017) 36:1461–73. doi: 10.1038/onc.2016.304
198. Aggelidakis J, Berdiaki A, Nikitovic D, Papoutsidakis A, Papachristou DJ, Tsatsakis AM, et al. Biglycan Regulates MG63 Osteosarcoma Cell Growth Through a LPR6/β-Catenin/IGFR-IR Signaling Axis. *Front Oncol* (2018) 8:470. doi: 10.3389/fonc.2018.00470
199. Hu L, Yt D, Jf Li, Lp Su, Yan M, Zg Z, et al. Biglycan Enhances Gastric Cancer Invasion by Activating FAK Signaling Pathway. *Oncotarget* (2014) 5:1885–96. doi: 10.18632/oncotarget.1871
200. Pinto F, Santos-Ferreira L, Pinto MT, Gomes C, Reis CA. The Extracellular Small Leucine-Rich Proteoglycan Biglycan Is a Key Player in Gastric Cancer Aggressiveness. *Cancers* (2021) 13:1330. doi: 10.3390/cancers13061330
201. Maishi N, Ohba Y, Akiyama K, Ohga N, Hamada Ji, Nagao-Kitamoto H, et al. Tumour Endothelial Cells in High Metastatic Tumours Promote Metastasis *via* Epigenetic Dysregulation of Biglycan. *Sci Rep* (2016) 6:1–13. doi: 10.1038/srep28039
202. Andrlová H, Mastroianni J, Madl J, Kern JS, Melchinger W, Dierbach H, et al. Biglycan Expression in the Melanoma Microenvironment Promotes Invasiveness *via* Increased Tissue Stiffness Inducing Integrin-β1 Expression. *Oncotarget* (2017) 8:42901–16. doi: 10.18632/oncotarget.17160
203. Sun H, Wang X, Zhang Y, Che X, Liu Z, Zhang L, et al. Biglycan Enhances the Ability of Migration and Invasion in Endometrial Cancer. *Arch Gynecol Obstetrics* (2016) 293:429–38. doi: 10.1007/s00404-015-3844-5
204. Weber CK, Sommer G, Michl P, Fensterer H, Weimer M, Gansauge F, et al. Biglycan is Overexpressed in Pancreatic Cancer and Induces G1-Arrest in Pancreatic Cancer Cell Lines. *Gastroenterology* (2001) 121:657–67. doi: 10.1053/gast.2001.27222
205. Niedworok C, Röck K, Kretschmer I, Freudenberger T, Nagy N, Szarvas T, et al. Inhibitory Role of the Small Leucine-Rich Proteoglycan Biglycan in Bladder Cancer. *PloS One* (2013) 8:e80084. doi: 10.1371/journal.pone.0080084
206. Rydström K, Joost P, Ehinger M, Edén P, Jerkeman M, Cavallin-Ståhl E, et al. Gene Expression Profiling Indicates That Immunohistochemical Expression of CD40 Is a Marker of an Inflammatory Reaction in the Tumor Stroma of Diffuse Large B-Cell Lymphoma. *Leukemia Lymphoma* (2012) 53:1764–8. doi: 10.3109/10428194.2012.666541
207. Schultze JL, Cardoso AA, Freeman GJ, Seamon MJ, Daley J, Pinkus GS, et al. Follicular Lymphomas can be Induced to Present Alloantigen Efficiently: A Conceptual Model to Improve Their Tumor Immunogenicity. *Proc Natl Acad Sci* (1995) 92:8200–4. doi: 10.1073/pnas.92.18.8200
208. French RR, Chan HC, Tutt AL, Glennie MJ. CD40 Antibody Evokes a Cytotoxic T-Cell Response That Eradicates Lymphoma and Bypasses T-Cell Help. *Nat Med* (1999) 5:548–53. doi: 10.1038/8426
209. Recktenwald CV, Leisz S, Steven A, Mimura K, Müller A, Wulfänger J, et al. HER-2/Neu-Mediated Down-Regulation of Biglycan Associated With Altered Growth Properties. *J Biol Chem* (2012) 287:24320–9. doi: 10.1074/jbc.M111.334425
210. Subbarayan K, Leisz S, Wickenhauser C, Bethmann D, Massa C, Steven A, et al. Biglycan-Mediated Upregulation of MHC Class I Expression in HER-2/

Neu-Transformed Cells. *Oncoimmunology* (2018) 7:e1373233. doi: 10.1080/2162402X.2017.1373233
211. Subbarayan K, Massa C, Lazaridou MF, Ulagappan K, Seliger B. Identification of a Novel miR-21-3p/TGF-β Signaling-Driven Immune Escape via the MHC Class I/biglycan Axis in Tumor Cells. *Clin Trans Med* (2021) 11:e306. doi: 10.1002/ctm2.306
212. Neill T, Schaefer L, Iozzo RV. Decorin as a Multivalent Therapeutic Agent Against Cancer. *Adv Drug Deliv Rev* (2016) 97:174–85. doi: 10.1016/j.addr.2015.10.016
213. Xu W, Neill T, Yang Y, Hu Z, Cleveland E, Wu Y, et al. The Systemic Delivery of an Oncolytic Adenovirus Expressing Decorin Inhibits Bone Metastasis in a Mouse Model of Human Prostate Cancer. *Gene Ther* (2015) 22:247–56. doi: 10.1038/gt.2014.110
214. Yang Y, Xu W, Neill T, Hu Z, Wang CH, Xiao X, et al. Systemic Delivery of an Oncolytic Adenovirus Expressing Decorin for the Treatment of Breast Cancer Bone Metastases. *Hum Gene Ther* (2015) 26:813–25. doi: 10.1089/hum.2015.098
215. Ständer M, Naumann U, Dumitrescu L, Heneka M, Löschmann P, Gulbins E, et al. Decorin Gene Transfer-Mediated Suppression of TGF-βSynthesis Abrogates Experimental Malignant Glioma Growth In Vivo. *Gene Ther* (1998) 5:1187–94. doi: 10.1038/sj.gt.3300709
216. Ma HI, Hueng DY, Shui HA, Han JM, Wang CH, Lai YH, et al. Intratumoral Decorin Gene Delivery by AAV Vector Inhibits Brain Glioblastomas and Prolongs Survival of Animals by Inducing Cell Differentiation. *Int J Mol Sci* (2014) 15:4393–414. doi: 10.3390/ijms15034393
217. Järvinen TA, Prince S. Decorin: A Growth Factor Antagonist for Tumor Growth Inhibition. *BioMed Res Int* (2015) 2015:1–11. doi: 10.1155/2015/654765
218. Roedig H, Damiescu R, Zeng-Brouwers J, Kutija I, Trebicka J, Wygrecka M, et al. Danger Matrix Molecules Orchestrate CD14/CD44 Signaling in Cancer Development. *Semin Cancer Biol* (2020) 62:31–47. doi: 10.1016/j.semcancer.2019.07.026

Conflict of Interest: The authors declare that the research was conducted in the absence of any commercial or financial relationships that could be construed as a potential conflict of interest.

Publisher's Note: All claims expressed in this article are solely those of the authors and do not necessarily represent those of their affiliated organizations, or those of the publisher, the editors and the reviewers. Any product that may be evaluated in this article, or claim that may be made by its manufacturer, is not guaranteed or endorsed by the publisher.

Copyright © 2021 Diehl, Huber, Trebicka, Wygrecka, Iozzo and Schaefer. This is an open-access article distributed under the terms of the Creative Commons Attribution License (CC BY). The use, distribution or reproduction in other forums is permitted, provided the original author(s) and the copyright owner(s) are credited and that the original publication in this journal is cited, in accordance with accepted academic practice. No use, distribution or reproduction is permitted which does not comply with these terms.

GLOSSARY

ALR	AIM2-like receptors
AMPK	AMP-activated protein kinase
ANGPT2	angiopoietin 2
CBL	casitas B-lineage lymphoma
CCL	chemokine C–C motif-ligand
CD	cluster of differentiation
CS/DS	chondroitin sulfate/dermatan sulfate
CXCL	chemokine C-X-C motif-ligand
DAMP	damage-associated molecular pattern
ECM	extracellular matrix
EGF	epidermal growth factor
EGFR	epidermal growth factor receptor
EMT	epithelial-mesenchymal transition
Epo	erythropoietin
Erk	extracellular signal-regulated kinase
FAK	Focal-adhesion kinase
GAG	glycosaminoglycan
HGF	hepatocyte growth factor
HIF-1α	hypoxia-inducible factor 1α
HSP70	heat shock protein 70
IGF-1R	insulin-like growth factor type 1 receptor
IL-10	interleukin 10
IL-1β	interleukin 1 beta
LC3	microtubule-associated protein 1A/1B-light chain 3
LRP6	low-density lipoprotein receptor-related protein 6
LRR	leucine-rich repeat
MAPK	mitogen-activated protein kinase
Met	mesenchymal-epithelial transition factor
MHC	major histocompatibility complex
miR	microRNA
mTOR	mammalian target of rapamycin
MYC	myelocytomatosis oncogene protein
MyD88	myeloid differentiation primary response 88
NF-κB	nuclear factor kappa-light-chain-enhancer of activated B-cells
NLRP3	NOD-like receptor protein 3
NLRs	NOD-like receptors
NOX	NADPH oxidase
PARP1	poly [ADP-ribose] polymerase 1
PCNA	proliferating cell nuclear antigen
PDCD4	programmed cell death protein 4
Peg3	paternally expressed 3
PGC-1α	peroxisome proliferator-activated receptor-γ co-activator 1-α
RAS	Ras GTPase/Rat sarcoma
Rho	RAS homolog family member A
ROCK1	Rho-associated coiled-coil kinase 1
ROS	reactive oxygen species
RTK	receptor tyrosine kinase
shRNA	short hairpin RNA
SLRP	small leucine-rich proteoglycan
TGF-β	transforming growth factor β
TGF-β1	transforming growth factor β isoform 1
Th	T helper
TIMP-3	metalloproteinases-3
TLR	Toll-like receptor
TME	tumor microenvironment
TNF-α	tumor necrosis factor alpha
TRIF	TIR-domain-containing adapter-inducing interferon-β
TSP-1	thrombospondin-1
VEGFA	vascular endothelial growth factor A
VEGFR	vascular endothelial growth factor receptor
VEGFR2	vascular endothelial growth factor receptor 2
VPS34	vacuolar protein sorting 34

frontiers in Oncology

ORIGINAL RESEARCH
published: 17 January 2022
doi: 10.3389/fonc.2021.826865

Cold Atmospheric Plasma Attenuates Breast Cancer Cell Growth Through Regulation of Cell Microenvironment Effectors

Christos A. Aggelopoulos[1], Anna-Maria Christodoulou[2†], Myrsini Tachliabouri[2†], Stauros Meropoulis[1], Maria-Elpida Christopoulou[2], Theodoros T. Karalis[2], Athanasios Chatzopoulos[2] and Spyros S. Skandalis[2]**

[1] Laboratory of Cold Plasma and Advanced Techniques for Improving Environmental Systems, Institute of Chemical Engineering Sciences, Foundation for Research and Technology Hellas (FORTH/ICE-HT), Patras, Greece, [2] Biochemistry, Biochemical Analysis & Matrix Pathobiology Res. Group, Laboratory of Biochemistry, Department of Chemistry, University of Patras, Patras, Greece

OPEN ACCESS

Edited by:
Martin Götte,
University of Münster, Germany

Reviewed by:
Manuela Viola,
University of Insubria, Italy
Ilona Kovalszky,
Semmelweis University, Hungary

***Correspondence:**
Christos A. Aggelopoulos
caggelop@iceht.forth.gr
Spyros S. Skandalis
skandalis@upatras.gr

†These authors have contributed equally to the work

Specialty section:
This article was submitted to Molecular and Cellular Oncology, a section of the journal Frontiers in Oncology

Received: 01 December 2021
Accepted: 22 December 2021
Published: 17 January 2022

Citation:
Aggelopoulos CA, Christodoulou A-M, Tachliabouri M, Meropoulis S, Christopoulou M-E, Karalis TT, Chatzopoulos A and Skandalis SS (2022) Cold Atmospheric Plasma Attenuates Breast Cancer Cell Growth Through Regulation of Cell Microenvironment Effectors. Front. Oncol. 11:826865. doi: 10.3389/fonc.2021.826865

Breast cancer exists in multiple subtypes some of which still lack a targeted and effective therapy. Cold atmospheric plasma (CAP) has been proposed as an emerging anti-cancer treatment modality. In this study, we investigated the effects of direct and indirect CAP treatment driven by the advantageous nanosecond pulsed discharge on breast cancer cells of different malignant phenotypes and estrogen receptor (ER) status, a major factor in the prognosis and therapeutic management of breast cancer. The main CAP reactive species in liquid (i.e. H_2O_2, NO_2^-/NO_3^-) and gas phase were determined as a function of plasma operational parameters (i.e. treatment time, pulse voltage and frequency), while pre-treatment with the ROS scavenger NAC revealed the impact of ROS in the treatment. CAP treatment induced intense phenotypic changes and apoptosis in both ER+ and ER- cells, which is associated with the mitochondrial pathway as evidenced by the increased Bax/Bcl-2 ratio and cleavage of PARP-1. Interestingly, CAP significantly reduced CD44 protein expression (a major cancer stem cell marker and matrix receptor), while differentially affected the expression of proteases and inflammatory mediators. Collectively, the findings of the present study suggest that CAP suppresses breast cancer cell growth and regulates several effectors of the tumor microenvironment and thus it could represent an efficient therapeutic approach for distinct breast cancer subtypes.

Keywords: CAP, breast cancer, estrogen receptor, tumor microenvironment, ROS, extracellular matrix

INTRODUCTION

Breast cancer is a highly heterogeneous disease that may exist in multiple subtypes. Its classification is critical for proper patient management and follow-up (1). Estrogen receptor alpha (ERα) expression profile is the prominent molecular feature for the discrimination of breast cancers, which are classified as ER-positive (ER+) and ER-negative (ER-). Almost 70% of breast cancers are ER+ and can be targeted with endocrine therapies. Others are classified as HER2-positive (they

express the HER2 receptor tyrosine kinase) against which anti-HER2 targeted therapies are applied, and triple-negative breast cancer (TNBC, due to the absence of ER, progesterone and HER2 receptors), which has the worst prognosis and lacks an effective targeted therapy (2–4). Further, breast cancers can be classified with regard to their extracellular matrix (ECM) expression pattern resulting in distinct ECM subtypes related with different clinical outcome (5). Current options of breast cancer treatment include surgery, chemotherapy and radiotherapy, which all present severe limitations as they are not selective and offer incomplete tumor ablation. Therefore, the development of new therapeutic approaches that would ablate incurable breast tumor subtypes is urgently needed.

A rapidly evolving technology showing a strong potential for biomedical applications is cold plasma operating at atmospheric pressure (Cold Atmospheric Plasma, CAP) (6). CAP is generated from electrical energy allowing the creation of high energy electrons and reactive oxygen and nitrogen species (ROS/RNS) such as $^1O_2$, OH radicals, NO_x, atomic O, O_3 and H_2O_2 which play critical role in transferring the reactivity from the gas discharge plasma zone to solutions/media (7), subsequently inducing specific biochemical responses. CAP has been used in several branches of modern medicine, such as in wound healing and sterilization (8). Notably, CAP has shown promising anticancer activity over the last decade (9–11). The *in vitro* application of this technology in numerous tumor cell lines resulted in the significant inhibition of cell growth, while it also attenuated the growth of subcutaneous xenograft tumors and melanoma in mice (9, 12, 13).

To date, many studies have concluded that the prominent factors contributing to the lethal CAP-mediated effects on cancer cells both *in vitro* and *in vivo* are the ROS/RNS generated during the complex interaction between plasma and cancer cells (14, 15). Fine tuning of the cellular levels of reactive species is critical for numerous cellular processes, such as metabolism, survival and differentiation, since they can act as mediators of various signaling pathways (16). Dysregulated ROS and/or RNS generation may have pro-tumorigenic effects by damaging nucleic acid and promoting genetic instability through induction of DNA strand breaks, which may induce the malignant transformation of tumor cells. On the other hand, excessive rise of intracellular ROS/RNS species appear anti-tumorigenic as they may induce irreversible damage in DNA, mitochondria and other vital components/structures of tumor cells as well as the activation of apoptotic mechanisms (16–20). In addition, several studies suggest the selective cancer cell apoptosis by CAP. For example, ROS produced in cancer cells at much higher levels than in normal cells, tend cancer cells to be more vulnerable than normal cells to ROS generated by CAP (21, 22).

Different setups for CAP cancer treatment have been extensively investigated with the prevailing devices being the plasma jet (9, 23, 24) and the dielectric barrier discharge (DBD) (22, 25, 26). Along with the basic principles of each device, the functions in the two devices are also different; by employing the jet device, the sample is faced as a separate, independent part of the system, while in the case of a DBD device, the sample constitutes a part of the discharge. Therefore, in case of a gentle treatment at a small area of the sample plasma jet device may be more suitable, while for treating a large area of sample and in a more intense mode, DBD could be considered more suitable (9). In addition, the main CAP discharge type reported to date includes AC-driven reactors. However, considering that the effectiveness of the treatment is closely related to the produced plasma reactive species, a rapid, effective and high production of reactive species is of eminent importance. In this context, recent efforts performed in reactors driven by nanosecond pulses (NSP) revealed its advantageous performance with respect to other plasma systems in terms of energy efficiency and production of plasma active particles (27).

In general, there are two different possible ways to perform a CAP-based cancer treatment, either through direct treatment of tumor cells or by an indirect treatment of culture solutions used for cells growth. In the present study, three approaches of DBD-CAP driven by the advantageous nanosecond pulsed discharge have been applied in breast cancer cells of different morphological and molecular features; the non-metastatic MCF-7/ER+ cells and the metastatic MDA-MB-231/ER- and Hs578T/ER- cells. The three DBD-CAP approaches included the direct treatment of the cell cultures, the indirect treatment of cell cultures using CAP-stimulated medium and the direct treatment of the cell cultures followed by the immediate change of the CAP-stimulated medium by fresh.

Collectively, we provide evidence that DBD-CAP suppresses breast cancer cell growth and metastatic potential by triggering cell apoptosis and regulating specific effectors of the tumor cell microenvironment such as ROS, matrix receptors, proteases and inflammatory mediators. The observed differential effects of the applied DBD-CAP approaches on the mammary tumor cell models used in the present study suggest that CAP-based technology could advance the therapy of distinct breast cancer subtypes of different ER profile and specific molecular features.

MATERIALS AND METHODS

CAP Device and Treatment Strategy

The depiction of the plasma device used to treat breast cancer cell lines along with a picture of the plane-to-plane DBD reactor operated with air is presented in **Figure 1A**. The HV electrode was a stainless-steel disc (28 mm diameter) covered by an acrylic glass cylinder (bottom thickness 1.5 mm, wall thickness 5 mm) acting as the discharge dielectric barrier. A petri dish (35 mm diameter) was filled with 1 mL of complete cell culture medium [Dulbecco's Modified Eagle's Medium (DMEM) with 10% FBS] and placed over a stainless-steel disc serving as the grounded electrode. The inter-electrode distance was ~6 mm, the distance between the dielectric surface and culture medium surface was ~1 mm and the air flow rate streamed above the culture medium surface was fixed at 1.0 liters per minute. The DBD reactor was driven by a high voltage (HV) generator (NPG-18/3500) able to produce positive nanosecond pulses (NSP) recorded on a Rigol MSO2302A, 300MHz oscilloscope using a Tektronix P6015A

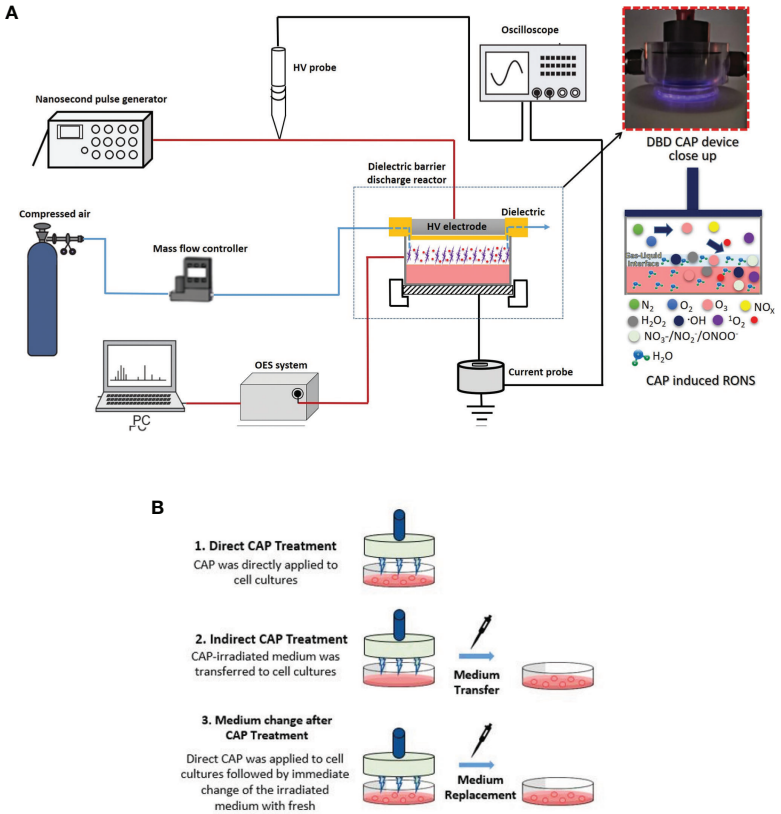

FIGURE 1 | Schematic illustration of **(A)** Dielectric Barrier Discharge (DBD) CAP device; **(B)** breast cancer cell treatment approaches: 1. Direct DBD-CAP treatment (DBD-CAP was directly applied to cell cultures); 2. Indirect DBD-CAP treatment (DBD-CAP-treated medium was transferred to cell cultures); 3. Medium change after DBD-CAP treatment (Direct DBD-CAP was applied to cell cultures followed by immediate change of the CAP-treated medium by fresh untreated).

voltage probe and a Pearson electronics 2877, 300 Hz-200 MHz wideband current transformer. The average discharge power (P) was estimated by multiplying the pulse repetition rate (f) by the discharge pulse energy (E_p), which was found by the integration of the instantaneous pulse voltage and current over the pulse duration (t) (28):

$$P = f \quad E_p = f \int_{pulse} V(t)I(t)dt \qquad (1)$$

where V(t) and I(t) are the voltage and current signals, respectively.

Optical emission spectroscopy (OES) was employed to identify the main plasma-induced reactive oxygen and nitrogen species (ROS/RNS) in the gas phase. The emission spectra of the air-DBD was recorded with a fiber optics spectrometer (AvaSpec-ULS2048CL-EVO, Avantes). The NSP-DBD treatments were repeated at two different pulse voltages (27.6 and 31.2 kV), pulse repetition rates (0.5 and 1.5 kHz) and treatment times (2 to 6 min) at room temperature.

Cell Culture and Reagents

Low metastatic MCF-7 (ER+) and highly metastatic MDA-MB-231 and Hs 578T (triple negative, ER-/PR-/HER2-) breast cancer cell lines (obtained from the ATCC) were utilized in the present study. For cell cultures, complete media (DMEM, #LM-D1109/500, Biosera) containing 10% fetal bovine serum and antimicrobial agents cocktail were used as described before (29). All chemicals were of the best commercially available grade.

DBD-CAP Treatment Approaches on Breast Cancer Cells

The schematic illustration of the DBD-CAP treatment approaches applied in the present study is depicted in **Figure 1B**. In each experiment, a certain number of breast cancer cells (280,000 for MCF-7, 220,000 for MDA-MB-231 and Hs578T) was seeded on a 35-mm dish (#G203-35, Kisker) in complete medium (1 mL). After 24 h incubation under the standard cell culture conditions (a humidified, 37°C, 5% CO_2 environment), the medium was replaced with 1 mL of fresh complete medium and the cell cultures were proceeded to DBD-CAP treatment. Three different treatment approaches were followed: (i) *Direct treatment*, where DBD-CAP was directly applied to cell cultures, (ii) *indirect treatment*, where cell-free DBD-CAP-treated medium (1 mL) was transferred to cell cultures, and (iii) *medium change*, where DBD-CAP was applied to cell cultures followed by immediate change of the CAP-treated medium by 1 mL of fresh untreated one. Following

24 h culture, cancer cells were proceeded to the various biochemical assays. For each treatment approach, a control group corresponding to cancer cells grown in 1 mL complete medium without DBD-CAP treatment was included.

Preparation of N-Acetyl-L-Cysteine (NAC)-DMEM and Pre-Treatment of Breast Cancer Cells

DMEM containing NAC (NAC-DMEM) at concentration of 5 mM was made by dissolving NAC powder (Sigma-Aldrich, A7250) in complete medium (DMEM with 10% FBS). Breast cancer cells were cultured for 24 h, as described above, and the medium was replaced with 1 mL of NAC-DMEM. After 2 h, cell cultures were proceeded to the DBD-CAP treatments.

pH and Temperature Measurement in Culture Media

Cell-free complete culture media were exposed to air NSP-DBD plasma for 2, 3, 4 and 6 min under the various abovementioned pulse voltages and pulse frequencies. Immediately after plasma treatment, the pH and temperature of the culture media were measured with a pH meter (Consort C830) and an infrared thermometer (Benetech GM900), respectively.

Measurement of Reactive Species in Culture Media (H_2O_2, NO_2^- and NO_3^-) and in Reactor Exhaust Gas (NO_x)

The concentrations of H_2O_2, nitrate ions (NO_3^-) and nitrite ions (NO_2^-) in cell-free complete culture media at the various investigated DBD-CAP conditions were measured with the suitable QUANTOFIX® test strips and quantified accurately with the QUANTOFIX® Relax unit (Macherey-Nagel, GmbH). Moreover, NO_x concentration in the plasma exhaust gas was measured with a gas analyzer (Optima 7).

Morphology/Phase Contrast Microscopy

For the observation of cell morphological changes, photographs of breast cancer cells (both the control groups and those subjected to the three DBD-CAP approaches) were captured at 3 h and 24 h after CAP treatment utilizing a color digital camera (CMOS) mounted on a phase contrast microscope (OLYMPUS CKX41, QImaging Micro Publisher 3.3RTV) through a 10x objective.

Cell Viability

To evaluate cell viability, control and DBD-CAP-treated cells were stained with crystal violet solution followed by optical density measurement at 570 nm as described before (29). As an alternative method, breast cancer cells (control and DBD-CAP-treated cells cultured for 24 h) were detached from the 35-mm dishes with trypsin-EDTA 1× in PBS for 3 min, collected and counted on a hemocytometer counting chamber according to standard protocols.

Fluorescence Microscopy

The assay was performed as described before (30). A green fluorescent phalloidin conjugate (Phalloidin-iFluor™ 488) (1:40, #00042, Biotium CF™488A) in 1% BSA/PBST was used to visualize actin cytoskeleton utilizing a fluorescent phase contrast microscope (OLYMPUS CKX41, QImaging Micro Publisher 3.3RTV) at 60×.

RNA Isolation, cDNA Synthesis, and Real Time RT-PCR

RNA isolation from control and DBD-CAP-treated cells, cDNA synthesis and real time PCR analysis were conducted according to the manufacturer's instructions. The relative mRNA expression of different gene transcripts (the corresponding primer sequences are presented in **Table 1**) was calculated as described in (30). The threshold cycle (Ct) number of each gene was normalized to the Ct of the normalizer (18S rRNA).

Western Blot Analysis

Western blot analysis was performed as described before (29). The primary antibodies used in the present study were: anti-PARP-1 (rabbit, 1:500, #ab6079, Abcam) and anti-α-tubulin (mouse, clone DM1A, 1:500, #T9026, Sigma-Aldrich). Detection of the proteins was performed according to the manufacturer's instructions.

Statistical Analysis

Reported values are expressed as mean ± standard deviation and are based on three (at least) independent experiments. GraphPad Prism unpaired t-test (95% confidence intervals) was used for the evaluation of statistical significant differences. Three significance levels are indicated, i.e. $*p<0.05$, $**p<0.01$ and $***p<0.001$.

RESULTS

Electrical and Optical Characteristics of the Discharge

The recorded NSP-DBD voltage and current waveforms during cell cultures treatment are shown in **Figure 2A**. Both voltage and

TABLE 1 | Primer sequences used for quantitative RT-PCR.

Gene	Primer Sequence (5'-3')	$T_{annealing}$
Bax	Sense: CTGAGCGAGTGTCTCAAGCG Anti-Sense: CCCCAGTTGAAGTTGCCGTC	60°C
Bcl-2	Sense: AAGAGCAGACGGATGGAAAAAGG Anti-Sense: GGGCAAATGCAAGTGAATG	60°C
CD44 total	Sense: ATAATTGCCGCTTTGCAGGTGTATT Anti-Sense: ATAATGGCAAGGTGCTATTGAAAGCCT	60°C
uPA	Sense: ACTACTACGGCTCTGAAGTCACCA Anti-Sense: GAAGTGTGAGACTCTCGTGTAGAC	60°C
MMP-1	Sense: CCTCGCTGGGAGCAAACA Anti-Sense: TTGGCAAATCTGGCGTGTAA	60°C
MT1-MMP	Sense: CATGGGCAGCGATGAAGTCT Anti-Sense: CCAGTATTTGTTCCCCTTGTAGAAGTA	60°C
IL-6	Sense: TCCAGAACAGATTTGAGAGTAGTG Anti-Sense: GCATTTGTGGTTGGGTCAGG	58°C
IL-8	Sense: GGCACAAACTTTCAGAGACAGCAG Anti-Sense: GTTTCTTCCTGGCTCTTGTCCTAG	61°C
18S RNA	Sense: CAGGTCTGTGATGCCCTTAGA Anti-Sense: GCTTATGACCGGCACTTACTG	60°C

current signals comprised by a sequence of pulses (31) with the rise time of the main positive HV pulse being ~4 ns and its duration ~15 ns at the full width at half maximum. The peak current was ~50 A resulted in an extremely high instantaneous power of ~1.2 MW (**Figure 2B**), but at the same time the average discharge power was very low and ranged from 1.8 to 4.8 W under the investigated pulse voltages and frequencies (inset of **Figure 2B**) due to the quite low duty cycle involved.

Various excited molecular and atomic plasma ROS/RNS can be detected based on their peaks on the optical emission spectra (OES) of the discharge. The recorded spectrum at 31.2 kV is presented in **Figure 2C** revealing the major plasma species generated in the air NSP-DBD system of this study. Mainly, emission peaks originating from the N_2 second positive system (N_2 SPS) in the range 315-405 nm, the N_2 first positive system (N_2 FPS) between 500 and 900 nm, and N_2^+ at 393 and 427 nm were observed (27). Furthermore, OH radical emissions (309 nm) (32) which is a strong oxidant and precursor for H_2O_2 production, NO gamma emission lines in the range 230-260 nm (33), atomic oxygen (O) line at 777 and 844 nm, and O_2^+ line at 527 nm were detected (34).

Quantification of Plasma-Generated NO_x in Gas Phase

During CAP process under air atmosphere, the dissolution of the produced gaseous NO_x in the cell culture media results in the formation of nitrites (NO_2^-) and nitrates (NO_3^-) that have been identified as reactive species playing a significant role in cancer cell death (35, 36). Thus, the concentration of the gaseous NO_x in the plasma exhaust gases under the different pulse voltages and frequencies were measured and presented in **Table 2**. NO concentration was not detected since in air-CAP nitrogen monoxide is rapidly converted to nitrogen dioxide (37) and therefore NO_x concentration is equal to NO_2 concentration at each experimental condition. It is apparent that NO_2 concentration increased with pulse voltage and repetition rate. At constant repetition rate of 0.5 kHz, NO_2 concentration increased from 132 to 173 ppm when pulse voltage increased from 27.6 to 31.2 kV whereas at pulse voltage 27.6 kV and pulse frequency 1.5 kHz, NO_2 concentration increased further to 239 ppm. The enhancement of the CAP-induced gaseous NO_2 concentration with pulse voltage and frequency is directly related to the enhanced electric field and discharge power (inset of **Figure 2B**).

Quantification of Hydrogen Peroxide (H_2O_2), Nitrite (NO_2^-) and Nitrate (NO_3^-) in Cell-Free Culture Media

To investigate plasma-induced ROS/RNS generation in cell-free culture media, a quantitative analysis with emphasis on the species H_2O_2, NO_2^- and NO_3^- was performed. Besides nitrite and nitrate ions, hydrogen peroxide has been also identified as a major specie of cancer treatment (38). The concentration of H_2O_2 at various NSP-DBD treatment times and over two different values of the applied pulse voltage and pulse

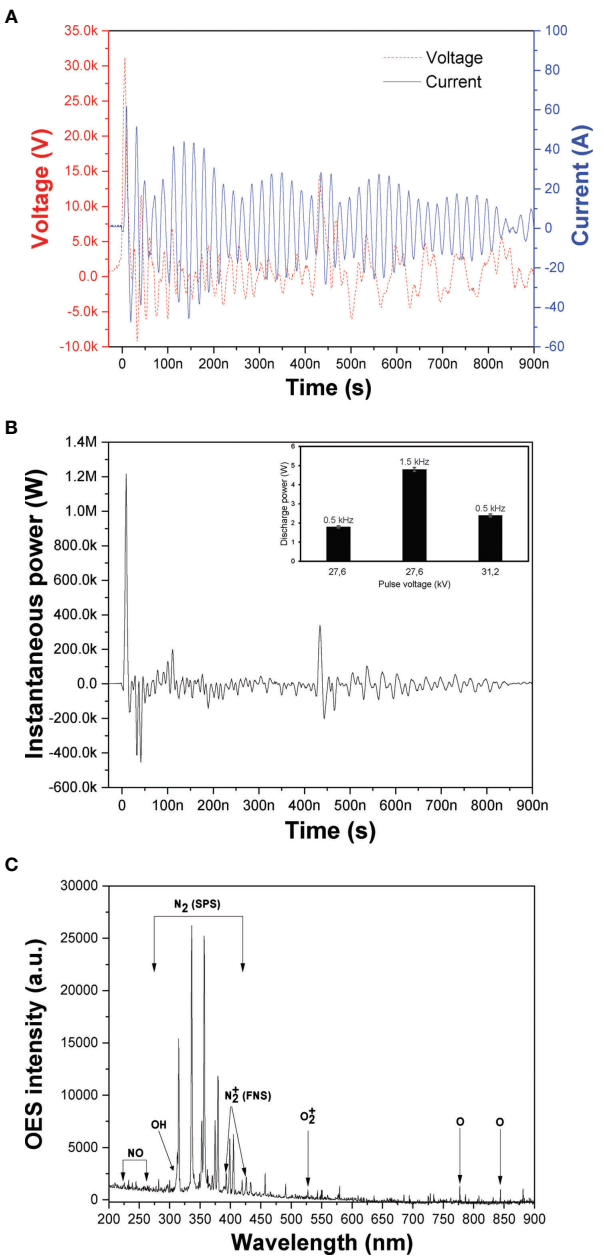

FIGURE 2 | DBD-CAP characterization. **(A)** Instantaneous voltage and current NSP-DBD signals obtained at V=31.2 kV and *f* = 0.5 kHz; **(B)** Instantaneous power signal calculated by multiplying the instantaneous pulse voltage and current (inset: average discharge power as a function of pulse voltage and frequency; **(C)** Optical emission spectrum to identify the major excited ROS/RNS in the NSP-DBD with air gas.

TABLE 2 | Concentration of plasma-generated NO_x in the exhaust gases.

Conditions	NO (ppm)	NO_2 (ppm)
0.5 kHz - 27.6 kV	–	132
0.5 kHz - 31.2 kV	–	173
1.5 kHz - 27.6 kV	–	239

repetition rate is depicted in **Figure 3A**. H_2O_2 concentration increased significantly (i) with treatment time under all investigated conditions and (ii) with both pulse voltage and frequency. At mild treatment conditions (pulse voltage 27.6 kV and pulse frequency 0.5 kHz), the NSP-DBD for 2 min induced H_2O_2 generation of 0.24 mM which enhanced to 0.53 mM and 0.62 mM after 4 min and 6 min of treatment, respectively. Under strong treatment conditions (either pulse frequency 0.5 kHz/pulse voltage 31.2 kV or pulse frequency 1.5 kHz/pulse voltage 27.6 kV) after 6 min of plasma exposure time, H_2O_2 concentration in culture media increased from 0.62 mM to 2.18 mM (0.5 kHz/31.2 kV) and to 3.56 mM (1.5 kHz/27.6 kV).

The dissolution of the gaseous NO_2 **(Table 2)** in the culture media results in the formation of nitrites, nitrates and hydrogen ions (39): $2\ NO_2\ (g) + H_2O \rightarrow NO_2^-\ (aq) + NO_3^-\ (aq) + 2\ H^+\ (aq)$. The concentration of NO_2^- and NO_3^- in cell-free culture media at various plasma exposure times is shown in **Figures 3B, C**, respectively. Similar to H_2O_2, both RNSs increased substantially with treatment time, pulse voltage and pulse frequency, whereas NO_3^- concentration was about one order of magnitude higher compared to that of NO_2^- under all investigated plasma conditions. More specifically, at mild CAP conditions, the concentration of NO_2^- was 0.21 mM after 2 min of treatment and increased to 0.41 mM at 6 min of treatment **(Figure 3B)**. Under strong DBD-CAP, NO_2^- level was further increased to 1.07 mM at 6 min of treatment (0.5 kHz/31.2 kV) whereas an even higher NO_2^- concentration was measured (1.25 mM) at higher pulse repetition rate (1.5 kHz/27.6 kV) for the same treatment time. NO_3^- concentration exhibited an analogous increase with treatment time, pulse voltage and frequency with its maximum (18 mM) measured under strong DBD-CAP (1.5 kHz/27.6 kV) after 6 min **(Figure 3C)**.

Estimation of pH and Temperature

It has been reported that the transfer of ROS/RNS generated by CAP in the aqueous phase affects the pH of the culture media and therefore it was measured for various treatment times under both mild and strong DBD-CAP **(Figure 4A)**. The pH of the cell-free culture media at 0.5 kHz was slightly changed from 8.3 (control) to 8.1 and 8.0 after 6 min of plasma treatment under both mild and strong DBD-CAP (pulse voltage 27.6 kV and 31.2 kV, respectively). At higher pulse frequency of 1.5 kHz (strong conditions), higher acidification was observed since pH was further decreased to 7.8 and 7.5 after 4 min and 6 min of treatment, respectively, which is due to the higher ROS/RNS concentration at 1.5 kHz compared to that at 0.5 kHz as already shown in **Figure 3**.

Another important parameter during cancer cells treatment by CAP is the change in temperature of culture media since temperature increase can inflict thermal damages in cells (40). The temperature of cell culture media was measured at various treatment times (2, 3, 4 and 6 min) of CAP treatment and 0.7 ± 0.1°C increase was detected after 6 min under mild DBD-CAP, whereas the corresponding increase under strong DBD-CAP (0.5 kHz/31.2 kV) was 1.0 ± 0.1°C **(Figure 4B)**. Therefore, the NSP-DBD device of this study operating even under strong treatment conditions overcomes the heating effect of other AC-driven plasma devices (41). Nevertheless, a higher increase of 4.2 ± 0.2°C was observed at 1.5 kHz/27.6 kV **(Figure 4B)**.

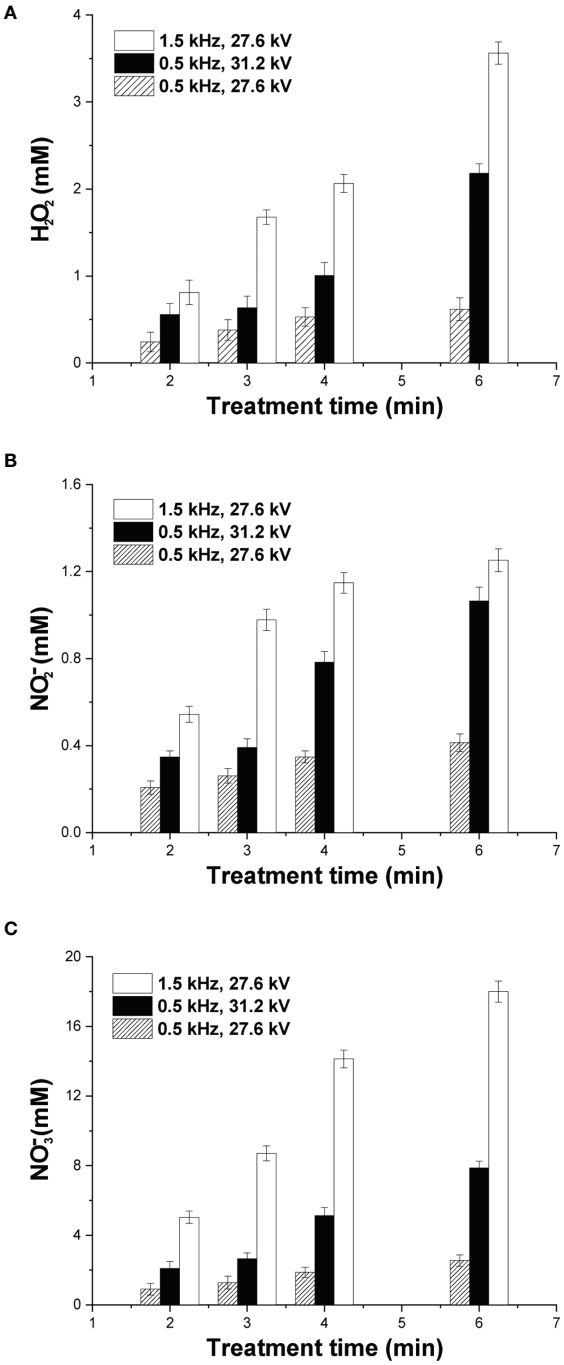

FIGURE 3 | Quantification of major DBD-CAP-originated ROS/RNS. Concentration of **(A)** H_2O_2; **(B)** NO_2^-; **(C)** NO_3^- in cell-free culture media (DMEM with 10% FBS) exposed to various plasma treatment times at different pulse voltages and frequencies. The values represent the mean ± SD of 3 (at least) independent experiments.

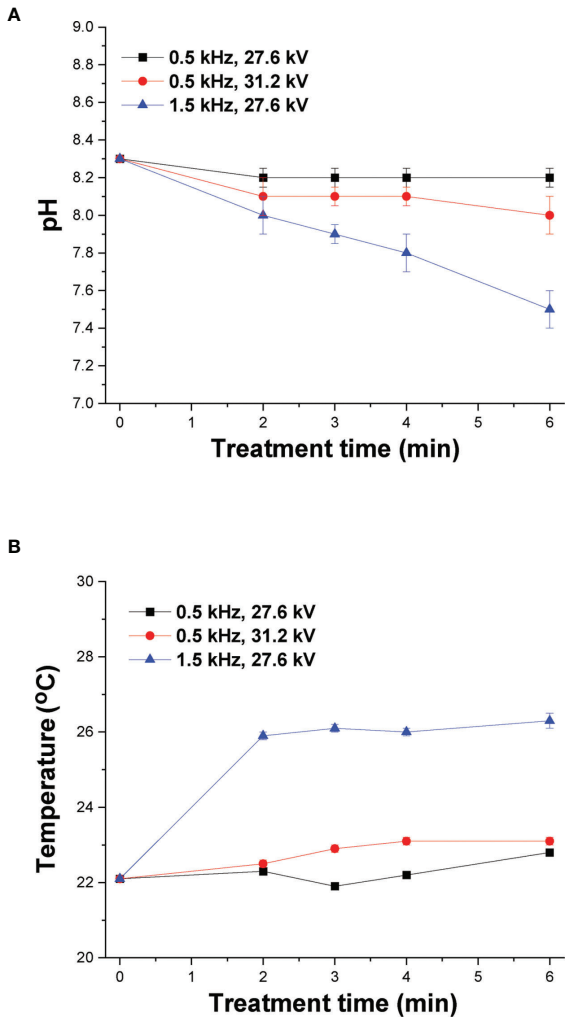

FIGURE 4 | DBD-CAP treatment does not affect cell cultured medium pH and temperature. Effect of plasma exposure time on **(A)** pH and **(B)** temperature of cell-free culture media (DMEM with 10% FBS) at different pulse voltages and frequencies of the NSP-DBD device. The values represent the mean ± SD of 3 (at least) independent experiments.

DBD-CAP Attenuates Breast Cancer Cell Growth

Direct treatment of MCF-7 (ER+, low metastatic), MDA-MB-231 and Hs578T (ER-, highly metastatic) breast cancer cells with mild (0.5 kHz/27.6 kV) or strong (1.5 kHz/27.6 kV or 0.5 kHz/31.2 kV) DBD-CAP conditions revealed a time- and dose-dependent effect on cell viability. Specifically, short (2 min) mild DBD-CAP induced 30-40% toxicity to all cell lines, which was further increased up to 60-80% when cells were subjected to longer (6 min) mild DBD-CAP treatment. Strong DBD-CAP of short treatment time (2 min) resulted in 60-80% cytotoxicity (at levels similar to those observed for the long mild DBD-CAP), which was further enhanced up to 70-90% when cells were subjected to strong DBD-CAP for 6 min (**Figures 5A**, **6A**, **7A**). Indirect treatment resulted in a similar strong effect on cell viability as shown by the increased cytotoxicity at all DBD-CAP conditions used in the present study (**Figures 5C**, **6C**, **7C**). Among cancer cells, Hs578T cells showed the highest toxicity (approx. 90%) when subjected to strong indirect DBD-CAP even with short treatment time (2 min) (**Figure 7C**). On the other hand, MDA-MB-231 cells showed a more resistant phenotype at both direct and indirect treatment approaches compared to the other two cell lines (**Figures 6A, C**).

To further investigate these observations, breast cancer cells were directly subjected to DBD-CAP under the same conditions as in direct/indirect treatment approaches and the culture medium was immediately replaced with fresh. This approach (medium change) resulted in the lowest cytotoxicity at all three breast cancer cell lines (**Figures 5E**, **6E**, **7E**). This was particularly evident for Hs578T cells, which exhibited remarkably lower cytotoxicity (approx. 60%) when medium was changed after strong DBD-CAP (**Figure 7E**) compared to direct or indirect approaches (**Figures 7A, C**, respectively) where cytotoxicity ranged from approx. 70 to 95%. On the other hand, the same approach revealed a significantly lower cytotoxicity for MDA-MB-231 cells (**Figure 6E**) which were the most resistant to all applied approaches.

Overall, these results revealed an important role of DBD-CAP-originated species within the medium in the inhibition of breast cancer cell growth.

DBD-CAP Affects Breast Cancer Cell Morphology

The observed significant reduction in cell viability prompted us to examine cell cytoskeleton changes upon DBD-CAP treatment. To this aim, we used Phalloidin-Fluor488 to visualize filamentous actin (F-actin). Treatment of cells with direct or indirect mild DBD-CAP (2 min) resulted in a moderate to strong actin cytoskeleton disorganization, which was more evident in MCF-7 (**Figures 5B, D**) and Hs578T (**Figures 7B, D**) cells. The changes in filamentous actin organization were significantly intensified in all three breast cancer cell lines upon treatment with direct or indirect strong DBD-CAP (2 min), which was followed by cell rounding and a dramatic loss of cells as expected (**Figures 5**, **6**, **7B, D**). On the other hand, only moderate changes in actin cytoskeleton were observed when the CAP-treated medium was immediately replaced by fresh (medium change approach) at both mild and strong DBD-CAP conditions while no significant loss of cells occurred in line with the low cytotoxicity observed for this approach (**Figures 5**, **6**, **7F**).

Pretreatment With NAC Partly Weakens DBD-CAP-Mediated Effects on Breast Cancer Cell Viability

It is known that the CAP-originated reactive species are the major anti-cancer effectors inhibiting the growth of tumor cells *in vitro*. Therefore, to further investigate the strong anti-cancer effect of DBD-CAP treatment, breast cancer cells were treated with the intracellular ROS scavenger NAC (5 mM) prior to mild (0.5 kHz/27.6 kV) DBD-CAP (direct, indirect or media change) for 4 min. The results revealed that NAC partly counteracted the significant reduction in cell viability, especially when indirect

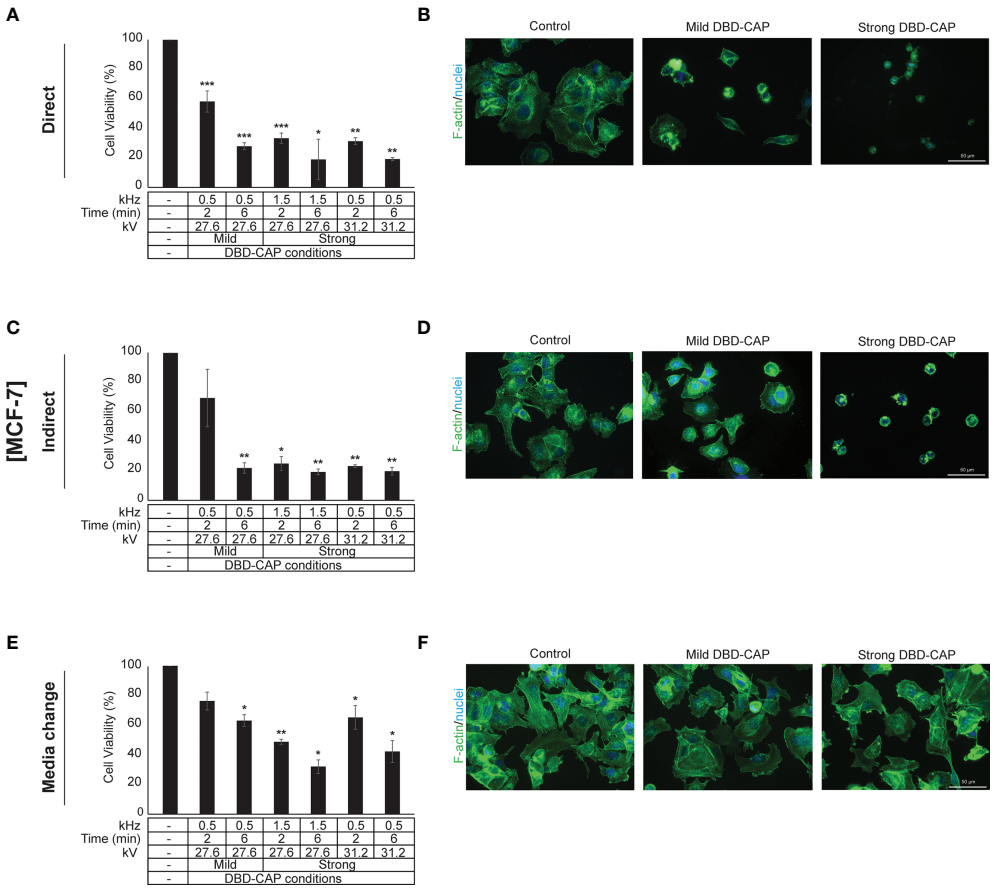

FIGURE 5 | DBD-CAP suppresses MCF-7 (ER+, low metastatic) breast cancer cell growth. **(A**, **C**, **E)** Assessment of % cell survival 24 h after treatment with mild (0.5 kHz/27.6 kV) or strong (1.5 kHz/27.6 kV or 0.5 kHz/31.2 kV) DBD-CAP (direct, indirect, media change) for 2 and 6 min. The values represent the mean ± SD of 3 (at least) independent experiments. Asterisks illustrate significant differences of the different treatment conditions compared to untreated (control) cells (*$p < 0.05$, **$p < 0.01$, ***$p < 0.001$). **(B, D, F)** Cell morphology after mild (0.5 kHz/27.6 kV) or strong (0.5 kHz/31.2 kV) DBD-CAP treatment for 2 min. Scale bars, 50 μm. Representative immunofluorescence images are shown (*F-actin*, green; *nuclei*, blue/DAPI).

treatment was applied to breast cancer cells **(Figure 8)**. These findings were confirmed by phase contrast microscopy, which revealed negligible changes in cell morphology when CAP-treated cells were pretreated with the ROS scavenger compared to the CAP-treated cells alone **(Supplementary Figure 1)**.

DBD-CAP Induces the Mitochondrial Apoptotic Pathway in Breast Cancer Cells

To examine whether the significant inhibition of breast cancer cell growth after DBD-CAP treatment was due to induction of cell apoptosis, we examined the mRNA levels of two key apoptosis-associated mitochondrial proteins, namely the proapoptotic Bax and the antiapoptotic Bcl-2, and evaluated the changes in their ratio since an elevated Bax/Bcl-2 ratio indicates the induction of the intrinsic cell apoptotic pathway (42). The results showed that the Bax/Bcl-2 ratio was significantly elevated (1,5- to 2,5-fold) in all three cell lines subjected to mild (0.5 kHz/27.6 kV) direct DBD-CAP compared to untreated cells (control) **(Figure 9A)**. To further investigate this observation, we performed immunoblotting analysis for poly [ADP-ribose] polymerase 1 (PARP-1) protein (43). Notably, DBD-CAP induced PARP-1 cleavage, a marker of apoptosis, as evidenced by the detection of the PARP-1 fragment (29-kDa, cPARP-1) in all cell lines **(Figure 9B)**.

DBD-CAP Affects the Expression of Matrix Effectors

Next, we investigated whether DBD-CAP would affect tumor cell microenvironment. To this aim, we treated cells with mild (0.5 kHz/27.6 kV) direct DBD-CAP that caused a moderate cytotoxicity and examined the expression of key matrix molecules involved in breast tumor cell malignant properties by qPCR analysis. Our findings showed that DBD-CAP resulted in a significant down-regulation of CD44 (the main cellular receptor for the polysaccharide hyaluronan and a prominent cancer stem cell marker) mRNA expression in all three breast cancer cell lines **(Figure 10A)**. Further, DBD-CAP treatment significantly modulated the expression of several proteases including matrix metalloproteases (MMP-1 and the membrane-associated MT1-

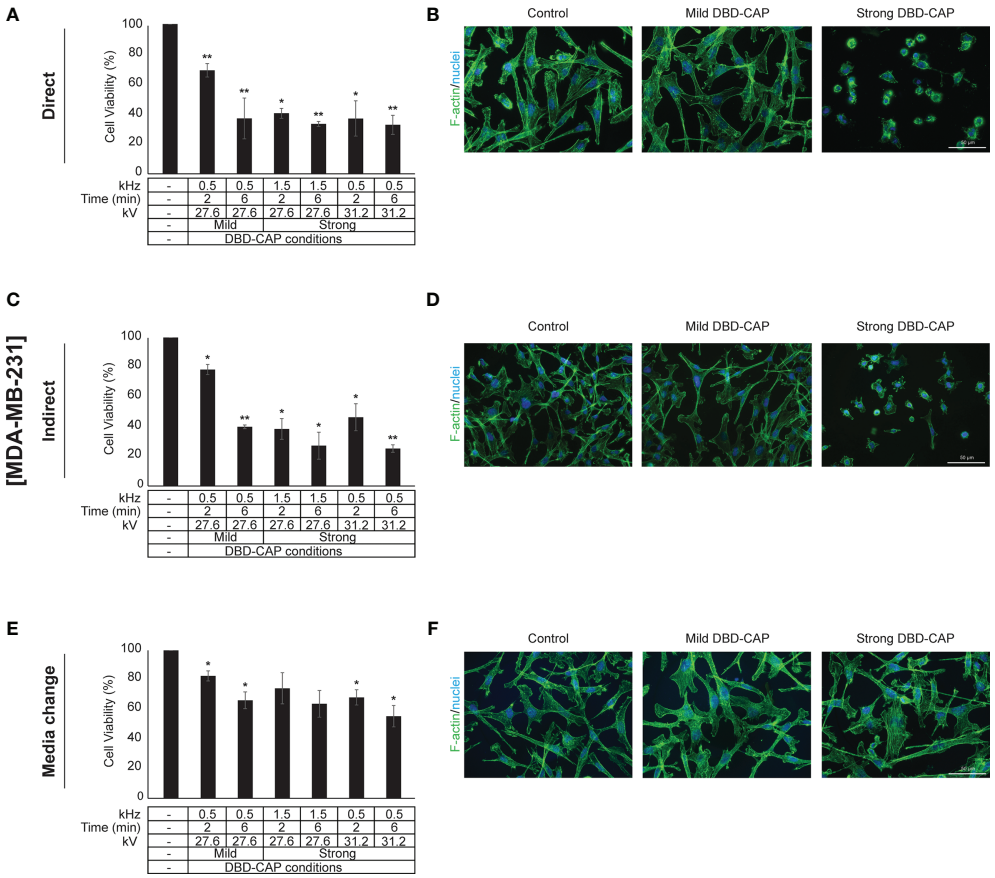

FIGURE 6 | DBD-CAP suppresses MDA-MB-231 (ER-, highly metastatic) breast cancer cell growth. **(A, C, E)** Assessment of % cell survival 24 h after treatment with mild (0.5 kHz/27.6 kV) or strong (1.5 kHz/27.6 kV or 0.5 kHz/31.2 kV) DBD-CAP (direct, indirect, media change) for 2 and 6 min. The values represent the mean ± SD of 3 (at least) independent experiments. Asterisks illustrate significant differences of the different treatment conditions compared to untreated (control) cells (*p < 0.05, **p < 0.01). **(B, D, F)** Cell morphology after mild (0.5 kHz/27.6 kV) or strong (0.5 kHz/31.2 kV) DBD-CAP treatment for 2 min. Scale bars, 50 μm. Representative immunofluorescence images are shown (*F-actin*, green; *nuclei*, blue/DAPI).

MMP) as well as uPA, a critical component of the plasminogen activation system that promotes MMP activation and degradation of most ECM proteins (**Figures 10B–D**, respectively). Notably, DBD-CAP treatment showed an opposite effect in the expression of the proteases between ER- and ER+ breast cancer cells. Specifically, DBD-CAP significantly down-regulated the mRNA levels of MMP-1, MT1-MMP and uPA in MDA-MB-231/ER- and Hs578T/ER- cells, while it up-regulated these proteases in MCF-7/ER+ cells. In a similar mode of action, DBD-CAP differentially affected the expression of inflammatory mediators such as interleukins IL-6 and IL-8 since they were also up-regulated in MCF-7/ER+ cells, while they were significantly suppressed in ER- cells (MDA-MB-231 and Hs578T) (**Figures 10E, F**).

DISCUSSION

Breast cancer derives from a number of distinct tumors of epithelial cells of the breast and it cannot accurately descried as a single disease (44, 45). ERα expression is a major criterion for the classification and clinical management of breast cancers. Although a high proportion is ER+ and responsive to antiestrogens-based treatment, ER- breast cancers (such as TNBC) still lack effective targeted therapies while they present high risk of recurrence and the worst prognosis. Conventional treatments for controlling cancer is mostly based on anti-cancer agents, exhibiting limited effectiveness, high-cost and numerous side-effects. It is therefore obvious that there is urgent need to adopt new technologies and methods to deal with this problem. The outstanding performance of CAP concerning its anti-cancer effects has already been shown in a number of *in vitro* studies for the treatment of different types of tumors (46, 47), including those of skin (33, 40, 48), pancreatic (49), colon (50), lung (51, 52) and breast (53–55). Nevertheless, although these studies have indicated the prevailing character of plasma as a promising tool in tumor therapy, the responsible effectors and the underlying molecular mechanisms remain unclear.

The critical role of ER in breast cancer pathobiology prompted us to design this study with the assumption that ER would provide a differential outcome on breast cancer subtypes

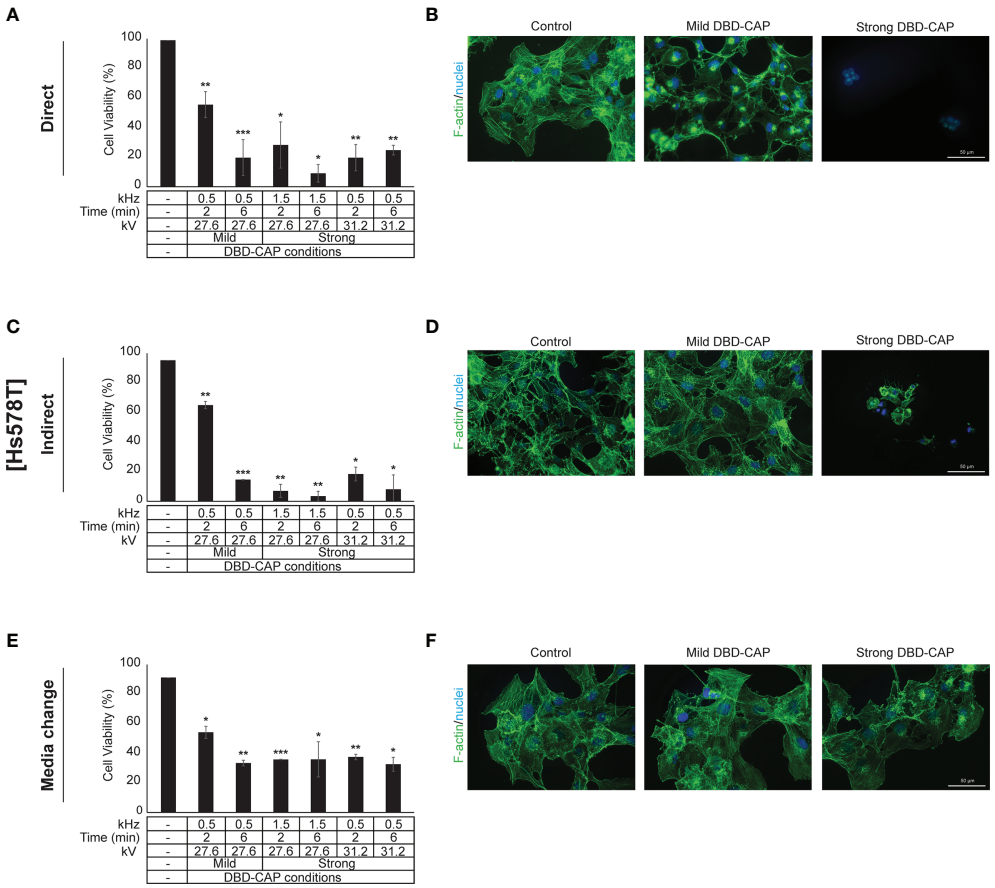

FIGURE 7 | DBD-CAP suppresses Hs578T (ER-, highly metastatic) breast cancer cell growth. **(A**, **C**, **E)** Assessment of % cell survival 24 h after treatment with mild (0.5 kHz/27.6 kV) or strong (1.5 kHz/27.6 kV or 0.5 kHz/31.2 kV) DBD-CAP (direct, indirect, media change) for 2 and 6 min. The values represent the mean ± SD of 3 (at least) independent experiments. Asterisks illustrate significant differences of the different treatment conditions compared to untreated (control) cells (*$p < 0.05$, **$p < 0.01$, ***$p < 0.001$). **(B**, **D**, **F)** Cell morphology after mild (0.5 kHz/27.6 kV) or strong (0.5 kHz/31.2 kV) DBD-CAP treatment for 2 min. Scale bars, 50 μm. Representative immunofluorescence images are shown (*F-actin*, green; *nuclei*, blue/DAPI).

after treatment with plasma. Thus, we investigated the effects of DBD-CAP on three breast cancer cell models of distinct ER status (MCF-7/ER+, MDA-MB-231/ER- and Hs578T/ER-).

The chemical factors in CAP alleged as the critical anti-cancer effectors involve the reactive species generated during plasma process (14, 56). Many studies highlight that the CAP-treated medium, defined as a solution containing most of the long-lived reactive species deriving from CAP, are capable to cause strong and selective anti-cancer effect both *in vitro* and *in vivo* (33, 52, 57–62). Long-lived reactive oxygen and nitrogen species (ROS/RNS), including H_2O_2, NO_2^-/HNO_2 and NO_3^-/HNO_3, and O_3 possessing long-lasting halftimes, are critical for the biochemical stimulation of plasma-activated medium (63). Peroxynitrite/peroxynitrous acid ($ONOO^-/ONOOH$) in CAP-treated medium has been also recognized as a quite effective agent based on chain reactions producing NO which is a beneficial specie for pathogen inactivation/cell apoptosis (Eqs. 1-10).

$$\cdot N + \cdot OH \rightarrow \cdot NO + \cdot H \quad (1)$$

$$\cdot H + NO_2^- \rightarrow \cdot NO + OH^- \quad (2)$$

$$N_2O_3 \leftrightarrow \cdot NO + \cdot NO_2 \quad (3)$$

$$HNO_2 + \cdot H \rightarrow \cdot NO + H_2O \quad (4)$$

$$HNO_2 + H_2O_2 \rightarrow ONOOH \leftrightarrow \cdot NO_2 + \cdot OH \quad (5)$$

$$NO_2^- + H_2O_2 \rightarrow ONOO^- \leftrightarrow \cdot NO + \cdot O_2^- \quad (6)$$

$$\cdot OH + ONOOH \rightarrow \cdot NO + O_2 + H_2O \quad (7)$$

$$\cdot NO_2 + . O \rightarrow \cdot NO + O_2 \quad (8)$$

$$\cdot N O_2 + \cdot N \rightarrow 2 \cdot NO \quad (9)$$

$$\cdot NO_2 + O_3 \rightarrow \cdot NO + O_2 \quad (10)$$

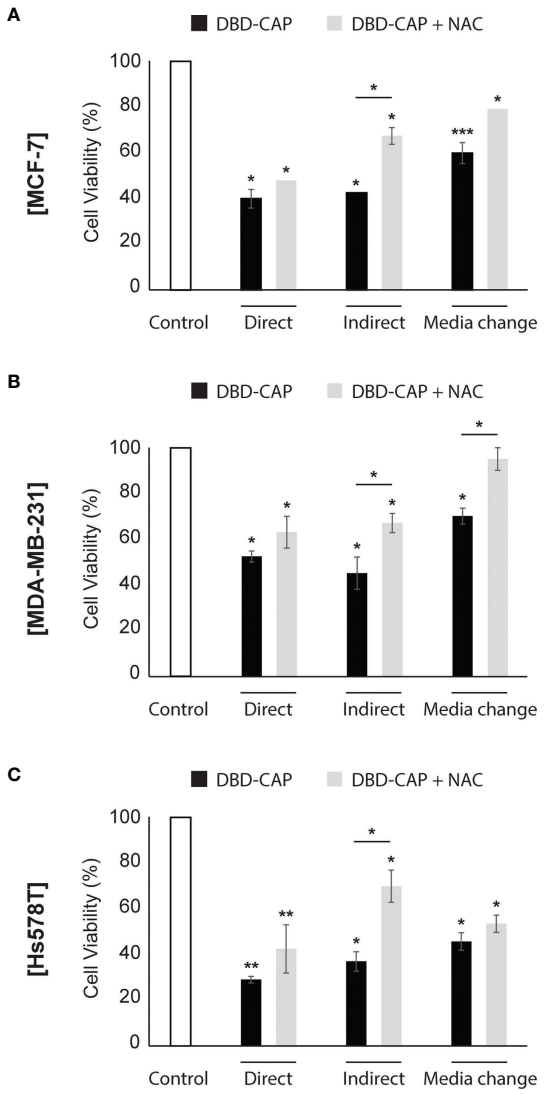

FIGURE 8 | ROS scavenger NAC partly inhibits DBD-CAP-mediated effects on breast cancer cell viability. Assessment of % cell survival 24 h after treatment of **(A)** MCF-7, **(B)** MDA-MB-231, **(C)** Hs578T with mild (0.5 kHz/ 27.6 kV) DBD-CAP (direct, indirect, media change) for 4 min in the absence or presence of NAC (pre-treatment with 5 mM NAC-DMEM for 2 h). The values represent the mean ± SD of 3 (at least) independent experiments. Asterisks illustrate significant differences of the different treatment conditions compared to untreated (control) cells as well as between DBD-CAP and DBD-CAP + NAC (*$p < 0.05$, **$p < 0.01$, ***$p < 0.001$).

The major ROS/RNS species generated in the gaseous plasma phase of our NSP-DBD system identified as N_2(SPS),N_2^+, OH, O, NO_2/NO_x and O_2^+ **(Figure 2C)** resulted in the formation of strong oxidants inside the cell culture media (e.g. H_2O_2, NO_2^- and NO_3^-). These species were found to increase substantially with treatment time, pulse voltage and pulse frequency **(Figure 3)** similarly to gaseous NO_2 concentration **(Table 2)**, which is indicative of the increase of ROS/RNS concentration at higher discharge power (inset of **Figure 2B**).

Transferring plasma inside the body is an important and challenging issue especially for tumors located in deeper areas. The present study deals with this issue by evaluating the effectiveness of three different CAP approaches (direct, indirect and media change) and clearly shows that indirect treatment of the cells (exposure of cells with DBD-CAP-stimulated medium) induced similar or, in some cases, higher cytotoxicity than the direct approach **(Figures 5**, **6**, **7)**. Therefore, the indirect approach could be used to treat deep tumors (including breast cancer) by injecting plasma-activated medium alone or in combination with a conventional therapy highlighting the important perspective to apply this technology in clinical practice in a more simplified way without directly subject the patients to plasma treatment. To further understand in depth the CAP-mediated mechanisms it is also useful to examine the cytotoxic effect of CAP treatment by renewing the medium immediately after CAP treatment. In our study, the observation that the medium change approach caused significant lower cytotoxicity to all breast cancer cell lines further supports the assumption that the cytotoxicity of CAP depends on the CAP-derived ROS/RNS (59).

Over the past decade, the importance of the plasma ROS/RNS in cytotoxicity has been investigated (9, 62, 64, 65). To that end, the most effective way to reveal the significance of the reactive species is by using specific chemical species (known as scavengers) added in the medium which can eliminate the CAP effect. CAP-generated ROS/RNS are trapped by these scavengers showing indirectly their importance in CAP treatment (66). In line with this, in the present study, we demonstrate that DBD-CAP-generated ROS contribute to the observed cytotoxicity since pre-treatment of the tumor cells with the ROS scavenger NAC weakened the toxic effects of the plasma **(Figure 8**, **Supplementary Figure 1)**.

With regard to cell morphology, in agreement with previous studies (67, 68), shortly after the treatment with plasma (direct or indirect) many tumor cells underwent morphological changes that ranged from moderate to strong depending on the cell type and the applied DBD-CAP conditions. Their shapes were changed from spread to contractive accompanied by a disorganized actin cytoskeleton and loss of cell polarization and cytoplasmic protrusions **(Figures 5**, **6**, **7B, D)**. The observed changes were dependent on plasma-derived reactive species since both the immediate change of the DBD-CAP-stimulated medium (medium change approach) **(Figures 5**, **6**, **7F)** and the treatment of tumor cells with the ROS scavenger NAC prior to DBD-CAP treatment **(Supplementary Figure 1)** resulted in minor cell morphological changes. As a consequence, DBD-CAP might affect proteins that are located on tumor cell membranes, including receptors, channels and transporters, thus affecting cell-cell and cell-matrix interactions and related functions. However, this remains to be investigated.

Regarding the physical parameters, the final temperature and pH of the medium covering the tumor cells is determined by its initial temperature or pH, composition, CAP treatment dose and the power of discharge (9, 41). In our experimental set up, temperature changes were not high enough to impose thermal

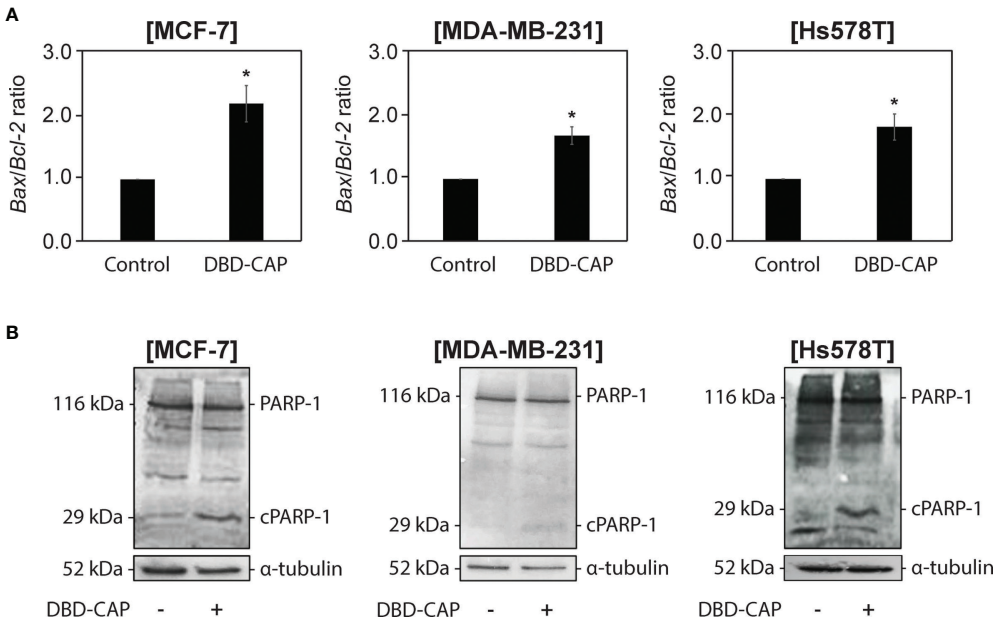

FIGURE 9 | DBD-CAP induces apoptosis in both ER+ and ER- breast cancer cells. **(A)** *Bax/Bcl-2* ratio as estimated from the relative expression of *Bax* and *Bcl-2* to *18S rRNA* (housekeeping gene) mRNA levels by quantitative qPCR analysis in MCF-7/ER+, MDA-MB-231/ER- and Hs578T/ER- cells treated with mild (0.5 kHz/27.6 kV) direct DBD-CAP for 4 min. The values represent the mean ± SD of 3 (at least) independent experiments. Asterisks illustrate significant differences between control (untreated) and DBD-CAP-treated cells (*$p < 0.05$). **(B)** Immunoblot analyses of PARP-1/cPARP-1 and α-tubulin (loading control) in MCF-7/ER+, MDA-MB-231/ER- and Hs578T/ER- untreated (left lane) or treated with mild (0.5 kHz/27.6 kV) direct DBD-CAP for 4 min (right lane). Representative blots are shown.

damages in cells (**Figure 4B**). Since the standard temperature in the incubator is 37°C, the slightly warmed medium after CAP treatment does not affect tumor cell growth and viability. Another important parameter that should be considered in order to understand the chemical essence of DBD-CAP cytotoxicity is pH. A slight acidification was detected especially when cells were subjected to higher pulse frequency (1.5 kHz/27.6 kV) due to the higher RNS (HNO_2/HNO_3/ONOOH) concentration at these conditions (**Figure 4A**). The negligible changes in the pH of the medium could be due to the existence of buffering chemicals in the media and are obviously not harmful for the cells in line with previous studies (9, 41).

CAP induces cancer cell death mainly *via* induction of apoptosis (11, 69). Apoptotic pathways may be extrinsic, which acts on cell surface death receptors, or intrinsic, which acts through mitochondria. The latter pathway is regulated by key apoptosis-related proteins, including cytochrome *c*, Bax and Bcl−2, which subsequently activate caspase−3 and PARP-1 protein (70). Bax translocates to the interior of mitochondria upon apoptosis induction and is important for apoptotic signaling (71). On the other hand, Bcl-2 protein negatively regulates cell apoptosis since it promotes cell survival (72). Notably, the ratio of Bax to Bcl-2 indicates induced or suppressed cell apoptosis rates (73). In this study, DBD-CAP resulted in the increase of the Bax/Bcl-2 ratio in both ER+ and ER- breast cancer cells (**Figure 9A**) suggesting that the observed cell apoptosis is dependent on alterations of these proteins expression and is associated with the mitochondrial apoptotic pathway. This is further supported by the finding that DBD-CAP induced degradation of PARP-1, which is also a marker of cell apoptosis (**Figure 9B**). Therefore, it is likely that upon rise of the Bax/Bcl−2 ratio in the mitochondrial membrane, cytochrome *c* is translocated from the mitochondria to the cytosol, resulting in activation of specific proteases (such as caspase−3) that cleave PARP-1. Interestingly, inhibition of PARP-1 activity compromises base excision repair and promotes synthetic lethality in tumor cells with homologous recombination (HR) defects. However, this is not the case for normal cells since they retain the ability to repair DNA through HR (74). These observations are consistent with the possibility that DBD-CAP selectively ablates tumor cells and indicate the potential of CAP as a promising anti-cancer treatment modality.

The present study suggests that the tumor-suppressive properties of DBD-CAP on mammary carcinoma cells occur, at least in part, due to modulation of the tumor cell microenvironment. Our findings revealed significant changes in the expression of specific extracellular matrix effectors with established roles in tumor growth and metastasis. In particular, DBD-CAP markedly down-regulated CD44, which is the major cellular receptor of the extracellular heteropolysaccharide hyaluronan, in both ER+ and ER- breast cancer cells (**Figure 10A**). Hyaluronan-CD44 interactions have a substantial impact on stemness properties of cancer stem cells and drug resistance through promotion of the epithelial-to-mesenchymal transition program, epigenetic control, oxidative stress resistance, and secretion of exosomes/extracellular vesicles (75). Given that CD44 is a prominent breast cancer stem cell marker (76), our results

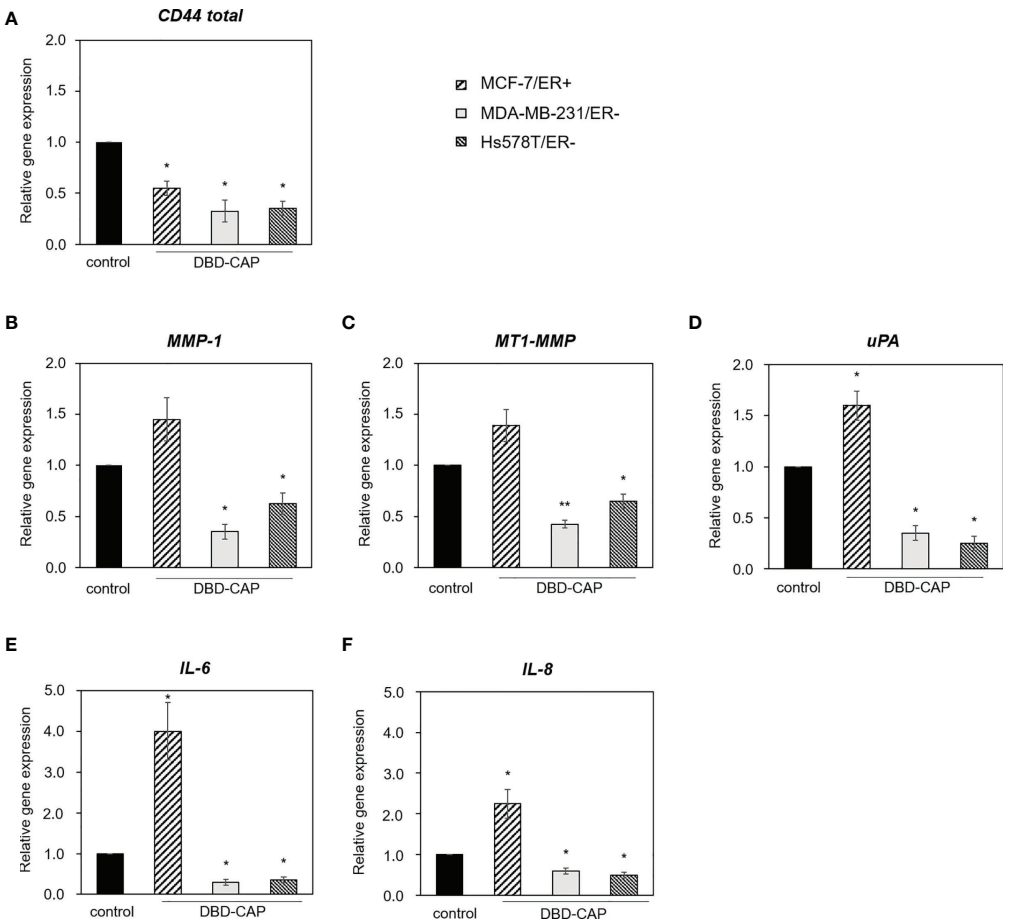

FIGURE 10 | DBD-CAP regulates the expression of matrix effectors in breast cancer cells. Quantitative qPCR analysis of **(A)** *CD44*, **(B)** *MMP-1*, **(C)** *MT1-MMP*, **(D)** *uPA*, **(E)** *IL-6* and **(F)** *IL-8* in MCF-7/ER+, MDA-MB-231/ER- and Hs578T/ER- cells treated with mild (0.5 kHz/27.6 kV) direct DBD-CAP for 4 min. The values represent the mean ± SD of 3 (at least) independent experiments. Asterisks illustrate significant differences between control (untreated) and DBD-CAP-treated cells (*$p < 0.05$, **$p < 0.01$).

suggest that CAP affects stem cell niche and suppresses breast cancer cell stemness. DBD-CAP was shown to affect also the proteolytic potential of tumor cells since it significantly down-regulated the expression of MMP-1, MT1-MMP and uPA in the metastatic ER- breast cancer cells **(Figures 10B–D)**. These proteases have been shown to be involved in cancer dissemination. For example, membrane-associated MT1-MMP, a key effector in invadopodia-dependent ECM degradation, interacts with CD44 in protrusions/invadopodia of ER- cells thus promoting proteolytic activities and tumor cell metastasis (77). Moreover, the inhibitory effect of DBD-CAP on uPA is of high interest since it is an established prognostic indicator in breast cancer and, together with PAI-1, comprise efficient predictors of distant metastases in a subset of early node-negative breast cancer patients (78, 79). However, these proteases were induced in ER+ cells (mainly uPA) **(Figures 10B, C, D),** indicating a differential effect of DBD-CAP on the proteolytic potential of breast cancer cells of different ER status. A similar differential effect was also evident for the inflammatory mediators IL-6 and IL-8, which were suppressed in ER- but induced in ER+ breast cancer cells **(Figures 10E, F)**. Although these findings need further investigation, they clearly demonstrate that CAP has a substantial impact on tumor cell microenvironment, while significant changes in specific matrix effectors seem to occur with regard to the ER expression profile. This seems reasonable given the role of ROS/RNS as major mediators of ECM remodeling during tumor progression (80).

Collectively, our data revealed important DBD-CAP-mediated changes in tumor cell viability and expression of specific matrix effectors not only between breast cancer cells of different ER status (i.e. MCF-7/ER+ *vs* MDA-MB-231/ER- and Hs578T/ER-) but also between cells of the same ER profile (i.e. MDA-MB-231/ER- *vs* Hs578T/ER-), since MDA-MB-231/ER- cells appeared more resistant to the applied DBD-CAP treatments than the Hs578T/ER- cells. This observation implies that different molecular mechanisms and effectors determine tumor cell behavior in the newly-formed plasma-induced microenvironment and this should be considered for the treatment of different breast cancer subtypes. Despite recent

advances in breast cancer classification that have resulted in efficient targeted therapies for a large cohort of patients, evidence support that there is a high heterogeneity among breast cancers even between those belonging to the same subtype (81, 82). This is reflected to the differences observed for the two ER- cell lines used in the present study, which could be explained from their different molecular characteristics and origin. The Hs578T originated from a carcinosarcoma of the breast (83) while MDA-MB-231 originated from invasive ductal carcinoma (84). Therefore, a precise classification and a targeted therapy for each individual tumor would highly benefit breast cancer patients.

In conclusion, the present study provides a new perspective to understand the interactions of CAP with the tumor cells and their surrounding microenvironment. Our data suggest that CAP operating under mild conditions inhibits the growth of metastatic breast cancer cells and, at the same time, it regulates the expression of extracellular matrix effectors with established roles in inflammation and cancer. Although these interactions need further investigation, we suggest that CAP could represent an effective therapeutic mean for the treatment of specific breast cancer subtypes with regard to their ER status.

DATA AVAILABILITY STATEMENT

The original contributions presented in the study are included in the article/**Supplementary Material**, further inquiries can be directed to the corresponding author/s.

AUTHOR CONTRIBUTIONS

SS and CA conceived the experiments. A-MC, MT, SM, M-EC, TK, and AC. conducted the experiments. SS and CA analyzed the results. All authors reviewed the manuscript. All authors contributed to the article and approved the submitted version.

FUNDING

This research was supported by Grant (project code: 80626) from the Research Committee of the University of Patras, Greece, *via* "C. CARATHEODORI" program. The publication of this article has been financed by the Research Committee of the University of Patras.

SUPPLEMENTARY MATERIAL

The Supplementary Material for this article can be found online at: https://www.frontiersin.org/articles/10.3389/fonc.2021.826865/full#supplementary-material

Supplementary Figure 1 | ROS scavenger NAC partly inhibits DBD-CAP-mediated effects on breast cancer cell viability. Morphology of **(A)** MCF-7, **(B)** MDA-MB-231, **(C)** Hs578T breast cancer cells after mild (0.5 kHz/27.6 kV) DBD-CAP (direct, indirect, media change) for 4 min in the absence or presence of NAC (pre-treatment with 5 mM NAC-DMEM for 2 h). Representative phase contrast images captured 24 h after DBD-CAP treatment are shown (magnification, *10X*).

REFERENCES

1. Russnes HG, Lingjaerde OC, Borresen-Dale AL, Caldas C. Breast Cancer Molecular Stratification: From Intrinsic Subtypes to Integrative Clusters. *Am J Pathol* (2017) 187:2152–62. doi: 10.1016/j.ajpath.2017.04.022
2. Prat A, Perou CM. Deconstructing the Molecular Portraits of Breast Cancer. *Mol Oncol* (2011) 5:5–23. doi: 10.1016/j.molonc.2010.11.003
3. Dieci MV, Orvieto E, Dominici M, Conte P, Guarneri V. Rare Breast Cancer Subtypes: Histological, Molecular, and Clinical Peculiarities. *Oncologist* (2014) 19:805–13. doi: 10.1634/theoncologist.2014-0108
4. Rakha EA, Reis-Filho JS, Ellis IO. Basal-Like Breast Cancer: A Critical Review. *J Clin Oncol* (2008) 26:2568–81. doi: 10.1200/JCO.2007.13.1748
5. Bergamaschi A, Tagliabue E, Sorlie T, Naume B, Triulzi T, Orlandi R, et al. Extracellular Matrix Signature Identifies Breast Cancer Subgroups With Different Clinical Outcome. *J Pathol* (2008) 214:357–67. doi: 10.1002/path.2278
6. Brany D, Dvorska D, Halasova E, Skovierova H. Cold Atmospheric Plasma: A Powerful Tool for Modern Medicine. *Int J Mol Sci* (2020) 21. doi: 10.3390/ijms21082932
7. Aggelopoulos CA. Recent Advances of Cold Plasma Technology for Water and Soil Remediation: A Critical Review. *Chem Eng J* (2022) 428:131657. doi: 10.1016/j.cej.2021.131657
8. Fridman G, Friedman G, Gutsol A, Shekhter AB, Vasilets VN, Fridman A. Applied Plasma Medicine. *Plasma Processes Polymers* (2008) 5:503–33. doi: 10.1002/ppap.200700154
9. Yan D, Sherman JH, Keidar M. Cold Atmospheric Plasma, a Novel Promising Anti-Cancer Treatment Modality. *Oncotarget* (2017) 8:15977–95. doi: 10.18632/oncotarget.13304
10. Keidar M, Walk R, Shashurin A, Srinivasan P, Sandler A, Dasgupta S, et al. Cold Plasma Selectivity and the Possibility of a Paradigm Shift in Cancer Therapy. *Br J Cancer* (2011) 105:1295–301. doi: 10.1038/bjc.2011.386
11. Ratovitski EA, Cheng X, Yan D, Sherman JH, Canady J, Trink B, et al. Anti-Cancer Therapies of 21st Century: Novel Approach to Treat Human Cancers Using Cold Atmospheric Plasma. *Plasma Processes Polymers* (2014) 11:1128–37. doi: 10.1002/ppap.201400071
12. Yajima I, Iida M, Kumasaka MY, Omata Y, Ohgami N, Chang J, et al. Non-Equilibrium Atmospheric Pressure Plasmas Modulate Cell Cycle-Related Gene Expressions in Melanocytic Tumors of RET-Transgenic Mice. *Exp Dermatol* (2014) 23:424–5. doi: 10.1111/exd.12415
13. Chernets N, Kurpad DS, Alexeev V, Rodrigues DB, Freeman TA. Reaction Chemistry Generated by Nanosecond Pulsed Dielectric Barrier Discharge Treatment Is Responsible for the Tumor Eradication in the B16 Melanoma Mouse Model. *Plasma Process Polym* (2015) 12:1400–9. doi: 10.1002/ppap.201500140
14. Graves DB. The Emerging Role of Reactive Oxygen and Nitrogen Species in Redox Biology and Some Implications for Plasma Applications to Medicine and Biology. *J Phys D: Appl Phys* (2012) 45:263001. doi: 10.1088/0022-3727/45/26/263001
15. Yan D, Cui H, Zhu W, Talbot A, Zhang LG, Sherman JH, et al. The Strong Cell-Based Hydrogen Peroxide Generation Triggered by Cold Atmospheric Plasma. *Sci Rep* (2017) 7:10831. doi: 10.1038/s41598-017-11480-x
16. Finkel T. Signal Transduction by Reactive Oxygen Species. *J Cell Biol* (2011) 194:7–15. doi: 10.1083/jcb.201102095
17. Szatrowski TP, Nathan CF. Production of Large Amounts of Hydrogen Peroxide by Human Tumor Cells. *Cancer Res* (1991) 51:794–8.
18. Barrera G. Oxidative Stress and Lipid Peroxidation Products in Cancer Progression and Therapy. *ISRN Oncol* (2012) 2012:137289. doi: 10.5402/2012/137289
19. Huang Q, Zhan L, Cao H, Li J, Lyu Y, Guo X, et al. Increased Mitochondrial Fission Promotes Autophagy and Hepatocellular Carcinoma Cell Survival Through the ROS-Modulated Coordinated Regulation of the NFKB and TP53 Pathways. *Autophagy* (2016) 12:999–1014. doi: 10.1080/15548627.2016.1166318

20. Chio IIC, Tuveson DA. ROS in Cancer: The Burning Question. *Trends Mol Med* (2017) 23:411–29. doi: 10.1016/j.molmed.2017.03.004
21. Tanaka H, Mizuno M, Ishikawa K, Toyokuni S, Kajiyama H, Kikkawa F, et al. Molecular Mechanisms of Non-Thermal Plasma-Induced Effects in Cancer Cells. *Biol Chem* (2019) 400:87–91. doi: 10.1515/hsz-2018-0199
22. Fridman G, Shereshevsky A, Jost MM, Brooks AD, Fridman A, Gutsol A, et al. Floating Electrode Dielectric Barrier Discharge Plasma in Air Promoting Apoptotic Behavior in Melanoma Skin Cancer Cell Lines. *Plasma Chem Plasma Process* (2007) 27:163–76. doi: 10.1007/s11090-007-9048-4
23. Weltmann KD, Kindel E, von Woedtke T, Hähnel M, Stieber M, Brandenburg R. Atmospheric-Pressure Plasma Sources: Prospective Tools for Plasma Medicine. *Pure Appl Chem* (2010) 82:1223–37. doi: 10.1351/PAC-CON-09-10-35
24. Kim JY, Kim S-O, Wei Y, Li J. A Flexible Cold Microplasma Jet Using Biocompatible Dielectric Tubes for Cancer Therapy. *Appl Phys Lett* (2010) 96:203701. doi: 10.1063/1.3431392
25. Kim SJ, Joh HM, Chung TH. Production of Intracellular Reactive Oxygen Species and Change of Cell Viability Induced by Atmospheric Pressure Plasma in Normal and Cancer Cells. *Appl Phys Lett* (2013) 103:153705. doi: 10.1063/1.4824986
26. Kaushik NK, Uhm H, Choi EH. Micronucleus Formation Induced by Dielectric Barrier Discharge Plasma Exposure in Brain Cancer Cells. *Appl Phys Lett* (2012) 100:084102. doi: 10.1063/1.3687172
27. Aggelopoulos CA, Meropoulis S, Hatzisymeon M, Lada ZG, Rassias G. Degradation of Antibiotic Enrofloxacin in Water by Gas-Liquid Nsp-DBD Plasma: Parametric Analysis, Effect of H2O2 and CaO2 Additives and Exploration of Degradation Mechanisms. *Chem Eng J* (2020) 398:125622. doi: 10.1016/j.cej.2020.125622
28. Aggelopoulos CA, Hatzisymeon M, Tataraki D, Rassias G. Remediation of Ciprofloxacin-Contaminated Soil by Nanosecond Pulsed Dielectric Barrier Discharge Plasma: Influencing Factors and Degradation Mechanisms. *Chem Eng J* (2020) 393:124768. doi: 10.1016/j.cej.2020.124768
29. Karalis TT, Chatzopoulos A, Kondyli A, Aletras AJ, Karamanos NK, Heldin P, et al. Salicylate Suppresses the Oncogenic Hyaluronan Network in Metastatic Breast Cancer Cells. *Matrix Biol Plus* (2020) 6-7:100031. doi: 10.1016/j.mbplus.2020.100031
30. Karalis TT, Heldin P, Vynios DH, Neill T, Buraschi S, Iozzo RV, et al. Tumor-Suppressive Functions of 4-MU on Breast Cancer Cells of Different ER Status: Regulation of Hyaluronan/HAS2/CD44 and Specific Matrix Effectors. *Matrix Biol* (2019) 78-79:118–38. doi: 10.1016/j.matbio.2018.04.007
31. Moss MS, Yanallah K, Allen RWK, Pontiga F. An Investigation of CO2 splitting Using Nanosecond Pulsed Corona Discharge: Effect of Argon Addition on CO2conversion and Energy Efficiency. *Plasma Sources Sci Technol* (2017) 26:035009. doi: 10.1088/1361-6595/aa5b1d
32. Jamróz P, Pohl P, Żyrnicki W. Spectroscopic Evaluation of a Low Power Atmospheric Pressure Mixed Argon–Helium Microwave Induced Plasma Combined With the Chemical Generation of Volatile Species for the Optical Emission Spectrometric Determination of Arsenic, Antimony and Mercury. *J Anal Atomic Spectrometry* (2012) 27:1772–9. doi: 10.1039/c2ja30063j
33. Yadav DK, Adhikari M, Kumar S, Ghimire B, Han I, Kim M-H, et al. Cold Atmospheric Plasma Generated Reactive Species Aided Inhibitory Effects on Human Melanoma Cells: An *In Vitro* and *In Silico* Study. *Sci Rep* (2020) 10:3396. doi: 10.1038/s41598-020-60356-0
34. Rezaei F, Abbasi-Firouzjah M, Shokri B. Investigation of Antibacterial and Wettability Behaviours of Plasma-Modified PMMA Films for Application in Ophthalmology. *J Phys D: Appl Phys* (2014) 47:085401. doi: 10.1088/0022-3727/47/8/085401
35. Chauvin J, Judée F, Yousfi M, Vicendo P, Merbahi N. Analysis of Reactive Oxygen and Nitrogen Species Generated in Three Liquid Media by Low Temperature Helium Plasma Jet. *Sci Rep* (2017) 7:4562. doi: 10.1038/s41598-017-04650-4
36. Mohades S, Laroussi M, Sears J, Barekzi N, Razavi H. Evaluation of the Effects of a Plasma Activated Medium on Cancer Cells. *Phys Plasmas* (2015) 22:122001. doi: 10.1063/1.4933367
37. Judée F, Simon S, Bailly C, Dufour T. Plasma-Activation of Tap Water Using DBD for Agronomy Applications: Identification and Quantification of Long Lifetime Chemical Species and Production/Consumption Mechanisms. *Water Res* (2018) 133:47–59. doi: 10.1016/j.watres.2017.12.035
38. Judée F, Fongia C, Ducommun B, Yousfi M, Lobjois V, Merbahi N. Short and Long Time Effects of Low Temperature Plasma Activated Media on 3D Multicellular Tumor Spheroids. *Sci Rep* (2016) 6:21421. doi: 10.1038/srep21421
39. Liu DX, Liu ZC, Chen C, Yang AJ, Li D, Rong MZ, et al. Aqueous Reactive Species Induced by a Surface Air Discharge: Heterogeneous Mass Transfer and Liquid Chemistry Pathways. *Sci Rep* (2016) 6:23737. doi: 10.1038/srep23737
40. Saadati F, Mahdikia H, Abbaszadeh H-A, Abdollahifar M-A, Khoramgah MS, Shokri B. Comparison of Direct and Indirect Cold Atmospheric-Pressure Plasma Methods in the B16F10 Melanoma Cancer Cells Treatment. *Sci Rep* (2018) 8:7689. doi: 10.1038/s41598-018-25990-9
41. Panngom K, Baik KY, Nam MK, Han JH, Rhim H, Choi EH. Preferential Killing of Human Lung Cancer Cell Lines With Mitochondrial Dysfunction by Nonthermal Dielectric Barrier Discharge Plasma. *Cell Death Dis* (2013) 4:e642–2. doi: 10.1038/cddis.2013.168
42. Cory S, Adams JM. The Bcl2 Family: Regulators of the Cellular Life-or-Death Switch. *Nat Rev Cancer* (2002) 2:647–56. doi: 10.1038/nrc883
43. Gupte R, Liu Z, Kraus WL. PARPs and ADP-Ribosylation: Recent Advances Linking Molecular Functions to Biological Outcomes. *Genes Dev* (2017) 31:101–26. doi: 10.1101/gad.291518.116
44. Makki J. Diversity of Breast Carcinoma: Histological Subtypes and Clinical Relevance. *Clin Med Insights Pathol* (2015) 8:23–31. doi: 10.4137/CPath.S31563
45. Polyak K. Breast Cancer: Origins and Evolution. *J Clin Invest* (2007) 117:3155–63. doi: 10.1172/JCI33295
46. Weltmann KD, von Woedtke T. Plasma Medicine—Current State of Research and Medical Application. *Plasma Phys Controlled Fusion* (2016) 59:014031. doi: 10.1088/0741-3335/59/1/014031
47. Mohammadi A, Mahsa S, Otaghsara T, Khadem M, Karimi M, Adel F, et al. A Review of New Method of Cold Plasma in Cancer Treatment. *Scholars Acad J Biosci (SAJB)* (2015) 3:222–30.
48. Gay-Mimbrera J, García MC, Isla-Tejera B, Rodero-Serrano A, García-Nieto AV, Ruano J. Clinical and Biological Principles of Cold Atmospheric Plasma Application in Skin Cancer. *Adv Ther* (2016) 33:894–909. doi: 10.1007/s12325-016-0338-1
49. Partecke LI, Evert K, Haugk J, Doering F, Normann L, Diedrich S, et al. Tissue Tolerable Plasma (TTP) Induces Apoptosis in Pancreatic Cancer Cells *In Vitro* and *In Vivo*. *BMC Cancer* (2012) 12:473. doi: 10.1186/1471-2407-12-473
50. Ruwan Kumara MHS, Piao MJ, Kang KA, Ryu YS, Park JE, Shilnikova K, et al. Non-Thermal Gas Plasma-Induced Endoplasmic Reticulum Stress Mediates Apoptosis in Human Colon Cancer Cells. *Oncol Rep* (2016) 36:2268–74. doi: 10.3892/or.2016.5038
51. Hou J, Ma J, Yu KN, Li W, Cheng C, Bao L, et al. Non-Thermal Plasma Treatment Altered Gene Expression Profiling in Non-Small-Cell Lung Cancer A549 Cells. *BMC Genomics* (2015) 16:435. doi: 10.1186/s12864-015-1644-8
52. Lin A, Truong B, Patel S, Kaushik N, Choi EH, Fridman G, et al. Nanosecond-Pulsed DBD Plasma-Generated Reactive Oxygen Species Trigger Immunogenic Cell Death in A549 Lung Carcinoma Cells Through Intracellular Oxidative Stress. *Int J Mol Sci* (2017) 18:966. doi: 10.3390/ijms18050966
53. Wang M, Holmes B, Cheng X, Zhu W, Keidar M, Zhang LG. Cold Atmospheric Plasma for Selectively Ablating Metastatic Breast Cancer Cells. *PloS One* (2013) 8:e73741. doi: 10.1371/journal.pone.0073741
54. Lee S, Lee H, Bae H, Choi EH, Kim SJ. Epigenetic Silencing of miR-19a-3p by Cold Atmospheric Plasma Contributes to Proliferation Inhibition of the MCF-7 Breast Cancer Cell. *Sci Rep* (2016) 6:30005–5. doi: 10.1038/srep30005
55. Lee S, Lee H, Jeong D, Ham J, Park S, Choi EH, et al. Cold Atmospheric Plasma Restores Tamoxifen Sensitivity in Resistant MCF-7 Breast Cancer Cell. *Free Radical Biol Med* (2017) 110:280–90. doi: 10.1016/j.freeradbiomed.2017.06.017
56. Keidar M, Yan D, Beilis II, Trink B, Sherman JH. Plasmas for Treating Cancer: Opportunities for Adaptive and Self-Adaptive Approaches. *Trends Biotechnol* (2018) 36:586–93. doi: 10.1016/j.tibtech.2017.06.013
57. Yan D, Talbot A, Nourmohammadi N, Cheng X, Canady J, Sherman J, et al. Principles of Using Cold Atmospheric Plasma Stimulated Media for Cancer Treatment. *Sci Rep* (2015) 5:18339. doi: 10.1038/srep18339
58. Yan D, Xu W, Yao X, Lin L, Sherman JH, Keidar M. The Cell Activation Phenomena in the Cold Atmospheric Plasma Cancer Treatment. *Sci Rep* (2018) 8:15418. doi: 10.1038/s41598-018-33914-w

59. Bauer G, Sersenová D, Graves DB, Machala Z. Cold Atmospheric Plasma and Plasma-Activated Medium Trigger RONS-Based Tumor Cell Apoptosis. *Sci Rep* (2019) 9:14210. doi: 10.1038/s41598-019-50291-0
60. Yan D, Sherman JH, Cheng X, Ratovitski E, Canady J, Keidar M. Controlling Plasma Stimulated Media in Cancer Treatment Application. *Appl Phys Lett* (2014) 105:224101. doi: 10.1063/1.4902875
61. Chauvin J, Gibot L, Griseti E, Golzio M, Rols M-P, Merbahi N, et al. Elucidation of *In Vitro* Cellular Steps Induced by Antitumor Treatment With Plasma-Activated Medium. *Sci Rep* (2019) 9:4866. doi: 10.1038/s41598-019-41408-6
62. Tanaka H, Mizuno M, Ishikawa K, Nakamura K, Kajiyama H, Kano H, et al. Plasma-Activated Medium Selectively Kills Glioblastoma Brain Tumor Cells by Down-Regulating a Survival Signaling Molecule, AKT Kinase. (2011) 1:265–77. doi: 10.1615/PlasmaMed.2012006275
63. Zhou R, Zhou R, Wang P, Luan B, Zhang X, Fang Z, et al. Microplasma Bubbles: Reactive Vehicles for Biofilm Dispersal. *ACS Appl Mater Interfaces* (2019) 11:20660–9. doi: 10.1021/acsami.9b03961
64. Ji W-O, Lee M-H, Kim G-H, Kim E-H. Quantitation of the ROS Production in Plasma and Radiation Treatments of Biotargets. *Sci Rep* (2019) 9:19837. doi: 10.1038/s41598-019-56160-0
65. Laroussi M, Lu X, Keidar M. Perspective: The Physics, Diagnostics, and Applications of Atmospheric Pressure Low Temperature Plasma Sources Used in Plasma Medicine. *J Appl Phys* (2017) 122:020901. doi: 10.1063/1.4993710
66. Vandamme M, Robert E, Lerondel S, Sarron V, Ries D, Dozias S, et al. ROS Implication in a New Antitumor Strategy Based on Non-Thermal Plasma. *Int J Cancer* (2012) 130:2185–94. doi: 10.1002/ijc.26252
67. Lee HJ, Shon CH, Kim YS, Kim S, Kim GC, Kong MG. Degradation of Adhesion Molecules of G361 Melanoma Cells by a Non-Thermal Atmospheric Pressure Microplasma. *New J Phys* (2009) 11:115026. doi: 10.1088/1367-2630/11/11/115026
68. Kim GJ, Kim W, Kim KT, Lee JK. DNA Damage and Mitochondria Dysfunction in Cell Apoptosis Induced by Nonthermal Air Plasma. *Appl Phys Lett* (2010) 96:021502. doi: 10.1063/1.3292206
69. Yan D, Talbot A, Nourmohammadi N, Sherman JH, Cheng X, Keidar M. Toward Understanding the Selective Anticancer Capacity of Cold Atmospheric Plasma—A Model Based on Aquaporins (Review). *Biointerphases* (2015) 10:040801. doi: 10.1116/1.4938020
70. Kroemer G, Reed JC. Mitochondrial Control of Cell Death. *Nat Med* (2000) 6:513–9. doi: 10.1038/74994
71. Narita M, Shimizu S, Ito T, Chittenden T, Lutz RJ, Matsuda H, et al. Bax Interacts With the Permeability Transition Pore to Induce Permeability Transition and Cytochrome C Release in Isolated Mitochondria. *Proc Natl Acad Sci USA* (1998) 95:14681–6. doi: 10.1073/pnas.95.25.14681
72. Ola MS, Nawaz M, Ahsan H. Role of Bcl-2 Family Proteins and Caspases in the Regulation of Apoptosis. *Mol Cell Biochem* (2011) 351:41–58. doi: 10.1007/s11010-010-0709-x
73. Chresta CM, Masters JR, Hickman JA. Hypersensitivity of Human Testicular Tumors to Etoposide-Induced Apoptosis Is Associated With Functional P53 and a High Bax:Bcl-2 Ratio. *Cancer Res* (1996) 56:1834–41.
74. Iglehart JD, Silver DP. Synthetic Lethality–A New Direction in Cancer-Drug Development. *N Engl J Med* (2009) 361:189–91. doi: 10.1056/NEJMe0903044
75. Skandalis SS, Karalis TT, Chatzopoulos A, Karamanos NK. Hyaluronan-CD44 Axis Orchestrates Cancer Stem Cell Functions. *Cell Signal* (2019) 63:109377. doi: 10.1016/j.cellsig.2019.109377
76. Ricardo S, Vieira AF, Gerhard R, Leitao D, Pinto R, Cameselle-Teijeiro JF, et al. Breast Cancer Stem Cell Markers CD44, CD24 and ALDH1: Expression Distribution Within Intrinsic Molecular Subtype. *J Clin Pathol* (2011) 64:937–46. doi: 10.1136/jcp.2011.090456
77. Zhao P, Xu Y, Wei Y, Qiu Q, Chew TL, Kang Y, et al. The CD44s Splice Isoform Is a Central Mediator for Invadopodia Activity. *J Cell Sci* (2016) 129:1355–65. doi: 10.1242/jcs.171959
78. Foekens JA, Peters HA, Look MP, Portengen H, Schmitt M, Kramer MD, et al. The Urokinase System of Plasminogen Activation and Prognosis in 2780 Breast Cancer Patients. *Cancer Res* (2000) 60:636–43.
79. De Cremoux P, Grandin L, Dieras V, Savignoni A, Degeorges A, Salmon R, et al. Urokinase-Type Plasminogen Activator and Plasminogen-Activator-Inhibitor Type 1 Predict Metastases in Good Prognosis Breast Cancer Patients. *Anticancer Res* (2009) 29:1475–82.
80. Nikitovic D, Corsini E, Kouretas D, Tsatsakis A, Tzanakakis G. ROS-Major Mediators of Extracellular Matrix Remodeling During Tumor Progression. *Food Chem Toxicol* (2013) 61:178–86. doi: 10.1016/j.fct.2013.06.013
81. Howlader N, Cronin KA, Kurian AW, Andridge R. Differences in Breast Cancer Survival by Molecular Subtypes in the United States. *Cancer Epidemiol Biomarkers Prev* (2018) 27:619–26. doi: 10.1158/1055-9965.EPI-17-0627
82. Sarmiento-Salinas FL, Delgado-Magallon A, Montes-Alvarado JB, Ramirez-Ramirez D, Flores-Alonso JC, Cortes-Hernandez P, et al. Breast Cancer Subtypes Present a Differential Production of Reactive Oxygen Species (ROS) and Susceptibility to Antioxidant Treatment. *Front Oncol* (2019) 9:480. doi: 10.3389/fonc.2019.00480
83. Hackett AJ, Smith HS, Springer EL, Owens RB, Nelson-Rees WA, Riggs JL, et al. Two Syngeneic Cell Lines From Human Breast Tissue: The Aneuploid Mammary Epithelial (Hs578T) and the Diploid Myoepithelial (Hs578Bst) Cell Lines. *J Natl Cancer Inst* (1977) 58:1795–806. doi: 10.1093/jnci/58.6.1795
84. Cailleau R, Young R, Olive M, Reeves WJJr. Breast Tumor Cell Lines From Pleural Effusions. *J Natl Cancer Inst* (1974) 53:661–74. doi: 10.1093/jnci/53.3.661

Conflict of Interest: The authors declare that the research was conducted in the absence of any commercial or financial relationships that could be construed as a potential conflict of interest.

Publisher's Note: All claims expressed in this article are solely those of the authors and do not necessarily represent those of their affiliated organizations, or those of the publisher, the editors and the reviewers. Any product that may be evaluated in this article, or claim that may be made by its manufacturer, is not guaranteed or endorsed by the publisher.

Copyright © 2022 Aggelopoulos, Christodoulou, Tachliabouri, Meropoulis, Christopoulou, Karalis, Chatzopoulos and Skandalis. This is an open-access article distributed under the terms of the Creative Commons Attribution License (CC BY). The use, distribution or reproduction in other forums is permitted, provided the original author(s) and the copyright owner(s) are credited and that the original publication in this journal is cited, in accordance with accepted academic practice. No use, distribution or reproduction is permitted which does not comply with these terms.

frontiers in Oncology

REVIEW
published: 21 January 2022
doi: 10.3389/fonc.2021.811434

The Impact of Hyaluronan on Tumor Progression in Cutaneous Melanoma

Piia Takabe[1], *Hanna Siiskonen*[2], *Aino Rönkä*[3], *Kirsi Kainulainen*[1] *and Sanna Pasonen-Seppänen*[1]*

[1] Institute of Biomedicine, University of Eastern Finland, Kuopio, Finland, [2] Department of Clinical Pathology, Kuopio University Hospital, Kuopio, Finland, [3] Department of Oncology, Kuopio University Hospital, Kuopio, Finland

The incidence of cutaneous melanoma is rapidly increasing worldwide. Cutaneous melanoma is an aggressive type of skin cancer, which originates from malignant transformation of pigment producing melanocytes. The main risk factor for melanoma is ultraviolet (UV) radiation, and thus it often arises from highly sun-exposed skin areas and is characterized by a high mutational burden. In addition to melanoma-associated mutations such as BRAF, NRAS, PTEN and cell cycle regulators, the expansion of melanoma is affected by the extracellular matrix surrounding the tumor together with immune cells. In the early phases of the disease, hyaluronan is the major matrix component in cutaneous melanoma microenvironment. It is a high-molecular weight polysaccharide involved in several physiological and pathological processes. Hyaluronan is involved in the inflammatory reactions associated with UV radiation but its role in melanomagenesis is still unclear. Although abundant hyaluronan surrounds epidermal and dermal cells in normal skin and benign nevi, its content is further elevated in dysplastic lesions and local tumors. At this stage hyaluronan matrix may act as a protective barrier against melanoma progression, or alternatively against immune cell attack. While in advanced melanoma, the content of hyaluronan decreases due to altered synthesis and degradation, and this correlates with poor prognosis. This review focuses on hyaluronan matrix in cutaneous melanoma and how the changes in hyaluronan metabolism affect the progression of melanoma.

Keywords: melanoma, hyaluronan, skin, UV radiation, tumor microenvironment

OPEN ACCESS

Edited by:
Nikos Karamanos, University of Patras, Greece

Reviewed by:
Linli Zhou, University of Cincinnati, United States
Davide Vigetti, University of Insubria, Italy

***Correspondence:**
Sanna Pasonen-Seppänen
sanna.pasonen@uef.fi

Specialty section:
This article was submitted to Molecular and Cellular Oncology, a section of the journal Frontiers in Oncology

Received: *08 November 2021*
Accepted: *31 December 2021*
Published: *21 January 2022*

Citation:
Takabe P, Siiskonen H, Rönkä A, Kainulainen K and Pasonen-Seppänen S (2022) The Impact of Hyaluronan on Tumor Progression in Cutaneous Melanoma. Front. Oncol. 11:811434. doi: 10.3389/fonc.2021.811434

INTRODUCTION

Cutaneous melanoma is a skin cancer that develops from melanocytes. Melanocytes reside in the basal layer of epidermis and synthesize melanin pigment that is transferred in melanosomes to the surrounding keratinocytes to form a protective shield against the harmful effects of UV. Family history, genetic factors, number of nevi and actinic damage have been identified as risk factors for melanoma (1). Solarium is one source for recreational UV exposure, but the impact of moderate solarium use on melanoma risk is still controversial (2). However, The World Health Organization has listed solar radiance as a carcinogen already in 2009 (3).

The American Cancer Society estimates that over 106 000 new melanomas will be diagnosed and over 7000 melanoma-related deaths will occur during this year (2021) (4). In other countries, also in

northern countries such as Finland, almost 2000 new melanomas and over 200 melanoma-related deaths occur annually, causing the incidence of 32.74/100 000 persons (5). Melanoma affects mostly people with a light skin type (Caucasians) and the incidence is 27.5/100,000 people compared to the incidence of 1.1/100,000 among people with a dark skin type (6). UV radiation is the most critical risk factor for melanoma development due to its high mutagenic properties. The rate of basal mutations in melanoma (100 mutations/Mb of entire exome) is higher in comparison to other cancers (7).

Hyaluronan is a glycosaminoglycan found in the extracellular space of most tissues, but it also forms a pericellular coat surrounding individual cells. Hyaluronan is involved in many biological and pathophysiological processes such as tissue homeostasis and integrity, fertilization, wound healing, inflammation, angiogenesis, and cancer. Hyaluronan is mainly produced as a high molecular weight (HMW) chain by hyaluronan synthases (HAS) and degraded to lower molecular weight (LMW) fragments or oligosaccharides by hyaluronidases (HYAL) or environmental factors such as reactive oxygen species (ROS) or UV radiation. The effects of hyaluronan on immune, non-malignant and malignant cells are size dependent. HMW hyaluronan has been shown to be relatively inert, and is more physiological, while its degradation products are more abundant during inflammation and angiogenesis, as reviewed in (8–11), and have been speculated to be biologically active and to modulate the tumor microenvironment (TME) (12).

The role of hyaluronan in cancers has been studied broadly. In cancers originating from simple epithelium such as breast and prostate cancer, the increase of hyaluronan in the tumor and the stroma indicates aggressive type of cancer and poor prognosis (13–17). In melanoma and cancers originating from stratified epithelium, however, poor prognosis is associated with the reduced amount of hyaluronan. Benign nevi and melanoma *in situ* contain abundant amounts of hyaluronan whereas in deep and metastatic melanomas the hyaluronan content is scarce. This is due to the reduced expression of HAS1 and 2 and the increased expression of HYAL2 in melanoma cells (18). The loss of HAS2 has shown to be associated with the poor prognosis and recurrence of melanoma (19). The role of hyaluronan in melanoma development and its progression is the focus of this review.

CUTANEOUS MELANOMA

The Structure of Skin and Melanocytes

Skin covers the human body and comprises over 20% of the body weight. In addition to providing a physical external barrier and insulation, it is also involved in the process of thermoregulation, pain sensation and chemical messaging (20). Keratinocytes are the main cell type in the avascular epidermis. Epidermis also contains pigment-producing melanocytes, which locate in the basal cell layer, Merkel cells, which are mechanoreceptors and Langerhans cells, which are antigen-presenting dendritic cells (21). The dermal compartment is separated from the epidermis by the basement membrane, and it contains blood and lymphatic vessels, nerve endings for mechanoreception, adnexal structures, and an abundant extracellular matrix (ECM). The ECM is composed of collagen, elastin, glycoproteins like fibronectin, proteoglycans like versican and glycosaminoglycans like hyaluronan, which all are mainly produced by fibroblasts. The subcutis or hypodermis resides deep in the dermis attaching the skin to the underlying skeletal muscles. Due to the structure and organization of the dermis it provides strength and support to the entire skin (20, 22).

In addition to skin, the neural crest-derived melanocytes can be found in hair follicles and in the uvea of the eye (23). Melanocytes produce mainly two types of melanin pigment, eumelanin and pheomelanin. Eumelanin (brown-black pigment) is produced during UV exposure to protect the skin from oxidative (UVA) and direct (UVB) DNA damage. Pheomelanin (yellow-red) is enriched among individuals with red hair and pale skin tone, who lack eumelanin synthesis and are more prone to develop melanoma due to spontaneous reactive oxygen species (ROS) production (24). The dendritic nature of melanocytes with their long axial protrusions and large surface area helps them to transfer melanin granules to adjacent keratinocytes for photoprotection. Melanocytes also have immunomodulatory properties in skin (25).

UV exposure causes the activation of two pathways in melanocytes, namely the immediate tanning pathway by UVA and the delayed tanning pathway by UVB (**Figure 1**). The immediate tanning pathway is non-photoprotective and leads to immediate and persistent pigment darkening whereas the delayed tanning pathway is photoprotective *via* increasing melanogenesis. In keratinocytes, UVB increases p53-mediated transcription of POMC (pro-opiomelanocortin) which is post-translationally processed leading to α-MSH (α-melanocyte stimulating hormone), ACTH (adrenal corticotropin hormone) and opioid peptide β-endorphin production. α-MCH is secreted from keratinocytes to the adjacent melanocytes and, then by activation of MC1R (melanocortin 1 receptor), it induces MITF-M (microphtalmia-associated transcription factor isoform M) transcription and melanosome production. After the maturation of melanosomes, they are transported into basal cell layer keratinocytes to form a protective perinuclear cap against harmful effects of UVR (26). Other mechanisms activated in melanocytes in response to UV-related damage are unfolded protein response (UPR) and integrated stress response (ISR). These mechanisms foster the renewal of homeostasis by activating factors with antioxidant activity, such as NRF2 (nuclear factor erythroid 2-related factor 2) that tackles the damaging effects of ROS. Failure in these repair mechanisms leads to the survival of damaged cells, their adaptation to the environment and promotion of carcinogenesis (27, 28).

The Classification of Melanoma

Cutaneous melanoma was earlier classified to four major clinical subtypes: superficially spreading melanoma (SSM), nodular melanoma (NM), acral lentiginous melanoma (ALM) and lentigo maligna melanoma (LMM) (29). Interestingly, the World Health Organization recently published a new classification based on the evolutionary pathways of each subtype. The new classification divides melanomas with relation to sun exposure (30). Melanoma

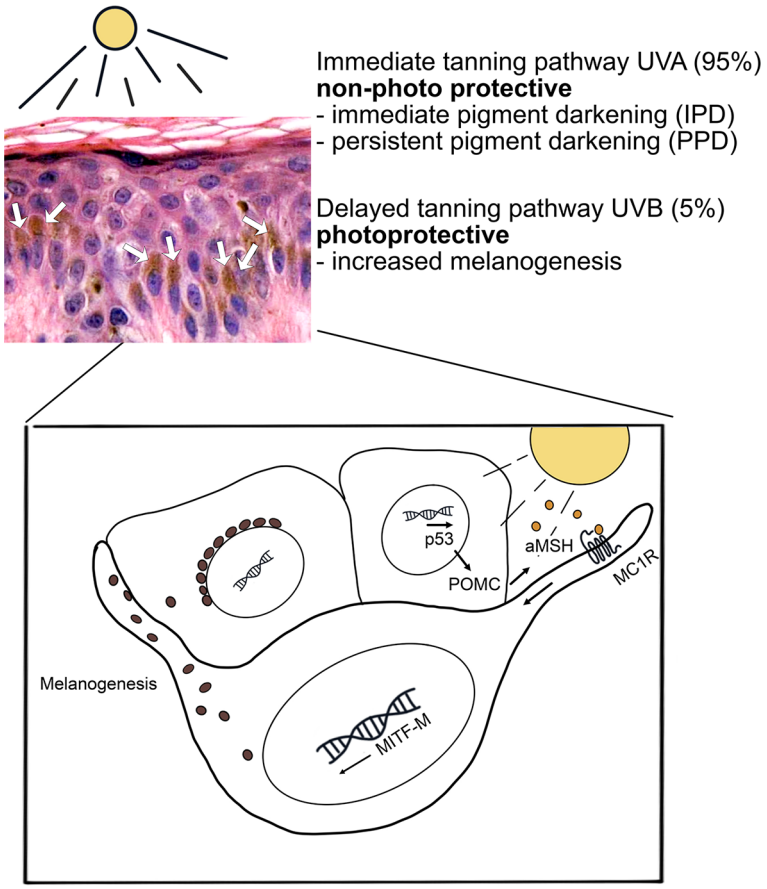

FIGURE 1 | UV-induced tanning pathways in melanocytes. UV radiation induces two tanning pathways in melanocytes. The UVA-induced immediate tanning pathway is non-photoprotective and leads to persistent pigment darkening. The photoprotective tanning pathway is activated firstly in keratinocytes by UVB. In keratinocytes, activated p53 pathway induces α-MSH production and secretion. Secreted α-MSH leads to MC1 receptor-mediated MITF-M activation in melanocytes and increase in melanogenesis. Mature melanosomes are transported into keratinocytes to form a protective perinuclear cap against UVR. Hematoxylin eosin staining of skin epidermis, several basal keratinocytes show accumulated melanin granules (brown color, white arrows) above the cell nuclei.

subtypes associated with cumulative solar damage (CSD) are superficially spreading melanoma (low-CSD melanoma), lentigo maligna melanoma (high-CSD melanoma) and desmoplastic melanoma. Melanoma subtypes that are not consistently associated with CSD are Spitz melanoma, acral melanoma, mucosal melanoma, melanoma arising in congenital or blue nevi and uveal melanoma. Nodular melanoma constitutes the third group in the new classification (30, 31). Melanomas associated with CSD are more common among Caucasians while non-CSD (without cumulative solar damage) melanomas affect more often the non-Caucasian population (32). High frequency of specific BRAF mutations and patients' younger age are characteristic for non-CSD. CSD melanomas arise in areas with chronic sun exposure such as face, ears, neck and lower extremities and are associated with high mutational burden. CSD is usually diagnosed in elder people (>60 years) associating with solar elastosis and other non-melanoma skin cancers (31).

SSMs emerge at younger age in comparison to NM or LMM. Typical manifestation of SSM is a flat, slowly growing, irregular lesion with multicolor pigmentation. Histologically, SSM presents with large pleomorphic epithelioid melanocytes showing nested groups of cells and single cells migrating intra-epidermally and/or in the superficial dermis. In contrast, typical for NM is a rapidly expanding nodule that may show ulceration and hemorrhage. Histologically, NM localize in the dermal component, likely combined to epidermal extension. LMM usually appears in chronically sun-exposed areas as a large, multicolor macule with irregular edges. The histological features include proliferation of atypical melanocytes, epidermal atrophy with the loss of rete ridges, severe dermal solar elastosis and dermal thinning. ALM occurs in the palms, soles and fingernail regions showing slowly growing macules like in LMM. Histologically ALM shows single atypical melanocytes scattered along the junctional epidermal layer (33).

Melanoma-Associated Mutations

Melanoma is associated with a broad range of somatic mutations (34). The basal mutation frequency in melanoma is one of the highest of all cancer types (100/Mb entire exome) and most of

them are point mutations of C → T (7). The most common mutation, found in around 50% of all melanoma cases, is the *BRAF* gene mutation, most often the $BRAF^{V600E}$ where valine is substituted with a glutamic acid (35). Interestingly, the $BRAF^{V600E}$ mutation can also be found in over 80% of benign nevi (36, 37) and is thought to be the driver mutation for the formation of acquired nevi (38). Other common mutations found in melanoma are *NRAS* (neuroblastoma RAS viral oncogene homolog), *c-Kit* (35) and *CDKN2A* (cyclin dependent kinase inhibitor 2A) the latter of which associates with familial atypical multiple mole melanoma syndrome (FAMMM) (39). Pigmentation and melanocyte differentiation related mutations in *MC1R* (melanocortin 1 receptor) and *MITF* (microphthalmia associated transcription factor) have also been found in melanoma. *MITF* regulates melanocyte proliferation, differentiation, and survival (40) and acts also as an oncogene regulating the functions of the tumor suppressor p16 and CDK2 (cyclin dependent kinase 2) (41, 42).

Other mutations occurring in melanoma are in genes encoding *CDK4* (cyclin-dependent kinase 4), *PTEN* (phosphatase and tensin homolog), *BAP1* (BRCA1 associated protein), *p53* and those associated with proper telomere function, such as *TERT* (telomerase reverse transcriptase) (39, 40, 43). In UV-related melanoma evolution the primary events depend on the age of the individual and the biological demeanor of the oncogenic initiating mutation in the nevi, such as BRAF. Then, the secondary events such as chronic irritation or irregular high dose UV exposure of mutation-bearing melanocytes damage the cell-cycle checkpoint regulatory system (G1/S phase) or telomerase function and result in even higher mutation burden and formation of melanoma cells (44, 45).

The aforementioned mutations often lead to the over-activation of signaling cascades involving MAPK (mitogen-activated protein kinase) and PI3K (phosphoinositol-3-kinase) pathways. Interestingly, these pathways activated in melanoma, act also closely in the regulation of hyaluronan synthesis (reviewed by Heldin et al. (2019) (46). The MAPK pathway (RAS/RAF/MEK/ERK) transduces extracellular signals from growth factors and hormones to proliferative responses, differentiation, and survival. PI3K(/AKT) signaling pathway is associated with cellular homeostasis. Loss of tumor suppressor gene *PTEN*, which acts as an inhibitor of AKT signaling, further increases the activation of PI3K signaling. The MAPK and PI3K pathways overlap in melanoma and therefore some signaling mediators such as NRAS act through both pathways. This complicates single-agent therapies since the other pathway can take over. Therefore, dual targeting is often needed (47, 48).

Melanomagenesis

Melanomagenesis (**Figure 2**) is a multistep process. Clustering of melanocytes forms a benign nevus without abnormal characteristics. These benign nevi can locate either in the epidermis (*junctional nevus*), or in dermis (*intradermal nevus*), or the nevus cell nests can be accumulated in both the epidermis and dermis (*compound nevus*). Melanocytic neoplasms arise from gain-of-function mutations in one or several primary oncogenes. The neoplastic changes usually occur as new lesions with dysplastic features in skin areas which have no previous melanocytic lesions (31). Dysplastic nevi embody cell hyperplasia, cytologic atypia and enlarged nuclei. They can remain in this regressed state for a long time or develop into radial growth phase (RGP) of melanoma. In this state, melanoma is still restricted to the epidermis by basement membrane and surgical excision is the preferred treatment of choice. The prognosis is good and the ten-year survival rate is over 90% (20, 49). When melanoma progresses from this step to the vertical growth phase (VGP) where melanoma cells invade through the basement membrane into dermis and are capable of metastasizing (locally or distantly), it has become the most aggressive type of skin cancer. At this point, the prognosis is inversely comparative to the depth of the neoplasm and the extent of lymph node metastases (50). The ten-year survival rates in stage III (lymph node positive) and deep (>4 mm) melanomas' have improved during recent years due to novel therapies, but the prognosis largely depends on the sex and age of the patient, the anatomical location of the tumor, and the stage of melanoma at the time of diagnosis (51).

Factors Affecting Melanomagenesis

One important function of UV is the induction of vitamin D precursor synthesis in the skin. For this purpose, the UV requirement is achieved already with the suberythematogenic doses (52). It has been estimated that 65% of all melanomas are caused by UV radiation. Excessive sun exposure during childhood is an important risk factor, but sunburns at any age increase the risk, as well as occupational exposure to UV for people who work outdoors (45). Acute UV exposure increases skin inflammation and DNA damages whereas chronic exposure induces immune cell infiltration and immune suppression leading eventually to malignant changes in melanocytes (26, 53). Within hours after UV exposure repair mechanisms start repairing the oxidative DNA damages (DNA single-strand breaks and DNA-protein crosslinks), and later on the cyclobutane pyrimidine dimers (CPDs). The CPDs are termed as UV signature mutations which induce C → T and CC → TT transitions mostly in the tumor suppressor p53 coding sequence (54). Reactive oxygen species (ROS) such as singlet oxygen, superoxide anion and hydrogen peroxide generated by chromophores, which absorb UVA- and UVB-photons, can also induce damages on nucleic acids, lipids or proteins (55). In addition to the DNA repair mechanisms, UV-induced damages launch multiple other repair mechanisms, such as secretion of paracrine factors (e.g. cytokines, chemokines and growth factors) by skin cells, activation of cellular protection mechanisms (e.g. cell-cycle checkpoints) and activation of cell death pathways and immune responses in damaged cells. At the cellular level, the most important function is the activation of tumor suppressor responses of p53 and p16 signaling pathways (45).

HYALURONAN

Hyaluronan and Its Synthesis

Hyaluronan is a peculiar polysaccharide with broad functions. Hyaluronan is involved in many physiological processes such as embryogenesis (56), wound healing (57), ECM organization (58–60), lubricant in the articular cartilage and synovial fluid (61, 62),

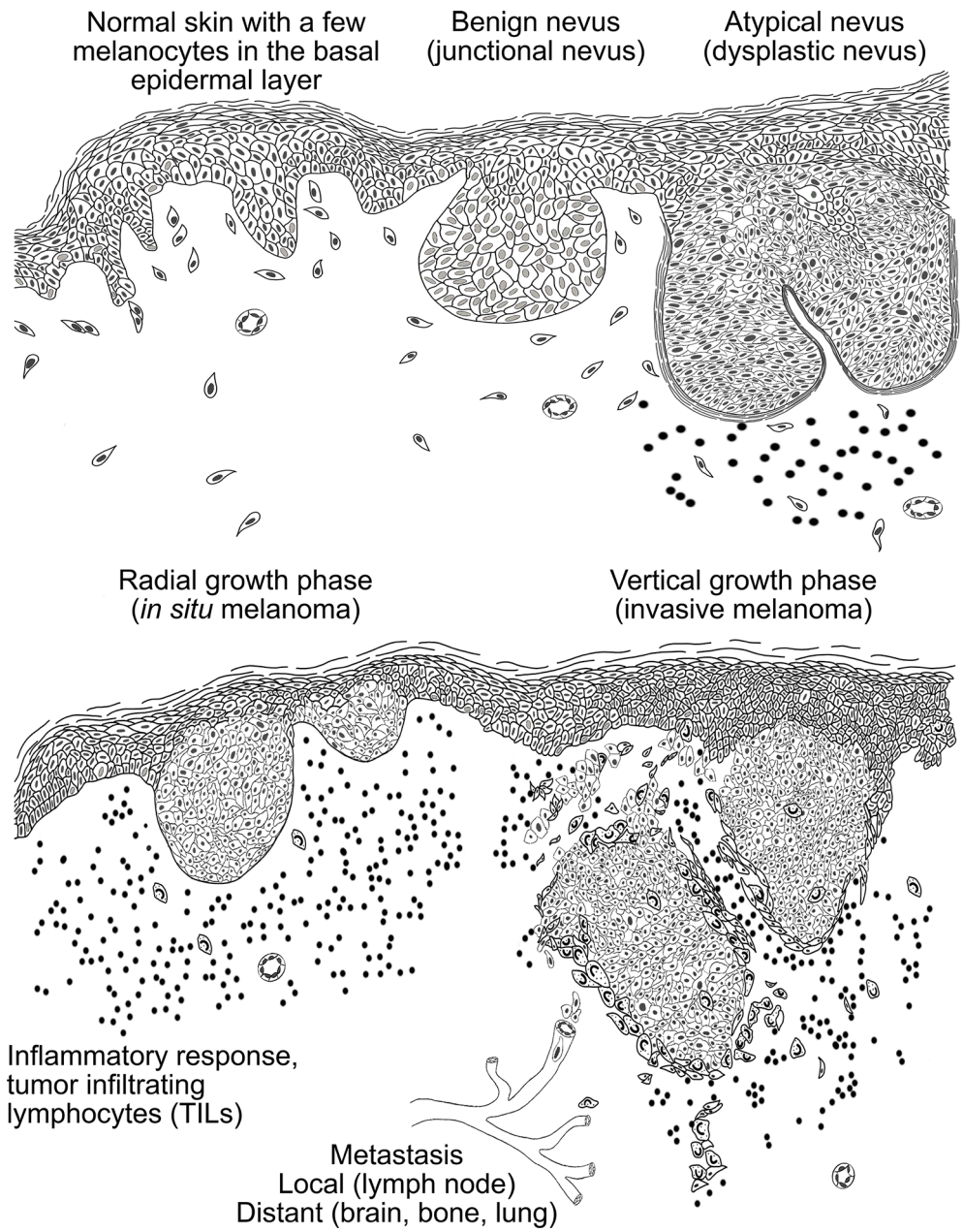

FIGURE 2 | A schematic presentation of the histopathogenesis of the melanocytic tumors. In normal skin, melanocytes are scattered along the basal cell layer. Melanocytes accumulation leads to the formation of benign nevi that can reside in the epidermis (junctional nevus), in the dermis (intradermal nevus) or nevus cells can be assembled in both (compound nevus). In dysplastic nevus melanocytes exhibit cell hyperplasia and show cytological and architectural atypia. Moreover, lymphocyte infiltration around the nevus is typical in dysplastic nevi. In the radial growth phase (RGP) melanoma is still restricted to the epidermis by basement membrane and associates with high lymphocyte infiltration. When melanoma cells start to invade through the basement membrane into the dermis, melanoma has reached the vertical growth phase (VGP). In this stage the melanoma cells are capable of metastasizing *via* blood and lymphatic capillaries to local lymph nodes and distant organs.

mammary gland morphogenesis (63) etc. Hyaluronan, composed of cytosolic UDP-*N*-acetylglucosamine (UDP-GlcNAc) and UDP-glucuronic acid (UDP-GlcUA) precursors, is produced as a linear chain at the plasma membrane by hyaluronan synthases (HAS1-3), which are glycosyltransferases (64, 65). Hyaluronan synthesis by HASes can start *de novo* as the synthases do not need a precursor for the initiation. They use self-primer UDP-GlcNAc and add the two sugar substrates by turns to the reducing end of the growing chain (64). HASes are membrane-spanning enzymes that hold the catalytic site at the inner side of the plasma membrane and synthesized hyaluronan is protruded through a pore-like structure to the cell surface

(64, 66). It is suggested that HASes can synthesize hyaluronan also intracellularly (67, 68), but the general perception is that HASes are functional and synthesize hyaluronan only at the plasma membrane (69). In normal physiology hyaluronan is produced as HMW size and can be up to 40,000 sugars long (8 MDa) (64). Extracellular and pericellular hyaluronan can be internalized *via* receptor-mediated (like CD44-mediated endocytosis) endocytosis for hyaluronan turnover and catabolism (70). Hyaluronan is degraded to LMW form either on the plasma membrane or in lysosomes by hyaluronidases (HYALs) (71), ROS (72) or UV (73). Albeit the mechanism of UV-induced hyaluronan degradation is less known. Moreover, TMEM2 (transmembrane protein 2) and HYBID (hyaluronan binding protein involved in hyaluronan depolymerization, also known as CEMIP or KIIAA1199) are also able to depolymerize hyaluronan (74, 75). TMEM2 degrades extracellular hyaluronan in a Ca^{2+} -dependent manner into intermediate-sized fragments which are thereafter internalized and completely degraded in the lysosomes (76). The HA degradation products, LMW hyaluronan, hyaluronan fragments (<250 kDa) and oligosaccharides (<20 kDa) are involved in inflammation (77, 78), wound healing (79) angiogenesis (80, 81) and in general they associate with pathological conditions, such as asthma and lung infections including coronavirus disease (82, 83) and cancer (84).

The enzymatic activity of the synthases also affects the molecular weight of the produced hyaluronan. It has been proposed that HAS1 and HAS2 synthesize higher molecular weight hyaluronan compared to HAS3 (85). However, recent studies have pointed out that HASes could be able to control the hyaluronan product size and the synthesis rate *in vivo* by separate enzyme submechanisms. This was shown in targeted mutation studies to B-X_7-B motifs in *Streptococcus eguisimilis* HAS, which indicated that the different regions in the HAS enzyme are involved in hyaluronan size control as well as its enzymatic activity (86).

Hyaluronan in Cancer

Understanding of hyaluronan in the inflammatory diseases and cancer is growing. Depending on which tissue type the cancer originates from, the increased/decreased content of hyaluronan in the tumor or stromal cells correlates with tumor aggressivity, poor prognosis, and recurrence of the cancer. Breast cancer, which originates from simple type of epithelium that contains low levels of hyaluronan in the normal state, shows increased hyaluronan content in the tumor cells and in the stroma, and the amount of hyaluronan associates with aggressive type of breast cancer and poor overall survival (14, 17). The trend is similar in other cancers originating from simple epithelia. Increased content of hyaluronan in the stroma of ovarian cancer (87, 88), prostate cancer (15, 16, 89) and pancreatic cancers (90) indicates poor prognosis. Similar findings have been demonstrated in gastric cancer parenchyma (91) and in tumor cells (92) and tumor interstitial fluid of colorectal cancer (93).

In cutaneous melanoma, hyaluronan metabolism is different compared to cancers originating from simple epithelia. The hyaluronan content varies depending on the stage of the tumor (**Figure 3**). Cultured skin melanocytes contain high amount of pericellular hyaluronan (94) similarly to the cells in the benign nevi (18). Moreover, the stroma between the melanocytic nests in the benign nevi shows intense staining for hyaluronan. In *dysplastic nevus*, where melanocytic cells show cytological and architectural atypia, the content of hyaluronan is elevated to local melanomas (melanoma *in situ*), where tumor cells show intense membraneous and cytoplasmic staining for hyaluronan.

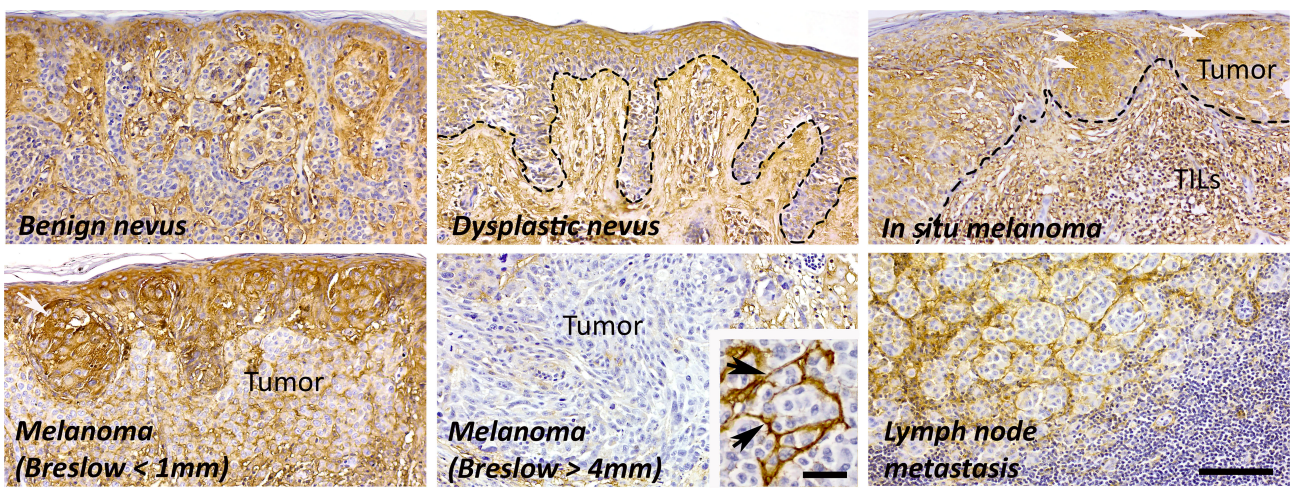

FIGURE 3 | The amount of hyaluronan in different stages of melanoma. In normal skin, both epidermis and dermis are highly hyaluronan positive, also melanocytes in the benign nevi show moderate or intense hyaluronan staining. The amount of hyaluronan increases in dysplastic nevi and in local tumors (white arrows) probably as part of the inflammatory reaction with elevated number of tumor infiltrating lymphocytes (TILs). In invasive melanoma, the amount of hyaluronan is decreased in tumor tissue but the stroma is strongly hyaluronan positive (black arrows). The hyaluronan staining pattern is similar in lymph node metastases and in deep melanomas (Breslow > 4 mm). Scale bar 100 μm, 40 μm in insert.

When melanoma progresses and tumor cells start to invade vertically, tumoral hyaluronan content decreases (melanoma, Breslow < 1mm) while the stroma remains hyaluronan positive (18). Especially in nodular type of tumors the stroma shows intensive staining for hyaluronan (melanoma, Breslow > 4mm, *insert*). Hyaluronan staining pattern in lymph node metastases is similar to deep melanomas. The reduction of hyaluronan in the tumor tissue has been shown to be due to the loss of HAS1 and HAS2, and increased HYAL2, and this associated with poor prognosis and shortened disease-specific survival in melanoma (19, 95).

The Effects of UVB on Hyaluronan Metabolism

Mouse studies have shown that chronic UV exposure with minimal erythemal dose induces the accumulation of hyaluronan in the epidermis, which correlates with epidermal hyperplasia (96). In organotypic keratinocyte cultures, UV-exposure was shown to increase hyaluronan metabolism by upregulating the expression of both HASes and HYALs simultaneously and by shifting the molecular weight of hyaluronan towards smaller size range (97). Studies with keratinocytes and dermal fibroblasts have shown different temporal expression patterns of HASes and HYALs after UVB-exposure (98). Immediate responses after UVB-exposure showed decrease in hyaluronan secretion in both cell types whereas 24 hours later keratinocytes showed increased hyaluronan synthesis while in dermal fibroblasts hyaluronan synthesis was still downmodulated. 24 hours after UVB-exposure the expression of *HAS1* and *HAS2* was upregulated in both cell types, and in addition the expression of *HYAL1* and *-2* was elevated in dermal fibroblasts indicating increased hyaluronan degradation after UVB exposure (98). The similar mechanism was also detected in photoexposed human skin, where LMW hyaluronan content was increased due to upregulated expression of HYALs compared to photoprotected skin (99). In addition to increased HYAL activity after UV exposure, UV induces oxidative stress *via* ROS production (100), which can further induce hyaluronan fragmentation (72, 101). Hyaluronan is able to scavenge toxic ROS (102, 103), or inhibit their formation, but at the same time hyaluronan is fragmented (103). Albeit it is not yet known how ROS-induced hyaluronan degradation and generation of LMW hyaluronan followed by inflammation in skin contributes to melanoma development in melanocytes, the research is supporting the idea that hyaluronan has a role in melanoma development and especially affecting the TME in melanoma (18, 19, 94, 104).

Hyaluronan in Inflammatory Reactions

As mentioned earlier, UV radiation induces various biological effects in the skin such as DNA damage, pigmentation and inflammation. Excessive exposure to UVB causes sunburn reaction together with inflammation. Several cell types, such as keratinocytes, fibroblasts, Langerhans cells, melanocytes and macrophages, participate in these inflammatory reactions by secreting inflammatory mediators and reshaping the tissue structure. During inflammation, the amount of hyaluronan is elevated (105, 106), and especially the LMW hyaluronan and hyaluronan fragments are associated with inflammation (107). They can activate intracellular signaling cascades and induce cytokine and chemokine production *via* receptor activation. LMW hyaluronan, for example, has shown to induce the production of IL-6, IL-8, CXCL1, CXCL2 and CXCL6 in dermal fibroblasts (108). Key receptors for LMW hyaluronan include CD44 (cluster of differentiation 44), RHAMM (receptor for hyaluronan-mediated motility), TLR2 (Toll-like receptor) and TLR4 (109). TLR4 activation leads to NF-κB-mediated signaling and production of inflammatory cytokines and chemokines such as IL-6, IL-8, CXCL-1 and CXCL-10 in melanocytes (94) and IL-8 and MMP-2 secretion in melanoma cells (110). Hyaluronan fragments of 4-16 oligosaccharides, in turn, have shown to induce the maturation of dendritic cells by autocrine production of TNF-α (81), and dendritic cell-associated hyaluronan appears to contribute to the antigen-specific activation of T-cells (111). We have recently shown in primary melanocytes that UVB-exposure mediated hyaluronan coat degradation promoted the expression of proinflammatory cytokines IL-6 and chemokines (IL-8, CXCL1, CXCL10) *via* TLR4 (94). Interestingly, in this model, the expression of proinflammatory cytokines and chemokines were suppressed by *HAS2* silencing, suggesting that HAS2 expression and hyaluronan fragments support the formation of pro-inflammatory state. In contrast, HMW hyaluronan (970 kDa) has been shown to protect epidermal keratinocytes against UVB-mediated TGF-β, IL-6 and IL-8 production (112). It is hypothesized that HMW hyaluronan has a protective role in skin against UV radiation and the fragmentation of hyaluronan acts as a damage-associated molecular pattern (DAMP) (113).

The effects of hyaluronan on immune, non-malignant and malignant cells are size-dependent. HMW hyaluronan has been shown to be relatively inert, whereas its degradation products have been speculated to be biologically active and modulate the TME towards pro- or anti-inflammatory states depending on the tumor stage. Hyaluronan and its fragments are thought to regulate macrophage polarization, although the exact mechanisms are still unresolved (114). Macrophages have an essential role in orchestrating the inflammatory responses and they are also a key component of TME in all stages of melanoma development (115, 116). In the TME, tumor associated macrophages (TAMs) are very plastic and are composed of several distinct populations that share features of both pro-inflammatory (M1) and immunosuppressive (M2) macrophages (117). Intermediate-size hyaluronan (50-1000 kDa) fragments have shown to activate monocyte polarization to immunosuppressive M2-type macrophages *via* the activation of TLR4 (118), but there are also contrasting studies showing that hyaluronan fragments induce M1 polarization of macrophages *via* TLR4 (119). In addition, TLR4 signaling pathway is responsible for inflammatory gene expression induced by hyaluronan fragments in several other cell types like dendritic cells, melanocytes and tumor cells (81, 94, 110, 119, 120).

In TME, enhanced hyaluronan production by stromal fibroblasts (104, 121) combined to increased hyaluronidase

activity from melanoma cells could produce broad pool of different types of hyaluronan fragments and oligosaccharides that maintain the inflammatory milieu. This is also supported by a study from Sapudom et al. (2020) where hyaluronidase added to decellularized fibroblast matrix, 3D fibroblast matrix and hyaluronan-functionalized 3D collagen matrix increased melanoma cell proliferation and invasion due to lower hyaluronan molecular size (122). It has also been shown that LMW hyaluronan promotes melanoma lymph node metastasis (123), soluble LMW hyaluronan contributes to melanoma cell proliferation (124), and shorter hyaluronan fragments induce TLR4-mediated signaling in melanoma and promote inflammation as well as invasiveness (110). Interestingly, in naked mole rats HAS2 produces exceptionally high molecular weight hyaluronan that is able to avoid fragmentation (125). These animals display longevity and are cancer-resistant, but when HAS2 is knocked down or HYAL2 is overexpressed the naked mole rat cells became prone to malignant transformation (125).

Current understanding suggests that hyaluronan fragments modify the adaptive immune responsiveness and shape the microenvironment (113). The formation of cancer inflammatory milieu recruits immune cells to the TME to shape it suitable for tumor progression. TLR4 has shown to be overexpressed in melanoma tumors and associate to decreased survival (126), which links hyaluronan and TLR4 in melanomagenesis. TLRs respond to acute inflammatory signals either from microbial sources (PAMPs, pathogen-associated molecular patterns) or self-derived stress signals (DAMPs), the role that also hyaluronan has been proposed to play. The activation of TLR signaling leads to NF-κB, AP-1 and/or IRF-3 mediated inflammatory response in healthy skin and in primary melanocytes and eventually skin carcinogenesis (94, 127). This suggests a role for hyaluronan metabolism, especially for UV-induced hyaluronan fragmentation *via* TLR4-mediated inflammation, in melanocyte transformation process towards cutaneous melanoma. Future research should aim at clarifying whether chronic UV-exposure together with hyaluronan fragmentation could mediate sustained inflammatory responses initiating cutaneous melanoma development. Even though hyaluronan can modulate immune responses, it may also act as a protective barrier in the TME and thus prevent immune cells to reach and recognize the tumor cells (128). And in this way hyaluronan may also promote the immune evasion of tumor cells.

MELANOMA TUMOR MICROENVIRONMENT

Composition of Different Cell Types in the Tumor Microenvironment

TME is inherently diverse surroundings consisting of not only the tumor and stromal cells but also immune cells, blood vessels and the ECM, which all affect the tumor progression. Considering the complexity of the TME, cancer therapies cannot focus only on the tumor cells (129, 130). Melanoma is one of the most immunogenic cancers and immune cells have a significant role in all stages of tumor progression, from the initiation to the metastatic processes and thus these cells are the main target of modern anti-melanoma therapy. Transformed melanocytic cells start to express tumor-specific antigens (TSA), which induce the infiltration of dendritic cells, which later activate the cells of innate and adaptive immunity. Dendritic cell maturation is needed to actuate the T-cell mediated anti-tumor response and natural killer cell activation (131). Lymphocytes infiltrate the tumor environment in response to chronic inflammation. These so-called tumor-infiltrating lymphocytes (TILs) appear to be a positive indicator for melanoma prognosis (132, 133). TILs are a heterogeneous population of lymphatic cells such as T-cells, natural killer cells and myeloid-derived suppressor cells (134). The presence of TILs promotes immune responses against tumor cells and can be thought as a predictive biomarker in melanoma. Computational meta-analysis of melanoma tumors indicated a favorable prognostic role for CD3+, CD4+, CD8+, FOXP3+ and CD20+ positive TILs in the overall survival when the amount of TILs in the tumor was high (135). A study by Erdag et al. (2012) categorized tumor microenvironments of metastatic melanoma into three immunotype subgroups A, B and C based on the number and localization of TILs (T-cells, B-cells, natural killer cells), mature dendritic cells and macrophages. The immunotype A had no immune cell infiltration and the median estimate of survival in this group was only 15 months. The immunotype B had infiltration of immune cells to regions proximal to intratumoral blood vessels with the median estimate of survival was 23 months. The last immunotype C had immune cell infiltration throughout the metastatic tumor with a median estimate of survival of 130 months (136). Although the number of TILs in melanoma as a prognostic biomarker, especially in the VGP, was established a long time ago (137), it is still a valid diagnostic predictor estimating patients' survival.

In contrast to TILs, tumor-associated macrophages (TAMs) can promote the dissemination of cancer cells and expansion of the tumor depending on their type. The categorization of TAMs is not unambiguous. Traditionally, TAMs are categorized as classically activated macrophages (M1) that secrete pro-inflammatory cytokines and have anti-tumor effects, and alternatively activated macrophages (M2) that produce anti-inflammatory cytokines and have protumor effects (138). As already mentioned earlier, in the TME, TAMs are composed of several distinct populations that share features of both pro-inflammatory and immunosuppressive macrophages and these cells induce and maintain pro-tumor inflammation, which promotes tumor growth, invasion, angiogenesis, stemness and immune suppression (139, 140). The precise mechanisms underlying TAM-mediated immune suppression in TME are still unknown but at least partly relate to their ability to inhibit cytotoxic activity of $CD8^+$ T cells *via* PD-1 (programmed cell death protein) (141). PD-1 is an immune checkpoint receptor that prevents overstimulation of immune responses upon engagement to its ligand, PD-L1 (142). In several cancers, including melanoma, the expression of PD-L1 is considered as a marker for immunosuppressive TME (143). During tumor

progression, TAMs start to overexpress PD-L1, like tumor cells, and thus are able to downmodulate the function of CD8+ lymphocytes and facilitate the immune evasion of tumor cells (144). Moreover, it has been shown *in vitro* that alternatively activated macrophages can suppress T-cell function by producing regulatory cytokines, such as TGFβ and IL-10, hence repress T-cell proliferation (145) and recruit regulatory T-cells to the immune suppressed TME, which further contributes to tumor progression (138).

Salmi et al. (2019) reported that the number of TAMs is higher in malignant melanocytic lesions compared to benign nevi and TAMs are localized especially in the tumor nests in deep melanomas. They also reported that the dysplastic nevi have higher number of CD163+ macrophages (M2 type macrophages) compared to benign nevi, which could predict immunosuppression and progression of melanoma (146). It is also known that these benign and dysplastic nevi as well as melanoma *in situ* express hyaluronan abundantly (18), but its role for macrophage polarization is still unknown. It has been shown that HMW hyaluronan suppresses M1 macrophage polarization and promotes the immunosuppressive activation in induced pulmonary inflammation (147). Kim et al. (2019) also showed *in vitro* that hyaluronan in the ECM induces M2-type polarization of THP-1 cells (148). The similar mechanism could also be involved in the formation of immunosuppressive microenvironment in melanoma, where increased hyaluronan synthesis at the early stage of melanoma could polarize macrophages toward immunosuppressive phenotype. Although it is generally thought that M2 type TAMs have protumor effects in the TME, the pro-inflammatory macrophages have also shown to secrete several protumor factors, like TNFα and IL1β, and are able to modify the TME suitable for cancer progression (149–151).

In addition to several immune related cells, TME contains fibroblasts which are mainly responsible for the production of complex extracellular matrix, which either suppresses or supports the tumor progression. In the early stages, in pro-inflammatory tumors, factors like IL-6, TNFα, PDGF and ROS secreted from tumor and immune cells can activate the stromal fibroblasts. Once activated these contractile and highly elongated cancer associated fibroblasts (CAFs) produce several cytokines and chemokines, synthesize and degrade matrix components and generate tensile forces, which all are needed for tissue remodeling for tumor cell growth and spreading (152).

Extracellular Matrix in Melanoma

The tumor ECM is a mixed territory of different types of proteins, glycoproteins, proteoglycans and glycosaminoglycans, which all have specific physiological and biochemical properties (153). The composition of ECM maintains the three-dimensional structure that keeps up tissue homeostasis, undergoes continuous remodeling and contains over 100 different proteins and bioactive molecules like growth factors, cytokines and extracellular vesicles (EVs) produced jointly by stromal cells and tumor cells (154). A typical ECM matrix in melanoma includes fibrillar and structural proteins, such as collagen types of I, III, VII, XV, XVIII, laminin 7, tenascin-C, fibronectin and hydrated gel-forming macromolecules like hyaluronan and proteoglycans, as well as integrins, which carry out the adhesive signaling (155). Excess of these ECM components, such as collagen and fibronectin, increase tissue fibrosis and hence matrix stiffness, which affects the metastatic potential of tumor cells and invasiveness (156). Li et al. (2019) showed in melanoma cells that increased matrix stiffness enhanced the metastatic potential of naturally less-metastatic melanoma cells. Their metastatic potential was comparable to melanoma cells with high metastatic potential in stiffer matrix. This indicates that the tumor-surrounding matrix has a high impact on oncogenesis and changes in the matrix might have greater effect on the metastatic process than tumor cells (157).

A rapidly growing cell mass causes dysfunctional tumor vasculature leading to hypoxic environment and low oxygen levels. Hypoxia can lead to specific changes in signaling pathways, such as ERK hyperactivation leading to increased invasiveness, angiogenesis, EMT changes, radiotherapy resistance, changes in the ECM composition, which all promote tumor progression. HIF (hypoxia-inducible factor) 1 and 2 are regulators of hypoxia-mediated responses in over 300 target genes. Hypoxic TME correlates with aggressive cancer phenotype associated with increased tumor plasticity and may induce cancer stem-like cells (158–160). The high metabolic activity of melanoma cells causes the production of acidic molecules to the TME, which affects the ECM composition. Acidification of the TME influences the tumor cell invasiveness, increases expression of EMT-related proteins and causes a selection of acid-resistant cells that show greater metastatic potential. Acidic TME also affects anticancer therapies and the absorption of mildly alkaline chemotherapeutics leading to melanoma cells drug resistance (159).

The composition of the ECM changes during tumor development. Many ECM molecules are expressed at low levels in benign nevi whereas their levels increase in metastatic melanoma, as shown with tenascin-C, fibronectin and different epitopes of heparan sulfate. Other glycosaminoglycans such as chondroitin sulfate and hyaluronan are highly expressed in the benign nevi and also abundant in melanomas either in the tumor nests or in the stroma (18, 161, 162). Recently, Mayorca-Guiliani et al. (2017) developed an ISDoT (*in situ* decellularization of tissues) technique where they could study the native tumor ECM in a mouse model. They could identify more than 200 ECM proteins as well as many secreted factors such as MMPs, versican and members of the S100 protein family from the decellularized tumor tissues, showing tumor-specific changes in the ECM composition in comparison to healthy tissue (163).

Phenotype switch is an important regulator between proliferative and invasive states of melanoma cells. Melanoma cells do not undergo normal EMT changes, however they utilize EMT and MET (mesenchymal-to-epithelial transition) states that are mediated by adhesion molecules such as Cadherin-11, Connexis, integrins, N-cadherin and MCAM (CD146) which all are indicators of progressed melanoma (164). Melanoma cell phenotype switch can also alter MITF expression, which in melanocytes regulates pigmentation. High MITF expression

sensitizes melanoma cells to BRAF and MEK inhibitors whereas the cells are more proliferative. However, low MITF expression increases drug resistance and induces invasive phenotype. Low expression or loss of MITF was also shown to increase glycosaminoglycan metabolism, ECM organization and structural organization in melanoma cells. Also, loss of MITF increased stem cell marker SOX2 that is important in melanoma cell self-renewal. Thereby, the level of MITF alters melanoma phenotype switch as well as matrix composition and interactions (164, 165).

Ubiquitous hyaluronan in the ECM provides the cells a suitable environment to migrate, divide, change their shape and adhere due to its viscous hygroscopic nature. In addition, hyaluronan facilitates signaling from the environment, but at the same time also orchestrates many unwanted functions in the ECM by permitting the cancer cells do the same (66, 166). Even though the role of hyaluronan is broadly studied in the context of melanoma cells *in vitro*, its function in primary melanocytes and early melanoma development is uncertain. Neither is known how the basal level of hyaluronan differs in different skin types or the alteration of hyaluronan in photoprotected areas versus photoexposed areas, as UV exposure has been shown to increase the hyaluronan content in epidermis (99). It is thought that hyaluronan in the ECM could act as a protective matrix and hinder the inflammatory reaction produced by ROS (10). The thicker hyaluronan content in the skin could shield from the harmful effects of UV, reduce the inflammatory reaction following it, and therefore protect the skin cells against carcinogenesis. When hyaluronan degradation was combined to UV-exposure in primary melanocytes, the inflammatory reaction following it was highly enhanced (94). This could indicate that thicker hyaluronan coat around the cells and in the ECM could moderate the inflammatory reaction following UV exposure. UV-induced conditions also associate with hyaluronan degradation, which further enhances the inflammation. The direct mechanism of hyaluronan fragmentation by UV is still unknown, but the activation of HYAL and/or ROS directly, by ROS-activated HYAL or direct fragmentation by UV have been suggested. Inflammation following UV exposure is also an acute defense mechanism to protect and dispose damaged cells (167), but in a chronic state it can lead to carcinogenesis.

Melanoma-Stroma Interaction

It is well known that the interaction between cancer cells and stroma is needed for tumor progression and metastasis. Already in 1889 Paget's theory of "seed and soil" emerged (168). Since that, different studies on melanoma-tumor stroma have emerged and nowadays is well acknowledged that the surrounding tumor stroma is equally important as the tumor itself. Our results (2012) as well as others have shown that melanoma cell-secreted factors (PDGF) induce stromal fibroblasts to produce hyaluronan by upregulating *HAS2 via* PDGFR-PI3K-AKT and p38 MAPK signaling (104, 121). In this study, PDGF -induced *HAS2* upregulation associated with activated phenotype of fibroblasts with elongated morphology, upregulation of proteolytic enzyme MMP1, MMP9 and MT1-MMP expressions and increased invasion into the matrix, suggesting that HAS2 is essential in activating the fibroblasts in the tumor stroma (104). The activated fibroblasts, so called cancer associated fibroblasts (CAFs), facilitate melanoma cell invasion by modifying the ECM suitable for tumor invasion (169). These *in vitro* results are in line with the patient data where Siiskonen et al. (2013) showed that hyaluronan staining in invasive and metastatic melanoma stroma is intense in comparison to almost negative tumor staining. They also showed that HYAL2 staining is elevated in invasive and metastatic melanoma samples, which could indicate that hyaluronan catabolism and thus the degradation of hyaluronan is increased in melanoma cells (18) (**Figure 4**). Increased hyaluronidase activity in melanoma cells has also been shown to induce angiogenesis (170) and cutaneous wound healing (171) likely attributed to hyaluronan fragments. As it has been shown that tumor cells secrete higher amounts of extracellular vesicles (exosomes, microvesicles) compared to non-transformed cells (172), their role in tumor-stroma interaction is essential. Recently Arasu et al. (2020) published a study where they reported that HAS3-induced hyaluronan coated extracellular vesicles (EV's) from melanoma cells induced EMT changes and increased proliferation of target cells, keratinocytes, similarly as CAF -derived hyaluronan has shown to promote melanoma cell proliferation (121, 173). In Arasu's study they hypothesized that hyaluronan coated EV's may form a positive feedback regulation which induces the tumorigenic potential of the target cells in the surroundings (173). This EV-mediated target cell activation has also been shown to be bidirectional. Cancer associated fibroblasts' (CAFs) exosome secretion was enhanced by melanoma cell-secreted exosomal miRNA. These CAF-derived exosomes promoted melanoma progression and metastasis (174). In addition, EV's can carry matrix-remodeling proteins, such as MMPs, TIMPs, ADAMTSs, hyaluronidases, heparanases, whose proteolytic activity can modify the composition of the ECM suitable for tumor progression (175).

Therapeutic Approaches in Melanoma

The therapeutic approaches in melanoma depend on the prognostic stage of the disease. The 8th American Joint Committee on Cancer staging and classification system (AJCC8) is the recommended standard for melanoma staging (176). The standard of care for local or locally advanced melanoma (AJCC8 stage I-III) is radical surgical excision with either sentinel lymph node biopsy or regional lymph node evacuation depending on the clinical preoperative lymph node status (176–179). Although surgical removal of oligometastases might be an option for selected patients with stage IV melanomas, the backbone of the treatment of metastatic melanoma is systemic oncological therapy with immunomodulating agents (immune check point inhibitors, ICIs) and/or BRAF-signaling route-targeted therapy. During recent years, these agents have also been available for the adjuvant treatment of high-risk stage IIIB-D and IV diseases, where the 5-year melanoma-specific survival is 85% or less (176, 180–185).

Considering the high immunogenicity of melanoma it is not surprising that the therapeutic options targeting the immune cell-TME signaling have turned out effective. Immune checkpoint inhibitors (nivolumab or pembrolizumab, PD-1 antibodies) enhance the anti-tumor immune response by

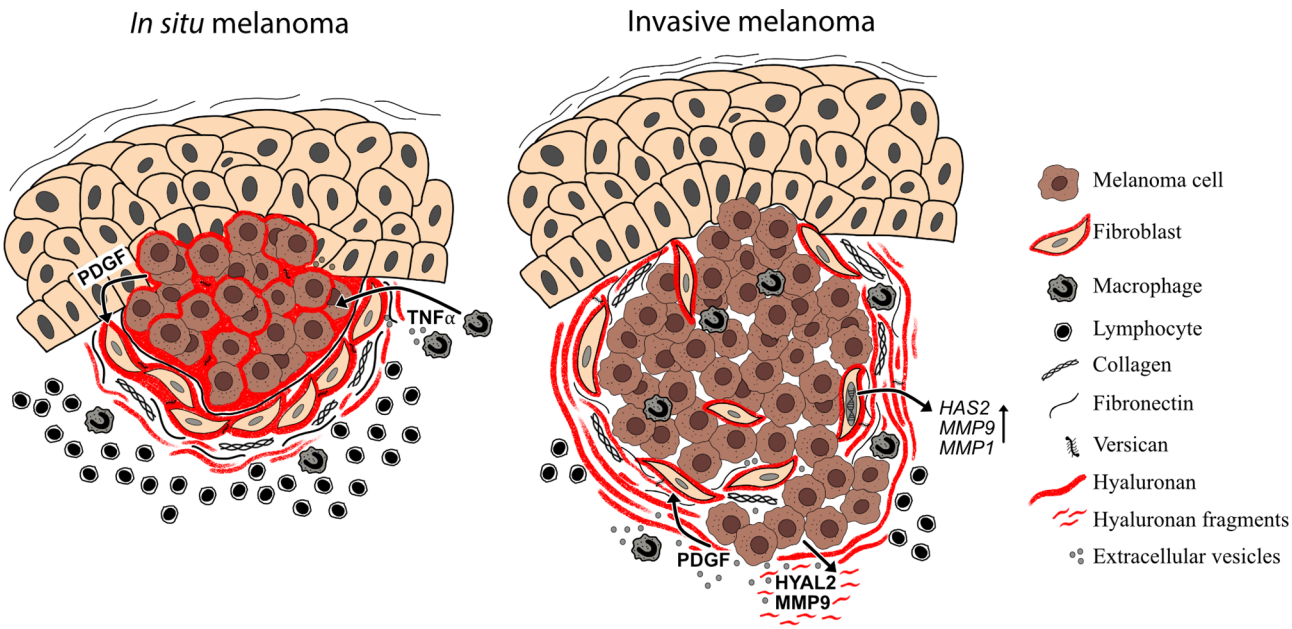

FIGURE 4 | Melanoma-stroma-ECM in superficial and deep melanomas. Superficial melanomas (*in situ* melanoma) have high tumoral hyaluronan content and the stroma contains also abundantly hyaluronan, which is produced by cancer associated fibroblasts. In addition to hyaluronan, melanoma stroma contains other ECM components such as type I collagen, fibronectin and versican. This hyaluronan-rich pericellular matrix surrounding the melanoma cells may mask the tumor cells from immune cell recognition. In deep melanomas (i.e. invasive melanomas), the tumoral hyaluronan content is decreased but stroma is still hyaluronan positive. The hyaluronan and hyaluronan fragment -rich matrix in the tumor stroma may, in turn, facilitate the invasion and metastasis of melanoma cells. In the TME, soluble growth factors (e.g. PDGF), cytokines (e.g. TNFα) and extracellular vesicles, produced by both tumor and stromal cells regulate the expression of HAS2, HYAL2 and MMPs.

blocking the signaling *via* suppressive immune checkpoint molecules PD-1, PD-L1 and CTLA-4 that are often expressed in the TME by tumor cells and immune cells, such as tumor associated macrophages (TAMs), as a mechanism of immune evasion. At best, immune checkpoint inhibitors can induce complete and durable tumor regression of metastatic diseases (186, 187). However, therapy resistance is common and severe, even fatal, autoimmune-mediated toxicities are associated with the therapy (186–188). Biomarkers predictive of the therapy result are therefore needed to estimate the response likelihood and to optimize the patient selection for therapy. So far, the only clinically used predictive biomarker of the efficacy for immune checkpoint inhibitor therapy, is the expression intensity of PD-L1 in the TME, but it has turned out to be suboptimal (188, 189). Other potential biomarkers are under investigation. These include the TME lymphocyte infiltration (190, 191) and tumor mutation burden (192). Moreover, as the structure of ECM in melanoma stroma may affect the therapy response, its potential as one of the predictive parameters should also be evaluated.

Hundreds of ongoing clinical trial studies are currently exploring other immunotherapeutic targets for future melanoma treatment (ClinicalTrials.org). The furthest developed novel anti-check point molecule, with recently released phase II/III results, is the LAG-3-inhibitor relatlimab, which has shown clinical efficacy in combination with nivolumab in metastatic melanoma (193). The interleukin 2 pathway agonist bempegaldesleukin, with the currently ongoing phase III clinical trial, and has shown promising phase II results in combination with nivolumab. An IL-6 antagonist, tocilizumab, is also studied in combination with nivolumab in a phase II study (Clinicaltrials.gov, NCT03999749).

A local treatment option for unresectable stage IIIB-IVM1a melanomas with (sub)cutaneous metastases is an oncolytic vaccine called talimogene laherparepvec (T-VEC; IMLYGIC®), a modified herpes virus vector that is injected locally in melanoma lesions and, in addition to direct cell destruction, enhances both local and distant immune responses. The use of T-VEC in advanced melanoma is also being evaluated in combination therapy approaches, e.g. together with ipilimumab and pembrolizumab (194, 195), with the aim of increased efficacy in patients with visceral metastases. Other vaccine therapies, including dendritic cell-based, peptide-based and vector-based vaccines are also in the testing phase and so far, the results have not been assuring (196). Instead, adoptive cell therapies (ACT) are a promising investigational option. The ACT approaches include tumor infiltrating lymphocytes (TILs) and chimeric antigen receptor (CAR) T-cell therapy (197).

THERAPEUTICALLY TARGETING HYALURONAN IN MELANOMA

Therapeutic targeting of hyaluronan degradation or combining it with other types of therapy have been studied in solid tumors

associating with high accumulation of hyaluronan in the tumor or in the stroma like in pancreatic cancer (198). *In vitro* studies have shown that hyaluronan-rich matrix constrains the access of immune cells, like CD8+ cytotoxic T cells, to the tumor area in tumors with high hyaluronan matrix such as breast and pancreatic cancer (199). Using a PEGylated recombinant human PH20 hyaluronidase (PEGPH20) in combination with trastuzumab or cetuximab, the immune cell infiltration was enhanced but also the used treatment, trastuzumab- or cetuximab-mediated antibody-dependent cell-mediated cytotoxicity against tumor cells was highly improved. Similar results were seen in mouse models (200). However, a phase I trial in pancreatic ductal adenocarcinoma patients using PEGPH20 in combination with gemcitabine resulted in unacceptable adverse effects such as musculoskeletal pain, peripheral edema and thromboembolic events (201). Moreover, the overall survival or the progression-free survival were not improved in phase III trials of pancreatic ductal adenocarcinoma with the treatment of PEGPH20 in combination neither with nab-paclitaxel nor gemcitabine. Patients also suffered higher grade adverse effects such as fatigue, muscle spasms and hyponatreamia (202). Nevertheless, in 2020, the FDA approved another type of hyaluronidase, hyaluronidase-zzxf from Phesco, to be used as a subcutaneous injection to increase dispersion and absorption of pertuzumab or trastuzumab to treat HER2-positive early stage and metastatic breast cancer (203).

Since the hyaluronan levels in advanced stage melanoma tumors are low or almost negative (18) in contrast to breast and pancreatic cancers, similar kind of hyaluronidase therapies most likely cannot be used. However, *in vitro* studies have shown that melanoma cells induce hyaluronan production in dermal fibroblasts (104, 121) and it also correlates with the hyaluronan levels in the stroma of melanoma (18), and this could be a potential target for therapy. Theoretically, targeting the stromal hyaluronan in melanoma might induce better immune cell recognition and T-cell infiltration, as was seen in pancreatic ductal adenocarcinoma (204). Bearing this in mind, new local photothermal therapies (PTT) in synergy with immune therapy have been tested by combining dissolved microneedles to hyaluronidase-modified semiconductor polymer nanoparticles containing poly(cyclopentadithiophene-*alt*-benzothiazole) and immune adjuvant polyinosinic-polycytidylic acid in mouse models. The approach enhanced the activation of immune cells, especially T-cell-mediated immune responses. Although, its use is currently limited only to superficial melanomas as a local treatment (205), it opens prospects to combine targeted hyaluronan degradation and immunotherapy to treat melanoma TME in the future. In addition, 4-methylumbelliferone (4-MU) is an interesting agent known to inhibit hyaluronan synthesis (206). 4-MU acts as a competitive substrate for UDP-glucuronosyltransferase -enzyme involved in hyaluronan synthesis (207), it inhibits hyaluronan synthesis by depleting its precursor sugar UDP-glucuronic acid and downregulating the expression of HAS2 and HAS3 (208). *In vitro*, 4-MU has shown to inhibit melanoma cell proliferation and invasion into collagen lattices (209). Recently, a topically applied 4-MU formulation was shown to decrease cutaneous hyaluronan content in a mouse model (210), opening interesting new approaches to treatment of conditions with altered hyaluronan metabolism, including melanoma.

CONCLUSIONS AND FUTURE PERSPECTIVES

Considering the yearly increasing numbers of new melanoma cases, the race in finding effective therapies remains tense. Preventive measures seem to be cost-effective (211) but they may not reach people at the greatest risk of developing skin cancer. Luckily, basic clinical research has taken huge steps during the past years and decades and enlightened the details of melanoma progression. Not only has our understanding of the several genes and signal transmitters involved in the pathogenesis of melanoma increased enormously, but we are also starting to realize the complexity of the microenvironment surrounding the evolving tumor. As reviewed here, hyaluronan, an abundant glycosaminoglycan surrounding skin cells, has also several functions affecting the development of melanoma. Hyaluronan may have controversial role in cancer as it is increased in certain cancer types but decreased in others. Although there are effective treatments available and promising therapies being studied in clinical trials, we still need a more detailed understanding of the complexity of the ECM, including hyaluronan, in melanoma progression. Future research should focus on investigating the gradual processes in the TME during tumor development and on finding new ways to modulate the matrix surrounding the tumor. The key to conquer cancer may not be just affecting the tumor cells or the immune reactions but also to modify the TME susceptible for treatment. Hyaluronan appears to be a potent molecular target for future therapeutic modalities and innovative research ideas should be supported. Considering the past advances in cancer biology, the breakthrough findings and the most effective treatments are yet to come.

AUTHOR CONTRIBUTIONS

Writing - Original Draft Preparation: PT. Writing - Review and Editing: PT, HS, AR, KK, SP-S. Figure Preparation: PT and SP-S. All authors contributed to the article and approved the submitted version.

FUNDING

This work was funded by the Academy of Finland (SP-S, grant number 324238), Sigrid Jusélius Foundation (SP-S) and Päivikki and Sakari Sohlberg Foundation (PT).

REFERENCES

1. Müller C, Wendt J, Rauscher S, Sunder-Plassmann R, Richtig E, Fae I, et al. Risk Factors of Subsequent Primary Melanomas in Austria. *JAMA Dermatol* (2019) 155(2):188–95. doi: 10.1001/jamadermatol.2018.4645
2. Reichrath J, Lindqvist PG, Pilz S, Marz W, Grant WB, Holick MF, et al. Sunbeds and Melanoma Risk: Many Open Questions, Not Yet Time to Close the Debate. *Anticancer Res* (2020) 40(1):501–9. doi: 10.21873/anticanres.13978
3. El Ghissassi SF, Baan R, Straif K, Grosse Y, Secretan B, Bouvard V, et al. A Review of Human Carcinogens–Part D: Radiation. *Lancet Oncol* (2009) 10 (8):751–2. doi: 10.1016/S1470-2045(09)70213-X
4. *Cancer Statistic Center* (2020). Available at: https://cancerstatisticscenter.cancer.org/?_ga=2.3063024.1776694736.1587709797-1973017240.1585132932#!/cancer-site/Melanoma%20of%20the%20skin (Accessed 06/03, 2021).
5. *Finnish Cancer Registry* (2021). Available at: https://cancerregistry.fi/statistics/cancer-statistics/ (Accessed 06/03, 2021).
6. Rigel DS. Epidemiology of Melanoma. *Semin Cutan Med Surg* (2010) 29 (4):204–9. doi: 10.1016/j.sder.2010.10.005
7. Lawrence MS, Stojanov P, Polak P, Kryukov GV, Cibulskis K, Sivachenko A, et al. Mutational Heterogeneity in Cancer and the Search for New Cancer-Associated Genes. *Nature* (2013) 499(7457):214–8. doi: 10.1038/nature12213
8. Liu M, Tolg C, Turley E. Dissecting the Dual Nature of Hyaluronan in the Tumor Microenvironment. *Front Immunol* (2019) 10:947. doi: 10.3389/fimmu.2019.00947
9. Avenoso A, Bruschetta G, D'Ascola A, Scuruchi M, Mandraffino G, Gullace R, et al. Hyaluronan Fragments Produced During Tissue Injury: A Signal Amplifying the Inflammatory Response. *Arch Biochem Biophys* (2019) 663:228–38. doi: 10.1016/j.abb.2019.01.015
10. Cowman MK. Hyaluronan and Hyaluronan Fragments. *Adv Carbohydr Chem Biochem* (2017) 74:1–59. doi: 10.1016/bs.accb.2017.10.001
11. Toole BP. Hyaluronan: From Extracellular Glue to Pericellular Cue. *Nat Rev Cancer* (2004) 4(7):528–39. doi: 10.1038/nrc1391
12. Wu M, Cao M, He Y, Liu Y, Yang C, Du Y, et al. A Novel Role of Low Molecular Weight Hyaluronan in Breast Cancer Metastasis. *FASEB J* (2015) 29(4):1290–8. doi: 10.1096/fj.14-259978
13. Auvinen P, Rilla K, Tumelius R, Tammi M, Sironen R, Soini Y, et al. Hyaluronan Synthases (HAS1-3) in Stromal and Malignant Cells Correlate With Breast Cancer Grade and Predict Patient Survival. *Breast Cancer Res Treat* (2014) 143(2):277–86. doi: 10.1007/s10549-013-2804-7
14. Auvinen P, Tammi R, Kosma VM, Sironen R, Soini Y, Mannermaa A, et al. Increased Hyaluronan Content and Stromal Cell CD44 Associate With HER2 Positivity and Poor Prognosis in Human Breast Cancer. *Int J Cancer* (2013) 132(3):531–9. doi: 10.1002/ijc.27707
15. Aaltomaa S, Lipponen P, Tammi R, Tammi M, Viitanen J, Kankkunen JP, et al. Strong Stromal Hyaluronan Expression Is Associated With PSA Recurrence in Local Prostate Cancer. *Urol Int* (2002) 69(4):266–72. doi: 10.1159/000066123
16. Lipponen P, Aaltomaa S, Tammi R, Tammi M, Ågren U, Kosma VM. High Stromal Hyaluronan Level is Associated With Poor Differentiation and Metastasis in Prostate Cancer. *Eur J Cancer* (2001) 37(7):849–56. doi: 10.1016/S0959-8049(00)00448-2
17. Auvinen P, Tammi R, Parkkinen J, Tammi M, Ågren U, Johansson R, et al. Hyaluronan in Peritumoral Stroma and Malignant Cells Associates With Breast Cancer Spreading and Predicts Survival. *Am J Pathol* (2000) 156 (2):529–36. doi: 10.1016/S0002-9440(10)64757-8
18. Siiskonen H, Poukka M, Tyynelä-Korhonen K, Sironen R, Pasonen-Seppänen S. Inverse Expression of Hyaluronidase 2 and Hyaluronan Synthases 1-3 is Associated With Reduced Hyaluronan Content in Malignant Cutaneous Melanoma. *BMC Cancer* (2013) 13:181–2407-13-181. doi: 10.1186/1471-2407-13-181
19. Poukka M, Bykachev A, Siiskonen H, Tyynelä-Korhonen K, Auvinen P, Pasonen-Seppänen S, et al. Decreased Expression of Hyaluronan Synthase 1 and 2 Associates With Poor Prognosis in Cutaneous Melanoma. *BMC Cancer* (2016) 16:313–016-2344-8. doi: 10.1186/s12885-016-2344-8
20. Ciarletta P, Foret L, Ben Amar M. The Radial Growth Phase of Malignant Melanoma: Multi-Phase Modelling, Numerical Simulations and Linear Stability Analysis. *J R Soc Interface* (2011) 8(56):345–68. doi: 10.1098/rsif.2010.0285
21. Prost-Squarcioni C, Fraitag S, Heller M, Boehm N. Functional Histology of Dermis. *Ann Dermatol Venereol* (2008) 135(1 Pt 2):1S5–20. doi: 10.1016/S0151-9638(08)70206-0
22. Montagna W, Kligman AM, Carlisle KS. *Atlas of Normal Human Skin. 1st ed*. New York: Springer-Verlag (1992).
23. Shain AH, Bastian BC. From Melanocytes to Melanomas. *Nat Rev Cancer* (2016) 16(6):345–58. doi: 10.1038/nrc.2016.37
24. Mitra D, Luo X, Morgan A, Wang J, Hoang MP, Lo J, et al. An Ultraviolet-Radiation-Independent Pathway to Melanoma Carcinogenesis in the Red Hair/Fair Skin Background. *Nature* (2012) 491(7424):449–53. doi: 10.1038/nature11624
25. Hong Y, Song B, Chen HD, Gao XH. Melanocytes and Skin Immunity. *J Investig Dermatol Symp Proc* (2015) 17(1):37–9. doi: 10.1038/jidsymp.2015.14
26. Chen H, Weng QY, Fisher DE. UV Signaling Pathways Within the Skin. *J Invest Dermatol* (2014) 134(8):2080–5. doi: 10.1038/jid.2014.161
27. Manga P, Choudhury N. The Unfolded Protein and Integrated Stress Response in Melanoma and Vitiligo. *Pigment Cell Melanoma Res* (2021) 34(2):204–11. doi: 10.1111/pcmr.12947
28. Yardman-Frank JM, Fisher DE. Skin Pigmentation and its Control: From Ultraviolet Radiation to Stem Cells. *Exp Dermatol* (2020) 30(4):560–71. doi: 10.1111/exd.14260
29. Clark W, Elder DE, Guerry D4, Epstein MN, Greene MH, Van Horn M. A Study of Tumor Progression: The Precursor Lesions of Superficial Spreading and Nodular Melanoma. *Hum Pathol* (1984) 15(12):1147–65. doi: 10.1016/S0046-8177(84)80310-X
30. Elder DE, Bastian BC, Cree IA, Massi D, Scolyer RA. The 2018 World Health Organization Classification of Cutaneous, Mucosal, and Uveal Melanoma: Detailed Analysis of 9 Distinct Subtypes Defined by Their Evolutionary Pathway. *Arch Pathol Lab Med* (2020) 144(4):500–22. doi: 10.5858/arpa.2019-0561-RA
31. Bastian BC. The Molecular Pathology of Melanoma: An Integrated Taxonomy of Melanocytic Neoplasia. *Annu Rev Pathol* (2014) 9:239–71. doi: 10.1146/annurev-pathol-012513-104658
32. Sarkar S, Gaddameedhi S. Solar UV-Induced DNA Damage Response: Melanocytes Story in Transformation to Environmental Melanomagenesis. *Environ Mol Mutagen* (2020) 61(7):736–51. doi: 10.1002/em.22370
33. Scolyer RA, Long GV, Thompson JF. Evolving Concepts in Melanoma Classification and Their Relevance to Multidisciplinary Melanoma Patient Care. *Mol Oncol* (2011) 5(2):124–36. doi: 10.1016/j.molonc.2011.03.002
34. Alexandrov LB, Nik-Zainal S, Wedge DC, Aparicio SA, Behjati S, Biankin AV, et al. Signatures of Mutational Processes in Human Cancer. *Nature* (2013) 500(7463):415–21. doi: 10.1038/nature12477
35. Testa U, Castelli G, Pelosi E. Melanoma: Genetic Abnormalities, Tumor Progression, Clonal Evolution and Tumor Initiating Cells. *Med Sci (Basel)* (2017) 5(4):28. doi: 10.3390/medsci5040028
36. Kiuru M, Tartar DM, Qi L, Chen D, Yu L, Konia T, et al. Improving Classification of Melanocytic Nevi: Association of BRAF V600E Expression With Distinct Histomorphologic Features. *J Am Acad Dermatol* (2018) 79 (2):221–9. doi: 10.1016/j.jaad.2018.03.052
37. Poynter JN, Elder JT, Fullen DR, Nair RP, Soengas MS, Johnson TM, et al. BRAF and NRAS Mutations in Melanoma and Melanocytic Nevi. *Melanoma Res* (2006) 16(4):267–73. doi: 10.1097/01.cmr.0000222600.73179.f3
38. Roh MR, Eliades P, Gupta S, Tsao H. Genetics of Melanocytic Nevi. *Pigment Cell Melanoma Res* (2015) 28(6):661–72. doi: 10.1111/pcmr.12412
39. Abdo JF, Sharma A, Sharma R. Role of Heredity in Melanoma Susceptibility: A Primer for the Practicing Surgeon. *Surg Clin North Am* (2020) 100(1):13–28. doi: 10.1016/j.suc.2019.09.006
40. Toussi A, Mans N, Welborn J, Kiuru M. Germline Mutations Predisposing to Melanoma. *J Cutan Pathol* (2020) 47(7):606–16. doi: 10.1111/cup.13689
41. Loercher AE, Tank EM, Delston RB, Harbour JW. MITF Links Differentiation With Cell Cycle Arrest in Melanocytes by Transcriptional Activation of INK4A. *J Cell Biol* (2005) 168(1):35–40. doi: 10.1083/jcb.200410115
42. Du J, Widlund HR, Horstmann MA, Ramaswamy S, Ross K, Huber WE, et al. Critical Role of CDK2 for Melanoma Growth Linked to its Melanocyte-

Specific Transcriptional Regulation by MITF. *Cancer Cell* (2004) 6(6):565–76. doi: 10.1016/j.ccr.2004.10.014
43. Yokoyama S, Woods SL, Boyle GM, Aoude LG, MacGregor S, Zismann V, et al. A Novel Recurrent Mutation in MITF Predisposes to Familial and Sporadic Melanoma. *Nature* (2011) 480(7375):99–103. doi: 10.1038/nature10630
44. Day CP, Marchalik R, Merlino G, Michael H. Mouse Models of UV-Induced Melanoma: Genetics, Pathology, and Clinical Relevance. *Lab Invest* (2017) 97(6):698–705. doi: 10.1038/labinvest.2016.155
45. Emri G, Paragh G, Tosaki A, Janka E, Kollar S, Hegedus C, et al. Ultraviolet Radiation-Mediated Development of Cutaneous Melanoma: An Update. *J Photochem Photobiol B* (2018) 185:169–75. doi: 10.1016/j.jphotobiol.2018.06.005
46. Heldin P, Lin CY, Kolliopoulos C, Chen YH, Skandalis SS. Regulation of Hyaluronan Biosynthesis and Clinical Impact of Excessive Hyaluronan Production. *Matrix Biol* (2019) 78-79:100–17. doi: 10.1016/j.matbio.2018.01.017
47. Leonardi GC, Falzone L, Salemi R, Zanghi A, Spandidos DA, Mccubrey JA, et al. Cutaneous Melanoma: From Pathogenesis to Therapy (Review). *Int J Oncol* (2018) 52(4):1071–80. doi: 10.3892/ijo.2018.4287
48. Jokinen E, Koivunen JP. MEK and PI3K Inhibition in Solid Tumors: Rationale and Evidence to Date. *Ther Adv Med Oncol* (2015) 7(3):170–80. doi: 10.1177/1758834015571111
49. Ross MI, Gershenwald JE. Evidence-Based Treatment of Early-Stage Melanoma. *J Surg Oncol* (2011) 104(4):341–53. doi: 10.1002/jso.21962
50. Rastrelli M, Tropea S, Rossi CR, Alaibac M. Melanoma: Epidemiology, Risk Factors, Pathogenesis, Diagnosis and Classification. *In Vivo* (2014) 28 (6):1005–11.
51. Lideikaite A, Mozuraitiene J, Letautiene S. Analysis of Prognostic Factors for Melanoma Patients. *Acta Med Litu* (2017) 24(1):25–34. doi: 10.6001/actamedica.v24i1.3460
52. Gilchrest BA. Sun Exposure and Vitamin D Sufficiency. *Am J Clin Nutr* (2008) 88(2):570S–7S. doi: 10.1093/ajcn/88.2.570S
53. Mignogna C, Scali E, Camastra C, Presta I, Zeppa P, Barni T, et al. Innate Immunity in Cutaneous Melanoma. *Clin Exp Dermatol* (2017) 42(3):243–50. doi: 10.1111/ced.13023
54. Kim SI, Pfeifer GP. The Epigenetic DNA Modification 5-Carboxylcytosine Promotes High Levels of Cyclobutane Pyrimidine Dimer Formation Upon UVB Irradiation. *Genome Instab Dis* (2021) 2(1):59–69. doi: 10.1007/s42764-020-00030-x
55. de Jager TL, Cockrell AE, Du Plessis SS. Ultraviolet Light Induced Generation of Reactive Oxygen Species. *Adv Exp Med Biol* (2017) 996:15–23. doi: 10.1007/978-3-319-56017-5_2
56. Hadas R, Gershon E, Cohen A, Atrakchi O, Lazar S, Golani O, et al. Hyaluronan Control of the Primary Vascular Barrier During Early Mouse Pregnancy is Mediated by Uterine NK Cells. *JCI Insight* (2020) 5(22): e135775. doi: 10.1172/jci.insight.135775
57. Xin Y, Xu P, Wang X, Chen Y, Zhang Z, Zhang Y. Human Foreskin-Derived Dermal Stem/Progenitor Cell-Conditioned Medium Combined With Hyaluronic Acid Promotes Extracellular Matrix Regeneration in Diabetic Wounds. *Stem Cell Res Ther* (2021) 12(1):49–020-02116-5. doi: 10.1186/s13287-020-02116-5
58. Parkes WS, Amargant F, Zhou LT, Villanueva CE, Duncan FE, Pritchard MT. Hyaluronan and Collagen Are Prominent Extracellular Matrix Components in Bovine and Porcine Ovaries. *Genes (Basel)* (2021) 12 (8):1186. doi: 10.3390/genes12081186
59. Knudson CB. Hyaluronan Receptor-Directed Assembly of Chondrocyte Pericellular Matrix. *J Cell Biol* (1993) 120(3):825–34. doi: 10.1083/jcb.120.3.825
60. Goldberg RL, Toole BP. Pericellular Coat of Chick Embryo Chondrocytes: Structural Role of Hyaluronate. *J Cell Biol* (1984) 99(6):2114–22. doi: 10.1083/jcb.99.6.2114
61. Ludwig TE, Hunter MM, Schmidt TA. Cartilage Boundary Lubrication Synergism is Mediated by Hyaluronan Concentration and PRG4 Concentration and Structure. *BMC Musculoskelet Disord* (2015) 16:386–015-0842-5. doi: 10.1186/s12891-015-0842-5
62. Schmidt TA, Gastelum NS, Nguyen QT, Schumacher BL, Sah RL. Boundary Lubrication of Articular Cartilage: Role of Synovial Fluid Constituents. *Arthritis Rheum* (2007) 56(3):882–91. doi: 10.1002/art.22446
63. Tolg C, Yuan H, Flynn SM, Basu K, Ma J, Tse KCK, et al. Hyaluronan Modulates Growth Factor Induced Mammary Gland Branching in a Size Dependent Manner. *Matrix Biol* (2017) 63:117–32. doi: 10.1016/j.matbio.2017.02.003
64. Weigel PH. Hyaluronan Synthase: The Mechanism of Initiation at the Reducing End and a Pendulum Model for Polysaccharide Translocation to the Cell Exterior. *Int J Cell Biol* (2015) 2015:367579. doi: 10.1155/2015/367579
65. Ontong P, Hatada Y, Taniguchi S, Kakizaki I, Itano N. Effect of a Cholesterol-Rich Lipid Environment on the Enzymatic Activity of Reconstituted Hyaluronan Synthase. *Biochem Biophys Res Commun* (2014) 443(2):666–71. doi: 10.1016/j.bbrc.2013.12.028
66. Passi A, Vigetti D, Buraschi S, Iozzo RV. Dissecting the Role of Hyaluronan Synthases in the Tumor Microenvironment. *FEBS J* (2019) 286(15):2937–49. doi: 10.1111/febs.14847
67. Vigetti D, Genasetti A, Karousou E, Viola M, Clerici M, Bartolini B, et al. Modulation of Hyaluronan Synthase Activity in Cellular Membrane Fractions. *J Biol Chem* (2009) 284(44):30684–94. doi: 10.1074/jbc.M109.040386
68. Wang A, Hascall VC. Hyperglycemia, Intracellular Hyaluronan Synthesis, Cyclin D3 and Autophagy. *Autophagy* (2009) 5(6):864–5. doi: 10.4161/auto.9041
69. Rilla K, Siiskonen H, Spicer AP, Hyttinen JM, Tammi MI, Tammi RH. Plasma Membrane Residence of Hyaluronan Synthase is Coupled to its Enzymatic Activity. *J Biol Chem* (2005) 280(36):31890–7. doi: 10.1074/jbc.M504736200
70. Kobayashi T, Chanmee T, Itano N. Hyaluronan: Metabolism and Function. *Biomolecules* (2020) 10(11):1525. doi: 10.3390/biom10111525
71. Stern R, Jedrzejas MJ. Hyaluronidases: Their Genomics, Structures, and Mechanisms of Action. *Chem Rev* (2006) 106(3):818–39. doi: 10.1021/cr050247k
72. Deguine V, Menasche M, Fraisse L, Ferrari P, Pouliquen Y, Robert L. Determination of Extracellular Matrix Degradation by Free Radicals Using Viscosity Measurement of Hyaluronan. *Clin Chim Acta* (1997) 262(1-2):147–52. doi: 10.1016/S0009-8981(97)06545-5
73. Schmut O, Ansari AN, Faulborn J. Degradation of Hyaluronate by the Concerted Action of Ozone and Sunlight. *Ophthalmic Res* (1994) 26(6):340–3. doi: 10.1159/000267499
74. Tobisawa Y, Fujita N, Yamamoto H, Ohyama C, Irie F, Yamaguchi Y. The Cell Surface Hyaluronidase TMEM2 is Essential for Systemic Hyaluronan Catabolism and Turnover. *J Biol Chem* (2021) 297(5):101281. doi: 10.1016/j.jbc.2021.101281
75. Yoshida H, Okada Y. Role of HYBID (Hyaluronan Binding Protein Involved in Hyaluronan Depolymerization), Alias KIAA1199/CEMIP, in Hyaluronan Degradation in Normal and Photoaged Skin. *Int J Mol Sci* (2019) 20 (22):5804. doi: 10.3390/ijms20225804
76. Yamamoto H, Tobisawa Y, Inubushi T, Irie F, Ohyama C, Yamaguchi Y. A Mammalian Homolog of the Zebrafish Transmembrane Protein 2 (TMEM2) is the Long-Sought-After Cell-Surface Hyaluronidase. *J Biol Chem* (2017) 292(18):7304–13. doi: 10.1074/jbc.M116.770149
77. Avenoso A, D'Ascola A, Scuruchi M, Mandraffino G, Calatroni A, Saitta A, et al. Hyaluronan in Experimental Injured/Inflamed Cartilage: *In Vivo* Studies. *Life Sci* (2018) 193:132–40. doi: 10.1016/j.lfs.2017.11.006
78. Soroosh A, Albeiroti S, West GA, Willard B, Fiocchi C, de la Motte CA. Crohn's Disease Fibroblasts Overproduce the Novel Protein KIAA1199 to Create Proinflammatory Hyaluronan Fragments. *Cell Mol Gastroenterol Hepatol* (2016) 2(3):358–68. doi: 10.1016/j.jcmgh.2015.12.007
79. Tolg C, Telmer P, Turley E. Specific Sizes of Hyaluronan Oligosaccharides Stimulate Fibroblast Migration and Excisional Wound Repair. *PLoS One* (2014) 9(2):e88479. doi: 10.1371/journal.pone.0088479
80. Cui X, Xu H, Zhou S, Zhao T, Liu A, Guo X, et al. Evaluation of Angiogenic Activities of Hyaluronan Oligosaccharides of Defined Minimum Size. *Life Sci* (2009) 85(15-16):573–7. doi: 10.1016/j.lfs.2009.08.010
81. Termeer CC, Hennies J, Voith U, Ahrens T, Weiss JM, Prehm P, et al. Oligosaccharides of Hyaluronan are Potent Activators of Dendritic Cells. *J Immunol* (2000) 165(4):1863–70. doi: 10.4049/jimmunol.165.4.1863
82. Queisser KA, Mellema RA, Middleton EA, Portier I, Manne BK, Denorme F, et al. COVID-19 Generates Hyaluronan Fragments That Directly Induce

Endothelial Barrier Dysfunction. *JCI Insight* (2021) 6(17):e147472. doi: 10.1172/jci.insight.147472
83. Liang J, Jiang D, Noble PW. Hyaluronan as a Therapeutic Target in Human Diseases. *Adv Drug Deliv Rev* (2016) 97:186–203. doi: 10.1016/j.addr.2015.10.017
84. Dominguez-Gutierrez PR, Kwenda EP, Donelan W, O'Malley P, Crispen PL, Kusmartsev S. Hyal2 Expression in Tumor-Associated Myeloid Cells Mediates Cancer-Related Inflammation in Bladder Cancer. *Cancer Res* (2021) 81(3):648–57. doi: 10.1158/0008-5472.CAN-20-1144
85. Itano N, Sawai T, Yoshida M, Lenas P, Yamada Y, Imagawa M, et al. Three Isoforms of Mammalian Hyaluronan Synthases Have Distinct Enzymatic Properties. *J Biol Chem* (1999) 274(35):25085–92. doi: 10.1074/jbc.274.35.25085
86. Baggenstoss BA, Harris EN, Washburn JL, Medina AP, Nguyen L, Weigel PH. Hyaluronan Synthase Control of Synthesis Rate and Hyaluronan Product Size are Independent Functions Differentially Affected by Mutations in a Conserved Tandem B-X7-B Motif. *Glycobiology* (2017) 27(2):154–64. doi: 10.1093/glycob/cww089
87. Hiltunen EL, Anttila M, Kultti A, Ropponen K, Penttinen J, Yliskoski M, et al. Elevated Hyaluronan Concentration Without Hyaluronidase Activation in Malignant Epithelial Ovarian Tumors. *Cancer Res* (2002) 62(22):6410–3.
88. Anttila MA, Tammi RH, Tammi MI, Syrjanen KJ, Saarikoski SV, Kosma VM. High Levels of Stromal Hyaluronan Predict Poor Disease Outcome in Epithelial Ovarian Cancer. *Cancer Res* (2000) 60(1):150–5.
89. Rizzardi AE, Vogel RI, Koopmeiners JS, Forster CL, Marston LO, Rosener NK, et al. Elevated Hyaluronan and Hyaluronan-Mediated Motility Receptor are Associated With Biochemical Failure in Patients With Intermediate-Grade Prostate Tumors. *Cancer* (2014) 120(12):1800–9. doi: 10.1002/cncr.28646
90. Tahkola K, Ahtiainen M, Mecklin JP, Kellokumpu I, Laukkarinen J, Tammi M, et al. Stromal Hyaluronan Accumulation is Associated With Low Immune Response and Poor Prognosis in Pancreatic Cancer. *Sci Rep* (2021) 11(1):12216–021-91796-x. doi: 10.1038/s41598-021-91796-x
91. Setälä LP, Tammi MI, Tammi RH, Eskelinen MJ, Lipponen PK, Ågren UM, et al. Hyaluronan Expression in Gastric Cancer Cells is Associated With Local and Nodal Spread and Reduced Survival Rate. *Br J Cancer* (1999) 79(7-8):1133–8. doi: 10.1038/sj.bjc.6690180
92. Ropponen K, Tammi M, Parkkinen J, Eskelinen M, Tammi R, Lipponen P, et al. Tumor Cell-Associated Hyaluronan as an Unfavorable Prognostic Factor in Colorectal Cancer. *Cancer Res* (1998) 58(2):342–7.
93. Schmaus A, Klusmeier S, Rothley M, Dimmler A, Sipos B, Faller G, et al. Accumulation of Small Hyaluronan Oligosaccharides in Tumour Interstitial Fluid Correlates With Lymphatic Invasion and Lymph Node Metastasis. *Br J Cancer* (2014) 111(3):559–67. doi: 10.1038/bjc.2014.332
94. Takabe P, Kärnä R, Rauhala L, Tammi M, Tammi R, Pasonen-Seppänen S. Melanocyte Hyaluronan Coat Fragmentation Enhances the UVB-Induced TLR-4 Receptor Signaling and Expression of Proinflammatory Mediators IL-6, IL-8, CXCL-1 and CXCL-10 *via* NF-kappaB Activation. *J Invest Dermatol* (2019) 139(9):1993–2003.e4. doi: 10.1016/j.jid.2019.03.1135
95. Karjalainen JM, Tammi RH, Tammi MI, Eskelinen MJ, Ågren UM, Parkkinen JJ, et al. Reduced Level of CD44 and Hyaluronan Associated With Unfavorable Prognosis in Clinical Stage I Cutaneous Melanoma. *Am J Pathol* (2000) 157(3):957–65. doi: 10.1016/S0002-9440(10)64608-1
96. Siiskonen H, Törrönen K, Kumlin T, Rilla K, Tammi MI, Tammi RH. Chronic UVR Causes Increased Immunostaining of CD44 and Accumulation of Hyaluronan in Mouse Epidermis. *J Histochem Cytochem* (2011) 59(10):908–17. doi: 10.1369/0022155411417874
97. Rauhala L, Hämäläinen L, Salonen P, Bart G, Tammi M, Pasonen-Seppänen S, et al. Low Dose Ultraviolet B Irradiation Increases Hyaluronan Synthesis in Epidermal Keratinocytes *via* Sequential Induction of Hyaluronan Synthases Has1-3 Mediated by P38 and Ca2+/calmodulin-Dependent Protein Kinase II (CaMKII) Signaling. *J Biol Chem* (2013) 288(25):17999–8012. doi: 10.1074/jbc.M113.472530
98. Averbeck M, Gebhardt CA, Voigt S, Beilharz S, Anderegg U, Termeer CC, et al. Differential Regulation of Hyaluronan Metabolism in the Epidermal and Dermal Compartments of Human Skin by UVB Irradiation. *J Invest Dermatol* (2007) 127(3):687–97. doi: 10.1038/sj.jid.5700614
99. Tzellos TG, Klagas I, Vahtsevanos K, Triaridis S, Printza A, Kyrgidis A, et al. Extrinsic Ageing in the Human Skin is Associated With Alterations in the Expression of Hyaluronic Acid and its Metabolizing Enzymes. *Exp Dermatol* (2009) 18(12):1028–35. doi: 10.1111/j.1600-0625.2009.00889.x
100. Halliday GM. Inflammation, Gene Mutation and Photoimmunosuppression in Response to UVR-Induced Oxidative Damage Contributes to Photocarcinogenesis. *Mutat Res* (2005) 571(1-2):107–20. doi: 10.1016/j.mrfmmm.2004.09.013
101. Uchiyama H, Dobashi Y, Ohkouchi K, Nagasawa K. Chemical Change Involved in the Oxidative Reductive Depolymerization of Hyaluronic Acid. *J Biol Chem* (1990) 265(14):7753–9. doi: 10.1016/S0021-9258(19)38993-8
102. Krasinski R, Tchorzewski H, Lewkowicz P. Antioxidant Effect of Hyaluronan on Polymorphonuclear Leukocyte-Derived Reactive Oxygen Species is Dependent on its Molecular Weight and Concentration and Mainly Involves the Extracellular Space. *Postepy Hig Med Dosw (Online)* (2009) 63:205–12.
103. Soltes L, Mendichi R, Kogan G, Schiller J, Stankovska M, Arnhold J. Degradative Action of Reactive Oxygen Species on Hyaluronan. *Biomacromolecules* (2006) 7(3):659–68. doi: 10.1021/bm050867v
104. Pasonen-Seppänen S, Takabe P, Edward M, Rauhala L, Rilla K, Tammi M, et al. Melanoma Cell-Derived Factors Stimulate Hyaluronan Synthesis in Dermal Fibroblasts by Upregulating HAS2 Through PDGFR-PI3K-AKT and P38 Signaling. *Histochem Cell Biol* (2012) 138(6):895–911. doi: 10.1007/s00418-012-1000-x
105. Wight TN, Frevert CW, Debley JS, Reeves SR, Parks WC, Ziegler SF. Interplay of Extracellular Matrix and Leukocytes in Lung Inflammation. *Cell Immunol* (2017) 312:1–14. doi: 10.1016/j.cellimm.2016.12.003
106. Petrey AC, de la Motte CA. Hyaluronan, a Crucial Regulator of Inflammation. *Front Immunol* (2014) 5:101. doi: 10.3389/fimmu.2014.00101
107. Tavianatou AG, Caon I, Franchi M, Piperigkou Z, Galesso D, Karamanos NK. Hyaluronan: Molecular Size-Dependent Signaling and Biological Functions in Inflammation and Cancer. *FEBS J* (2019) 286(15):2883–908. doi: 10.1111/febs.14777
108. Vistejnova L, Safrankova B, Nesporova K, Slavkovsky R, Hermannova M, Hosek P, et al. Low Molecular Weight Hyaluronan Mediated CD44 Dependent Induction of IL-6 and Chemokines in Human Dermal Fibroblasts Potentiates Innate Immune Response. *Cytokine* (2014) 70(2):97–103. doi: 10.1016/j.cyto.2014.07.006
109. Schwertfeger KL, Cowman MK, Telmer PG, Turley EA, McCarthy JB. Hyaluronan, Inflammation, and Breast Cancer Progression. *Front Immunol* (2015) 6:236. doi: 10.3389/fimmu.2015.00236
110. Voelcker V, Gebhardt C, Averbeck M, Saalbach A, Wolf V, Weih F, et al. Hyaluronan Fragments Induce Cytokine and Metalloprotease Upregulation in Human Melanoma Cells in Part by Signalling *via* TLR4. *Exp Dermatol* (2008) 17(2):100–7. doi: 10.1111/j.1600-0625.2007.00638.x
111. Mummert ME, Mummert D, Edelbaum D, Hui F, Matsue H, Takashima A. Synthesis and Surface Expression of Hyaluronan by Dendritic Cells and its Potential Role in Antigen Presentation. *J Immunol* (2002) 169(8):4322–31. doi: 10.4049/jimmunol.169.8.4322
112. Hašová M, Crhák T, Šafránková B, Dvořaková J, Muthný T, Velebný V, et al. Hyaluronan Minimizes Effects of UV Irradiation on Human Keratinocytes. *Arch Dermatol Res* (2011) 303(4):277–84. doi: 10.1007/s00403-011-1146-8
113. Muto J, Sayama K, Gallo RL, Kimata K. Emerging Evidence for the Essential Role of Hyaluronan in Cutaneous Biology. *J Dermatol Sci* (2019) 94(1):190–5. doi: 10.1016/j.jdermsci.2019.01.009
114. Rayahin JE, Buhrman JS, Zhang Y, Koh TJ, Gemeinhart RA. High and Low Molecular Weight Hyaluronic Acid Differentially Influence Macrophage Activation. *ACS Biomater Sci Eng* (2015) 1(7):481–93. doi: 10.1021/acsbiomaterials.5b00181
115. Pieniazek M, Matkowski R, Donizy P. Macrophages in Skin Melanoma-the Key Element in Melanomagenesis. *Oncol Lett* (2018) 15(4):5399–404. doi: 10.3892/ol.2018.8021
116. Wang T, Herlyn M. The Macrophage: A New Factor in UVR-Induced Melanomagenesis. *J Invest Dermatol* (2013) 133(7):1711–3. doi: 10.1038/jid.2013.93
117. Chanmee T, Ontong P, Konno K, Itano N. Tumor-Associated Macrophages as Major Players in the Tumor Microenvironment. *Cancers (Basel)* (2014) 6(3):1670–90. doi: 10.3390/cancers6031670

118. Zhang B, Du Y, He Y, Liu Y, Zhang G, Yang C, et al. INT-HA Induces M2-Like Macrophage Differentiation of Human Monocytes *via* TLR4-miR-935 Pathway. *Cancer Immunol Immunother* (2019) 68(2):189–200. doi: 10.1007/s00262-018-2261-6
119. Sokolowska M, Chen LY, Eberlein M, Martinez-Anton A, Liu Y, Alsaaty S, et al. Low Molecular Weight Hyaluronan Activates Cytosolic Phospholipase A2alpha and Eicosanoid Production in Monocytes and Macrophages. *J Biol Chem* (2014) 289(7):4470–88. doi: 10.1074/jbc.M113.515106
120. Black KE, Collins SL, Hagan RS, Hamblin MJ, Chan-Li Y, Hallowell RW, et al. Hyaluronan Fragments Induce IFNbeta *via* a Novel TLR4-TRIF-TBK1-IRF3-Dependent Pathway. *J Inflammation (Lond)* (2013) 10(1):23. doi: 10.1186/1476-9255-10-23
121. Willenberg A, Saalbach A, Simon JC, Anderegg U. Melanoma Cells Control HA Synthesis in Peritumoral Fibroblasts *via* PDGF-AA and PDGF-CC: Impact on Melanoma Cell Proliferation. *J Invest Dermatol* (2012) 132 (2):385–93. doi: 10.1038/jid.2011.325
122. Sapudom J, Nguyen KT, Martin S, Wippold T, Moller S, Schnabelrauch M, et al. Biomimetic Tissue Models Reveal the Role of Hyaluronan in Melanoma Proliferation and Invasion. *Biomater Sci* (2020) 8(5):1405–17. doi: 10.1039/C9BM01636H
123. Du Y, Cao M, Liu Y, He Y, Yang C, Wu M, et al. Low-Molecular-Weight Hyaluronan (LMW-HA) Accelerates Lymph Node Metastasis of Melanoma Cells by Inducing Disruption of Lymphatic Intercellular Adhesion. *Oncoimmunology* (2016) 5(11):e1232235. doi: 10.1080/2162402X.2016.1232235
124. Sapudom J, Ullm F, Martin S, Kalbitzer L, Naab J, Moller S, et al. Molecular Weight Specific Impact of Soluble and Immobilized Hyaluronan on CD44 Expressing Melanoma Cells in 3D Collagen Matrices. *Acta Biomater* (2017) 50:259–70. doi: 10.1016/j.actbio.2016.12.026
125. Tian X, Azpurua J, Hine C, Vaidya A, Myakishev-Rempel M, Ablaeva J, et al. High-Molecular-Mass Hyaluronan Mediates the Cancer Resistance of the Naked Mole Rat. *Nature* (2013) 499(7458):346–9. doi: 10.1038/nature12234
126. Eiro N, Ovies C, Fernandez-Garcia B, Alvarez-Cuesta CC, Gonzalez L, Gonzalez LO, et al. Expression of TLR3, 4, 7 and 9 in Cutaneous Malignant Melanoma: Relationship With Clinicopathological Characteristics and Prognosis. *Arch Dermatol Res* (2013) 305(1):59–67. doi: 10.1007/s00403-012-1300-y
127. Dickinson SE, Wondrak GT. TLR4 in Skin Cancer: From Molecular Mechanisms to Clinical Interventions. *Mol Carcinog* (2019) 58(7):1086–93. doi: 10.1002/mc.23016
128. Caon I, Bartolini B, Parnigoni A, Carava E, Moretto P, Viola M, et al. Revisiting the Hallmarks of Cancer: The Role of Hyaluronan. *Semin Cancer Biol* (2020) 62:9–19. doi: 10.1016/j.semcancer.2019.07.007
129. Henke E, Nandigama R, Ergun S. Extracellular Matrix in the Tumor Microenvironment and Its Impact on Cancer Therapy. *Front Mol Biosci* (2020) 6:160. doi: 10.3389/fmolb.2019.00160
130. Junttila MR, de Sauvage FJ. Influence of Tumour Micro-Environment Heterogeneity on Therapeutic Response. *Nature* (2013) 501(7467):346–54. doi: 10.1038/nature12626
131. Antohe M, Nedelcu RI, Nichita L, Popp CG, Cioplea M, Brinzea A, et al. Tumor Infiltrating Lymphocytes: The Regulator of Melanoma Evolution. *Oncol Lett* (2019) 17(5):4155–61. doi: 10.3892/ol.2019.9940
132. Taylor RC, Patel A, Panageas KS, Busam KJ, Brady MS. Tumor-Infiltrating Lymphocytes Predict Sentinel Lymph Node Positivity in Patients With Cutaneous Melanoma. *J Clin Oncol* (2007) 25(7):869–75. doi: 10.1200/JCO.2006.08.9755
133. Spatz A, Gimotty PA, Cook MG, van den Oord JJ, Desai N, Eggermont AM, et al. Protective Effect of a Brisk Tumor Infiltrating Lymphocyte Infiltrate in Melanoma: An EORTC Melanoma Group Study. *2007 ASCO Annu Meeting Proceedings: J Clin Oncol* (2007) 25(18_suppl):8519. doi: 10.1200/jco.2007.25.18
134. Lee N, Zakka LR, Mihm MC, Schatton T. Tumour-Infiltrating Lymphocytes in Melanoma Prognosis and Cancer Immunotherapy. *Pathology* (2016) 48 (2):177–87. doi: 10.1016/j.pathol.2015.12.006
135. Fu Q, Chen N, Ge C, Li R, Li Z, Zeng B, et al. Prognostic Value of Tumor-Infiltrating Lymphocytes in Melanoma: A Systematic Review and Meta-Analysis. *Oncoimmunology* (2019) 8(7):1593806. doi: 10.1080/2162402X.2019.1593806
136. Erdag G, Schaefer JT, Smolkin ME, Deacon DH, Shea SM, Dengel LT, et al. Immunotype and Immunohistologic Characteristics of Tumor-Infiltrating Immune Cells are Associated With Clinical Outcome in Metastatic Melanoma. *Cancer Res* (2012) 72(5):1070–80. doi: 10.1158/0008-5472.CAN-11-3218
137. Clark WHJr, Elder DE, Guerry D4, Braitman LE, Trock BJ, Schultz D, et al. Model Predicting Survival in Stage I Melanoma Based on Tumor Progression. *J Natl Cancer Inst* (1989) 81(24):1893–904. doi: 10.1093/jnci/81.24.1893
138. Cassetta L, Kitamura T. Macrophage Targeting: Opening New Possibilities for Cancer Immunotherapy. *Immunology* (2018) 155(3):285–93. doi: 10.1111/imm.12976
139. Cho U, Kim B, Kim S, Han Y, Song YS. Pro-Inflammatory M1 Macrophage Enhances Metastatic Potential of Ovarian Cancer Cells Through NF-kappaB Activation. *Mol Carcinog* (2018) 57(2):235–42. doi: 10.1002/mc.22750
140. Song W, Thakor P, Vesey DA, Gobe GC, Morais C. Conditioned Medium From Stimulated Macrophages Inhibits Growth But Induces an Inflammatory Phenotype in Breast Cancer Cells. *BioMed Pharmacother* (2018) 106:247–54. doi: 10.1016/j.biopha.2018.06.126
141. Kitamura T, Qian BZ, Pollard JW. Immune Cell Promotion of Metastasis. *Nat Rev Immunol* (2015) 15(2):73–86. doi: 10.1038/nri3789
142. Okazaki T, Honjo T. PD-1 and PD-1 Ligands: From Discovery to Clinical Application. *Int Immunol* (2007) 19(7):813–24. doi: 10.1093/intimm/dxm057
143. Patel SP, Kurzrock R. PD-L1 Expression as a Predictive Biomarker in Cancer Immunotherapy. *Mol Cancer Ther* (2015) 14(4):847–56. doi: 10.1158/1535-7163.MCT-14-0983
144. Zou W, Wolchok JD, Chen L. PD-L1 (B7-H1) and PD-1 Pathway Blockade for Cancer Therapy: Mechanisms, Response Biomarkers, and Combinations. *Sci Transl Med* (2016) 8(328):328rv4. doi: 10.1126/scitranslmed.aad7118
145. Oishi S, Takano R, Tamura S, Tani S, Iwaizumi M, Hamaya Y, et al. M2 Polarization of Murine Peritoneal Macrophages Induces Regulatory Cytokine Production and Suppresses T-Cell Proliferation. *Immunology* (2016) 149(3):320–8. doi: 10.1111/imm.12647
146. Salmi S, Siiskonen H, Sironen R, Tyynelä-Korhonen K, Hirschovits-Gerz B, Valkonen M, et al. The Number and Localization of CD68+ and CD163+ Macrophages in Different Stages of Cutaneous Melanoma. *Melanoma Res* (2019) 29(3):237–47. doi: 10.1097/CMR.0000000000000522
147. Shi Q, Zhao L, Xu C, Zhang L, Zhao H. High Molecular Weight Hyaluronan Suppresses Macrophage M1 Polarization and Enhances IL-10 Production in PM2.5-Induced Lung Inflammation. *Molecules* (2019) 24(9):1766. doi: 10.3390/molecules24091766
148. Kim H, Cha J, Jang M, Kim P. Hyaluronic Acid-Based Extracellular Matrix Triggers Spontaneous M2-Like Polarity of Monocyte/Macrophage. *Biomater Sci* (2019) 7(6):2264–71. doi: 10.1039/C9BM00155G
149. Wu H, Zhang X, Han D, Cao J, Tian J. Tumour-Associated Macrophages Mediate the Invasion and Metastasis of Bladder Cancer Cells Through CXCL8. *PeerJ* (2020) 8:e8721. doi: 10.7717/peerj.8721
150. Eyre R, Alférez DG, Santiago-Gómez A, Spence K, McConnell JC, Hart C, et al. Microenvironmental IL1beta Promotes Breast Cancer Metastatic Colonisation in the Bone *via* Activation of Wnt Signalling. *Nat Commun* (2019) 10(1):5016. doi: 10.1038/s41467-019-12807-0
151. Brenner D, Blaser H, Mak TW. Regulation of Tumour Necrosis Factor Signalling: Live or Let Die. *Nat Rev Immunol* (2015) 15(6):362–74. doi: 10.1038/nri3834
152. Poltavets V, Kochetkova M, Pitson SM, Samuel MS. The Role of the Extracellular Matrix and Its Molecular and Cellular Regulators in Cancer Cell Plasticity. *Front Oncol* (2018) 8:431. doi: 10.3389/fonc.2018.00431
153. Hui L, Chen Y. Tumor Microenvironment: Sanctuary of the Devil. *Cancer Lett* (2015) 368(1):7–13. doi: 10.1016/j.canlet.2015.07.039
154. Naba A, Clauser KR, Hoersch S, Liu H, Carr SA, Hynes RO. The Matrisome: In Silico Definition and In Vivo Characterization by Proteomics of Normal and Tumor Extracellular Matrices. *Mol Cell Proteomics* (2012) 11(4): M111.014647. doi: 10.1074/mcp.M111.014647
155. Botti G, Cerrone M, Scognamiglio G, Anniciello A, Ascierto PA, Cantile M. Microenvironment and Tumor Progression of Melanoma: New Therapeutic Prospectives. *J Immunotoxicol* (2013) 10(3):235–52. doi: 10.3109/1547691X.2012.723767

156. Pickup MW, Mouw JK, Weaver VM. The Extracellular Matrix Modulates the Hallmarks of Cancer. *EMBO Rep* (2014) 15(12):1243–53. doi: 10.15252/embr.201439246
157. Li Y, Fanous MJ, Kilian KA, Popescu G. Quantitative Phase Imaging Reveals Matrix Stiffness-Dependent Growth and Migration of Cancer Cells. *Sci Rep* (2019) 9(1):248–018-36551-5. doi: 10.1038/s41598-018-36551-5
158. D'Aguanno S, Mallone F, Marenco M, Del Bufalo D, Moramarco A. Hypoxia-Dependent Drivers of Melanoma Progression. *J Exp Clin Cancer Res* (2021)f 40(1):159–021-01926-6. doi: 10.1186/s13046-021-01926-6
159. Dratkiewicz E, Simiczyjew A, Mazurkiewicz J, Zietek M, Matkowski R, Nowak D. Hypoxia and Extracellular Acidification as Drivers of Melanoma Progression and Drug Resistance. *Cells* (2021) 10(4):862. doi: 10.3390/cells10040862
160. Bedogni B, Powell MB. Hypoxia, Melanocytes and Melanoma - Survival and Tumor Development in the Permissive Microenvironment of the Skin. *Pigment Cell Melanoma Res* (2009) 22(2):166–74. doi: 10.1111/j.1755-148X.2009.00553.x
161. Frey K, Fiechter M, Schwager K, Belloni B, Barysch MJ, Neri D, et al. Different Patterns of Fibronectin and Tenascin-C Splice Variants Expression in Primary and Metastatic Melanoma Lesions. *Exp Dermatol* (2011) 20 (8):685–8. doi: 10.1111/j.1600-0625.2011.01314.x
162. Smetsers TF, van de Westerlo EM, ten Dam GB, Clarijs R, Versteeg EM, van Geloof WL, et al. Localization and Characterization of Melanoma-Associated Glycosaminoglycans: Differential Expression of Chondroitin and Heparan Sulfate Epitopes in Melanoma. *Cancer Res* (2003) 63(11):2965–70.
163. Mayorca-Guiliani AE, Madsen CD, Cox TR, Horton ER, Venning FA, Erler JT. ISDoT: In *Situ* Decellularization of Tissues for High-Resolution Imaging and Proteomic Analysis of Native Extracellular Matrix. *Nat Med* (2017) 23 (7):890–8. doi: 10.1038/nm.4352
164. Smart JA, Oleksak JE, Hartsough EJ. Cell Adhesion Molecules in Plasticity and Metastasis. *Mol Cancer Res* (2021) 19(1):25–37. doi: 10.1158/1541-7786.MCR-20-0595
165. Dilshat R, Fock V, Kenny C, Gerritsen I, Lasseur RMJ, Travnickova J, et al. MITF Reprograms the Extracellular Matrix and Focal Adhesion in Melanoma. *Elife* (2021) 10:e63093. doi: 10.7554/eLife.63093
166. Tammi MI, Oikari S, Pasonen-Seppänen S, Rilla K, Auvinen P, Tammi RH. Activated Hyaluronan Metabolism in the Tumor Matrix - Causes and Consequences. *Matrix Biol* (2019) 78–79:147–64. doi: 10.1016/j.matbio.2018.04.012
167. Bennett MF, Robinson MK, Baron ED, Cooper KD. Skin Immune Systems and Inflammation: Protector of the Skin or Promoter of Aging? *J Investig Dermatol Symp Proc* (2008) 13(1):15–9. doi: 10.1038/jidsymp.2008.3
168. Villanueva J, Herlyn M. Melanoma and the Tumor Microenvironment. *Curr Oncol Rep* (2008) 10(5):439–46. doi: 10.1007/s11912-008-0067-y
169. Zhou L, Yang K, Andl T, Wickett RR, Zhang Y. Perspective of Targeting Cancer-Associated Fibroblasts in Melanoma. *J Cancer* (2015) 6(8):717–26. doi: 10.7150/jca.10865
170. Liu D, Pearlman E, Diaconu E, Guo K, Mori H, Haqqi T, et al. Expression of Hyaluronidase by Tumor Cells Induces Angiogenesis *In Vivo*. *Proc Natl Acad Sci U S A* (1996) 93(15):7832–7. doi: 10.1073/pnas.93.15.7832
171. Fronza M, Caetano GF, Leite MN, Bitencourt CS, Paula-Silva FW, Andrade TA, et al. Hyaluronidase Modulates Inflammatory Response and Accelerates the Cutaneous Wound Healing. *PLoS One* (2014) 9(11):e112297. doi: 10.1371/journal.pone.0112297
172. Tickner JA, Urquhart AJ, Stephenson SA, Richard DJ, O'Byrne KJ. Functions and Therapeutic Roles of Exosomes in Cancer. *Front Oncol* (2014) 4:127. doi: 10.3389/fonc.2014.00127
173. Arasu UT, Deen AJ, Pasonen-Seppanen S, Heikkinen S, Lalowski M, Karna R, et al. HAS3-Induced Extracellular Vesicles From Melanoma Cells Stimulate IHH Mediated C-Myc Upregulation *via* the Hedgehog Signaling Pathway in Target Cells. *Cell Mol Life Sci* (2020) 77(20):4093–115. doi: 10.1007/s00018-019-03399-5
174. Shelton M, Anene CA, Nsengimana J, Roberts W, Newton-Bishop J, Boyne JR. The Role of CAF Derived Exosomal microRNAs in the Tumour Microenvironment of Melanoma. *Biochim Biophys Acta Rev Cancer* (2021) 1875(1):188456. doi: 10.1016/j.bbcan.2020.188456
175. Nawaz M, Shah N, Zanetti BR, Maugeri M, Silvestre RN, Fatima F, et al. Extracellular Vesicles and Matrix Remodeling Enzymes: The Emerging Roles in Extracellular Matrix Remodeling, Progression of Diseases and Tissue Repair. *Cells* (2018) 7(10):167. doi: 10.3390/cells7100167
176. Gershenwald JE, Scolyer RA, Hess KR, Sondak VK, Long GV, Ross MI, et al. Melanoma Staging: Evidence-Based Changes in the American Joint Committee on Cancer Eighth Edition Cancer Staging Manual. *CA Cancer J Clin* (2017) 67(6):472–92. doi: 10.3322/caac.21409
177. Sondak VK. Clinical Problems in the Immunotherapy Surgery and Radiation Therapy of Melanoma. *Am Soc Clin Oncol* (2017). Educational book. Available at: https://ascopubs.org/toc/edbk/37
178. Thompson JF, Scolyer RA, Kefford RF. Cutaneous Melanoma. *Lancet* (2005) 365(9460):687–701. doi: 10.1016/S0140-6736(05)17951-3
179. Han D, Zager JS, Shyr Y, Chen H, Berry LD, Iyengar S, et al. Clinicopathologic Predictors of Sentinel Lymph Node Metastasis in Thin Melanoma. *J Clin Oncol* (2013) 31(35):4387–93. doi: 10.1200/JCO.2013.50.1114
180. Eggermont AMM, Blank CU, Mandala M, Long GV, Atkinson V, Dalle S, et al. Adjuvant Pembrolizumab Versus Placebo in Resected Stage III Melanoma. *N Engl J Med* (2018) 378(19):1789–801. doi: 10.1056/NEJMoa1802357
181. Hauschild A, Dummer R, Schadendorf D, Santinami M, Atkinson V, Mandala M, et al. Longer Follow-Up Confirms Relapse-Free Survival Benefit With Adjuvant Dabrafenib Plus Trametinib in Patients With Resected BRAF V600-Mutant Stage III Melanoma. *J Clin Oncol* (2018) 36 (35):3441–9. doi: 10.1200/JCO.18.01219
182. Weber JS, Mandalà M, Del Vecchio M, Gogas H, Arance AM, Cowey CL, et al. Adjuvant Therapy With Nivolumab (NIVO) Versus Ipilimumab (IPI) After Complete Resection of Stage III/IV Melanoma: Updated Results From a Phase III Trial (CheckMate 238). *J Clin Oncol* (2018) 36(Suppl. 15):9502. doi: 10.1200/JCO.2018.36.15_suppl.9502
183. Robert C, Long GV, Brady B, Dutriaux C, Maio M, Mortier L, et al. Nivolumab in Previously Untreated Melanoma Without BRAF Mutation. *N Engl J Med* (2015) 372(4):320–30. doi: 10.1056/NEJMoa1412082
184. Robert C, Schachter J, Long GV, Arance A, Grob JJ, Mortier L, et al. Pembrolizumab Versus Ipilimumab in Advanced Melanoma. *N Engl J Med* (2015) 372(26):2521–32. doi: 10.1056/NEJMoa1503093
185. Robert C, Karaszewska B, Schachter J, Rutkowski P, Mackiewicz A, Stroiakovski D, et al. Improved Overall Survival in Melanoma With Combined Dabrafenib and Trametinib. *N Engl J Med* (2015) 372(1):30–9. doi: 10.1056/NEJMoa1412690
186. Robert C, Ribas A, Schachter J, Arance A, Grob JJ, Mortier L, et al. Pembrolizumab Versus Ipilimumab in Advanced Melanoma (KEYNOTE-006): *Post-Hoc* 5-Year Results From an Open-Label, Multicentre, Randomised, Controlled, Phase 3 Study. *Lancet Oncol* (2019) 20(9):1239–51. doi: 10.1016/S1470-2045(19)30388-2
187. Hodi FS, Chiarion-Sileni V, Gonzalez R, Grob JJ, Rutkowski P, Cowey CL, et al. Nivolumab Plus Ipilimumab or Nivolumab Alone Versus Ipilimumab Alone in Advanced Melanoma (CheckMate 067): 4-Year Outcomes of a Multicentre, Randomised, Phase 3 Trial. *Lancet Oncol* (2018) 19(11):1480–92. doi: 10.1016/S1470-2045(18)30700-9
188. Haanen JBAG, Carbonnel F, Robert C, Kerr KM, Peters AU, Larkin J, et al. Management of Toxicities From Immunotherapy: ESMO Clinical Practice Guidelines for Diagnosis, Treatment and Follow-Up. *Ann Oncol* (2018) 29 (Suppl 4):iv264–6. doi: 10.1093/annonc/mdy162
189. Doroshow DB, Bhalla S, Beasley MB, Sholl LM, Kerr KM, Gnjatic S, et al. PD-L1 as a Biomarker of Response to Immune-Checkpoint Inhibitors. *Nat Rev Clin Oncol* (2021) 18(6):345–62. doi: 10.1038/s41571-021-00473-5
190. Buder-Bakhaya K, Hassel JC. Biomarkers for Clinical Benefit of Immune Checkpoint Inhibitor Treatment-A Review From the Melanoma Perspective and Beyond. *Front Immunol* (2018) 9:1474. doi: 10.3389/fimmu.2018.01474
191. Barnes TA, Amir E. HYPE or HOPE: The Prognostic Value of Infiltrating Immune Cells in Cancer. *Br J Cancer* (2017) 117(4):451–60. doi: 10.1038/bjc.2017.220
192. Snyder A, Makarov V, Merghoub T, Yuan J, Zaretsky JM, Desrichard A, et al. Genetic Basis for Clinical Response to CTLA-4 Blockade in Melanoma. *N Engl J Med* (2014) 371(23):2189–99. doi: 10.1056/NEJMoa1406498
193. Lipson EJ, Tawbi HA, Schadendorf D, Ascierto PA, Matamala L, Gutiérrez EC, et al. Relatlimab (RELA) Plus Nivolumab (NIVO) Versus NIVO in First-Line Advanced Melanoma: Primary Phase III Results From RELATIVITY-

047 (CA224-047). *J Clin Oncol* (2021) 39(Suppl. 15):9503. doi: 10.1200/JCO.2021.39.15_suppl.9503
194. van Akkooi ACJ, Haferkamp S, Papa S, Franke V, Pinter A, Weishaupt C, et al. A Retrospective Chart Review Study of Real-World Use of Talimogene Laherparepvec in Unresectable Stage IIIB-IVM1a Melanoma in Four European Countries. *Adv Ther* (2021) 38(2):1245–62. doi: 10.1007/s12325-020-01590-w
195. Johnson DB, Puzanov I, Kelley MC. Talimogene Laherparepvec (T-VEC) for the Treatment of Advanced Melanoma. *Immunotherapy* (2015) 7(6):611–9. doi: 10.2217/imt.15.35
196. Rodriguez-Cerdeira C, Carnero Gregorio M, Lopez-Barcenas A, Sanchez-Blanco E, Sanchez-Blanco B, Fabbrocini G, et al. Advances in Immunotherapy for Melanoma: A Comprehensive Review. *Mediators Inflammation* (2017) 2017:3264217. doi: 10.1155/2017/3264217
197. Sarnaik AA, Hamid O, Khushalani NI, Lewis KD, Medina T, Kluger HM, et al. Lifileucel, a Tumor-Infiltrating Lymphocyte Therapy, in Metastatic Melanoma. *J Clin Oncol* (2021) 39(24):2656–66. doi: 10.1200/JCO.21.00612
198. Hosein AN, Brekken RA, Maitra A. Pancreatic Cancer Stroma: An Update on Therapeutic Targeting Strategies. *Nat Rev Gastroenterol Hepatol* (2020) 17(8):487–505. doi: 10.1038/s41575-020-0300-1
199. Sharma NS, Gupta VK, Garrido VT, Hadad R, Durden BC, Kesh K, et al. Targeting Tumor-Intrinsic Hexosamine Biosynthesis Sensitizes Pancreatic Cancer to Anti-PD1 Therapy. *J Clin Invest* (2020) 130(1):451–65. doi: 10.1172/JCI127515
200. Singha NC, Nekoroski T, Zhao C, Symons R, Jiang P, Frost GI, et al. Tumor-Associated Hyaluronan Limits Efficacy of Monoclonal Antibody Therapy. *Mol Cancer Ther* (2015) 14(2):523–32. doi: 10.1158/1535-7163.MCT-14-0580
201. Hingorani SR, Harris WP, Beck JT, Berdov BA, Wagner SA, Pshevlotsky EM, et al. Phase Ib Study of PEGylated Recombinant Human Hyaluronidase and Gemcitabine in Patients With Advanced Pancreatic Cancer. *Clin Cancer Res* (2016) 22(12):2848–54. doi: 10.1158/1078-0432.CCR-15-2010
202. Van Cutsem E, Tempero MA, Sigal D, Oh DY, Fazio N, Macarulla T, et al. Randomized Phase III Trial of Pegvorhyaluronidase Alfa With Nab-Paclitaxel Plus Gemcitabine for Patients With Hyaluronan-High Metastatic Pancreatic Adenocarcinoma. *J Clin Oncol* (2020) 38(27):3185–94. doi: 10.1200/JCO.20.00590
203. Gao JJ, Osgood CL, Gong Y, Zhang H, Bloomquist EW, Jiang X, et al. FDA Approval Summary: Pertuzumab, Trastuzumab, and Hyaluronidase-Zzxf Injection for Subcutaneous Use in Patients With HER2-Positive Breast Cancer. *Clin Cancer Res* (2021) 27(8):2126–9. doi: 10.1158/1078-0432.CCR-20-3474
204. Blair AB, Kim VM, Muth ST, Saung MT, Lokker N, Blouw B, et al. Dissecting the Stromal Signaling and Regulation of Myeloid Cells and Memory Effector T Cells in Pancreatic Cancer. *Clin Cancer Res* (2019) 25(17):5351–63. doi: 10.1158/1078-0432.CCR-18-4192
205. He T, Luo Y, Zhang Q, Men Z, Su T, Fan L, et al. Hyalase-Mediated Cascade Degradation of a Matrix Barrier and Immune Cell Penetration by a Photothermal Microneedle for Efficient Anticancer Therapy. *ACS Appl Mater Interfaces* (2021) 13(23):26790–9. doi: 10.1021/acsami.1c06725
206. Nagy N, Kuipers HF, Frymoyer AR, Ishak HD, Bollyky JB, Wight TN, et al. 4-Methylumbelliferone Treatment and Hyaluronan Inhibition as a Therapeutic Strategy in Inflammation, Autoimmunity, and Cancer. *Front Immunol* (2015) 6:123. doi: 10.3389/fimmu.2015.00123
207. Kakizaki I, Kojima K, Takagaki K, Endo M, Kannagi R, Ito M, et al. A Novel Mechanism for the Inhibition of Hyaluronan Biosynthesis by 4-Methylumbelliferone. *J Biol Chem* (2004) 279(32):33281–9. doi: 10.1074/jbc.M405918200
208. Kultti A, Pasonen-Seppänen S, Jauhiainen M, Rilla KJ, Kärnä R, Pyöriä E, et al. 4-Methylumbelliferone Inhibits Hyaluronan Synthesis by Depletion of Cellular UDP-Glucuronic Acid and Downregulation of Hyaluronan Synthase 2 and 3. *Exp Cell Res* (2009) 315(11):1914–23. doi: 10.1016/j.yexcr.2009.03.002
209. Edward M, Quinn JA, Pasonen-Seppänen SM, McCann BA, Tammi RH. 4-Methylumbelliferone Inhibits Tumour Cell Growth and the Activation of Stromal Hyaluronan Synthesis by Melanoma Cell-Derived Factors. *Br J Dermatol* (2010) 162(6):1224–32. doi: 10.1111/j.1365-2133.2010.09699.x
210. Steen EH, Short WD, Li H, Parikh UM, Blum A, Templeman N, et al. Skin-Specific Knockdown of Hyaluronan in Mice by an Optimized Topical 4-Methylumbelliferone Formulation. *Drug Delivery* (2021) 28(1):422–32. doi: 10.1080/10717544.2021.1886376
211. Trager MH, Queen D, Samie FH, Carvajal RD, Bickers DR, Geskin LJ. Advances in Prevention and Surveillance of Cutaneous Malignancies. *Am J Med* (2020) 133(4):417–23. doi: 10.1016/j.amjmed.2019.10.008

Conflict of Interest: The authors declare that the research was conducted in the absence of any commercial or financial relationships that could be construed as a potential conflict of interest.

Publisher's Note: All claims expressed in this article are solely those of the authors and do not necessarily represent those of their affiliated organizations, or those of the publisher, the editors and the reviewers. Any product that may be evaluated in this article, or claim that may be made by its manufacturer, is not guaranteed or endorsed by the publisher.

Copyright © 2022 Takabe, Siiskonen, Rönkä, Kainulainen and Pasonen-Seppänen. This is an open-access article distributed under the terms of the Creative Commons Attribution License (CC BY). The use, distribution or reproduction in other forums is permitted, provided the original author(s) and the copyright owner(s) are credited and that the original publication in this journal is cited, in accordance with accepted academic practice. No use, distribution or reproduction is permitted which does not comply with these terms.

frontiers in Oncology

ORIGINAL RESEARCH
published: 27 January 2022
doi: 10.3389/fonc.2022.803899

Differential Impact of Membrane-Bound and Soluble Forms of the Prognostic Marker Syndecan-1 on the Invasiveness, Migration, Apoptosis, and Proliferation of Cervical Cancer Cells

Katharina Hilgers[1†], *Sherif Abdelaziz Ibrahim*[2], *Ludwig Kiesel*[1], *Burkhard Greve*[3], *Nancy A. Espinoza-Sánchez*[1,3‡] *and Martin Götte*[1*‡]

[1] Department of Gynecology and Obstetrics, Münster University Hospital, Münster, Germany, [2] Department of Zoology, Faculty of Science, Cairo University, Giza, Egypt, [3] Department of Radiotherapy-Radiooncology, Münster University Hospital, Münster, Germany

OPEN ACCESS

Edited by:
Panagiota S. Filippou, Teesside University, United Kingdom

Reviewed by:
Ilona Kovalszky, Semmelweis University, Hungary
Chiara Falciani, University of Siena, Italy

***Correspondence:**
Martin Götte
mgotte@uni-muenster.de

†Present address:
Katharina Hilgers, Diamond Aesthetics, Düsseldorf, Germany

‡These authors share senior authorship

Specialty section:
This article was submitted to Molecular and Cellular Oncology, a section of the journal Frontiers in Oncology

Received: *28 October 2021*
Accepted: *03 January 2022*
Published: *27 January 2022*

Citation:
Hilgers K, Ibrahim SA, Kiesel L, Greve B, Espinoza-Sánchez NA and Götte M (2022) Differential Impact of Membrane-Bound and Soluble Forms of the Prognostic Marker Syndecan-1 on the Invasiveness, Migration, Apoptosis, and Proliferation of Cervical Cancer Cells. Front. Oncol. 12:803899. doi: 10.3389/fonc.2022.803899

Cervical cancer ranks fourth among the most commonly diagnosed malignant tumors in women worldwide. Previously published evidence suggested a possible connection between the expression of the membrane-bound heparan sulfate proteoglycan syndecan-1 (Sdc-1) and the development of cervical carcinoma. Sdc-1 serves as a matrix receptor and coreceptor for receptor tyrosine kinases and additional signaling pathways. It influences cell proliferation, adhesion, and migration and is seen as a modulator of the tumor microenvironment. Following proteolytic cleavage of its extracellular domain in a process called shedding, Sdc-1 can act as a paracrine effector. The loss of Sdc-1 expression is associated with low differentiation of cervical carcinoma and with an increased rate of lymph node metastases. Here, we analyzed the clinical impact of Sdc-1 expression by analysis of public gene expression datasets and studied the effect of an overexpression of Sdc-1 and its membrane-bound and soluble forms on the malignant properties of the human cervical carcinoma cell line HeLa through functional analysis. For this purpose, the HeLa cells were stably transfected with the control plasmid pcDNA3.1 and three different Sdc-1-DNA constructs,encoding wild-type, permanently membrane-bound, and constitutively soluble Sdc-1. In clinical specimens, Sdc-1 mRNA was more highly expressed in local tumor tissues than in normal and metastatic cervical cancer tissues. Moreover, high Sdc-1 expression correlated with a poor prognosis in Kaplan-Meier survival analysis, suggesting the important role of Sdc-1 in the progression of this type of cancer. *In vitro*, we found that the soluble, as well as the permanently membrane-bound forms of Sdc-1 modulated the proliferation and the cell cycle, while membrane-bound Sdc1 regulated HeLa cell apoptosis. The overexpression of Sdc-1 and its soluble form increased invasiveness. *In vitro* scratch/wound healing assay, showed reduced Sdc-1-dependent cell motility which was linked to the Rho-

GTPase signaling pathway. In conclusion, in cervical cancer Sdc-1 modulates pathogenetically relevant processes, which depend on the membrane-association of Sdc-1.

Keywords: syndecan-1, proteoglycan, cervical cancer, shedding, prognosis, metastasis

INTRODUCTION

Cervical cancer represents a major public health problem worldwide. More than 500,000 new cases and approximately 250,000 deaths are reported each year, making cervical cancer the fourth most common type of cancer in women (1). The persistence of Human Papilloma Virus infection is the main factor driving pre-neoplastic lesions and increased risk of cervical cancer, however infection alone is not sufficient to cause cancer (2). Evidence suggests that the microenvironment plays a very important role in the development and progression of cervical cancer. For example, immunosuppression is mediated by the adenosinergic pathway and the presence of immunomodulatory mesenchymal stromal cells (3, 4). Also, the remodeling of the extracellular matrix (ECM) by fibroblasts through the production of laminin is important for cervical cancer cell invasion (5). On the other hand, the ECM receptor Syndecan-1 (Sdc-1) is differentially expressed in cervical intraepithelial neoplasias and carcinoma *in situ* (6). This cell surface heparan sulfate proteoglycan is one of four members of the Sdc family expressed in mouse and human tissues (7). Sdc-1 has well-documented roles in regulating inflammation by modulating the expression and activity of cytokines, chemokines, growth factors, and adhesion molecules through its heparin-related heparan sulfate chains, thus functioning as a signaling co-receptor for different signaling pathways including Rho, Wnt, Hedgehog, Notch, and STAT3 (8, 9). The Sdc-1 protein contains a cytoplasmic, an extracellular, and a hydrophobic transmembrane domain. The short highly conserved cytoplasmic domain mediates oligomerization, binding to Type 2 PDZ domains, intracellular interactions with cytoskeleton, and modulation of signal transduction (9). The extracellular domain harbours attachment sites for HS and can be substituted with chondroitin sulfate chains (7). With the extracellular domain Sdc-1 acts as a matrix receptor for collagen, fibronectin, and laminin isoforms. Notably, Sdc ectodomains can be shed by proteolytic cleavage mediated by a variety of proteases, including matrix metalloproteinases (MMPs), ADAMs, and gamma-secretase, resulting in the conversion of the membrane-bound molecule into a soluble paracrine effector (9). In cancer, Sdc-1 is involved in the regulation of cell migration, cell-cell and cell-matrix interactions, growth-factor, chemokine, and integrin activity, and in the regulation of protease activity (7, 9–11). Importantly, several preclinical and clinical studies have demonstrated that therapies targeting Sdc-1 can inhibit the aggressive behavior of tumor cells (7, 12). Thus, this protein has emerged as a novel target for the development of selective and more potent therapies. Although some studies indicate that Sdc-1 can act both anti- or pro-tumorigenic (13–17), the mechanisms by which Sdc-1 participates in the pathogenesis and progression of tcervical cancer are still unknown. In this study, we analyzed the dysregulation and prognostic impact of Sdc-1 expression in clinical specimens of cervical cancer utilizing publically available transcriptomic datasets. Then, we analyzed the role of Sdc-1 in the proliferation, cell cycle, migration, and invasion characteristics of the well-established cervical cancer cell model line HeLa. Importantly, we studied the individual contributions of membrane-bound and soluble Sdc-1 forms in these processes and the relation between Sdc-1 and RhoGTPases in the invasive characteristics of HeLa cells. Understanding the mechanisms by which different forms of Sdc-1 promote these processes could help to better understand the behavior of cervical cancer cells and to find specific therapeutic targets.

MATERIALS AND METHODS

TNMplot and KM Plot Analysis

To compare the expression of Sdc-1 between non-tumor tissue, tumor, and metastases, we used the TNMplot online tool https://tnmplot.com/analysis/, accessed on 15 September 2021. This platform uses data generated by gene arrays from the Gene Expression Omnibus of the National Center for Biotechnology Information (NCBI-GEO) or RNA-seq from The Cancer Genome Atlas (TCGA), Therapeutically Applicable Research to Generate Effective Treatments (TARGET), and The Genotype-Tissue Expression (GTEx) repositories. Statistical significance was computed using Mann–Whitney or Kruskal–Wallis tests. False Discovery Rate (FDR) was computed using the Benjamini–Hochberg method. The database contains 56,938 samples, including 33,520 samples from 3180 gene chip-based studies (453 metastatic, 29,376 tumorous, and 3691 normal samples), 11,010 samples from TCGA (394 metastatic, 9886 tumorous, and 730 normal), 1193 samples from TARGET (1 metastatic, 1180 tumorous and 12 normal) and 11,215 normal samples from GTEx (18). Survival analysis was performed using the Pan-cancer database of the KMPlot online tool (19), selecting the Cervical squamous cell carcinoma subset (n=304 patients). The median of gene expression was used as a cutoff (median 23526, expression range 298 – 129355). All of the clinical data of the current study are publicly available and have been reviewed in the original studies, therefore there was no necessity for additional ethical review approval processes. The original datasets are described in references (18, 19).

Cell Culture and Generation of Stably Transfected Cell Lines

The HeLa cell line was purchased from ATCC/LGC Promochem (Wesel, Germany) and cultured in RPMI (Sigma, cat. No. D8758, Deisenhofen, Germany); containing 10% Fetal Calf Serum (FCS, Biochrom GmbH, Cat. No. S0615, Berlin, Germany) and 1% penicillin/streptomycin (Sigma, cat. No. P433) and maintained in a humidified atmosphere of 5% CO_2 at 37°C. Cells were stably transfected with a pcDNA3.1 control plasmid (Invitrogen, Karlsruhe, Germany) or a plasmid allowing for the overexpression of wild-type (WT), a constitutively membrane-bound (Sdc-1-388), and a constitutively shed form (Sdc-1-392) of murine Sdc-1 in the vector pReceiver-M02 under control of the cytomegalovirus promoter (RZPD/ImaGenes, Berlin, Germany) as previously described (10, 20). Stable clones were selected using 1 mg/ml G418. HeLa cells were cultured in RPMI-1640 medium containing 10% FCS, 1% penicillin/streptomycin and 600 mg/ml G418 in a humidified atmosphere of 5% CO_2 at 37°C. Successful transfections were confirmed by qPCR.

Quantitative Real-Time PCR

Total RNA isolation was performed with OLS RNA Kits (OMNI Life Science GmbH & Co. KG, Hamburg, Deutschland) according to the manufacturer's instructions, and reverse transcribed into cDNA using the First-strand cDNA Synthesis Kit (Thermo Scientific, cat. No. K1612, Waltham, MA, USA) according to the supplier's protocols. Quantitative real-time PCR was performed in duplicates for each target gene using Universal TaqManR PCR Mastermix (Applied Biosystems, cat. No. 4305719, Foster City, CA, USA), and gene expression levels were measured in an ABI 7300 Real-time PCR detection system (Applied Biosystems, CA, USA). Gene expression was analyzed using the $2^{-\Delta\Delta CT}$ method and samples were normalized to the expression of *18SRNA*. The ID of the TaqMan probes are: *18srRNA* (hs99999901s1, bp 604, Gen bank accession no. X03205.1), Human *Sdc-1* (hs00174579m1, bp 317 exon boundary 1-2, Gen bank mRNA AJ551176.1), Mouse *Sdc-1* (Mm00448918m1,bp 429, exon boundary 2-3, Gen bank mRNA AK132236.1), *MMP2* (hs00234422m1, bp 1793, exon boundary 12-13, Gen bank mRNA AK301536.1), *ECAD* (hs00170423m1, bp 451, exon boundary 3-4, Gen bank mRNA AB025105.1), *TIMP1* (hs00171558_m1, bp 515, exon boundary 5-6, Gen bank mRNA A10416.1), *BAK* (hs00832876g1 bp 1330, exon 6, Gen bank mRNA AK091807.1), *Bad* (hs00188930m1, bp 188, exon boundary 1-2, Gen bank mRNA AB451254.1), and *BCL2* (hs00153350m1, bp 977, exon boundary 2-3, Gen bank mRNA BC027258.1) (Assays by Applied Biosystems, CA, USA).

Cell Proliferation Assay

Cell proliferation was evaluated using alamarBlueR-System (Thermo Scientific, cat. No. A50100). A total of 5000 cells/well were seeded in 96-well plates and maintained in RPMI medium supplemented with 10% FCS. After 24 h, 20µl alamarBlueR-substrate was added. Following the manufacturer's protocol, after 6 h the colorimetric change was analyzed.

Cell Cycle Analysis

For DAPI staining, cell pellets were resuspended in 1 mL of 4,6-diamidino-2-phenylindole (DAPI) (CyStain UV Ploidy, cat. no. 05-5001, Sysmex, Norderstedt, Germany) and after 5-min incubation at RT, cells were analyzed by flow cytometry (CyFlow space, Sysmex/Partec, Münster, Germany). Excitation was carried out with a 375-nm UV laser and fluorescence emission was measured at 455 nm in FL4. Data analysis was performed with FlowJo software (LLC).

Apoptosis Assay

Cells were stained with the Annexin V/propidium iodide (PI) (Thermo Fisher Scientific, cat. No. V13242), as detailed by the manufacturer and as previously described (21). Measurement was performed on a flow cytometer using FloMax software (Quantum Analysis, Münster, Germany) to visualize and manage flow data. For interpretation, the fourth quartile in the measurement graph indicated apoptotic cells, where cells are positive for Annexin V. Annexin V binds to phosphatidylserine when cell membranes lose lipid asymmetry during apoptosis, but are negative for propidium iodide as cell membranes remained intact (22).

Invasion Assay

Transfected cells were diluted to 50.000 cells/mL in RPMI media containing serum. Then, 500 µL (corresponding to 25.000 cells) were transferred to Matrigel-coated inserts (Corning®, cat. no. 354230; Bedford, MA). This was followed by a 24-hour incubation period at 37°C, 7.5% CO_2. After carefully removing RPMI media and replaces by 500 µL of RPMI without serum, the invasion was triggered by adding 750 µL of RPMI medium with FCS as a chemoattractant factor into the lower compartment of the chamber. After 24 hours, all media was removed, and the cells on top of the Matrigel were removed with "cotton-wool" sticks and washed in PBS for 1 minute. After removing the PBS, the cells were stained in 1% toluidine blue in BORAX (Sigma, cat. No. T3260) for 6 minutes and washed with H_2O. Two non-overlapping pictures were taken under a Zeiss Axiophot (Zeiss, Jena, Germany) bright-field microscope (magnification 10X) and invaded cells were counted.

Wound Healing Assay

Cells were cultivated in 6-well plates for 72 hours in triplicate. After that, the cells were washed one time with 1X PBS, and then a scratched area was created using a sterile 200 µL pipette tip on 90% confluence, followed by incubation in serum-free RPMI medium for 24 hours. Cells migrated into the wound surface were determined under the microscope at time intervals of 0, 6, 8.5, and 23 hours. Images of scratched areas were captured with Zeiss Axiophot bright-field microscope (magnification 10X). The ratio of cell migration was calculated as the percentage of the remaining cell-free area compared with the area of the initial scratched area using the Axio Vision program (Carl Zeiss Microscopy GmbH, Göttingen, Germany). With a 10 X scaling, a contour was drawn around the cells at the edge of the scratch and the wound area was calculated in μm^2, supported

by the software. Some assays were performed in the presence or absence of 10 µM of the Rho kinase (ROCK) inhibitor Y-27632 (Stem Cell Technologies, cat. No. 72302).

Immunofluorescence Microscopy and Immunocytochemistry

Cells (25,000) were cultured in 8-well slides. After the cells adhered, the medium was removed completely, and then, cells were fixed with 3.7% paraformaldehyde (Merck KGaA, K42464803, Darmstadt, Germany) for 10 minutes, followed by a 5-minute incubation in 0.1% Triton X-100 (Carl Roth GmbH and Co. KG, 3051.3, Austria) to allow permeabilization. Cells were washed twice with 1X PBS for 5 minutes each and incubated for 30 minutes with 10% Aurion BSA (AURION, 60613/3, Wageningen, Netherlands). For immunofluorescence microscopy, the cells were incubated with the primary Rabbit-anti-human RhoB (Santa Cruz Biotechnology, Santa Cruz, California, USA) in Dako antibody diluent (1:50, Agilent Technologies, S2022, California, USA) for 1 hour at room temperature (RT). After that, cells were incubated for 30 min at RT with the secondary IgG anti-rabbit conjugated with AlexaFluor 488 (cat. No. A48282, Thermo Fisher Scientific, USA) diluted at 1:600 in DAKO antibody diluent. For staining of actin filaments, cells were incubated for 30-minutes with Phalloidin CruzFluor™ 594 Conjugate 1000X (1:500, Santa Cruz Biotechnology, cat. No. sc-363795, Texas, USA) in Dako antibody diluent. Then, samples were washed three times with PBS for 5 minutes each and incubated with DAPI diluted 1:5000 in PBS for an additional 1 minute, followed by rinsing with PBS. Coverslips were mounted with Vectashield Medium (Vector Laboratories, Cat. No. H-1000-10, California, USA). Samples were examined by fluorescence microscopy (Olympus BX 61, Camera Regina 4000 R). The image sections were reproduced at 400X magnification using the Q Capture 2.73.0 Media Cybernetics Image Pro® software (Bethesda, USA). For each cell line, several images were photographed from the three independent experiments. For immunocytochemistry of murine Sdc-1, cells were cultured and processed analogously up to the stage of primary antibody incubation. Cells were then stained with rat-anti-mouse Sdc-1 mAb 281-2 (BD Pharmingen, San Jose, CA, 1:1000 in PBS/1% bovine serum albumin (BSA)), Endogenous peroxidase was quenched with methanol/0.6% H_2O_2, followed by three washes with PBS. Murine Sdc-1 was detected using the Vectastain ABC kit (anti-rat), Vector Laboratories Inc., Burlingame, CA), and the AEC substrate (DAKO, Glostrup, Denmark), followed by counterstaining with Mayer's Hemalum (Merck, Darmstadt, Germany). Sections were observed with a Zeiss Axiovert 100 microscope equipped with an Axiophot Mrc camera.

Flow Cytometry for Syndecan-1

To detect cell surface Sdc-1, HeLa cells were detached using 1.5 mM ethylenediaminetetraacetic acid (EDTA) in Ca/Mg-free PBS buffer for 10 min at 37°C with gentle agitation. Cells were washed in PBS and resuspended in cold buffer containing 1% FCS. A total of 2 x 10^5 cells per sample were used for a single analysis. Following centrifugation, cells were resuspended in PBS/2% BSA and incubated for 15 min at 25°C with 10 µl of anti-human Sdc-1 (CD138)-PE (eBioscience, Inc., San Diego, CA, USA) or an isotype control IgG. Stained cells were analyzed by a cube-8 flow cytometer (Sysmex/Partec, Muenster, Germany).

Dot Blot Assay for Shed Syndecan-1

To detect soluble (shed) human and murine Sdc-1, cell culture supernatants were collected from the transfected HeLa cell lines grown for 5 days in 75 cm^2 flasks (12 ml medium, 6 x 10^6 cells at time of harvesting). 600µl of cleared (10 000g, 4°C, 10 min) cell culture supernatants were loaded on nitrocellulose membranes using a microfiltration apparatus (Bio-Rad, Hercules, CA). Membranes were blocked for 60 min with 3% non-fat dry milk, 0.5% bovine serum albumin, 150 mM NaCl, 50 mM Tris-HCl, pH 7.4, and incubated for 16 h at 4°C with the rat-anti-mouse Sdc-1 antibody 281-2 (BD Pharmingen, San Jose, CA 1:100 in PBS/1% BSA) at 4°C or the mouse anti-human Sdc-1 antibody DL-101 (1:100 in PBS/1%BSA, Santa Cruz Biotechnology, Santa Cruz, CA, USA). Immunoreactivity was visualized with HRP–conjugated secondary antibodies (1:5000 in PBS/1%BSA, Sigma, Deisenhofen, Germany). Antibodies were detected by enhanced chemiluminescence according to the manufacturer's instructions using SuperSignal™West Pico PLUS Chemiluminescent Substrate (Thermo Scientific™, cat. no. 34580, Foster City, CA, USA) in a FUSION SL (Vilber Lourmat, Marne-la-Vallée Cedex, France) device. Digitalized images were analyzed densitometrically using ImageJ software (National Institutes of Health, Bethesda, MD), and expressed as percentage of the vector control cells.

Statistical Analyses

Statistical analysis of *in vitro* data was performed with GraphPad Prism 4.02 (GraphPad Software, La Jolla, CA). GraphPad Prism 4.02 was used to perform two-tailed t-tests, one-way ANOVA with Dunn´s posttest, or nonparametric Friedman's test with Dunn's posttest, where appropriate. Data of the TNM Plotter resource were analysed using Mann-Whitney Test or Kruskal–Wallis test as appropriate, whereas data of the KM Plotter resource were analysed by Cox proportional hazards regression analysis calculatinge log-rank P values, and hazard ratios (HR) with the "survival" R package v2.38. Data were considered significant, when P-values were below 0.05.

RESULTS

Sdc-1 Is Highly Expressed in Cervical Carcinoma, and Correlates With a Poor Overall Survival

Previous studies have indicated a dysregulation of Sdc-1 expression in cervical carcinoma tissues (6, 13–17). To further investigate the clinicopathological relevance of aberrant Sdc-1 expression in this disease, we made use of large public gene expression datasets. Using the RNA Seq-based gene expression data of the TNMplot online tool (18), we found that the

expression of Sdc-1 in 3 paired samples of adjacent normal cervical tissue cervical squamous cell carcinoma and endocervical adenocarcinoma was strongly, yet non-significantly upregulated in the malignant tissue (**Figure 1A**). Further analysis of a larger number of cancerous tissues (n=304) and metastases (n=2) showed a trend for a higher expression compared to normal tissues (n=3) (p=0.0669, Kruskal-Wallis-test) (**Figure 1B**). Post-hoc analysis by Dunn test revealed a p-value of $1.65x10^{-03}$ for the comparison of normal tissue and tumors, a p-value of $1.75x10^{-01}$ comparing tumor tissue and metastases, and a p-value of $1,15x10^{-01}$-for the comparison of normal and metastatic tissue. We next utilized gene chip-based mRNA expression data of 304 cervical carcinoma patients and correlated the high vs low expression of Sdc-1 with patient survival using the cervical carcinoma subset of the KM Plotter pan-cancer database (19). Using the median as cutoff, a high expression of Sdc-1 was found to significantly correlate with a poor overall survival (HR = 1.74 (1.07 − 2.82), logrank P = 0.024) (**Figure 1C**). Overall, these data confirm previous evidence for a dysregulation of Sdc-1 expression in cervical cancer, and provide novel evidence for its utility as a prognostic marker in mRNA-based analyses.

Overexpression of Membrane-Bound and Soluble Sdc-1 Affects Proliferation and the Cell Cycle, While Membrane-Bound Sdc-1 Increases Apoptosis of HeLa Cells

Previous studies using heterologous overexpression of membrane-bound and soluble forms of murine Sdc-1 in human breast cancer cells had provided valuable insights on their differential role in invasive growth of breast cancer cells (10). To understand the roles of the wild type (Sdc1-WT), membrane-bound (Sdc1-388), and soluble Sdc-1 (Sdc1-392) in the progression of cervical cancer, the human cervical cancer cell line HeLa was stably transfected with three different Sdc-1 DNA constructs and a control vector (**Figure 2A**), as previously described (10). The control plasmid pcDNA3.1 does not contain an insert. The Wild-Type Sdc-1 plasmid overexpresses murine Sdc-1 under the strong CMV promoter. Murine and human Sdc-1 share 70% amino acid sequence identity in their extracellular, 96% in their cytoplasmic, and 100% in their transmembrane domains (10, 23). The construct Sdc1-392 encodes only the extracellular domain of Sdc-1 and the construct Sdc1-388 enables the overexpression of a constitutively membrane-bound (non-cleavable) form, in which the shedding site is replaced by CD4 sequences (10). To verify overexpression of Sdc-1, the expression of murine Sdc-1 constructs was quantified by qRT-PCR. As expected, the control plasmid did not express murine Sdc-1 (**Figure 2B**). We confirmed a slight overexpression of the murine Sdc1-WT, while the constitutively membrane-bound and soluble murine Sdc-1 were detected at almost the same levels as the endogenous human Sdc-1 (**Figure 2B**). Therefore, these results confirm that the transfection was successful, and that the altered Sdc-1 constructs were ectopically expressed at levels comparable to endogenous human Sdc-1. We next confirmed the presence of human Sdc-1 protein at the cell surface of the transfected cells using flow cytometry (**Figure 2C**). In all cell lines, human Sdc-1 levels clearly exceeded background expression levels, with cells expressing the heterologous constructs exceeding the levels of the vector control (2.64% vs 4.11-8,44%). We next studied the expression of the heterologous murine constructs by immunocytochemistry (**Figure 2D**). Vector control cells showed only a neglible background staining for murine Sdc-1. Murine Sdc-1 was distributed at the cell surface and cytoplasm of WT-Sdc1 cells, and showed a more pronounced membranous staining in Sdc1-388 cells. Cytoplasmic staining in these cells may mark passage through the secretory pathway. In contrast, no membranous murine Sdc-1 staining was seen in Sdc1-392 cells, where cytoplasmic and nuclear staining of Sdc-1 were observed (**Figure 2D**). To study the levels of soluble, shed Sdc-1 in our cell models, we employed a dot-blot analysis of conditioned media (**Figures 2E, F**). Even after long exposure times, signals of shed Sdc-1 were only slightly detectable above background levels, demanding cautious interpretation of the results. All cells shed comparable amounts of human Sdc-1 into the media, with a slight (approx. 10%), yet significant increase noted in cells overexpressing shed murine Sdc-1 (Sdc1-392) (**Figure 2E**). With respect to murine Sdc-1, results showed greater variability. While both Sdc1-WT and Sdc1-392 cells showed clearly increased soluble murine Sdc-1 levels over vector controls, the increase was only significant in the case of Sdc1-WT cells (**Figure 2F**). Overall, the results demonstrate the presence of membrane-bound and soluble human Sdc-1 on our cell models, and a proper expression and localisation of the heterologous murine Sdc-1 constructs over a background of endogenous human Sdc-1.

Due to the capacity of Sdc-1 to act as ligands or co-receptors for various signal-transducing receptors, affecting pathways associated with the hallmarks of cancer, namely proliferation, cell cycle, and apoptosis (24, 25), we performed functional analysis related to these processes. We observed that both soluble (Sdc1-392) and constitutive membrane-bound Sdc-1 (Sdc1-388) moderately inhibited HeLa cell proliferation. Compared with vector controls, membrane-bound Sdc1-388 decreased proliferation to 89% and soluble Sdc-1-392 decreased proliferation to 92%. Murine Sdc1-WT overexpression did not affect proliferation (**Figure 3A**). **Figure 3B** shows that the overexpression of membrane-bound Sdc1-388 affected apoptosis. The percentage of apoptotic cells was 13.9% in membrane-bound Sdc-1-388 cells compared to the control with 6.75%, the soluble Sdc1-392 with 9.67%, and Sdc1-WT with 8.49% (**Figure 3B**). Regarding the cell cycle, the overexpression of soluble Sdc1-392 and membrane-bound Sdc1-388 led to a significant shift of the HeLa cells from the S-phase to the G2M-phase (**Figure 3C**). Approximately, 22% of control cells (vector and Sdc1-WT) are in the S-phase, while 18.6% of membrane-bound Sdc-1-388 and 18.5% of soluble Sdc-1-392 were in the S-phase. Interestingly, a clear shift to the G2M phase was observed from a 12.4% control to a 15.25% of membrane-bound Sdc1-388 and 15.53% of soluble Sdc1-392 in HeLa cells (**Figure 3C**). Since the membrane-bound Sdc1-388 affected apoptosis, we evaluated the

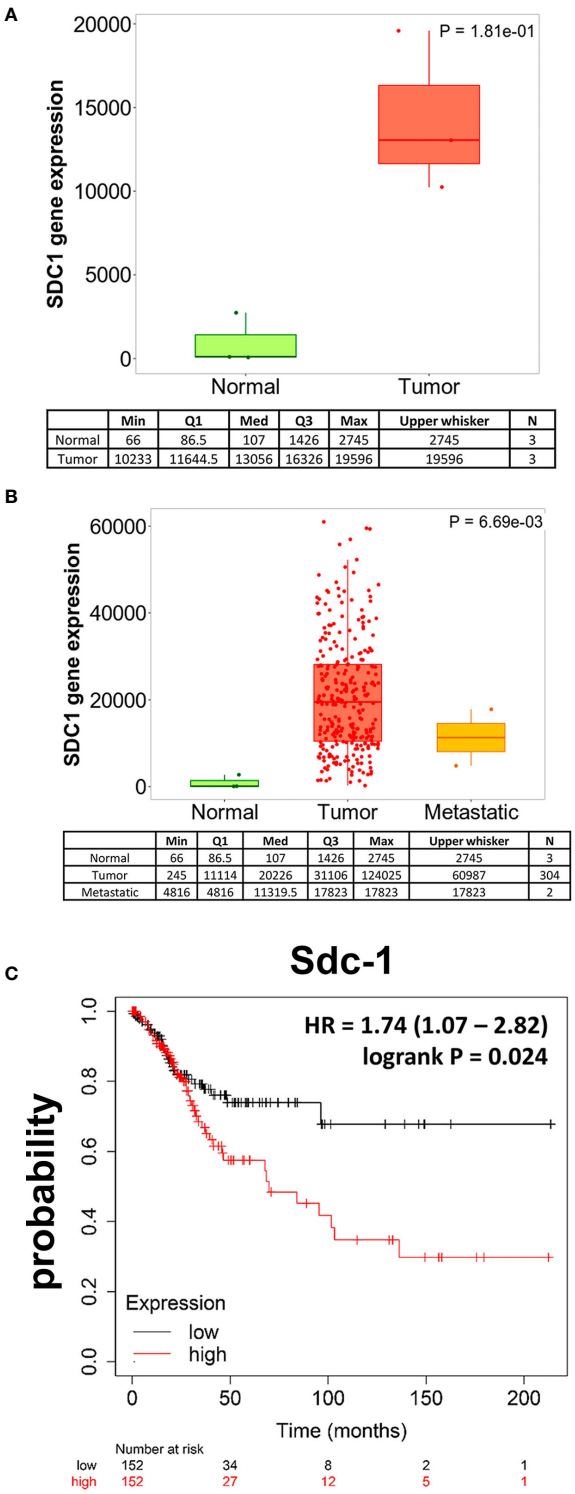

	Min	Q1	Med	Q3	Max	Upper whisker	N
Normal	66	86.5	107	1426	2745	2745	3
Tumor	10233	11644.5	13056	16326	19596	19596	3

	Min	Q1	Med	Q3	Max	Upper whisker	N
Normal	66	86.5	107	1426	2745	2745	3
Tumor	245	11114	20226	31106	124025	60987	304
Metastatic	4816	4816	11319.5	17823	17823	17823	2

FIGURE 1 | Sdc-1 is dysregulated in cervical carcinoma, and its high expression correlates with poor overall survival. Boxplots of SDC-1 gene expression in cervical cancer tissue when comparing paired normal and tumor RNA Seq data of three patients. **(A)** and when comparing normal, tumor and metastasis RNA Seq data **(B)**. The quantile cutoff values (minimum, 1st quartile, median, 3rd quartile, maximum) and the number of analyzed samples are presented. **(C)** Kaplan-Meier Survival analysis of 304 cervical carcinoma patients stratified by high or low expression of Sdc-1. **(A)** p=0.181 (not significant), Mann-Whitney-Test. **(B)** p=0.069 (Kruskal-Wallis test, trend for significance), *post hoc*-analysis p-values (Dunn's test): $p=1.65x10^{-03}$ normal tissue compared to tumors (significant), p=0.175 tumor tissue compared to metastases (not significant), p=0.115 normal tissue compared to metastatic tissue. **(C)** p=0.024 (significant), Cox regression analysis log rank p-value.

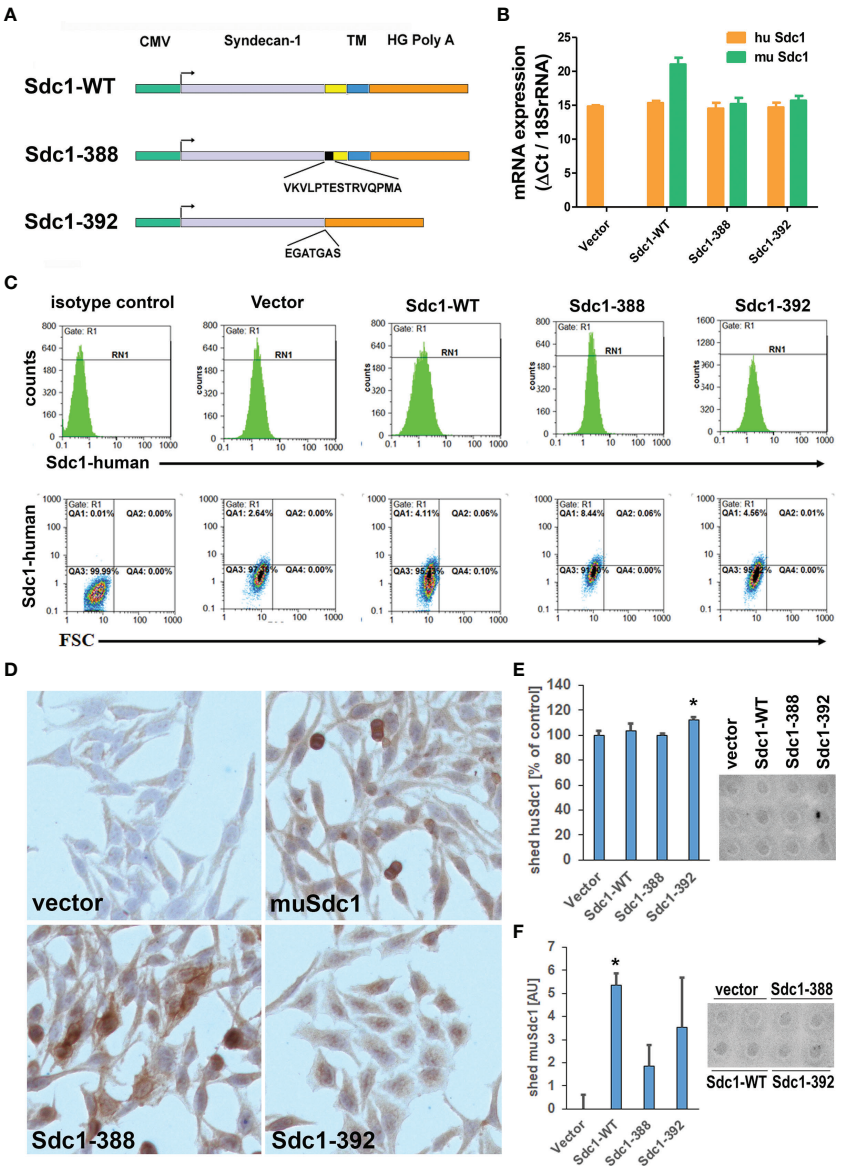

FIGURE 2 | Characterisation of HeLa cells overexpressing wild-type, constitutively membrane bound (Sdc-388) and constitutively shed (Sdc1-392) Sdc-1. **(A)** Schematic representation of the plasmid Sdc-1 cDNA inserts, CMV, cytomegalovirus promoter; yellow box, juxta-membrane domain; Black box, non-cleavable CD4 sequence; blue box, transmembrane and cytoplasmic domain, orange box, poly-A-tail; Sdc1-WT murine wild-type form; Sdc1-388, uncleavable construct 388;Sdc1-392, constitutively shed construct 392. **(B)** Quantitative PCR analysis of murine (mu Sdc-1 and human (Hu Sdc-1) Sdc1 expression. Sdc-1 expression was related to the housekeeping gene 18SrRNA. $n \geq 3$, error bars = SEM. **(C)** Detection of human Sdc-1 protein expression at the surface of the transfected HeLa cell lines using flow cytometry. Cells were stained for isotype control mouse IgG1-PE and mouse anti-human Sdc-1 (CD138)-PE and the cells were subjected to flow cytometry. Human Sdc-1 is expressed at the cell surface of all cell types. **(D)** Immunocytochemistry for murine Sdc-1, demonstrating expression of murine Sdc-1 in Sdc1-WT, Sdc-1-388 and Sdc-1 392 transfected cells (brown-red staining). Original magnification 10x. **(E, F)** Detection of shed human **(E)** and murine **(F)** Sdc-1 in cell culture supernatants of the transfected cell lines. Conditioned media were collected from the cell lines indicated and 600 µl were subjected to a dotblot assay and quantified by Image J densitometric analysis. Left panels = quantification, right panels= representative dot-blots, n>3, *= $p<0.05$ Sdc1-392 compared to vector control (t-test). The cell lines shed comparable amounts of human Sdc-1 into the culture media, with a moderately, yet significantly enhanced amount in Sdc1-392 cells. Shed amounts of murine Sdc-1 were variable, with Sdc1-WT cells showing significantly increased levels of shed murine Sdc-1 compared to vector control (n>3, *$p<0.05$, t-test).

expression levels of apoptosis-related genes in the Sdc1-388 HeLa cells such as *Bad*, *Bak*, and *Bcl-2* by qRT-PCR. No significant alteration in gene expression was detected, suggesting that transcriptional changes of these markers as a cause of increased apoptosis can be excluded (**Figure 3D**). These results suggest that both the membrane and soluble forms of Sdc-1 have an impact on proliferation, apoptosis, and the cell cycle in cervical cancer cells.

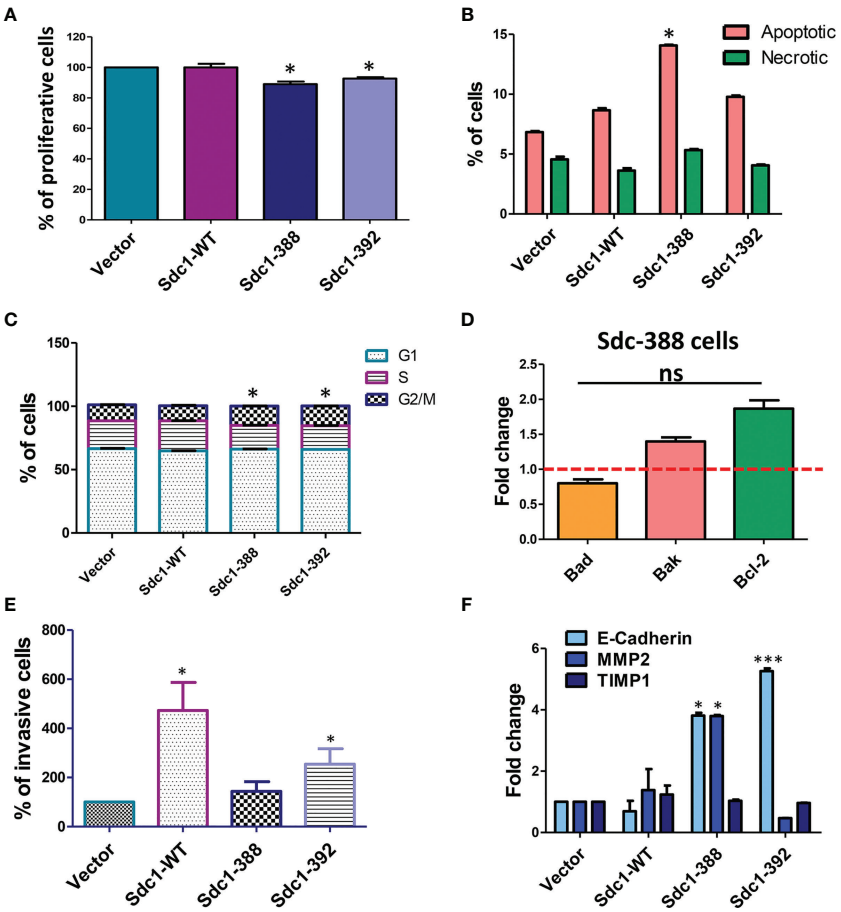

FIGURE 3 | Role for soluble and membrane bound forms of Sdc-1 in HeLa cell proliferation, cell cycle progression, apoptosis and invasion. **(A)** Differential effect of membrane-bound and soluble Sdc-1 on breast cancer cell proliferation. Control vector-transfected HeLa and HeLa cells stably overexpressing WT (Sdc1-WT), constitutively membrane-bound (Sdc1-388) or the soluble ectodomain (Sdc1-392) of Sdc1 were subjected to an Alamar Blue cell proliferation assay $^*P < 0.05$ (One-way ANOVA with Dunn's *post hoc* test) for Sdc1-388 compared to vector control and Sdc1-392 compared to vector control $n \geq 3$, error bars = SEM. Changes in apoptosis **(B)** and cell cycle progression **(C)** after the stable transfection of HeLa cells as quantified by using Annexin V/propidium iodide **(B)** and by DNA staining **(C)** and followed by flow cytometry. $^*P < 0.05$ (One-way ANOVA with Dunn's *post hoc* test) for Sdc1-388 compared to vector control, and Sdc1-392 compared to vector control, $n \geq 3$, error bars = SEM. **(D)** quantitative Real-Time PCR of the expression of the apoptosis markers Bad, Bak and Bcl-2 in the HeLa Sdc1-388 transfected cells. Data are expressed as fold change versus control vector-transfected cells. ns, no significant p value for all group comparisons (one-way ANOVA with Dunn's *post hoc* test). n≥3, error bars = SEM. **(E)** Stably transfected HeLa cells were subjected to a matrigel invasion assay. Quantification of invasive cells relative to control vector-transfected cells. *p <0.05 Sdc1-WT compared to vectror controls and SDc1-392 compared to vector controls, (one-way ANOVA with Dunn's *post hoc* test), n≥4, error bars = SEM. **(F)** quantitative RT-PCR analysis of E-cadherin, MMP2 and TIMP1 compared with vector controls. *p <0.05, MMP2 Sdc1-388 compared to vector controls, E-cadherin Sdc1-388 compared to vector controls, ***p <0.001, E-cadherin Sdc1-392 compared to vector controls (one-way ANOVA with Dunn's *post hoc* test), n≥3, error bars = SEM.

Overexpression of Sdc1-WT and Soluble Sdc1-392 Increases Cervical Cancer Cell Invasiveness

Previously, we observed that the depletion of Sdc-1 in breast and colon cancer cells increases their migration and invasion capacity (24, 26), while in endometriotic cells the expression of Sdc-1 promotes their invasive potential (27). Moreover, membrane-bound and Sdc-1-WT promoted invasion of breast cancer cells *in vitro* (11). To analyse a possible role of Sdc-1 in the invasion capacity of the transfected HeLa cells, we performed matrigel invasion assays. Overexpression of Sdc1-WT and soluble Sdc1-392 significantly increased the invasion capacity of HeLa cells (430% and 230%, respectively) compared with vector control cells (100%). Overexpression of membrane-bound Sdc1-388 did not affect invasiveness (**Figure 3E**). To investigate if Sdc-1 in its different forms influences the expression of invasion-related factors, we analyzed the expression levels of *E-cad*, *MMP2*, and tissue inhibitor of metalloproteinases 1 (*TIMP-1*), which are also associated with the metastasis of cervical cancer cells (28, 29) by qRT-PCR. In cells transfected with the membrane-bound Sdc1-388, we observed a significant overexpression in both *E-cad* and *MMP2*. Moreover, *E-cad* was also overexpressed in the Sdc1-392-

transfected cells, while no gene expression changes were noted with respect to cells overexpressing Sdc-1-WT (**Figure 3F**).

Sdc-1 Overexpression Inhibits Migration of HeLa Cells in Rho-GTPase-Dependent Mechanism

We next performed migration assays to analyze if changes in invasive growth may be linked to an altered migration capacity of the Sdc-1-manipulated HeLa cells. For this purpose, a scratch area was created in the transfected HeLa cells, and after 6, 8, and 23 h closing of the cell-free area was analyzed. At 6 hours, the membrane-bound Sdc1-388 and soluble Sdc1-392 cells showed less migration capacity relative to control and Sdc1-WT cells, while at 8 h only the membrane-bound Sdc1-388 cells were less migratory compared to the other cells (**Figure 4A**). At 23 h the vector cells have a higher migration capacity relative to Sdc1-WT, membrane-bound Sdc1-388, and soluble Sdc1-392 HeLa cells, which displayed a decreased migratory phenotype (**Figure 4A**). These results suggest that the wild-type and the soluble form of Sdc-1 have an impact on the invasion, while all forms of Sdc-1 influence the migration capacity of cervical cancer cells. We previously found that the depletion of Sdc-1 in the triple-negative breast cancer MDA-MB-231 cell line leads to an increase in migration and invasion which was dependent on the expression and activity of Rho-GTPase (24). To decipher the role of Sdc-1 and Rho in the migration capacity of cervical cancer cells, the transfected HeLa cells were cultured in the presence of the specific inhibitor of Rho-Kinases (ROCK) Y-27632. Interestingly, due to the pharmacological blockade of the Rho signaling pathway, the Sdc-1-specific effect on cell migration could be inhibited (**Figure 4B**). This suggests that the Sdc-1-dependent changes in migration of cervical cancer cells depend on the Rho signaling pathway. Finally, since Sdc-1 influences the motility of the HeLa cells in a Rho-dependent manner, we performed immunofluorescence staining to examine the distribution of RhoB in the HeLa-transfected cells. Phalloidin staining demonstrated actin fiber formation that was particularly prominent at the margins of cell groups, demonstrating cytoskeletal remodeling of the cervical cancer cells. Moreover, in all cell lines, RhoB showed a cytoplasmic localisation (**Figure 4C**). However, we found that the overexpression of the soluble Sdc1-392 induced an increased localization of RhoB at the cell-cell boundaries, which indicates an increased membrane localization (**Figure 4C**, arrow), and could influence the activation of the GTPase signal. On the other hand, overexpression of membrane-bound Sdc1-388 induced cell rounding that could indicate the presence of apoptotic cells (**Figure 4C**, arrow), which is in agreement with the result of apoptosis analysis (**Figure 3B**).

DISCUSSION

Sdc-1 plays an important role in the progression of different types of cancers by regulating the hallmarks of cancer such as

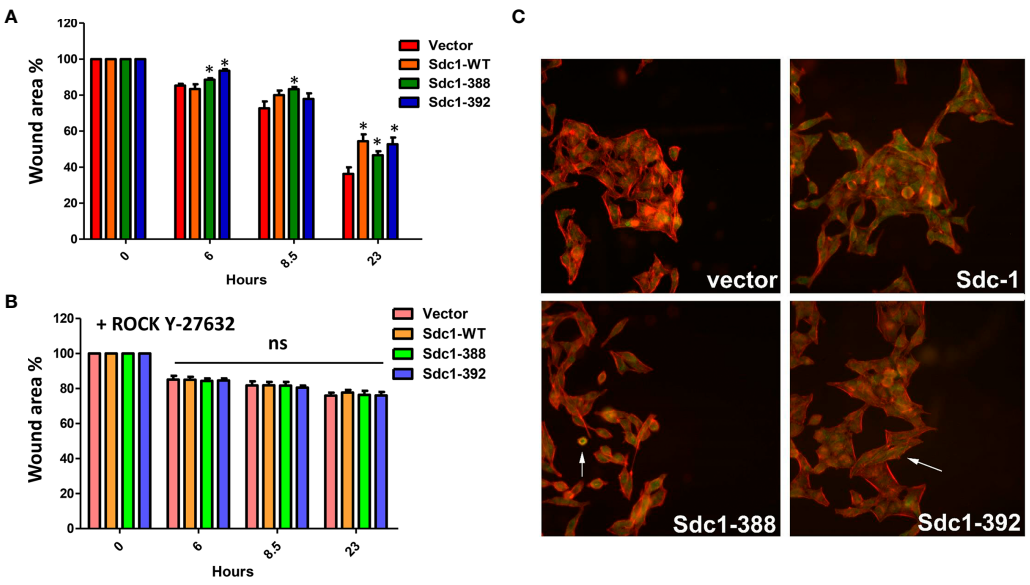

FIGURE 4 | Migration of HeLa cells is decreased by all forms of Sdc-1 in a Rho-GTPase dependent manner. **(A)** The Scratch/wound area of the four cell lines is shown as a percentage of the wound area at time 0h, 6h, 8.5h and 23h. The ability of all three cell constructs to migrate is reduced compared to the control cell line. * = p <0.05 (nonparametric Friedman's test with Dunn's posttest) for Sdc1-388 compared to vector control (t=6h, 8.5h, 23h), for Sdc1-WT vs vector control (t=23h) and for Sdc1-392 vs vector control (t=6h, 23h), n≥3, error bars = SEM. **(B)** Stably transfected HeLa cells were treated with the Rho kinase (ROCK) inhibitor Y-27632 and then a Scratch/wound area was created. The area of the three cell constructs and vector was quantified at 0h, 6h, 8.5h and 23h. ns, no significant difference compared to vector control (nonparametric Friedman's test with Dunn's posttest). n≥3, error bars = SEM. **(C)** Confocal immunofluorescence microscopic analysis of RhoB protein in HeLa transfected cells. green, RhoB; red, actin-binding protein phalloidin for cytoskeletal staining; blue, DAPI staining for nucleus. Representative images are presented. 40x magnification.

proliferation, angiogenesis, apoptosis, invasion, and metastasis (7, 9, 25, 30, 31). Despite all this evidence, little is known about how Sdc-1 affects the progression of cervical cancer. On one hand, it has been observed that the cervix exhibits a differential expression of Sdc-1 depending on the type of cell and epithelium as well as, in non-neoplastic and neoplastic lesions and the histological grade of the tumor (13, 16). Low Sdc-1 expression was observed in the progression of cervical intraepithelial neoplasia (CIN) grade I to grade III, while in poorly differentiated squamous cell carcinomas, Sdc-1 was almost absent (13). Immunohistochemical analysis of cervix tumor tissues showed that the cell surface Sdc-1 expression was higher on stromal fibroblasts than in cancer cells and that patients with high cell surface Sdc-1 expression had significantly better survival (14). In another study, the authors observed that intensity of Sdc-1 staining was higher in the normal epithelium, followed by CIN, and by invasive squamous cell carcinoma (15). Importantly, an inverse correlation between the expression of Sdc-1 in the primary site and lymph node metastasis was observed (15), suggesting that Sdc-1 has a different role in the different stages of development of cervical cancer. In our study, we found that Sdc-1 mRNA showed a trend for a higher expression in local tumor tissues than in normal and metastatic cervical cancer tissues, and a significant correlation with poor survival of cervical carcinoma patients (**Figure 1**). These data suggest an important role of Sdc-1 in the progression of this type of cancer. In a cohort of 124 samples of primary invasive carcinoma of the cervix, a high expression of Sdc-1 was observed in 39% of the samples which was associated with the grade of differentiation and squamous histology but was not associated with the disease-free survival (16). In a different study, from 121 samples of cervical cancer, 101 (83.5%) were positive for Sdc-1 being the histological type, and grade those that showed statistical significance with Sdc-1 expression (32). In this case, high Sdc-1 expression in the cytoplasm was related to better patient survival (32). These results suggest that in cervical cancer, Sdc-1 plays an important role in the development and maintenance of the primary tumor. Therefore, it would be important to carry out more studies that involve a greater number of samples including primary and metastatic tumors. To know more about the role of Sdc-1 in processes associated with malignancy, we analyzed the effect of the overexpression of Sdc-1 and its membrane-bound and soluble form on the malignant properties of the human cervical carcinoma cell line HeLa through functional analysis. We previously showed that in breast cancer cells, the membrane-bound and the soluble form of Sdc-1 exert different functions (10). Here, we found that the soluble, as well as the permanently membrane-bound state of Sdc-1, decreased the proliferation and the cell cycle progression of HeLa cells (**Figures 3A, C**). In breast cancer cells, the overexpression of WT Sdc-1 increased cell proliferation, whereas overexpression of the soluble form Sdc1 inhibits proliferation (10). It has been observed that Sdc-1 shedding potentially affects tumor growth and metastasis (30). This suggests that the soluble form of Sdc-1 has an important role in proliferation, but its role is tumor type-dependent. We also observed that the soluble, as well as the permanently membrane-bound state of Sdc-1, modulated the cell cycle from S to G2/M phase. Interestingly, in mesothelioma Sdc-1 promotes an arrest in the G1 phase by modifying the heparan sulfate composition (33). Regarding apoptosis, in endometrial cells, Sdc-1 expression prevents their apoptosis (34). In agreement, in myeloma Sdc-1 functions as an inhibitory factor of apoptosis. Also, inhibiting IGF1R, which is captured by Sdc-1, a reduction in size and vasculature of myeloma tumor xenografts was observed (35). On the contrary, we here observed that the membrane-bound Sdc1-388 promotes the apoptosis of HeLa cells (**Figure 3B**). Again, the effect of Sdc-1 on apoptosis seems to be dependent on the type of tumor but also on its membrane localisation.

In our study, the overexpression of Sdc-1 and its soluble form Sdc1-392 increased HeLa cell invasiveness (**Figure 3E**). In concordance, soluble Sdc-1 promoted the invasion of breast cancer cells (10). In contrast to our findings in breast cancer cells (10), we observed an increase in the expression of *E-cad* and no changes in TIMP expression in the cells transfected with the soluble form (**Figure 3F**). This suggests that in cervical cancer cells, the soluble form of Sdc-1 has different downstream targets. However, it should be noted that loss of expression of E-cadherin did not affect pancreatic tumor cell motility and metastasis (36). Further, elevated E-cadherin expression enhances invasion and passive dissemination of SUM149 inflammatory breast cancer cells *via* induction of cell-cell adhesion and formation of tumor clusters or emboli (37, 38). Moreover, in head and neck squamous cell carcinoma the cells with the higher levels of Sdc-1 are less migratory and invasive (39), while the increase in soluble Sdc-1 favors migration and angiogenesis in myeloma (40). Interestingly, the progression of CIN to early invasive cervical cancer was associated with low levels of Sdc-1 (17). Distinguishing the role of membrane-bound and soluble Sdc-1 with respect to invasive behavior, it is surprising that MMP2 was downregulated in the most invasive cell type (WT-Sdc-1), whereas it was upregulated in moderately invasive Sdc1-388 cells (**Figure 3F**). We can only speculate if upregulation of MMP2 in Sdc1-388 cells may have been balanced by the upregulation of anti-invasive E-cadherin, which may have also contributed to a weaker pro-invasive effect in the Sdc1-392 cells compared to Sdc1-WT (**Figures 3E, F**). Regarding migration, our *in vitro* scratch/wound healing assay showed reduced Sdc-1-dependent motility of the HeLa cells which was mediated by the Rho-GTPase signaling pathway (**Figure 4**). These results appear counter-intuitive considering the effect of the different forms of Sdc-1 on invasion, but demonstrate the complexity of Sdc-1-dependent functions, which may affect cell adhesion, cell matrix-interactions, cytokine and chemokine activity, a modulation of proteolytic factors and expression changes in cell adhesion molecules (7, 9, 10). It is also conceivable that the murine forms of Sdc-1 may have influenced the functional status of endogenous human Sdc-1 in our assays. For example, in Sdc1-392 cells, nuclear localization of Sdc-1 appeared to be more prominent compared to the other forms (**Figure 2D**), which may have influenced E-cadherin expression and EMT (41). Also, the presence of uncleavable murine Sdc-1 could have resulted in increased compensatory shedding of endogenous Sdc-1, however, we could not find experimental evidence for this hypothesis (**Figure 2E**). Our data suggest that the migration phenotype may depend on cytoskeletal activity modulated by

Sdc-1, whereas factors such as proteolysis and homotypic cell-cell adhesion may be of higher relevance for the invasion phenotype. Furthermore, in the matrigel invasion assay, Sdc-1-dependent interactions with this basement-membrane like extracellular matrix are of relevance, whereas this matrix was absent in the cell motility assay. It was demonstrated that, interacting with focal adhesions, Sdc-1 modulates regeneration of the tumor cell cytoskeleton in a rho-GTPase-dependent manner (42). Studies on MDA-MB-231 breast cancer cells found an association between Sdc-1 and Rho-GTPase in the regulation of cell motility, and in contrast to HeLa cells, MDA-MB-231 cell motility was increased *via* the Rho signaling pathway upon pathway upon Sdc-1 depletion (24). Moreover, data in an experimental model of lung injury has demonstrated that exosomes enriched in Sdc-1 ameliorate lung edema and inflammation *via* a mechanism that involves Rho-kinase signaling and cytoskeletal restructuring (43). In addition, calcification-independent vascular effects of osteoprotegerin have been ascribed to an activation of Sdc-1, and included osteoprotegerin-dependent activation of Rho kinase (44). Clinically, different functions of Sdc-1 between cervical and breast cancer have been observed. Whereas high Sdc-1 expression in mammary carcinoma is related to poor prognosis (32, 45), low Sdc-1 expression in cervical carcinoma is associated with poor differentiation and poor prognosis (6, 13). We showed that in HeLa cells, soluble Sdc-1 overexpression leads to changes in Rho B localization (**Figure 4C**). Since Sdc-1 and Rho-Kinases regulate cell motility, we suggest soluble Sdc-1 placing Rho B into a different activated status, affecting a change of localization to cell-cell borders. Different forms of Rho Kinases need to be relocated when they change from inactive cytoplasmatic form to activated plasma membrane form (42, 46). The involvement of Rho kinases in changes of cell-cell adhesion (42, 46) and the participation of Sdc-1 in the formation of focal adhesions is well known (9).

Some caveats are associated with the present study. Our study focused on clinicopathological data and a model cell line-based *in vitro* analysis. In the clinicopathological datasets, healthy tissue and metastatic samples were limited, requiring cautious interpretation of some of our results. Regarding the mechanistic data, further xenograft studies could help to corroborate our results in a setting that includes the tumor microenvironment, and could expand our study to find out, e.g., how Sdc-1 in its different forms affects angiogenesis, a mechanism which could promote metastases of the cervical cancer cells. We did not analyse the glycosylation status of our cells, which may have acted as a confounder. However, previous work in breast cancer cells applying the same methodological approach had not revealed major changes in heparan sulfate structure (10). Furthermore, future studies could address if Sdc-1 can function as a co-receptor for Human Papilloma Viruses as an important pathogenetic mechanism in cervical cancer (47). Finally, the role of Sdc-1 in the progression to a malignant phenotype apparently depends not only on its expression in the tumor cells, but also in the stroma, providing a rationale for studies in a co-culture setting.

In conclusion, In HeLa cervical cancer cells, membrane-bound and soluble forms of Sdc-1 modulate cell proliferation, apoptosis, motility, and invasiveness. These observations suggest an important role for Sdc-1 in the progression of cervical cancer. The observation of decreased cell motility in Sdc-1 overexpressing HeLa cells (**Figure 4**) is consistent with clinical data on Sdc-1-dependent lymph node metastasis, as a previous study on 106 tissue specimens showed an inverse correlation between Sdc-1 expression in the primary site of cervical carcinomas and lymph node metastases (15). Therefore, reduced cell motility in Sdc-1 expressing cervical carcinoma cells may contribute to a reduction in metastatic behaviour. However, the function of Sdc-1 appears to be context-dependent, as we observed increased invasiveness of Sdc-1 WT and Sdc1-392 HeLa cells in the Matrigel invasion chamber assay (**Figure 3E**, see discussion above). Sdc-1 modulates cell motility in a Rho-GTPase-dependent manner. The membrane-bound and the soluble Sdc-1 can be assigned different functions, the detailed analysis of which appears worthwhile in future studies. Understanding the mechanisms by which Sdc-1 promotes these processes could help to better understand the behavior of cervical cancer and find specific therapeutic targets.

DATA AVAILABILITY STATEMENT

The original contributions presented in the study are included in the article/supplementary material. Further inquiries can be directed to the corresponding author.

AUTHOR CONTRIBUTIONS

KH performed the *in vitro* experiments and analyzed the data. NE-S performed flow cytometry. SI and BG supervised the data and provided the expertise on cell proliferation, apoptosis, invasion and migration assays analysis. LK provided the general support, co-supervised KH, and was involved in the data interpretation. MG conceived and coordinated the study. NE-S and MG performed database analysis, generated the figures and wrote the manuscript. All authors contributed to the article and approved the submitted version.

FUNDING

This work was supported by EU H2020 MSCA-RISE project no. 645756 GLYCANC (to MG, SI) and the Deutsche Forschungsgemeinschaft DFG GO 1392/8-1 (to MG) and GR4743/5-1 (to BG).

ACKNOWLEDGMENTS

We would like to acknowledge Birgit Pers and Annette van Dülmen for expert technical assistance.

REFERENCES

1. Ferlay J, Colombet M, Soerjomataram I, Mathers C, Parkin DM, Piñeros M, et al. Estimating the Global Cancer Incidence and Mortality in 2018: GLOBOCAN Sources and Methods. *Int J Cancer* (2019) 144:1941–53. doi: 10.1002/ijc.31937
2. Roden RBS, Stern PL. Opportunities and Challenges for Human Papillomavirus Vaccination in Cancer. *Nat Rev Cancer* (2018) 18:240–54. doi: 10.1038/nrc.2018.13
3. Muñóz–Godínez R, De Lourdes Mora–García M, Weiss–Steider B, Montesinos–Montesinos JJ, Del Carmen Aguilar–Lemarroy A, García–Rocha R, et al. Detection of CD39 and a Highly Glycosylated Isoform of Soluble CD73 in the Plasma of Patients With Cervical Cancer: Correlation With Disease Progression. *Mediators Inflamm* (2020) 2020:1678780. doi: 10.1155/2020/1678780
4. García–Rocha R, Moreno–Lafont M, Mora–García ML, Weiss–Steider B, Montesinos JJ, Piña–Sánchez P, et al. Mesenchymal Stromal Cells Derived From Cervical Cancer Tumors Induce TGF–β1 Expression and IL–10 Expression and Secretion in the Cervical Cancer Cells, Resulting in Protection From Cytotoxic T Cell Activity. *Cytokine* (2015) 76:382–90. doi: 10.1016/j.cyto.2015.09.001
5. Fullár A, Dudás J, Oláh L, Hollósi P, Papp Z, Sobel G, et al. Remodeling of Extracellular Matrix by Normal and Tumor–Associated Fibroblasts Promotes Cervical Cancer Progression. *BMC Cancer* (2015) 15:256. doi: 10.1186/s12885–015–1272–3
6. Sobel G, Szabó I, Páska C, Kiss A, Kovalszky I, Kádár A, et al. Changes of Cell Adhesion and Extracellular Matrix (ECM) Components in Cervical Intraepithelial Neoplasia. *Pathol Oncol Res* (2005) 11:26–31. doi: 10.1007/BF03032402
7. Karamanos NK, Piperigkou Z, Theocharis AD, Watanabe H, Franchi M, Baud S, et al. Proteoglycan Chemical Diversity Drives Multifunctional Cell Regulation and Therapeutics. *Chem Rev* (2018) 118:9152–232. doi: 10.1021/acs.chemrev.8b00354
8. Aquino RS, Teng YHF, Park PW. Glycobiology of Syndecan–1 in Bacterial Infections. *Biochem Soc Trans* (2018) 46:371–7. doi: 10.1042/BST20170395
9. Hassan N, Greve B, Espinoza–Sánchez NA, Götte M. Cell–Surface Heparan Sulfate Proteoglycans as Multifunctional Integrators of Signaling in Cancer. *Cell Signal* (2021) 77:109822. doi: 10.1016/j.cellsig.2020.109822
10. Nikolova V, Koo CY, Ibrahim SA, Wang Z, Spillmann D, Dreier R, et al. Differential Roles for Membrane–Bound and Soluble Syndecan–1 (CD138) in Breast Cancer Progression. *Carcinogenesis* (2009) 30:397–407. doi: 10.1093/carcin/bgp001
11. Iba K, Albrechtsen R, Gilpin B, Fröhlich C, Loechel F, Zolkiewska A, et al. The Cysteine–Rich Domain of Human ADAM 12 Supports Cell Adhesion Through Syndecans and Triggers Signaling Events That Lead to β1 Integrin–Dependent Cell Spreading. *J Cell Biol* (2000) 149:1143–55. doi: 10.1083/jcb.149.5.1143
12. Ramani VC, Purushothaman A, Stewart MD, Thompson CA, Vlodavsky I, Au JLS, et al. The Heparanase/Syndecan–1 Axis in Cancer: Mechanisms and Therapies. *FEBS J* (2013) 280:2294–306. doi: 10.1111/febs.12168
13. Inki P, Stenbäck F, Grenman S, Jalkanen M. Immunohistochemical Localization of Syndecan–1 in Normal and Pathological Human Uterine Cervix. *J Pathol* (1994) 172:349–55. doi: 10.1002/path.1711720410
14. Karászi K, Vigh R, Máthé M, Fullár A, Oláh L, Füle T, et al. Aberrant Expression of Syndecan–1 in Cervical Cancers. *Pathol Oncol Res* (2020) 26:2255–64. doi: 10.1007/s12253–020–00816–0
15. Numa F, Hirabayashi K, Kawasaki K, Sakaguchi Y, Sugino N, Suehiro Y, et al. Syndecan–1 Expression in Cancer of the Uterine Cervix: Association With Lymph Node Metastasis. *Int J Oncol* (2002) 20:39–43. doi: 10.3892/ijo.20.1.39
16. Rintala M, Inki P, Klemi P, Jalkanen M, Grénman S. Association of Syndecan–1 With Tumor Grade and Histology in Primary Invasive Cervical Carcinoma. *Gynecol Oncol* (1999) 75:372–8. doi: 10.1006/gyno.1999.5595
17. Shinyo Y, Kodama J, Hasengaowa, Kusumoto T, Hiramatsu Y. Loss of Cell–Surface Heparan Sulfate Expression in Both Cervical Intraepithelial Neoplasm and Invasive Cervical Cancer. *Gynecol Oncol* (2005) 96:776–83. doi: 10.1016/j.ygyno.2004.11.004
18. Bartha Á, Győrffy B. Tnmplot.Com: A Web Tool for the Comparison of Gene Expression in Normal, Tumor and Metastatic Tissues. *Int J Mol Sci* (2021) 22:1–12. doi: 10.3390/ijms22052622
19. Nagy Á, Munkácsy G, Győrffy B. Pancancer Survival Analysis of Cancer Hallmark Genes. *Sci Rep* (2021) 11:6047. doi: 10.1038/s41598–021–84787–5
20. Vijaya Kumar A, Brézillon S, Untereiner V, Sockalingum GD, Kumar Katakam S, Mohamed HT, et al. HS2ST1–Dependent Signaling Pathways Determine Breast Cancer Cell Viability, Matrix Interactions, and Invasive Behavior. *Cancer Sci* (2020) 111:2907–22. doi: 10.1111/cas.14539
21. Greve B, Dreffke K, Rickinger A, Könemann S, Fritz E, Eckardt–Schupp F, et al. Multicentric Investigation of Ionising Radiation–Induced Cell Death as a Predictive Parameter of Individual Radiosensitivity. *Apoptosis* (2009) 14:226–35. doi: 10.1007/s10495–008–0294–6
22. Crowley LC, Marfell BJ, Scott AP, Waterhouse NJ. Quantitation of Apoptosis and Necrosis by Annexin V Binding, Propidium Iodide Uptake, and Flow Cytometry. *Cold Spring Harb Protoc* (2016) 2016:pdb.prot087288. doi: 10.1101/PDB.PROT087288
23. Mali M, Andtfolk H, Miettinen HM, Jalkanen M. Suppression of Tumor Cell Growth by Syndecan–1 Ectodomain. *J Biol Chem* (1994) 269:27795–8. doi: 10.1016/s0021–9258(18)46853–6
24. Ibrahim SA, Yip GW, Stock C, Pan JW, Neubauer C, Poeter M, et al. Targeting of Syndecan–1 by Microrna Mir–10b Promotes Breast Cancer Cell Motility and Invasiveness *via* a Rho–Gtpase– and E–Cadherin–Dependent Mechanism. *Int J Cancer* (2012) 131:E884–96. doi: 10.1002/ijc.27629
25. Hanahan D, Weinberg RA. Hallmarks of Cancer: The Next Generation. *Cell* (2011) 144:646–74. doi: 10.1016/j.cell.2011.02.013
26. Kumar Katakam S, Tria V, Sim WC, Yip GW, Molgora S, Karnavas T, et al. The Heparan Sulfate Proteoglycan Syndecan–1 Regulates Colon Cancer Stem Cell Function *via* a Focal Adhesion Kinase—Wnt Signaling Axis. *FEBS J* (2021) 288:486–506. doi: 10.1111/febs.15356
27. Ponandai–Srinivasan S, Saare M, Boggavarapu NR, Frisendahl C, Ehrström S, Riethmüller C, et al. Syndecan–1 Modulates the Invasive Potential of Endometrioma *via* TGF–B Signalling in a Subgroup of Women With Endometriosis. *Hum Reprod* (2020) 35:2280–93. doi: 10.1093/humrep/deaa164
28. Murakami A, Nakagawa T, Fukushima C, Torii M, Sueoka K, Nawata S, et al. Relationship Between Decreased Expression of Squamous Cell Carcinoma Antigen 2 and E–Cadherin in Primary Cervical Cancer Lesions and Lymph Node Metastasis. *Oncol Rep* (2008) 19:99–104. doi: 10.3892/or.19.1.99
29. Azevedo Martins JM, Rabelo–Santos SH, Do Amaral Westin MC, Zeferino LC. Tumoral and Stromal Expression of MMP–2, MMP–9, MMP–14, TIMP–1, TIMP–2, and VEGF–a in Cervical Cancer Patient Survival: A Competing Risk Analysis. *BMC Cancer* (2020) 20:660. doi: 10.1186/s12885–020–07150–3
30. Yang Y, MacLeod V, Miao HQ, Theus A, Zhan F, Shaughnessy JD, et al. Heparanase Enhances Syndecan–1 Shedding: A Novel Mechanism for Stimulation of Tumor Growth and Metastasis. *J Biol Chem* (2007) 282:13326–33. doi: 10.1074/jbc.M611259200
31. Nassar E, Hassan N, El–Ghonaimy EA, Hassan H, Abdullah MS, Rottke TV, et al. Syndecan–1 Promotes Angiogenesis in Triple–Negative Breast Cancer Through the Prognostically Relevant Tissue Factor Pathway and Additional Angiogenic Routes. *Cancers (Basel)* (2021) 13:2318. doi: 10.3390/cancers13102318
32. Kim YI, Lee A, Lee BH, Kim SY. Prognostic Significance of Syndecan–1 Expression in Cervical Cancers. *J Gynecol Oncol* (2011) 22:161–7. doi: 10.3802/jgo.2011.22.3.161
33. Heidari–Hamedani G, Vivès RR, Seffouh A, Afratis NA, Oosterhof A, van Kuppevelt TH, et al. Syndecan–1 Alters Heparan Sulfate Composition and Signaling Pathways in Malignant Mesothelioma. *Cell Signal* (2015) 27:2054–67. doi: 10.1016/j.cellsig.2015.07.017
34. Boeddeker SJ, Baston–Buest DM, Altergot–Ahmad O, Kruessel JS, Hess AP. Syndecan–1 Knockdown in Endometrial Epithelial Cells Alters Their Apoptotic Protein Profile and Enhances the Inducibility of Apoptosis. *Mol Hum Reprod* (2014) 20:567–78. doi: 10.1093/molehr/gau009
35. Beauvais DLM, Jung O, Yang Y, Sanderson RD, Rapraeger AC. Syndecan–1 (CD138) Suppresses Apoptosis in Multiple Myeloma by Activating IGF1 Receptor: Prevention by Synstatinigf1r Inhibits Tumor Growth. *Cancer Res* (2016) 76:4981–93. doi: 10.1158/0008–5472.CAN–16–0232
36. Liu X, Huang H, Remmers N, Hollingsworth MA. Loss of E–Cadherin and Epithelial to Mesenchymal Transition Is Not Required for Cell Motility in Tissues or for Metastasis. *Tissue Barriers* (2014) 2:e969112. doi: 10.4161/21688362.2014.969112
37. Hoffmeyer MR, Wall KM, Dharmawardhane SF. *In Vitro* Analysis of the Invasive Phenotype of SUM 149, an Inflammatory Breast Cancer Cell Line. *Cancer Cell Int* (2005) 5:11. doi: 10.1186/1475–2867–5–11

38. Ibrahim SA, Gadalla R, El–Ghonaimy EA, Samir O, Mohamed HT, Hassan H, et al. Syndecan–1 Is a Novel Molecular Marker for Triple Negative Inflammatory Breast Cancer and Modulates the Cancer Stem Cell Phenotype *via* the IL–6/STAT3, Notch and EGFR Signaling Pathways. *Mol Cancer* (2017) 16:57. doi: 10.1186/s12943–017–0621–z
39. Ishikawa T, Kramer RH. Sdc1 Negatively Modulates Carcinoma Cell Motility and Invasion. *Exp Cell Res* (2010) 316:951–65. doi: 10.1016/j.yexcr.2009.12.013
40. Purushothaman A, Uyama T, Kobayashi F, Yamada S, Sugahara K, Rapraeger AC, et al. Heparanase–Enhanced Shedding of Syndecan–1 by Myeloma Cells Promotes Endothelial Invasion and Angiogenesis. *Blood* (2010) 115:2449–57. doi: 10.1182/blood–2009–07–234757
41. Kumar–Singh A, Parniewska MM, Giotopoulou N, Javadi J, Sun W, Szatmári T, et al. Nuclear Syndecan–1 Regulates Epithelial–Mesenchymal Plasticity in Tumor Cells. *Biol (Basel)* (2021) 10:521. doi: 10.3390/biology10060521
42. Morgan MR, Humphries MJ, Bass MD. Synergistic Control of Cell Adhesion by Integrins and Syndecans. *Nat Rev Mol Cell Biol* (2007) 8:957–69. doi: 10.1038/nrm2289
43. Zhang C, Guo F, Chang M, Zhou Z, Yi L, Gao C, et al. Exosome–Delivered Syndecan–1 Rescues Acute Lung Injury *via* a FAK/P190rhogap/Rhoa/ROCK/NF–Kappab Signaling Axis and Glycocalyx Enhancement. *Exp Cell Res* (2019) 384:111596. doi: 10.1016/j.yexcr.2019.111596
44. Alves–Lopes R, Neves KB, Strembitska A, Harvey AP, Harvey KY, Yusuf H, et al. Osteoprotegerin Regulates Vascular Function Through Syndecan–1 and NADPH Oxidase–Derived Reactive Oxygen Species. *Clin Sci (Lond)* (2021) 135:2429–44. doi: 10.1042/CS20210643
45. Barbareschi M, Maisonneuve P, Aldovini D, Cangi MG, Pecciarini L, Mauri FA, et al. High Syndecan–1 Expression in Breast Carcinoma Is Related to an Aggressive Phenotype and to Poorer Prognosis. *Cancer* (2003) 98:474–83. doi: 10.1002/cncr.11515
46. Crosas–Molist E, Samain R, Kohlhammer L, Orgaz JL, George SL, Maiques O, et al. Rho Gtpase Signaling in Cancer Progression and Dissemination. *Physiol Rev* (2022) 102:455–510. doi: 10.1152/physrev.00045.2020
47. Vanajothi R, Srikanth N, Vijayakumar R, Palanisamy M, Bhavaniramya S, Premkumar K. HPV–Mediated Cervical Cancer: A Systematic Review on Immunological Basis, Molecular Biology and Immune Evasion Mechanisms. *Curr Drug Targets* (2021). doi: 10.2174/1389450123666211221160632

Conflict of Interest: The authors declare that the research was conducted in the absence of any commercial or financial relationships that could be construed as a potential conflict of interest.

Publisher's Note: All claims expressed in this article are solely those of the authors and do not necessarily represent those of their affiliated organizations, or those of the publisher, the editors and the reviewers. Any product that may be evaluated in this article, or claim that may be made by its manufacturer, is not guaranteed or endorsed by the publisher.

Copyright © 2022 Hilgers, Ibrahim, Kiesel, Greve, Espinoza-Sánchez and Götte. This is an open-access article distributed under the terms of the Creative Commons Attribution License (CC BY). The use, distribution or reproduction in other forums is permitted, provided the original author(s) and the copyright owner(s) are credited and that the original publication in this journal is cited, in accordance with accepted academic practice. No use, distribution or reproduction is permitted which does not comply with these terms.

frontiers in Oncology

ORIGINAL RESEARCH
published: 03 February 2022
doi: 10.3389/fonc.2022.819883

SPOCK1 Promotes the Development of Hepatocellular Carcinoma

*Lóránd Váncza[1], Katalin Karászi[1], Bálint Péterfia[2], Lilla Turiák[3], Katalin Dezső[1], Anna Sebestyén[1], Andrea Reszegi[1], Gábor Petővári[1], András Kiss[4], Zsuzsanna Schaff[4], Kornélia Baghy[1] and Ilona Kovalszky[1]**

[1] 1st Department of Pathology and Experimental Cancer Research, Semmelweis University, Budapest, Hungary, [2] Faculty of Information Technology and Bionics, Pázmány Péter Catholic University, Budapest, Hungary, [3] MS Proteomics Research Group, Research Centre for Natural Sciences, Eötvös Loránd Research Network, Budapest, Hungary, [4] 2nd Department of Pathology, Semmelweis University, Budapest, Hungary

OPEN ACCESS

Edited by:
Alberto Passi,
University of Insubria, Italy

Reviewed by:
Nikolaos A. Afratis,
Weizmann Institute of Science, Israel
Stéphane Brezillon,
UMR7369 Matrice extracellulaire et dynamique cellulaire (MEDyC), France

***Correspondence:**
Ilona Kovalszky
kovalszky.ilona@med.semmelweis-univ.hu;
kovalelastic@gmail.com

Specialty section:
This article was submitted to Molecular and Cellular Oncology, a section of the journal Frontiers in Oncology

Received: *22 November 2021*
Accepted: *10 January 2022*
Published: *03 February 2022*

Citation:
Váncza L, Karászi K, Péterfia B, Turiák L, Dezső K, Sebestyén A, Reszegi A, Petővári G, Kiss A, Schaff Z, Baghy K and Kovalszky I (2022) SPOCK1 Promotes the Development of Hepatocellular Carcinoma. Front. Oncol. 12:819883. doi: 10.3389/fonc.2022.819883

The extracellular matrix proteoglycan SPOCK1 is increasingly recognized as a contributor to the development and progression of cancers. Here, we study how SPOCK1, which is present in non-tumorous hepatocytes at low concentrations, promotes the development and progression of malignant hepatocellular tumors. Although SPOCK1 is an extracellular matrix proteoglycan, its concentration increases in the cytoplasm of hepatocytes starting with very low expression in the normal cells and then appearing in much higher quantities in cells of cirrhotic human liver and hepatocellular carcinoma. This observation is similar to that observed after diethylnitrosamine induction of mouse hepatocarcinogenesis. Furthermore, syndecan-1, the major proteoglycan of the liver, and SPOCK1 are in inverse correlation in the course of these events. In hepatoma cell lines, the cytoplasmic SPOCK1 colocalized with mitochondrial markers, such as MitoTracker and TOMM20, a characteristic protein of the outer membrane of the mitochondrion and could be detected in the cell nucleus. SPOCK1 downregulation of hepatoma cell lines by siRNA inhibited cell proliferation, upregulated p21 and p27, and interfered with pAkt and CDK4 expression. A tyrosine kinase array revealed that inhibition of SPOCK1 in the liver cancer cells altered MAPK signaling and downregulated several members of the Sarc family, all related to the aggressivity of the hepatoma cell lines. These studies support the idea that SPOCK1 enhancement in the liver is an active contributor to human and rodent hepatocarcinogenesis and cancer progression. However, its mitochondrial localization raises the possibility that it has a currently unidentified physiological function in normal hepatocytes.

Keywords: hepatocellular cancer (HCC), SPOCK1 in the liver, SPOCK1 and syndecan-1, SPOCK1 in mitochondrion, effect of SPOCK1 inhibition and overexpression

1 INTRODUCTION

Several factors influence the contest between cancer and its prevention as well as treatment. Pollution of the environment, sedentary lifestyle, inappropriate food consumption, etc., go together with the inappropriate response of our body to injured molecules that gain oncogenic potentials. Among the factors, the current tumor management still fails to consider the importance of extracellular matrix (ECM) and stromal components of cancers, although they are known to be active participants in the development and progression of malignant tumors (1–3).

In the last 30 years, several publications proved the role of proteoglycans in the physiology and pathology of the liver. Although according to the literature syndecan-1 is the major heparan sulfate proteoglycan of the healthy liver, all four members of the family have been reported in increased amounts in various chronic liver diseases, such as liver fibrosis, cirrhosis (4, 5), cholestasis (6), non-alcoholic fatty liver disease (NAFLD) (7), and cancer (8, 9). Glypican-3 is a typical marker of hepatocellular carcinoma, detected not only in the tumor cells but also in the circulation (10). The fact that it is hardly expressed in the normal healthy liver makes glypican-3 a potential therapeutic target (11). In the healthy liver, agrin and perlecan are the components of basement membranes of the blood vessels; their increased amounts can be detected not only there but also in the connective tissue of the liver cirrhosis and cancer (12). The importance of agrin was suggested in the early phase of cancer development (11). In contrast with published data (13), versican, the only hyalectan ECM proteoglycan, is deposited mainly in the stroma of liver cancer according to the Human Protein Atlas.

SPOCK1/Testican-1 was discovered in 1992, isolated from the seminal plasma (14), and then cloned from brain tissue in 1997 (15). The limited information about the protein verifies its presence in the brain (16), the neuromuscular synapsis (17), the ECM, the endothelial cells, and evidently the testis. Through MT1-MMP, SPOCK1 inhibits MMP2 (18) and a couple of other proteases (19). It is involved in the mechanism of sepsis (20). Since the first study reported its oncogenic role in 2011, a number of accounts described the implication of SPOCK1 in the poor outcome in almost all types of cancers, from glioblastoma to prostate tumors (21–24). The mechanism of its action is still not completely understood; inhibition of apoptosis, upregulation of the Akt pathway, and involvement in epithelial–mesenchymal transition (EMT) are speculated, among others (23, 25–28). SPOCK1 is also implicated in the development and progression of liver cancer (29).

In spite of these reports, SPOCK1 is still considered as an ECM proteoglycan, and interestingly hardly any account paid attention that it can be detected in tumor cells of surgically removed human cancer tissues, and also in the cytoplasm of cancer cell lines (30). Human Protein Atlas provides several examples of cancer tissues expressing ample amounts of SPOCK1 in the tumor cells. The presence of SPOCK1 in epithelial tumors indicates that SPOCK1 likely can be found in resident non-tumorous epithelial cells, although in very low amounts. Based on this background, we investigated if a) healthy or diseased hepatocytes express SPOCK1 and b) SPOCK1 plays a mechanistic role during hepatocarcinogenesis and cancer progression. To this end, we performed a series of assays on an experimental hepatocarcinogenesis model, studied human liver cancers, and quantified how SPOCK1 silencing or upregulation influenced the aggressiveness of hepatoma cell lines.

2 MATERIALS AND METHODS

2.1 Materials

If it is not indicated otherwise, all materials were purchased from Merck KGaA (Darmstadt, Germany). For the antibodies used see **Supplementary Table 1**.

2.2 Cell Culture

HepG2 (ATCC HB-8065) was obtained from American Type Culture Collection (ATCC, Manassas, VA, USA); HLE (JCRB0404) and Huh7 (JCRB0403) were obtained from the Japanese Collection of Research Bioresources Cell Bank. Cell lines were maintained in Dulbecco's Modified Eagle Medium (DMEM) Low Glucose (D5546) supplemented with 10% fetal bovine serum (FBS; FB-1001B/500, Biosera, Kansas City, MO, USA), 2 mM of L-glutamine (XC-T1715/100; Biosera), 100 unit/ml of penicillin, and 100 µg/ml of streptomycin (P0781-100ML).

2.3 Double-Fluorescent Immunocytochemistry: SPOCK1 and TOMM20

Cells were plated on coverslips in 6-well plates (2×10^5 cell/well) and cultivated in a complete growth medium for 24 h. Cells were washed three times with phosphate-buffered saline (PBS; containing 137 mM of NaCl, 2.7 mM of KCl, 10 mM of Na_2HPO_4, and 1.8 mM of KH_2PO_4, pH 7.5) and then fixed with ice-cold methanol for 10 min. Fixed cells were washed three times with PBS followed by blocking with 5% w/v bovine serum albumin (BSA) in PBS. SPOCK1 and TOMM20 primary antibodies were applied overnight in 1% w/v of BSA at 4^{O}C. Next day, the coverslips were washed three times with PBS and incubated with fluorescent-labeled Alexa Fluor 488 and Alexa Fluor 568-conjugated secondary antibodies in 1% w/v of BSA containing DAPI (1:200; D9542) for 1 h at room temperature. The cells were washed and mounted using Fluoromount (F4680; Merck KGaA). In the case of the negative controls, the primary antibodies were omitted.

2.4 SPOCK1 Silencing in HLE and Huh7 Cell Lines

The transfection was performed using Lipofectamine™ 3000 Transfection Reagent (L3000008, Life Technologies, Carlsbad, CA, USA) and ON-TARGETplus Human SPOCK1 siRNA (L-013724-01-0005, Dharmacon Inc., Lafayette, CO, USA). The target sequences of the SPOCK1 siRNA were as follows: "CCUACAAAGAACAUCGUAA", "GGGUUGGACCUUCG AAUUU", "CGAUGGAGCCACAUUAAUA", and "GGUGU AAUGAGGAGGGCUA". To perform the transfection, cells

were seeded in 6-well plates at a density of 1.5×10^5 cell/well from Huh7 and 1×10^5 cell/well from HLE and cultured for 24 h in a complete growth medium. In each well, 6 µl of transfection reagent and 50 pmol of SPOCK1 siRNA or 50 pmol of scrambled siRNA as negative control were used. Transfection efficacy was controlled with GAPDH siRNA. Twenty-four hours after the transfection, the medium was changed to a fresh growth medium. Forty-eight hours after transfection, the cells and conditioned medium were collected for follow-up experiments.

2.5 Expression Plasmids and Transfection of HepG2 Cells

The expression plasmid for wild-type SPOCK1 was constructed by PCR cloning. Briefly, full-length ORF encoding human SPOCK1 was PCR-amplified with Phusion High-Fidelity polymerase in two steps. For the first PCR, outer primers (F-out: 5′ GGCGGCGTGTGGCAGGAG 3′ and R-out: 3′ TAGAGAGCAACAATGGAGAAGAGACC 5′) were used in 30 cycles, using cDNA from HLE cells as a template. For the second PCR, inner primers (ORF-F: 5′ TTTTTGGATCCGAA ATGCCTGCTATCGCGGTG 3′ and ORF-R: 3′ TTTTTC TCGAGCTACCATATGTACCCGACCTCATC 5′) were used, and the template was the purified product of the first PCR. Gel extracted fragment of the second PCR was inserted into a pcDNA^{TM}4/TO mammalian expression plasmid (Invitrogen, Carlsbad, CA, USA) using *Bam*HI and *Xho*I sites. The transfection was performed using Neon Transfection System (MPK5000, Life Technologies) with 2×10^5 cells in a 100-µl pipette tip with 5 µg of SPOCK1 pcDNA^{TM}4/TO and empty vector pcDNA^{TM}4/TO using the following settings of the machine: 1,200 V, 50 ms, and 1 pulse. The cells were seeded in 6-well plates in DMEM supplemented with 20% FBS and 2 mM of L-glutamine. Stable transfectants were selected in a selective medium (complete growth medium supplemented with 500 µg/ml of Zeocin). Stably transfected monoclonal cell lines were generated by isolating individual colonies. The colony with the highest SPOCK1 expression was selected and expanded for further experiments.

2.6 Western Blotting

Cell cultures at 70%–80% confluency were harvested in lysis buffer containing 20 mM of Tris, 150 mM of NaCl, 2 mM of EDTA (pH 8), and 0.5% Triton X-100 supplemented with protease and phosphatase inhibitors (P8340). The protein concentration was measured using Protein Assay Dye Reagent Concentrate (500-0006, Bio-Rad, CA, USA). An equal amount of protein (20 µg) was separated by 10% sodium dodecyl sulfate (SDS)–polyacrylamide gel electrophoresis (TGX FastCast Acrylamide Kit, 10%, #1610173, Bio-Rad, CA, USA) and transferred to polyvinylidene difluoride (PVDF) membrane (IPVH00010, Merck Millipore, Burlington, MA, USA) using Trans-Blot Turbo Transfer System (1704150, Bio-Rad). The membrane was incubated with Blotting-Grade Blocker (#170-6404, Bio-Rad) for 2 h at room temperature and with primary antibody overnight at 4°C. After being washed three times in Tris-buffered saline containing 0.1% v/v Tween-20 (TBST containing 8.7 g of NaCl; 2.4 g of Tris; 0.05% Tween-20), the membrane was incubated with horseradish peroxidase (HRP)-conjugated secondary antibody for 1 h at room temperature, then washed three times in TBST, and visualized with SuperSignal^{TM} West Pico PLUS Chemiluminescent Substrate (34580, Life Technologies). Images were performed using iBright FL1000 Imaging Systems (Life Technologies) and analyzed with ImageJ software.

2.7 Human Phospho-Kinase Array

Human Phospho-Kinase Array (ARY003B, R&D Systems, Minneapolis, MN, USA) was used for the detection of relative phosphorylation levels of 43 potential kinase phosphorylation sites. The assay was performed according to the manufacturer's instructions, and 400 µg of protein of SPOCK1-silenced and control samples was used on each array. The signal detection was performed using iBright FL1000 Imaging Systems and analyzed with Carpentier G. Protein Array Analyze for ImageJ (2010) available online: http://rsb.info.nih.gov/ij/macros/toolsets/Protein Array Analyzer.txt

2.8 Bromodeoxyuridine Assay

Forty-eight hours after transfection, the culture medium was changed to fresh medium supplemented with 10 µM of bromodeoxyuridine (BrdU) (B5002, Merck KGaA) and incubated for 30 min at 37°C. The cells were fixed with ice-cold methanol for 10 min, washed three times with PBS, and incubated with 2 M of HCl for 10 min at room temperature. After being washed, the cells were incubated with an Anti-BrdU antibody for 1 h at room temperature. Finally, the cells were incubated with fluorescent-labeled Alexa Fluor 488 and DAPI (1:200) and mounted using Fluoromount. The stained slides were scanned with 3DHistech Pannoramic Confocal scanner and analyzed using CaseViewer CellQuant 2.2 (3DHISTECH Ltd., Budapest, Hungary).

2.9 Migration Assay

The cells were plated on coverslips and transfected with either SPOCK1 or scrambled siRNA as described before. Twenty-four hours after transfection, the cells were incubated with a complete growth medium containing 10 µg/ml of Mitomycin C (M5353, Merck KGaA, Darmstadt, Germany) for 3 h and then washed two times with PBS. The scratch was created using a 200-µl pipette tip. The debris was removed, and the cells were grown in a complete growth medium containing 1% FBS. The cells were fixed at 0-, 24-, and 48-h time points using methanol as described before and stained with H&E. The slides were scanned with Pannoramic P1000 scanner (3DHISTECH Ltd., Budapest, Hungary).

2.10 Invasion Assay

The invasiveness of the cell lines was studied using CytoSelect^{TM} 24-Well Cell Invasion Assay (CBA-110, Cell Biolabs Inc., San Diego, CA, USA). The cells were transfected as described before; 24 h after transfection, 1×10^6 cells were plated onto each insert. The assay was performed according to the manufacturer's instructions.

2.11 Generation of Human Syndecan-1-Transgenic (hSDC$^{+/+}$) Mice and Diethylnitrosamine-Induced Hepatocarcinogenesis

Diethylnitrosamine (DEN) hepatocarcinogenesis model was carried out as was described previously (9). Animal experiments were approved by the Ethics Committee of the Animal Health Care and Control Institute, Csongrád County, Hungary (protocol code XVI/03047-2/2008).

2.12 Immunohistochemistry

The surgical materials were collected and used according to the instructions of Semmelweis University Regional and Institutional Committee of Science and Research Ethics (TUKEB permit number: 155/2012), Medical Research Council Committee of Science and Research Ethics (permit number: 61303-2/2018/EKU). Human, mouse, rat liver, and human bone marrow formalin-fixed and paraffin-embedded tissue sections were deparaffinized and rehydrated. Heat-induced antigen retrieval was carried out by BOND Epitope Retrieval Solution 1 (AR9961, Leica Biosystems, Newcastle, UK). Endogenous peroxidase was blocked with 10% H_2O_2 in methanol for 20 min at room temperature. Sections were washed in TBST followed by blocking the non-specific protein binding with Novocastra Protein Block (RE71102, Leica Biosystems) for 10 min at room temperature. After a wash step, the sections were incubated with SPOCK1 and CHD1L primary antibodies overnight at 4°C. The next day, the sections were washed and incubated with HISTO-Labeling System for 30 min at room temperature (30011.R500, Department of Immunology and Biotechnology, Pécs, Hungary). The reactions were visualized using diaminobenzidine 1:50 (ImmPACT DAB, SK-4105, Vector Laboratories, Burlingame, CA, USA) followed by counterstain with hematoxylin. The sections were dehydrated and covered using BIOMOUNT (BMT-500, BIOGNOST D.O.O, Zagreb, Croatia). Stained slides were scanned at ×20 magnification with Pannoramic P1000 scanner, and the quantitative analysis was performed using CaseViewer DensitoQuant 2.2 (3DHISTECH Ltd., Budapest, Hungary).

2.13 Automated Western Blotting System (WES™)

The samples were analyzed using WES™ (ProteinSimple, San Jose, CA, USA, a Bio-Techne Brand) automated capillary-based electrophoresis instrument. Cell lysates were prepared as described at the Western blotting and were further diluted in 0.1× Sample Buffer (ProteinSimple, 042-195), and the concentration was set to 1 μg/μl. Conditioned media were collected and concentrated using 10,000 NMWL centrifugal filters (Amicon Ultra-4, UFC801024, Merck Millipore, Burlington, MA, USA). Fluorescent Master Mix was added to the samples in a 1:4 ratio followed by 5-min incubation at 95°C. The samples, blocking reagent (Antibody Diluent; 042-203, ProteinSimple), diluted primary antibody (see **Supplementary Table 1**), secondary antibody (042-206, ProteinSimple), chemiluminescent substrate, and wash buffer were loaded into WES capillary plate according to the manufacturer's instruction. Five micrograms of protein from cell lysate and 5 μl of conditioned medium were separated using 12–230 kDa of Separation Module (SM-W004, ProteinSimple) with the following settings: separation (395V, 30 min), blocking (5 min), incubation with primary antibody (30 min), incubation with secondary antibody (30 min), and chemiluminescent detection (15 min). The results were analyzed, and the pictures were edited using Compass software (San Jose, CA, USA).

2.14 Quantitative Real-Time PCR

Total RNA was isolated using RNeasy Plus Mini Kit (74134, Qiagen, Germany). For reverse transcription, 1 μg of RNA was used, and the assay was performed with High Capacity cDNA Reverse Transcription Kit (4368814, Life Technologies) according to the manufacturer's instructions. The mRNA level was quantified using a SPOCK1 TaqMan Gene Expression Assay (assay ID: *Hs00270274_m1*; Life Technologies) and TaqMan Fast Advanced Master Mix (4444556, Life Technologies) with the following protocol: 2 min, 50°C UNG incubation; 2 min, 95°C polymerase activation; 40 cycles of 1 s, 95°C denaturation; and 20 sec, 60°C annealing and elongation. The relative quantification was normalized to endogenous β-actin (4326315E, Life Technologies) expression.

2.15 Hepatocyte Isolation

Hepatocytes were isolated from the liver of F344 rats. The breeding animals were purchased from Charles River Laboratories (Écully, France). The animals were housed in plastic cages (556 × 334 mm, AnimaLab, Poznań, Poland) and kept under standard conditions: 12 h of light–dark cycles, constant temperature (23°C), and humidity (22%). Standard rodent chow (V1535000, SSNIFF, Soest, Germany; 15-mm pellets) was provided *ad libitum*.

Hepatocyte isolation was performed using a two-step collagenase perfusion method as described before (31). The cells were filtered through a 100-μm nylon filter, and then the suspension was centrifuged 3 times for 5 min at 50*g* to separate hepatocytes from non-parenchymal cells. The cells were kept on ice for 6 h. Hepatocytes were plated on glass slides every hour for immunocytochemistry. The smears were air-dried and then fixed with ice-cold methanol for 10 min. SPOCK1 fluorescent immunocytochemistry was performed as described before.

2.16 Statistical Analysis

Statistical analysis was calculated, and bar charts were drawn using the GraphPad Prism v8.01 (GraphPad Software, La Jolla, CA, USA) software. Results were analyzed by unpaired Student's *t*-test, and significance was defined as $^{*}p < 0.05$, $^{**}p < 0.01$, and $^{***}p < 0.001$.

3 RESULTS

3.1 SPOCK1 in Healthy, Cirrhotic, and Tumorous Human Livers

A pilot survey of a few human liver specimens revealed modest cytoplasmic positivity in the hepatocytes of seemingly healthy

human livers. While SPOCK1 expression was high in the cirrhotic hepatocytes, the staining intensity in cancer cells was heterogeneous. The cytoplasm of the endothelial cell displayed intense cytoplasmic positivity; however, except for the blood vessels, the connective tissue was negative. SPOCK1 reaction in the liver cells was an unexpected finding. Apparently, although the expression of SPOCK1 is very low in healthy hepatocytes, their injuries facilitate the upregulation of the proteoglycan, and its expression increases in liver cirrhosis and hepatocellular carcinoma. SPOCK1 expression was assessed on human liver cirrhosis and hepatocellular carcinoma of various etiologies. Compared with control livers, significant upregulation could be detected in both hepatitis C virus (HCV)-infected cirrhotic and tumorous livers (**Figures 1**, **2**).

In the next step, an experimental hepatocarcinogenesis model was designed, by utilizing the genotoxic diethylnitrosamine as a proxy carcinogen to follow the changes of SPOCK1 during the process of tumor development (**Figure 3**). The results provided clear evidence that SPOCK1 is hardly detectable in the liver of 6-month-old healthy mice. Weak cytoplasmic staining of the hepatocytes could be deciphered only around the blood vessels. On the contrary, SPOCK1 was well detectable in the transformed hepatocytes without fatty change. These findings support the hypothesis that even if SPOCK1 expression is very low in the normal liver, it is upregulated during carcinogenesis. Furthermore, the process was facilitated by the upregulation of CHD1L, a known oncogenic factor of the proteoglycan (32).

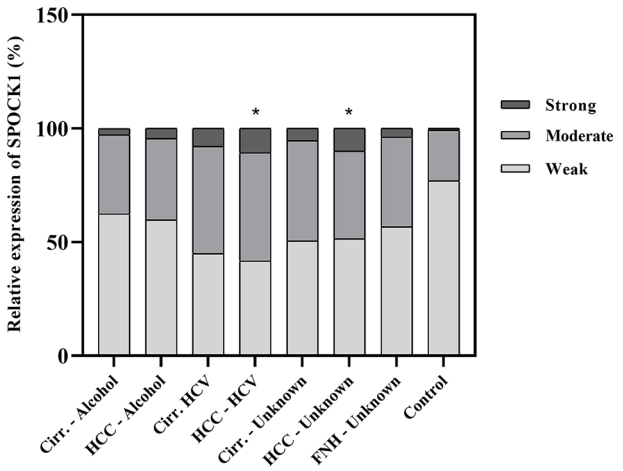

FIGURE 2 | Quantitative assessment of the expression of SPOCK1 protein in liver cirrhosis and cancer of various origins. Significant increase in cancer specimens. n = 76, *p < 0.05.

3.2 SPOCK1 Expression Is Rapidly Activated in Isolated Hepatocytes

SPOCK1 expression was also studied in healthy rat livers. Similar to that in the mouse liver, the proteoglycan was hardly

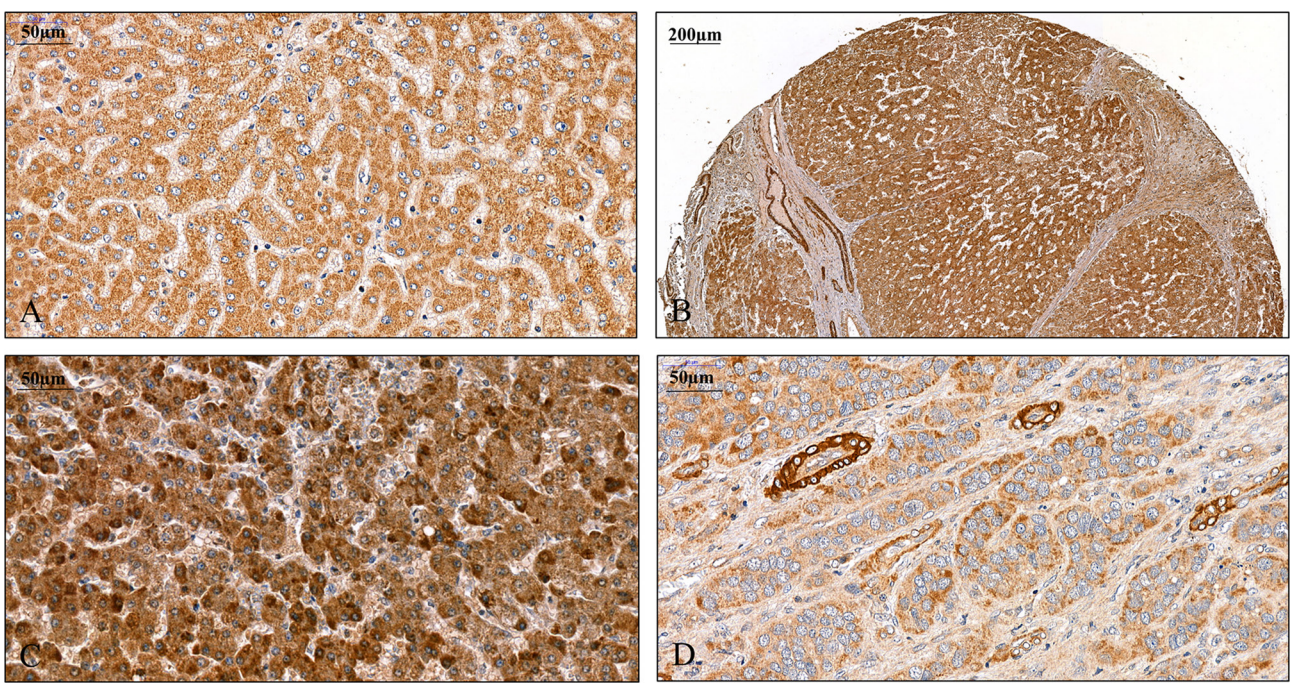

FIGURE 1 | Detection of SPOCK1 protein on human liver specimens. **(A)** Normal liver, moderate staining in the cytoplasm of hepatocytes. **(B)** Cirrhotic liver with intensive staining in the cytoplasm. Endothelial cells of the blood vessels also show the presence of high levels of SPOCK1. Areas of connective tissue are devoid of SPOCK1. **(C)** Hepatocellular carcinoma, the tumor cells are loaded with the proteoglycan. **(D)** Hepatocellular carcinoma, the staining intensity is modest in tumor cells, whereas the cytoplasm of endothelial cells shows high protein levels.

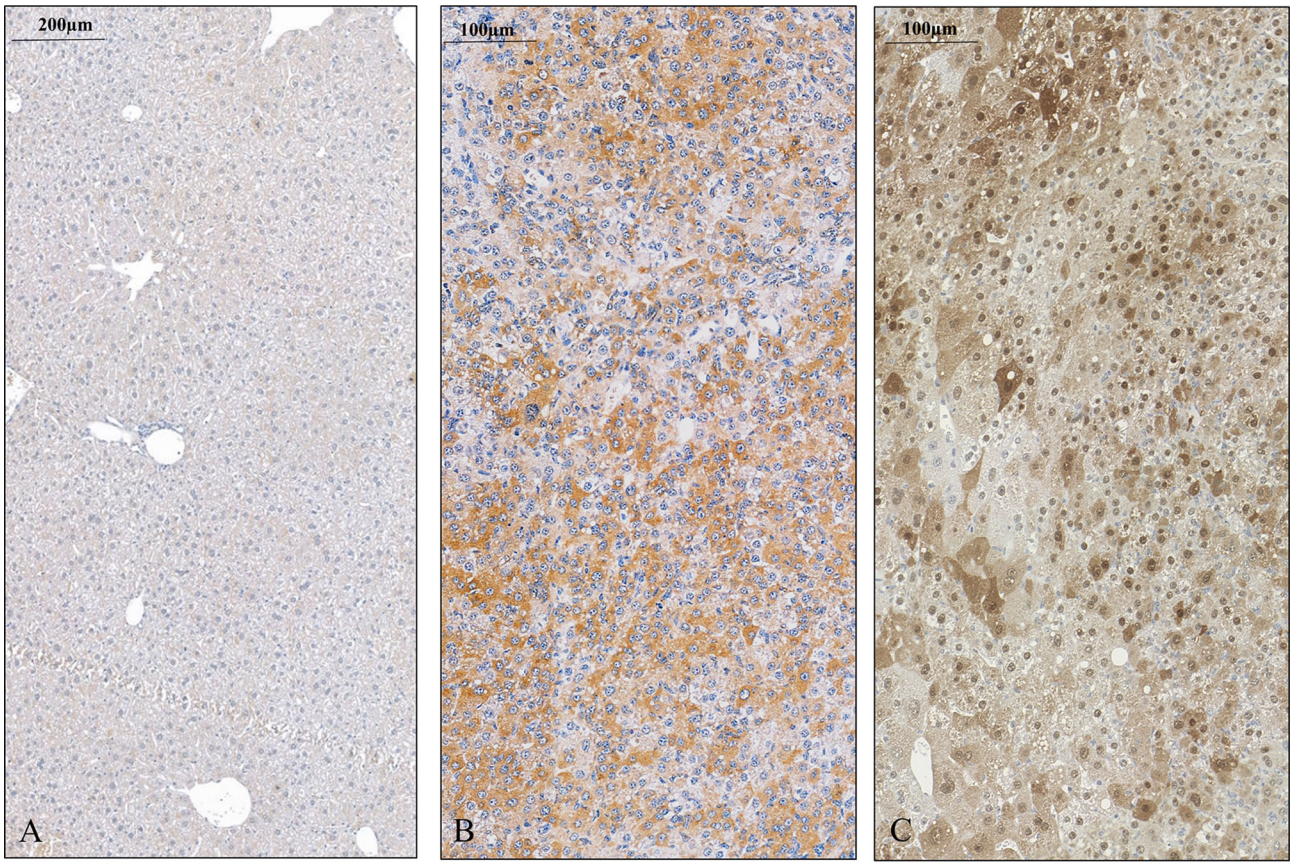

FIGURE 3 | SPOCK1 expression in control mouse liver and hepatocellular cancer. **(A)** Healthy liver with low amounts of SPOCK1 around the central veins. **(B)** SPOCK1 detection in diethylnitrosamine (DEN) induced hepatocellular cancer and transformed liver cells that contain ample amounts of proteoglycan. **(C)** Expression of CHD1L, the transcription factor of SPOCK1, in the same liver. The protein is detectable in both the nucleus and the cytoplasm.

detectable. To evaluate if cellular stress activates the synthesis of the proteoglycan in normal hepatocytes or it is the sign of impaired secretion, hepatocytes were isolated from rat livers, and the expression of SPOCK1 was followed in time.

Immediately after isolation, a proportion of the cells displayed wide cytoplasm with weak SPOCK1 positivity. Nevertheless, in some cells with similar nuclei, the cytoplasm shrank, exhibiting intensive SPOCK1 positivity. Over time, the number of these SPOCK1-positive cells kept increasing, whereas their cytoplasm was shrinking. After plating, the intensity of SPOCK1 expression gradually decreased, and by the end of the third day, it turned back to the state observed immediately after isolation (**Figure 4**). Taken together, SPOCK1 expression in human fetal livers was comparable with that of normal mouse and rat livers, whereas normoblasts in the sinusoids and the bone marrow were strongly positive (**Figure 5**).

3.3 SPOCK1 Localizes in the Mitochondria of Human Hepatoma Cell Lines

The granular cytoplasmic SPOCK1 reaction raised the possibility that the proteoglycan localizes in the mitochondria; thus, double fluorescent immunostainings were carried out with SPOCK1 antibody together either with TOMM20 or mitochondrial marker (MitoTracker-red, M22425) on hepatoma cell lines (**Figure 6**). We observed that SPOCK1 was present in the mitochondria, and it colocalized with both MitoTracker and TOMM20 (Translocase of Outer Membrane of Mitochondrion). This finding indicates that SPOCK1 belongs to the proteins that TOMM20 is ready to transfer from the cytoplasm to the mitochondria.

3.4 Functional Assays to Detect the Effect of SPOCK1 Silencing

To assess the role of SPOCK1 in the regulation of cell proliferation, its effect on DNA synthesis was investigated by BrdU uptake. The amount of the incorporated thymidine analog indicated the activity of DNA synthesis in tumor cells. Control cells were compared with SPOCK1 siRNA silenced and SPOCK1 expression vector-transfected tumor cells following BrdU uptake for 30 min. As an effect of SPOCK1 inhibition, the number of labeled cell nuclei decreased to 25% and 50%, respectively, in siRNA-treated HLE and HUH7 cells and increased to about 130% in SPOCK1-transfected HepG2 cells (**Figure 7**).

Migration and invasion of HLE and Huh7 tumor cells in control and SPOCK1 siRNA silenced samples showed that siRNA inhibited both migration and invasion of HLE cells. On

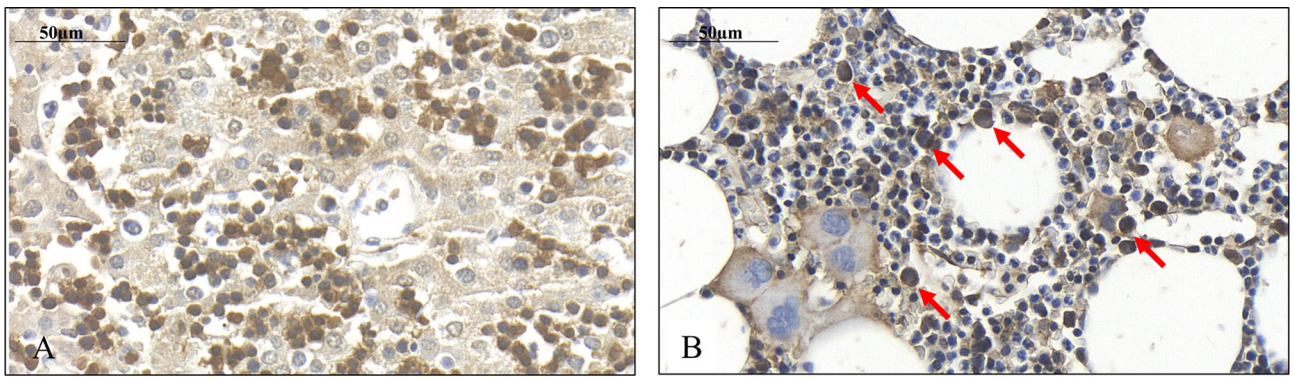

FIGURE 4 | Presence of SPOCK1 in fetal human liver. **(A)** The weak cytoplasmic staining exhibits a good correlation with SPOCK1 intensity in normal mouse liver; normoblasts in the sinusoids display strong staining. **(B)** SPOCK1-positive normoblasts are detectable in the bone marrow marked with arrows.

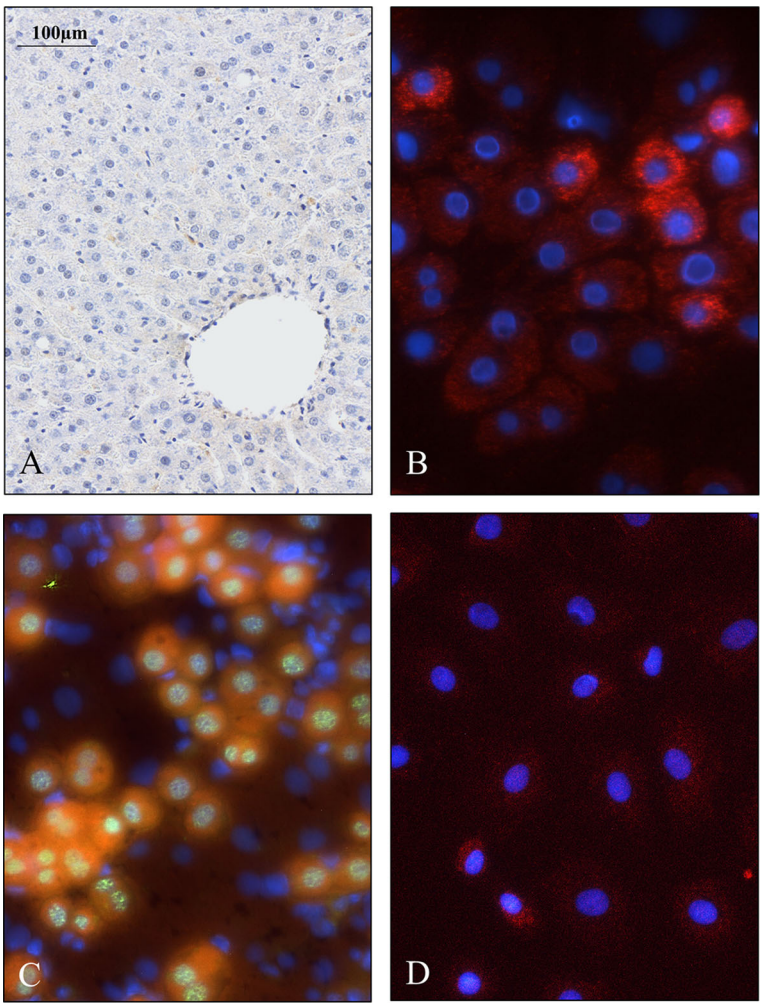

FIGURE 5 | Weak SPOCK1 staining in healthy rat liver, fast upregulation of SPOCK1 during hepatocyte isolation. **(A)** SPOCK1 protein cannot be detected in healthy rat liver. **(B, C)** Upregulation of SPOCK1 as a function of time in isolated hepatocytes. **(C)** HNF4α (Hepatocyte Nuclear Factor 4 *Alpha*) can be detected in the nucleus. **(D)** After 3 days of culture, the proteoglycan expression returns to the original low levels.

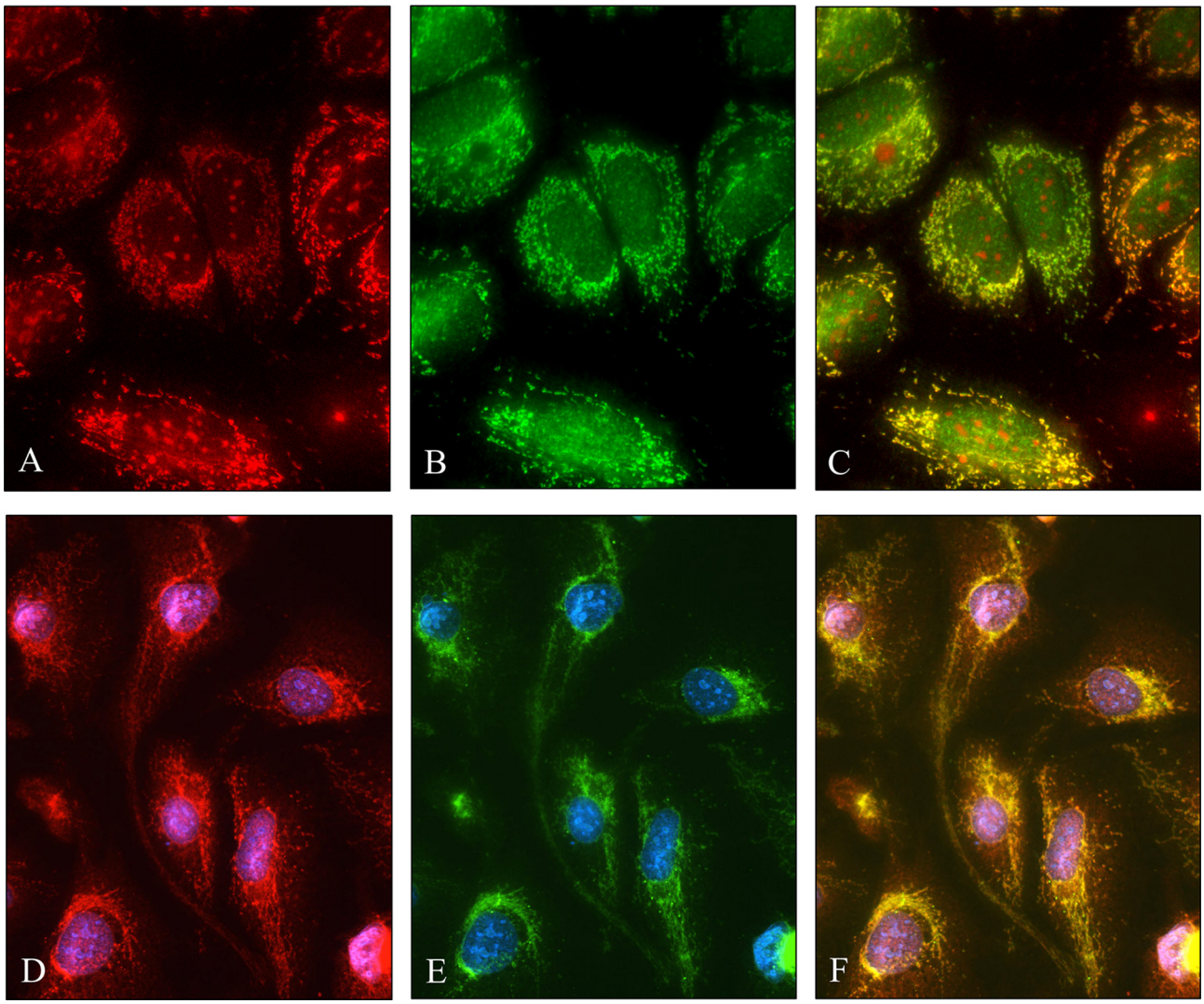

FIGURE 6 | Colocalization of SPOCK1 with a mitochondrion marker and TOMM20 mitochondrial protein. **(A)** Staining of HuH7 hepatoma cells with MitoTracker. **(B)** SPOCK1 alone. **(C)** The MitoTracker-red and SPOCK1 (green) stainings are aligned. **(D, E)** Immunostaining of HLE cells with SPOCK1 (red) and TOMM20 (green); the two proteins are fully aligned **(F)**. Original magnification, ×40.

the contrary, the differentiated control Huh7 cells neither migrate nor invade collagen as it was already determined previously. Thus, we could not detect any difference with these methods between its control and silenced cells (**Figure 8**).

3.5 Effect of SPOCK1 Silencing on Regulatory Proteins of Hepatoma Cell Lines

3.5.1 Phosphokinase Arrays

HLE and HuH7 hepatoma cells were transfected with SPOCK1 siRNA. Subsequently, their cell homogenates were incubated with the premade filters containing specific antibodies against phosphokinase proteins. SPOCK1 silencing significantly downregulated the activated EGF receptor in both HLE and HuH7 cell lines, together with decreased phosphorylation of ERK1/2, MSK1/2, and CREB (S133), observed in the MAPK pathway. Additionally, 3 proteins from the SRC family, Src, Lyn, and Yes were also downregulated in HLE cells. The EGFR downregulation resulted in significant inhibition of both the ERK and p38 pathways and different Src family members in the Huh7 cells. Inhibition of the mTOR pathway was less detectable in the two cell lines (**Figure 9**).

3.5.2 Western Blotting

Besides those, as revealed on the phosphokinase array, SPOCK1 silencing influenced several other regulatory proteins. Phospho-Akt(T308), CDK4, and cleaved caspase-3 expression decreased, while the expression of cyclin-dependent kinase inhibitors p21 and p27 increased. The modest inhibition of cleaved caspase-3 indicated that SPOCK1 can interfere with the apoptotic machinery (**Figure 10**).

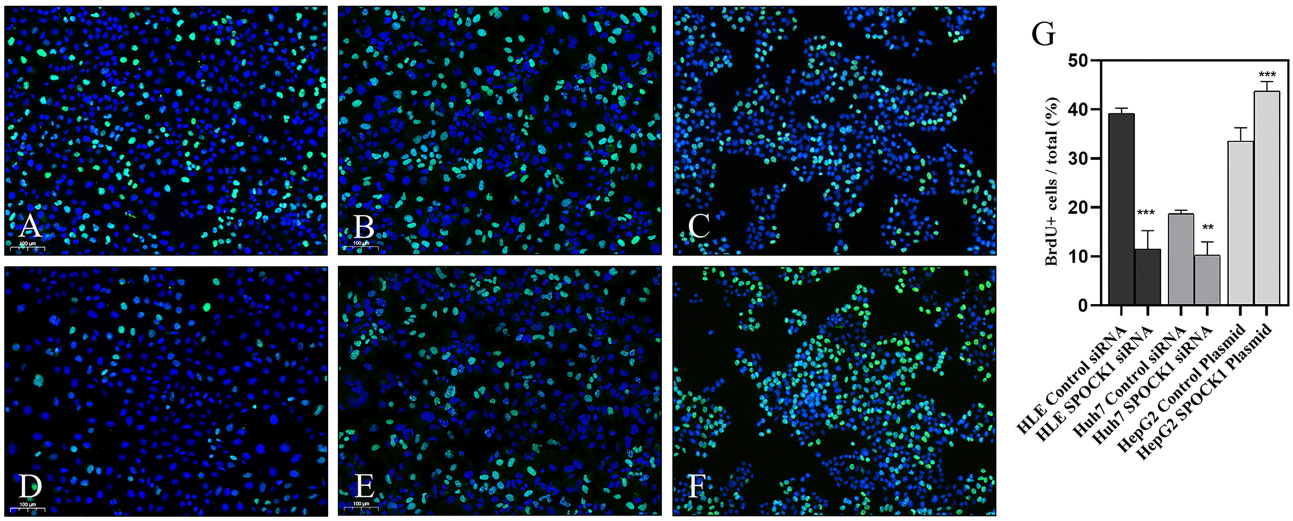

FIGURE 7 | BrdU uptake was studied in HLE and HuH7 cells after silencing SPOCK1 and HepG2 cells overexpressing the proteoglycan. Silencing of SPOCK1 inhibits its upregulation by transfection, promoting BrdU uptake. **(A)** HLE, **(B)** HuH7, and **(C)** HepG2 control cell lines. **(D)** HLE and **(E)** HuH7 cell lines transfected with siRNA. **(F)** HepG2 cell line transfected with the SPOCK1 expression vector. **(G)** Quantitation of the fluorescent nuclei. Green BrdU, blue DAPI. Original magnification, ×20. **p < 0.01, ***p < 0.001.

3.5.3 Detection of SPOCK1 After Silencing or Transfection of Hepatoma Cell Lines

SPOCK1 mRNA decreased in SPOCK1-silenced and increased in SPOCK1-transfected hepatoma cell lines. However, intracellular SPOCK1 protein expression was constant, and it was only the culture medium where the effect of downregulation or upregulation could be detected on the protein level (**Figure 11** and **Table 1**).

3.6 SPOCK1 and Syndecan-1 Compete in the Liver and in Hepatocellular Cancer

We studied if the presence or overexpression of syndecan-1 the major transmembrane heparan sulfate proteoglycan of the liver can interfere with the tumor-induced upregulation of SPOCK1. Without DEN exposure, no difference could be detected between wild type and $hSDC^{+/+}$ by immunostaining (**Figures 3A**, **12A**). However, Western blotting revealed that $hSDC^{+/+}$ transgenic control livers expressed a lower amount of SPOCK1 (**Figures 12C, D**). Similarly, $hSDC^{+/+}$ tumors contained less SPOCK1 than tumors developed in wild-type livers (**Figures 3B**, **12B**). In normal human liver, syndecan-1 and SPOCK1 are well separated, with the former being detected on the cell surface of hepatocytes and the latter in their cytoplasm. In contrast, in human liver cancer, syndecan-1 expression decreases, or even disappears, whereas the cytoplasm is filled with SPOCK1 (**Figure 13**).

4 DISCUSSION

4.1 Uncertainties Related to SPOCK1

Although SPOCK1 was discovered in 1997, the first reports related to its oncogenic potential were published after 2010, describing the implication of the proteoglycan in gastric cancer (33). In the past 10 years, many more accounts have called attention to the oncogenic potential of SPOCK1. However, it is still uncertain if SPOCK1 has physiological functions outside the central nervous system and where it localizes *in vivo*. Is it an ECM protein? Or similar to serglycin (34), can it be detected in the cells of epithelial origin? The first assessment of the role of SPOCK1 in tissue metabolism was published last year. According to this report, SPOCK1 regulates adipogenesis-related genes, participates in thermoregulation, induces adipocyte differentiation, and is likely to be involved in the development of obesity and type 2 diabetes (35). Furthermore, SPOCK1 transgenic mice develop fatty liver.

Our work indicates that except for endothelial cells of blood vessels, neither hepatocytes nor the connective tissue of the healthy liver expresses abundant amounts of SPOCK1. However, our results demonstrated that intensive cytoplasmic SPOCK1 expression occurs in normal hepatocytes after their isolation, which most probably is related to cellular stress. The support of these presumptions needs further evaluation. This is in contrast with a recent report emphasizing that SPOCK1 is expressed presumably in activated hepatic stellate cells (HSCs). However, in the published paper, SPOCK1 immunostaining was localized in the cytoplasm of hepatocytes (30, 36), whereas the connective tissue was almost free of immunoreaction. Our studies on human liver specimens support the notion that SPOCK1 is upregulated in cirrhotic liver and hepatocellular carcinoma, but the localization is not stromal. Cultured HSCs do express SPOCK1 in their cytoplasm (36), and we could confirm this in LX2 immortalized HSC cells.

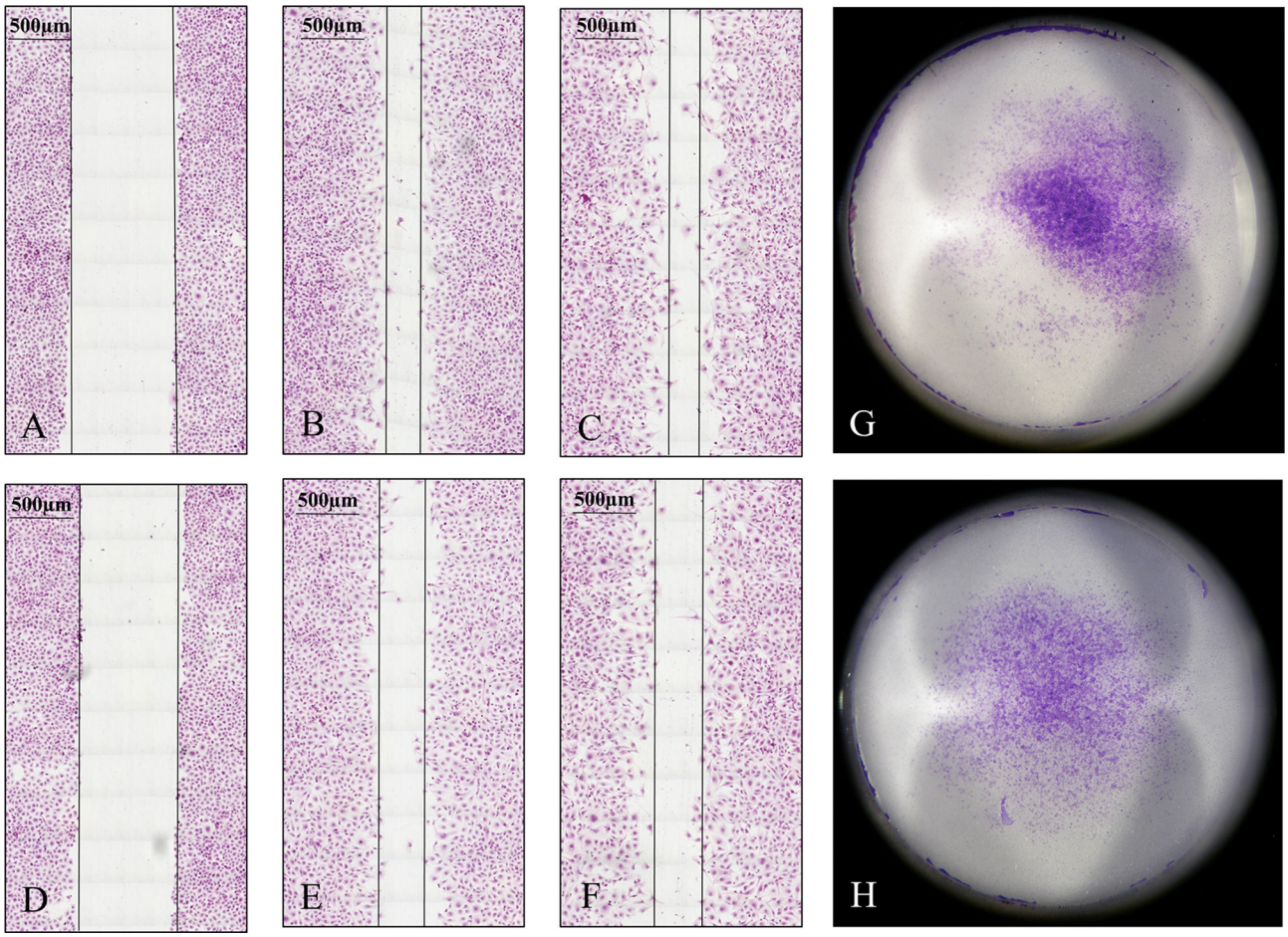

FIGURE 8 | Migration and invasion assays of HLE cells. The tumor cells were observed for 48 h in the migration assay. Silencing of SPOCK1 by siRNA inhibited the migration of the tumor cells. **(A–C)** Control cells at 0, 24, and 48 h time points. **(D–F)** SPOCK1 siRNA transfected cells at 0, 24, and 48 h time points. Invasion assay of control **(G)** and SPOCK1-silenced **(H)** HLE cells. Silencing inhibited both the migration and invasion of the tumor cells. As control Huh7 cells neither migrate nor invade collagen, no difference between the control and silenced cells could be detected.

4.2 SPOCK1 in Human Tumors, Intracellular or Stromal?

Immunohistochemical analysis of 76 surgically removed liver specimens revealed that the expression of SPOCK1 is a characteristic feature of human liver cirrhosis and cancer, and its accumulation occurs in the cytoplasm of hepatocytes and the cells of hepatocellular carcinoma. The most significant increase was observed in hepatitis C-infected cirrhotic and tumorous specimens. In general, several tumors of epithelial origin express SPOCK1 in the cytoplasm, including prostate cancer (36, 37), breast cancer (38), gastric cancer (22), and several others (27). In the case of non-small cell lung cancer, the presence of SPOCK1 contributes to the resistance of the third-generation tyrosine kinase inhibitor (39). SPOCK1 can also be the regulator of brain metastasis of lung cancers (40), raising the opportunity to use the protein as a predictive tumor marker. Taken together, SPOCK1 is claimed to be an oncogene, involved in major oncogenic events, such as cell cycle regulation, DNA synthesis, migration, invasion, and EMT (27). This summary supports our findings presented here.

4.3 SPOCK1 and Liver Cancer

Thus, our results on the human hepatocellular cancer (HCC) and mouse hepatocarcinogenesis models, together with literature data, provided confirmation for the presence of SPOCK1 in diseased hepatocytes of cirrhotic liver and cancer cells (29). In support of earlier studies, the transcription factor of SPOCK1 was also upregulated in the experimental hepatocarcinogenesis model. However, the expression of cytoplasmic SPOCK1 in seemingly normal human livers needs explanation, especially as this finding is the opposite of what we found in healthy rodent livers. Our hypothesis is that during the significantly increased lifespan, the human liver is

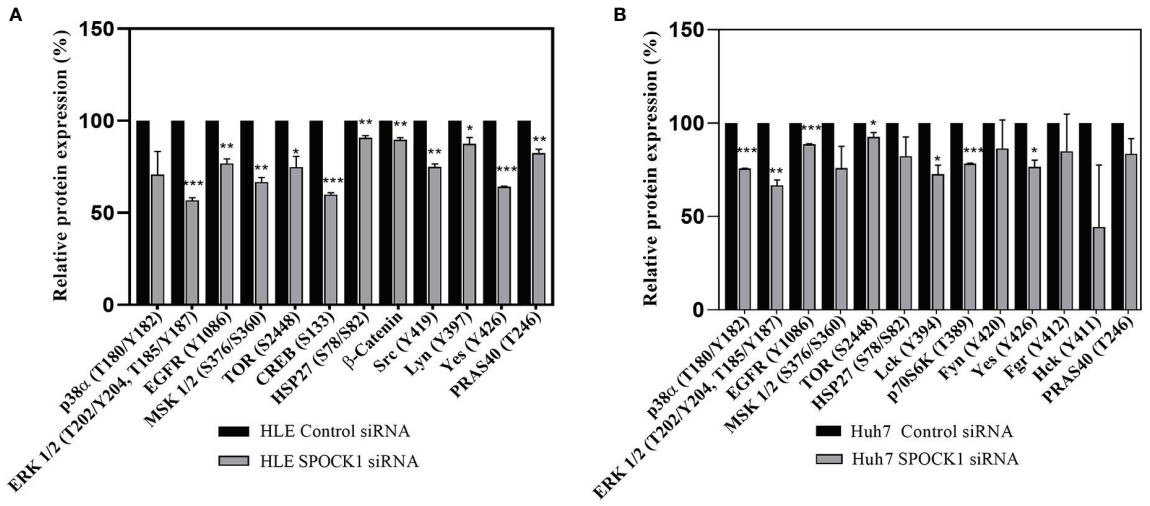

FIGURE 9 | Phosphotyrosine kinase arrays of HLE **(A)** and Huh7 **(B)** cells showing the changes as an effect of SPOCK1 silencing by siRNA. Downregulation of SPOCK1 was accompanied by decreased activation of EGFR, and MAPK pathways in both HLE and HuH7 cell lines together with several members of the Sarc family. The inhibition was more effective in the highly aggressive HLE cell line where MSK1, Creb, mTOR, and β-catenin were also affected. *p < 0.05, **p < 0.01, ***p < 0.001.

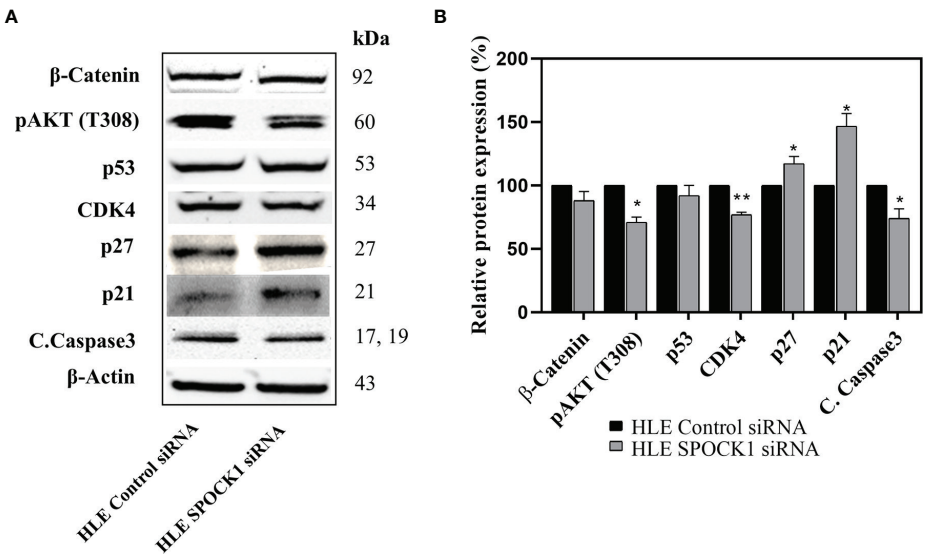

FIGURE 10 | Western blotting of control and SPOCK1 siRNA silenced HLE cells. **(A)** Additional consequences of SPOCK1 downregulation. Inhibition of the proteoglycan resulted in the downregulation of pAkt (T308), and CDK4 cyclin-dependent kinase, accompanied by the elevated expression of p21 and p27 cyclin-dependent kinase inhibitors. **(B)** Quantitative evaluation. *p < 0.05, **p < 0.01.

exposed to stressful injuries, capable of upregulating the proteoglycan. Indeed, the expression of SPOCK1 in the cytoplasm of fetal human livers was comparable with that of normal mouse and rat livers. In stress situations in our experiments, isolated hepatocytes from rat livers exhibited rapid transient upregulation of SPOCK1 in the cytoplasm.

4.4 *In Vitro* Models

HLE, HuH7, and HepG2 cell lines express considerable amounts of SPOCK1 in the cytoplasm, mainly localized in the mitochondria. At this point, it is uncertain if it interferes with the mitochondrial function of these hepatoma cells. The potential of SPOCK1 to inhibit apoptosis has been published

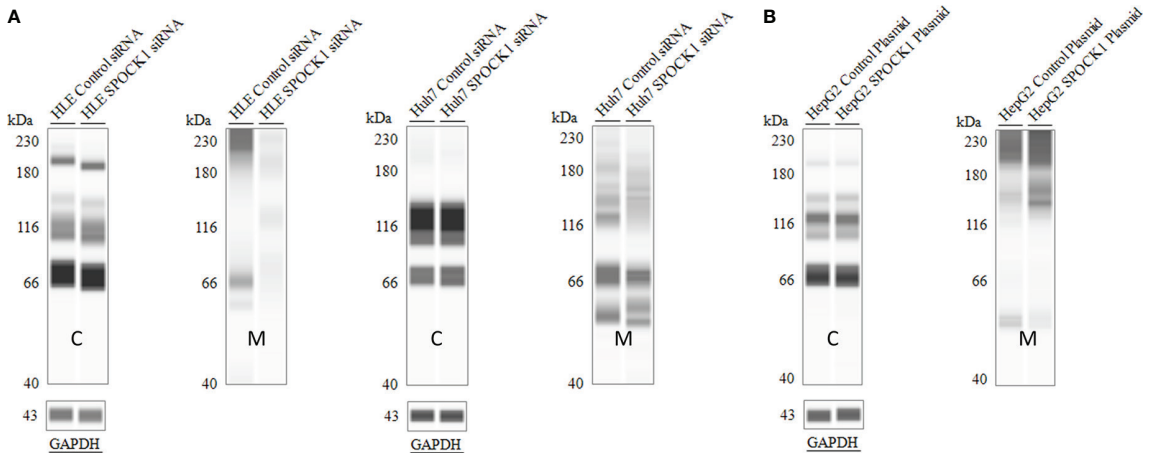

FIGURE 11 | SPOCK1 downregulation and upregulation were mirrored only by the amount of the secreted proteoglycan. WES of SPOCK1-silenced **(A)** and SPOCK1-transfected **(B)** cells were separated and run parallel with the part of the proteins secreted into the culture medium. The intracellular concentration of the protein remained constant, and only the amounts secreted to the medium represented the changes. C, tumor cells; M, culture medium.

TABLE 1 | Downregulation of SPOCK1 mRNA in HLE and Huh7 cells by SPOCK1 siRNA and its upregulation after transfection by SPOCK1 construct of HepG2.

Cell line	Relative quantification (fold change)	95% CI
HLE	0.07	0.046–0.109
Huh7	0.292	0.139–0.613
HepG2	30.517	16.698–55.771

Data indicate the fold changes.

(29, 41), and this function of SPOCK1 is related to the effect of its transcription factor CHD1L (42).

To detect the mechanistic function of SPOCK1, we followed the migration and invasion in the HLE and Huh7 cell lines after silencing with SPOCK1 siRNA. Both migration and invasion were successfully inhibited in the highly aggressive HLE cell line, but Huh7 cells neither migrate nor invade collagen. The mechanism behind this phenomenon needs further evaluation. To investigate if SPOCK1 has the potential to interfere with DNA synthesis, we downregulated its expression with siRNA or, alternatively, overexpressed it by using a SPOCK1 construct. From these assays, we learned that the proteoglycan interfered with the DNA synthesis, as its downregulation hampered the incorporation, whereas its elevated amount supported the uptake of BrdU. SPOCK1 inhibition pointed to CREB and CDK4, as both proteins were downregulated by SPOCK1 silencing, suggesting that they regulate the proteoglycan (43). So far, no report has evaluated the relationship between CREB and SPOCK1. However, as more than 4,000 proteins contain creb binding cre element in their promoters, SPOCK1 is likely equipped with this feature (44, 45). The CREB transcription factor is regulated *via* several tyrosine kinase receptor-activated pathways, and SPOCK1 silencing resulted in decreased EGFR activation followed by downregulation of the MAPK pathway (45). This explains not only the decreased action of CREB but also the lower levels of CDK4 cyclin-dependent kinase. These, together with the elevation of p21 and p27 cyclin-dependent kinase inhibitors, support the notion that SPOCK1 downregulation inhibits proliferation (46). One so far unknown consequence of SPOCK1 silencing is the inhibition of the members of the Src family. This family contains several non-receptor tyrosine kinase proteins, known to be implicated in cancer progression (47) including their involvement in migration, invasion, and proliferation. The HBX protein of the hepatitis B virus needs the action of Src to activate the signaling of RAS (48). C-Src is frequently upregulated in liver cancer and promotes the upregulation of the Hippo pathway (49). As SPOCK1 silencing inhibits the activation of Src, it is possible that this function similarly affects the Hippo pathway. In addition, it was recently reported that the Src protein in the liver interferes with the mitochondrial OXIPHOS complex (50). Considering that TOMM20 is an active player of mitochondrial metabolism and presumably responsible for the mitochondrial uptake of SPOCK1, closer scrutiny of their relationship may provide further clarification of the processes involved. Although our phosphokinase array revealed significant downregulation of Yes and other members of the Src family, its expression in HCC is still under debate (51, 52) without mechanistic data. According to a more recent report, inhibition of Yes by miR-210 decreases the proliferative capacity of hepatoma cells (53).

4.5 SPOCK1 Intracellular or Extracellular?

Although mRNA expression of SPOCK1 depends upon the experimental conditions when using hepatoma cell lines, the intracellular presence of the protein is not influenced either by silencing or transfection. This indicates that SPOCK1 is secreted to the culture media. Certainly, SPOCK1 concentration in the culture medium changes according to the actual experimental conditions; it is decreased after silencing and increased after SPOCK1 transfection, supporting the idea that SPOCK1 is a secreted

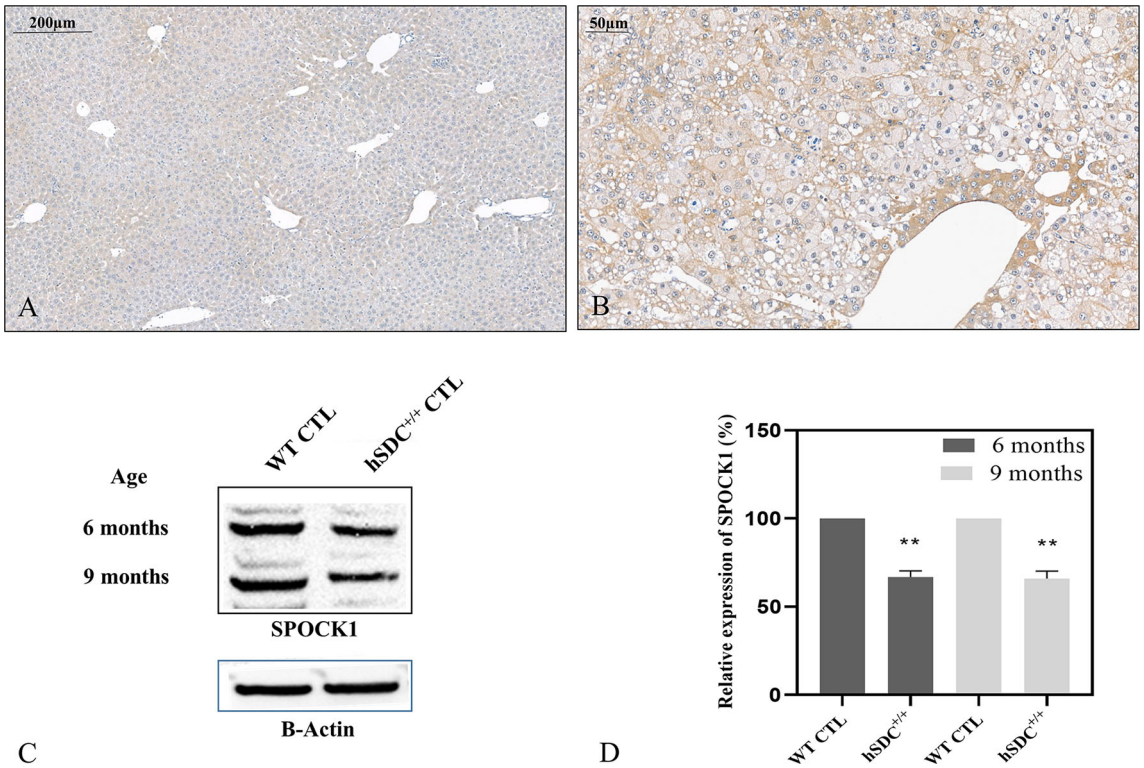

FIGURE 12 | SPOCK1 expression in hSDC-1$^{+/+}$ transgenic control liver and its diethylnitrosamine (DEN)-induced cancer. **(A)** Weak SPOCK1 positivity was detected around the central veins in hSDC-1$^{+/+}$ control liver. **(B)** Hepatocellular cancer 11 months after DEN exposure in the hSDC-1$^{+/+}$ liver. The intensity of SPOCK1 staining is still modest, except around the central veins. Western blotting **(C, D)** supports the results of immunohistochemistry; SPOCK1 expression in hSDC-1$^{+/+}$ control livers is lower than that in wild-type liver throughout the whole experiments. **p < 0.01.

proteoglycan (36). However, its synthesis was not restricted to stromal cells, as opposed to an earlier report (36). These findings are in direct contradiction with those we detected in human livers, where the cytoplasm of cirrhotic and transformed hepatocytes was loaded with considerable amounts of SPOCK1. This raises several questions: is the signal peptide injured? Are there other structural alterations of the proteoglycan? Do cancer cells need more intracellular SPOCK1 for their functions? Is the proteoglycan removed into the circulation? Further studies are needed to answer these questions.

4.6 Overexpression of SPOCK1 Coincides With Downregulation of Syndecan-1 in Human Hepatocellular Carcinoma

In experimental hepatocarcinogenesis, syndecan-1 overexpression provides protection against the development of cancer, and in addition to other factors, the downregulation of SPOCK1 could be observed throughout the experimental period (9). Since in human HCCs syndecan-1 lacks the protective effect, we assume that the increased syndecan-1 expression is a requirement for the protection against the harmful effects of SPOCK1. Further studies are necessary to understand those events that regulate the interaction of the two proteoglycans. Potential mechanisms can involve forced shedding of syndecan-1 and/or its decreased synthesis. The effect seems to be related to tumor aggressiveness because cells of well-differentiated tumors can rescue their cell surface syndecan-1. In contrast, no detectable amounts of the proteoglycan were found on the surface of micrometastases. Concerning other proteoglycans, no publications were found in PubMed about their interaction with SPOCK1.

Syndecan-1 is the most studied proteoglycan of the liver. Besides it functions as a lipoprotein receptor (54), it interferes with lipid metabolism by inhibiting the synthesis of FASN and modulating the Akt-mTOR and Wnt signaling, in this way protecting again NAFLD and experimental carcinogenesis (9). Its expression increases in liver fibrogenesis and liver cirrhosis (55), and its activity as the receptor of HCV is also confirmed (56).

Recently, syndecan-4 was also published to be a serum marker of NAFLD (7) and also acts as a receptor of HCV (57), not only infecting the hepatocytes but also responsible for the submission of the virus from men to men infecting anal Langerhans cells (58). Besides syndecan-1, syndecan-4 also regulates the Wnt signaling (59). By masking the functional domain of osteopontin, syndecan-4 inhibits the development of osteopontin-induced acute liver injury (60).

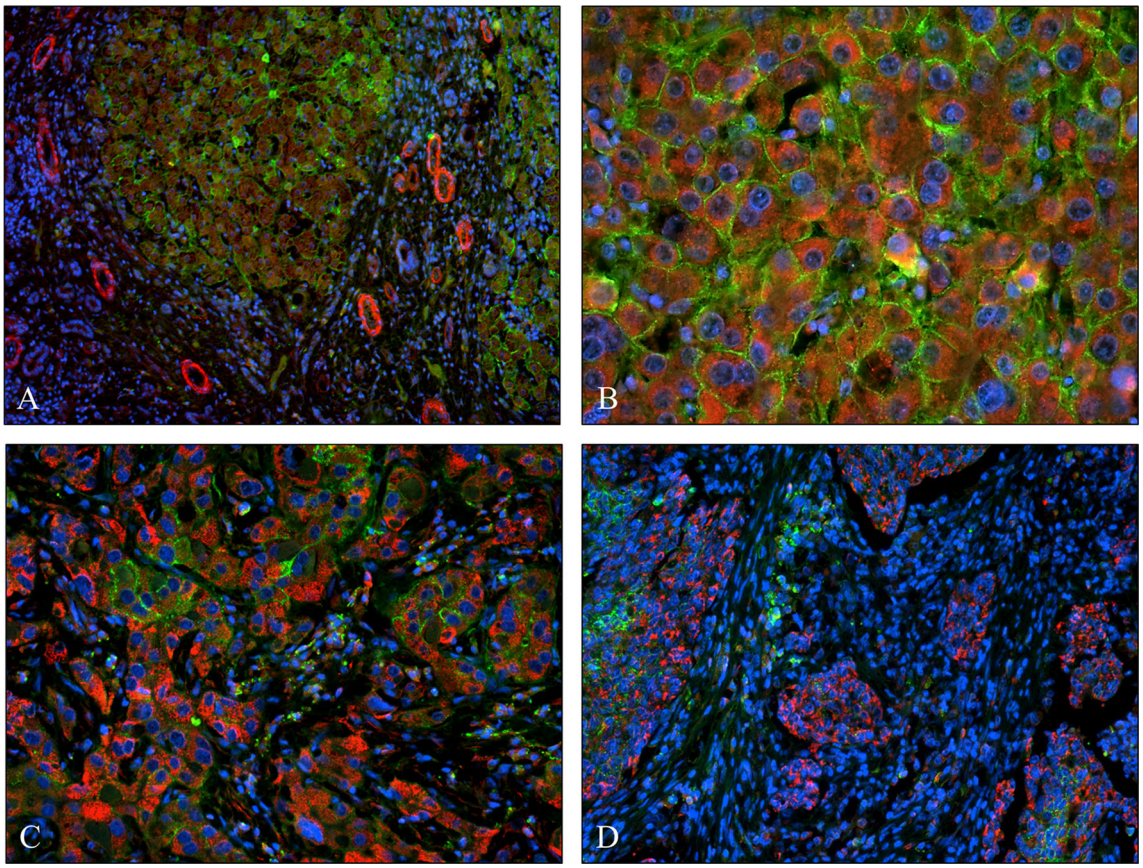

FIGURE 13 | Co-expression of syndecan-1 and SPOCK1 in human liver cirrhosis and hepatocellular cancers. **(A)** Cirrhotic remodeling of the liver structure. A modest amount of SPOCK1 in the cytoplasm of hepatocytes (red), with syndecan-1 on the surface of the same cells (green). SPOCK1 containing endothelial cells of blood vessels are present in the stroma. **(B)** Well-differentiated hepatocellular cancer (HCC) with intensive cytoplasmic SPOCK1 staining and large amounts of syndecan-1 on the surface of tumor cells. **(C)** HCC with de-differentiated cancer cells. Intensive SPOCK1 expression in the cytoplasm; syndecan-1 vanished from the majority of cancer cells. **(D)** Micro metastases of HCC migrating in the tumor stroma. While SPOCK1 can be detected in large amounts, syndecan-1 protein cannot be observed.

4.7 Possible Cooperation of Liver Proteoglycans in the Promotion of Cancer

In preexisting literature, only glypican-3 and agrin have been recognized as proteoglycans with oncogenic potential in the liver. Based on the data presented herein, SPOCK1 will likely join this company. Glypican-3 is a cell membrane-anchored proteoglycan (61), while agrin is present in the basement membranes of tumor vasculature, bile ducts, and the portal area (62). According to our results, SPOCK1 is present in the mitochondria of the HCC cells. Due to their distinct localization, a direct interaction between these proteoglycans is improbable; their effects may nevertheless combine. Glypican exerts its action *via* the Wnt pathway by upregulating β-catenin, facilitating the transcription of proteins with oncogenic potential while simultaneously downregulating Hedgehog signaling (63). Agrin regulates focal adhesion integrity, facilitates migration, and promotes EMT by signaling through the Musk receptor (64). Furthermore, it is involved in the downregulation of the Hypo pathway *via* transducing matrix stiffness by utilizing both Musk and integrin receptors (65). SPOCK1 can stimulate the mTOR pathway (38) and utilize Wnt signaling (28, 66). Additionally, the fact that it promotes resistance against third-generation TK inhibitors in lung cancer (39) indicates its involvement in EGFR signaling. The potential cooperation of glypican-3, agrin, and SPOCK1 in liver oncogenesis should be elucidated in future experimental models.

4.8 Conclusion

Data collected in the last 12 years indicate that SPOCK1 is a proteoglycan with oncogenic potential. Its presence in tumor cells increases with tumor aggressiveness, and it can influence the function of receptor tyrosine kinases, intracellular phosphokinases, and DNA synthesis and alleviates the protective potential of syndecan-1 against HCC. Most likely, after secretion to the ECM, SPOCK1 establishes interaction with TGFβ1 and promotes EMT (67). SPOCK1 may additionally interact with other, currently unidentified, proteins and cellular mechanisms

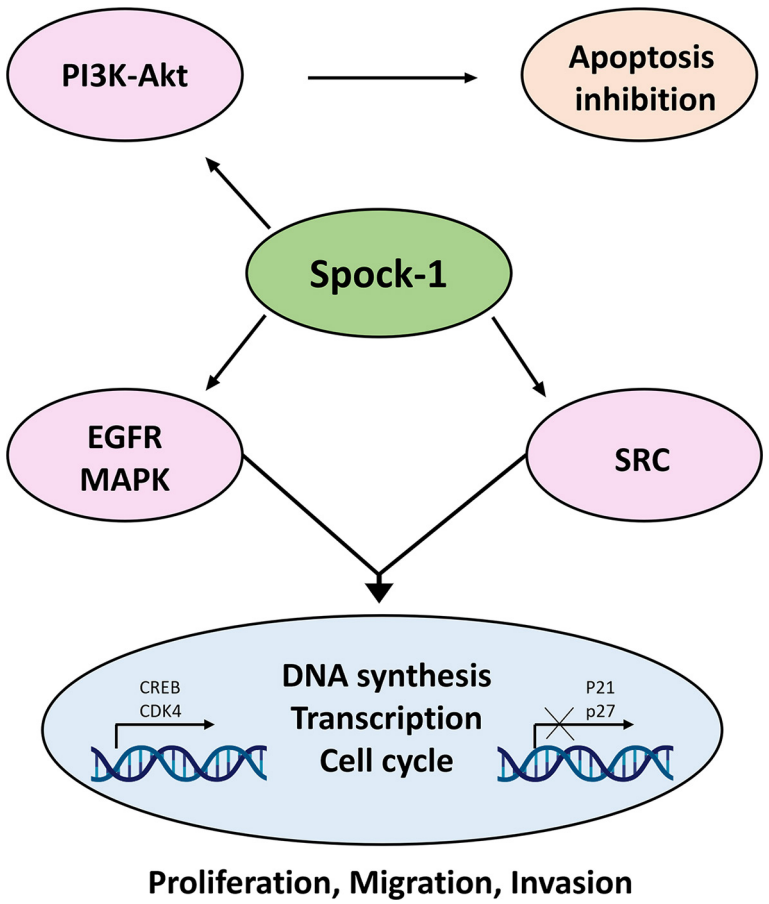

FIGURE 14 | Action of SPOCK1 in hepatoma cell lines. In harmony with previous results, Spock-1 stimulates the Akt-mTOR pathway. Akt activation results in apoptosis inhibition. The mitochondrial localization of the proteoglycan may interfere in other ways as well with the apoptotic activity, which needs further evaluation. SPOCK1 silencing resulted in the downregulation of the EGFR tyrosine kinase receptor and members of the Sarc tyrosine kinase family, indicating the stimulatory potential of the proteoglycan on the signaling activity, partly through the MAPK pathway. Furthermore, SPOCK1 inhibition pointed to a decrease of two nuclear proteins CREB and CDK4; the former is a multivalent transcription factor with strong oncogenic potential, and the latter is the stimulator of cell cycle. Both nuclear proteins can be upregulated *via* MAPK signaling. Furthermore, CREB establishes interaction with several nuclear factors, facilitates DNA synthesis, and regulates chromatin function as well. Its action is in a good agreement with the effect of SPOCK1 on DNA synthesis, cell migration, and invasion (43).

(**Figure 14**). Because in human and experimental hepatocellular carcinoma its stromal expression was hardly detected after secretion, SPOCK1 is likely to be cleared by the circulation. This finding may serve as a diagnostic tool in the not too distant future.

DATA AVAILABILITY STATEMENT

The original contributions presented in the study are included in the article/**Supplementary Material**. Further inquiries can be directed to the corresponding author.

ETHICS STATEMENT

The studies involving human participants were reviewed and approved by Semmelweis University Regional and Institutional Committee of Science and Research Ethics (TUKEB permit number: 155/2012) and Medical Research Council Committee of Science and Research Ethics (permit number: 61303-2/2018/EKU). Written informed consent for participation was not required for this study in accordance with the national legislation and the institutional requirements. The animal study was reviewed and approved by the Ethics Committee of the Animal Health Care and Control Institute, Csongrád County (protocol code XVI/03047-2/2008).

AUTHOR CONTRIBUTIONS

Conceptualization: KB, ZS, LT, LV, and IK. Methodology: KK, BP, AR, and IK. Data curation: LV and IK. Formal analysis: LV, AR, KK, and IK. Funding acquisition: KB, AK, KD and IK. Investigation: LV, AK, KK, LT, GP, BP, and IK. Resources: AS

and IK. Validation: KD, AS, KB, and IK. Writing: LV and IK. Writing—review and editing: KD, KB, and IK. Visualization: AR, GP, and IK. Supervision: ZS, AK, and IK. Project administration: IK. All authors listed have made a substantial, direct, and intellectual contribution to the work and approved it for publication.

FUNDING

This work was supported by the Hungarian Scientific Research Fund (grants 67925, 100904 and 119283 to I.K. and FK 138673 to K.D.) and European Union Horizon 2020 Marie Skłodowska-Curie Actions (MSCA) Research and Innovation Staff Exchange Evaluations (RISE) project (grant 645756): "GLYCANC—Matrix glycans as multifunctional pathogenesis factors and therapeutic targets in cancer" (to I.K. and K.B.), EFOP-3.6.3-VEKOP-16-2017-00009 (to L.V.).

ACKNOWLEDGMENTS

We are grateful to László Ötvös for editorial assistance.

SUPPLEMENTARY MATERIAL

The Supplementary Material for this article can be found online at: https://www.frontiersin.org/articles/10.3389/fonc.2022.819883/full#supplementary-material

REFERENCES

1. You W, Henneberg M. Cancer Incidence Increasing Globally: The Role of Relaxed Natural Selection. *Evolutionary Appl* (2017) 11(2):140–52. doi: 10.1111/eva.12523
2. Valkenburg KC, de Groot AE, Pienta KJ. Targeting the Tumour Stroma to Improve Cancer Therapy. *Nat Rev Clin Oncol* (2018) 15(6):366–81. doi: 10.1038/s41571-018-0007-1
3. Pape J, Magdeldin T, Stamati K, Nyga A, Loizidou M, Emberton M, et al. Cancer-Associated Fibroblasts Mediate Cancer Progression and Remodel the Tumouroid Stroma. *Br J Cancer* (2020) 123(7):1178–90. doi: 10.1038/s41416-020-0973-9
4. Sebestyén A, Gallai M, Knittel T, Ambrust T, Ramadori G, Kovalszky I. Cytokine Regulation of Syndecan Expression in Cells of Liver Origin. *Cytokine* (2000) 12(10):1557–60. doi: 10.1006/cyto.2000.0754
5. Regős E, Abdelfattah HH, Reszegi A, Szilák L, Werling K, Szabó G, et al. Syndecan-1 Inhibits Early Stages of Liver Fibrogenesis by Interfering With Tgfβ1 Action and Upregulating MMP14. *Matrix Biol J Int Soc Matrix Biol* (2018) 68-69:474–89. doi: 10.1016/j.matbio.2018.02.008
6. Roskams T, Rosenbaum J, De Vos R, David G, Desmet V. Heparan Sulfate Proteoglycan Expression in Chronic Cholestatic Human Liver Diseases. *Hepatol (Baltimore Md)* (1996) 24(3):524–32. doi: 10.1053/jhep.1996.v24.pm0008781318
7. Xia SJ, Tang LZ, Li WH, Xu ZS, Zhang LL, Cheng FG, et al. Serum Syndecan-4 is Associated With Nonalcoholic Fatty Liver Disease. *J Digestive Dis* (2021) 22(9):536–44. doi: 10.1111/1751-2980.13037
8. Regős E, Karászi K, Reszegi A, Kiss A, Schaff Z, Baghy K, et al. Syndecan-1 in Liver Diseases. *Pathol Oncol Res POR* (2020) 26(2):813–9. doi: 10.1007/s12253-019-00617-0
9. Reszegi A, Karászi K, Tóth G, Rada K, Váncza L, Turiák L, et al. Overexpression of Human Syndecan-1 Protects Against the Diethylnitrosamine-Induced Hepatocarcinogenesis in Mice. *Cancers* (2021) 13(7):1548. doi: 10.3390/cancers13071548
10. Filmus J, Capurro M. Glypican-3: A Marker and a Therapeutic Target in Hepatocellular Carcinoma. *FEBS J* (2013) 280(10):2471–6. doi: 10.1111/febs.12126
11. Guo M, Zhang H, Zheng J, Liu Y. Glypican-3: A New Target for Diagnosis and Treatment of Hepatocellular Carcinoma. *J Cancer* (2020) 11(8):2008–21. doi: 10.7150/jca.39972
12. Tátrai P, Egedi K, Somorácz A, van Kuppevelt TH, Ten Dam G, Lyon M, et al. Quantitative and Qualitative Alterations of Heparan Sulfate in Fibrogenic Liver Diseases and Hepatocellular Cancer. *J Histochem Cytochem Off J Histochem Soc* (2010) 58(5):429–41. doi: 10.1369/jhc.2010.955161
13. Bukong TN, Maurice SB, Chahal B, Schaeffer DF, Winwood PJ. Versican: A Novel Modulator of Hepatic Fibrosis. *Lab invest; J Tech Methods Pathol* (2016) 96(3):361–74. doi: 10.1038/labinvest.2015.152
14. Bonnet F, Perin JP, Maillet P, Jolles P, Alliel PM. Characterization of a Human Seminal Plasma Glycosaminoglycan-Bearing Polypeptide. *Biochem J* (1992) 288(Pt 2):565–9. doi: 10.1042/bj2880565
15. Charbonnier F, Périn JP, Roussel G, Nussbaum JL, Alliel PM. [Cloning of Testican/SPOCK in Man and Mouse. Neuromuscular Expression Perspectives in Pathology]. *C R Seances Soc Biol Fil* (1997) 191(1):127–33.
16. Cifuentes-Diaz C, Alliel PM, Charbonnier F, de la Porte S, Molgó J, Goudou D, et al. Regulated Expression of the Proteoglycan SPOCK in the Neuromuscular System. *Mech Dev* (2000) 94(1-2):277–82. doi: 10.1016/s0925-4773(00)00285-9
17. Bonnet F, Périn JP, Charbonnier F, Camuzat A, Roussel G, Nussbaum JL, et al. Structure and Cellular Distribution of Mouse Brain Testican. Association With the Postsynaptic Area of Hippocampus Pyramidal Cells. *J Biol Chem* (1996) 271(8):4373–80. doi: 10.1074/jbc.271.8.4373
18. Hausser HJ, Decking R, Brenner RE. Testican-1, an Inhibitor of Pro-MMP-2 Activation, Is Expressed in Cartilage. *Osteoarthritis Cartilage* (2004) 12(11):870–7. doi: 10.1016/j.joca.2004.07.008
19. Edgell CJ, BaSalamah MA, Marr HS. Testican-1: A Differentially Expressed Proteoglycan With Protease Inhibiting Activities. *Int Rev Cytol* (2004) 236:101–22. doi: 10.1016/s0074-7696(04)36003-1
20. Lee Y, Lee W, Chang HH, Kim SW, Kim J, Bae JS. Testican-1, as a Novel Diagnosis of Sepsis. *J Cell Biochem* (2018) 119(5):4216–23. doi: 10.1002/jcb.26661
21. Chen D, Zhou H, Liu G, Zhao Y, Cao G, Liu Q. SPOCK1 Promotes the Invasion and Metastasis of Gastric Cancer Through Slug-Induced Epithelial-Mesenchymal Transition. *J Cell Mol Med* (2018) 22(2):797–807. doi: 10.1111/jcmm.13357
22. Chen Q, Yao YT, Xu H, Chen YB, Gu M, Cai ZK, et al. SPOCK1 Promotes Tumor Growth and Metastasis in Human Prostate Cancer. *Drug Des Devel Ther* (2016) 10:2311–21. doi: 10.2147/dddt.S91321
23. Shu YJ, Weng H, Ye YY, Hu YP, Bao RF, Cao Y, et al. SPOCK1 as a Potential Cancer Prognostic Marker Promotes the Proliferation and Metastasis of Gallbladder Cancer Cells by Activating the PI3K/AKT Pathway. *Mol Cancer* (2015) 14(1):12. doi: 10.1186/s12943-014-0276-y
24. Yu F, Li G, Gao J, Sun Y, Liu P, Gao H, et al. SPOCK1 Is Upregulated in Recurrent Glioblastoma and Contributes to Metastasis and Temozolomide Resistance. *Cell Prolif* (2016) 49(2):195–206. doi: 10.1111/cpr.12241
25. Veenstra VL, Damhofer H, Waasdorp C, Steins A, Kocher HM, Medema JP, et al. Stromal SPOCK1 Supports Invasive Pancreatic Cancer Growth. *Mol Oncol* (2017) 11(8):1050–64. doi: 10.1002/1878-0261.12073
26. Fan LC, Jeng YM, Lu YT, Lien HC. SPOCK1 Is a Novel Transforming Growth Factor-β-Induced Myoepithelial Marker That Enhances Invasion and Correlates With Poor Prognosis in Breast Cancer. *PloS One* (2016) 11(9):e0162933. doi: 10.1371/journal.pone.0162933
27. Han J, Rong Y, Gao X. Multiomic Analysis of the Function of SPOCK1 Across Cancers: An Integrated Bioinformatics Approach. *J Int Med Res* (2021) 49(6):300060520962659. doi: 10.1177/0300060520962659

28. Wang T, Liu X, Tian Q, Liang T, Chang P. Reduced SPOCK1 Expression Inhibits Non-Small Cell Lung Cancer Cell Proliferation and Migration Through Wnt/β-Catenin Signaling. *Eur Rev Med Pharmacol Sci* (2018) 22 (3):637–44. doi: 10.26355/eurrev_201802_14288
29. Li Y, Chen L, Chan TH, Liu M, Kong KL, Qiu JL, et al. SPOCK1 Is Regulated by CHD1L and Blocks Apoptosis and Promotes HCC Cell Invasiveness and Metastasis in Mice. *Gastroenterology* (2013) 144(1):179–91.e4. doi: 10.1053/j.gastro.2012.09.042
30. Annaval T, Wild R, Crétinon Y, Sadir R, Vivès RR, Lortat-Jacob H. Heparan Sulfate Proteoglycans Biosynthesis and Post Synthesis Mechanisms Combine Few Enzymes and Few Core Proteins to Generate Extensive Structural and Functional Diversity. *Molecules* (2020) 25(18):4215. doi: 10.3390/molecules25184215
31. Seglen PO. Preparation of Isolated Rat Liver Cells. *Methods Cell Biol* (1976) 13:29–83. doi: 10.1016/s0091-679x(08)61797-5
32. Xiong X, Lai X, Li A, Liu Z, Ma N. Diversity Roles of CHD1L in Normal Cell Function and Tumorigenesis. *Biomark Res* (2021) 9(1):16. doi: 10.1186/s40364-021-00269-w
33. Marimuthu A, Jacob HK, Jakharia A, Subbannayya Y, Keerthikumar S, Kashyap MK, et al. Gene Expression Profiling of Gastric Cancer. *J Proteomics Bioinf* (2011) 4(4):74–82. doi: 10.4172/jpb.1000170
34. Korpetinou A, Papachristou DJ, Lampropoulou A, Bouris P, Labropoulou VT, Noulas A, et al. Increased Expression of Serglycin in Specific Carcinomas and Aggressive Cancer Cell Lines. *BioMed Res Int* (2015) 2015:690721. doi: 10.1155/2015/690721
35. Alshargabi R, Shinjo T, Iwashita M, Yamashita A, Sano T, Nishimura Y, et al. SPOCK1 Induces Adipose Tissue Maturation: New Insights Into the Function of SPOCK1 in Metabolism. *Biochem Biophys Res Commun* (2020) 533 (4):1076–82. doi: 10.1016/j.bbrc.2020.09.129
36. Du Z, Lin Z, Wang Z, Liu D, Tian D, Xia L. SPOCK1 Overexpression Induced by Platelet-Derived Growth Factor-BB Promotes Hepatic Stellate Cell Activation and Liver Fibrosis Through the Integrin α5β1/PI3K/Akt Signaling Pathway. *Lab invest; J Tech Methods Pathol* (2020) 100(8):1042–56. doi: 10.1038/s41374-020-0425-4
37. Chen ML, Ho CJ, Yeh CM, Chen SL, Sung WW, Wang SC, et al. High SPOCK1 Expression Is Associated With Advanced Stage, T Value, and Gleason Grade in Prostate Cancer. *Med (Kaunas)* (2019) 55(7):343. doi: 10.3390/medicina55070343
38. Xu M, Zhang X, Zhang S, Piao J, Yang Y, Wang X, et al. SPOCK1/SIX1axis Promotes Breast Cancer Progression by Activating AKT/mTOR Signaling. *Aging* (2020) 13(1):1032–50. doi: 10.18632/aging.202231
39. Gao Y, Yu M, Ma M, Zhuang Y, Qiu X, Zhao Q, et al. SPOCK1 Contributes to the Third-Generation EGFR Tyrosine Kinase Inhibitors Resistance in Lung Cancer. *J Cell Biochem* (2019) 120(8):12566–73. doi: 10.1002/jcb.28523
40. Singh M, Venugopal C, Tokar T, Brown KR, McFarlane N, Bakhshinyan D, et al. RNAi Screen Identifies Essential Regulators of Human Brain Metastasis-Initiating Cells. *Acta Neuropathol* (2017) 134(6):923–40. doi: 10.1007/s00401-017-1757-z
41. Li J, Ke J, Fang J, Chen JP. A Potential Prognostic Marker and Therapeutic Target: SPOCK1 Promotes the Proliferation, Metastasis, and Apoptosis of Pancreatic Ductal Adenocarcinoma Cells. *J Cell Biochem* (2020) 121(1):743–54. doi: 10.1002/jcb.29320
42. Cheng W, Su Y, Xu F. CHD1L: A Novel Oncogene. *Mol Cancer* (2013) 12 (1):170. doi: 10.1186/1476-4598-12-170
43. Steven A, Seliger B. Control of CREB Expression in Tumors: From Molecular Mechanisms and Signal Transduction Pathways to Therapeutic Target. *Oncotarget* (2016) 7(23):35454–65. doi: 10.18632/oncotarget.7721
44. Johannessen M, Moens U. Multisite Phosphorylation of the cAMP Response Element-Binding Protein (CREB) by a Diversity of Protein Kinases. *Front Biosci* (2007) 12:1814–32. doi: 10.2741/2190
45. Wang H, Xu J, Lazarovici P, Quirion R, Zheng W. cAMP Response Element-Binding Protein (CREB): A Possible Signaling Molecule Link in the Pathophysiology of Schizophrenia. *Front Mol Neurosci* (2018) 11:255. doi: 10.3389/fnmol.2018.00255
46. Scheiblecker L, Kollmann K, Sexl V. CDK4/6 and MAPK-Crosstalk as Opportunity for Cancer Treatment. *Pharm (Basel)* (2020) 13(12):418. doi: 10.3390/ph13120418
47. Kumar A, Jaggi AS, Singh N. Pharmacology of Src Family Kinases and Therapeutic Implications of Their Modulators. *Fundam Clin Pharmacol* (2015) 29(2):115–30. doi: 10.1111/fcp.12097
48. Klein NP, Schneider RJ. Activation of Src Family Kinases by Hepatitis B Virus HBx Protein and Coupled Signaling to Ras. *Mol Cell Biol* (1997) 17(11):6427–36. doi: 10.1128/mcb.17.11.6427
49. Yang J, Zhang X, Liu L, Yang X, Qian Q, Du B. C-Src Promotes the Growth and Tumorigenesis of Hepatocellular Carcinoma *via* the Hippo Signaling Pathway. *Life Sci* (2021) 264:118711. doi: 10.1016/j.lfs.2020.118711
50. Hunter CA, Koc H, Koc EC. C-Src Kinase Impairs the Expression of Mitochondrial OXPHOS Complexes in Liver Cancer. *Cell Signal* (2020) 72:109651. doi: 10.1016/j.cellsig.2020.109651
51. Nonomura T, Masaki T, Morishita A, Jian G, Uchida N, Himoto T, et al. Identification of C-Yes Expression in the Nuclei of Hepatocellular Carcinoma Cells: Involvement in the Early Stages of Hepatocarcinogenesis. *Int J Oncol* (2007) 30(1):105–11. doi: 10.3892/ijo.30.1.105
52. Feng H, Masaki T, Nonomura T, Morishita A, Jian G, Nakai S, et al. Activation of C-Yes in Hepatocellular Carcinoma: A Preliminary Study. *World J Gastroenterol* (2006) 12(35):5743–5. doi: 10.3748/wjg.v12.i35.5743
53. Tan W, Lim SG, Tan TM. Up-Regulation of microRNA-210 Inhibits Proliferation of Hepatocellular Carcinoma Cells by Targeting YES1. *World J Gastroenterol* (2015) 21(46):13030–41. doi: 10.3748/wjg.v21.i46.13030
54. Stanford KI, Bishop JR, Foley EM, Gonzales JC, Niesman IR, Witztum JL, et al. Syndecan-1 Is the Primary Heparan Sulfate Proteoglycan Mediating Hepatic Clearance of Triglyceride-Rich Lipoproteins in Mice. *J Clin Invest* (2009) 119(11):3236–45. doi: 10.1172/jci38251
55. Charchanti A, Kanavaros P, Koniaris E, Kataki A, Glantzounis G, Agnantis NJ, et al. Expression of Syndecan-1 in Chronic Liver Diseases: Correlation With Hepatic Fibrosis. *In Vivo (Athens Greece)* (2021) 35(1):333–9. doi: 10.21873/invivo.12264
56. Shi Q, Jiang J, Luo G. Syndecan-1 Serves as the Major Receptor for Attachment of Hepatitis C Virus to the Surfaces of Hepatocytes. *J Virol* (2013) 87(12):6866–75. doi: 10.1128/jvi.03475-12
57. Lefèvre M, Felmlee DJ, Parnot M, Baumert TF, Schuster C. Syndecan 4 Is Involved in Mediating HCV Entry Through Interaction With Lipoviral Particle-Associated Apolipoprotein E. *PloS One* (2014) 9(4):e95550. doi: 10.1371/journal.pone.0095550
58. Nijmeijer BM, Eder J, Langedijk CJM, Kaptein TM, Meeussen S, Zimmermann P, et al. Syndecan 4 Upregulation on Activated Langerhans Cells Counteracts Langerin Restriction to Facilitate Hepatitis C Virus Transmission. *Front Immunol* (2020) 11:503. doi: 10.3389/fimmu.2020.00503
59. Astudillo P, Carrasco H, Larraín J. Syndecan-4 Inhibits Wnt/β-Catenin Signaling Through Regulation of Low-Density-Lipoprotein Receptor-Related Protein (LRP6) and R-Spondin 3. *Int J Biochem Cell Biol* (2014) 46:103–12. doi: 10.1016/j.biocel.2013.11.012
60. Kon S, Ikesue M, Kimura C, Aoki M, Nakayama Y, Saito Y, et al. Syndecan-4 Protects Against Osteopontin-Mediated Acute Hepatic Injury by Masking Functional Domains of Osteopontin. *J Exp Med* (2008) 205(1):25–33. doi: 10.1084/jem.20071324
61. Takahashi Y, Dungubat E, Kusano H, Ganbat D, Tomita Y, Odgerel S, et al. Application of Immunohistochemistry in the Pathological Diagnosis of Liver Tumors. *Int J Mol Sci* (2021) 22(11):5780. doi: 10.3390/ijms22115780
62. Tátrai P, Dudás J, Batmunkh E, Máthé M, Zalatnai A, Schaff Z, et al. Agrin, a Novel Basement Membrane Component in Human and Rat Liver, Accumulates in Cirrhosis and Hepatocellular Carcinoma. *Lab invest; J Tech Methods Pathol* (2006) 86(11):1149–60. doi: 10.1038/labinvest.3700475
63. Kolluri A, Ho M. The Role of Glypican-3 in Regulating Wnt, YAP, and Hedgehog in Liver Cancer. *Front Oncol* (2019) 9:708. doi: 10.3389/fonc.2019.00708
64. Chakraborty S, Lakshmanan M, Swa HL, Chen J, Zhang X, Ong YS, et al. An Oncogenic Role of Agrin in Regulating Focal Adhesion Integrity in Hepatocellular Carcinoma. *Nat Commun* (2015) 6:6184. doi: 10.1038/ncomms7184
65. Chakraborty S, Njah K, Pobbati AV, Lim YB, Raju A, Lakshmanan M, et al. Agrin as a Mechanotransduction Signal Regulating YAP Through the Hippo Pathway. *Cell Rep* (2017) 18(10):2464–79. doi: 10.1016/j.celrep.2017.02.041
66. Yang J, Yang Q, Yu J, Li X, Yu S, Zhang X. SPOCK1 Promotes the Proliferation, Migration and Invasion of Glioma Cells Through PI3K/AKT

and Wnt/β-Catenin Signaling Pathways. *Oncol Rep* (2016) 35(6):3566–76. doi: 10.3892/or.2016.4757
67. Sun LR, Li SY, Guo QS, Zhou W, Zhang HM. SPOCK1 Involvement in Epithelial-To-Mesenchymal Transition: A New Target in Cancer Therapy? *Cancer Manage Res* (2020) 12:3561–9. doi: 10.2147/cmar.S249754

Conflict of Interest: The authors declare that the research was conducted in the absence of any commercial or financial relationships that could be construed as a potential conflict of interest.

Publisher's Note: All claims expressed in this article are solely those of the authors and do not necessarily represent those of their affiliated organizations, or those of the publisher, the editors and the reviewers. Any product that may be evaluated in this article, or claim that may be made by its manufacturer, is not guaranteed or endorsed by the publisher.

Copyright © 2022 Váncza, Karászi, Péterfia, Turiák, Dezső, Sebestyén, Reszegi, Petővári, Kiss, Schaff, Baghy and Kovalszky. This is an open-access article distributed under the terms of the Creative Commons Attribution License (CC BY). The use, distribution or reproduction in other forums is permitted, provided the original author(s) and the copyright owner(s) are credited and that the original publication in this journal is cited, in accordance with accepted academic practice. No use, distribution or reproduction is permitted which does not comply with these terms.

frontiers in Cell and Developmental Biology

ORIGINAL RESEARCH
published: 09 February 2022
doi: 10.3389/fcell.2021.816230

Comprehensive Analysis of the Expression and Prognosis for ITGBs: Identification of ITGB5 as a Biomarker of Poor Prognosis and Correlated with Immune Infiltrates in Gastric Cancer

Dongliang Liu[1], Shaojun Liu[2], Yu Fang[2], Liu Liu[2] and Kongwang Hu[1]**

[1]*Department of General Surgery, The First Affiliated Hospital of Anhui Medical University, Hefei, China,* [2]*Department of General Surgery, The First Hospital Affiliated to the University of Science and Technology of China, Hefei, China*

Background: Integrin β superfamily members (ITGBs) are documented to play important roles in various biological processes, and accumulating evidence suggests that ITGBs are associated with carcinogenic effects in several malignancies. Gastric cancer (GC) is a complicated and highly heterogeneous disease; however, the expression and prognostic values of eight ITGBs and potential mechanism in GC remain largely unclear.

Methods: The expression and prognostic significance of ITGBs in GC were systematically analyzed through Gene Expression Profiling Interactive Analysis, Human Protein Atlas, Kaplan–Meier Plotter, and cBioPortal databases. Then, the mRNA transcription data and corresponding clinical data of GC were downloaded from the Gene Expression Omnibus database as a testing cohort, and differentially expressed and prognostic genes were identified. The correlation between ITGB5 expression and overall survival and various clinical parameters were found by using univariate/multivariable Cox regression and Kaplan–Meier survival analysis. Additionally, differential analysis of gene expression profiles in low- and high-ITGB5 expression groups and pathway enrichment analysis was performed. Finally, the correlation of ITGB5 expression with immune infiltrates in GC was clarified.

Results: Compared with adjacent normal tissue, the results reveal that the mRNA levels of ITGB1-2 and ITGB4-8 are significantly higher in GC, and immunohistochemistry results show the consistency between RNA and protein expression levels. Cox regression and Kaplan–Meier survival analysis indicate that high ITGB5 expression contributes to a poor prognosis and could be an independent prognostic factor in GC patients. Besides this, gene functional enrichment analysis indicates that ITGB5 expression is significantly associated with extracellular matrix organization, cell-substrate adhesion, and ossification. The KEGG pathway analysis of ITGB5 shows a close association between ITGB5 and focal adhesion, ECM-receptor interaction, phagosome, and PI3K-Akt signaling pathway. Last, the infiltrating level of $CD4^+$ T cells, macrophages, and dendritic cells are positively related to the expression of ITGB5, especially macrophages, and lower levels of macrophages predict a better prognosis in GC in our study.

OPEN ACCESS

Edited by:
Nikos Karamanos,
University of Patras, Greece

Reviewed by:
Vasiliki Zolota,
University of Patras, Greece
Miguel Lopez-Ramirez,
University of California, San Diego, United States

****Correspondence:***
Liu Liu
liuwkjy@126.com
Kongwang Hu
hukw@sina.com

Specialty section:
This article was submitted to Molecular and Cellular Oncology, a section of the journal Frontiers in Cell and Developmental Biology

Received: *16 November 2021*
Accepted: *27 December 2021*
Published: *09 February 2022*

Citation:
Liu D, Liu S, Fang Y, Liu L and Hu K (2022) Comprehensive Analysis of the Expression and Prognosis for ITGBs: Identification of ITGB5 as a Biomarker of Poor Prognosis and Correlated with Immune Infiltrates in Gastric Cancer. Front. Cell Dev. Biol. 9:816230. doi: 10.3389/fcell.2021.816230

Conclusion: Our findings investigate that ITGB5 may function as a valid biomarker of prognosis, and high expression of ITGB5 predicts poor prognosis for patients with GC. Besides this, it might be a potential target of precision therapy against GC.

Keywords: ITGBs, gastric cancer, ITGB5, prognosis, immune infiltrate

INTRODUCTION

Gastric cancer (GC) is the fifth most common cancer and the third leading cause of cancer-related deaths globally (Ferlay et al., 2019). Despite the improvement in radiological diagnosis and surgical techniques, a low 5-year survival rate of patients with advanced GC remains a challenge because of the late presentation, high metastasis, and recurrence rate. The American Joint Committee on Cancer (AJCC) TNM staging system, which is based on tumor infiltration depth (pT), number of lymph node metastases (pN), and the presence of distant metastasis are the main reference index for predicting the prognosis of patients (Compton, 2007). The 8th edition of the AJCC TNM staging system for GC was published in October 2016 and officially implemented in January 1, 2018, in which the N3a and N3b categories were separately introduced into different TNM subgroups (Ilhan et al., 2016). However, due to epigenetic changes, multiple genetic alterations, and the tumor microenvironment, GC is a complicated and highly heterogeneous disease and results in variable prognosis in patients. In addition, there are still significant differences in the survival outcomes of patients with the same clinicopathological characteristics, which means that the current TNM staging system cannot reflect the intrinsic tumor heterogeneity. Hence, further exploration of a specific biomarker is an unmet medical need for improving the diagnosis and prognosis of GC.

The family of integrin is a transmembrane glycoprotein widely existing in the cell membrane, and it consists of α and β subunits by noncovalent bonds. To date, eight members of the Integrin β (ITGB) family of proteins have been identified in organisms. Integrin has a two-way signal transduction function due to its particular transmembrane structure, which interacts with the extracellular matrix (ECM) to activate related signaling pathways and play a pivotal role in the regulation of various biological behavior, including proliferation, adhesion, migration, and differentiation (Chung and Kim, 2008; Ginsberg, 2014; Bianconi et al., 2016). Deregulation of integrin signaling is reported to associate with carcinogenic effects in several malignancies (Shen et al., 2019; Song et al., 2020). Lin et al. (2018) reports that ITGB5 is highly expressed in hepatocellular carcinoma (HCC), and miR-185 regulates the expression of β-catenin through the ITGB5-dependent manner and affects the proliferation and migration of HCC cells. In pancreatic cancer, ITGB4 is demonstrated to be associated with epithelial-mesenchymal transition. Overexpression of ITGB4 promotes pancreatic carcinogenesis and regulates the MEK1-ERK1/2 signal pathway (An et al., 2016). Cui et al. (2018) found that ITGB8 promotes ovarian carcinogenesis, and overexpression of ITGB8 was associated with drug resistance. Similar findings are observed in other types of cancer (Laudato et al., 2017; Huang et al., 2019; Shen et al., 2019). However, the prognostic value and potential biological functions of the entire ITGBs in GC are still largely elusive.

Herein, this study aimed to identify the expression and prognostic values of the eight ITGBs and search for the potential therapeutic biomarker of GC patient survival. Furthermore, we explore the underlying mechanisms based on ITGB5-related GC genes using a pathway enrichment analysis. Finally, the correlation of ITGB5 expression with immune infiltrates in GC is clarified by Tumor IMmune Estimation Resource (TIMER).

MATERIALS AND METHODS

Data Download and Preprocessing

The expression and prognostic significance of ITGBs in GC were systematically analyzed through Gene Expression Profiling Interactive Analysis (GEPIA) (http://www.gepia.cancer-pku.cn/ http://www. gepia.cancer-pku.cn/) and cBioPortal databases (https://cbioportal.org). The expression of ITGBs in GC was displayed using boxplots with statistical significance evaluated using the Wilcoxon test and marked with an asterisk. Correlation between mRNA expression of ITGBs and tumor stages in patients with GC was generated and displayed, and the Kaplan–Meier curves were plotted to assess the survival and prognostic values of ITGBs. Data from cBioPortal was selected to analyze genetic changes of gastric cancer, and genetic alterations among diverse types of GC were shown in different colors.

Immunohistochemical Staining Evaluation

The Human Protein Atlas (HPA) (https://www.proteinatlas.org/) aimed to map all the human proteins in cells, tissues, and organs using an integration of various -omics technologies, and consists of six separate parts, each focusing on a particular aspect of the genome-wide analysis of the human proteins. In this study, immunohistochemistry (IHC) images of the ITGBs protein expression in clinical samples of patients with normal and GC tissues were searched in HPA.

Identification of Differentially Expressed and Prognostic Genes

The mRNA transcription data and corresponding clinical data of GC were downloaded from the GEO database as a testing cohort, and the data set with fewer than 60 samples or with incomplete follow-up information was excluded from our selection. Age, overall survival (OS), gender, grade, and TNM stage were obtained. Subsequently, the gene expression profile (GSE84437) was filtered from theGEO database, which contained 357 GC tissues. We combined all this information into a matrix file using Perl language (http://www.perl.

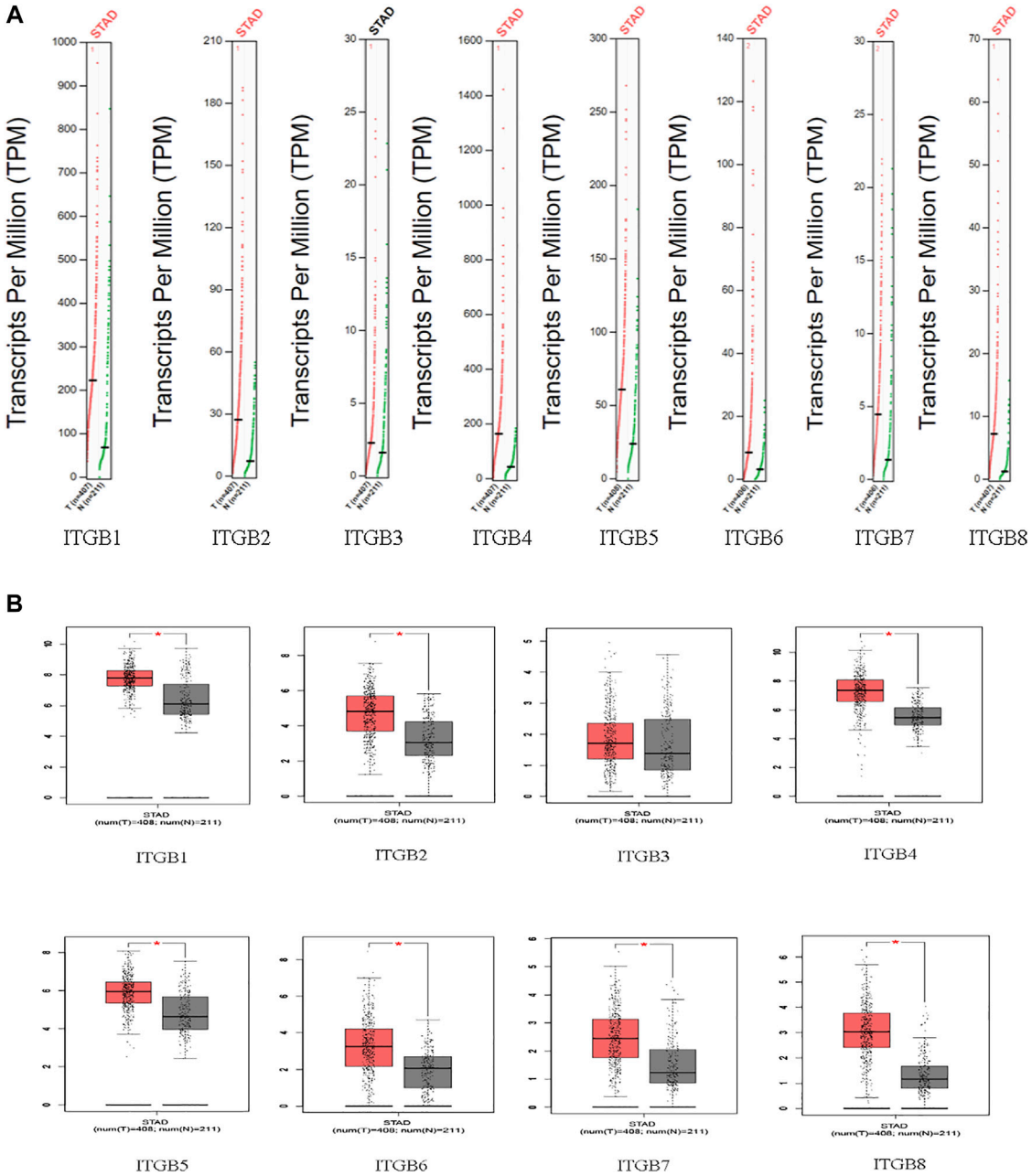

FIGURE 1 | The expression of ITGBs in GC [**(A)** scatter diagram; **(B)** box plot] (GEPIA).

org/). Transcriptome data were subjected to differential analysis, and differentially expressed and prognostic genes were identified based on the GEO database using the "survival package" and "limma package" in R software.

Prognosis Analysis and the Association of ITGB5 Expression with Clinical Features in GC

Univariate/multivariable Cox regression and Kaplan–Meier survival analysis were used to analyze the relationships between low- and high-ITGB5 expression and OS rate and various clinical features. The prognostic value of ITGB5 mRNA expression was verified using an online database, Kaplan–Meier Plotter (www.kmplot.com), which contains survival information and expression data of GC patients.

Functional Enrichment Analysis and Immune Cell Infiltration

Functional enrichment analysis was conducted in R studio to identify important key genes and significantly enriched

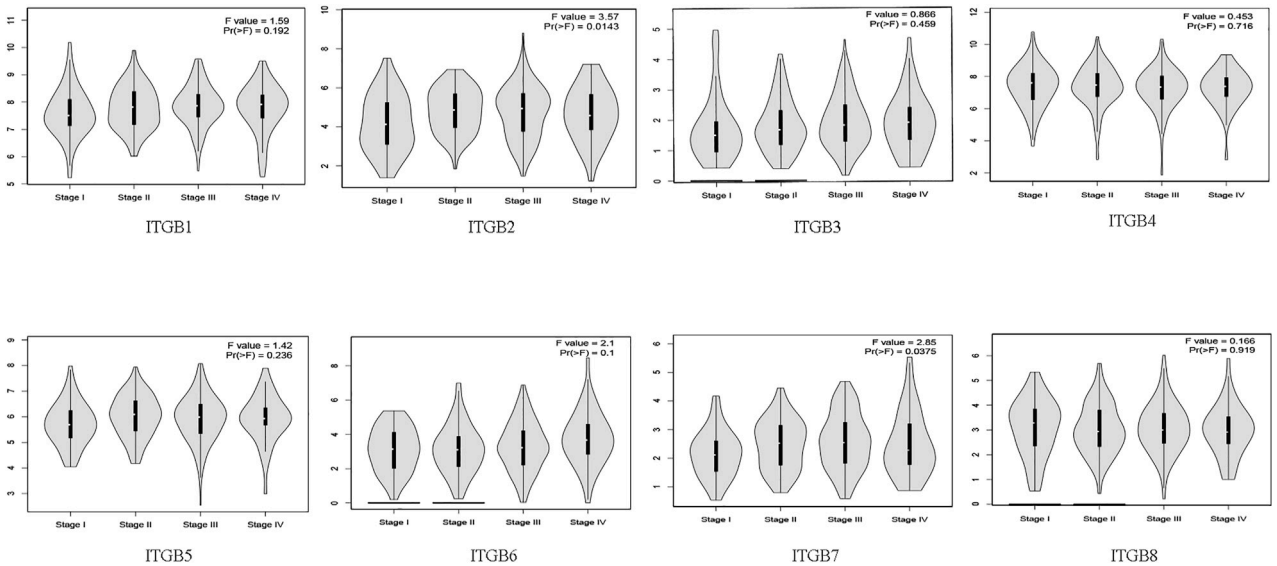

FIGURE 2 | Correlation between mRNA expression of ITGBs and tumor stages in patients with GC (GEPIA).

pathways involved in oncogenesis and tumor progression of GC. The heatmap and volcano plot of the differentially expressed genes were drawn using the "pheatmap package" and "ggplot2 package." Then, we transformed the gene symbols into gene IDs *via* the "Biomanager" and "org. Hs.eg.db" package. Pathway enrichment analysis based on the Gene Ontology (GO) and Kyoto Encyclopedia of Genes and Genomes (KEGG) pathway by using the "ggplot2," "cluster Profiler," and "enrich plot" packages. Furthermore, we explore the correlation between immune cell infiltration and ITGB5 in GC by using the "gene" and "survival" modules in TIMER.

Statistical Analysis

R version 4.0.5 and Perl version 5.28 were used to complete the statistic work. The Kaplan–Meier method with the log-rank test was used to analyze the survival rate. The univariate/multivariate Cox proportional hazard regression model was used to analyze the significant transcription factors affecting OS. p values $< .05$ indicate statistical significance.

RESULTS

Transcriptional Levels of ITGBs in Patients with GC

The mRNA expression of ITGBs in normal and GC tissues was analyzed using GEPIA. Based on a wide variety of data sets, the results reveal that the mRNA levels of ITGB1, ITGB2, ITGB4, ITGB5, ITGB6, ITGB7, and ITGB8 were significantly higher in GC than in normal tissues. Besides this, ITGB3 was confirmed with a similar expression in GC compared with normal tissues (**Figures 1A,B**).

Correlation Between mRNA Expression of ITGBs and Pathological Stages in Patients with GC

The results indicate that significant statistical differences between tumor stages I–IV were identified in the ITGB2 and ITGB7 groups. There was no association between the other ITGB members and pathological stage ($p > .05$; **Figure 2**).

Survival Analysis and Prognostic Values of ITGBs in Patients with GC

We investigated correlations between ITGB expression levels and patient prognosis using GEPIA. The results reveal that the expression levels of ITGA1, ITGA3, and ITGB5 were remarkably correlated with OS in GC patients (**Figure 3**). However, no significant difference was observed in DFS in most ITGB family members except ITGB6.

IHC Analysis of ITGBs in GC

IHC was used to examine the protein expression of ITGBs in normal and GC tissues. According to the degree of staining, we found that ITGB1, ITGB2, ITGB4, ITGB5, ITGB6, and ITGB8 proteins were more highly expressed in the GC tissues than in the normal tissues (**Figure 4**), and these findings were consistent with the mRNA expression. Unfortunately, there is no available protein expression of ITGB7.

Distinction of Prognostic and Differentially Expressed Genes

A total of 172 genes were identified and analyzed for prognosis of GC (**Supplementary Table S1**), and 334 differentially expressed GC-related genes, which were analyzed from the GEO database, are listed in **Supplementary Table S2**. ITGB5 exists in both

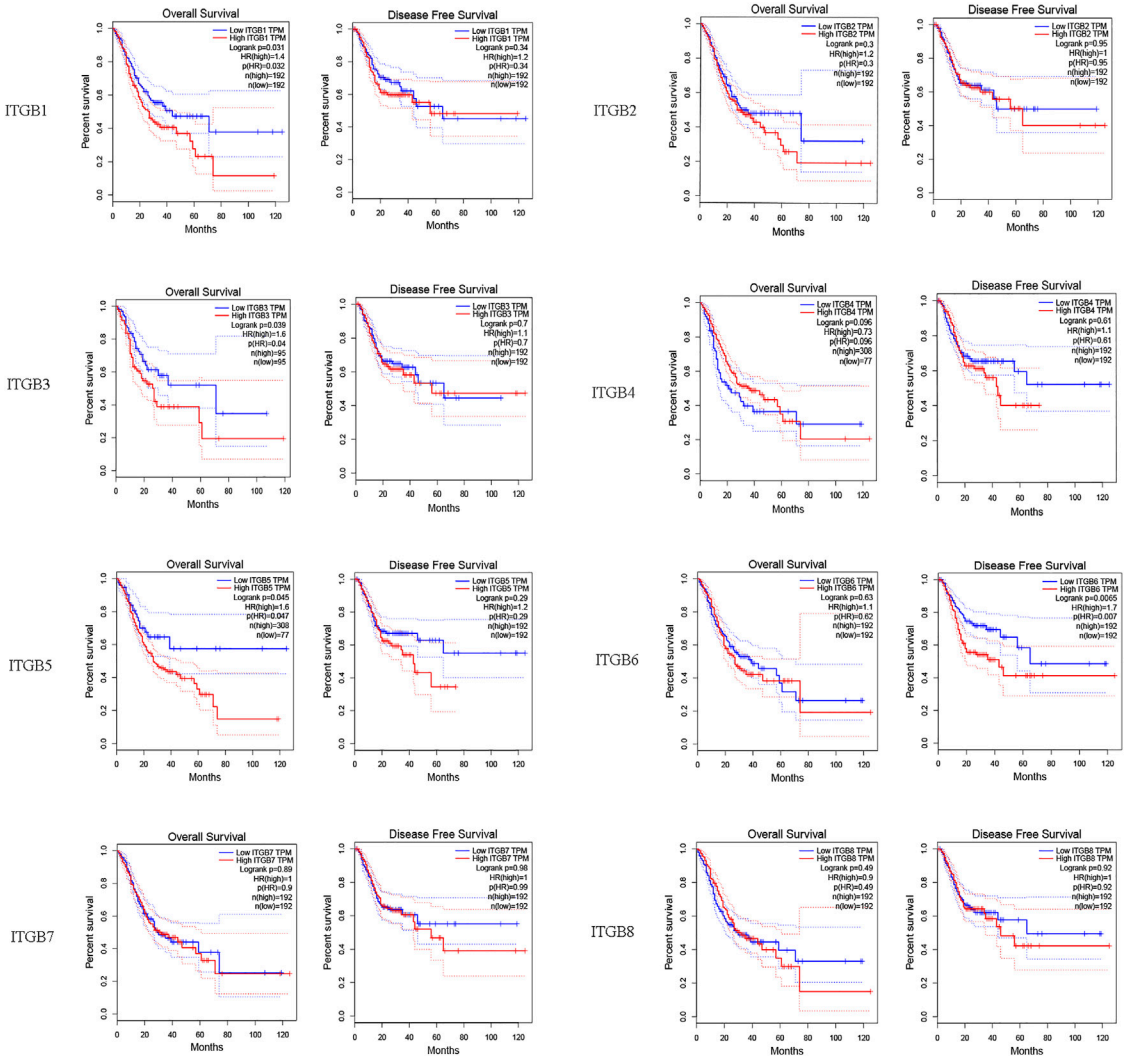

FIGURE 3 | Survival analysis and prognostic values of ITGBs in patients with GC (GEPIA).

Supplementary Tables S1, S2. Thus, we selected ITGB5 for further analysis. The heatmap and volcano plot show that the ITGB5 interactive genes in GC between the low- and high-ITGB5 expression groups were mainly upregulated genes (**Figures 5A,B**). The expressions of ITGB5 among various cancer types are shown in **Figure 6A** as determined by GEPIA. Subcellular location and immunofluorescence images of ITGB5 expression in GC cells were discovered from HPA (**Figure 6B**). We analyzed the ITGB5 mutation by using the cBioPortal for GC, and the detailed mutation information of ITGB5 in GC is described in **Figures 6C–E**.

ITGB5 Expression Predicted Survival and Could Be Used as an Independent Prognostic Biomarker in GC Patients

To explore the relationship between ITGB5 expression and prognosis, the expression levels of ITGB5 in patients were divided into low- and high-expression groups according to the median value of ITGB5 expression levels in the GEO database. We found that high ITGB5 expression was significantly associated with shorter survival time than those with low ITGB5 expression in GC (**Figure 7A**). To explore the independence of ITGB5, univariate and multivariate Cox analyses were performed using the entire GEO cohort. The univariate analysis demonstrated that age, stage, and ITGB5 level were independently associated with OS in GC ($p < .001$) (**Figure 7B**), and the results show that ITGB5 level could be an independent survival predictor of OS in multivariate analyses ($p < .001$) (**Figure 7C**). Thus, ITGB5 level may serve as an independent predictive and prognostic factor. Conversely, there were significant correlations between the ITGB5 level and T/N stage (**Figures 7D–G**). The prognostic value of ITGB5 mRNA expression was further verified by using an online database, Kaplan–Meier Plotter (**Figure 8**). The correlation between ITGB5 expression and various clinical

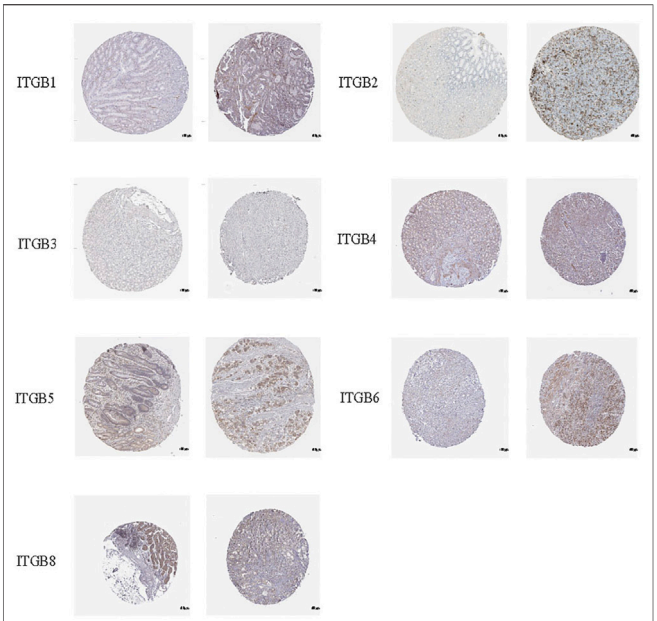

FIGURE 4 | IHC analysis of ITGBs in GC (the HPA database).

parameters was found by using univariate and multivariable Cox regression. As shown in **Figures 7B,C**, ITGB5 expression, age, T stage, and N stage are all significantly correlated with OS and are independent prognostic factors. Therefore, ITGB5 could be used as an independent prognostic biomarker in GC patients. Besides this, we performed a nomogram on the foundation of the GEO data set to anticipate the 1-, 2-, and 3-year OS of each GC patient (**Supplementary Figure S1A**), and the calibration curve of the 3-year OS was obtained, which compared well with the ideal model (**Supplementary Figure S1B**).

Functional Enrichment Analysis of the Differentially Expressed Genes in GC Patients

The functions of ITGB5 and the differentially expressed genes significantly associated with GC were predicted by analyzing the GO and KEGG pathway. GO enrichment analysis predicted the functional effect of target genes on account of three aspects, including molecular functions (MF), biological processes (BP), and cellular components (CC). We found that GO:0030198 (extracellular matrix organization), GO:0043062 (extracellular structure organization), GO:0031589 (cell-substrate adhesion), GO:0001503 (ossification), and GO:0007178 (transmembrane receptor protein serine/threonine kinase signaling pathway) were significantly regulated in GC (**Figures 9A**, **10**). In the KEGG pathway analysis, 16 pathways related to the functions of ITGB5 interactive genes were discovered, and the top five pathways identified were focal adhesion, protein digestion and absorption, ECM-receptor interaction, phagosome, and PI3K-Akt signaling pathway (**Figure 9B**). The PI3K-Akt signaling pathway was involved in the development of GC (**Figures 11A,B**). These findings indicate that ITGB5 has potential value in the development and metastasis of GC.

RELATIONSHIP BETWEEN THE ITGB5 EXPRESSION AND THE TUMOR-INFILTRATING IMMUNE CELLS

We used the TIMER algorithm to investigate whether ITGB5 expression is associated with immune infiltration in GC and the abundance of six tumor-infiltrating immune cells (B cells, $CD4^+$ T cells, $CD8^+$ T cells, macrophages, neutrophils, and dendritic cells). The results shown in **Figure 12A** indicate that the

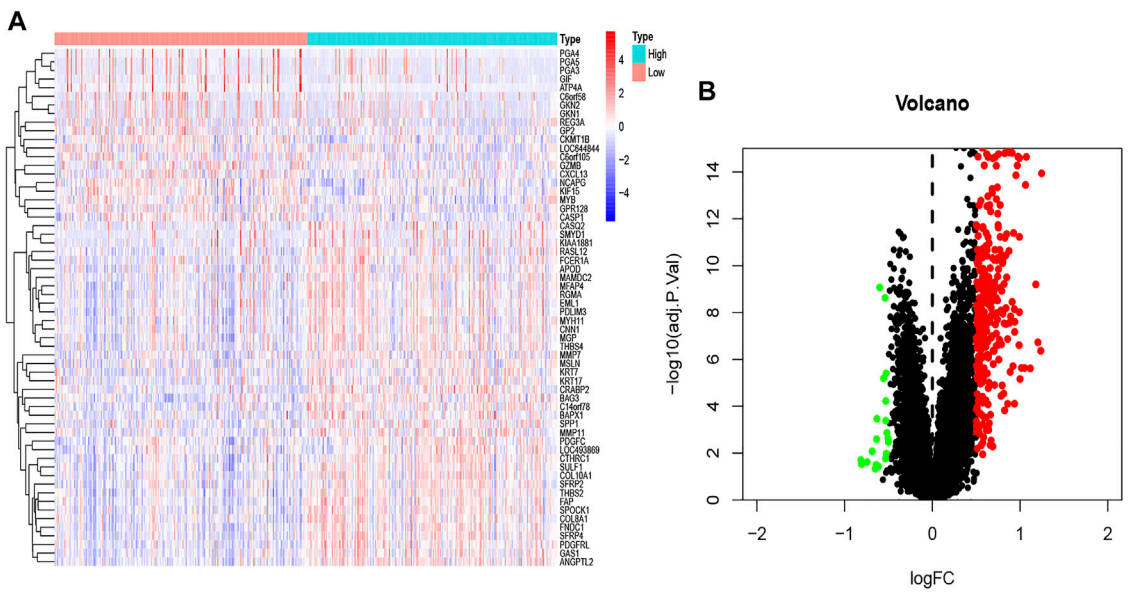

FIGURE 5 | The heatmap **(A)** and volcano plot **(B)** of mRNA expression changes based on ITGB5 in GC samples from the GEO database.

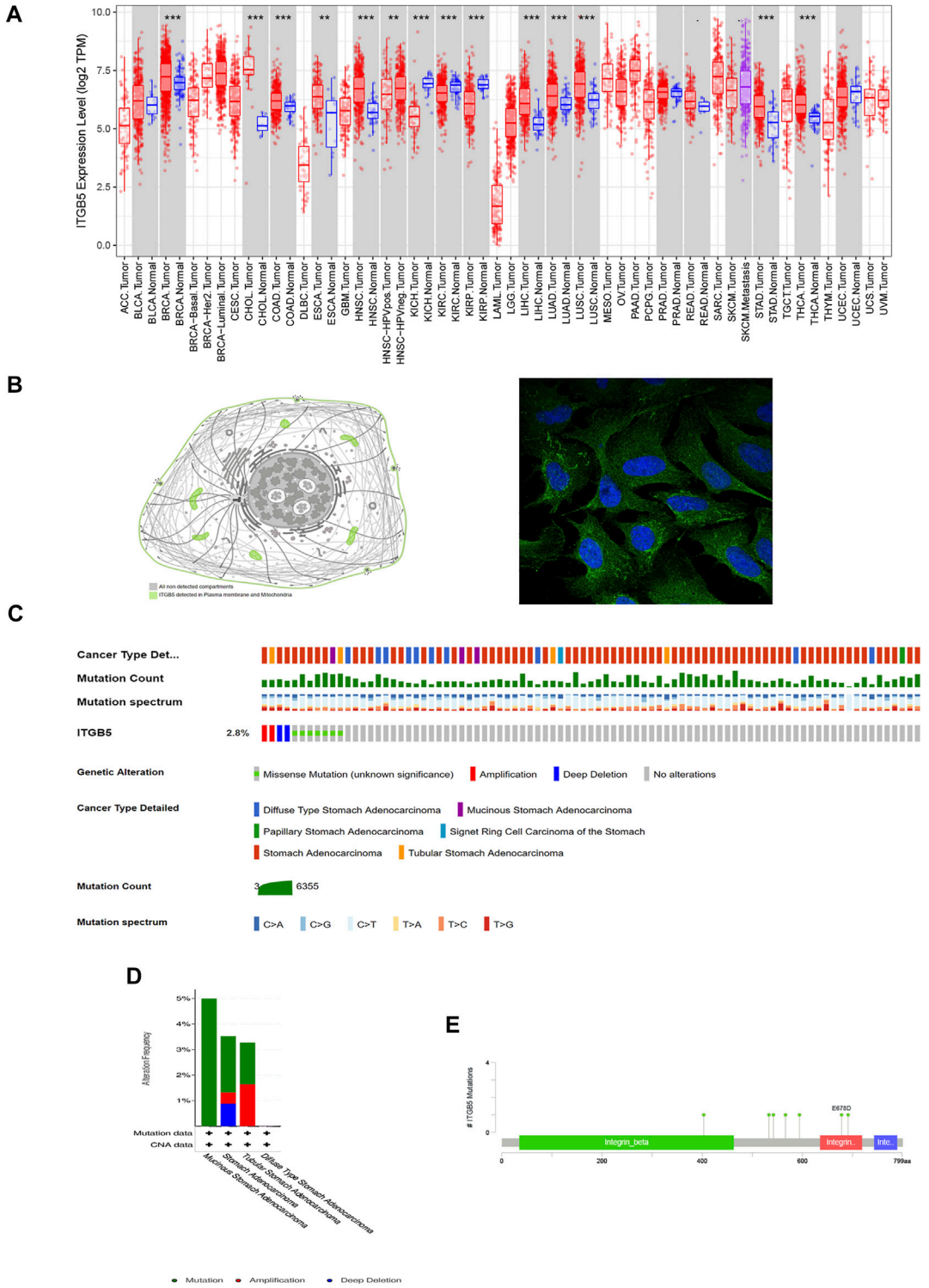

FIGURE 6 | Basic characteristic of ITGB5. **(A)** Expression of ITGB5 in different types of cancer. **(B)** Subcellular location and immunofluorescence images of ITGB5 expression in GC cells from HPA. **(C–E)** Detailed mutation information of ITGB5 in GC.

expression of ITGB5 is positively correlated with $CD4^+$ T cells (cor = 0.155, p = 2.91e-03), macrophages (cor = 0.314, p = 6.51e-10), and dendritic cells (cor = 0.132, p = 1.06e-02), whereas it was negatively correlated with B cells (cor = −0.109, p = 3.71e-02). The macrophage infiltration significantly correlated with the prognosis of GC patients in KM survival analysis

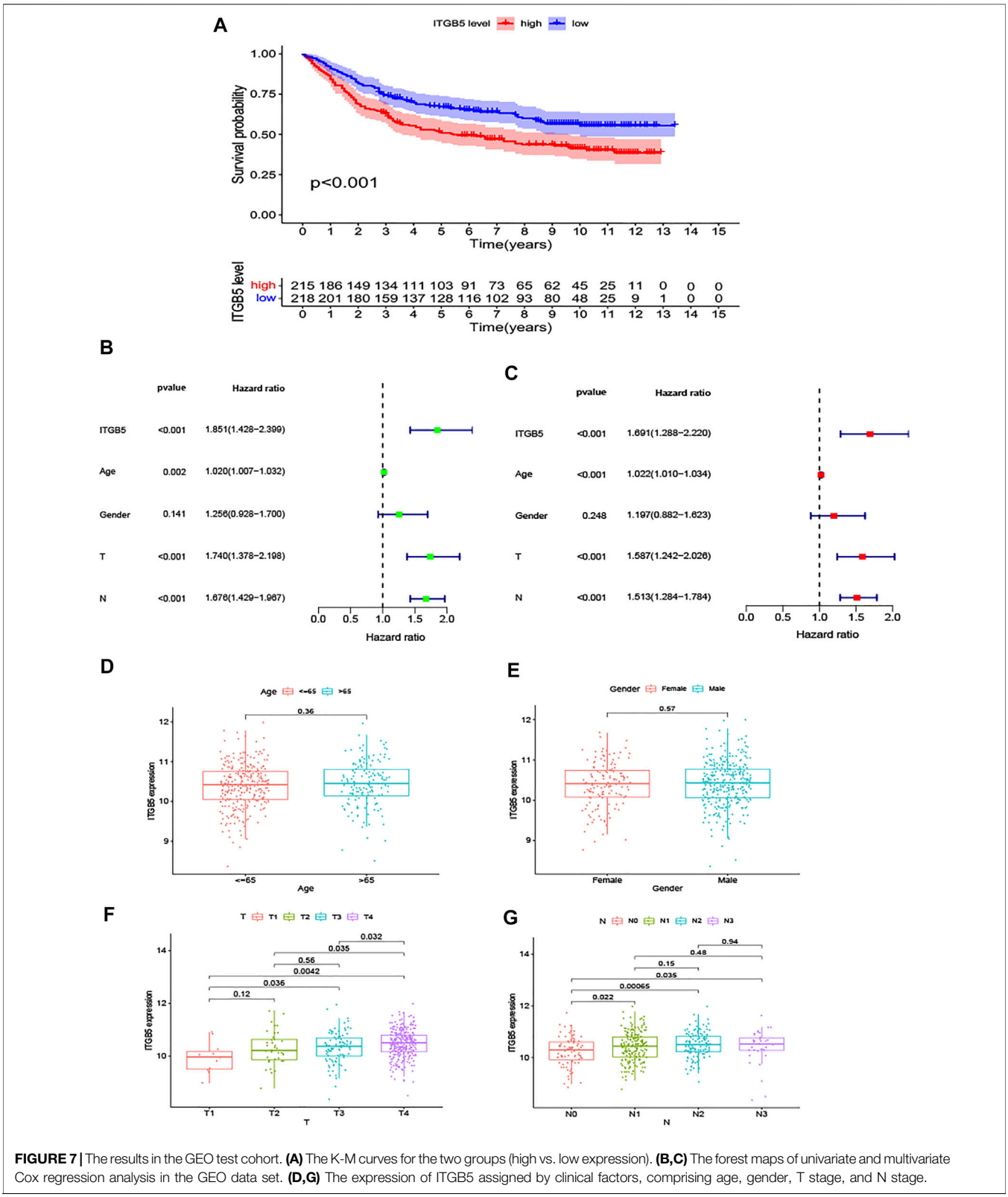

FIGURE 7 | The results in the GEO test cohort. **(A)** The K-M curves for the two groups (high vs. low expression). **(B,C)** The forest maps of univariate and multivariate Cox regression analysis in the GEO data set. **(D,G)** The expression of ITGB5 assigned by clinical factors, comprising age, gender, T stage, and N stage.

(**Figure 12B**). Moreover, we plotted the correlation between ITGB5 expression and gene markers of macrophage, and the ITGB5 expression was significantly correlated with macrophage markers, including M1 macrophages markers (NOS2, IL1B, CD86), M2 macrophages markers (CSF1R, MRC1, CD163), and tumor-associated macrophage markers (MARCO, CSF1R,

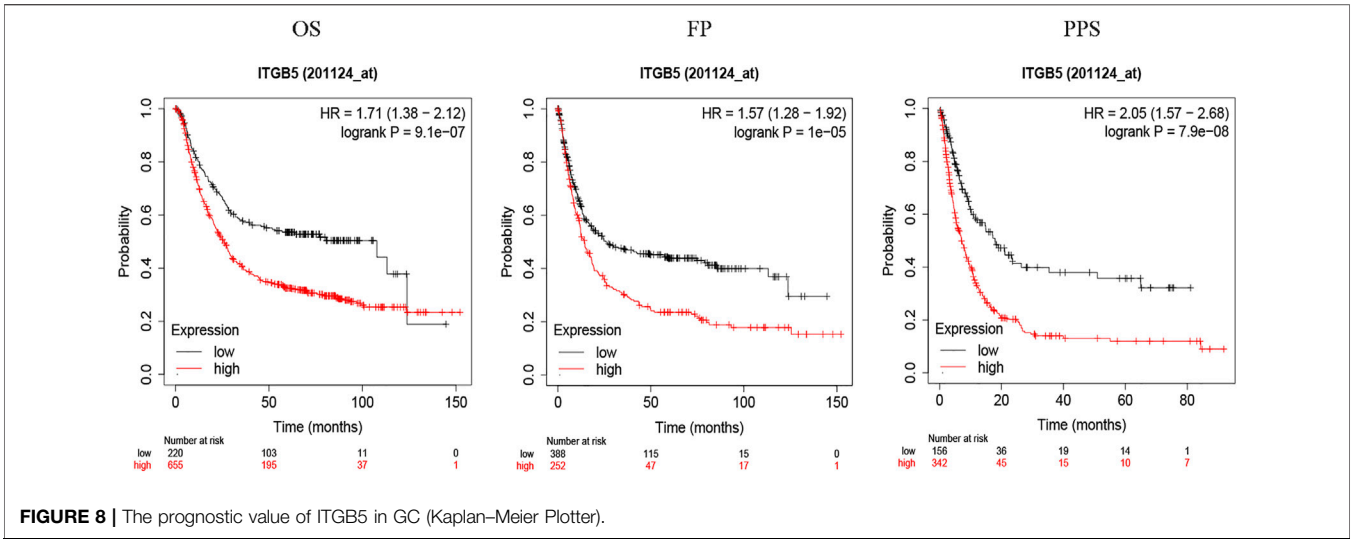

FIGURE 8 | The prognostic value of ITGB5 in GC (Kaplan–Meier Plotter).

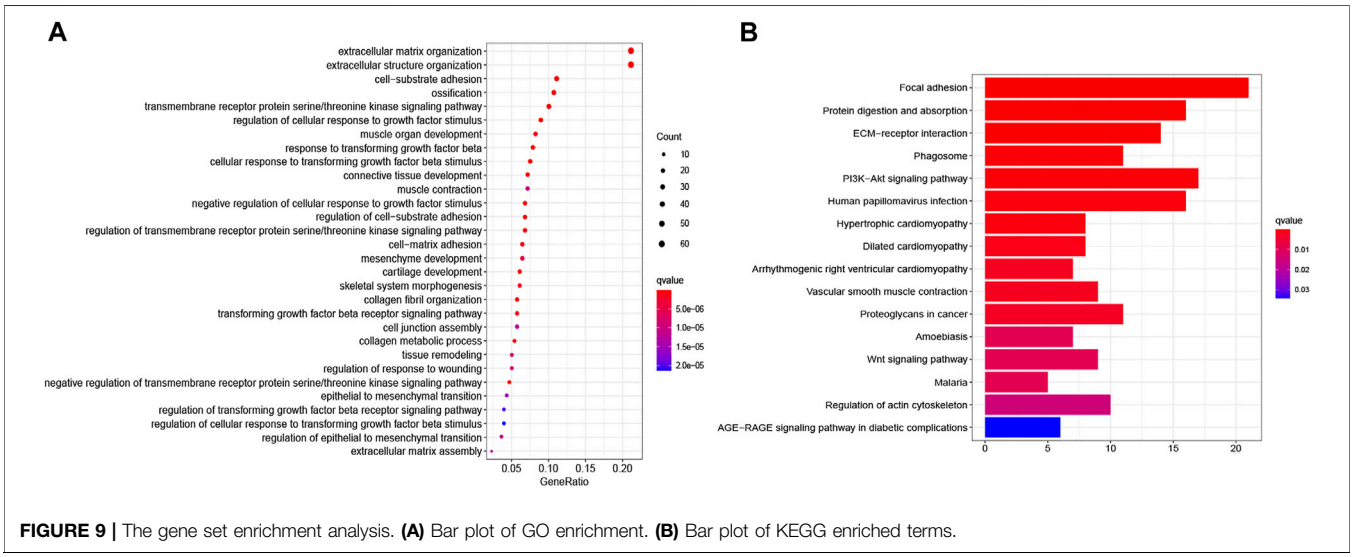

FIGURE 9 | The gene set enrichment analysis. **(A)** Bar plot of GO enrichment. **(B)** Bar plot of KEGG enriched terms.

CD40) (**Figures 13A–C**). The upper findings imply that ITGB5 might involve in infiltration of macrophages and affect patient prognosis *via* regulating immune infiltrates in GC (**Figure 14**).

DISCUSSION

Although the past 20 years have been characterized by the expansion of clarifying the molecular mechanism of GC and an advance in diagnostic and therapeutic methods for managing GC patients, the survival outcomes remained poor (Liu et al., 2020; Sugawara et al., 2021). Hence, searching for specific molecular biomarkers for the tumorigenesis and pathogenesis of GC had important significance in the diagnosis and treatment of patients. Since their discovery in the late 1980s, the ITGB superfamily members are demonstrated to be involved in the regulation of cancer development and progression (Cooper and Giancotti, 2019). The role of ITGBs in the tumorigenesis and pathogenesis of various cancer types has increasingly received attention (Sharma et al., 2020; Fujita et al., 2021; Nurzat et al., 2021; Paindelli et al., 2021). Here, in this paper, we evaluate the utility of ITGBs as biomarkers in GC, and we utilize bioinformatics tools for investigating the underlying mechanisms by ITGB5 affected GC.

We explored the mRNA levels of ITGB superfamily members in GC, and all ITGBs except ITGB3 were significantly higher in primary tumors compared with normal tissues in GC. The IHC results show the consistency between RNA and protein expression levels. Furthermore, we investigated correlations between ITGB expression levels and patient prognosis using GEPIA. The results reveal that the expression levels of ITGA1 and ITGB5 were remarkably associated with OS in GC patients. Similar findings were reported in other types of cancers (Yang et al., 2014; Laudato et al., 2017). Xu et al. (2010) established a

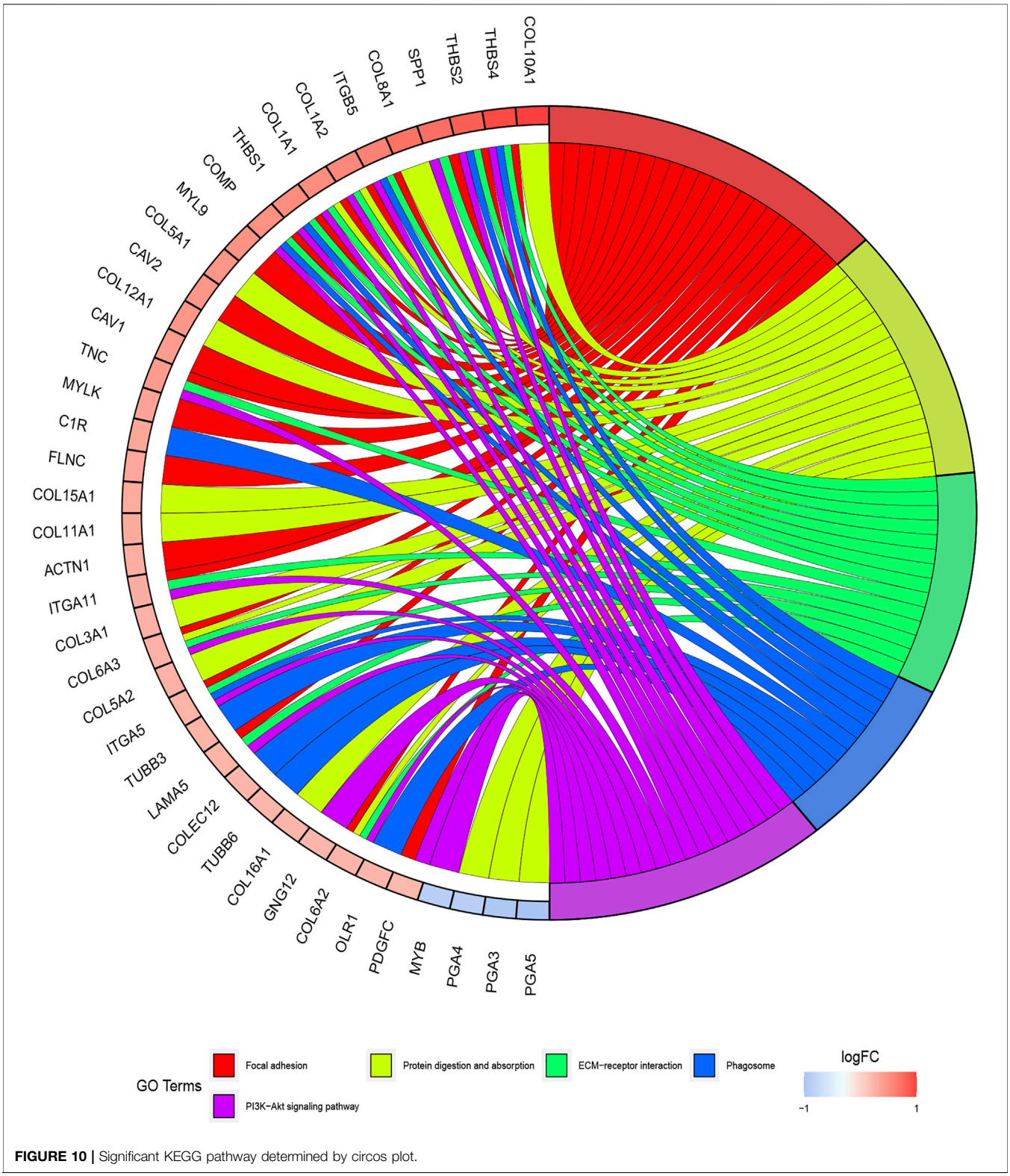

FIGURE 10 | Significant KEGG pathway determined by circos plot.

model that can measure the ITGB5 and ITGB1 expression to predict the survival of GC patients. Taken together, ITGA1 and ITGB5 could be utilized as promising prognostic biomarkers in GC patients. The GEO data set is used as the training and test sets, and we further identified prognosis-related genes. Classified according to GC and normal tissues, we screened differentially expressed GC driver genes. ITGB5 exists in both prognosis-related and differentially expressed genes. Thus, we selected

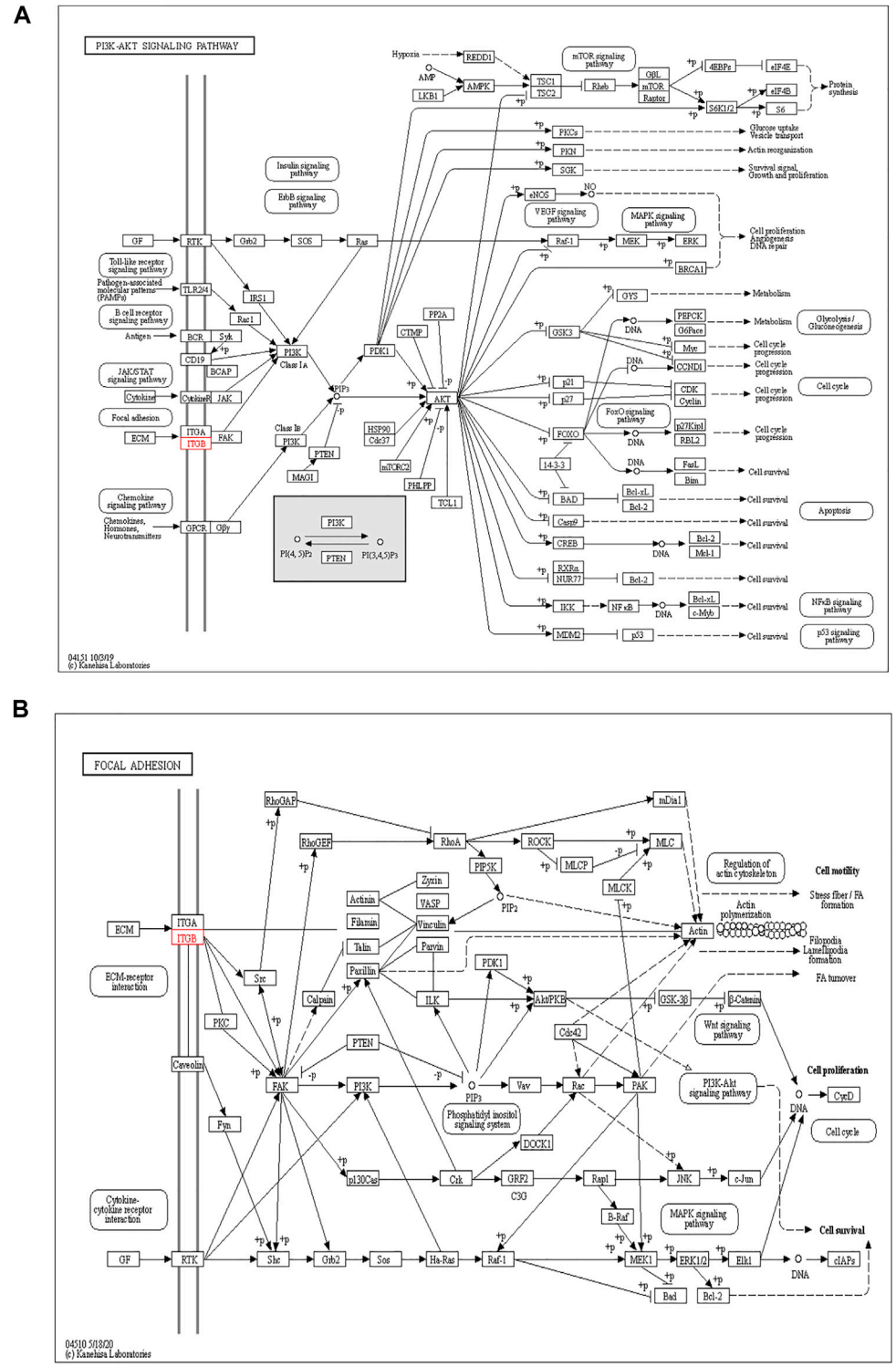

FIGURE 11 | PI3K-Akt signaling pathway **(A)** and focal adhesion procedure **(B)** regulated by ITGBs.

ITGB5 for further analysis. Hirano et al. conducted an *in silico* analysis and found that a high integrin β5 mRNA expression level was correlated with a poor prognosis of patients with GC (Hirano et al., 2020). Similarly, Wang et al. (2020) also suggests that increased ITGB5 level in clinical specimens predicts poor prognosis in GC. We discovered ITGB5 expression upregulated in GC tissues, and the high ITGB5 expression group was positively correlated with advanced tumor stage

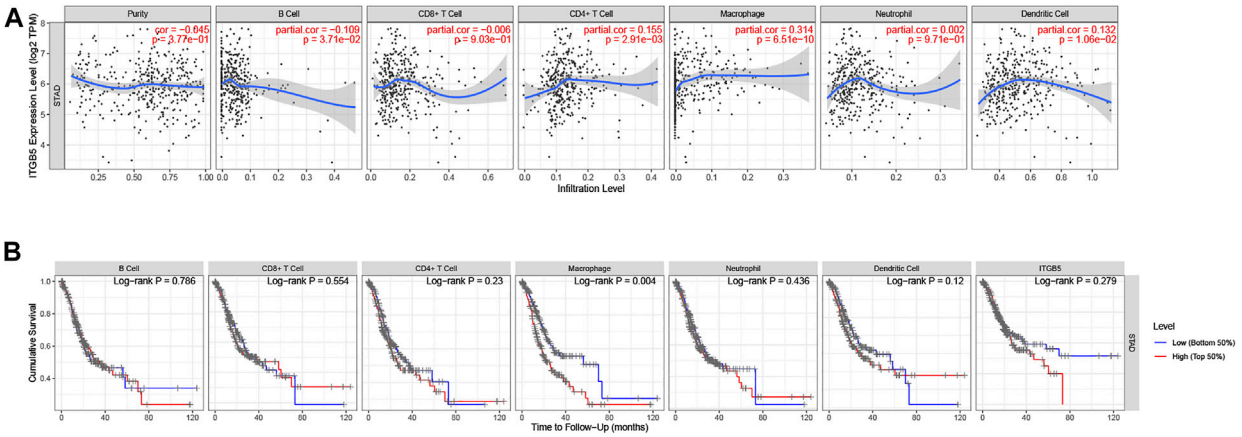

FIGURE 12 | Immune correlation analysis of ITGB5 based on immune infiltration in GC. **(A)** Correlation of ITGB5 expression with immune cell infiltration. **(B)** Prognostic value of immune cell infiltration in GC.

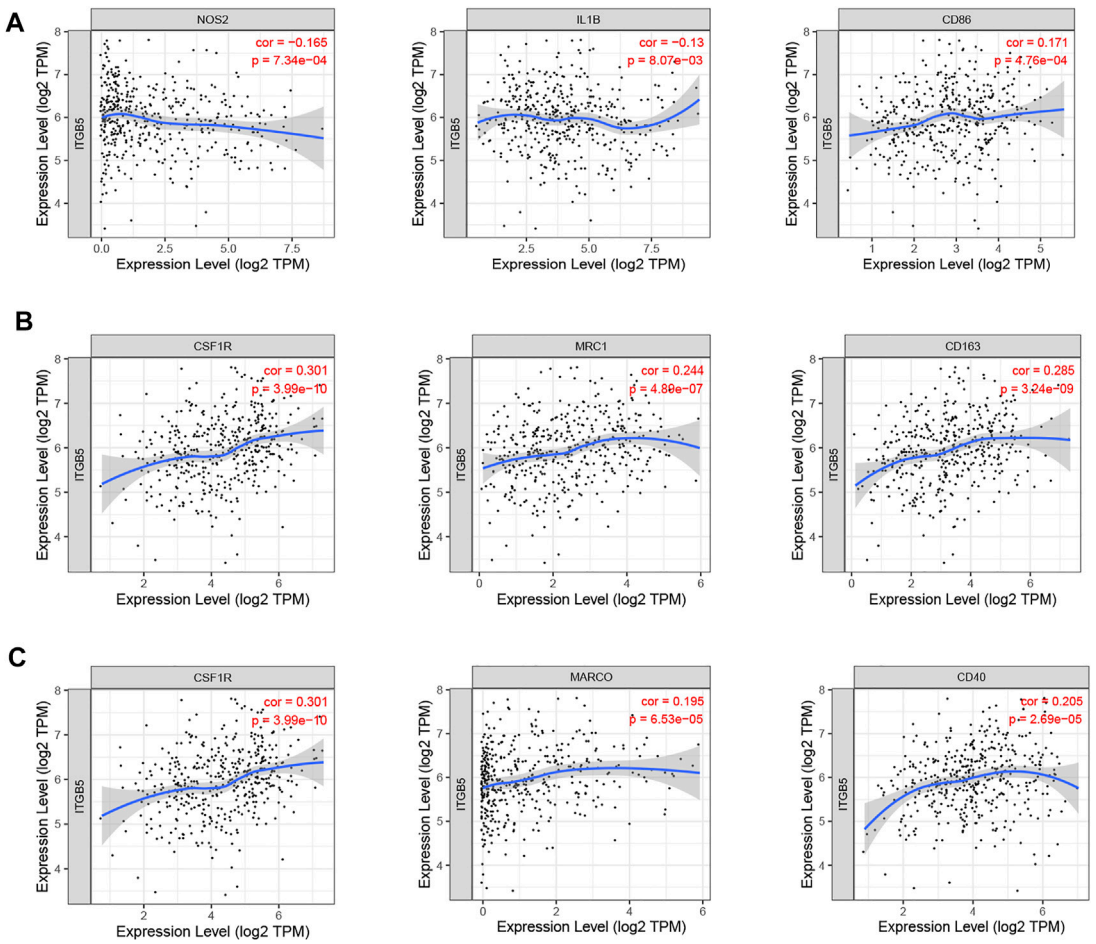

FIGURE 13 | Correlation between ITGB5 expression and gene markers of macrophage in GC. **(A)** ITGB5 and M1 macrophages. **(B)** ITGB5 and M2 macrophages. **(C)** ITGB5 and tumor-associated macrophages.

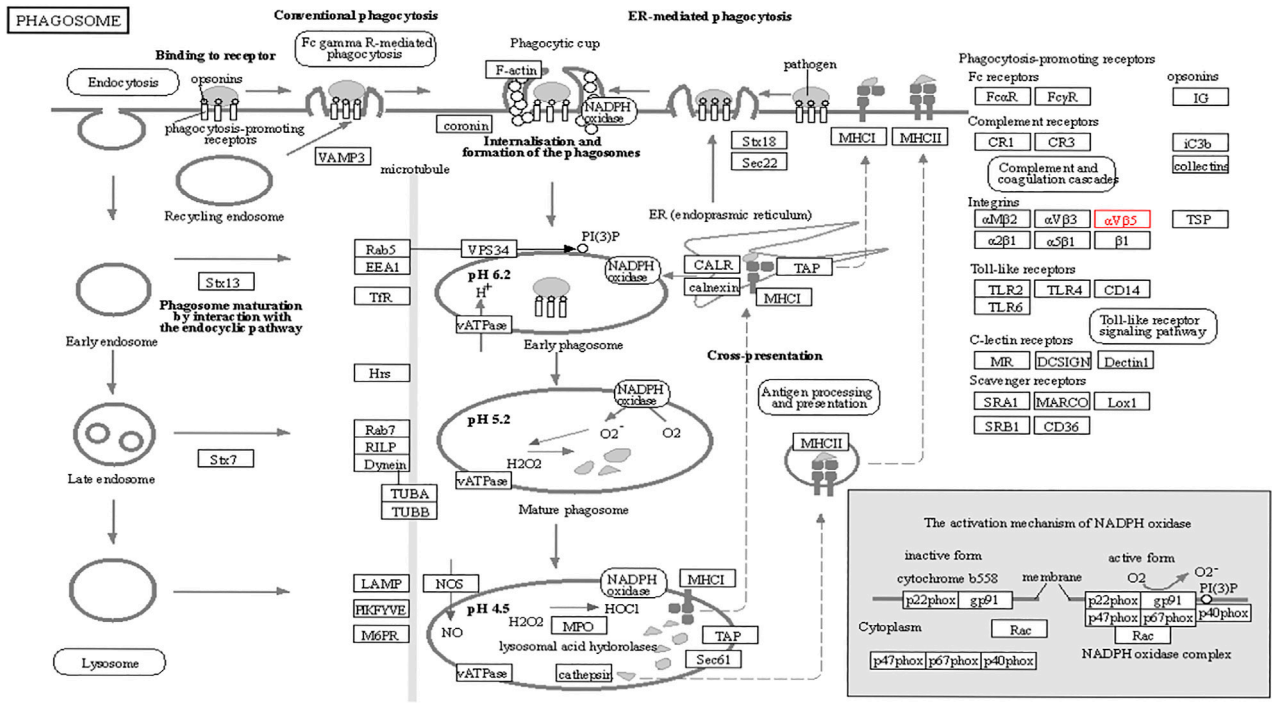

FIGURE 14 | Phagosome pathway regulated by ITGB5.

and positive lymph nodes, which caused a worse prognosis in GC. Our study confirms a high ITGB5 expression level could act as a good predictor of poor prognosis for patients with GC.

However, few studies focus on ITGB5 in GC, and its role in the development and metastasis of GC is not yet fully elucidated (Kawahar et al., 1995; Böger et al., 2015; Lv et al., 2021). ITGB5, encoding integrin-β5, was localized to the plasma membrane and mitochondria, which was supposed to be associated with the initiation and progression of the tumor by mediating links between the ECM and cells (Zhang et al., 2019). According to the enrichment of GO collection, we found that ITGB5 expression is significantly associated with ECM organization, extracellular structure organization, cell-substrate adhesion, and ossification. Exploring the molecular mechanisms of ITGB5 in GC contributed to investigating the novel targeted therapy approach. The KEGG pathway analysis of ITGB5 shows a close association between ITGB5 and focal adhesion, protein digestion and absorption, ECM-receptor interaction, phagosome, and PI3K-Akt signaling pathway. Several studies already report that ITGBs mediate the interaction between ECM and cells and are involved in cell adhesion and migration (Wilisch-Neumann et al., 2013; Lian et al., 2016). Cell adhesion molecules act as one of the main mediators between the ECM and cell. Changes in cell adhesion molecules may affect a variety of signaling pathways, leading to the occurrence and development of tumors (Deville and Cordes, 2019). Previous findings indicate that the focal adhesion signaling pathway plays an important role in the process of epithelial to mesenchymal transition in pancreatic cancer (Ning et al., 2014). Wang et al. (2016a) reports that the focal adhesion signaling pathway activated by ITGB5 can alter cell glycolysis and induce cisplatin resistance in cervical and breast cancer. Meanwhile, for the first time, we demonstrate that ITGB5 overexpression was significantly associated with upregulation of the focal adhesion signaling pathway, indicating the potential role of ITGB5 in the focal adhesion signaling pathway in GC. We also found that the PI3K-Akt signaling pathway is upregulated. The anomalous activation of the PI3K/Akt signal pathway presents in variable tumors, and plenty of studies verify that the PI3K-Akt signal pathway is involved in regulating GC cell growth, proliferation, migration, differentiation, apoptosis, and energy metabolism (Lin et al., 2019; Rong et al., 2020; Xu et al., 2020). However, the research about its mechanism through ITGB5 in GC is insufficient, and there is no direct evidence to confirm that the upregulation of this pathway affiliates with the prognosis of GC. Indeed, the results suggest that we need further work on the relationship between the ITGB5 and PI3K-Akt in GC.

Cellular immunity plays a considerable role in the antitumor process. B cells, T cells, macrophages, neutrophils, and dendritic cells are the main effector cells of the immune system. The infiltrating condition of these immune cells and their differences in forecasting the prognosis of GC has not been discussed yet. To further study the function of ITGB5 in GC, we analyzed whether ITGB5 expression is associated with immune infiltration by using the TIMER algorithm, and the results show that the content of these special immune cells activated was statistically different. In our paper, we find the infiltrating level of $CD4^+$ T cells, macrophages, and dendritic cells were positively related to the expression of ITGB5, especially macrophages, and a low level of macrophages predicts a better prognosis in GC in our study. Besides this, we explored the

correlation between ITGB5 expression and gene markers of macrophage, and the ITGB5 expression was significantly correlated with macrophage markers, including M1 macrophage markers (NOS2, IL1B, CD86), M2 macrophage markers (CSF1R, MRC1, CD163), and tumor-associated macrophage markers (MARCO, CSF1R, CD40). Macrophages as a fundamental innate immune population perform various supportive functions specialized to different tissue components, and aberrance in macrophage functions leads substantially to the development and progression of several diseases, including cancer (Ngambenjawong et al., 2017). Tumor-associated macrophages, M1 and M2 macrophage phenotypes, are generally considered to directly or indirectly promote tumor proliferation and metastasis in GC and are positively correlated with invasion depth and tumor stage (Ishigami et al., 2003). The M1 macrophages can stimulate apoptosis, suppress proliferation and the development of neovascularization, whereas M2 macrophages can accelerate both cancer growth and metastasis (Wu et al., 2015; Wang et al., 2016b). In recent years, researchers have expanded their studies to figure out both M1 and M2 phenotypes within microenvironments. High levels of M1 macrophages predict better prognosis, whereas increasing levels of M2 macrophages indicate poor outcomes (Ma et al., 2010; Yuan et al., 2014; Mei et al., 2016). Liu et al. (2020) summarize that the high infiltrating levels of M2 macrophages and total tumor-associated macrophages might be negative prognostic factors for patients with GC. In our present study, M2 macrophages were positively and M1 macrophages negatively related to the expression of ITGB5. The total tumor-associated macrophages were positively correlated with the level of ITGB5, which indicates higher M2 macrophage infiltration, thus supporting the view that ITGB5 may play a vital role in the progression of GC via promoting M2 macrophage polarization and inhibiting antitumor immunity. This might explain, to a certain degree, why GC patients with high expression of ITGB5 had poor prognoses. Along with the existing evidence, the results of our study confirm that ITGB5 might act a critical role in the immune mechanism of cancer.

To the best of our knowledge, this is the first study to comprehensively identify the oncologic and prognostic values of the eight ITGBs. The upper results demonstrate that ITGB5 has potential value in the tumorigenesis and pathogenesis of GC, which might involve infiltration of macrophages and affect patient prognosis *via* regulating immune infiltrates in GC. However, this study has some limitations that should be considered. On the one hand, our study is based on the specimens from one database and may have a bias by the potential heterogeneity. On the other hand, this study was only at the level of bioinformatics analysis, and *in vitro* and *in vivo* experiments about the underlying mechanism of ITGB5 in GC should be performed.

In conclusion, ITGB5 seems to be a valuable prognostic biomarker and a pivotal regulator of immune infiltrates in GC patients, which might be a potential target of precision therapy against GC. However, the molecular mechanism and the related signal pathways of ITGB5 in GC remain unclear, which requires further exploration.

DATA AVAILABILITY STATEMENT

The original contributions presented in the study are included in the article/**Supplementary Material**, further inquiries can be directed to the corresponding authors.

AUTHOR CONTRIBUTIONS

DL and LL were involved in the study conception and design. DL and SL performed the data acquisition. LL and YF performed the analysis and interpretation of the data. DL and KH drafted the manuscript. DL and KH critically revised the manuscript.

ACKNOWLEDGMENTS

We appreciate the public databases including GEO, GEPIA, Human Protein Atlas, Kaplan-Meier Plotter, cBioPortal and Tumor IMmune Estimation Resource for allowing access to their data.

SUPPLEMENTARY MATERIAL

The Supplementary Material for this article can be found online at: https://www.frontiersin.org/articles/10.3389/fcell.2021.816230/full#supplementary-material

REFERENCES

An, X.-Z., Zhao, Z.-G., Luo, Y.-X., Zhang, R., Tang, X.-Q., Hao, D.-L., et al. (2016). Netrin-1 Suppresses the MEK/ERK Pathway and ITGB4 in Pancreatic Cancer. *Oncotarget.* 7 (17), 24719–24733. doi:10.18632/oncotarget.8348

Bianconi, D., Unseld, M., and Prager, G. W. (2016). Integrins in the Spotlight of Cancer. *Int. J. Mol. Sci.* 17 (12), 2037. doi:10.3390/ijms17122037

Böger, C., Warneke, V. S., Behrens, H.-M., Kalthoff, H., Goodman, S. L., Becker, T., et al. (2015). Integrins αvβ3 and αvβ5 as Prognostic, Diagnostic, and Therapeutic Targets in Gastric Cancer. *Gastric Cancer.* 18 (4), 784–795. doi:10.1007/s10120-014-0435-2

Chung, J., and Kim, T. H. (2008). Integrin-Dependent Translational Control: Implication in Cancer Progression. *Microsc. Res. Tech.* 71 (5), 380–386. doi:10.1002/jemt.20566

Compton, C. C. (2007). Optimal Pathologic Staging: Defining Stage II Disease. *Clin. Cancer Res.* 13 (22 Pt 2), 6862s–70s. doi:10.1158/1078-0432.CCR-07-1398

Cooper, J., and Giancotti, F. G. (2019). Integrin Signaling in Cancer: Mechanotransduction, Stemness, Epithelial Plasticity, and Therapeutic Resistance. *Cancer Cell.* 35 (3), 347–367. doi:10.1016/j.ccell.2019.01.007

Cui, Y., Wu, F., Tian, D., Wang, T., Lu, T., Huang, X., et al. (2018). miR-199a-3p Enhances Cisplatin Sensitivity of Ovarian Cancer Cells by Targeting ITGB8. *Oncol. Rep.* 39 (4), 1649–1657. doi:10.3892/or.2018.6259

Deville, S. S., and Cordes, N. (2019). The Extracellular, Cellular, and Nuclear Stiffness, a Trinity in the Cancer Resistome-A Review. *Front. Oncol.* 9, 1376. doi:10.3389/fonc.2019.01376

Ferlay, J., Colombet, M., Soerjomataram, I., Mathers, C., Parkin, D. M., Piñeros, M., et al. (2019). Estimating the Global Cancer Incidence and Mortality in 2018: GLOBOCAN Sources and Methods. *Int. J. Cancer.* 144 (8), 1941–1953. doi:10.1002/ijc.31937

Fujita, M., Sasada, M., Eguchi, M., Iyoda, T., Okuyama, S., Osawa, T., et al. (2021). Induction of Cellular Senescence in Fibroblasts through β1-integrin Activation by Tenascin-C-Derived Peptide and its Protumor Effect. *Am. J. Cancer Res.* 11 (9), 4364–4379.

Ginsberg, M. H. (2014). Integrin Activation. *BMB Rep.* 47 (12), 655–659. doi:10.5483/bmbrep.2014.47.12.241

Hirano, T., Shinsato, Y., Tanabe, K., Higa, N., Kamil, M., Kawahara, K., et al. (2020). FARP1 Boosts CDC42 Activity from Integrin αvβ5 Signaling and Correlates with Poor Prognosis of Advanced Gastric Cancer. *Oncogenesis.* 9 (2), 13. doi:10.1038/s41389-020-0190-7

Huang, L., Hu, C., Chao, H., Wang, R., Lu, H., Li, H., et al. (2019). miR-29c Regulates Resistance to Paclitaxel in Nasopharyngeal Cancer by Targeting ITGB1. *Exp. Cell Res.* 378 (1), 1–10. doi:10.1016/j.yexcr.2019.02.012

Ilhan, E., Ureyen, O., and Meral, U. M. (2016). Ongoing Problems Concerning 7th TNM Staging System and Proposals for 8th TNM Staging System of Gastric Cancer. *pg.* 4 (4), 223–225. doi:10.5114/pg.2016.64069

Ishigami, S., Natsugoe, S., Tokuda, K., Nakajo, A., Okumura, H., Matsumoto, M., et al. (2003). Tumor-Associated Macrophage (TAM) Infiltration in Gastric Cancer. *Anticancer Res.* 23 (5A), 4079–4083.

Kawahar, E., Ooi, A., and Nakanishi, I. (1995). Integrin Distribution in Gastric Carcinoma: Association of β3 and β5 Integrins with Tumor Invasiveness. *Pathol. Int.* 45 (7), 493–500. doi:10.1111/j.1440-1827.1995.tb03491.x

Laudato, S., Patil, N., Abba, M. L., Leupold, J. H., Benner, A., Gaiser, T., et al. (2017). P53-induced miR-30e-5p Inhibits Colorectal Cancer Invasion and Metastasis by Targeting ITGA6 and ITGB1. *Int. J. Cancer.* 141 (9), 1879–1890. doi:10.1002/ijc.30854

Lian, P.-L., Liu, Z., Yang, G.-Y., Zhao, R., Zhang, Z.-Y., Chen, Y.-G., et al. (2016). Integrin αvβ6 and Matrix Metalloproteinase 9 Correlate with Survival in Gastric Cancer. *Wjg.* 22 (14), 3852–3859. doi:10.3748/wjg.v22.i14.3852

Lin, J.-X., Xie, X.-S., Weng, X.-F., Qiu, S.-L., Yoon, C., Lian, N.-Z., et al. (2019). UFM1 Suppresses Invasive Activities of Gastric Cancer Cells by Attenuating the Expression of PDK1 through PI3K/AKT Signaling. *J. Exp. Clin. Cancer Res.* 38 (1), 410. doi:10.1186/s13046-019-1416-4

Lin, Z., He, R., Luo, H., Lu, C., Ning, Z., Wu, Y., et al. (2018). Integrin-β5, a miR-185-Targeted Gene, Promotes Hepatocellular Carcinoma Tumorigenesis by Regulating β-catenin Stability. *J. Exp. Clin. Cancer Res.* 37 (1), 17. doi:10.1186/s13046-018-0691-9

Liu, X., Cao, Y., Li, R., Gu, Y., Chen, Y., Qi, Y., et al. (2020). Poor Clinical Outcomes of Intratumoral Dendritic Cell-Specific Intercellular Adhesion Molecule 3-grabbing Non-integrin-positive Macrophages Associated with Immune Evasion in Gastric Cancer. *Eur. J. Cancer.* 128, 27–37. doi:10.1016/j.ejca.2020.01.002

Lv, Y., Shan, Y., Song, L., Zhao, Y., Lai, R., Su, J., et al. (2021). Type I Collagen Promotes Tumor Progression of Integrin β1 Positive Gastric Cancer through a BCL9L/β-Catenin Signaling Pathway. *Aging.* 13 (14), 19064–19076. doi:10.18632/aging.203355

Ma, J., Liu, L., Che, G., Yu, N., Dai, F., and You, Z. (2010). The M1 Form of Tumor-Associated Macrophages in Non-Small Cell Lung Cancer Is Positively Associated with Survival Time. *BMC Cancer* 10, 112. doi:10.1186/1471-2407-10-112

Mei, J., Xiao, Z., Guo, C., Pu, Q., Ma, L., Liu, C., et al. (2016). Prognostic Impact of Tumor-Associated Macrophage Infiltration in Non-small Cell Lung Cancer: A Systemic Review and Meta-Analysis. *Oncotarget.* 7 (23), 34217–34228. doi:10.18632/oncotarget.9079

Ngambenjawong, C., Gustafson, H. H., and Pun, S. H. (2017). Progress in Tumor-Associated Macrophage (TAM)-Targeted Therapeutics. *Adv. Drug Deliv. Rev.* 114, 206–221. doi:10.1016/j.addr.2017.04.010

Ning, Z., Wang, A., Liang, J., Xie, Y., Liu, J., Yan, Q., et al. (2014). USP22 Promotes Epithelial-Mesenchymal Transition via the FAK Pathway in Pancreatic Cancer Cells. *Oncol. Rep.* 32 (4), 1451–1458. doi:10.3892/or.2014.3354

Nurzat, Y., Su, W., Min, P., Li, K., Xu, H., and Zhang, Y. (2021). Identification of Therapeutic Targets and Prognostic Biomarkers Among Integrin Subunits in the Skin Cutaneous Melanoma Microenvironment. *Front. Oncol.* 11, 751875. doi:10.3389/fonc.2021.751875

Paindelli, C., Casarin, S., and Wang, F. (2021). Enhancing Radium 223 Treatment Efficacy by Anti-beta 1 Integrin Targeting. *J. Nucl. Med.* doi:10.2967/jnumed.121.262743

Rong, L., Li, Z., Leng, X., Li, H., Ma, Y., Chen, Y., et al. (2020). Salidroside Induces Apoptosis and Protective Autophagy in Human Gastric Cancer AGS Cells through the PI3K/Akt/mTOR Pathway. *Biomed. Pharmacother.* 122, 109726. doi:10.1016/j.biopha.2019.109726

Sharma, R., Kameswaran, M., and Dash, A. (2020). ComparativeIn VitroCytotoxicity Studies of177Lu-CHX-A″-DTPA-Trastuzumab and177Lu-CHX-A″-DTPA-F(ab′)2-Trastuzumab in HER2-Positive Cancer Cell Lines. *Cancer Biother. Radiopharm.* 35 (3), 177–189. doi:10.1089/cbr.2019.2882

Shen, J., Xu, J., Chen, B., Ma, D., Chen, Z., Li, J.-C., et al. (2019). Elevated Integrin α6 Expression Is Involved in the Occurrence and Development of Lung Adenocarcinoma, and Predicts a Poor Prognosis: a Study Based on Immunohistochemical Analysis and Bioinformatics. *J. Cancer Res. Clin. Oncol.* 145 (7), 1681–1693. doi:10.1007/s00432-019-02907-1

Song, J., Yang, P., and Lu, J. (2020). Upregulation of ITGBL1 Predicts Poor Prognosis and Promotes Chemoresistance in Ovarian Cancer. *Cancer Biomark.* 27 (1), 51–61. doi:10.3233/CBM-190460

Sugawara, K., Yamashita, H., Yajima, S., Oshima, Y., Mitsumori, N., Fujisaki, M., et al. (2021). Prognosis of Hemodialysis Patients Undergoing Surgery for Gastric Cancer: Results of a Multicenter Retrospective Study. *Surgery.* 170 (1), 249–256. doi:10.1016/j.surg.2021.01.014

Wang, J. F., Wang, Y., Zhang, S. W., Chen, Y. Y., Qiu, Y., Duan, S. Y., et al. (2020). Expression and Prognostic Analysis of Integrins in Gastric Cancer. *J. Oncol.* 2020, 8862228. doi:10.1155/2020/8862228

Wang, S., Xie, J., Li, J., Liu, F., Wu, X., and Wang, Z. (2016a). Cisplatin Suppresses the Growth and Proliferation of Breast and Cervical Cancer Cell Lines by Inhibiting Integrin β5-mediated Glycolysis. *Am. J. Cancer Res.* 6 (5), 1108–1117.

Wang, X. L., Jiang, J. T., and Wu, C. P. (2016b). Prognostic Significance of Tumor-Associated Macrophage Infiltration in Gastric Cancer: a Meta-Analysis. *Genet. Mol. Res.* 15 (4), gmr15049040. doi:10.4238/gmr15049040

Wilisch-Neumann, A., Kliese, N., Pachow, D., Schneider, T., Warnke, J.-P., Braunsdorf, W. E., et al. (2013). The Integrin Inhibitor Cilengitide Affects Meningioma Cell Motility and Invasion. *Clin. Cancer Res.* 19 (19), 5402–5412. doi:10.1158/1078-0432.ccr-12-0299

Wu, M.-H., Lee, W.-J., Hua, K.-T., Kuo, M.-L., and Lin, M.-T. (2015). Macrophage Infiltration Induces Gastric Cancer Invasiveness by Activating the β-Catenin Pathway. *PLoS One.* 10 (7), e0134122. doi:10.1371/journal.pone.0134122

Xu, L., Chen, J., Jia, L., Chen, X., Awaleh Moumin, F., and Cai, J. (2020). SLC1A3 Promotes Gastric Cancer Progression via the PI3K/AKT Signalling Pathway. *J. Cell. Mol. Med.* 24 (24), 14392–14404. doi:10.1111/jcmm.16060

Xu, Z.-Y., Chen, J.-S., and Shu, Y.-Q. (2010). Gene Expression Profile Towards the Prediction of Patient Survival of Gastric Cancer. *Biomed. Pharmacother.* 64 (2), 133–139. doi:10.1016/j.biopha.2009.06.021

Yang, Z., Zhou, X., Liu, Y., Gong, C., Wei, X., Zhang, T., et al. (2014). Activation of Integrin β1 Mediates the Increased Malignant Potential of Ovarian Cancer Cells Exerted by Inflammatory Cytokines. *Acamc.* 14 (7), 955–962. doi:10.2174/1871520614666140613123108

Yuan, Z.-Y., Luo, R.-Z., Peng, R.-J., Wang, S.-S., and Xue, C. (2014). High Infiltration of Tumor-Associated Macrophages in Triple-Negative Breast Cancer Is Associated with a Higher Risk of Distant Metastasis. *Ott.* 7, 1475–1480. doi:10.2147/ott.s61838

Zhang, L.-y., Guo, Q., Guan, G.-f., Cheng, W., Cheng, P., and Wu, A.-h. (2019). Integrin Beta 5 Is a Prognostic Biomarker and Potential Therapeutic Target in Glioblastoma. *Front. Oncol.* 9, 904. doi:10.3389/fonc.2019.00904

Conflict of Interest: The authors declare that the research was conducted in the absence of any commercial or financial relationships that could be construed as a potential conflict of interest.

Publisher's Note: All claims expressed in this article are solely those of the authors and do not necessarily represent those of their affiliated organizations, or those of the publisher, the editors and the reviewers. Any product that may be evaluated in this article, or claim that may be made by its manufacturer, is not guaranteed or endorsed by the publisher.

Copyright © 2022 Liu, Liu, Fang, Liu and Hu. This is an open-access article distributed under the terms of the Creative Commons Attribution License (CC BY). The use, distribution or reproduction in other forums is permitted, provided the original author(s) and the copyright owner(s) are credited and that the original publication in this journal is cited, in accordance with accepted academic practice. No use, distribution or reproduction is permitted which does not comply with these terms.

frontiers | Frontiers in Oncology

ORIGINAL RESEARCH
published: 14 April 2022
doi: 10.3389/fonc.2022.868868

Serglycin Is Involved in TGF-β Induced Epithelial-Mesenchymal Transition and Is Highly Expressed by Immune Cells in Breast Cancer Tissue

*Marta Tellez-Gabriel[1], Xavier Tekpli[2], Trine M. Reine[3], Beate Hegge[1], Stephanie R. Nielsen[1], Meng Chen[4], Line Moi[1,5], Lisa Svartdal Normann[6,7], Lill-Tove R. Busund[1,5], George A. Calin[4,8], Gunhild M. Mælandsmo[1,6], Maria Perander[1], Achilleas D. Theocharis[9], Svein O. Kolset[10] and Erik Knutsen[1,11]**

[1] Department of Medical Biology, Faculty of Health Sciences, UiT-The Arctic University of Norway, Tromsø, Norway, [2] Department of Medical Genetics, Oslo University Hospital, Oslo, Norway, [3] Department of Interphase Genetics, Institute for Cancer Genetics and Informatics, Oslo University Hospital, Oslo, Norway, [4] Department of Translational Molecular Pathology, The University of Texas MD Anderson Cancer Center, Houston, TX, United States, [5] Department of Clinical Pathology, University Hospital of North Norway, Tromsø, Norway, [6] Department of Tumor Biology, Institute for Cancer Research, Oslo University Hospital, Oslo, Norway, [7] Department of Research and Innovation, Vestre Viken Hospital Trust, Drammen, Norway, [8] Center for RNA Interference and Non-Coding RNAs, The University of Texas MD Anderson Cancer Center, Houston, TX, United States, [9] Biochemistry, Biochemical Analysis & Matrix Pathobiology Research Group, Laboratory of Biochemistry, Department of Chemistry, University of Patras, Patras, Greece, [10] Department of Nutrition, University of Oslo, Oslo, Norway, [11] Centre for Clinical Research and Education, University Hospital of North Norway, Tromsø, Norway

OPEN ACCESS

Edited by:
Martin Götte,
University of Münster, Germany

Reviewed by:
Elvira V. Grigorieva,
Institute of Molecular Biology and Biophysics (RAS), Russia
Davide Vigetti,
University of Insubria, Italy

***Correspondence:**
Erik Knutsen
erik.knutsen@uit.no

Specialty section:
This article was submitted to Molecular and Cellular Oncology, a section of the journal Frontiers in Oncology

Received: *03 February 2022*
Accepted: *21 March 2022*
Published: *14 April 2022*

Citation:
Tellez-Gabriel M, Tekpli X, Reine TM, Hegge B, Nielsen SR, Chen M, Moi L, Normann LS, Busund L-TR, Calin GA, Mælandsmo GM, Perander M, Theocharis AD, Kolset SO and Knutsen E (2022) Serglycin Is Involved in TGF-β Induced Epithelial-Mesenchymal Transition and Is Highly Expressed by Immune Cells in Breast Cancer Tissue. Front. Oncol. 12:868868. doi: 10.3389/fonc.2022.868868

Serglycin is a proteoglycan highly expressed by immune cells, in which its functions are linked to storage, secretion, transport, and protection of chemokines, proteases, histamine, growth factors, and other bioactive molecules. In recent years, it has been demonstrated that serglycin is also expressed by several other cell types, such as endothelial cells, muscle cells, and multiple types of cancer cells. Here, we show that serglycin expression is upregulated in transforming growth factor beta (TGF-β) induced epithelial-mesenchymal transition (EMT). Functional studies provide evidence that serglycin plays an important role in the regulation of the transition between the epithelial and mesenchymal phenotypes, and it is a significant EMT marker gene. We further find that serglycin is more expressed by breast cancer cell lines with a mesenchymal phenotype as well as the basal-like subtype of breast cancers. By examining immune staining and single cell sequencing data of breast cancer tissue, we show that serglycin is highly expressed by infiltrating immune cells in breast tumor tissue.

Keywords: proteoglycans (PG), serglycin (SRGN), transforming growth factor beta (TGF- β), epithelial-mesenchymal transition (EMT), breast cancer, tumor infiltrating immune cells, Single cell sequencing

INTRODUCTION

The extracellular matrix (ECM) is important in regulating cellular behavior and in diverse processes such as development, tissue formation, inflammation, and disease. The ECM is a complex tissue constituent, where its make-up varies between tissues and cells A major component of the ECM is the collagens, comprising more than 20 different members with large structural and functional

differences. Other important ECM members are fibronectin, laminin, elastin, and proteoglycans (PGs) (1). The latter family of macromolecules contains both extracellular types such as agrin, versican, perlecan, and decorin, whereas important cell surface PGs are syndecans and glypicans. Serglycin is an intracellular PG, but with important extracellular functions when released from e.g. immune cells (2). PGs are unique among the ECM family of macromolecules as they are heavily glycosylated and sulfated, which contribute to their unique structures and functions. The core proteins are decorated with negatively charged glycosaminoglycan (GAG) chains, which are important for the interactions with partner molecules such as growth factors, proteases, and chemokines (3).

The role of PGs has been studied in relation to cartilage and bone functions, regulation of blood coagulation, extravasation of immune cells, cardiovascular disease, and cancer (4). Serglycin was initially defined as a hematopoietic PG (5), and a series of studies have focused on the role of serglycin in inflammation (2). However, serglycin has now been demonstrated to be expressed by diverse cell types such as muscle cells, chondrocytes, endothelial cells, and several types of cancer cells (6). Several PGs have been associated with epithelial-mesenchymal transition (EMT) (7–23), a naturally occurring, transdifferentiation program by which polarized epithelial cells lose their adherent and tight cell–cell junctions, enhance their migratory capacity, and increase their resistance to apoptosis (24). EMT is important in embryonic development, wound healing, and mammary gland development, and it is induced by a range of extracellular cues including a variety of growth factors, like transforming growth factor beta (TGF-β), and malignancy-associated cellular stress (25–27). The transition is orchestrated by several transcription factors, including Snail, Slug, TWIST, and ZEB (26). In cancer, the process of EMT is of fundamental importance, as EMT has been associated with dissemination, invasion, metastasis to distant organs, chemotherapy resistance, dormancy, and relapse (28–30). Overexpression of serglycin in the breast cancer cell line MCF7 induced expression of mesenchymal markers fibronectin and vimentin and the EMT transcription factor Snail, accompanied with a change to a more mesenchymal like morphology (31). Further, drug resistance towards the chemotherapeutics doxorubicin and methotrexate was increased with induced expression of serglycin (31). Using immunohistochemistry, serglycin was demonstrated to be present in breast cancer tissue, and serglycin was highly expressed in the aggressive MDA-MB-231 cell line (32). The MDA-MB-231 breast cancer cell line has been associated with a mesenchymal phenotype and has a high migratory potential (33, 34). High serglycin expression was also observed in highly metastatic nasopharyngeal cells (35). Furthermore, invasiveness and mobility of the cells was shown to be dependent on the glycosylated form of serglycin in breast cancer (32). In addition, the implication of serglycin in highly aggressive tumor cells was also studied in the glioblastoma cell line LN-18 (12). Silencing of the serglycin gene (*SRGN*) resulted in less proliferation, colony formation, stemness accompanied by astrocytic differentiation, and diminished tumor cell growth *in vivo*.

In this study, we have examined several TGF-β induced EMT RNA-Seq experiments, and we find that serglycin is upregulated by TGB-β stimulation. Disruption of the open reading frame (ORF) of the serglycin gene, *SRGN*, resulted in reduced and delayed induction of EMT. In breast cancer cell lines, serglycin expression is significantly associated with a mesenchymal phenotype. However, *in vivo*, we find serglycin expression to be highly related to infiltration of immune cells in the breast tumor tissue. Here, we have examined mRNA expression of serglycin in two breast cancer cohorts and a single cell sequencing data set, as well as the protein expression in a tumor microarray (TMA) by immunohistochemistry. Overall, our results presented show that serglycin is one of many important molecules in the complicated network of factors determining the transition from the epithelial to the mesenchymal phenotype, and suggest that serglycin in tumor tissue is mainly produced by infiltrating immune cells.

MATERIAL AND METHODS

Cell Culturing

BT474, BT549, Hs578T, MCF7, MDA-MB-231, MDA-MB-468, SK-BR-3, and T-47D, cells were purchased from the American Type Culture Collection (ATCC). HMLE cells were a kind gift from Robert Weinberg, Whitehead Institute for Biomedical Research and Department of Biology, Massachusetts Institute of Technology. BT474, BT549, MDA-MB-231, MDA-MB-468, SK-BR-3, and T-47D were cultured in RPMI 1640 (Sigma-Aldrich) supplemented with 10% fetal bovine serum (FBS) (Biochrom) and 1% penicillin-streptomycin (Sigma-Aldrich). BT549 cells were grown in the presence of 0.001 mg/ml insulin (Sigma-Aldrich) and T-47D were grown in the presence of 0.006 mg/ml insulin (Sigma-Aldrich). Hs578T were cultured in Dulbecco's Modified Eagle's Medium (DMEM; Sigma-Aldrich) supplemented with 10% FBS, 1% penicillin-streptomycin, and 0.01 mg/ml insulin. MCF7 were cultivated in Minimum Essential Medium Eagle (MEM; Sigma-Aldrich) supplemented with 10% FBS, 1% penicillin-streptomycin, and 0.01 mg/ml insulin. HMLE cells were grown in a 1:1 mixture of MEBM (Lonza) with DMEM/F12 (Sigma-Aldrich) supplemented with 10 ng/ml EGF, 0.5 µg/ml hydrocortisone, 0.01 mg/ml insulin, and 1% penicillin-streptomycin. All cell lines were incubated in a 5% CO2 humidified incubator at 37°C.

Generation of Epithelial and Mesenchymal Cell Subpopulations of HMLE Cells

HMLE cells were separated into an epithelial and a mesenchymal subpopulation by immunomagnetic separation. Magnetic beads (Immunomagnetic M450 Dynabeads®, ThermoFisher Scientific) were coated with anti-EpCAM (MOC31, IQ Products). Trypsinized cells (1 ml) were mixed with 30 µl of coated beads and incubated on a rotating rack at 4°C for 30 min. The beads with epithelial cells and cell suspension containing mesenchymal cells were subsequently separated using a magnet rack.

RNA Isolation, cDNA Synthesis, and RT-qPCR

From the breast cancer cell lines, RNA was isolated using the GenElute™ Mammalian Total RNA Miniprep Kit (Merck) according to the protocol provided by the manufacturer.

cDNA synthesis of total RNA was performed with SuperScript™ VI Reverse Transcriptase (ThermoFisher Scientific). 5.0 µM of random hexamer primer (P/N100026484, ThermoFisher Scientific) and approximately 200 ng of template were used for the reaction.

For RT-qPCR of cDNA from total RNA, 5 ng cDNA was mixed with FastStart Essential DNA Green Master (Roche Life Science) and 0.25 µM forward and reverse primer. All primer sequences are provided in **Table 1**. The LightCycler® 96 was used for quantification, and the formulas $2^{-\Delta\Delta Cq}$ or $2^{-\Delta Cq}$ were used to calculate fold change or expression values, respectively, using GAPDH as an internal reference.

Transient Transfections

Lipofectamine® 2000 (ThermoFisher Scientific) was used for transfection according to the protocol provided by the manufacturer. 25 µM siRNA or control siRNA was used for transfections. Cells were incubated for 48, 72, and 96 hours after transfection before harvesting. The following siRNA and control siRNA were used: siSRGN#1 (ThermoFisher Scientific, 4392420-S11041), siSRGN#2 (ThermoFisher Scientific 4392420-S11043), and Silencer® Negative Control No. 1 siRNA, (ThermoFisher Scientific, AM4611).

CRISPR/Cas9 Knockout

For generation of serglycin knockout cells, a synthetic single guide RNAs (sgRNAs) in complex with Cas9, targeting the protein coding sequence of *SRGN* (guide sequence: CTG AGT CTT ACC TTG AAC TGA GG, exon 1) were transfected by electroporation according to previously described protocol (36). sgRNAs and Cas9 2NLS Nuclease were purchased from Synthego and electroporation was performed using the Cell Line Nucleofector™ Kit V (Lonza). 100.000 cells were diluted in 50 µl electroporation buffer containing 3.6 µM of sgRNA and 0.8 µM Cas9 enzyme and electroporated using the program P-020 (Amaxa™ Nucleofector™ II). Cells were transferred immediately after electroporation to full media and left to recover for 1 week, before single cell colonies were generated by seeding of single cells using Flow cytometry. Screening for knockout clones were done by sanger sequencing of the target region using the forward primer AAA TGC AGT CGG CTT GTC CT and reverse primer CCC AAC AGT CAA AGG TGC CA. For sanger sequencing, the BigDye™ Terminator v3.1 Cycle Sequencing Kit (ThermoFisher Scientific) was used according to the manual provided by the manufacturer. Analysis of sanger sequences was done using the ICE Analysis by Synthego (https://ice.synthego.com/#/).

TABLE 1 | Primer list used for RT-qPCR.

Gene	Forward primer sequence	Reverse primer sequence
SRGN	GCTACTCAAATGCAGTCGGC	CCCATTGGTACCTGGCTCTC
CDH2	GGCTTCTGGTGAAATCGCAT	AAGAGGCTGTCCTTCATGCAC
VIM	GAACGCCAGATGCGTGAAAT	AAGGTGACGAGCCATTTCCT
TWIST	ATTCAAAGAAACAGGGCGTGGG	AGAATGCAGAGGTGTGAGGATG
ZEB1	GCGCTTCTCACACTCTGG	GCGCTTCTCACACTCTGG
ZEB2	ACTTGCAGAGCATTACCCC	ACTTGCAGAGCATTACCCC
GAPDH	GAGCGAGATCCCTCCAAAAT	AAATGAGCCCCAGCCTTCT

TGF-β and EGF Stimulation

70.000 cells were seeded in a twelve well plate for each time point. Three wells per time point were stimulated with either 10 ng/ml recombinant human TGF-β (ThermoFisher Scientific, PHG9214) or 20 ng/ml EGF (R&B Systems). If reaching confluency, cells were split, and 70.000 cells were reseeded for each condition. Splitting was never performed less than three days before harvesting, to allow cells to recover.

Analysis of Publicly Available RNA-Seq Data

Three publicly available RNA-Seq experiments where EMT had been induced by TGF-β were downloaded from the Sequence Read Archive (SRA) at NCBI. The bioproject numbers are: PRJNA474381 (37), PRJNA513977 (38), PRJNA260526 (39).

RNA-Seq analyses were performed with the CLC Genomic Workbench 21 following the RNA-Seq analysis pipeline. In short, raw reads were trimmed for quality and the presence of the Illumina adaptor, before being mapped to the human reference genome GRCh38 with Ensembl v104 annotation. Expression values were normalized as Trimmed Mean of the M-values (TMM) adjusted counts per million (CPM). Calculation of significantly differentially expressed genes was done using the Differential Expression for RNA-Seq tool provided in the CLC Genomic Workbench and were defined as >2.0 fold change with <0.05 FDR adjusted p-value.

Gene Expression, Survival, Correlation, and Copy Number Analyses in Breast Cancer Cohorts

Breast cancer cell line RNA-Seq expression data and subtype information was downloaded from the Cancer Cell Line Encyclopedia (https://sites.broadinstitute.org/ccle/) (40). For the TCGA cohort, gene expression data and associated subtype information were obtained using R package TCGAbiolinks (41, 42). Gene expression levels were measured using $\log_2$ transformed fragments per kilobase of transcripts per million mapped reads (FPKM). A total of 1079 breast cancer primary tumor samples were included. According to the PAM50 classifier, the number of samples per subtypes were: 1) luminal A (n=506); 2) luminal B (n=207); 3) basal-like (n=190); 4) HER2-enriched (n=82); and 5) normal-like (n=40). PAM50 subtype classification and median centered mRNA expression data of primary tumors from 364 breast cancer patients included in the OSLO2 study were used for expression analyses for the OSLO2 cohort. The OSLO2 study is approved by Regional committees for medical and health research ethics of Norway (approval number 2016/433). The significant differences in gene expression between the five molecular subtypes of breast cancer

were examined in both cohorts using One-way ANOVA in GraphPad Prism 9.

Survival analysis was performed using GraphPad Prism 9 using the extracted TCGA cohort data. Patients were divided into a high and low group based on the median expression of *SRGN*.

Correlations between *SRGN* and other genes were analyzed by Pearson correlation in R programing environment (R 4.0.5). The p value of 0.05 ($p < 0.05$), and absolute value of the correlation coefficient above 0.6 (abs (correlation) >0.6) were used for selecting correlated genes with *SRGN*. Gene Set Enrichment Analysis (GSEA) was performed using the web interface (https://www.gsea-msigdb.org/gsea/index.jsp) (43, 44).

Copy number profiling data was obtained from the UCSC Xena platform (https://xenabrowser.net/datapages/). Copy number was measured experimentally using whole genome microarray at a TCGA genome characterization center. Subsequently, the GISTIC2 method was applied using the TCGA FIREHOSE pipeline to produce gene-level copy number estimates. GISTIC2 further thresholded the estimated values to -2, -1, 0, 1, 2, representing homozygous deletion, single copy deletion, diploid normal copy, low-level copy number amplification, or high-level copy number amplification, respectively. Genes were mapped onto the human genome coordinates using UCSC xena HUGO probeMap (45). The estimated values -2 and -1 are classified into loss. The estimated value 1 and 2 are classified into gain. A total of 1042 breast cancer copy number profiling were included in this study. According to the PAM50 classifier, the number of samples per subtypes were: luminal A (n=541); 2) luminal B (n=201); 3) basal-like (n=182); 4) HER2-enriched (n=80); and 5) normal-like (n=38).

Single Cell RNA-Seq Data Analysis

The publicly available dataset E-MTAB-8107 was used for single cell analysis, which includes 18 breast cancer patients (46). Count matrix of single cell RNA-Seq was analyzed using the Seurat package in R (v4.0.2) to obtain UMAP. The count matrix was already filtered for dying cells by the authors. It was further normalized and scaled regressing out potential confounding factors such as: number of UMIs, number of gene detected in the cell, and percentage of mitochondrial RNA. After scaling, variably expressed genes were used to construct principal components (PCs) and PCs covering the highest variance in the dataset were selected based on elbow and Jackstraw plots to build the UMAP. Clusters were calculated by the FindClusters function with a resolution chosen at 1.2, and visualized using the UMAP dimensional reduction method. Cell type annotation from the authors was used to visualize the distribution of different cell types on UMAP.

Clinical Samples and Immunostaining

Two tumor micro array (TMA) slides, including a total of 88 patients from the Clinical and Multi-omic (CAMO) cohort were used for immunostaining. The TMA contained samples of both tumor tissue in the invasive front and in the center of the tumor. Patient clinical data was defined as previously described (47). The use of the tissue samples and data was in accordance with the ethical approval from the Regional committees for medical and health research ethics of Norway (approval numbers 2010/1931 and 2013/2271). FFPE sections were baked in a dry oven at 60° C overnight and deparaffinized and rehydrated in xylene and alcohol. The Envison FLEX + system/Dako Autostainer Link 48 (Agilent Technologies) was used for the immunohistochemistry procedure. Antigen retrieval was performed in a commercial pressure chamber (pt-link, Dako) with a heating of 97°C for 20 minutes in Tris/EDTA buffer pH 9. Slides were then allowed to cool to 65°C and permeabilized in TBST (Tris-buffered saline solution containing Tween 20, pH 7.6, Envision Flex Wash Buffer) for 5 minutes. Peroxidase block was performed for 5 minutes in Envision Flex peroxidase block solution followed by protein blocking in 5% BSA for 10 minutes. After incubation with primary anti-serglycin (generated in the lab of Achilleas Theocharis) 1:10 000 for 30 min in room temperature, slides were washed in TBST and incubated with secondary anti-rabbit antibody and linker for 15 minutes. Following a wash in TBST, slides were incubated with EnVision FLEX/HRP (dextran polymer conjugated with horseradish peroxidase) for 20 minutes and washed for 5 minutes. Immunostaining was developed in DAB chromogen solution for 30 minutes. Finally, after washing in TBST, the slides were immediately counterstained with Shandon instant hematoxylin TID, and mounted using eukitt. The immune staining was documented using the Aperio scanner. Only samples defined as luminal A (ER+, HER2-, and Ki67 ≤30) or triple negative (ER-, PR-, HER-) were evaluated. Due to sample loss or poor-quality samples, 42 patients were included in the final scoring. Serglycin expression was scored from 0-3: 0 - no staining, 1 - low intensity, 2 - medium intensity, 3 – high intensity.

RESULTS

Serglycin Is Transcriptionally Upregulated During TGF-β Induced Epithelial-Mesenchymal Transition

Both during normal development and in carcinogenesis, TGF-β is a potent inducer of epithelial-mesenchymal transition (EMT). TGF-β is also important in the regulation of synthesis of many extracellular matrix (ECM) proteins, including several proteoglycans (PGs) (48). In wound healing, TGF-β plays a major role in inducing EMT and inflammation and in in the remodeling of the ECM (49). To investigate the role of proteoglycans (PGs) in TGF-β induced EMT, we mined publicly available RNA-Seq experiments, in which epithelial cells had been stimulated with TGF-β. Our inclusion criteria were: 1) Cells have a normal non-cancerous epithelial origin, 2) the sequencing experiment should include a minimum of two replicates per sample, and 3) the data is published with a complete method description. Three such datasets were identified; PRJNA474381 (37), PRJNA513977 (38), and PRJNA260526 (39). Differential gene expression analysis was performed using the CLC Genomic workbench, and for all three datasets, Gene set enrichment analysis identified EMT as the

most significantly enriched hallmark (**Figure 1A**). The data was used to examine the expression of 42 PGs, and we identified eight as significantly differently expressed (**Figure 1B**). Many of the significantly differently expressed PGs have previously been associated with EMT: *SDC2* (8, 9), *SDC4* (10, 11), *SRGN* (12–14), *VCAN* (15–17), *DCN* (18), *LUM* (19), *SPOCK1* (20–23). One of the most significantly differently expressed genes was serglycin (*SRGN*), with a fold change of 59.7 (p=8.8E-80), 4.1 (p=1.6E-23), and 17.7 (p=7.0E-72) (**Figure 1C**). As TGF-β has a functional role in controlling the inflammatory responses (50) and serglycin is an important inflammatory PG, we decided to focus on serglycin in our further studies. To validate the observed induction of serglycin by TGF-β, we treated the HMLE cell line with TGF-β for six days. HMLE is a normal breast epithelial cell line which is known to undergo EMT when stimulated by TGF-β (51, 52). RT-qPCR analysis of *SRGN* showed a 5.9-fold induction (p=0.004) in the HMLE cells after TGF-β stimulation (**Figure 1D**).

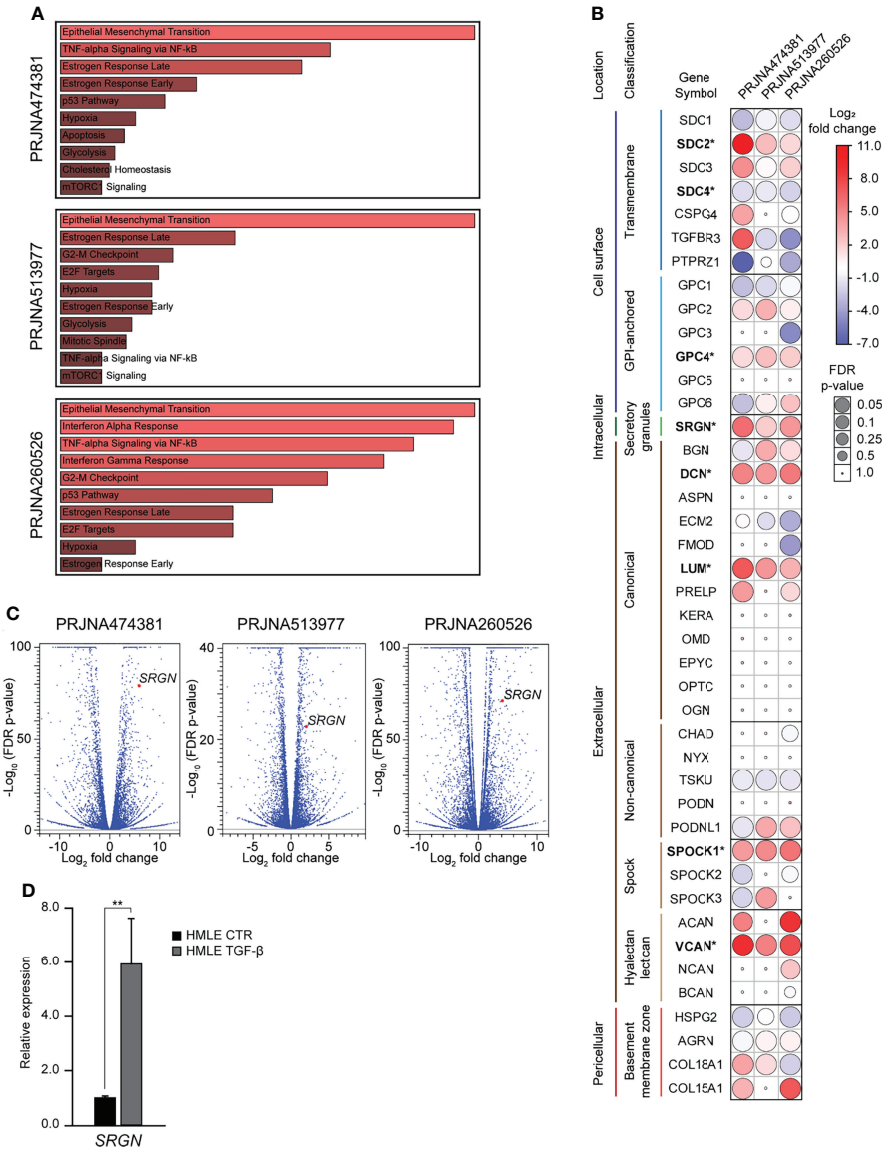

FIGURE 1 | Serglycin is transcriptionally upregulated during TGF-β induced epithelial-mesenchymal transition. **(A–C)** Analysis of RNA-Seq data from three publicly available data sets. **(A)** Gene set enrichment analysis for differentially expressed genes. Length and color represent the significance of that specific gene-set. **(B)** Expression of 42 genes encoding proteoglycans. Bold gene symbols marked with * were defined as differently expressed in all three datasets and with the same direction of change. Color (blue-white-red) symbolizes fold change, while the size of circles symbolizes false discovery rate (FDR) corrected p-value. **(C)** Volcano plot including all analyzed genes. *SRGN* is marked as a red dot in all three plots. **(D)** RT-qPCR data showing *SRGN* expression in TGF- β induced HMLE cells. The experiment includes three biological replicates and is representative for one of a minimum of three independent experimental setups. Error bars represent standard deviation. (**p ≤ 0.01).

Knockout of Serglycin Causes a Delay in EMT-Associated Gene Expression and Morphology

To examine the functional role of serglycin in TGF-β induced EMT, we generated two HMLE knockout clones by CRISPR/Cas9. The two clones had unique frameshift mutations confirmed by Sanger sequencing (**Figure 2A**). As expected, the serglycin knockout clones had a significantly reduced baseline expression of *SRGN* (**Figure 2B**), as mRNA stability is often reduced by frameshift mutations (53). Further, when treating with TGF-β, the serglycin knockout cells showed no evident induction of *SRGN*, as compared to the wild type HMLE cell line (**Figure 2B**). Importantly, the loss of *SRGN* was accompanied by a reduced induction of N-cadherin (*CDH2*) and the EMT transcription factor *ZEB1* (**Figures 2C, D**). Induction of *SRGN* expression in the normal HMLE cells preceded induction of both *CDH2* and *ZEB1*, and all together these results indicate that upregulation of *SRGN* might be an important early event for efficient EMT induction in HMLE cells. Further, we observed more cells with an elongated mesenchymal phenotype and the growth pattern of the cells were more scattered with less contact with other cells in the wild type control cells as compared to the serglycin knock out cells after TGF-β treatment (**Figure 2E**). As *ZEB1* expression was reduced in the serglycin knockout clones, we examined the relationship between ZEB1 and serglycin in TGF-β induced EMT. One of the previously examined publicly RNA-Seq datasets (PRJNA513977) had included sequencing of an epithelial ZEB1 knockout cell line treated with TGF-β. Knockout of ZEB1 was sufficient to inhibit induction of *SRGN* (**Figure 2F**), indicating that ZEB1 might be a positive regulator of serglycin. Finally, to examine whether serglycin plays a key role in maintaining an EMT phenotype, we transiently transfected mesenchymal HMLE cells with two different *SRGN*-targeting siRNAs. Although the siRNAs significantly silenced the *SRGN* expression, the expressions of key EMT marker genes including *CDH2*, *VIM*, *TWIST*, *ZEB1*, and *ZEB2* remained unchanged 72 hours post-transfection (**Figure 2G**). This suggests that loss of serglycin is not sufficient to revert an established mesenchymal phenotype in the HMLE cell model.

Breast Cancer Cell Lines With a Mesenchymal Phenotype and the Basal-Like Subtype of Breast Cancer Express High Levels of Serglycin

Elevated levels of TGF-β, both in the plasma and at the invasive front, have been associated with metastasis in breast cancer patients (54–56), and TGF-β has been proposed as a target for cancer therapy (57, 58). Furthermore, many transcription factors and pathways that regulate EMT have been found to be activated in breast tumors (59). To evaluate the association of serglycin expression with EMT in breast cancer, we started by examining RNA-Seq data from 48 breast cancer cell lines deposited to the Cancer Cell Line Encyclopedia (40). The breast cancer cell lines were clustered based on the expression of 194 genes included in the EMT hallmark gene dataset according to the Molecular Signatures Database v7.4 (43, 60) (**Figure 3A**). The clustering gave three main clusters: Mesenchymal (M), partial EMT (P), and epithelial (E) (**Figure 3A**). By examining serglycin mRNA levels, we found that *SRGN* is highest expressed in cell lines defined as mesenchymal, while no or very low expression is identified in epithelial like cells (**Figures 3A, B**). We confirmed by RT-qPCR the higher expression in the mesenchymal breast cancer cell lines Hs578T, MDA-MB-231, and BT549, versus the plastic MDA-MB-468 and the epithelial T-47D, SK-BR-3, BT474, and MCF7 breast cancer cell lines (**Figure 3C**). SK-BR-3, an epithelial like breast cancer cell line, can be induced to go through EMT by EGF stimulation, and show a low baseline expression of *SRGN*. We therefore examined *SRGN* expression in SK-BR-3 during EMT and found that *SRGN* was induced by EGF treatment together with N-cadherin (*CDH2*) and *ZEB1* (**Figure 3D**).

As serglycin is important for EMT and expressed by mesenchymal like breast cancer cell lines, we went on to examine the expression of *SRGN* in two breast cancer cohorts, TCGA and OSLO2. In both cohorts, *SRGN* is highest expressed in the basal-like subtype of breast cancer (**Figure 3E**), a subtype associated with triple negative breast tumors and tumors with a mesenchymal phenotype (61, 62). However, the expression of *SRGN* was not associated with survival, neither for all patients nor for patients with the basal-like subtype (**Figure 3F**). To examine whether the higher expression of *SRGN* in the basal-like subtype could be a consequence of gene amplification, we analyzed copy-number of *SRGN*. Perhaps surprisingly, a higher incidence of allele loss was seen for the luminal B and basal-like subtypes (30.8% and 36.8%, respectively) as compared with the other subtypes (**Figure 3G**). Generally, allele loss was not seen to be more abundant in patients with lower expression of *SRGN*, and allele gain was not more prominent amongst patients with high expression of *SRGN* (**Figure 3G**), indicating that copy number variation does not influence *SRGN* expression in breast tumor tissue.

Serglycin Is Expressed by Non-Neoplastic Cells in Breast Tumor Tissue

The higher *SRGN* genomic loss in the basal-like subtype and the non-enrichment for allele loss in low expressing patients, prompted us to further investigate the association between the basal-like subtype and *SRGN* expression. We therefore performed immune staining on 42 breast cancer patients, either defined as luminal A (ER+, HER2-, and Ki67 ≤30) or triple negative (ER-, PR-, HER-) (**Figure 4A**). In both subtypes, we detected expression of serglycin in both the cancer cells and in infiltrating immune cells. For the cancer cells, a non-significant, but higher expression was observed in the luminal A subtype as compared to the triple negative (**Figure 4A**). In contrast, we observed a significantly higher number of infiltrating immune cells and a significantly higher expression of serglycin in the immune cells in the triple negative subtype as compared to the luminal A subtype (**Figure 4A**). This may indicate that the increased expression of serglycin in the basal-like subtype is a consequence of immune infiltration in the tumor tissue. By performing a co-expression analysis, we found that genes that correlated with *SRGN* expression in the basal-like cases from the TCGA cohort were not enriched for genes associated with EMT, but for genes enriched with the hallmarks Allograft rejection, Inflammatory response, and Complement (**Figure 4B**), which are all associated

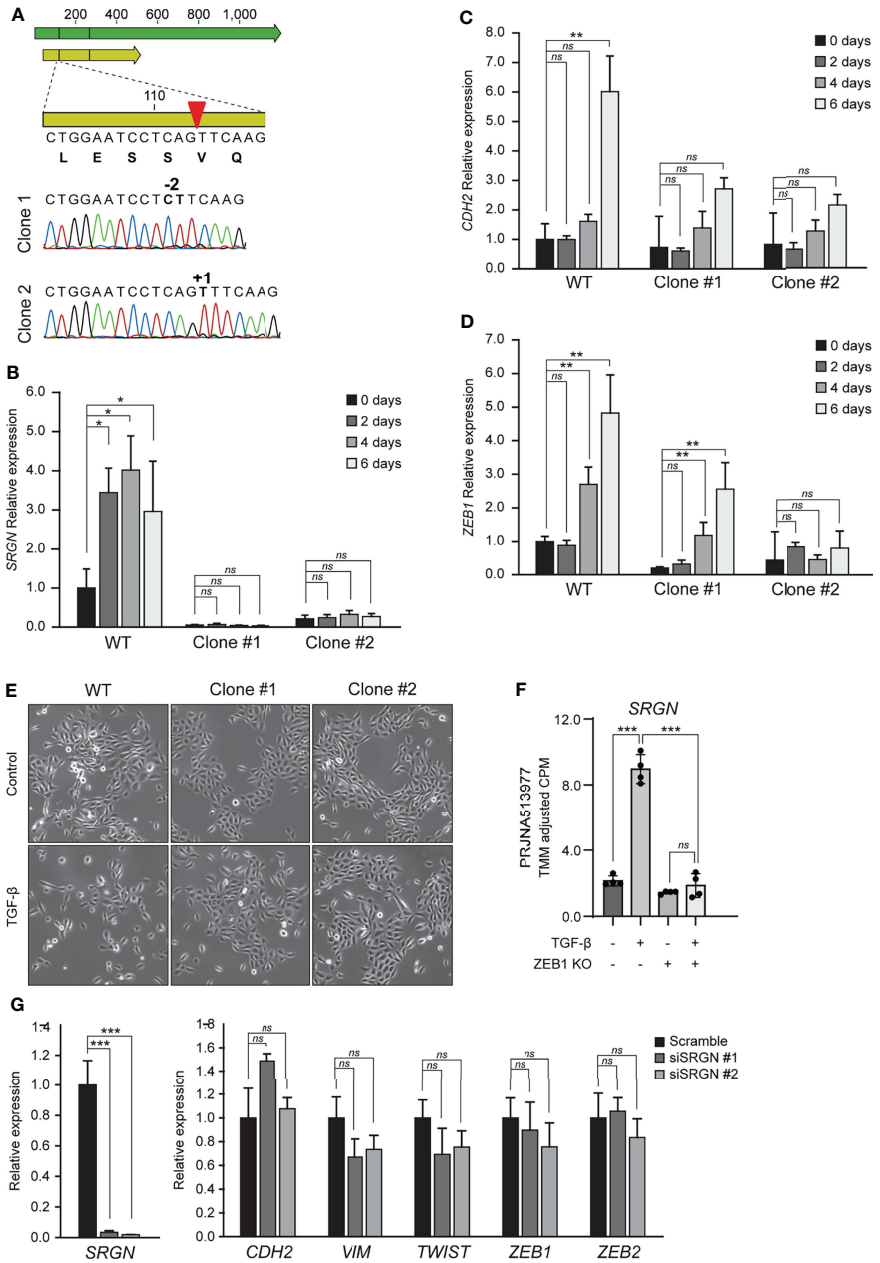

FIGURE 2 | Knockout of serglycin causes a delay in EMT-associated gene expression and morphology. **(A)** Confirmation of CRISPR/Cas9 generation of serglycin knockout clones by Sanger sequencing (bottom part of figure). Green arrow, mRNA; yellow arrow, open reading frame; red arrow, CRISPR/Cas9 target site. **(B–D)** HMLE epithelial cells were stimulated with 10 ng/ml TGF-β for 2, 4, and 6 days and **(B)** *SRGN*, **(C)** *CDH2*, and **(D)** *ZEB1* expression were evaluated by RT-qPCR. **(E)** HMLE epithelial cells were stimulated with 10 ng/ml TGF-β 4 days before imaged using a brightfield microscope. **(F)** Expression of *SRGN* in MCF10A wild type and ZEB1 knockout cells, with and without TGF-β stimulation. **(G)** HMLE mesenchymal cells were transfected for 72 hours with control (scramble) or two siRNAs, siSRGN #1, or siSRGN #2, specifically targeting *SRGN*. *SRGN* expression and expression of mesenchymal marker genes or EMT transcription factors were evaluated by RT-qPCR. For **(B–D)**, and **(G)** the experiments include three biological replicates and are representative for one of a minimum of three independent experimental setups. Error bars represent standard deviation. (***p ≤ 0.001; **p ≤ 0.01; *p ≤ 0.05; ns, not significant).

with an immune response. In addition, the following hallmarks for signaling pathways/molecules were found to be enriched: IFN-γ, STAT5, IFN-α, KRAS, JAK/STAT3, and TNF-α (**Figure 4B**). The observed high expression of serglycin in immune cells, and the association towards an immune response, prompted us to examine *SRGN* expression in a publicly available breast cancer single cell RNA-Seq data set (46). Here, expression analysis showed that *SRGN* is highly expressed in dendritic cells, T-cells, myeloid cells, and mast cells in the tumor tissue, and with lowly detectable expression of *SRGN* in the cancer cells (**Figure 4C**).

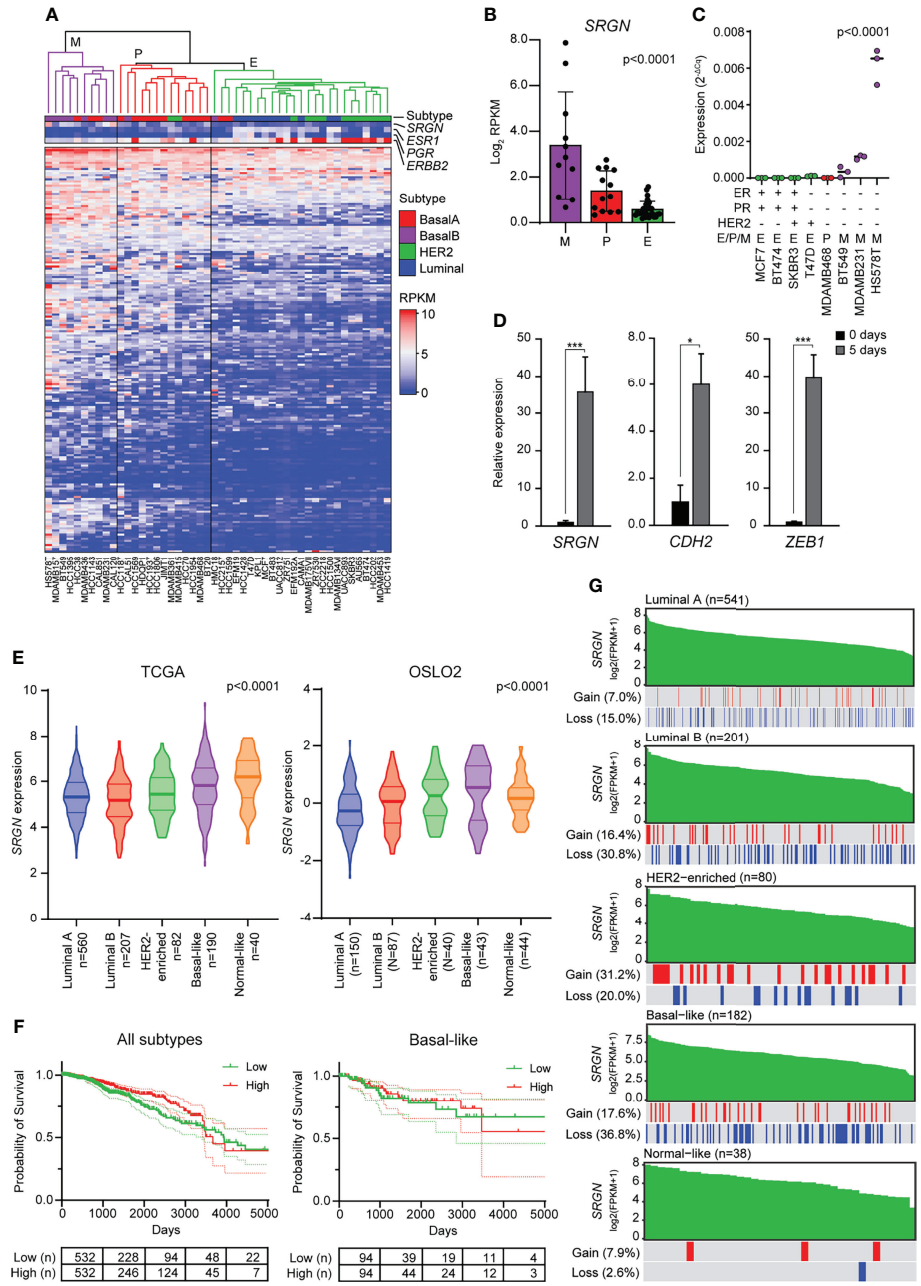

FIGURE 3 | Breast cancer cell lines with a mesenchymal phenotype and the basal-like subtype of breast cancer express high levels of serglycin. **(A)** Hierarchical clustering of 48 breast cancer cell lines based on 194 genes included in the EMT hallmark gene dataset. Subtype and expression of *SRGN*, *ESR1*, *PGR*, and *ERBB2* are shown separately above the heatmap. E, epithelial; P, partial EMT; M, mesenchymal; RPKM, reads per kilobase per million. **(B)** *SRGN* expression in cell lines defined as epithelial **(E)**, partial EMT (P), or mesenchymal (M) based on hierarchical clustering. **(C)** *SRGN* expression in breast cancer cell lines evaluated by RT-qPCR. E, epithelial; P, partial EMT; M, mesenchymal. **(D)** SK-BR-3 cells were stimulated with 20 ng/ml EGF for 5 days. *SRGN*, *CDH2*, and *ZEB1* expression were evaluated by RT-qPCR. The experiment includes three biological replicates and is representative for one of a minimum of three independent experimental setups. Error bars represent standard deviation.**(E)** *SRGN* expression in the TCGA and OSLO2 cohorts. **(F)** Probability of survival for either all breast cancer patients or only patient with the basal-like subtype from the TCGA cohort. High and low expression is based on the median expression value of *SRGN*. Dotted lines represent the 95% confidence interval **(G)** Serglycin copy number gain or loss for patients included in the TCGA cohort. Green bars represent *SRGN* expression, arranged from high to low expression within each subtype. A red line indicates a copy number gain while a blue line represents a copy number loss in the patient with the specific expression value bar seen above in green. FPKM, fragments per kilobase per million. (***p ≤ 0.001; *p, ≤ 0.05).

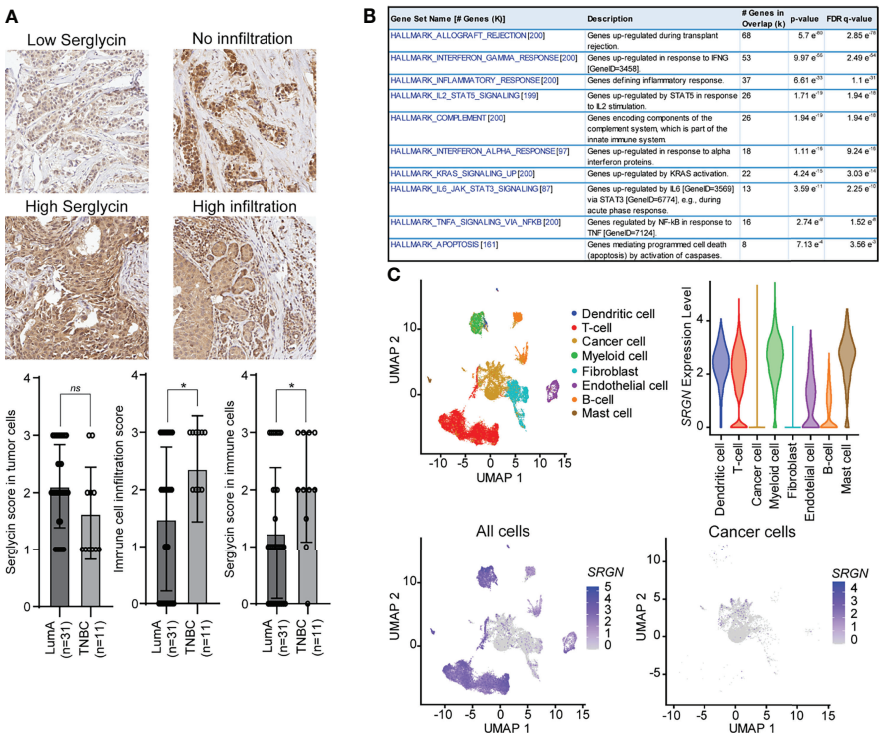

FIGURE 4 | Serglycin is expressed by non-neoplastic cells in breast tumor tissue. **(A)** Immune staining for serglycin in breast cancer patients defined as either luminal A (LumA) or triple negative breast cancer (TNBC). Images representing low (score 1) and high (score 3) serglycin expression in cancer cells, and no (score 0) or high immune cell infiltration (score 3) are included. Bar plots includes quantification of expression of serglycin in either tumor cells or immune cells as well as quantification of immune infiltration in the tumor tissue. Error bars represent semi-standard deviation. **(B)** Gene set enrichment analysis for genes that show a high correlation with *SRGN* expression in patients with the basal-like subtype from the TCGA cohort. **(C)** *SRGN* expression in single cell RNA-Seq data including 18 patients with different subtypes. Top left: Visualization of the different cell types in the UMAP plot. Top right: *SRGN* expression visualized as violine plots per cell type. Bottom left: UMAP plot of *SRGN* expression in all cell types. Bottom right: UMAP plot of *SRGN* expression in only cancer cells. (*p ≤ 0.05; ns, not significant).

DISCUSSION

EMT in cancer is associated with the acquisition of cancer stem cell-like properties and increased migratory and metastatic abilities, antitumor drug resistance, and immunosuppression. Several stimuli induce EMT in cancer cells including growth factors like TGF-β and EGF, hypoxia, ECM stiffness, cell-cell and cell-ECM interactions, and epigenomic factors (63, 64). We demonstrate that *SRGN* expression is upregulated in different epithelial cells that undergo EMT as response to TGF-β stimulation (**Figure 5**). *SRGN* knockdown in mesenchymal cells is not able to revert an acquired mesenchymal phenotype, but serglycin knockout in epithelial cells exhibit a delay or lower response to TGF-β induced EMT. These data suggest that serglycin is an important player in the EMT reprogramming in epithelial cells, but not essential for cells to maintain a mesenchymal phenotype. The induction of *SRGN* also preceded *CDH2* and *ZEB1*, indicating that *SRGN* induction is an early event in EMT. However, knockout of ZEB1 inhibited *SRGN* induction by TGF-β, suggesting that ZEB1 might be a potentially important transcription factor for serglycin (**Figure 5**). By examining the UCSC Genome Browser, two ZEB1 binding sites are located in the promotor region of serglycin. The potential directly regulation of serglycin by ZEB1 should therefore be experimentally validated. Aggressive breast cancer cells with mesenchymal traits such as MDA-MB-231 and Hs578T, as well as basal-like breast tumors, express high levels of *SRGN*, in contrast to epithelial breast cancer cells and respective luminal subtypes of breast cancer. Altogether, our data point to serglycin as a novel, highly significant marker for breast mesenchymal cells. *SRGN* expression was also found to be induced in the epithelial breast cancer cell line SK-BR-3 through induction of EMT by EGF, which demonstrates the strong association between serglycin and EMT, both in normal as well as in cancer cells.

Previous studies have shown that expression of serglycin in the epithelial breast cancer cell line MCF7 (32) and in non-small cell lung cancer cells (NSCLC) (65) evokes their malignant properties, and that chondroitin sulfate chains attached on the serglycin core protein are required for this regulation. Increased expression of serglycin in epithelial breast cancer cells drives EMT, chemoresistance, proteolytic potential, invasion, and metastasis both *in vitro* and *in vivo* (31, 66–68). Serglycin is constitutively secreted by breast cancer cells acting in an autocrine manner *via* binding to cell surface receptors such as CD44, a key mesenchymal and breast cancer stem cell marker gene, and integrins, possibly through its chondroitin sulfate (CS) chains (69) (**Figure 5**).

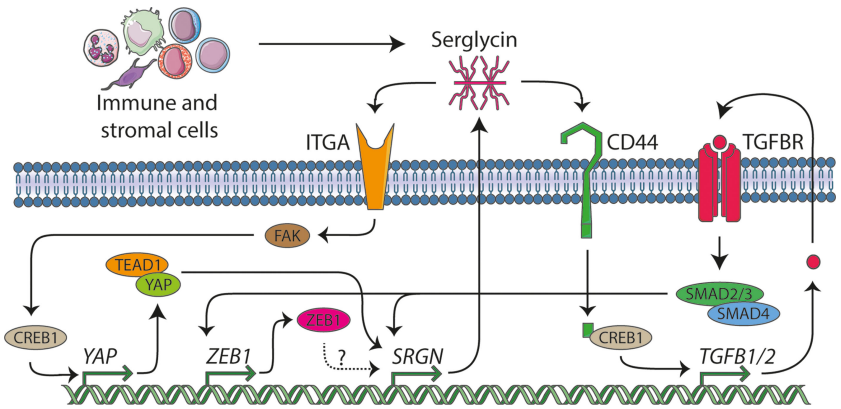

FIGURE 5 | The serglycin signaling network. In this manuscript we identify serglycin to be a TGF-β responsive gene that is induced during epithelial mesenchymal transition (EMT), and we propose that ZEB1 might be a potential transcription factor that can induce serglycin expression. From previous publication, serglycin has been shown to be able to act in an autocrine manner through the TGF-β pathway and *via* the YAP transcriptional co-activator. Several lines of evidence show that immune and stromal cells are major contributors of serglycin in the tumor microenvironment, and we hypothesize that expression of serglycin in the tumor microenvironment can stimulate breast cancer cells to undergo EMT.

Binding of serglycin to CD44 activates multiple signaling pathways including CD44/CREB1 to induce TGF-β2 secretion that in turn upregulates *SRGN* expression *via* Smad3 signaling (66), as well as by activating β-catenin signaling (67). Secreted serglycin also triggers ITGA5/FAK/CREB1 signaling to increase the transcription of YAP (68) (**Figure 5**). Reciprocally, YAP/TEAD1 complex promotes the transcription of *SRGN* to form a feed-forward circuit. Furthermore, YAP/RUNX1 complex induces the transcription of HDAC2 to induce chemoresistance and stemness in breast cancer cells (68). Serglycin also promotes IL-8 secretion in breast cancer cells activating IL-8/CXCR2 signaling and underlying signaling cascades such as PI3K, Src, and Rac1 (31). Similarly, to breast cancer, serglycin triggers signaling pathways that evoke malignant properties and EMT in many other cancer types. The serglycin/CD44 signaling axis induces the expression of Nanog and activates NF-κB/claudin-1 axis in NSCLC (70) and triggers MAPK/β-catenin signaling in nasopharyngeal cancer cells (71) to foster EMT, cancer cell stemness, and drug resistance.

Over the last few years, an increasing number of studies have shown that upregulation of serglycin in many tumors is associated with aggressive tumor cells properties (6). In breast cancer, serglycin has been demonstrated to be associated with chemotherapy resistance (31, 72). Here, we describe that *SRGN* expression in the basal-like subtype of breast cancer is correlated to the expression of genes involved in inflammatory response. Previous reports have also highlighted the role of serglycin in regulation of the biosynthesis of inflammatory mediators and growth factors in immune cells, platelets, endothelial, and tumor cells (2, 69). Serglycin also controls the proteolytic potential of tumor cells *via* regulating the expression and activity of MMPs (6, 12, 31, 73). Both inflammatory mediators and MMPs are known to be involved in EMT and in the advancement of the malignant phenotype of breast cancer cells (74, 75). We have demonstrated that the high expression of *SRGN* in the generally aggressive basal-like breast cancer subtype is not a consequence of gene amplification, but rather surprisingly, the subtype shows a higher probability for allele loss. This may imply that the bulk of serglycin expression comes from stromal cells (**Figure 5**). Several cell types populate the tumor stroma, with the most predominant being immune cells, cancer-associated fibroblasts, and endothelial cells. Breast cancer single cell RNA-Seq data indicate that *SRGN* is highly expressed mostly in stromal cells and lymphocytes, including myeloid, dendritic, mast cells, T-lymphocytes, endothelial cells, and B-lymphocytes. Cancer cells and fibroblasts exhibit low *SRGN* expression in the analyzed sample cohort. This points toward infiltrating immune cells being the major source of serglycin in breast tumor tissue. It is well known that serglycin is constitutively expressed by immune cells such as macrophages, lymphocytes, and mast cells and its expression is upregulated upon their activation (2, 76). Mast cells infiltrate the glioma microenvironment and secrete high levels of serglycin, and the process is associated with poor survival (77). Co-culture of mast cells with glioma cells induces the expression of serglycin, CD44, ZEB1, vimentin, CXCL10, CXCL12, and TNF-α in glioma cells and IL-6 and CXCL1 in mast cells, creating an inflammatory milieu that induce glioma cell aggressiveness (77). In glioblastoma, serglycin works in an autocrine manner, and suppression of serglycin potently reduces their malignant properties, pro-neoplastic signaling, and stemness, and evokes astrocytic differentiation (12). This demonstrates a key role for serglycin in glioma progression, and demonstrates how serglycin, either *via* induction by an inflammatory response or by direct secretion by immune cells is of major importance for cancer progression. Serglycin is also upregulated in cancer-associated fibroblasts in hypoxic conditions and its secretion activates Wnt/β-catenin signaling, leading to enhanced cancer cell stemness, chemoresistance, and tumor growth (78).

It is proposed that cancer cells that are subjected to partial EMT and remain in a hybrid state where they co-express both epithelial and mesenchymal markers, have the greatest

malignant and metastatic potential (63, 79). Furthermore, subpopulations of cancer cells composed of epithelial, hybrid, or mesenchymal cells have been found to be localized in specific microenvironments where distinct stromal cells reside (79). Tumor areas specifically populated by the hybrid or mesenchymal cancer cells have an increased number of immune cells, particularly monocytes and macrophages, lymphocytes, and endothelial cells, highlighting the association of EMT induction with the inflammatory environment. Interestingly, cancer cells express increased levels of chemokines and other pro-inflammatory and pro-angiogenic molecules that attract stromal cells and coordinates their niche formation and spatial organization (79). Further, serglycin has recently been identified to be involved in inflammatory reactions in adipose tissue (80). Altogether, our data and previously published data on serglycin, EMT, and cancer, may imply that serglycin participates in an immune cell-cancer cell crosstalk, acting as a regulatory molecule that links inflammation and induced oncogenic signaling and EMT in breast cancer cell (**Figure 5**). Future studies should therefore investigate the molecular mechanisms behind this potential crosstalk, *via* serglycin, between the breast cancer cells and the infiltrating immune cells and if expression of serglycin by the immune cells can induce EMT in the breast cancer cells.

DATA AVAILABILITY STATEMENT

The original contributions presented in the study are included in the article/supplementary material. Further inquiries can be directed to the corresponding author.

ETHICS STATEMENT

The studies involving human participants were reviewed and approved by Regional committees for medical and health research ethics of Norway. The patients/participants provided their written informed consent to participate in this study.

AUTHOR CONTRIBUTIONS

MT-G, TR, BH, SN, and EK conducted experiments. XT, MC, LN, and EK collected and analyzed data. LM, L-TB, GM, MP, AT, SK, and EK provided material or patient samples. MP, AT, SK, and EK wrote the manuscript. All authors revised and approved the manuscript.

FUNDING

EK is funded by Helse Nord (HNF1585-21), SK is funded by the Throne Holst Foundation, LN is funded by Helse Sør-Øst (2017034), and GM is funded by the Norwegian Cancer Society (#190257).

ACKNOWLEDGMENTS

We thank Professor Dr. Robert A. Weinberg, Whitehead Institute for Biomedical Research and Department of Biology, Massachusetts Institute of Technology, Cambridge, Massachusetts USA, for the kind gift of HMLE cells.

REFERENCES

1. Theocharis AD, Manou D, Karamanos NK. The Extracellular Matrix as a Multitasking Player in Disease. *FEBS J* (2019) 286(15):2830–69. doi: 10.1111/febs.14818
2. Kolset SO, Pejler G. Serglycin: A Structural and Functional Chameleon With Wide Impact on Immune Cells. *J Immunol* (2011) 187(10):4927–33. doi: 10.4049/jimmunol.1100806
3. Couchman JR, Pataki CA. An Introduction to Proteoglycans and Their Localization. *J Histochem Cytochem* (2012) 60(12):885–97. doi: 10.1369/0022155412464638
4. Manon-Jensen T, Itoh Y, Couchman JR. Proteoglycans in Health and Disease: The Multiple Roles of Syndecan Shedding. *FEBS J* (2010) 277(19):3876–89. doi: 10.1111/j.1742-4658.2010.07798.x
5. Kolset SO, Gallagher JT. Proteoglycans in Haemopoietic Cells. *Biochim Biophys Acta* (1990) 1032(2-3):191–211. doi: 10.1016/0304-419X(90)90004-K
6. Manou D, Karamanos NK, Theocharis AD. Tumorigenic Functions of Serglycin: Regulatory Roles in Epithelial to Mesenchymal Transition and Oncogenic Signaling. *Semin Cancer Biol* (2020) 62:108–15. doi: 10.1016/j.semcancer.2019.07.004
7. Couchman JR. Syndecan-1 (CD138), Carcinomas and EMT. *Int J Mol Sci* (2021) 22(8):4227. doi: 10.3390/ijms22084227
8. Hua R, Yu J, Yan X, Ni Q, Zhi X, Li X, et al. Syndecan-2 in Colorectal Cancer Plays Oncogenic Role *via* Epithelial-Mesenchymal Transition and MAPK Pathway. *BioMed Pharmacother* (2020) 121:109630. doi: 10.1016/j.biopha.2019.109630
9. Contreras HR, Ledezma RA, Vergara J, Cifuentes F, Barra C, Cabello P, et al. The Expression of Syndecan-1 and -2 is Associated With Gleason Score and Epithelial-Mesenchymal Transition Markers, E-Cadherin and Beta-Catenin, in Prostate Cancer. *Urol Oncol* (2010) 28(5):534–40. doi: 10.1016/j.urolonc.2009.03.018
10. Toba-Ichihashi Y, Yamaoka T, Ohmori T, Ohba M. Up-Regulation of Syndecan-4 Contributes to TGF-Beta1-Induced Epithelial to Mesenchymal Transition in Lung Adenocarcinoma A549 Cells. *Biochem Biophys Rep* (2016) 5:1–7. doi: 10.1016/j.bbrep.2015.11.021
11. Chen LL, Gao GX, Shen FX, Chen X, Gong XH, Wu WJ. SDC4 Gene Silencing Favors Human Papillary Thyroid Carcinoma Cell Apoptosis and Inhibits Epithelial Mesenchymal Transition *via* Wnt/beta-Catenin Pathway. *Mol Cells* (2018) 41(9):853–67. doi: 10.14348/molcells.2018.0103
12. Manou D, Bouris P, Kletsas D, Gotte M, Greve B, Moustakas A, et al. Serglycin Activates Pro-Tumorigenic Signaling and Controls Glioblastoma Cell Stemness, Differentiation and Invasive Potential. *Matrix Biol Plus* (2020) 6-7:100033. doi: 10.1016/j.mbplus.2020.100033
13. Xu Y, Xu J, Yang Y, Zhu L, Li X, Zhao W. SRGN Promotes Colorectal Cancer Metastasis as a Critical Downstream Target of HIF-1alpha. *Cell Physiol Biochem* (2018) 48(6):2429–40. doi: 10.1159/000492657
14. Humtsoe JO, Koya E, Pham E, Aramoto T, Zuo J, Ishikawa T, et al. Transcriptional Profiling Identifies Upregulated Genes Following Induction of Epithelial-Mesenchymal Transition in Squamous Carcinoma Cells. *Exp Cell Res* (2012) 318(4):379–90. doi: 10.1016/j.yexcr.2011.11.011
15. Yang L, Wang L, Yang Z, Jin H, Zou Q, Zhan Q, et al. Up-Regulation of EMT-Related Gene VCAN by NPM1 Mutant-Driven TGF-Beta/cPML Signalling Promotes Leukemia Cell Invasion. *J Cancer* (2019) 10(26):6570–83. doi: 10.7150/jca.30223
16. Zhang Y, Zou X, Qian W, Weng X, Zhang L, Zhang L, et al. Enhanced PAPSS2/VCAN Sulfation Axis is Essential for Snail-Mediated Breast Cancer

Cell Migration and Metastasis. *Cell Death Differ* (2019) 26(3):565–79. doi: 10.1038/s41418-018-0147-y
17. Xia L, Huang W, Tian D, Zhang L, Qi X, Chen Z, et al. Forkhead Box Q1 Promotes Hepatocellular Carcinoma Metastasis by Transactivating ZEB2 and VersicanV1 Expression. *Hepatology* (2014) 59(3):958–73. doi: 10.1002/hep.26735
18. Mao L, Yang J, Yue J, Chen Y, Zhou H, Fan D, et al. Decorin Deficiency Promotes Epithelial-Mesenchymal Transition and Colon Cancer Metastasis. *Matrix Biol* (2021) 95:1–14. doi: 10.1016/j.matbio.2020.10.001
19. Li LF, Chu PH, Hung CY, Kao WW, Lin MC, Liu YY, et al. Lumican Regulates Ventilation-Induced Epithelial-Mesenchymal Transition Through Extracelluar Signal-Regulated Kinase Pathway. *Chest* (2013) 143(5):1252–60. doi: 10.1378/chest.12-2058
20. Cui X, Wang Y, Lan W, Wang S, Cui Y, Zhang X, et al. SPOCK1 Promotes Metastasis in Pancreatic Cancer *via* NF-kappaB-Dependent Epithelial-Mesenchymal Transition by Interacting With IkappaB-Alpha. *Cell Oncol (Dordr)* (2021) 45(1):69–84. doi: 10.1007/s13402-021-00652-7
21. Liu HX, Cao YY, Qu JY. SPOCK1 Promotes the Proliferation and Migration of Colon Cancer Cells by Regulating the NF-kappaB Pathway and Inducing EMT. *Neoplasma* (2021) 68(4):702–10. doi: 10.4149/neo_2021_201031N1158
22. Alshargabi R, Sano T, Yamashita A, Takano A, Sanada T, Iwashita M, et al. SPOCK1 is a Novel Inducer of Epithelial to Mesenchymal Transition in Drug-Induced Gingival Overgrowth. *Sci Rep* (2020) 10(1):9785. doi: 10.1038/s41598-020-66660-z
23. Chen D, Zhou H, Liu G, Zhao Y, Cao G, Liu Q. SPOCK1 Promotes the Invasion and Metastasis of Gastric Cancer Through Slug-Induced Epithelial-Mesenchymal Transition. *J Cell Mol Med* (2018) 22(2):797–807. doi: 10.1111/jcmm.13357
24. Thiery JP. Epithelial-Mesenchymal Transitions in Tumour Progression. *Nat Rev Cancer* (2002) 2(6):442–54. doi: 10.1038/nrc822
25. Kotiyal S, Bhattacharya S. Breast Cancer Stem Cells, EMT and Therapeutic Targets. *Biochem Biophys Res Commun* (2014) 453(1):112–6. doi: 10.1016/j.bbrc.2014.09.069
26. Thiery JP, Acloque H, Huang RY, Nieto MA. Epithelial-Mesenchymal Transitions in Development and Disease. *Cell* (2009) 139(5):871–90. doi: 10.1016/j.cell.2009.11.007
27. Lamouille S, Xu J, Derynck R. Molecular Mechanisms of Epithelial-Mesenchymal Transition. *Nat Rev Mol Cell Biol* (2014) 15(3):178–96. doi: 10.1038/nrm3758
28. De Angelis ML, Francescangeli F, Zeuner A. Breast Cancer Stem Cells as Drivers of Tumor Chemoresistance, Dormancy and Relapse: New Challenges and Therapeutic Opportunities. *Cancers (Basel)* (2019) 11(10):1569. doi: 10.3390/cancers11101569
29. De Angelis ML, Francescangeli F, La Torre F, Zeuner A. Stem Cell Plasticity and Dormancy in the Development of Cancer Therapy Resistance. *Front Oncol* (2019) 9:626. doi: 10.3389/fonc.2019.00626
30. Visvader JE, Lindeman GJ. Cancer Stem Cells: Current Status and Evolving Complexities. *Cell Stem Cell* (2012) 10(6):717–28. doi: 10.1016/j.stem.2012.05.007
31. Bouris P, Manou D, Sopaki-Valalaki A, Kolokotroni A, Moustakas A, Kapoor A, et al. Serglycin Promotes Breast Cancer Cell Aggressiveness: Induction of Epithelial to Mesenchymal Transition, Proteolytic Activity and IL-8 Signaling. *Matrix Biol J Int Soc Matrix Biol* (2018) 74:35–51. doi: 10.1016/j.matbio.2018.05.011
32. Korpetinou A, Skandalis SS, Moustakas A, Happonen KE, Tveit H, Prydz K, et al. Serglycin Is Implicated in the Promotion of Aggressive Phenotype of Breast Cancer Cells. *PloS One* (2013) 8(10):e78157. doi: 10.1371/journal.pone.0078157
33. Gordon LA, Mulligan KT, Maxwell-Jones H, Adams M, Walker RA, Jones JL. Breast Cell Invasive Potential Relates to the Myoepithelial Phenotype. *Int J Cancer* (2003) 106(1):8–16. doi: 10.1002/ijc.11172
34. Tan TZ, Miow QH, Miki Y, Noda T, Mori S, Huang RY, et al. Epithelial-Mesenchymal Transition Spectrum Quantification and its Efficacy in Deciphering Survival and Drug Responses of Cancer Patients. *EMBO Mol Med* (2014) 6(10):1279–93. doi: 10.15252/emmm.201404208
35. Li XJ, Ong CK, Cao Y, Xiang YQ, Shao JY, Ooi A, et al. Serglycin is a Theranostic Target in Nasopharyngeal Carcinoma That Promotes Metastasis. *Cancer Res* (2011) 71(8):3162–72. doi: 10.1158/0008-5472.CAN-10-3557
36. Rosenlund IA, Calin GA, Dragomir MP, Knutsen E. CRISPR/Cas9 to Silence Long Non-Coding RNAs. *Methods Mol Biol* (2021) 2348:175–87. doi: 10.1007/978-1-0716-1581-2_12
37. Shinde A, Hardy SD, Kim D, Akhand SS, Jolly MK, Wang WH, et al. Spleen Tyrosine Kinase-Mediated Autophagy Is Required for Epithelial-Mesenchymal Plasticity and Metastasis in Breast Cancer. *Cancer Res* (2019) 79(8):1831–43. doi: 10.1158/0008-5472.CAN-18-2636
38. Watanabe K, Panchy N, Noguchi S, Suzuki H, Hong T. Combinatorial Perturbation Analysis Reveals Divergent Regulations of Mesenchymal Genes During Epithelial-to-Mesenchymal Transition. *NPJ Syst Biol Appl* (2019) 5:21. doi: 10.1038/s41540-019-0097-0
39. Tian B, Li X, Kalita M, Widen SG, Yang J, Bhavnani SK, et al. Analysis of the TGFbeta-Induced Program in Primary Airway Epithelial Cells Shows Essential Role of NF-Kappab/RelA Signaling Network in Type II Epithelial Mesenchymal Transition. *BMC Genomics* (2015) 16:529. doi: 10.1186/s12864-015-1707-x
40. Ghandi M, Huang FW, Jane-Valbuena J, Kryukov GV, Lo CC, McDonald ER3rd, et al. Next-Generation Characterization of the Cancer Cell Line Encyclopedia. *Nature* (2019) 569(7757):503–8. doi: 10.1038/s41586-019-1186-3
41. Anders S, Pyl PT, Huber W. HTSeq–a Python Framework to Work With High-Throughput Sequencing Data. *Bioinformatics* (2015) 31(2):166–9. doi: 10.1093/bioinformatics/btu638
42. Colaprico A, Silva TC, Olsen C, Garofano L, Cava C, Garolini D, et al. TCGAbiolinks: An R/Bioconductor Package for Integrative Analysis of TCGA Data. *Nucleic Acids Res* (2016) 44(8):e71. doi: 10.1093/nar/gkv1507
43. Subramanian A, Tamayo P, Mootha VK, Mukherjee S, Ebert BL, Gillette MA, et al. Gene Set Enrichment Analysis: A Knowledge-Based Approach for Interpreting Genome-Wide Expression Profiles. *Proc Natl Acad Sci USA* (2005) 102(43):15545–50. doi: 10.1073/pnas.0506580102
44. Mootha VK, Lindgren CM, Eriksson KF, Subramanian A, Sihag S, Lehar J, et al. PGC-1alpha-Responsive Genes Involved in Oxidative Phosphorylation are Coordinately Downregulated in Human Diabetes. *Nat Genet* (2003) 34(3):267–73. doi: 10.1038/ng1180
45. Mermel CH, Schumacher SE, Hill B, Meyerson ML, Beroukhim R, Getz G. GISTIC2.0 Facilitates Sensitive and Confident Localization of the Targets of Focal Somatic Copy-Number Alteration in Human Cancers. *Genome Biol* (2011) 12(4):R41. doi: 10.1186/gb-2011-12-4-r41
46. Qian J, Olbrecht S, Boeckx B, Vos H, Laoui D, Etlioglu E, et al. A Pan-Cancer Blueprint of the Heterogeneous Tumor Microenvironment Revealed by Single-Cell Profiling. *Cell Res* (2020) 30(9):745–62. doi: 10.1038/s41422-020-0355-0
47. Moi L, Braaten T, Al-Shibli K, Lund E, Busund LR. Differential Expression of the miR-17-92 Cluster and miR-17 Family in Breast Cancer According to Tumor Type; Results From the Norwegian Women and Cancer (NOWAC) Study. *J Transl Med* (2019) 17(1):334. doi: 10.1186/s12967-019-2086-x
48. Yang SN, Burch ML, Tannock LR, Evanko S, Osman N, Little PJ. Transforming Growth Factor-Beta Regulation of Proteoglycan Synthesis in Vascular Smooth Muscle: Contribution to Lipid Binding and Accelerated Atherosclerosis in Diabetes. *J Diabetes* (2010) 2(4):233–42. doi: 10.1111/j.1753-0407.2010.00089.x
49. Penn JW, Grobbelaar AO, Rolfe KJ. The Role of the TGF-Beta Family in Wound Healing, Burns and Scarring: A Review. *Int J Burns Trauma* (2012) 2(1):18–28.
50. Tauriello DVF, Sancho E, Batlle E. Overcoming TGFbeta-Mediated Immune Evasion in Cancer. *Nat Rev Cancer* (2022) 22(1):25–44. doi: 10.1038/s41568-021-00413-6
51. Ramadoss S, Chen X, Wang CY. Histone Demethylase KDM6B Promotes Epithelial-Mesenchymal Transition. *J Biol Chem* (2012) 287(53):44508–17. doi: 10.1074/jbc.M112.424903
52. Katsuno Y, Meyer DS, Zhang Z, Shokat KM, Akhurst RJ, Miyazono K, et al. Chronic TGF-Beta Exposure Drives Stabilized EMT, Tumor Stemness, and Cancer Drug Resistance With Vulnerability to Bitopic mTOR Inhibition. *Sci Signal* (2019) 12(570):eaau8544. doi: 10.1126/scisignal.aau8544
53. Lykke-Andersen S, Jensen TH. Nonsense-Mediated mRNA Decay: An Intricate Machinery That Shapes Transcriptomes. *Nat Rev Mol Cell Biol* (2015) 16(11):665–77. doi: 10.1038/nrm4063

54. Chod J, Zavadova E, Halaska MJ, Strnad P, Fucikova T, Rob L. Preoperative Transforming Growth Factor-Beta 1 (TGF-Beta 1) Plasma Levels in Operable Breast Cancer Patients. *Eur J Gynaecol Oncol* (2008) 29(6):613–6.
55. Kong FM, Anscher MS, Murase T, Abbott BD, Iglehart JD, Jirtle RL. Elevated Plasma Transforming Growth Factor-Beta 1 Levels in Breast Cancer Patients Decrease After Surgical Removal of the Tumor. *Ann Surg* (1995) 222(2):155–62. doi: 10.1097/00000658-199508000-00007
56. Lv ZD, Kong B, Li JG, Qu HL, Wang XG, Cao WH, et al. Transforming Growth Factor-Beta 1 Enhances the Invasiveness of Breast Cancer Cells by Inducing a Smad2-Dependent Epithelial-to-Mesenchymal Transition. *Oncol Rep* (2013) 29(1):219–25. doi: 10.3892/or.2012.2111
57. Liu Q, Chen G, Moore J, Guix I, Placantonakis D, Barcellos-Hoff MH. Exploiting Canonical TGFbeta Signaling in Cancer Treatment. *Mol Cancer Ther* (2022) 21(1):16–24. doi: 10.1158/1535-7163.MCT-20-0891
58. Imamura T, Hikita A, Inoue Y. The Roles of TGF-Beta Signaling in Carcinogenesis and Breast Cancer Metastasis. *Breast Cancer* (2012) 19 (2):118–24. doi: 10.1007/s12282-011-0321-2
59. Ye X, Brabletz T, Kang Y, Longmore GD, Nieto MA, Stanger BZ, et al. Upholding a Role for EMT in Breast Cancer Metastasis. *Nature* (2017) 547 (7661):E1–3. doi: 10.1038/nature22816
60. Liberzon A, Birger C, Thorvaldsdottir H, Ghandi M, Mesirov JP, Tamayo P. The Molecular Signatures Database (MSigDB) Hallmark Gene Set Collection. *Cell Syst* (2015) 1(6):417–25. doi: 10.1016/j.cels.2015.12.004
61. Bertucci F, Finetti P, Cervera N, Esterni B, Hermitte F, Viens P, et al. How Basal are Triple-Negative Breast Cancers? *Int J Cancer* (2008) 123(1):236–40. doi: 10.1002/ijc.23518
62. Sarrio D, Rodriguez-Pinilla SM, Hardisson D, Cano A, Moreno-Bueno G, Palacios J. Epithelial-Mesenchymal Transition in Breast Cancer Relates to the Basal-Like Phenotype. *Cancer Res* (2008) 68(4):989–97. doi: 10.1158/0008-5472.CAN-07-2017
63. Williams ED, Gao D, Redfern A, Thompson EW. Controversies Around Epithelial-Mesenchymal Plasticity in Cancer Metastasis. *Nat Rev Cancer* (2019) 19(12):716–32. doi: 10.1038/s41568-019-0213-x
64. Zheng X, Dai F, Feng L, Zou H, Feng L, Xu M. Communication Between Epithelial-Mesenchymal Plasticity and Cancer Stem Cells: New Insights Into Cancer Progression. *Front Oncol* (2021) 11:617597. doi: 10.3389/fonc.2021.617597
65. Guo JY, Chiu CH, Wang MJ, Li FA, Chen JY. Proteoglycan Serglycin Promotes Non-Small Cell Lung Cancer Cell Migration Through the Interaction of Its Glycosaminoglycans With CD44. *J BioMed Sci* (2020) 27 (1):2. doi: 10.1186/s12929-019-0600-3
66. Zhang Z, Deng Y, Zheng G, Jia X, Xiong Y, Luo K, et al. SRGN-TGFbeta2 Regulatory Loop Confers Invasion and Metastasis in Triple-Negative Breast Cancer. *Oncogenesis* (2017) 6(7):e360. doi: 10.1038/oncsis.2017.53
67. Cao L, Luo FF, Huang HB, Huang TJ, Hu H, Zheng LS, et al. The Autoregulatory Serglycin/CD44 Axis Drives Stemness-Like Phenotypes in TNBC in a Beta-Catenin-Dependent Manner. *Clin Trans Med* (2021) 11(2): e311. doi: 10.1002/ctm2.311
68. Zhang Z, Qiu N, Yin J, Zhang J, Liu H, Guo W, et al. SRGN Crosstalks With YAP to Maintain Chemoresistance and Stemness in Breast Cancer Cells by Modulating HDAC2 Expression. *Theranostics* (2020) 10(10):4290–307. doi: 10.7150/thno.41008
69. Korpetinou A, Skandalis SS, Labropoulou VT, Smirlaki G, Noulas A, Karamanos NK, et al. Serglycin: At the Crossroad of Inflammation and Malignancy. *Front Oncol* (2014) 3:327. doi: 10.3389/fonc.2013.00327
70. Guo JY, Hsu HS, Tyan SW, Li FY, Shew JY, Lee WH, et al. Serglycin in Tumor Microenvironment Promotes Non-Small Cell Lung Cancer Aggressiveness in a CD44-Dependent Manner. *Oncogene* (2017) 36(17):2457–71. doi: 10.1038/onc.2016.404
71. Chu Q, Huang H, Huang T, Cao L, Peng L, Shi S, et al. Extracellular Serglycin Upregulates the CD44 Receptor in an Autocrine Manner to Maintain Self-Renewal in Nasopharyngeal Carcinoma Cells by Reciprocally Activating the MAPK/beta-Catenin Axis. *Cell Death Dis* (2016) 7(11):e2456. doi: 10.1038/cddis.2016.287
72. Du Q, Yuan Z, Huang X, Huang Y, Zhang J, Li R. miR-26b-5p Suppresses Chemoresistance in Breast Cancer by Targeting Serglycin. *Anticancer Drugs* (2021) 33(3):308–19. doi: 10.1097/CAD.0000000000001268
73. Zhu Y, Lam AKY, Shum DKY, Cui D, Zhang J, Yan DD, et al. Significance of Serglycin and its Binding Partners in Autocrine Promotion of Metastasis in Esophageal Cancer. *Theranostics* (2021) 11(6):2722–41. doi: 10.7150/thno.49547
74. Baram T, Rubinstein-Achiasaf L, Ben-Yaakov H, Ben-Baruch A. Inflammation-Driven Breast Tumor Cell Plasticity: Stemness/EMT, Therapy Resistance and Dormancy. *Front Oncol* (2020) 10:614468. doi: 10.3389/fonc.2020.614468
75. Gialeli C, Theocharis AD, Karamanos NK. Roles of Matrix Metalloproteinases in Cancer Progression and Their Pharmacological Targeting. *FEBS J* (2011) 278(1):16–27. doi: 10.1111/j.1742-4658.2010.07919.x
76. Uhlin-Hansen L, Wik T, Kjellen L, Berg E, Forsdahl F, Kolset SO. Proteoglycan Metabolism in Normal and Inflammatory Human Macrophages. *Blood* (1993) 82(9):2880–9. doi: 10.1182/blood.V82.9.2880.2880
77. Roy A, Attarha S, Weishaupt H, Edqvist PH, Swartling FJ, Bergqvist M, et al. Serglycin as a Potential Biomarker for Glioma: Association of Serglycin Expression, Extent of Mast Cell Recruitment and Glioblastoma Progression. *Oncotarget* (2017) 8(15):24815–27. doi: 10.18632/oncotarget.15820
78. Xie J, Qi X, Wang Y, Yin X, Xu W, Han S, et al. Cancer-Associated Fibroblasts Secrete Hypoxia-Induced Serglycin to Promote Head and Neck Squamous Cell Carcinoma Tumor Cell Growth *In Vitro* and *In Vivo* by Activating the Wnt/beta-Catenin Pathway. *Cell Oncol* (2021) 44(3):661–71. doi: 10.1007/s13402-021-00592-2
79. Pastushenko I, Brisebarre A, Sifrim A, Fioramonti M, Revenco T, Boumahdi S, et al. Identification of the Tumour Transition States Occurring During EMT. *Nature* (2018) 556(7702):463–8. doi: 10.1038/s41586-018-0040-3
80. Doncheva AI, Norheim FA, Hjorth M, Grujic M, Paivandy A, Dankel SN, et al. Serglycin Is Involved in Adipose Tissue Inflammation in Obesity. *J Immunol* (2021) 208(1):121–32. doi: 10.4049/jimmunol.2100231

Conflict of Interest: The authors declare that the research was conducted in the absence of any commercial or financial relationships that could be construed as a potential conflict of interest.

The handling editor declared a past co-authorship with the author ADT.

Publisher's Note: All claims expressed in this article are solely those of the authors and do not necessarily represent those of their affiliated organizations, or those of the publisher, the editors and the reviewers. Any product that may be evaluated in this article, or claim that may be made by its manufacturer, is not guaranteed or endorsed by the publisher.

Copyright © 2022 Tellez-Gabriel, Tekpli, Reine, Hegge, Nielsen, Chen, Moi, Normann, Busund, Calin, Mælandsmo, Perander, Theocharis, Kolset and Knutsen. This is an open-access article distributed under the terms of the Creative Commons Attribution License (CC BY). The use, distribution or reproduction in other forums is permitted, provided the original author(s) and the copyright owner(s) are credited and that the original publication in this journal is cited, in accordance with accepted academic practice. No use, distribution or reproduction is permitted which does not comply with these terms.

frontiers | Frontiers in Oncology

ORIGINAL RESEARCH
published: 27 April 2022
doi: 10.3389/fonc.2022.869417

MCF10CA Breast Cancer Cells Utilize Hyaluronan-Coated EV-Rich Trails for Coordinated Migration

*Niina Aaltonen[1], Heikki Kyykallio[1], Sylvain Tollis[1], Janne Capra[1], Jaana M. Hartikainen[2], Johanna Matilainen[1], Sanna Oikari[1] and Kirsi Rilla[1]**

[1] Institute of Biomedicine, University of Eastern Finland, Kuopio, Finland, [2] Institute of Clinical Medicine, Clinical Pathology and Forensic Medicine, University of Eastern Finland, Kuopio, Finland

Invasion of tumor cells through the stroma is coordinated in response to migratory cues provided by the extracellular environment. One of the most abundant molecules in the tumor microenvironment is hyaluronan, a glycosaminoglycan known to promote many hallmarks of tumor progression, including the migratory potential of tumor cells. Strikingly, hyaluronan is also often found to coat extracellular vesicles (EVs) that originate from plasma membrane tentacles of tumor cells crucial for migration, such as filopodia, and are abundant in tumor niches. Thus, it is possible that hyaluronan and hyaluronan-coated EVs have a cooperative role in promoting migration. In this work, we compared the hyaluronan synthesis, EV secretion and migratory behavior of normal and aggressive breast cell lines from MCF10 series. Single live cell confocal imaging, electron microscopy and correlative light and electron microscopy experiments revealed that migrating tumor cells form EV-rich and hyaluronan -coated trails. These trails promote the pathfinding behavior of follower cells, which is dependent on hyaluronan. Specifically, we demonstrated that plasma membrane protrusions and EVs left behind by tumor cells during migration are strongly positive for CD9. Single cell tracking demonstrated a leader-follower behavior, which was significantly decreased upon removal of pericellular hyaluronan, indicating that hyaluronan promotes the pathfinding behavior of follower cells. Chick chorioallantoic membrane assays *in ovo* suggest that tumor cells behave similarly in 3D conditions. This study strengthens the important role of extracellular matrix production and architecture in coordinated tumor cell movements and validates the role of EVs as important components and regulators of tumor matrix. The results suggest that tumor cells can modify the extracellular niche by forming trails, which they subsequently follow coordinatively. Future studies will clarify in more detail the orchestrated role of hyaluronan, EVs and other extracellular cues in coordinated migration and pathfinding behavior of follower cells.

Keywords: hyaluronan, breast cancer, extracellular vesicle (EV), migration, filopodia

Abbreviations: CAM, chick chorioallantoic membrane assay; CLEM, correlative light and electron microscopy; ECM, extracellular matrix; EV, extracellular vesicle; HAS, hyaluronan synthase; NTA, nanoparticle tracking analysis; SEM, Scanning electron microscopy; TEM, transmission electron microscopy.

OPEN ACCESS

Edited by:
Alberto Passi, University of Insubria, Italy

Reviewed by:
Maurizio Onisto, University of Padua, Italy
Demitrios Vynios, University of Patras, Greece

***Correspondence:**
Kirsi Rilla
kirsi.rilla@uef.fi

Specialty section:
This article was submitted to Molecular and Cellular Oncology, a section of the journal Frontiers in Oncology

Received: *04 February 2022*
Accepted: *28 March 2022*
Published: *27 April 2022*

Citation:
Aaltonen N, Kyykallio H, Tollis S, Capra J, Hartikainen JM, Matilainen J, Oikari S and Rilla K (2022) MCF10CA Breast Cancer Cells Utilize Hyaluronan-Coated EV-Rich Trails for Coordinated Migration. Front. Oncol. 12:869417. doi: 10.3389/fonc.2022.869417

INTRODUCTION

Understanding the mechanisms that drive tumor cell migration is essential in efforts for identifying strategies for effective cancer therapies. All steps within tumor progression; growth, vascularization, intravasation, extravasation, invasion, and metastasis require migration of cells. Tumor cell migration is a complex process which involves reorganization of the intracellular actin cytoskeleton and its modulators (1), components of the cell adhesion machinery (2, 3) and extracellular environment that coordinates cellular motility (4). For effective migration cells both interact with, and often modify their surrounding extracellular matrix (ECM) (5).

Hyaluronan is an abundant molecule of the tumor ECM with a fundamental role in tumor progression and regulation of migration (6). Interestingly, hyaluronan is associated with formation of filopodia (7), which are crucial in tumor cell migration *via* sensing the environment and interactions with the ECM (5). Additionally, hyaluronan induces the secretion of extracellular vesicles (EVs) (8) and accumulates on their surface, forming a thick coating on EVs (9). EVs are plasma membrane-derived particles produced by all cell types into the extracellular space and body fluids, regulating both normal physiology and pathological conditions (10). Tumor derived EVs affect the formation of tumor microenvironments and mediate cellular interactions during cancer progression (11). Lately, the contribution of EVs in tumor cell migration has received increased attention (12). Moreover, hyaluronan-coated EVs are shedding from tips of filopodia (8, 13, 14), calling for a direct testing of the role of hyaluronan and EVs in regulating the migratory capacity and invasive potential of tumor cells.

EVs have been suggested to be related to multiple aspects of cell motility, including directional sensing, cell adhesion, ECM degradation, and leader-follower behavior (12). For example, it has been shown that EV secretion is essential for promoting adhesion formation during tumor cell migration (15), and for coordination of directional cell migration (16). Coordinated cell migration relies on cellular interactions through soluble and contact-mediated signals and chemotactic gradients. During coordinated migration, leader cells facilitate the directed migration of followers, either directly by generating pulling forces *via* intercellular contacts, or indirectly by modifying the composition of the extracellular matrix (17). This kind of coordination between migrating cells is a hallmark of cancer invasion and metastasis, immune responses, angiogenesis, wound healing, and morphogenesis during embryonic development (18). All the data described above suggest an association between EVs, coordinated migration, filopodia and hyaluronan, but so far, no studies have directly demonstrated this connection.

To understand this connection in more detail, we utilized MCF10 cell series as a model of breast cancer cell migratory behavior. MCF10A cell line is a spontaneously immortalized non-malignant breast epithelial cells line that is considered normal, with no invasiveness, and no ability to form tumors in immunodeficient mice (19), while MCF10CA is the most malignant and aggressive cell line from the MCF10 series with high metastatic potential (20). We demonstrated that aggressive breast cancer cells not just produce higher numbers of EVs and more hyaluronan than normal cells, but also form trails that are coated with hyaluronan and EVs originating from cellular protrusions. Our live imaging experiments and tracking analyses in single cell level revealed that tumor cells migrate in more coordinated way than normal cells, which is attenuated when hyaluronan is enzymatically digested. We demonstrated a similar trail formation tendency of tumor cells in 3D cultures and chorioallantoic membrane (CAM) assays. The results of this study introduce a novel mechanism for hyaluronan as a guide for coordinated migration and support the role EVs as facilitators of migration.

MATERIALS AND METHODS

Cell Culture

MCF10 human breast cell lines, MCF10A and MCF10CA, were cultured in DMEM/F12 medium (Gibco, Thermo Fischer Scientific, Waltham, MA, USA) supplemented with 5% horse serum (Invitrogen, Carlsbad, CA, USA), 2 mM glutamine (EuroClone, Pavia, Italy), 100 µg/mL streptomycin sulfate, 100 U/mL penicillin (EuroClone), 0.5 µg/mL epidermal growth factor (EGF, Sigma), 0.5 µg/mL hydrocortisone (Sigma), 0.1 µg/mL cholera toxin (Sigma), and 10 µg/mL insulin (Sigma). Both cell lines were passaged twice a week at the following split ratios (MCF10CA 1:20; MCF10A 1:25) using 0.05% trypsin (w/v) 0.02% EDTA (w/v) (Biochrom AG, Berlin,Germany). For experiments with the EV isolation, serum was purified by centrifugation at 110,000× g for 16 h and sterile-filtered with 0.22 µm syringe filters (Guangzhou Jet Bio-Filtration Co., Ltd., Guangdong, China).

Immunostainings and Vital Stainings

The cells were cultured on 8-well Ibidi chamber slides (Ibidi GmbH, Martinsried, Germany) and fixed with 4% paraformaldehyde in PB for 20 min. The fixed cells were permeabilized for 15 min with 0.1% Triton X-100 with 1% BSA, blocked with 1% BSA for 20 min at room temperature. For detection of actin, cells were incubated for 20 min with Phalloidin-iFluor 594 Reagent (Abcam, Cambridge, UK), washed with PB, and stored at 4°C. For staining of CD44, cells were incubated overnight at 4°C with anti-CD44 antibody (1:100, Novus Biologicals, Abingdon, Oxon). After washing, the cells were incubated for 2 h with Texas red-labeled secondary antibody (l:500; Vector Laboratories Inc., Burlingame, CA, USA). For HA staining, cells were incubated overnight at 4°C with 3 µg/ml of biotinylated HA-binding complex (bHABC). After washing, the cells were incubated for 2 h with Alexa Fluor® 488-streptavidin (1:500, Vector, Burlingame, CA, USA). Nuclei were labeled with 4′,6-diamidino-2-phenylindole (DAPI, 1 µg/mL, Sigma-Aldrich, St. Louis, MO, USA).

For staining of pericellular HA coat of live cells, a fluorescently labeled (Alexa Fluor® 680) HA binding complex (fHABC) was used as described previously (21). Live cell cultures grown on chambered cover glasses were incubated for 2 h at 37°C with 10 µg/ml of fluorescent HABC in culture medium.

CellMask™ Deep Red plasma membrane stain (1.25 μg/ml, Molecular Probes, Eugene, OR, USA) was added to the cultures immediately before imaging to label the plasma membranes. For staining of CD9 in live cultures, a FITC-labeled CD9 antibody (1:200, BioLegend, San Diego, CA, USA) was used, and nuclei were labeled with NucBlue™ (Molecular Probes) or DRAQ5™ (Biostatus Ltd., Leicesterchire, UK) DNA labels.

Confocal Imaging

The fluorescent images were obtained with a Zeiss Axio Observer inverted microscope (40 × NA 1.3 oil objective) equipped with a Zeiss LSM 800 confocal module (Carl Zeiss Microimaging GmbH, Jena, Germany). Image processing, including three-dimensional rendering, was performed using the ZEN software (Carl Zeiss Microimaging GmbH).

Quantitative Real-Time RT-PCR (qRT-PCR)

Total RNA from the cells was isolated using Tri Reagent (Molecular Research Center Inc., Cincinnati, OH, USA). The cDNAs were synthesized using the Verso cDNA kit (Thermo Scientific, San Jose, CA, USA). The quantitative real-time PCR was performed with Fast Start Universal SYBR Green mix (Roche Applied Science, Indianapolis, IN, USA) using the Stratagene Mx3000P real-time PCR system (Agilent Technologies, Santa Clara, CA, USA). The primer sequences were the same as used in (13). Relative mRNA expression levels were compared by using the 2−ΔΔC(T) method, with Ribosomal protein, Large, P0 (RPLP0) as reference gene.

Hyaluronan Assay

Subconfluent cell cultures were used to measure the cellular hyaluronan secretion levels. After change of fresh medium, the cells were cultured for 48 h before the cells were counted and the media harvested for the sandwich-type hyaluronan assay as described previously (21).

Hyaluronan Size Determination

Hyaluronan size determinations were performed using Sephacryl S-1000 (1 × 30 cm) column with 100 mM ammonium bicarbonate as a buffer. The protocol was modified from Tammi et al. (22). The column was calibrated with 2500 kDa, 500 kDa and 150 kDa hyaluronan (Hyalose, Oklahoma City, OK, USA). Cell culture medium samples in volume of 1 ml were injected into column directly (MCF10CA) or after lyophilization and dilution to volume of 1.2 ml by 100 mM ammonium bicarbonate (MCF10A). From each sample, 40 fractions (0.8 ml) were collected. Two consecutive fractions were combined and lyophilized. The dried samples were dissolved into 1% BSA-PBS and analyzed for their hyaluronan content by hyaluronan assay as described above.

EV Isolation and Nanoparticle Tracking Analysis (NTA)

The conditioned culture media from MCF10 cells were filtered with 5 μm syringe filter (Sartorius, Goettingen, Germany) to remove cell debris. Filtered media were centrifuged at 10,000× g for 90 min at 4°C and the supernatants were centrifuged at 110,000 × g for 90 min at 4°C. Pellets from both centrifugation steps were suspended into sterile filtered PBS and combined. The size distribution and number of the EVs in isolates from MCF10 culture media were analyzed with the Nanoparticle Tracking Analyzer (Malvern Instruments Ltd., Malvern, UK) with a NS300 view unit. The following settings were used for data acquisition: camera level 13, acquisition time 30 s, and detection threshold 3. Data analysis was performed with the NTA v3.1 software (NanoSight, Amesbury, UK).

Transmission Electron Microscopy

The EV preparations were layered onto carbon-coated glow-discharged copper grids. Grids were fixed in 2% paraformaldehyde for 10 min and contrasted using 2% neutral uranyl acetate for 10–15 min and embedded in 1.8% methylcellulose (25 Cp)/0.4% uranyl acetate. Imaging was performed with JEOL JEM 2100F transmission electron microscope (Jeol Ltd., Tokyo, Japan) operated at 200 kV.

CAM tumors were prefixed with 2.5% glutaraldehyde in 0.1 M phosphate buffer for 4h at room temperature. After an overnight wash in 0.1 M phosphate buffer, pH 7.4 and 1 h wash in H_2O, the tumors were postfixed in 1% osmium tetraoxide and 2.22% CaCl2 in H2O and stained with 1% uranyl acetate. The tumors were dehydrated and embedded in LX-112 resin (Ladd Research Industries, Burlington, VT) and polymerized at 60°C for 48 h. The 70 nm sections were stained with 1% uranyl acetate and imaged with JEOL JEM-2100F transmission electron microscope (Jeol Ltd., Tokyo, Japan) at 200 kV.

Correlative Light and Electron Microscopy

For correlative light and electron microscopy, cells were seeded on 13 mm cover glasses coated with Poly-D-Lysine (Sigma-Aldrich) and grown overnight. The cells were fixed and stained with CD44 antibody and bHABC probe as described above. After confocal imaging of the fluorescent stainings, cells were processed for scanning electron microscopy. Shortly, the cells were routinely dehydrated in ascending series of ethanol and hexamethyldisilazane, and finally, coated with a thin layer of gold. After processing, cells were re-localized by utilizing gridded glass bottom culture dishes and imaged with a Zeiss Sigma HD| VP (Carl Zeiss Microscopy GmbH, Oberkochen, Germany) scanning electron microscope operated at 3 kV. Adobe® Photoshop was utilized to overlay of the SEM images with confocal images

Proliferation Rate and Tracking and Analysis of Coordinated Migration

MCF10A and MCF10CA cells were seeded on the 96-well plate (2500, 3500 or 4000 cells/well). The following day, growth media was replaced with fresh growth media containing IncuCyte® NucLight®Rapid Red Reagent (Essen BioSciences, Hertfordshire, UK) and *Streptomyces* hyaluronidase (10 TRU/ml) in selected wells. The cells were imaged every 20 min for a total of 24 h using Incucyte® S3 Live-Cell Imaging System (Essen BioSciences Ltd., Hertfordshire, UK) and Incucyte S3 2021C

software (Essen BioSciences, Hertfordshire, UK) was used to count the numbers of cells and the level of confluency.

Image Analysis of Single Cell Migration

For the analysis of collective migration, MCF10A and MCF10CA cells were imaged every 20 min for 8 h, yielding a 25 time-points/frames movie for each field of view (FOV). Several FOVs were imaged for each condition, during each experiment. Cell motion was analyzed within each FOV separately as follows. First, single cell trajectories (**Figure S1A**) were extracted from the movies with the TrackMate plugin in ImageJ and computed the displacement vector of each cell along its trajectory at each time-point (See **Supplemental Material** for details). Second, for each pair of cells i and j the angle $\theta_{i\text{-}j,k}$ made by their displacement vectors was computed at each time-point k: $\theta_{i\text{-}j,k}=0$ means that cells are moving exactly in the same direction at this instant of time, while $\theta_{i\text{-}j,k}=\pi$ means that they are moving in opposite directions. Since each FOV encompassed several hundreds of cells, hundreds of thousands of such displacement angles $\theta_{i\text{-}j,k}$ were obtained for each FOV. Third, the distribution of the displacement angles was computed, as illustrated for two typical FOVs of normal cells (**Figure S1B**, top) and cancer cells (**Figure S1B**, bottom). From this distribution, the correlation index (CI) was computed for each FOV as the ratio between the peak (around $\theta=0$) and the basal (around $\theta=\pi$) occurrence levels (**Supplemental Material** and **Figure S1B**). Therefore, equally distributed displacements (100% uncorrelated motion, flat distribution) yield CI~1, and strongly correlated collective motion corresponds to a majority of colinear displacements $\theta_{i\text{-}j,k}\sim0$ and large CI values. This analysis was performed in Matlab R2019b (the Mathworks) using custom dedicated scripts.

Data Processing and Statistics

As illustrated on **Figure S1B** the CI as defined above was larger for cancer cells compared to normal cells and for untreated cancer cells compared to hyaluronan-degrading enzyme-treated cancer cells in most FOVs, and across all replicate experiments. However, we observed differences in the scaling of the CI across different replicate experiments, which could stem from different cell densities or culture conditions across experiments. Hence, to be able to aggregate data from multiple replicates without artefactually increasing data variance, we normalized the CI of each FOV of each experiment to the median CI across all control FOVs of the same experiment (normal cells for **Figure 5A**, or untreated cancer cells for **Figure 6G**), yielding the normalized CI shown on those Figure panels.

To assess the statistical significances of the differences in median CI across conditions, we performed Wilcoxon rank tests using Matlab's ranksum function. The differences in CI for cancer versus normal cells and treated versus untreated cancer cells were statistically significant with p-values close to 0.01. To further demonstrate that such p-values were unlikely to originate by chance from the variability in our data coupled with a limited number of FOVs, we randomized the CI values for sample and control FOVs and repeated the Wilcoxon ranksum tests for 100 randomization trials. P-values lower than 0.05 were obtained in only 2-3% of the trials, limiting to this extent the odds that our conclusions arise from sample-to-sample variability and limited sampling (limited number of FOVs).

Chick Chorioallantoic Membrane (CAM) Assays

Fertilized white Leghorn chicken eggs were incubated at 37°C under constant humidity, starting at embryo development day 0 (EDD0). Separation of the CAM was induced on EDD4 by piercing the eggshell. On EDD8 cells were collected, suspended in PBS, and Corning® Matrigel® Matrix GFR Phenol Red Free (Thermo Fisher Scientific Inc., Göteborg, Sweden) (1:1), and implanted on the CAM (10^6 cells per egg). On EDD13, the tumors were photographed *in ovo* and excised. Tumor area was measured on photographs from 8-10 eggs per cell line.

Tumors were fixed in 3% paraformaldehyde, embedded in paraffin and cut in 5 µm sections. The sections were deparaffinized and rehydrated with routine protocols (xylene for 2 × 5 min, absolute EtOH for 2 × 2 min, 94% EtOH for 2 × 2 min), and washed with dH2O for 20 s. The deparaffinized sections were subjected to antigen retrieval by incubation in 10 mM citrate buffer, pH 6.0 for 15 min in a pressure cooker at 120°C. To block endogenous peroxidase, the sections were treated for 5 min with 1% H2O2. After washing with 0.1 M Na-phosphate buffer, pH 7.4 (PB), the sections were incubated in 1% bovine serum albumin (BSA) in PB for 30 min to block nonspecific binding. For hyaluronan staining, sections were incubated overnight with biotinylated complex of HA-binding region of bovine articular cartilage aggrecan G1 domain and link protein (bHABC) diluted in 1% BSA. The intensity of HA staining was quantified using the color deconvolution algorithm for DAB in ImageJ and the optical density was calculated with the formula log (max intensity/mean intensity). For staining of mitotic cells, sections were incubated overnight with primary antibody against proliferation marker protein Ki-67 (Dako, Glostrup, Denmark) and after washing, for 1 h with biotinylated antimouse secondary antibody (1:1000, Vector Laboratories). Stainings were visualized with the avidin–biotin peroxidase method (Vectastain Kit, Vector Laboratories) followed by incubation for 5 min in 0.05% diaminobenzidine (Sigma) and 0.03% hydrogen peroxide in PB, yielding a brown reaction product. The nuclei were stained with Mayer's hematoxylin. Stained sections were imaged with Zeiss Axio Imager M2 light microscope (Carl Zeiss Microimaging GmbH, Zeiss, Jena, Germany). Stained sections were scanned by Nanozoomer XR digital slide scanner (Hamamatsu Photonics K.K., Hamamatsu City, Japan) at 20× and evaluated by the automated Oncotopix image analysis software v2018.2 (VisioPharm, Hoersholm, Denmark) provided by the Biobank of Eastern Finland.

For fluorescent stainings, the deparaffinized CAM tumor sections were treated with 50 mM glycine for 20 min at room temperature to quench any autofluorescence. The sections were blocked with 1% bovine serum albumin for 30 min, followed by an overnight incubation at 4°C with the primary antibodies against CD44 (Novus Biologicals). After washing, the sections were incubated for 1 h with the secondary antibodies (1:1000, Texas Red anti-rabbit IgG, Vector and 1:1000, Dylight 488-streptavidin, Vector). Nuclei were labelled with DAPI (1 µg/ml,

Sigma-Aldrich). The sections were mounted in Vectashield (Vector H-1000, Vector) and the samples were imaged with confocal microscope.

Statistical Analyses

Statistical analyses were carried out using the GraphPad Prism version 5.00 for Windows (Graph-Pad Software, San Diego, CA, USA). The significance of differences between groups was tested using Mann–Whitney test or Student's t-test. Differences were considered significant when $p < 0.05$.

RESULTS

MCF10CA Tumor Cells Produce Higher Levels of Hyaluronan and Have Increased HAS3 Expression Levels as Compared to MCF10A Normal Breast Epithelial Cells

To compare the hyaluronan production activity of non-malignant MCF10A breast epithelial cells and malignant MCF10CA cells, hyaluronan secretion levels in the culture media were analyzed by hyaluronan assay and size analysis. MCF10CA cells secreted significantly higher levels of hyaluronan than MCF10A cells (**Figure 1A**), with an increased fraction of high molecular weight hyaluronan (85.5% and 65.9%, was high molecular weight in MCF10CA, and MCF10A, respectively) than normal MCF10A cells (**Figure 1B**). To find out, which of the three isoforms of hyaluronan synthases are mainly responsible for this increase, we analyzed the relative expression levels of HAS isoenzymes in both cell lines by qPCR. Both cell lines expressed all HAS isoenzymes, but the expression level of HAS3 was clearly higher in MCF10CA cells as compared to the levels of MCF10A cells (**Figure 1C**). Localization of pericellular hyaluronan was studied in live cells with fHABC hyaluronan binding probe. MCF10CA cells formed larger hyaluronan coats around them than MCF10A cells (**Figures 1D, E**). Interestingly, hyaluronan seemed to form trails on the substratum between individual MCF10CA cells (arrowheads in **Figure 1E**). We next studied the morphology of fixed, phalloidin-stained cells. We found that the cytoskeletal organization differed between the two cell lines, with denser actin peripheral accumulation and higher number of filopodia in MCF10CA cells compared to MCF10A cells (**Figures 1F, G**), in agreement with previous findings (23). Higher number of both lateral and dorsal filopodia in MCF10CA cells was confirmed by scanning electron microscopy that reveals the cells' surface morphology (**Figures 1H, I**).

Tumor Cells Secrete More EVs Than Normal Cells and Form Trails Rich in Hyaluronan and Hyaluronan-Coated EVs

We next sought to compare the EV production activity of the two MCF10 cell lines. In this purpose, we first isolated EVs from culture media and performed NTA analysis where isolated vesicles were counted and sized. We found that MCF10CA cells produced significantly more EVs (about 2.5-fold, **Figure 2A**), but of similar size (**Figures 2B, C**), than MCF10A

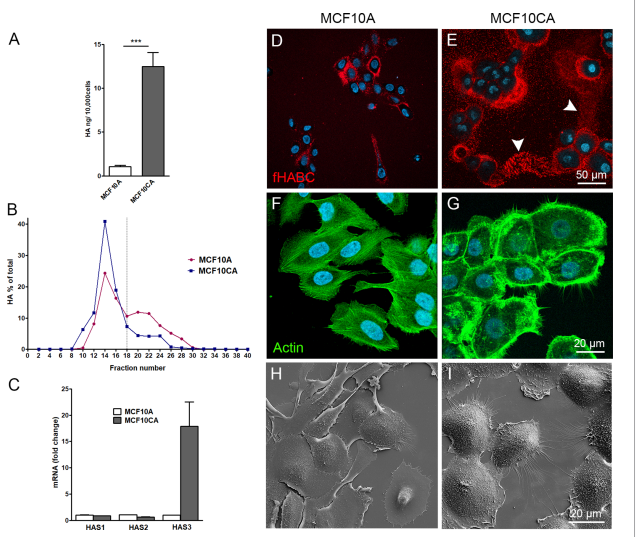

FIGURE 1 | MCF10CA cells synthesize more hyaluronan and express higher levels of HAS3 than MCF10A cells. Hyaluronan secretion levels by MCF10A and MCF10CA cell lines analyzed by hyaluronan assay **(A)** and analysis of relative molecular weight distribution of produced hyaluronan **(B)**. Relative expression levels of HAS isoenzymes **(C)**. Confocal images of live MCF10A **(D)** and MCF10CA **(E)** cells stained with fHABC to detect pericellular hyaluronan (arrowheads in E indicate HA-rich trails) and fixed cell stained with phalloidin to show actin cytoskeleton of MCF10A **(F)** and MCF10CA **(G)**. Scanning electron microscopic images of MCF10A **(H)** and MCF10CA **(I)**. Blue = nuclei in **(D–G)**. The data represent means ± SE of 6 independent experiments in **(A)** ± SE of 3 independent experiments in **(B, C)** ***$p < 0.001$, Mann–Whitney test.

cells. Likewise, both cell lines produced typical cup-shaped EVs with similar morphology as revealed by transmission electron microscopy (arrows in **Figures 2D, E**). Hence, the number - but not the size or shape - of EVs was upregulated in cancer cells.

We next aimed to confirm these findings in live MCF10 cells. In this purpose, MCF10A and MCF10CA subconfluent monolayer cultures were stained *in situ* with the CellMask® plasma membrane marker (that also labeled EVs), FITC-labeled antibody for the EV-marker CD9, and the fHABC probe to detect hyaluronan. In agreement with our fixed cells data (**Figures 1D, E, H, I**), MFC10A cells exhibited substantially less filopodia than MCF10CA (**Figures 3A–D**, **E–H** respectively). EVs seemed to originate from those plasma membrane protrusions (arrows in **Figures 3A, E**). Some EVs were also detected on the bottom of the plate (arrow in **Figure 3A**), in particular in MCF10CA cancer cells where a high number plate-adherent EVs were arranged as trails next to cells with high number of long plasma membrane protrusions (arrows in **Figure 3E**). Double staining with CD9 and fHABC (**Figures 3B, C, F, G**) showed that the filopodia and EVs were strongly positive for CD9, and that the trails generated by MCF10CA cells were hyaluronan-rich and localized in the same areas than CD9-positive protrusions and EVs (**Figures 3F, G**). These structures were all less pronounced in MCF10A cells, with some filopodia, EVs and a weak hyaluronan

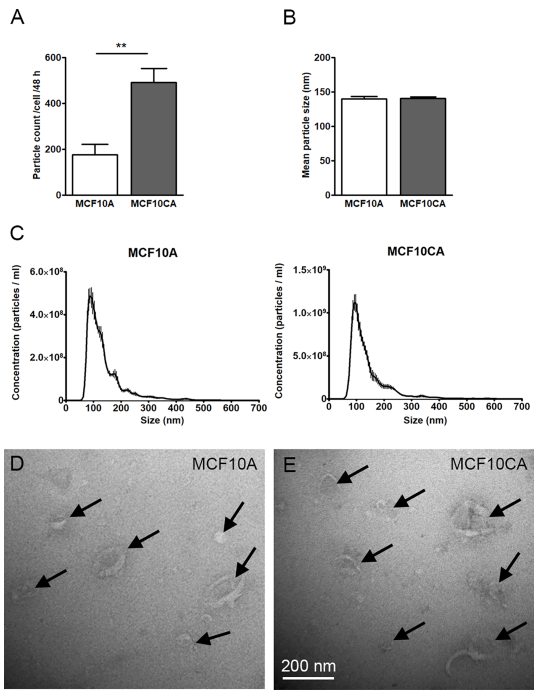

FIGURE 2 | MCF10CA cell produce more EVs than MCF10A cells. Particle counts **(A)**, mean particle sizes **(B)** and size distributions **(C)** of EV isolates from MCF10 cell lines analyzed by NTA. TEM images from the same isolates are shown in **(D, E)**. The data represent means ± SE of 5-6 independent experiments in **(A, B)** and means ± SE of 5-6 independent experiments in **(C)** **p < 0.01, Mann–Whitney test. Arrows point EVs in panels **(D, E)**.

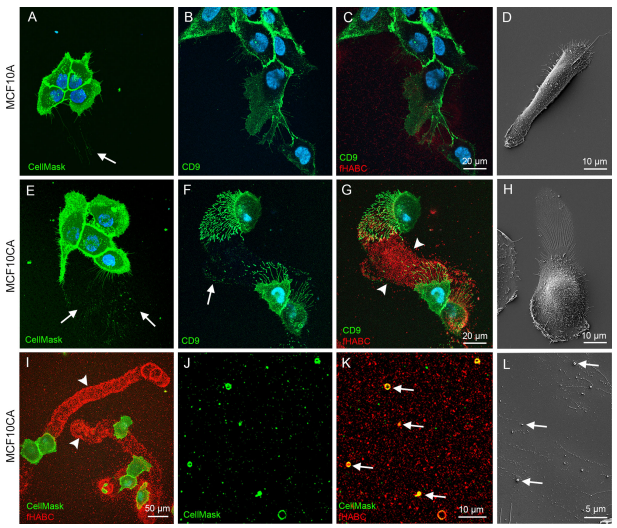

FIGURE 3 | MCF10CA cells form hyaluronan-rich trails that contain plasma membrane-derived vesicles. Live MCF10 cells stained with CellMask® to label lipid membranes **(A, E)** and FITC-conjugated antibody against EV marker CD9 **(B, F)** co-stained with fHABC to visualize hyaluronan **(C, G)**. A lower-magnification image **(G)** of double-staining with CellMask and fHABC shows the trails of up to several hundreds of micrometers long coated with hyaluronan. Scanning electron microscopic images of MCF10A **(D)** and MCF10CA **(H)**. Panel **(I)** shows a lower magnification overview of trails of MCF10CA cells. A higher-magnification images of the trail-areas show HA-coated (red) EVs (green) of different diameter **(J, K)**. A higher magnification scanning electron microscopic image from the trail area **(L)**. Arrows in all panels point membrane-derived vesicles and arrowheads show hyaluronan-rich trails.

staining (**Figures 3B, C**). Scanning electron microscopy corroborated fluorescence imaging findings, showing a lower number of protrusions and EVs in MCF10A cell cultures (**Figure 3D**), as compared to MCF10CA cells with clear trails of filopodia and EVs (**Figure 3H**). A lower magnification overview of MCF10CA cells labeled with CellMask (pseudo colored green) and fHABC (red) revealed the huge length of hyaluronan-rich trails, reaching up to several hundreds of micrometers (**Figure 3I**). A higher magnification image from trail area of the same live MCF10CA cell culture shows EVs of variable size (**Figure 3J**), most of which carried hyaluronan (arrows in **Figure 3K**). In addition to EV-associated hyaluronan, also "free" hyaluronan was detected in trail areas (**Figure 3K**). A higher magnification scanning electron microscopic image from the trail area revealed single EVs of variable size (arrows in **Figure 3L**). Hence, tumor cells generate hyaluronan-, EV- and hyaluronan-coated EV-rich trails on their neighbor substrate.

Next, we aimed to visualize the ultrastructure of hyaluronan-rich trails formed by MCF10CA cells in more detail with correlative light and electron microscopy (CLEM). The fluorescence staining with CD44 antibody and bHABC probe to detect hyaluronan indicated that fixation decreased the number and length of filopodia as compared to live cells (**Figure 3**), as previously shown (23). Intensity of hyaluronan staining on trails was also diminished in fixed cells, but clearly visible trails with hyaluronan positivity were detected (**Figures 4A, C, E, G**). Correlation of the SEM and fluorescence images and higher resolution imaging from selected areas (white boxes in 4A, C, E, and G) indicated that the hyaluronan-rich trails contained EVs and also other ECM material that was adhered to the bottom of the plate and left as "slime trails" behind migrating cells, (**Figures 4B, D, F, H**).

Tumor Cells Migrate in a More Coordinated Way Than Normal Cells

We next interrogated the functional relationship between cancer-associated hyaluronan/EV-rich trails and the ability of cancer cells to coordinate their motion. To quantify coordinated cellular motion, we imaged MCF10A and MCF10CA cells overtime in an Incucyte Live-Cell Imaging System. For each field of view (FOV), we computed single-cell trajectories and defined a FOV-based correlation index (CI), that measures the degree of collinearity between the displacement directions of all pairs of cells across the FOV and all time-points (*Methods*). The CI defined a FOV-based global metric of collective cell motion. The median CI was 48% larger for FOVs showing cancer cells than for FOVs showing normal cells (**Figure 5A**, Wilcoxon rank-test p-value p=0.0151, N=11 FOVs per cell type). This increase in

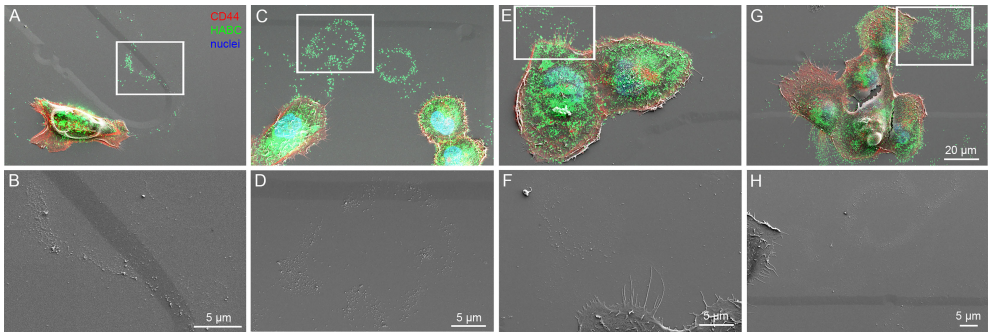

FIGURE 4 | Visualization of HA-positive trails with correlative light and electron microscopy (CLEM). Single cells or groups of cells are presented as overlay images of confocal 3D projections from CD44 and fHABC stainings and scanning electron microscopy **(A, C, E, G)** and high magnification SEM images from the selected areas indicated by white boxes are shown in **(B, D, F, H)**.

correlated motion index was not due to the limited number of FOVs (*Methods*). Therefore, collective cell motion is more coordinated in cancer cells than in normal cells (**Figure 5A**).

Then we sought to investigate correlations between coordinated motion and hyaluronan trails. We utilized time lapse live cell imaging combined with fHABC staining to monitor simultaneously single cell motion and the appearance of trails (selected time points: **Figure 5B**; full movies: **Supplementary Movies 1** and **2**). On the left panels of **Figure 5B**, a group of 4 cells that have produced a hyaluronan rich coating around them. Asterisk indicates a hyaluronan-rich area, which the migrating cell follows and reaches the area at 100 min time point. On the right, one leader cell is followed by a follower cell along the leader's trajectory. These analyses strongly suggest that the follower cell tracks the hyaluronan-coated trail that the leader cell leaves behind.

Hyaluronidase Digestion Decreases the Coordinated Migration Behavior of Tumor Cells

To test this hypothesis, we sought to investigate how the leader-followed behavior of MCF10CA cells is dependent on hyaluronan. In this purpose, we degraded the extracellular hyaluronan with the *Streptomyces* hyaluronidase, and compared MCF10CA motion coordination in presence and absence (control) of hyaluronan-digesting enzyme treatment of the extracellular medium. After 4 h digestion, most of the hyaluronan that in control untreated cells was abundant around CD9-positive plasma membrane protrusions and trails (**Figure 6B**) had disappeared (**Figure 6E**). Also, the plasma membrane protrusions and EVs decreased in hyaluronidase-treated cells (**Figure 6D**) as compared to control cells (**Figure 6A**). However, as previously shown (24), many of the lateral filopodia supported by the substratum were not dependent on hyaluronan coating (**Figures 6C, F**). Hence, hyaluronidase treatment effectively disrupted hyaluronan accumulation in cell trails.

Then, we repeated our time-lapse imaging experiments of moving cancer cells and quantification of the motion correlation in the presence of hyaluronidase-treatment to assess whether the coordinated motion of MCF10CA cells was dependent upon the presence of hyaluronan in trails. HYAL-treatment decreased the median CI by 28% (**Figure 6G**, Wilcoxon rank-text p-value p=0.0068, N=25 and 20 FOVs for untreated and treated cells respectively). Hence, extracellular hyaluronan promotes the coordination of cell motion in cancer cells.

Cancer Cells Create Hyaluronan/EV-Rich Trails and Long Protrusions Also *In Ovo*

To mimic *in vivo* conditions, we cultured the MCF10 cells in chick chorioallantoic membrane (CAM) assays. Transplantation of both MCF10CA and MCF10A cells onto the CAM membrane of fertilized eggs resulted in tumor formation. The MCF10A cells formed small islands while MCF10CA tumors were formed by clearly bigger islands and chords (**Figure 7A**). As expected, MCF10CA cells showed a significantly higher proliferative index (**Figure 7B**) and formed significantly bigger tumors as compared to those of MCF10A cells (**Figure 7C**). Especially tumor cell-associated hyaluronan was high in MCF10CA tumors but was also increased in the stromal areas of the tumors formed by MCF10CA cells, while MCF10A cells had a less intense staining (**Figure 7A**). The hyaluronan staining of tumor sections was analyzed, and there was a significant increase in the optical density of staining in MCF10CA tumors as compared to MCF10A tumors (**Figure 7D**), which is in line with the results of the monolayer cell cultures.

CAM MCF10CA tumor paraffin sections were double stained with CD44 antibody and HABC for a more detailed analysis by confocal microscopy. Again, hyaluronan staining was very intense around and between tumor cells (**Figures 8A, B**), and hyaluronan-rich trails were detected in the stromal areas (arrowheads in **Figures 8A, B**), resembling the trails seen in monolayer cultures. Additionally, higher magnification revealed hyaluronan-positive particles (arrows in **Figure 8B**), which suggests the presence of hyaluronan-coated EVs. Because detection of thin plasma membrane protrusions and EVs in paraffin sections is challenging, transmission electron microscopy was utilized for more detailed morphological analysis of the cultures. Electron microscopy revealed EVs of

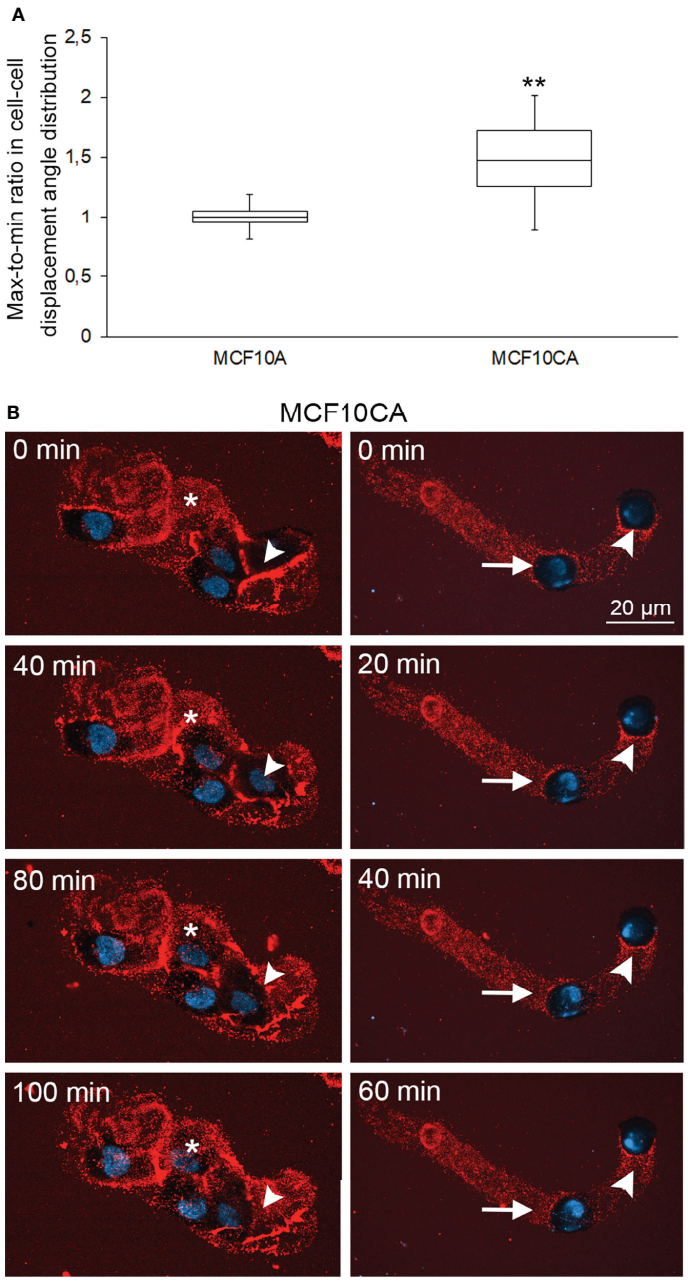

FIGURE 5 | Collective cell motion is more coordinated in cancer cells than in normal cells. Whisker and box plot showing the distribution of correlation index (CI) for MCF10A (left) and MCF10CA (right) cells **(A)**. Plots were constructed using data from 11 FOVs from 2 experiments for each cell type, totalizing several hundreds of cells. The CI of each FOV was normalized to the median CI of normal cells for the same experiment. **: Wilcoxon rank-text p-value p=0.0151. Two examples of collective migration of live MCF10CA cells along trails are shown in **(B)**. Asterisks (*) indicate the hyaluronan-rich area that the migrating cell follows, and arrowheads show the trail that a moving cell leaves behind (left panel in B and **Supplementary Movie 2**). The right panel in B and **Supplementary Movie 2** show an example of leader-follower behavior, where the original position (0 min) of the leader cell is indicated by an arrowhead and the follower cell by an arrow. Red = hyaluronan and blue = nuclei.

variable size and morphology in the extracellular matrix (arrows in **Figures 8C–F**) and the very long plasma membrane protrusions (arrowheads in **Figures 8D, E**) that follow the orientation of bundles of collagen fibers (asterisks in **Figures 8D, E**). EVs were especially abundant in the proximity of plasma membrane protrusions pointing towards the stroma (**Figure 8F**). This data suggest that cancer cells also create hyaluronan/EV-rich trails to coordinate motion in 3D environments.

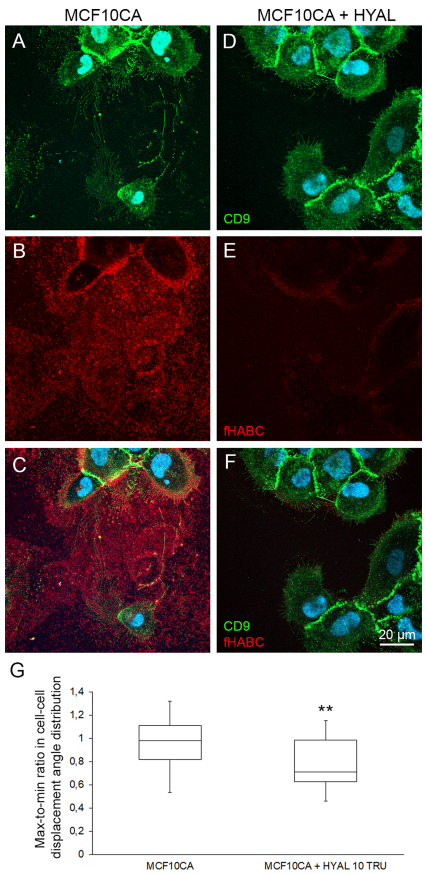

FIGURE 6 | Pericellular hyaluronan promotes the coordination of cell motion in cancer cells. Comparison of live MCF10CA control cells **(A–C)** and hyaluronidase-digested cells **(D–F)** stained with FITC-labeled CD9 and fHABC. Blue = nuclei. Whisker and box plot showing the distribution of correlation index (CI) for untreated (left) and hyaluronan-degrading enzyme-treated (right) cancer cells **(G)**. Plots were constructed using data from 25 and 20 FOVs from 4 experiments for each condition respectively, totalizing several hundreds of cells. The CI for each FOV was normalized to the median CI of untreated cells for the same experiment. **: Wilcoxon rank-text p-value p=0.0068.

DISCUSSION

The Leader-Follower Behavior of Cancer Cells Is Guided by Trails Left Behind by Leader Cells

In this study, we have discovered that aggressive MCF10CA breast cancer cells were forming trails coated with hyaluronan and EVs, and showed that "follower" cells stepped in those trails for coordinated, directional cell migration. The hyaluronan-coated trails discovered in this work resemble the EV containing "slime trails" introduced by Sung et al. (16), that are left behind migrating leader cells and promote the pathfinding behavior of follower cells in a paracrine manner (15). EVs contain multiple motility-promoting cargoes which might facilitate migration (15), although resolving how the effect of EVs is mediated would require more detailed investigation. It may be possible that the migrating cells internalize the EVs while they migrate over EV trails and use their motility-promoting cargoes to enhance their migratory capacity.

Cell-cell contacts and adhesion to the substratum or extracellular matrix are thought to be crucial for cell migration. This is particularly important during collective cell migration to maintain cells in contact with their neighbors while moving directionally (25, 26). Here we demonstrated a coordinated migration without direct cell-cell contacts, where single cells migrate in a coordinated way by following the ECM cues left by leader cells. Cellular adhesion to the ECM becomes particularly important for this kind of solitary migrating cells, including immune cells or metastatic tumor cells escaping the local tumor tissue.

Plasma membrane protrusions, especially filopodia are involved in substrate tethering and environment sensing of invasive tumor cells, and it is well known that migrating cancer cells assemble filopodia also in 3D environment (5). EVs are released from retraction fibers of migrating cells, as demonstrated using the pHluorin-CD63 EV marker (27). In agreement, we observed in this work very long filopodia or retraction fibers especially at the rear end of migrating breast cancer cells. From those filopodia, EVs were shedding as revealed by the CD9 marker, in line with the previous findings of filopodia as sources for EV shedding (28).

Role of Hyaluronan in Coordinated Migration

The extracellular cues play a crucial role in paracrine interactions between the tumor cells and the ECM, either disabling or enabling tumor progression (4). These involve both mechanical and chemical migratory cues that regulate cell migratory behavior (25, 29). Hyaluronan expression in cancer is a predictor of poor prognosis (30), and its role in many processes related to cancer progression, including migration is well known (6). Hyaluronan secreted by leader cells can therefore provide in principle migratory cues to the follower cells.

Our results showed that breast tumor cells produced higher amounts of hyaluronan with higher average molecular weight than their normal counterparts, and that hyaluronan was positively affecting coordinated migration. In fibroblasts, it was shown that short hyaluronan chains stimulate migration (31), while in contrast high molecular weight hyaluronan in the ECM reduces migration of glioblastoma stem cells (32) and MDA-MB-231 breast cancer cells (33). Hence, it is possible that the effect of hyaluronan on migration is cell type/tissue-dependent. High expression levels of adhesion receptor CD44, which binds hyaluronan with high affinity, has been observed and shown to promote collective invasion in breast cancer (34, 35). This result could provide a mechanistic basis to explain the role of hyaluronan in coordinated migration. Interestingly, CD44- and integrin αVβ5-positive EVs released from retracting filopodia of trabecular meshwork cells were arranged in 'trails' (36). In addition to hyaluronan (37), tumor cells produce high amounts of mucins (38) on their cell surface, which creates a

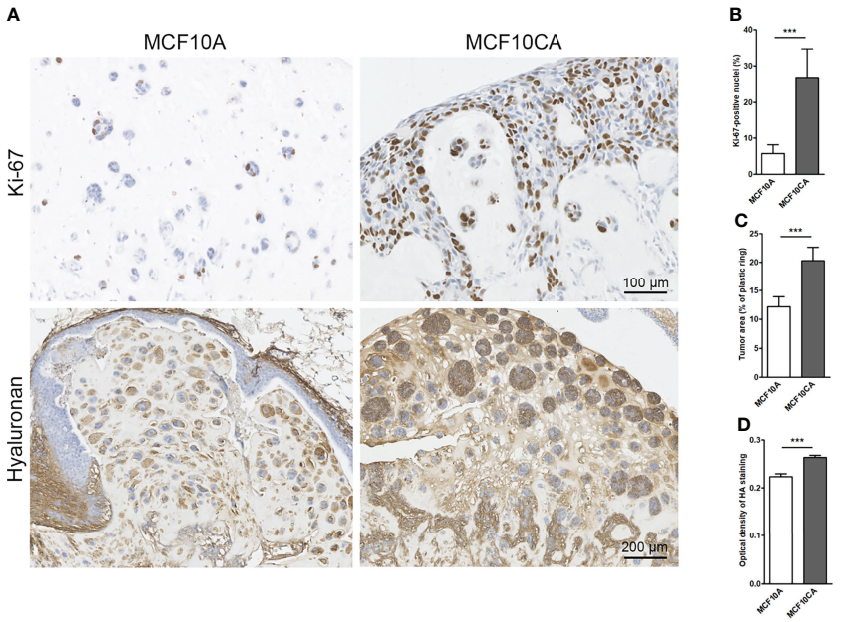

FIGURE 7 | MCF10CA cells have a higher proliferation index, and they form bigger tumors with higher hyaluronan content than MCF10A cells in CAM model. Representative images of Ki-67-stainings (brown) and hyaluronan stainings (brown) of MCF10A and MCF10CA tumor sections **(A)** The proportion of Ki-67-positive nuclei in both tumor groups is shown in **(B)**, the average tumor area is shown in **(C)** and optical density of HA staining visualized with DAB in **(D)**; n = 8 in MCF10A and n = 10 in MCF10CA groups. **p < 0.001.

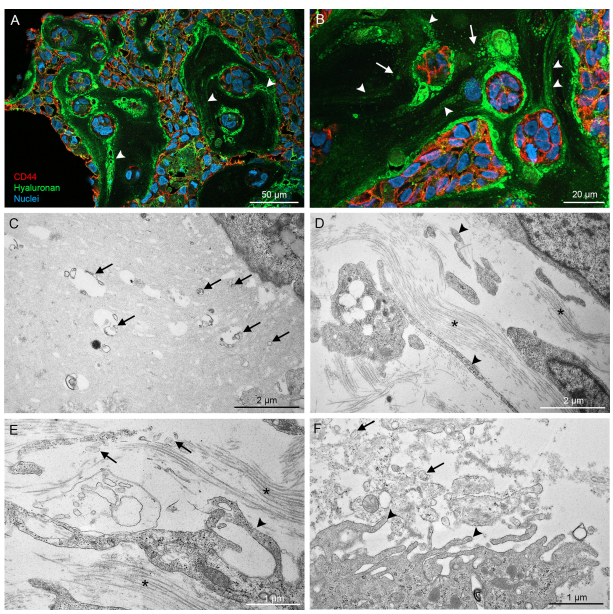

FIGURE 8 | High resolution imaging of CAM tumor sections shows that hyaluronan-rich trails are formed in tumors *in ovo*. Confocal 3D projections from CAM tumor paraffin sections **(A, B)** derived from MCF10CA cells show high amount of hyaluronan between and around tumor cells and hyaluronan-rich trails (arrowheads in **A, B**). TEM images **(C–F)** show the numerous EVs of variable size and shape in the stromal areas (arrows in **C–F**). Asterisks (*) in **(D, E)** indicate collagen bundles.

niche promoting tumor growth and survival. Our study does not exclude that other ECM proteins, possibly *via* interactions with cellular adhesion molecules including integrins, may play a role in facilitating the migration along these trails.

EVs as Facilitators of Migration

Interestingly, hyaluronan synthesis is associated with enhanced EV shedding, which has been shown either by overexpressing hyaluronan synthases (8, 39, 40) or by removal of the glycocalyx by hyaluronidase digestion (41). Specific glycocalyx compositions such as mucin biopolymers and long-chain polysaccharides are secreted by tumor cells and drive formation of protrusions and secretion of EVs (41). We showed here that when cultured in identical conditions, aggressive MCF10CA cancer cells produce more EVs than their corresponding, close to normal breast epithelial cells. Although there is evidence that tumor cells produce more actively EVs compared with their nonmalignant counterparts (42, 43) some reports show no differences on the levels of plasma EVs between cancer patients and healthy people (44). The complexity of plasma samples with EVs from many cell types, as well as methodological pitfalls, may interfere with analysis of this data and obfuscate the differences between cancer and healthy patients. In addition, the secretion of EVs in cancer cells migration could also be cell type/tissue-dependent.

Many recent findings suggest that tumor EVs can prime premetastatic niches (45). Furthermore, EV secretion rate is enhanced in migrating cells as compared to non-moving cells and directional cell migration is dependent on EV secretion (16). There is recent evidence on EV shedding from retraction fibers as "footprints" (13), or "adhesive exosome trails" (27).

Directional Tumor Cell Movements in 3D Environment

Fibroblasts are major producers of the ECM and often drive the collective migration of tumor cells through direct intercellular contact (46) and by protease- and force-mediated matrix remodeling (47). Typically, carcinoma cells move within tracks in the ECM behind the leading fibroblast (47). However, the results of this study support the findings (4) that in addition to cancer associated fibroblasts, cancer cells themselves may also produce and modify ECM to guide their own collective migration.

Mechanical properties of the tumor niche regulate tumor cell migration (32). ECM modeling and alignment are strongly correlated with promotion of cancer invasion, and cell invasion is oriented along collagen fibers, suggesting that alignment of collagen fibers relative to tumors regulates invasion (48). It has been reported that hyaluronan can alter the orientation of collagen network (32). Recent data suggest that increased hyaluronan concentration swells the size of collagen network pores, which are filled with hyaluronan molecules (33). This may be due to the high water binding capacity of hyaluronan, which increases the hydrostatic pressure to create space between collagen fibers. The ability of tumor cells to acquire a distinct "leader" cell phenotype may be triggered by these hyaluronan-rich "voids" formed between dense collagen networks. According to the data of our study, filopodia seemed to follow the orientation of collagen fibers. This suggests that hyaluronan, cellular protrusions and EVs *via* their molecular interactions such as MMP activity may create spaces between collagen fibers to facilitate or attract follower cell invasion. Interestingly, in a recent work, increased pressure of the ECM was shown to drive coordinated cellular motion, by a rapid burst-like streams of cervical cancer cells emerging in matrices with low collagen concentration (49). It is thus possible that also hyaluronan has a role in the regulation of pressure by creating areas of lower collagen concentrations to facilitate bursts of cancer cell invasion.

Final Conclusions

This study showed that aggressive breast cancer cells migrate in a more coordinated way than normal cells. During migration, they leave trails containing EVs secreted from plasma membrane protrusions and hyaluronan, which guide the migration of follower cells. These trails tended to follow the direction of collagen fibers in 3D conditions. This study introduces a novel mechanism for hyaluronan as a guide for coordinated migration and supports the role EVs as facilitators of migration.

DATA AVAILABILITY STATEMENT

The raw data supporting the conclusions of this article will be made available by the authors, without undue reservation.

AUTHOR CONTRIBUTIONS

NA, SO, and KR contributed to conception and design of the study. NA, HK, ST, JC, JH, JM, SO, and KR performed the imaging, laboratory analyses and analysis of the results. NA, HK, ST, and SO performed the statistical analysis. KR wrote the first draft of the manuscript. NA, HK, and ST wrote sections of the manuscript. All authors contributed to manuscript revision, read, and approved the submitted version.

FUNDING

This research was financially supported by Academy of Finland GeneCellNano Flagship (grant 337120), Jane and Aatos Erkko Foundation, Juselius Foundation and Mizutani Foundation.

ACKNOWLEDGMENTS

Taija Hukkanen, Eija Rahunen, Virpi Miettinen, Aija Kekkonen and Helena Keniläinen are acknowledged for their expert technical assistance. We are thankful for the opportunity to use the facilities of the SIB Labs and UEF Cell and Tissue Imaging Unit, Biocenter Kuopio and Biocenter Finland.

SUPPLEMENTARY MATERIAL

The Supplementary Material for this article can be found online at: https://www.frontiersin.org/articles/10.3389/fonc.2022.869417/full#supplementary-material

Supplementary Figure 1 | Schematics of the correlation index definition. **(A)** Exemplary FOV showing normal cell trajectories as output by TrackMate, at times Tk (top) and Tk+1 (bottom). Two exemplary cells labeled Ci and Cj are shown for illustrative purposes. The displacement vectors Di,k and Dj,k of the cells Ci and Cj respectively are shown as arrows on the bottom panel, together with the displacement angle θi-j,k made by the directions of these two displacements. Similar displacement angles were obtained for all pairs of cells and all time-points to obtain the distributions shown in **(B)**. **(B)** exemplary distributions of displacement angles for two FOVs representing normal cells (top) and cancer cells (bottom). The ranges of displacement values used to compute the peak occurrence (PO) and basal occurrence (BO), as well as the formula for the CI are indicated in red.

Supplementary Movie 1 | An example video of trajectories of MCF10A cell cultures. The video was recorded for 12 h.

Supplementary Movie 2 | An example video of trajectories of MCF10CA cell cultures. The video was recorded for 12 h.

Supplementary Movie 3 | Time lapse movie of MCF10CA cells labeled with fHABC and NucBlue™. shows the coordinated movements of follower and leader cells along the hyaluronan-coated trails. Movie shows fHABC and NucBlue™ signals in MCF10CA cell culture during 100 min. The frames were collected in every 60 s and the movie plays at 7 frames/s.

Supplementary Movie 4 | A time-lapse movie shows the coordinated movements of follower and leader cells along the hyaluronan-coated trails. Movie shows fHABC and NucBlue™ signals in MCF10CA cell culture during 60 min. The frames were collected in every 60 s, the movie plays at 7 frames/s and the total time is 60 minutes. The focus drift was adjusted a couple of times during the imaging.

REFERENCES

1. Yamaguchi H, Wyckoff J, Condeelis J. Cell Migration in Tumors. *Curr Opin Cell Biol* (2005) 17:559–64. doi: 10.1016/J.CEB.2005.08.002
2. Sahai E, Garcia-Medina R, Pouysségur J, Vial E. Smurf1 Regulates Tumor Cell Plasticity and Motility Through Degradation of RhoA Leading to Localized Inhibition of Contractility. *J Cell Biol* (2007) 176:35–42. doi: 10.1083/JCB.200605135
3. Sieg DJ, Hauck CR, Ilic D, Klingbeil CK, Schaefer E, Damsky CH, et al. FAK Integrates Growth-Factor and Integrin Signals to Promote Cell Migration. *Nat Cell Biol* (2000) 2:249–56. doi: 10.1038/35010517
4. Eble JA, Niland S. The Extracellular Matrix in Tumor Progression and Metastasis. *Clin Exp Metastasis* (2019) 36:171–98. doi: 10.1007/S10585-019-09966-1
5. Jacquemet G, Hamidi H, Ivaska J. Filopodia in Cell Adhesion, 3D Migration and Cancer Cell Invasion. *Curr Opin Cell Biol* (2015) 36:23–31. doi: 10.1016/j.ceb.2015.06.007
6. Caon I, Bartolini B, Parnigoni A, Caravà E, Moretto P, Viola M, et al. Revisiting the Hallmarks of Cancer: The Role of Hyaluronan. *Semin Cancer Biol* (2020) 62:9–19. doi: 10.1016/J.SEMCANCER.2019.07.007
7. Kultti A, Rilla K, Tiihonen R, Spicer AP, Tammi RH, Tammi MI. Hyaluronan Synthesis Induces Microvillus-Like Cell Surface Protrusions. *J Biol Chem* (2006) 281:15821–8. doi: 10.1074/jbc.M512840200
8. Rilla K, Pasonen-Seppänen S, Deen AJ, Koistinen VVT, Wojciechowski S, Oikari S, et al. Hyaluronan Production Enhances Shedding of Plasma Membrane-Derived Microvesicles. *Exp Cell Res* (2013) 319:2006–18. doi: 10.1016/j.yexcr.2013.05.021
9. Rilla K, Siiskonen H, Tammi M, Tammi R. Hyaluronan-Coated Extracellular Vesicles- A Novel Link Between Hyaluronan and Cancer. *Adv Cancer Res* (2014) 123:121–48. doi: 10.1016/B978-0-12-800092-2.00005-8
10. Yates AG, Pink RC, Erdbrügger U, Siljander PR, Dellar ER, Pantazi P, et al. In Sickness and in Health: The Functional Role of Extracellular Vesicles in Physiology and Pathology *In Vivo*. *J Extracellular Vesicles* (2022) 11(1): e12151. doi: 10.1002/JEV2.12190
11. Eguchi T, Sheta M, Fujii M, Calderwood SK. Cancer Extracellular Vesicles, Tumoroid Models, and Tumor Microenvironment. *Semin Cancer Biol* (2022) S1044-579X(22)00003-7. doi: 10.1016/J.SEMCANCER.2022.01.003
12. Sung BH, Parent CA, Weaver AM. Extracellular Vesicles: Critical Players During Cell Migration. *Dev Cell* (2021) 56:1861–74. doi: 10.1016/J.DEVCEL.2021.03.020
13. Arasu UT, Kärnä R, Härkönen K, Oikari S, Koistinen A, Kröger H, et al. Human Mesenchymal Stem Cells Secrete Hyaluronan-Coated Extracellular Vesicles. *Matrix Biol* (2017) 64:54–68. doi: 10.1016/j.matbio.2017.05.001
14. Franchi M, Piperigkou Z, Karamanos KA, Franchi L, Masola V. Extracellular Matrix-Mediated Breast Cancer Cells Morphological Alterations, Invasiveness, and Microvesicles/Exosomes Release. *Cells* (2020) 9(9):2031. doi: 10.3390/cells9092031
15. Sung BH, Weaver AM. Exosome Secretion Promotes Chemotaxis of Cancer Cells. *Cell Adh Migr* (2017) 11:187–95. doi: 10.1080/19336918.2016.1273307
16. Sung BH, Ketova T, Hoshino D, Zijlstra A, Weaver AM. Directional Cell Movement Through Tissues Is Controlled by Exosome Secretion. *Nat Commun* (2015) 6:7164. doi: 10.1038/ncomms8164
17. Mayor R, Etienne-Manneville S. The Front and Rear of Collective Cell Migration. *Nat Rev Mol Cell Biol* (2016) 17:97–109. doi: 10.1038/NRM.2015.14
18. Grada A, Otero-Vinas M, Prieto-Castrillo F, Obagi Z, Falanga V. Research Techniques Made Simple: Analysis of Collective Cell Migration Using the Wound Healing Assay. *J Invest Dermatol* (2017) 137:e11–6. doi: 10.1016/j.jid.2016.11.020
19. Dawson PJ, Wolman SR, Tait L, Heppner GH, Miller FR. MCF10AT: A Model for the Evolution of Cancer From Proliferative Breast Disease. *Am J Pathol* (1996) 148:313–9.
20. Santner SJ, Dawson PJ, Tait L, Soule HD, Eliason J, Mohamed AN, et al. Malignant MCF10CA1 Cell Lines Derived From Premalignant Human Breast Epithelial MCF10AT Cells. *Breast Cancer Res Treat* (2001) 65:101–10. doi: 10.1023/A:1006461422273
21. Rilla K, Tiihonen R, Kultti A, Tammi M, Tammi R. Pericellular Hyaluronan Coat Visualized in Live Cells With a Fluorescent Probe Is Scaffolded by Plasma Membrane Protrusions. *J Histochem Cytochem* (2008) 56:901–10. doi: 10.1369/jhc.2008.951665
22. Tammi RH, Tammi MI, Hascall VC, Hogg M, Pasonen S, MacCallum DK. A Preformed Basal Lamina Alters the Metabolism and Distribution of Hyaluronan in Epidermal Keratinocyte "Organotypic" Cultures Grown on Collagen Matrices. *Histochem Cell Biol* (2000) 113:265–77. doi: 10.1007/S004180000128
23. Kyykallio H, Oikari S, Bueno Álvez M, Gallardo Dodd CJ, Capra J, Rilla K. The Density and Length of Filopodia Associate With the Activity of Hyaluronan Synthesis in Tumor Cells. *Cancers* (2020) 12:1–14. doi: 10.3390/cancers12071908
24. Koistinen V, Kärnä R, Koistinen A, rjonen A, Tammi M, Rilla K. Cell Protrusions Induced by Hyaluronan Synthase 3 (HAS3) Resemble Mesothelial Microvilli and Share Cytoskeletal Features of Filopodia. *Exp Cell Res* (2015) 337:179–91. doi: 10.1016/j.yexcr.2015.06.016
25. Vicente-Manzanares M, Aguilar-Cuenca R, Llorente-Gonzalez C, Vicente C. Microfilament-Coordinated Adhesion Dynamics Drives Single Cell Migration and Shapes Whole Tissues. *F1000Research* (2017) 6:160. doi: 10.12688/F1000RESEARCH.10356.1/DOI
26. Friedl P, Gilmour D. Collective Cell Migration in Morphogenesis, Regeneration and Cancer. *Nat Rev Mol Cell Biol* (2009) 10:445–57. doi: 10.1038/nrm2720
27. Sung BH, von Lersner A, Guerrero J, Krystofiak ES, Inman D, Pelletier R, et al. A Live Cell Reporter of Exosome Secretion and Uptake Reveals Pathfinding Behavior of Migrating Cells. *Nat Commun* (2020) 11(1):2092. doi: 10.1038/s41467-020-15747-2

28. Rilla K. Diverse Plasma Membrane Protrusions Act as Platforms for Extracellular Vesicle Shedding. *J Extracellular Vesicles* (2021) 10:e12148. doi: 10.1002/jev2.12148
29. Das T, Safferling K, Rausch S, Grabe N, Boehm H, Spatz JP. A Molecular Mechanotransduction Pathway Regulates Collective Migration of Epithelial Cells. *Nat Cell Biol* (2015) 17(3):276–87. doi: 10.1038/ncb3115
30. Tammi MI, Oikari S, Pasonen-Seppänen S, Rilla K, Auvinen P, Tammi RH. Activated Hyaluronan Metabolism in the Tumor Matrix — Causes and Consequences. *Matrix Biol* (2018) 78–79:147–64. doi: 10.1016/j.matbio.2018.04.012
31. Tolg C, Telmer P, Turley E. Specific Sizes of Hyaluronan Oligosaccharides Stimulate Fibroblast Migration and Excisional Wound Repair. *PloS One* (2014) 9(2):e88479. doi: 10.1371/JOURNAL.PONE.0088479
32. Herrera-Perez M, Voytik-Harbin SL, Rickus JL. Extracellular Matrix Properties Regulate the Migratory Response of Glioblastoma Stem Cells in Three-Dimensional Culture. *Tissue Eng Part A* (2015) 21:2572–82. doi: 10.1089/TEN.TEA.2014.0504
33. Unnikandam Veettil SR, Hwang D, Correia J, Bartlett MD, Schneider IC. Cancer Cell Migration in Collagen-Hyaluronan Composite Extracellular Matrices. *Acta Biomaterialia* (2021) 130:183–98. doi: 10.1016/J.ACTBIO.2021.06.009
34. Yang C, Cao M, Liu Y, He Y, Du Y, Zhang G, et al. Inducible Formation of Leader Cells Driven by CD44 Switching Gives Rise to Collective Invasion and Metastases in Luminal Breast Carcinomas. *Oncogene* (2019) 38:7113–32. doi: 10.1038/S41388-019-0899-Y
35. Uchino M, Kojima H, Wada K, Imada M, Onoda F, Satofuka H, et al. Nuclear Beta-Catenin and CD44 Upregulation Characterize Invasive Cell Populations in Non-Aggressive MCF-7 Breast Cancer Cells. *BMC Cancer* (2010) 10:414. doi: 10.1186/1471-2407-10-414
36. Keller KE, Kopczynski C. Effects of Netarsudil on Actin-Driven Cellular Functions in Normal and Glaucomatous Trabecular Meshwork Cells: A Live Imaging Study. *J Clin Med* (2020) 9:3524. doi: 10.3390/jcm9113524
37. Turley EA, Wood DK, McCarthy JB. Carcinoma Cell Hyaluronan as a "Portable" Cancerized Prometastatic Microenvironment. *Cancer Res* (2016) 76:2507–12. doi: 10.1158/0008-5472.CAN-15-3114
38. Kufe DW. Mucins in Cancer: Function, Prognosis and Therapy. *Nat Rev Cancer* (2009) 9:874–85. doi: 10.1038/NRC2761
39. Melero-Fernandez de Mera RM, Arasu UT, Kärnä R, Oikari S, Rilla K, Vigetti D, et al. Effects of Mutations in the Post-Translational Modification Sites on the Trafficking of Hyaluronan Synthase 2 (HAS2). *Matrix Biol* (2019) 80:85–103. doi: 10.1016/j.matbio.2018.10.004
40. Arasu UT, Deen AJ, Pasonen-Seppänen S, Heikkinen S, Lalowski M, Kärnä R, et al. HAS3-Induced Extracellular Vesicles From Melanoma Cells Stimulate IHH Mediated C-Myc Upregulation *via* the Hedgehog Signaling Pathway in Target Cells. *Cell Mol Life Sci* (2020) 77(20):4093–115. doi: 10.1007/s00018-019-03399-5
41. Shurer CR, Kuo JC-H, Roberts LM, Gandhi JG, Colville MJ, Enoki TA, et al. Physical Principles of Membrane Shape Regulation by the Glycocalyx. *Cell* (2019) 177:1757–70.e21. doi: 10.1016/j.cell.2019.04.017
42. Graves LE, Ariztia E v., Navari JR, Matzel HJ, Stack MS, Fishman DA. Proinvasive Properties of Ovarian Cancer Ascites-Derived Membrane Vesicles. *Cancer Res* (2004) 64:7045–9. doi: 10.1158/0008-5472.CAN-04-1800
43. Vasconcelos MH, Caires HR, Ābols A, Xavier CPR, Linē A. Extracellular Vesicles as a Novel Source of Biomarkers in Liquid Biopsies for Monitoring Cancer Progression and Drug Resistance. *Drug Resistance Updates: Rev Commentaries Antimicrobial Anticancer Chemother* (2019) 47:100647. doi: 10.1016/J.DRUP.2019.100647
44. Menck K, Bleckmann A, Wachter A, Hennies B, Ries L, Schulz M, et al. Characterisation of Tumour-Derived Microvesicles in Cancer Patients' Blood and Correlation With Clinical Outcome. *J Extracellular Vesicles* (2017) 6 (1):1340745. doi: 10.1080/20013078.2017.1340745
45. Ghoroghi S, Mary B, Asokan N, Goetz JG, Hyenne V. Tumor Extracellular Vesicles Drive Metastasis (It's a Long Way From Home). *FASEB BioAdvances* (2021) 3:930. doi: 10.1096/FBA.2021-00079
46. Conti S, Kato T, Park D, Sahai E, Trepat X, Labernadie A. CAFs and Cancer Cells Co-Migration in 3D Spheroid Invasion Assay. *Methods Mol Biol (Clifton NJ)* (2021) 2179:243–56. doi: 10.1007/978-1-0716-0779-4_19
47. Gaggioli C, Hooper S, Hidalgo-Carcedo C, Grosse R, Marshall JF, Harrington K, et al. Fibroblast-Led Collective Invasion of Carcinoma Cells With Differing Roles for RhoGTPases in Leading and Following Cells. *Nat Cell Biol 2007 9:12* (2007) 9:1392–400. doi: 10.1038/ncb1658
48. Provenzano PP, Eliceiri KW, Campbell JM, Inman DR, White JG, Keely PJ. Collagen Reorganization at the Tumor-Stromal Interface Facilitates Local Invasion. *BMC Med* (2006) 4(1):38. doi: 10.1186/1741-7015-4-38
49. Raghuraman S, Schubert A, Bröker S, Jurado A, Müller A, Brandt M, et al. Pressure Drives Rapid Burst-Like Coordinated Cellular Motion From 3D Cancer Aggregates. *Adv Sci (Weinheim Baden-Wurttemberg Germany)* (2022) 6:2104808. doi: 10.1002/ADVS.202104808

Conflict of Interest: The authors declare that the research was conducted in the absence of any commercial or financial relationships that could be construed as a potential conflict of interest.

Publisher's Note: All claims expressed in this article are solely those of the authors and do not necessarily represent those of their affiliated organizations, or those of the publisher, the editors and the reviewers. Any product that may be evaluated in this article, or claim that may be made by its manufacturer, is not guaranteed or endorsed by the publisher.

Copyright © 2022 Aaltonen, Kyykallio, Tollis, Capra, Hartikainen, Matilainen, Oikari and Rilla. This is an open-access article distributed under the terms of the Creative Commons Attribution License (CC BY). The use, distribution or reproduction in other forums is permitted, provided the original author(s) and the copyright owner(s) are credited and that the original publication in this journal is cited, in accordance with accepted academic practice. No use, distribution or reproduction is permitted which does not comply with these terms.

frontiers | Frontiers in Oncology

ORIGINAL RESEARCH
published: 31 May 2022
doi: 10.3389/fonc.2022.914838

Chondroitin Sulfates Control Invasiveness of the Basal-Like Breast Cancer Cell Line MDA-MB-231 Through ROR1

Satomi Nadanaka[1], *Jun-ichi Tamura*[2] *and Hiroshi Kitagawa*[1]*

[1] Laboratory of Biochemistry, Kobe Pharmaceutical University, Kobe, Japan, [2] Department of Agricultural, Life and Environmental Sciences, Faculty of Agriculture, Tottori University, Tottori, Japan

OPEN ACCESS

Edited by:
Nikos Karamanos, University of Patras, Greece

Reviewed by:
Davide Vigetti, University of Insubria, Italy
Mauro Sergio Pavao, Federal University of Rio de Janeiro, Brazil
Chrysostomi Gialeli, Lund University, Sweden

***Correspondence:**
Hiroshi Kitagawa
kitagawa@kobepharma-u.ac.jp

Specialty section:
This article was submitted to Molecular and Cellular Oncology, a section of the journal Frontiers in Oncology

Received: *07 April 2022*
Accepted: *02 May 2022*
Published: *31 May 2022*

Citation:
Nadanaka S, Tamura J and Kitagawa H (2022) Chondroitin Sulfates Control Invasiveness of the Basal-Like Breast Cancer Cell Line MDA-MB-231 Through ROR1. Front. Oncol. 12:914838. doi: 10.3389/fonc.2022.914838

Extracellular and cell surface chondroitin sulfates (CSs) regulate cancer cell properties, including proliferation and invasion. Thus, it is necessary to understand the mechanisms underlying their roles in cancer. Although we have shown that CS has an inherent ability to enhance the invasive activity of the human triple-negative breast cancer cell line MDA-MB-231, its molecular mechanism remains elusive. Here, we focused on receptor tyrosine kinase-like orphan receptor 1 (ROR1) and dickkopf WNT signaling pathway inhibitor 1 (DKK1). MDA-MB-231 cells express high levels of ROR1; their invasive potential depends on ROR1 signaling. Although accumulating evidence has demonstrated that ROR1 is associated with aggressive breast-cancer phenotypes, the whole picture of its biological function remains poorly understood. In this study, we examined whether CS controls ROR1 function. Surface plasmon resonance analysis indicated that CSs were bound to ROR1 in the presence of WNT5A. The invasive activity of MDA-MB-231 cells enhanced by CSs was completely suppressed by *ROR1* knockdown. In addition, knockdown of the CS biosynthetic enzymes CHST11 and CHST15 inhibited invasive activity, even in the presence of ROR1. These results suggest that CS is required to induce an ROR1-dependent, aggressive MDA-MB-231 phenotype. ROR1 signaling in MDA-MB-231 cells activated c-Jun N-terminal kinase (JNK), leading to increased invasive potential; moreover, exogenous CSs activated JNK. MDA-MB-231 cells express DKK1, a tumor suppressor factor that binds to CS, at high levels. Knockdown of *DKK1* enhanced CS-stimulated tumor invasion activity of MDA-MB-231 cells, suggesting that DKK1 sequesters CS to block ROR1/JNK signaling. These results showed that CSs promotes cancer aggressiveness through the ROR1–JNK axis in MDA-MB-231 cells.

Keywords: proteoglycan, chondroitin sulfate, breast cancer, receptor tyrosine kinase-like orphan receptor 1, Dickkopf 1

INTRODUCTION

Tumor-associated glycocalyx plays a key role in the promotion and regulation of breast cancer progression and metastasis (1). The glycosaminoglycan chondroitin sulfate (CS) is present on the cell surface and in the extracellular matrix (ECM), including the glycocalyx. There is ample evidence for a pro-tumorigenic role for CS in the enhancement of cell proliferation, motility, and metastasis (2–5).

Chondroitin sulfate proteoglycans (CS-PGs) consist of a core protein and covalently attached CS chains. CS is a linear sulfated polymer of repeating disaccharide units of glucuronic acid (GlcA) and *N*-acetylgalactosamine (GalNAc) [-GlcA-GalNAc-]$_n$. During the synthesis of the chondroitin backbone, multiple sulfotransferases catalyze the transfer of a sulfate group from 3'-phosphoadenosine 5'-phosphate, the universal donor in sulfation reactions, to their respective sulfation sites on GalNAc or GlcA residues in the CS chain. Based on the substrate preferences of chondroitin sulfotransferases identified to date, the biosynthetic scheme for CS-type sulfation can be separated into initial 4-*O*-sulfation and 6-*O*-sulfation pathways. In the initial step, the non-sulfated O unit [GlcA-GalNAc] serves as a common acceptor substrate for two types of sulfotransferases, chondroitin 4-*O*-sulfotransferases (CHST11 and CHST12) (6–8) and chondroitin 6-*O*-sulfotransferse-1 (CHST3), forming monosulfated A [GlcA-GalNAc(4-*O*-sulfate)] and C [GlcA-GalNAc(6-*O*-sulfate)] units, respectively. Subsequent sulfation of the A and C units also occurs *via* GalNAc 4-sulfate 6-*O*-sulfotransferase (CHST15) or CS-specific uronyl 2-*O*-sulfotransferase (UST), producing disulfated disaccharide E [GlcA-GalNAc(4,6-*O*-disulfate)] and D [GlcA(2-*O*-sulfate)-GalNAc(6-*O*-sulfate)] units, respectively (9). Of these sulfotransferases, it has been reported that the expression of CHST11 and CHST15 is upregulated in breast cancer cells (10). Moreover, the expression of *CHST11* has been correlated with breast-cancer progression (11). Specific sulfation patterns are hypothesized to underlie the distinct functional roles of CS not only under physiological conditions but also in tumor development and progression (12, 13).

Interestingly, it has been reported that the invasive activity of basal-like subtypes (MDA-MB-231 and BT-549 cells) is elevated by treatment with chondroitin sulfate E (CS-E), the major component of which is the E-unit (14). This result prompted us to hypothesize that there is a CS-E receptor in some cancer cells. We previously showed that N-cadherin functions as a receptor for CS-E in BT-549 cells, enhancing invasion activity by upregulating matrix metallopeptidase 9 *via* N-cadherin–catenin signaling. In another basal-like subtype of MDA-MB-231 cells, invasive activity was enhanced by treatment with CS-E; however, MDA-MB-231 cells do not express N-cadherin. In addition, CS-E had no effect on β-catenin-dependent transcription in MDA-MB-231 cells (14), suggesting that CS-E increases invasive activity mediated by non-canonical Wnt signaling. MDA-MB-231 cells express high levels of receptor tyrosine kinase-like orphan receptor 1 (ROR1), a receptor for non-canonical Wnt ligands such as WNT5A (15). ROR1 is associated with CS-dependent invasiveness of MDA-MB-231 cells. In addition, MDA-MB-231 cells express high levels of the Wnt signal modulator, Dickkopf-1 (DKK1), which binds directly to CS-E (14). Although DKK1 is a secreted inhibitor of β-catenin-dependent Wnt signaling, recent studies have shown that its elevated expression correlates with poor prognosis in a range of cancers (16). Here, we show that ROR1-dependent invasion activity is controlled by CSs in MDA-MB-231 cells. In addition, this study suggests that DKK1 exhibits tumor suppressor activity by blocking the tumor invasion activity of CS-E and by inhibiting β-catenin-dependent Wnt signaling.

MATERIALS AND METHODS

Cell Culture and Stable Transfection

The human breast cancer cell line MDA-MB-231 (#92020424) was purchased from the European Collection of Cell Culture (ECACC) (Salisbury, UK). MCF7 cells (ATCC® HTB-22™) were obtained from the American Type Culture Collection (ATCC). Both lines were cultured in Roswell Park Memorial Institute (RPMI) 1640 supplemented with 10% heat-inactivated fetal bovine serum (FBS), 100 units/ml penicillin, 100 μg/ml streptomycin, and 1% L-glutamine.

The expression plasmids [pcDNA3.1(+)-ROR1] were transfected into MCF7 cells using Lipofectamine 3000 (Thermo Fisher Scientific, Waltham, MA), according to the manufacturer's instructions. Transfectants were cultured in the presence of 300 μg/ml G418. Colonies surviving in the presence of 300 μg/ml G418 were collected, and ROR1-expressing cell populations were enriched using 2 μg of anti-ROR1 antibody (Clone 4A5, Cat. No. 564464, BD Biosciences, Franklin Lakes, NJ, USA) and 1.5 mg of Dynabeads™ Protein G (Cat. No. 10003D, Invitrogen, Waltham, MA). The pooled ROR1-expressing clones were propagated for experiments.

Plasmid Construction

A human ROR1 Flexi clone (FXC20341) was obtained from Kazusa Genome Technologies, Inc. (Chiba, Japan). For the expression of ROR1, polymerase chain reaction (PCR) was performed using the following primers and pF1KE3329-human ROR1 as a template: forward, 5'-GCTGGCTAGCGT TTA**ATG**CACCGGCCGCGCCGCCG-3' [underline, homologous to the pcDNA3.1(+) vector sequence; bold, start codon]; reverse, 5'-GGTTTAAACGGGCCCTTACAGTTCTG CAGAAATCATAGATTCG-3' [underline, homologous to the pcDNA3.1(+) vector sequence]. pCDNA3.1(+)-ROR1 was constructed using an In-Fusion® HD cloning kit (TaKaRa Bio Inc., Shiga, Japan). Linearized pcDNA3.1(+)was generated by inverse PCR using the following primers and KOD One PCR master mix (TOYOBO, Osaka, Japan): forward, 5'-TAAACGCTAGCCAGC-3', reverse, 5'-GGGCCCGTTTAAACC-3'.

Real-Time PCR

Total RNA was isolated from cells using Sepasol®-RNA I Super G (Nacalai Tesque, Inc., Kyoto, Japan). For reverse transcription, 1 μg of total RNA was treated with Moloney murine leukemia

virus reverse transcriptase (Promega, Madison, WI, USA) using random primers [nondeoxyribonucleotide mixture; $pd(N)_9$] (Takara Bio Inc., Shiga, Japan). Quantitative real-time PCR was conducted using FastStart DNA Master Plus SYBR Green I in a LightCycler® 96 (Roche Applied Science, Penzberg, Germany), according to the manufacturer's protocol. The data processing was based on standard curves, and target-to-reference ratios were calculated using the relative quantification analysis module of the LigtCycler® 96 software. The amplification efficiency was calculated based on the slope of the standard curve (target DNA was amplified with 90%–110% efficiency). Amplified DNA product was checked by post-PCR melting curve analysis. The housekeeping gene *GAPDH* was used as an internal control for quantification. Primers are listed in **Table 1**.

Knockdowns

Cells were transfected with Silencer® Select siRNAs targeting *ROR1* (assay ID s9755), *WNT5A* (assay ID: s14873), *CHST11* (assay ID: s27032 and s27033), *CHST15* (assay IDs: s28015 and s28017), and *DKK1* (assay ID: s22721) purchased from Thermo Fisher Scientific. Forty-two hours after transfection, cells were subjected to invasion and migration assays.

Invasion and Migration Assays

Invasion was assessed using Corning® BioCoat™ Matrigel® invasion chambers, according to the manufacturer's instructions. Cells were collected by treatment with trypsin/EDTA, washed twice with phosphate-buffered saline (PBS), pelleted, and resuspended in medium containing 0.2% fetal bovine serum or 0.1% bovine serum albumin. Cells (5×10^4/ml) were incubated in the presence or absence of 50 μg/ml CS-E (Seikagaku Corporation, Tokyo, Japan) or 10 μM JNK inhibitor SP600125 (Cat. No. 129-56-6, Cayman Chemical Company, Ann Arbor, MI) for 20 min at 25°C, added to the upper chamber, and allowed to invade for 22 h at 37°C in a CO_2 incubator. Complete medium containing 10% fetal bovine serum or 200 ng/ml recombinant human/mouse Wnt-5A (Cat. No. 645-WN/CF) was placed in the bottom well as chemoattractant. Migration was assessed using Corning® BioCoat™ control inserts according to the manufacturer's instructions. Cells (5×10^4/ml) were prepared as described above.

Immunoblotting

Cells were treated with 50 μg/ml CS-E or CS-A (Seikagaku Corporation, Tokyo, Japan), 50 μg/ml synthesized hexasaccharides GalNAc(4-*O*-sulfate,6-*O*-sulfate)-GlcA-GalNAc(4-*O*-sulfate,6-*O*-sulfate)-GlcA-GalNAc(4-*O*-sulfate,6-*O*-sulfate)-GlcA-*O*-*p*-methoxyphenyl (E-E-E 6-mer), or GalNAc-GlcA-GalNAc-GlcA-GalNAc-GlcA-O-p-methoxyphenyl (O-O-O 6-mer) for the indicated times. Cells were solubilized in M-PER (Thermo Fisher Scientific) containing a protease inhibitor cocktail (Nacalai Tesque, Inc., Kyoto, Japan) and 10 μM proteasome inhibitor (MG132; PEPTIDE Institute. Inc., Osaka, Japan) for 30 min on ice. Lysates were centrifuged at 16,500×*g* for 15 min. Proteins were separated on Bullet PAGE precast gels, 5-15% (Nacalai Tesque, Inc.), transferred to polyvinylidene fluoride (PVDF) membranes, and incubated overnight with primary antibodies against phosphor-c-Jun N-terminal kinase (JNK) (T183/Y185) (clone 81E11, Cat. No. 4668S, Cell Signaling Technology, Danvers, MA, USA), actin (clone AC-40, Cat. No. A3853, Sigma-Aldrich, St. Louis, MO), Ror1 (clone D6T8C, Cat. No. 16540S, Cell Signaling Technology), phospho-cortactin (Y421) (Cat. No. 4569S, Cell Signaling Technology), and cortactin (clone H222, Cat. No. 3503S; Cell Signaling Technology).

Flow Cytometry

Cells (1×10^6) were fixed with PBS containing 4% paraformaldehyde on ice for 30 min. After washing with PBS, cells were incubated with PBS containing 2% BSA on ice for 30 min and then stained with anti-ROR1 antibody (dilution ratio, 1:100) (Clone 4A5, Cat. No. 564464, BD Biosciences, Franklin Lakes, NJ, USA) on ice. After 1 h, cells were washed and incubated with mouse IgG2b antibody conjugated with Alexa™488 (dilution ratio, 1:400) (Thermo Fisher Scientific) on ice for 1 h. Cells were analyzed using a BD Accuri™ C6 flow cytometer (BD Biosciences).

TABLE 1 | Primers used for real-time PCR.

Gene Name	5'-primer	3'-primer	References
hWNT1	5'-ACCGAGGCTGTCGAGAAACG-3'	5'-GCCGGTAGTCACACGTGCAG-3'	(14)
hWNT2	5'-GCTCACCCCCGAGGTCAACT-3'	5'-CCTGGCTAATGGCACGCATC-3'	(14)
hWNT3A	5'-ACAACAATGAGGCTGGG-3'	5'-ATCTCCGAGGCACTGTCATA-3'	(14)
hWNT4	5'-CTCCACACTCGACTCCTTGC-3'	5'-CCGAAGAGATGGCGTACACG-3'	PrimerBank ID156630997c2
hWNT5A	5'-TCGACTATGGCTACCGCTTTG-3'	5'-CACTCTCGTAGGAGCCCTTG-3'	PrimerBank ID3371506361c3
hWNT5B	5'-CATGGCCTACATAGGGGAGG -3'	5'-CTGTGCTGCAATTCCACCG-3'	PrimerBank ID17402920c2
hWNT6	5'-GGCAGCCCCTTGGTTATGG-3'	5'-CTCAGCCTGGCACAACTCG-3'	PrimerBank ID53729353c1
hWNT7A	5'-CTGTGGCTGCGACAAAGAGAA-3'	5'-GCCGTGGCACTTACATTCC-3'	PrimerBank ID34328912c1
hWNT11	5'-GGAGTCGGCCTTCGTGTATG-3'	5'-GCCCGTAGCTGAGGTTGTC-3'	PrimerBank ID17017973c1
hDKK-1	5'-GTGCGCAGAGGACGAGGAGT-3'	5'-GTGACGCATGCAGCGTTTTC-3'	(14)
hROR1	5'-CAGTCAGTGCTGAATTAGTGCC-3'	5'-TCATCGAGGGTCAGGTAAGAAT-3'	PrimerBank ID 134152685c1
hROR2	5'-GTGCGGTGGCTAAAGAATGAT-3'	5'-ATTCGCAGTCGTGAACCATATT-3'	PrimerBank ID 317008621c2
hCHST11	5'-AAACGCCAGCGGAAGAA-3'	5'-GGGATGGCAGAGTGAGTAGA-3'	(7)
hCHST15	5'-TCGTGTGGACAGTAAGCAGAT-3'	5'-TGTAAGAAGCCATTACCAAGGTC-3'	PrimerBank ID 311893349c1

Disaccharide Analysis of CSs From Human Breast Cancer Cell Lines

CSs isolated and purified from human breast cancer MDA-MB-231 and MCF7 cells were analyzed as previously described (6, 7, 17–19).

Biacore Analysis

Real-time binding was assessed as described previously (19), using Biacore X100 (Cytiva, Tokyo, Japan). Recombinant human ROR1-Fc chimera (Cat. No. 9490-RO, R&D Systems) was immobilized on a CM5 series chip (Cytiva) using the amine-coupling method. ROR1 injection was stopped when the surface plasmon resonance reached ~ 3,200 RU. For ROR1 binding assays, WNT5A (0, 0.038, 0.075, 0.15, 0.30, and 0.60 μM), WNT5A/CS-E (0, 0.036/0.25, 0.071/0.50, 0.15/1.0, 0.29/2.0, and 0.57/4.0 μM), recombinant human DKK1 (Cat. No. 5439-DK/CF, R&D Systems) (0, 0.038, 0.075, 0.15, and 0.3 μM), or DKK1/CS-E (0, 0.038/0.28, 0.075/0.55, 0.15/1.1, and 0.3/2.1 μM) were sequentially injected at a flowrate of 30 μl/min for 120 s at 25°C; the dissociation time was set for 130 s. Binding reactions were performed in 50 mM Tris–HCl buffer (pH 7.5).

Statistical Analysis

Data are expressed as means ± one standard deviation. Statistical significance was determined using Student's *t*-test or one-way ANOVA, with Tukey's honestly significant difference (HSD) test.

RESULTS

Invasion-Promoting Activity of CS-E Is Mediated by WNT5A/ROR1/JNK Signaling

We have shown that the invasive activity of basal-like subtypes (MDA-MB-231 and BT-549 cells) is elevated by treatment with chondroitin sulfate E (CS-E) (13). Because MDA-MB-231 cells express mRNAs for the receptors in the canonical Wnt signaling pathway, LRP5 and LRP6, at low levels (13), we hypothesized that the receptors for the non-canonical Wnt signaling pathway, ROR1 and ROR2, are targeted by CS-E in MDA-MB-231 cells. Quantitative real-time PCR (qRT-PCR) indicated that ROR1 was predominantly expressed in MDA-MB-231 cells (**Figure 1A**). Because it is known that Ror1 is a receptor for WNT5A and WNT5B (20), their gene expression levels were examined (**Figure 1A**). Among the Wnt ligands examined, *WNT5A* mRNA was expressed at the highest

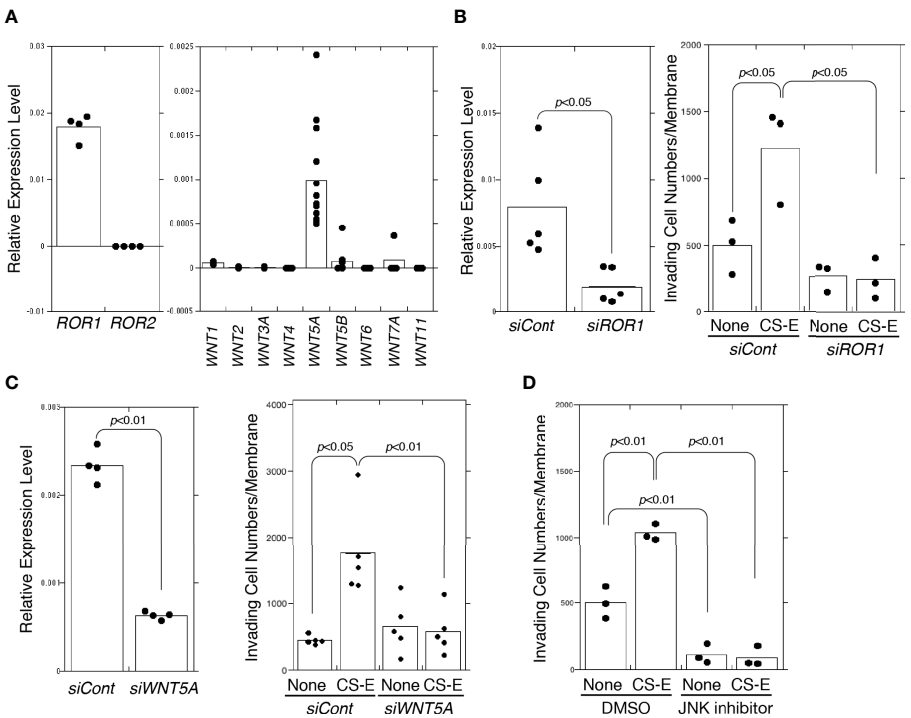

FIGURE 1 | CS-E-elicited invasiveness *via* WNT5A-ROR1-JNK signaling. **(A)** Expression levels of ROR1 (n=4), ROR2 (n=4), WNT1 (n=3), WNT2 (n=3), WNT3A (n=3), WNT4 (n=4), WNT5A (n=13), WNT5B (n=8), WNT6 (n=4), WNT7A (n=4), and WNT11 (n=4) in MDA-MB-231 cells measured by qPCR. **(B)** *ROR1* expression after *ROR1* knockdown (*siROR1*) (n=5) or control cells (*siCont*) (n=5) measured by qPCR. Invasiveness of *siROR1*-treated cells (*siROR1*) (n=3) or control cells (*siCont*) (n=3) was measured in the absence or presence of 50 μg/ml CS-E. Data were analyzed using Student's *t*-test. **(C)** Left graph: *WNT5A* mRNA expression decreased at the mRNA level following siRNA-induced knockdown in MDA-MB-231 by qPCR (n=4). Expression data were normalized to those of *GAPDH*. Right graph: invasiveness of *WNT5A*-knockdown (siWNT5A) and control cells (siCont) measured in the absence or presence of 50 μg/ml of CS-E (n=5). Data were analyzed using Student's *t*-test. **(D)** MDA-MB-231 cells treated with DMSO or 10 μM JNK inhibitor SP600125, assessed for invasiveness in the absence or presence of 50 μg/ml CS-E.

level in MDA-MB-231 cells. To determine whether ROR1 is involved in invasion activity enhanced by treatment with CS-E, *ROR1* was knocked down. The invasion potential of MDA-MB-231 cells was significantly upregulated in response to CS-E, whereas MDA-MB-231 cells became less responsive to CS-E after *ROR1* knockdown (**Figure 1B**). Next, we examined the effect of *WNT5A* knockdown on invasiveness elicited by CS-E (**Figure 1C**) but did not observe an increase. As WNT5A signals are transduced through RORs to activate the c-Jun N-terminal kinase (JNK) pathway (21–23), we determined whether an inhibitor of JNK, SP600125, altered invasiveness in MDA-MB-231 cells (**Figure 1D**). As expected, CS-E did not promote invasiveness in the presence of JNK inhibitor. These results suggest that CS-E enhances the invasive activity of MDA-MB-231 cells through the WNT5A–ROR1–JNK signaling axis.

CSs activate JNK in a Sulfation Pattern-Dependent Manner

Treatment with CS-E polymers for 10 min significantly elevated JNK phosphorylation (**Figure 2A**). The CS-E polymers used in this study contained 72% E, 18.4% A, 8.7% C, and 6.6% O units. To determine whether the E-disaccharide unit is required to activate JNK, we used chemically synthesized hexasaccharide sequences, including the E-E-E-containing sequence GalNAc(4-*O*-sulfate,6-*O*-sulfate)-GlcA-GalNAc(4-*O*-sulfate,6-*O*-sulfate)-GlcA-GalNAc(4-*O*-sulfate,6-*O*-sulfate)-GlcA-*O*-*p*-methoxyphenyl (E-E-E 6-mer). The E-E-E 6-mer also activated JNK in MDA-MB-231 cells (**Figure 2B**). These results suggest that the E units in the CS chains play an important role in the activation of JNK.

As described in *Introduction*, CS exhibits highly diverse structural variations that contribute to its functional diversity. Therefore, we determined whether CS-E specifically elicits JNK phosphorylation. Chondroitin sulfate A (CS-A) polymers used in this study contained 74.5% A units, 23.7% C units, 1.9% O units, 1.8% D units, and 0% E units. CS-A polymers did not activate JNK (**Figure 2C**). In addition, chemically synthesized non-sulfated hexasaccharides GalNAc-GlcA-GalNAc-GlcA-GalNAc-GlcA-*O*-*p*-methoxyphenyl (O-O-O 6-mer) did not activate JNK (**Figure 2D**). These results suggest that CS controls JNK activation in a sulfation-pattern-dependent manner.

E Unit-Containing CS Chains Enhance Invasiveness

As shown in **Figure 3A**, the disaccharide unit of CS, GlcA-GalNAc, is sulfated by the indicated sulfotransferases. The E unit is synthesized by CHST11 (carbohydrate sulfotransferase 11, C4ST-1) and CHST15 (carbohydrate sulfotransferase 15, GALNAC4S-6ST). The expression levels of these sulfotransferases in MDA-MB-231 cells were examined (**Figure 3B**). The CS chains produced in MDA-MB-231 cells contained 63.5% A, 21.8% O, 7.9% C, 4.5% E, and 2.2% D units (**Figure 3C**). To downregulate the expression of the A and E units, *CHST11* was knocked down; this strongly decreased the invasiveness of MDA-MB-231 cells (**Figure 3D**). When only E units were decreased by CHST15 knockdown, the invasiveness was suppressed (**Figure 3E**). These results suggest that a specific sulfation pattern, the E unit, is associated with the high invasive potential of MDA-MB-231 cells.

Increased Invasiveness Elicited by Expression of ROR1 Is Diminished by *CHST15* Knockdown in MCF7 Cells

MCF7 is a less-aggressive, non-invasive cell line that is normally considered to have low metastatic potential (24). MCF7 cells expressed low levels of ROR2, WNT5A, and WNT5B (**Figure 4A**). Endogenous ROR1 (**Figures 4A, C**) and DKK1 proteins (13) were not detected in MCF7 cells, so ROR1-

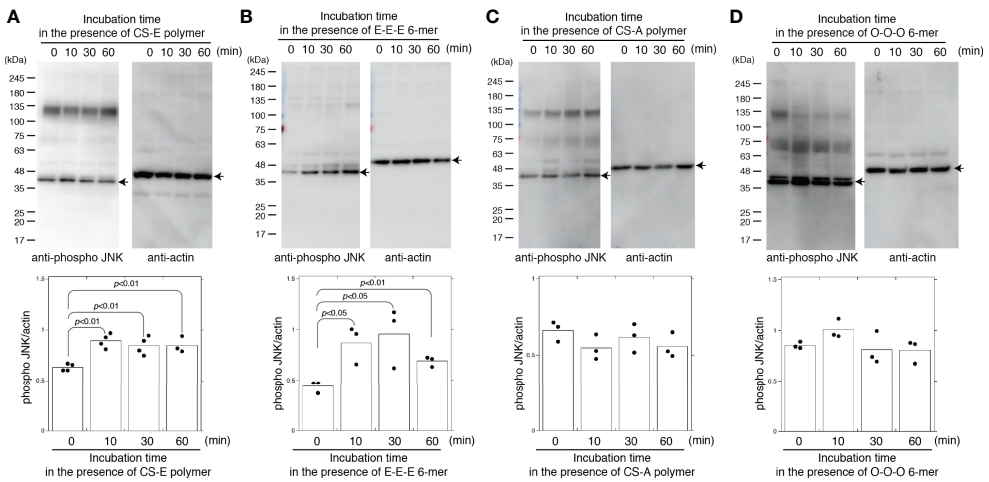

FIGURE 2 | CS-E and chemically-synthesized E unit-containing hexasaccharides specifically activate JNK. MDA-MB-231 cells were treated with 50 μg/ml of CS-E polymers **(A)**, 50 μg/ml chemically synthesized hexasaccharides consisting of three E units (E-E-E 6 mer) **(B)**, 50 μg/ml of CS-A polymers **(C)**, or 50 μg/ml chemically synthesized hexasaccharides consisting of three O units (O-O-O 6 mer) **(D)** at the indicated times. Phosphorylated JNK and actin levels were assessed by immunoblotting (top of each panel) and quantified by densitometry (bottom of each panel) (n≧3). Representative protein bands are indicated by arrows. Statistical significance was assessed using Student's *t*-test.

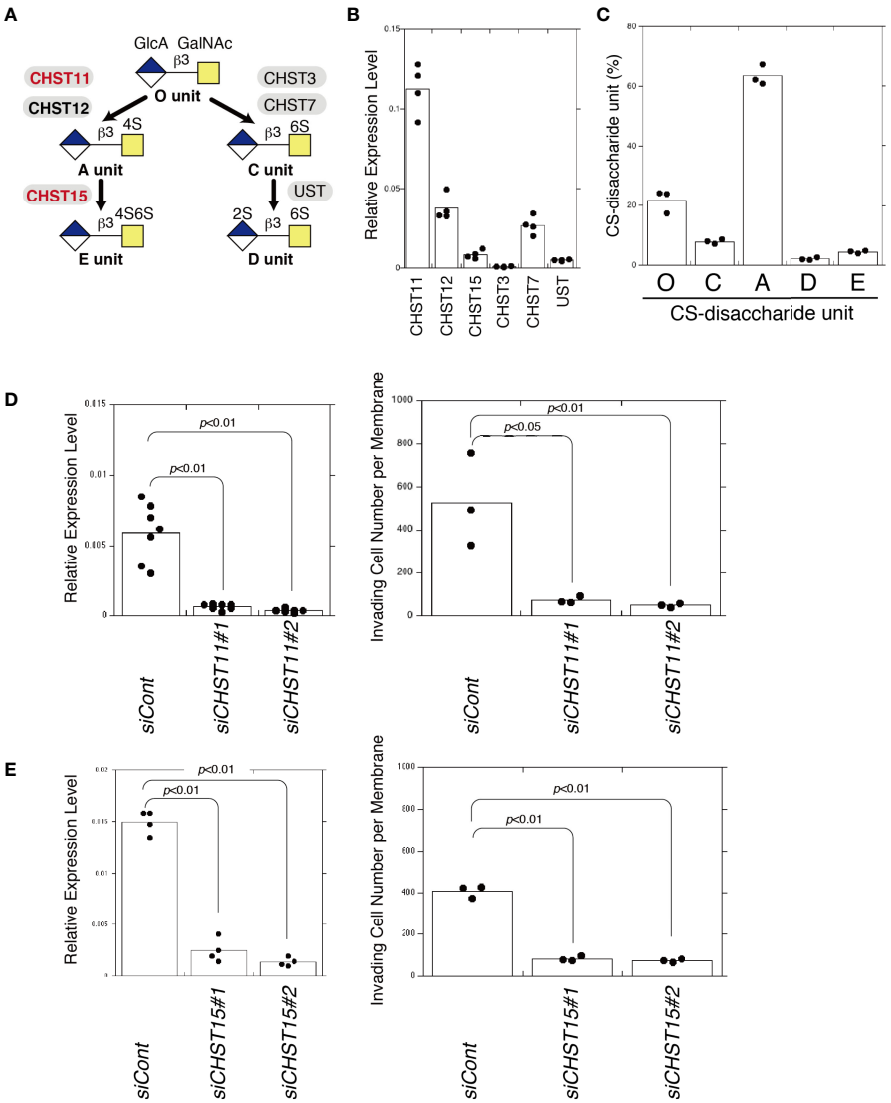

FIGURE 3 | Decreased E unit biosynthesis decreases invasiveness. **(A)** Diagram of sulfation pathways. The C4-position of the GalNAc residue in the O unit is sulfated by CHST11 and CHST12 to form an A unit. Subsequently, the A unit is converted to an E unit by CHST15. **(B)** mRNA expression levels of chondroitin sulfotransferases, *CHST11*, *CHST12*, *CHST15*, *CHST3*, *CHST7*, and *UST* in MDA-MB-231 cells measured by qPCR (*n=4*). **(C)** Composition of CS-disaccharide units of sulfated CS chains isolated from MDA-MB-231 cells analyzed using HPLC (n=3). **(D)** *CHST11* mRNA expression decreased following two kinds of siRNA-induced knockdown (*siCHST11#1* and *siCHST11#2*) in MDA-MB-231 cells, measured using qPCR (n=7). Expression data were normalized to those of *GAPDH*. Right graph: Invasiveness of *CHST11* knocked down cells (*siCHST11#1* or *siCHST11#2*) (n=3) or control cells (*siCont*) (n=3). **(E)** *CHST15* mRNA expression decreased at the mRNA level following knockdowns by *siCHST15#5* and *siCHST15#7* in MDA-MB-231 cells measured using qPCR (n=4). Expression data were normalized to those of *GAPDH*. Right graph, invasiveness of *CHST15* knocked down cells (*siCHST15#1* or *siCHST15#2*) (n=3) or control cells (*siCont*) (n=3). Data were analyzed using the Tukey–Kramer multiple comparison.

expressing cells were generated. ROR1 surface expression in MCF7 cells stably transfected with an empty vector (MCF7-empty cells) or stably expressing ROR1 (MCF7-ROR1 cells) was confirmed by flow cytometry (**Figure 4B**). Immunoblotting showed that MCF7-ROR1 cells expressed ROR1 at high levels (**Figure 4C**). As shown in **Figure 4D**, MCF7 cells produced CSs containing 20% E. Next, we examined whether the E unit was required for ROR1-mediated migration activity using MCF7-ROR1 cells. The migration potential of MCF7 cells was increased by ROR1 expression. This increase was attenuated by *CHST15* knockdown (**Figure 4E**). In addition, enhanced migration stimulated by treatment with WNT5A was suppressed by knockdown of *CHST15* (**Figure 4F**). Hasan et al. reported that WNT5A stimulates ROR1-dependent cortactin phosphorylation and enhances cell migration (25). We found that CS-E increased the phosphorylation of cortactin by WNT5A and that *CHST15* knockdown inhibited cortactin phosphorylation (**Figure 4G**). These results suggest that CSs regulate ROR1-mediated migration of breast cancer cells.

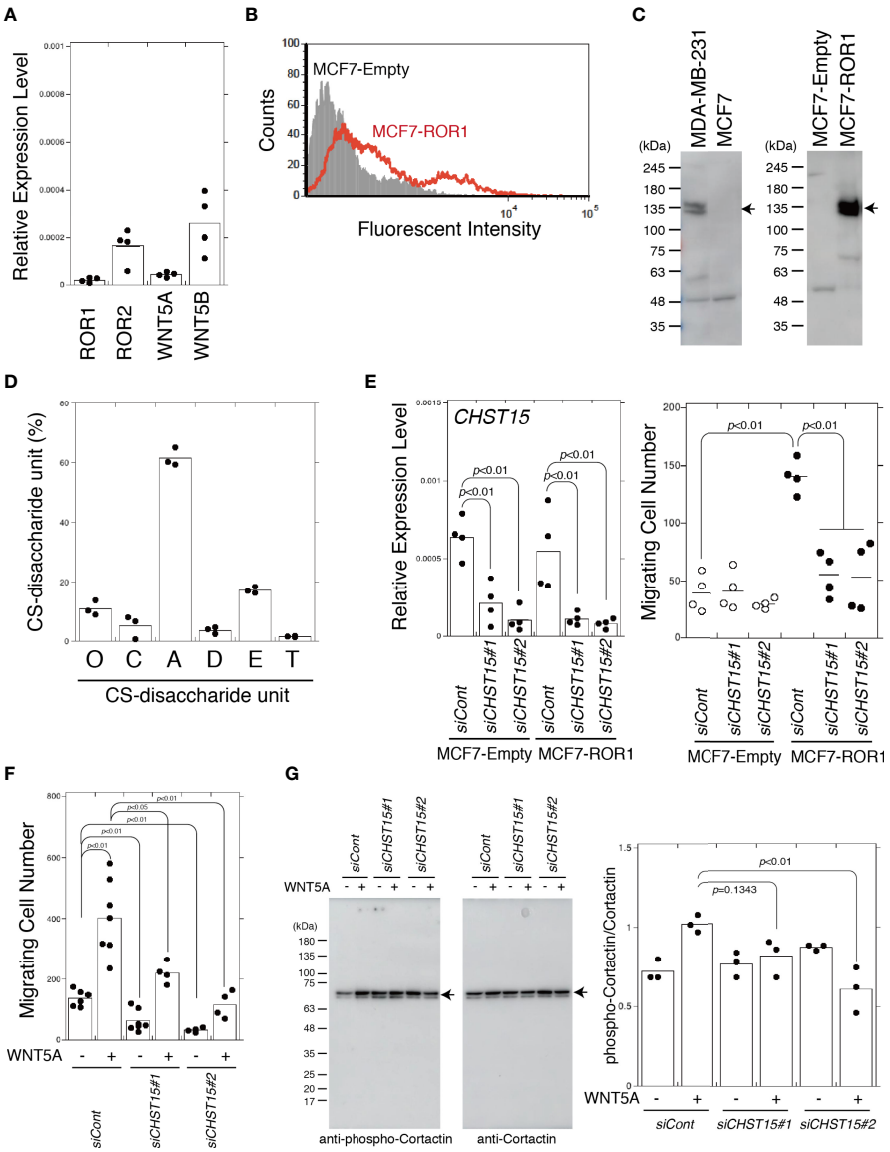

FIGURE 4 | MCF7 cells acquire invasiveness by expression of ROR1 and lose it by knockdown of *CHST15*. **(A)** mRNA expression levels of chondroitin sulfotransferase genes, *ROR1*, *ROR2*, *WNT5A*, and *WNT5B* in MDA-MB-231 cells measured by qPCR (*n=4*). **(B)** ROR1 surface expression by MCF7-empty cells (shaded area) and MCF7-Ror1 cells (red line) measured by flow cytometry. **(C)** Left, ROR1 expression in MDA-MB-231 and MCF7 cells measured by immunoblotting. Right, ROR1 expression MCF7 cells stably transfected with an empty vector (MCF7-Empty) or an ROR1 expression plasmid (MCF7-ROR1) analyzed by immunoblotting. **(D)** CS-disaccharide composition of sulfated CS chains from MCF7 cells analyzed using HPLC (n=3). **(E)** Left, *CHST15* mRNA expression following siRNA-induced knockdown (*siCHST15#1* or *siCHST15#2*) in MCF7-empty cells and MCF7-ROR1 cells measured using qPCR (n=4). Expression data were normalized to those of *GAPDH*. Right, migration of *CHST15* knocked down cells (*siCHST15#1* or *siCHST15#2*) (n=4) and control cells (*siCont*) (n=4) measured using a Transwell assay. **(F)** *CHST15* knocked down MCF7-ROR1 cells (*siCHST15#1* or *siCHST15#2*) or control cells (*siCont*) serum-starved and treated with (+) or without (–) 200 ng/ml of WNT5A. **(G)** *CHST15* knocked down MCF7-ROR1 cells (*siCHST15#1* or *siCHST15#2*) or control cells (*siCont*) treated with or without 100 ng/ml of WNT5a for 5 min, lysed, and subjected to immunoblotting using anti-phospho-cortactin and anti-cortactin antibodies. Right graph, relative levels of phosphorylated cortactin, standardized against total cortactin (n=4). Statistical significance was assessed using Student's *t*-test.

CS-E Directly Interacts With ROR1 in the Presence of Either WNT5A or DKK1

By surface plasmon resonance (SPR) analysis, neither WNT5A nor CS-E bound to ROR1 (**Figures 5A, B**). In contrast, CS-E premixed with WNT5A at a molar ratio of 7:1 did bind ROR1 (**Figures 5A, B**).

As it has been previously shown that DKK1 binds to CS-E (13), we hypothesized that DKK1 was able to bind to ROR1 by forming a

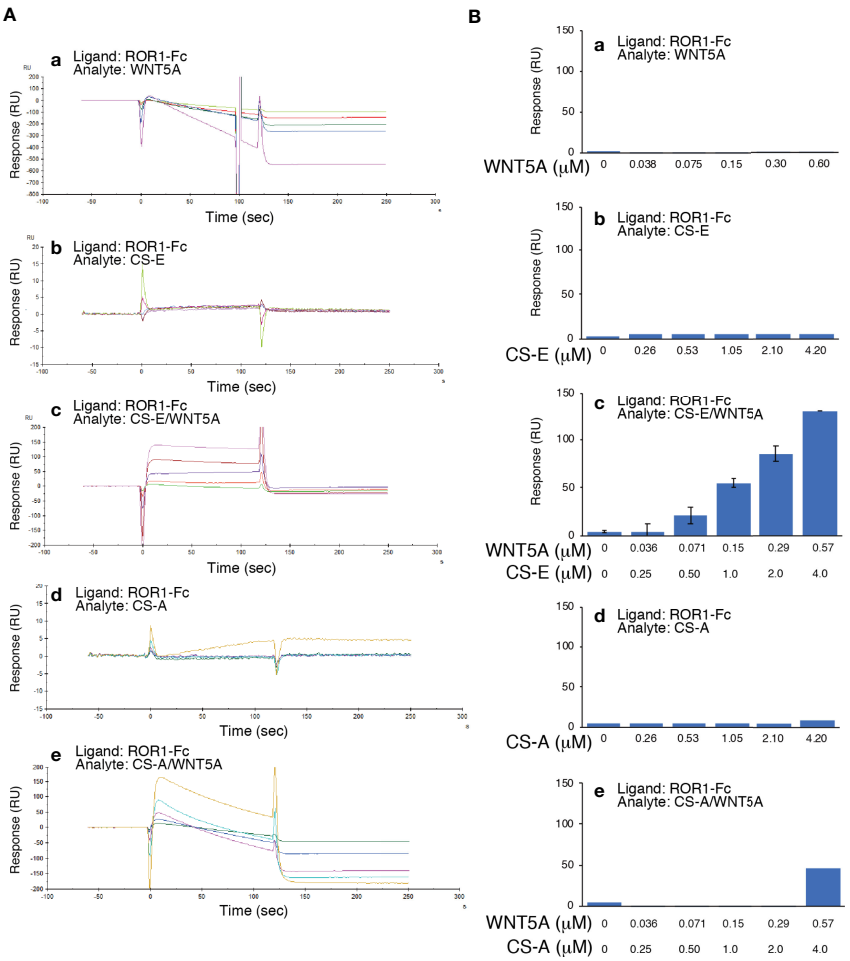

FIGURE 5 | WNT5A binds ROR1 in the presence of CS-E. **(A)** Raw sensor grams. ROR1 was immobilized in a flow cell of a CM5 sensor chip. WNT5A (a), CS-E (b), WNT5A pre-mixed with CS-E (c), CS-A (d), and WNT5A pre-treated with CS-A (e) were used as analytes. **(B)** Response-unit quantification of binding.

complex with CS-E. DKK1 is known to bind to LDL receptor-related proteins 5 and 6 (LRP5/6), which function as coreceptors in the canonical WNT signaling pathway, but no direct interaction between DKK1 and ROR1 has been shown. SPR indicated that DKK1 weakly bound to ROR1 in the concentration range of 0.0375 to 0.15 μM (**Figures 6A, B**). Binding of DKK1 to ROR1 was not reproducibly observed at 0.3 μM DKK1. CS-E was premixed with DKK1 at a molar ratio of 7:1, after which it was bound to ROR1 in a concentration-dependent manner, while DKK1 did not bind to ROR1 in the presence of CS-A (**Figures 6A, B**). These results suggested that DKK1 binds to ROR1 in the presence of CS-E.

We next examined whether CS-E increased the invasiveness of MDA-MB-231 cells by forming a complex with DKK1. Unexpectedly, *DKK1* knockdown enhanced CS-E-elicited invasiveness (**Figure 6D**). These results suggest that ROR1-dependent invasion signaling is blocked by binding of the DKK1/CS-E complex to ROR1 and that DKK1 exerts anti-tumorigenic effects by blocking the tumor invasion activity of CS-E as well as by inhibiting β-catenin-dependent Wnt signaling.

DISCUSSION

ROR1 as a Potential CS Target

Focusing on the roles of CS in regulating cancer hallmark capabilities, we show here the involvement of ROR1, known as a receptor for WNT5A, in CS-E-mediated upregulation of invasion activity in MDA-MB-231 cells (14). Particular attention has been paid to the functional and clinical significance of ROR1 in many malignancies, including breast cancer. ROR1 is present in breast cancer specimens, but not in normal breast tissues (26), and high expression of ROR1 in breast cancer is associated with aggressive phenotype (27, 28). Several therapeutic strategies targeting ROR1 have been developed and evaluated in clinical trials (15).

ROR1 is a transmembrane receptor that contains extracellular, transmembrane, and cytoplasmic domains. The extracellular region includes immunoglobulin-like, cysteine-rich (CRD), and Kringle domains. Although ligands for ROR1 have not been identified for many years, it is now known that

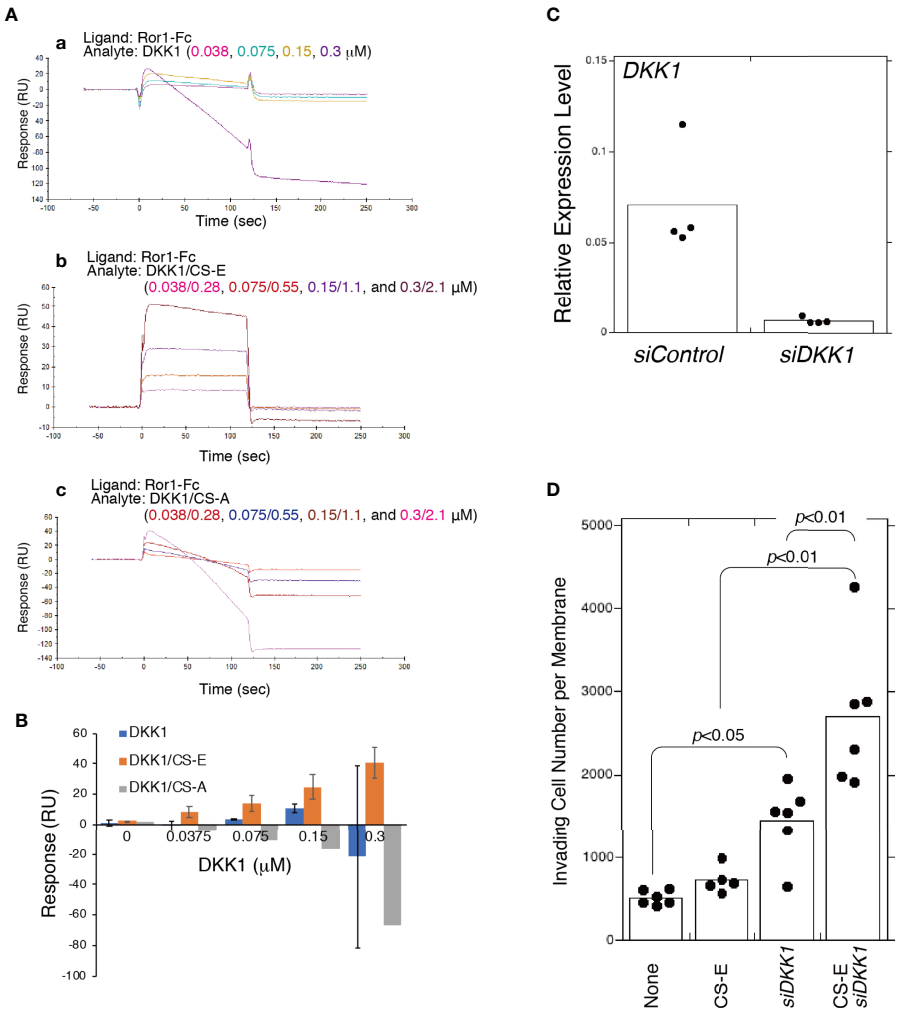

FIGURE 6 | CS-E-elicited invasiveness is enhanced by the absence of DKK1. **(A)** Raw sensor grams. ROR1 was immobilized in a flow cell of a CM5 sensor chip. DKK1 alone **(a)**, DKK1 premixed with CS-E at a 1:7 molar ratio **(b)**, and DKK1 premixed with CS-A at a 1:7 molar ration **(c)** were used as analytes. **(B)** Response-unit quantification of binding. **(C)** *DKK1* mRNA expression in MDA-MB-231 cells transfected with *siDKK1* or control siRNA (*siCont*) measured using qPCR (n=4). Expression data were normalized to those of *GAPDH*. **(D)** Invasiveness of *DKK1* knocked down MDA-MB-231 cells (*siDKK1*) or control cells (*siCont*) treated with or without CS-E (n>5). Data were analyzed using a Tukey–Kramer multiple comparison.

ROR1 is a receptor for WNT5A/B and WNT16, with WNT5A as the primary ligand (15, 29, 30). The CRD of ROR1 is thought to interact with WNT5A (31, 32). Although Fukuda et al. showed *in vitro* binding of ROR1 to WNT5A using immunoprecipitated WNT5A expressed in CHO cells (27), the possibility that CSs mediate binding between ROR1 and WNT5A cannot be excluded. We analyzed the direct interaction between recombinant ROR1 and WNT5A using Biacore, but unexpectedly, we observed no binding in the absence of CS (**Figure 5**). The cell-surface chondroitin sulfate proteoglycan functions as a coreceptor in WNT5A–ROR1 signaling (**Figure 7**). Further studies are needed to clarify whether CS-E universally act on WNT5A-ROR1 signaling using other ROR1-positive and estrogen-negative cell lines.

CS Sulfation and Cell Signaling in Cancer

Extensive evidence supports the importance of tumor-associated CSs in promoting aggressive and metastatic behavior of malignant cells by engaging transmembrane receptors (4, 33). In addition, it has been reported that cancer-cell surface CS chains facilitate downstream signal transduction through specific binding to adhesion molecules, including selectins and N-cadherin (14, 34). CS activity is governed by specific sulfation patterns. As mentioned in *Introduction*, CS is modified by sulfation by multiple sulfotransferases, including CHST11 and CHST15, which are involved in the synthesis of E units and are upregulated in breast cancer cells (4, 10). Although E units have low abundance in mammals, they play a critical role in regulating tumor progression and metastasis (35, 36). We have previously

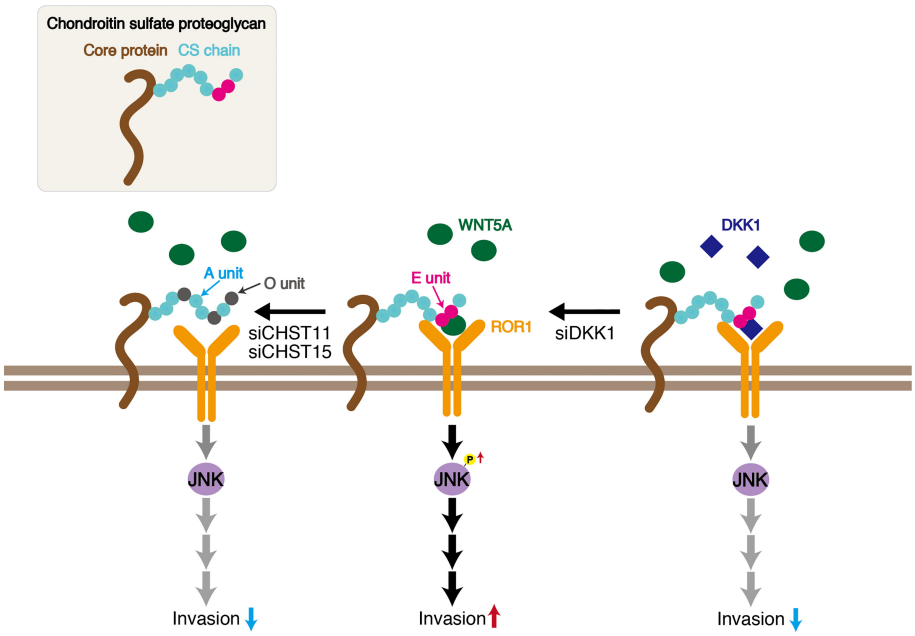

FIGURE 7 | Schematic of CS-E enhancement of invasive activity of the triple-negative breast cancer MDA-MB-231 cell line. CS chains bind WNT5A and ROR1 through E units, signaling cancer cells to activate JNK1. Decreasing E units by knockdown of *CHST11* and *CHST15* inhibits WNT5A–ROR1–JNK signaling. DKK1 suppresses CS tumor promoting activity by binding to E units.

reported that CSs rich in E units (CS-E) utilize N-cadherin as a receptor and control β-catenin signaling *via* N-cadherin in the human basal-like breast cancer cell line BT-549. In this study, we showed that the E unit is required for the binding of WNT5A to ROR1 (**Figure 7**). CSs rich in A-units (CS-A) did not mediate the interaction between WNT5A and ROR1. A decline in the expression levels of CHST11 and CHST15, which are involved in the synthesis of E units, suppresses the invasive activity of MDA-MB-231 cells (**Figure 7**). Thus, CS-E likely contributes to breast cancer malignancy. Further studies are needed to elucidate whether cancer-cell-derived CS-E promotes tumor growth and metastasis *in vivo*.

Changes in the degree of sulfation and/or the pattern of CSs and the expression level of Chn sulfotransferases are associated with cancer; these changes have been proposed as cancer biomarkers (37). Furthermore, the degree of sulfation and/or the pattern of CSs exhibit person-to-person variations. In addition, the same cancers at different stages are associated with different sulfation changes (38). Thus, identifying tumor subtypes using CS sulfation patterns may have potential applications in patient stratification for therapy. CS sulfation patterns are thus key components in future diagnostic and therapeutic strategies and provide novel targets for improved and personalized cancer therapy (39).

Another CS-E Partner Protein, DKK1

DKK1 was originally characterized as a secreted inhibitor of canonical WNT signaling. It binds to LRP5/6 coreceptors with high affinity and blocks β-catenin-dependent WNT signaling (40). MDA-MB-231 cells express high levels of DKK1 but LRP5/6 at low levels (14). We have previously shown that DKK1 binds to CS-E in a sulfation-dependent manner (14). Furthermore, recent studies have shown that elevated DKK1 expression contributes to tumor growth and poor prognosis in a range of cancers, suggesting a role in tumor aggressiveness independent of WNT signaling (16). Cytoskeleton-associated protein 4 (CKAP4) is a novel DKK1 receptor that binds to DKK1 to activate AKT signaling and enhance cancer cell proliferation (41). These findings prompted us to hypothesize that DKK1 binds to an unidentified receptor in the presence of CS-E to enhance the invasive potential of MDA-MB-231 cells. However, knockdown of *DKK1* increased invasive activity (**Figures 6**, **7**). Interestingly, invasiveness enhanced by exogenously added CS-E was further increased by knockdown of *DKK1* (**Figure 6**). These results suggested that DKK1 suppresses the tumor-promoting activity of CS-E by binding to CS-E. The ability of CS-E to function as a tumor promoter likely depends on the expression level of CS-E partner proteins such as N-cadherin, ROR1, and DKK1.

DATA AVAILABILITY STATEMENT

The raw data supporting the conclusions of this article will be made available by the authors, without undue reservation.

AUTHOR CONTRIBUTIONS

SN performed research and analyzed data. JT synthesized hexasaccharides. SN and HK wrote the manuscript. SN and HK conceived and designed the study. HK coordinated the study. All authors contributed to the article and approved the submitted version.

FUNDING

This work was supported in part by Grants-in-Aid for Scientific Research on Innovative Areas 23110003 (to HK) and Scientific Research (B) 25293014 and 20H03386 (to HK) and (C) 17K07353 and 21K06089 (to SN), and by the Support Program for Strategic Research Foundation at Private Universities 2012–2016 (to HK) from the Ministry of Education, Culture, Sports, Science, and Technology, Japan.

ACKNOWLEDGMENTS

We thank Hiroki Kinouchi, Aiko Yoshioka, Ayaka Akamatsu, Naho Otsuka, Saori Nishimura, and Koki Hamabe for technical support.

REFERENCES

1. Kang H, Wu Q, Sun A, Liu X, Fan Y, Deng X. Cancer Cell Glycocalyx and Its Significance in Cancer Progression. *Int J Mol Sci* (2018) 19:2484. doi: 10.3390/ijms19092484
2. Yang J, Price MA, Neudauer CL, Wilson C, Ferrone S, Xia H, et al. Melanoma Chondroitin Sulfate Proteoglycan Enhances FAK and ERK Activation by Distinct Mechanisms. *J Cell Biol* (2004) 165:881–91. doi: 10.1083/jcb.200403174
3. Yang J, Price MA, Li GY, Bar-Eli M, Salgia R, Jagedeeswaran R, et al. Melanoma Proteoglycan Modifies Gene Expression to Stimulate Tumor Cell Motility, Growth, and Epithelial-to-Mesenchymal Transition. *Cancer Res* (2009) 69:7538–47. doi: 10.1158/0008-5472.CAN-08-4626
4. Cooney CA, Jousheghany F, Yao-Borengasser A, Phanavanh B, Gomes T, Kieber-Emmons AM, et al. Chondroitin Sulfates Play a Major Role in Breast Cancer Metastasis: A Role for CSPG4 and CHST11 Gene Expression in Forming Surface P-Selectin Ligands in Aggressive Breast Cancer Cells. *Breast Cancer Res* (2011) 13:R58. doi: 10.1186/bcr2895
5. Willis CM, Kluppel M. Chondroitin Sulfate-E is a Negative Regulator of a Pro-Tumorigenic Wnt/beta-Catenin-Collagen 1 Axis in Breast Cancer Cells. *PloS One* (2014) 9:e103966. doi: 10.1371/journal.pone.0103966
6. Nadanaka S, Ishida M, Ikegami M, Kitagawa H. Chondroitin 4-O-Sulfotransferase-1 Modulates Wnt-3a Signaling Through Control of E Disaccharide Expression of Chondroitin Sulfate. *J Biol Chem* (2008) 283:27333–43. doi: 10.1074/jbc.M802997200
7. Nadanaka S, Kinouchi H, Taniguchi-Morita K, Tamura J, Kitagawa H. Down-Regulation of Chondroitin 4-O-Sulfotransferase-1 by Wnt Signaling Triggers Diffusion of Wnt-3a. *J Biol Chem* (2011) 286:4199–208. doi: 10.1074/jbc.M110.155093
8. Nadanaka S, Kinouchi H, Kitagawa H. Histone Deacetylase-Mediated Regulation of Chondroitin 4-O-Sulfotransferase-1 (Chst11) Gene Expression by Wnt/beta-Catenin Signaling. *Biochem Biophys Res Commun* (2016) 480:234–40. doi: 10.1016/j.bbrc.2016.10.035
9. Mikami T, Kitagawa H. Biosynthesis and Function of Chondroitin Sulfate. *Biochim Biophys Acta* (2013) 1830:4719–33. doi: 10.1016/j.bbagen.2013.06.006
10. Iida J, Dorchak J, Clancy R, Slavik J, Ellsworth R, Katagiri Y, et al. Role for Chondroitin Sulfate Glycosaminoglycan in NEDD9-Mediated Breast Cancer Cell Growth. *Exp Cell Res* (2015) 330:358–70. doi: 10.1016/j.yexcr.2014.11.002
11. Hazan RB, Phillips GR, Qiao RF, Norton L, Aaronson SA. Exogenous Expression of N-Cadherin in Breast Cancer Cells Induces Cell Migration, Invasion, and Metastasis. *J Cell Biol* (2000) 148:779–90. doi: 10.1083/jcb.148.4.779
12. Kitagawa H. Using Sugar Remodeling to Study Chondroitin Sulfate Function. *Biol Pharm Bull* (2014) 37:1705–12. doi: 10.1248/bpb.b14-00613
13. Nadanaka S, Kitagawa H. Exostosin-Like 2 Regulates FGF2 Signaling by Controlling the Endocytosis of FGF2. *Biochim Biophys Acta Gen Subj* (2018) 1862:791–9. doi: 10.1016/j.bbagen.2018.01.002
14. Nadanaka S, Kinouchi H, Kitagawa H. Chondroitin Sulfate-Mediated N-Cadherin/Beta-Catenin Signaling is Associated With Basal-Like Breast Cancer Cell Invasion. *J Biol Chem* (2018) 293:444–65. doi: 10.1074/jbc.M117.814509
15. Zhao Y, Zhang D, Guo Y, Lu B, Zhao ZJ, Xu X, et al. Tyrosine Kinase ROR1 as a Target for Anti-Cancer Therapies. *Front Oncol* (2021) 11:680834. doi: 10.3389/fonc.2021.680834
16. Kagey MH, He X. Rationale for Targeting the Wnt Signalling Modulator Dickkopf-1 for Oncology. *Br J Pharmacol* (2017) 174:4637–50. doi: 10.1111/bph.13894
17. Kitazawa K, Nadanaka S, Kadomatsu K, Kitagawa H. Chondroitin 6-Sulfate Represses Keratinocyte Proliferation in Mouse Skin, Which is Associated With Psoriasis. *Commun Biol* (2021) 4:114. doi: 10.1038/s42003-020-01618-5
18. Nadanaka S, Zhou S, Kagiyama S, Shoji N, Sugahara K, Sugihara K, et al. EXTL2, a Member of the EXT Family of Tumor Suppressors, Controls Glycosaminoglycan Biosynthesis in a Xylose Kinase-Dependent Manner. *J Biol Chem* (2013) 288:9321–33. doi: 10.1074/jbc.M112.416909
19. Nadanaka S, Hashiguchi T, Kitagawa H. Aberrant Glycosaminoglycan Biosynthesis by Tumor Suppressor EXTL2 Deficiency Promotes Liver Inflammation and Tumorigenesis Through Toll-Like 4 Receptor Signaling. *FASEB J* (2020) 34:8385–401. doi: 10.1096/fj.201902076R
20. Menck K, Heinrichs S, Baden C, Bleckmann A. The WNT/ROR Pathway in Cancer: From Signaling to Therapeutic Intervention. *Cells* (2021) 10:142. doi: 10.3390/cells10010142
21. Oishi I, Suzuki H, Onishi N, Takada R, Kani S, Ohkawara B, et al. The Receptor Tyrosine Kinase Ror2 Is Involved in non-Canonical Wnt5a/JNK Signalling Pathway. *Genes Cells* (2003) 8:645–54. doi: 10.1046/j.1365-2443.2003.00662.x
22. Pukrop T, Klemm F, Hagemann T, Gradl D, Schulz M, Siemes S, et al. Wnt 5a Signaling is Critical for Macrophage-Induced Invasion of Breast Cancer Cell Lines. *Proc Natl Acad Sci USA* (2006) 103:5454–9. doi: 10.1073/pnas.0509703103
23. Klemm F, Bleckmann A, Siam L, Chuang HN, Rietkotter E, Behme D, et al. Beta-Catenin-Independent WNT Signaling in Basal-Like Breast Cancer and Brain Metastasis. *Carcinogenesis* (2011) 32:434–42. doi: 10.1093/carcin/bgq269
24. Comsa S, Cimpean AM, Raica M. The Story of MCF-7 Breast Cancer Cell Line: 40 Years of Experience in Research. *Anticancer Res* (2015) 35:3147–54.
25. Hasan MK, Widhopf GF 2nd, Zhang S, Lam SM, Shen Z, Briggs SP, et al. Wnt5a Induces ROR1 to Recruit Cortactin to Promote Breast-Cancer Migration and Metastasis. *NPJ Breast Cancer* (2019) 5:35. doi: 10.1038/s41523-019-0131-9
26. Zhang S, Chen L, Cui B, Chuang HY, Yu J, Wang-Rodriguez J, et al. ROR1 is Expressed in Human Breast Cancer and Associated With Enhanced Tumor-Cell Growth. *PloS One* (2012) 7:e31127. doi: 10.1371/journal.pone.0031127
27. Fukuda T, Chen L, Endo T, Tang L, Lu D, Castro JE, et al. Antisera Induced by Infusions of Autologous Ad-CD154-Leukemia B Cells Identify ROR1 as an Oncofetal Antigen and Receptor for Wnt5a. *Proc Natl Acad Sci U.S.A.* (2008) 105:3047–52. doi: 10.1073/pnas.0712148105
28. Balakrishnan A, Goodpaster T, Randolph-Habecker J, Hoffstrom BG, Jalikis FG, Koch LK, et al. Analysis of ROR1 Protein Expression in Human Cancer and Normal Tissues. *Clin Cancer Res* (2017) 23:3061–71. doi: 10.1158/1078-0432.CCR-16-2083
29. Karvonen H, Perttila R, Niininen W, Hautanen V, Barker H, Murumagi A, et al. Wnt5a and ROR1 Activate Non-Canonical Wnt Signaling *via* RhoA in

TCF3-PBX1 Acute Lymphoblastic Leukemia and Highlight New Treatment Strategies *via* Bcl-2 Co-Targeting. *Oncogene* (2019) 38:3288–300. doi: 10.1038/s41388-018-0670-9
30. Sheikh MA, Kong X, Haymart B, Kaatz S, Krol G, Kozlowski J, et al. Comparison of Temporary Interruption With Continuation of Direct Oral Anticoagulants for Low Bleeding Risk Procedures. *Thromb Res* (2021) 203:27–32. doi: 10.1016/j.thromres.2021.04.006
31. Masiakowski P, Yancopoulos GD. The Wnt Receptor CRD Domain Is Also Found in MuSK and Related Orphan Receptor Tyrosine Kinases. *Curr Biol* (1998) 8:R407. doi: 10.1016/S0960-9822(98)70263-5
32. Saldanha J, Singh J, Mahadevan D. Identification of a Frizzled-Like Cysteine Rich Domain in the Extracellular Region of Developmental Receptor Tyrosine Kinases. *Protein Sci* (1998) 7:1632–5. doi: 10.1002/pro.5560070718
33. Theocharis AD, Skandalis SS, Tzanakakis GN, Karamanos NK. Proteoglycans in Health and Disease: Novel Roles for Proteoglycans in Malignancy and Their Pharmacological Targeting. *FEBS J* (2010) 277:3904–23. doi: 10.1111/j.1742-4658.2010.07800.x
34. Kastana P, Choleva E, Poimenidi E, Karamanos N, Sugahara K, Papadimitriou E. Insight Into the Role of Chondroitin Sulfate E in Angiogenesis. *FEBS J* (2019) 286:2921–36. doi: 10.1111/febs.14830
35. Vallen MJ, Schmidt S, Oosterhof A, Bulten J, Massuger LF, Van Kuppevelt TH. Primary Ovarian Carcinomas and Abdominal Metastasis Contain 4,6-Disulfated Chondroitin Sulfate Rich Regions, Which Provide Adhesive Properties to Tumour Cells. *PloS One* (2014) 9:e111806. doi: 10.1371/journal.pone.0111806
36. Li J, Sparkenbaugh EM, Su G, Zhang F, Xu Y, Xia K, et al. Enzymatic Synthesis of Chondroitin Sulfate E to Attenuate Bacteria Lipopolysaccharide-Induced Organ Damage. *ACS Cent Sci* (2020) 6:1199–207. doi: 10.1021/acscentsci.0c00712
37. Weyers A, Yang B, Yoon DS, Park JH, Zhang F, Lee KB, et al. A Structural Analysis of Glycosaminoglycans From Lethal and Nonlethal Breast Cancer Tissues: Toward a Novel Class of Theragnostics for Personalized Medicine in Oncology? *OMICS* (2012) 16:79–89. doi: 10.1089/omi.2011.0102
38. Soares Da Costa D, Reis RL, Pashkuleva I. Sulfation of Glycosaminoglycans and Its Implications in Human Health and Disorders. *Annu Rev BioMed Eng* (2017) 19:1–26. doi: 10.1146/annurev-bioeng-071516-044610
39. Mereiter S, Balmana M, Campos D, Gomes J, Reis CA. Glycosylation in the Era of Cancer-Targeted Therapy: Where Are We Heading? *Cancer Cell* (2019) 36:6–16. doi: 10.1016/j.ccell.2019.06.006
40. Bafico A, Liu G, Yaniv A, Gazit A, Aaronson SA. Novel Mechanism of Wnt Signalling Inhibition Mediated by Dickkopf-1 Interaction With LRP6/Arrow. *Nat Cell Biol* (2001) 3:683–6. doi: 10.1038/35083081
41. Kimura H, Fumoto K, Shojima K, Nojima S, Osugi Y, Tomihara H, et al. CKAP4 is a Dickkopf1 Receptor and Is Involved in Tumor Progression. *J Clin Invest* (2016) 126:2689–705. doi: 10.1172/JCI84658

Conflict of Interest: The authors declare that the research was conducted in the absence of any commercial or financial relationships that could be construed as potential conflicts of interest.

Publisher's Note: All claims expressed in this article are solely those of the authors and do not necessarily represent those of their affiliated organizations, or those of the publisher, the editors and the reviewers. Any product that may be evaluated in this article, or claim that may be made by its manufacturer, is not guaranteed or endorsed by the publisher.

Copyright © 2022 Nadanaka, Tamura and Kitagawa. This is an open-access article distributed under the terms of the Creative Commons Attribution License (CC BY). The use, distribution or reproduction in other forums is permitted, provided the original author(s) and the copyright owner(s) are credited and that the original publication in this journal is cited, in accordance with accepted academic practice. No use, distribution or reproduction is permitted which does not comply with these terms.

frontiers | Frontiers in Oncology

ORIGINAL RESEARCH
published: 03 June 2022
doi: 10.3389/fonc.2022.917633

ESR2 Drives Mesenchymal-to-Epithelial Transition in Triple-Negative Breast Cancer and Tumorigenesis *In Vivo*

Zoi Piperigkou[1,2], Anastasios Koutsandreas[1], Marco Franchi[3], Vasiliki Zolota[4], Dimitrios Kletsas[5], Alberto Passi[6] and Nikos K. Karamanos[1,2*]*

[1] Biochemistry, Biochemical Analysis and Matrix Pathobiology Research Group, Laboratory of Biochemistry, Department of Chemistry, University of Patras, Patras, Greece, [2] Foundation for Research and Technology-Hellas (FORTH)/Institute of Chemical Engineering Sciences (ICE-HT), Patras, Greece, [3] Department for Life Quality Study, University of Bologna, Rimini, Italy, [4] Department of Pathology, School of Medicine, University of Patras, Patras, Greece, [5] Laboratory of Cell Proliferation and Ageing, Institute of Biology, National Centre for Scientific Research (N.C.S.R). "Demokritos", Athens, Greece, [6] Department of Medicine and Surgery, University of Insubria, Varese, Italy

OPEN ACCESS

Edited by:
Daniele Vergara,
University of Salento, Italy

Reviewed by:
Akshita Bhatt,
St. Jude Children's Research Hospital, United States
Wanessa Altei,
Barretos Cancer Hospital, Brazil

***Correspondence:**
Zoi Piperigkou
zoipip@upatras.gr
Nikos K. Karamanos
n.k.karamanos@upatras.gr

Specialty section:
This article was submitted to Molecular and Cellular Oncology, a section of the journal Frontiers in Oncology

Received: 11 April 2022
Accepted: 09 May 2022
Published: 03 June 2022

Citation:
Piperigkou Z, Koutsandreas A, Franchi M, Zolota V, Kletsas D, Passi A and Karamanos NK (2022) ESR2 Drives Mesenchymal-to-Epithelial Transition in Triple-Negative Breast Cancer and Tumorigenesis In Vivo. Front. Oncol. 12:917633. doi: 10.3389/fonc.2022.917633

Estrogen receptors (ERs) have pivotal roles in the development and progression of triple-negative breast cancer (TNBC). Interactions among cancer cells and tumor microenvironment are orchestrated by the extracellular matrix that is rapidly emerging as prominent contributor of fundamental processes of breast cancer progression. Early studies have correlated ERβ expression in tumor sites with a more aggressive clinical outcome, however ERβ exact role in the progression of TNBC remains to be elucidated. Herein, we introduce the functional role of ERβ suppression following isolation of monoclonal cell populations of MDA-MB-231 breast cancer cells transfected with shRNA against human *ESR2* that permanently resulted in 90% reduction of ERβ mRNA and protein levels. Further, we demonstrate that clone selection results in strongly reduced levels of the aggressive functional properties of MDA-MB-231 cells, by transforming their morphological characteristics, eliminating the mesenchymal-like traits of triple-negative breast cancer cells. Monoclonal populations of shERβ MDA-MB-231 cells undergo universal matrix reorganization and pass on a mesenchymal-to-epithelial transition state. These striking changes are encompassed by the total prevention of tumorigenesis *in vivo* following ERβ maximum suppression and isolation of monoclonal cell populations in TNBC cells. We propose that these novel findings highlight the promising role of ERβ targeting in future pharmaceutical approaches for managing the metastatic dynamics of TNBC breast cancer.

Keywords: breast cancer, ESR2, estrogen receptor beta, tumorigenesis, extracellular matrix

INTRODUCTION

Human cancers arise from multistep processes that make their way from normalcy to the acquisition of particular hallmark traits during complex tumorigenic signaling cascades (1). Breast cancer is characterized by a great heterogeneity in its molecular subtypes, therefore important breakthroughs reducing relapse and providing higher quality years of life may be accomplished in treatment approaches.

Estrogens as master regulators of breast cancer susceptibility, mediate their effects in target tissues through two estrogen receptors (ERs), ERα and ERβ. ERs and their variants exert distinct functions following activation in response to ligand binding and trigger genomic and non-genomic signaling cascades (2). Many lines of evidence suggest that in breast cancer, ER-evoked signaling is closely connected to extracellular matrix (ECM) remodeling that stimulates cancer progression, metastasis and drug resistance (3). The role of tumor ECM has long been recognized as a dynamic 3D structural and functional network of biomolecules that dynamically interact to reinforce cancer cell properties (4). Major matrix components of this functional bioscaffold consist, among other constituents, of collagen, proteoglycans (PGs), glycosaminoglycans (GAGs), adhesive glycoproteins, fibrils and degrading enzymes, that actively communicate to orchestrate ECM renewal, cell morphology and functional properties of cancer cells (5–7). The integrity of ECM composition is critical for normal tissue homeostasis, since altered expression of ECM macromolecules in the tumor microenvironment (TME) affects cancer cell survival, growth, migration, and invasion to adjacent tissues (8, 9). The triple-negative breast carcinoma (TNBC), accounting for up to 20% of breast carcinomas, is the aggressive molecular subtype of breast cancer, characterized by the absence of ERα, progesterone receptor (PgR), and HER2. Population-based studies show that TNBC is more common to younger age groups of premenopausal African American and Hispanic women compared to Caucasian American women (10).

There is increasing evidence that the second ER isoform, ERβ, which is localized in myoepithelial cells as well as in the surrounding stroma and endothelial cells, is highly expressed and correlated to worse survival rates in TNBC patients (3, 11). The discovery of ERβ in 1996 as the second nuclear receptor for steroid/thyroid hormones (i.e., 17β-estradiol, E2), after ERα, reserved a new era in the diagnosis, survival estimation and therapeutic targeting of breast cancer (12). While less well established, ERβ dynamically communicates with major matrix components, including PGs and epidermal growth factor receptor (EGFR) to stimulate cancer cell behavior, epithelial-to-mesenchymal transition (EMT) and stem-like characteristics (13–15).

EMT is an evolutionarily conserved developmental program in which cells gradually unbend tight cell junctions due to the decreased expression of epithelial proteins (i.e., E-cadherin) and gain mesenchymal traits through epigenetic alterations, reorganized cytoskeleton and the expression of mesenchymal matrix markers, such as fibronectin and vimentin (16). This process is the driving force of cancer cells to increased motility and initiation of metastasis, through matrix remodeling and the activation of signaling cascades (i.e., Notch, TGFβ) and a possible mechanistic basis for anticancer drug resistance (17, 18).

The daunting consequences of TNBC arise from matrix extensive reorganization and EMT activation builds the aggressive cancer cell behavior that establishes the initiation of metastasis. These functional capabilities acquired by TNBC cells may be the motive power to advance modern TNBC targeting approaches for the diagnosis and personalized therapeutic management. Recent work has revealed some encouraging data correlating *ESR2* suppression in TNBC cells with a less aggressive cell phenotype (14, 19, 20). Similar to other receptors for steroid hormones, ERβ, encoded by *ESR2* gene, is expressed as a pool of five alternatively spliced variants; the wild-type, ERβ1 and also ERβ2, ERβ3, ERβ4 and ERβ5, which exist in normal and disease states (2). In breast cancer tissues, the most common ERβ variants are ERβ1, ERβ4 and ERβ5, which may be dimerized in order to boost signal transduction processes (21, 22). This explains that shERβ MDA-MB-231 cells demonstrated phenotypic heterogeneity that was reflected in deviant phenotype and *ESR2* mRNA levels; from 70% to 80% inconstant decrease in *ESR2* levels and intrigued us to achieve higher ERβ gene and protein suppression rates to exclude the impact of ERβ variants on heterogenous profile of ERβ-suppressed cells.

Herein, we report for the first time that the isolation of monoclonal cell populations, characterized by ERβ knockdown, led to cultures with a constant epithelial-like behavior. Certainly, such clues force further investigation ERβ as a power player of the tumor microenvironment of TNBC cells. This prompted us to further elucidate the functional effects of ERβ knockdown as compared to parental breast cancer cell lines with distinct ER status, as well as the *in vivo* tumorigenic effects of monoclonal shERβ MDA-MB-231 cell populations. A detailed molecular understanding of ERβ functions is critical in identifying its promising role in TNBC targeting.

MATERIALS AND METHODS

Cell Cultures, Transfections and Selection of Monoclonal Cell Populations

MDA-MB-231 (high metastatic potential; ERβ-positive) and MCF-7 (low metastatic potential; ERα-positive) breast cancer cell lines were obtained from the American Type Culture Collection (ATCC). MDA-MB-231 cells were routinely cultured in a humidified 95% air/5% CO_2 incubator at 37°C in complete medium [Dulbecco's Modified Eagle's Medium (DMEM) supplemented with 10% fetal bovine serum (FBS), 1.0 mM sodium pyruvate, 2 mM L-glutamine and a cocktail of antimicrobial agents (100 IU/ml penicillin, 100 μg/ml streptomycin, 10 μg/ml gentamicin sulfate and 2.5 μg/ml amphotericin B)]. Cells were harvested by trypsinization with 0.05% (w/v) trypsin in PBS containing 0.02% (w/v) Na_2EDTA. Transfections of MDA-MB-231 cells with shRNA against human *ESR2* or non-targeting shRNA control were performed as

previously described by Piperigkou et al. (14), and ERβ suppression was monitored with real-time PCR analysis and western blot analysis.

Since the cultures of stably transfected shERβ MDA-MB-231 cells were heterogenous in respect of *ESR2* levels, the isolation of monoclonal cell populations (clone selection) was performed to identify single clones with the highest *ESR2* suppression levels, as follows. Briefly, 10 cells/ml of shERβ MDA-MB-231 cells were seeded in a 96-well culture plate adding 100 μl per well (i.e., 1 cell per well), the number of cells per well after 24 hours was assessed and the wells with only 1 cell were noted. The monoclonal population has been expanded and passaged to 6-well plates. A portion of cells was examined for the levels of ESR2 suppression and expression stability and the cultures were further expanded. Finally, suppressed clones (~90% ESR2/ERβ suppression) were freezed down and named "clone shERβ MDA-MB-231" cells). Notably, during the freeze-thaw cycle of clone shERβ MDA-MB-231 cells the suppression rates of *ESR2* and ERβ are totally stable, as confirmed by real-time PCR and western blot analysis, respectively.

Chemicals and Reagents

DMEM, FBS, L-glutamine, penicillin, streptomycin were all obtained from Biosera (Nuaillé, France). All other chemicals used were of the best commercially available grade.

RNA Isolation, Reverse Transcription and Real-Time qPCR Analysis

Total cellular RNA was isolated using NucleoSpin RNA II Kit (Macherey-Nagel, Duren, Germany). The amount of isolated RNA was quantified by measuring its absorbance at 260 nm. Total RNA was reverse transcribed using the PrimeScript 1st strand cDNA synthesis kit perfect real time (Takara Bio Inc., Japan). Real-time qPCR analysis was conducted in 20 μl reaction mixture, according to manufacturer's instructions (KAPA Taq ReadyMix DNA Polymerase, KAPA BIOSYSTEMS, Wilmington, Massachusetts). The amplification was performed utilizing Rotor Gene Q (Qiagen, USA). All reactions were performed in triplicates and a standard curve was always included for each pair of primers for assay validation. In addition, a melting curve analysis was always performed for detecting the SYBR Green-based objective amplicon. To provide quantification, the point of product accumulation in the early logarithmic phase of the amplification plot was defined by assigning a fluorescence threshold above the background, defined as the threshold cycle (Ct) number. Relative expression of different gene transcripts was calculated by the ΔΔCt method. The Ct value of any gene of interest was normalized to the Ct of the normalizer (GAPDH). Fold changes (arbitrary units) were determined as $2^{-\Delta\Delta Ct}$. Primer sequences of the tested genes are presented in **Supplementary Table 1**. All primers were purchased from Eurofins Genomics (Ebersberg, Germany).

Tumorigenicity Assay

An equal number (106) of MDA-MB-231 or clone shERβ MDA-MB-231 cells was inoculated in the back of seven 5-weeks-old SCID female mice. Four weeks later, the animals were sacrificed, and the tumors formed following MDA-MB-231 inoculations were removed. The tumor volume was calculated with the Caliper method, using the formula tumor volume = 1/2(length × width^2) (23). Tumor samples developed from MDA-MB-231 cells were mechanically homogenized in the presence of liquid nitrogen and stored in -80°C. All animal studies were conducted according to the institutional guidelines conforming to international standards and the protocols were approved by the relevant committee of the Veterinary Direction, Greek Ministry of Rural Development and Food (Permission No. 193900).

Immunohistochemistry

Serial 3μm paraffin sections were cut from tissue blocks, mounted on poly-L-lysine-coated slides and subjected to immunohistochemical staining. Briefly, the sections were initially dried for 24 hours at 60°C, deparaffinized in xylene and dehydrated in gradient alcohol. Antigen retrieval was performed at 600W in a microwave for 20 minutes. Endogenous peroxidase blocking was performed by incubating the slides in a 3% H_2O_2 solution for 15 minutes. Sections were then incubated with the following primary antibodies against: ERα, clone 6F11 (Leica Biosystems), Ki-67 IHC MIB-1 (DAKO, mouse monoclonal, 1:50), HER2 (DAKO, Rabbit polyclonal, 1:300), E-cadherin (DAKO, mouse monoclonal, 1:50), vimentin, clone V9 (Leica Biosystems). Dako EnVision polymer (Dako EnVision Mini Flex, Dako Omnis, Angilent Technology Inc., California, USA, GV823) was used for signal detection. Diaminobenzidine (Dako Omnis, GV823) was used as a chromogen and Harris hematoxylin was used for nuclear counterstaining. Positive and negative controls for antibody validation were used according to the manufacturer's instructions.

Western Blot Analysis

Cell monolayers were washed with cold PBS and lysed with Lysis Buffer: 25 mM Hepes, pH 7.5, 150 mM NaCl, 5 mM EDTA, 10% (v/v) glycerol, 1% (v/v) Triton X-100, containing protease inhibitor cocktail (#20-201 Chemicon, Millipore, CA) and 0.5 mM sodium orthovanadate (S6508, Sigma-Aldrich, Inc). Samples were reduced with β-mercaptoethanol in Laemmli sample buffer, separated by SDS-PAGE in 12% poly-acrylamide gels and transferred to polyvinylidene difluoride (PVDF) membranes (Macherey Nagel, Germany). The membranes were blocked in 5% (w/v) non-fat dry milk in Tris-buffered saline pH 7.4 containing 0.05% Tween-20 (TBS-T) for 2 hours at room temperature and were then incubated with primary antibodies for 16 hours at 4°C. After three washes in TBS-T, membranes were further incubated with peroxidase-conjugated secondary goat anti-rabbit IgG (A0545, Sigma-Aldrich, Inc) or anti-mouse IgG (A4416, Sigma-Aldrich, Inc) for 90 minutes at room temperature. Detection of the immunoreactive proteins was performed by chemiluminescence horseradish peroxidase substrate Super Signal (Pierce, Thermoscientific), according to the manufacturer's instructions. Primary antibodies used in immunoblotting include ERβ (ab3576, abcam), p-ERK1/2 (9101, Cell Signaling Technology, dilution 1:1000), total ERK1/2 (9102,

Cell Signaling Technology, dilution 1:1000) and α-tubulin (T9026, Sigma-Aldrich Inc., dilution 1:7500). ImageJ software has been used for measuring the band density.

Immunofluorescence and Phase-Contrast Microscopy

For immunofluorescence microscopy, parental and transfected breast cancer cells were seeded on glass coverslips in 24-well plates and grown to confluence. Cells were first washed twice with phosphate-buffered saline (PBS) buffer, fixed in 4% formaldehyde in PBS buffer, washed three times with PBS-Tween buffer, permeabilized with freshly made 0.5% Triton X-100 in PBS, washed three times with PBS-Tween buffer and blocked with 5% BSA in PBS. Slides were stained for E-cadherin, vimentin and F-actin with the following primary antibodies: E-cadherin (ECCD-2, Takara, dilution 1:200) and Alexa-Fluor 568-labeled phalloidin (Invitrogen Corporation, Carlsbad, USA, dilution 1:100. Then the appropriate Alexa Fluor-488 anti-mouse (A-11032, Invitrogen, dilution 1:2000) secondary antibody was used for E-cadherin staining and the coverslips were mounted on microscope slides. Stained slides with the appropriate secondary antibodies alone were used as negative controls. For phase-contrast microscopy, images of live cells growing on the culture dish were collected on an OLYMPUS CKX41 microscope equipped with a CMOS color digital camera (SC30). Cell circularity was monitored using the ImageJ plugin that calculates object circularity using the formula: circularity= $4pi(area/perimeter^2)$. This formula was applied to each cell of 10 representative digital images of parental and transfected breast cancer cells. A circularity value of 1.0 indicates a perfect circle. As the value approaches 0.0, it indicates an increasingly elongated polygon.

Scanning Electron Microscopy

Parental and transfected breast cancer cells seeded in culture flasks for 48 hours, were firstly rinsed with a phosphate buffer solution to prevent cells detachment and then fixed in a Karnovsky's solution for 20 minutes. Flasks with adhering cells were again rinsed three times with 0.1% cacodylate buffer, post-fixed in 1% OsO_4 in cacodylate buffer for 20 minutes, dehydrated with increasing concentrations of ethanol, and finally dehydrated with hexamethyldisilazane (Sigma-Aldrich Inc.) for 15 minutes. The specimens were mounted on appropriate stubs, coated with a 5nm palladium gold film (Emitech 550 sputter-coater) to be observed under a SEM (Philips 515, Eindhoven, The Netherlands) operating in secondary-electron mode.

Cell Viability Assay

Parental and transfected breast cancer cells were seeded in the presence of FBS into 96-well plates at a density of 5,000 cells/well and then the cells were incubated in serum-free culture medium. Premix WST-1 (water-soluble tetrazolium salt) Cell Proliferation Assay System (Takara Bio Inc., Japan) was added after 24 hours at a ratio 1:10. The assay is based on the reduction of WST-1 by viable cells, producing a soluble formazan salt absorbing at 450 nm (reference wavelength at 650 nm).

Wound Healing Assay

Parental and transfected breast cancer cells were seeded in 12-well cell culture plates at a density of 25,000 cells/well. Breast cancer confluent cell layers were serum starved for 16 hours and then wounded by scratching with a sterile 100 μl pipette tip. Detached cells were removed by washing twice with PBS and fresh culture medium, in the absence of FBS, was added. The wound closure was monitored at 0 and 24 hours using a digital camera connected to a microscope. Wound surface area was quantified by image analysis (Image J software).

Collagen Invasion Assay

The invasive potential of parental and transfected breast cancer cells was evaluated as previously described (24). In brief, the collagen type I solution with final concentration of 1 mg/ml was prepared by mixing the precooled components: 4 volumes collagen type I (stock concentration 3 mg/ml), 5 volumes of CMF-HBSS, 1 volume of MEM (10x), 1 volume of 0.25 M $NaHCO_3$, 2.65 volumes of standard medium and 0.3 volumes of 1M NaOH. The solution was gently mixed and added to one well of 12-well plate, spread homogeneously and let gelify in a humidified atmosphere of 10% CO_2 at 37°C for at least 1 hour. Cells were serum-starved overnight and then seeded at a density of $6x10^4$ cells/well on top of collagen I type gels and cultured for 24 hours. Digital images were obtained with 10x objective and the evaluation of cell invasion was conducted according to the experimental protocol (24).

Cell Adhesion Assays

In order to evaluate the adhesion potential of breast cancer cells, the following adhesion protocol was performed, as previously described (25). Briefly, 96-well plate was coated with collagen type I (40 μg/ml) and kept at 4°C. After 12 hours, the solution was removed, and the plate was air-dried; 3% BSA in PBS solution was added in each well, for 30 minutes, to block non-specific adsorption. Then the solution was removed, and the plate was washed with PBS and air-dried. Cells treated for 24 hours prior to the adhesion assay were detached with PBS-EDTA 1x and resuspended in serum-free medium with 0.1% BSA. and seeded at a density of $2x10^4$ cells/well. Cells were incubated for 30 min, to allow adhesion to the surface. Non-adherent cells were removed with serum free medium, and then cells were incubated with medium supplemented with 10% FBS for 2 hours for recovery. Premix WST-1 (water-soluble tetra-zolium salt) Cell Proliferation Assay System (Takara Bio Inc., Göteborg, Sweden) was then added at a ratio 1:10, and the absorbance at 450 nm was measured (reference wavelength at 650 nm).

Prognostic Power of *ESR2*

Data on the *ESR2* isoform structure, the interactive bodymap, the signature-based statistics for normal/cancer comparison, and Kaplan-Meier overall survival were collected byGEPIA2, the online server for large-scale analysis of cancer-related genomic datasets (26). GEPIA2 is a highly cited resource for analyzing the RNA sequencing expression data of 9,736 tumors and 8,587 normal samples from the TCGA and the GTEx databases, using a

standard processing pipeline applying the bioinformatics tools CIBERSORT, EPIC and quanTIseq, and performing multiple downstream analyses. Tumor/normal differential expression analysis, profiling according to cancer types, patient survival analysis was performed.2. Kaplan-Meier overall survival analysis performed using the TCGA dataset for breast cancer invasive carcinoma. The statistical difference between the curves can be measured by the log-rank test. The package "survival" of the R statistical environment was used to calculate hazard ratio (HR), 95% confidence intervals (CI), and log-rank p-values.

Statistical Analysis

Reported values are expressed as mean ± standard deviation (SD) of experiments in triplicate. Three independent biological samples have been used in each experimental set. Statistically significant differences were evaluated using the analysis of variance (two-way ANOVA) test and were considered statistically significant at the level of at least $p \leq 0.05$. Statistical analysis and graphs were made using GraphPad Prism 8.2.1. software.

RESULTS

ESR2 Predicts Overall Survival Rates in Breast Cancer Patients

ER status is the most important discriminator of breast cancers highlighting the cardinal role of ERs as biomarkers in breast cancer progression (27). Functional studies indicate that the structural organization of main ERβ subtype suggest the ligand-induced conformational changes that explain distinct genomic and non-genomic transcriptional actions (**Figure 1A**) (3). Interactive bodymap indicates that *ESR2* is aberrantly expressed in several tumor tissues (**Figure 1B**). Regarding breast cancer, *ESR2* expression is 2-fold higher in invasive breast carcinoma as compared to normal breast tissues (**Figure 1C**). Notably, Kaplan-Meier survival analysis revealed that high levels of *ESR2* in patients with invasive breast carcinoma, demonstrate a significantly lower overall survival, as compared to breast tumors with low *ESR2* expression (**Figure 1D**). This suggests the crucial role of ERβ in prognosis of aggressive breast cancer and that its targeting may be beneficial for effective management of this malignancy.

Expression Traits of Matrix Signaling Mediators Following *ESR2* Suppression

Recent work deduced that the highest possible ERβ suppression should be achieved to avoid the heterogenous genotypic and phenotypic experimental observations resulting from the ERβ variants in MDA-MB-231 TNBC cells. The mature antisense sequences that have been developed to suppress *ESR2* target three sites: 3' untranslated region (UTR), non-coding and open reading frame (ORF). These regions are common among ERβ variants. In the direction of avoiding disorientations of still present ERβ variants, we proceeded to isolation of monoclonal cell populations in shERβ MDA-MB-231 cells as to achieve higher *ESR2* suppression rates and phenotypic homogeneity, and we named the monoclonal cell cultures, clone shERβ MDA-MB-231 cells. Indeed, clone selection in shERβ MDA-MB-231cells resulted in 90% decrease in *ESR2* levels, as compared to MDA-MB-231 cells (**Figure 2A**). Notably, *ESR2*

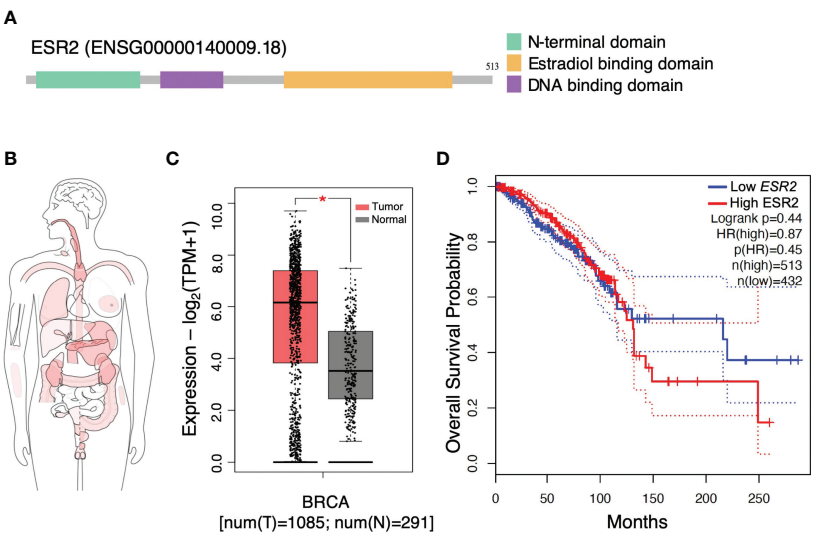

FIGURE 1 | Gene structure and expression profiling of estrogen receptor beta gene (*ESR2*). **(A)** Structure of *ESR2* alternatively spliced transcript variant aberrantly expressed in breast cancer. **(B)** Interactive bodymap presenting median expression of *ESR2* in tumor samples. Scale: $\log_2$(TPM+1); $p \leq 0.05$. **(C)** The gene expression profile across tumor samples and paired normal tissues. **(D)** *ESR2* expression is correlated to worse prognosis in breast cancer patients. GEPIA2 tool was utilized to perform these meta-analysis tests. Kaplan-Meier overall survival analysis performed using the TCGA dataset for breast cancer invasive carcinoma. The statistical difference between the curves [P value and hazard ratio (HR) value] has been calculated by the log-rank test. BRCA, breast cancer; HR, hazard ratio; TPM, transcripts per million. Asterisk (*) indicate statistically significant differences ($p \leq 0.05$).

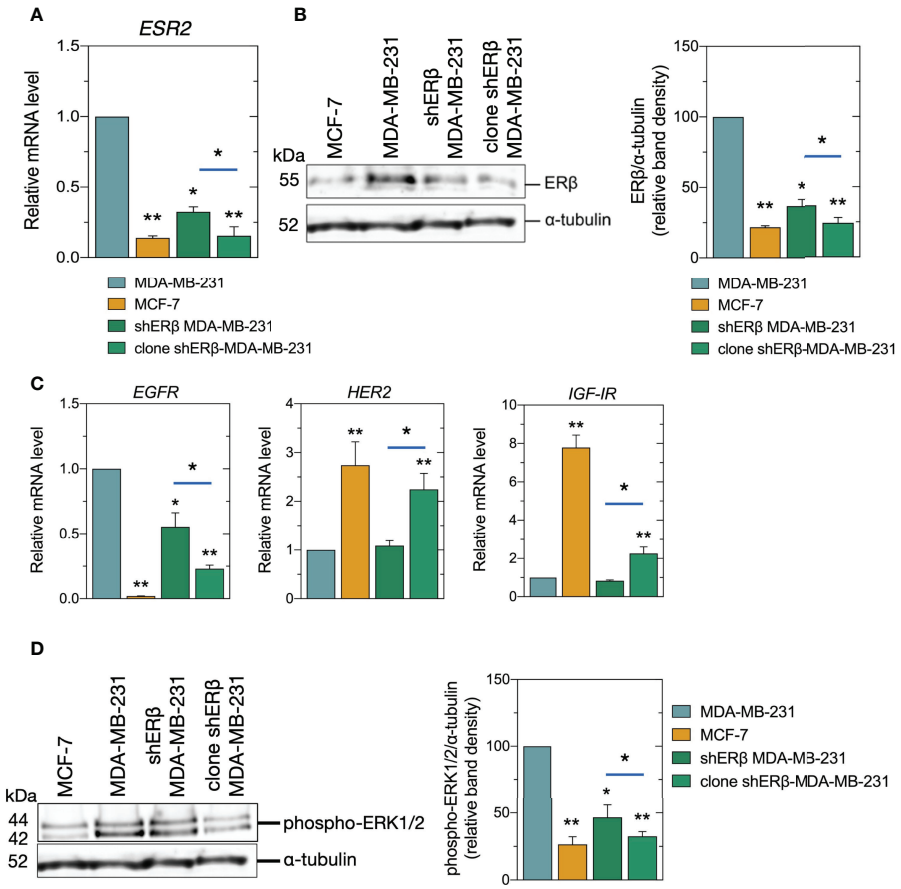

FIGURE 2 | Expression of *ESR2*, ERβ protein levels, and signaling mediators in breast cancer cells. **(A)** Real-time PCR analysis of *ESR2* in MCF-7, MDA-MB-231, shERβ MDA-MB-231 and clone shERβ MDA-MB-231 cells. **(B)** Immunoblots of ERβ and α-tubulin in the four cell lines (left panel) and quantification of protein bands (right panel). **(C)** Real-time PCR analysis of *EGFR*, *HER2* and *IGF-IR*. **(D)** Immunoblots of phospho-ERK1/2 (p44/42) and α-tubulin (left panel) and quantification of protein bands (right panel). The data are presented as the mean ± SD values (n=3). Asterisks (*), (**) indicate statistically significant differences ($p \leq 0.05$ and $p \leq 0.01$, respectively).

expression levels in clone shERβ MDA-MB-231 cells seem to resemble ERα-positive and ERβ-negative MCF-7 breast cancer cells (**Figure 2A**). These results have been confirmed by ERβ protein detection; not to mention the statistically significant 70% decrease in ERβ protein levels in clone shERβ MDA-MB-231 cells as compared to the heterogenous cultures of shERβ MDA-MB-231 cells (**Figure 2B**).

The ligand-independent ER actions include the phosphorylation of growth factor receptors and the subsequent activation of protein kinase signaling pathways to regulate transcription (28). Therefore, we further evaluated the expression and activity levels of major matrix signaling molecules, as growth factor receptors and mitogen-activated protein kinases (MAPK). It has been established that the most clinically aggressive subtypes of breast cancer, are also associated with *EGFR* overexpression (29, 30), while in ERα-positive breast cancer, IGF-IR is present at high levels and its action is correlated to ER status (31). In this study, we confirmed that the less aggressive breast cancer cell line, namely MCF-7, demonstrated a slight *EGFR* expression, and 7-fold *IGF-IR* and 2.5-fold *HER2* increased levels, respectively, as compared to MDA-MB-231 cells (**Figure 2C**). Most importantly, we demonstrated that clone shERβ MDA-MB-231 cells demonstrated 75% reduced *EGFR* levels, and a 2-fold increase in *HER2* and *IGF-IR* levels as compared to MDA-MB-231 cells, resembling the expression profile of epithelial cell line (**Figure 2C**). Notably, we did not note any significant alteration in *ESR1* levels in clone shERβ MDA-MB-231 cells. Finally, as shown in **Figure 2D**, the isolation of monoclonal population of shERβ MDA-MB-231 cells resulted in 65% reduction in the phosphorylated levels of ERK1/2 MAPK, as compared to MDA-MB-231 cells, that can be further connected to the less aggressive phenotype of this cell type.

ER Status Drives Morphological Characteristics and Metastatic Potential of Breast Cancer Cells

The inherent aggressive character of cancer cells dictates the initiation of metastasis, caused by an extensive matrix remodeling, loss of tissue organization and abnormal cell behavior (32). Changes in tumor microenvironment play

critical roles in the migrating capability of cancer cells through the EMT program where cancer cells develop mesenchymal morphology and increased invasive capacity (33, 34). SEM analysis of MDA-MB-231 2D cultures revealed different phenotypes: mainly isolated, elongated cells with lamellipodia and filopodia protrusions, but also "cobblestone"-shaped cells and a few isolated globular-like ones (**Figure 3A**). Microvilli, microvesicles and intercellular connections were also detected on the surface of MDA-MB-231 cells, explaining the highly mobile nature of TNBC cells (35). On the other hand, the epithelial morphology of ERα-positive MCF-7 cells is pursued by the formation of cell-cell contacts, tight cell junctions and cell aggregates as confirmed by SEM analysis in 2D cultures (**Figure 3A**). Ultrastructural investigations confirmed that ERβ suppression induced the development of more round and flattened cells, significant loss of cytoplasmic protrusions and cell-cell contacts as well as the tendency to form cell aggregates. Notably, when we selected and cultured monoclonal cell populations of shERβ MDA-MB-231 cells we noticed a profound elimination of cytoplasmic protrusions and the establishment of cell cultures with flattened cells (**Figure 3A**). Notably, the high suppression rates of *ESR2* have been connected with the establishment of cultures with grouped cells exhibiting a small nucleus and large cytoplasm, no evident cytoplasmic protrusions (**Figure 3A**, right panel) and evident cell-cell contacts. Moreover, tight junctions and few microvesicles were detectable on the surface of clone shERβ MDA-MB-231 cells (**Figure 3A**, right panel).

We further analyzed the morphological characteristics of breast cancer cells with different ER status, in respect of cell circularity (**Figure 3B**). It is well established that the architecture of tumor microenvironment constructs cancer cell characteristics, thus predicting the tumor biological behavior and invasive potential (4, 36, 37). Of note, as the value of circularity approaches 0.0, it indicates an increasingly elongated polygon; a circularity value of 1.0 indicates a perfect circle. Formation analysis in our models at first confirmed that the mesenchymal-like MDA-MB-231 cells demonstrate the lowest circularity level of 0.2. Intriguingly, the monoclonal cell populations of shERβ MDA-MB-231 cells demonstrated a 0.8 circularity rate that is much higher than that of shERβ MDA-MB-231 cells and clearly approaches MCF-7 cells' circularity (**Figure 3B**). The above data confirm the value of ERβ in the morphology, growth and invasive properties of breast cancer cells. MDA-MB-231 breast cancer cells are characterized by increased rates of cell viability, motility and invasive capacity,

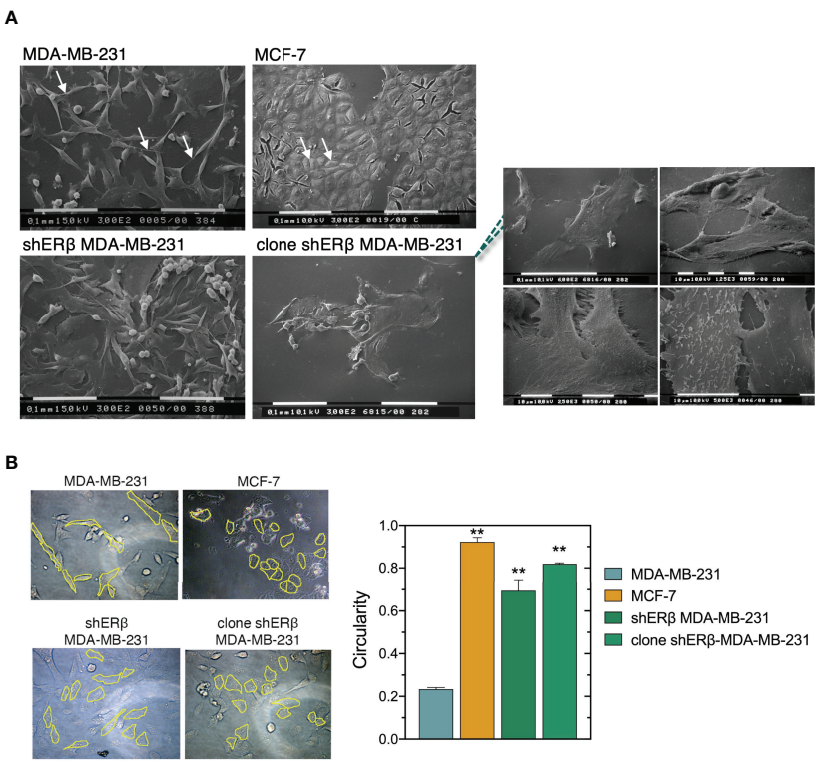

FIGURE 3 | ERβ-dependent cellular morphological characteristics. **(A)** Scanning electron microscopy (SEM) of MDA-MB-231 cells shows elongated cells with long filopodia (arrows), whereas MCF-7 cultures consist of grouped cobblestone/flattened cells with tight cell junctions (arrows). ERβ-suppressed cells demonstrate phenotypic heterogeneity similar to MDA-MB-231 cells. However, the majority of ERβ-suppressed cells look like flattened with cell-cell contacts and less cytoplasmic processes. Monoclonal populations of ERβ-suppressed cells mainly contain grouped and very flattened cells with small nucleus and large cytoplasm, no microvesicles or cytoplasmic protrusions (right panel) and many cell-cell junctions. **(B)** Circularity of the different breast cancer cellular models as quantified by Image J software. The data are presented as the mean ± SD values (n=3). Asterisk, (**) indicate statistically significant differences $p \leq 0.01$.

followed by significant loss in cell adhesive efficiency (**Figures 4A–D**). The aggressive behavior of ERβ-positive MDA-MB-231 cells confirms their mesenchymal-like characteristics (**Figure 3A**). The striking phenotypic changes in clone shERβ MDA-MB-231 cells were guided by critical alterations in functional properties of these cells. In particular, clone shERβ MDA-MB-231 cells demonstrated harsh decrease in viability, motility and invasive capacities, along with a profound increase in adhesion capability, as compared to aggressive ERβ-positive MDA-MB-231 cells (**Figures 4A–D**). Intriguingly, these changes were much more evident than in heterogenous shERβ MDA-MB-231 cells, approaching the levels of epithelial MCF-7 cells. Collectively, these novel data suggest the prominent role of ERβ suppression in the establishment of a permanently less aggressive phenotype as depicted in the monoclonal cell populations of clone shERβ MDA-MB-231 cells.

Reprogramming EMT and ECM Degradation in Monoclonal Cultures of shERβ MDA-MB-231 Cells

The conversion of early-stage tumors into invasive malignancies is a hallmark in tumorigenesis and is mediated by the actions of matrix degrading enzymes, as the proteolytic MMPs, that directly mediate EMT program (7). In this study, we revealed that *ESR2* high suppression rates in monoclonal shERβ MDA-MB-231 cells decreased the mRNA levels of MMP7 and MMP14, 70% and 55%, respectively, as compared to the highly invasive MDA-MB-231 cells (**Figure 5A**), whereas it led to a 3-fold increase in MMP9 levels (**Figure 5A**), an epithelial-derived MMP that acts as tumor suppressor in many types of cancer (38, 39). These changes in clone shERβ MDA-MB-231 cells co-existed with *TIMP1* and *TIMP2* decrease at 75% and 60%, respectively as compared to MDA-MB-231 cells (**Figure 5B**). Our data pinpointed that the expression profile of clone shERβ MDA-MB-231 cells in respect of *MMPs* and *TIMPs* resembles that of low metastatic MCF-7 breast cancer cells (**Figure 5A**, **B**). Furthermore, as shown in **Figures 5C, D**, the 90% *ESR2* suppression in monoclonal shERβ MDA-MB-231 cells resulted in a 2.5-fold increase in E-cadherin mRNA and protein levels, the major protein in adherens junctions, serving as an epithelial marker (40). Immunofluorescence analysis revealed the characteristic E-cadherin expression dots, in the monoclonal populations of shERβ MDA-MB-231 cells. These cells express this glycoprotein in cell junctions, as compared to MDA-MB-231 cells where E-cadherin staining is negative (**Figure 5D**, yellow frames). Notably, E-cadherin protein expression is more evident in clone shERβ MDA-MB-231 cells than in heterogenous shERβ MDA-MB-231 cells (**Figure 5D**). These results confirm the adhesive profile of clone shERβ MDA-MB-231 cells as depicted in **Figure 4D**. E-cadherin protein expression in MCF-7 epithelial cells with tight junctions confirmed the existence of this cell adhesion molecule in cell junctions (**Figure 5D**). *ESR2* depletion resulted also in a 50% reduction in *fibronectin* levels, as compared to MDA-MB-231 cells (**Figure 5C**). Fibronectin that promotes EMT and serves as a scaffold for fibrillar ECM (41), explaining its high mRNA levels in aggressive ERβ-positive MDA-MB-231 cells compared to the 70% decrease in MCF-7 epithelial cells (**Figure 5C**). This screening highlights the ERβ-mediated switch of the mesenchymal-to-epithelial transition (MET) trait in homogenous monoclonal cultures of shERβ MDA-MB-23 cells.

The invasive capacity of breast carcinoma cells is broadly connected to their phenotype, which determines EMT, cell-matrix and cancer cell-stroma interactions, critical to initiate a premetastatic niche (42). Striking alterations in morphological characteristics, lamellipodia deletion (**Figure 3A**), E-cadherin

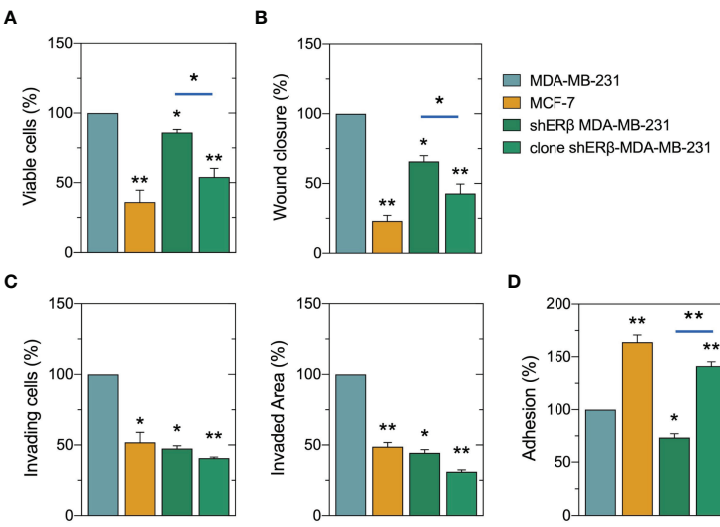

FIGURE 4 | Evaluation of ERβ suppression on cell functional properties of breast cancer cells. Monoclonal populations of shERβ-MDA-MB-231 cells demonstrate much lower levels of viability **(A)**, motility **(B)** and invasiveness **(C)** and in increased adhesive capacity **(D)** as compared to shERβ MDA-MB-231 cells. The data are presented as the mean ± SD values (n=3). Asterisks (*), (**) indicate statistically significant differences ($p \leq 0.05$ and $p \leq 0.01$, respectively).

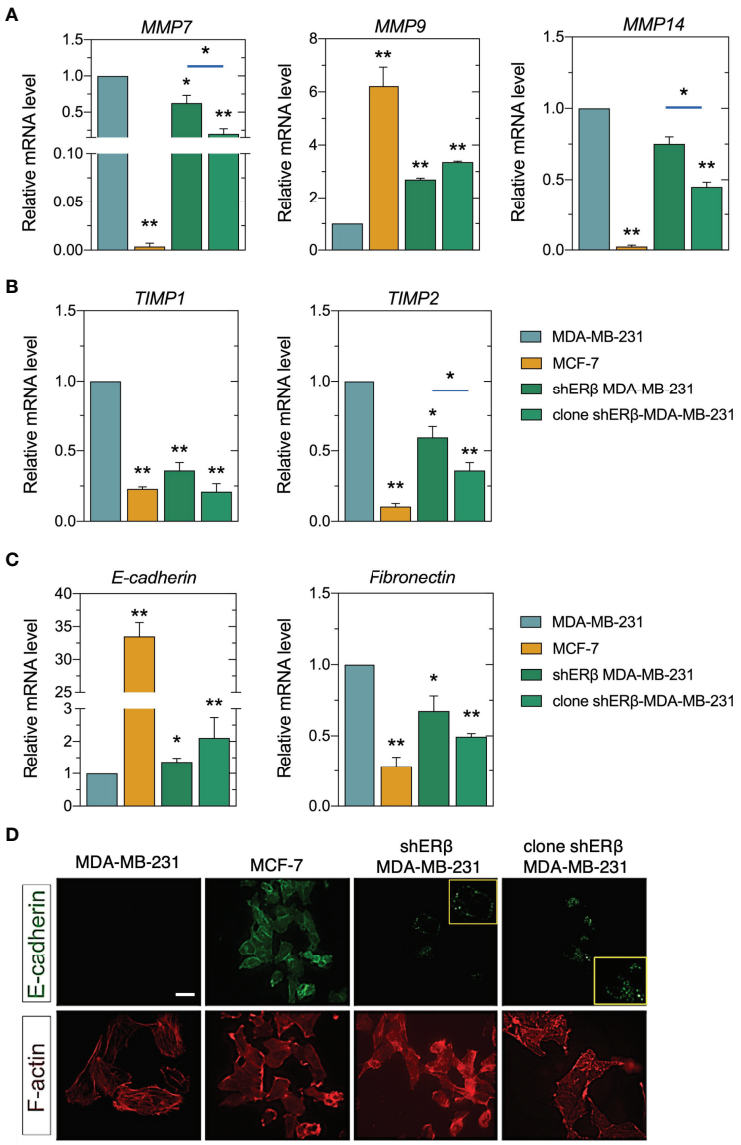

FIGURE 5 | ERβ regulates matrix composition in breast cancer cells. **(A)** Real-time qPCR analysis of major MMPs (*MMP7*, *MMP9*, *MMP14*) and their endogenous inhibitors (*TIMP1*, *TIMP2*) **(B)**. **(C)** Real-time qPCR analysis of EMT biomarkers, *E-cadherin* and *fibronectin*. The mRNA levels were studied using GAPDH as reference gene. Asterisks (*), (**) indicate statistically significant differences ($p \leq 0.05$ and $p \leq 0.01$, respectively). **(D)** Immunofluorescence analysis of E-cadherin (green) and F-actin (red). Scale bar, 10μm.

increment along with *fibronectin* loss, has led to robust cytoskeleton rearrangement in clone shERβ MDA-MB-231 cells (**Figure 5D**). F-actin staining for cytoskeleton revealed a clearly condensed cytoskeleton network in these cells, resembling F-actin microtubule network of MCF-7 cells, as compared to the characteristic mesenchymal-like cytoskeleton of MDA-MB-231 cells. All things considered, these findings highlight that *ESR2* could play a role in matrix remodeling, hence the expression of certain MMPs (i.e., MMP7, MMP9, MMP14) are critical factors for the degradation and reorganization of ECM components. *ESR2* also drives cytoskeletal rearrangement, and the expression profiles of major EMT markers.

ERβ Maximum Suppression Prevents *In Vivo* ERβ-Evoked Tumorigenesis

On account of the intrigued role of ERβ in mediating MET process by altering cellular characteristics and functions, F-actin cytoskeleton rearrangement and ECM reorganization, the *in vivo* tumorigenic capacity of this ER was assessed. 10^6 MDA-MB-231 and clone shERβ MDA-MB-231 cells were injected in two sites in the back of three female SCID mice and tumor formation was monitored for four weeks (**Figure 6A**). Intriguingly, after four weeks, *in vivo* tumor formation was observed exclusively in sites where MDA-MB-231 cells were injected (**Figure 6A**). The size and expression profile of MDA-MB-231-formed tumors was

calculated with *ex vivo* size measurements (**Figures 6B, C**) and immunochistochemistry analysis of major TNBC markers, including ERα, PgR, HER2, Ki-67, E-cadherin and vimentin (**Figure 6D**). Specifically, MDA-MB-231-generated tumors express vimentin and Ki-67, whereas the loss of ERα, PgR, HER2 and E-cadherin confirmed the aggressive phenotype of MDA-MB-231 cells and the necessity of targeting the ER that mediates this behavior, namely ERβ. In light of these facts, we conclude that ERβ directly controls *in vivo* tumorigenesis and the aggressive profile of TNBC cells, as the capacity of MDA-MB-231 cells to form tumors is vanished following *ESR2* practically total suppression, highlighting the importance of its molecular targeting.

DISCUSSION

The complex structure of solid tumors together with the interactions of cancer cells with the surrounding stroma and matrix components stimulate the initiation of a premetastatic niche that promotes metastasis to distant sites (8, 43–45)

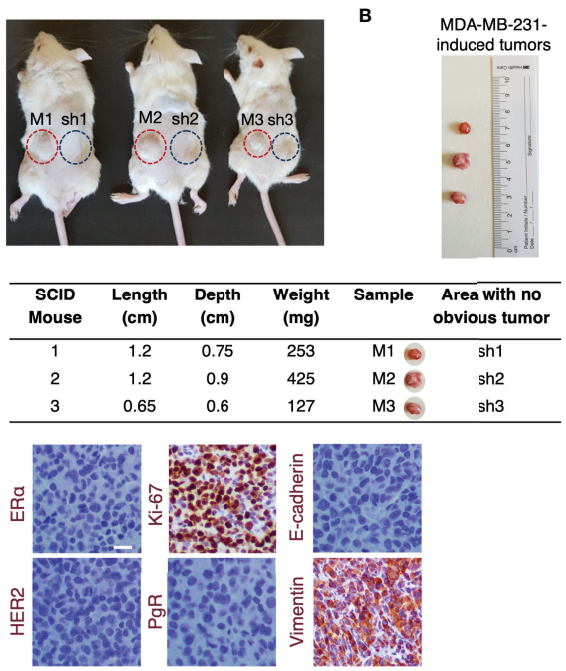

SCID Mouse	Length (cm)	Depth (cm)	Weight (mg)	Sample	Area with no obvious tumor
1	1.2	0.75	253	M1	sh1
2	1.2	0.9	425	M2	sh2
3	0.65	0.6	127	M3	sh3

FIGURE 6 | The highest *ESR2* suppression in MDA-MB-231 cells prevents tumorigenesis *in vivo*. **(A)** 10^6 MDA-MB-231 (red cycles) and clone shERβ MDA-MB-231 (blue cycles) cells were inoculated in two sites in the back of three female SCID mice. Tumor formation was observed only in sites where MDA-MB-231 cells were injected (M1, M2, M3) and no obvious tumors were detected following injections with clone shERβ MDA-MB-231 cells (sh1, sh2, sh3). **(B)** Size of the three tumors extracted from mice following injections with MDA-MB-231 cells (M1, M2, M3) for four weeks and **(C)** *ex vivo* tumor measurements. **(D)** Immunohistochemical analysis of specific breast cancer markers (i.e., ERα, PgR, HER2, Ki-67, E-cadherin, vimentin) in the MDA-MB-231 tumor tissue confirms the mesenchymal phenotype of tumor cells. Positive staining is indicated with brown. Scale bar, 10μm.

(**Figure 7A**). Alterations in the expression profiles of ECM structural components, including among others, PGs, hyaluronan, growth factor receptors, MMPs, and signaling stimulators, foresee the variations in cancer cell behavior, and construct the homes for metastasis (7, 46–48). Even though the significance of ERβ is less clarified in breast cancer progression than its isoform, ERα, probably due to the existence of several alternatively spliced ERβ variants; however, the potential of ERβ targeting in aggressive breast cancer subtypes, as TNBC, has gained attention over the years (49). In this study, we reported that high *ESR2* expression rates have been correlated to decreased overall survival rates in breast cancer patients diagnosed with invasive breast carcinoma. Recent reports indicate that ERβ target genes mostly regulate cell survival, movement, and growth (50), and that ERβ signaling pathway intersects with EGFR cascade to mediate TNBC cell morphology and stemness (13, 15). These data have been corroborated by the strong implication of ERβ in EMT process since it acts as EMT promoter by activating the TGFβ/Smad3 pathway to promote tumor growth and invasion in metastatic renal cell carcinoma (51). We demonstrated that ERβ maximum suppression (90%) leaded to transformed MDA-MB-231 clones that slightly express *EGFR*, whereas the expression rates of *IGF-IR* and *HER2* have been induced. Notably, IGF-IR signaling is reported to drastically lower the aggressive potential of breast cancer cells (31). The intracellular signaling pathway of EGFR receptor tyrosine kinase, includes the activation of Ras/MAPKs and PI3K/AKT and is involved in various aspects of breast cancer cell growth (52). Here we report that the slight *EGFR* expression is correlated with a robust decrease in ERK1/2 phosphorylation in monoclonal shERβ MDA-MB-231 cells, compared to the excessive phosphorylation in the invasive MDA-MB-231 cells. In previous studies, we have demonstrated that the distinct ER status of breast cancer cells is correlated to different microRNA (miRNA) epigenetic signatures and that specific miRNAs (i.e., miR-10b, miR-145 and miR-200b) are possible biomarkers for regulating breast cancer cell behavior by interacting with matrix mediators (19, 20, 53, 54). Especially for ERβ, this ER is the epigenetic mediator of miR-10b, miR-145 and miR-92, specific miRNAs implicated in breast cancer progression (19, 55). These findings clearly indicate the potential of ERβ-targeting in aggressive breast cancer, however little is known about its implication in tumor formation *in vivo*.

Enzymatic proteolysis is critical for matrix functionality and integrity, tissue homeostasis and cell signaling. Matrix degradation is predominantly orchestrated by bioactive MMPs that are not only responsible for ECM remodeling, but they also control the activities of other matrix components, suggesting their fundamental role in complex biological processes during cancer progression (7, 56). Moreover, it is well established that extensive or even dysregulated matrix remodeling generate molecular cues to promote tumorigenic processes. In datasets of primary breast tumors, high expression levels of a subset of MMPs, including MMP7 and MMP14, are correlated to poor prognosis and decreased survival rates (7, 57, 58). However, MMP9 expression varies among the molecular subtypes of breast

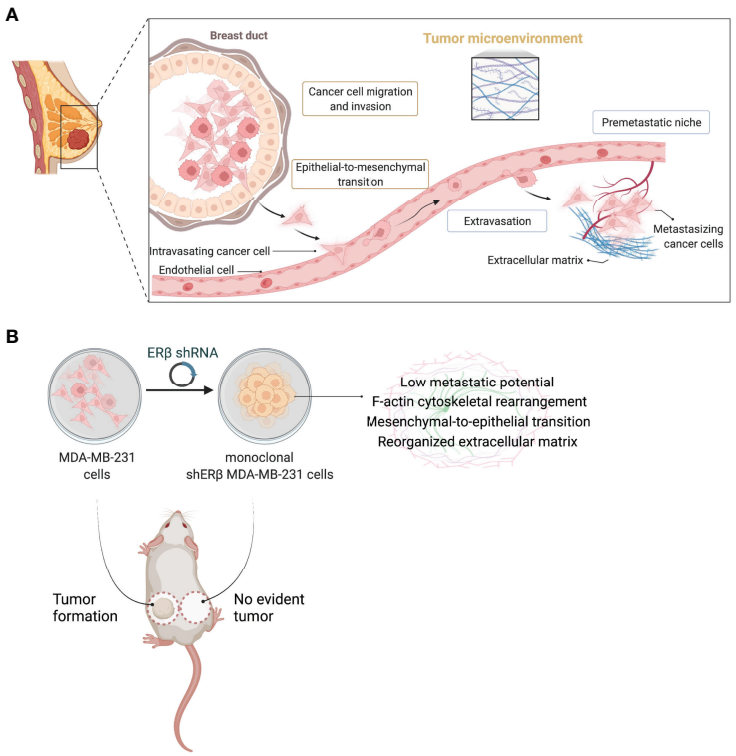

FIGURE 7 | ERβ globally mediates the behavior of triple-negative breast cancer cells. **(A)** Schematic depiction of major steps during breast cancer metastasis from a primary breast tumor of mesenchymal-like cancer cells, as the ERβ-positive triple-negative breast cancer (TNBC) cells. ERβ-dependent epithelial-to-mesenchymal transition alters the behavior of TNBC cells to advance high dynamics to invade endothelial barrier and enter blood stream. Intravasated cells follow the opposite process in order to be transferred through the blood stream. The extravasation of metastatic cancer cells creates a favourable microenvironment for premetastatic niche formation in secondary tissues and distant organs that is characterized by extensive matrix remodelling and the activation of the angiogenic switch. **(B)** Schematic representation delineating the cardinal role of ERβ in modulating the invasive phenotype of MDA-MB-231 TNBC cells. ERβ suppression and isolation of monoclonal populations transforms MDA-MB-231 cells into a less aggressive subtype that prevents *in vivo* tumorigenesis. Please consult the manuscript for additional details. Created with BioRender.com.

carcinoma (39, 59). Clearly, ERβ has a critical role in reducing the expression levels of MMPs, *MMP7* and *MMP14*, and their endogenous inhibitors, *TIMP1* and *TIMP2*, underscoring the notion that ERβ-evoked MMPs elevated levels in TNBC cells is cardinal for the initiation of the premetastatic niche in these cells. Intriguingly, monoclonal populations of shERβ MDA-MB-231 cells demonstrate a strong increase in *MMP9* levels following the profile of the MCF-7 breast cancer cells of low metastatic potential. This suggests that TNBC has a stronger clinical value in predicting metastasis rather than any of the other biological factors examined.

The formation of cell junctions is controlled by interactions of the transmembrane glycoproteins, mainly E-cadherin and intracellular components as β-catenin. The multifunctional complex of cell junctions includes the organization of actin cytoskeleton and the stabilization of cell-cell adhesion (60, 61). ERβ has an active role in regulating major EMT modulators, as its absence in monoclonal populations of shERβ MDA-MB-231 cells clearly boosted E-cadherin protein expression in the newly formed cell-cell junctions that these cells form. In respect to this observation, *fibronectin*, a fibrillar protein regulating cell-matrix adhesion and fibro-proliferative condition in diseased tissues (62), is diminished compared to the aggressive MDA-MB-231 TNBC cells, depicting that the ERβ-dependent mesenchymal characteristics connected to EMT initiation have been lost. Lamelipodia and long filopodia dynamics consist the cell motor pool mediating cell adhesion, motility, EMT and invasive capacity of breast cancer cells (63–65). Notably, ERβ-suppression in monoclonal cell populations of shERβ MDA-MB-231 cells clearly transformed TNBC cells to those with a less aggressive phenotype as explained by the fact that these cells lost the invasive morphology of MDA-MB-231 cells that is explained by the spindle-like shape and the long filopodia and lamellipodia cellular protrusions. Intriguingly, clone shERβ MDA-MB-231 cells gained the acquired morphological characteristics of MCF-7 epithelial-like cells, implying the flattened shape, loss of cellular protrusions and the formation of cell aggregates (**Figure 7B**). This transformation in clone shERβ MDA-MB-231 cells resulted in robust F-actin cytoskeletal rearrangement and the establishment of condensed F-actin network that is related to the decreased viability, motility and invasion to collagen type I of these cells (66). In addition, previous studies suggest that

actin dynamics directs the suppression of cell invasion in HER2-positive and ERα-positive tumors (67). Together, these findings suggest that ERβ is required for the establishment of actin structures and cellular characteristics during TNBC progression.

Collectively, the main goal of this study focused on unravelling the effects of highest possible ERβ suppression in ERβ-positive MDA-MB-231 TNBC cells on matrix composition, EMT program and *in vivo* tumor growth. The pioneering discovery of this study summarized that ERβ serves as one of the major biomolecules in this aggressive subtype of breast carcinoma and that its suppression is capable of leading to the total prevention of tumorigenesis (**Figure 7**). The molecular axis enclosing ERβ, matrix effectors (i.e., cell receptors and MMPs), and principal EMT mediators (i.e., E-cadherin and fibronectin), is critical for breast cancer progression and definitely affects response to endocrine therapy.

The apparent advantage of precise ERβ inhibition in guiding a paradigmatic shift to a less aggressive cell population with no apparent dynamics in forming tumors *in vivo* may be of great clinical interest opening new horizons in research of personalized therapeutics for TNBC. Exploiting the pharmacological targeting of ERβ as a powerful biomarker in TNBC may be among the bio-tools for improving the management and survival rates of breast cancer patients.

DATA AVAILABILITY STATEMENT

The raw data supporting the conclusions of this article will be made available by the authors, without undue reservation.

ETHICS STATEMENT

The animal study was reviewed and approved by N.C.S.R "Demokritos" institutional guidelines conforming to international standards and the protocols were approved by the relevant committee of the Veterinary Direction, Greek Ministry of Rural Development and Food (Permission No. 193900).

AUTHOR CONTRIBUTIONS

ZP and NK contributed to the conception and design of the work; ZP, MF, AP, DK, and NK involved in methodology; ZP, AK, MF, and VZ performed formal analysis, acquisition, and data interpretation; ZP prepared the original draft and figures; NK substantively revised draft and supervised the study. All authors have read, reviewed and agreed to the published version of the manuscript.

FUNDING

ZP acknowledges funding by the Horizon 2020 project NMBP-TO-IND-2018-2020 (MIS953152), and NKK by the Action for the Strategic Development on the Research and Technological Sector (MIS5033644), funded by the Operational Programme 'Competitiveness, Entrepreneurship and Innovation' (NSRF 2014-2020), and co-financed by Greece and the European Union (European Regional Development Fund).

ACKNOWLEDGMENTS

We acknowledge support by Dr. Konstantina Kyriakopoulou for her kind comments and suggestions during discussions on the results of this study.

SUPPLEMENTARY MATERIAL

The Supplementary Material for this article can be found online at: https://www.frontiersin.org/articles/10.3389/fonc.2022.917633/full#supplementary-material

REFERENCES

1. Hanahan D. Hallmarks of Cancer: New Dimensions. *Cancer Discovery* (2022) 12:31–46. doi: 10.1158/2159-8290.CD-21-1059
2. Thomas C, Gustafsson J-Å. The Different Roles of ER Subtypes in Cancer Biology and Therapy. *Nat Rev Cancer* (2011) 11:597–608. doi: 10.1038/nrc3093
3. Piperigkou Z, Karamanos NK. Estrogen Receptor-Mediated Targeting of the Extracellular Matrix Network in Cancer. *Semin Cancer Biol* (2020) 62:116–24. doi: 10.1016/j.semcancer.2019.07.006
4. Karamanos NK, Theocharis AD, Piperigkou Z, Manou D, Passi A, Skandalis SS, et al. A Guide to the Composition and Functions of the Extracellular Matrix. *FEBS J* (2021) 288:6850–912. doi: 10.1111/febs.15776
5. Karamanos NK, Theocharis AD, Neill T, Iozzo RV. Matrix Modeling and Remodeling: A Biological Interplay Regulating Tissue Homeostasis and Diseases. *Matrix Biol* (2019) 75–76:1–11. doi: 10.1016/j.matbio.2018.08.007
6. Theocharis AD, Manou D, Karamanos NK. The Extracellular Matrix as a Multitasking Player in Disease. *FEBS J* (2019) 286:2830–69. doi: 10.1111/febs.14818
7. Piperigkou Z, Kyriakopoulou K, Koutsakis C, Mastronikolis S, Karamanos NK. Key Matrix Remodeling Enzymes: Functions and Targeting in Cancer. *Cancers (Basel)* (2021) 13:1441. doi: 10.3390/cancers13061441
8. Karamanos NK, Piperigkou Z, Passi A, Götte M, Rousselle P, Vlodavsky I. Extracellular Matrix-Based Cancer Targeting. *Trends Mol Med* (2021) 27:P1000–13. doi: 10.1016/j.molmed.2021.07.009
9. Karamanos NK, Piperigkou Z, Theocharis AD, Watanabe H, Franchi M, Baud S, et al. Proteoglycan Chemical Diversity Drives Multifunctional Cell Regulation and Therapeutics. *Chem Rev* (2018) 118:9152–232. doi: 10.1021/acs.chemrev.8b00354
10. Yan S, Dey P, Ziegler Y, Jiao X, Hoon Kim S, Katzenellenbogen JA, et al. Comprehensive Molecular Portraits of Human Breast Tumours. *Nature* (2012) 490:61–70. doi: 10.1038/nature11412
11. Liu X-Z, Rulina A, Choi MH, Pedersen L, Lepland J, Takle ST, et al. C/EBPB-Dependent Adaptation to Palmitic Acid Promotes Tumor Formation in Hormone Receptor Negative Breast Cancer. *Nat Commun* (2022) 13:69. doi: 10.1038/s41467-021-27734-2
12. Kuiper GG, Enmark E, Pelto-Huikko M, Nilsson S, Gustafsson JA. Cloning of a Novel Receptor Expressed in Rat Prostate and Ovary. *Proc Natl Acad Sci* (1996) 93:5925–30. doi: 10.1073/pnas.93.12.5925

13. Kyriakopoulou K, Riti E, Piperigkou Z, Koutroumanou Sarri K, Bassiony H, Franchi M, et al. Egfr/Erβ-Mediated Cell Morphology and Invasion Capacity Are Associated With Matrix Culture Substrates in Breast Cancer. *Cells* (2020) 9:2255. doi: 10.3390/cells9102256
14. Piperigkou Z, Bouris P, Onisto M, Franchi M, Kletsas D, Theocharis AD, et al. Estrogen Receptor Beta Modulates Breast Cancer Cells Functional Properties, Signaling and Expression of Matrix Molecules. *Matrix Biol* (2016) 56:4–23. doi: 10.1016/j.matbio.2016.05.003
15. Kyriakopoulou K, Kefali E, Piperigkou Z, Riethmüller C, Greve B, Franchi M, et al. EGFR is a Pivotal Player of the E2/Erβ – Mediated Functional Properties, Aggressiveness, and Stemness in Triple-Negative Breast Cancer Cells. *FEBS J* (2021) 289:1552–74. doi: 10.1111/febs.16240
16. Bracken CP, Goodall GJ. The Many Regulators of Epithelial–Mesenchymal Transition. *Nat Rev Mol Cell Biol* (2022) 23:89–90. doi: 10.1038/s41580-021-00442-x
17. Yousefnia S, Seyed Forootan F, Seyed Forootan S, Nasr Esfahani MH, Gure AO, Ghaedi K. Mechanistic Pathways of Malignancy in Breast Cancer Stem Cells. *Front Oncol* (2020) 10:452. doi: 10.3389/fonc.2020.00452
18. Tang L, Chen Y, Chen H, Jiang P, Yan L, Mo D, et al. DCST1-AS1 Promotes TGF-β-Induced Epithelial–Mesenchymal Transition and Enhances Chemoresistance in Triple-Negative Breast Cancer Cells *via* ANXA1. *Front Oncol* (2020) 10:280. doi: 10.3389/fonc.2020.00280
19. Piperigkou Z, Franchi M, Götte M, Karamanos NK. Estrogen Receptor Beta as Epigenetic Mediator of miR-10b and miR-145 in Mammary Cancer. *Matrix Biol* (2017) 64:94–111. doi: 10.1016/j.matbio.2017.08.002
20. Piperigkou Z, Franchi M, Riethmüller C, Götte M, Karamanos NK. miR-200b Restrains EMT and Aggressiveness and Regulates Matrix Composition Depending on ER Status and Signaling in Mammary Cancer. *Matrix Biol Plus* (2020) 6–7:100024. doi: 10.1016/j.mbplus.2020.100024
21. Yan S, Dey P, Ziegler Y, Jiao X, Kim SH, Katzenellenbogen JA, et al. Contrasting Activities of Estrogen Receptor Beta Isoforms in Triple Negative Breast Cancer. *Breast Cancer Res Treat* (2021) 185:281–92. doi: 10.1007/s10549-020-05948-0
22. Sellitto A, D'Agostino Y, Alexandrova E, Lamberti J, Pecoraro G, Memoli D, et al. Insights Into the Role of Estrogen Receptor β in Triple-Negative Breast Cancer. *Cancers (Basel)* (2020) 12:1477. doi: 10.3390/cancers12061477
23. Tomayko MM, Reynolds CP. Determination of Subcutaneous Tumor Size in Athymic (Nude) Mice. *Cancer Chemother Pharmacol* (1989) 24:148–54. doi: 10.1007/BF00300234
24. de Wever O, Hendrix A, de Boeck A, Westbroek W, Braems G, Emami S, et al. Modeling and Quantification of Cancer Cell Invasion Through Collagen Type I Matrices. *Int J Dev Biol* (2010) 54:887–96. doi: 10.1387/ijdb.092948ow
25. Mobley JL, Shimizu Y. Measurement of Cellular Adhesion Under Static Conditions. *Curr Protoc Immunol* (2000) 37. doi: 10.1002/0471142735.im0728s37
26. Tang Z, Kang B, Li C, Chen T, Zhang Z. GEPIA2: An Enhanced Web Server for Large-Scale Expression Profiling and Interactive Analysis. *Nucleic Acids Res* (2019) 47:W556–60. doi: 10.1093/nar/gkz430
27. Nicolini A, Ferrari P, Duffy MJ. Prognostic and Predictive Biomarkers in Breast Cancer: Past, Present and Future. *Semin Cancer Biol* (2018) 52:56–73. doi: 10.1016/j.semcancer.2017.08.010
28. Wilkenfeld SR, Lin C, Frigo DE. Communication Between Genomic and non-Genomic Signaling Events Coordinate Steroid Hormone Actions. *Steroids* (2018) 133:2–7. doi: 10.1016/j.steroids.2017.11.005
29. Kyriakopoulou K, Kefali E, Piperigkou Z, Bassiony H, Karamanos NK. Advances in Targeting Epidermal Growth Factor Receptor Signaling Pathway in Mammary Cancer. *Cell Signalling* (2018) 51:99–109. doi: 10.1016/j.cellsig.2018.07.010
30. Masuda H, Zhang D, Bartholomeusz C, Doihara H, Hortobagyi GN, Ueno NT. Role of Epidermal Growth Factor Receptor in Breast Cancer. *Breast Cancer Res Treat* (2012) 136:331–45. doi: 10.1007/s10549-012-2289-9
31. Afratis NA, Bouris P, Skandalis SS, Multhaupt HA, Couchman JR, Theocharis AD, et al. IGF-IR Cooperates With Erα to Inhibit Breast Cancer Cell Aggressiveness by Regulating the Expression and Localisation of ECM Molecules. *Sci Rep* (2017) 7:40138. doi: 10.1038/srep40138
32. Zhao Y, Zheng X, Zheng Y, Chen Y, Fei W, Wang F, et al. Extracellular Matrix: Emerging Roles and Potential Therapeutic Targets for Breast Cancer. *Front Oncol* (2021) 11:650453. doi: 10.3389/fonc.2021.650453
33. Spill F, Reynolds DS, Kamm RD, Zaman MH. Impact of the Physical Microenvironment on Tumor Progression and Metastasis. *Curr Opin Biotechnol* (2016) 40:41–8. doi: 10.1016/j.copbio.2016.02.007
34. Vargas DA, Bates O, Zaman MH. Computational Model to Probe Cellular Mechanics During Epithelial-Mesenchymal Transition. *Cells Tissues Organs* (2013) 197:435–44. doi: 10.1159/000348415
35. Franchi M, Piperigkou Z, Karamanos K-A, Franchi L, Masola V. Extracellular Matrix-Mediated Breast Cancer Cells Morphological Alterations, Invasiveness, and Microvesicles/Exosomes Release. *Cells* (2020) 9:2031. doi: 10.3390/cells9092031
36. Da Q, Deng S, Li J, Yi H, Huang X, Yang X, et al. Quantifying the Cell Morphology and Predicting Biological Behavior of Signet Ring Cell Carcinoma Using Deep Learning. *Sci Rep* (2022) 12:183. doi: 10.1038/s41598-021-03984-4
37. Gavert N, Ben-Ze'ev A. Epithelial–mesenchymal Transition and the Invasive Potential of Tumors. *Trends Mol Med* (2008) 14:199–209. doi: 10.1016/j.molmed.2008.03.004
38. Pujada A, Walter L, Patel A, Bui TA, Zhang Z, Zhang Y, et al. Matrix Metalloproteinase MMP9 Maintains Epithelial Barrier Function and Preserves Mucosal Lining in Colitis Associated Cancer. *Oncotarget* (2017) 8:94650–65. doi: 10.18632/oncotarget.21841
39. Yousef EM, Tahir MR, St-Pierre Y, Gaboury LA. MMP-9 Expression Varies According to Molecular Subtypes of Breast Cancer. *BMC Cancer* (2014) 14:609. doi: 10.1186/1471-2407-14-609
40. Hartsock A, Nelson WJ. Adherens and Tight Junctions: Structure, Function and Connections to the Actin Cytoskeleton. *Biochim Biophys Acta (BBA)* (2008) 1778:660–9. doi: 10.1016/j.bbamem.2007.07.012
41. Park J, Schwarzbauer JE. Mammary Epithelial Cell Interactions With Fibronectin Stimulate Epithelial-Mesenchymal Transition. *Oncogene* (2014) 33:1649–57. doi: 10.1038/onc.2013.118
42. Rolli CG, Seufferlein T, Kemkemer R, Spatz JP. Impact of Tumor Cell Cytoskeleton Organization on Invasiveness and Migration: A Microchannel-Based Approach. *PLos One* (2010) 5:e8726. doi: 10.1371/journal.pone.0008726
43. Hanahan D, Coussens LM. Accessories to the Crime: Functions of Cells Recruited to the Tumor Microenvironment. *Cancer Cell* (2012) 21:309–22. doi: 10.1016/j.ccr.2012.02.022
44. Baghban R, Roshangar L, Jahanban-Esfahlan R, Seidi K, Ebrahimi-Kalan A, Jaymand M, et al. Tumor Microenvironment Complexity and Therapeutic Implications at a Glance. *Cell Communication Signaling* (2020) 18:59. doi: 10.1186/s12964-020-0530-4
45. Peinado H, Zhang H, Matei IR, Costa-Silva B, Hoshino A, Rodrigues G, et al. Pre-Metastatic Niches: Organ-Specific Homes for Metastases. *Nat Rev Cancer* (2017) 17:302–17. doi: 10.1038/nrc.2017.6
46. Kokoretsis D, Maniaki E, Kyriakopoulou K, Koutsakis C, Piperigkou Z, Karamanos NK. Hyaluronan as "Agent Smith" in Cancer Extracellular Matrix Pathobiology: Regulatory Roles in Immune Response, Cancer Progression and Targeting. *IUBMB Life* (2022). doi: 10.1002/iub.2608
47. Iozzo RV, Theocharis AD, Neill T, Karamanos NK. Complexity of Matrix Phenotypes. *Matrix Biol Plus* (2020) 6–7:100038. doi: 10.1016/j.mbplus.2020.100038
48. Theocharis AD, Karamanos NK. Proteoglycans Remodeling in Cancer: Underlying Molecular Mechanisms. *Matrix Biol* (2019) 75–76:220–59. doi: 10.1016/j.matbio.2017.10.008
49. Austin D, Hamilton N, Elshimali Y, Pietras R, Wu Y, Vadgama J. Estrogen Receptor-Beta is a Potential Target for Triple Negative Breast Cancer Treatment. *Oncotarget* (2018) 9:33912–30. doi: 10.18632/oncotarget.26089
50. Hamilton N, Márquez-Garbán D, Mah V, Fernando G, Elshimali Y, Garbán H, et al. Biologic Roles of Estrogen Receptor-β and Insulin-Like Growth Factor-2 in Triple-Negative Breast Cancer. *BioMed Res Int* (2015) 2015:1–15. doi: 10.1155/2015/925703
51. Song W, He D, Chen Y, Yeh C, Hsu I, Huang Q, et al. Targeting Newly Identified Erβ/TGF-β1/SMAD3 Signals With the FDA-Approved Anti-Estrogen Faslodex or an Erβ Selective Antagonist in Renal Cell Carcinoma. *Mol Oncol* (2018) 12:2055–71. doi: 10.1002/1878-0261.12377
52. Maennling AE, Tur MK, Niebert M, Klockenbring T, Zeppernick F, Gattenlöhner S, et al. Molecular Targeting Therapy Against EGFR Family

in Breast Cancer: Progress and Future Potentials. *Cancers (Basel)* (2019) 11:1826. doi: 10.3390/cancers11121826
53. Piperigkou Z, Tzaferi K, Makrokanis G, Cheli K, Karamanos NK. The microRNA-Cell Surface Proteoglycan Axis in Cancer Progression. *Am J Physiol-Cell Physiol* (2022) 322:C825–32. doi: 10.1152/ajpcell.00041.2022
54. Zolota V, Tzelepi V, Piperigkou Z, Kourea H, Papakonstantinou E, Argentou M-I, et al. Epigenetic Alterations in Triple-Negative Breast Cancer—the Critical Role of Extracellular Matrix. *Cancers (Basel)* (2021) 13:713. doi: 10.3390/cancers13040713
55. Al-Nakhle H, Burns PA, Cummings M, Hanby AM, Hughes TA, Satheesha S, et al. Estrogen Receptor β1 Expression Is Regulated by miR-92 in Breast Cancer. *Cancer Res* (2010) 70:4778–84. doi: 10.1158/0008-5472.CAN-09-4104
56. Mohan V, Das A, Sagi I. Emerging Roles of ECM Remodeling Processes in Cancer. *Semin Cancer Biol* (2020) 62:192–200. doi: 10.1016/j.semcancer.2019.09.004
57. Cheng T, Chen P, Chen J, Deng Y, Huang C. Landscape Analysis of Matrix Metalloproteinases Unveils Key Prognostic Markers for Patients With Breast Cancer. *Front Genet* (2022) 12:809600. doi: 10.3389/fgene.2021.809600
58. Radisky ES. Matrix Metalloproteinases as Drivers and Therapeutic Targets in Breast Cancer. *Front Biosci* (2015) 20:4364. doi: 10.2741/4364
59. Jiang H, Li H. Prognostic Values of Tumoral MMP2 and MMP9 Overexpression in Breast Cancer: A Systematic Review and Meta-Analysis. *BMC Cancer* (2021) 21:149. doi: 10.1186/s12885-021-07860-2
60. Halbleib JM, Nelson WJ. Cadherins in Development: Cell Adhesion, Sorting, and Tissue Morphogenesis. *Genes Dev* (2006) 20:3199–214. doi: 10.1101/gad.1486806
61. Gumbiner BM. Regulation of Cadherin-Mediated Adhesion in Morphogenesis. *Nat Rev Mol Cell Biol* (2005) 6:622–34. doi: 10.1038/nrm1699
62. Salajegheh A. "Fibronectin.,". In: *Angiogenesis in Health, Disease and Malignancy*. Cham: Springer International Publishing (2016). p. 121–5. doi: 10.1007/978-3-319-28140-7_19
63. Ehrlich JS, Hansen MDH, Nelson WJ. Spatio-Temporal Regulation of Rac1 Localization and Lamellipodia Dynamics During Epithelial Cell-Cell Adhesion. *Dev Cell* (2002) 3:259–70. doi: 10.1016/S1534-5807(02)00216-2
64. Franchi M, Piperigkou Z, Riti E, Masola V, Onisto M, Karamanos NK. Long Filopodia and Tunneling Nanotubes Define New Phenotypes of Breast Cancer Cells in 3D Cultures. *Matrix Biol Plus* (2020) 6–7:100026. doi: 10.1016/j.mbplus.2020.100026
65. Karamanou K, Franchi M, Vynios D, Brézillon S. Epithelial-To-Mesenchymal Transition and Invadopodia Markers in Breast Cancer: Lumican a Key Regulator. *Semin Cancer Biol* (2020) 62:125–33. doi: 10.1016/j.semcancer.2019.08.003
66. Yamaguchi H, Condeelis J. Regulation of the Actin Cytoskeleton in Cancer Cell Migration and Invasion. *Biochim Biophys Acta (BBA)* (2007) 1773:642–52. doi: 10.1016/j.bbamcr.2006.07.001
67. Padilla-Rodriguez M, Parker SS, Adams DG, Westerling T, Puleo JI, Watson AW, et al. The Actin Cytoskeletal Architecture of Estrogen Receptor Positive Breast Cancer Cells Suppresses Invasion. *Nat Commun* (2018) 9:2980. doi: 10.1038/s41467-018-05367-2

Conflict of Interest: The authors declare that the research was conducted in the absence of any commercial or financial relationships that could be construed as a potential conflict of interest.

Publisher's Note: All claims expressed in this article are solely those of the authors and do not necessarily represent those of their affiliated organizations, or those of the publisher, the editors and the reviewers. Any product that may be evaluated in this article, or claim that may be made by its manufacturer, is not guaranteed or endorsed by the publisher.

Copyright © 2022 Piperigkou, Koutsandreas, Franchi, Zolota, Kletsas, Passi and Karamanos. This is an open-access article distributed under the terms of the Creative Commons Attribution License (CC BY). The use, distribution or reproduction in other forums is permitted, provided the original author(s) and the copyright owner(s) are credited and that the original publication in this journal is cited, in accordance with accepted academic practice. No use, distribution or reproduction is permitted which does not comply with these terms.

frontiers | Frontiers in Oncology

REVIEW
published: 17 June 2022
doi: 10.3389/fonc.2022.908247

Revisiting the Tenascins: Exploitable as Cancer Targets?

Richard P. Tucker[1] *and Martin Degen*[2*]

[1] Department of Cell Biology and Human Anatomy, University of California, Davis, Davis, CA, United States, [2] Laboratory for Oral Molecular Biology, Department of Orthodontics and Dentofacial Orthopedics, University of Bern, Bern, Switzerland

For their full manifestation, tumors require support from the surrounding tumor microenvironment (TME), which includes a specific extracellular matrix (ECM), vasculature, and a variety of non-malignant host cells. Together, these components form a tumor-permissive niche that significantly differs from physiological conditions. While the TME helps to promote tumor progression, its special composition also provides potential targets for anti-cancer therapy. Targeting tumor-specific ECM molecules and stromal cells or disrupting aberrant mesenchyme-cancer communications might normalize the TME and improve cancer treatment outcome. The tenascins are a family of large, multifunctional extracellular glycoproteins consisting of four members. Although each have been described to be expressed in the ECM surrounding cancer cells, tenascin-C and tenascin-W are currently the most promising candidates for exploitability and clinical use as they are highly expressed in various tumor stroma with relatively low abundance in healthy tissues. Here, we review what is known about expression of all four tenascin family members in tumors, followed by a more thorough discussion on tenascin-C and tenascin-W focusing on their oncogenic functions and their potential as diagnostic and/or targetable molecules for anti-cancer treatment purposes.

Keywords: tenascins, extracellular matrix, tumor stroma, biomarker, anti-cancer therapy

OPEN ACCESS

Edited by:
Alberto Passi,
University of Insubria, Italy

Reviewed by:
Sherif Abdelaziz Ibrahim,
Cairo University, Egypt
Nikolaos A. Afratis,
National and Kapodistrian University of Athens, Greece

***Correspondence:**
Martin Degen
martin.degen@zmk.unibe.ch

Specialty section:
This article was submitted to Molecular and Cellular Oncology, a section of the journal Frontiers in Oncology

Received: *30 March 2022*
Accepted: *16 May 2022*
Published: *17 June 2022*

Citation:
Tucker RP and Degen M (2022) Revisiting the Tenascins: Exploitable as Cancer Targets? Front. Oncol. 12:908247. doi: 10.3389/fonc.2022.908247

1 INTRODUCTION

The extracellular matrix (ECM) is a complex meshwork of various cell-secreted macromolecules that regulates the development and homeostasis of tissues. In humans, the ECM is broadly composed of a mixture of proteins, polysaccharides, and water that, depending on the specific composition, reflect the physiological requirements for a given tissue (1). The main building blocks of the ECM are (i) collagens, (ii) glycoproteins, (iii) proteoglycans, and (iv) elastin. Collagens include the most abundant fibrous proteins of our body. They maintain the structural integrity of tissues by providing tensile strength. Glycoproteins are responsible for either linking different ECM molecules or mediating cell-ECM interactions, while proteoglycans include gel-like elements within the ECMs that allow a tissue to resist compressive forces. Finally, elastin, as its name indicates, is responsible for tissue elasticity (2). The human genome harbors 274 genes encoding for the proteins of the core matrisome (3). Although typical ECM-like domains were already present in the proteins of unicellular organisms, the complexity and diversity of the matrisome mainly arose during the transition from unicellular (protozoa) to multicellular (metazoa) animals. The emergence of more complex and multicellular organisms required major evolutionary innovations, which were

accompanied by the creation of more specialized and sophisticated ECM frameworks. Extensive elaborations of ECM proteins by exon shuffling, multiplications, and gene family expansions provided the rich repertoire of ECM molecules required for building the various structures (4, 5).

Initially, the ECM was mainly perceived as an inert physical scaffold for cells. However, this view has changed considerably during recent decades. Not only does the ECM provide structural and mechanical support for tissue integrity, but it is also responsible for the mobilization and availability of growth factors and cytokines (4). Additionally, the three-dimensional (3D) network provides specific biochemical and biomechanical properties that are sensed by specialized transmembrane receptors, such as integrins, syndecans and discoidin domain receptors, which can bind specific motifs in ECM proteins. Receptor ligation results in its activation, triggering signaling cascades that regulate various vital cellular processes, including cell adhesion, migration, proliferation, survival, and differentiation. Moreover, the ECM is subject to specific modifications and remodeling, which tailors the ECM to the unique needs of tissues. Therefore, each tissue is surrounded by an ECM that is fine-tuned in its composition and arrangement, providing the necessary cues for tissue homeostasis.

Since tissue homeostasis is often disrupted in cancers, the ECM surrounding cancer cells is significantly different from the one found in healthy conditions (6, 7). The role of the tumor microenvironment (TME) on cancer cells has only recently begun to be appreciated. Earlier cancer research was focused on the individual cancer cell, oncogenes and tumor suppressors; novel mutations and hyperactive signaling pathways were then identified and exploited as anti-cancer therapies. While this approach revolutionized cancer treatment, it seems clear today that cancers need to be viewed as complex heterogeneous tissues. Apart from cancer cells, cancers also depend on supporting components present in the TME that are not malignant themselves. These include the vasculature, immune cells, fibroblasts, and the ECM. Cellular sources of this tumor-specific ECM might be tumor cells themselves, but more often this matrix is derived from cancer-associated fibroblasts (CAFs). CAFs are believed to evolve from the activation of quiescent fibroblasts by epithelial-mesenchymal interactions, often involving cancer cell-derived growth factors (8). Hence, while carcinoma growth is initiated by transformed epithelial cells, cancers continuously tailor and orchestrate their microenvironment for their specific needs. Consequently, a unique composition and mix of ECM molecules is created, which provides feedback to malignant cells allowing the modulation of various hallmarks of cancers (9–11).

There is mounting evidence that the tumor ECM plays an active role in driving malignancy (9). Hence, novel anti-cancer drugs might be more powerful if they not only aim to eliminate cancers cells, but also try to normalize the TME. Such an approach requires a better understanding of the aberrant tumor cell-stroma crosstalk as well as a better understanding of the tumor-specific ECM molecules that are present. At least two members of the tenascin family of ECM glycoproteins, tenascin-C (TN-C) and tenascin-W (TN-W), are highly expressed in most solid cancers, but are expressed at much lower levels in normal tissues. Both of these tenascins provide multifunctional pro-tumorigenic activities (12). Therefore, tenascins, as specific components of tumor-permissive ECMs, are interesting candidates for potential exploitation for cancer therapies. Herein, we will briefly revisit the tenascin family with a focus on their structure and patterns of expression in physiological as well as in cancerous conditions. We will further focus on their cancer-related functions providing the basis for their exploitability and value for translational applications and clinical benefit.

2 A BRIEF ENCOUNTER WITH THE TENASCINS

Tenascins are a family of modular ECM glycoproteins (**Figure 1**). The family members share both a basic domain architecture and a common evolutionary ancestor. Near their amino-termini most tenascins have a coiled-coil domain that supports trimerization. This is followed by one or more EGF-like domains, numerous fibronectin-type III (FNIII) repeats, and a fibrinogen-like globe (FBG) at their carboxy-termini. The founding member of the tenascin family is TN-C, with the C designating "cytotactin", which was one of its original monikers. This was followed by descriptions of tenascin-R (TN-R), tenascin-X (TN-X) and TN-W (31, 32). While the roles of the EGF domains remain to be clarified, one or more of a tenascin's FNIII repeats typically contains integrin-binding motifs (33, 34), and tenascin FBGs bind to and activate toll-like receptor 4 (TLR4) (35). Tenascins are only found in chordates, with all four family members present in bony fishes and tetrapods (36).

After considering each member of the tenascin family, this review emphasizes what we have learned about the two tenascins that are most abundant in the TME: TN-C and TN-W. In humans, TN-C has 14 EGF-like domains and 8 constant FNIII repeats. Between the 5^{th} and 6^{th} constant FNIII repeats alternative splicing can add up to 9 additional FNIII repeats, resulting in hundreds of TN-C variants with significantly different molecular weights (32, 37). The potential to exploit differential expression patterns of TN-C isoforms in normal tissues and in cancer is described below. Human TN-W has just three EGF-like domains and 9 FNIII repeats. There is no evidence of alternative splicing in TN-W (32). In addition to trimerization *via* the coiled-coil domain, the amino-termini of TN-C and TN-W have free cysteine residues that support the formation of hexamers from two trimers (i.e., hexabrachions). As well as being integrin ligands, both TN-C and TN-W can bind to Wnt3a (38).

TN-C and TN-W are both widely expressed during embryonic development. For example, TN-C is found around migrating neural crest cells, at sites of branching morphogenesis and epithelial-mesenchymal interactions, and throughout the central nervous system in zones where glial precursors are proliferating and migrating. TN-C and TN-W are both

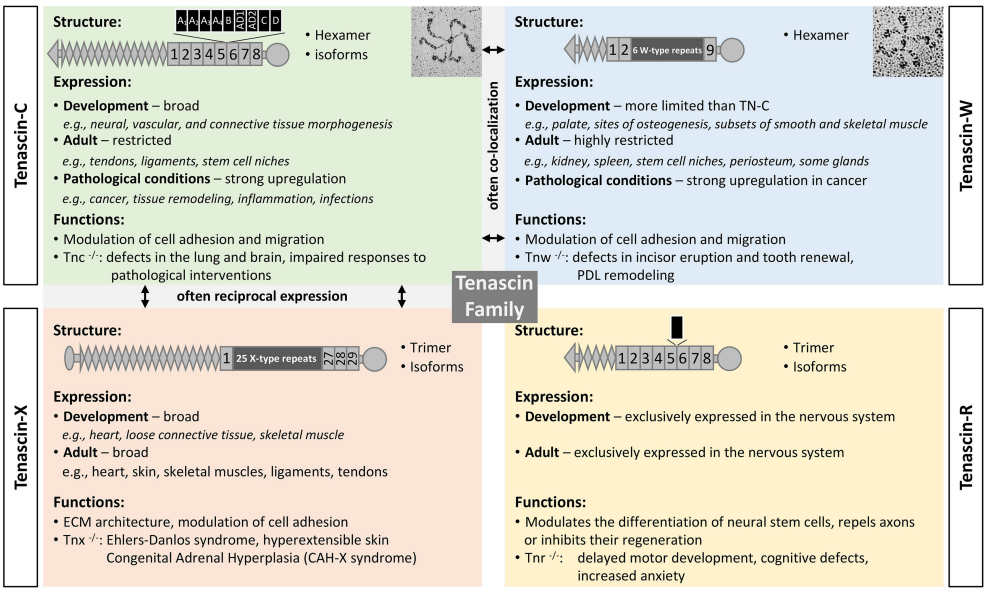

FIGURE 1 | The tenascin family. A brief description of the four tenascin members, including their structure and alternative splicing, major sites of expression, and functions. Original rotary shadowing micrograph for TN-C is from Chiquet-Ehrismann et al. (13) and for TN-W from Scherberich et al. (14) both with permission. The following symbols have been used to describe the structural domains: EGF-like domains (diamonds), FNIII domains (boxes), fibrinogen globe (circle). FNIII repeats shown above the structure are subject to alternative splicing (black boxes). Selected references: for TN-C (15–17), TN-X (18–21), TN-R (22–24), TN-W (25–27), and for tenascins in general (28–30).

expressed at sites of smooth muscle morphogenesis as well as chondrogenesis and osteogenesis, where their expression patterns often partially overlap (32, 37). In the adult, both remain highly expressed in dense connective tissues (28) and in certain stem cell niches (39), but they are largely absent from most other tissues (**Figure 2**).

3 EXPRESSION OF THE TENASCIN MEMBERS IN CANCER

The TME plays an active role in cancer progression. Therefore, full awareness of the composition and expression patterns of tumor-specific ECM, compared to the matrix of corresponding healthy tissues, is of high clinical importance. Tumor-specific ECM molecules might be harnessed and targeted in combination with more classical anti-cancer treatment approaches for the benefit of patients. Almost 40 years ago, TN-C was identified as an ECM protein enriched in the stroma of glioma (42). As other members of the tenascin family were identified, each was studied in turn to see if it was also expressed in tumor stroma. The next section will focus on the expression patterns of all four members of the tenascin family in solid cancers.

3.1 TN-C: "The Founding Member"

As described above, TN-C is transiently expressed in a highly spatio-temporal manner in various tissues during development (**Figure 2**). In the adult, its expression is only preserved in a few tissues that mainly have to withstand tensile stress (e.g., tendons, ligaments) (28). A robust re-expression in solid cancers is one of the most intriguing features of TN-C. One of the earliest studies analyzing tumor-specific TN-C expression was performed in mouse models of mammary breast cancer (43). These data described TN-C as an ECM molecule present in malignant breast cancer, but absent in the normal healthy mammary parenchyma as well as in benign tumors of the breast. This initial discovery fueled subsequent studies analyzing various cancers for the presence of TN-C, which resulted in an extremely rich literature on its expression in human tumors. TN-C has been identified in the tumor stroma of basically all cancer types analyzed, including cancers derived from breast, brain, uterus, ovary, prostate, pancreas, colorectal, kidney, biliary tract, stomach, gastric, osteosarcoma, oral cavity, urinary tract, skin tissue and many more [for reviews see (44–47)]. This abundant tumor-specific TN-C expression is compelling as TN-C is only mildly expressed in normal adult tissues, although most of them are not completely deprived of it. In certain cancers, such as renal cell carcinoma, brain and lung cancer, TN-C is expressed adjacent to CD31-positive vascular endothelial cells (48). TN-C is not only abundantly expressed in the tissues of cancer patients, but also detectable in their sera. Several studies reported increased TN-C levels in serum of cancer patients compared to healthy controls in non-small cell lung cancer, squamous cell carcinoma of the head and neck, colorectal cancer, breast cancer, and ovarian cancer (49–52).

The *TNC* gene is subject to extensive alternative splicing within its FNIII repeats (**Figure 1**). Hence, many different TN-C isoforms can be produced, with the larger isoforms with

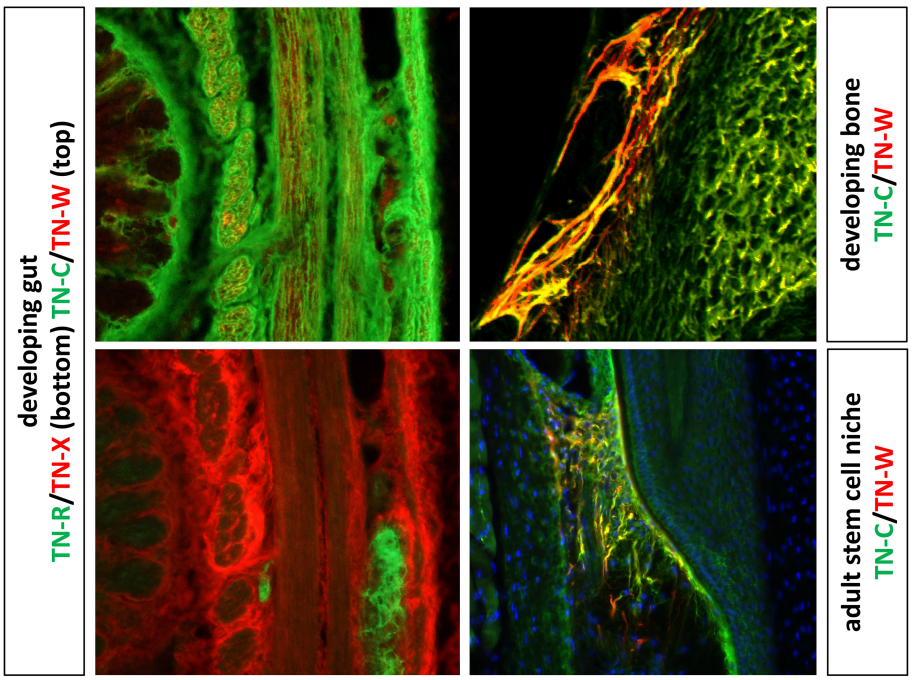

FIGURE 2 | The images to the left show double label immunohistochemistry of the developing gut with antibodies to TN-C, TN-W, TN-R and TN-X. TN-C expression is widespread, while TN-W is found in small patches in a subset of the smooth muscle. TN-R is limited to the autonomic ganglia of the gut, while TN-X is concentrated in the epimysium surrounding bundles of smooth muscle. On the top right is a section of a developing ulna immunostained with antibodies to TN-C and TN-W. Both are strongly expressed in developing bone, with partially overlapping patterns (yellow). On the bottom right is a section though the whisker follicle stem cell niche of an adult mouse. The patterns of TN-C and TN-W expression are more limited in the adult, but they are found in partly overlapping patterns in this stem cell niche. Original images of the developing gut and bone from Meloty-Kapella et al. (40) and adult stem cell niches from Tucker et al. (41) with permission.

additional FNIII repeats typically present during development and in tumors. Indeed, the TN-C isoform spectrum present in the ECM surrounding cancer cells significantly differs from the one in normal ECM (53–56). Consequently, not only general detection of TN-C in tumor stroma is important, but also knowledge about the precise expression of tumor-specific TN-C isoforms is relevant for translational use, as different isoforms in the stroma might affect cancer cell behavior in a distinct way (57). While alternative splicing adds another level of complexity to the multifunctional activities of TN-C, tumor-specific TN-C isoforms also represent promising exploitable targets for anti-cancer therapies (58, 59).

The observation of a tight regulation of TN-C expression during development, in the adult, and in cancers prompted numerous studies trying to elucidate the regulatory mechanisms for this multifunctional ECM molecule. Many factors have been identified, both *in vivo* and *in vitro*, that lead to induction of TN-C. Inducing stimuli include patterning genes during development such as paired-related homeobox 1, as well as growth factors (e.g., PDGF, TGFβ1, FGF2), inflammatory cytokines (e.g., IL1α, IL1β), biophysical properties of the microenvironment (e.g., hypoxia, ECM stiffness), mechanical stress, activated signaling pathways, and micro RNAs (miRNAs). In contrast, glucocorticoids are known to repress TN-C, though the exact molecular mechanism underlying this repression is not clear (60, 61). While some of these regulatory mechanisms might also be relevant for TN-C expression in tumors (e.g., TGFβ1 in breast cancer), the transcription factor SOX4 has been shown to induce TN-C in many malignancies (62). In addition, a crosstalk between TN-C and Notch signaling has also been described in glioma (63). The proximal *TNC* promoter contains a crucial RBPJκ binding element and in glioblastoma, TN-C was shown to be trans-activated by Notch2 signaling in an RBPJκ-dependent manner. How alternative splicing of the *TNC* is gene is regulated is not well understood. Apart from some specific splice factors (e.g., Sam68), certain growth factors/cytokines as well as biophysical properties of the microenvironment might also be involved in the splicing regulation of *TNC* (64–67). Clearly, regulation of *TNC* is a very complex process that reflects its highly specific expression pattern both in physiological conditions as well as in cancers.

TNC mRNA has been detected both in stromal as well as in cancer cells. Epithelial-mesenchymal interactions between cancer cells and stromal cells results in the differentiation of quiescent fibroblasts into CAFs, which show a unique gene expression profile. TN-C is one of the specific proteins that is secreted and incorporated into a tumor-permissive ECM by CAFs (8). Furthermore, hyperplastic endothelial cells are also a source for TN-C, which showed strong *TNC* expression in astrocytoma but not in vessels of normal brains (68). Similarly, *TNC* was also identified as a gene highly enriched in endothelial

cells isolated from a panel of malignant compared to normal tissues (69). However, TN-C expression has also been found in many cancer cells, including cancers of the breast, brain, skin, colon, pharynx, and larynx as well as in oral squamous cell carcinoma (46). The strongest TN-C positivity is often observed in the cancer cells at the periphery of malignant nests suggesting a role for this tenascin in driving invasion and migration (70). The importance of epithelial-mesenchymal interaction for TN-C expression is illustrated by the fact that in co-culture experiments cancer cells are able to induce TN-C expression in otherwise TN-C-negative fibroblasts (71), while TN-C-negative cancer cells start to express this tenascin when co-cultured with embryonic mesenchyme (72).

3.2 TN-R: "The Brain-Specific Member"

TN-R shows a very tissue-specific expression pattern during development and in the adult as it is only detectable in the nervous system (**Figure 2**) (22, 73). Relatively few studies focused on the expression and function of TN-R in cancers, and its expression was only revealed in brain cancer. As often is the case with a low number of studies and lack of functional analyses, the expression as well as the role of TN-R in brain cancer remains controversial. Although TN-R was found to be expressed in fetal cerebellum, TN-R was not detectable in the most common malignant brain tumor in children, medulloblastoma, as assessed by a cDNA microarray as well as immunohistochemistry (74). In contrast, analysis by high resolution northern blot displayed *TNR* in both astrocytoma and meningioma (75). Ayachi et al. show by quantitative real-time PCR (qPCR) and *in situ* hybridization (ISH) that *TNR* was over-expressed in pilocytic astrocytoma and ganglioglioma, two non-invasive tumors, while in low-grade infiltrative glioma and glioblastoma, *TNR* expression was moderate and negative, respectively (76). These results suggest that TN-R could act as a suppressor of glioma invasion. But clearly, more studies are required to allow a conclusive verdict to be given about the role of TN-R in brain and in other cancers.

Regulation of *TNR* remains not well-understood at the moment. Some growth factors and cytokines, including PDGF and NGF, have been shown to induce TN-R *in vitro*. TN-R is mainly produced by oligodendrocytes. Co-culturing these cells with either astrocytes, neurons, or conditioned medium from activated microglia modulates TN-R expression (60). Whether any of these or related mechanisms play a role in aberrant TN-R expression in cancer is not known.

3.3 TN-X – "The Controversial Member"

TN-X is found in epimysium and loose connective tissues (**Figure 2**) (32). As with TN-R, only a few studies have addressed TN-X expression in tumor-specific ECMs, and the results of these studies have proven to be controversial. TN-X levels were found to be elevated in the tumor stroma of malignant mesothelioma, ovarian cancer, and low-grade astrocytoma. In the latter, TN-X was expressed in the adventita and the perivascular niche (77–80). In mesothelioma, high TN-X expression allowed the differential diagnosis between malignant mesothelioma and lung adenocarcinoma (78) as well as between malignant mesothelioma and ovarian carcinoma/peritoneal serous carcinoma (77). TN-X is also expressed by Hodgkin lymphoma-derived Reed Sternberg cells (81). Additionally, elevated TN-X concentrations were detectable in serum of breast cancer and ovarian cancer patients compared to control serum (79). Contradictory results were observed in high-grade astrocytoma, malignant nerve sheath tumors, melanoma, and cancers of the uterus (leiomyoma) (80, 82–84). In these malignancies, TN-X was markedly reduced compared to their corresponding normal tissues or to their benign forms. The most elaborate study on TN-X expression in cancer, which used *in silico* analyses of expression data as well as immunohistochemical screening of tissue microarrays, was recently published (85). In this study, TN-X was found to be downregulated in the six cancers with highest incidence and mortality in the world (lung, breast, colon, prostate, stomach, and liver) as well as in all other cancers tested. Notably, diminished TN-X levels were found in the cancers reported to have upregulated TN-X expression by others (see above). Only in brain cancers (astrocytoma, glioblastoma multiforme and oligodendroglioma) was TN-X found to be enriched compared to healthy tissue. For lung adenocarcinoma and breast cancer, clinical data matching the *in silico* datasets were also available, which allowed to establish a negative correlation between TN-X expression and tumor stage as well as patient survival. These data suggest that TN-X levels are reduced in most cancers and that TN-X might represent a promising prognostic biomarker (85). Tumor-specific TN-X downregulation was also shown in another study examining The Cancer Genome Atlas for ECM molecule dysregulation in a large panel of malignancies (86). While 58 of the 249 ECM molecules analyzed were dysregulated in cancers, *TNXB* was found to be the most significantly downregulated gene overall. However, all these data have to be interpreted carefully since (i) TN-X RNA and protein levels did not always correlate; (ii), TN-X downregulation was not observed in every clinical specimen analyzed from the same cancer type; (iii) TN-X was still readily detectable in cancer tissues. However, these observations definitely warrant additional studies looking at TN-X expression and function in cancers.

Very limited data are available regarding *TNXB* gene regulation. So far, there is no evidence that *TNXB* responds to any growth factors or cytokines, which is in contrast to the other tenascin members. This is somewhat surprising since several putative binding sites for Sp1/Sp3 transcription factors were identified close to the transcription start site and found to be functional and required for driving *TNXB* expression. However, the upstream signaling pathways remain elusive. As with other tenascin family members, it is known that glucocorticoids have a negative effect on *TNXB* levels. However, details remain unresolved (60).

3.4 TN-W: "The Most Tumor-Specific Member"

TN-W is the newest member of the tenascin family, which was often found co-expressed or at least in the vicinity of TN-C during development (**Figure 2**) (25, 26). Since TN-C has been known for its high expression in the tumor stroma of breast cancer, initial studies on TN-W in tumors focused on this tissue as well. Using different breast cancer mouse models, TN-W was found to be enriched in the tumor stroma surrounding breast

cancer cells. However, tumor stroma was only positive for TN-W in the models with a high likelihood to metastasize and not in the non-metastatic ones (87). Encouraged by these findings in mice, the human orthologue was cloned, expressed, and antibodies raised against it. The first tissues analyzed resulted in intriguing observations. In healthy normal breast and colorectal tissues, TN-W was not detectable at all, while their corresponding cancerous tissues displayed a robust and highly significant *de novo* expression of TN-W (52, 88). Screening of additional human tumor types confirmed these initial observations: TN-W was strongly enriched in the stroma of brain (glioblastoma, oligodendroglioma, astrocytoma), prostate, kidney (clear cell carcinoma, papillary carcinoma, chromophobe renal carcinoma, and oncocytoma), ovarian, prostate, pancreas, biliary tract (liver carcinoma, gallbladder carcinoma), and lung cancers as well as in melanoma (48, 89, 90). Most significantly, TN-W was not detectable in the corresponding healthy tissues. However, TN-W expression in tumors was heterogenous, varying from low to very high levels, but was significantly increased compared to the normal tissues in most of the cases tested. For some metastatic melanoma patients, lymph node metastases as well as metastases from diverse locations (spleen, lung and skin) were found to be TN-W positive (87.5% of lymph node metastases, and 85% of other metastases) (48). Similar to TN-C, TN-W was often found to be expressed in close proximity to the vasculature as assessed by co-staining of TN-W with endothelial cell markers CD31/Pecam-1, von-Willebrand-factor, and Desmin in at least kidney, lung, breast, colon, ovary, and brain cancers (48, 90). Elevated concentrations of TN-W could also be measured in the serum of breast and colon cancer patients compared to healthy controls using a sensitive TN-W sandwich ELISA (52).

Although the list of solid cancers with prominent upregulation of TN-W is constantly growing, some very elementary questions about TN-W in tumor stroma remain. For instance, what is the cellular source of its expression? It is believed that TN-W is mainly expressed by stromal cells mediated by epithelial-mesenchymal interactions. This statement is supported by immunohistochemical analyses of TN-W that never revealed any TN-W expression in cancer cells as well as by *in vitro* experiments unsuccessfully trying to detect endogenous TN-W in numerous cancer cell lines of various origin (26). The concept of stromal cell origin of TN-W was reinforced by observations that bone marrow-derived stromal cells exclusively expressed TN-W when co-cultured with malignant cells in a xenograft model of breast cancer cell displaying metastatic propensity toward bone (91). However, a recent study screening for *TNW* transcripts in 20 biliary tract cancer cell lines is challenging the idea about pure stromal cell origin of TN-W (89). While most of the cells displayed very modest or negligible *TNW* levels, Huh-28 cells, an intrahepatic cholangiocarcinoma cell line, showed high levels of *TNW*. These results were further confirmed by immunoblotting and immunocytochemistry. Notably, when cultured alone, TN-W in Huh-28 cells was mainly observed to be intracellular without being organized and incorporated into the ECM. However, when co-cultured with bone marrow-derived stromal cells, Huh28-derived TN-W organized into ECM fibrils surrounding nests of tumor cells, a situation that closely mimics the situation of tumors *in vivo* (89). Therefore, there is strong evidence that proper epithelial-mesenchymal crosstalk is required for formation of TN-W-positive fibrils, but also that cancer cells themselves might represent a cellular source for TN-W, which is similar to the situation for TN-C. Additional experiments, such as ISH on tumor samples, are required to fully elucidate the cell types responsible for TN-W expression and to know whether the cellular source might differ among distinct tumors.

Another open question about TN-W expression in tumor stroma concerns the regulatory mechanisms of its *de novo* expression. Most of the available knowledge on this topic has been gained in *in vitro* studies of mouse and chicken cells. Growth factors, such as BMP2, BMP7, and TNFα induce TN-W in mouse embryonic fibroblasts, mouse cranial fibroblasts, mouse C2C12 myoblasts, HC11 normal mouse mammary gland epithelial cells, mouse bone marrow-derived Kusa-A1 cells as well as in primary chicken osteoblasts (14, 92, 93). In addition, Wnt5a seems also indirectly involved in triggering TN-W expression through p38/MAPK signaling (94). However, the molecule that acts as the upstream inducer has not been identified. In contrast, none of these factors have been shown to be able to activate *TNW* in human cells. Today, we only know that TGFβ1 signaling has an inducing effect on TN-W. Breast cancer cells secrete TGFβ1 into the tumor stroma, where the growth factor is sensed by bone marrow-derived stromal cells, which leads to a Smad4-dependent induction of *TNW* in the stromal cells (91). Negative impact on *TNW* transcripts has been attributed to glucocorticoids, which is similar to their effect on *TNC* and *TNXB* (60). More studies and research are required to better understand cancer-specific expression of TN-W.

There is not much evidence available for the presence of specific TN-W isoforms or TN-W modifications. The only observation in this regard was gained in the Huh-28 cells, which showed a TN-W protein with a higher molecular weight than expected (89). Whether this result hints at a tumor-specific isoform, modification, or multimerization of TN-W in this cell line and whether it has any relevance *in vivo* remains to be seen.

4 POTENTIAL CANCER-PROMOTING ACTIVITIES OF TENASCINS

As mentioned before, tenascins are multifunctional matricellular proteins with a highly specific pattern of expression during development and in cancer. Although each family member might be involved in cancers to some extent (see above), currently there is only robust and consistent data about expression and function in tumors for two of the family members: TN-C and TN-W. Therefore, we put the focus in the following chapters on TN-C and TN-W and try to emphasize their role in regulating various cellular processes required for tumor progression (**Figure 3**).

4.1 Modulation of Cell Adhesion

The potential to modulate cell adhesion is probably one of the most described and studied characteristics of TN-C. TN-C is an anti-adhesive molecule, which, as substratum, does not promote attachment and spreading of either epithelial cells (e.g., breast cancer cells) or fibroblasts (95). The most prominent feature of TN-C is its inhibitory effect on fibronectin (FN)-mediated cell adhesion (13). Attachment and spreading on FN requires cells to engage synergistically both the heparan sulfate proteoglycan receptor syndecan-4 and integrin α5β1. However, TN-C can bind to FN at a heparin binding motif located around the 13th FNIII repeat, which leads to a competitive hindrance of syndecan-4 binding to FN. Consequently, the presence of TN-C (such as in tumors) inhibits cell spreading and increases cell proliferation (96). Similar, but less consistent and less understood properties, have been found for TN-W in regulating cell adhesion. Initially, a TN-W substratum was found to be anti-adhesive for human breast cancer cells, while it promoted human fibroblast attachment, but not proper spreading. However, for both cell types, the presence of TN-W did not interfere with FN-mediated attachment (88). Different results were observed in primary chicken osteoblasts, mouse C2C12 myoblasts, embryonic fibroblasts, and whisker follicle stem cells, for which TN-W was able to interfere with FN-mediated cell spreading when soluble or used as substratum (41, 97). These results suggest that the activity of TN-W to modulate cell adhesion and spreading is cell-type specific. For cancer cells, TN-W seems to be anti-adhesive and not able to interfere with FN-mediated cell attachment, while for normal cells, TN-W shares the anti-adhesive properties of TN-C towards FN-mediated cell spreading. However, the mechanistical details underlying the latter observation remain unknown, as direct TN-W/FN interactions have yet to be reported.

4.2 Cell Proliferation

In vitro, cancer cell lines can be stimulated to become hyperproliferative by the addition of recombinant TN-C (45). This is most likely the consequence of TN-C impairing cell adhesion to FN by blocking the binding site of syndecan-4 (96). As a result, tumor cell proliferation was enhanced in the presence of TN-C. Gene expression profiling revealed the mechanistical details for this effect: TN-C disrupts the actin cytoskeleton by downregulation of tropomyosin 1, while it was able to de-repress and activate Wnt and MAPK signaling, respectively (98). Besides having a pro-proliferative effect on cancer cells, TN-C is also able to stimulate proliferation of endothelial and smooth muscle cells (45). The mitogenic activity of TN-C is supported *in vivo* by immunohistochemistry showing TN-C co-expression with the proliferation marker Ki-67/Mib-1 in many invasive carcinomas (99), and the observation that TN-C is associated with proliferative epithelial cells in regenerating epithelia (100). A study by Swindle et al. also revelaed that select EGF-like repeats of TN-C might promote proliferation in an EGFR-dependent way by activating downstream MAPK signaling (101). In contrast, there are not many studies available on the effect of TN-W on cell proliferation. While an anti-proliferative activity was reported for TN-W in the murine osteoblastic cells MC3T3 (92), treatment of MDA-MB231-1833 breast cancer cells with

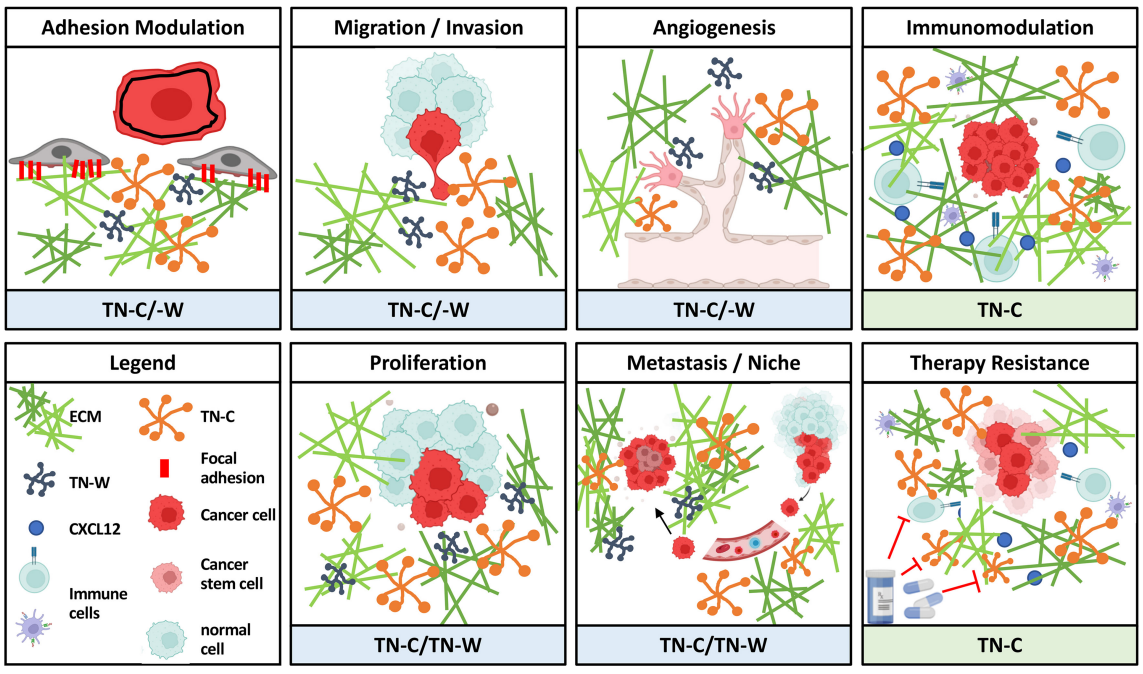

FIGURE 3 | Overview of oncogenic activities of TN-C and TN-W. As matricellular proteins, TN-C and TN-W can influence various cellular processes involved in tumor progression by modulating the interplay between stromal and epithelial cells or other cells. Schemes were created using www.biorender.com.

different concentrations of recombinant TN-W resulted in a significant increase of BrdU incorporation, suggesting that TN-W is able to stimulate cancer cell proliferation (91).

4.3 Cell Migration/Invasion

In clinical specimens, TN-C is often expressed in the intratumoral stroma but also at the invasive front of the tumor nests (46). TN-C expression at the invasive front is correlated with aggressive tumor behavior and poor prognosis and is suggestive of a role for TN-C in promoting migration and invasion of cancer cells (45, 46). These observations could be recapitulated *in vitro* by showing increased motility of various cell types, including cancer cells, fibroblasts, endothelia cells, and smooth muscle cells, in the presence of soluble TN-C or TN-C as substratum (102–104). Again, the TN-C-mediated cell adhesion modulating effect might explain the mechanisms underlying the pro-migratory outcome. In the presence of TN-C, cancer cells cannot properly spread, favoring an intermediate state of adhesions with suppressed Rho activation and actin-rich filipodia, which enhances their motile behavior (105). In contrast, lack of TN-C allows cell spreading and the formation of stable focal adhesions with stress fibers. Similar pro-migratory properties can be attributed to TN-W, although the molecular mechanisms have not been elucidated yet. First evidence for this finding has been gained in the highly metastatic murine mammary cancer cell line 4T1, which showed a faster migratory behavior across a transwell filter coated with TN-W (87). A follow-up study using human T47D breast cancer cells lines confirmed this result and showed that treatment of the cells with soluble TN-W increased their migratory phenotype (88). Accordingly, the migration of chicken osteoblasts across filters coated with TN-W was stimulated and TN-W added to the medium increased osteoblast migration when cultured on FN-coated filters when compared to controls (106).

Another prominent feature that is linked to altered motile behavior is the process of epithelial-mesenchymal-transition (EMT). While EMT is crucial during development, cancers often use this process for invasion and their dissemination into distant organs (107). TN-C has been found to be able to promote EMT. In MCF7 breast cancer cells, TN-C induced EMT-like morphological changes, which, on a molecular level, included the delocalization of E-cadherin and β-catenin correlating with tyrosine-protein kinase SRC activation and the SRC-mediated phosphrorylation of FAK (108). Subsequently, these changes were accompanied by cell detachment from the substratum and an enhanced migratory cell phenotype. In clinical breast cancer specimens, a frequent upregulation and co-localization of TN-C with the mesenchymal marker vimentin was observed at the invasive fronts of cancers in those cells having a more scattered and mesenchymal-like morphology. Such a cancer fingerprint could be correlated to increased malignancy in breast cancer (109). These data suggest an active role for TN-C in promoting EMT-like features. In regard to this, a recent *in vitro* study identified the highly conserved C-terminal FBG of TN-C and TN-W as activators of latent TGFβ (110). Subsequently, the mature TGFβ is presented to cells, which elicits an intracellular smad-dependent signaling cascade. Since TGFβ is a potent inducer of EMT (111), these data indicate that the FBGs of tenascins might be able to promote a TGFβ-mediated EMT. Whether this process plays an active role in TN-C- and/or TN-W-rich tumor stroma remains to be elucidated. However, EMT-promotion by tenascins represent intriguing options for them to drive cancer progression.

4.4 Metastasis and the "Cancer Stem Cell" Niche

Metastasis is a complex multistep process by which cancer cells gain the power to escape from the primary tumor mass, disseminate into the vasculature and throughout the body, and finally home and colonize distant organ sites to form secondary cancers (112). On this journey, cancer cells must overcome several hurdles and challenges. Successfully disseminated cancer cells often are able to produce a specific microenvironment, a so-called niche, that protects them and enables them longer survival in a hostile environment during their metastatic journey (70, 113). The invasive front of tumors has been suggested to be rich in cancer-initiating cells ("cancer stem cells") and the same region is known to express high levels of TN-C, indicating that TN-C might be a component of the metastatic niche (70). Disseminating breast cancer cells that express their own TN-C have survival advantages early on until the CAFs take over and produce TN-C, creating a niche that supports their fitness by modulating stemness-like signaling pathways such as Wnt and Notch (70, 114). A more recent study promotes TN-C as a specific and highly-expressed molecule of the lymph node pre-metastatic niche in muscle invasive bladder cancer (115). In this niche, TN-C induction by CAFs is believed to be triggered by cytokines present within tumor cell-derived extracellular vesicles (EV). Hence, infiltrating tumor cells secrete EVs with signaling cues that prepare a TN-C-rich niche, which provides survival advantages (115). Similar findings have recently emerged for TN-W (91). Breast cancer cells on their way to metastasize to bone are surrounded by a specific niche, established by epithelial-mesenchymal interactions. Cancer cell-derived TGFβ1 induces *de novo* expression of TN-W in the stromal cells, providing an important component for the metastatic niche. Accordingly, aberrant presence of TN-W in the metastatic niche, shaped and tailored by the cancer cells, provides the stimuli for increased cancer cell proliferation and migration, thereby increasing the risk for bone metastases (91). *In vitro* studies in biliary tract cancers revealed that TN-W fibrils are only formed in the presence of stromal cells (89). This observation might reflect such a metastatic niche as well. In there, TN-W can carry out its potential oncogenic activities leading to the successful dissemination of the cancer cells.

TN-C is also believed to influence metastasis by its very specific organization in the tumor matrix networks. Together with additional ECM proteins, TN-C remodels the ECM to form channel-forming, migratory tracks, which provides signaling cues for the survival of cancer cells and supports dissemination of cancer cells during the metastatic process (116, 117). Notably, periostin (POSTN), another matricellular ECM molecule associated with the metastatic niche (118), interacts with TN-C and is responsible for TN-C incorporation into this specialized ECM organizational units. While doing so, POSTN might enhance collagen cross-linking, which leads to the formation of

migratory tracks during metastasis (119). Functionally, both POSTN and TN-C are known to be able to activate Wnt signaling in cancer cells by recruiting Wnt ligands and the downregulation of the Wnt signaling pathway inhibitor DKK1, respectively (98, 118). The education of stromal cells to produce POSTN and TN-C by infiltrating cancer cells represents a crucial step during the metastatic process, which might be exploitable for anti-cancer therapies.

4.5 Angiogenesis

TN-C as well as TN-W are found associated with endothelial cells in various cancers suggesting that both tenascins might play a role in promoting tumor angiogenesis. *In vitro*, both tenascins trigger an elongated morphology and motility of human umbilical vein endothelial cells (HUVEC), properties related to angiogenic endothelial cells (90). Presence of either TN-W or TN-C in a collagen gel induces endothelial cell sprouts in gel-embedded HUVEC spheroids compared to collagen alone (90). Similarly, injection of malignant melanoma cells into TN-C-deficient mice revealed significantly less vascularization within the tumor mass (120). All these data point towards an active role for TN-C and TN-W in promoting angiogenesis in cancers. Indeed, TN-C in the TME contributes to the angiogenic switch in neuroendocrine tumors (121) and belongs to the AngioMatrix signature (a panel of 110 ECM genes) that correlates with poor prognosis in glioma patients (122). In addition, a higher vessel density, but less functional vessels, are also observations attributed to high TN-C levels in tumors (121). How TN-W triggers angiogenesis mechanistically has yet to be addressed. For TN-C, it is known that its presence in the mesenchyme results in increased levels of the pro-angiogenic factor VEGF in A375 melanoma cell transplant experiments (120) and TN-C is able to repress Wnt signaling by DKK1 in tumor and endothelial cells creating a proangiogenic TME (121). Increased complexity was revealed by a more recent study showing that TN-C can regulate both pro- and anti-angiogenic factors (123). Direct contact of TN-C with endothelial cells inhibits YAP signaling by disrupting actin polymerization. Since YAP signaling is required for the induction of pro-angiogenic genes (e.g., *CTGF* and *CYR61*), endothelial cell survival, proliferation, and vessel formation is impaired. In contrast, brain cancer cells exposed to TN-C respond by secretion of pro-angiogenic signals promoting tubulogenesis of endothelial cells. Hence, TN-C can play multiple and opposing roles during tumor angiogenesis depending on the cells with which it interacts.

4.6 Immunomodulation

Although it has been known that TN-C is able to shape innate and adaptive immunity (124, 125), its impact on tumor immunity is not fully elucidated yet. Studies have revealed that the C-terminal FBG of TN-C as well as of TN-W is able to activate TLR4 on either macrophages or fibroblasts (35, 126). TLR4 is a key component of the innate immune system and when activated stimulates the secretion of pro-inflammatory cytokines such as IL6, IL8, or TNFα (127). *In vivo* relevance for TLR4 activation by the FBG of TN-C was established in an orthotopic grafting model of breast cancer (128). Application of a therapeutic monoclonal antibody raised against the FBG of TN-C blocked TLR4 activation and reduced primary tumor growth and metastasis (128). The same authors reported a dual role for TN-C on tumor immunity depending on its cellular source: while tumor cell-derived TN-C polarized macrophages towards a pathogenic, immune-suppressive phenotype, host stromal cell-derived TN-C promoted immunity by recruiting anti-tumoral macrophages. Additional roles for TN-C in modulating the immune system in cancers are only recently emerging. In a mouse model, prostate cancer-initiating cells were protected from immune surveillance by over-expressing TN-C, which in turn was able to inhibit T-cell proliferation and effector functions (129). Similar results were obtained in a study in brain cancer. There, TN-C is packaged into exosomes derived from brain tumor-initiating cells and released into the microenvironment, where it can suppress systemic T-cell responses through an α5β1 or αvβ6 integrin-dependent inhibition of T-cell activation and proliferation (130). Both studies promote TN-C as a molecule providing protection for cancer-initiating cells from host-derived immune surveillance. Moreover, TN-C was recently shown to contribute to an immune-suppressive microenvironment in oral squamous cell carcinoma by mobilizing dendritic cells in the tumor stroma through binding CCL21 (131). Similarly, TN-C was responsible for the induction of CXCL12, which in turn immobilized $CD8^+$ tumor infiltrating T lymphocytes (CD8 TIL) in the matrix. Trapped in the TN-C-rich matrix, CD8 TIL could not combat and kill breast cancer cells, suggesting a role for TN-C in anti-tumor immunity escape (132). The newest discovery that the FBGs of both TN-C and TN-W can activate latent TGFβ renews speculation about a potential involvement of tenascins in tumor immunomodulation (110) since TGFβ is a potent suppressor of immune responses (133). Data on the effect of TN-W in immunomodulation remain absent apart from the potential of its FBG to activate TLR4 and TGFβ. Whether such activities might play a role in tumor progression has to be addressed in the future.

4.7 Therapy-Related Activities

Cancer therapy resistance represents a major hurdle and some evidence suggests that TN-C might be involved in this process. In a melanoma model, knockdown of TN-C not only significantly diminished the stem cell-like cells in melanoma spheres, but also lowered their resistance to doxorubicin treatment (134). Therefore, it can be assumed that TN-C is a driver of melanoma progression as it provides protective cues for therapy-resistant melanoma-initiating cells. A tumor-specific large TN-C isoform was shown to confer gemcitabine resistance in pancreatic cancer cells by the canonical phosphatidylinositol 3-kinase/AKT/NF-κB signaling pathway by its interaction with Annexin2 (135). In a study aiming to determine changes of stromal proteins in breast cancer following neoadjuvant chemotherapy, TN-C was identified as a molecule being important for conferring cancer cell resistance to doxorubicin- and docetaxel-based neoadjuvant chemotherapy by activating the integrinβ1/mTOR pathway (136). Moreover, a correlation of high *TNC* expression with tamoxifen resistance was identified in a clinical study analyzing 1286 primary breast tumors by qPCR (137).

Having reviewed the functions of TN-C in tumor immunity, TN-C might also affect the success rate of anti-cancer immunotherapies. Regarding this, a recent study identified a molecular mechanism explaining the observation that triple-negative breast cancers (TNBC) often do not respond to T-cell-mediated immunotherapies (138). In TNBC, defective autophagy-mediated TN-C degradation results in TN-C accumulation, which impairs T-cell-mediated tumor cytotoxicity. This phenotype could be reversed by inhibition of TN-C suggesting an important role for TN-C in autophagy deficiency-mediated immunosuppression. Consequently, blocking TN-C by specific anti-TN-C antibodies could boost the efficiency of immunotherapies in TNBC.

In addition to chemo- and immunotherapies, radiotherapy is a frequent cancer treatment option. Radiotherapy triggers DNA damage leading to the death of rapidly dividing cancer cells. However, tissues adjacent to the tumor and other normal cells are also affected. Ionization can lead to the modulation of the ECM and indeed, TN-C has been found to be induced upon this treatment (47). Moreover, it is known that ionization also stimulates an inflammatory reaction, fibrosis, and hypoxia. These conditions are known to mediate high TN-C expression (28). With all the knowledge we have gained about the tumor-promoting activities of TN-C, radiation, while killing cancer cells, might also create a pro-tumorigenic stroma. Whether or not this radiation-induced TN-C plays a role in potential tumor relapses, or secondary tumor formations after radio-treatment, remains to be investigated. Nothing is known yet about TN-W function in therapy resistance.

5 CAN WE MAKE USE OF THE PROMINENT EXPRESSION OF TNC AND TNW IN TUMOR STROMA?

Having summarized the expression patterns of TN-C and TN-W in tumors as well as their potential tumor-promoting activities, we plan to shed light on the possibilities they offer to be harnessed for clinical use and for the benefit of cancer patients.

5.1 Diagnostic and/or Prognostic Tumor Biomarker

Cancers are most dangerous when they are able to form distant metastases. Unfortunately, some cancers are only detected when such metastases have already formed rendering therapy even more challenging. In order to prevent this, there is an urgent need for diagnostic tumor markers that recognize premalignant lesion with high specificity and sensitivity. The best-case scenario would be that in adult healthy tissues a potential biomarker is not detectable, while its levels are sharply elevated in early premalignant dysplasia. This would allow an early detection of dysplastic and pre-malignant tissues. Both TN-C and TN-W seem to be interesting cancer biomarker candidates as they are often over-expressed in the tumor stroma (**Figure 4A**). However, the two tenascins differ significantly in their expression in healthy and noncancerous tissues. A recent screening of a healthy tissue microarray revealed limited basal TN-W expression. Apart for some expression in spleen, kidney, and some adult stem cell niches (e.g., hair follicles), as has been already observed in the initial mouse studies, TN-W was also weakly present in the female reproductive system and in certain glands (89). In contrast, TN-C is readily detectable in a larger array of healthy tissues (**Figure 4A**). Moreover, it is well established that TN-C upregulation is not restricted to cancers, but that abundant TN-C expression is a prominent feature of many other pathological conditions. These include inflammatory diseases (e.g. arthritis and asthma), infections (e.g. viral infections), and tissue remodeling processes such as wound healing and fibrosis (28). This is in stark contrast to TN-W, for which there is no evidence for *de novo* expression in pathological conditions other than cancers. Even in conditions with strong TN-C expression such as healing wounds and inflammatory bowel diseases, TN-W is not detectable (**Figure 4B**). These observations promote TN-W as a better and more tumor-specific tissue biomarker than TN-C (48). However, we have mentioned that TN-C is subject to alternative splicing generating very tissue- and condition-specific isoforms. Therefore, it might be also worth studying tumor-specific expression of distinct TN-C isoforms. It is known that certain splice variants, especially the variants with additional FNIII domains, are expressed in cancerous conditions. Hence, even if normal healthy tissue is expressing TN-C, detection of tumor-specific TN-C isoforms might still be of clinical value as a diagnostic readout.

TN-C and TN-W can also be detected in elevated concentrations in serum of cancer patients. But similar to the situation in tissues, increased TN-C levels in serum are also found in additional pathologies. Some of the conditions known to have increased serum TN-C levels include spondylitis, sepsis, myocardial defects, traumatic brain injuries, rheumatic diseases, pulmonary hypertension, Alzheimer's disease, systemic lupus, idiopathic inflammatory myositis, muscular dystrophy, chronic hepatitis C infection, and chronic renal diseases (139–146). Common to most of these conditions is the fact that they involve an inflammatory reaction. Therefore, it is not surprising that TN-C in serum correlates with C- reactive protein, a common inflammation marker, and represents a questionable tumor biomarker (147, 148). As mentioned above, the presence of certain TN-C splice variants in serum may still have some value as a marker of cancer. In contrast, to date elevated TN-W has only been detected in the serum of cancer patients (52).

Numerous studies also assessed the prognostic value of TN-C. Although these results are often ambiguous, there seems to be a clear trend towards a positive correlation between TN-C levels and local tumor recurrence, the metastatic potential, and poor prognosis in many aggressive human cancers. This correlation was observed in clinical specimens of brain, breast, colon, head and neck, and lung cancer (45). Why this observation is not valid for other cancers is not understood, but it might reflect the multifunctional roles of TN-C and tumor heterogeneity. There

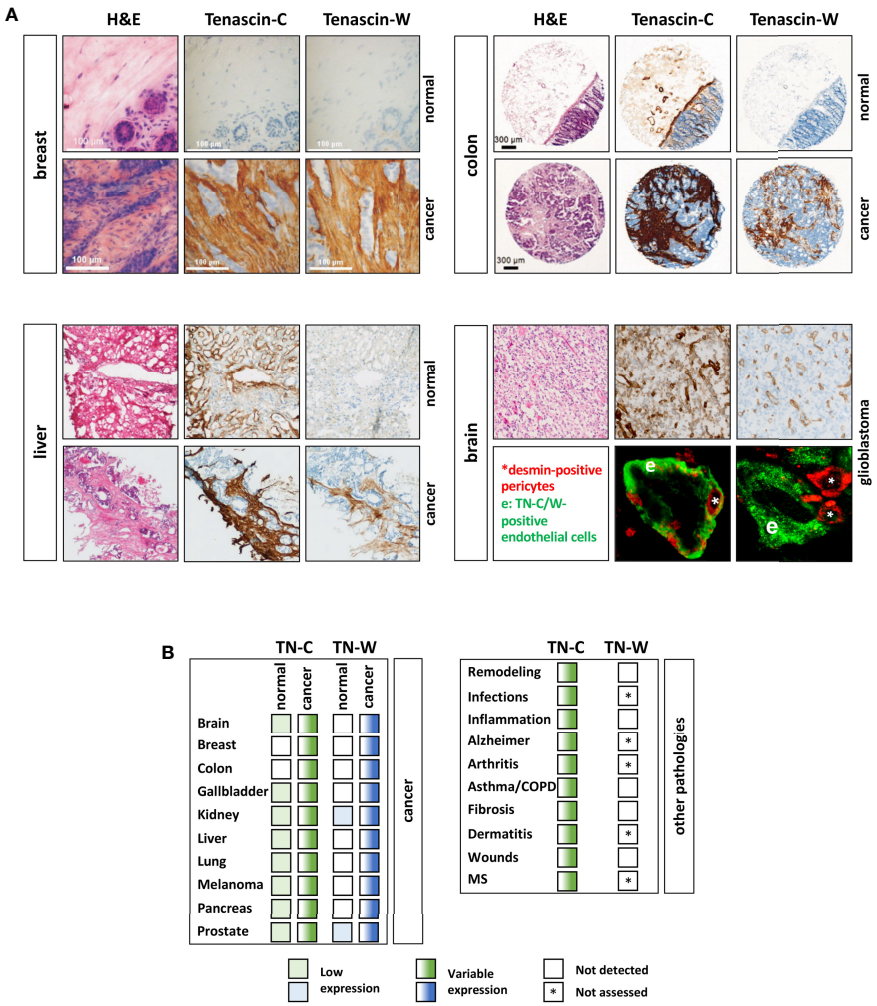

FIGURE 4 | TN-C and TN-W expression in human cancers. **(A)** Examples of immunohistochemical analyses of TN-C and TN-W in human breast, liver, and colorectal cancer as well as in adjacent normal tissues. Note that while TN-W is not expressed in healthy tissues, TN-C is detectable in colon and liver. In glioblastoma TN-C and TN-W show strong expression around vessel-like structures (top). Double immunofluorescence staining of TN-W or TN-C (green) with desmin (red) shows that TN-C encloses all pericytes, while TN-W staining is adjacent to them. Original images of breast tissue from Degen et al. (88), of liver tissue from Hendaoui et al. (89), of colon tissue from Degen et al. (52), and of brain tissue from Martina et al. (90) with permission. **(B)** Table of all cancer/normal tissues that have been analyzed so far for TN-W and TN-C by immunohistochemistry and/or immunoblotting (left). Right table shows non-cancerous conditions with TN-C upregulation and non-detectable (white box) TN-W expression. Fully colored boxes: expressed; gradient-colored boxes: variable expression ranging from low (light) to high (dark). * not assessed yet; MS, multiple sclerosis.

are also two studies that report a correlation of serum TN-C with prognostic factors of cancers: In non-small cell lung cancer patients TN-C serum levels correlated with larger tumor size, lymph node metastases and patient's overall survival (51), while serum TN-C levels in grade 3 breast cancer were significantly higher than in grade 1-2 tumors (50). Moreover, TN-C is known to be a substrate for various matrix metalloproteinases and serine proteases, which can lead to TN-C fragmentation (149). Significantly more small TN-C fragments were found in lung cancer patients who had a higher risk to develop lymph node as well as poor overall survival suggesting that TN-C degradation might be a marker for the metastatic potential of lung tumors (150, 151). Unfortunately, little has been done to date to study the prognostic value of TN-W. Initially, TN-W was found to be mainly enriched in mouse models of mammary cancer that metastasize (87). However, such a correlation could not be confirmed in human breast cancer where TN-W was more strongly expressed in low-grade tumors than in high-grade tumors (88). In lung cancer, TN-W showed a tendency towards higher expression in high-grade compared to low-grade cancers. Similarly, the more severe clear cell carcinoma expressed more TN-W (and TN-C) than the less severe oncocytoma (48). In colorectal carcinoma patients with tumor recurrence, serum TN-W levels were higher than in those without recurrence (52). Although these data suggest some prognostic value of TN-W in certain malignancies, the number

of cases analyzed for TN-W are too small to draw any definite conclusions yet.

5.2 Modulating Tumor-Specific Tenascin Expression

TN-C and TN-W are enriched in most solid human tumors. Both molecules also share a broad spectrum of tumor-promoting activities (**Figure 3**). Reversing their high expression in tumors could be a promising concept to normalize the TME thereby impairing its effect on promoting tumor progression. This approach should be attempted in combination with more classical, cancer cell-targeting therapies with the ultimate goal to limit the metastasis of, and to kill, cancer cells. To target tumor-expression of tenascins and prevent TN-C and TN-W from joining the TME, there are broadly two options: pharmacological inhibition and gene-based approaches.

5.2.1 Pharmacological and Natural Inhibitors

A simple concept for reducing the expression levels of tenascins includes the inhibition of the signaling pathways required for to their activation. However, this approach requires full knowledge about how tenascins are regulated in tumors. While for TN-C several pathways have been reported to lead to its induction (e.g. TGFβ signaling), knowledge of TN-W regulation in tumors remains sparse. In addition, inhibiting such important and canonical pathways will likely have unwanted side effects and therefore, does not represent a feasible approach to target tenascins in tumor stroma.

The use of miRNAs might represent an alternative approach to target tenascins. miRNAs are regulators of post-transcriptional gene regulation, which are also known to play a critical role in different cancer types as their dysregulation has been shown to affect the hallmarks of cancer (152). Therefore, tenascin-specific miRNA could be utilized in combination with additional treatment strategies to increase treatment success against cancer. A major challenge for this approach is the efficient delivery of these agents to target cells, which might require antibodies or peptides. Several miRNAs have been identified to suppress TN-C levels in cancers: miRNA-198 in colorectal cancer (153), miRNA-335 in breast cancer (154), miRNA-150 in head and neck squamous cell carcinoma (155), and miRNA-218 in glioma (156). In brain cancer, miRNA-107 indirectly diminishes TN-C levels by targeting Notch2, a direct inducer of TN-C (157). So far, no data exist about a possible regulation of TN-W by miRNAs.

Glucocorticoids are known repressors of both TN-C and TN-W (60). Therefore, the use of corticoids, which dampen tenascin expression, might represent a promising addition to the treatment cocktail of specific cancer types. Such an approach is applied in the treatment of castration-resistant prostate cancer patients, who receive dexamethasone as monotherapy or as part of their chemotherapeutic cocktail (158, 159). However, the effects of a widespread use of dexamethasone either to attenuate the side effects of chemotherapy or to combat malignancies might be double-edged as it has been shown that the glucocorticoid can enhance lung metastasis of breast cancer cells (160).

Recently, an approach to reduce TN-C in the tumor stroma of pancreatic cancer involved interfering with the aberrant cancer cell-mesenchymal crosstalk, which is required for stellate cell activation (161). These activated stellate cells are responsible for TN-C secretion into the stroma, in which TN-C can activate oncogenic signaling cascades (Wnt/β-catenin *via* inhibition of DKK1 and YAP/TAZ signaling) leading to tumor progression. The metastasis suppressor, N-myc downstream-regulated gene-1 (NDRG1) is able to dampen tumorigenesis by inhibiting these two pathways as well as by decreasing TGFβ production by cancer cells. The latter factor is required for stellate cell activation, which enables TN-C synthesis. Consequently, upregulation of NDRG1 might have the power to normalize the TME by impairing stellate cell activation thereby preventing induction of TN-C. Interestingly, the anti-cancer compounds thiosemicarbazone potently upregulate NDRG1, which both prevents aberrant epithelial-stellate cell crosstalk and synthesis of TN-C.

5.2.2 Gene-Based Approaches

Another strategy for anti-cancer treatment includes the use of RNA interference (RNAi) technologies. With RNAi, it is possible to specifically target a gene that is known to play a key role in tumor progression. As such it is not surprising that several attempts used RNAi to target TN-C in cancers (**Table 1**). Double-stranded RNAs specific for the TN-C sequence (ATN-RNA) were used to inhibit its expression in glioma, which are rich in TN-C. ATN-RNA was injected into the brain of 11 patients after initial tumor surgery, and treatment specificity and effects were assessed (162). Thereafter, the study was extended to 46 patients with grade II, III, and IV glioma (163, 164). Both the well-being as well as progression-free and overall survival of the patients were significantly increased in the ATN-RNA treated patients compared to the ones only obtaining brachytherapy. Although promising, this treatment only provided small advantages in survival prolongation. Whether the foreign dsRNA elicited an immune response affecting the patient's outcome was not assessed. A recent study used the same approach *in vitro* to show proof of concept for ATN-RNA application in breast cancer (165). ATN-RNA treatment significantly downregulated TN-C in MDA-MB-231 cells and reduced many TN-C-mediated activities for tumor progression, such as cancer cell proliferation and migration. Although, the ATN-RNA approach shows some apparent benefits, systemic delivery of RNAi to the patients remains one of the most difficult challenges in the clinic. We are not aware of any RNAi approaches targeting TN-W in the tumor stroma.

5.2.2.1 Function Blocking Antibodies

In an effort to develop novel and better tools to detect human TN-C, recombinant single-domain nanobodies (Nbs) have been recently raised in the dromedary (166). Nbs possess favorable properties over regular antibodies as they present a high stability, solubility, specificity as well as low immunogenicity. These Nbs recognized the 5th FNIII repeat of TN-C and were able to specifically detect TN-C in formalin-fixed and paraffin-embedded tumor sections. The Nbs also abolished certain pro-

TABLE 1 | Strategies for targeting TN-C in cancer treatment.

TN-C	COMPOUND	APPLICATION	CANCER TYPE/ MODEL	CLINICAL TRIALS	OUTCOME	REF
INTERFERENCE RNA	ATN-RNA (anti TN-C dsRNA)	Injection into the brain after tumor resection	Glioma	11 patients	Significant extension of survival	(162)
	ATN-RNA (anti TN-C dsRNA)	Injection into the brain after tumor resection	Glioma, grade II, III, and IV	46 patients	Increased overal well-being and survival	(163, 164)
	ATN-RNA (anti TN-C dsRNA)	"Proof of concept" in MDA-MB-231 cells	Breast cancer cells	preclinical	Reduced tumor cell proliferation and migration	(165)
FUNCTION BLOCKING ANTIBODIES	Single domain nanobodies (Nbs)	"Proof of concept" in KRIB cells	Osteosarcoma cells	preclinical	TN-C function-blocking	(166)
PEPTIDES	PL1 (targeting FN-EDB and TN-C-C) loaded with pro-apoptotic payload	10 injections every other day	Xenograft mose model of glioma (U87-MG)	preclinical	Reduced tumor size and prolonged median survival	(167)
	PL3 (targeting TN-C-C and NRP1) loaded with pro-apoptotic payload	10 injections every other day	Xenograft mose model of glioma (U87-MG)	preclinical	Prolonged survival	(168)
	Ft peptide (targeting TN-C and NRP1) loaded with paclitaxel	Intravenously administered every 2 weeks for 3 times	Xenograft mose model of glioma (U87-MG)	preclinical	Prolonged survival	(169)
APTAMERS	^{99}mTc-TTA1	Tumor imaging and targeted delivery of payload	Xenograft mouse models	preclinical	Specific uptake into tumors (glioma)	(170–172)
	GBI-10	SELEX for TN-C	–	–	Several TN-C-specific sequences were bound	(173)
	^{18}F-Fb-TN-C	PET tracer based on a TN-C ssDNA aptamer	Xenograft models (glioma, lung, melanoma cell lines)	preclinical	Tumor-specific uptake with high tumor-background ratio	(174)
	^{64}Cu-NOTA-TN-C	PET tracer based on a TN-C ssDNA aptamer	Xenograft models (glioma, lung, melanoma cell lines)	preclinical	Tumor-specific uptake with high tumor-background ratio	(174)
	SMART	Cancer imaging probe	Cell lines *in vitro*	preclinical	Enhanced specificity and signal intensity when compared to "mono" probes	(175)
ANTIBODY-DRUG-CONJUGATES	Tenatumomab-^{131}I (sigma-tau i.f.r. S.p.A.)	RI	Various solid cancers	Phase I; NCT02602067; terminated	Uptake of drug into the tumor lesion was negligible	
	81C6-^{131}I (Neuradiab, Bradmer Pharmaceuticals)	RI after resection followed by systemic chemotherapy	Primary or metastatic brain cancer	Phase I/II	Low toxicity and prolonged survival	(176, 177)
	81C6-^{131}I (Neuradiab, Bradmer Pharmaceuticals)	RI combined with temozolomide	Glioma, grade IV	Phase III; NCT00615186; terminated	Delay in site initiation and funding considerations	
	81C6-^{131}I (Neuradiab, Bradmer Pharmaceuticals)	RI after resection	Recurrent brain and central nervous system tumors	Phase I; NCT00002753; completed	Unknown	
	81C6-^{131}I (Neuradiab, Bradmer Pharmaceuticals)	Bolus injection vs. microinfusion	Primary brain and central nervous system tumors	Phase I/II; NCT00003478; completed	Unknown	
	81C6-^{131}I (Neuradiab, Bradmer Pharmaceuticals)	RI after resection	Primary or metastatic brain cancer	Phase I/II; NCT00002752; completed	Unknown	
	81C6-^{131}I (Neuradiab, Bradmer Pharmaceuticals)	RI after tumor resection combined with carmustine or irinotecan	Primary brain cancers	Phase I; NCT00003484; completed	Unknown	
	81C6-^{131}I (Neuradiab, Bradmer Pharmaceuticals)	Combined with bevacizumab (Avastin)	Glioma, grade IV	Phase II; NCT00906516; unknown	Unknown	
	81C6-^{211}At (Bradmer Pharmaceuticals)	RI after resection	Primary or metastatic brain cancer	Phase I/II; NCT00003461; completed	Unknown	
	81C6-^{211}At (Bradmer Pharmaceuticals)	RI after resection follwed by systemic chemotherapy	Primary or metastatic brain cancer	Phase I/II	Tolerable toxicity and promising response	(178)

(Continued)

TABLE 1 | Continued

TN-C	COMPOUND	APPLICATION	CANCER TYPE/ MODEL	CLINICAL TRIALS	OUTCOME	REF
	F16-IL2 (Teleukin, Philogen)	Combined with doxorubicin	Advanced solid tumors, breast cancer	Phase I/II; NCT01131364; terminated	Safe administration	(179)
	F16-IL2 (Teleukin, Philogen)	Combined with paclitaxel	Solid tumors, breast cancer, metastatic melanoma, lung cancer	Phase I/II; NCT01134250; completed	Safe administration/disease stabilization	(180)
	F16-IL2 (Teleukin, Philogen)	Combined with cytarabine	AML, relapse, adult	Phase I; NCT0297032; active	Marked reduction of AML lesions; clinical improval	(181)
	F16-IL2 (Teleukin, Philogen)	Combined with paclitaxel	Merkel Cell Carcinoma	Phase II; NCT02054884; terminated	Terminated due to lack of enrollment	
	F16-IL2 (Teleukin, Philogen)	Combined with anti-CD33 antibody BI 836858	AML relapse after allogeneic stem cell transplantation	Phase I; NCT03207191; completed	Unknown	
	F16-IL2 (Teleukin, Philogen)	Combined with temozolomide	Xenograft mose model of glioma (U87-MG)	preclinical	Complete remission	(182)
	F16-^{131}I (Tenarad, Philogen)	RI	Solid tumors, Hodgkin's lymphoma	Phase I/II; NCT01240720; completed	Partial response/stabilization; tolerable toxicity	(183)
	F16-^{124}I (Philogen)	RI	Head and neck cancer	Phase 0	Tumor-specific uptake and good tolerance	(184)
	BC-2-^{131}I; BC-4-^{131}I	RI	Glioma, recurrent	Phase II; -; completed	Partial stabilization	(185)
	BC-4-biotin + avidin + ^{99}Y-biotin	Pre-targeted antibody-guided RI	Glioma	Phase I; -; completed	Stabilization	(186)
PEPTIDE-ANTIBODY	iRGD peptide fused to TN-C-C antibody G11	Tail vein injection	Xenograft mose model of glioma (U87-MG)	preclinical	Improved homing to blood vessels, extravasation, and penetration of tumor parenchyma	(187)

Summary of the strategies mentioned in the text for TN-C-targeted approaches in cancer treatment. If available, the NTC identifiers are indicated (www.clinicaltrials.gov). Table was adapted from reference (47). Note that so far there are no clinical trials aimed to target cancer-specific TN-W, TN-R or TN-X. RI, Radioimmunotherapy; AML, Acute Myeloid Leukemia; IL2, Interleukin-2; SELEX, Systematic Evolution of Ligands by Exponential Enrichment; SMART, Simultaneously Multiple Aptamers and RGD Targeting; RGD, arginine-glycine-aspartic acid; PET, Positron Emission Tomography; ds, double-stranded; ss, single-stranded; TN-C, Tenascin-C; TN-C-C, Tenascin-C with extradomain C; FN-EDB, Fibronectin with extradomain B; NRP1, Neuropilin-1; REF, References.

tumorigenic functions of TN-C, such as cell adhesion modulation on a FN substratum as well as stromal retention of dendritic cells DC2.4 by CCL21/TN-C. These results promote the newly developed TN-C-specific Nbs as novel molecular tools for detecting TN-C in tumors (diagnostic biomarker) as well as for their potential use as anti-cancer treatment options by blocking the oncogenic functions of TN-C (**Table 1**). Although TN-W-specific single-domain antibodies have been developed in the dromedary as well (188), so far they only have been tested for the specific detection and imaging of TN-W and not for blocking its functions.

5.2.2.2 Affinity Ligands to TN-C and TN-W as Anti-Cancer Strategy

Well-known challenges faced by conventional cytotoxic anti-cancer drugs are their side effects in normal tissues and the barriers in the organism that the drugs need to cross to reach the target site. Specificity is lacking and high drug doses are required for reaching the required local compound concentration. For these reasons, drug-targeting strategies represent promising new avenues for anti-cancer treatment. High-affinity targeting ligands, such as antibodies, peptides, and aptamers can be used that specifically recognize a molecule overexpressed at the target site. By coupling active pharmacological molecules, it should be possible to maximize the therapeutic effects by specific drug delivery. The idea of targeted therapy was initially developed by Ehrlich more than 100 years ago, who proposed to kill pathogens without harming the body [reviewed by (189)]. This simple concept can be and is currently applied to cancer therapy where malignancies must be specifically targeted and eliminated. TN-C, including tumor-specific isoforms, and TN-W represent very promising targets for high-affinity ligands as they are both explicitly enriched in various tumor stroma and as ECM proteins represent quite stable antigens. The benefits in doing so are twofold: TN-C and TN-W are expressed and accessible in the TME (target site), and their levels represent excellent biomarkers for treatment success. As indicated before, available data so far speak in favor of TN-W being superior to TN-C as a tumor biomarker. This holds true both in regard to its tumor-specific expression and to its more significant threshold defining the stage of transformation from normal to malignant tissues as compared to TN-C. However, as it was identified almost 40 years ago, there is much more known about TN-C biology, function, and expression and more TN-C-specific tools have been developed for studying and targeting TN-C in animal models, preclinical, and clinical trials than for TN-W. Indeed, TN-C targeting approaches are actively exploited in *in vivo*

models as well as in clinical trials for delivering drugs (e.g., cytokines, radionuclides) specifically to distinct cancer tissues (**Table 1**). Several different tumor-homing agents have been used to target TN-C, including antibody fragments, monoclonal antibodies, peptides, and aptamers. Optimally, the ligand should possess high-binding affinity for TN-C and low immunogenicity. We present a short overview about the most promising approaches, tools and studies, which utilize TN-C as delivery address for anti-cancer payloads.

5.2.2.2.1 Peptides. During the last two years several novel peptide-based approaches for TN-C-targeted anti-cancer therapies have been developed. A peptide PL1 that targets bi-specifically the oncofetal FN isoform (FN-EDB) and a large TN-C isoform (TN-C-C) was identified and shown to home exclusively to the TME as well as to glioblastoma and prostate carcinoma cells in xenografts models (167). When loaded with a pro-apoptotic peptide, the PL1-targeted model nanocarrier was able to shrink glioblastoma in mice and significantly increase their survival. The same authors also developed a specific, octameric PL3 peptide targeting TN-C and cell- and tissue-penetration receptor NRP1. Promisingly, nanoparticles containing PL3-targeted anticancer payloads proved to be very useful in detection and systemic therapy in prostate carcinoma, glioma, and melanoma cells and in the corresponding xenograft mouse models, as the animal significantly survived for longer periods (168). A similar approach was applied by Kang et al. They also used the combination of TN-C and NRP1 as homing addresses for targeting the tumor ECM and neovasculature, respectively. When loaded with paclitaxel, the synergistic dual-targeting nanocarrier showed higher cytotoxic effects and apoptosis rate compared with mono-targeting approaches in glioma models (169).

5.2.2.2.2 Aptamers. Aptamers are short single-stranded oligonucleotides (DNA or RNA) and represent an alternative approach for targeting approaches in tumors. They possess high affinity and selectivity for a specific target, while there is low immunogenicity, amenability to modifications and conjugations, as well as favorable pharmacokinetics. Several TN-C-specific aptamers have been developed that can be used as imaging tools [^{99}mTc-TTA1 (170–172) and GBI-10 aptamers (173)] and PET tracers [^{18}F-Fb-TN-C and ^{64}Cu-NOTA-TN-C aptamers (174)] to localize and detect tumor-specific TN-C expression allowing the planning of personalized treatment strategies as well as tumor monitoring. Aptamers are usually taken up by a variety of solid tumors and are rapidly cleared from the blood and other nontarget tissues, which add to their beneficial properties. A multimodal nanoparticle-based Simultaneously Multiple Aptamers and RGD Targeting (SMART) cancer imaging probe, which is able to simultaneously target nucleolin (AS1411 aptamer), integrin $a_v\beta3$ (RGD), and TN-C (TTA1 aptamer) hes been described by Ko et al. (175). This probe showed enhanced tumor targeting efficacy and a better signal-to-noise ratio compared to mono-biomarker targeting approaches in various cancers (175). Moreover, TN-C targeting aptamers can also be used as vehicles for delivering radioisotopes or chemical agents to cancerous tissues and present novel potential therapeutic applications. So far, clinical trials with aptamers targeting TN-W have not been reported.

5.2.2.2.3 Antibodies. Antibody-drug-conjugate (ADC) technology aims to home a toxic agent specifically into the tumor using target-specific antibodies. Several ADCs have shown impressive results in treating cancers, which resulted in the approval of 11 different ADCs by the FDA that target hematologic as well as solid malignancies (190). Four crucial features might decide the success or failure of ADC applications: (i) specific tumor targeting; (ii) the property of the antibody itself; (iii) the nature of the cytotoxic payload; and (iv) the method used for linking the payload to the antibody. As described, TN-C and especially tumor-specific large TN-C isoforms (as well as TN-W) represent interesting tumor marker candidates for ADCs. Indeed, several monoclonal antibodies recognizing isoforms of TN-C are in preclinical and clinical stages. For instance, ^{131}I- and ^{211}At-labeled chimeric 81C6 monoclonal antibody (Neuradiab recognizing TN-C-C/D) as monotreatment or in combination with other compounds for the treatment of patients with non-Hodgkin lymphoma, with recurrent glioma, with primary or metastatic brain cancer showed encouraging initial results with relatively low toxicity (176–178). Additional TN-C-specific antibodies have been tested in recurrent malignant glioma patients (antibodies BC-2-^{131}I, BC-4-^{131}I; clinical phase II) and in anaplastic astrocytoma and glioblastoma patients (BC4-biotin + avidin + ^{99}Y-biotin; clinical phase I) and revealed disease stabilization with partial remission (185, 186). Another promising tool consisting of a fully humanized antibody F16 recognizing the variable FNIII domain A1 of TN-C has been developed by Philogen (191). In the small immunoprotein format (SIP), F16 was able to recognize TN-C in several different cancers such as glioblastoma, lymphoma, melanoma, head and neck, and renal cell carcinoma (182, 192–196). The promising biodistribution of F16 prompted its testing for radionuclide as well as cytokine/chemokine combination therapy. F16-^{124}I has been applied in four head and neck cancer patients resulting in a tumor-specific signal in all patients within 24 hours (184). Phase I/II clinical dose finding and efficacy trials (www.clinicaltrials.gov; NCT01240720) have been performed with F16-^{131}I (Tenarad) in eight Hodgkin lymphoma patients (183). Treatment of the patients with F16-^{131}I did not cause any severe toxicity problems and was effective in providing clinical benefit in the majority of the patients. Apart from radiotherapies, F16SIP is currently also evaluated for its potential as combinatory treatment option when coupled to IL2, which elicits an immune response that is able to kill cancer cells. So far, F16-IL2 (Teleukin, Philogen) has been applied in combination with paclitaxel for breast cancer, melanoma, non-small lung cancer [NCT01134250 (180)] as well as in metastatic Merkel cell carcinoma patients (NCT02054884), together with low doses of cytarabine in AML patients with advanced disease (NCT02957032 (181), and simultaneously with doxorubicin in advanced solid tumor and metastatic breast cancer patients (NCT01131364). Initial results for the studies using F16-IL2 are promising as it can be safely and repeatedly administered to patients with lung cancer in combination with paclitaxel (180) and to patients with different solid and metastatic breast cancer together with doxorubicin (179). The strong safety profile and the appear-

ance of early signs of clinical activity of F16-IL2 warrant further studies.

Tumor-homing, extravasation, and penetration of cancer drugs can be improved by conjugation to tumor penetrating iRGD peptides, which is a widely used approach (197–199). Several clinical trials are ongoing in pancreas, colon, and digestive cancers testing the effect of iRGD alone [NCT05052567 (not yet recruiting)] in combination with anti-cancer drugs nabpaclitaxel and gemcitabine [NCT03517176 (completed), NCT05042128 (not yet recruiting)], or with panitumumab [NCT05121038 (recruiting)]. Recently, a study analyzed the effect of genetic fusion of the iRGD peptide to recombinant anti-TN-C-C single-chain antibody clone G11 (58) in U87-MG glioma tumor models compared to the parental antibody (187). Comparative biodistribution studies revealed improved homing to blood vessels, extravasation, and tumor penetration in the presence of the iRGD peptide (187). Such an approach using a tumor-penetrating peptide-functionalized TN-C antibody could be more efficient in delivering therapeutic agents into solid tumor lesions and may develop into a useful strategy for affinity targeting of solid tumors.

6 CONCLUDING REMARKS

Tenascins are a family of matricellular proteins that show intriguing expression patterns. During development they are expressed widely in various tissues reflecting their important role in organ and tissue development. In most healthy adult tissues their levels of expression are greatly diminished. Upon disturbance of tissue homeostasis, which often accompanies the initiation of a tumor (200), TN-C and TN-W are sharply upregulated in the TME. There, they make use of their multifunctionality and interact with several other ECM proteins and cell surface receptors, eliciting signaling pathways that drive tumor progression (201).

In the embryo and in the TME tenascins are part of a complex microenvironment with many other ECM molecules and growth factors. With these many potential interaction partners available, tenascins have multiple possibilities to influence cell fate. This enormous complexity makes the study of the real *in vivo* effects and functions of tenascins in physiological as well in pathological conditions challenging. Can we really study tenascin function in a 2D tissue culture dish? Is the use of 3D conditions or Matrigel of any advantage to determine the *in vivo* function of these molecules? What all these study models have in common is the limitation that none can fully recapitulate the microenvironment as it exists *in vivo*. Still, the proper understanding and a thorough characterization of the tenascin members is of utmost importance. Even if the study conditions do not fully reflect the complexity of the *in vivo* situation, much has been and still can be learned from these experimental approaches. This is especially true for TN-C and TN-W, which are both prominently over-expressed in tumor stroma. The many pre-clinical and clinical studies trying to harness their tumor-specific expression for diagnostic and therapeutic use could not have been done without understanding the basics about TN-C and TN-W biology.

Fundamental to the study of TN-C and TN-W in clinical settings is the availability of excellent antibodies for their detection. For both proteins, outstanding antibodies have been raised (88, 147, 188), and more recent efforts generated TN-C-specific Nbs (166), which might be highly useful for future studies and clinical trials. Unfortunately, research on TN-W lags behind the research focused on its older brother, TN-C. In contrast to TN-C, TN-W function has not been thoroughly elucidated yet and there still remains a lot to be learned about the role of TN-W in tumors, which might clarify why it is expressed at a high level in many cancers. A better understanding of TN-W function and regulation, as well as its interactions with cellular receptors in tumors, might also provide the basis for more attempts in using it as a cancer biomarker or therapeutic target. This, of course, raises the questions about the importance of TN-C and TN-W in tumor ECM. Is it feasible to expect better cancer management or a normalization of the TME by targeting one specific aberrantly expressed ECM protein present in the tumor stroma, such as TN-C, while we know that the TME consists of a 3D meshwork with seemingly countless components? Perhaps after targeting TN-C in tumors stroma, TN-W can compensate for its absence and, therefore, a positive treatment effect is only short-lived or only achieved if both tenascins are targeted. The clinical trials with drug-delivery vehicles targeting TN-C produced some encouraging results in their initial phases (see above). Certainly, it is worth continuing this path of research and making use of their highly regulated expression in tumors. In this regard, TN-W might also represent an interesting and promising tumor-specific homing address for drug delivery: (i) TN-W is often expressed around blood vessels in the tumor stroma, which are often leaky making antibody administration feasible; (ii) TN-W is not known to be upregulated in pathologies other than cancers; and (iii) TN-W is generally not expressed in normal tissues with some few exceptions. However, we are currently not aware of such attempts. It also remains to be understood why among patients suffering from the same type of tumor, TN-W and TN-C expression is very heterogenous. Some patients display very high levels of the tenascins, while other patients only show modest expression [see for example (88)]. Which biochemical, biophysical or clinical properties dictate their regulation of expression in cancer?

Herein, we attempted to summarize some of the knowledge about the tenascin family of ECM proteins in health and cancer. Although we have learned much over the last 40 years, there is still much to be discovered. We are still far from being able to depict the full picture of the specific roles of each of the tenascin members and how they are incorporated into complex ECM networks, and how they are precisely regulated in health and disease. This is true for all four members. As of today, TN-C and TN-W are the most promising family members to be exploited for anti-cancer treatment. However, this does not diminish the potential roles that TN-R and TN-X might play in tumorigenesis. Clearly, more work is required to address and recognize the pleiotropic roles of all tenascin members in physiological as well as in pathological conditions. Only a broader understanding of tenascin biology might give us the chance to use them as

exploitable matricellular proteins for cancer diagnosis and monitoring as well as for anti-cancer therapies.

AUTHOR CONTRIBUTIONS

RT wrote the first draft of the abstract and section 2, MD wrote the first draft of the remaining sections. Both authors contributed to the figures and the final draft. All authors contributed to the article and approved the submitted version.

FUNDING

Open access publication fees have been paid by the University of Bern, Switzerland.

ACKNOWLEDGMENTS

We apologize to all colleagues whose work could not be mentioned due to space restrictions.

REFERENCES

1. Frantz C, Stewart KM, Weaver VM. The Extracellular Matrix at a Glance. *J Cell Sci* (2010) 123(Pt 24):4195–200. doi: 10.1242/jcs.023820
2. Karamanos NK, Theocharis AD, Piperigkou Z, Manou D, Passi A, Skandalis SS, et al. A Guide to the Composition and Functions of the Extracellular Matrix. *FEBS J* (2021) 288(24):6850–912. doi: 10.1111/febs.15776
3. Naba A, Clauser KR, Ding H, Whittaker CA, Carr SA, Hynes RO. The Extracellular Matrix: Tools and Insights for the "Omics" Era. *Matrix Biol* (2016) 49:10–24. doi: 10.1016/j.matbio.2015.06.003
4. Hynes RO. The Extracellular Matrix: Not Just Pretty Fibrils. *Science* (2009) 326(5957):1216–9. doi: 10.1126/science.1176009
5. Ozbek S, Balasubramanian PG, Chiquet-Ehrismann R, Tucker RP, Adams JC. The Evolution of Extracellular Matrix. *Mol Biol Cell* (2010) 21(24):4300–5. doi: 10.1091/mbc.E10-03-0251
6. Mueller MM, Fusenig NE. Friends or Foes - Bipolar Effects of the Tumour Stroma in Cancer. *Nat Rev Cancer* (2004) 4(11):839–49. doi: 10.1038/nrc1477
7. Shekhar MP, Pauley R, Heppner G. Host Microenvironment in Breast Cancer Development: Extracellular Matrix-Stromal Cell Contribution to Neoplastic Phenotype of Epithelial Cells in the Breast. *Breast Cancer Res* (2003) 5(3):130–5. doi: 10.1186/bcr580
8. Kalluri R, Zeisberg M. Fibroblasts in Cancer. *Nat Rev Cancer* (2006) 6 (5):392–401. doi: 10.1038/nrc1877
9. Bonnans C, Chou J, Werb Z. Remodelling the Extracellular Matrix in Development and Disease. *Nat Rev Mol Cell Biol* (2014) 15(12):786–801. doi: 10.1038/nrm3904
10. Lu P, Weaver VM, Werb Z. The Extracellular Matrix: A Dynamic Niche in Cancer Progression. *J Cell Biol* (2012) 196(4):395–406. doi: 10.1083/jcb.201102147
11. Pickup MW, Mouw JK, Weaver VM. The Extracellular Matrix Modulates the Hallmarks of Cancer. *EMBO Rep* (2014) 15(12):1243–53. doi: 10.15252/embr.201439246
12. Brellier F, Chiquet-Ehrismann R. How Do Tenascins Influence the Birth and Life of a Malignant Cell? *J Cell Mol Med* (2012) 16(1):32–40. doi: 10.1111/j.1582-4934.2011.01360.x
13. Chiquet-Ehrismann R, Kalla P, Pearson CA, Beck K, Chiquet M. Tenascin Interferes With Fibronectin Action. *Cell* (1988) 53(3):383–90. doi: 10.1016/0092-8674(88)90158-4
14. Scherberich A, Tucker RP, Samandari E, Brown-Luedi M, Martin D, Chiquet-Ehrismann R. Murine Tenascin-W: A Novel Mammalian Tenascin Expressed in Kidney and at Sites of Bone and Smooth Muscle Development. *J Cell Sci* (2004) 117(Pt 4):571–81. doi: 10.1242/jcs.00867
15. Saga Y, Yagi T, Ikawa Y, Sakakura T, Aizawa S. Mice Develop Normally Without Tenascin. *Genes Dev* (1992) 6(10):1821–31. doi: 10.1101/gad.6.10.1821
16. Mackie EJ, Tucker RP. The Tenascin-C Knockout Revisited. *J Cell Sci* (1999) 112(Pt 22):3847–53. doi: 10.1242/jcs.112.22.3847
17. Chiquet M. Tenascin-C: From Discovery to Structure-Function Relationships. *Front Immunol* (2020) 11:611789. doi: 10.3389/fimmu.2020.611789
18. Burch GH, Gong Y, Liu W, Dettman RW, Curry CJ, Smith L, et al. Tenascin-X Deficiency Is Associated With Ehlers-Danlos Syndrome. *Nat Genet* (1997) 17(1):104–8. doi: 10.1038/ng0997-104
19. Mao JR, Taylor G, Dean WB, Wagner DR, Afzal V, Lotz JC, et al. Tenascin-X Deficiency Mimics Ehlers-Danlos Syndrome in Mice Through Alteration of Collagen Deposition. *Nat Genet* (2002) 30(4):421–5. doi: 10.1038/ng850
20. Tucker RP, Chiquet-Ehrismann R. The Regulation of Tenascin Expression by Tissue Microenvironments. *Biochim Biophys Acta* (2009) 1793(5):888–92. doi: 10.1016/j.bbamcr.2008.12.012
21. Valcourt U, Alcaraz LB, Exposito JY, Lethias C, Bartholin L. Tenascin-X: Beyond the Architectural Function. *Cell Adh Migr* (2015) 9(1-2):154–65. doi: 10.4161/19336918.2014.994893
22. Anlar B, Gunel-Ozcan A. Tenascin-R: Role in the Central Nervous System. *Int J Biochem Cell Biol* (2012) 44(9):1385–9. doi: 10.1016/j.biocel.2012.05.009
23. Weber P, Bartsch U, Rasband MN, Czaniera R, Lang Y, Bluethmann H, et al. Mice Deficient for Tenascin-R Display Alterations of the Extracellular Matrix and Decreased Axonal Conduction Velocities in the Cns. *J Neurosci* (1999) 19(11):4245–62. doi: 10.1523/JNEUROSCI.19-11-04245.1999
24. Pesheva P, Probstmeier R, Skubitz AP, McCarthy JB, Furcht LT, Schachner M. Tenascin-R (J1 160/180 Inhibits Fibronectin-Mediated Cell Adhesion–Functional Relatedness to Tenascin-C. *J Cell Sci* (1994) 107(Pt 8):2323–33. doi: 10.1242/jcs.107.8.2323
25. Degen M, Scherberich A, Tucker RP. Tenascin-W: Discovery, Evolution, and Future Prospects. *Front Immunol* (2020) 11:623305. doi: 10.3389/fimmu.2020.623305
26. Tucker RP, Degen M. The Expression and Possible Functions of Tenascin-W During Development and Disease. *Front Cell Dev Biol* (2019) 7:53. doi: 10.3389/fcell.2019.00053
27. Imhof T, Balic A, Heilig J, Chiquet-Ehrismann R, Chiquet M, Niehoff A, et al. Pivotal Role of Tenascin-W (-N) in Postnatal Incisor Growth and Periodontal Ligament Remodeling. *Front Immunol* (2020) 11:608223. doi: 10.3389/fimmu.2020.608223
28. Chiquet-Ehrismann R, Chiquet M. Tenascins: Regulation and Putative Functions During Pathological Stress. *J Pathol* (2003) 200(4):488–99. doi: 10.1002/path.1415
29. Hsia HC, Schwarzbauer JE. Meet the Tenascins: Multifunctional and Mysterious. *J Biol Chem* (2005) 280(29):26641–4. doi: 10.1074/jbc.R500005200
30. Jones FS, Jones PL. The Tenascin Family of Ecm Glycoproteins: Structure, Function, and Regulation During Embryonic Development and Tissue Remodeling. *Dev Dyn* (2000) 218(2):235–59. doi: 10.1002/(SICI)1097-0177(200006)218:2<235::AID-DVDY2>3.0.CO;2-G
31. Tucker RP, Drabikowski K, Hess JF, Ferralli J, Chiquet-Ehrismann R, Adams JC. Phylogenetic Analysis of the Tenascin Gene Family: Evidence of Origin Early in the Chordate Lineage. *BMC Evol Biol* (2006) 6:60. doi: 10.1186/1471-2148-6-60
32. Chiquet-Ehrismann R, Tucker RP. Tenascins and the Importance of Adhesion Modulation. *Cold Spring Harb Perspect Biol* (2011) 3(5):a004960. doi: 10.1101/cshperspect.a004960
33. Tucker RP, Chiquet-Ehrismann R. Tenascin-C: Its Functions as an Integrin Ligand. *Int J Biochem Cell Biol* (2015) 65:165–8. doi: 10.1016/j.biocel.2015.06.003
34. Yoshida T, Akatsuka T, Imanaka-Yoshida K. Tenascin-C and Integrins in Cancer. *Cell Adh Migr* (2015) 9(1-2):96–104. doi: 10.1080/19336918.2015.1008332

35. Zuliani-Alvarez L, Marzeda AM, Deligne C, Schwenzer A, McCann FE, Marsden BD, et al. Mapping Tenascin-C Interaction With Toll-Like Receptor 4 Reveals a New Subset of Endogenous Inflammatory Triggers. *Nat Commun* (2017) 8(1):1595. doi: 10.1038/s41467-017-01718-7
36. Adams JC, Chiquet-Ehrismann R, Tucker RP. The Evolution of Tenascins and Fibronectin. *Cell Adh Migr* (2015) 9(1-2):22–33. doi: 10.4161/19336918.2014.970030
37. Midwood KS, Chiquet M, Tucker RP, Orend G. Tenascin-C at a Glance. *J Cell Sci* (2016) 129(23):4321–7. doi: 10.1242/jcs.190546
38. Hendaoui I, Tucker RP, Zingg D, Bichet S, Schittny J, Chiquet-Ehrismann R. Tenascin-C Is Required for Normal Wnt/Beta-Catenin Signaling in the Whisker Follicle Stem Cell Niche. *Matrix Biol* (2014) 40:46–53. doi: 10.1016/j.matbio.2014.08.017
39. Chiquet-Ehrismann R, Orend G, Chiquet M, Tucker RP, Midwood KS. Tenascins in Stem Cell Niches. *Matrix Biol* (2014) 37:112–23. doi: 10.1016/j.matbio.2014.01.007
40. Meloty-Kapella CV, Degen M, Chiquet-Ehrismann R, Tucker RP. Avian Tenascin-W: Expression in Smooth Muscle and Bone, and Effects on Calvarial Cell Spreading and Adhesion *in Vitro*. *Dev Dyn* (2006) 235 (6):1532–42. doi: 10.1002/dvdy.20731
41. Tucker RP, Ferralli J, Schittny JC, Chiquet-Ehrismann R. Tenascin-C and Tenascin-W in Whisker Follicle Stem Cell Niches: Possible Roles in Regulating Stem Cell Proliferation and Migration. *J Cell Sci* (2013) 126(Pt 22):5111–5. doi: 10.1242/jcs.134650
42. Bourdon MA, Wikstrand CJ, Furthmayr H, Matthews TJ, Bigner DD. Human Glioma-Mesenchymal Extracellular Matrix Antigen Defined by Monoclonal Antibody. *Cancer Res* (1983) 43(6):2796–805.
43. Mackie EJ, Chiquet-Ehrismann R, Pearson CA, Inaguma Y, Taya K, Kawarada Y, et al. Tenascin Is a Stromal Marker for Epithelial Malignancy in the Mammary Gland. *Proc Natl Acad Sci U S A* (1987) 84 (13):4621–5. doi: 10.1073/pnas.84.13.4621
44. Midwood KS, Hussenet T, Langlois B, Orend G. Advances in Tenascin-C Biology. *Cell Mol Life Sci* (2011) 68(19):3175–99. doi: 10.1007/s00018-011-0783-6
45. Orend G, Chiquet-Ehrismann R. Tenascin-C Induced Signaling in Cancer. *Cancer Lett* (2006) 244(2):143–63. doi: 10.1016/j.canlet.2006.02.017
46. Lowy CM, Oskarsson T. Tenascin C in Metastasis: A View From the Invasive Front. *Cell Adh Migr* (2015) 9(1-2):112–24. doi: 10.1080/19336918.2015.1008331
47. Spenle C, Saupe F, Midwood K, Burckel H, Noel G, Orend G. Tenascin-C: Exploitation and Collateral Damage in Cancer Management. *Cell Adh Migr* (2015) 9(1-2):141–53. doi: 10.1080/19336918.2014.1000074
48. Brellier F, Martina E, Degen M, Heuze-Vourc'h N, Petit A, Kryza T, et al. Tenascin-W Is a Better Cancer Biomarker Than Tenascin-C for Most Human Solid Tumors. *BMC Clin Pathol* (2012) 12:14. doi: 10.1186/1472-6890-12-14
49. Pauli C, Stieber P, Schmitt UM, Andratschke M, Hoffmann K, Wollenberg B. The Significance of Tenascin-C Serum Level as Tumor Marker in Squamous Cell Carcinoma of the Head and Neck. *Anticancer Res* (2002) 22(5):3093–7.
50. Didem T, Faruk T, Senem K, Derya D, Murat S, Murat G, et al. Clinical Significance of Serum Tenascin-C Levels in Epithelial Ovarian Cancer. *Tumour Biol* (2014) 35(7):6777–82. doi: 10.1007/s13277-014-1923-z
51. Gebauer F, Gelis S, Zander H, Meyer KF, Wolters-Eisfeld G, Izbicki JR, et al. Tenascin-C Serum Levels and Its Prognostic Power in Non-Small Cell Lung Cancer. *Oncotarget* (2016) 7(15):20945–52. doi: 10.18632/oncotarget.7976
52. Degen M, Brellier F, Schenk S, Driscoll R, Zaman K, Stupp R, et al. Tenascin-W, a New Marker of Cancer Stroma, Is Elevated in Sera of Colon and Breast Cancer Patients. *Int J Cancer* (2008) 122(11):2454–61. doi: 10.1002/ijc.23417
53. Adams M, Jones JL, Walker RA, Pringle JH, Bell SC. Changes in Tenascin-C Isoform Expression in Invasive and Preinvasive Breast Disease. *Cancer Res* (2002) 62(11):3289–97.
54. Hindermann W, Berndt A, Borsi L, Luo X, Hyckel P, Katenkamp D, et al. Synthesis and Protein Distribution of the Unspliced Large Tenascin-C Isoform in Oral Squamous Cell Carcinoma. *J Pathol* (1999) 189(4):475–80. doi: 10.1002/(SICI)1096-9896(199912)189:4<475::AID-PATH462>3.0.CO;2-V
55. Dueck M, Riedl S, Hinz U, Tandara A, Moller P, Herfarth C, et al. Detection of Tenascin-C Isoforms in Colorectal Mucosa, Ulcerative Colitis, Carcinomas and Liver Metastases. *Int J Cancer* (1999) 82(4):477–83. doi: 10.1002/(SICI)1097-0215(19990812)82:4<477::AID-IJC2>3.0.CO;2-5
56. Borsi L, Carnemolla B, Nicolo G, Spina B, Tanara G, Zardi L. Expression of Different Tenascin Isoforms in Normal, Hyperplastic and Neoplastic Human Breast Tissues. *Int J Cancer* (1992) 52(5):688–92. doi: 10.1002/ijc.2910520504
57. Hancox RA, Allen MD, Holliday DL, Edwards DR, Pennington CJ, Guttery DS, et al. Tumour-Associated Tenascin-C Isoforms Promote Breast Cancer Cell Invasion and Growth by Matrix Metalloproteinase-Dependent and Independent Mechanisms. *Breast Cancer Res* (2009) 11(2):R24. doi: 10.1186/bcr2251
58. Silacci M, Brack SS, Spath N, Buck A, Hillinger S, Arni S, et al. Human Monoclonal Antibodies to Domain C of Tenascin-C Selectively Target Solid Tumors *in Vivo*. *Protein Eng Des Sel* (2006) 19(10):471–8. doi: 10.1093/protein/gzl033
59. Galler K, Junker K, Franz M, Hentschel J, Richter P, Gajda M, et al. Differential Vascular Expression and Regulation of Oncofetal Tenascin-C and Fibronectin Variants in Renal Cell Carcinoma (Rcc): Implications for an Individualized Angiogenesis-Related Targeted Drug Delivery. *Histochem Cell Biol* (2012) 137(2):195–204. doi: 10.1007/s00418-011-0886-z
60. Chiovaro F, Chiquet-Ehrismann R, Chiquet M. Transcriptional Regulation of Tenascin Genes. *Cell Adh Migr* (2015) 9(1-2):34–47. doi: 10.1080/19336918.2015.1008333
61. Degen M, Goulet S, Ferralli J, Roth M, Tamm M, Chiquet-Ehrismann R. Opposite Effect of Fluticasone and Salmeterol on Fibronectin and Tenascin-C Expression in Primary Human Lung Fibroblasts. *Clin Exp Allergy* (2009) 39(5):688–99. doi: 10.1111/j.1365-2222.2009.03220.x
62. Scharer CD, McCabe CD, Ali-Seyed M, Berger MF, Bulyk ML, Moreno CS. Genome-Wide Promoter Analysis of the Sox4 Transcriptional Network in Prostate Cancer Cells. *Cancer Res* (2009) 69(2):709–17. doi: 10.1158/0008-5472.CAN-08-3415
63. Sivasankaran B, Degen M, Ghaffari A, Hegi ME, Hamou MF, Ionescu MC, et al. Tenascin-C Is a Novel Rbpjkappa-Induced Target Gene for Notch Signaling in Gliomas. *Cancer Res* (2009) 69(2):458–65. doi: 10.1158/0008-5472.CAN-08-2610
64. Borsi L, Allemanni G, Gaggero B, Zardi L. Extracellular Ph Controls Pre-Mrna Alternative Splicing of Tenascin-C in Normal, But Not in Malignantly Transformed, Cells. *Int J Cancer* (1996) 66(5):632–5. doi: 10.1002/(SICI)1097-0215(19960529)66:5<632::AID-IJC9>3.0.CO;2-U
65. Borsi L, Balza E, Castellani P, Carnemolla B, Ponassi M, Querze G, et al. Cell-Cycle Dependent Alternative Splicing of the Tenascin Primary Transcript. *Cell Adhes Commun* (1994) 1(4):307–17. doi: 10.3109/15419069409097262
66. Moritz S, Lehmann S, Faissner A, von Holst A. An Induction Gene Trap Screen in Neural Stem Cells Reveals an Instructive Function of the Niche and Identifies the Splicing Regulator Sam68 as a Tenascin-C-Regulated Target Gene. *Stem Cells* (2008) 26(9):2321–31. doi: 10.1634/stemcells.2007-1095
67. Zhao Y, Young SL. Tgf-Beta Regulates Expression of Tenascin Alternative-Splicing Isoforms in Fetal Rat Lung. *Am J Physiol* (1995) 268(2 Pt 1):L173–80. doi: 10.1152/ajplung.1995.268.2.L173
68. Zagzag D, Friedlander DR, Dosik J, Chikramane S, Chan W, Greco MA, et al. Tenascin-C Expression by Angiogenic Vessels in Human Astrocytomas and by Human Brain Endothelial Cells *in Vitro*. *Cancer Res* (1996) 56(1):182–9.
69. Seaman S, Stevens J, Yang MY, Logsdon D, Graff-Cherry C, St Croix B. Genes That Distinguish Physiological and Pathological Angiogenesis. *Cancer Cell* (2007) 11(6):539–54. doi: 10.1016/j.ccr.2007.04.017
70. Oskarsson T, Acharyya S, Zhang XH, Vanharanta S, Tavazoie SF, Morris PG, et al. Breast Cancer Cells Produce Tenascin C as a Metastatic Niche Component to Colonize the Lungs. *Nat Med* (2011) 17(7):867–74. doi: 10.1038/nm.2379
71. Chiquet-Ehrismann R, Kalla P. Pearson CA. Participation of Tenascin and Transforming Growth Factor-Beta in Reciprocal Epithelial-Mesenchymal Interactions of Mcf7 Cells and Fibroblasts. *Cancer Res* (1989) 49(15):4322–5.
72. Hiraiwa N, Kida H, Sakakura T, Kusakabe M. Induction of Tenascin in Cancer Cells by Interactions With Embryonic Mesenchyme Mediated by a Diffusible Factor. *J Cell Sci* (1993) 104(Pt 2):289–96. doi: 10.1242/jcs.104.2.289
73. Rathjen FG, Hodge R. Early Days of Tenascin-R Research: Two Approaches Discovered and Shed Light on Tenascin-R. *Front Immunol* (2020) 11:612482. doi: 10.3389/fimmu.2020.612482

74. Park PC, Taylor MD, Mainprize TG, Becker LE, Ho M, Dura WT, et al. Transcriptional Profiling of Medulloblastoma in Children. *J Neurosurg* (2003) 99(3):534–41. doi: 10.3171/jns.2003.99.3.0534
75. Carnemolla B, Leprini A, Borsi L, Querze G, Urbini S, Zardi L. Human Tenascin-R. Complete Primary Structure, Pre-Mrna Alternative Splicing and Gene Localization on Chromosome 1q23-Q24. *J Biol Chem* (1996) 271 (14):8157–60. doi: 10.1074/jbc.271.14.8157
76. El Ayachi I, Baeza N, Fernandez C, Colin C, Scavarda D, Pesheva P, et al. Kiaa0510, the 3'-Untranslated Region of the Tenascin-R Gene, and Tenascin-R Are Overexpressed in Pilocytic Astrocytomas. *Neuropathol Appl Neurobiol* (2010) 36(5):399–410. doi: 10.1111/j.1365-2990.2010.01074.x
77. Yuan Y, Nymoen DA, Stavnes HT, Rosnes AK, Bjorang O, Wu C, et al. Tenascin-X Is a Novel Diagnostic Marker of Malignant Mesothelioma. *Am J Surg Pathol* (2009) 33(11):1673–82. doi: 10.1097/PAS.0b013e3181b6bde3
78. Nakayama K, Seike M, Noro R, Takeuchi S, Matsuda K, Kunugi S, et al. Tenascin Xb Is a Novel Diagnostic Marker for Malignant Mesothelioma. *Anticancer Res* (2019) 39(2):627–33. doi: 10.21873/anticanres.13156
79. Kramer M, Pierredon S, Ribaux P, Tille JC, Petignat P, Cohen M. Secretome Identifies Tenascin-X as a Potent Marker of Ovarian Cancer. *BioMed Res Int* (2015) 2015:208017. doi: 10.1155/2015/208017
80. Hasegawa K, Yoshida T, Matsumoto K, Katsuta K, Waga S, Sakakura T. Differential Expression of Tenascin-C and Tenascin-X in Human Astrocytomas. *Acta Neuropathol* (1997) 93(5):431–7. doi: 10.1007/s004010050636
81. Wallentine JC, Kim KK, Seiler CE3rd, Vaughn CP, Crockett DK, Tripp SR, et al. Comprehensive Identification of Proteins in Hodgkin Lymphoma-Derived Reed-Sternberg Cells by Lc-Ms/Ms. *Lab Invest* (2007) 87(11):1113–24. doi: 10.1038/labinvest.3700672
82. Geffrotin C, Horak V, Crechet F, Tricaud Y, Lethias C, Vincent-Naulleau S, et al. Opposite Regulation of Tenascin-C and Tenascin-X in Melim Swine Heritable Cutaneous Malignant Melanoma. *Biochim Biophys Acta* (2000) 1524(2-3):196–202. doi: 10.1016/s0304-4165(00)00158-6
83. Levy P, Ripoche H, Laurendeau I, Lazar V, Ortonne N, Parfait B, et al. Microarray-Based Identification of Tenascin C and Tenascin Xb, Genes Possibly Involved in Tumorigenesis Associated With Neurofibromatosis Type 1. *Clin Cancer Res* (2007) 13(2 Pt 1):398–407. doi: 10.1158/1078-0432.CCR-06-0182
84. Lee SO, Lee SY, Lee SR, Ju W, Kim SC. Tenascin-X and Leukemia Inhibitory Factor Receptor Are Down-Regulated in Leiomyoma Compared With Normal Myometrium. *J Gynecol Oncol* (2008) 19(2):139–44. doi: 10.3802/jgo.2008.19.2.139
85. Liot S, Aubert A, Hervieu V, Kholti NE, Schalkwijk J, Verrier B, et al. Loss of Tenascin-X Expression During Tumor Progression: A New Pan-Cancer Marker. *Matrix Biol Plus* (2020) 6-7:100021. doi: 10.1016/j.mbplus.2020.100021
86. Chakravarthy A, Khan L, Bensler NP, Bose P, De Carvalho DD. Tgf-Beta-Associated Extracellular Matrix Genes Link Cancer-Associated Fibroblasts to Immune Evasion and Immunotherapy Failure. *Nat Commun* (2018) 9 (1):4692. doi: 10.1038/s41467-018-06654-8
87. Scherberich A, Tucker RP, Degen M, Brown-Luedi M, Andres AC, Chiquet-Ehrismann R. Tenascin-W Is Found in Malignant Mammary Tumors, Promotes Alpha8 Integrin-Dependent Motility and Requires P38mapk Activity for Bmp-2 and Tnf-Alpha Induced Expression *in Vitro*. *Oncogene* (2005) 24(9):1525–32. doi: 10.1038/sj.onc.1208342
88. Degen M, Brellier F, Kain R, Ruiz C, Terracciano L, Orend G, et al. Tenascin-W Is a Novel Marker for Activated Tumor Stroma in Low-Grade Human Breast Cancer and Influences Cell Behavior. *Cancer Res* (2007) 67(19):9169–79. doi: 10.1158/0008-5472.CAN-07-0666
89. Hendaoui I, Lahmar A, Campo L, Mebarki S, Bichet S, Hess D, et al. Tenascin-W Is a Novel Stromal Marker in Biliary Tract Cancers. *Front Immunol* (2020) 11:630139. doi: 10.3389/fimmu.2020.630139
90. Martina E, Degen M, Ruegg C, Merlo A, Lino MM, Chiquet-Ehrismann R, et al. Tenascin-W Is a Specific Marker of Glioma-Associated Blood Vessels and Stimulates Angiogenesis *in Vitro*. *FASEB J* (2010) 24(3):778–87. doi: 10.1096/fj.09-140491
91. Chiovaro F, Martina E, Bottos A, Scherberich A, Hynes NE, Chiquet-Ehrismann R. Transcriptional Regulation of Tenascin-W by Tgf-Beta Signaling in the Bone Metastatic Niche of Breast Cancer Cells. *Int J Cancer* (2015) 137(8):1842–54. doi: 10.1002/ijc.29565
92. Kimura H, Akiyama H, Nakamura T, de Crombrugghe B. Tenascin-W Inhibits Proliferation and Differentiation of Preosteoblasts During Endochondral Bone Formation. *Biochem Biophys Res Commun* (2007) 356 (4):935–41. doi: 10.1016/j.bbrc.2007.03.071
93. d'Amaro R, Scheidegger R, Blumer S, Pazera P, Katsaros C, Graf D, et al. Putative Functions of Extracellular Matrix Glycoproteins in Secondary Palate Morphogenesis. *Front Physiol* (2012) 3:377. doi: 10.3389/fphys.2012.00377
94. Morgan JM, Wong A, Yellowley CE, Genetos DC. Regulation of Tenascin Expression in Bone. *J Cell Biochem* (2011) 112(11):3354–63. doi: 10.1002/jcb.23265
95. Midwood KS, Orend G. The Role of Tenascin-C in Tissue Injury and Tumorigenesis. *J Cell Commun Signal* (2009) 3(3-4):287–310. doi: 10.1007/s12079-009-0075-1
96. Huang W, Chiquet-Ehrismann R, Moyano JV, Garcia-Pardo A, Orend G. Interference of Tenascin-C With Syndecan-4 Binding to Fibronectin Blocks Cell Adhesion and Stimulates Tumor Cell Proliferation. *Cancer Res* (2001) 61(23):8586–94.
97. Brellier F, Martina E, Chiquet M, Ferralli J, van der Heyden M, Orend G, et al. The Adhesion Modulating Properties of Tenascin-W. *Int J Biol Sci* (2012) 8(2):187–94. doi: 10.7150/ijbs.8.187
98. Ruiz C, Huang W, Hegi ME, Lange K, Hamou MF, Fluri E, et al. Growth Promoting Signaling by Tenascin-C [Corrected]. *Cancer Res* (2004) 64 (20):7377–85. doi: 10.1158/0008-5472.CAN-04-1234
99. Vollmer G. Biologic and Oncologic Implications of Tenascin-C/Hexabrachion Proteins. *Crit Rev Oncol Hematol* (1997) 25(3):187–210. doi: 10.1016/s1040-8428(97)00004-8
100. Yoshimura E, Majima A, Sakakura Y, Sakakura T, Yoshida T. Expression of Tenascin-C and the Integrin Alpha 9 Subunit in Regeneration of Rat Nasal Mucosa After Chemical Injury: Involvement in Migration and Proliferation of Epithelial Cells. *Histochem Cell Biol* (1999) 111(4):259–64. doi: 10.1007/s004180050356
101. Swindle CS, Tran KT, Johnson TD, Banerjee P, Mayes AM, Griffith L, et al. Epidermal Growth Factor (Egf)-Like Repeats of Human Tenascin-C as Ligands for Egf Receptor. *J Cell Biol* (2001) 154(2):459–68. doi: 10.1083/jcb.200103103
102. Schenk S, Chiquet-Ehrismann R, Battegay EJ. The Fibrinogen Globe of Tenascin-C Promotes Basic Fibroblast Growth Factor-Induced Endothelial Cell Elongation. *Mol Biol Cell* (1999) 10(9):2933–43. doi: 10.1091/mbc.10.9.2933
103. McKean DM, Sisbarro L, Ilic D, Kaplan-Alburquerque N, Nemenoff R, Weiser-Evans M, et al. Fak Induces Expression of Prx1 to Promote Tenascin-C-Dependent Fibroblast Migration. *J Cell Biol* (2003) 161(2):393–402. doi: 10.1083/jcb.jcb.200302126
104. Ishigaki T, Imanaka-Yoshida K, Shimojo N, Matsushima S, Taki W, Yoshida T. Tenascin-C Enhances Crosstalk Signaling of Integrin Alphavbeta3/Pdgfr-Beta Complex by Src Recruitment Promoting Pdgf-Induced Proliferation and Migration in Smooth Muscle Cells. *J Cell Physiol* (2011) 226(10):2617–24. doi: 10.1002/jcp.22614
105. Wenk MB, Midwood KS, Schwarzbauer JE. Tenascin-C Suppresses Rho Activation. *J Cell Biol* (2000) 150(4):913–20. doi: 10.1083/jcb.150.4.913
106. Meloty-Kapella CV, Degen M, Chiquet-Ehrismann R, Tucker RP. Effects of Tenascin-W on Osteoblasts *in Vitro*. *Cell Tissue Res* (2008) 334(3):445–55. doi: 10.1007/s00441-008-0715-4
107. Derynck R, Weinberg RA. Emt and Cancer: More Than Meets the Eye. *Dev Cell* (2019) 49(3):313–6. doi: 10.1016/j.devcel.2019.04.026
108. Nagaharu K, Zhang X, Yoshida T, Katoh D, Hanamura N, Kozuka Y, et al. Tenascin C Induces Epithelial-Mesenchymal Transition-Like Change Accompanied by Src Activation and Focal Adhesion Kinase Phosphorylation in Human Breast Cancer Cells. *Am J Pathol* (2011) 178 (2):754–63. doi: 10.1016/j.ajpath.2010.10.015
109. Dandachi N, Hauser-Kronberger C, More E, Wiesener B, Hacker GW, Dietze O, et al. Co-Expression of Tenascin-C and Vimentin in Human Breast Cancer Cells Indicates Phenotypic Transdifferentiation During Tumour Progression: Correlation With Histopathological Parameters, Hormone Receptors, and Oncoproteins. *J Pathol* (2001) 193(2):181–9. doi: 10.1002/1096-9896(2000)9999:9999<::AID-PATH752>3.0.CO;2-V

110. Aubert A, Mercier-Gouy P, Aguero S, Berthier L, Liot S, Prigent L, et al. Latent Tgf-Beta Activation Is a Hallmark of the Tenascin Family. *Front Immunol* (2021) 12:613438. doi: 10.3389/fimmu.2021.613438
111. Xu J, Lamouille S, Derynck R. Tgf-Beta-Induced Epithelial to Mesenchymal Transition. *Cell Res* (2009) 19(2):156–72. doi: 10.1038/cr.2009.5
112. Lambert AW, Pattabiraman DR, Weinberg RA. Emerging Biological Principles of Metastasis. *Cell* (2017) 168(4):670–91. doi: 10.1016/j.cell.2016.11.037
113. Descot A, Oskarsson T. The Molecular Composition of the Metastatic Niche. *Exp Cell Res* (2013) 319(11):1679–86. doi: 10.1016/j.yexcr.2013.04.017
114. Winkler J, Abisoye-Ogunniyan A, Metcalf KJ, Werb Z. Concepts of Extracellular Matrix Remodelling in Tumour Progression and Metastasis. *Nat Commun* (2020) 11(1):5120. doi: 10.1038/s41467-020-18794-x
115. Silvers CR, Messing EM, Miyamoto H, Lee YF. Tenascin-C Expression in the Lymph Node Pre-Metastatic Niche in Muscle-Invasive Bladder Cancer. *Br J Cancer* (2021) 125(10):1399–407. doi: 10.1038/s41416-021-01554-z
116. Spenle C, Gasser I, Saupe F, Janssen KP, Arnold C, Klein A, et al. Spatial Organization of the Tenascin-C Microenvironment in Experimental and Human Cancer. *Cell Adh Migr* (2015) 9(1-2):4–13. doi: 10.1080/19336918.2015.1005452
117. Tomko LA, Hill RC, Barrett A, Szulczewski JM, Conklin MW, Eliceiri KW, et al. Targeted Matrisome Analysis Identifies Thrombospondin-2 and Tenascin-C in Aligned Collagen Stroma From Invasive Breast Carcinoma. *Sci Rep* (2018) 8(1):12941. doi: 10.1038/s41598-018-31126-w
118. Malanchi I, Santamaria-Martinez A, Susanto E, Peng H, Lehr HA, Delaloye JF, et al. Interactions Between Cancer Stem Cells and Their Niche Govern Metastatic Colonization. *Nature* (2011) 481(7379):85–9. doi: 10.1038/nature10694
119. Kii I, Nishiyama T, Li M, Matsumoto K, Saito M, Amizuka N, et al. Incorporation of Tenascin-C Into the Extracellular Matrix by Periostin Underlies an Extracellular Meshwork Architecture. *J Biol Chem* (2010) 285 (3):2028–39. doi: 10.1074/jbc.M109.051961
120. Tanaka K, Hiraiwa N, Hashimoto H, Yamazaki Y, Kusakabe M. Tenascin-C Regulates Angiogenesis in Tumor Through the Regulation of Vascular Endothelial Growth Factor Expression. *Int J Cancer* (2004) 108(1):31–40. doi: 10.1002/ijc.11509
121. Saupe F, Schwenzer A, Jia Y, Gasser I, Spenle C, Langlois B, et al. Tenascin-C Downregulates Wnt Inhibitor Dickkopf-1, Promoting Tumorigenesis in a Neuroendocrine Tumor Model. *Cell Rep* (2013) 5(2):482–92. doi: 10.1016/j.celrep.2013.09.014
122. Langlois B, Saupe F, Rupp T, Arnold C, van der Heyden M, Orend G, et al. Angiomatrix, a Signature of the Tumor Angiogenic Switch-Specific Matrisome, Correlates With Poor Prognosis for Glioma and Colorectal Cancer Patients. *Oncotarget* (2014) 5(21):10529–45. doi: 10.18632/oncotarget.2470
123. Rupp T, Langlois B, Koczorowska MM, Radwanska A, Sun Z, Hussenet T, et al. Tenascin-C Orchestrates Glioblastoma Angiogenesis by Modulation of Pro- and Anti-Angiogenic Signaling. *Cell Rep* (2016) 17(10):2607–19. doi: 10.1016/j.celrep.2016.11.012
124. Marzeda AM, Midwood KS. Internal Affairs: Tenascin-C as a Clinically Relevant, Endogenous Driver of Innate Immunity. *J Histochem Cytochem* (2018) 66(4):289–304. doi: 10.1369/0022155418757443
125. Udalova IA, Ruhmann M, Thomson SJ, Midwood KS. Expression and Immune Function of Tenascin-C. *Crit Rev Immunol* (2011) 31(2):115–45. doi: 10.1615/critrevimmunol.v31.i2.30
126. Midwood K, Sacre S, Piccinini AM, Inglis J, Trebaul A, Chan E, et al. Tenascin-C Is an Endogenous Activator of Toll-Like Receptor 4 That Is Essential for Maintaining Inflammation in Arthritic Joint Disease. *Nat Med* (2009) 15(7):774–80. doi: 10.1038/nm.1987
127. Medzhitov R, Janeway CAJr. Decoding the Patterns of Self and Nonself by the Innate Immune System. *Science* (2002) 296(5566):298–300. doi: 10.1126/science.1068883
128. Deligne C, Murdamoothoo D, Gammage AN, Gschwandtner M, Erne W, Loustau T, et al. Matrix-Targeting Immunotherapy Controls Tumor Growth and Spread by Switching Macrophage Phenotype. *Cancer Immunol Res* (2020) 8(3):368–82. doi: 10.1158/2326-6066.CIR-19-0276
129. Jachetti E, Caputo S, Mazzoleni S, Brambillasca CS, Parigi SM, Grioni M, et al. Tenascin-C Protects Cancer Stem-Like Cells From Immune Surveillance by Arresting T-Cell Activation. *Cancer Res* (2015) 75 (10):2095–108. doi: 10.1158/0008-5472.CAN-14-2346
130. Mirzaei R, Sarkar S, Dzikowski L, Rawji KS, Khan L, Faissner A, et al. Brain Tumor-Initiating Cells Export Tenascin-C Associated With Exosomes to Suppress T Cell Activity. *Oncoimmunology* (2018) 7(10):e1478647. doi: 10.1080/2162402X.2018.1478647
131. Spenle C, Loustau T, Murdamoothoo D, Erne W, Beghelli-de la Forest Divonne S, Veber R, et al. Tenascin-C Orchestrates an Immune-Suppressive Tumor Microenvironment in Oral Squamous Cell Carcinoma. *Cancer Immunol Res* (2020) 8(9):1122–38. doi: 10.1158/2326-6066.CIR-20-0074
132. Murdamoothoo D, Sun Z, Yilmaz A, Riegel G, Abou-Faycal C, Deligne C, et al. Tenascin-C Immobilizes Infiltrating T Lymphocytes Through Cxcl12 Promoting Breast Cancer Progression. *EMBO Mol Med* (2021) 13(6):e13270. doi: 10.15252/emmm.202013270
133. Li MO, Wan YY, Sanjabi S, Robertson AK, Flavell RA. Transforming Growth Factor-Beta Regulation of Immune Responses. *Annu Rev Immunol* (2006) 24:99–146. doi: 10.1146/annurev.immunol.24.021605.090737
134. Fukunaga-Kalabis M, Martinez G, Nguyen TK, Kim D, Santiago-Walker A, Roesch A, et al. Tenascin-C Promotes Melanoma Progression by Maintaining the Abcb5-Positive Side Population. *Oncogene* (2010) 29 (46):6115–24. doi: 10.1038/onc.2010.350
135. Gong XG, Lv YF, Li XQ, Xu FG, Ma QY. Gemcitabine Resistance Induced by Interaction Between Alternatively Spliced Segment of Tenascin-C and Annexin A2 in Pancreatic Cancer Cells. *Biol Pharm Bull* (2010) 33 (8):1261–7. doi: 10.1248/bpb.33.1261
136. Wang T, Srivastava S, Hartman M, Buhari SA, Chan CW, Iau P, et al. High Expression of Intratumoral Stromal Proteins Is Associated With Chemotherapy Resistance in Breast Cancer. *Oncotarget* (2016) 7 (34):55155–68. doi: 10.18632/oncotarget.10894
137. Helleman J, Jansen MP, Ruigrok-Ritstier K, van Staveren IL, Look MP, Meijer-van Gelder ME, et al. Association of an Extracellular Matrix Gene Cluster With Breast Cancer Prognosis and Endocrine Therapy Response. *Clin Cancer Res* (2008) 14(17):5555–64. doi: 10.1158/1078-0432.CCR-08-0555
138. Li ZL, Zhang HL, Huang Y, Huang JH, Sun P, Zhou NN, et al. Autophagy Deficiency Promotes Triple-Negative Breast Cancer Resistance to T Cell-Mediated Cytotoxicity by Blocking Tenascin-C Degradation. *Nat Commun* (2020) 11(1):3806. doi: 10.1038/s41467-020-17395-y
139. Bubova K, Prajzlerova K, Hulejova H, Gregova M, Mintalova K, Husakova M, et al. Elevated Tenascin-C Serum Levels in Patients With Axial Spondyloarthritis. *Physiol Res* (2020) 69(4):653–60. doi: 10.33549/physiolres.934414
140. Yuan W, Zhang W, Yang X, Zhou L, Hanghua Z, Xu K. Clinical Significance and Prognosis of Serum Tenascin-C in Patients With Sepsis. *BMC Anesthesiol* (2018) 18(1):170. doi: 10.1186/s12871-018-0634-1
141. Hasanzadeh Z, Nourazarian A, Nikanfar M, Laghousi D, Vatankhah AM, Sadrirad S. Evaluation of the Serum Dkk-1, Tenascin-C, Oxidative Stress Markers Levels and Wnt Signaling Pathway Genes Expression in Patients With Alzheimer's Disease. *J Mol Neurosci* (2021) 71(4):879–87. doi: 10.1007/s12031-020-01710-9
142. Zavada J, Uher M, Svobodova R, Olejarova M, Husakova M, Ciferska H, et al. Serum Tenascin-C Discriminates Patients With Active Sle From Inactive Patients and Healthy Controls and Predicts the Need to Escalate Immunosuppressive Therapy: A Cohort Study. *Arthritis Res Ther* (2015) 17:341. doi: 10.1186/s13075-015-0862-4
143. Page TH, Charles PJ, Piccinini AM, Nicolaidou V, Taylor PC, Midwood KS. Raised Circulating Tenascin-C in Rheumatoid Arthritis. *Arthritis Res Ther* (2012) 14(6):R260. doi: 10.1186/ar4105
144. Niebroj-Dobosz I, Madej-Pilarczyk A, Marchel M, Sokolowska B, Hausmanowa-Petrusewicz I. Circulating Tenascin-C Levels in Patients With Dilated Cardiomyopathy in the Course of Emery-Dreifuss Muscular Dystrophy. *Clin Chim Acta* (2011) 412(17-18):1533–8. doi: 10.1016/j.cca.2011.04.033
145. Tanaka H, El-Karef A, Kaito M, Kinoshita N, Fujita N, Horiike S, et al. Circulating Level of Large Splice Variants of Tenascin-C Is a Marker of Piecemeal Necrosis Activity in Patients With Chronic Hepatitis C. *Liver Int* (2006) 26(3):311–8. doi: 10.1111/j.1478-3231.2005.01229.x

146. Horstrup JH, Gehrmann M, Schneider B, Ploger A, Froese P, Schirop T, et al. Elevation of Serum and Urine Levels of Timp-1 and Tenascin in Patients With Renal Disease. *Nephrol Dial Transplant* (2002) 17(6):1005–13. doi: 10.1093/ndt/17.6.1005
147. Schenk S, Muser J, Vollmer G, Chiquet-Ehrismann R. Tenascin-C in Serum: A Questionable Tumor Marker. *Int J Cancer* (1995) 61(4):443–9. doi: 10.1002/ijc.2910610402
148. Schenk S, Muser J, Vollmer G, Chiquet-Ehrismann R. Tenascin-C in Serum: An Acute-Phase Protein or a Carcinoma Marker? *Int J Cancer* (1995) 60 (1):145. doi: 10.1002/ijc.2910600121
149. Imai K, Kusakabe M, Sakakura T, Nakanishi I, Okada Y. Susceptibility of Tenascin to Degradation by Matrix Metalloproteinases and Serine Proteinases. *FEBS Lett* (1994) 352(2):216–8. doi: 10.1016/0014-5793(94) 00960-0
150. Kusagawa H, Onoda K, Namikawa S, Yada I, Okada A, Yoshida T, et al. Expression and Degeneration of Tenascin-C in Human Lung Cancers. *Br J Cancer* (1998) 77(1):98–102. doi: 10.1038/bjc.1998.15
151. Cai M, Onoda K, Takao M, Kyoko IY, Shimpo H, Yoshida T, et al. Degradation of Tenascin-C and Activity of Matrix Metalloproteinase-2 Are Associated With Tumor Recurrence in Early Stage Non-Small Cell Lung Cancer. *Clin Cancer Res* (2002) 8(4):1152–6.
152. Peng Y, Croce CM. The Role of Micrornas in Human Cancer. *Signal Transduct Target Ther* (2016) 1:15004. doi: 10.1038/sigtrans.2015.4
153. Murakami T, Kikuchi H, Ishimatsu H, Iino I, Hirotsu A, Matsumoto T, et al. Tenascin C in Colorectal Cancer Stroma Is a Predictive Marker for Liver Metastasis and Is a Potent Target of Mir-198 as Identified by Microrna Analysis. *Br J Cancer* (2017) 117(9):1360–70. doi: 10.1038/bjc.2017.291
154. Tavazoie SF, Alarcon C, Oskarsson T, Padua D, Wang Q, Bos PD, et al. Endogenous Human Microrna That Suppress Breast Cancer Metastasis. *Nature* (2008) 451(7175):147–52. doi: 10.1038/nature06487
155. Koshizuka K, Nohata N, Hanazawa T, Kikkawa N, Arai T, Okato A, et al. Deep Sequencing-Based Microrna Expression Signatures in Head and Neck Squamous Cell Carcinoma: Dual Strands of Pre-Mir-150 as Antitumor Mirnas. *Oncotarget* (2017) 8(18):30288–304. doi: 10.18632/oncotarget.16327
156. Dang S, Zhang R, Tian S, Hou P, Li G, Ji M. Microrna218 Inhibits the Malignant Phenotypes of Glioma by Modulating the Tnc/Akt/Ap1/Tgfbeta1 Feedback Signaling Loop. *Int J Mol Med* (2021) 48(5):205. doi: 10.3892/ijmm.2021.5038
157. Chen L, Zhang R, Li P, Liu Y, Qin K, Fa ZQ, et al. P53-Induced Microrna-107 Inhibits Proliferation of Glioma Cells and Down-Regulates the Expression of Cdk6 and Notch-2. *Neurosci Lett* (2013) 534:327–32. doi: 10.1016/j.neulet.2012.11.047
158. Venkitaraman R, Lorente D, Murthy V, Thomas K, Parker L, Ahiabor R, et al. A Randomised Phase 2 Trial of Dexamethasone Versus Prednisolone in Castration-Resistant Prostate Cancer. *Eur Urol* (2015) 67(4):673–9. doi: 10.1016/j.eururo.2014.10.004
159. Holder SL, Drabick J, Zhu J, Joshi M. Dexamethasone May Be the Most Efficacious Corticosteroid for Use as Monotherapy in Castration-Resistant Prostate Cancer. *Cancer Biol Ther* (2015) 16(2):207–9. doi: 10.1080/15384047.2014.1002687
160. Zhang Y, Shi G, Zhang H, Xiong Q, Cheng F, Wang H, et al. Dexamethasone Enhances the Lung Metastasis of Breast Cancer *Via* a Pi3k-Sgk1-Ctgf Pathway. *Oncogene* (2021) 40(35):5367–78. doi: 10.1038/s41388-021-01944-w
161. Geleta B, Tout FS, Lim SC, Sahni S, Jansson PJ, Apte MV, et al. Targeting Wnt/Tenascin C-Mediated Cross Talk Between Pancreatic Cancer Cells and Stellate Cells *Via* Activation of the Metastasis Suppressor Ndrg1. *J Biol Chem* (2022) 298(3):101608. doi: 10.1016/j.jbc.2022.101608
162. Zukiel R, Nowak S, Wyszko E, Rolle K, Gawronska I, Barciszewska MZ, et al. Suppression of Human Brain Tumor With Interference Rna Specific for Tenascin-C. *Cancer Biol Ther* (2006) 5(8):1002–7. doi: 10.4161/cbt.5.8.2886
163. Wyszko E, Rolle K, Nowak S, Zukiel R, Nowak M, Piestrzeniewicz R, et al. A Multivariate Analysis of Patients With Brain Tumors Treated With Atn-Rna. *Acta Pol Pharm* (2008) 65(6):677–84.
164. Rolle K, Nowak S, Wyszko E, Nowak M, Zukiel R, Piestrzeniewicz R, et al. Promising Human Brain Tumors Therapy With Interference Rna Intervention (Irnai). *Cancer Biol Ther* (2010) 9(5):396–406. doi: 10.4161/cbt.9.5.10958
165. Wawrzyniak D, Grabowska M, Glodowicz P, Kuczynski K, Kuczynska B, Fedoruk-Wyszomirska A, et al. Down-Regulation of Tenascin-C Inhibits Breast Cancer Cells Development by Cell Growth, Migration, and Adhesion Impairment. *PloS One* (2020) 15(8):e0237889. doi: 10.1371/journal.pone.0237889
166. Dhaouadi S, Ben Abderrazek R, Loustau T, Abou-Faycal C, Ksouri A, Erne W, et al. Novel Human Tenascin-C Function-Blocking Camel Single Domain Nanobodies. *Front Immunol* (2021) 12:635166. doi: 10.3389/fimmu.2021.635166
167. Lingasamy P, Tobi A, Haugas M, Hunt H, Paiste P, Asser T, et al. Bi-Specific Tenascin-C and Fibronectin Targeted Peptide for Solid Tumor Delivery. *Biomaterials* (2019) 219:119373. doi: 10.1016/j.biomaterials.2019.119373
168. Lingasamy P, Tobi A, Kurm K, Kopanchuk S, Sudakov A, Salumae M, et al. Tumor-Penetrating Peptide for Systemic Targeting of Tenascin-C. *Sci Rep* (2020) 10(1):5809. doi: 10.1038/s41598-020-62760-y
169. Kang T, Zhu Q, Jiang D, Feng X, Feng J, Jiang T, et al. Synergistic Targeting Tenascin C and Neuropilin-1 for Specific Penetration of Nanoparticles for Anti-Glioblastoma Treatment. *Biomaterials* (2016) 101:60–75. doi: 10.1016/j.biomaterials.2016.05.037
170. Hicke BJ, Marion C, Chang YF, Gould T, Lynott CK, Parma D, et al. Tenascin-C Aptamers Are Generated Using Tumor Cells and Purified Protein. *J Biol Chem* (2001) 276(52):48644–54. doi: 10.1074/jbc.M104651200
171. Schmidt KS, Borkowski S, Kurreck J, Stephens AW, Bald R, Hecht M, et al. Application of Locked Nucleic Acids to Improve Aptamer *in Vivo* Stability and Targeting Function. *Nucleic Acids Res* (2004) 32(19):5757–65. doi: 10.1093/nar/gkh862
172. Hicke BJ, Stephens AW, Gould T, Chang YF, Lynott CK, Heil J, et al. Tumor Targeting by an Aptamer. *J Nucl Med* (2006) 47(4):668–78.
173. Daniels DA, Chen H, Hicke BJ, Swiderek KM, Gold L. A Tenascin-C Aptamer Identified by Tumor Cell Selex: Systematic Evolution of Ligands by Exponential Enrichment. *Proc Natl Acad Sci U S A* (2003) 100(26):15416–21. doi: 10.1073/pnas.2136683100
174. Jacobson O, Yan X, Niu G, Weiss ID, Ma Y, Szajek LP, et al. Pet Imaging of Tenascin-C With a Radiolabeled Single-Stranded DNA Aptamer. *J Nucl Med* (2015) 56(4):616–21. doi: 10.2967/jnumed.114.149484
175. Ko HY, Choi KJ, Lee CH, Kim S. A Multimodal Nanoparticle-Based Cancer Imaging Probe Simultaneously Targeting Nucleolin, Integrin Alphavbeta3 and Tenascin-C Proteins. *Biomaterials* (2011) 32(4):1130–8. doi: 10.1016/j.biomaterials.2010.10.034
176. Reardon DA, Akabani G, Coleman RE, Friedman AH, Friedman HS, Herndon JE2nd, et al. Salvage Radioimmunotherapy With Murine Iodine-131-Labeled Antitenascin Monoclonal Antibody 81c6 for Patients With Recurrent Primary and Metastatic Malignant Brain Tumors: Phase Ii Study Results. *J Clin Oncol* (2006) 24(1):115–22. doi: 10.1200/JCO.2005.03.4082
177. Reardon DA, Zalutsky MR, Akabani G, Coleman RE, Friedman AH, Herndon JE2nd, et al. A Pilot Study: 131i-Antitenascin Monoclonal Antibody 81c6 to Deliver a 44-Gy Resection Cavity Boost. *Neuro Oncol* (2008) 10(2):182–9. doi: 10.1215/15228517-2007-053
178. Zalutsky MR, Reardon DA, Akabani G, Coleman RE, Friedman AH, Friedman HS, et al. Clinical Experience With Alpha-Particle Emitting 211at: Treatment of Recurrent Brain Tumor Patients With 211at-Labeled Chimeric Antitenascin Monoclonal Antibody 81c6. *J Nucl Med* (2008) 49 (1):30–8. doi: 10.2967/jnumed.107.046938
179. Catania C, Maur M, Berardi R, Rocca A, Giacomo AM, Spitaleri G, et al. The Tumor-Targeting Immunocytokine F16-Il2 in Combination With Doxorubicin: Dose Escalation in Patients With Advanced Solid Tumors and Expansion Into Patients With Metastatic Breast Cancer. *Cell Adh Migr* (2015) 9(1-2):14–21. doi: 10.4161/19336918.2014.983785
180. De Braud FG, Catania C, Onofri A, Pierantoni C, Cascinu S, Maur M, et al. Combination of the Immunocytokine F16-Il2 With Doxorubicin or Paclitaxel in Patients With Solid Tumors: Results From Two Phase Ib Trials. *J Clin Oncol* (2011) 29(15):Strategies for targeting TN-C in cancer treatment. doi: 10.1200/jco.2011.29.15_suppl.2595
181. Gutbrodt KL, Schliemann C, Giovannoni L, Frey K, Pabst T, Klapper W, et al. Antibody-Based Delivery of Interleukin-2 to Neovasculature Has Potent Activity Against Acute Myeloid Leukemia. *Sci Transl Med* (2013) 5 (201):201ra118. doi: 10.1126/scitranslmed.3006221

182. Pedretti M, Verpelli C, Marlind J, Bertani G, Sala C, Neri D, et al. Combination of Temozolomide With Immunocytokine F16-Il2 for the Treatment of Glioblastoma. *Br J Cancer* (2010) 103(6):827–36. doi: 10.1038/sj.bjc.6605832
183. Aloj L, D'Ambrosio L, Aurilio M, Morisco A, Frigeri F, Caraco C, et al. Radioimmunotherapy With Tenarad, a 131i-Labelled Antibody Fragment Targeting the Extra-Domain A1 of Tenascin-C, in Patients With Refractory Hodgkin's Lymphoma. *Eur J Nucl Med Mol Imaging* (2014) 41(5):867–77. doi: 10.1007/s00259-013-2658-6
184. Heuveling DA, de Bree R, Vugts DJ, Huisman MC, Giovannoni L, Hoekstra OS, et al. Phase 0 Microdosing Pet Study Using the Human Mini Antibody F16sip in Head and Neck Cancer Patients. *J Nucl Med* (2013) 54(3):397–401. doi: 10.2967/jnumed.112.111310
185. Riva P, Arista A, Tison V, Sturiale C, Franceschi G, Spinelli A, et al. Intralesional Radioimmunotherapy of Malignant Gliomas. *Effective Treat Recurrent Tumors Cancer* (1994) 73(3 Suppl):1076–82. doi: 10.1002/1097-0142(19940201)73:3+<1076::aid-cnr2820731347>3.0.co;2-z
186. Paganelli G, Bartolomei M, Ferrari M, Cremonesi M, Broggi G, Maira G, et al. Pre-Targeted Locoregional Radioimmunotherapy With 90y-Biotin in Glioma Patients: Phase I Study and Preliminary Therapeutic Results. *Cancer Biother Radiopharm* (2001) 16(3):227–35. doi: 10.1089/10849780152389410
187. Lingasamy P, Laarmann AH, Teesalu T. Tumor Penetrating Peptide-Functionalized Tenascin-C Antibody for Glioblastoma Targeting. *Curr Cancer Drug Targets* (2021) 21(1):70–9. doi: 10.2174/1568009620666201001112749
188. Dhaouadi S, Murdamoothoo D, Tounsi A, Erne W, Benabderrazek R, Benlasfar Z, et al. Generation and Characterization of Dromedary Tenascin-C and Tenascin-W Specific Antibodies. *Biochem Biophys Res Commun* (2020) 530(2):471–8. doi: 10.1016/j.bbrc.2020.05.077
189. Strebhardt K, Ullrich A. Paul Ehrlich's Magic Bullet Concept: 100 Years of Progress. *Nat Rev Cancer* (2008) 8(6):473–80. doi: 10.1038/nrc2394
190. Tong JTW, Harris PWR, Brimble MA, Kavianinia I. An Insight Into Fda Approved Antibody-Drug Conjugates for Cancer Therapy. *Molecules* (2021) 26(19). doi: 10.3390/molecules26195847
191. Brack SS, Silacci M, Birchler M, Neri D. Tumor-Targeting Properties of Novel Antibodies Specific to the Large Isoform of Tenascin-C. *Clin Cancer Res* (2006) 12(10):3200–8. doi: 10.1158/1078-0432.CCR-05-2804
192. Pedretti M, Soltermann A, Arni S, Weder W, Neri D, Hillinger S. Comparative Immunohistochemistry of L19 and F16 in Non-Small Cell Lung Cancer and Mesothelioma: Two Human Antibodies Investigated in Clinical Trials in Patients With Cancer. *Lung Cancer* (2009) 64(1):28–33. doi: 10.1016/j.lungcan.2008.07.013
193. Schliemann C, Wiedmer A, Pedretti M, Szczepanowski M, Klapper W, Neri D. Three Clinical-Stage Tumor Targeting Antibodies Reveal Differential Expression of Oncofetal Fibronectin and Tenascin-C Isoforms in Human Lymphoma. *Leuk Res* (2009) 33(12):1718–22. doi: 10.1016/j.leukres.2009.06.025
194. Berndt A, Kollner R, Richter P, Franz M, Voigt A, Berndt A, et al. A Comparative Analysis of Oncofetal Fibronectin and Tenascin-C Incorporation in Tumour Vessels Using Human Recombinant Sip Format Antibodies. *Histochem Cell Biol* (2010) 133(4):467–75. doi: 10.1007/s00418-010-0685-y
195. Frey K, Fiechter M, Schwager K, Belloni B, Barysch MJ, Neri D, et al. Different Patterns of Fibronectin and Tenascin-C Splice Variants Expression in Primary and Metastatic Melanoma Lesions. *Exp Dermatol* (2011) 20 (8):685–8. doi: 10.1111/j.1600-0625.2011.01314.x
196. Schwager K, Villa A, Rosli C, Neri D, Rosli-Khabas M, Moser G. A Comparative Immunofluorescence Analysis of Three Clinical-Stage Antibodies in Head and Neck Cancer. *Head Neck Oncol* (2011) 3:25. doi: 10.1186/1758-3284-3-25
197. Sha H, Li R, Bian X, Liu Q, Xie C, Xin X, et al. A Tumor-Penetrating Recombinant Protein Anti-Egfr-Irgd Enhance Efficacy of Paclitaxel in 3d Multicellular Spheroids and Gastric Cancer *in Vivo*. *Eur J Pharm Sci* (2015) 77:60–72. doi: 10.1016/j.ejps.2015.05.020
198. Sha H, Zou Z, Xin K, Bian X, Cai X, Lu W, et al. Tumor-Penetrating Peptide Fused Egfr Single-Domain Antibody Enhances Cancer Drug Penetration Into 3d Multicellular Spheroids and Facilitates Effective Gastric Cancer Therapy. *J Control Release* (2015) 200:188–200. doi: 10.1016/j.jconrel.2014.12.039
199. Zhu A, Sha H, Su S, Chen F, Wei J, Meng F, et al. Bispecific Tumor-Penetrating Protein Anti-Egfr-Irgd Efficiently Enhances the Infiltration of Lymphocytes in Gastric Cancer. *Am J Cancer Res* (2018) 8(1):91–105.
200. Henke E, Nandigama R, Ergun S. Extracellular Matrix in the Tumor Microenvironment and Its Impact on Cancer Therapy. *Front Mol Biosci* (2019) 6:160. doi: 10.3389/fmolb.2019.00160
201. Gerarduzzi C, Hartmann U, Leask A, Drobetsky E. The Matrix Revolution: Matricellular Proteins and Restructuring of the Cancer Microenvironment. *Cancer Res* (2020) 80(13):2705–17. doi: 10.1158/0008-5472.CAN-18-2098

Conflict of Interest: The authors declare that the research was conducted in the absence of any commercial or financial relationships that could be construed as a potential conflict of interest.

Publisher's Note: All claims expressed in this article are solely those of the authors and do not necessarily represent those of their affiliated organizations, or those of the publisher, the editors and the reviewers. Any product that may be evaluated in this article, or claim that may be made by its manufacturer, is not guaranteed or endorsed by the publisher.

Copyright © 2022 Tucker and Degen. This is an open-access article distributed under the terms of the Creative Commons Attribution License (CC BY). The use, distribution or reproduction in other forums is permitted, provided the original author(s) and the copyright owner(s) are credited and that the original publication in this journal is cited, in accordance with accepted academic practice. No use, distribution or reproduction is permitted which does not comply with these terms.

frontiers | Frontiers in Oncology

REVIEW
published: 17 June 2022
doi: 10.3389/fonc.2022.909450

CD44 In Sarcomas: A Comprehensive Review and Future Perspectives

Enrique Fernández-Tabanera[1,2,3], *Raquel M. Melero-Fernández de Mera*[1,2] *and Javier Alonso*[1,2*]

[1] Unidad de Tumores Sólidos Infantiles, Instituto de Investigación de Enfermedades Raras (IIER), Instituto de Salud Carlos III (ISCIII), Madrid, Spain, [2] Centro de Investigación Biomédica en Red de Enfermedades Raras, Instituto de Salud Carlos III (U758; CB06/07/1009; CIBERER-ISCIII), Madrid, Spain, [3] Universidad Nacional de Educación a Distancia (UNED), Madrid, Spain

It is widely accepted that the tumor microenvironment, particularly the extracellular matrix, plays an essential role in the development of tumors through the interaction with specific protein-membrane receptors. One of the most relevant proteins in this context is the transmembrane protein CD44. The role of CD44 in tumor progression, invasion, and metastasis has been well established in many cancers, although a comprehensive review concerning its role in sarcomas has not been published. CD44 is overexpressed in most sarcomas and several *in vitro* and *in vivo* experiments have shown a direct effect on tumor progression, dissemination, and drug resistance. Moreover, CD44 has been revealed as a useful marker for prognostic and diagnostic (CD44v6 isoform) in osteosarcoma. Besides, some innovative treatments such as HA-functionalized liposomes therapy have become an excellent CD44-mediated intracellular delivery system for osteosarcoma. Unfortunately, the reduced number of studies deciphering the prognostic/diagnostic value of CD44 in other sarcoma subgroups, neither than osteosarcoma, in addition to the low number of patients involved in those studies, have produced inconclusive results. In this review, we have gone through the information available on the role of CD44 in the development, maintenance, and progression of sarcomas, analyzing their implications at the prognostic, therapeutic, and mechanistic levels. Moreover, we illustrate how research involving the specific role of CD44 in the different sarcoma subgroups could suppose a chance to advance towards a more innovative perspective for novel therapies and future clinical trials.

Keywords: CD44, sarcoma, cancer therapy, biomarker, CD44-ICD, signalling transduction, epithelial mesenchymal transition (EMT), extracellular matrix (ECM)

OPEN ACCESS

Edited by:
Alberto Passi,
University of Insubria, Italy

Reviewed by:
Alessandro De Vita,
Scientific Institute of Romagna for the Study and Treatment of Tumors (IRCCS), Italy
Hashem Obaid Alsaab,
Taif University, Saudi Arabia

***Correspondence:**
Javier Alonso
fjalonso@isciii.es

Specialty section:
This article was submitted to Molecular and Cellular Oncology, a section of the journal Frontiers in Oncology

Received: *31 March 2022*
Accepted: *02 May 2022*
Published: *17 June 2022*

Citation:
Fernández-Tabanera E, Melero-Fernández de Mera RM and Alonso J (2022) CD44 In Sarcomas: A Comprehensive Review and Future Perspectives. Front. Oncol. 12:909450. doi: 10.3389/fonc.2022.909450

1 INTRODUCTION

Sarcomas are a heterogeneous group of tumors originating from mesenchymal cells. These rare malignancies account for approximately 10% of childhood solid tumors arising in soft and bone tissues (1), and 2% of cancers diagnosed in adult individuals (representing an overall annual incidence of approximately six adult cases per 100,000 people in Europe) (2, 3). Sarcomas are mostly detected in the extremities (approximately 60%) and the trunk (around 18%) (4), but they can arise

from any part of the body (retroperitoneum-12%, head and neck-9%, and mediastinum-1%). Metastases, when detected, are located predominantly in the lung, although are rarely present at the time of diagnosis (around 10% of the cases) (5–7).

According to the World Health Organization (WHO), there are more than 100 histological subtypes of sarcomas with different clinical characteristics (8). This classification considers the histology but also key genetic alterations, which are found within specific sarcomas. During the last decades, our understanding of the molecular mechanisms that underlie most of the sarcomas has been largely determined, contributing to improving diagnosis and treatment. The genetic alterations more frequently detected in sarcomas are: tyrosine-kinase activating mutations (9), gene fusions of growth factors or kinases (e.g., involving ALK, ROS1 or NTRK family) (10–12), gene fusions involving transcriptions factors (e.g., EWSR1-FLI1, PAX3-FOXO1) (13, 14), inactivation of tumor suppressor genes (e.g., NF1, PTEN or TP53) (15–17), gene amplification (e.g. MDM2 and MDM2/CDK4 co-amplification) (18) and epigenetic dysregulation (19, 20).

In addition to genetic alterations, other factors are also involved in the initiation, maintenance, and progression of cancer cells (21). Thereby, it is now widely accepted that the tumor microenvironment plays an essential role in tumor maintenance and progression. Particularly, the extracellular matrix (ECM) regulates many aspects related to the processes of cancer cell invasion, cancer cell dissemination, and the establishment of distant foci of metastasis. The components of the ECM interact with specific protein membrane receptors activating signaling pathways involved in migration, epithelial-mesenchymal transition (EMT), mesenchymal-epithelial transition (MET), and stemness (22). Collagens, proteoglycans, laminins, fibronectins, glycosaminoglycans, as the hyaluronic acid, or matricellular proteins, as periostin, are extracellular components present in the ECM. All of them are able to interact with specific receptors modulating the malignant phenotype, the metastatic processes, or the resistance to drugs (23, 24). One of the more relevant actors in this scenario is the transmembrane protein CD44, which interacts with many ECM components, triggering multiple signaling cascades within tumor cells. The role of CD44 in tumor progression and particularly in the processes of invasion and metastasis has been well established in many cancers mainly of epithelial origin, which have been the subject of excellent reviews (25–27). However, as far as we know, no comprehensive review compiling the data concerning the role of CD44 in sarcomas has been published. In this review, we have gone through the information available on the role of CD44 in the development, maintenance, and progression of sarcomas and analyzed their implications at the prognostic, therapeutic, and mechanistic levels.

2 CD44: STRUCTURE, LIGANDS, AND SIGNALING

2.1 CD44 Structure

The gene encoding human CD44 protein is located on the short arm of chromosome 11 and it is composed of 18 exons (HGNC:1681). Several exons (exons 6-14) undergo alternative splicing generating different isoforms (CD44v2-v10) (**Figure 1**) (25, 28). The isoform CD44v1 is not present in humans due to the absence of one exon in comparison to the CD44 gene in mice, which is composed of 19 exons instead 18 (28). The CD44 standard isoform, called CD44s (29), is composed of exons 1-5 (N-terminal and ligand binding domain) and exons 15-18 (C-terminal domain), thus excluding all the alternatively spliced exons. There are three differentiated regions in this complex cell-surface glycoprotein (**Figure 2**): i) the ectodomain, constituted by exons 1-16. It includes the alternatively spliced regions and thus their length is variable. This domain interacts with numerous extracellular ligands; ii) the transmembrane domain (TM, exon 17) and iii) the intracellular domain (ICD, exon 18) which interacts with kinases and other signaling molecules (27, 30) (UniProt accession number: P16070).

2.2 CD44 Ligands

The extracellular domain of CD44 has been shown to interact with several ligands as for example hyaluronic acid (HA),

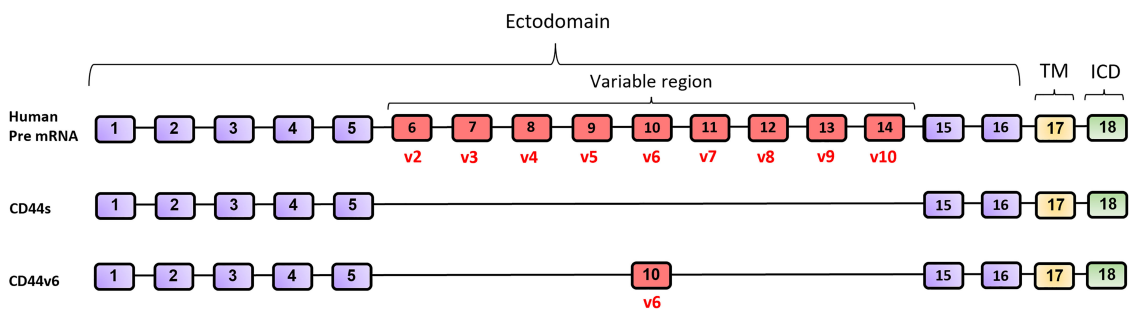

FIGURE 1 | Diagram of full-length CD44 pre-mRNA, CD44s and CD44v6 mRNA in human. CD44 is encoded by 18 exons (ENSEMBL accession number #ENSG00000026508. https://www.ensembl.org/). CD44 isoform 1 (CD44v1) is not present in humans. Exons marked in purple color are always expressed in the ectodomain of all CD44 isoforms. Up to nine exon variants can be inserted by alternative splicing to compose the variable region (Exons 6-14 in red). Exon 17 (yellow) codes for the transmembrane domain (TM) and exon 18 (green) codes for the intracellular domain (ICD).

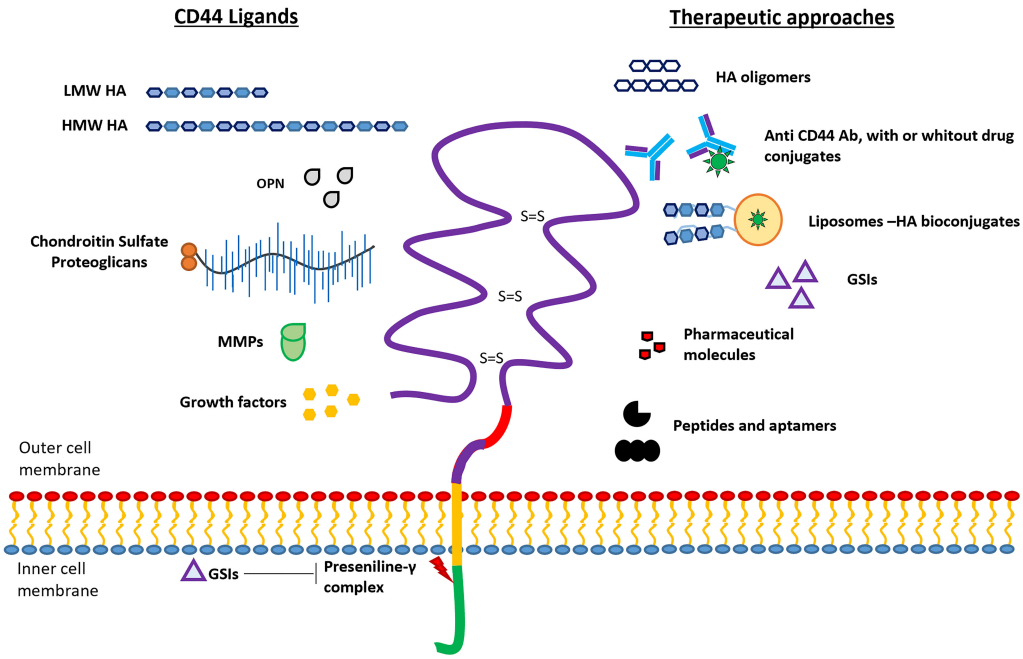

FIGURE 2 | Schematic representation of CD44 protein structure. The four domains of CD44 glycoprotein are represented with different colors: ectodomain (purple), variable domain (red), transmembrane domain (yellow), and intracellular domain (green). Ligands interacting with the ectodomain (left), and the different therapeutic approaches (right) are schematically represented. Presenilin-γ complex promotes the ICD cleavage which can be blocked by using γ-secretase inhibitors (GSIs).

osteopontin (OPN), serglycin/sulfated proteoglycans, fibronectin, collagen, and matrix metalloproteases (MMPs) (**Figure 2**). The binding of these ligands to CD44 triggers diverse cellular signaling cascades, some of which have been studied in sarcomas (see below) (25, 27, 31–37). The bioavailability of these biomolecules at the tumor or metastatic sites can modulate cancer progression through the activation of specific pathways. In this section, we analyzed briefly the effects triggered by CD44-ligand interactions.

2.2.1 Hyaluronic Acid (HA)

HA is a primary ECM constituent (commonly found in connective tissue and bone marrow) and the major ligand for CD44 (36). HA is a linear polymer of disaccharide units of β-1,3-N-acetyl glucosamine and β-1,4-glucuronic acid that is synthesized by the hyaluronan synthase proteins (HAS1-3) (38). The CD44/HA binding region resides in the N-terminal domain, located in residues 21-178, and is stabilized by three cysteine disulfide cross-links (39) (**Figure 2**). Interestingly, the molecular weight of HA, which can vary between dozens (≈5 KDa) and thousands of units (2,000 KDa), affects the binding of HA to CD44 and consequently to the effects that it causes in tumor cells (35). High molecular weight HA (HMW-HA, >500kDa) causes cell cycle arrest and reduces proliferation, neo-angiogenesis, and inflammation (35, 40), while low molecular weight HA (LMW-HA, 1-500 kDa) induces proliferation, ECM degradation processes (mediated by metalloproteases) and cell migration and invasion (35, 41). Ras, MAPK, PI3K, Nanog-Stat3, Oct4-Sox2-Nanog, c-Met or c-Src kinase signaling are some of the pathways directly modulated through CD44-HA binding (42–45). Merlin-ERM (ezrin-radixin-moesin) family of proteins, acts as a tumor suppressor by inhibiting the CD44-HA signaling (46).

2.2.2 Osteopontin (OPN)

OPN is an acidic phosphoprotein mainly secreted in plasma by macrophages and activated T cells and into the bone matrix by osteoblasts, among other cell types. This protein has been shown to be of predictive value in several types of cancers (47) and to be specifically upregulated in primary cultures from giant cell tumors of bone and desmoplastic fibroma samples (48). The CD44 residues implied in OPN binding involve the region containing amino acids 121 to 140 (47). The CD44/OPN interaction (32) supports tumor progression through the activation of the phosphatidylinositol 3-kinase/Akt signaling pathway (49), increasing consequently cell survival. Several cells, such as MDA-MB-435 or LCC15-MB among other breast cancer cell lines produce increased levels of this protein (50), which provide them with a growth advantage. HIF-2α (Hypoxia-Inducible Factor 2α) expression is also regulated by CD44-OPN interaction through a CBP/p300-dependent mechanism (mediated by CD44-ICD) and it has been demonstrated to promote stem-like properties and tumoral aggressiveness in glioma cells (51).

2.2.3 Proteoglycans

Several proteoglycans are being shown to interact with CD44. For example, serglycin a proteoglycan characterized by repeats of Serine-Glycine dipeptide, is primarily expressed in hematopoietic

tissue (52). However, this proteoglycan can be secreted by many cancer cells (e.g., nasopharyngeal carcinoma cells, myeloma cells, non-small cell lung cancers) (53, 54). CD44-Serglycin interaction maintains tumoral cell stemness through CD44 upregulation (as part of a positive feedback loop) mediated by MAPK/β-catenin pathway activation in nasopharyngeal carcinoma cells (55). Another proteoglycan, the versican, which is secreted by tumor stromal fibroblasts and cancer cells, binds to HA and generates HA/versican aggregations through its N-terminal region that contains a G1 domain (56), composed of an immunoglobulin-like domain (57, 58). The macromolecular complexes CD44/HA/versican promoted the invasion events in ovarian cancer cells (59). Another proteoglycan, aggrecan, a major component of cartilage, interacts with CD44, mediates cell adhesion, and induces CD44 oligomerization, which may lead to the triggering of the phosphorylation of Src kinases, activation of Rho-like GTPases or NF-κB activation cascades (60).

2.2.4 Fibronectin and Collagen

Fibronectin and collagens are abundantly present in the ECM and are mostly found in connective tissues. The interaction of fibronectin with CD44 facilitates the extravasation of cells and the adhesion processes, allowing cancer cells to adhere more efficiently to ECM within a metastatic microenvironment (61). On the other hand, collagens are the main components of the ECM which must be degraded so that tumor cells can colonize other tissues and organs. CD44 can upregulate serine protease and collagen-degrading enzymatic expression and its activity to achieve it (62) (see the paragraph below matrix metalloproteinases). Additionally, CD44 and type IV collagen interactions have been involved to participate in cell adhesion processes in colorectal carcinoma cell lines (KM-12c, CCL 188, and MIP-101) (63).

2.2.5 Matrix Metalloproteinases (MMPs)

MMPs are a group of calcium-dependent zinc-containing endopeptidases, which are responsible for tissue remodeling and degradation of ECM components, including collagens, elastins, gelatin, matrix glycoproteins, and proteoglycans (64). Malignant cells produce high levels of these proteins, which allow them to degrade ECM components faster than normal cells (65). The tumor invasiveness promoted by MMP-9 seems to be mediated by the binding of the proteolytically active metalloprotease to the CD44 ectodomain (66). Alternatively, the migration in rounded-amoeboid cells is supported through a non-catalytic mechanism based on actomyosin contractility modifications *via* CD44-MMP9 interaction (65). The metalloproteinase MT1-MMP, also known as MMP14, colocalizes with CD44 forming a complex through the hemopexin-like (PEX) domain in the MT1-MMP and the CD44-ICD, whose interaction is indispensable for degrading the extracellular matrix barrier during cancer invasion and is also involved in the CD44 ectodomain cleavage (see below) (67, 68).

2.3 Signaling Pathways Activated Through CD44

CD44-dependent signalling pathway activation takes place through two different mechanisms: i) the interaction between adaptor molecules and the intracellular domain (CD44-ICD) (28, 37) and ii) through the direct translocation of the CD44-ICD to the nucleus (37, 69, 70).

i) The CD44-ICD domain lacks kinase activity but it can interact with adaptor molecules like ankyrin and ERM (ezrin-radixin-moesin protein family) (**Figure 3**), which link CD44 to the actin-cytoskeleton network. These interactions trigger changes in the tumor cell cytoskeletal architecture and cell signaling (e.g., c-Met activation, Ras-MAPK cascade, Snail/β-catenin translocation, or PI3K-AKT pathway activation), playing a role in the regulation of epithelial-mesenchymal transition mechanisms (EMT) and the activation of angiogenesis, proliferation, and invasion mechanisms (70, 71).

ii) On the other hand, CD44-ICD can translocate to the cell nucleus thanks to the transportin1-specific nuclear localization signal (residues DRKPS) present at its N-terminal region and there (**Figure 3**) (71, 72). At the nucleus, CD44-ICD regulates the expression of some genes through the formation of different complexes with CBP/p300, Runx2, or Stat3 (42, 70, 73–76). Among the genes that have been shown to be regulated by CD44-ICD are some stemness factors (e.g., Nanog, Sox2, or Oct4), activators of cell proliferation (e.g. Cyclin D1 or c-myc), regulators of EMT (e.g., MMP-9 or Twist1) or CD44 itself (51, 69, 70, 73, 74, 76, 77).

The translocation of CD44-ICD to the nucleus is preceded by a sequential cleavage (**Figure 3**) of the CD44 protein (69). The ectodomain cleavage produced between the variable region and the transmembrane domain could be activated by three different pathways; i) the protein kinase C (PKC) which activates the ADAM Metallopeptidase Domain 17 (ADAM17); ii) the calcium influx which activates the ADAM10; iii) the interleukin 1, TGFβ1, or interferon γ which induces the expression of MT1-MMP (MMP14) activating proMMP-2 (78, 79), and promoting cell migration and invasiveness (80–82). Subsequently, a mechanism called regulated intramembrane proteolysis (RIP), which is driven by the presenilin-γ-secretases is activated. The presenilin-γ-secretase complex, constituted by presenilin 1 and presenilin 2 γ-secretases, recognizes the proteolytic cleavage sites at the CD44 transmembrane domain (residues Ala278-Leu279 and Ile287-Ala288) and detaches the intracellular domain from the rest of the protein (83), releasing the CD44-ICD domain to the cytoplasm (70, 73, 84). Interestingly, this sequential proteolytic cleavage can be promoted by CD44-ligand interactions (26, 35, 79, 83, 85), while the CD44-ICD releasing can be inhibited by γ-secretase inhibitors (GSI) (69, 77) or by merlin protein. Merlin recognizes the same motif recognized by ERM (71) and can provide a tumor suppressor state by blocking the cleavage site (46).

3 MSCS, CSCS, AND DIFFERENTIATED TISSUES: CD44 EXPRESSION AND INFLUENCE DURING CELL DIFFERENTIATION AND SARCOMAGENESIS

Sarcomas are thought to arise from mesenchymal stem cells (MSCs) or derived progenitors, from which normal differentiated cells are

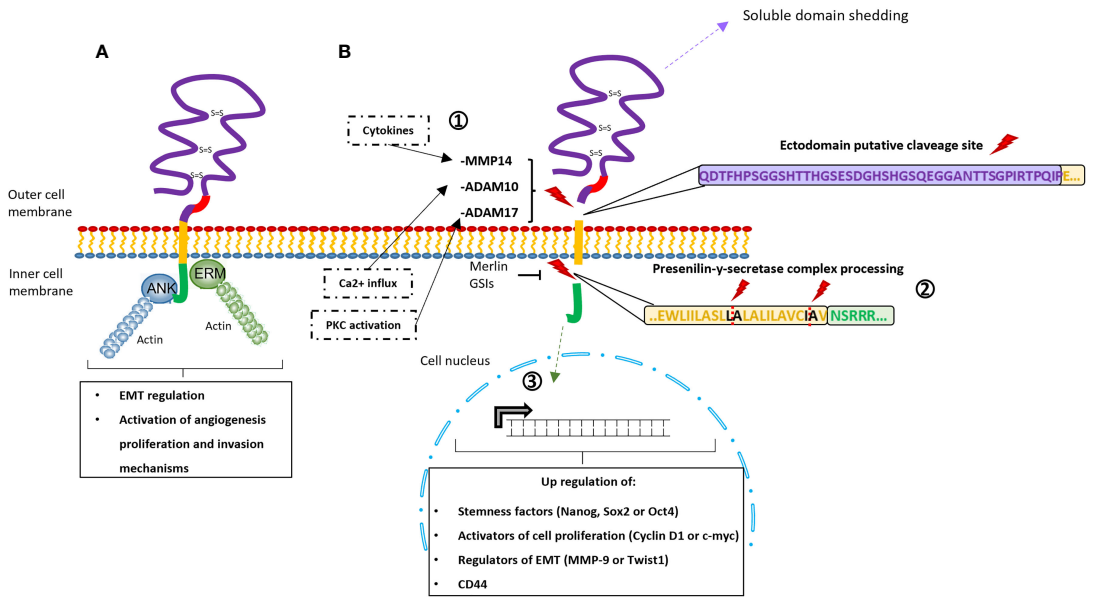

FIGURE 3 | Schematic representation of the signaling pathways activated through CD44. **(A)** Interaction between adaptor molecules Ankyrin (blue) and Ezrin-Radixin-Moesin (green) with the intracellular domain CD44-ICD. This interaction triggers modifications in the cytoskeletal disposition and the activation of specific pathways (e.g., c-Met activation, Ras-MAPK cascade, Snail/β-catenin translocation, or PI3K-AKT pathway activation). As consequence, this *via* is involved in epithelial-mesenchymal transition mechanisms (EMT) and the activation of angiogenesis, proliferation, and invasion mechanisms. **(B)** Schematic representations of CD44-ICD signaling via, including the sequential proteolytic cleavage of the CD44 protein. 1) The ectodomain shedding is induced by PKC, Ca2+ influx or cytokines that activate the MMPs (ADAM17, ADAM10 and MMP14, respectively). 2) The presenilin-γ-secretase complex is activated and processes the ICD through the specific cleavage sites in the transmembrane domain (residues L-A and residues I-A). GSIs (γ-secretase inhibitors) and the merlin protein can inhibit this second proteolytic processing. 3) The ICD is released and translocated to the nucleus upregulating stemness factors, activators of cell proliferation, epithelial-mesenchymal transition mechanisms (EMT) regulators and CD44 itself.

also produced (for example adipo-, chondro-, myogenic, and osteocytic cells) (86). Therefore, the study of the similarities and differences among different grades of cell differentiation, that is, mesenchymal stem cells, sarcoma cells, and normal differentiated cells, is important to understand the role of CD44 in sarcomas.

3.1 CD44 Expression in MSCs, Sarcoma (CSCs), and Differentiated Tissues

MSCs presents different surface markers including STRO-1, CD166, CD146, CD106, CD105, CD90, CD73, CD54, CD44, CD34, CD29 and CD13 (87, 88). CD44 shows high expression in MSCs as well as in sarcomas (89–92). Interestingly, CD44 has been shown to be expressed in the subpopulation of cancer stem cells (CSCs), which can reconstitute the tumor mass. CSCs and MSCs share similar stem-like properties and features. These similitudes among the characteristics of MSC (stemness, healing, regeneration processes, and cell recruitment) and cancer stem cells CSCs (potential for tumor initiation, EMT, tumoral progression, and stemness) with increased CD44 expression have already been broadly described in different cancers (28, 70, 93–97). Concordantly, CD44 is expressed at high levels in most sarcomas (**Figure 4**). The available data from the public database (DEPMAP Portal, https://depmap.org/portal/) confirms that CD44 expression was elevated in all sarcoma cell lines available in the dataset, with the unique notable exception of Ewing sarcoma, which expresses low levels of CD44 in comparison to the rest of sarcoma cell lines. Controversially, Skubitz et al., performed a CSCs characterization of stem cell markers in 31 soft tissue sarcoma from patients and determined that neither CD44, ALDH1, or CD133 were useful for sarcoma (CSCs) identification in these samples (98).

On the other hand, the CD44 protein is detected in the most differentiated tissues according to the Human Protein Atlas database (https://www.proteinatlas.org/). In consequence, CD44 shows a reduced tissue specificity due to its ubiquitous nature. Despite its ubiquity, CD44 is predominantly found in epithelial cells, bone marrow, and lymphoid tissue. Mesenchymal-derived tissues such as chondrocytes and bone cells have been demonstrated to express CD44 and modulate its expression in specific biological processes (cell-cell and/or cell-matrix attachment, morphological changes observed from osteoblasts to osteocytes, osteoclastogenesis, regulatory function in chondrocytes) (99–101). Additionally, CD44 seems to be involved in the processes of MSCs differentiation (101–105). Interestingly, CD44 expression was suggested to be reduced during the process of differentiation from MSCs to differentiated mature cells (103, 106). Thus, Huynh et al., monitored the process of chondrogenic differentiation from MSCs derived from bone marrow. They analysed the changes in the mRNA profile during differentiation and described several MSC markers, such as CD44,

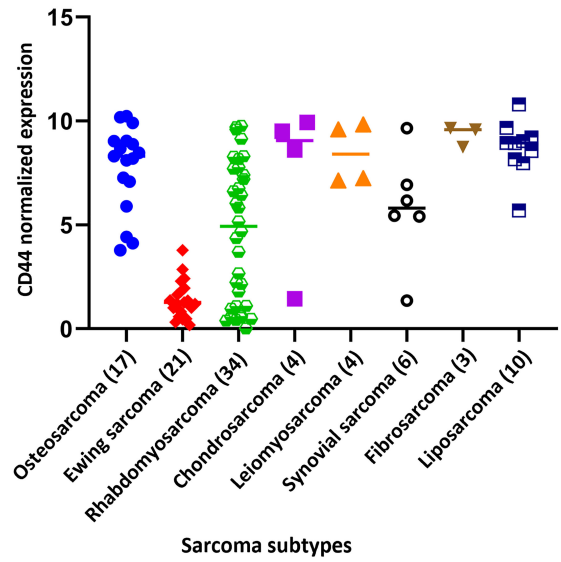

FIGURE 4 | CD44 normalized expression of the different cell line sarcoma subtypes. Data extracted from DEPMAP Portal (https://depmap.org/portal/). The number of cell lines in each sarcoma subtype is indicated in brackets.

ENG, NT5E, or THY1, that progressively decreased during the differentiation process, while well-established chondrogenic markers (e.g., COL2A1, ACAN, COL9A1, COL11A1, COMP) were up regulated as the process of cell differentiation progressed (106). Moroes et al., studied the effect of CD90 and CD44 on differentiation processes induced in mesenchymal stem cells. The silencing of CD90 decreased the expression of CD44 which promoted the osteogenic and adipogenic differentiation of MSCs *in vitro*, thus associating the expression of high levels of CD44 and CD90 to the stemness state of MSCs (103, 107). Alternatively, the impairments in maturation processes involving high levels of CD44 were tested in neural differentiation experiments from MSCs and astrocytes precursor cells. Increased expression of CD44 inhibited oligodendrocytes differentiation and arrested the cells at the glial progenitor state. The *in vivo* research performed in a CD44 misexpression transgenic mouse model (CNP-CD44 mouse), supported that the CD44 overexpression blocked the oligodendrocyte maturation (108, 109). Complementary, Naruse et al., demonstrated that despite the widespread expression of CD44 in progenitor cells at early embryonic stages, the CD44 expression in adults was restricted to a specific mature subtype of cells (granule neurons). Thus, supporting the role of CD44 in the maintenance of stemness properties, but being able to promote differentiation of specific subtypes of neurons and astrocytes (110).

In summary, there is a relatively high expression level of CD44 in MSCs and sarcomas according to different studies and publicly available datasets. The differences in CD44 expression among the stem-like cells (MSCs and CSCs/sarcomas) and differentiated tissues suggest a down-regulation event of CD44 upon differentiation into mature cells, acquiring a new basal level of CD44, corresponding to its novel biological functions, which is susceptible of up/down-regulation.

3.2 CD44 and Tumor Microenvironment

The mesenchymal cell microenvironment has been demonstrated to be crucial for the development of multiple functions of mesenchymal stem cells (MSCs). This microenvironment provides components for cell regeneration and self-renewal potential maintenance (111, 112). For instance, abundant quantities of HA are produced by MSCs to maintain their stemness (70). Injure healing processes and tissue regeneration are typical MSCs-driven processes, for which MSCs recruitment is mandatory, and CD44s-HA interaction seems to be a determinant mechanism to promote cell migration (113). Therefore, CD44 and the microenvironment play an important role in the processes performed by these cells and as consequence in their derived tumors.

Functionally, the high expression of CD44 benefits CSCs in several situations. CD44 works as a co-receptor for growth factors (CD44v3 co-receipts FGF and VEFG, while CD44v6 co-receipts EGF and HGF) and cytokines in the tumoral niche, potentiating receptor tyrosine kinase or CD44-mediated signalling (37, 114) and triggering TGF-β up-regulation and the induction of Snail and Twist (115, 116). These two genes are considered key regulators of EMT and cancer progression (117–119). Snail has also been associated with cell cycle regulation, apoptosis evasion, cell adhesion, neuroendocrine differentiation, and chemoresistance (118–120). Twist is thought to promote metastasis, although the mechanisms implied are poorly understood (121, 122). Additionally, CD44-regulated transcription factors related to stem cell expression programs (Sox2, Klf4, Oct4, and Nanog), are commonly identified in MSCs and tumors (115), when CD44 has been knocked-down the expression of these markers (Oct4, Nanog, and Sox2) are notably reduced (123). Consequently, the transcriptional networks mediated by these factors are crucial for stemness properties observed during tissue development (70, 124, 125).

The hypoxic low-ROS (reactive oxygen species) environment is also associated with proliferation and the maintenance of self-renewal capacities in cancer stem cells (CSCs) and solid tumors (126, 127). In this situation, CD44 has a specific function. HIF-1α induced by hypoxia promotes glycolytic metabolism, angiogenesis (128), and CD44, CD44v6/v7/v8 expression (129). CD44 regulates ROS-mediated cytotoxicity in tumors through two different mechanisms (70). The interaction of CD44-ICD-PKM2 (pyruvate kinase isoenzyme type M2) increases PKM2 phosphorylation (suppressing its activity) which promotes the activation of glycolytic metabolism, driving the CSCs to a pro-antioxidant status (130). Low PKM2 activity increases the levels of reduced NADPH which favors the regeneration of reduced glutathione GSH (131, 132). Alternatively, the interaction CD44-XCT (subunit of the cystine-glutamate transporter Xc), promotes cystine uptake for the synthesis of GSH (133). As consequence, oxidative stress is controlled and reduced, providing a favorable environment for CSCs. The relevance of this mechanism has supposed its targeting through xCT inhibitors, like the sulfasalazine. This molecule has been tested in a dose-

escalation clinical study with advanced gastric cancer patients, showing the inhibition of the proliferation in CD44v-positive cancer cells, both *in vitro* and *in vivo* (134).

4 FUNCTIONAL CHARACTERIZATION OF CD44 IN SARCOMA CELL LINES

Most of the studies carried out to understand the functionality of CD44 in cancer have been performed in epithelial tumors, although some relevant works focused specifically on sarcomas.

4.1 Chondrosarcoma

Some studies performed in chondrosarcoma cell lines have contributed to understanding the role of CD44 in these tumors and clarifying the signal transduction cascade triggered upon CD44 stimulation. Suzuki et al., reported that LMW-HA (molecular weight 3.5 kDa) can stimulate CD44 and subsequently, increase c-Met expression and c-Met phosphorylation in the chondrosarcoma cell line HCS-2/8 (45). In a similar study, using the same chondrosarcoma cell line, Kobayashi et al., demonstrated that the mRNA and protein of the urokinase-type plasminogen activator (uPA) and theurokinase-type plasminogen activator receptor (uPAR) were upregulated after CD44 stimulation with LMW-HA. Moreover, it was shown that CD44 stimulation with LMW-HA induced MAPK pathway activation, *via* phosphorylation of MEK1/2, ERK1/2, and c-Jun. Additionally, the signalling cascade derived from the interaction of HA with CD44 could be disrupted at different points; by using anti-CD44 antibodies, MAP kinase inhibitors, neutralizing anti-uPAR pAb, anti-catalytic anti-uPA mAb, or amiloride (135). These results provide a novel therapeutical alternative and suggest that there could exist an autocrine loop; CD44 stimulation - MAP kinase cascade activation (including c-Met) - uPA/uPAR overexpression, in chondrosarcoma cells that can boost their invasiveness.

4.2 Osteosarcoma

Gene silencing and CRISPR/Cas9-mediated knockout have been used to elucidate the role of CD44 in osteosarcoma pathogenesis, particularly in relation to resistance to treatment and metastasis formation. Knocking-out of CD44 using CRISPR/Cas9 system in the drug-resistant osteosarcoma cell lines KHOSR2 and U-2OSR2 (both resistant to Doxorubicin) showed significant inhibition of migration, invasion, proliferation, and resistance to doxorubicin (136). In another study, CRISPR/Cas9 was also used to knocking-out CD44 in the human osteosarcoma cell lines MNNG/HOS and 143B, both highly metastatic. This study showed the inhibition of cell proliferation and tumor-sphere formation in 3D cultures upon CD44 inactivation (137). CD44 inactivation, through a siRNA strategy, performed by Kong et al., in MG63 and U2OS cells showed a reduction in proliferation rate and inhibited the cell migration and the invasive capability (138). It was suggested that this effect could be a consequence of the downregulation of cathepsin S (a lysosomal cysteine protease of papain subfamily) upon CD44 knocking out. Concordantly, a similar study performed by Gvozdenovic et al., in 143B osteosarcoma cell line using an shRNA-silencing approach to downregulate CD44 expression, resulted in a decrease in the adhesion of osteosarcoma cells to HA, migration, and a diminished capacity to growth anchorage independent in soft agar. However, CD44 silencing favored the growth of the primary tumor and the appearance of pulmonary metastasis in an intratibial xenograft model (139), highlighting the existence of controversial results between *in vitro* and *in vivo* situations. Immunohistochemistry analysis of intratibial primary tumor and lung metastasis showed notably lower levels of merlin, a tumor suppressor protein, compared to the same cell lines in *in vitro* conditions. Therefore, this enhanced malignant phenotype *in vivo* could be associated with the impairment of the adhesion properties to ECM due to CD44 depletion or the reduced expression of merlin in *in vivo* conditions. The authors explained that since 143-B cells were obtained through Ki-Ras transformation (140), the enhanced Ras-driven metastatic behavior is evidenced because of merlin protein expression lacked *in vivo*. Although the mechanism involved in merlin downregulation in osteosarcoma cells has not been yet elucidated, a possible explanation could be deduced from studies carried out in breast cancer cells. In breast cancer cells, the phosphorylation of merlin which promotes its proteasomal degradation is a process initiated by OPN and mediated by the Akt pathway (141), thus suppressing completely the antitumoral activity of merlin. Interestingly, the CD44 expression in osteosarcoma CSCs has been determined to be affected by pimozide treatment (a STAT5 inhibitor). This drug reduced considerably the expression of CD44 among other stem cell markers (CD133, Oct-4, and ABCG2) in KHOS/NP and SJSA-1 cell lines and, in consequence, impaired the growth and stemness of CSCs (142). The available data from the depmap portal (https://depmap.org/portal/) showed some differences in CD44 expression among osteosarcoma cell lines. Thus, MG63, OS252, C396, and HS888T cell lines showed the highest levels of CD44 expression, while NOS1 and HSOS1 had the lowest levels.

In addition to the experimental strategies described above, the study of miRNAs and long non-coding mRNAs that can downregulate CD44 levels have been also useful to determine the role of CD44 in osteosarcoma pathogenesis. For example, ectopic expression of miR-34a represses the expression of CD44 in two osteosarcoma cell sublines (F5M2 with highly metastatic potential and F4 with a low metastatic potential), inhibiting their migration and invasive ability (143). Another miRNA, the miR-199a-3p that targets directly the 3′-UTR region of CD44, produces a reduction in the levels of CD44 mRNA. Interestingly, miR-199a-3p levels are notably reduced in osteosarcoma cells and tumors compared to normal osteoblast. The overexpression of miR-199a-3p in KHOS and U-2OS inhibited CD44 mRNA levels and significantly increased the sensitivity of these cells to doxorubicin (144). In other studies, *in vitro* knockdown of the oncogenic long non-coding RNA GAPLINC (Gastric adenocarcinoma predictive long intergenic non-coding) in HOS and Saos-2 osteosarcoma cell lines, reduced migration and invasion by inhibiting considerably CD44 expression, although it does not impair cell proliferation (145). In

summary, these studies suggest that the CD44-miR-199a-3p axis and GAPLINC regulation are relevant regulators in the development of metastasis, tumor recurrence, and drug resistance in osteosarcoma cells mediated by CD44.

4.3 Ewing Sarcoma

Ewing sarcoma, an extremely rare sarcoma that arises mainly during childhood and adolescence, presents a notably reduced expression of CD44 compared to the rest of the sarcoma cell lines (**Figure 4**). The explanation for this difference could rely on the CD44 gene regulation, which contains an element recognized by the ETS-1 (v-ets erythroblastosis virus E26 oncogene homolog 1) family transcription factors. Ewing sarcoma is genetically characterized by a balanced chromosomal translocation, in which a member of the FET gene family (FUS, EWSR1, or TAF15) is fused with an ETS transcription factor (FLI1, ERG, ETV1, ETV4, or FEV, among others) (146). The EWSR1–FLI1 chimeric protein can recognize the domain on the CD44 promotor and regulates its expression. An assay performed in the A673 cell line with an shRNA silencing approach for EWSR1-FLI1 showed that EWSR1-FLI1 inhibition induces CD44, CD59, CD73, CD29, and CD54 surface antigen expression, among others (147). Therefore, the lower CD44 levels find in this rare cancer are due to the high basal expression levels of the EWSR1-ETS1. This phenomenon, regarding the downregulation of CD44 in comparison to other sarcomas, could be determinant for the tumor growth, dissemination, and drug resistance in this sarcoma subtype. Thus, further research is required to define the role of CD44 in Ewing sarcoma.

Beyond this observation, the role of CD44 in the progression, metastasis, or drug resistance of Ewing sarcoma remains unclear. Recently, Paulis et al., showed that CD44 was involved in a phenomenon known as 'vasculogenic mimicry', defined as the ability of some cells to transdifferentiate into cells with endothelial characteristics and constitute vasculogenic networks independent of angiogenesis, which is associated with tumor aggressiveness and poor prognosis. The authors used two derived Ewing sarcoma cell lines (EW7 and SIM.EW27) and two breast cancer cell lines (MDA-MB-231 and MCF-7) to study key molecules involved in the vasculogenic mimicry. The authors concluded that CD44/c-Met signalling cascade, highly overexpressed in the aggressive cell lines (EW7 and MDA-MB-231), is crucial for vasculogenic mimicry (148). Overexpression of CD44 (CD44s and CD44v6 isoform) in the EW7 and MDA-MB-231 cell lines (highly metastatic) compared to the low-invasive cell lines (SIM.EW27 and MCF-7) was related to increased aggressiveness and to the promotion of the formation of vasculogenic structures *in vitro*. Accordingly, knocking-out CD44 by siRNA reduced the CD44 RNA level and the protein expression to approximately 40% in EW7 cells. As result, the migration capacity was markedly reduced, as well as the vascular-like networks. Tumor samples from patients analyzed in this study also supported the association among vasculogenic structures and 'blood lakes' formation and CD44 expression. CD44 was detected by immunochemistry in 14 out of 15 Ewing sarcoma tissues whose score was positive for the presence of blood lakes (149).

4.4 Fibrosarcoma

Several studies involving fibrosarcoma cell lines have been performed to elucidate the role of the receptors for hyaluronic acid-mediated motility (RHAMM, another HA receptor) and HA interactions in fibrosarcoma. Kouvidi et al., determined the effect of HA/RHAMM signalling on the ability of HT1080 fibrosarcoma cell line to adhere to fibronectin. On one hand, the adhesion properties of HT1080 cells significantly increased ($p \leq 0.01$) with LMW-HA treatment, while HMW-HA inhibited them. On the other hand, the HT1080 RHAMM-deficient cells had a diminished adherence capacity compared with control cells. Additionally, *in vitro* experiments established that the activation of FAK and ERK1/2 signalling pathways, triggered through the RHAMM/HA interaction, regulated cell adhesion properties in HT1080 fibrosarcoma cells (150). Hatano et al., reported that, in *in vitro* conditions, RHAMM interacted with ERK (as previously explained), increasing the proliferative ability of fibroma cells. However, this process involved the interaction of CD44 with the epidermal growth factor receptor (EGFR) (151). Therefore, the axis CD44/RHAMM seems to mediate proliferation and metastatic dissemination due to the modification of adhesiveness to ECM components.

The specific contribution of CD44 in metastatic dissemination was studied in murine models (152). Culp et al., overexpressed the human CD44s (standard isoform) on the nonmetastatic cell lines: sis-transformed Balb/c 3T3 cells and ras-revertant IIIA4 cells. Afterward, the cells were implanted in athymic nude mice. The result of the experiment demonstrated that the increased expression of human CD44s in the mice model promoted micrometastasis events of the lungs (152).

The functional studies performed in different sarcomas demonstrate that CD44 plays a relevant role in sarcomagenesis and tumor progression. Ligand-dependent processes, proliferation events, migration/adhesion capacities, or drug resistance were shown to be regulated through specific mechanisms in which CD44, ECM components, and microenvironment have a direct or indirect effect. Although several studies have shown a relevant role of CD44 in a reduced number of sarcomas, there is a clear lack of studies in other types of sarcomas such as myxofibrosarcoma, synovial sarcoma, or rhabdomyosarcoma, among others. This highlights the existence of a poorly developed field of research that needs to be completed to define in detail the role that CD44 plays in these types of cancer.

5 PROGNOSTIC VALUE OF CD44 EXPRESSION IN SARCOMAS

Several studies have analyzed the prognostic value of CD44 expression in sarcomas (**Table 1**). Given that sarcomas are rare cancers, and therefore it may be difficult to accumulate a relevant number of cases, several of these studies have been carried out with

TABLE 1 | Summary of sarcoma subtype studies analyzing CD44 expression alone or in combination with other biomarkers in patient samples.

Sarcoma subtype	Study	Number of samples	CD44 isoform detected	Detection technique	Additional markers tested	Clinical conclusion
Myxofibrosarcoma	Matuschek et al.	34	Increased CD44s Low CD44v6	Quantitative PCR	–	Improved clinical outcome
	Tsuchie et al.	44	Increased CD44s	Inmunohistochemical	–	Poor event free survival and local recurrence in patients with lung metastasis
Synovial Sarcoma	Sneath et al.	56	CD44 expression	Inmunohistochemical	–	No correlation with prognosis
	Zhou et al.	20	CD44 expression	Inmunohistochemical	CD133, CD29, Nestin and ALDH1	CD44 was not correlated with prognosis, but ALDH1 positive cases showed a poorer prognosis
Rhabdomyosarcoma	Saxon et al.	12	CD44 expression	Inmunohistochemical	ECM proteins (laminin, fibronectin, tenascin and thrombospondin)	No correlation among the markers tested with metastasis or with the level of tumor differentiation
	Humphrey et al.	28	CD44 expression	Inmunohistochemical	–	CD44 positive patients presented improved outcome
Chondrosarcoma	Heyse et al.	30	CD44 overexpression	Inmunohistochemical	–	Correlation with tumor grading, metastatic potential, and survival
	Roxeman et al.	16	CD44 expression	Inmunohistochemical	ECM components, growth factors, p53, among others	Preferential CD44 splicing: CD44+/CD44v3– in the chondrogenic component of dedifferentiated peripheral chondrosarcoma and CD44–/CD44v3+ in secondary peripheral chondrosarcomas
Osteosarcoma	Boldrini et al.	34	CD44 expression	Inmunohistochemical	Ezrina	No correlation was established
	Gvozdenovic et al.	53	CD44 expression	Inmunohistochemical	–	Failed as an independent predictor
	Liu et al.	329	CD44 expression	Meta-analysis	–	CD44 expression did not correlate with overall survival or metastasis
	Xiao et al.	96	CD44 expression	Inmunohistochemical	–	Useful biomarker to predict chemoresistance. Supported by functional studies
	Liu et al.	548	CD44 expression	Meta-analysis	–	Useful in the prediction of poor survival and metastatic potential
	Kuryu et al.	44	CD44s and CD44v3, v4, v5, v6, v7, v9, and v10	Inmunohistochemical	–	CD44v6 was correlated to patient prognosis
	Deng et al.	110	CD44v6	Inmunohistochemical	CDH11 and β-catenin	CD44V6, CDH11, and β-catenin were associated with overall survival
	Gao et al.	114	CD44 expression	Inmunohistochemical	–	Poor outcome and drug response
	Kim et al.	59	CD44 expression	Inmunohistochemical	IGF1R and ABCG2	CD44 and ABCG2 can be used in combination with IGF1R as prognosis and efficient treatment factors
	Zhang et al.	486	CD44v6	Meta-analysis	–	CD44v6 over-expression correlates with poor outcome and metastasis
	Zhang et al.	463	CD44v6	Meta-analysis	–	CD44v6 could act as a diagnostic marker for osteosarcoma

a series of patients consisting of various tumor types. Henderson et al., analyzed the expression of CD44 by immunohistochemistry in a series of 23 soft tissue sarcomas (8 liposarcomas, 4 myxofibrosarcoma, 4 undifferentiated pleiomorphic sarcomas, 1 alveolar soft parts sarcoma, 1 extraskeletal mesenchymal chondrosarcoma, 1 leiomyosarcoma, 1 malignant peripheral nerve sheath tumor, 1 extraskeletal osteosarcoma, 1 synovial sarcoma, and 1 primitive neuro-ectodermal tumor. Their results suggest that increased CD44 expression was associated with a worse disease specific survival (p=0.056, univariant analysis). In the same article, the authors analyzed by multivariate analysis 74 cases of soft tissue sarcoma from The Cancer Genome Atlas program (TCGA) that included clinical and genomic data (https://www.cancer.gov/about-nci/organization/ccg/research/structural-genomics/tcga). It was shown that CD44 copy number variations predicted worse disease specific survival (p=0.007). Thus, the authors concluded that increased expression of CD44 was correlated with worse outcomes in soft tissue sarcomas (153). In another study, Kahara et al., analyzed by immunohistochemistry the expression of several CD44 isoforms in a series of 47 sarcomas

(18 malignant fibrous histiocytomas, 13 synovial sarcomas, 7 malignant schwannomas, and 9 liposarcomas). Isoforms CD44v3, v4, v5, v6, v7, and v9 were frequently detected, whereas CD44v10 was not expressed in any of the samples analyzed. CD44v6 isoform was commonly detected in high-grade tumors and both CD44v6 and v9 expression correlated negatively with metastasis-free survival (154). Kebudi et al., also studied the relevance of CD44 levels in serum (measured by ELISA), in the context of pediatric sarcomas (18 rhabdomyosarcomas, 22 Ewing sarcoma, and 15 osteosarcomas). In this study, the differences observed between the serum levels of CD44 in children with sarcoma and healthy controls were not significant ($p>0.05$), as result, a non-diagnostic or prognosis value was established (155).

5.1 Studies Performed on Specific Sarcoma Subtypes

5.1.1 Myxofibrosarcoma

Myxofibrosarcoma is one of the most common and aggressive soft tissue sarcomas, commonly developed in the limbs. A multivariate study focused on the analysis of CD44 isoforms in 34 adult patients with myxofibrosarcoma showed that increased expression of CD44s and reduced expression of CD44v6 isoform correlated significantly with an improved outcome ($p<0.05$ and $p<0.02$, respectively) (156). Additionally, a recent multivariate analysis designed to identify possible relationships between CD44s expression and clinic-pathological factors carried out in 44 retrospectively enrolled myxofibrosarcoma patients, showed that increased expression of CD44s correlated negatively with event-free survival and local recurrence. Additionally, in the subgroup of patients with distant metastasis, the CD44 expression was significantly elevated in patients with lung metastasis compared to patients with lymph node metastasis ($p=0.044$) (157).

5.1.2 Synovial Sarcoma

Synovial sarcoma is an aggressive soft tissue sarcoma, whose initiation and progression rely on the fusion gene SYT-SSX (158). This tumor has a low incidence, and it is predominantly detected in the lower extremities of young adults (8). This tumor is formed by mesenchymal spindle cells, but it is not related to the synovial membrane. Studies of immunohistochemistry determined that CD44 expression did not correlate with prognosis (survival, local recurrence, or metastasis) in synovial sarcoma (159). The uselessness of CD44 levels in synovial sarcoma prognosis has also been supported by Zhou et al., where stem cell-associated markers (CD133, CD29, CD44, nestin) and ALDH1 were characterized immunohistochemically in 20 synovial sarcomas. No relationship was settled down between these markers and clinical parameters (age, gender, sites, tumor size, histological type, tumor stage, and distant metastases). However, this study confirmed that ALDH1 positive synovial sarcomas had a significantly poorer prognosis compared to ALDH1 negative synovial sarcomas (160), providing an alternative prognosis marker to CD44.

5.1.3 Rhabdomyosarcoma

Rhabdomyosarcoma is a malignant soft tissue tumor that arises from muscle cells. It commonly arises during childhood. There are two main types of rhabdomyosarcomas that differ in their molecular and clinical characteristics. Alveolar rhabdomyosarcomas are characterized by the presence of reciprocal translocations that result in chimeric proteins that fusion the PAX3 or PAX7 genes with the transcription factor FOXO1. By contrast, embryonal rhabdomyosarcomas are characterized by chromosomal losses and gains (161). Humphrey et al., analyzed by immunohistochemistry, a series of 28 rhabdomyosarcomas (8 alveolar and 20 embryonal) and showed that CD44 positive patients had improved outcomes compared with CD44 negative tumors ($p=0.001$, Fisher test) (162). By contrast, a study performed by Saxon et al., in 12 pediatric rhabdomyosarcoma tumor-derived cells (five alveolars, six embryonal, and one botryoid subtype) reported no association between the expression of ECM proteins (laminin, fibronectin, thrombospondin, tenascin) and CD44 with metastatic events at clinical presentation (163).

5.1.4 Chondrosarcoma

Chondrosarcoma is a type of sarcoma that develops from chondrocyte progenitors, primarily affecting the cartilage of the femur, arm, pelvis, or knee. Heyse et al., determined that the levels of CD44s increased with the malignant grade of the tumor and that the overexpression of CD44 correlated with metastatic potential and survival (164). This study included 22 conventional chondrosarcomas, two dedifferentiated chondrosarcomas, two extraskeletal chondrosarcomas, and one periostal, mesenchymal, clear cell, and myxoid chondrosarcoma each. In another study, Rozeman et al., analyzed sixteen chondrosarcomas by immunohistochemistry for CD44, different ECM components, and growth factors. The study suggested the existence of a differential pattern of CD44 isoform. Thus, CD44 positive and CD44v3 negative expressions were found in the chondrogenic component of dedifferentiated peripheral chondrosarcoma, whereas in secondary peripheral chondrosarcomas was detected the expression of CD44 negative– and CD44v3 positive isoforms (165). Dedifferentiated peripheral chondrosarcoma is a rare subtype of chondrosarcoma arising superimposed on the cartilage cap of a pre-existing osteochondroma (8). These findings suggest that different CD44 isoforms can be associated with different grades of chondrogenic differentiation in chondrosarcomas. No data about the correlation of clinical parameters with CD44 expression were present in this study.

5.1.5 Osteosarcoma

Osteosarcoma is one of the most common sarcomas observed during childhood and adolescence (8). Approximately 30% of patients develop pulmonary metastasis (166). Some parameters well-established that affect the patient outcome are the anatomic location of the primary tumor, tumor size, dissemination processes, and response to induction chemotherapy (167). These tumors are the sarcomas in which more studies on CD44 have been carried out although the role of CD44 as a prognostic marker in osteosarcoma patients is controversial. Some studies, including one meta-analysis of 329 patients from six different studies (168), conclude that there is no significant association between prognostic or metastatic recurrence with CD44 expression levels (168–170). However, recent studies,

including other meta-analyses of 548 osteosarcoma patients from nine studies, have concluded that CD44 expression may predict survival, metastasis recurrence, and drug resistance (136, 137). This agrees with *in vitro* studies carried out in different osteosarcoma cell lines (KHOS doxorubicin resistant, U2-OS doxorubicin resistant, MNNG/HOS, and 143B) that demonstrated that CD44 promotes cell migration, cell invasiveness, and drug resistance (136, 137, 139, 170).

Other studies focused on osteosarcoma have revealed that overexpression of CD44v6 (171, 172), CD133 (173), CD133/CD44 combination (174), CDH11 (172), β-catenin (172), GAPLINC (145), CD44-miR-199a-3p axis (144) and the combination CD44/IGF1R/ABCG2 (175) could provide valuable information as prognostic markers in this sarcoma. Supporting the role of the CD44v6 marker in osteosarcoma, two meta-analyses (both with more than 460 osteosarcoma cases) focused on the prognostic utility of this specific CD44 isoform revealed that its overexpression is associated with the overall survival rate and the occurrence of metastatic events and could be used as a complementary diagnostic marker in osteosarcoma (176, 177). However, the authors explained that the diagnostic utility of CD44v6 presented some limitations due to the low number of articles involved in the meta-analysis and the heterogeneity among them (because of the cut-off values, control groups, assay kits, and other aspects). Interestingly, the CD44v6 variant is one of the CD44 isoforms that more frequently correlates with tumor progression in other malignancies. For example, poor prognosis, presence of metastasis, or disease progression have been correlated with CD44v6 expression changes (alone or in combination with other isoforms) in gastric carcinoma (178, 179), non-small cell lung carcinoma (180, 181), hepatocarcinoma (182), acute myeloid leukemia (183), non-Hodgkin's lymphoma (184, 185), pancreatic adenocarcinoma (186), primary pancreatic cancer (187) and uterine cervical carcinoma (188). Therefore, the CD44v6 variant seems to play a critical role in disease progression and could provide useful prognostic information in osteosarcoma, among other malignancies.

The combination of CD44 with other surface markers can provide additional information about the malignant potential of osteosarcoma cells. For example, in nude mice intratibial xenograft model performed with Saos-2 osteosarcoma cell line, CD133+/CD44+ cells were potentially more metastatic (174). A multivariate analysis performed on 90 osteosarcomas and 20 osteochondromas, indicated the clinical stage, metastasis status, and the relationship between the expression of CD44V6, CDH11, and β-catenin correlated with improved outcome (172). GAPLINC showed an indirect regulation of CD44 due to both mRNAs are negatively regulated by the same microRNA, the miR211-3p. GAPLINC overexpression in osteosarcoma was shown to correlate with advanced Enneking stage, distant metastasis, and poor outcome (145), providing an additional novel biomarker. The expression of CD44/IGF1R/ABCG2, tumoral markers related to prognosis and drug resistance, have also been analyzed, alone and in combination, in order to obtain information about their contribution to the patient prognosis. Thus, the Insulin Growth Factor 1 receptor (IGFR1) has been shown to be a prognostic factor for metastasis in osteosarcoma (189). The analysis of the expression pattern in 59 osteosarcomas showed that IGF1R expression is highly correlated with ABCG2 expression and with CD44 expression in osteosarcoma patients under 10 years old (175).

6 THERAPEUTIC APPROACHES TARGETING CD44

CD44 can be considered a suitable therapeutic target in many malignancies by blocking the activation of the signalling pathways in which this protein is involved, or by using its overexpression to drive, specifically, the pharmacological treatment. In fact, several strategies targeting CD44 have already been developed which include small molecular inhibitors, peptides, aptamers, blocking antibodies, secretase inhibitors, drug delivery systems, CD44 decoys, and HA oligomers (**Table 2**).

6.1 Inhibition of CD44 Expression

Since CD44 is expressed at high levels in most types of sarcoma, inhibition of CD44 expression could have therapeutic usefulness. In this sense, several compounds have been shown to regulate the expression of CD44, both directly and indirectly (218). Silibinin, a flavonolignan composed of two diastereomers (silibinin A and B), strongly inhibited the activity of the CD44 promoter in the prostate (PC-3M) and pancreatic cancer cell lines (BxPC-3 and PANC-1) (190, 191). Zerumbone, a sesquiterpenoid and cyclic ketone, suppressed EGF-dependent CD44 expression through inhibition of the STAT3 pathway in breast cancer cell lines (SKBR3 and MDA-MB468) (192). Additionally, the inhibition of the STAT3 pathway (through the selective blocking of STAT3 phosphorylation) was obtained with the combination of curcumin and epigallocatechin gallate in a pharmacological treatment, which reduced the CD44+ population of CSCs in MDA-MB-231 and MCF7 breast cancer cell lines (193). Therefore, the use of Sibilin, Zerumbone, or curcumin/epigallocatechin notably reduced the population of CD44+ tumor cells (breast cancer, pancreatic cancer, and prostate cancer), suggesting a novel approach for the treatment of sarcomas.

6.2 Inhibition of γ-Secretases

As described above, CD44-ICD is released upon cleavage of CD44 by γ-secretases and, subsequently, it is translocated to the nucleus where upregulates the expression of specific target genes implied in stemness, migration/invasiveness, or cell proliferation. The cleavage mechanism requires, inexorably, the activity of the presenilin-γ-secretases (aspartyl proteases). Thus, direct inhibition of these enzymes with γ-secretase inhibitors (GSIs) is a particularly interesting approach to block CD44-mediated signalling because these inhibitors can block CD44-ICD release and, consequently, interfere with the gene regulatory functions of CD44-ICD. The γ-secretase complex processes the precursor of amyloid protein (APP) and cleavages the intracellular domain of NOTCH signaling protein (NOTCH-ICD), analogously, to CD44-ICD. Several γ-secretase complex inhibitors (GSIs) have been developed and deployed for the treatment of Alzheimer's with variable success (219) and there

TABLE 2 | Summary of therapeutic approaches targeting CD44.

Pharmacological approach	Agent	Mechanism of action	Stage of development	Refs
Small molecular inhibitors	Silibinin	Inhibits the activity of the CD44 promoter reducing its expression.	Preclinically tested in prostate, pancreatic, and breast cancer cells	(190, 191)
	Zerumbone	Suppresses EGF-dependent CD44 expression through inhibition of the STAT3 pathway.	Preclinically tested in breast cancer cells.	(192)
	Curcumin and epigallocatechin gallate	Reduces CD44 expression through the inhibition of the STAT3 pathway (blocks the STAT3 phosphorylation).	Alternative approach like Zerumbone. Not tested yet.	(193)
GSI (γ-secretase inhibitors)	PF-3084014 (Nirogacestat)	Blocks CD44-ICD releasing and subsequently interfere with CD44-ICD-dependent functions.	Phase II. Clinical benefit in patients with refractory, progressive desmoid tumors who receive long-term treatment (NCT01981551).	(194)
	LY-450139 (Semagacestat)		Phase I. Clinical activity in heavily pretreated patients with breast cancer and leiomyosarcoma (NCT01695005).	(195)
	BMS-906024		Preclinically tested. Decreases cell proliferation in *in vivo* studies using cell line- and patient-derived lung adenocarcinoma xenografts.	(196)
Antibodies conjugated with anti-tumor drugs	RO5429083 (Roche)	Immunoconjugates antibody that binds to the constant region of the extracellular domain, favoring the antitumoral drug uptake.	Phase I. Tested in patients with metastatic and/or locally advanced CD44-expressing malignant solid tumors (NCT01358903).	(197, 198)
	U36 indium-111	Monoclonal antibody labeled with indium-111 that targets CD44 and had been suggested the possible use in the detection of this cancer.	Preclinically characterized in head and neck carcinoma xenografts mice models expressing CD44v6 isoform.	(199)
	Bivatuzumab mertansine	Humanized monoclonal antibody against CD44v6 and a cytotoxic agent (mertansine).	Phase I. Tested in head and neck carcinoma patients with variable therapeutic response and a severe skin toxicity	(200, 201)
Antibodies blocking CD44	H4C4	Decreases the capacity of self-renewal and tumor initiation through STAT3 signaling inhibition and the downregulation of the stem cell self-renewal gene Nanog.	Preclinically tested. Reduces tumor growth, metastasis, and post-radiation tumor recurrence in human pancreatic mice xenografts.	(202)
	IM7	Inhibits HA-CD44 mediated signaling in human umbilical vein endothelial cells.	Preclinically tested. Additionally, decreases cell migration and invasion capacities in breast cancer cell lines.	(203, 204)
	KM201		Preclinically tested in human umbilical vein endothelial cells.	(203)
Peptides and aptamers	PEP-1	Reduces CD44 expression levels in mice models for gastric cancer.	Preclinically tested.	(205)
	PCK3145	Seems to interfere with the tyrosine kinase activity associated with the VEGF signalling axis in endothelial cells inhibiting angiogenesis processes.	Preclinically tested. Demonstrated to reduce bone metastases and prostate tumor growth tumor in rats inoculated with MAT-Ly-Lu-B-2 cell line.	(206–208)
	Apt1 (RNA aptamer)	Used to functionalize the surface of PEGylated liposomes, increasing cellular uptake of CD44 positive cell lines.	Preclinically tested in cell lines: A549 (lung cancer) and MDA-MB-231 (breast cancer).	(209)
	CD44-EpCAM (double-stranded RNA aptamer)	Blocks simultaneously CD44 and EpCAM, reducing tumor progression and promoting apoptosis.	Preclinically tested. *In vitro* and *in vivo* xenograft models of ovarian tumor cells (OVCAR8).	(210)
Ligand chemotherapy delivery systems	Chol-SS-mPEG/HA-L	HA-coated redox responsive liposome, whose cytoplasmic drug release system is triggered by GSH.	Preclinically tested in xenograft models of osteosarcoma. The results showed: a reduction of tumor growth and increased animal survival.	(211)
	HA-LsDOX	Promotes the sulfhydration and ubiquitination of proteins and activates the pro-apoptotic CHOP-mediated signaling.		(212)

(Continued)

TABLE 2 | Continued

Pharmacological approach	Agent	Mechanism of action	Stage of development	Refs
	ALN–HA–SS–L–L/DOX	Equipped with bone- and CD44-dual-targeting and redox cleavage characteristics, its efficacy seems to increase with the coadministration of internalizing RGD.		(213)
	HA-es-ZnPP	Photodynamic therapy based on a hyaluronan conjugated zinc protoporphyrin *via* an ester bond, with a tumor environment-responsive mechanism.	Preclinically tested *in vitro* and in a mouse sarcoma S180 solid tumor model, demonstrating prolonged circulation time, enhanced cell permeability and retention and anticancer effect.	(214)
	ALN-HA-C18/curcumin	Dual-targeting delivery therapy combining the active bone accumulating ability and the curcumin inhibition effect on CD44 expression.	Tested preclinically in MG-63 cells and in *in vivo* model. The results showed a reduction of tumor growth in osteosarcoma mouse model.	(215)
Hyaluronic Acid oligomers	HA-mers	Bind CD44, competing by and displacing the biological HA polymer and can inhibit HA synthesis.	Preclinically tested. Promoted apoptosis and reduced both cell viability, cell proliferation, cell motility, and decreased the retention of endogenous HA in murine (LM-8) and human (MG-63) osteosarcoma cells. Its intratumoral injection in xenograft models suppressed dissemination events in the lung. A similar effect has been observed in other cancers such as melanoma, carcinoma, or glioma.	(94, 216, 217)

has been a repositioning of these molecules as candidate drugs against cancer and immune diseases. Since GSIs are also active inhibiting CD44-ICD cleavage (220), the CD44-ICD downstream signalling could be effectively affected and consequently, CD44-mediated cell migration and invasion mechanisms. Many of these inhibitors have been extensively tested in clinical trials and currently, it is an active development field. For example, the GSI PF-3084014 (Nirogacestat) was well tolerated in patients with advanced cancer and demonstrated promising clinical benefit in patients with refractory, progressive desmoid tumors who receive long-term treatment (NCT01981551) (194). Another of these GSIs, LY450139 (Semagacestat), was also well-tolerated and demonstrated evidence of clinical activity in heavily pretreated patients with breast cancer and leiomyosarcoma (NCT01695005) (195). In preclinical studies, the potent GSI BMS-906024 showed enhanced antitumor activity in combination with paclitaxel versus either drug alone, decreasing cell proliferation and increasing apoptosis in *in vivo* studies using cell line- and patient-derived lung adenocarcinoma xenografts (196). However, this approach has not been tested to date in sarcomas and may represent an attractive treatment strategy.

6.3 Blocking CD44 With Antibodies

Antibodies targeting CD44 are being tested in preclinical and clinical trials for many types of cancer. These antibodies can be conjugated with anti-tumor drugs to target cells overexpressing CD44 to favor the antitumoral drug uptake or act as blockers of CD44-mediated signalling. There have been developed several molecule-conjugated antibodies. The Roche radioimmunoconjugate RO5429083 (RG7356) antibody targets a conformational-dependent epitope of CD44 (in the constant region of the extracellular domain), and it is being tested in clinical trials to treat neoplasms (NCT01358903) and acute myelogenous leukemia (NCT01641250) (197, 198). Another anti-CD44 monoclonal antibody, called U36, labeled with indium-111, was tested in head and neck carcinoma xenografts that expressed CD44v6 isoform. The authors of this study suggested the possible use of this antibody as a cancer detection tool (199). Bivatuzumab mertansine is the combination of a humanized monoclonal antibody against CD44v6 and a cytotoxic agent (mertansine), which has been tested in a phase I trial in head and neck carcinoma (200, 201). However, the therapeutic response in these trials was variable and severe skin toxicity was detected due to the binding of the antibody to the CD44v6 isoform located on the keratinocyte's membrane.

Alternatively, CD44 blocking antibodies have also been developed. H4C4, a monoclonal antibody that recognizes the extracellular domain of CD44 (from residue 69 to residue 90), reduced tumor growth, metastasis, and post-radiation tumor recurrence in human pancreatic mice xenografts (202). This antibody affected both bulk tumor cells and tumor initiating cells, decreasing the capacity of self-renewal and tumor initiation through STAT3 signalling inhibition and the downregulation of the stemness gene Nanog (202). The CD44 blocking monoclonal antibodies IM7 (that recognizes the constant region of the ECD, specifically residues 145-186) and KM201 (that binds to a region that is close to the HA binding domain) abrogate the VEGF secretion mechanism through the inhibition of the HA-CD44 signalling in human umbilical vein endothelial cells (203). Additionally, Uchino et al., demonstrated that the IM7 antibody decreased cell migration and invasion capacities in breast cancer cells (MCF-7-14 cells and its clone CL6, and MDA-MB-231 cells) using *in vitro* conditions (204). Therefore, there is an untested group of anti-CD44 blocking antibodies, which may have therapeutic potential in the context of sarcomas, but further research is needed.

6.4 Blocking CD44 With Peptides and Aptamers

Another therapeutic strategy could be based on the use of peptides and aptamers to block CD44 interactions or reduce CD44 expression. These molecules have a great affinity and specificity to target proteins and thus are excellent tools to inhibit their functions. Several peptides and RNA aptamers directed against CD44 have already been tested in many cancer models (221). The peptide PEP-1 (a short amphipathic peptide that blocks the interaction CD44/HA) reduced the CD44 expression levels in mice models of gastric cancer (205). PCK3145, a synthetic peptide corresponding to amino acids 31-45 of prostate secretory protein 94 (PSP94), was demonstrated to reduce bone metastases and prostate tumor growth tumor in rats injected with MAT-Ly-Lu-B-2 cell line (206). The mechanism of action of this antitumoral peptide is not completely understood, but it seems the peptide interferes with the tyrosine kinase activity associated with the VEGF signalling axis in endothelial cells inhibiting angiogenesis processes (*in vivo* testing with Mat Ly Lu rat prostate cancer cells) (207) and reduces the levels of plasma matrix metalloproteinase MMP-9 (a CD44 ligand). Annabi et al., studied the antitumoral effect of this peptide in the fibrosarcoma cell line HT1080 and showed that it inhibited cell adhesiveness to HA, laminin-1, and type-I collagen. PCK3145 inhibited the secretion of MMP-9 and triggered the shedding of the ectodomain of CD44 from the cell surface preventing the interaction of CD44 with MMP-9 (208). The RNA aptamer (Apt1) was used to functionalize the surface of PEGylated liposomes. This combination, Apt1-Liposome, allowed a better cellular uptake of the conjugated molecule in CD44 positive cell lines A549 (lung cancer) and MDA-MB-231 (breast cancer) (209). Finally, CD44-EpCAM (Epithelial Cell Adhesion Molecule) aptamer is a double-stranded RNA adaptor which acts blocking both, CD44 and EpCAM, simultaneously reducing tumor progression and promoting apoptosis, both *in vitro* and *in vivo* xenograft models of ovarian tumor cells (OVCAR8) (210).

6.5 CD44-Ligand Chemotherapy Delivery Systems

In addition, several strategies exploit the ability of CD44 to interact with a variety of extracellular proteins (25). For example, the interaction of CD44 with HA, its principal ligand, can be used to maximize the uptake of chemotherapy delivery systems on cells overexpressing CD44. Chemotherapeutic agent-encapsulated liposomes, or covalently bound HA-bioconjugates, were selectively taken up by tumor cells after systemic delivery and reduced specific gene expression in several xenograft models (222–224). Several of these innovative tools based on HA-functionalized liposomes have become an excellent CD44-mediated intracellular delivery system for doxorubicin (DOX) or photodynamic anticancer therapy in osteosarcomas: Chol-SS-mPEG/HA-L (211), HA-LsDOX (212), ALN–HA–SS–L–L/DOX (213), and HA-es-ZnPP (214). Chol-SS-mPEG/HA-L is an HA-coated redox responsive liposome, whose cytoplasmic drug release system is triggered by GSH. The HA-LsDOX liposomes mechanism consists in the release of the drug into the endoplasmic reticulum, promoting protein sulfhydration and ubiquitination, and activating CHOP-mediated pro-apoptotic signalling. ALN-HA-SS-L-L/DOX is a liposome with dual bone and CD44 targeting abilities and redox sensitivity whose efficacy appears to be increased by the co-administration of internalizing RGD (Arg-Gly-Asp motif). HA-es-ZnPP, a hyaluronan conjugated zinc protoporphyrin *via* an ester bond with a tumor environment-responsive mechanism, was tested *in vitro* and in a mouse sarcoma S180 solid tumor model. This nanoprobe for photodynamic anticancer approach combined with a xenon light source, demonstrated prolonged circulation time and enhanced cell permeability and retention. Consequently, an improved anticancer therapy effect without apparent side effects.

The micelles with HA functionalization have been used in other drug–gene combinations therapies to co-delivery the antitumor treatments (e.g., siRNA against overexpressed cancerous genes, anticancer drugs-Paclitaxel, doxorubicin, superparamagnetic iron oxide nanoparticles-SPIONs…) (225–228). The synergistic effect of these micelles on cell cytotoxicity was tested in the MDA-MB-231 breast cancer cell (229) and OVCAR8TR ovarian cancer cells (230, 231), both overexpressing CD44. Additionally, a dual-targeting platform for CD44 has already been tested in hepatic tumors (e.g., HA- glycyrrhetinic acid -conjugated polymer to target liver) (232, 233) and breast cancer (e.g., HA-folic acid micelles for cells overexpressing the folic acid receptor) (234). These multiple targeting strategies showed better consistency and increased cellular uptake, thus enhanced cytotoxicity. In the study performed by Xi Y et al. curcumin was used in a dual-targeting delivery therapy combining the active bone accumulating ability with tumor CD44 targeting capacity in alendronate-hyaluronic acid-octadecanoic acid (ALN-HA-C18) micelles (215). The curcumin loaded in ALN-HA-C18 micelles showed increased cytotoxic activity against MG-63 cells and reduced tumor growth in the osteosarcoma mouse model compared to the free drug. Nanoparticles labeled with CD133-EGFR aptamers were determined to inhibit tumor growth in the osteosarcoma mouse model (235). Thereby, novel combinations of dual-targeting such as CD133-CD44 aptamers, both overexpressed in osteosarcoma CSCs, are potentially susceptible to being tested in these malignancies. Overall, these innovative delivery packages showed an increased tissue specificity, enhanced anticancer effect and great potential in clinical developments and delivery systems, supposing a therapeutic alternative superficially explored in sarcomas.

In summary, these studies indicate that treatment with HA-functionalized liposomes or photodynamic therapy reduced tumor growth and increased survival time in xenograft models of osteosarcoma, becoming a promising osteosarcoma-targeted therapy. Beyond its biological properties, HA nanomedicine is limited by the reduced methods for chemical conjugation, the fluctuant cellular uptake caused by the chemical characteristics of HA, and the unavoidable biological degradation when it enters *in vivo* (228). Therefore, the effects of these limitations need to be further studied to ensure minimum adverse responses and maximum clinical efficacy.

6.6 Blocking CD44 With CD44 Ligands

Finally, another way to block the CD44 function is by blocking CD44-HA interactions. The soluble CD44 ectodomain has been

demonstrated to compete with the CD44-HA interaction on malignant cells, inhibiting tumor progression and invasiveness (236). Conversely, another strategy is to use HA-oligomers to block CD44-HA interactions. HA oligomers are small molecule chains composed of a variable number of units (6-12 mers). These molecules have been shown to suppress signalling pathways involved in drug resistance against different therapeutic agents (237, 238). Several studies have shown that HA disaccharides bind CD44, competing by and displacing the biological HA polymer (239, 240) and can inhibit HA synthesis (241). Despite its therapeutic potential there are few studies addressing the therapeutic possibilities of these molecules in sarcomas. Hosono et al., studied the effect of hyaluronan oligosaccharides on tumor growth in murine (LM-8) and human (MG-63) osteosarcoma cells. Hyaluronan octamers promoted apoptosis and reduced both cell viability, cell proliferation and cell motility, and decreased the retention of endogenous HA. The intratumoral injection of these molecules in xenograft models produced a reduction of HA accumulation in the tumor, suppressing the dissemination of tumor cells to the lung (216). A similar effect has been observed in other cancers such as melanoma, carcinoma, or glioma (94, 217). HA oligomers therapies provide a viable alternative for blocking the CD44-HA interactions in sarcomas which has been only superficially explored, so that clinical trials should be performed to confirm this antitumoral approach.

7 CONCLUSIONS

CD44 has a key role, along with ECM components, in sarcoma tumor development, metastasis, and drug resistance. Understanding CD44 signalling is crucial to comprise the multifactorial role of this protein in several processes, such as activation of different pathways, upregulation of several genes, or modification of cytoskeletal structures that promote EMT mechanisms, among others.

MSCs are thought to give rise to sarcomas. As consequence, several molecular mechanisms, transcription factors, metabolic pathways, and cell markers are shared among MSCs, CSCs and sarcomas. CD44, in this context, provides the elements to maintain the stemness and to take advantage of the tumoral microenvironment in hypoxia conditions. Studies focused on MSCs, and sarcomas have shown CD44 to be highly expressed in these tissues compared to mature cells. Thus, it has been proposed that during cell differentiation, expression of CD44 could be downregulated, and conversely, high levels of CD44 are necessary to maintain the cells in a stemness state.

Further research involving the sarcoma functional mechanisms could be really enriching in the characterization context of sarcoma, as well as, in the therapeutic approaches targeting CD44. Some of the innovative treatment tools such as peptides, aptamers, HA oligomers, pharmacological substances, and chemotherapy delivery systems, among others, have been developed from the discovery and well-understanding of the CD44 structure, the signalling pathways and the interactions involved.

The data from the characterization of osteosarcomas have revealed that CD44 (concretely CD44v6 isoform) is a potential and promising marker for prognosis and diagnosis. There is a low number of detailed studies deciphering the prognostic/diagnostic value of CD44 in sarcomas (excluding osteosarcoma which is one of the most studied and common sarcomas). In addition, sarcoma-specific studies involving a greater number of patients are necessary to confirm the influence of CD44 variant expression on the patients' prognosis (regardless of the utility of CD44v6 as a prognostic marker in osteosarcoma). The complexity and distinct molecular origin of the different sarcoma subgroups have made impossible to apply a unified characterization or prognosis criterion, and therefore they should be studied separately. In addition, the reduced number of studies focused on CD44, and the low number of patients involved in the different sarcoma subgroups have produced inconclusive results. As consequence, the combination of different characterization markers will be more precise and will provide relevant information to determine patients' outcomes, neither than the use of CD44 individually.

To conclude, more research about the contribution of CD44 in sarcomas could contribute to understand the pathogenesis of these rare cancers, and evolve towards novel therapies and future clinical trials.

AUTHOR CONTRIBUTIONS

Writing original draft preparation, EF-T; writing - review and editing, EF-T, RM-FM, and JA; supervision, JA; funding acquisition, JA. All authors have read and agreed to the published version of the manuscript.

FUNDING

This review was funded by the Instituto de Salud Carlos III, grant numbers PI20CIII/00020, DTS18CIII/00005, Asociacion Pablo Ugarte, grant numbers TRPV205/18; Asociación Candela Riera, Asociación Todos Somos Iván & Fundación Sonrisa de Alex, grant numbers TVP333-19, TVP-1324/15; ASION, grant number TVP141/17. R.M.M-FdM is supported for a grant of the Spanish Center for Biomedical Network Research on Rare Diseases (CIBERER).

REFERENCES

1. Williams RF, Fernandez-Pineda I, Gosain A. Pediatric Sarcomas. *Surg Clinics North America. W.B. Saunders;* (2016) 96:1107–25. doi: 10.1016/j.suc.2016.05.012
2. Stiller CA, Trama A, Serraino D, Rossi S, Navarro C, Chirlaque MD, et al. Descriptive Epidemiology of Sarcomas in Europe: Report From the RARECARE Project. *Eur J Cancer* (2013) 49(3):684–95. doi: 10.1016/j.ejca.2012.09.011
3. Dufresne A, Brahmi M, Karanian M, Blay JY. Using Biology to Guide the Treatment of Sarcomas and Aggressive Connective-Tissue Tumours. *Nat Rev Clin Oncol* (2018) 15:443–58. doi: 10.1038/s41571-018-0012-4
4. Lawrence W, Donegan WL, Natarajan N, Mettlin C, Beart R, Winchester D. Adult Soft Tissue Sarcomas: A Pattern of Care Survey of the American

College of Surgeons. *Ann Surg* (1987) 205(4):349–59. doi: 10.1097/00000658-198704000-00003
5. Christie-Large M, James SLJ, Tiessen L, Davies AM, Grimer RJ. Imaging Strategy for Detecting Lung Metastases at Presentation in Patients With Soft Tissue Sarcomas. *Eur J Cancer* (2008) 44(13):1841–5. doi: 10.1016/j.ejca.2008.06.004
6. Vezeridis MP, Moore R, Karakousis CP. Metastatic Patterns in Soft-Tissue Sarcomas. *Arch Surg* (1983) 118(8):915–8. doi: 10.1001/archsurg.1983.01390080023007
7. Potter DA, Glenn J, Kinsella T, Glatstein E, Lack EE, Restrepo C, et al. Patterns of Recurrence in Patients With High-Grade Soft-Tissue Sarcomas. *J Clin Oncol* (2016) 3(3):353–66. doi: 10.1200/JCO.1985.3.3.353
8. Fletcher CDM, Bridge JA, Hogendoorn PCW, Mertens F. *WHO Classification of Tumours of Soft Tissue and Bone*, *4th ed*, Vol. 5. World Health Organization, 2013.
9. Hyman DM, Puzanov I, Subbiah V, Faris JE, Chau I, Blay J-Y, et al. Vemurafenib in Multiple Nonmelanoma Cancers With BRAF V600 Mutations. *New Engl J Med* (2015) 373(8):726–36. doi: 10.1056/NEJMoa1502309
10. Simon MP, Pedeutour F, Sirvent N, Grosgeorge J, Minoletti F, Coindre JM, et al. Deregulation of the Platelet-Derived Growth Factor B-Chain Gene *via* Fusion With Collagen Gene COL1A1 in Dermatofibrosarcoma Protuberans and Giant-Cell Fibroblastoma. *Nat Genet* (1997) 15(1):95–8. doi: 10.1038/ng0197-95
11. Hyman DM, Laetsch TW, Kummar S, DuBois SG, Farago AF, Pappo AS, et al. The Efficacy of Larotrectinib (LOXO-101), a Selective Tropomyosin Receptor Kinase (TRK) Inhibitor, in Adult and Pediatric TRK Fusion Cancers. *J Clin Oncol* (2017) 35(15_suppl):LBA2501–LBA2501. doi: 10.1200/JCO.2017.35.18_suppl.LBA2501
12. Mariño-Enríquez A, Wang WL, Roy A, Lopez-Terrada D, Lazar AJF, Fletcher CDM, et al. Epithelioid Inflammatory Myofibroblastic Sarcoma: An Aggressive Intra-Abdominal Variant of Inflammatory Myofibroblastic Tumor With Nuclear Membrane or Perinuclear Alk. *Am J Surg Pathol* (2011) 35(1):135–44. doi: 10.1097/PAS.0b013e318200cfd5
13. Delattre O, Zucman J, Melot T, Garau XS, Zucker J-M, Lenoir GM, et al. The Ewing Family of Tumors – A Subgroup of Small-Round-Cell Tumors Defined by Specific Chimeric Transcripts. *New Engl J Med* (1994) 331(5):294–9. doi: 10.1056/NEJM199408043310503
14. Prieur A, Tirode F, Cohen P, Delattre O. EWS/FLI-1 Silencing and Gene Profiling of Ewing Cells Reveal Downstream Oncogenic Pathways and a Crucial Role for Repression of Insulin-Like Growth Factor Binding Protein 3. *Mol Cell Biol* (2004) 24(16):7275–83. doi: 10.1128/MCB.24.16.7275-7283.2004
15. Kawaguchi KI, Oda Y, Saito T, Takahira T, Yamamoto H, Tamiya S, et al. Genetic and Epigenetic Alterations of the PTEN Gene in Soft Tissue Sarcomas. *Hum Pathol* (2005) 36(4):357–63. doi: 10.1016/j.humpath.2005.01.017
16. Kenerson H, Folpe AL, Takayama TK, Yeung RS. Activation of the mTOR Pathway in Sporadic Angiomyolipomas and Other Perivascular Epithelioid Cell Neoplasms. *Hum Pathol* (2007) 38(9):1361–71. doi: 10.1016/j.humpath.2007.01.028
17. Gibault L, Ferreira C, Pérot G, Audebourg A, Chibon F, Bonnin S, et al. From PTEN Loss of Expression to RICTOR Role in Smooth Muscle Differentiation: Complex Involvement of the mTOR Pathway in Leiomyosarcomas and Pleomorphic Sarcomas. *Modern Pathol* (2012) 25(2):197–211. doi: 10.1038/modpathol.2011.163
18. Coindre JM, Pédeutour F, Aurias A. Well-Differentiated and Dedifferentiated Liposarcomas. *Virchows Archiv. Springer Verlag;* (2010) 456:167–79. doi: 10.1007/s00428-009-0815-x
19. Huang L, Xu J, Wood DJ, Zheng MH. Gene Expression of Osteoprotegerin Ligand, Osteoprotegerin, and Receptor Activator of NF-κb in Giant Cell Tumor of Bone: Possible Involvement in Tumor Cell-Induced Osteoclast-Like Cell Formation. *Am J Pathol* (2000) 156(3):761–7. doi: 10.1016/S0002-9440(10)64942-5
20. Kadoch C, Copeland RA, Keilhack H. PRC2 and SWI/SNF Chromatin Remodeling Complexes in Health and Disease. *Vol. 55 Biochem Am Chem Society;* (2016) :1600–14. doi: 10.1021/acs.biochem.5b01191
21. Hanahan D, Weinberg RA. Hallmarks of Cancer: The Next Generation. *Cell Cell Press;* (2011) 144:646–74. doi: 10.1016/j.cell.2011.02.013
22. Avnet S, Cortini M. Role of Pericellular Matrix in the Regulation of Cancer Stemness. *Stem Cell Rev Rep* (2016) 12:464–75. doi: 10.1007/s12015-016-9660-x
23. Winkler J, Abisoye-Ogunniyan A, Metcalf KJ, Werb Z. Concepts of Extracellular Matrix Remodelling in Tumour Progression and Metastasis. *Nat Commun Nat Rese* (2020) 11:1–19. doi: 10.1038/s41467-020-18794-x
24. González-González L, Alonso J. Periostin: A Matricellular Protein With Multiple Functions in Cancer Development and Progression. *Front Oncol* (2018) 8:225. doi: 10.3389/fonc.2018.00225
25. Chen C, Zhao S, Karnad A, Freeman JW. The Biology and Role of CD44 in Cancer Progression: Therapeutic Implications. *J Hematol Oncol* (2018) 11:1–23. doi: 10.1186/s13045-018-0605-5
26. Senbanjo LT, Chellaiah MA. CD44: A Multifunctional Cell Surface Adhesion Receptor Is a Regulator of Progression and Metastasis of Cancer Cells. *Front Cell Dev Biol* (2017) 5(MAR):18. doi: 10.3389/fcell.2017.00018
27. Xu H, Tian Y, Yuan X, Wu H, Liu Q, Pestell RG, et al. The Role of CD44 in Epithelial–Mesenchymal Transition and Cancer Development. *OncoTargets Ther* (2015) 8:3783–92. doi: 10.2147/OTT.S95470
28. Xu H, Niu M, Yuan X, Wu K, Liu A. CD44 as a Tumor Biomarker and Therapeutic Target. *Exp Hematol Oncol* (2020) 9:1–14. doi: 10.1186/s40164-020-00192-0
29. Orian-Rousseau V, Sleeman J. CD44 is a Multidomain Signaling Platform That Integrates Extracellular Matrix Cues With Growth Factor and Cytokine Signals. *In: Adv Cancer Res* (2014), 231–54. doi: 10.1016/B978-0-12-800092-2.00009-5
30. Idzerda RL, Carter WG, Nottenburg C, Wayner EA, Gallatin WM, John TS. Isolation and DNA Sequence of a cDNA Clone Encoding a Lymphocyte Adhesion Receptor for High Endothelium. *Proc Natl Acad Sci U S A.* (1989) 86(12):4659–63. doi: 10.1073/pnas.86.12.4659
31. Faassen AE, Schrager JA, Klein DJ, Oegema TR, Couchman JR, McCarthy JB. A Cell Surface Chondroitin Sulfate Proteoglycan, Immunologically Related to CD44, is Involved in Type I Collagen-Mediated Melanoma Cell Motility and Invasion. *J Cell Biol* (1992) 116(2):521–31. doi: 10.1083/jcb.116.2.521
32. Weber GF, Ashkar S, Glimcher MJ, Cantor H. Receptor-Ligand Interaction Between CD44 and Osteopontin (Eta-1). *Science* (1996) 271(5248):509–12. doi: 10.1126/science.271.5248.509
33. Toyama-Sorimachi N, Sorimachi H, Tobita Y, Kitamura F, Yagita H, Suzuki K, et al. A Novel Ligand for CD44 is Serglycin, a Hematopoietic Cell Lineage-Specific Proteoglycan. *Possible involvement lymphoid Cell adherence activation J Biol Chem* (1995) 270(13):7437–44. doi: 10.1074/jbc.270.13.7437
34. Knutson JR, Iida J, Fields GB, McCarthy JB. CD44/chondroitin Sulfate Proteoglycan and α2β1 Integrin Mediate Human Melanoma Cell Migration on Type IV Collagen and Invasion of Basement Membranes. *Mol Biol Cell* (1996) 7(3):383–96. doi: 10.1091/mbc.7.3.383
35. Liu M, Tolg C, Turley E. Dissecting the Dual Nature of Hyaluronan in the Tumor Microenvironment. *Front Immunol Front Media S.A.;* (2019) 10:947. doi: 10.3389/fimmu.2019.00947
36. Misra S, Heldin P, Hascall VC, Karamanos NK, Skandalis SS, Markwald RR, et al. Hyaluronan-CD44 Interactions as Potential Targets for Cancer Therapy. *FEBS J* (2011) 278:1429–43. doi: 10.1111/j.1742-4658.2011.08071.x
37. Ponta H, Sherman L, Herrlich PA. CD44: From Adhesion Molecules to Signalling Regulators. *Nat Rev Mol Cell Biol* (2003) 4, 33–45. doi: 10.1038/nrm1004
38. Weigel PH. Hyaluronan Synthase: The Mechanism of Initiation at the Reducing End and a Pendulum Model for Polysaccharide Translocation to the Cell Exterior. *Int J Cell Biol* (2015) 2015:15. doi: 10.1155/2015/367579
39. Takeda M, Ogino S, Umemoto R, Sakakura M, Kajiwara M, Sugahara KN, et al. Ligand-Induced Structural Changes of the CD44 Hyaluronan-Binding Domain Revealed by NMR. *J Biol Chem* (2006) 281(52):40089–95. doi: 10.1074/jbc.M608425200
40. Enegd B, King JAJ, Stylli S, Paradiso L, Kaye AH, Novak U, et al. Overexpression of Hyaluronan Synthase-2 Reduces the Tumorigenic Potential of Glioma Cells Lacking Hyaluronidase Activity. *Neurosurgery* (2002) 50(6):1311–8. doi: 10.1097/00006123-200206000-00023

41. Schwertfeger KL, Cowman MK, Telmer PG, Turley EA, McCarthy JB. Hyaluronan, Inflammation, and Breast Cancer Progression. *Front Immunol Front Media S.A.* (2015) 6. doi: 10.3389/fimmu.2015.00236
42. Bourguignon LYW, Spevak CC, Wong G, Xia W, Gilad E. Hyaluronan-CD44 Interaction With Protein Kinase Cϵ Promotes Oncogenic Signaling by the Stem Cell Marker Nanog and the Production of microRNA-21, Leading to Down-Regulation of the Tumor Suppressor Protein PDCD4, Anti-Apoptosis, and Chemotherapy Resistance in Breast Tumor Cells. *J Biol Chem* (2009) 284(39):26533–46. doi: 10.1074/jbc.M109.027466
43. Lv L, Liu HG, Dong SY, Yang F, Wang QX, Guo GL, et al. Upregulation of CD44v6 Contributes to Acquired Chemoresistance *via* the Modulation of Autophagy in Colon Cancer SW480 Cells. *Tumor Biol* (2016) 37(7):8811–24. doi: 10.1007/s13277-015-4755-6
44. Ju SY, Chiou SH, Su Y. Maintenance of the Stemness in CD44+ HCT-15 and HCT-116 Human Colon Cancer Cells Requires miR-203 Suppression. *Stem Cell Res* (2014) 12(1):86–100. doi: 10.1016/j.scr.2013.09.011
45. Suzuki M, Kobayashi H, Kanayama N, Nishida T, Takigawa M, Terao T. CD44 Stimulation by Fragmented Hyaluronic Acid Induces Upregulation and Tyrosine Phosphorylation of C-Met Receptor Protein in Human Chondrosarcoma Cells. *Biochim Biophys Acta - Mol Cell Res* (2002) 1591 (1–3):37–44. doi: 10.1016/S0167-4889(02)00246-X
46. Bai Y, Liu YJ, Wang H, Xu Y, Stamenkovic I, Yu Q. Inhibition of the Hyaluronan-CD44 Interaction by Merlin Contributes to the Tumor-Suppressor Activity of Merlin. *Oncogene* (2007) 26(6):836–50. doi: 10.1038/sj.onc.1209849
47. Marroquin CE, Downey L, Guo H, Kuo PC. Osteopontin Increases CD44 Expression and Cell Adhesion in RAW 264.7 Murine Leukemia Cells. *Immunol Lett* (2004) 95(1):109–12.
48. de Vita A, Vanni S, Miserocchi G, Fausti V, Pieri F, Spadazzi C, et al. A Rationale for the Activity of Bone Target Therapy and Tyrosine Kinase Inhibitor Combination in Giant Cell Tumor of Bone and Desmoplastic Fibroma: Translational Evidences. *Biomedicines* (2022) 10(2):372. doi: 10.3390/biomedicines10020372
49. Lin YH, Yang-Yen HF. The Osteopontin-CD44 Survival Signal Involves Activation of the Phosphatidylinositol 3-Kinase/Akt Signaling Pathway. *J Biol Chem* (2001) 276(49):46024–30. doi: 10.1074/jbc.M105132200
50. Sharp JA, Sung V, Slavin J, Thompson EW, Henderson MA. Tumor Cells are the Source of Osteopontin and Bone Sialoprotein Expression in Human Breast Cancer. *Lab Investigation; J Tech Methods Pathol* (1999) 79(7):869–77.
51. Pietras A, Katz AM, Ekström EJ, Wee B, Halliday JJ, Pitter KL, et al. Osteopontin-CD44 Signaling in the Glioma Perivascular Niche Enhances Cancer Stem Cell Phenotypes and Promotes Aggressive Tumor Growth. *Cell Stem Cell* (2014) 14(3):357–69. doi: 10.1016/j.stem.2014.01.005
52. Kolset SO, Tveit H. Serglycin - Structure and Biology. *Cell Mol Life Sci Cell Mol Life Sci;* (2008) 65:1073–85. doi: 10.1007/s00018-007-7455-6
53. Li XJ, Qian CN. Serglycin in Human Cancers. *Chin J Cancer* (2011) 30 (9):585. doi: 10.5732/cjc.011.10314
54. Guo JY, Hsu HS, Tyan SW, Li FY, Shew JY, Lee WH, et al. Serglycin in Tumor Microenvironment Promotes non-Small Cell Lung Cancer Aggressiveness in a CD44-Dependent Manner. *Oncogene* (2017) 36:17. doi: 10.1038/onc.2016.404
55. Chu Q, Huang H, Huang T, Cao L, Peng L, Shi S, et al. Extracellular Serglycin Upregulates the CD44 Receptor in an Autocrine Manner to Maintain Self-Renewal in Nasopharyngeal Carcinoma Cells by Reciprocally Activating the MAPK/β-Catenin Axis. *Cell Death Dis* (2016) 7(11):e2456–e2456. doi: 10.1038/cddis.2016.287
56. Merrilees MJ, Zuo N, Evanko SP, Day AJ, Wight TN. G1 Domain of Versican Regulates Hyaluronan Organization and the Phenotype of Cultured Human Dermal Fibroblasts. *J Histochem Cytochem* (2016) 64 (6):353. doi: 10.1369/0022155416643913
57. LeBaron RG, Zimmermann DR, Ruoslahti E. Hyaluronate Binding Properties of Versican. *J Biol Chem* (1992) 267(14):10003–10. doi: 10.1016/S0021-9258(19)50191-0
58. Mauri P, Scarpa A, Nascimbeni AC, Benazzi L, Parmagnani E, Mafficini A, et al. Identification of Proteins Released by Pancreatic Cancer Cells by Multidimensional Protein Identification Technology: A Strategy for Identification of Novel Cancer Markers. *FASEB J* (2005) 19(9):1125–7. doi: 10.1096/fj.04-3000fje
59. Ween MP, Oehler MK, Ricciardelli C. Role of Versican, Hyaluronan and CD44 in Ovarian Cancer Metastasis. *Int J Mol Sci MDPI AG;* (2011) 12:1009–29. doi: 10.3390/ijms12021009
60. Fujimoto T, Kawashima H, Tanaka T, Hirose M, Toyama-Sorimachi N, Matsuzawa Y, et al. CD44 Binds a Chondroitin Sulfate Proteoglycan, Aggrecan. *Int Immunol* (2001) 13(3):359–66. doi: 10.1093/intimm/13.3.359
61. Mcfarlane S, Mcfarlane C, Montgomery N, Hill A, Waugh DJJ. CD44-Mediated Activation of α5β1-Integrin, Cortactin and Paxillin Signaling Underpins Adhesion of Basal-Like Breast Cancer Cells to Endothelium and Fibronectin-Enriched Matrices. *Oncotarget* (2015) 6(34):36762. doi: 10.18632/oncotarget.5461
62. Montgomery N, Hill A, McFarlane S, Neisen J, O'Grady A, Conlon S, et al. CD44 Enhances Invasion of Basal-Like Breast Cancer Cells by Upregulating Serine Protease and Collagen-Degrading Enzymatic Expression and Activity. *Breast Cancer Res* (2012) 14:3. doi: 10.1186/bcr3199
63. Ishii S, Ford R, Thomas P, Nachman A, Steele G, Jessup JM. CD44 Participates in the Adhesion of Human Colorectal Carcinoma Cells to Laminin and Type IV Collagen. *Surg Oncol* (1993) 2(4):255–64. doi: 10.1016/0960-7404(93)90015-Q
64. Verma RP, Hansch C. Matrix Metalloproteinases (MMPs): Chemical-Biological Functions and (Q)SARs. *Bioorganic Medicinal Chem Bioorg Med Chem;* (2007) 15:2223–68. doi: 10.1016/j.bmc.2007.01.011
65. Orgaz JL, Pandya P, Dalmeida R, Karagiannis P, Sanchez-Laorden B, Viros A, et al. Diverse Matrix Metalloproteinase Functions Regulate Cancer Amoeboid Migration. *Nat Commun* (2014) 5(1):1–13. doi: 10.1038/ncomms5255
66. Yu Q, Stamenkovic I. Localization of Matrix Metalloproteinase 9 to the Cell Surface Provides a Mechanism for CD44-Mediated Tumor Invasion. *Genes Dev* (1999) 13(1):35–48. doi: 10.1101/gad.13.1.35
67. Mori H, Tomari T, Koshikawa N, Kajita M, Itoh Y, Sato H, et al. CD44 Directs Membrane-Type 1 Matrix Metalloproteinase to Lamellipodia by Associating With its Hemopexin-Like Domain. *EMBO J* (2002) 21(15):3949. doi: 10.1093/emboj/cdf411
68. Nagano O, Saya H. Mechanism and Biological Significance of CD44 Cleavage. *Cancer Sci* (2004) 95(12):930–5. doi: 10.1111/j.1349-7006.2004.tb03179.x
69. Okamoto I, Kawano Y, Murakami D, Sasayama T, Araki N, Miki T, et al. Proteolytic Release of CD44 Intracellular Domain and its Role in the CD44 Signaling Pathway. *J Cell Biol* (2001) 155(5):755–62. doi: 10.1083/jcb.200108159
70. Yan Y, Zuo X, Wei D. Concise Review: Emerging Role of CD44 in Cancer Stem Cells: A Promising Biomarker and Therapeutic Target. *Stem Cells Trans Med* (2015) 4(9):1033–43. doi: 10.5966/sctm.2015-0048
71. Tsukita S, Oishi K, Sato N, Sagara J, Kawai A, Tsukita S. ERM Family Members as Molecular Linkers Between the Cell Surface Glycoprotein CD44 and Actin-Based Cytoskeletons. *J Cell Biol* (1994) 126(2):391–401. doi: 10.1083/jcb.126.2.391
72. Janiszewska M, de Vito C, Le Bitoux MA, Fusco C, Stamenkovic I. Transportin Regulates Nuclear Import of CD44. *J Biol Chem* (2010) 285 (40):30548. doi: 10.1074/jbc.M109.075838
73. Su YJ, Lai HM, Chang YW, Chen GY, Lee JL. Direct Reprogramming of Stem Cell Properties in Colon Cancer Cells by CD44. *EMBO J* (2011) 30 (15):3186–99. doi: 10.1038/emboj.2011.211
74. Bourguignon LYW, Earle C, Wong G, Spevak CC, Krueger K. Stem Cell Marker (Nanog) and Stat-3 Signaling Promote MicroRNA-21 Expression and Chemoresistance in Hyaluronan/CD44-Activated Head and Neck Squamous Cell Carcinoma Cells. *Oncogene* (2012) 31(2):149–60. doi: 10.1038/onc.2011.222
75. Senbanjo LT, Aljohani H, Majumdar S, Chellaiah MA. Characterization of CD44 Intracellular Domain Interaction With RUNX2 in PC3 Human Prostate Cancer Cells. *Cell Commun Signaling* (2019) 17(1):1–13. doi: 10.1186/s12964-019-0395-6
76. Senbanjo LT, AlJohani H, AlQranei M, Majumdar S, Ma T, Chellaiah MA. Identification of Sequence-Specific Interactions of the CD44-Intracellular Domain With RUNX2 in the Transcription of Matrix Metalloprotease-9 in Human Prostate Cancer Cells. *Cancer Drug Resist* (2020) 3(3):586. doi: 10.20517/cdr.2020.21
77. Cho Y, Lee HW, Kang HG, Kim HY, Kim SJ, Chun KH. Cleaved CD44 Intracellular Domain Supports Activation of Stemness Factors and Promotes

Tumorigenesis of Breast Cancer. *Oncotarget* (2015) 6(11):8709–21. doi: 10.18632/oncotarget.3325
78. Medrano-González PA, Rivera-Ramírez O, Montaño LF, Rendón-Huerta EP. Proteolytic Processing of CD44 and Its Implications in Cancer. *Stem Cells Int* (2021) 2021. doi: 10.1155/2021/6667735
79. Okamoto I, Kawano Y, Tsuiki H, Sasaki JI, Nakao M, Matsumoto M, et al. CD44 Cleavage Induced by a Membrane-Associated Metalloprotease Plays a Critical Role in Tumor Cell Migration. *Oncogene* (1999) 18(7):1435–46. doi: 10.1038/sj.onc.1202447
80. Kajita M, Itoh Y, Chiba T, Mori H, Okada A, Kinoh H, et al. Membrane-Type 1 Matrix Metalloproteinase Cleaves CD44 and Promotes Cell Migration. *J Cell Biol* (2001) 153(5):893–904. doi: 10.1083/jcb.153.5.893
81. Rao JS. Molecular Mechanisms of Glioma Invasiveness: The Role of Proteases. *Nat Rev Cancer* (2003) 3:7. doi: 10.1038/nrc1121
82. Takahashi K, Eto H, Tanabe KK. Involvement of CD44 in Matrix Metalloproteinase-2 Regulation in Human Melanoma Cells. *Int J Cancer*. (1999) 80:387–95. doi: 10.1002/(SICI)1097-0215(19990129)80:3<387::AID-IJC9>3.0.CO;2-T
83. Lammich S, Okochi M, Takeda M, Kaether C, Capell A, Zimmer AK, et al. Presenilin-Dependent Intramembrane Proteolysis of CD44 Leads to the Liberation of Its Intracellular Domain and the Secretion of an Abeta-LikePeptide. *J Biol Chem* (2002) 277(47):44754–9. doi: 10.1074/jbc.M206872200
84. Pelletier L, Guillaumot P, Frêche B, Luquain C, Christiansen D, Brugière S, et al. γ-Secretase-Dependent Proteolysis of CD44 Promotes Neoplastic Transformation of Rat Fibroblastic Cells. *Cancer Res* (2006) 66(7):3681–7. doi: 10.1158/0008-5472.CAN-05-3870
85. Sugahara KN, Murai T, Nishinakamura H, Kawashima H, Saya H, Miyasaka M. Hyaluronan Oligosaccharides Induce CD44 Cleavage and Promote Cell Migration in CD44-Expressing Tumor Cells. *J Biol Chem* (2003) 278 (34):32259–65. doi: 10.1074/jbc.M300347200
86. Heo JS, Choi Y, Kim HS, Kim HO. Comparison of Molecular Profiles of Human Mesenchymal Stem Cells Derived From Bone Marrow, Umbilical Cord Blood, Placenta and Adipose Tissue. *Int J Mol Med* (2016) 37(1):115–25. doi: 10.3892/ijmm.2015.2413
87. Mafi P, Hindocha S, Mafi R, Griffin M, Khan WS. Adult Mesenchymal Ste Cells and Cell Surface Characterization: A Systematic Review of the Literature. *Open Orthop J* (2011) 5(Suppl 2):253–60. doi: 10.2174/1874325001105010253
88. Lv FJ, Tuan RS, Cheung KMC, Leung VYL. Concise Review: The Surface Markers and Identity of Human Mesenchymal Stem Cells. *Stem Cells* (2014) 32(6):1408–19. doi: 10.1002/stem.1681
89. Genadry KC, Pietrobono S, Rota R, Linardic CM. Soft Tissue Sarcoma Cancer Stem Cells: An Overview. *Front Oncol Front Media S.A.;* (2018) 8:475. doi: 10.1007/BF00307793
90. Gibbs CP, Kukekov VG, Reith JD, Tchigrinova O, Suslov ON, Scott EW, et al. Stem-Like Cells in Bone Sarcomas: Implications for Tumorigenesis. *Neoplasia* (2005) 7(11):967–76. doi: 10.1593/neo.05394
91. di Fiore R, Santulli A, Drago Ferrante R, Giuliano M, de Blasio A, Messina C, et al. Identification and Expansion of Human Osteosarcoma-Cancer-Stem Cells by Long-Term 3-Aminobenzamide Treatment. *J Cell Physiol* (2009) 219(2):301–13. doi: 10.1002/jcp.21667
92. Martínez-Delgado P, Lacerenza S, Obrador-Hevia A, Lopez-Alvarez M, Mondaza-Hernandez JL, Blanco-Alcaina E, et al. Cancer Stem Cells in Soft-Tissue Sarcomas. *Cells* (2020) 9(6):1449. doi: 10.3390/cells9061449
93. Geng S, Guo Y, Wang Q, Li L, Wang J. Cancer Stem-Like Cells Enriched With CD29 and CD44 Markers Exhibit Molecular Characteristics With Epithelial-Mesenchymal Transition in Squamous Cell Carcinoma. *Arch Dermatol Res* (2013) 305(1):35–47. doi: 10.1007/s00403-012-1260-2
94. Thapa R, Wilson GD. The Importance of CD44 as a Stem Cell Biomarker and Therapeutic Target in Cancer. *Stem Cells Int* (2016) 2016:15. doi: 10.1155/2016/2087204
95. Morath I, Hartmann TN, Orian-Rousseau V. CD44: More Than a Mere Stem Cell Marker. *Int J Biochem Cell Biol* (2016) 81(Pt A):166–73. doi: 10.1016/j.biocel.2016.09.009
96. Skandalis SS, Karalis TT, Chatzopoulos A, Karamanos NK. Hyaluronan-CD44 Axis Orchestrates Cancer Stem Cell Functions. *Cell Signalling*. (2019) 63:109377. doi: 10.1016/j.cellsig.2019.109377
97. Williams K, Motiani K, Giridhar PV, Kasper S. CD44 Integrates Signaling in Normal Stem Cell, Cancer Stem Cell and (Pre)Metastatic Niches. *Exp Biol Med Exp Biol Med (Maywood);* (2013) 238:324–38. doi: 10.1177/1535370213480714
98. Skubitz KM, Wilson JD, Cheng EY, Lindgren BR, Boylan KLM, Skubitz APN. Effect of Chemotherapy on Cancer Stem Cells and Tumor-Associated Macrophages in a Prospective Study of Preoperative Chemotherapy in Soft Tissue Sarcoma. *J Transl Med* (2019) 17(1):1–13. doi: 10.1186/s12967-019-1883-6
99. Nakamura H, Kenmotsu SI, Sakai H, Ozawa H. Localization of CD44, the Hyaluronate Receptor, on the Plasma Membrane of Osteocytes and Osteoclasts in Rat Tibiae. *Cell Tissue Res*(1995) 280(2):225–33. doi: 10.1007/BF00307793
100. Li Y, Zhong G, Sun W, Zhao C, Zhang P, Song J, et al. CD44 Deficiency Inhibits Unloading-Induced Cortical Bone Loss Through Downregulation of Osteoclast Activity. *Sci Rep* (2015) 5:1. doi: 10.1038/srep16124
101. Albrecht C, Schlegel W, Eckl P, Jagersberger T, Sadeghi K, Berger A, et al. Alterations in CD44 Isoforms and HAS Expression in Human Articular Chondrocytes During the De- and Re-Differentiation Processes. *Int J Mol Med* (2009) 23(2):253–9. doi:10.3892/ijmm_00000124
102. Xu Y, Wang YQ, Wang AT, Yu CY, Luo Y, Liu RM, et al. Effect of CD44 on Differentiation of Human Amniotic Mesenchymal Stem Cells Into Chondrocytes *via* Smad and ERK Signaling Pathways. *Mol Med Rep* (2020) 21(6):2357. doi: 10.3892/mmr.2020.11044
103. Moraes D. What the Relationship Between CD90 E CD44 in Mesenchymal Stem Cells? *Cytotherapy* (2018) 20(5):S47. doi: 10.1016/j.jcyt.2018.02.124
104. Hughes DE, Salter DM, Simpson R. CD44 Expression in Human Bone: A Novel Marker of Osteocytic Differentiation. *J Bone Mineral Res* (1994) 9 (1):39–44. doi: 10.1002/jbmr.5650090106
105. Wu SC, Chen CH, Chang JK, Fu YC, Wang CK, Eswaramoorthy R, et al. Hyaluronan Initiates Chondrogenesis Mainly *via* CD44 in Human Adipose-Derived Stem Cells. *J Appl Physiol* (2013) 114(11):1610–8. doi: 10.1152/japplphysiol.01132.2012
106. Huynh NP, Zhang B, Guilak F. High-Depth Transcriptomic Profiling Reveals the Temporal Gene Signature of Human Mesenchymal Stem Cells During Chondrogenesis. *FASEB J* (2019) 33(1):358–72. doi: 10.1096/fj.201800534R
107. Moraes DA, Sibov TT, Pavon LF, Alvim PQ, Bonadio RS, da Silva JR, et al. A Reduction in CD90 (THY-1) Expression Results in Increased Differentiation of Mesenchymal Stromal Cells. *Stem Cell Res Ther* (2016) 7:1. doi: 10.1186/s13287-016-0359-3
108. Okolicsanyi RK, Camilleri ET, Oikari LE, Yu C, Cool SM, van Wijnen AJ, et al. Human Mesenchymal Stem Cells Retain Multilineage Differentiation Capacity Including Neural Marker Expression After Extended *In Vitro* Expansion. *PloS One* (2015) 10(9):e0137255. doi: 10.1371/journal.pone.0137255
109. Liu Y, Han SS, Wu Y, Tuohy TM, Xue H, Cai J. CD44 Expression Identifies Astrocyte-Restricted Precursor Cells. *Dev Biol* (2004) 276(1):31–46. doi: 10.1016/j.ydbio.2004.08.018
110. Naruse M, Shibasaki K, Yokoyama S, Kurachi M, Ishizaki Y. Dynamic Changes of CD44 Expression From Progenitors to Subpopulations of Astrocytes and Neurons in Developing Cerebellum. *PloS One* (2013) 8(1): e53109. doi: 10.1371/journal.pone.0053109
111. Jensen T, Vadasz S, Phoenix K, Claffey K, Parikh N, Finck C. Descriptive Analysis of Tumor Cells With Stem Like Phenotypes in Metastatic and Benign Adrenal Tumors. *J Pediatr Surg* (2015) 50(9):1493–501. doi: 10.1016/j.jpedsurg.2015.04.012
112. Vega FM, Colmenero-Repiso A, Gómez-Muñoz MA, Rodríguez-Prieto I, Aguilar-Morante D, Ramírez G, et al. CD44-High Neural Crest Stem-Like Cells are Associated With Tumour Aggressiveness and Poor Survival in Neuroblastoma Tumours. *EBioMedicine* (2019) 49:82–95. doi: 10.1016/j.ebiom.2019.10.041
113. Zhu H, Mitsuhashi N, Klein A, Barsky LW, Weinberg K, Barr ML, et al. The Role of the Hyaluronan Receptor CD44 in Mesenchymal Stem Cell Migration in the Extracellular Matrix. *Stem Cells* (2006) 24(4):928–35. doi: 10.1634/stemcells.2005-0186
114. Zhao P, Damerow MS, Stern P, Liu AH, Sweet-Cordero A, Siziopikou K, et al. CD44 Promotes Kras-Dependent Lung Adenocarcinoma. *Oncogene* (2013) 32(43):5186–90. doi: 10.1038/onc.2012.542

115. Chanmee T, Ontong P, Kimata K, Itano N. Key Roles of Hyaluronan and its CD44 Receptor in the Stemness and Survival of Cancer Stem Cells. *Front Oncol Front Media S.A.;* (2015) 5:1. doi: 10.3389/fonc.2015.00180
116. Chanmee T, Ontong P, Mochizuki N, Kongtawelert P, Konno K, Itano N. Excessive Hyaluronan Production Promotes Acquisition of Cancer Stem Cell Signatures Through the Coordinated Regulation of Twist and the Transforming Growth Factor β (TGF-β)-Snail Signaling Axis. *J Biol Chem* (2014) 289(38):26038–56. doi: 10.1074/jbc.M114.564120
117. Kidan N, Khamaisie H, Ruimi N, Roitman S, Eshel E, Dally N, et al. Ectopic Expression of Snail and Twist in Ph+ Leukemia Cells Upregulates CD44 Expression and Alters Their Differentiation Potential. *J Cancer* (2017) 8 (19):3952–68. doi: 10.7150/jca.19633
118. Guarino M, Rubino B, Ballabio G. The Role of Epithelial-Mesenchymal Transition in Cancer Pathology. *Pathol* (2007) 39(3):305–18. doi: 10.1080/00313020701329914
119. Emadi Baygi M, Soheili ZS, Schmitz I, Sameie S, Schulz WA. Snail Regulates Cell Survival and Inhibits Cellular Senescence in Human Metastatic Prostate Cancer Cell Lines. *Cell Biol Toxicol* (2010) 26(6):553–67. doi: 10.1007/s10565-010-9163-5
120. Fontana F, Raimondi M, Marzagalli M, Sommariva M, Limonta P, Gagliano N. Epithelial-To-Mesenchymal Transition Markers and CD44 Isoforms Are Differently Expressed in 2D and 3D Cell Cultures of Prostate Cancer Cells. *Cells* (2019) 8(2):143. doi: 10.3390/cells8020143
121. Yang J, Mani SA, Donaher JL, Ramaswamy S, Itzykson RA, Come C, et al. Twist, a Master Regulator of Morphogenesis, Plays an Essential Role in Tumor Metastasis. *Cell* (2004) 117(7):927–39. doi: 10.1016/j.cell.2004.06.006
122. Matsuo N, Shiraha H, Fujikawa T, Takaoka N, Ueda N, Tanaka S, et al. Twist Expression Promotes Migration and Invasion in Hepatocellular Carcinoma. *BMC Cancer* (2009) 9(1):1–12. doi: 10.1186/1471-2407-9-240
123. Shigeishi H, Biddle A, Gammon L, Emich H, Rodini CO, Gemenetzidis E, et al. Maintenance of Stem Cell Self-Renewal in Head and Neck Cancers Requires Actions of GSK3b Influenced by CD44 and RHAMM. *Stem Cells* (2013) 31(10):2073–83. doi: 10.1002/stem.1418
124. Marangoni E, Lecomte N, Durand L, de Pinieux G, Decaudin D, Chomienne C, et al. CD44 Targeting Reduces Tumour Growth and Prevents Post-Chemotherapy Relapse of Human Breast Cancers Xenografts. *Br J Cancer* (2009) 100(6):918–22. doi: 10.1038/sj.bjc.6604953
125. Jin L, Hope KJ, Zhai Q, Smadja-Joffe F, Dick JE. Targeting of CD44 Eradicates Human Acute Myeloid Leukemic Stem Cells. *Nat Med* (2006) 12(10):1167–74. doi: 10.1038/nm1483
126. Jang YY, Sharkis SJ. A Low Level of Reactive Oxygen Species Selects for Primitive Hematopoietic Stem Cells That may Reside in the Low-Oxygenic Niche. *Blood* (2007) 110(8):3056–63. doi: 10.1182/blood-2007-05-087759
127. Zhou D, Shao L, Spitz DR. Reactive Oxygen Species in Normal and Tumor Stem Cells. In: *Adv Cancer Res* (2014) 122:1–67. doi:10.1016/B978-0-12-420117-0.00001-3
128. Mohyeldin A, Garzón-Muvdi T, Quiñones-Hinojosa A. Oxygen in Stem Cell Biology: A Critical Component of the Stem Cell Niche. *Cell Stem Cell Cell Stem Cell;* (2010) 7:150–61. doi: 10.1016/j.stem.2010.07.007
129. Krishnamachary B, Penet MF, Nimmagadda S, Mironchik Y, Raman V, Solaiyappan M, et al. Hypoxia Regulates CD44 and Its Variant Isoforms Through HIF-1α in Triple Negative Breast Cancer. *PloS One* (2012) 7(8): e44078. doi: 10.1371/journal.pone.0044078
130. Tamada M, Nagano O, Tateyama S, Ohmura M, Yae T, Ishimoto T, et al. Modulation of Glucose Metabolism by CD44 Contributes to Antioxidant Status and Drug Resistance in Cancer Cells. *Cancer Res* (2012) 72(6):1438–48. doi: 10.1158/0008-5472.CAN-11-3024
131. Christofk HR, vander Heiden MG, Harris MH, Ramanathan A, Gerszten RE, Wei R, et al. The M2 Splice Isoform of Pyruvate Kinase is Important for Cancer Metabolism and Tumour Growth. *Nat* (2008) 452(7184):230–3. doi: 10.1038/nature06734
132. Tamada M, Suematsu M, Saya H. Pyruvate Kinase M2: Multiple Faces for Conferring Benefits on Cancer Cells. *Clin Cancer Res Clin Cancer Res;* (2012) 18:5554–61. doi: 10.1158/1078-0432.CCR-12-0859
133. Ishimoto T, Nagano O, Yae T, Tamada M, Motohara T, Oshima H, et al. CD44 Variant Regulates Redox Status in Cancer Cells by Stabilizing the xCT Subunit of System Xc- and Thereby Promotes Tumor Growth. *Cancer Cell* (2011) 19(3):387–400. doi: 10.1016/j.ccr.2011.01.038
134. Shitara K, Doi T, Nagano O, Imamura CK, Ozeki T, Ishii Y, et al. Dose-Escalation Study for the Targeting of CD44v+ Cancer Stem Cells by Sulfasalazine in Patients With Advanced Gastric Cancer (EPOC1205). *Gastric Cancer* (2017) 20(2):341–9. doi: 10.1007/s10120-016-0610-8
135. Kobayashi H, Suzuki M, Kanayama N, Nishida T, Takigawa M, Terao T. CD44 Stimulation by Fragmented Hyaluronic Acid Induces Upregulation of Urokinase-Type Plasminogen Activator and its Receptor and Subsequently Facilitates Invasion of Human Chondrosarcoma Cells. *Int J Cancer.* (2002) 102(4):379–89. doi: 10.1002/ijc.10710
136. Xiao Z, Wan J, Nur AA, Dou P, Mankin H, Liu T, et al. Targeting CD44 by CRISPR-Cas9 in Multi-Drug Resistant Osteosarcoma Cells. *Cell Physiol Biochem* (2018) 51(4):1879–93. doi: 10.1159/000495714
137. Liu T, Yan Z, Liu Y, Choy E, Hornicek FJ, Mankin H, et al. CRISPR-Cas9-Mediated Silencing of CD44 in Human Highly Metastatic Osteosarcoma Cells. *Cell Physiol Biochem* (2018) 46(3):1218–30. doi: 10.1159/000489072
138. Kong L, Ji H, Gan X, Cao S, Li Z, Jin Y. Knockdown of CD44 Inhibits Proliferation, Migration and Invasion of Osteosarcoma Cells Accompanied by Downregulation of Cathepsin s. *J Orthopaedic Surg Res* (2022) 17(1):154. doi: 10.1186/s13018-022-03048-x
139. Gvozdenovic A, Arlt MJE, Campanile C, Brennecke P, Husmann K, Born W, et al. Silencing of CD44 Gene Expression in Human 143-B Osteosarcoma Cells Promotes Metastasis of Intratibial Tumors in SCID Mice. *PloS One* (2013) 8(4):e60329. doi: 10.1371/journal.pone.0060329
140. Rhim JS, Cho HY, Huebner RJ. Non-Producer Human Cells Induced by Murine Sarcoma Virus. *Int J Cancer* (1975) 15(1):23–9. doi: 10.1002/ijc.2910150104
141. Morrow KA, Das S, Metge BJ, Ye K, Mulekar MS, Tucker JA, et al. Loss of Tumor Suppressor Merlin in Advanced Breast Cancer is Due to Post-Translational Regulation. *J Biol Chem* (2011) 286(46):40376–85. doi: 10.1074/jbc.M111.250035
142. Subramaniam D, Angulo P, Ponnurangam S, Dandawate P, Ramamoorthy P, Srinivasan P, et al. Suppressing STAT5 Signaling Affects Osteosarcoma Growth and Stemness. *Cell Death Dis* (2020) 11(2):1–15. doi: 10.1038/s41419-020-2335-1
143. Zhao H, Ma B, Wang Y, Han T, Zheng L, Sun C, et al. miR-34a Inhibits the Metastasis of Osteosarcoma Cells by Repressing the Expression of CD44. *Oncol Rep* (2013) 29(3):1027–36. doi: 10.3892/or.2013.2234
144. Gao Y, Feng Y, Shen JK, Lin M, Choy E, Cote GM, et al. CD44 is a Direct Target of miR-199a-3p and Contributes to Aggressive Progression in Osteosarcoma. *Sci Rep* (2015) 5:1–9. doi: 10.1038/srep11365
145. Liao S, Zhou S, Wang C. GAPLINC is a Predictor of Poor Prognosis and Regulates Cell Migration and Invasion in Osteosarcoma. *Biosci Rep* (2018) 38 (5): BSR20181171. doi: 10.1042/BSR20181171
146. Grünewald TGP, Cidre-Aranaz F, Surdez D, Tomazou EM, de Álava E, Kovar H, et al. Ewing Sarcoma. *Nat Rev Dis Primers* (2018) 4(1): 5. doi: 10.1038/s41572-018-0003-x
147. Tirode F, Laud-Duval K, Prieur A, Delorme B, Charbord P, Delattre O. Mesenchymal Stem Cell Features of Ewing Tumors. *Cancer Cell* (2007) 11 (5):421–9. doi: 10.1016/j.ccr.2007.02.027
148. Paulis YWJ, Huijbers EJM, van der Schaft DWJ, Soetekouw PMMB, Pauwels P, Tjan-Heijnen VCG, et al. CD44 Enhances Tumor Aggressiveness by Promoting Tumor Cell Plasticity. *Oncotarget* (2015) 6(23):19634–46. doi: 10.18632/oncotarget.3839
149. Van Der Schaft DW, Hillen F, Pauwels P, Kirschmann DA, Castermans K, oude Egbrink MGA, et al. Tumor Cell Plasticity in Ewing Sarcoma, an Alternative Circulatory System Stimulated by Hypoxia. *Cancer Res* (2005) 65 (24):11520–8. doi: 10.1158/0008-5472.CAN-05-2468
150. Kouvidi K, Berdiaki A, Nikitovic D, Katonis P, Afratis N, Hascall VC, et al. Role of Receptor for Hyaluronic Acid-Mediated Motility (RHAMM) in Low Molecular Weight Hyaluronan (LMWHA)-Mediated Fibrosarcoma Cell Adhesion. *J Biol Chem* (2011) 286(44):38509. doi: 10.1074/jbc.M111.275875
151. Hatano H, Shigeishi H, Kudo Y, Higashikawa K, Tobiume K, Takata T, et al. RHAMM/ERK Interaction Induces Proliferative Activities of Cementifying Fibroma Cells Through a Mechanism Based on the CD44–EGFR. *Lab Invest* (2011) 91:3. doi: 10.1038/labinvest.2010.176
152. Kogerman P, Sy MS, Culp LA. Counter-Selection for Over-Expressed Human CD44s in Primary Tumors Versus Lung Metastases in a Mouse Fibrosarcoma Model. *Oncogene* (1997) 15(12):1407–16. doi: 10.1038/sj.onc.1201306

153. Henderson T, Chen M, Darrow MA, Li CS, Chiu CL, Monjazeb AM, et al. Alterations in Cancer Stem-Cell Marker CD44 Expression Predict Oncologic Outcome in Soft-Tissue Sarcomas. *J Surg Res* (2018) 223:207–14. doi: 10.1016/j.jss.2017.11.016
154. Kahara N, Ozaki T, Doi T, Nishida K, Kawai A, Shibahara M, et al. CD44 Expression in Soft Tissue Sarcomas. *Virchows Archiv.* (2000) 436(6):574–8. doi: 10.1007/s004289900159
155. Kebudi R, Ayan I, Yasasever V, Demokan S, Görgün Ö. Are Serum Levels of CD44 Relevant in Children With Pediatric Sarcomas? *Pediatr Blood Cancer.* (2006) 46(1):62–5. doi: 10.1002/pbc.20554
156. Matuschek C, Lehnhardt M, Gerber PA, Poremba C, Hamilton J, Lammering G, et al. Increased CD44s and Decreased CD44v6 RNA Expression are Associated With Better Survival in Myxofibrosarcoma Patients: A Pilot Study. *Eur J Med Res* (2014) 19(1):1–7. doi: 10.1186/2047-783X-19-6
157. Tsuchie H, Emori M, Miyakoshi N, Nagasawa H, Okada K, Nanjyo H, et al. Prognostic Impact of CD44 Expression in Patients With Myxofibrosarcoma. *In Vivo.* (2019) 33(6):2095–102. doi: 10.21873/invivo.11709
158. Fligman I, Lonardo F, Jhanwar SC, Gerald WL, Woodruff J, Ladanyi M. Molecular Diagnosis of Synovial Sarcoma and Characterization of a Variant SYT-SSX2 Fusion Transcript. *Am J Pathol* (1995) 147(6):1592–9.
159. Sneath RJ, Mangham DC. CD44 Isoform Expression in Synovial Sarcoma Correlates With Epitheliogenesis But Not Prognosis. *Histopathology* (2000) 37(2):166–74. doi: 10.1046/j.1365-2559.2000.00953.x
160. Zhou Y, Chen D, Qi Y, Liu R, Li S, Zou H, et al. Evaluation of Expression of Cancer Stem Cell Markers and Fusion Gene in Synovial Sarcoma: Insights Into Histogenesis and Pathogenesis. *Oncol Rep* (2017) 37(6):3351–60. doi: 10.3892/or.2017.5617
161. Parham DM, Barr FG. Classification of Rhabdomyosarcoma and its Molecular Basis. *Adv Anatomic Pathol Adv Anat Pathol;* (2013) 20:387–97. doi: 10.1097/PAP.0b013e3182a92d0d
162. Humphrey G, Hazel DL, MacLennan K, Lewis I. Expression of CD44 by Rhabdomyosarcoma: A New Prognostic Marker? *Br J Cancer.* (1999) 80(5–6):918–21. doi: 10.1038/sj.bjc.6690442
163. Saxon BR, Byard RW, Han P. Cellular Expression of Adhesion Factors in Childhood Rhabdomyosarcoma. *Pediatr Pathol Lab Med* (1997) 17(2):259–66. doi: 10.1080/15513819709168570
164. Heyse TJ, Malcherczyk D, Moll R, Timmesfeld N, Wapelhorst J, Fuchs-Winkelmann S, et al. CD44: Survival and Metastasis in Chondrosarcoma. *Osteoarthr Cartil* (2010) 18(6):849–56. doi: 10.1016/j.joca.2010.02.007
165. Rozeman LB, de Bruijn IHB, Bacchini P, Staals EL, Bertoni F, Bovée JVMG, et al. Dedifferentiated Peripheral Chondrosarcomas: Regulation of EXT-Downstream Molecules and Differentiation-Related Genes. *Modern Pathol* (2009) 22(11):1489–98. doi: 10.1038/modpathol.2009.120
166. Misaghi A, Goldin A, Awad M, Kulidjian AA. Osteosarcoma: A Comprehensive Review. *SICOT J* (2018) 4:12. doi: 10.1051/sicotj/2017028
167. Mankin HJ, Hornicek FJ, Rosenberg AE, Harmon DC, Gebhardt MC. Survival Data for 648 Patients With Osteosarcoma Treated at One Institution. *Clin Orthopaedics Related Res* (2004) 429):286–91. doi: 10.1097/01.blo.0000145991.65770.e6
168. Liu Y, Wu Y, Gu S, Sun Z, Rui Y, Wang J, et al. Prognostic Role of CD44 Expression in Osteosarcoma: Evidence From Six Studies. *Diagn Pathol* (2014) 9(1):1–5. doi: 10.1186/1746-1596-9-140
169. Boldrini E, Peres SV, Morini S, de Camargo B. Immunoexpression of Ezrin and CD44 in Patients With Osteosarcoma. *J Pediatr Hematology/Oncology.* (2010) 32(6):e213–7. doi: 10.1097/MPH.0b013e3181e5e247
170. Gvozdenovic A, Arlt MJE, Campanile C, Brennecke P, Husmann K, Li Y, et al. CD44 Enhances Tumor Formation and Lung Metastasis in Experimental Osteosarcoma and is an Additional Predictor for Poor Patient Outcome. *J Bone Mineral Res* (2013) 28(4):838–47. doi: 10.1002/jbmr.1817
171. Kuryu M, Ozaki T, Nishida K, Shibahara M, Kawai A, Inoue H. Expression of CD44 Variants in Osteosarcoma. *J Cancer Res Clin Oncol* (1999) 125 (11):646–52. doi: 10.1007/s004320050329
172. Deng Z, Niu G, Cai L, Wei R, Zhao X. The Prognostic Significance of CD44V6, CDH11, and β -Catenin Expression in Patients With Osteosarcoma. *BioMed Res Int* (2013) 2013:9. doi: 10.1155/2013/496193
173. Tirino V, Desiderio V, Paino F, de Rosa A, Papaccio F, Fazioli F, et al. Human Primary Bone Sarcomas Contain CD133 + Cancer Stem Cells Displaying High Tumorigenicity *In Vivo*. *FASEB J* (2011) 25(6):2022–30. doi: 10.1096/fj.10-179036
174. He A, Yang X, Huang Y, Feng T, Wang Y, Sun Y, et al. CD133+CD44+ Cells Mediate in the Lung Metastasis of Osteosarcoma. *J Cell Biochem* (2015) 116 (8):1719–29. doi: 10.1002/jcb.25131
175. Kim CK, Oh S, Kim SJ, Leem SH, Heo J, Chung SH. Correlation of IGF1R Expression With ABCG2 and CD44 Expressions in Human Osteosarcoma. *Genes Genomics* (2018) 40(4):381–8. doi: 10.1007/s13258-017-0639-z
176. Zhang Y, Ding C, Wang J, Sun G, Cao Y, Xu L, et al. Prognostic Significance of CD44V6 Expression in Osteosarcoma: A Meta-Analysis. *J Orthop Surg Res* (2015) 10:187. doi: 10.1186/s13018-015-0328-z
177. Zhang Y, Lun L, Zhu B, Wang Q, Ding C, Hu Y, et al. Diagnostic Accuracy of CD44V6 for Osteosarcoma: A Meta-Analysis. *J Orthopaedic Surg Res* (2016) 11(1):1–9. doi: 10.1186/s13018-016-0470-2
178. Martin TA, Harrison G, Mansel RE, Jiang WG. The Role of the CD44/ezrin Complex in Cancer Metastasis. *Crit Rev Oncol Hematol* (2003) 46(2):165–86. doi: 10.1016/s1040-8428(02)00172-5.
179. Castellà EM, Ariza A, Pellicer I, Fernández-Vasalo A, Ojanguren I. Differential Expression of CD44v6 in Metastases of Intestinal and Diffuse Types of Gastric Carcinoma. *J Clin Pathol* (1998) 51(2):134–7. doi: 10.1136/jcp.51.2.134
180. Zhao S, He JL, Qiu ZX, Chen NY, Luo Z, Chen BJ, et al. Prognostic Value of CD44 Variant Exon 6 Expression in non-Small Cell Lung Cancer: A Meta-Analysis. *Asian Pacific J Cancer Prev* (2014) 15(16):6761–6. doi: 10.7314/APJCP.2014.15.16.6761
181. Tran TA, Kallakury BVS, Sheehan CE, Ross JS. Expression of CD44 Standard Form and Variant Isoforms in non-Small Cell Lung Carcinomas. *Hum Pathol* (1997) 28(7):809–14. doi: 10.1016/S0046-8177(97)90154-4
182. Endo K, Terada T. Protein Expression of CD44 (Standard and Variant Isoforms) in Hepatocellular Carcinoma: Relationships With Tumor Grade, Clinicopathologic Parameters, P53 Expression, and Patient Survival. *J Hepatol* (2000) 32(1):78–84. doi: 10.1016/S0168-8278(00)80192-0
183. Legras S, Günthert U, Stauder R, Curt F, Oliferenko S, Kluin-Nelemans HC, et al. A Strong Expression of CD44-6v Correlates With Shorter Survival of Patients With Acute Myeloid Leukemia. *Blood* (1998) 91(9):3401–13. doi: 10.1182/blood.V91.9.3401
184. Stauder R, Eisterer W, Thaler J, Günthert U. CD44 Variant Isoforms in non-Hodgkin's Lymphoma: A New Independent Prognostic Factor. *Blood* (1995) 85(10):2885–99. doi: 10.1182/blood.V85.10.2885.bloodjournal85102885
185. Ristamäki R, Joensuu H, Söderström K -O, Jalkanen S. CD44v6 Expression in non-Hodgkin's Lymphoma: An Association With Low Histological Grade and Poor Prognosis. *J Pathol* (1995) 176(3):259–67. doi: 10.1002/path.1711760308
186. Gansauge F, Gansauge S, Zobywalski A, Scharnweber C, Link KH, Nussler AK, et al. Differential Expression of CD44 Splice Variants in Human Pancreatic Adenocarcinoma and in Normal Pancreas. *Cancer Res* (1995) 55(23):5499–503.
187. Gotoda T, Matsumura Y, Kondo H, Saitoh D, Shimada Y, Kosuge T, et al. Expression of CD44 Variants and its Association With Survival in Pancreatic Cancer. *Jpn J Cancer Res* (1998) 89(10):1033–40. doi: 10.1111/j.1349-7006.1998.tb00493.x
188. Ayhan A, Baykal C, Al A, Ayhan A. Altered CD44 Variant 6 Expression in FIGO Stage IB Cervical Carcinoma. *Gynecologic Oncol* (2001) 83(3):569–74. doi: 10.1006/gyno.2001.6406
189. Cao Y, Roth M, Piperdi S, Montoya K, Sowers R, Rao P, et al. Insulin-Like Growth Factor 1 Receptor and Response to Anti-IGF1R Antibody Therapy in Osteosarcoma. *PloS One* (2014) 9(8):e106249. doi: 10.1371/journal.pone.0106249
190. Handorean AM, Yang K, Robbins EW, Flaig TW, Iczkowski KA. Silibinin Suppresses CD44 Expression in Prostate Cancer Cells. *Am J Transl Res* (2009) 1(1):80–6.
191. Nambiar D, Prajapati V, Agarwal R, Singh RP. *In Vitro* and *In Vivo* Anticancer Efficacy of Silibinin Against Human Pancreatic Cancer BxPC-3 and PANC-1 Cells. *Cancer Lett* (2013) 334(1):109–17. doi: 10.1016/j.canlet.2012.09.004
192. Kim S, Kil WH, Lee J, Oh SJ, Han J, Jeon M, et al. Zerumbone Suppresses EGF-Induced CD44 Expression Through the Inhibition of STAT3 in Breast Cancer Cells. *Oncol Rep* (2014) 32(6):2666–72. doi: 10.3892/or.2014.3514

193. Chung SS, Vadgama JV. Curcumin and Epigallocatechin Gallate Inhibit the Cancer Stem Cell Phenotype *via* Down-Regulation of STAT3-Nfκb Signaling. *Anticancer Res* (2015) 35(1):39–46.
194. Kummar S, Coyne GOS, Do KT, Turkbey B, Meltzer PS, Polley E, et al. Clinical Activity of the γ-Secretase Inhibitor PF-03084014 in Adults With Desmoid Tumors (Aggressive Fibromatosis). *J Clin Oncol* (2017) 35 (14):1561–9. doi: 10.1200/JCO.2016.71.1994
195. Massard C, Azaro A, Soria JC, Lassen U, le Tourneau C, Sarker D, et al. First-In-Human Study of LY3039478, an Oral Notch Signaling Inhibitor in Advanced or Metastatic Cancer. *Ann Oncol* (2018) 29(9):1911–7. doi: 10.1093/annonc/mdy244
196. Morgan KM, Fischer BS, Lee FY, Shah JJ, Bertino JR, Rosenfeld J, et al. Gamma Secretase Inhibition by BMS-906024 Enhances Efficacy of Paclitaxel in Lung Adenocarcinoma. *Mol Cancer Ther* (2017) 16(12):2759–69. doi: 10.1158/1535-7163.MCT-17-0439
197. Menke-van der Houven van Oordt CW, Gomez-Roca C, van Herpen C, Coveler AL, Mahalingam D, Verheul HMW, et al. First-In-Human Phase I Clinical Trial of RG7356, an Anti-CD44 Humanized Antibody, in Patients With Advanced, CD44-Expressing Solid Tumors. . *Oncotarget* (2016) 7 (48):80046–58. doi: 10.18632/oncotarget.11098
198. Vey N, Delaunay J, Martinelli G, Fiedler W, Raffoux E, Prebet T, et al. Phase I Clinical Study of RG7356, an Anti-CD44 Humanized Antibody, in Patients With Acute Myeloid Leukemia. *Oncotarget* (2016) 7(22):32532–42. doi: 10.18632/oncotarget.8687
199. Sandström K, Nestor M, Ekberg T, Engström M, Anniko M, Lundqvist H. Targeting CD44v6 Expressed in Head and Neck Squamous Cell Carcinoma: Preclinical Characterization of an 111In-Labeled Monoclonal Antibody. *Tumor Biol* (2008) 29(3):137–44. doi: 10.1159/000143399
200. Riechelmann H, Sauter A, Golze W, Hanft G, Schroen C, Hoermann K, et al. Phase I Trial With the CD44v6-Targeting Immunoconjugate Bivatuzumab Mertansine in Head and Neck Squamous Cell Carcinoma. *Oral Oncol* (2008) 44(9):823–9. doi: 10.1016/j.oraloncology.2007.10.009
201. Tijink BM, Buter J, de Bree R, Giaccone G, Lang MS, Staab A, et al. A Phase I Dose Escalation Study With Anti-CD44v6 Bivatuzumab Mertansine in Patients With Incurable Squamous Cell Carcinoma of the Head and Neck or Esophagus. *Clin Cancer Res* (2006) 12(20 PART 1):6064–72. doi: 10.1158/1078-0432.CCR-06-0910
202. Li L, Hao X, Qin J, Tang W, He F, Smith A, et al. Antibody Against CD44s Inhibits Pancreatic Tumor Initiation and Postradiation Recurrence in Mice. *Gastroenterol* (2014) 146(4):1108–1118.e12. doi: 10.1053/j.gastro.2013.12.035
203. Murphy JF, Lennon F, Steele C, Kelleher D, Fitzgerald D, Long A. Engagement of CD44 Modulates Cyclooxygenase Induction, VEGF Generation, and Cell Proliferation in Human Vascular Endothelial Cells. *FASEB J* (2005) 19(3):1–17. doi: 10.1096/fj.03-1376fje
204. Uchino M, Kojima H, Wada K, Imada M, Onoda F, Satofuka H, et al. Nuclear β-Catenin and CD44 Upregulation Characterize Invasive Cell Populations in non-Aggressive MCF-7 Breast Cancer Cells. *BMC Cancer* (2010) 10:414. doi: 10.1186/1471-2407-10-414
205. Khurana SS, Riehl TE, Moore BD, Fassan M, Rugge M, Romero-Gallo J, et al. The Hyaluronic Acid Receptor CD44 Coordinates Normal and Metaplastic Gastric Epithelial Progenitor Cell Proliferation. *J Biol Chem* (2013) 288 (22):16085–97. doi: 10.1074/jbc.M112.445551
206. Shukeir N, Arakelian A, Chen G, Garde S, Ruiz M, Panchal C, et al. A Synthetic 15-Mer Peptide (PCK3145) Derived From Prostate Secretory Protein can Reduce Tumor Growth, Experimental Skeletal Metastases, and Malignancy-Associated Hypercalcemia. *Cancer Res* (2004) 64(15):5370–7. doi: 10.1158/0008-5472.CAN-04-0788
207. Lamy S, Ruiz MT, Wisniewski J, Garde S, Rabbani SA, Panchal C, et al. A Prostate Secretory Protein94-Derived Synthetic Peptide PCK3145 Inhibits VEGF Signalling in Endothelial Cells: Implication in Tumor Angiogenesis. *Int J Cancer* (2006) . 118(9):2350–8. doi: 10.1002/ijc.21615
208. Annabi B, Bouzeghrane M, Currie JC, Hawkins R, Dulude H, Daigneault L, et al. A PSP94-Derived Peptide PCK3145 Inhibits MMP-9 Secretion and Triggers CD44 Cell Surface Shedding: Implication in Tumor Metastasis. *Clin Exp Metastasis* (2005) 22(5):429–39. doi: 10.1007/s10585-005-2669-1
209. Alshaer W, Hillaireau H, Vergnaud J, Ismail S, Fattal E. Functionalizing Liposomes With Anti-CD44 Aptamer for Selective Targeting of Cancer Cells. *Bioconjugate Chem* (2015) 26(7):1307–13. doi: 10.1021/bc5004313
210. Zheng J, Zhao S, Yu X, Huang S, Liu HY. Simultaneous Targeting of CD44 and EpCAM With a Bispecific Aptamer Effectively Inhibits Intraperitoneal Ovarian Cancer Growth. *Theranostics* (2017) 7(5):1373–88. doi: 10.7150/thno.17826
211. Chi Y, Yin X, Sun K, Feng S, Liu J, Chen D, et al. Redox-Sensitive and Hyaluronic Acid Functionalized Liposomes for Cytoplasmic Drug Delivery to Osteosarcoma in Animal Models. *J Controlled Release.* (2017) 261:113–25. doi: 10.1016/j.jconrel.2017.06.027
212. Gazzano E, Buondonno I, Marengo A, Rolando B, Chegaev K, Kopecka J, et al. Hyaluronated Liposomes Containing H2S-Releasing Doxorubicin are Effective Against P-Glycoprotein-Positive/Doxorubicin-Resistant Osteosarcoma Cells and Xenografts. *Cancer Letters.* (2019) 456:29–39. doi: 10.1016/j.canlet.2019.04.029
213. Feng S, Wu ZX, Zhao Z, Liu J, Sun K, Guo C, et al. Engineering of Bone- and CD44-Dual-Targeting Redox-Sensitive Liposomes for the Treatment of Orthotopic Osteosarcoma. *ACS Appl Mater Interfaces* (2019) 11(7):7357–68. doi: 10.1021/acsami.8b18820
214. Gao S, Islam R, Fang J. Tumor Environment-Responsive Hyaluronan Conjugated Zinc Protoporphyrin for Targeted Anticancer Photodynamic Therapy. *J Pers Med* (2021) 11(2):1–15. doi: 10.3390/jpm11020136
215. Xi Y, Jiang T, Yu Y, Yu J, Xue M, Xu N, et al. Dual Targeting Curcumin Loaded Alendronate-Hyaluronan- Octadecanoic Acid Micelles for Improving Osteosarcoma Therapy. *Int J Nanomedicine* (2019) 14:6425. doi: 10.2147/IJN.S211981
216. Hosono K, Nishida Y, Knudson W, Knudson CB, Naruse T, Suzuki Y, et al. Hyaluronan Oligosaccharides Inhibit Tumorigenicity of Osteosarcoma Cell Lines MG-63 and LM-8 *In Vitro* and *In Vivo via* Perturbation of Hyaluronan-Rich Pericellular Matrix of the Cells. *Am J Pathol* (2007) 171 (1):274–86. doi: 10.2353/ajpath.2007.060828
217. Gilg AG, Tye SL, Tolliver LB, Wheeler WG, Visconti RP, Duncan JD, et al. Targeting hyaluronan interactions in malignant gliomas and their drug-resistant multipotent progenitors. *Clin Cancer Res* (2008) 14(6):1804–13. doi: 10.1158/1078-0432.CCR-07-1228
218. Hu Y, Fu L. Targeting Cancer Stem Cells: A New Therapy to Cure Cancer Patients. *Am J Cancer Res* (2012) 2(3):340–56.
219. Xia W. γ-Secretase and its Modulators: Twenty Years and Beyond. *Neurosci Letters. Elsevier Ireland Ltd;* (2019) 701:162–9. doi: 10.1016/j.neulet.2019.02.011
220. Ran Y, Hossain F, Pannuti A, Lessard CB, Ladd GZ, Jung JI, et al. γ-Secretase Inhibitors in Cancer Clinical Trials are Pharmacologically and Functionally Distinct. *EMBO Mol Med* (2017) 9(7):950–66. doi: 10.15252/emmm.201607265
221. Orian-Rousseau V, Ponta H. Perspectives of CD44 Targeting Therapies. *Arch Toxicol* (2015) 89(1):3–14. doi:10.1007/s00204-014-1424-2
222. Dalla Pozza E, Lerda C, Costanzo C, Donadelli M, Dando I, Zoratti E, et al. Targeting Gemcitabine Containing Liposomes to CD44 Expressing Pancreatic Adenocarcinoma Cells Causes an Increase in the Antitumoral Activity. *Biochim Biophys Acta - Biomembranes* (2013) 1828(5):1396–404. doi: 10.1016/j.bbamem.2013.01.020
223. Peer D, Margalit R. Loading Mitomycin C Inside Long Circulating Hyaluronan Targeted Nano-Liposomes Increases its Antitumor Activity in Three Mice Tumor Models. *Int J Cancer* (2004) 108(5):780–9. doi: 10.1002/ijc.11615
224. Peer D, Margalit R. Tumor-Targeted Hyaluronan Nanoliposomes Increase the Antitumor Activity of Liposomal Doxorubicin in Syngeneic and Human Xenograft Mouse Tumor Models. *Neoplasia* (2004) 6(4):343–53. doi: 10.1593/neo.03460
225. Cheng D, Cao N, Chen J, Yu X, Shuai X. Multifunctional Nanocarrier Mediated Co-Delivery of Doxorubicin and siRNA for Synergistic Enhancement of Glioma Apoptosis in Rat. *Biomater* (2012) 33(4):1170–9. doi: 10.1016/j.biomaterials.2011.10.057
226. Šmejkalová D, Nešporová K, Huerta-Angeles G, Syrovátka J, Jirák D, Gálisová A, et al. Selective *In Vitro* Anticancer Effect of Superparamagnetic Iron Oxide Nanoparticles Loaded in Hyaluronan Polymeric Micelles. *Biomacromolecules* (2014) 15(11):4012–20. doi: 10.1021/bm501065q
227. Wickens JM, Alsaab HO, Kesharwani P, Bhise K, Amin MCIM, Tekade RK, et al. Recent Advances in Hyaluronic Acid-Decorated Nanocarriers for Targeted Cancer Therapy. *Drug Discovery Today* (2017) 22(4):665–80. doi: 10.1016/j.drudis.2016.12.009

228. Cai J, Fu J, Li R, Zhang F, Ling G, Zhang P. A Potential Carrier for Anti-Tumor Targeted Delivery-Hyaluronic Acid Nanoparticles. *Carbohydr Polym* (2019) 208:356–64. doi: 10.1016/j.carbpol.2018.12.074
229. Yin T, Wang L, Yin L, Zhou J, Huo M. Co-Delivery of Hydrophobic Paclitaxel and Hydrophilic AURKA Specific siRNA by Redox-Sensitive Micelles for Effective Treatment of Breast Cancer. *Biomater* (2015) 61:10–25. doi: 10.1016/j.biomaterials.2015.05.022
230. Yang X, Iyer AK, Singh A, Milane L, Choy E, Hornicek FJ, et al. Cluster of Differentiation 44 Targeted Hyaluronic Acid Based Nanoparticles for MDR1 siRNA Delivery to Overcome Drug Resistance in Ovarian Cancer. *Pharm Res* (2015) 32(6):2097–109. doi: 10.1007/s11095-014-1602-1
231. Yang X, Lyer AK, Singh A, Choy E, Hornicek FJ, Amiji MM, et al. MDR1 siRNA Loaded Hyaluronic Acid-Based CD44 Targeted Nanoparticle Systems Circumvent Paclitaxel Resistance in Ovarian Cancer. *Sci Rep* (2015) 5:1–9. doi: 10.1038/srep08509
232. Ahmed M, Narain R. Carbohydrate-Based Materials for Targeted Delivery of Drugs and Genes to the Liver. *Nanomedicine (Lond)* (2015) 10(14):2263–88. doi: 10.2217/nnm.15.58
233. Wang Y, Du H, Zhai G. Recent Advances in Active Hepatic Targeting Drug Delivery System. *Curr Drug Targets* (2014) 15(6):573–99. doi: 10.2174/1389450115666140309232100
234. Liu Y, Sun J, Cao W, Yang J, Lian H, Li X, et al. Dual Targeting Folate-Conjugated Hyaluronic Acid Polymeric Micelles for Paclitaxel Delivery. *Int J Pharm* (2011) 421(1):160–9. doi: 10.1016/j.ijpharm.2011.09.006
235. Chen F, Zeng Y, Qi X, Chen Y, Ge Z, Jiang Z, et al. Targeted Salinomycin Delivery With EGFR and CD133 Aptamers Based Dual-Ligand Lipid-Polymer Nanoparticles to Both Osteosarcoma Cells and Cancer Stem Cells. *Nanomedicine* (2018) 14(7):2115–27. doi: 10.1016/j.nano.2018.05.015
236. Ahrens T, Sleeman JP, Schempp CM, Howells N, Hofmann M, Ponta H, et al. Soluble CD44 Inhibits Melanoma Tumor Growth by Blocking Cell Surface CD44 Binding to Hyaluronic Acid. *Oncogene* (2001) 20(26):3399–408. doi: 10.1038/sj.onc.1204435
237. Toole BP, Slomiany MG. Hyaluronan, CD44 and Emmprin: Partners in Cancer Cell Chemoresistance. *Drug Resist Updates* (2008) 11(3):110–21. doi: 10.1016/j.drup.2008.04.002
238. Toole B, Ghatak S, Misra S. Hyaluronan Oligosaccharides as a Potential Anticancer Therapeutic. *Curr Pharm Biotechnol* (2008) 9(4):249–52. doi: 10.2174/138920108785161569
239. Lesley J, Hascall VC, Tammi M, Hyman R. Hyaluronan Binding by Cell Surface CD44. *J Biol Chem* (2000) 275(35):26967–75. doi: 10.1016/S0021-9258(19)61467-5
240. Underhill CB, Toole BP. Binding of Hyaluronate to the Surface of Cultured Cells. *J Cell Biol* (1979) 82(2):475–84. doi: 10.1083/jcb.82.2.475
241. Slomiany MG, Dai L, Bomar PA, Knackstedt TJ, Kranc DA, Tolliver L, et al. Abrogating Drug Resistance in Malignant Peripheral Nerve Sheath Tumors by Disrupting Hyaluronan-CD44 Interactions With Small Hyaluronan Oligosaccharides. *Cancer Res* (2009) 69(12):4992–8. doi: 10.1158/0008-5472.CAN-09-0143

Conflict of Interest: The authors declare that the research was conducted in the absence of any commercial or financial relationships that could be construed as a potential conflict of interest.

Publisher's Note: All claims expressed in this article are solely those of the authors and do not necessarily represent those of their affiliated organizations, or those of the publisher, the editors and the reviewers. Any product that may be evaluated in this article, or claim that may be made by its manufacturer, is not guaranteed or endorsed by the publisher.

Copyright © 2022 Fernández-Tabanera, Melero-Fernández de Mera and Alonso. This is an open-access article distributed under the terms of the Creative Commons Attribution License (CC BY). The use, distribution or reproduction in other forums is permitted, provided the original author(s) and the copyright owner(s) are credited and that the original publication in this journal is cited, in accordance with accepted academic practice. No use, distribution or reproduction is permitted which does not comply with these terms.

frontiers | Frontiers in Oncology

TYPE Mini Review
PUBLISHED 22 July 2022
DOI 10.3389/fonc.2022.956926

Check for updates

OPEN ACCESS

EDITED BY
Nikos Karamanos,
University of Patras, Greece

REVIEWED BY
Nuno Coelho,
Fibrocor Therapeutics Inc., Canada
Hamid Morjani,
Universitéde Reims Champagne-Ardenne,
France

*CORRESPONDENCE
Serge Roche
serge.roche@crbm.cnrs.fr
Audrey Sirvent
audrey.sirvent@crbm.cnrs.fr

SPECIALTY SECTION
This article was submitted to Molecular and Cellular Oncology, a section of the journal Frontiers in Oncology

RECEIVED 30 May 2022
ACCEPTED 28 June 2022
PUBLISHED 22 July 2022

CITATION
Sirvent A, Espie K, Papadopoulou E, Naim D and Roche S (2022) New functions of DDR1 collagen receptor in tumor dormancy, immune exclusion and therapeutic resistance. *Front. Oncol.* 12:956926. doi: 10.3389/fonc.2022.956926

COPYRIGHT
© 2022 Sirvent, Espie, Papadopoulou, Naim and Roche. This is an open-access article distributed under the terms of the Creative Commons Attribution License (CC BY). The use, distribution or reproduction in other forums is permitted, provided the original author(s) and the copyright owner(s) are credited and that the original publication in this journal is cited, in accordance with accepted academic practice. No use, distribution or reproduction is permitted which does not comply with these terms.

New functions of DDR1 collagen receptor in tumor dormancy, immune exclusion and therapeutic resistance

Audrey Sirvent*, Kevin Espie, Evangelia Papadopoulou, Dana Naim and Serge Roche*

Centre de Recherche en Biologie cellulaire de Montpellier (CRBM), Centre National de la Recherche Scientifique (CNRS), Univ. Montpellier, Montpellier, France

The tumor microenvironment facilitates cancer progression and therapeutic resistance. Tumor collagens and their architecture play an essential role in this process. However, little is known about the mechanisms by which tumor cells sense and respond to this extracellular matrix environment. Recently, the Discoidin Domain Receptor 1 (DDR1), a collagen receptor and tyrosine kinase has emerged as an important player in this malignant process, although the underlying signaling mechanisms remain unclear. Here, we review new DDR1 functions in tumor dormancy following dissemination, immune exclusion and therapeutic resistance induced by stromal collagens deposition. We also discuss the signaling mechanisms behind these tumor activities and the therapeutic strategies aiming at targeting these collagens-dependent tumor responses.

KEYWORDS

Keywords: collagen, tumor microenvironment, receptor, tyrosine kinase, immune evasion, metastasis, tumor dormancy, therapeutic resistance

Tumor collagens

Extracellular matrix (ECM) components from the tumor microenvironment (TME) play an important role in epithelial tumor development (1, 2). Specifically, aberrant deposition of collagens, the most abundant components of tumor ECM, defines a bad prognosis marker in several cancer patients and contributes to their tumor progression (3). TME collagens are secreted by cancer-associated fibroblasts (CAF), tumor-associated macrophages (TAM) and tumor cells themselves, and are deposited within or around the tumor and at the metastatic site. They are modified by components secreted by tumor and stromal cells in the TME that modulate their organization, resulting in wavy or fibrotic and aligned fibers. For instance, TME acidification and secretion of metalloproteases, collage :e cross-linkage and stabilization of insoluble collagen

deposited in tumor tissues (4, 5). Other post-translational modifications may participate in collagens' organization locally, as reported for Peptidyl Arginine Deaminase activity that promotes dense collagen fibers at the metastatic niche (6). Besides the nature of TME collagens, these architectures define important prognostic markers of the disease. Consistent with this notion, deposition of a dense and reticulated collagen induces tumor stiffness, resulting in enhanced tumor growth, reduced immune infiltration, and promote metastatic colonization (4, 5).

The collagen receptor DDR1

The mechanism by which tumor cells respond to the heterogeneous collagen-enriched microenvironment is not clearly established. Collagens bind to 6 receptor types (i.e Integrins, DDRs, Lairs, GPVI receptors, and OSCAR) (7). While integrins may play a role in this process (8), several of these tumor responses also implicate DDR1 (9, 10). DDR1 belongs to the DDRs family of the receptor tyrosine kinase (RTK), which includes DDR1 and DDR2 (11, 12). DDRs exhibit a similar modular structure to RTKs (*i.e.* extracellular domain with ligand binding, short transmembrane domain, and large cytoplasmic tail containing a kinase domain); however, unlike other RTKs,DDRs bind to the ECM collagens, and theirr kinase activation kinetic is slow but sustained over time (11, 12). Although the underlying mechanism is not fully understood, DDR1 regulation involves its aggregation into large clusters where collagen induces the lateral association of receptor dimers (*i.e.* receptor clustering) and phosphorylation between dimers (13–15). DDR1 is activated by most collagen types, including I and IV, which are abundant in the basement membrane (11, 12). DDR1 is preferentially expressed in epithelial tissues and acts as a cellular sensor of the collagen-enriched microenvironment by modulating growth and adhesive receptors signaling (12). In physiological conditions, *DDR1* deficient mice revealed an important function of DDR1 in mammary gland development as well as pancreatic and kidney tissue homeostasis (16–21). Whether DDR1 displays similar function in other epithelial tissues is unknown. DDR1 is upregulated in many epithelial cancers and plays important roles during tumor development. Positive and negative functions were reported depending on the cancer type, the tumor stage and the nature/organization of collagens matrix (11, 12, 22–24). DDR1 has been involved in tumor growth, dissemination and metastasis development, implicating an interplay between DDR1 signaling and collagen remodeling, and these functions have been extensively discussed in previous reviews (11, 12, 22–24). Here we discuss recent findings uncovering additional DDR1 functions in tumor dormancy following dissemination, immune exclusion and therapeutic resistance governed by specific TME collagen-enriched matrices.

DDR1 in cancer dormancy and metastatic reactivation

Metastatic development is an inefficient multistep process characterized by local tumor cell invasion of the stroma surrounding the tumor, followed by dissemination in the blood or lymphatic circulation and colonization of distant tissues (25, 26). While metastatic development is initiated by disseminated tumor cells (DTCs) with cancer stem cell properties, this whole process is supported by the aberrant tumor cell communication with their microenvironment (i.e. the front of the primary tumor, the stroma, the blood vessels and the metastatic niche of the colonized tissue) (25, 26). In this context, aberrant collagen deposition plays an essential role throughout this malignant process and DDR1 contributes to tumor cell responses to these collagen-enriched microenvironments. For instance, DDR1 promotes local invasion of epithelial cancer cells into collagen fibers deposited at the front of the tumor, both in a single or collective mode (27, 28). DDR1 is also essential for homing and colonization of epithelial cancer in the lungs and the bones (10, 29). Similarly, DDR1 upregulation enables liver metastatis of colon cancer cells (30). This metastatic function may be activated by the collagens deposited at the metastatic site from CAFs, TAMs, DTCs and cancer exosomes secereted by the primary tumor (23).

Recently, Di Martino uncovered an additional important function of DDR1 in this metastatic process, through the maintenance of DTCs in a quiescence state (31) (**Figure 1A**). It is known that tumor cell dissemination can occur both at early stages of tumorigenesis (i.e. when the primary tumor is not macrosopically detectable) and during cancer progression (26). These DTCs become non-proliferative (i.e. dormant state) at the metastatic site for long periods of time and are reactivated by specific signals to induce metastatic development (26). This process is at the origin of the clinical manifestation where patients develop metastasis years after the removal of the primary tumor by surgery and chemotherapy. The authors assessed the contribution of local ECM components in the induction of this cellular dormant state by using well-established dormant and proliferative models of human head and neck squamous cacrinoma cells and murine mammary tumor cell-lines in mouse xenograft assays. By comparing collagens' architecture and composition in both situations, they found a deposition of wavy collagens (i.e. with low degree of linear orientation) enriched in collagen III surrounding dormant tumor cells and showed that this ECM impacts their non-proliferative state. In sharp contrat, proliferative DTCs were surrounded by an extracellular matrix enriched in ECM glycoproteins with aligned collagen fibers. Interestingly, collagen III was provided by landed DTCs, suggesting a self-protective non-proliferative program. Next, the authors demonstrated that DDR1 mediates this collagen III-dependent

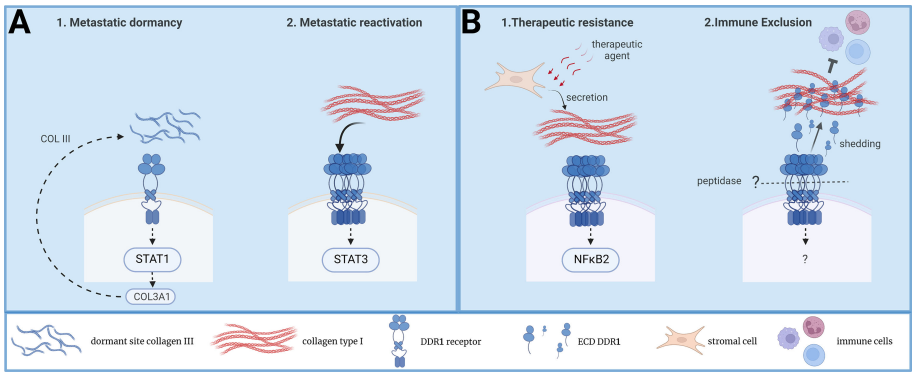

FIGURE 1
New functions of DDR1 collagen receptor in tumor dormancy, immune exclusion and therapeutic resistance. **(A)** A model on DDR1 signaling during DTC dormancy and metastatic reactivation induced by TME collagens. **(B)** A model on DDR1 signaling during therapeutic resistance and immune exclusion induced TME collagens.

dormant state. Interestingly, DDR1 dormant signaling was dependent upon its binding to collagen III but independent of its kinase activity. Importantly, they identified a feedforward loop where DDR1 induces *COLA31* expression by a Stat1-dependent mechanism. From this, they propose that *COL3A1* expression remodels the ECM in a wavy collagen architecture to maintain the cells into a dormant state (**Figure 1A**). In agreement with this idea, DDR1 downregulation reactivated DTCs proliferation. Of note, the authors observed that DDR1 was also essential for survival of proliferative DTCs, consistent with a DDR1 function also during metastatic reactivation (10). In this context, DDR1 survival signaling was kinase-dependent and involved Stat3 signaling. Collectively these results support a model where DDR1 regulates both cell dormancy and metastatic reactivation, depending on the architecture of the ECM deposited at the metastatic niche (collagen III-enriched wavy ECM versus collagen I-enriched linear ECM) (**Figure 1A**).

DDR1 in tumor immune exclusion

Immune evasion is an important feature of aggressive tumors and the ECM deposited at the TME contributes to this pathogenic effect (5). While a dense ECM network surrounding the tumor may prevent immune infiltration (5), the underlying mechanism is largely unclear. Recently, Sun et al. reported a central role of DDR1 in this malignant process (32) (**Figure 1B**). By using murine models of mammary tumor cells, they could show that DDR1 ablation prevented tumor development in immuno-competent, but not in immune-deficient mice, thus uncovering a new DDR1 function in tumor immune evasion. This effect was attributed to an immune exclusion effect rather than an inhibition of infiltrated cytotoxic lymphocytes. Importantly, the authors reported an inverse correlation between DDR1 tumor expression and CD8+ T tumoral levels in a cohort of breast cancer patients, highlighting the clinical relevance of their findings. While transcriptomic analysis were not very insightful, functional rescue assays uncovered an unsuspected mechanism behind this new DDR1 tumor function. It is known that DDR1 can be subjected to membrane shedding leading to the release of the whole extracellular domain (ECD-DDR1) (12). Surprisingly, expression of ECD-DDR1 alone was sufficient to promote substantial tumor immune exclusion. Mechanistically, this response was associated with a higher order of dense collagen fibers deposited at the ECM, suggestive of ECD-DDR1 function in ECM remodeling. This hypothesis was next validated by showing that ECD-DDR1, in its multimeric form, efficiently remodels collagen fibers and reduces T cells motility in culture. *In vivo*, injection of purified ECD-DDR1 reduced tumor immune infiltration in tumor xenografts. Finally, they could validate DDR1 as a therapeutic target for tumor immunotherapy by generating a blocking anti-DDR1 antibody. This antibody promoted immune infiltration and reduced tumor development *in vivo*. Unlike tumor xenograft animals, *DDR1* knock-out in genetically modified MMTV-PyMT mice promotes spontaneous mammary tumor development, consistent with a DDR1 negative function during tumor initiation (33). Still, their DDR1 antibody gave a similar anti-tumor effect, suggesting that DDR1 may have a tumor-promoting function at later stages of tumor development. This novel study further confirms previous results showing a function for DDR1 in tumor evasion and resistance to anti-Programmed cell Death protein 1 (PD1) immunotherapy (34). However, it uncovers an additional mechanism by which DDR1 contributes to immune evasion, i.e. the remodeling of TME collagen-enriched matrix unfavorable of immune infiltration. Whether this mechanism is conserved in other epithelial cancers is however unknown. Overall, this study further highlights the important role of DDR1 in tumor immune

gure 1B).

DDR1 in induced therapeutic tumor resistance

Tumor cells have a remarkable capacity to adapt to different environments and to cellular stresses (e.g. oxidative, oncogenic, and therapeutic) (2). This cellular plasticity is at the origin of the clinical manifestation of cancer patients that become resistant to therapy, resulting in treatment failure. While tumor adaptation can be induced by therapeutic resistant mutations in tumor cells, it can be induced by genetic-independent mechanisms, which involve the TME (3). In this context, Berestjuk et al. reported a central role of DDR1 and DDR2 in this adaptation process (35) (**Figure 1B**). By addressing the influence of TME ECM in the induced resistance of melanoma cells to anti-BRAFV600E therapy, they could show that the ECM produced by CAFs confers a drug-protective action to melanoma cells in culture. This drug tolerance effect was attributed to the aligned and dense collagen I fibers. The authors noticed a high expression of DDR1 and DDR2 in melanoma that was associated with a bad prognosis. Additionally, they associated DDR1/2 expression with melanoma progression and with the invasive and therapy-resistant phenotype. From this, they hypothesized that DDRs would mediate this drug resistance response. Consistently, interaction of melanoma cells with CAFs' ECMs induces activation and linear clustering of DDR1/2. Functionally, inhibition of DDR1/2 expression or activity overcome ECM-mediated melanoma cell resistance to the targeted therapy *in vitro*. *In vivo*, mice treatment with imatinib, a tyrosine kinase inhibitor (TKi) known to target DDR1/2 activity (36, 37), improved anti-BRAFV600E drug efficacy and delayed tumor relapse. Interestingly, this anti-tumor effect was associated with a diminution of drug-induced collagen remodeling, suggestive of a feedforward loop between DDR1/2 and collagens. However, additional imatinib drug targets (e.g. stromal PDGFR and DDR2) may contribute to the normalization of collagen deposition. Finally, while MAPK signaling was not modified by this resistance mechanism, proteomic analysis pointed to a pro-survival NIK/IKKα/NF-κB2 pathway downstream this DDR1/2 drug resistance effect (**Figure 1B**). Interestingly, this study suggest that DDR1 and DDR2 can signal in a concerted fashion. While the underlying mechanism is unclear, it may likely involve receptor hetero-dimerization. This new DDR1 activity was corroborated in KRAS-mutant lung cancer upon treatment with platinum (38). In this study, DDR1 was found upregulated during chemotherapy and its expression levels correlated with poor response to chemotherapy in lung cancer patients. Importantly, pharmacological DDR1 inhibition gave a synergistic effect with chemotherapy in a number of lung cancer experimental models tested. Whether this DDR1 function was induced by collagen remodeling during therapeutic treatment was not investigated. However, the authors discussed a tetraspanin TM4SF1-dependent mechanism of DDR1 upregulation, previously reported in lung cancer metastasis (39). In summary, these new studies confirm an important function of DDR1 in tumor adaptation to therapy, which implicates TME ECM remodeling.

Discussion and future direction

These recent findings bring new insights into the complex signaling mechanisms behind DDR1 tumor activities. Both kinase-dependent and independent DDR1 tumor signaling were reported, although their underlying mechanisms remain unclear (12, 23). Interestingly the work of Di Martino suggests that the nature of collagen-enriched ECM (wavy versus dense aligned collagen) would discriminate between DDR1 kinase-independent dormant versus kinase-dependent survival signaling. Specifically, aligned collagen fibers would promote high DDR1 clustering, which is necessary for DDR1 kinase activation (13). However, it is likely that additional factors (ECM, cytokine, receptors) may be involved in this process. Consistent with this idea, in resistant melanoma cells, DDR2 may contribute to DDR1 clustering, enabling kinase-dependent signaling. Similarly, TM4SF1 may act as a co-receptor for DDR1 function during metastatic reactivation (10). While TM4SF1 also induces DDR1 clustering, receptor phospho-signaling was relayed by cytoplasmic protein kinases, such as PKCalpha/JAK2 in metastatic breast cancer (10) and PKCtheta/SYK in metastatic pancreatic cancer (40). These new findings suggest that the combination of collagen-induced DDR1 clustering and their association with specific co-receptors may influence DDR1 phospho-signaling. Sun et al. provided an additional kinase-independent DDR1 signaling mechanism in tumor immune exclusion (32). This activity is mediated by receptor shedding, previously identified as a negative mechanism of DDR1 signaling (12). Importantly, this study brings the first pro-tumoral function of this known molecular process. However, this attractive model raises several important mechanistic questions. For instance, it is unclear whether the endogenous level of ECD-DDR1 produced from the tumor is consistent with its remodeling effect observed in overexpressing system. It is likely that additional factors may contribute to this response. Similarly, additional DDR1 signaling may contribute to this tumor effect and the activity of a shedding-resistant DDR1 allele would be informative in this regard. While ADAM10 and MMPs (41, 42) were involved in DDR1 shedding, the nature of proteases triggering this new DDR1 activity was not addressed, while of potential therapeutic interest. Finally, this model does not address how receptor shedding would cope with its cytoplasmic signaling capacity to mediate collagen DDR1 pro-tumoral activities. For instance, a role of DDR1 was reported in mechanical remodelling of collagen I by tumor cells, which depends on DDR1 clustering and association with

myosin (14, 43). It is thus likely that this signaling mechanism also participates in this pathological effect. In this scenario, the shredded DDR1-ECD would be left on collagens after cells reorganize it and would contribute to the DDR1 tumor function reported by Sun et al. (32). Clearly, further investigation is needed in the future to decipher these complex DDR1 tumor signaling mechanisms.

Finally, these recent reports may have important therapeutic consequences on the design of DDR1-based cancer therapies. First of all, they confirm the interest of therapeutically targeting DDR1 to reduce tumor immune evasion, metastatic development and thepareutic resistance in several cancer types. Second, these observations may help in optimising a strategy to chemically inhibit these diverse DDR1 pathogenic activities. For instance, a tumor with dense and aligned collagen fibers could be predictive of DDR1-kinase dependent signaling that could be targeted by TKi. While specific DDR1 kinase inhibitors did not reach the clinic yet, several clinically available TKi (e.g. imatinib, nilotinib, dasatinib) were shown to effectively inhibit DDR1/2 (22) and could be used for this purpose. However, this strategy may not be effective on kinase-independent DDR1 tumor functions. A complementary approach would involve an anti-DDR1 immunotherapy, as demonstrated in experimental settings addressing tumor immune evasion (32, 34). While this approach would target both kinase-dependent and independent DDR1 functions, several adverse effects could be predicted, such as metastatic reactivation of dormant DTCs. Besides, not all tumor-types may be dependent upon TME collagens to mediate immune evasion. For instance, in pancreatic cancer, TME collagen depletion from CAFs led to an increased tumor immune supression consistent with anti-tumor function of TME collagens (44). Whether DDR1 has a role in this anti-tumor effect is currently unknown. Clearly, further investigation is needed to clarify the role of TME collagens and its receptor DDR1 in cancer agressiveness.

In conclusion, these new studies add additional important DDR1 functions in cancer development and confirm this receptor as an attractive target in oncology. Mechanistic insight into these new functions may help to develop effective DDR1-based therapy in order to improve anti-tumor effects of the currently used therapy. Finally, additional exciting new findings on DDR1 tumor function may be expected in the future, such as tumor cell metabolism, another hallmark of cancer (1, 2) influenced by TME collagens (45).

Author contributions

SR drafted the first version of the manuscript and KE and EP the figure. All the authors have critically reviewed and approved the manuscript.

Funding

This work was supported by the Association pour la Recherche contre le Cancer ARC, Montpellier SIRIC Grant «INCa-DGOS-Inserm 6045», CNRS, and the University of Montpellier. SR is an INSERM investigator.

Conflict of interest

The authors declare that the research was conducted in the absence of any commercial or financial relationships that could be construed as a potential conflict of interest.

Publisher's note

All claims expressed in this article are solely those of the authors and do not necessarily represent those of their affiliated organizations, or those of the publisher, the editors and the reviewers. Any product that may be evaluated in this article, or claim that may be made by its manufacturer, is not guaranteed or endorsed by the publisher.

References

1. Hanahan D, Weinberg RA. Hallmarks of cancer: The next generation. *Cell* (2011) 144:646–74. doi: 10.1016/j.cell.2011.02.013

2. Hanahan D. Hallmarks of cancer: New dimensions. *Cancer Discov* (2022) 12:31–46. doi: 10.1158/2159-8290.CD-21-1059

3. Pickup MW, Mouw JK, Weaver VM. The extracellular matrix modulates the hallmarks of cancer. *EMBO Rep* (2014) 15:1243–53. doi: 10.15252/embr.201439246

4. Xu S, Xu H, Wang W, Li S, Li H, Li T, et al. The role of collagen in cancer: From bench to bedside. *J Transl Med* (2019) 17:309. doi: 10.1186/s12967-019-2058-1

5. Cox TR. The matrix in cancer. *Nat Rev Cancer* (2021) 21:217–38. doi: 10.1038/s41568-020-00329-7

6. Yuzhalin AE, Gordon-Weeks AN, Tognoli ML, Jones K, Markelc B, Konietzny R, et al. Colorectal cancer liver metastatic growth depends on PAD4-driven citrullination of the extracellular matrix. *Nat Commun* (2018) 9:4783. doi: 10.1038/s41467-018-07306-7

7. Leitinger B, Hohenester E. Mammalian collagen receptors. *Matrix Biol* (2007) 26:146–55. doi: 10.1016/j.matbio.2006.10.007

8. Hamidi H, Ivaska J. Every step of the way: integrins in cancer progression and metastasis. *Nat Rev Cancer* (2018) 18:533–48. doi: 10.1038/s41568-018-0038-z

9. Vogel W, Brakebusch C, Fässler R, Alves F, Ruggiero F, Pawson T. Discoidin domain receptor 1 is activated independently of beta(1) integrin. *J Biol Chem* (2000) 275:5779–84. doi: 10.1074/jbc.275.8.5779

10. Gao H, Chakraborty G, Zhang Z, Akalay I, Gadiya M, Gao Y, et al. Multi-organ site metastatic reactivation mediated by non-canonical discoidin domain receptor 1 signaling. *Cell* (2016) 166:47–62. doi: 10.1016/j.cell.2016.06.009

11. Valiathan RR, Marco M, Leitinger B, Kleer CG, Fridman R. Discoidin domain receptor tyrosine kinases: new players in cancer progression. *Cancer Metastasis Rev* (2012) 31:295–321. doi: 10.1007/s10555-012-9346-z

12. Leitinger B. Discoidin domain receptor functions in physiological and pathological conditions. *Int Rev Cell Mol Biol* (2014) 310:39–87. doi: 10.1016/[illegible]180-6.00002-5

13. Juskaite V, Corcoran DS, Leitinger B. Collagen induces activation of DDR1 through lateral dimer association and phosphorylation between dimers. *eLife* (2017) 6. doi: 10.7554/eLife.25716

14. Coelho NM, Arora PD, van Putten S, Boo S, Petrovic P, Lin AX, et al. Discoidin domain receptor 1 mediates myosin-dependent collagen contraction. *Cell Rep* (2017) 18:1774–90. doi: 10.1016/j.celrep.2017.01.061

15. Yeung DA, Shanker N, Sohail A, Weiss BA, Wang C, Wellmerling J, et al. Clustering, spatial distribution, and phosphorylation of discoidin domain receptors 1 and 2 in response to soluble collagen I. *J Mol Biol* (2019) 431:368–90. doi: 10.1016/j.jmb.2018.11.015

16. Vogel WF, Aszódi A, Alves F, Pawson T. Discoidin domain receptor 1 tyrosine kinase has an essential role in mammary gland development. *Mol Cell Biol* (2001) 21:2906–17. doi: 10.1128/MCB.21.8.2906-2917.2001

17. Gross O, Beirowski B, Harvey SJ, McFadden C, Chen D, Tam S, et al. DDR1-deficient mice show localized subepithelial GBM thickening with focal loss of slit diaphragms and proteinuria. *Kidney Int* (2004) 66:102–11. doi: 10.1111/j.1523-1755.2004.00712.x

18. Ruggeri JM, Franco-Barraza J, Sohail A, Zhang Y, Long D, Pasca di Magliano M, et al. Discoidin domain receptor 1 (DDR1) is necessary for tissue homeostasis in pancreatic injury and pathogenesis of pancreatic ductal adenocarcinoma. *Am J Pathol* (2020) 190:1735–51. doi: 10.1016/j.ajpath.2020.03.020

19. Rauner G, Jin DX, Miller DH, Gierahn TM, Li CM, Sokol ES, et al. Breast tissue regeneration is driven by cell-matrix interactions coordinating multi-lineage stem cell differentiation through DDR1. *Nat Commun* (2021) 12:7116. doi: 10.1038/s41467-021-27401-6

20. Chiusa M, Hu W, Liao H-J, Su Y, Borza CM, de Caestecker MP, et al. The extracellular matrix receptor discoidin domain receptor 1 regulates collagen transcription by translocating to the nucleus. *J Am Soc Nephrol* (2019) 30:1605–24. doi: 10.1681/ASN.2018111160

21. Ngai D, Mohabeer AL, Mao A, Lino M, Bendeck MP. Stiffness-responsive feedback autoregulation of DDR1 expression is mediated by a DDR1-YAP/TAZ axis. *Matrix Biol* (2022) 110:129–40. doi: 10.1016/j.matbio.2022.05.004

22. Rammal H, Saby C, Magnien K, Van-Gulick L, Garnotel R, Buache E, et al. Discoidin domain receptors: Potential actors and targets in cancer. *Front Pharmacol* (2016) 7:55. doi: 10.3389/fphar.2016.00055

23. Lafitte M, Sirvent A, Roche S. Collagen kinase receptors as potential therapeutic targets in metastatic colon cancer. *Front Oncol* (2020) 10:125. doi: 10.3389/fonc.2020.00125

24. Gao Y, Zhou J, Li J. Discoidin domain receptors orchestrate cancer progression: A focus on cancer therapies. *Cancer Sci* (2021) 112:962–9. doi: 10.1111/cas.14789

25. Vanharanta S, Massagué J. Origins of metastatic traits. *Cancer Cell* (2013) 24:410–21. doi: 10.1016/j.ccr.2013.09.007

26. Massagué J, Ganesh K. Metastasis-initiating cells and ecosystems. *Cancer Discov* (2021) 11:971–94. doi: 10.1158/2159-8290.CD-21-0010

27. Hidalgo-Carcedo C, Hooper S, Chaudhry SI, Williamson P, Harrington K, Leitinger B, et al. Collective cell migration requires suppression of actomyosin at cell-cell contacts mediated by DDR1 and the cell polarity regulators Par3 and Par6. *Nat Cell Biol* (2011) 13:49–58. doi: 10.1038/ncb2133

28. Juin A, Di Martino J, Leitinger B, Henriet E, Gary A-S, Paysan L, et al. Discoidin domain receptor 1 controls linear invadosome formation *via* a Cdc42-tuba pathway. *J Cell Biol* (2014) 207:517–33. doi: 10.1083/jcb.201404079

29. Valencia K, Ormazábal C, Zandueta C, Luis-Ravelo D, Antón I, Pajares MJ, et al. Inhibition of collagen receptor discoidin domain receptor-1 (DDR1) reduces cell survival, homing, and colonization in lung cancer bone metastasis. *Clin Cancer Res* (2012) 18:969–80. doi: 10.1158/1078-0432.CCR-11-1686

30. Jeitany M, Leroy C, Tosti P, Lafitte M, Le Guet J, Simon V, et al. Inhibition of DDR1-BCR signalling by nilotinib as a new therapeutic strategy for metastatic colorectal cancer. *EMBO Mol Med* (2018) 10. doi: 10.15252/emmm.201707918

31. Di Martino JS, Nobre AR, Mondal C, Taha I, Farias EF, Fertig EJ, et al. A tumor-derived type III collagen-rich ECM niche regulates tumor cell dormancy. *Nat Cancer* (2022) 3:90–107. doi: 10.1038/s43018-021-00291-9

32. Sun X, Wu B, Chiang H-C, Deng H, Zhang X, Xiong W, et al. Tumour DDR1 promotes collagen fibre alignment to instigate immune exclusion. *Nature* (2021) 599:673–8. doi: 10.1038/s41586-021-04057-2

33. Takai K, Drain AP, Lawson DA, Littlepage LE, Karpuj M, Kessenbrock K, et al. Discoidin domain receptor 1 (DDR1) ablation promotes tissue fibrosis and hypoxia to induce aggressive basal-like breast cancers. *Genes Dev* (2018) 32:244–57. doi: 10.1101/gad.301366.117

34. Zhong X, Zhang W, Sun T. DDR1 promotes breast tumor growth by suppressing antitumor immunity. *Oncol Rep* (2019) 42:2844–54. doi: 10.3892/or.2019.7338

35. Berestjuk I, Lecacheur M, Carminati A, Diazzi S, Rovera C, Prod'homme V, et al. Targeting discoidin domain receptors DDR1 and DDR2 overcomes matrix-mediated tumor cell adaptation and tolerance to BRAF-targeted therapy in melanoma. *EMBO Mol Med* (2022) 14:e11814. doi: 10.15252/emmm.201911814

36. Bantscheff M, Eberhard D, Abraham Y, Bastuck S, Boesche M, Hobson S, et al. Quantitative chemical proteomics reveals mechanisms of action of clinical ABL kinase inhibitors. *Nat Biotechnol* (2007) 25:1035–44. doi: 10.1038/nbt1328

37. Rix U, Hantschel O, Dürnberger G, Remsing Rix LL, Planyavsky M, Fernbach NV, et al. Chemical proteomic profiles of the BCR-ABL inhibitors imatinib, nilotinib, and dasatinib reveal novel kinase and nonkinase targets. *Blood* (2007) 110:4055–63. doi: 10.1182/blood-2007-07-102061

38. Nokin M-J, Darbo E, Travert C, Drogat B, Lacouture A, San José S, et al. Inhibition of DDR1 enhances *in vivo* chemosensitivity in KRAS-mutant lung adenocarcinoma. *JCI Insight* (2020) 5:137869. doi: 10.1172/jci.insight.137869

39. Ye L, Pu C, Tang J, Wang Y, Wang C, Qiu Z, et al. Transmembrane-4 l-six family member-1 (TM4SF1) promotes non-small cell lung cancer proliferation, invasion and chemo-resistance through regulating the DDR1/Akt/ERK-mTOR axis. *Respir Res* (2019) 20:106. doi: 10.1186/s12931-019-1071-5

40. Deng J, Kang Y, Cheng C-C, Li X, Dai B, Katz MH, et al. DDR1-induced neutrophil extracellular traps drive pancreatic cancer metastasis. *JCI Insight* (2021) 6:146133. doi: 10.1172/jci.insight.146133

41. Fu H-L, Sohail A, Valiathan RR, Wasinski BD, Kumarasiri M, Mahasenan KV, et al. Shedding of discoidin domain receptor 1 by membrane-type matrix metalloproteinases. *J Biol Chem* (2013) 288:12114–29. doi: 10.1074/jbc.M112.409599

42. Shitomi Y, Thøgersen IB, Ito N, Leitinger B, Enghild JJ, Itoh Y. ADAM10 controls collagen signaling and cell migration on collagen by shedding the ectodomain of discoidin domain receptor 1 (DDR1). *Mol Biol Cell* (2015) 26:659–73. doi: 10.1091/mbc.E14-10-1463

43. Coelho NM, Wang A, McCulloch CA. Discoidin domain receptor 1 interactions with myosin motors contribute to collagen remodeling and tissue fibrosis. *Biochim Biophys Acta Mol Cell Res* (2019) 1866:118510. doi: 10.1016/j.bbamcr.2019.07.005

44. Chen Y, Kim J, Yang S, Wang H, Wu C-J, Sugimoto H, et al. Type I collagen deletion in αSMA+ myofibroblasts augments immune suppression and accelerates progression of pancreatic cancer. *Cancer Cell* (2021) 39:548–65.e6. doi: 10.1016/j.ccell.2021.02.007

45. Zanotelli MR, Zhang J, Ortiz I, Wang W, Chada NC, Reinhart-King CA. Highly motile cells are metabolically responsive to collagen density. *Proc Natl Acad Sci USA* (2022) 119:e2114672119. doi: 10.1073/pnas.2114672119

frontiers | Frontiers in Oncology

TYPE Original Research
PUBLISHED 27 July 2022
DOI 10.3389/fonc.2022.918419

Check for updates

OPEN ACCESS

EDITED BY
Alberto Passi,
University of Insubria, Italy

REVIEWED BY
Taize M. Augusto,
Faculty of Medicine of Jundiai, Brazil
Paul J. Higgins,
Albany Medical College, United States
Neta Ilan,
Technion Israel Institute of Technology, Israel

*CORRESPONDENCE
Maurizio Onisto
maurizio.onisto@unipd.it
Valentina Masola
valentina.masola@unipd.it

SPECIALTY SECTION
This article was submitted to Molecular and Cellular Oncology, a section of the journal Frontiers in Oncology

RECEIVED 12 April 2022
ACCEPTED 27 June 2022
PUBLISHED 27 July 2022

CITATION
Masola V, Franchi M, Zaza G, Atsina FM, Gambaro G and Onisto M (2022) Heparanase regulates EMT and cancer stem cell properties in prostate tumors. *Front. Oncol.* 12:918419. doi: 10.3389/fonc.2022.918419

COPYRIGHT
© 2022 Masola, Franchi, Zaza, Atsina, Gambaro and Onisto. This is an open-access article distributed under the terms of the Creative Commons Attribution License (CC BY). The use, distribution or reproduction in other forums is permitted, provided the original author(s) and the copyright owner(s) are credited and that the original publication in this journal is cited, in accordance with accepted academic practice. No use, distribution or reproduction is permitted which does not comply with these terms.

Heparanase regulates EMT and cancer stem cell properties in prostate tumors

Valentina Masola[1*], Marco Franchi[2], Gianluigi Zaza[3], Francesca Mansa Atsina[4], Giovanni Gambaro[5] and Maurizio Onisto[1*]

[1]Department of Biomedical Sciences, University of Padova, Padova, Italy, [2]Department of Life Quality Sciences, University of Bologna, Rimini, Italy, [3]Department of Medical and Surgical Sciences, University of Foggia, Foggia, Italy, [4]University Hospital of Verona, Verona, Italy, [5]Renal Unit, Department of Medicine, University Hospital of Verona, Verona, Italy

Prostate cancer displays a certain phenotypic plasticity that allows for the transition of cells from the epithelial to the mesenchymal state. This process, known as epithelial–mesenchymal transition (EMT), is one of the factors that give the tumor cells greater invasive and migratory capacity with subsequent formation of metastases. In addition, many cancers, including prostate cancer, are derived from a cell population that shows the properties of stem cells. These cells, called cancer stem cells (CSCs) or tumor-initiating cells, not only initiate the tumor process and growth but are also able to mediate metastasis and drug resistance. However, the impact of EMT and CSCs in prostate cancer progression and patient survival is still far from fully understood. Heparanase (HPSE), the sole mammalian endoglycosidase capable of degrading heparan sulfate (HS), is also involved in prostate cancer progression. We had previously proved that HPSE regulates EMT in non-cancerous pathologies. Two prostate cancer cell lines (DU145 and PC3) were silenced and overexpressed for HPSE. Expression of EMT and stemness markers was evaluated. Results showed that the expression of several EMT markers are modified by HPSE expression in both the prostate cancer cell lines analyzed. In the same way, the stemness markers and features are also modulated by HPSE expression. Taken together, the present findings seem to prove a new mechanism of action of HPSE in sustaining prostate cancer growth and diffusion. As for other tumors, these results highlight the importance of HPSE as a potential pharmacological target in prostate cancer treatment.

KEYWORDS

prostate cancer, heparanase, epithelial to mesenchymal transition, cancer stem cells, *in vitro*

Introduction

Of all the existing cancers, prostate cancer is the one that has globally recorded the greatest growth in cases over the last 30 years in both developing and developed countries. Being a male cancer that occurs mainly in old age, the aging of the population is one of the factors that have contributed most to the increase in cases (1). It is estimated that prostate cancer will increase to nearly 2.3 million new cases and 740,000 deaths per year by 2040 simply as a result of population growth and aging (2, 3). The severity of the disease is conferred by the ability of cancer cells to disseminate and metastasize, affecting various organs and tissues—specifically, bone tissue in 84% of cases, distant lymph nodes in 10.6%, the liver in 10.2%, and the thorax in 9.1% (4).

Two phenomena that contribute to the progression and metastasis of this neoplasm are the epithelium–mesenchymal transition process (EMT) and the presence of tumor stem cells. The EMT is a reversible cell-differentiation process during which the morphological and phenotypic conversion of polarized epithelial cells into mesenchymal cells occurs. These cells have a greater migratory capacity, greater resistance to apoptosis, increased expression of mesenchymal markers, and resistance to senescence. This change involves the loss of the junction systems that hold epithelial cells together and the loss of baso-apical polarity and various rearrangements of the cytoskeletal apparatus (5, 6).

The EMT process has also been shown to be present in prostate cancer, and among the various factors that seem to be involved in promoting this change, androgens and estrogens with their related signaling, hypoxia, transforming growth factor beta (TGF-β), and epidermal growth factor (EGF) must be mentioned (7).

These factors promote the activation of the PI3K/AKT and MAPK signaling pathway—thus activating the downstream effectors such as GSK3β and NF-kB, which increase the activity of SNAI-1 and Twist and consequently induce the expression of mesenchymal proteins (8).

Cancer stem cells, according to the American Association for Cancer Research, are described as "a cell within a tumor that possesses the capacity to self-renew and to cause the heterogeneous lineages of cancer cells that comprise the tumor" (9).

Consequently, in line with this definition, CSCs possess both the ability to expand the population of cancer stem cells and, after differentiation, to give rise to other types of neoplastic cells that will make up a large part of the tumor mass. Since non-stem cells in cancer have a limited capacity for proliferation, the only cells with unlimited potential are cancer stem cells, which are thus able to guide the growth and metastatic process (10). For this reason, CSCs that have very long division times, and which are relatively insensitive to drug therapies aimed at targeting rapidly proliferating cells, may be one of the sources of cancer recurrence (11). Over the last few years, experimental evidence has accumulated in favor of the existence of CSC in prostate cancer and its role in tumor and metastatic progression (12). CSCs of the prostate can originate from basal or luminal-type progenitor/stem cells that will develop into tumors with markedly different biological and clinical characteristics in terms of aggressiveness and response to chemotherapy treatments and androgen-deprivation therapy (ADT) (13, 14). Since prostatic CSCs play a fundamental role in ADT resistance, it is currently considered essential to develop new anti-CSC strategies to compensate for treatment failure and disease recurrence (15).

More recently, it has been suggested that the expression of HPSE, the only enzyme capable of degrading the heparan sulfate (HS) chains of HS-proteoglycans (HSPGs), is associated with the characteristics of CSCs in Hodgkin's lymphoma cells (16) and in myeloma (17).

HS is a highly sulfated linear polysaccharide, attached to the core protein of heparan sulfate proteoglycans (18, 19). HS proteoglycans are ubiquitously found both at the cell surface (i.e., syndecans and glypicans) and in the extracellular matrix (ECM) (18) where they regulate ECM structure and cell–ECM interaction (20, 21). In addition, HS regulates the activity of several molecules (cytokines, growth factors, etc.) (22–25). Currently, heparanase (HPSE) is defined as a multitasking protein capable of performing enzymatic-degradative activity towards HS chains, but which, at the same time, also manifests non-enzymatic activities (26). Through its cutting activity of the side chains of heparane sulfates (HS), it contributes both to the remodeling of the extracellular matrix and to the release and diffusion of various bioactive molecules linked to HS such as growth factors, cytokines, and enzymes. Considering that heparanase is not only produced and secreted by cancer cells but also by endothelial cells and activated immune cells and platelets, it is not surprising that its activity has a strong impact on the tumor microenvironment, thanks to those factors linked to HS, which, once released, promote tumor growth, neo-angiogenesis, and the formation of a metastatic niche (27). As a proof of concept, it has been shown that heparanase overexpression in transgenic mice (Hpa-Tg) makes the tumor microenvironment more conducive to neoplastic development in various experimental models of *in vivo* tumorigenesis (28, 29).

Since prostate cancer also has an increased expression of HPSE (30), we decided to verify whether this increase could be able to regulate EMT and cancer stem cells properties of prostate cancer.

Methods

Cell lines

DU145 (ATCC® HTB-81™) and PC3 (ATCC® CRL-1435™) prostate cancer cell lines were cultured in Roswell

Park Memorial Institute (RPMI) containing 10% fetal bovine serum and supplemented with 1% penicillin/streptomycin. Cells were maintained in a humidified environment containing 5% CO_2 at 37°C, and the culture medium was replaced every 2 days.

Transfection of HPSE overexpressing and shRNA plasmid

In order to stably obtain HPSE-overexpressing DU145 cells, we used a plasmid-coding HPSE ORF purchased from OriGene, and as a negative control, we used the corresponding empty vector.

To stably obtain HPSE-silenced PC3 cells, we used four different shRNAs targeting human heparanase (NM_006665) purchased from OriGene as described earlier (31, 32). As a negative control, we used an shRNA pRS non-effective GFP plasmid (TR30003).

DU145 and PC3 cells were seeded in six-well plates and when they reached 70%–80% of confluence, they were transfected with Lipofectamine 3000 (Invitrogen) according to the manufacturer's instructions. Forty-eight hours after transfection, DU145 cells overexpressing HPSE were selected with 500 μg/ml G418 (Sigma), and PC3 cells silenced for HPSE were selected with 0.75 μg/ml of puromycin (Sigma). Single clones were isolated and analyzed for HPSE expression. The ones with the highest overexpression/silencing rate were used in the subsequent experiments.

RNA isolation and real-time qPCR analysis

Total RNA was extracted from cells by Trizol reagent (Invitrogen) according to the manufacturer's instructions (33). RNA yield and purity were checked using a Nanodrop spectrophotometer (EuroClone), and total RNA from each sample was reverse transcribed into cDNA using Moloney Murine Leukemia Virus Reverse Transcriptase (Sigma-Aldrich). Real-time PCR was performed on a StepOne™ Real-Time PCR System (Thermo Fisher) using SensiFAST SYBR Hi-Rox (Bioline). The comparative Ct method (ΔΔCt) was used to quantify gene expression, and the relative quantification was calculated as $2^{-\Delta\Delta Ct}$. The presence of non-specific amplification products was excluded by melting curve analysis. Statistical analyses on real-time PCR data were performed using the Relative Expression Software Tool (REST) (34). The forward and reverse primer sequences were reported in Table 1.

Western blotting and immunofluorescence

Cells were lysed in radioimmunoprecipitation assay buffer (RIPA) buffer composed of 150 mM NaCl, 50 mM TRIS_HCl (pH 8), 0.5% sodium deoxycholate, 0.1% sodium dodecyl sulfate (SDS), and 1% Triton-X with Complete Protease Inhibitor Mixture (Roche Applied Science, Penzberg, Germany). In brief, equal amounts of proteins were treated in reducing sample buffer and denatured for 10 min at 100°C. Protein samples were then resolved in 10% sodium dodecyl sulfate–polyacrylamide gel electrophoresis (SDS–PAGE) and electrotransferred to nitrocellulose membranes. Non-specific binding was blocked for 1 h at room temperature with non-fat milk (5%) in TBST buffer (50 mM Tris–HCl, pH 7.4, 150 mM NaCl and 0.1% Tween 20). Membranes were exposed to primary antibodies GAPDH (sc-47778 Santa Cruz), HPSE (MA1-83806 HP3/17, Thermo Fisher), E-cadherin (E-CAD) (GTX10443 GeneTex), vimentin (VIM) (sc-7557 Santa Cruz), α-SMA (A5228 Sigma), SOX2 (GTX101507 GeneTex), OCT4 (GTX627419 GeneTex), and NANOG (GTX100863 GeneTex), overnight at 4°C and incubated with a secondary peroxidase-

TABLE 1 Primer sequences used for real-time PCR .

Gene	Forward Sequence (5'–3')	Reverse Sequence (5'–3')	Product Length (bp)
GAPDH	ACACCCACTCCTCCACCTTT	TCCACCACCCTGTTGCTGTA	112
HPSE	ATTTGAATGGACGGACTGC	GTTTCTCCTAACCAGACCTTC	136
E-CAD	TTCTGCTGCTCTTGCTGTTT	TGGCTCAAGTCAAAGTCCTG	142
VIM	AAAACACCCTGCAATCTTTCAGA	CACTTTGCGTTCAAGGTCAAGAC	74
α-SMA	GAAGAAGAGGACAGCACTG	TCCCATTCCCACCATCAC	143
TGF-β	CGTGGAGCTGTACCAGAAAT	GATAACCACTCTGGCGAGTC	90
SDC1	GAAGATCAAGATGGCTCTGGG	GTTCTGGAGACGTGGGAATAG	145
SOX2	AGCTACAGCATGATGCAGGA	GGTCATGGAGTTGTACTGCA	126
OCT4	CCTCACTTCACTGCACTGG	CAGGTTTTCTTTCCCTAGCT	164
NANOG	CAGTCTGGACACTGGCTGAA	CTCGCTGATTAGGCTCCAAC	149
CD133	TCAGTGAGAAAGTGGCATCG	GCTTTTCCTATGCCAAACCA	121

conjugated antibody for 1 h at room temperature. The signal was detected with Luminata™ Forte Western HRP Substrate (Millipore) according to the manufacturer's instructions, and the signal was acquired with Mini HD9 (UVItec, Cambridge, UK). Immunofluorescence cells were fixed in 4% paraformaldehyde for 15 min, permeabilized with 0.2% Triton X-100 in phosphate-buffered saline (PBS) for 5 min, and blocked with 3% bovine serum albumin (BSA) in PBS at room temperature for 30 min. Cells were then incubated overnight at 4°C with the primary antibodies in PBS with 1% BSA and then washed three times for 5 min with PBS before incubation for 1 h at 37°C with the secondary antibody, again in PBS with 1% BSA. Cell nuclei were visualized with a Hoechst 33258. Images were obtained with a confocal LeicaSP5 microscope.

Colony formation assay

WT and HPSE-silenced/overexpressing prostate cancer cells were seeded in 35-mm culture dishes (1,000 cells per well) and incubated with RPMI supplemented with 10% FBS for 7–10 days (35, 36). The media was renewed every 2 days. The colonies were fixed using paraformaldehyde and stained with 0.1% crystal violet. Cell colony-forming ability was assessed by counting the number of colonies. A colony was defined when the number of cells was more than 50.

Hanging drop assay

To assess the spheroid-formation capacity and compare the spheroid size of the cells, 500 cells in DMEM-F12 complete medium were placed as drops (20 µl each) into the lid of a Petri dish. The lid was then rapidly re-inverted onto the culture dish that was filled with 10 ml of sterile PBS to prevent evaporation of the drops. The hanging drop cultures were incubated at 37°C in a humidified atmosphere with 5% CO_2 for 1 week. Pictures of the spheroids inside the drop were taken using a Leica MZ16F stereomicroscope, and their comparative size was obtained measuring the area occupied by the spheres using the software NIH ImageJ.

Results

Establishment of HPSE overexpressing/silenced prostate cancer cell lines

In order to investigate the function of HPSE in prostate cancer, we choose to use two prostate cancer cell lines because they display very different morphological aspects related to EMT. DU145 has a more epithelial phenotype, whereas PC3 cells are elongated and spindle-shaped like mesenc

Starting from this evidence, we decided to overexpress HPSE in DU145 and to silence it in PC3 (Supplementary Figure S1). HPSE was overexpressed in DU145 cells and silenced in PC3 cells. Results confirmed a significant HPSE upregulation in DU145 cells both at gene and protein level confirmed by WB and immunofluorescence (Figure 1) with respect to DU145 control cells transfected with the empty vector (CTR). CTR cells displayed HPSE expression levels comparable to wt DU145 cells (data not shown). Furthermore, HPSE was silenced by shRNA in PC3 cells by more than 50% both at gene and protein levels (Figure 1).

HPSE regulates EMT in prostate cancer cells

In order to investigate whether HPSE is able to modulate EMT, the expression levels of epithelial and mesenchymal markers were measured in DU145 and PC3 cells. Gene expression analyses indicated a decrease in epithelial marker E-cadherin in HPSE overexpressing DU145 cells compared with the control. Also observed was a marked increase in the expression levels of vimentin, α-SMA, SNAI1, and TGF-β compared with the control (Figure 2A). By contrast, in HPSE-silenced PC3 cells, E-cadherin gene expression was increased, and the expression of mesenchymal markers was reduced (Figure 2C). The reduction in E-cadherin and the increase in vimentin and a-SMA in HPSE-overexpressing DU145 cells were also confirmed at protein level by WB and by immunofluorescence (Figures 2B, E). On the other hand, the reduction in vimentin and a-SMA in HPSE-silenced PC3 cells was also confirmed at protein level (Figures 2D, E). These results indicate that HPSE likely promotes EMT in prostate cancer cells.

HS proteoglycans has an important role on prostate epithelium–stroma architecture (34). In particular, syndecans, a family of heparan sulfate proteoglycans that are present on the cell surface, are involved in the control of cell proliferation, apoptosis, and transformation. In prostate cancer, the expression of syndecan-1 in epithelial cells decreases when cells are transformed and acquire invasive properties. This decreased expression is associated with a bad prognosis (37–39).

In addition, HPSE cleaves HS chains on syndecan-1, and a tight relationship between HPSE and syndecan-1 has been documented in tumor and non-tumor models (19, 32, 40, 41).

Results showed that syndecan-1 gene expression was reduced in HPSE-overexpressing DU145 cells, and, in contrast, syndecan-1 expression was increased in HPSE-silenced PC3 cells.

HPSE regulates stemness features in prostate cancer cells

Numerous studies have shown that the key regulators in the stemness of embryonic stem cells, including

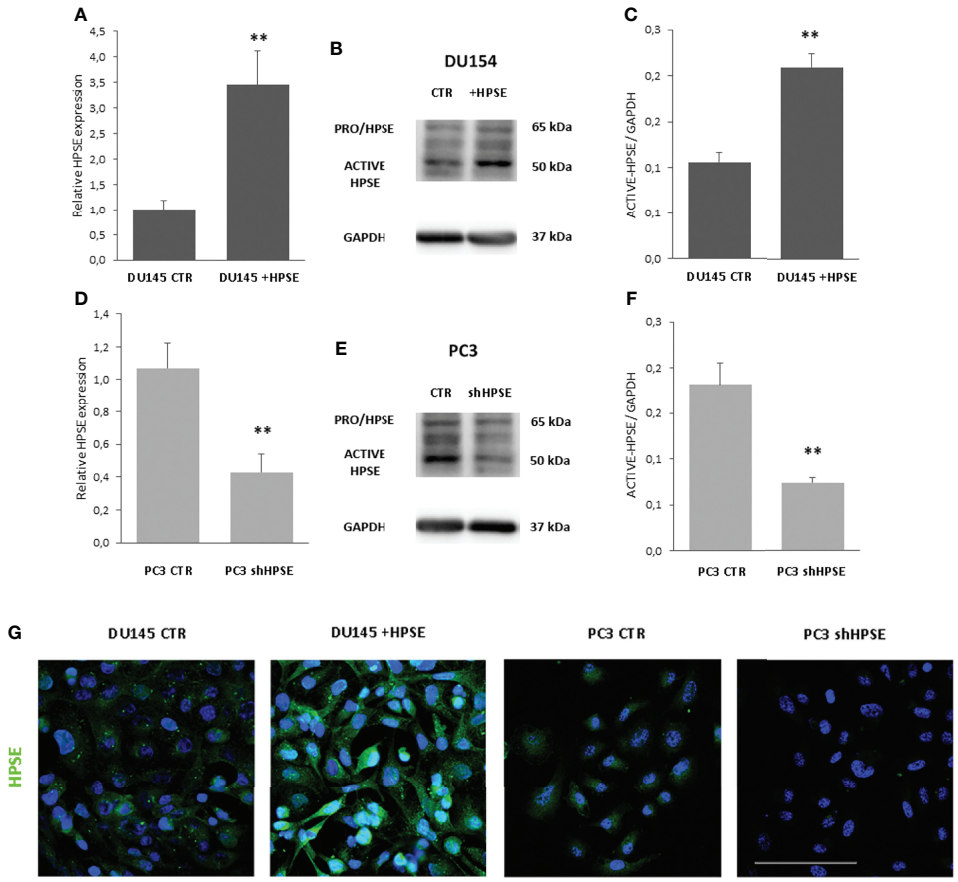

FIGURE 1
HPSE overexpression and silencing in prostate cancer cells. HPSE gene expression was evaluated by real-time PCR on DU145 **(A)** and PC3 **(D)** cells. Data were normalized to GAPDH expression. Means ± SD (error bars), n=6. **p < 0.001 vs. CTR. WB analysis of HPSE in DU145 **(B)** and PC3 **(E)** and relative quantification **(C, F)**. **(G)** HPSE immunofluorescence in DU145 and PC3 cells (green). Nuclei were counterstained with Hoechst 33342. Scale bar = 100 μm.

Oct4, Sox2, and Nanog, along with their activation targets, are commonly overexpressed in cancer stem cells in several malignancies (42–44). In addition, a series of molecules, including CD44, CD133, integrin α2β1, ALDH1A1, and Bmi1, involved in the regulation of cancer stem cell self-renewal, metastasis, and drug resistance, have also been confirmed in prostate cancer (45, 46). Results showed that the stemness markers SOX2, OCT4, NANOG, and CD133 were upregulated both at gene and protein level in HPSE-overexpressing DU145 cells compared with the control. By contrast, the same markers were significantly reduced in HPSE-silenced PC3 cells compared with the control (Figure 3).

Two important characteristics of cancer stem cells are the capacity to grow starting from a single cell and to form a sphere in an independent anchoring system.

Colony formation is the ability of cancer stem cells to form colonies when seeded on cell culture dishes at very low concentrations after limiting dilutions (47). Resu[illegible] that HPSE overexpression in DU145 cells increases the number of colonies compared to control cells and that HPSE silencing in PC3 significantly limited the ability to form colonies (**Figures 4A, B**).

To assess the spontaneous sphere formation efficiency of cancer stem cells, we used the hanging drop method (48, 49). Both cell lines were able to form similar circular spheres. HPSE overexpression in DU145 cells increased the sphere perimeter, whereas HPSE silencing in PC3 cells exerted the opposite effects (**Figures 4C, D**).

Discussion

The malignant growth and progression of tumor disease are supported by key features of cancer cells that have collectively been referred to as "hallmarks of cancer." To the initial six [illegible] (supporting proliferative signaling, evading growth

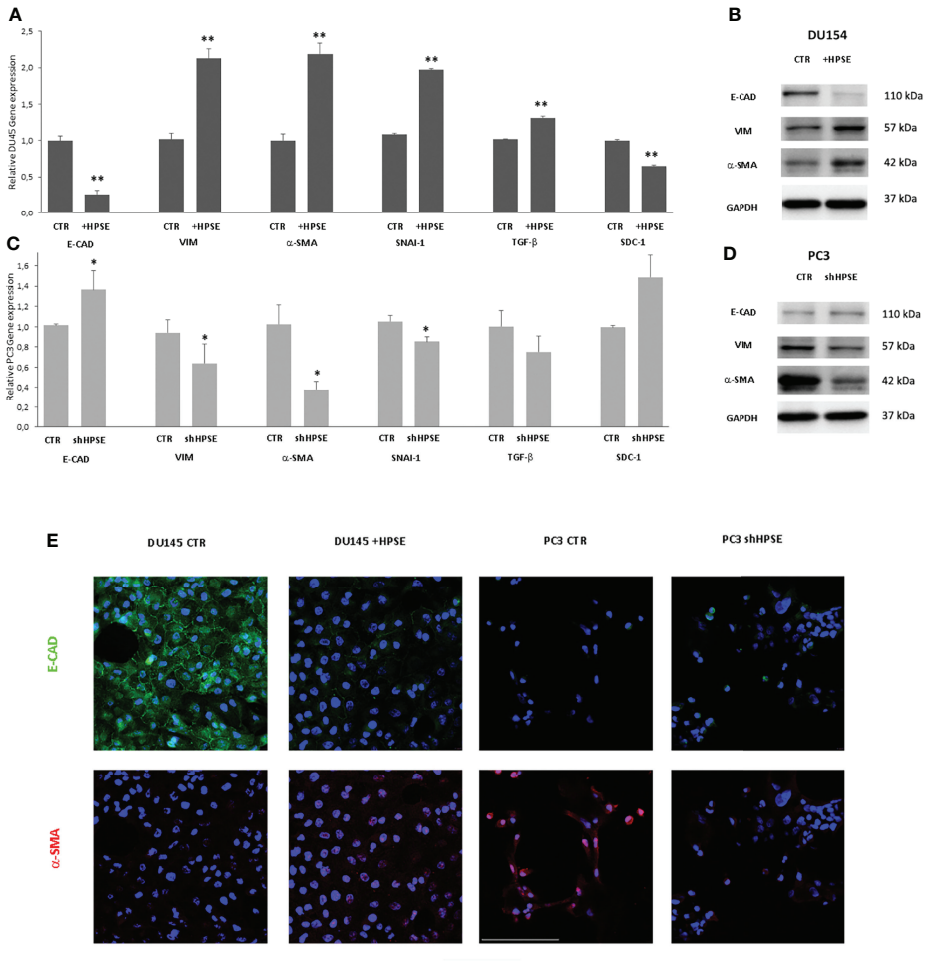

FIGURE 2
EMT markers expression in prostate cancer cells. E-CAD, VIM, α-SMA, TGF-β, and SDC-1 gene expression was evaluated by real-time PCR in DU145 **(A)** and PC3 **(C)** cells. Data were normalized to GAPDH expression. Means ± SD (error bars), n=6. **p < 0.001, *p<0.05 vs. CTR. E-CAD, VIM, a-SMA, and protein level were quantified by WB in DU145 **(B)** and PC3 **(D)** cells. GAPDH was included as loading control. **(E)** E-CAD (green) and α-SMA (red) immunofluorescence in DU145 and PC3 cells. Nuclei were counterstained with Hoechst 33342. Scale bar = 100 µm.

suppressors, replicative immortality, resistance to cell death, inducing angiogenesis, and activating invasion and metastasis), four other "enabling features" have more recently been added, such as instability and mutation of the genome, tumor-promoting inflammation, deregulated energy metabolism, and escape from immune destruction (50). Since it is now consolidated evidence that all tumors examined to date overexpress HPSE, some authors have proposed that with its multiple roles within the tumor microenvironment, heparanase can regulate each of these distinctive characteristics of cancer and, in turn, highlight the need for therapies aimed at its inhibition (51).

Starting from this evidence, our goal was to evaluate how the overexpression and silencing of heparanase in prostate cancer cells affect stemness characteristics and epithelium–mesenchymal transition (EMT)—two of the classic tumor "hallmark

EMT is thought to be activated in cancer cells, linked to their dissociation from the primary tumor and their intravasation into blood vessels (52). However, the impact of EMT in cancer progression and patient survival is still far from fully understood.

EMT was originally described during morphogenesis and later was observed in several pathological events, including fibrosis and cancer metastasis (53). During EMT, epithelial cells lose adherence junctions and (54) apical–basal polarity and acquire a mesenchymal phenotype with an enhanced motility. In response to various signals (55–58), epithelial cells upregulate a group of transcription factors to orchestrate EMT, and the main ones are SNAI-1 and TWIST. EMT can be considered to be a continuum process (59), and cells with this hybrid phenotype have been referred to as "metastable" (60), reflecting the flexibility of these cells in inducing or reversing the

ss (61).

10.3389/fonc.2022.918419

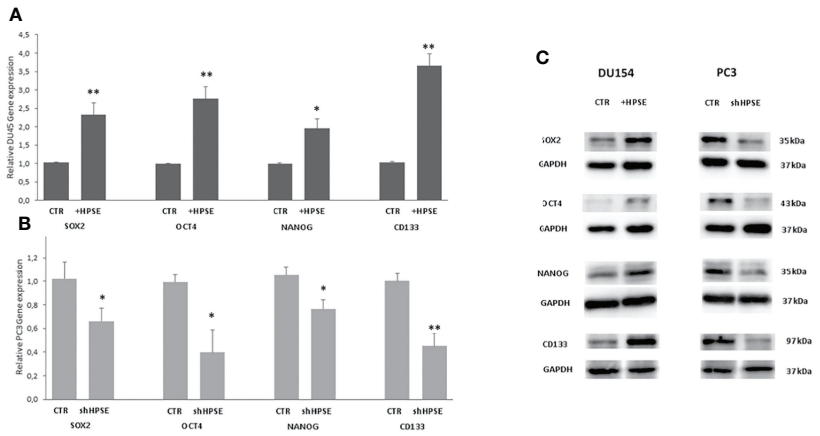

FIGURE 3
Stemness markers expression in prostate cancer cells. SOX2, OCT4, NANOG, and CD133 gene expression were evaluated by real-time PCR in DU145 **(A)** and PC3 **(B)** cells. Data were normalized to GAPDH expression. Means ± SD (error bars), n=6. **p < 0.001, *p<0.05 vs. **(C)** SOX2, OCT4, and NANOG protein level were quantified by WB in DU145 and PC3 cells. GAPDH was included as loading control.

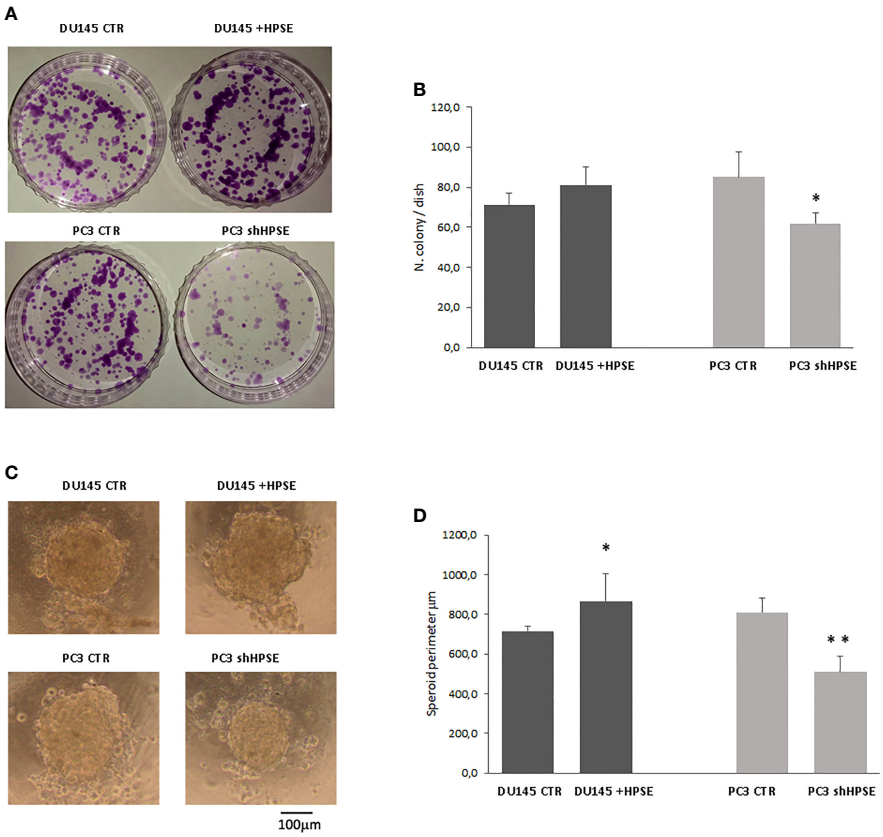

FIGURE 4
Stemness properties in prostate cancer cells. Representative images of colony **(A)** and sphere **(C)** assays evaluated in DU145 and PC3 cells. **(B, D)** Bars represent the quantification of colony and sphere assay respectively and are expressed as mean ± SD values; n=8. **p < 0.001, *p<0.05 vs. CTR.

Heparanase is the sole mammalian endoglycosidase capable of degrading glycosaminoglycan HS. The enzymatic cleavage of HS by HPSE results in ECM remodeling and releasing these bioactive mediators, producing a rapid tissue response to local or systemic stimuli. These effects profoundly affect multiple pathophysiological processes such as tumor progression, inflammation, and fibrosis (62–65). Since uncontrolled HS degradation results in significant tissue damage, HPSE expression is tightly regulated (19, 66, 67), whereas it is overexpressed in malignant tumors (66, 68).

Prostate cancer is responsible for more gender-specific cancer-related deaths in men than any other cancer (1). Zhou et al. (69) have shown that HPSE overexpression can facilitate tumor invasion and accelerate bone destruction caused by prostate cancer metastasis. Expression of HPSE has also been evaluated in prostate neoplasia; its malignant transformation has been shown to be associated with heparanase-1 increased expression at both mRNA and protein levels (70). These authors have also correlated HPSE expression with the degree of metastasizing tumors and suggested its use as a potential marker for diagnosis of the prostate metastatic process (70).

We and other previous literature support the contention that heparanase is needed for pathological organ fibrosis, and this action is exerted thorough the regulation of EMT. *In vitro* and *in vivo* studies have shown that HPSE regulates renal EMT induced by FGF-2, TGF-beta, and hypoxia (71–74). We have also proved that HPSE regulates high glucose-induced EMT of mesothelial cells (75). In addition, it has been proven that HPSE participates in lung fibrosis by regulating EMT (76), and it probably also has a role in the liver (33).

We induced HPSE overexpression in DU145 cell line and its silencing, by shRNA, in PC3 cell line. The silencing/overexpression rate was confirmed both at gene and protein levels. Results showed that HPSE is an EMT inducer in prostate cancer. Indeed, the epithelial marker E-cadherin was reduced in HPSE-overexpressing DU145 cells and upregulated in HPSE-silenced PC3 cells with respect to control. In contrast, the expression of mesenchymal markers a-SMA and vimentin was increased in HPSE-overexpressing DU45 cells and reduced in HPSE-silenced PC3 cells with respect to control.

Moreover, we have proved that HPSE regulates the expression of TGF-β (one of the principal EMT activators) and the levels of its associated transcription factor SNAI-1. Specifically, TGF-b and SNAI-1 were increased in HPSE-overexpressing DU145 cells and reduced in HPSE-silenced PC3 cells with respect to control.

During malignant transformation depletion of epithelial cell surface, syndecan-1 profoundly alters cell morphology and anchorage-dependent growth: thus, syndecan-1 is necessary in maintaining the epithelial phenotype. TGF-β can induce EMT by activating SNAI-1, which in turn, represses the expression of syndecan-1. A coordinated loss of syndecan-1 and E-cadherin has been documented in many epithelial malignancies compared to their benign counterparts. In the prostate, changes in syndecan-1 expression are linked to EMT (77). It has been described that syndecan-1 expression is lower in PC3 and DU145 prostate cancer cell lines than in normal prostate epithelial cells (78).

Here, we have shown that HPSE expression modulates syndecan-1: HPSE overexpression reduced syndecan-1 in DU145 cells, and HPSE silencing increased syndecan-1 expression in PC3 cell line.

Recently, EMT has been linked to stem cell phenotype (79), since cancer cells with EMT characteristics acquires stem-cell-like features, such as self-renewal and slow proliferation (80, 81). Cancer stem cells acquire more complete EMT molecular characteristics and exhibit more aggressive abilities. Specifically, prostate cancer stem cells display increased EMT markers and increased tumorigenesis, migration, and invasion ability (82). Cancer stem cells have a specific gene signature, and the principal markers are SOX2, OCT4, and NANOG. Additionally, other genes involved in maintaining self-renewal capacity in prostate cancer include CD-133 and CD-44 (83, 84).

Here, we have proved that HPSE expression modulates prostate CSCs. Specifically, the stemness markers SOX2, OCT4, NANOG, and CD133 were upregulated both at gene and protein levels in HPSE-overexpressing DU145 cells and reduced in HPSE-silenced PC3 cells compared with the control. In addition, functional assays confirmed a role of HPSE in prostate cancer stemness: HPSE increases the capacity to grow starting from a single cell and to form a sphere in an independent anchoring system. Future studies could also characterize the potential role of HPSE in self-renewal capacity of prostate CSCs.

Here, we report that the expression of several EMT markers is controlled by HPSE expression in prostate cancer. Moreover, stemness markers and features of CSCs are also modulated by HPSE. Collectively, these results proved an additional mechanism by means of which HPSE can contribute to prostate cancer progression and metastasis, and further studies will be necessary to clarify its potential as a pharmacological goal.

Data availability statement

The original contributions presented in the study are included in the article/Supplementary Material. Further inquiries can be directed to the corresponding authors.

Author contributions

VM, MO, and GG conceptualized this study. GZ and MF contributed to the design and implementation of the research. VM and FA carried out the experiment. VM and MO wrote the

manuscript. All authors have read and agreed to the published version of the manuscript.

Funding

This work was supported by a grant provided by the University of Padova (BIRD192859/19).

Conflict of interest

The authors declare that the research was conducted in the absence of any commercial or financial relationships that could be construed as a potential conflict of interest.

The handling editor AP declared a past co-authorship with the authors MF, MO, VM.

Publisher's note

All claims expressed in this article are solely those of the authors and do not necessarily represent those of their affiliated organizations, or those of the publisher, the editors and the reviewers. Any product that may be evaluated in this article, or claim that may be made by its manufacturer, is not guaranteed or endorsed by the publisher.

Supplementary material

The Supplementary Material for this article can be found online at: https://www.frontiersin.org/articles/10.3389/fonc.2022.918419/full#supplementary-material

References

1. Dy GW, Gore JL, Forouzanfar MH, Naghavi M, Fitzmaurice C. Global burden of urologic cancers, 1990-2013. *Eur Urol* (2017) 71(3):437–46. doi: 10.1016/j.eururo.2016.10.008

2. Zhou CK, Check DP, Lortet-Tieulent J, Laversanne M, Jemal A, Ferlay J, et al. Prostate cancer incidence in 43 populations worldwide: An analysis of time trends overall and by age group. *Int J Cancer* (2016) 138(6):1388–400. doi: 10.1002/ijc.29894

3. Culp MB, Soerjomataram I, Efstathiou JA, Bray F, Jemal A. Recent global patterns in prostate cancer incidence and mortality rates. *Eur Urol* (2020) 77(1):38–52. doi: 10.1016/j.eururo.2019.08.005

4. Gandaglia G, Abdollah F, Schiffmann J, Trudeau V, Shariat SF, Kim SP, et al. Distribution of metastatic sites in patients with prostate cancer: A population-based analysis. *Prostate* (2014) 74(2):210–6. doi: 10.1002/pros.22742

5. Lamouille S, Xu J, Derynck R. Molecular mechanisms of epithelial-mesenchymal transition. *Nat Rev Mol Cell Biol* (2014) 15(3):178–96. doi: 10.1038/nrm3758

6. Kalluri R, Weinberg RA. The basics of epithelial-mesenchymal transition. *J Clin Invest* (2009) 119(6):1420–8. doi: 10.1172/JCI39104

7. Montanari M, Rossetti S, Cavaliere C, D'Aniello C, Malzone MG, Vanacore D, et al. Epithelial-mesenchymal transition in prostate cancer: an overview. *Oncotarget* (2017) 8(21):35376–89. doi: 10.18632/oncotarget.15686

8. Di Zazzo E, Galasso G, Giovannelli P, Di Donato M, Bilancio A, Perillo B, et al. Estrogen receptors in epithelial-mesenchymal transition of prostate cancer. *Cancers (Basel)* (2019) 11(10):1418. doi: 10.3390/cancers11101418

9. Clarke MF, Dick JE, Dirks PB, Eaves CJ, Jamieson CHM, Jones DL, et al. Cancer stem cells–perspectives on current status and future directions: AACR workshop on cancer stem cells. *Cancer Res* (2006) 66(19):9339–44. doi: 10.1158/0008-5472.CAN-06-3126

10. Clarke MF, Fuller M. Stem cells and cancer: two faces of eve. *Cell* (2006) 124(6):1111–5. doi: 10.1016/j.cell.2006.03.011

11. Dean M, Fojo T, Bates S. Tumour stem cells and drug resistance. *Nat Rev Cancer* (2005) 5(4):275–84. doi: 10.1038/nrc1590

12. Li JJ, Shen MM. Prostate stem cells and cancer stem cells. *Cold Spring Harb Perspect Med* (2019) 9(6):a030395. doi: 10.1101/cshperspect.a030395

13. Wang ZA, Shen MM. Revisiting the concept of cancer stem cells in prostate cancer. *Oncogene* (2011) 30(11):1261–71. doi: 10.1038/onc.2010.530

14. Shen MM, Wang X, Economides KD, Walker D, Abate-Shen C. Progenitor cells for the prostate epithelium: roles in development, regeneration, and cancer. *Cold Spring Harb Symp Quant Biol* (2008) 73:529–38. doi: 10.1101/sqb.2008.73.050

15. Seruga B, Ocana A, Tannock IF. Drug resistance in metastatic castration-resistant prostate cancer. *Nat Rev Clin Oncol* (2011) 8(1):12–23. doi: 10.1038/nrclinonc.2010.136

16. Troschel FM, Linsenmaier M, Borrmann K, Eich HT, Götte M, Greve B. Heparanase expression is associated with cancer stem cell radioresistance in hodgkin's lymphoma cells. *Anticancer Res* (2021) 41(7):3299–308. doi: 10.21873/anticanres.15117

17. Tripathi K, Ramani VC, Bandari SK, Amin R, Brown EE, Ritchie JP, et al. Heparanase promotes myeloma stemness and *in vivo* tumorigenesis. *Matrix Biol* (2020) 88:53–68. doi: 10.1016/j.matbio.2019.11.004

18. Parish CR, Freeman C, Hulett MD. Heparanase: a key enzyme involved in cell invasion. *Biochim Biophys Acta* (2001) 1471(3):M99–108. doi: 10.1016/S0304-419X(01)00017-8

19. Ramani VC, Purushothaman A, Stewart MD, Thompson CA, Vlodavsky I, Au JL-S, et al. The heparanase/syndecan-1 axis in cancer: mechanisms and therapies. *FEBS J* (2013) 280(10):2294–306. doi: 10.1111/febs.12168

20. Theocharis AD, Skandalis SS, Tzanakakis GN, Karamanos NK. Proteoglycans in health and disease: novel roles for proteoglycans in malignancy and their pharmacological targeting. *FEBS J* (2010) 277(19):3904–23. doi: 10.1111/j.1742-4658.2010.07800.x

21. Bishop JR, Schuksz M, Esko JD. Heparan sulphate proteoglycans fine-tune mammalian physiology. *Nature* (2007) 446(7139):1030–7. doi: 10.1038/nature05817

22. Kato M, Wang H, Kainulainen V, Fitzgerald ML, Ledbetter S, Ornitz DM, et al. Physiological degradation converts the soluble syndecan-1 ectodomain from an inhibitor to a potent activator of FGF-2. *Nat Med* (1998) 4(6):691–7. doi: 10.1038/nm0698-691

23. Rider CC, Mulloy B. Heparin, heparan sulphate and the TGF-β cytokine superfamily. *Molecules* (2017) 22(5):458–60. doi: 10.3390/molecules22050713

24. Meneghetti MCZ, Hughes AJ, Rudd TR, Nader HB, Powell AK, Yates EA, et al. Heparan sulfate and heparin interactions with proteins. *J R Soc Interface* (2015) 12(110):0589. doi: 10.1098/rsif.2015.0589

25. Parish CR. The role of heparan sulphate in inflammation. *Nat Rev Immunol* (2006) 6(9):633–43. doi: 10.1038/nri1918

26. Masola V, Bellin G, Gambaro G, Onisto M. Heparanase: A multitasking protein involved in extracellular matrix (ECM) remodeling and intracellular events. *Cells* (2018) 7(12):236. doi: 10.3390/cells7120236

27. Masola V, Zaza G, Gambaro G, Franchi M, Onisto M. Role of heparanase in tumor progression: Molecular aspects and therapeutic options. *Semin Cancer Biol* (2020) 62:86–98. doi: 10.1016/j.semcancer.2019.07.014

28. Boyango I, Barash U, Naroditsky I, Li J-P, Hammond E, Ilan N, et al. Heparanase cooperates with ras to drive breast and skin tumorigenesis. *Cancer Res* (2014) 74(16):4504–14. doi: 10.1158/0008-5472.CAN-13-2962

29. Weissmann M, Arvatz G, Horowitz N, Feld S, Naroditsky I, Zhang Y, et al. Heparanase-neutralizing antibodies attenuate lymphoma tumor growth and metastasis. *Proc Natl Acad Sci U S A* (2016) 113(3):704–9. doi: 10.1073/pnas.1519453113

30. Barbosa GO, Cervigne NK, Carvalho HF, Augusto TM. Heparanase 1 involvement in prostate physiopathology. *Cell Biol Int* (2017) 41(11):1194–202. doi: 10.10748

31. Masola V, Gambaro G, Tibaldi E, Onisto M, Abaterusso C, Lupo A. Regulation of heparanase by albumin and advanced glycation end products in proximal tubular cells. *Biochim Biophys Acta* (2011) 1813(8):1475–82. doi: 10.1016/j.bbamcr.2011.05.004

32. Masola V, Gambaro G, Tibaldi E, Brunati AM, Gastaldello A, D'Angelo A, et al. Heparanase and syndecan-1 interplay orchestrates fibroblast growth factor-2-induced epithelial-mesenchymal transition in renal tubular cells. *J Biol Chem* (2012) 287(2):1478–88. doi: 10.1074/jbc.M111.279836

33. Secchi MF, Crescenzi M, Masola V, Russo FP, Floreani A, Onisto M. Heparanase and macrophage interplay in the onset of liver fibrosis. *Sci Rep* (2017) 7(1):14956. doi: 10.1038/s41598-017-14946-0

34. Masola V, Bonomini M, Onisto M, Ferraro PM, Arduini A, Gambaro G. Biological effects of XyloCore, a glucose sparing PD solution, on mesothelial cells: Focus on mesothelial-mesenchymal transition, inflammation and angiogenesis. *Nutrients* (2021) 13(7):2282. doi: 10.3390/nu13072282

35. Zhang Y, Jin Z, Zhou H, Ou X, Xu Y, Li H, et al. Suppression of prostate cancer progression by cancer cell stemness inhibitor napabucasin. *Cancer Med* (2016) 5(6):1251–8. doi: 10.1002/cam4.675

36. Wang M, Ren D, Guo W, Huang S, Wang Z, Li Q, et al. N-cadherin promotes epithelial-mesenchymal transition and cancer stem cell-like traits *via* ErbB signaling in prostate cancer cells. *Int J Oncol* (2016) 48(2):595–606. doi: 10.3892/ijo.2015.3270

37. Contreras HR, Ledezma RA, Vergara J, Cifuentes F, Barra C, Cabello P, et al. The expression of syndecan-1 and -2 is associated with Gleason score and epithelial-mesenchymal transition markers, e-cadherin and beta-catenin, in prostate cancer. *Urol Oncol ottobre* (2010) 28(5):534–40. doi: 10.1016/j.urolonc.2009.03.018

38. Barbosa GO, Biancardi MF, Carvalho HF. Heparan sulfate fine-tunes stromal-epithelial communication in the prostate gland. *Dev Dyn* (2021) 250 (5):618–28. doi: 10.1002/dvdy.281

39. Contreras HR. [Syndecans in the diagnosis and prognosis of prostate cancer]. *Rev Med Chil Jan* (2010) 138(1):95–101. doi: 10.4067/S0034-98872010000100014

40. Rangarajan S, Richter JR, Richter RP, Bandari SK, Tripathi K, Vlodavsky I, et al. Heparanase-enhanced shedding of syndecan-1 and its role in driving disease pathogenesis and progression. *J Histochem Cytochem* (2020) 68(12):823–40. doi: 10.1369/0022155420937087

41. Teixeira FCOB, Götte M. Involvement of syndecan-1 and heparanase in cancer and inflammation. *Adv Exp Med Biol* (2020) 1221:97–135. doi: 10.1007/978-3-030-34521-1_4

42. Jeter CR, Liu B, Liu X, Chen X, Liu C, Calhoun-Davis T, et al. NANOG promotes cancer stem cell characteristics and prostate cancer resistance to androgen deprivation. *Oncogene* (2011) 30(36):3833–45. doi: 10.1038/onc.2011.114

43. Chiou S-H, Wang M-L, Chou Y-T, Chen C-J, Hong C-F, Hsieh W-J, et al. Coexpression of Oct4 and nanog enhances malignancy in lung adenocarcinoma by inducing cancer stem cell-like properties and epithelial-mesenchymal transdifferentiation. *Cancer Res* (2010) 70(24):10433–44. doi: 10.1158/0008-5472.CAN-10-2638

44. Boumahdi S, Driessens G, Lapouge G, Rorive S, Nassar D, Le Mercier M, et al. SOX2 controls tumour initiation and cancer stem-cell functions in squamous-cell carcinoma. *Nature* (2014) 511(7508):246–50. doi: 10.1038/nature13305

45. Lin X, Farooqi AA, Qureshi MZ, Romero MA, Tabassum S, Ismail M. Prostate cancer stem cells: Viewing signaling cascades at a finer resolution. *Arch Immunol Ther Exp (Warsz)* (2016) 64(3):217–23. doi: 10.1007/s00005-016-0383-0

46. Li T, Su Y, Mei Y, Leng Q, Leng B, Liu Z, et al. ALDH1A1 is a marker for malignant prostate stem cells and predictor of prostate cancer patients' outcome. *Lab Invest* (2010) 90(2):234–44. doi: 10.1038/labinvest.2009.127

47. Franken NAP, Rodermond HM, Stap J, Haveman J, van Bree C. Clonogenic assay of cells in vitro. *Nat Protoc* (2006) 1(5):2315–9. doi: 10.1038/nprot.2006.339

48. Chen K, Li X, Li N, Dong H, Zhang Y, Yoshizawa M, et al. Spontaneously formed spheroids from mouse compact bone-derived cells retain highly potent stem cells with enhanced differentiation capability. *Stem Cells Int* (2019) 2019:8469012. doi: 10.1155/2019/8469012

49. Foty R. A simple hanging drop cell culture protocol for generation of 3D spheroids. *J Vis Exp* (2011) 51):2720. doi: 10.3791/2720

50. Hanahan D, Weinberg RA. Hallmarks of cancer: the next generation. *Cell* (2011) 144(5):646–74. doi: 10.1016/j.cell.2011.02.013

51. Jayatilleke KM, Hulett MD. Heparanase and the hallmarks of cancer. *J Transl Med* (2020) 18(1):453. doi: 10.1186/s12967-020-02624-1

52. Thiery JP, Acloque H, Huang RYJ, Nieto MA. Epithelial-mesenchymal transitions in development and disease. *Cell* (2009) 139(5):871–90. doi: 10.1016/j.cell.2009.11.007

53. Yeung KT, Yang J. Epithelial-mesenchymal transition in tumor metastasis. *Mol Oncol* (2017) 11(1):28–39. doi: 10.1002/1878-0261.12017

54. Nieto MA. Epithelial plasticity: a common theme in embryonic and cancer cells. *Science* (2013) 342(6159):1234850. doi: 10.1126/science.1234850

55. Strutz F, Zeisberg M, Ziyadeh FN, Yang C-Q, Kalluri R, Müller GA, et al. Role of basic fibroblast growth factor-2 in epithelial-mesenchymal transformation. *Kidney Int* (2002) 61(5):1714–28. doi: 10.1046/j.1523-1755.2002.00333.x

56. Moustakas A, Heldin C-H. Mechanisms of TGFβ-induced epithelial-mesenchymal transition. *J Clin Med* (2016) 5(7):63. doi: 10.3390/jcm5070063

57. Lo H-W, Hsu S-C, Xia W, Cao X, Shih J-Y, Wei Y, et al. Epidermal growth factor receptor cooperates with signal transducer and activator of transcription 3 to induce epithelial-mesenchymal transition in cancer cells *via* up-regulation of TWIST gene expression. *Cancer Res* (2007) 67(19):9066–76. doi: 10.1158/0008-5472.CAN-07-0575

58. Gonzalez DM, Medici D. Signaling mechanisms of the epithelial-mesenchymal transition. *Sci Signal* (2014) 7(344):re8. doi: 10.1126/scisignal.2005189

59. Nieto MA, Huang RY-J, Jackson RA, Thiery JP. EMT: 2016. *Cell* (2016) 166 (1):21–45. doi: 10.1016/j.cell.2016.06.028

60. Lee JM, Dedhar S, Kalluri R, Thompson EW. The epithelial-mesenchymal transition: new insights in signaling, development, and disease. *J Cell Biol* (2006) 172(7):973–81. doi: 10.1083/jcb.200601018

61. Rosanò L, Spinella F, Di Castro V, Decandia S, Nicotra MR, Natali PG, et al. Endothelin-1 is required during epithelial to mesenchymal transition in ovarian cancer progression. *Exp Biol Med (Maywood)* (2006) 231(6):1128–31. doi: 10.3181/00379727-232-2311128

62. Secchi MF, Masola V, Zaza G, Lupo A, Gambaro G, Onisto M. Recent data concerning heparanase: focus on fibrosis, inflammation and cancer. *Biomol Concepts* (2015) 6(5–6):415–21. doi: 10.1515/bmc-2015-0021

63. Lv Q, Zeng J, He L. The advancements of heparanase in fibrosis. *Int J Mol Epidemiol Genet* (2016) 7(4):137–40.

64. Sanderson RD, Elkin M, Rapraeger AC, Ilan N, Vlodavsky I. Heparanase regulation of cancer, autophagy and inflammation: new mechanisms and targets for therapy. *FEBS J* (2017) 284(1):42–55. doi: 10.1111/febs.13932

65. Masola V, Zaza G, Onisto M, Lupo A, Gambaro G. Impact of heparanase on renal fibrosis. *J Transl Med* (2015) 13:181. doi: 10.1186/s12967-015-0538-5

66. Meirovitz A, Goldberg R, Binder A, Rubinstein AM, Hermano E, Elkin M. Heparanase in inflammation and inflammation-associated cancer. *FEBS J* (2013) 280(10):2307–19. doi: 10.1111/febs.12184

67. Ilan N, Elkin M, Vlodavsky I. Regulation, function and clinical significance of heparanase in cancer metastasis and angiogenesis. *Int J Biochem Cell Biol* (2006) 38(12):2018–39. doi: 10.1016/j.biocel.2006.06.004

68. Nadir Y, Brenner B. Heparanase multiple effects in cancer. *Thromb Res* (2014) 133 Suppl 2:S90–94. doi: 10.1016/S0049-3848(14)50015-1

69. Zhou Y, Song B, Qin W-J, Zhang G, Zhang R, Luan Q, et al. Heparanase promotes bone destruction and invasiveness in prostate cancer. *Cancer Lett* (2008) 268(2):252–9. doi: 10.1016/j.canlet.2008.04.008

70. Kutsenko OS, Kovner AV, Mostovich LA, Kunin IS, Nepomnyashchikh RD, Prudnikova TY, et al. Expression of heparanase-1 in prostate gland tumors. *Bull Exp Biol Med* (2012) 152(3):344–7. doi: 10.1007/s10517-012-1524-z

71. Masola V, Onisto M, Zaza G, Lupo A, Gambaro G. A new mechanism of action of sulodexide in diabetic nephropathy: inhibits heparanase-1 and prevents FGF-2-induced renal epithelial-mesenchymal transition. *J Transl Med* (2012) 10:213. doi: 10.1186/1479-5876-10-213

72. Masola V, Zaza G, Secchi MF, Gambaro G, Lupo A, Onisto M. Heparanase is a key player in renal fibrosis by regulating TGF-β expression and activity. *Biochim Biophys Acta* (2014) 1843(9):2122–8. doi: 10.1016/j.bbamcr.2014.06.005

73. Masola V, Zaza G, Gambaro G, Onisto M, Bellin G, Vischini G, et al. Heparanase: A potential new factor involved in the renal epithelial mesenchymal transition (EMT) induced by Ischemia/Reperfusion (I/R) injury. *PLoS One* (2016) 11(7):e0160074. doi: 10.1371/journal.pone.0160074

74. Abassi Z, Hamoud S, Hassan A, Khamaysi I, Nativ O, Heyman SN, et al. Involvement of heparanase in the pathogenesis of acute kidney injury: nephroprotective effect of PG545. *Oncotarget* (2017) 8(21):34191–204. doi: 10.18632/oncotarget.16573

75. Masola V, Granata S, Bellin G, Gambaro G, Onisto M, Rugiu C, et al. Specific heparanase inhibition reverses glucose-induced mesothelial-to-mesenchymal transition. *Nephrol Dial Transplant* (2017) 32(7):1145–54. doi: 10.1093/ndt/gfw403

76. He L, Sun F, Wang Y, Zhu J, Fang J, Zhang S, et al. HMGB1 exacerbates bronchiolitis obliterans syndrome *via* RAGE/NF-κB/HPSE signaling to enhance latent TGF-β release from ECM. *Am J Transl Res* (2016) 8(5):1971–84.

77. Szatmári T, Ötvös R, Hjerpe A, Dobra K. Syndecan-1 in cancer: Implications for cell signaling, differentiation, and prognostication. *Dis Markers* (2015) 2015:796052. doi: 10.1155/2015/796052

78. Hu Y, Sun H, Owens RT, Gu Z, Wu J, Chen YQ, et al. Syndecan-1-dependent suppression of PDK1/Akt/bad signaling by docosahexaenoic acid induces apoptosis cer. *Neoplasia* (2010) 12(10):826–36. doi: 10.1593/neo.10586

79. Mani SA, Guo W, Liao M-J, Eaton EN, Ayyanan A, Zhou AY, et al. The epithelial-mesenchymal transition generates cells with properties of stem cells. *Cell* (2008) 133(4):704–15. doi: 10.1016/j.cell.2008.03.027

80. Pirozzi G, Tirino V, Camerlingo R, Franco R, La Rocca A, Liguori E, et al. Epithelial to mesenchymal transition by TGFβ-1 induction increases stemness characteristics in primary non small cell lung cancer cell line. *PLoS One* (2011) 6(6): e21548. doi: 10.1371/journal.pone.0021548

81. Bisson I, Prowse DM. WNT signaling regulates self-renewal and differentiation of prostate cancer cells with stem cell characteristics. *Cell Res* (2009) 19(6):683–97. doi: 10.1038/cr.2009.43

82. Luo Y, Cui X, Zhao J, Han Y, Li M, Lin Y, et al. Cells susceptible to epithelial-mesenchymal transition are enriched in stem-like side population cells from prostate cancer. *Oncol Rep* (2014) 31(2):874–84. doi: 10.3892/or.2013.2905

83. Desai B, Ma T, Zhu J, Chellaiah MA. Characterization of the expression of variant and standard CD44 in prostate cancer cells: identification of the possible molecular mechanism of CD44/MMP9 complex formation on the cell surface. *J Cell Biochem* (2009) 108(1):272–84. doi: 10.1002/jcb.22248

84. Richardson GD, Robson CN, Lang SH, Neal DE, Maitland NJ, Collins AT. CD133, a novel marker for human prostatic epithelial stem cells. *J Cell Sci* (2004) 117(Pt 16):3539–45. doi: 10.1242/jcs.01222

frontiers | Frontiers in Oncology

ORIGINAL RESEARCH
published: 02 August 2022
doi: 10.3389/fonc.2022.906415

Interplay Between Chemotherapy-Activated Cancer Associated Fibroblasts and Cancer Initiating Cells Expressing CD44v6 Promotes Colon Cancer Resistance

Shibnath Ghatak[1,2*†], *Vincent C. Hascall*[3†], *Nikos Karamanos*[4], *Roger R. Markwald*[1] *and Suniti Misra*[1,2*]

[1] Department of Regenerative Medicine and Cell Biology, Medical University of South Carolina, Charleston, SC, United States, [2] Department Natural Sciences, Trident Technical College, North Charleston, SC, United States, [3] Department of Biomedical Engineering/ND20, Cleveland Clinic, Cleveland, OH, United States, [4] Department of Chemistry, University of Patras, Matrix Pathobiology Research Group, Patras, Greece

OPEN ACCESS

Edited by:
Xiuwei Yang,
University of Kentucky, United States

Reviewed by:
Lynne-Marie Postovit,
University of Alberta, Canada
Xin Zhang,
University of Oklahoma Health Sciences Center, United States

***Correspondence:**
Suniti Misra
suniti.misra@tridenttech.edu;
sunitimisra1972@gmail.com
Shibnath Ghatak
shibnath.ghatak@tridenttech.edu;
ghataks852@gmail.com

[†]These authors share first authorship

Specialty section:
This article was submitted to Molecular and Cellular Oncology, a section of the journal Frontiers in Oncology

Received: 28 March 2022
Accepted: 22 June 2022
Published: 02 August 2022

Citation:
Ghatak S, Hascall VC, Karamanos N, Markwald RR and Misra S (2022) Interplay Between Chemotherapy-Activated Cancer Associated Fibroblasts and Cancer Initiating Cells Expressing CD44v6 Promotes Colon Cancer Resistance. Front. Oncol. 12:906415. doi: 10.3389/fonc.2022.906415

Cancer-initiating cells (CICs) drive colorectal tumor growth by their supportive niches where CICs interact with multiple cell types within the microenvironment, including cancer-associated fibroblasts (CAFs). We investigated the interplay between the CICs and the clinically relevant chemotherapeutic FOLFOX that creates the persistent tumorigenic properties of colorectal CICs, and stimulates the microenvironmental factors derived from the CAFs. We found that the CICs expressing an immunophenotype (CD44v6[+]) promote FOLFOX-resistance and that the CIC-immunophenotype was enhanced by factors secreted by CAFs after FOLFOX treatment These secreted factors included periostin, IL17A and WNT3A, which induced CD44v6 expression by activating WNT3A/β-catenin signaling. Blocking the interaction between CICs with any of these CAF-derived factors through tissue-specific conditional silencing of CD44v6 significantly reduced colorectal tumorigenic potential. To achieve this, we generated two unique vectors (floxed-pSico-CD44v6 shRNA plus *Fabpl-Cre*) that were encapsulated into transferrin coated PEG-PEI/(nanoparticles), which when introduced *in vivo* reduced tumor growth more effectively than using CD44v6-blocking antibodies. Notably, this tissue-specific conditional silencing of CD44v6 resulted in long lasting effects on self-renewal and tumor growth associated with a positive feedback loop linking WNT3A signaling and alternative-splicing of CD44. These findings have crucial clinical implications suggesting that therapeutic approaches for modulating tumor growth that currently focus on cell-autonomous mechanisms may be too limited and need to be broadened to include mechanisms that recognize the interplay between the stromal factors and the subsequent CIC-immunophenotype enrichment. Thus, more specific therapeutic approaches may be required to block a chemotherapy induced remodeling of a microenvironment that acts as a paracrine regulator to enrich CD44v6 (+) in colorectal CICs

Keywords: colorectal cancer (CRC), cancer initiating cells (CICs), cancer associate fibroblasts (CAFs), CD44v6, periostin, IL17A, WNT3A, CD44v6-therapy

INTRODUCTION

Human colorectal cancer is a widely studied human tumor type for which the steps from small adenomas to metastatic colorectal cancer (CRC) are clearly defined. In the face of recent progress in cancer therapy and increased knowledge of tumor biology, CRC ranked second in women after breast cancer and third in men after prostate and lung cancers (1). CRC-associated death is primarily caused by cancer recurrence and metastasis. CRC recurrence is defined as local, regional, and distant metastatic recurrence after a disease-free period (2). Moreover, five-year survival in CRC ranges from 90% in early localized stages to less than 10% in advanced, metastatic cases (3, 4).

The vast majority of tumors (90%) are linked to somatic mutations and environmental factors, whereas only a minority of all cancers are caused by germline mutations. Recent studies provide evidence that tumors exist as complex tissues composed of heterogeneous, aberrant cell types containing a hierarchy of cells that differ in morphology, gene expression, proliferative capacity, and invasiveness (5). A small subset of cancer cells known as cancer initiating cells (CICs) display cellular hierarchies from which tumor clones originate with tumor initiation ability, self-renewal capacity, long-term repopulation potential, cell death evasion capacity, and demonstration of extensive proliferating capacity to differentiate into multi cell types (6–11). CICs do not simply survive in seclusion, but rather live in a tumor microenvironment known as "niche". The niche is the cellular environment in which the CICs exist and interact within the extracellular matrix (ECM) with mesenchymal fibroblast cells called cancer associated fibroblasts (CAFs) (12–15). Additionally, immune cells (16), endothelial cells (17), and paracrine signaling molecules such as growth factors (18), matricellular proteins (19) and cytokines (20) are found in the microenvironment of these niches (21, 22). We hypothesize that paracrine factors secreted by CAFs in the CIC niche interact with specific isoforms (variants) of CD44 receptors on CICs to govern tumor growth.

CD44 is a multi-structural and multi-functional transmembrane glycoprotein that is encoded by a single gene containing 20 exons, ten of which are alternatively spliced to generate the numerous CD44 splice variants (CD44v) (23, 24). The standard isoform of CD44 (CD44s) has no variant exons, is small, and is nearly ubiquitous in vertebrate cells (25). Even though CD44s, CD44v6 and CD44v4-10, are detected in the human gut epithelium (26), experiments using knock-in mice that express either CD44v4-10 or CD44s isoforms have demonstrated that CD44v isoforms, but not the CD44s isoform, promote adenoma formation in Apc/Min/+ mice (26). CD44v6 acts as a coreceptor for many growth factors and cytokines produced by cells in the tumor microenvironment, including HGF (27), VEGF (28), EGF (29) and TGFβ1 (30, 31). We and others have shown that CD44 receptors can serve as a signaling platform that integrates cellular microenvironmental cues with growth factor and cytokine induced receptor tyrosine kinase or non-tyrosine kinase signals and transduces these signals to membrane-associated cytoskeletal proteins (27, 28, 32–36). This regulates a variety of genes related to apoptosis resistance including MDR1 (37–40), suggesting a mechanism that could explain CIC's chemoresistance.

While cytokines and chemokines within the tumor environment are well known paracrine and autocrine signaling factors, in this study, we have focused on stromal proteins secreted by CAFs whose roles are less understood in the context of the tumor microenvironment associated with CD44v6(+)-CICs. One of the stromal factors is periostin (PN), a matricellular protein (41). It is frequently upregulated in various types of human cancers, including CRC (41–45). PN is observed mainly in tumor stroma and at a minor level in the cytoplasm of cancer cells, and stromal PN has a key role in regulating CIC maintenance and expansion during metastatic colonization by increasing WNT signaling (19). Similarly, CAFs create a chemo-resistant niche in CRC by releasing cytokines, including IL17A, a colorectal CIC maintenance factor (20). Likewise, the functional expression of WNT activity defines CRC stem cells and is regulated by the microenvironment (12, 46). WNT-pathway activation results in nuclear accrual of its main effector protein, β-catenin, which interacts with transcriptional regulators including leukocyte enhancer factor-1 (LEF-1) and T cell factor (TCF), which leads to WNT responsive gene expression (47).

Although much work has been done on molecular structure and tumorigenic functions of CD44v6, most of these functions are contributed by tumor cells instead of CICs. Thus, in this study, we present evidence for the role of CD44v6(+) expressed by CICs in communicating within the tumor microenvironment and in regulating CIC stemness properties to sustain drug resistance, which has not been clearly understood. We showed that FOLFOX therapy induces reorganization of the tumor microenvironment that supports a cellular hierarchy in CRC, enriching the undifferentiated highly tumorigenic CD44v6(+)CIC subpopulation through secreted factors derived from CAFs. We found that human colorectal tumor tissue contains cancer initiating cells defined by CD44v6 expression that are exclusively tumorigenic and highly resistant to standard chemotherapy, and the CIC tumorigenic potential is stimulated significantly. Our data also suggest that combinations of 5-fluorouracil [5-FU], oxaliplatin [OXA], and leucovorin induce reorganization of the tumor microenvironment that supports a cellular hierarchy in CRC, enriching the undifferentiated highly tumorigenic CD44v6(+)CIC subpopulation through secreted factors derived from CAFs. FOLFOX stimulation increased the ability of CAFs to stimulate a relative proportion of fibroblasts to the epithelial component (α SMA versus EpCAM). Subsequently CAFs create a chemo-resistant niche by releasing pre-dominantly PN, WNT3A and IL17A. Exogenous addition of either PN, IL17A or WNT3A increased CIC tumorigenic function and maintenance. Especially, these

Abbreviations: CD44s, Standard isoform of CD44 having no variant exons; CD44v, CD44 splice variant; CD44v6, variant 6 of CD44; PN, periostin; CIC, cancer initiating cell; CAF, cancer initiating fibroblast; CRC, colorectal cancer; 5-FU, 5-fluorouracil; OXA, oxaliplatin; FOLFOX, 5-FU plus OXA plus leucovorin; ALDH1, aldehyde dehydrogenase; LRP6, low-density lipoprotein receptor-related protein; TCF, T-cell factor; LEF, lymphoid enhancer factor; Tf, transferrin; Nano (Tf-PEG-PEI [nanoparticles]); MDR1, multidrug resistance protein 1; IP, immunoprecipitation; WB, Western Blotting; DN, dominant negative; sh, shRNA; SQ, sub cutaneous.

factors were overexpressed by colorectal CAFs in response to FOLFOX with expression validated directly in patient-derived specimens. Periostin and IL17A sustain a WNT3A induced maintenance of CD44v6(+) CICs. Additionally, our data also revealed that the tumorigenic potential of these CICs together with the CAFs subpopulation significantly increased in secondary and tertiary subcutaneous xenograft tumors. In contrast, tumorigenic potential of Non-CICs plus CAFs was completely lost in secondary, tertiary and quaternary subcutaneous xenograft tumors suggesting that non-CICs are differentiated non-tumorigenic cells. These results provide evidence that drug resistance and long-term tumorigenic potential are restricted to the CD44v6 expressing CIC population, and chemotherapy induces remodeling of the tumor microenvironment to support the tumor cellular hierarchy through secreted factors. These results have central clinical significances as most chemotherapeutic methods focus on blocking cell-autonomous mechanisms without reflecting on the crosstalk between CICs and CAFs that may promote the specific CD44v6-signaling required for maintenance of CIC resistance and tumor recurrence through sustained WNT3A/β-catenin/TCF4 signaling.

MATERIALS AND METHODS

Institutional Review Board (IRB) Statement

The Medical University of South Carolina (MUSC) IRB determined that this research project meets the criteria for "Not Human Subjects".

Institutional Animal Care and Use Committee (IACUC) Statement

All animal studies described were approved by the Medical University of South Carolina (MUSC) IACUC (protocol # IACUC – 2019-00829; Approval period 08/03/2020- 09/24/20221) and conducted in accordance with the National Institutes of Health Guide for the Care and Use of Animals.

Materials

Dulbecco's Modified Eagle's Medium (DMEM), Eagle's Minimum Essential Medium (EMEM), McCoy's 5A Medium, F-12K Medium, Leibovitz's L-15 Medium, L- Glutamine, Sodium pyruvate, Penicillin (100 μg/ml) and Streptomycin (100 μg/ml), sodium pyruvate, 0.05% EDTA solution (Versene), Phosphate buffered saline (PBS, Calcium and Magnesium free), and 0.05% Trypsin were from Corning Inc. Fetal Bovine Serum (FBS) was from Atlanta Biologicals. Amphotericin B- Hyclone was from *Thermo Fisher Scientific*, Waltham, MA, USA. Nonidet P-40, EGTA, sodium orthovanadate, glycerol, phenylmethylsulphonyl fluoride, leupeptin, pepstatin A, aprotinin and HEPES were from Sigma-Aldrich, Inc. St. Louis, MO, USA. Recombinant human WNT3A protein (5036-WN) periostin protein (CF 3548-F2), IL-17A protein (CF 317-ILB) were from R&D Systems, Inc. Minneapolis, MN, USA. The anti-Active-β-catenin antibody (05-665, anti-ABC antibody clone 8E7)from Millipore Sigma, Burlington, MA, USA, and the anti- β-catenin antibody (610153, mouse IgG1, BD, Tempe, Arizona, USA) were used for total β-catenin detection in western blotting analysis. The antibodies p-LRP6 (Serine 1490) (#2568, Rabbit IgG), LRP6 (#2560, Rabbit mAb clone C5C7), TCF4 antibody (#2569, Rabbit mAb clone C48H11) were from Cell Signaling Technology, Inc. Danvers, MA, USA. P-Glycoprotein (MDR1) western blotting antibody (PA5-28801, Rabbit Polyclonal against Human) was from Invitrogen-*Thermo Fisher Scientific*, Waltham, MA, USA. β β–Tubulin Antibody (D-10) (sc-5274, Mouse monoclonal IgG_{2b} κ, SCBT), Mouse anti-rabbit IgG-HRP (sc-2357, IgG, SCBT), Rabbit anti mouse IgG-HRP (sc-358914, IgG, SCBT), and Western blotting Luminol reagent (sc-2048, SCBT) were purchased from Santa Cruz Biotechnology Inc., Dallas, Texas, USA. Blocking antibodies for CD44v6 (BBA13, Monoclonal Mouse IgG_1 Clone # 2F10, R&D), and isotype control (MAB002, IgG1, R&D) were from R&D Systems, Inc. Minneapolis, MN USA. The mouse IgG1 antibodies were from R&D Systems, Inc. Minneapolis, MN, USA. Blocking antibody for protein WNT3A (703666) was from R&D Systems, Inc. Minneapolis, MN USA. Rabbit monoclonal IgG clone 1H12L14) was from *Thermo Fisher Scientific.* Waltham, MA, USA. Blocking antibody for periostin (OC-20) was from Adipogen Corporation, San Diego, CA, USA. Blocking antibody for IL17A Monoclonal (eBioMM17F3), and the mouse IgG1 antibodies were from R&D Systems, Inc. Minneapolis, MN USA. pcDNA3-WNT3A-V5 was a gift from Marian Waterman (Addgene plasmid # 35927; http://n2t.net/addgene:35927; RRID : Addgene #3 5927). Periostin cDNA was a gift from Dr. Akira Kudo, School of Dentistry, Showa University, Tokyo, Japan.

Cell Line

SW480(CCL-228) was maintained in Leibovitz's L-15 medium that was purchased from ATCC (Manassas, Virginia, USA) in a humidified atmosphere in the presence of 10% FBS, Penicillin (100 μg/ml) and Streptomycin (100 μg/ml) in 5% CO_2 at 37° C.

Generation of FOLFOX Resistant Cells

To determine the mechanisms of FOLFOX resistance, we selected SW480 cells out of 7 cell lines (as shown in in our companion paper (48), which have low basal levels of CD44v6 gene expression. Using this cell line, we determined the IC_{50} values for 5-Flourouracil (5-FU) and for oxaliplatin (OXA) (as shown in in our companion paper (48), because these molecules are the components of FOLFOX. To determine these IC_{50} values, cells were separately pretreated with various concentrations of 5-FU, or OXA, or vehicle. After a 24-h incubation at 37° C, growth assays were analyzed as described below. The 50% inhibitory concentration (IC_{50}) was identified as a concentration of drug required to achieve a 50% growth inhibition relative to untreated controls. The average IC_{50} value for SW480 cells for 5-FU is 47 μM and for OXA is 9.6 μM. FOLFOX resistance cells were generated by incubating the sensitive parental SW480 cells (SW480-S) with increasing concentrations from 1x FOLFOX (50 μM 5-FU + 10 μM OXA + 1 μM leucovorin) to 5 x FOLFOX over 3 days. This exposure and withdrawal cycle was repeated five times for each dose of FOLFOX. The surviving cells were cultured in normal

medium for 5 days. The resistances of these resistant clones were compared to sensitive pairs by determining the numbers of colonies in soft agar growth with 1x FOLFOX - 5x FOLFOX treatments.

Cell Viability and Apoptosis Assays

Five thousand cells were plated in triplicate into 96-well plates containing appropriate growth media and incubated overnight. After 16 hours growth, cultures were incubated in media containing no serum for 16 hours at 37°C in 5% CO_2, 95% air. Vehicle or chemotherapy drug was added to the plate. In each experiment, a total of five plates (6 wells/treatment) were used. Experiments were repeated 3 times. The growth of the cells was determined by measuring increases in readings of ATP levels for viability (CellTiter-Glo, Promega). Cell apoptosis was determined by the Caspase-Glo® 3/7 assay (Promega) using DEVD-amino luciferin substrate. The luminescent signal is proportional to caspase 3/7 activity and was measured using a luminometer (Perkin Elmer).

Tissue Collection and Isolation of CICs

All human drug resistant human CRC tissues were acquired from primary human colorectal tumor patient specimens undergoing colorectal resection, in agreement with human experimental guidelines and the ethical standards of the institutional review board (IRB). Human protocols were approved by the Institutional Review Board of the Medical University of South Carolina. The IRB has determined that this research project meets the criteria for 'Non Human Subjects' research. Patient-derived (PD) biopsies collected from 5-FU resistant (PD-5FUR), Oxaliplatin (PD-OXAR), and FOLFOX (PD-FR) tumor specimens and our FOLFOX resistant (FR), Oxaliplatin resistant (OXA-R), 5-flurouracil resistant (5-FUR) cell clones. SW480-S (sensitive) cells were maintained through subcutaneous (SQ) xenografts in the flanks of immunocompromised [NOD-SCID/IL2Rγnull (NSG)] mice and in SCID mice, respectively. Fresh tumors from normal colonic tissue and colorectal PD-FR, PD-OXAR, PD-5FUR, SW480-FR, SW480-OXAR, SW480-5FUR, and SW480-S SQ tumors were rinsed with DMEM (Life Technologies) supplemented with 200 units/mL of penicillin, 200 μg/mL of streptomycin, and 4 units/mL of amphotericin B, followed by incubation with 300 units/ml of collagenase (Worthington Biochemical) at 37° C for 3 hours. A single cell suspension was obtained by filtration through a 40 μm filter. After discarding lymphocytes by gradient centrifugation, the cells were processed for sphere formation (see below for methods), and sphere-propagated cells were subjected to fluorescence-activated cell sorting (FACS) buffer [Phosphate-buffered saline (PBS) + 2% BSA + 1 mM EDTA + 0.1% sodium azide], incubated with Fc blocking reagent (Millenia Biotech), and stained with directly conjugated antibodies by incubating on ice for 20 minutes.

Flow cytometry was done in a cell sorter. To enrich for CICs, single cells were labeled with a phycoerythrin (PE)-conjugated monoclonal antibody against CD44v6 (Miltenyi Biotec), and then analyzed for the expression of Fluorescein-5-isothiocyanate (FITC)-conjugated monoclonal antibody against EpCAM (R&D Systems). Purified CD44v6+/EpCAM+ and CD44v6-/EpCAM+ cells from various tumors were cultured separately and grown in fresh CIC growth medium. CICs were cultured in serum-free media with basic fibroblast growth factor (bFGF, 10 ng/ml; R&D Systems) and epidermal growth factor (EGF, 10 ng/ml; R&D Systems) for 2 weeks. Then, the cultured CD44v6+/EpCAM+ and CD44v6-/EpCAM+ cells were subjected to flow cytometric analysis for isolation of CD44v6 +EpCAM+ALDH1+CD133+ (designated as CICs), and CD44v6-EpCAM+ALDH1+CD133+ (designated as Non-CICs) using appropriate fluorescence-conjugated antibodies as described in our companion paper (48). CICs were cultured in serum-free media with basic fibroblast growth factor (bFGF, 10 ng/ml; R&D Systems) and epidermal growth factor (EGF, 10 ng/ml; R&D Systems).

Tissue Collection and Isolation of CAFs

Single cell suspensions from a dissociated FOLFOX resistant (FR) patient colorectal tumor (PD-FR) were sorted by FACS using PDGFR-α-PE and EpCAM-FITC. Percentages of EpCAM (-)/PDGFR-α(+) (CAFs) and EpCAM(+)/PDGFR-α(+) (Non-CAFs) in total unsorted cell populations were quantified. The integrities of EpCAM(-)/PDGFRα(+) gated CAFs from the dissociated CRC cells from the patient colorectal tumors (PD-5FUR, PD-OXAR, PD-FR) and from the sensitive and FOLFOX resistant SW480/SQ tumor tissues were confirmed by QPCR analyses for CAF-associated markers FSP1, FAP, PDGFR-α, and epithelial cell marker EpCAM (negative control). EpCAM (-)/PDGFR-α(+) cells referred to as 'CAFs' were isolated from the indicated tumor tissues. The high PDGFRα positive population was gated in a range of 4–20% (depending on the percentage of the total positive cell population of each sample) of the tail of the positive cells. These EpCAM(-)/PDGFR-α(+) cell populations (CAFs) were cultured in DMEM with 10% BSA for 12 days, and were sorted by FACS using α-SMA-PE and EpCAM-FITC antibodies. The percentages of the sorted α-SMA(+)/PDGFR-α(+) cells in total unsorted CAFs are designated as enrichment of active CAFs. Dead cells were eliminated by using the viability dye DAPI. Isotype controls were used to establish proper gates.

Tumor Sphere Formation

We followed the tumor sphere formation assay protocol from the Creative Bio-array (Shirley, NY, USA). An optimized serum substitute (1 x B27 supplement) (from Creative Bio array) was freshly added to tumor formation medium (500 ml Dulbecco's Modified Eagle Medium/F12) containing 20 ng/ml epidermal growth factor, 10 ng/ml basic fibroblast growth factor, 5 μg/ml insulin, and 0.4% bovine serum albumin. After harvesting the cells, 200 live cells/200 μl of tumor sphere medium were suspended on ice and mixed well for plating. PBS was added to the first and last columns (column 1 and 12) of the 96-well plate to help minimize medium evaporation. This leaves 10 wells available for each row. 200 μL aliquots of the cells were suspended in tumor sphere medium and added into each well

(200 cells per well). For each treatment, CICs were seeded into the wells of 2 rows for a total of 20 wells. Vehicle or 20 ng/ml of WNT3A, or PN, or IL17A, or a chemotherapeutic drug was added. The upper and lower edges of the 96-well plate were sealed with laboratory tape to avoid evaporation of medium, and cells were placed in an incubator set to 37°C and cultured in 5% CO_2 for 10 -14 days. These proteins/cytokines were added in optimum media for 24 hours, and this addition was renewed every 3 days. The medium was changed after 48 hours. After stipulated times of incubation, tumor sphere numbers were counted under a phase-contrast microscope using the 40X magnification lens. Data are presented as a percentage of wells containing tumor spheres compared to the total number of wells.

Cell Lysis, Immunoprecipitation and Immunoblot Analysis

Cells were cultured until they were 75% confluent. They were then washed twice at 4° Cwith phosphate-buffered saline (PBS), and harvested with 0.05% Versene. The cells were pelleted by centrifugation at 5,000 x g for 2 minutes at 4°C. The pellets were treated for 30 minutes with the lysis buffer containing 1% Nonidet P-40, 0.3 M NaCl, 1.5 mM MgCl2, 0.2 mM EDTA, 5 mM sodium orthovanadate, 10% (v/v) glycerol, 100 µg/ml phenylmethylsulphonyl fluoride (PMSF), 1 µg/ml leupeptin, 1 µg/ml pepstatin A, 1 µg/ml aprotinin, and 50 mM HEPES, pH 7.5. For immunoprecipitation, the cell extracts (1 mg total proteins) were precleaned by rotation for 1 h with 20 µl of protein G-Sepharose beads (Santa Cruz, CA). The precleaned supernatant was incubated with antibody needed for each specific experiment overnight. After incubation with 20 µl of protein G-Sepharose beads for 1 h, the suspension was centrifuged, and pellets were washed and collected as immunoprecipitation complexes. Western blotting was done as previously described (31, 49–51). Images were recorded using a luminescent image analyzer, and the intensities of the bands were quantitated by densitometry (NIH Image J software). Each protein was analyzed in samples from at least three independent experiments from each set of tumor cells, CICs and CAFs.

Lipid-Raft Isolation

All procedures were done at 4° C. Cells were scraped into buffer containing 1% cold Triton X-100 buffer (20 mM Tris-HCl, pH 7.4, 150 mM NaCl, 1% Triton X-100, 1% deoxycholate, 0.1% sodium dodecyl sulfate [SDS], 1 mM EGTA, 1 mM sodium orthovanadate with a cocktail of protease inhibitors at final concentrations of 0.2 mM aminoethyl-benzene sulfonyl fluoride, 1 µg/ml aprotinin, 3 µM E-64, 10 µg/ml leupeptin, 2 µM pepstatin, and 50 µg/ml calpain inhibitor I) and lysed on ice for 30 minutes. After centrifugation at 800 x g to remove nuclei and cell debris, lysates were subjected to sucrose gradient fractionation as described previously (52). An equal volume of each fraction was boiled in SDS-Lammeli sample buffer and subjected to western blotting analyses as described previously (30, 31, 49, 50, 53, 54). On the other hand, the Triton-insoluble rafts and Triton-soluble fractions were diluted with an equal volume of extraction buffer (25 mM HEPES, pH 7.6, 0.3 M NaCl, 1.5 mM MgCl2, 0.2 mM EDTA, 1% Nonidet P-40, and 0.5 mM dithiothreitol) and subjected to immunoprecipitation as described previously (31, 49, 55, 56).

Biotin Labelling of Cell Surface Receptors and Internalization Assays

For cell surface protein labelling, cells were treated in the presence or absence of FOLFOX or WNT3A conditioned media at 37°C for the times indicated and washed three times with ice-cold phosphate-buffered saline (PBS; pH 8.0) to remove any contaminating proteins. Biotinylation followed by immunoprecipitation and western blotting was done as described in our companion paper (48). For internalization assays, cell surface proteins were biotin-labelled as described in our companion paper (48). The amounts of receptor bound to beads were determined by SDS–PAGE and immunoblot analysis.

Transient Transfection and Luciferase Reporter Assay

For the transient assays, 1.0 x 10^5 cells were transfected using Lipofectamine LTX 2000 (Invitrogen) with 1 µg of each Luciferase construct and 100 ng of pRL-SV40 vector (Promega), according to the manufacturer's instructions. Firefly and Renilla Luciferase activities were measured in cell lysates 48 hours after transfection using the DualGlo Luciferase Assay System (Promega) on a Veritas TM Microplate Luminometer (Perkin-Elmer) following the manufacturer's protocol and as shown in our companion paper and as described previously (48, 55). All experiments were done in triplicate. Ratios of Renilla luciferase readings to firefly luciferase readings were taken for each experiment, and triplicates were averaged. The average values of the tested constructs were normalized to the activity of the empty pGL3-basic vector, which was arbitrarily set at value 1.

β-Catenin/TCF Reporter Assays

All reporter gene assays were done in 96-well plates. PD-FR/CICs or CD44v6 overexpressing SW480-FR/SQ/Non-CICs (Non-CICs/CD44v6) (1.0 × 10^4/well) were transfected with Super TOPFlash reporter (25 ng) and TK-Renilla (5 ng), and with the respective plasmid DNA as indicated using Lipofectamine™ 3000 transfection reagent according to the manufacturer's protocol. Each transfection was adjusted to 150 ng DNA/transfection with pcDNA3.1 empty vector. Where indicated, cells were transfected at 50–70% confluency with shRNA constructs using Lipofectamine™ 3000 transfection Reagentin 6 cm petri dishes according to the manufacturer's protocol 24 h before seeding the cells for the reporter assays. 50 ng/ml of WNT3A was added 24 h after DNA transfection. Cells were lysed 72 h after DNA transfection with 1 × Passive Lysis Buffer (Promega), and the luciferase activity was measured using the Luminescence counter (PerkinElmer). TOPFLASH experiments were normalized to co-transfected Renilla gene expression. In parallel to the reporter assay, transfected CICs and Non-CICs/CD44v6 cells were subjected to western blotting

analysis to detect the proteins involved in CD44v6-β-catenin-MDR1 signaling.

RNA Extraction and cDNA Synthesis

RNA extraction and cDNA synthesis were done following published work (57). Total RNA was isolated from cells using the RNeasy mini kit (Qiagen) according to the standard protocol provided by the manufacturer, with on-column DNA digestion. Five hundred ng of RNA was used for cDNA synthesis. One µl primer, 1 µl buffer (from 10X ezDNase™ Buffer), 0.5 µl RNase inhibitor, 1 µl dNTP (10 mM) and 0.5 µl Reverse Transcriptase (Thermo Fisher Scientific) and 6 µl Nuclease-free Water were mixed in a microtube (0.2 ml) to make 10 µL DNA digestion reaction mix for each RT-PCR reaction for cDNA synthesis. The synthesis was done at 50° C for 60 minutes in a thermal cycler (Bio Rad).

Primer Design and Semiquantitative RT-PCR

Design of primers and semiquantitative RT-PCR were performed following published works (55, 57, 58). Primers were designed by online Primer Quest Tool (https://www.idtdna.com/PrimerQuest/Home/Index). The quality of designed primers was analyzed by Oligoaniline Tool software. The semi-quantitative PCR primer sequences used for CD44 exon specific PCR are given in **Tables 1**, **2**. The semiquantitative PCR primer sequences used for proteins and cytokines of CAFs are presented in **Table 3**. Semi-quantitative PCR was done using different amounts of cDNA of RNA samples. One µl of forward (F) and of reverse (R) primers were used. For each sample, PCR was repeated three times. The reaction contained 1 µl of each cDNA sample, 0.5 µl of each primer, 5 µl Taq DNA Polymerase 2× Master Mix Red (Amplicon Co.) and 3 µl dd water in a final volume of 10 µl. Before the main reactions, the PCR conditions, including thermal conditions, and the number of cycles and the cDNA concentrations, were optimized. During the main PCR cycles, temperature conditions included one initial denaturation cycle (3 min at 95° C) followed by 35 cycles with a denaturation step for 5 sec at 95°C and a combined annealing and extension step for 35 sec at 61°C. The PCR products were electrophoresed on agarose 2.5%, stained with ethidium bromide and photographed. The analysis of band intensities was done by ImageJ software.

Primer Design and Quantitative Real-Time RT–PCR

Design of primers and RT–qPCR were done following previously described protocols (55, 58). Total RNA was isolated from cells after various treatments and transfections as described in the figure legends for each specified experiment using the RNeasy mini kit (Qiagen) according to the standard protocol provided by the manufacturer, with on-column DNA digestion. RNA integrity and concentration were analyzed using Bioanalyzer, and 100 ng of RNA was retrotranscribed into cDNA using the First Strand cDNA synthesis kit from Roche Applied Science (Qiagen). SYBR Green technology (Bio-Rad) was used for all real-time PCR experiments. Amplification was done with the real-time PCR analyzer (Bio-Rad). The PCR mixture (25 µl) contained 12.5 µl of 2 SYBR Green PCR Master Mix (Bio-Rad), 5 µl of diluted RT product (1:20), and 0.5 µM sense and antisense primer sets. The real-time PCR assays were done in three individual experiments with duplicate samples using standard conditions in a CFX96 real-time PCR detection machine. After incubations at 95° C for 3 minutes, the amplification protocol consisted of 50 cycles of denaturing at 95° C for 10 sec, followed by annealing and extension at 60° C for 30 sec. The standard curve was made from a series dilution of template cDNA. Expression levels of tested genes were calculated after normalization with the housekeeping gene *GAPDH* or β-actin. The QPCR primers used in this study in analyses of various genes associated with fibroblast specific markers as well as for PN, IL17A and WNT3A, are presented in **Table 4**. The QPCR primers used in this study in analyses of various genes associated with CIC stemness factors are presented in **Table 5**.

RNA Silencing and Confirmation of the Specificity of shRNA

For determining shRNA sequences, coding nucleotide sequences were used of the genes obtained from the National Institutes of Health database, website (www.ncbi.nlm.nih.gov). The hairpin shRNAs to target transcript sequences were designed using the Broad Institute GPP Web Portal (http://portals.broadinstitute.org/gpp/public/). The sequences for cloning in pSico/pSicoR vectors were designed following instructions described in the Jackson Lab website (http://web.mit.edu/jacks-lab/protocols). The resulting pSicoR-CD44v6 shRNA1 (CD44v6 sh1), pSicoR-CD44v6 shRNA2 (CD44v6 sh2), pSicoR-WNT3A shRNA1 (WNT3A sh1), pSicoR-WNT3A shRNA2 (WNT3A sh2) transfectants constitutively silence respectively CD44v6, WNT3A and β-catenin RNAs in the cells. The pSicoR-Non targeted shRNA (NT sh) was used as a control to the above shRNA transfectants for shRNA sequences used in this study. The specificities of the prepared shRNAs were confirmed (31, 49) as described in our companion paper (48). The primers for various shRNAs used in this study are given in **Table 6**.

Chromatin Immunoprecipitation (ChIP) Assay

The chromatin immunoprecipitation (ChIP) assay was done using the ChIP assay kit (Upstate Biotechnology) following the manufacturer's directions (44). Details of the ChIP assay and the primers used for ChIP PCR studies are presented in **Table 7**, and were described in our companion paper (48).

In Vivo Tumorigenic Potential of the CAFs to Affect the Tumorigenic Capacity of CICs

CICs and CAFs were isolated from subcutaneous SW480-FR/SQ xenografts in SCID mice (using an approved IACUC protocol). Tumorigenic potentials of CICs alone or in combination with CAFs (DMSO or FOLFOX treated) were determined by subcutaneous implantation in the flanks of six-week-old SCID female mice from the Jackson Laboratory. The CAFs were

TABLE 1 | CD44 exon specific PCR examined using 5' primers complementary to individual variable exons and a primer to the 3' constitutive exon 7.

Genes	Accession number	Primers	
		Forward sequence (5'-3')	Reverse sequence (5'-3')
C_5		AAGACATCTACCCCAGCAAC	
C_7			TTTGCTC CACCTTCTTGACTCC
h-CD44V2	NM_001001389.2	GAT GAG CAC TAG TGC TAC AG	TTTGCTCCACCTTCTTGACTCC
h-CD44V3	NM_001001390.2	ACG TCT TCA AAT ACC ATC TC	TTTGCTCCACCTTCTTGACTCC
h-CD44V4	NM_001001391.2	TCA ACC ACA CCA CGG GCT TT	TTTGCTCCACCTTCTTGACTCC
h-CD44V5	NM_00100139.2.2	GTA GAC AGA AAT GGC ACC AC	TTTGCTCCACCTTCTTGACTCC
h-CD44V6	NM_001202555.2	CAG GCA ACT CCT AGT AGT AC	TTTGCTCCACCTTCTTGACTCC
h-CD44V7	NM_001202556.2	CAG CCT CAG CTC ATA CCA G	TTTGCTCCACCTTCTTGACTCC
h-CD44V8	NM_001202557.2	TCC AGT CAT AGT ACA ACG CT	TTTGCTCCACCTTC TTGACTCC
h-CD44V9	XM_011520485.2	CAG AGC TTC TCT ACA TCA CA	TTTGCTCCACCTTCTTGACTCC
h-CD44V10	XM_005253238.3	GGT GGA AGA AGA GAC CCA AA	TTTGCTCCACCTTC TTGACTCC
h-C044C5V6		ATCCCTGC TACCATCCAGGCAAC	TTTGCTCCACC TTCTTGACTCC
h-CD44s	X155 150 (EMBL/Genebank)	AAGACATCTACCCCAGCAAC	TTTGCTCCACCTTCTTGACTCC
h-GAPDH	NM_002046.7	ACC ACA GTC CAT GCC ATC A	TCC ACC ACC CTG TTG CTG TA

treated with DMSO or FOLFOX (50 μM 5-FU + 10 μM OXA + 1 μM leucovorin) for 3 days. Tumorigenic potentials of CICs alone (4 x 10 ^{3}), or CICs (4 x 10^3) + CAFs (4 x 10^4) pre-treated with DMSO, or CICs (4 x 10^3) + CAFs (4 x 10^4) pre-treated with FOLFOX were determined by SQ implantation as described above. Twenty-five mice per cell types were used. The appearances of tumors were monitored, and five mice were sacrificed every 2 weeks. Tumors were removed and weighed to evaluate the tumor development (**Figure 8**).

In Vivo Evaluation of the CIC Tumor Growth Dependence on PN, WNT3A, IL17A and CD44v6

CICs (2 x 10^4) and CAFs (6 × 10^4) together were implanted subcutaneously (SQ) into immunocompromised mice (using an approved IACUC protocol). When tumors reached ~0.3 cm^3 in volume, treatment was initiated. Four arms were included: 1) isotype control (2 mg/kg antibody, 3 times/wk for 2 wks followed by 1 time/wk for 2 wks); 2) FOLFOX chemotherapy alone (1x FOLFOX, 3 times/wk for 2 wks, followed by 1 time/wk for 2 wks); 3) PN, or IL17A, or WNT3A, or CD44v6 blocking antibody therapy alone (2 mg/kg antibody, 3 times/wk for 2 wks, followed by 1 time/wk for 2 wks); and 4) a combination of the blocking antibodies and FOLFOX chemotherapy (5 mice per each time point, 0 wk, 2 wks, 4 wks and 6 wks). Mice were weighed, and the tumor volumes were measured by caliper every other day for 6 weeks. Every two weeks mice were sacrificed, and tumors were collected.

Conditional Knockdown of CD44v6

To test whether CD44v6 is a good therapeutic target, an *in vivo* approach to deliver shRNA specifically targeting CD44v6 was developed. Two vectors (floxed pSico-CD44v6shRNA + pFabpl-Cre) were engineered and encapsulated into transferrin (Tf)-coated nanoparticles (59, 60). The shRNA vectors are inherently inactive due to the presence of a Lox-Stop-Lox cassette prior to the start codon. When injected intraperitoneally (i.p.), there is ubiquitous cellular uptake of these vectors. However, only cells expressing FABPL (i.e. intestinal epithelium specific) will express the Cre protein and activate the shRNAs. First, we prepared transferrin (Tf)-PEG-PEI nanoparticles and encapsulated both plasmids (floxed pSico-CD44v6shRNA + pFabpl-Cre) into them following our published procedure (59). Our pSico-CD44v6shRNA in SW480-FR cells was validated in **Figure 9**.

Preparation of Transferrin (Tf)-Coated PEG-PEI (Nanoparticle)

The transferrin (Tf)-PEG-PEI/Nanoparticle (Nano) was prepared as validated in our previous studies (31, 49, 59). Briefly, transferrin was linked with N-hydroxy succinimide/

TABLE 2 | CD44 exon specific PCR examined using 3' primers complementary to v6 and vs exons and a primer to the 5' constitutive exon 5.

Genes	Accession number	Primers	
		Forward sequence (5'-3')	Reverse sequence (5'-3')
C_5		CATCCCAGACGAAGACAGTC	
h-CD44V6	NM_001202555.2		CAG GCA ACT CCT AGT AGT AC
h-CD44V8	NM_001202557.2		GTIGTCATTGAAAGAGG TCCT
h-CD44s	X155150 (EMBL/Genebank)	CATCCCAGACGAAGACAG TC	TTIGCTCCACCTTCTTGACTCC
h-GAPDH	NM_002046.7	ACC ACA GTC CAT GCC ATC A	TCC ACC ACC CTG TIG CTG TA
C_7			TTIGCTCCACCTTCTTGACTCC

TABLE 3 | Semiquantitative RT-PCR primers for Cytokines, growth factors, PN and relates receptors.

Genes	Accession number	Primers	
		Forward sequence (5'-3')	Reverse sequence (5'-3')
IL-17A	NM_002190.3	AGATTACTACAACCGATCCACCT	GGGGACAGAGTTCATGTGGTA-
IL-17R	NM_014339.7	AGTTCCACCAGCGATCCAAC	GTCTGAGGCAGTCA TIGAGGC
I L-23A	NM_016584.3	CTCAGGGACAACAGTCAGTIC	ACAGGGCTATCAGGGAGCA
IL-23R	NM_ 144701.3	ACATGCTTCTATGTACTGCACTG	TGTGTCTATGTAGGTGAGCTICC
RORα	NM_134261.3	CTTGCCGTAGGGATGTCTCG	GAAGTTCCGTCAGC CCGTI
Periostin	NM_006475.3	CTCATAGTCGTATCAGGGGTCG	ACACAGTCGTITICTGTCCAC
Integrin b1	NM_002211.4	CCTACTTCTGCACGATGTGATG	CCTTTGCTACGGTTGGTTACATI
PDGF α	NM_002607.6	GCAAGACCAGGACGGTCATTI	GGCACTTGACACTG CTCGT
TGFβ1	NM_000660.7	GGCCAGATCCTGTCCAAGC	GTGGGTTTCCACCATIAGCAC
TGFβ2	NM_001135599.4	CCATCCCGCCCACTTTCTAC	AGCTCAATCCGTIGTTCAGGC
G-CSF	X03438.1	GCTGCTTGAGCCAACTCCATA	GAACGCGGTACGACACCTC
WNT3A	NM_033131.4	AGCTACCCGATCTG GTGGTC	CAAACTCGATGTCCTCGCTAC
WNT5A	NM_003392.7	ATTCTTGGTGGTCGCTAGGTA	CGCCTTCTCCGATGTACTGC
SDF-1	AY874118.1	ATTCTCAACACTCCAAACTGTGC	ACTTTAGCTTCGGGTCAATGC
EGF	NM_001963.6	TGGATGTGCTIGATAAG CGG	ACCATGTCCTTTCCAGTGTGT
HGF	NM_000601.6	GCTATCGGGGTAAAGACCTACA	CGTAGCGTACCTCTGGATTGC
FGF	NM_000800.5	ACACCGACGGGCTTITATACG	CCCATTCTTCTIGAGGCCAAC
IL1β	NM_000576.3	AGCTACGAATCTCCGACCAC	CGTTATCCCATGTGTCGAAGAA
IL4	NM_000589.4	CCAACTGCTICCCCCTCTG	TCTGTIACG GTCAACTCGGTG
IL8	M28130.1	TTTTGCCAAGGAGTG CTAAAGA	AACCCTCTG CACCCAGTITIC
TNFα	NM_000594.4	CCTCTCTCTAATCAGCCCTCT	GAGGACCTGGGAGTAGATGAG
VEGFA	NM_001171623.2	AGGGCAGAATCATCACGAAGT	AGGGTCTCGATTGGATGGCA
IFNγ	NM_000619.3	TCGGTAACTGACTTGAATGTCCA	TCGCTTCCCTGTITIAGCTGC
PGE2	NM_004878.5	GTGACCGAGTICGG CAATAAG	CGGACAATGTAGTCAAAGGACG
IGF1	NM_001111283.3	GCTCTTCAGTICGTGTGTGGA	GCCTCCTIAGA TCACAG CTCC
IGF1R	NM_000875.5	TCGACATCCGCAACGACTATC	CCAGGGCGTAGTIGTAGAAGAG
CD44v6	NM_001202555.2	CTGCCGCTTTGCAGGTGTA	CATTGTGGG CAAGGTGCTATI
COX2	M90100.1	TAAGTGCGATIGTACCCGGAC	TTTGTAGCCATAGTCAGCA TIGT
FLT	NM_002019.4	GAAAACGCATAATCTG GGACAGT	GCGTGGTGTGCTTATTTGGA
MCP-1	NM_002982.4	CAGCCAGATGCAATCAATGCC	TGGAATCCTGAACCCACTICT
STAT3	NM_139276.3	CAGCAGCTTGACACACGGTA	AAACACCAAAGTGGCATGTGA
GAPDH	NM_002046.7	GGAGCGAGATCCCTCCAAAAT	GGCTGTTGTCATACTTCTCATGG

PEG/maleimide and then allowed to react with a mercaptopropionate-modified branched PEI to form Tf-PEG-PEI (59). The pSico-CD44v6 shRNA, or pFabpl-Cre plasmid were jointly encapsulated in the purified Tf-PEG-PEI conjugate (size: ~80 ± 31 nm).

Validation of pSico-CD44v6shRNA in Cells

In order to use shRNA for target genes in *in vivo* experiments, pSicoR-CD44v6 shRNA, pSicoR-WNT3A shRNA, and pSicoR-β-catenin shRNA were prepared as described in our previous study (59) in the RNA silencing section. The abilities of pSico and pSicoR vectors to conditionally silence endogenous CD44v6 genes were demonstrated by their ability to inhibit expression of the human CD44v6 expressionin SW480-FR cells (**Figures 9A–C**, and **Figures 9D–F**). PCR was done to amplify the recombined and unrecombined genomic plasmid DNAs from SW480-FR cells.

TABLE 4 | Real-time PCR (QPCR) primers for various genes used in this study.

Genes	Accession number	Primers	
		Forward sequence (5'-3')	Reverse sequence (5'-3')
IL17A	NM_002190.3	AAGACCTCATTGGTGTCACTGCTAC	ATCTCTCAGGGTCCTCATTGCG
Periostin	NM_006475.3	TGTTGCCCTGGTTATATGAG	ACTCGGTGCAAAGTAAGTGA
WNT3A	NM_033131.4	GGATACTTCTTACTCCTCTGCAG	AATGGCGTGGACAAAGGCCGACT
PDGFR α	NM_006206.6	GGTGGTCACAGGTG	CTTAAGGCTCTCAGGA
EpCAM	NM_002354.3	GCCAGTGTACTTCAGTTGGTGC	CCCTTCAGGTTTTGCTCTTCTCC
FAP	NM_004460.5	TGTGCATTGTCTTACGCCCT	CCGATCAGGTGATAAGCCGT
FSP1	NM_002961.3	TTGGGGAAAAGGACAGATGAAG	TGAAGGAGCCAGGGTGGAAAAA
α-SMA	NM_001100.4	CTATGCCTCTGGACGCACAACT	CAGATCCAGACGCATGATGGCA
GAPDH	NM_002046.7	GAAGGTGAAGGTCG	CTTCCCGTTCTCAG
β-actin	NM_001904.4	AGAAAATCTGGCACCACACC	AGAGGCGTACAGGGATAGCA

TABLE 5 | Real-time PCR (QPCR) primers for various genes associated with CICs stemness functions.

Genes	Primers	
	Forward sequence (5'–3')	Reverse sequence (5'–3')
SOX-2	GGACTGAGAGAAAGAAGAGGAGAG	CGCCGCCGATGATTGTTATTA
OCT4	GGAGGAAGCTGACAACAATGA	CTCTCACTCGGTTCTCGATACT
c-MYC	AAGCTGAGGCACACAAAGA	GCTTGGACAGGTTAGGAGTAAA
TWIST1	AGACTCTGGAGCTGGATAACT	GCCTGTCTCGCTTTCTCTTT
ALDH1	CTTGGAATTTCCCGTTGGTTATG	GAGAGCAGTGAGAGGAGTTTG
MDR1	TGCTGGTTGCTGCTTACA	GCCTATCTCCTGTCGCATTATAG
CD44v6	GACAGAATCCCTGCTACCAATAG	TCCTTCGTGTGTGGGTAATG
GAPDH	GAAGGTGAAGGTCG	CTTCCCGTTCTCAG
β-actin	AGAAAATCTGGCACCACACC	AGAGGCGTACAGGGATAGCA

*Validation of pSico-CD44v6shRNA in Cells In order to use shRNA for target genes in in vivo experiments, pSicoR-CD44v6 shRNA, pSicoR-WNT3A shRNA, and pSicoR- b-catenin shRNA were prepared as described in our previous study (59) in the RNA silencing section. The abilities of pSico and pSicoR vectors to conditionally silence endogenous CD44v6 genes were demonstrated by their ability to inhibit expression of the human CD 44 v6 expressionin SW 480- FR cells (**Figures 9A–C**, and **Figures 9D–F**). PCR was done to amplify the recombined and unrecombined genomic plasmid DNAs from SW480-FR cells.*

In Vivo Distribution of shRNA in Tissues

Distributions of shRNA against the firefly luciferase gene (pSico-Firefly luciferase shRNA/Nano) plus pFabpl-Cre/Nano were determined in various organs of C57Bl/6 mice (n = 4) that were previously injected (i.p.) with reporter plasmids expressing firefly luciferase and renilla luciferase. Twelve hours after their injection, pSico-Firefly luciferase shRNA/Nano plus pFabpl-Cre/Nano were injected (i.p.) Thirty-six hours later, cells from SQ tumors, intestine, colon, kidney and liver tissues were lysed, and the ratios between firefly and renilla luciferase activities were calculated. Distributions of the tissue specific delivery of luciferase-shRNAs were determined by measuring activities of luciferase-shRNA in various tissues as indicated above. Three independent experiments were performed. Western blot analyses of extracts from the various treated tumors collected at the end of the experiment were analyzed for CD44v6 and MDR1 expressions (β-tubulin was used as an internal standard).

In Vivo Targeting of CD44V6 by Genetic Modification to Inhibit CICs Tumor Growth in Mice

Study design: 2 x 10^4 CICs and 6 × 10^4 CAFs were isolated from SW480-FR SQ tumors, and PD-FR tumor specimens were implanted together into 8-week-old female SCID mice and NSG mice. When tumors reached ~0.3 cm^3 in volume, treatment was initiated. Ten arms were included: Group 1: [(100 μg) of pSico NT shRNA-Nano (3 x per wk for 4 wks)]; Group 2: [(100 μg) of pFabpl Cre-Nano (3 x per wk for 4 wks)]**;** Group 3: 1 x FOLFOX [(3 x per wk for 4 wks)] with pSico NT shRNA-Nano (3 x per wk for 4 wks)]**;** Group 4: 1 x FOLFOX [(3 x per wk for 4 wks] with pFabpl Cre-Nano (3 x per wk for 4 wks); Groups 5, 7, and 9: (pSico v6 shRNA plus Fabpl Cre)-Nano [(each plasmid 20 μg, Group 5); (each plasmid 50 μg, Group 7); (each plasmid 100 μg, Group 9) (3 x per wk. for 4 wks)]; Groups 6, 8 and 10: ([pSico v6 shRNA plus Fabpl Cre]-Nano + 1 x FOLFOX [3 x per wk for 4 wks]); [(each plasmid 20 μg plus FOLFOX, Group 6); (each plasmid 50 μg plus FOLFOX, Group 8); (each plasmid 100 μg plus FOLFOX, Group 10) (3 x per wk. for 4 wks)]. Seven SCID mice per group were used. Mice were weighed every other day, and the tumor volumes were measured by caliper every day. Mice were sacrificed every week for 4 weeks, and tumor weights were taken.

Statistics

A two-tailed Student's t-Test was used to compare mean value between sensitive and resistant cells using the following parameters: mean ΔΔCT values for QPCR; mean colony number for soft agar growth assays; mean densitometry values for QPCR and WB; mean percentage of cell viability assay (CellTiter-Glo) and FACS analysis; mean luminescence for ATP activity in cell growth, Caspase Glow assays in Apoptosis measurements; and mean tumor weight in xenograft studies. Chi-squared analysis was used to compare incidences between sensitive and resistant cells for the following assays: number of positive wells containing tumor spheres in the sphere formation assay, and numbers of mice developing tumors in xenograft studies. For experiments involving three or more groups, statistical significance was calculated with GraphPad Prism Software (version 8) using a 1-way or 2-way ANOVA with a Bonferroni's posttest, Student's *t* test, or log-rank (Mantel-Cox) test where appropriate (Graph-Pad Software Inc.). Data are represented as the mean ± SD.

Ethics Statement

The animal study was approved by the Institutional Animal Care and Use Committee (IACUC) at the Medical University of South Carolina (MUSC). Procedures for animal studies were conducted in accordance with the National Institutes of Health Guide for the Care and Use of Animals IACUC-2017-00250 (approval date: 2019/03/14-2021/03/29).

Data Availability Statement

All the data are included within the manuscript. The names of the repository/repositories and accession number(s) can be found in the article supporting information. Coding nucleotide sequences of the genes were obtained from the NCBI, National Institutes of Health, website (www.ncbi.nlm.nih.gov). Hairpin shRNAs were designed to target a transcript sequence using the Broad Institute GPP Web Portal (http://portals.broadinstitute.

TABLE 6 | shRNA sequence in pSico and pSicoR vectors (https://web.mit.edu/jacks-lab/protocols/).

Genes	Primers	
	Sense sequence (5'-3')	Antisense sequence (5'-3')
CD44v6 shRNA1	TCCTCCCAGTATGACACATATTTTCAAGAGAAATATGTGTCATACTGGGAGGTTTTTTC	TCGAGAAAAAAACCTCCCAGTATGACACATATTTCTCTTGAAAATATGTGTCATACTGGGAGGA
CD44 shRNA2	T GGACCAATTACCATAACTATTTCAAGAGA AATAGTTATGGTAATTGGTCCTTTTTTC	TCGAGAA AAAAGGACCAATTACCATAACTATTTCTCTTGAAAATAGTTATGGTAATTGGTCCA
WNT3A shRNA 1	TGTAGCGAGGACATCGAGTTTGTTCAAGAGACAAACTCGATGTCCTCGCTACTTTTTTTC	TCGAGAAAAAAGTAGCGAGGACATCGAGTTTGTCTCTTGAACAAACTCGATGTCCTCGCTACA
WNT3A shRNA 2	TGAACTACGTGGAGATCATGCTTCAAGAGAGCATGATCTCCACGTAGTTCCTTTTTTTC	TCGAGAAAAAAAGGAACTACGTGGAGATCATGCCTCTTGAACATGATCTCCACGTAGTTCCA
βcatenin shRNA 1	TATCTGTCTGCTCTAGTAATAATTCAAGAGATTATTACTAGAGCAGACAGATTTTTTTC	TCGAGAAAAAAATCTGTCTGCTCTAGTAATAATCTCTTGAATTATTACTAGAGCAGACAGATA
βcatenin shRNA 2	TTCTAACCTCACTTGCAAATAATTTCAAGAGAATTATTGCAAGTGAGGTTAGATTTTTTC	TCGAGAAAAAAATCTAACCTCACTTGCAATAATTCTCTTGAAATTATTGCAAGTGAGGTTAGAA
Caveolin-1 shRNA1	TACCTTCACTGTGACGAAATATTCAAGAGA TATTTCGTCACAGTGAAGGTGTTTTTTC	TCGAGAAAAAAACACCTTCACTGTGACGAAATATCTCTTGAATATTTCGTCACAGTGAAGGTGA
Caveolin-1 shRNA2	T ACCTTCACTGTGACGAAATATTCAAGAGA TATTTCGTCACAGTGAAGGTG TTTTTTC	TCGAGAAAAAAATCAACTTGCAGAAAGAAATATCTCTTGAATATTTCTTTCTGCAAGTTGATA
Clathrin shRNA1	TTGACTATGGAGTCTGACAAATTTCAAGAGA ATTTGTCAGACTCCATAGTCA TTTTTTC	TCGAGAAAAAATGACTATGGAGTCTGACAAATTTCTCTTGAAAATTTGTCAGACTCCATAGTCAA
Clathrin shRNA2	TACTATGGAGTCTGACAAATTTTCAAGAGA AATTTGTCAGACTCCATAGTC TTTTTTC	TCGAGAAAAAAGACTATGGAGTCTGACAAATTTCTCTTGAAAATTTGTCAGACTCCATAGTCA
Firefly luciferase shRNA1	TGCCCTGGTTCCTGGAACAATTTTCAAGAGA AATTGTTCCAGGAACCAGGGCTTTTTTC	TCGAGAAAAAAGCCCTGGTTCCTGGAACAATTTTCTCTTGAAAATTGTTCCAGGAACCAGGGCA
Firefly luciferase shRNA2	TTGAGTATTTCTGTCTGATTTTTCAAGAGA AATCAGACAGAAATACTCAC TTTTTTC	TCGAGAAAAAAGTGAGTATTTCTGTCTGATTTTCTCTTGAAAATCAGACAGAAATACTCACA

org/gpp/public/). Primers were designed by online Primer Quest Tool (https://www.idtdna.com/PrimerQuest/Home/Inde.

RESULTS

FOLFOX-stimulated Enrichment of CAFs Promotes Expression of CD44v6, Which Defines Highly Tumorigenic Potential of CICs

The majority of studies indicate that cancer stem cells (CSCs) in solid tumors divide symmetrically, do not display multipotency, and are unable to generate an entire array of lineages (61). Subsequently, the CSCs are termed as cancer initiating cells (CICs) to define this subset of cells with self-renewal and tumorigenic potential (62, 63). Furthermore, the hierarchical model suggests that the CIC is the cell-of-origin of tumor cells. During cancer treatment, chemotherapy inflicts strong selective pressures on cancer cells to gain characteristics that promote the recruitment of pro-tumorigenic tumor microenvironment cells. Chemotherapeutics modulate the composition, or function of the tumor microenvironment cells thereby further altering the selective pressures to which cancer cells are exposed. This promotes resistance to apoptosis through the ECM adhesion proteins, integrins and CD44/CD44v6, which integrates cellular microenvironmental cues with stromal-secreted growth factors and cytokines including WNT, IL-6, IL17A, SDF-1, HGF, FGF, and TGF-ß leading to the activation of several tumor survival pathways (48). We therefore generated FOLFOX resistant (FR) CRC cells from their sensitive (S) pairs (see details in preparing these FR cells described in materials and methods and in our companion paper (48). Next, the responses of CAFS from biopsies of a group of colorectal patients resistant to 5-FU (PD-5FUR), Oxaliplatin (PD-OXAR), FOLFOX (PD-FR) and their sensitive pairs of CRC cells derived from SQ tumors were analyzed. Viable CAFs were isolated from freshly resected PD-colon tumor tissues and from SQ/FR and SQ/S tumor samples by FACS using platelet-derived growth factor receptor-α (PDGFR-α) and EpCAM antibodies (**Figure 1A**). Data in **Figure 1B** show that unsorted PD-FR cells contain ~20% of EpCAM (–)/PDGFRα(+) (hereafter referred to as CAFs) and slightly more than 20% EpCAM(+)PDGFRα(+) cells (henceforth referred to as Non-CAFs). The PD/SQ-derived and FR/SQ tumor-derived CAFs expressed high levels of fibroblast mRNA markers (via QPCR analyses) αSMA, PDGFRα and FAP, but very little or no epithelial cell marker EPCAM (**Figure 1C**). The data in **Figure 1C** also demonstrated that fibroblast markers, including αSMA and PDGFRα, increased in FOLFOX resistant (FR) cells. Moreover, the basal level of αSMA in all indicated CAFs isolated from chemo-resistant colon tumors significantly increased compared to CAFs isolated from the corresponding sensitive (S) SQ tumor cells (**Figure 1C**). **Figure 1D** shows quantitative measures of the fibroblast component α-SMA versus the epithelial component EpCAM with or without FOLFOX treatment (measured by FACS sorting). The results show that CAFs derived from SQ/FR tumor cells enrich the

TABLE 7 | ChIP PCR primers for MDR1 and CD44v6 promoters.

Genes	Primers	
	Forward sequence (5'–3')	**Reverse sequence (5'–3')**
MDR1 (A) [-644- (-447)]	TAGGTCTTTCCACTAAAGTC	AGAGGACTTCACACTATCCA
MDR1 (B) [-1218- (-980)]	TTTCTTTCATTCCATTTATC	AAGTCTTCATATCCATATAA
MDR1 (C) [-1301- (-1056)]	AATGTAAGAATTTAAAATGC	CTTTGAAAAGGCTAGGAGAA
CD44v6 (A) [-1618- (-1370)]	AGAAGTCCTGGCATGGTTCC	TCTTCAGGGGAAGCCTTTTGA
CD44v6 (B) [-1997- (-1793)]	GGATGACTTACTTGTCCCTGT	ACTCACAAGCAGGCCATTACCA

proportion of fibroblasts to the epithelial component (αSMA/EpCAM), compared to SQ/5-FUR, SQ/OXAR and SQ/S tumor cells. The αSMA versus EpCAM ratio is further increased with FOLFOX treated CAFS in all the tumor types (**Figure 1D**), confirming that CAFs are enriched in post-FOLFOX therapy on tumors.

CD44v6 Expression Establishes a Highly Tumorigenic Colorectal Population

It has been previously demonstrated that colorectal CICs are enriched in tumor spheres or in freshly fractionated ALDH(+), or CD133(+), or EpCAM(+) cells (48, 55, 64). Moreover, since ALDH, CD133 and EpCAM are well known colorectal CIC markers (55, 64–67), we determined whether a sphere-propagated CD44v6(+)ALDH(+)CD133(+)EpCAM(+) (CICs) subpopulation of cells demonstrate distinct drug resistance properties. Since our focus in this study is on CD44v6 function in mediating communication between CAFS-derived factors and CICs isolated from resistant and sensitive colorectal cells, first we compared the expressions of different CD44 variant isoforms in our sensitive and resistant SW480 cells and designed a series of forward primers, which base pair with v3, v4, v5, v6, v7, v8, v9 and v10 exons independently (**Figure 2A**). The reverse primer formed a base pair with a constant exon (c7). As shown in **Figures 2B, C**, CD44 exon specific RT-PCRs were examined using 5' primers complementary to individual variable exons and a primer to

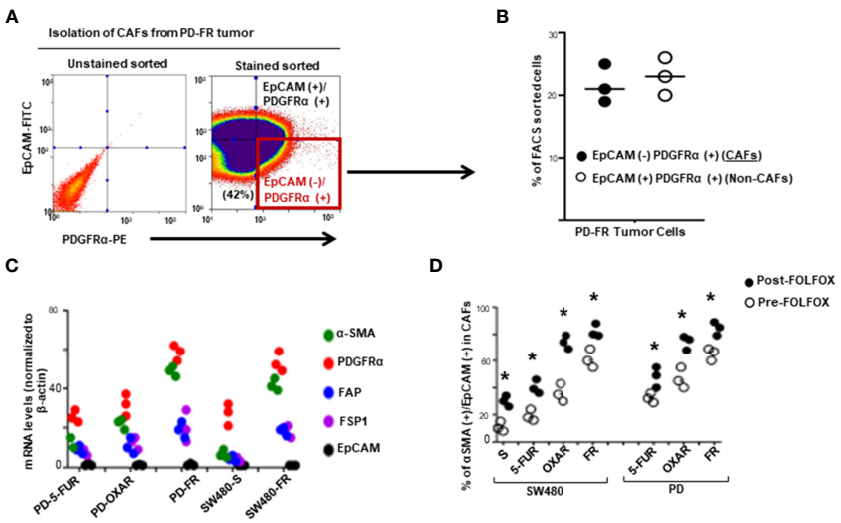

FIGURE 1 | Cancer associated fibroblasts (CAFs) account for tumor resistance to FOLFOX. **(A)**, Single cell suspensions isolated from a dissociated colorectal tumor (PD-FR) from a FOLFOX resistant (FR) patient were sorted by FACS using PDGFR-α-PE and EpCAM-FITC. CAFs were analyzed by FACS using: (i) the epithelial marker EpCAM-FITC; and (ii) the functional fibroblast cell immunophenotype by PDGFR-α-PE. **(B)**, Percentages of EpCAM [-]/PDGFR-α [+] (CAFs) and of EpCAM [+] /PDGFR-α [+]) (Non-CAFs) in total unsorted cell populations were quantified. **(C)**, The integrities of CAFs (EpCAM [-]/PDGFR-α [+]) from the dissociated patient colorectal specimens (PD-5FUR, PD-OXAR, PD-FR), and from the sensitive and FOLFOX resistant SW480/subcutaneous (SQ) tumor tissues were confirmed by QPCR analyses for CAF-associated markers FSP1, FAP and PDGFR-α, and for epithelial cell marker EpCAM (negative control), and for □ SMA. **(D)**, CAFs from the PD- 5FUR, PD-OXAR, PD-FR, SW480-S and SW489-FR (SQ) tumors were cultured in DMEM with 10% BSA and were further sorted by FACS using α SMA-FITC and PDGFR-α-PE antibodies. The percentages of the sorted α SMA (+)/PDGFR-α [+] cells in total EpCAM [-]/PDGFR-α [+] cells were quantified. Data are presented as Mean ± SD from six independent replicates in three independent experiments. **(D)**, *, $P < 0.05$ was considered significant, percent CAFs with post-FOLFOX treatment compared with pre-FOLFOX-treated cells after normalization to CAFs of serum starved untreated SW480 controls. Student's t-test was used to assess the significance.

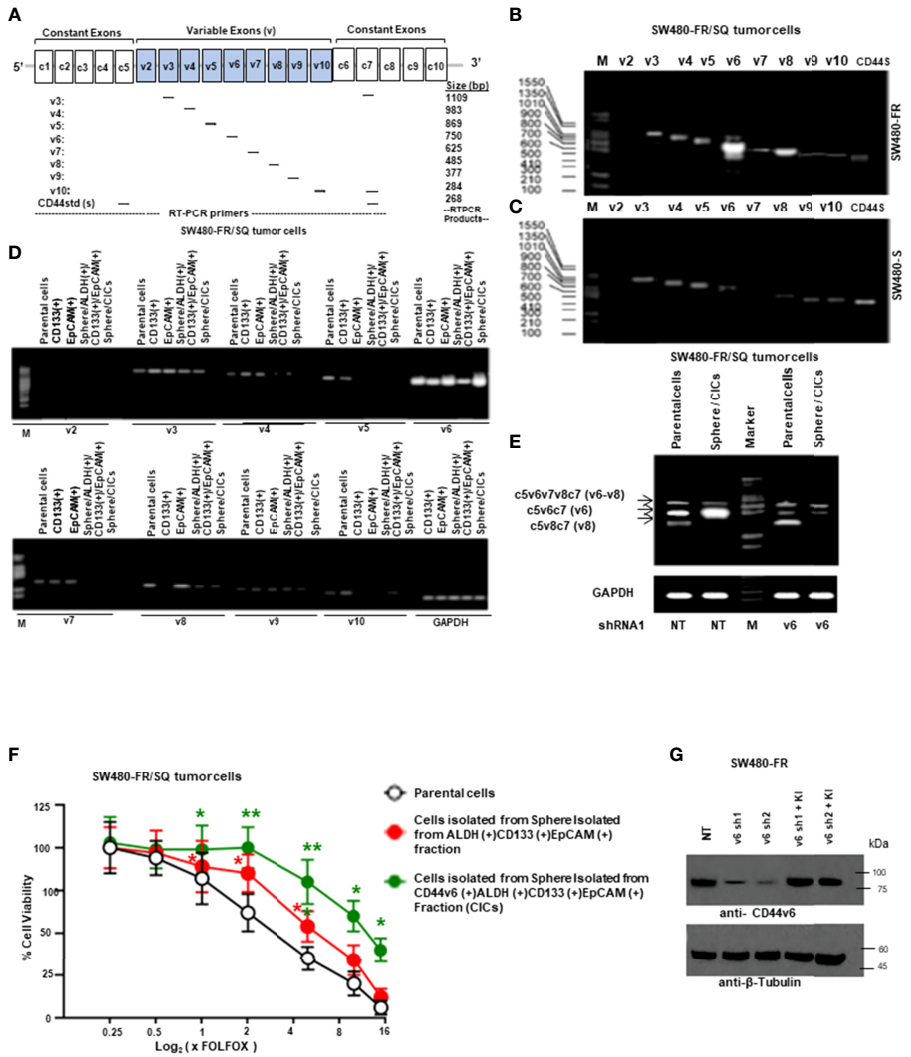

FIGURE 2 | CD44v6 appeared considerably higher in FACS sorted CD133+, ALDH+ and EpCAM+ cells, and in sphere-propagated ALDH+/CD133+/EpCAM+ cells relative to bulk primary cells. **(A)**, Constant and variable exons are shown for the PCR primers used to amplify CD44 variable (v) and standard (s) isoforms in the human CD44 gene. Primer positions are shown. The expected sizes of the PCR products are indicated. The primers for both the CD44v6 and standard isoforms (CD44s) predominantly generate one PCR product (c5v6c7 [v6] for CD44v6, and C5C7 for CD44s), whereas the primers for the v8 variants amplify two splice variants C5v6v7v8C7 (v6-v8) and C5v8C7 (v8). These PCR products are depicted in panels **(B, E)** experiments. **(B)**, SW480-FR cells show a differential expression profile of CD44 isoforms when compared with that of the SW480-S cells **(C)**. **(D)**, RT-PCR analyses are shown of CD44 variants (v2-v10) in parental cells, freshly purified CD133+ cells, EpCAM+ cells, sphere-propagated FACS sorted ALDH1+CD133+EpCAM+, and CD44v6+ALDH1+CD133+EpCAM+ (sphere/CICs) from cells SW480-FR/SQ tumor cells. Normalization was done by using GAPDH as a housekeeping control gene. **(E)** RT-PCRs are shown for CD44v6, CD44v6-v8, and CD44v8 on Non-targeted control shRNA (NTshRNA) cells and on CD44v6shRNA1 overexpressed in parental cells and in sphere/CICs. GAPDH was used as a housekeeping control gene. **(F)**, FOLFOX sensitivity was measured in parental cells, in freshly isolated sphere/ALDH1+CD133+EpCAM+ cells, and in sphere/CICs isolated from SW480-FR/SQ tumors grown in serum free medium that were treated with various concentrations of FOLFOX. An ATP based assay (CellTiter-Glo) measured cell viability compared with control cells (without FOLFOX treatment) as 100%. Error bars represent calculated SDs (n = 3). **(G)** Validations of two shRNAs for CD44v6 used in panel **(E)** were done by the indicated shRNA mediated knockdown and the corresponding knock-in (KI) gene transfections as described in Methods. Target proteins were analyzed by WB analysis (β-tubulin, internal control). Data are presented as Mean ± SD from n = 3–5 independent replicates in three independent experiments. All semi quantitative RT-PCR and western blot data are representative of three experiments. *, $P < 0.05$, **, $P < 0.01$ were considered significant, percent cell viability in ALDH (+)/CD133 (+)/EpCAM (+), and from CD44v6 (+)/ALDH (+)/CD133 (+)/EpCAM (+) fractions compared with control parental cell. Student's t-test was used to assess the significance.

the 3' constitutive exon 7 (c7) (primers are shown in **Table 1**). The results demonstrated that although SW480-S and SW480-FR cells expressed similar CD44 isoforms, the CD44v6 isoforms in resistant cells are significantly higher compared to sensitive cells. In addition, as shown in **Figure 2D**, although several of the variable CD44 exons were uniformly translated across SW480-FR/SQ tumor subsets, mRNA levels of CD44v6 appeared considerably higher in bulk parental primary

tumors cells, freshly purified CD133(+) cells, EpCAM(+) cells, Sphere-propagated FACS sorted ALDH1(+)CD133(+)EpCAM (+) cells (Sphere/ALDH1(+)/CD133+/EpCAM+) cells, and in Sphere-propagated FACS sorted CD44v6(+)ALDH1(+)CD133 (+)EpCAM(+) cells (Sphere/CICs) from SW480-FR/SQ tumor cells (**Figure 2D**). Analysis of CD44v6-containing isoforms in these cells further suggested that CD44v6 is translated in the same subset of SW480-FR cells (**Figure 2D**). Intriguingly, CD44v6 is significantly expressed more in sphere-propagated cells than in their corresponding parental primary tumors cells (**Figure 2E**), and knocking down CD44v6 with specific shRNA downregulates all CD44v6-containing isoforms (**Figure 2E**, validation of CD44v6 shRNA is shown in **Figure 2G**). Since CD44v6, ALDH, CD133 and EpCAM are well known colorectal CIC markers (55, 64–67), analysis of FOLFOX sensitivity in Sphere/CICs, in Sphere-propagated CD44v6(+)/ALDH1 (+)/CD133(+)/EpCAM(+) (Sphere/CICs) cells, and in Sphere-propagated ALDH1(+)/CD133(+)/EpCAM(+) cells were compared to parental SW480-FR cells (**Figure 2F**). Results in **Figure 2F** further suggested that Sphere/CICs are more resistant than in their corresponding Sphere/ALDH1 (+)/CD133(+)/EpCAM(+) cells and in parental primary tumor cells. Taking into consideration; 1) the strong elevation of the expression of CD44v6 isoform in FR cells compared to sensitive cells (**Figures 2B, C**); and 2) that sphere/CICs located in tumor spheres are more resistant compared to Sphere/ ALDH1(+)/CD133(+)/EpCAM(+) cells and primary parental tumor cells (**Figure 2F**), we concluded that CD44v6 splicing likely defines a colorectal CIC population with increased drug resistance properties.

Given that FOLFOX significantly increased the percentage of CAFs (αSMA[+]/EpCAM[+]) after drug (FOLFOX) treatment (as seen in **Figure 1D**), next, we determined whether FOLFOX treatment induces microenvironmental signals to instruct the tumorigenic potential of CICs. Thus, the effects of CAFs on viability of CICs were determined in co-culture experiments in which CICs and CAFs were either in close contact or in proximity, but not in direct contact, and by co-culture with conditioned media (CM) from the CAFs. Co-culture with FOLFOX-treated PD-FR/CAFs, or with their CM increased the PD-FR/CIC viability compared with DMSO (vehicle)-treated control (**Figures 3A, B**). Thus, CM from FOLFOX-treated PD-FR/CAFs contains secreted factors that promote PD-FR/CIC growth independent of contact. CAFs under both experimental conditions demonstrated a paracrine effect through secreted factors from CAFs pre-treated with FOLFOX to promote growth of CICs (**Figures 3A, B**). Interestingly, normal fibroblasts, which are not CAFs, used as control, did not increase CIC viability significantly upon FOLFOX treatment relative to untreated cells (**Figure 3A**). In agreement with the co-culture data, FOLFOX-treated CAFs enhanced the ability of CICs to initiate tumors and increase tumor growth rates in immunocompromised mice (**Figures 3C, D**). Moreover, xenografts generated by CICs co-implanted with FOLFOX-treated CAFs displayed increased SQ tumor incidence with increased tumor size (**Figures 3C, D**) and tumor numbers, and they reduced the latency of tumor formation by CICs (**Figure 3E**).

In a further step, we evaluated the effect of FOLFOX-treated CAFs on re-transplant ability of isolated colorectal patient tumor CD44v6(+)EpCAM(+)CD133(+)ALDH1(+) cells (CD44v6(+) CICs). 2 x 10^3 CICs alone or in combination with 6 x 10^3 CAFs pretreated with FOLFOX were subcutaneously implanted in immunocompromised mice. As shown in **Figures 3F, G**, in the immunocompromised mice models of colorectal cancer, as many as 5 x 10^5 patient-derived non CICs (CD44v6(-) cells), did not induce tumor formation. In contrast, 5 x 10^5 unfractionated bulk cells or as few as 2 x 10^3 CICs resuspended in Matrigel generated visible tumors after 3 weeks (**Figures 3F–G**). In concordance with the cell culture results, FOLFOX induced enrichment of CAFs (as shown in **Figure 1D**) increased the ability of CICs to initiate tumors in immunocompromised mice (**Figures 3F, G**). Interestingly, in spite of the higher number of CICs present in 5 x 10^5 unfractionated bulk tumor cells, tumor formation following injection of purified CICs co-implanted with FOLFOX-treated-CAFs was faster and more efficient than tumor formation obtained with the low number of CICs (**Figures 3F, G**). To investigate whether colorectal CD44v6(+) CICs co-implanted with FOLFOX-treated-CAFs display long-term tumorigenic potential, we assessed their ability to generate tumors after serial transplantations. For this purpose, indicated cells from primary SQ tumors were transplanted into secondary mice (**Figures 3F–G**). Indeed, injected CICs with FOLFOX-treated-CAFs engrafted and generated tumors that grew rapidly compared to CICs alone and required the mouse to be sacrificed within 6 weeks after implantation. Furthermore, CICs, or CICs plus FOLFOX-treated-CAFs tumor cells obtained from secondary xenografts were subsequently transplanted into third-generation mice. Thus, the CICs, alone or CICs with the FOLFOX-treated-CAF population in CRC tumors were able to generate serial xenografts showing a virtually unlimited growth potential. Interestingly, the presence of FOLFOX-treated-CAFs showed increased tumor incidence and reduced latency of tumor formation with increased size in each serial transplantation. Thus, data in **Figures 1–3** demonstrate that FOLFOX-therapy activates CAFs to secrete biological components in the microenvironment that stimulate CIC maintenance. Furthermore, the response to FOLFOX by these CAFs appears to be preconditioned by the tumor microenvironment since normal fibroblasts treated with FOLFOX could not induce CIC viability to the same degree (**Figure 3**, and data not shown).

FOLFOX Stimulated Cytokine Secretion of CAFs Maintains the Viability and Tumorigenic Potential of CICs

The data in **Figure 3** provide evidence that cytotoxic (FOLFOX) therapy induces remodeling of the tumor microenvironment to enrich the CAF secretome with biologically important components to support the tumorigenic potential of CICs. Therefore, using published microarray data in metastatic CRC associated fibroblasts (68), we made comparative analyses of CAF secreted cytokines, PN and some inflammatory proteins, and receptors including

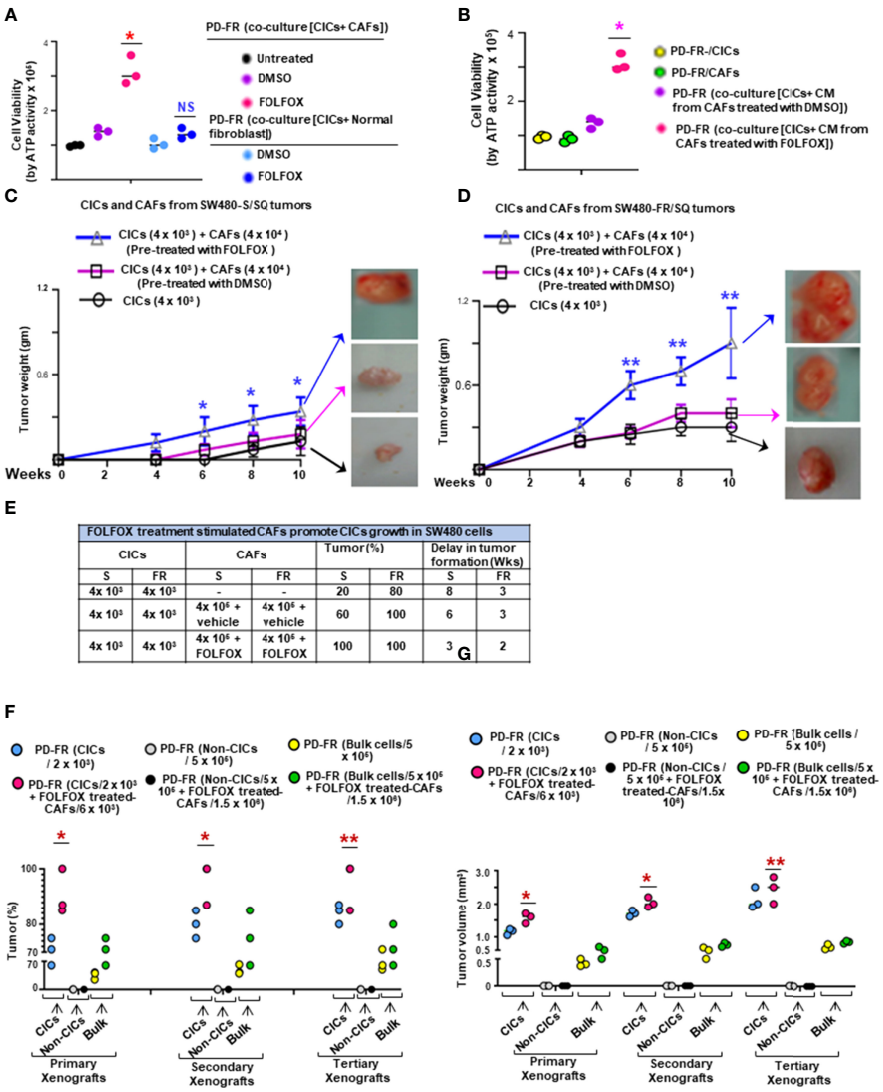

E

FOLFOX treatment stimulated CAFs promote CICs growth in SW480 cells							
CICs		CAFs		Tumor (%)		Delay in tumor formation (Wks)	
S	FR	S	FR	S	FR	S	FR
4x 10³	4x 10³	-	-	20	80	8	3
4x 10³	4x 10³	4x 10⁶ + vehicle	4x 10⁶ + vehicle	60	100	6	3
4x 10³	4x 10³	4x 10⁶ + FOLFOX	4x 10⁶ + FOLFOX	100	100	3	2

FIGURE 3 | FOLFOX-stimulated CAFs promote CIC growth. (A, B), The effect of CAFs on CICs was measured by co-culture of PD-FR/CICs with PD-FR/CAFs (A) and conditioned media (CM) treatment **(B)**. **(A)**, 1.5 x 105 PD-FR CICs were cultured with 3 x 105 PD-FR CAFs or with 3 x 105 normal fibroblasts pre-treated with vehicle (DMSO) or with FOLFOX-therapy for 12 days. Cellular viability was measured by the ATP Glo assay. **(B)**, 1.5 x 105 PD-FR/CICs, and 3 x 105 PD-FR CAFs were treated with vehicle (DMSO) or with FOLFOX for 72 hours. Conditioned media (CM) from CAFs were collected and used to culture CICs for 12 days. Cellular viability was measured by the ATP Glo assay. **(C, D)**, The abilities of the CAFs (4 x 104) to affect the tumor growth of CICs (4 x 103) from three different batches of SW480-S. **(C)** and of SW480-FR **(D)** were tested for tumorigenic potential. SW480-FR/SQ CAFs that were pre-treated with vehicle (DMSO) or with FOLFOX for 72 hours were subcutaneously co-implanted in immunocompromised mice. Tumors were harvested every week to evaluate their latency, and weights were measured to evaluate their development. **(E)**, The contributions of SW480-S/CAFs and SW480-FR/CAFs to post-FOLFOX treated tumor growth (tumor %) in their CICs were assessed by measuring tumor 10 weeks after implantation of the CICs and CAFs into immunocompromised mice. **(F)**, Numbers of SQ tumors formed by injections of the indicated numbers of CICs, Non-CICs, and unfractionated bulk tumor cells with and without addition of FOLFOX treated CAFs from the PD-FR cells are shown. FACS sorted CICs (2 x 103), Non-CICs (5 x 105), and the unfractionated bulk tumor cells (5 x 105), with and without FOLFOX treated CAFs (6 x 103 or 1.5 x 106 cells) from PD-FR tumor cells were resuspended in Matrigel and implanted in immunocompromised mice. The same cells from the first generation of SQ tumors were further implanted into immunocompromised mice to generate second generation of xenograft tumors. The experiments were repeated to generate tumors into a third generation of xenograft tumors. Only CICs and the unfractionated bulk tumor cells were capable of inducing first generation xenograft tumors formations. Isolation of second and third generation xenograft tumors displayed similar results (n = 5 analyzed patients derived cells, 8 mice group and experiments were performed in triplicates), Tumor percent (percentage of tumor bearing mice) **(F)** and tumor volumes **(G)** from experiment **(F)** were evaluated. Data are presented as Mean ± SD from n = 5 analyzed patients derived cells, 8 mice/group and experiments independent replicates in three independent experiments. **(A, B)**, *, $P < 0.05$ was considered significant, percent cell viability with FOLFOX treatment compared with DMSO treated coculture after normalization to that of untreated coculture. Student's t-test was used to assess the significance. **(C, D)**, Tumor growth stimulation data with pre-treatment with FOLFOX compared with DMSO-treated CICs + CAFs after normalization to tumor growth of CICs represent means ± SD.; n = 5-8; *, $P < 0.05$. **, $P < 0.01$ were considered significant; **(F, G)**, Tumor (%) and tumor volume of primary, or secondary, and tertiary xenografts from CICs-tumor compared to Bulk-tumor populations. *, $P < 0.05$, **, $P < 0.01$ were considered significant; ANOVA, followed by Bonferroni's post-hoc test was used to assess the significance in experiments **(C, G)**

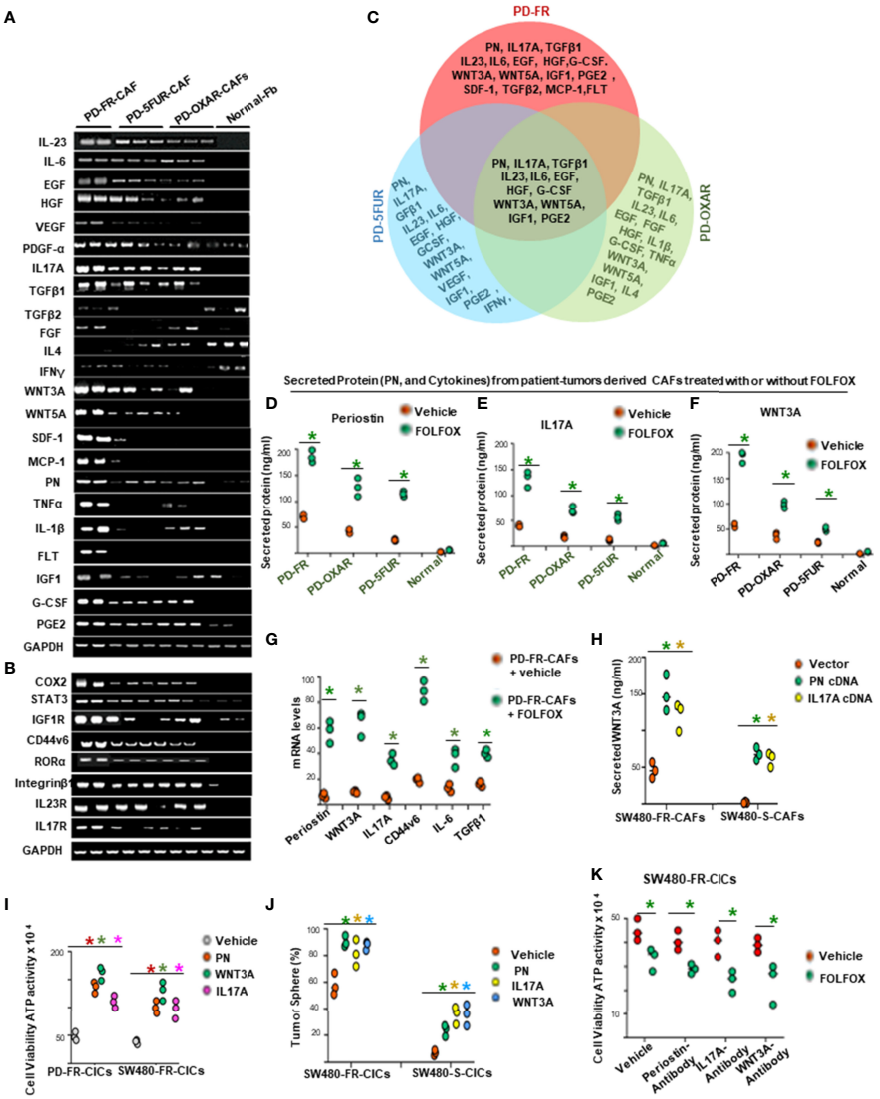

FIGURE 4 | FOLFOX induces cytokine secretion in CAFs. **(A, B)**, Basal mRNA expression levels of PN and the indicated growth factors, and of growth promoting cytokines and related molecules **(A, B)**, were analyzed by semi quantitative RT-PCR in eight indicated CAFs isolated from drug resistant patient tissues and from three normal fibroblasts (Fb). GAPDH was the reference gene. **(C)**, Venn diagram shows common cytokines isolated from PD-5FUR, PD-OXAR and PD-FR from the experiment in **(A)**. **(D–F)**, CAFs derived from three patient colorectal tumor (PD)-tissues and one normal intestinal fibroblast cell line were analyzed for their PN and two dominant cytokines (IL17A and WNT3A) after FOLFOX treatment. **(G)**, QPCR analyses are shown of PN and 4 major cytokines (WNT3A, IL17A, IL6 and TGFβ1) and of CD44v6 in patient tumor CAFs treated with DMSO or FOLFOX for 72 hours. GAPDH was the reference gene. **(H)**, PN and IL17A stimulated WNT3A production in CAFs isolated from sensitive and FR tumors of SW480 were assessed by transfecting these freshly isolated CAFs by vector control, PN and IL17A expression plasmids for 72 hours. Secretion of WNT3A was measured by an ELISA assay. **(I)**, Effects of PN, IL17A and WNT3A on cell viability were assessed by using ATP Glo assay on PD-FR CICs and SW480-FR CICs. The effects were assessed in these different specimens by culturing 104 CICs with vehicle, or with 20 ng/ml of PN, IL17A or WNT 3A for 12 hours. **(J)** Percentages of colon tumor sphere formation are shown in tumor spheres isolated fromCICs of FR-resistant and sensitive cells of SW480 in the absence and presence of 50 ng/ml of either PN, or IL17A or WNT3A proteins. **(K)**, Effects of the autocrine PN, IL17A and WNT3A production in growth of tumor spheres-derived CICs (CICs) were examined by studying the effects of blockade of PN, or IL17A or WNT3A on the tumor-initiating capacity of 1 x 104 CICs. The effects were evaluated in CICs by 12-day cultures with vehicle or FOLFOX alone. Cell viabilities (# of viable cells) were measured by ATP Glo assay. Data are presented as Mean ± SD from n = 3–5 independent replicates in three independent experiments. All semi quantitative RT-PCR data are representative of three experiments. **(D–F)**, *P < 0.05 was considered significant, Secreted protein of FOLFOX treated groups compared to vehicle control group. (G), *P < 0.05, was considered significant, FOLFOX treated groups compared to vehicle control group. **(G)** *P < 0.05 was considered significant, the mRNA levels of FOLFOX treated CAFs were compared with vehicle treated CAFs. **(H)**, *P < 0.05 was considered significant, secreted WNT3A in PN, and IL17A overexpressed CAFs compared with vector control. **(I)**, *P < 0.01 was considered significant, percent cell viability stimulation with PN, WNT3A, and IL17A treatment compared with vehicle-treated cells after normalization to growth of untreated controls. **(J)**, *P < 0.05 was considered significant, percent tumor sphere stimulation with PN, WNT3A, and IL17A treatment compared with vehicle-treated CICs from S-CICs, and FR-CICs of SW480 cells after normalization to untreated controls. **(K)**, *P < 0.01 was considered significant, percent cell viability stimulation with FOLFOX treatment group compared with vehicle-treated CICs that were pre-treated with PN-, or IL17A-, and WNT3A-antibodies. Student's t-test was used to assess the significance.

CD44v6, and transcription factor expressions in PD-5FUR/CAFs, PD-OXAR/CAFs and PD-FR/CAFs, as well as in normal fibroblasts (Normal-Fb) without further FOLFOX treatment (**Figures 4A, B**). **Figure 4A** (and data not shown) show several molecules that are exclusive to each CAF, and there were only 12 cytokines and matricellular protein molecules common to all three patient-tumor derived CAFs shown in the Venn diagram (**Figure 4C**). To further characterize the CAFs and compare their putative effects on CIC growth, conditioned media without serum (CM) from the three CAF and the normal fibroblast cultures were compared at baseline (without FOLFOX treatment) or after treatment with FOLFOX. Data in **Figures 4D–F** show that FOLFOX treatment significantly increased secretion of three dominant secreted factors (PN, IL17A and WNT3A) from their basal levels among the top five stromal secreted factors (PN, IL17A, WNT3A, IL-6 and TGF-β) in patient-derived PD-FR/CAFs, PD-OXAR/CAFs and PD-5FUR/CAFs (**Figure 4G**). Particularly, cytokine expression from normal fibroblasts was always lower than in CAFs basally and following FOLFOX treatment, highlighting the generally altered function of CAFs (**Figure 4D–G**, and data not shown). Regulation of these major secreted factors (PN, IL17A and WNT3A) by FOLFOX appears to occur at the level of transcription, as large increases compared to their basal levels were detectable for each of these target factors compared to IL-6 and TGF-β (**Figure 4G**). We also show that PN and IL17A were only present at ~2-7 ng/ml in sensitive cells, versus the constitutively high endogenous level (~40-59 ng/ml) observed in resistant cells (data not shown). Moreover, results of **Figures 4H, F**, and Supplemental **Figure 1A** indicate that both PN and IL17A induced WNT3A mRNA expression and secretion. Therefore, in the present study, we focused on PN, WNT3A and IL17A. Overall, these data strongly suggest that CAFs respond to FOLFOX treatment by secreting paracrine signaling factors, including matricellular proteins, cytokines, and growth factors.

In order to determine the involvement of these stromal-factors on CIC maintenance, we analyzed the autocrine production of the three stromal-secreted factors in PD-FR/CICs that were previously treated with vehicle or FOLFOX in the absence of CAFS. The results showed insignificant or only moderate levels of autocrine productions of PN, WNT3A and IL17A by CICs compared to their levels in CAFs (**Supplementary Figure 1B**, versus **Figures 4D–F**), and treatment with FOLFOX greatly increased the gene expressions and secreted proteins by these three paracrine factors (**Figures 4H**, and **Supplementary Figure 1A**). Moreover, each of these three stromal-secreted factors (PN, WNT3A or IL17A) directly augmented CICs viability in the absence of CAFs (ATP activity, **Figure 4I**) with reduced apoptosis (apoptosis data not shown). Further, these three CAF-secreted factors stimulated tumorigenic potential of CICs as measured by tumor sphere formation in CICs from sensitive and FR tumors of SW480 (**Figure 4J**). Note that the basal tumorigenic activity of SW480-FR-CICs was much higher compared to SW480-S-CICs, and treatment with each of the three stromal-secreted factors (PN, WNT3A and IL17A) increased tumor sphere formation ability relative to vehicle treated CICs (**Figure 4J**). These results provide evidence that these CAF-derived factors might directly regulate CIC maintenance. Moreover, both PN and IL17A increase WNT3A secretion (as in **Figures 4H** and **Supplementary Figure 1A**) indicating that WNT3A signaling may have a crucial role in tumor cellular hierarchy. To further elucidate the possible role for autocrine effects of PN, IL17A and WNT3A on CICs, we investigated the effects of blocking each of these stromal factors on the viability of CICs (measured by Cell Titer-Glo assay) and on the tumorigenic potential of CICs (measured by quantitation of tumor spheres) in the absence of CAFs using a blocking antibody for each of the stromal factors (**Figures 4K** and **Supplementary Figure 1C**). Only moderate levels of viability and tumorigenic potential were noted as a result of PN, or IL17A or WNT3A blocking antibodies in CICs (**Figuress 4K** and **Supplementary Figure 1C**), suggesting that CAF-derived PN, IL17A and WNT3A (**Figures 4D–F**) have a major affect compared to autocrine production of these factors in CICs. Further, blocking IL17A, PN or WNT3A only reduced tumor sphere formation in CICs isolated from resistant cells, while having no effect in CICs derived from sensitive cells (**Supplementary Figure 1C**) indicating that PN, WNT3A and IL17A induced tumorigenic activity is confined to the role of increased CAFs after FOLFOX treatment (as seen in **Figure 1D**).

PN and IL17A Can Contribute to CIC Maintenance Through WNT3A-CD44v6 Signaling

Given that CAFs derived from resistant tumor cells (PD-5FUR, PD-OXAR and PD-FR CAFs) also express significant levels of CD44v6 compared to its absence in normal-fibroblasts (as seen in **Figure 4B**), we determined if CD44v6 induces WNT3A activation in CAFs since it regulates WNT3A/β-catenin signaling in CICs (48). Thus, first, WNT3A expression was analyzed in FOLFOX treated PD-FR CAFs in which CD44v6 was knocked down, and the results show that CD44v6 regulates WNT3A production in FOLFOX treated PD-FR/CAFs (**Figure 5A**). Furthermore, this regulation of CD44v6 on WNT3A is through IL17A and PN in FR-tumor cell derived CAFs (**Figure 5B**), and this regulation of CD44v6 on WNT3A, PN and IL17A was not found in sensitive S-tumor cell derived CAFs (data not shown). Second, to investigate whether CD44v6 variants are important for β-catenin-MDR1 signaling, we examined the effects of WNT3A and FOLFOX on activation of CD44v6 splicing and β-catenin-MDR1 signaling in oxaliplatin resistant SW480-OXAR/SQ tumor cells. To detect the effects on CD44v6 and CD44v8, exon specific PCRs were examined using two different 3' primers paired to either the v6 or v8 exon respectively, and to a primer to the 5' constitutive exon 5 (c5) (as shown in schematic diagram **Figure 5C**; primers are shown in **Table 2**). As shown in **Figure 5D**, following WNT3A or FOLFOX addition, the expression of CD44v6

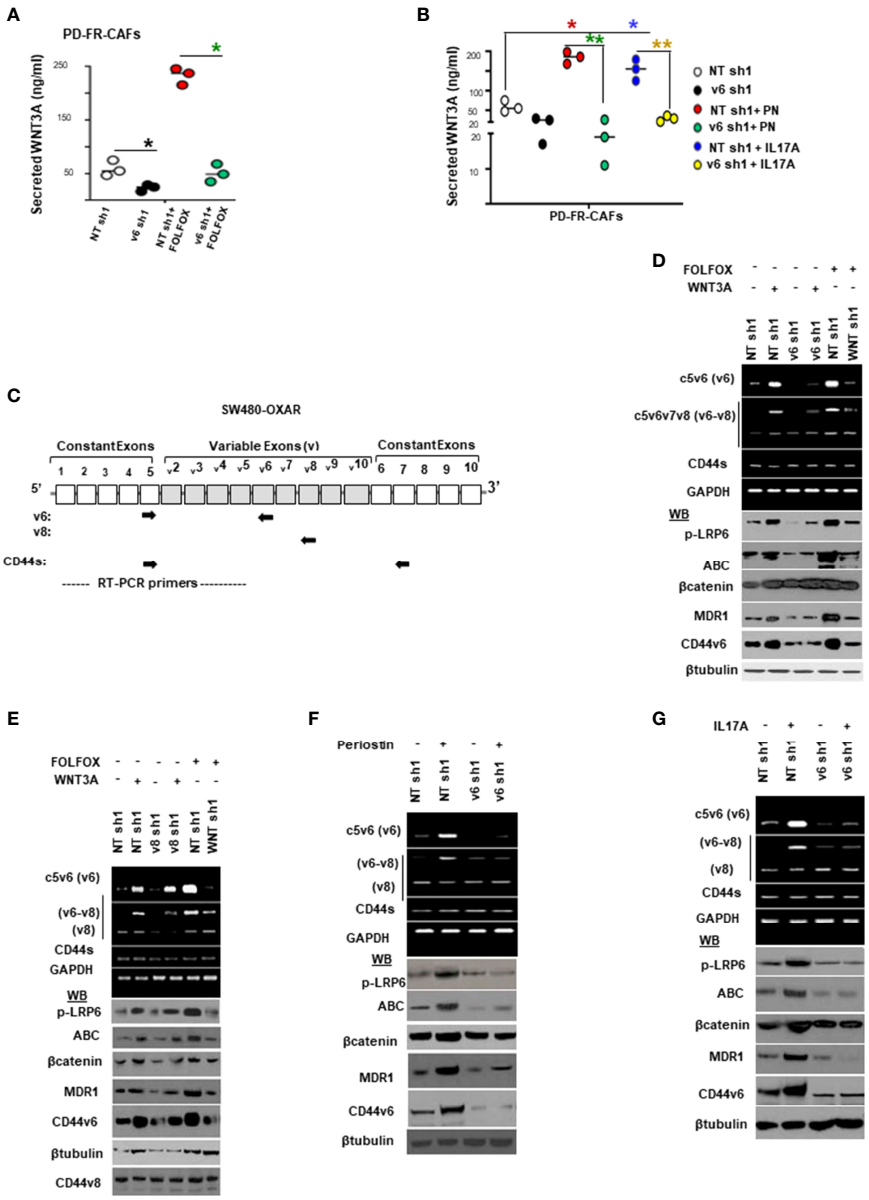

FIGURE 5 | FOLFOX induces CD44v6 expression, which is critically regulated by the WNT pathway stimulated by PN and/or IL17A. **(A)**, Confirmation of involvement of CD44v6 expression in regulating WNT3A production was assessed in PD-FR CAFs by examining the effects of blockade of CD44v6 using specific shRNAs on 10^4 SW480-FR/CAFs in the absence and presence of FOLFOX. The effects were evaluated by measuring secreted WNT3A in cultures by ELISA. **(B)**, Involvement of CD44v6 in regulating PN and IL17A induced WNT3A production was assessed in PD-FR CAFs by examining the effects of blockade of CD44v6 using specific shRNAs in the absence and presence of PN or IL17A. The effects were evaluated by measuring secreted WNT3A in cultures by ELISA. **(C)**, Schematic illustration of the CD44 gene is shown. Both constitutive **(C)** and variable (v) exons are represented. The PCR primers used to amplify CD44 variable (v) and standard (s) isoforms are shown as black arrows. The primers for both the v6 and standard isoforms (CD44s) predominantly generate one PCR product [C5v6 (v6) for CD44v6, and C5C7 for CD44s], whereas the primers for the v8 variants amplify two splice variants C5v6v7v8 (v6-v8) and C5v8 (v8). These PCR products are depicted in panels **(D–G)** experiments. The primers for both the v6 and standard isoforms predominantly generate one PCR product [c5v6 (v6)], whereas the primers for the v8 variants amplify two splice variants C5v6v7v8 (v6-v8), and C5v8 (v8). **(D, E)**, WNT3A shRNA, or CD44v6 shRNA1 **(D)**, but not CD44v8 shRNA1 **(E)** Upper panels: Semi-quantitative RT-PCR analyses are shown for CD44 variants in SW480-OXAR SQ tumor cells transfected with NT sh, or v6 sh1 or WNT3A sh1 followed by WNT3A or FOLFOX stimulation for 12 hours. Lower panels: Western blot analyses are shown for p-LRP6, active β–catenin, total β–catenin, MDR1, CD44v6 or β-tubulin. **(E)**, Upper panels: Semi-quantitative RT-PCR analyses are shown for CD44 variants in SW480-OXAR SQ tumor cells transfected with NT sh, or v8sh1, or WNT3A sh1 followed by WNT3A or FOLFOX stimulation for 12 hours. Lower panels: Western blot analyses are shown for p-LRP6, active β–catenin, total β–catenin, MDR1, CD44v6 or β-tubulin. **(F, G)**, Upper panels: Semi-quantitative RT-PCR analyses are shown for CD44 variants in SW480-OXAR SQ tumor cells transfected with NT sh or v6 sh1 followed by PN or IL17A stimulation for 12 hours. Lower panels: Western blot analyses are shown for p-LRP6 (S1490), active β–catenin, total β–catenin, MDR1, CD44v6 or β-tubulin. Data in A, B, represent means ± SD; n = 3–6 independent replicates in three independent experiments. **(A)**, *$p < 0.05$ was considered significant, inhibition of WNT3A secretion in v6 shRNA1 groups compared to NT shRNA1 controls. **(B)**, *$p < 0.05$, **$p < 0.01$ were considered significant, Inhibition of WNT3A secretion in v6 shRNA1 +PN and v6 shRNA1 +IL17A groups compared to NT shRNA1 controls. All Western blots and semi quantitative RT-PCR data are representative of three experiments.

variants increased significantly, whereas the expressions of the CD44v8 isoform or the standard CD44s isoform were not increased. Along with the CD44v6-containing isoform, the activation of β-catenin modulators, including p-LRP6, active β-catenin and MDR1 expressions were upregulated. Knocking down CD44v6 or WNT3A inhibited the induction of CD44v6 and WNT/β-catenin-MDR1 signaling (**Figure 5D**). The residual expressions of CD44 variants after WNT3A knockdown suggests that other signaling cascades, in addition to WNT/β-catenin, may also regulate v6 splicing of CD44 (**Figure 5D**). However, the levels of the v8 variant and of CD44s (with no variant exon) were almost identical after treatment with either v6 shRNA expressing cells (**Figure 5D**) or to the levels of control shRNA (NT-shRNA) treated cells. Treating cells with CD44v8shRNA and either WNT3A or FOLFOX inhibited the up-regulation of all the examined CD44v8-containing variants, but not the CD44v6 variants, and not the activation of p-LRP6, active-β-catenin and MDR1 expressions (**Figure 5E**). WNT3A, or FOLFOX stimulated isoforms containing v6 were silenced by WNT3A shRNA, or CD44v6 shRNA (**Figure 5D**), but not by CD44v8 shRNA (**Figure 5E**). This indicates that CD44v6 signaling, but not CD44v8 signaling, is required for WNT3A-, or FOLFOX-induced WNT/β-catenin-MDR1 signaling (**Figure 5E**). The v6–v8 variant amplified in the same experimental RT-PCR analysis maintained down-regulated levels (42 ± 5.0% of NT shRNA levels) because this variant contained the v6 exon targeted by v6 shRNA1 (**Figure 5E**). These results (**Figures 5D, E**) show that the CD44v6 containing isoform and CD44v6/LRP6/β-catenin/MDR1 signaling triggered by stromal secreted WNT3A might be important for drug resistance in CICs.

To gain insight into how PN and IL17A are related to the mechanisms that control viability of CICs and tumorigenic potentiality, we determined whether PN and IL17A coordinated with WNT to activate WNT-CD44v6-MDR1 signaling as described in our companion paper (48). Thus, we measured expressions of CD44 variants by RT-PCR, and levels of p-LRP6 (S1490), active β-catenin and MDR1 by WB after PN and IL17A stimulation in SW480-FR cells. As shown in **Figures 5F–G**, following addition of PN (**Figure 5F**) or IL17A (**Figure 5G**), expressions of CD44v6 and v6-containing variants increased, while the standard form (CD44s) remained unchanged. Activation of LRP6, active β-catenin and MDR1 also increased following PN or IL17A treatment, which was abrogated following v6 shRNA1 transfection. The expressions of variants containing the v6 exon were increased by greater than three (3.7 ± 0.54) and six (6 ± 0.53) fold respectively. Increases of 1.8 ± 0.33 and 2.6 ± 0.53 fold were observed for the v6–8 for PN and IL17A addition respectively (**Figures 5F, G**). Expression of CD44v6shRNA1 in PN- and IL17A-treated cells inhibited the up-regulation of all the CD44v6-containing variants. In addition, the interaction between either PN or IL17A with CD44v6-downstream signaling activities were measured by LRP6 phosphorylation, and by expressions of active β-catenin and MDR1 proteins (**Figures 5F, G**). TOPFlash carries TCF-binding sites, which are directly activated by the TCF4/β-catenin complex (69, 70). The data in **Figures 6A–C** indicate that PN, IL17A or WNT3A treatment in CICs from sensitive and chemo-resistant colorectal tumors induces the TOPFlash reporter activity. In each case each of these paracrine factors increases the reporter activity from their basal activity levels, and the combined treatment further stimulates the transactivation of the TOPFlash reporter (**Figures 6A–C**).

Given that TCF4 binding sites are present in the CD44v6 promoter sequence as described in our companion paper (48), we determined whether FOLFOX induced increased expression of CD44v6 depends on TCF4. Thus, a dominant-negative TCF-DN was co-transfected in resistant SW480-FR cells, and their CD44v6 expression in nuclear fractions was strongly inhibited (**Figure 6D**). Furthermore, WNT3A signaling activity is increased in the CD44v6 (+)CIC population isolated from SW480-5FUR, SW480-OXAR and SW480-FR SQ tumor cells overexpressing WNT3A, as analyzed by FACS (**Figure 6E**). Flow cytometry analysis showed that following the enrichment of CICs in WNT3A transfectants, a majority of CICs were present in sorted SW480-FR/SQ tumor cells expressing constitutively high WNT3A activity (**Figure 6E**), and this WNT3A activity is required for maintenance of the CIC immunophenotype (CD44v6 [high+]) by promoting tumor sphere formation in CICs (**Figure 6F**). Validations of CD44v6 shRNAs, CD44v8 shRNAs and WNT3A shRNAs were done following our previously published paper (31, 49) and are shown in **Figures 2G**, **6G**, and **6H**. Thus, PN, WNT3A and IL17A act as CIC niche components that can promote CIC maintenance and expansion by augmenting WNT-CD44v6-β-catenin-MDR1-signaling. This can trigger therapeutic resistance in CICs and their ability to generate virtually unlimited growth potential in serial xenografts established by injecting CICs in combination with CAFs subcutaneously in immunocompromised mice (as seen in **Figure 3F–G**).

PN and IL17A Induce Association of Nuclear β-catenin/TCF4 With CD44v6 and MDR1 to Modulate Drug Resistance

PN and IL17A mediation of a WNT3A/β-catenin pathway regulates CD44v6 expression and vice versa (as seen in **Figures 5A,B,D–G**), and enriches CD44v6 in CICs (**Figures 6D**). In searching for a possible linkage between PN and IL17A with WNT/β-catenin signaling to regulate CD44v6 expression and CIC survival/self-renewal, we analyzed transient transfection assays using SW480-FR cells with constructs containing TCF binding sites within the MDR1 promoter cloned into a luciferase reporter plasmid (see the schematic model of MDR1 luciferase reporter in **Figure 7A**). This construct was transfected with or without manipulations of TCF4 knockdown followed by either PN or IL17A co-transfection, and luciferase activities were measured for the PGL3-mdr1 constructs (**Figure 7B**). The results showed an ~8-fold decrease of basal PGL3-mdr1 luciferase activity by knocking down TCF4 (**Figure 7B**). In a further step, to determine the linkage between PN and IL17A with WNT/β-catenin signaling to regulate CD44v6 gene expression, we analyzed transient transfection assays using SW480-FR cells with constructs containing TCF binding sites within the MDR1

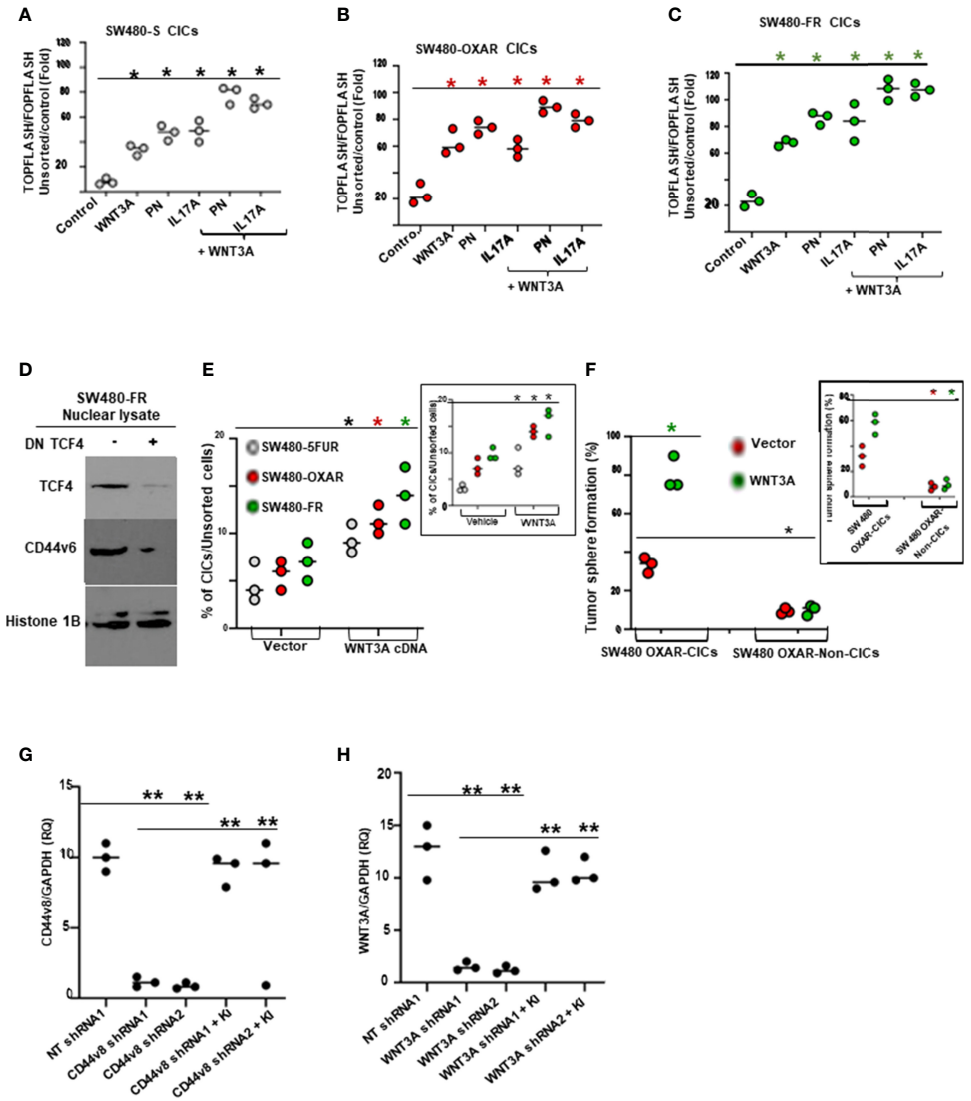

FIGURE 6 | FOLFOX induces b-catenin/TCF4 luciferase activity and tumor sphere formation in CICs stimulated by PN and/or IL17A, and TCF4 regulates CD44v6 expression. **(A–C)**, WNT reporter (TOPFLASH/FOPFLASH) activities were determined in SW480-S **(H)**, SW480-OXAR **(I)** and SW480-FR **(J)** CICs in response to culturing with vehicle (Control), or with PN, or IL17A or WNT3A alone (20 ng/ml), or in combination PN + WNT3A or IL17A + WNT3A. **(D)**, Dominant negative TCF4 mediated down regulation of TCF4 inhibits CD44v6 expression in nuclear lysates of SW480-FR SQ tumor cells. **(E)**, Flow cytometry analyses of percent enrichment of CICs are shown for unsorted cells from SW480-5FUR/SQ, SW480-OXAR/SQ and SW480-FR/SQ cells overexpressing WNT3A or vector control. **(F)**, Percentages of colon tumor sphere formation were measured in a sphere-formation assay for CICs and Non-CICs in SW480-OXAR SQ tumor cells overexpressing WNT3A or vector control. **(G,H)**, The effects of shRNA-mediated knockdown of CD44v8 and WNT3A using specific shRNAs in SW480-FR cells on the expressions of CD44v8 mRNA and WNT3A mRNA, as determined by real-time PCR (at 24 h; RQ, relative quantification) were done by the indicated shRNA mediated knockdown and the corresponding knock-in (KI) gene transfections as described in Methods. Target mRNAs were analyzed by QRT-PCR analysis (GAPDH, internal control). Data in **A–C, E–H**, represent means ± SD; n = 3–6 independent replicates in three independent experiments; **(A–C)**, *$p < 0.05$ was considered significant, stimulation of TOPFLASH/ FOPFLASH activities in treatment groups compared to control groups. **(D)**, Western blot data are representative of three experiments. **(E)**, *$p < 0.05$ was considered significant, stimulation of % of CICs by WNT3A over expression or exogenously added WNT3A group (inset) compared to respective control groups. , **(F)**, *$p < 0.05$ was considered significant, stimulation of tumor sphere formation in WNT3A over expression or exogenously added WNT3A group (inset) compared to respective control groups. **(G, H)**, **$p < 0.01$ was considered significant, Fold inhibition of CD44v8 and WNT3A mRNA in shRNAs overexpressing groups compared to corresponding NT shRNA groups; Fold restoration of CD44v8 and WNT3A mRNA in corresponding shRNA + Knock-in (KI) groups compared to corresponding shRNA groups. Student's t-test was used to assess the significance.

promoter cloned into a luciferase reporter plasmid. The cells were transfected with or without manipulations of TCF4 knock down followed by either PN or IL17A co-transfection, and luciferase activities were measured for the PGL3-mdr1 constructs (scheme in **Figure 7A**). The results showed that either PN or IL17A overexpression increases this promoter activity ~3 fold and ~3.5 fold respectively (**Figure 7B**). In contrast, the MDR1 promoter luciferase constructs negatively responded to co-transfection of

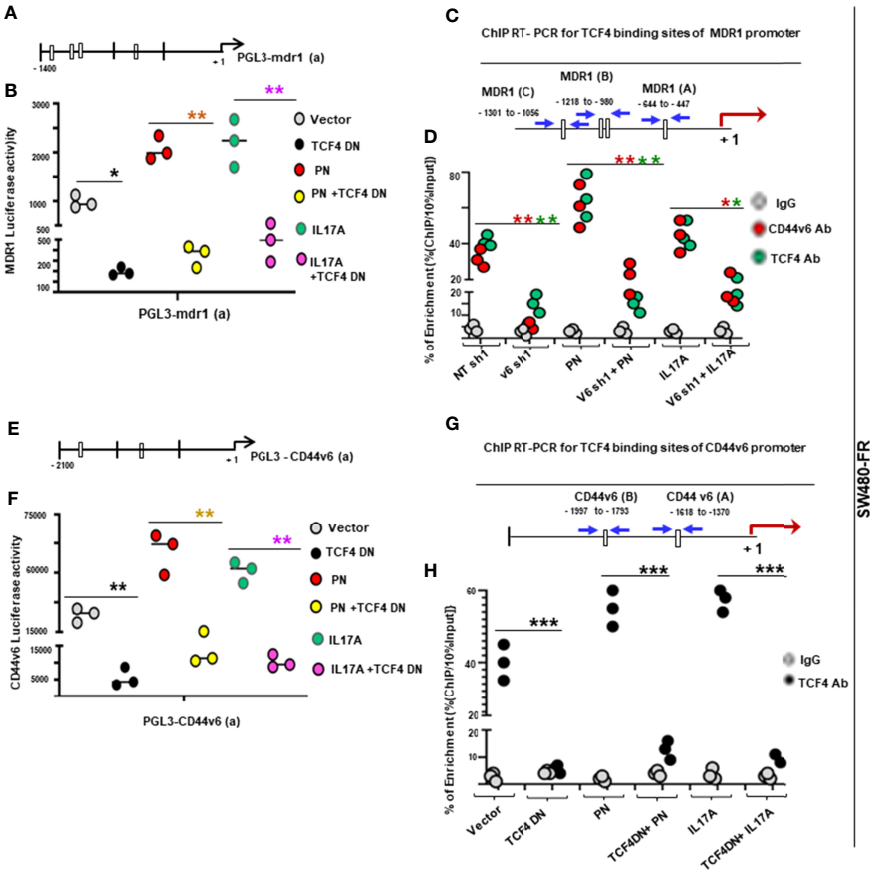

FIGURE 7 | PN and IL17A induce association of nuclear β-catenin/TCF4 with CD44v6 and MDR1 to modulate drug resistance. **(A, B)**, PN and IL17A induced MDR1 promoter luciferase activities were measured in SW480-FR cells using the indicated pGL3-mdr1 (a) reporter containing TCF4 binding sites (CTTTGA). **(A)**, The scheme shows the pGL3-mdr1 (a) reporter constructs with TCF binding sites. **(B)**, MDR1 luciferase activity reporter assays are shown for SW480-FR cells overexpressing a dominant negative TCF4-DN construct for 48 hours followed by co-transfection with or without PN or IL17A expression vectors. **(C)**, The sketch map shows the predicted TCF4 binding sites (CTTTGA) within the indicated MDR1 promoter (blue arrows). The transcriptional start site (red arrow) was at "+1", and ATG is at the translation start site. The putative TCF4 binding sites (MDR1 (A), MDR1 (B) and MDR1 (C) are shown, and their locations are labeled. **(D)**, ChIP PCR primers, designated for MDR1 **(A)** as shown in **(C)**, were used for amplification of the potential TCF4 binding sites of the MDR1 gene. ChIP assays were done using either anti-CD44v6, anti β-catenin or irrelevant IgG antibody as negative control in SW480-FR cells overexpressing specific shRNAs against CD44v6 or Non-targeted shRNA (NT-sh) with or without co-transfection with PN or IL17A constructs. Input: total genomic DNA was used as control for the PCR. **(E, F)**, PN and IL17A induced CD44v6 promoter luciferase activities were measured in SW480-FR cells using the indicated pGL3-CD44v6 (a) reporter containing TCF4 binding sites. **(E)**, The sketch map of predicted TCF4 binding sites (CTTTGA) within the CD44v6 promoter luciferase construct (CD44v6 [a]) is shown. **(F)**, CD44v6 luciferase activity reporter assays are shown for SW480-FR cells overexpressing dominant negative (DN) TCF4 for 48 hours followed by co-transfection with or without PN or IL17A expression vectors. **(G, H)**, PN or IL17A induced CD44v6 gene expression regulated by TCF4 in SW480-FR cells is shown. **(G)**, The sketch map shows the predicted TCF4 binding sites (CTTTGA) within the indicated CD44v6 promoter (blue arrows). The transcriptional start site was at "+1", and ATG is at the translation start site (red arrow). The putative TCF4 binding sites [CD44v6 **(A)**] and CD44v6 **(B)** are shown, and their locations are labeled. **(H)**, ChIP PCR primers, designated for CD44v6 **(A)** as shown in **(G)**, were used for amplification of the potential TCF4 binding sites of the CD44v6 gene. ChIP assays were done using either anti-TCF4 or irrelevant IgG antibody as negative control in SW480-FR cells overexpressing a dominant negative TCF4-DN construct for 48 hours followed by co-transfection with or without PN or IL17A expression vectors. Data presented in **(B, D, F, H** are Mean ± SD.; n = 3–5 independent replicates in three independent experiments; **(B)**, *, $P < 0.05$, **, $P < 0.01$ were considered significant, Inhibition in MDR1 luciferase activity in TCF4 DN, or PN + TCF4 DN, or IL17A + TCF4 DN overexpressed groups compared to vector control group. **(D)**, *, $P < 0.05$, **, $P < 0.01$ were considered significant, Inhibition of percent of enrichment of MDR1 mRNA in v6 shRNA1 (v6 sh1), v6 sh1+PN, v6 sh1+IL17A groups compared with , NT sh1, or PN, or IL17A overexpressed groups. **(E)**, *, $P < 0.05$, **, $P < 0.01$ were considered significant, Inhibition in CD44 luciferase activity in TCF4 DN, or PN + TCF4 DN, or IL17A + TCF4 DN overexpressed groups compared to vector control group. **(F)**, *, $P < 0.05$, **, $P < 0.01$, ***, $P < 0.001$ were considered significant, Inhibition of percent of enrichment of CD44v6 transcripts in TCF4 DN, or PN + TCF4 DN, or IL17A + TCF4 DN overexpressed groups compared to vector control group. Student's t-test was used to assess the significance.

dominant-negative TCF4-DN in cells pre-transfected with PN or IL17A constructs (**Figure 7B**). These reductions provide evidence that TCF promoter binding and activation of MDR1 is mediated through both PN and IL17A stimulated TCF4 in the nucleus. In agreement with these results, ChIP assays were done using CD44v6-immunoprecipitated (IP) DNA, and TCF4-IP'd DNA, and input DNAs were amplified using primers covering the indicated TCF4 binding sites (see the schematic model of MDR1 promoter

containing TCF4 binding sites in **Figure 7C**). ChIP assays (**Figure 7D**) showed robust binding of *β*-catenin/TCF4 to MDR1 sites in the SW480-FR cells. Results also showed a robust binding activity for CD44v6 to the DNA fragment where TCF4 binds (**Figure 7D**). Knockdown of CD44v6 reduced endogenous *β*-catenin/TCF4 binding to the *MDR1* promoter in response to PN and IL17A in SW480-FR cells (**Figure 7D**), thus validating the results from the luciferase reporter assay (**Figure 7B**) that CD44v6 and β-catenin co-regulate MDR1 expression in response to PN and IL17A in FOLFOX resistant cells. ChIP assays showed that at basal level, *β*-catenin/TCF4 bound weakly to TCF binding sites of the *MDR1* promoter in sensitive cells compared to robust binding activity in resistant cells (data not shown). These data provide evidence that in the presence of CD44v6, TCF4-mediated transactivation of *MDR1* was up-regulated from basal activity to CD44v6-regulated activity *via* TCF4 in response to PN and IL17A.

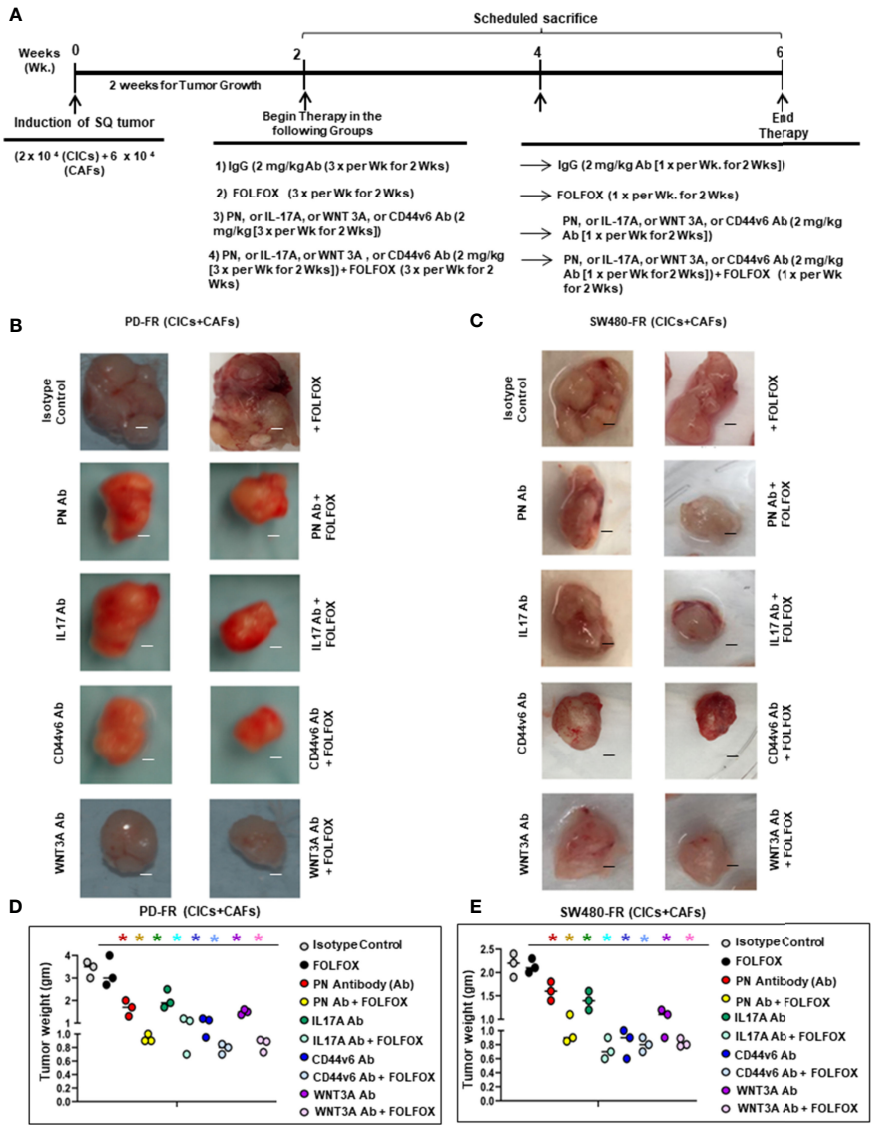

FIGURE 8 | FOLFOX induced PN, WNT3A and IL17A signaling regulates CIC growth *in vivo*. **(A),** Timeline is shown for antibody treatments with and without FOLFOX in xenograft tumors implanted by a mixture of CICs plus CAFs from PD-FR human tissues **(B, D)** and from SW480-FR xenograft tumor cells **(C, E)**. The dependences of CICs on IL17A, WNT3A, PN and CD44v6 were evaluated *in vivo*. 2 x10^4 CICs and 6 x 10^4 CAFs were injected into mice. When tumors reached to approximately 0.3 cm^3 in volume, treatments were initiated. Detailed treatment procedure is in Methods. Mice were weighed, and the tumor volumes were measured every other day for 4 weeks. **(B, C),** Representative tumors from three experiments are shown from mice treated as indicated. **(D, E),** Tumor weights from the experiments in **(B, C)** for each tumor set at the end of treatment after 4 weeks are shown. Data presented in **(D, E)** are Mean ± SD.; n = 5 mice/group independent replicates in three independent experiments; **(B)**, *, $P < 0.05$ were considered significant, inhibition in tumor growth represented by tumor weight and tumor volume in treatment groups compared to IgG control groups. ANOVA, followed by Bonferroni's post-hoc test was used to assess the significance. Scale bars, 1 cm.

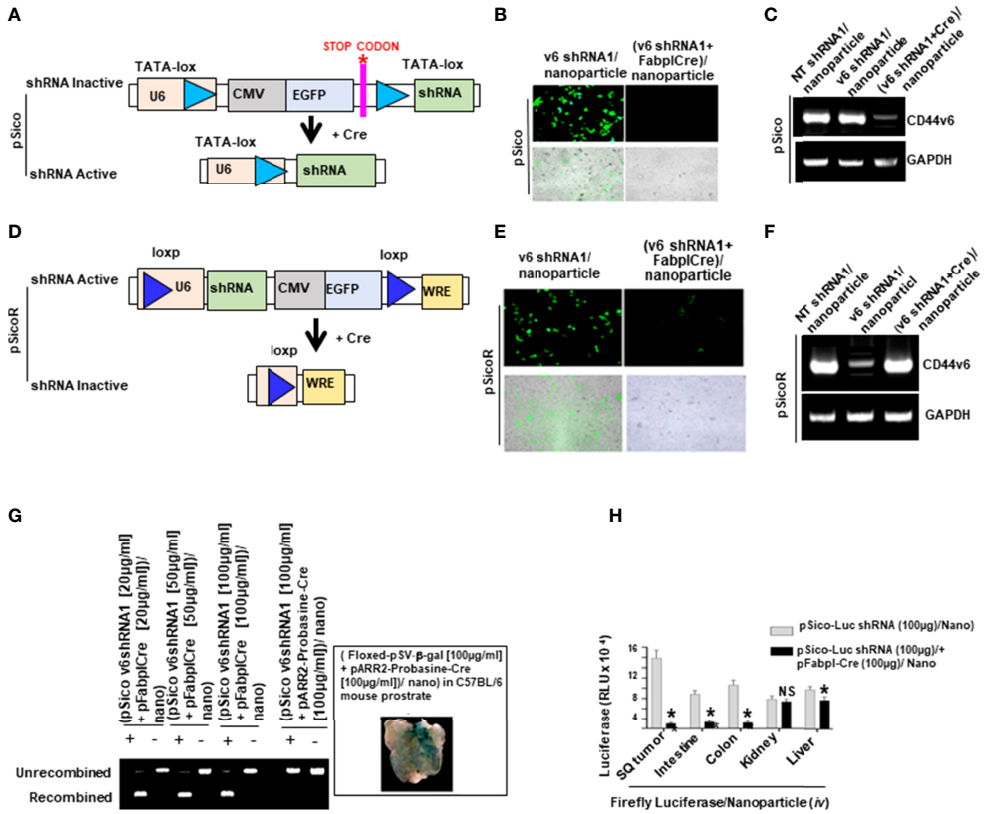

FIGURE 9 | Confirming the inducible CRE system used tissue specific knockdown of CD44v6 to inhibit subcutaneous (SQ) tumor growth. **(A–D)**, Schematic representations of pSico, and pSicoR after Cre-mediated recombination to synthesize active shRNA are shown. **(B–E)**, SW480-FR/SQ tumor cells from the transfection of the cells with (pSico-v6shRNA1 plus the pFabpl-Cre)/transferrin (Tf)-PEG-PEI) (Nanoparticles [Nano]) and with the (pSicoR-v6shRNA1 plus pFabpl-Cre)/Nano and were analyzed by epifluorescence microscopy to detect GFP. Similar cell densities and identical exposure times were used for all images. (See Materials and Methods for details in nanoparticles). **(C, F)**, Total RNAs extracted from the transfected cells were analyzed for CD44v6 and GAPDH mRNAs by semi-quantitative PCR. **(G)**, SW480-FR cells were transfected with pSico v6 shRNA plus Fabpl-Cre/Nano, or with pSicoR v6shRNA plus Fabpl-Cre/Nano. PCR detection is shown for Cre-mediated recombination of pSico-CD44v6 shRNA in tumor Genomic DNAs extracted from mice 4 days after shRNA plus indicated Cre/Nano treatments to xenograft tumors induced by SW480-FR cells. (# of mice/experiment = 5; # of experiments = 2). Note that pSico v6 shRNA plus Probasin Cre/Nano did not have any effect on colon tumors. Inset shows the functionality of Floxed-pSVβ-galactoside/ plus pARR2-Probasin Cre/nanoparticles in the prostate gland. **(H)**, Validation for tissue specific delivery of shRNA/nanoparticles was done by verifying distributions of shRNA against the firefly luciferase gene (pSico-Firefly luciferase shRNA plus pFabpl-Cre)/Nano, and are shown in various organs of C57/Bl mice (n = 4), which were previously injected with reporter plasmids expressing firefly luciferase and renilla luciferase (i.p.). The luciferase activities of the tumor extracts and the indicated tissues were measured. Note that luciferase-shRNA is active in colon tumors and in normal colon and intestine tissues due to the functionality of pFabpl-Cre. Data presented are Mean ± SD.; n = 5 mice/group independent replicates in two **(G)** and three **(H)** independent experiments. All semi quantitative RT-PCR and Epifluorescence microscopy data are representative of three experiments. **(H)**, *, $P < 0.05$ was considered significant, inhibition in luciferase activity in (pSico-Luc sh (100µg) + pFabpl-Cre (100µg))/ Nano compared to pSico-Luciferase shRNA (100µg)/Nano group. Student's t-test was used to assess the significance in **(H)**.

When stabilized β-catenin enters the nucleus, it interacts with transcriptional regulators, including TCF4, which leads to WNT/β-catenin responsive gene expression (69). Thus, the results in **Figure 7D** indicate that PN and/or IL17A regulate β-catenin/TCF4 binding to a *MDR1* promoter in a CD44v6-regulated manner in FOLFOX resistant cells.

Several putative TCF binding sites were located 2 kb upstream of the transcriptional start site of the CD44v6 gene (see the schematic model of CD44v6 luciferase reporter in **Figure 7E**). A CD44v6 luciferase assay was used to directly examine the interaction between PN and IL17A induced β-catenin/TCF4 and the CD44v6 promoter. The luciferase activities in SW480-FR cells transfected with dominant negative TCF4-DN were significantly lower than vector group, while PN and IL17A overexpression significantly increased the luciferase activity (**Figure 7F**). Further, this result also indicates that PN and IL17A induced CD44v6 promoter activity requires WNT/TCF4 binding to the CD44v6 promoter. This provides evidence that PN and IL17A stimulated the β-catenin/TCF4-mediated increase in CD44v6 transcription activity. To further validate these results, conventional ChIP analyses were done, and they provided direct evidence for the ability of PN and IL17A to stimulate TCF4 to bind to the promoter of CD44v6 (see the scheme in **Figure 7G**, and CD44v6 transcription activity in **Figure 7H**). The data in **Figure 7** indicate that PN and IL17A

promote both CD44v6 and MDR1 gene expressions through a β-catenin/TCF4 pathway. Overall, the above results (**Figure 7**) indicate that FOLFOX treatment mediates PN and IL17A, which recruit a WNT3A pathway that promotes CD44v6 expression (as seen in **Figures 5**, and in MDR1 and CD44v6 transcription activities in **Figure 7**), and CD44v6 regulates WNT3A production (as seen in **Figures 5A, B** and β-catenin signaling through PN and IL17A (as seen in **Figures 5D–G**) in response to FOLFOX treatment. Taken together our results provide evidence for a positive feed-back loop between CD44v6 and β-catenin/TCF4 that activates MDR1 gene expression and CD44v6 splicing, and mediates FOLFOX resistance (as seen in **Figures 2F**, **5** and **7**).

Stromal Secreted Factors Can Maintain CIC Growth and Tumorigenic Function

To address the contributions of PN, WNT3A, IL17A or CD44v6 in the *in vivo* SQ growth of CICs, a neutralizing antibody for each of these factors was used in combination with 1 x FOLFOX (schematic model detailing the experimental procedures (**Figure 8A**) used in the experiment of **Figure 8B**). Tumors were established by injecting CICs in combination with CAFs subcutaneously in immunocompromised mice. Administration of neutralizing antibodies for PN, or WNT3A, or IL17A, or CD44v6 increased the efficacy of FOLFOX-chemotherapy on reducing tumor growth (**Figures 8B–E**). These results confirm that FOLFOX resistance depends primarily on secreted factors including PN, WNT3A and/or IL17A in CAFs, as well as on CD44v6 in both CICs and CAFs. These data provide evidence that the central roles of PN, WNT3A and/or IL17A are to serve more as paracrine signals to have crucial roles in driving FOLFOX resistance in CICs and in promoting tumor growth. Together our data support a pattern in which FOLFOX-therapy stimulates CAFs and activates CIC maintenance (as seen in **Figure 1D**, and **Figure 3**) in the microenvironment to stimulate paracrine signals (as seen in **Figure 4**) for induction of CIC growth (as seen in **Figures 3C–G**) and SQ tumor growth when implanted with CAFs and CICs (**Figures 8B–E**).

Tissue Specific Inhibition of CD44v6 *In Vivo* Inhibits MDR1 Expression and CRC Progression by Retaining FOLFOX Sensitivity

There is no small molecule inhibitor for CD44v6 commercially available. For genetic targeting of CD44v6, we tested the effect of pSico-CD44v6shRNA plus pFabpl-Cre by intraperitoneal treatment with nanoparticle delivery systems engineered to express CD44v6shRNA in the SW480-FR/CICs plus PD-FR/CAFS implanted xenograft tumors in immunocompromised mice. The purpose was to transactivate a conditionally silenced pSico- plasmid with a CD44v6 shRNA oligonucleotide (pSico-CD44v6shRNA) by Cre-recombinase that is produced in response to an intestine/colon tissue-specific pFabpl promoter. The principle is as follows. The recombinase, produced under the influence of a tissue-specific promoter in the cells, will eliminate the (CMV-EGFP)-cassette from U6-$(CMV\text{-}EGFP)^{flox/flox}$-CD44v6 shRNA from the pSico-CD44v6shRNA, and then the U6 promoter will induce synthesis of CD44v6 shRNA. Normal cells in the intestine/colon will not be affected because they rely mostly on the standard CD44s expression, which does not have any variant exons of CD44. Even if cells in other organs express CD44v6shRNA, knockdown of CD44v6 will not be produced due to lack of response to the tissue-specific promoter. Unused plasmids in other organs will be progressively destroyed by cytoplasmic nucleases, and the nanoparticles will be cleared because PEG and PEI are biodegradable, thus avoiding any toxicity problem (31, 49), It has been shown that Transferrin (Tf)-receptors are highly expressed in colon tumors (59).

First, to assess the contributions of CD44v6 in colorectal CICs and CAFs implanted SQ tumors, we generated pSico-CD44v6shRNA plus pFabpl-Cre plasmids and encapsulated them in a Tf-polyethylene glycol (PEG)-polyethylene imine (PEI) nanoparticles following our previous study (59). The pSico-CD44v6shRNA was used in *in vivo* experiments in the presence of Fabpl-Cre to constitutively silence endogenous CD44v6 (schematic representation of pSico is shown in **Figure 9A**). The same CD44v6shRNA sequence was cloned in a pSicoR vector (**Figure 9D** schematic representation of pSicoR) and was used to constitutively silence endogenous CD44v6 in the absence of Fabpl-Cre in *in vitro* experiments. As a control, non targeted (NT) shRNA was also cloned in these vectors. Second, before applying our pSico-CD44v6shRNA1 plus Fabpl-Cre in *in vivo* experiments, we validated our Cre-regulated v6-shRNA1/nanoparticles in SW480-FR cells, which were transfected with either pSico-CD44v6shRNA1 with or without Fabpl-Cre containing nanoparticles. High-efficiency transduction by either vector was achieved as indicated by uniform GFP expression (**Figure 9B** for pSico-CD44v6shRNA1 and **Figure 9E** for pSicoR-CD44v6shRNA1 with or without Fabpl-Cre nanoparticles). Validation of the v6shRNA1 was done in **Figure 2G** following our previously published papers (31, 49). CD44v6shRNA1 expression by this vector was functionally consistent in inducing large reductions of CD44v6 gene expression, which was Cre-dependent (**Figures 9B, C** for pSico-CD44v6shRNA1 and **Figures 9E, F** for pSicoR-CD44v6shRNA1 with or without Fabpl-Cre nanoparticles). The results of **Figures 9A–H** validate the use of Fabpl-Cre- and pSico-CD44v6shRNA1, and pSicoR-CD44v6shRNA1 nanoparticles for silencing CD44v6 expression in *in vitro* and in *in vivo* experiments.

Further we validated the inclusion of a pFabpl-Cre plasmid in our conditional silencing of CD44v6 in *in vivo* tumors derived from CICs plus CAFs isolated from SW480-FR tumor cells. As shown in **Figure 9G**, shRNA knockdown of CD44v6 in CICs plus CAFs implanted to form SW480-FR/SQ tumors depended on the inclusion of a pFabpl-Cre plasmid and induced nearly complete recombination due to loss of GFP. In contrast a pARR2-Probasin-Cre plasmid, which is specific for prostate tissue, could not induce a recombination of the pSico-CD44v6-shRNA plasmid and did not show any effect in colon tissue. The inset (**Figure 9G**) shows that pARR2-Probasin Cre releases β-galactosidase from a conditional β-gal plasmid in the mouse prostate, further validating tissue specific delivery of the plasmid when a tissue specific Cre is in the right place. In addition, we validated tissue specificity of pFabpl-Cre

dependent knockdown of another gene (firefly luciferase gene). **Figure 9H** shows that the *in vivo* transfection and pFabpl-Cre dependent knockdown of the firefly luciferase gene was specific to colorectal tumor tissue, as well as to small and large intestines, but not to kidney or liver. This indicates that the nanoparticles carrying plasmids activate only in specific tissues that are dependent on promoter driven Cre expression. The *in vivo* knockdown of the luciferase gene was strikingly greater in SQ tumors with similarity between colon and intestine tumors (**Figure 9H**), indicating that the transferrin-coated nanoparticles carrying plasmids accumulate into the colon tumors more than into normal intestine/colon cells because of increased expression of transferrin receptor by these tumors as well as by expression of pFabpl-Cre mediated conditional silencing of the firefly luciferase gene (59, 71).

We next used the transferrin-nanoparticle delivery of pSicoCD44v6 shRNA plus Fabpl-Cre to determine whether silencing the expression of CD44v6, or of CD44v6-containing variants, can inhibit the tumor cell survival and growth by reducing WNT-CD44v6-MDR1 signaling. The pSicoCD44v6 shRNA1 plus Fabpl-Cre nanoparticles were used *in vivo* to examine the therapeutic potential of targeting CD44v6 in tumors implanted from CICs plus CAFs isolated from a FOLFOX resistant SW480-FR/SQ tumor, and from a patient-derived tumor specimen (PD-FR) (**Figure 10A**, schematic model). Details of the experimental procedures used are in **Figure 10B**. For this experiment, xenograft tumors were established by injecting SW480-FR/CICs in combination with SW480-FR/CAFs, and with PD-FR/CICs in combination with PD-FR/CAFs subcutaneously into immunocompromised mice (schematic model indicated in **Figure 10A**). Cre-mediated conditional silencing of endogenous CD44v6 was used in combination with FOLFOX therapy. Tissue samples from the experiments in **Figure 10B** were used in the follow-up experiments in the **Figures 10B–H**. Administration of Cre-mediated CD44v6shRNA nanoparticles prevented tumor growth (**Figures 10B–D**) and strongly inhibited CD44v6 and MDR1 expressions (**Figure 10E**) in a dose-dependent manner. Moreover, 100 μg/ml plasmid concentration + 1 x FOLFOX had the predominant effect in reducing tumor growth and inhibiting MDR1 expression (**Figures 10B–F**). In agreement with our recent study (55), knocking down CD44v6 reduced stemness related genes including c-Myc, TWIST1, OCT4, SOX2 and ABCB1 (MDR1) substantially in tumors generated from CICs plus CAFs (**Figure 10H**). Moreover, our data in **Figures 10G, H** support our hypothesis that CD44v6-WNT/β-catenin signaling regulates the stemness of CICs expressing CD44v6 (**Figure 10H**), and that blocking CD44v6 tissue specifically by conditional silencing has a dramatic effect on reduction of tumor growth (**Figures 10B–D**) by blocking WNT/β-catenin specific TOPFlash promoter activity in tumor lysates (**Figure 10G**). Importantly, pSico-v6shRNA1/Nano i.p. administration showed no evidence of toxicity within these experiments or in previous studies using Cre-mediated CD44v6shRNA1 nanoparticles (31, 49). These results provide direct relevance for CD44v6 as a therapeutic target to maintain FOLFOX sensitivity and reduce colon tumor growth by reducing MDR1 expression.

DISCUSSION

Many studies have shown that CICs may be accountable for tumor resistance to conventional chemotherapy (8, 72). When the resistance is increased through the crosstalk between CICs and the tumor microenvironment, that resistance concept acts through two ways for tumor progression in CICs: intrinsic and extrinsic pathways. The intrinsic mechanisms involve gene mutation, while the extrinsic mechanisms incorporate the production of distinct growth factors and cytokines by the tumor microenvironment leading to the activation of specific signaling pathways (22). This study revealed that paracrine factors secreted by TME cells such as CAFs induce WNT-CD44v6 signaling in CICs to further drive tumor growth in xenograft tumors implanted with CICs combined with CAFs. Interestingly, administration of cytotoxic drugs, including FOLFOX, induces secretion of paracrine factors by CAFs derived from colorectal cancer specimens from patients after cytotoxic drug treatment compared to normal fibroblasts (**Figures 4D–F**).This concept is important because several studies carefully used modified normal fibroblasts in place of CAFs with CRC cell lines to dissect out tumor-stromal interactions (12, 13, 73, 74). Most lethal colorectal tumors are diagnosed at more advanced stages. Thus we used a clinically relevant approach based on CAFs and CICs directly derived from fresh tumors of drug resistant human patient tissues (PD-FUR, or PD-OXAR or PD-FR), or from CAFs and CICs derived from our resistant cell implanted SQ tumors. Using these fresh specimens from patients, we showed a significant increase in CAFs occurrence in cytotoxic drug treated tumors (**Figure 1D**). Interestingly, the CICs isolated from cytotoxic drug treated patient specimens produced very low levels of secretome (secreted factors) (**Supplemental Figure 1A**). Thus, if CAFs truly do evolve from lethal chemotherapy resistant tumors upon drug exposure, then data acquired from modified normal colon fibroblasts may not reflect an accurate picture of the functions of CAFs in supporting CIC growth. Based on data in this study, we postulate that the secretome from CAFs used in our study supports that cytotoxic therapy induced CIC growth/maintenance drives CRC recurrence and mortality.

Most cancers originate from cells that gained cancer-initiating capacity or cancer stemness. These cells are known as CICs that are plastic in nature. Stemness functions of CICs are influenced by extrinsic factors secreted from stroma. Sustained drug resistance and tumorigenic potential of CICs is on TME and especially on the niche-microenvironment where CICs reside. Niches are specialized microenvironments that regulate the fate of CICs by providing cues in the form of both CIC-TME cell contacts and by secreted stromal factors. Here we demonstrate that tumorigenic colorectal cells are included in a rare population of undifferentiated CICs that express CD44v6 (**Figures 2D, E**). Our companion paper (48) revealed that the CIC immunophenotype ($CD44v6^{high+}$) within a tumor is responsible for tumor formation, progression, and resistance to FOLFOX therapies. The interaction between CICs and their tumor niches is strongly linked to the CIC survival/self-renewal (75). Through this tumor-stroma interaction, CICs

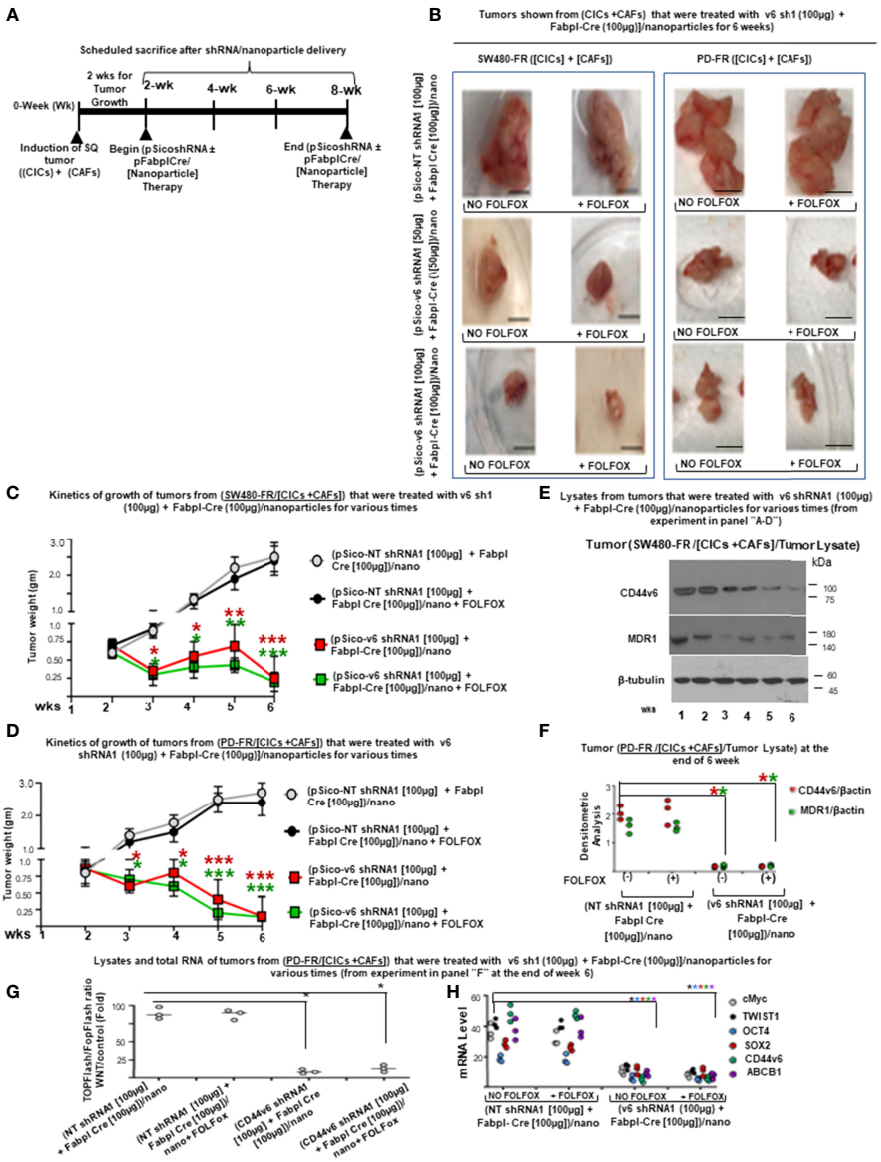

FIGURE 10 | Tissue specific knockdown of CD44v6 by pFabpl-Cre inhibits subcutaneous (SQ) tumor growth of implanted CICs plus CAFs from SW480-FR/SQ tumors and from PD-FR/SQ tumors. **(A)**, Timeline is shown for pSico-v6-shRNA/Nano particle treatment with and without pFabpl-Cre/Nano in xenograft tumors derived from CICs plus CAFs from SW480-FR/SQ tumors and PD-FR/SQ tumors. **(B)**, The dependence of tumors derived from CICs and CAFs on CD44v6 was evaluated in vivo. 2 x 104 FACS sorted CAM(+)CD44v6(+)CD133(+)ALDH1(+) CICs and 6 x 104 CAFs (EpCAM [-]/PDGFR-α were injected into mice. When tumors reached to approximately 0.3 cm3 in volume, treatment was initiated. Detailed treatment procedure is in Methods. Seven immunocompromised mice per group were used. Mice were weighed every other day, and the tumor weights were measured every week for 4 weeks. Representative tumors following sacrifice from three experiments are shown from mice treated as indicated in the schedule of treatment **(A)**. **(C, D)**, Kinetics of relative tumor weights with time are shown during in vivo SQ tumor growth at the indicated weeks that were generated by CICs plus CAFs from SW480-FR/SQ tumors **(C)** and from PD-FR/SQ tumors **(D)** injected (i.p.) with pSico-NT shRNA/Nano, pSico-v6 shRNA/Nano, and (pSico-v6 sh plus pFabpl-Cre)/Nano. Treatments were performed at weeks (wks) 2, 3, 4, and 5 and tumor growth was measured at wks 3, 4, 5, and 6 after treatments. **(E)**, Western blot analyses using CD44v6, MDR1 and β-catenin antibodies in extracts from the various treated xenograft tumors derived from CICs plus CAFs from SW480-FR/SQ tumors collected at 6 weeks from the experiment in **(A–C)** are shown. **(F)**, Densitometric ratios are shown of CD44v6/β -actin and MDR1/β -actin in the Western blot analyses using CD44v6, MDR1 and β–catenin antibodies in extracts from the various treated xenograft tumors derived from CICs plus CAFs and from PD-FR/SQ tumors collected at 6 weeks from the experiment in **(A, B, D)**. The results are means ± SE from four independent experiments (n = 6 mice) **(G)**, QPCR analyses of the indicated stemness related transcription factors from the total RNA from the various treated tumors collected at 6 weeks in **(A, B, D)** are shown. **(H)**, WNT3A/β-catenin reporter activities in the lysates from the tumors collected at 6 weeks from experiments in (A, B, D) are shown. Data **(C, D–H)** are presented as mean ± SD (n = 7); *P < 0.05 compared to appropriate control group. Western blot data (E) are representative of three experiments. Tumor data are presented as mean ± SD (n = 7 mice/group in four independent experiments); **(C–H)**, *P < 0.05. **P < 0.01, ***P were considered significant, Inhibition of tumor growth in (v6 shRNA + pFabpl Cre)/nano, and in (v6 shRNA + pFabpl Cre)/nano plus FOLFOX compared with (NT shRNA + pFabpl Cre)/nano, and in (NT shRNA + pFabpl Cre)/nano plus FOLFOX groups respectively Western blot data are representative of four independent experiments. ANOVA, followed by Bonferroni's post-hoc test was used to assess the significance in C and D. Student's t-test was used to assess the significance in **(E–H)**. Scale bars, 1 cm.

can preserve the tumor heterogeneity that underlies their important malignant behaviors and therapy resistance (76). Based on this backdrop, our present study revealed that colorectal tumors respond to FOFOX therapy by stimulation of supporting CAFs in the tumor-microenvironment to provide cues in the form of secreted factors (PN and IL17A) to stimulate WNT3A signals to maintain CICs. Our data also suggest that FOLFOX stimulation increased the frequency of CAFs measured by stimulating a relative proportion of fibroblasts to the epithelial component (αSMA versus EpCAM). Subsequently, the CAFs create a niche that is chemo resistant by releasing predominantly PN, WNT3A and IL17A. Exogenous addition of either PN, IL17A or WNT3A increased CIC tumorigenic function and maintenance. Especially, these factors were overexpressed by colorectal CAFs in response to FOLFOX with their expression validated directly in patient-derived specimens. Periostin and IL17A sustain a WNT3A-CD44v6 induced CD44v6(+) CIC-maintenance that is shared by WNT ligands. Additionally, our data also revealed that the tumorigenic potential of these CICs together with the CAF subpopulation significantly increased in secondary and tertiary subcutaneous xenograft tumors. In contrast, tumorigenic potential of Non-CICs plus CAFs was completely lost in secondary, tertiary and quaternary subcutaneous xenograft tumors suggesting that Non-CICs are differentiated non-tumorigenic cells. These results provide evidence that drug resistant and long-term tumorigenic potential are restricted to the CD44v6 expressing CIC population, and chemotherapy induces remodeling of the tumor microenvironment to support the tumor cellular hierarchy through secreted factors.

First, using primary cultures derived from the tumors of patients who were treated with cytotoxic regimens (PD-5FUR, PD-OXAR and PD-FR), we showed how FOLFOX induced enrichment of CAFs induces maintenance of CICs for self-renewal capacity as they can be clonally expanded, are exclusively tumorigenic, and are able to differentiate. As PN and IL17A provide important instructive signals from supportive CAFs to stimulate WNT3A, and because CD44v6 regulates these factors in the microenvironment, we focused our attention on these molecules within the CAF's-secretome. Freshly isolated patient-derived CD44v6+CICs were highly tumorigenic, and as few as 2 x 10^3 CD44v6+CICs were capable of inducing orthotopic tumor formation in immunocompromised mice. In contrast, as many as 5 x 10^5 CD44v6 (–) Non-CICs did not result in any tumor formation. Interestingly, when freshly derived CAFs from FOLFOX-resistant tumors were combined with CICs, the resultant tumors attained long term tumorigenic potential with shorter latency, and increased self-renewal capacity as they can be clonally expanded (**Figures 3F–G**).

Second, these factors (PN and IL17A) from CAFs recruit WNT3A ligands and thereby stimulation of WNT-CD44v6 signaling in CICs, which instructs the cellular hierarchy. In our companion paper (48), we showed for the first time that CD44v6 regulated a WNT/β-catenin axis, which in turn further transactivates MDR1 and CD44v6 gene expressions in CD44v6 (+) CICs. Activation of WNT-CD44v6 signaling has a key role in maintaining the CIC pool in the gut and in promoting self-renewal of colorectal-CICs (64, 77, 78). Stromal elements contribute significantly to maintain the undifferentiated status and the clonogenic activity of the tumorigenic cells (12–14, 79). Our results revealed that this property is not confined only to WNT, but is shared by PN and IL17A through FOLFOX, which augments β-catenin activation in colorectal CICs expressing CD44v6 (**Figure 5**).

Third, our results show the direct relevance of PN, WNT3A and IL17A as dominant paracrine signals for the interplay between CICs and CAFs in tumorigenesis. Since CD44v6 regulated WNT3A, as well as IL17A and PN production in CAFs (**Figures 5A, B**), we showed that targeting either WNT3A, or IL17A, or CD44v6 or PN in the CICs + CAFs implanted PD-FR and SW480-FR SQ tumors in immune-deficient mice was effective in reducing colon tumor growth (**Figures 10B–E** versus **Figures 8B–E**). Importantly, these results further indicate that IL17A signaling also has a functional role in CIC-CAF interactions independent of adaptive immune cell functions.

Fifth, we showed that our cell-specific delivery approach (59) to target the CD44v6-induced signaling pathway in colon cancer cells inhibited colon tumor growth (**Figure 10**) significantly compared to the CD44v6 neutralizing antibody mediated reduced tumor growth (**Figure 8**). This cell-specific targeting approach has several advantages and may be easily designed to target other CD44variant-expressing cancer cells, or any cell-surface receptor-expressing cancer cells where the receptor is both a functional marker and a therapeutic target of CICs.

CONCLUSION

We found that human colorectal CICs that are defined by CD44v6 expression are exclusively tumorigenic and highly resistant to FOLFOX-therapy. Colorectal-tumor progression is initially triggered by CD44v6(+) CICs. The interactions between CD44v6(+) CICs and their niche are supported by periostin and IL17A (**Figure 11**). Periostin and IL17A simulate WNT3A, which is crucial for augmenting CD44v6(+) CICs that promotes long-lasting tumorigenic potential. It is most intriguing that in an *in vivo* model of orthotopic colorectal cancer, implantation of CAFs with CD44v6(-) Non-CICs virtually abrogated the primary-tumor formation, whereas CAFs with CD44v6(+) CIC populations can reproduce the original tumor in permissive recipients. Since FOLFOX-therapy treated CAFs and CICs express increased levels of CD44v6 that regulates periostin, IL17A and WNT3A, the depletion of CD44v6 from tumors by tissue specific delivery of CD44v6 shRNA almost abrogated the stemness phenotype of CICs with significant inhibition effects on their tumorigenic potential (**Figure 11**). Therefore, we demonstrate that CD44v6 is a CIC marker and a therapeutic target. In summary, the drug resistance ability of colorectal CICs is increased by supported

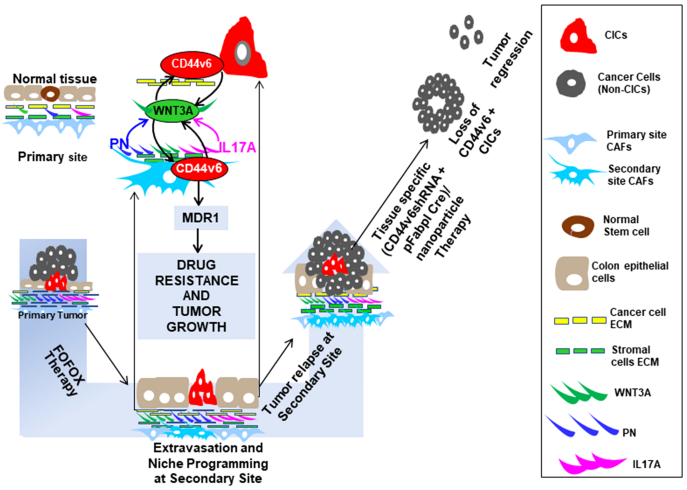

FIGURE 11 | Conclusion Figure. Colon cancer associated fibroblast derived PN and IL17A promote WNT3A induced CD44v6 expression in cancer initiating cells (CICs). CD44v6 positive CICs induce drug resistance and colorectal tumorigenesis by enhancing CD44v6/βcatenin nuclear localization and MDR1 gene expression in CICs. CD44v6 regulated PN, IL17A and WNT3A derived from chemotherapy induced CAFs that contribute to CIC maintenance through induction of the CD44v6 receptor. CD44v6 regulated PN, IL17A and WNT3A mediates the crosstalk between CICs and their niche to permit tumor growth and drug resistance. Importantly, this work identifies that tissue specific knockdown of CD44v6 inhibits functions of CICs and their interaction with CAFs, and thereby significantly suppresses tumor growth.

microenvironmental signals that promote the expression of CD44v6, and this indicates that CD44v6 is a molecule that could be clinically exploited both as a biomarker and an effective therapeutic modulator of CRC.

DATA AVAILABILITY STATEMENT

All the data are included within the manuscript. The names of the repository/repositories and accession number(s) can be found in the article supporting information. Coding nucleotide sequences of the genes were obtained from the NCBI, National Institutes of Health, website (www.ncbi.nlm.nih.gov). Hairpin shRNAs were designed to target a transcript sequence using the Broad Institute GPP Web Portal (http://portals.broadinstitute.org/gpp/public/). Primers were designed by online Primer Quest Tool (https://www.idtdna.com/PrimerQuest/Home/Inde).

ETHICS STATEMENT

The animal study was reviewed and approved by Institutional Review Board (IRB) Statement. The Medical University of South Carolina (MUSC) IRB determined that this research project meets the criteria for "Not Human Subjects". All animal studies described were approved by Institutional Animal Care and Use Committee (IACUC) (protocol # IACUC – 2019-00829; Approval period 08/03/2020- 09/24/ 20221) at the Medical University of South Carolina (MUSC) and conducted in accordance with the National Institutes of Health Guide for the Care and Use of Animals. Procedures for animal studies were conducted in accordance with the National Institutes of Health Guide for the Care and Use of Animals IACUC-2017-00250 (approval date: 2019/03/14-2021/03/29).

AUTHOR CONTRIBUTIONS

The experiments of this work were designed and carried out by SM and SG. The paper was written by SM and SG. VH reviewed, edited the multiple versions of the drafts and final versions of the text, figures, figure legends, participated in designing experiments and supplied reagents. RM edited the drafts, provided reagents, and participated in designing experiments. NK helped in editing the drafts and participated in designing experiments. All authors contributed to the article and approved the submitted version.

FUNDING

This work was supported by the: 1) 1R03CA167722-01A1 (to SM and SG); 2) 1K12HL141952-02 (to VH); 3) 2P20GM10399; NIH IDeA Network for SC Biomedical Research Excellence, 4) 02 P30 GM13195901, 5) **19TPA34900016** (to RM); and 6) SCTR grant (UL1 TR001450 for SM). The costs of publication of this article will be defrayed in part by the payment of page charges. This article must therefore be hereby marked "*advertisement*" in accordance with 18 U.S.C. Section 1734 solely to indicate this fact.

ACKNOWLEDGEMENTS

The prostate specific pARR2Probasin Cre construct was a gift from Dr. Robert J Matusik, Department of Cell and Developmental Biology, Vanderbilt University, Nashville, TN, USA.

SUPPLEMENTARY MATERIAL

The Supplementary Material for this article can be found online at: https://www.frontiersin.org/articles/10.3389/fonc.2022.906415/full#supplementary-material

Supplementary Figure 1 | Exogenous addition of PN and IL17A induces WNT3A secretion and tumor sphere formation in CAFs. **(A)**, Exogenous addition of 20 ng/ml of PN, or IL17A stimulated WNT3A production in CAFs isolated from sensitive and FR tumors of SW480 were assessed by measuring secretion of WNT3A by an ELISA assay. **(B)**, Autocrine expression of two dominant cytokines (IL17A and WNT3A) and of PN were assessed by using ELISA assays on PD-FR CICs (Sphere/CICs) treated with vehicle (DMSO) or with 1 x FOLFOX for 72 hours. **(C)** Percentages of colon tumor sphere formation are shown in CICs of FR-resistant and sensitive cells of SW480 in the absence and presence of 100 ng/ml of either PN-blocking antibody, IL17A-blocking antibody or WNT3A-blocking antibody. Data are presented as Mean ± SD (n = 4 replicates from three independent experiments *, $P < 0.05$ was considered significant, **(A, B)**, stimulation of secreted protein in treatment groups were compared with vehicle controls; **(C)**, Inhibition of percent of tumor sphere formation in PN, IL17A and WNT3A antibody treated groups compared with IgG control group. Student's t-test was used to assess the significance.

REFERENCES

1. Ferlay J, Soerjomataram I, Dikshit R, Eser S, Mathers C, Rebelo M, et al. Cancer Incidence and Mortality Worldwide: Sources, Methods and Major Patterns in GLOBOCAN 2012. *Int J Cancer* (2015) 136(5):E359–86. doi: 10.1002/ijc.29210
2. Duineveld LA, van Asselt KM, Bemelman WA, Smits AB, Tanis PJ, van Weert HC, et al. Symptomatic and Asymptomatic Colon Cancer Recurrence: A Multicenter Cohort Study. *Ann Fam Med* (2016) 14(3):215–20. doi: 10.1370/afm.1919
3. Coppede F, Lopomo A, Spisni R, Migliore L. Genetic and Epigenetic Biomarkers for Diagnosis, Prognosis and Treatment of Colorectal Cancer. *World J Gastroenterol* (2014) 20(4):943–56. doi: 10.3748/wjg.v20.i4.943
4. Haggar FA, Boushey RP. Colorectal Cancer Epidemiology: Incidence, Mortality, Survival, and Risk Factors. *Clin Colon Rectal Surg* (2009) 22 (4):191–7. doi: 10.1055/s-0029-1242458
5. Singh AK, Arya RK, Maheshwari S, Singh A, Meena S, Pandey P, et al. Tumor Heterogeneity and Cancer Stem Cell Paradigm: Updates in Concept, Controversies and Clinical Relevance. *Int J Cancer* (2015) 136(9):1991–2000. doi: 10.1002/ijc.28804
6. de Sousa e Melo F, Kurtova AV, Harnoss JM, Kljavin N, Hoeck JD, Hung J, et al. A Distinct Role for Lgr5(+) Stem Cells in Primary and Metastatic Colon Cancer. *Nature* (2017) 543(7647):676–80. doi: 10.1038/nature21713
7. Bu Y, Cao D. The Origin of Cancer Stem Cells. *Front Biosci (Schol Ed)* (2012) 4:819–30. doi: 10.2741/s302
8. Valent P, Bonnet D, De Maria R, Lapidot T, Copland M, Melo JV, et al. Cancer Stem Cell Definitions and Terminology: The Devil is in the Details. *Nat Rev Cancer* (2012) 12(11):767–75. doi: 10.1038/nrc3368
9. Clarke MF, Dick JE, Dirks PB, Eaves CJ, Jamieson CH, Jones DL, et al. Cancer Stem Cells–Perspectives on Current Status and Future Directions: AACR Workshop on Cancer Stem Cells. *Cancer Res* (2006) 66(19):9339–44. doi: 10.1158/0008-5472.CAN-06-3126
10. Nguyen LV, Vanner R, Dirks P, Eaves CJ. Cancer Stem Cells: An Evolving Concept. *Nat Rev Cancer* (2012) 12(2):133–43. doi: 10.1038/nrc3184
11. Kreso A, O'Brien CA, van Galen P, Gan OI, Notta F, Brown AM, et al. Variable Clonal Repopulation Dynamics Influence Chemotherapy Response in Colorectal Cancer. *Science* (2013) 339(6119):543–8. doi: 10.1126/science.1227670
12. Vermeulen L, De Sousa EMF, van der Heijden M, Cameron K, de Jong JH, Borovski T, et al. Wnt Activity Defines Colon Cancer Stem Cells and is Regulated by the Microenvironment. *Nat Cell Biol* (2010) 12(5):468–76. doi: 10.1038/ncb2048
13. Vermeulen L, Sprick MR, Kemper K, Stassi G, Medema JP. Cancer Stem Cells–Old Concepts, New Insights. *Cell Death Differ* (2008) 15(6):947–58. doi: 10.1038/cdd.2008.20
14. Medema JP, Vermeulen L. Microenvironmental Regulation of Stem Cells in Intestinal Homeostasis and Cancer. *Nature* (2011) 474(7351):318–26. doi: 10.1038/nature10212
15. Karamanos NK, Piperigkou Z, Passi A, Gotte M, Rousselle P, Vlodavsky I. Extracellular Matrix-Based Cancer Targeting. *Trends Mol Med* (2021) 27 (10):1000–13. doi: 10.1016/j.molmed.2021.07.009
16. Holzel M, Bovier A, Tuting T. Plasticity of Tumour and Immune Cells: A Source of Heterogeneity and a Cause for Therapy Resistance? *Nat Rev Cancer* (2013) 13(5):365–76. doi: 10.1038/nrc3498
17. Lu J, Ye X, Fan F, Xia L, Bhattacharya R, Bellister S, et al. Endothelial Cells Promote the Colorectal Cancer Stem Cell Phenotype Through a Soluble Form of Jagged-1. *Cancer Cell* (2013) 23(2):171–85. doi: 10.1016/j.ccr.2012.12.021
18. Luraghi P, Reato G, Cipriano E, Sassi F, Orzan F, Bigatto V, et al. MET Signaling in Colon Cancer Stem-Like Cells Blunts the Therapeutic Response to EGFR Inhibitors. *Cancer Res* (2014) 74(6):1857–69. doi: 10.1158/0008-5472.CAN-13-2340-T
19. Malanchi I, Santamaria-Martinez A, Susanto E, Peng H, Lehr HA, Delaloye JF, et al. Interactions Between Cancer Stem Cells and Their Niche Govern Metastatic Colonization. *Nature* (2011) 481(7379):85–9. doi: 10.1038/nature10694
20. Lotti F, Jarrar AM, Pai RK, Hitomi M, Lathia J, Mace A, et al. Chemotherapy Activates Cancer-Associated Fibroblasts to Maintain Colorectal Cancer-Initiating Cells by IL-17a. *J Exp Med* (2013) 210(13):2851–72. doi: 10.1084/jem.20131195
21. Sneddon JB, Werb Z. Location, Location, Location: The Cancer Stem Cell Niche. *Cell Stem Cell* (2007) 1(6):607–11. doi: 10.1016/j.stem.2007.11.009
22. Plaks V, Kong N, Werb Z. The Cancer Stem Cell Niche: How Essential is the Niche in Regulating Stemness of Tumor Cells? *Cell Stem Cell* (2015) 16 (3):225–38. doi: 10.1016/j.stem.2015.02.015
23. Screaton GR, Bell MV, Jackson DG, Cornelis FB, Gerth U, Bell JI. Genomic Structure of DNA Encoding the Lymphocyte Homing Receptor CD44 Reveals at Least 12 Alternatively Spliced Exons. *Proc Natl Acad Sci U.S.A.* (1992) 89 (24):12160–4. doi: 10.1073/pnas.89.24.12160
24. Zoller M. CD44: Can a Cancer-Initiating Cell Profit From an Abundantly Expressed Molecule? *Nat Rev Cancer* (2011) 11(4):254–67. doi: 10.1038/nrc3023
25. Naor D, Wallach-Dayan SB, Zahalka MA, Sionov RV. Involvement of CD44, a Molecule With a Thousand Faces, in Cancer Dissemination. *Semin Cancer Biol* (2008) 18(4):260–7. doi: 10.1016/j.semcancer.2008.03.015
26. Zeilstra J, Joosten SP, van Andel H, Tolg C, Berns A, Snoek M, et al. Stem Cell CD44v Isoforms Promote Intestinal Cancer Formation in Apc(min) Mice Downstream of Wnt Signaling. *Oncogene* (2014) 33(5):665–70. doi: 10.1038/onc.2012.611
27. Orian-Rousseau V, Chen L, Sleeman JP, Herrlich P, Ponta H. CD44 is Required for Two Consecutive Steps in HGF/c-Met Signaling. *Genes Dev* (2002) 16(23):3074–86. doi: 10.1101/gad.242602
28. Tremmel M, Matzke A, Albrecht I, Laib AM, Olaku V, Ballmer-Hofer K, et al. A CD44v6 Peptide Reveals a Role of CD44 in VEGFR-2 Signaling and Angiogenesis. *Blood* (2009) 114(25):5236–44. doi: 10.1182/blood-2009-04-219204
29. Cheng C, Yaffe MB, Sharp PA. A Positive Feedback Loop Couples Ras Activation and CD44 Alternative Splicing. *Genes Dev* (2006) 20(13):1715–20. doi: 10.1101/gad.1430906
30. Ghatak S, Bogatkevich GS, Atnelishvili I, Akter T, Feghali-Bostwick C, Hoffman S, et al. Overexpression of C-Met and CD44v6 Receptors Contributes to Autocrine TGF-Beta1 Signaling in Interstitial Lung

Disease. *J Biol Chem* (2014) 289(11):7856–72. doi: 10.1074/jbc.M113.505065
31. Ghatak S, Markwald RR, Hascall VC, Dowling W, Lottes RG, Baatz JE, et al. Transforming Growth Factor Beta1 (TGFbeta1) Regulates CD44V6 Expression and Activity Through Extracellular Signal-Regulated Kinase (ERK)-Induced EGR1 in Pulmonary Fibrogenic Fibroblasts. *J Biol Chem* (2017B) 292(25):10465–89. doi: 10.1074/jbc.M116.752451
32. Misra S, Toole BP, Ghatak S. Hyaluronan Constitutively Regulates Activation of Multiple Receptor Tyrosine Kinases in Epithelial and Carcinoma Cells. *J Biol Chem* (2006) 281(46):34936–41. doi: 10.1074/jbc.C600138200
33. Bourguignon LY, Zhu H, Chu A, Iida N, Zhang L, Hung MC. Interaction Between the Adhesion Receptor, CD44, and the Oncogene Product, P185her2, Promotes Human Ovarian Tumor Cell Activation. *J Biol Chem* (1997) 272 (44):27913–8. doi: 10.1074/jbc.272.44.27913
34. Orian-Rousseau V. CD44, a Therapeutic Target for Metastasising Tumours. *Eur J Cancer* (2010) 46(7):1271–7. doi: 10.1016/j.ejca.2010.02.024
35. Karousou E, Misra S, Ghatak S, Dobra K, Gotte M, Vigetti D, et al. Roles and Targeting of the HAS/hyaluronan/CD44 Molecular System in Cancer. *Matrix Biol* (2017) 59:3–22. doi: 10.1016/j.matbio.2016.10.001
36. Misra S, Heldin P, Hascall VC, Karamanos NK, Skandalis SS, Markwald RR, et al. Hyaluronan-CD44 Interactions as Potential Targets for Cancer Therapy. *FEBS J* (2011) 278(9):1429–43. doi: 10.1111/j.1742-4658.2011.08071.x
37. Safa AR. Resistance to Cell Death and Its Modulation in Cancer Stem Cells. *Crit Rev Oncog* (2016) 21(3-4):203–19. doi: 10.1615/CritRevOncog.2016016976
38. Misra S, Ghatak S, Toole BP. Regulation of MDR1 Expression and Drug Resistance by a Positive Feedback Loop Involving Hyaluronan, Phosphoinositide 3-Kinase, and Erbb2. *J Biol Chem* (2005) 280(21):20310–5. doi: 10.1074/jbc.M500737200
39. Misra S, Ghatak S, Zoltan-Jones A, Toole BP. Regulation of Multidrug Resistance in Cancer Cells by Hyaluronan. *J Biol Chem* (2003) 278 (28):25285–8. doi: 10.1074/jbc.C300173200
40. Orian-Rousseau V, Sleeman J. CD44 is a Multidomain Signaling Platform That Integrates Extracellular Matrix Cues With Growth Factor and Cytokine Signals. *Adv Cancer Res* (2014) 123:231–54. doi: 10.1016/B978-0-12-800092-2.00009-5
41. Morra L, Moch H. Periostin Expression and Epithelial-Mesenchymal Transition in Cancer: A Review and an Update. *Virchows Arch* (2011) 459 (5):465–75. doi: 10.1007/s00428-011-1151-5
42. Morra L, Rechsteiner M, Casagrande S, Duc Luu V, Santimaria R, Diener PA, et al. Relevance of Periostin Splice Variants in Renal Cell Carcinoma. *Am J Pathol* (2011) 179(3):1513–21. doi: 10.1016/j.ajpath.2011.05.035
43. Morra L, Rechsteiner M, Casagrande S, von Teichman A, Schraml P, Moch H, et al. Characterization of Periostin Isoform Pattern in non-Small Cell Lung Cancer. *Lung Cancer* (2012) 76(2):183–90. doi: 10.1016/j.lungcan.2011.10.013
44. Tischler V, Fritzsche FR, Wild PJ, Stephan C, Seifert HH, Riener MO, et al. Periostin is Up-Regulated in High Grade and High Stage Prostate Cancer. *BMC Cancer* (2010) 10:273. doi: 10.1186/1471-2407-10-273
45. Deng X, Ao S, Hou J, Li Z, Lei Y, Lyu G. Prognostic Significance of Periostin in Colorectal Cancer. *Chin J Cancer Res* (2019) 31(3):547–56. doi: 10.21147/j.issn.1000-9604.2019.03.16
46. Zeilstra J, Joosten SP, Dokter M, Verwiel E, Spaargaren M, Pals ST. Deletion of the WNT Target and Cancer Stem Cell Marker CD44 in Apc(Min/+) Mice Attenuates Intestinal Tumorigenesis. *Cancer Res* (2008) 68(10):3655–61. doi: 10.1158/0008-5472.CAN-07-2940
47. Wielenga VJ, Smits R, Korinek V, Smit L, Kielman M, Fodde R, et al. Expression of CD44 in Apc and Tcf Mutant Mice Implies Regulation by the WNT Pathway. *Am J Pathol* (1999) 154(2):515–23. doi: 10.1016/S0002-9440(10)65297-2
48. Ghatak S, Hascall VC, Karamanos N, Markwald RR, Misra S. Chemotherapy Induces Feedback Up-Regulation of CD44v6 in Colorectal Cancer Initiating Cells Through β-Catenin/MDR1 Signaling to Sustain Chemoresistance. *Front Oncol* (2022):MS ID-906260. doi: 10.3390/ijms22020753
49. Ghatak S, Hascall VC, Markwald RR, Feghali-Bostwick C, Artlett CM, Gooz M, et al. Transforming Growth Factor Beta1 (TGFbeta1)-Induced CD44V6-NOX4 Signaling in Pathogenesis of Idiopathic Pulmonary Fibrosis. *J Biol Chem* (2017A) 292(25):10490–519. doi: 10.1074/jbc.M116.752469
50. Ghatak S, Hascall VC, Markwald RR, Misra S. Stromal Hyaluronan Interaction With Epithelial CD44 Variants Promotes Prostate Cancer Invasiveness by Augmenting Expression and Function of Hepatocyte Growth Factor and Androgen Receptor. *J Biol Chem* (2010) 285(26):19821–32. doi: 10.1074/jbc.M110.104273
51. Ghatak S, Misra S, Norris RA, Moreno-Rodriguez RA, Hoffman S, Levine RA, et al. Periostin Induces Intracellular Cross-Talk Between Kinases and Hyaluronan in Atrioventricular Valvulogenesis. *J Biol Chem* (2014) 289 (12):8545–61. doi: 10.1074/jbc.M113.539882
52. von Haller PD, Donohoe S, Goodlett DR, Aebersold R, Watts JD. Mass Spectrometric Characterization of Proteins Extracted From Jurkat T Cell Detergent-Resistant Membrane Domains. *Proteomics* (2001) 1(8):1010–21. doi: 10.1002/1615-9861(200108)1:8<1010::AID-PROT1010>3.0.CO;2-L
53. Graham JM. OptiPrep Density Gradient Solutions for Mammalian Organelles. *ScientificWorldJournal* (2002) 2:1440–3. doi: 10.1100/tsw.2002.840
54. Macdonald JL, Pike LJ. A Simplified Method for the Preparation of Detergent-Free Lipid Rafts. *J Lipid Res* (2005) 46(5):1061–7. doi: 10.1194/jlr.D400041-JLR200
55. Ghatak S, Hascall VC, Markwald RR, Misra S. FOLFOX Therapy Induces Feedback Upregulation of CD44v6 Through YB-1 to Maintain Stemness in Colon Initiating Cells. *Int J Mol Sci* (2021) 22(2):753–90. doi: 10.3390/ijms22020753
56. Ghatak S, Misra S, Toole BP. Hyaluronan Constitutively Regulates ErbB2 Phosphorylation and Signaling Complex Formation in Carcinoma Cells. *J Biol Chem* (2005) 280(10):8875–83. doi: 10.1074/jbc.M410882200
57. Andoorfar S, Hosseini Tafreshi SA, Rezvani Z. Assessment of the Expression Level of miRNA Molecules Using a Semi-Quantitative RT-PCR Approach. *Mol Biol Rep* (2019) 46(5):5057–62. doi: 10.1007/s11033-019-04959-5
58. Misra S, Ghatak S, Moreno-Rodrigue R, Norris R, Hascall V, RR M. Periostin/Filamin-A: A Candidate Centralregulatory Axis for Valve Fibrogenesisand Matrix Compaction. *Front Cell Dev Biol (Accepted)* (2021) 10(3389). doi: 10.3389/fcell.2021.649862
59. Misra S, Hascall VC, De Giovanni C, Markwald RR, Ghatak S. Delivery of CD44 shRNA/Nanoparticles Within Cancer Cells: Perturbation of Hyaluronan/CD44v6 Interactions and Reduction in Adenoma Growth in Apc Min/+ MICE. *J Biol Chem* (2009) 284(18):12432–46. doi: 10.1074/jbc.M806772200
60. Ghatak S, Hascall VC, Berger FG, Penas MM, Davis C, Jabari E, et al. Tissue-Specific shRNA Delivery: A Novel Approach for Gene Therapy in Cancer. *Connect Tissue Res* (2008) 49(3):265–9. doi: 10.1080/03008200802147845
61. Kreso A, Dick JE. Evolution of the Cancer Stem Cell Model. *Cell Stem Cell* (2014) 14(3):275–91. doi: 10.1016/j.stem.2014.02.006
62. Kreso A, van Galen P, Pedley NM, Lima-Fernandes E, Frelin C, Davis T, et al. Self-Renewal as a Therapeutic Target in Human Colorectal Cancer. *Nat Med* (2014) 20(1):29–36. doi: 10.1038/nm.3418
63. Hill RP, Perris R. "Destemming" Cancer Stem Cells. *J Natl Cancer Inst* (2007) 99(19):1435–40. doi: 10.1093/jnci/djm136
64. Todaro M, Gaggianesi M, Catalano V, Benfante A, Iovino F, Biffoni M, et al. CD44v6 is a Marker of Constitutive and Reprogrammed Cancer Stem Cells Driving Colon Cancer Metastasis. *Cell Stem Cell* (2014) 14(3):342–56. doi: 10.1016/j.stem.2014.01.009
65. O'Brien CA, Pollett A, Gallinger S, Dick JE. A Human Colon Cancer Cell Capable of Initiating Tumour Growth in Immunodeficient Mice. *Nature* (2007) 445(7123):106–10. doi: 10.1038/nature05372
66. Huang EH, Hynes MJ, Zhang T, Ginestier C, Dontu G, Appelman H, et al. Aldehyde Dehydrogenase 1 is a Marker for Normal and Malignant Human Colonic Stem Cells (SC) and Tracks SC Overpopulation During Colon Tumorigenesis. *Cancer Res* (2009) 69(8):3382–9. doi: 10.1158/0008-5472.CAN-08-4418
67. Deng S, Yang X, Lassus H, Liang S, Kaur S, Ye Q, et al. Distinct Expression Levels and Patterns of Stem Cell Marker, Aldehyde Dehydrogenase Isoform 1 (ALDH1), in Human Epithelial Cancers. *PLoS One* (2010) 5(4):e10277. doi: 10.1371/journal.pone.0010277
68. Nakagawa H, Liyanarachchi S, Davuluri RV, Auer H, Martin EWJr., de la Chapelle A, et al. Role of Cancer-Associated Stromal Fibroblasts in Metastatic Colon Cancer to the Liver and Their Expression Profiles. *Oncogene* (2004) 23 (44):7366–77. doi: 10.1038/sj.onc.1208013
69. MacDonald BT, Tamai K, He X. Wnt/beta-Catenin Signaling: Components, Mechanisms, and Diseases. *Dev Cell* (2009) 17(1):9–26. doi: 10.1016/j.devcel.2009.06.016
70. Logan CY, Nusse R. The Wnt Signaling Pathway in Development and Disease. *Annu Rev Cell Dev Biol* (2004) 20:781–810. doi: 10.1146/annurev.cellbio.20.010403.113126

71. Misra S, Hascall VC, Karamanos NK, Markwald RR, Ghatak S. Targeting the tumor microenvironment in cancer progression. *Extracellular Matrix: Pathobiology and Signaling* edited by N Karamanos, Berlin, Boston: De Gruyter, (2012) 723–40. doi: 10.1515/9783110258776.723
72. Gottesman MM, Pastan I. Biochemistry of Multidrug Resistance Mediated by the Multidrug Transporter. *Annu Rev Biochem* (1993) 62:385–427. doi: 10.1146/annurev.bi.62.070193.002125
73. Dallas NA, Xia L, Fan F, Gray MJ, Gaur P, van Buren G, et al. Chemoresistant Colorectal Cancer Cells, the Cancer Stem Cell Phenotype, and Increased Sensitivity to Insulin-Like Growth Factor-I Receptor Inhibition. *Cancer Res* (2009) 69(5):1951–7. doi: 10.1158/0008-5472.CAN-08-2023
74. Dylla SJ, Beviglia L, Park IK, Chartier C, Raval J, Ngan L, et al. Colorectal Cancer Stem Cells are Enriched in Xenogeneic Tumors Following Chemotherapy. *PLoS One* (2008) 3(6):e2428. doi: 10.1371/journal.pone.0002428
75. Peitzsch C, Tyutyunnykova A, Pantel K, Dubrovska A. Cancer Stem Cells: The Root of Tumor Recurrence and Metastases. *Semin Cancer Biol* (2017) 44:10–24. doi: 10.1016/j.semcancer.2017.02.011
76. Ben-Porath I, Thomson MW, Carey VJ, Ge R, Bell GW, Regev A, et al. An Embryonic Stem Cell-Like Gene Expression Signature in Poorly Differentiated Aggressive Human Tumors. *Nat Genet* (2008) 40(5):499–507. doi: 10.1038/ng.127
77. Todaro M, Alea MP, Di Stefano AB, Cammareri P, Vermeulen L, Iovino F, et al. Colon Cancer Stem Cells Dictate Tumor Growth and Resist Cell Death by Production of Interleukin-4. *Cell Stem Cell* (2007) 1(4):389–402. doi: 10.1016/j.stem.2007.08.001
78. Leedham SJ, Rodenas-Cuadrado P, Howarth K, Lewis A, Mallappa S, Segditsas S, et al. A Basal Gradient of Wnt and Stem-Cell Number Influences Regional Tumour Distribution in Human and Mouse Intestinal Tracts. *Gut* (2013) 62 (1):83–93. doi: 10.1136/gutjnl-2011-301601
79. Bissell MJ, Labarge MA. Context, Tissue Plasticity, and Cancer: Are Tumor Stem Cells Also Regulated by the Microenvironment? *Cancer Cell* (2005) 7 (1):17–23. doi: 10.1016/j.ccr.2004.12.013

Conflict of Interest: The authors declare that the research was conducted in the absence of any commercial or financial relationships that could be construed as a potential conflict of interest.

Publisher's Note: All claims expressed in this article are solely those of the authors and do not necessarily represent those of their affiliated organizations, or those of the publisher, the editors and the reviewers. Any product that may be evaluated in this article, or claim that may be made by its manufacturer, is not guaranteed or endorsed by the publisher.

Copyright © 2022 Ghatak, Hascall, Karamanos, Markwald and Misra. This is an open-access article distributed under the terms of the Creative Commons Attribution License (CC BY). The use, distribution or reproduction in other forums is permitted, provided the original author(s) and the copyright owner(s) are credited and that the original publication in this journal is cited, in accordance with accepted academic practice. No use, distribution or reproduction is permitted which does not comply with these terms.

frontiers | Frontiers in Oncology

TYPE Original Research
PUBLISHED 08 August 2022
DOI 10.3389/fonc.2022.981009

Check for updates

OPEN ACCESS

EDITED BY
Nikos Karamanos,
University of Patras, Greece

REVIEWED BY
Ruud Bank,
University Medical Center Groningen, Netherlands
David Dolivo,
Northwestern University, United States

*CORRESPONDENCE
Ritva Heljasvaara
ritva.heljasvaara@oulu.fi

SPECIALTY SECTION
This article was submitted to Molecular and Cellular Oncology, a section of the journal Frontiers in Oncology

RECEIVED 29 June 2022
ACCEPTED 12 July 2022
PUBLISHED 08 August 2022

CITATION
Martínez-Nieto GA, Teppo H-R, Petrelius N, Izzi V, Devarajan R, Petäistö T, Liu H, Kim KS, Karppinen S-M, Ruotsalainen H, Koivunen J, Mäki JM, Walker GC, Pihlajaniemi T, Gullberg D and Heljasvaara R (2022) Upregulated integrin α11 in the stroma of cutaneous squamous cell carcinoma promotes skin carcinogenesis. *Front. Oncol.* 12:981009. doi: 10.3389/fonc.2022.981009

COPYRIGHT
© 2022 Martínez-Nieto, Teppo, Petrelius, Izzi, Devarajan, Petäistö, Liu, Kim, Karppinen, Ruotsalainen, Koivunen, Mäki, Walker, Pihlajaniemi, Gullberg and Heljasvaara. This is an open-access article distributed under the terms of the Creative Commons Attribution License (CC BY). The use, distribution or reproduction in other forums is permitted, provided the original author (s) and the copyright owner(s) are credited and that the original publication in this journal is cited, in accordance with accepted academic practice. No use, distribution or reproduction is permitted which does not comply with these terms.

Upregulated integrin α11 in the stroma of cutaneous squamous cell carcinoma promotes skin carcinogenesis

Guillermo A. Martínez-Nieto[1], Hanna-Riikka Teppo[2,3,4], Noora Petrelius[1], Valerio Izzi[1,5,6], Raman Devarajan[1], Tiina Petäistö[1], Hengshuo Liu[7], Kris S. Kim[8], Sanna-Maria Karppinen[1], Heli Ruotsalainen[1], Jarkko Koivunen[1], Joni M. Mäki[1], Gilbert C. Walker[8], Taina Pihlajaniemi[1], Donald Gullberg[7] and Ritva Heljasvaara[1,7]*

[1]ECM-Hypoxia Research Unit, Faculty of Biochemistry and Molecular Medicine, University of Oulu, Oulu, Finland, [2]Cancer Research and Translational Medicine Research Unit, University of Oulu, Oulu, Finland, [3]Medical Research Center, Oulu University Hospital and University of Oulu, Oulu, Finland, [4]Department of Pathology, Oulu University Hospital, Oulu, Finland, [5]Research Unit of Biomedicine, University of Oulu, Oulu, Finland, [6]Finnish Cancer Institute, Helsinki, Finland, [7]Matrix Biology Group, Department of Biomedicine, Centre for Cancer Biomarkers, University of Bergen, Bergen, Norway, [8]Department of Chemistry, University of Toronto, Toronto, ON, Canada

Integrin α11β1 is a collagen-binding integrin that is needed to induce and maintain the myofibroblast phenotype in fibrotic tissues and during wound healing. The expression of the α11 is upregulated in cancer-associated fibroblasts (CAFs) in various human neoplasms. We investigated α11 expression in human cutaneous squamous cell carcinoma (cSCC) and in benign and premalignant human skin lesions and monitored its effects on cSCC development by subjecting α11-knockout (*Itga11*$^{-/-}$) mice to the DMBA/TPA skin carcinogenesis protocol. α11-deficient mice showed significantly decreased tumor cell proliferation, leading to delayed tumor development and reduced tumor burden. Integrin α11 expression was significantly upregulated in the desmoplastic tumor stroma of human and mouse cSCCs, and the highest α11 expression was detected in high-grade tumors. Our results point to a reduced ability of α11-deficient stromal cells to differentiate into matrix-producing and tumor-promoting CAFs and suggest that this is one causative mechanism underlying the observed decreased tumor growth. An unexpected finding in our study was that, despite reduced CAF activation, the α11-deficient skin tumors were characterized by the presence of thick and regularly aligned collagen bundles. This finding was attributed to a higher expression of TGFβ1 and collagen crosslinking lysyl oxidases in the *Itga11*$^{-/-}$ tumor stroma. In summary, our data suggest that α11β1 operates in a complex interactive tumor environment to regulate ECM synthesis and collagen organization and thus foster cSCC growth. Further studies with advanced experimental models are still needed to define the exact roles and molecular mechanisms of stromal α11β1 in skin tumorigenesis.

10.3389/fonc.2022.981009

KEYWORDS

cancer-associated fibroblast, extracellular matrix, collagen, lysyl oxidase, myofibroblast, DMBA/TPA, tumor microenvironment

Introduction

The dynamic interactions of tumor cells with the surrounding tumor microenvironment (TME), consisting of various stromal cells, soluble factors, and the extracellular matrix (ECM), critically regulate all steps of tumorigenesis (1, 2). The non-vascular, non-inflammatory stromal cells within the TME are designated cancer-associated fibroblasts (CAFs) (3). Recent single-cell RNA sequencing (scRNA-seq), proteomics and flow cytometry approaches have revealed extraordinary heterogeneity and plasticity among CAFs subpopulations (2–4). The three major subtypes of CAFs, originally identified in pancreatic adenocarcinoma (PDAC), are myofibroblastic CAFs (myCAFs), inflammatory CAFs (iCAFs), and antigen-presenting CAFs (apCAFs) (5, 6). The biomarkers expressed in the different subsets of CAFs include alpha-smooth muscle actin (αSMA), fibroblast-specific protein 1 (FSP-1), platelet-derived growth factor receptors α and β (PDGFRα/β), and fibroblast-activating protein (FAP). CAFs are often characterized by the synthesis of ECM proteins, including fibrillar collagens, proteoglycans, matricellular proteins, and ECM-modifying enzymes, contributing to tumor fibrosis (2, 7). A current challenge in TME research involves identifying, characterizing, and targeting tumor-promoting CAF subtypes (2–4).

Cell-ECM interactions and signalling through αβ heterodimeric integrin receptors regulate the properties and functions of tumor cells, as well as the various cell types found in the TME. Tumor stromal integrins regulate tumor stiffness, matrix reorganization, tumor angiogenesis, CAF activation, and metastasis (8–10). The vertebrate integrin family is composed of 18 α subunits and 8 β subunits which can form 24 different αβ heterodimers. Integrin α11β1, together with α1β1, α2β1, and α10β1, constitute a subgroup that can bind collagens and associate exclusively with the β1 subunit (11). The first report demonstrating the importance of fibroblast-derived integrin α11 in cancer focused on non-small-cell lung cancer (NSCLC) and showed that α11β1 is highly expressed in the tumor stroma and promotes tumorigenesis through the induction of insulin growth factor 2 expression in CAFs (12). Later studies on NSCLC demonstrated that α11β1 signaling leads to the upregulation of lysyl oxidase like-1 (LOXL1) and, subsequently, increased collagen crosslinking, stromal stiffness, and tumor growth and progression (13, 14). High α11 expression in CAFs has been reported in many other solid tumors, such as head and neck squamous cell carcinoma (HNSCC) and breast cancer and PDAC, in which it is associated with a poor prognosis (15–17). Mechanistically, α11β1 has been shown to regulate the PDGFRβ/JNK signaling axis in breast cancer CAFs, leading to ECM remodeling and CAF-induced tumor cell invasion (16). In PDAC *in vitro* systems, the knockdown of α11 in pancreatic stellate cells inhibited cell contractility, migration, and differentiation and reduced the expression of several ECM components (17).

Cutaneous squamous cell carcinoma (cSCC) is the second most common human cancer. It is principally caused by ultraviolet light, increasing the incidence of this cancer type in sun-exposed areas of the body (18, 19). Although early detection and surgery can prevent complications, primary cSCC can frequently recur and metastasize, with an 5% average rate of metastasis. The accumulation of genetic mutations in epithelial cells fosters the progression of the disease from precancerous actinic keratosis lesions to cSCC *in situ*, to the invasive form of cSCC and, finally, to metastatic cSCC. The stromal compartment plays an important role in cSCC progression, and changes in ECM composition and properties, as well as inflammatory and immune cells, contribute to a milieu that favors tumorigenesis (20, 21).

The expression of β1-integrins and their ligands is known to correlate with tumor progression in human cSCC, and the roles of major epidermal β1 integrins (α2β1, α3β1) are widely studied (19, 22). In contrast, the data regarding the functions and significance of β1-integrins in CAFs are still limited (23). To advance our understanding of integrin α11β1 in cSCC, we analyzed the expression of the α11 subunit in human cSCC samples and in benign and premalignant human skin lesions *via* immunohistochemistry (IHC) and subjected mice deficient in the α11 subunit to the broadly used murine model of skin cancer, the multistep chemical skin carcinogenesis protocol involving 7,12-dimethylbenz[α]anthracene (DMBA) and 12-*O*-tetradecanoylphorbol-13-acetate (TPA) treatments (24). Our studies demonstrate, for the first time, the upregulation of integrin α11 in CAFs in human and mouse cSCC, as well as its tumor-promoting role in an experimental mouse model of skin carcinogenesis. We also describe interesting alterations in the skin tumor stroma on account of α11 ablation in mice.

Materials and methods

Human samples and immunohistochemistry

Formalin-fixed, paraffin-embedded (FFPE) human skin tissue samples were collected from the archives of the Department of Pathology, Oulu University Hospital, Finland, and consisted of 19 seborrheic keratosis samples, 14 actinic keratosis samples, five squamous carcinomas *in situ* (also known as Bowen's disease), 15 keratoacanthoma samples, and 29 cSCC samples (total n = 82). Diagnoses were made according to the current WHO classification (25). The use of skin specimens was approved by the Finnish National Supervisory Authority for Welfare and Health (V/12456/2019) and the Ethical Committee of the Northern Ostrobothnia Hospital District (Dnr. 100/2018). Studies were carried out in accordance with the provisions of the Helsinki Declaration (1983).

Skin tissues were stained with a previously validated monoclonal anti-human integrin α11 antibody (clone 210F4B6A4) (26) using an Envision FLEX+ kit (Dako, K800221-2). 3.5 µm-thick FFPE sections were dried at 55°C for 48h, deparaffinized in xylene (3 min, 3 times), and rehydrated through graded ethanol solutions. Antigen retrieval was performed using Tris-EDTA pH 9 (EnVision FLEX Target Retrieval Solution, high pH; Dako, K801021-2) by boiling with microwaves at 850W for 2 min and 150W for 15 min. After boiling, the sections were allowed to cool at room temperature (RT) and washed using distilled water and EnVision FLEX Wash Buffer for 10 min. The sections were incubated in the peroxidase blocking solution of the kit for 8 min and washed with EnVision FLEX Wash Buffer for 10 min. After washing, the sections were incubated with the primary α11 antibody for 1 h at RT at a 1:1000 dilution following overnight incubation at +4°C, incubated again at RT for 60 min, and then washed with EnVision FLEX Wash Buffer for 10 min. Then, the samples were incubated with secondary antibody (EnVision FLEX+ mouse linker) and visualized using EnVision FLEX/HRP and DAB according to the manufacturer's instructions. After being rinsed with distilled water, sections were counterstained with hematoxylin, rinsed, dehydrated, cleared, and mounted. The samples were imaged using a Hamamatsu NanoZoomer S60 whole-slide digital scanner in the 20× mode. In dermal spindle-shaped cells, the staining intensity was evaluated as one of the following expressions: absent (0), weak (1), moderate (2), or strong (3). The quantity of each intensity level was recorded: <10% (1), 10–50% (2), or >50% (3). Subsequently a staining index (SI) score (0–9) was obtained by multiplying the score for intensity by the quantity percentage group. The unambiguous α11 signal in myoepithelial cells around the sweat glands served as a positive control. Hematoxylin-eosin (H&E)-stained samples were used for cSCC grading.

Mice

Integrin-α11-knockout mice (*Itga11*^{tm1Dgul}, MGI:3714472) (27) were backcrossed to the FVB/N (Harlan, The Netherlands) strain for at least five generations. The mice were maintained in a pathogen-free facility, group-housed with corncob bedding and enrichments at 21°C with a 12:12-hour light:dark cycle and given *ad libitum* water and standard rodent chow. Mice were maintained and animal experiments were conducted in the Laboratory Animal Centre of the University of Oulu (OULAC), following the the regulations for the protection of vertebrate animals used for experimental and other scientific purposes (European Convention Treaty ETS No. 23, European Community Council Directive 2010/63/EU, and Finnish Government Decree 564/2013).

Chemical skin carcinogenesis and hyperplasia models

Skin carcinogenesis experiments were approved by the National Animal Experiment Board of Finland (license ESAVI/1188/04.10.07/2016). Skin tumors were induced in seven-week-old *Itga11*$^{+/+}$(n = 25) and *Itga11*$^{-/-}$ (n = 21) male mice with topical DMBA (Sigma-Aldrich) and TPA (Sigma-Aldrich) treatments (24). The dorsal skin of the mice was shaved and treated with a single dose of DMBA (100 µg in 100 µl acetone), followed by weekly TPA treatments (5 µg in 100 µl acetone), which continued until the mice were removed from the experiment at predetermined time points (15, 20, 25, and 30 weeks) or on the basis of humane endpoints (engraved or ulcerative cSCCs, tumors with a diameter over 10 mm, or excessive tumor load per mouse). During the treatments and tumor monitoring, the mice were housed in single cages to avoid fights and skin wounding, which can have an impact on tumorigenesis. Tumor growth was monitored once per week, and tumor number, size and macroscopic appearance were recorded. Tumor incidence (percentage of mice with a tumor) and cumulative tumor multiplicity (number of papillomas divided by the total number of mice alive at the time when the first mouse was removed from the experiment because of humane endpoints) were recorded and tumors were dissected for further analyses. H&E-stained carcinoma samples were analysed and graded by a pathologist in a blinded manner. To label the actively proliferating tumor cells, 100 µg/kg of 5-bromo-2-deoxyuridine (BrdU, Abcam) was injected intraperitoneally into the mice two hours before sacrifice.

To induce epidermal hyperplasia, the shaved dorsal skin of seven-week-old male mice was treated six times, at two-day intervals, with 5 µg of TPA in acetone, and skin samples were collected for analyses. Mouse skin treated with acetone was used as a control.

Mice were euthanized with CO_2 inhalation and cervical dislocation. Tissues were dissected and fixed in fresh phosphate-buffered 4% paraformaldehyde (PFA) for 24 hours at +4°C, washed for one hour under running tap water, dehydrated in ethanol of increasing concentration, cleared with xylene, and embedded in paraffin. Alternatively, the dissected tissues were embedded in OCT compound (Tissue-Tek, Sakura Finetechnical) and frozen for cryo-sectioning.

Immunofluorescence staining

Immunofluorescence was used to visualize integrin α11-, Ki67-, cytokeratin 5- (CK5), NG2-, PDGFRβ-, LOX-, and αSMA-positive cells in 5 µm-thick cryosections (Supplementary Table S1). Staining with rabbit polyclonal anti-integrin α11 antibody (1:200 dilution) (13, 28) was performed overnight at +4°C, after a 10 min methanol-acetone fixation at −20°C and blocking with 10% goat serum in PBS for one hour at RT. For monoclonal anti-Ki67 antibody ethanol-fixed (10 min at −20°C) cryo-sections were used, and antigen retrieval with 1% Triton-X and blocking with goat 10% serum for one hour at RT preceded the overnight incubation with the primary antibody +4°C. For the CK5, NG2, PDGFRβ, LOX, and αSMA antibodies, the blocking solution contained 1% BSA and 22.5 mg/ml glycin in PBS/0.1% Tween. Appropriate goat anti-rabbit Alexa Fluor 488 (1:300, Invitrogen) and goat anti-rat or donkey anti-mouse Cy3 (1:200, Jackson ImmunoResearch) secondary antibodies were used for the detection. To visualize αSMA in PFA-fixed tissues by immunofluorescence, antigen retrieval was accomplished by treating the 5 µm-thick sections in Tris/EDTA in boiling water for 10 min, followed by blocking in 10% goat serum for one hour at RT and overnight incubation with Cy3-conjugated anti-αSMA antibody. To detect BrdU, sections were blocked with 5% donkey serum, treated with 2M HCl (30 min) and 0.1M sodium borate (10 min), and then stained with anti-5-Bromo-2-Deoxyuridine antibody, followed by the application of donkey anti-mouse Cy3 (1:200, Jackson ImmunoResearch). Cell nuclei were labelled with DAPI (1:300, Sigma-Aldrich). A confocal microscope Zeiss LSM 700 or 780 was used for imaging. The intensities of the fluorescent PDGFRβ, αSMA, and LOX signals in the tumors were quantified from 20× confocal microscopy images in a blind manner using Fiji ImageJ analysis software.

Analysis of collagen content

To analyze the content of fibrillar collagen in skin tumors, Masson trichrome and picrosirius red stainings were performed as described previously (29). PFA-fixed tumor sections were dewaxed in xylene; rehydrated with decreasing ethanol series; and treated with a nuclear stain (Celestine blue and Harris' hematoxylin), acid fuchsin, phosphomolybdic acid, and methyl blue stain (all reagents from Sigma–Aldrich). For picrosirius red staining, PFA-fixed tumor sections were treated with 0.2% phosphomolybdic acid for 5 min, followed by staining with 0.1% Direct Red 80/Sirius Red F3B (Sigma–Aldrich) in saturated picric acid for 1 h at RT. Both protocols were finished *via* dehydration with an ethanol series, clearing with xylene, and mounting with Pertex (Sigma–Aldrich). The Masson's trichrome-stained sections were imaged with a Leica DM LB2 microscope, and picrosirius red-stained sections were imaged under bright and polorized light with an Olympus BX51 microscope (Olympys, Tokyo, Japan). Fiji ImageJ software was used for birefringence signal quantification, and the ratio of thick versus thin collagen fibers was calculated as described previously (30).

Transmission electron microscopy

Papillomas were dissected from mice; cut into 1 mm^3 cubes; fixed with 1% glutaraldehyde, 4% formaldehyde, and 0.1 M phosphate buffer (pH 7.4) for 12 hours at RT; post-fixed in 1% osmium tetroxide for 15 min; dehydrated in acetone; and embedded in Epon LX 112 (Ladd Research Industries). 80 nm sections were examined using a Tecnai G2 Spirit transmission electron microscope, and images were captured using Veleta or Quemesa CCD cameras (Olympus Soft Imaging Solutions). A total of six papillomas from different individuals, three per genotype, were analyzed using TEM.

Fluorescence-activated cell sorting

Mouse skin pieces were dissected and digested in 0.25% collagenase I (w/v) in DMEM for 2 hours at +37°C, disaggregated with vigorous pipetting, and passed through a 40 µM cell strainer. The resulting single-cell suspension was analyzed for different cell populations using FACSCalibur running the CellQuest Pro software (BD Biosciences). Fibroblast and immune cell populations were analysed with antibodies listed in Supplementary Table S2. Data were examined using FlowJo software (FlowJo LLC).

In vitro adipogenesis assay

Mesenchymal (MSC) progenitors were isolated from the stromal vascular fraction (SVF) of the mouse inguinal fat pads and differentiated into mature adipocytes using a standard protocol (31, 32), with minor modifications. Six-week-old mice were euthanized, sprayed with ethanol, and opened in a laminar hood. Inguinal fat pads were collected from four to five mice per genotype and pooled in cold phosphate buffered saline (PBS). Fat tissues were

minced and digested with 2.5 mg/ml of collagenase D (Roche) and 3.1 U/ml of Dispase II (Sigma-Aldrich) in 10 mM $CaCl_2$/PBS for 45 min at 37°C with regular shaking. Digestion was terminated by adding complete preadipocyte medium consisting of DMEM/F12 supplemented with 10% FBS, 1% penicillin/streptomycin and 0.1mg/ml primocin (*In vivo*Gen). The cellular suspension was filtered through 100 µm cell strainer to remove undigested tissue debris and centrifuged at 600 x g for 5 min at +4°C. SVF cells were suspended in preadipocyte medium, the suspension was filtered through a 40 µm cell strainer, and cells were seeded on a 10 cm culture plate in the complete preadipocyte medium. On the next day, the cells were washed four times with PBS and then cultured in complete preadipocyte medium. The culture medium was changed every day until the cells reached 90% confluence. Cells were divided and allowed to grow to confluence, and two days post-confluence, adipocyte differentiation was induced by adding preadipocyte medium supplemented with 5µg/ml insulin (Sigma-Aldrich), 1µM rosiglitazone (Cayman), 0.5mM isobutylmethylxanthine (Sigma-Aldrich), and 1µM dexamethasone (Sigma-Aldrich). After 48 h of induction, the cells were maintained in medium containing 1µM rosiglitazone and 5µg/ml insulin, and cell differentiation was monitored for 6 days, changing the maintenance medium daily. Cell samples were collected for RNA analyses every two days, and Oil Red-O staining was performed at the end of the experiment to measure to lipid accumulation. The medium was collected on Day 6 to measure the glycerol concentration. Cells were imaged using the Olympus CellSens imaging system with a 10× objective and supplemented with the Olympus XM10 CCD camera (Tokyo, Japan). The adipogenesis assay was repeated with at least three primary cell preparations per genotype.

Quantitative real-time polymerase chain reaction

Total RNA was extracted from snap-frozen mouse tumors and hyperplastic skin with TriPure reagent (Roche), followed by the RNeasy mini kit (Qiagen). A total of 0.5 µg RNA, pooled from at least five papillomas collected from five individuals of each genotype at a selected time point, was used to synthesize cDNA by using the iScript cDNA synthesis kit (Bio-Rad). Samples were analysed for the mRNA expression of α1 chains of collagen I (*Col1a1*) and III (*Col3a1*), prolyl 4-hydoxylases-1 (*Pdha1*) and -2 (*Pdha2*), αSMA (*Acta2*), PDGFRα (*Pdgfra*), PDGFRβ (*Pdgfrb*), and tenascin-C (*Tnc*). The PCR primers are listed in Supplementary Table 3. The qPCR was performed with iTaq SYBR Green Supermix with ROX reagents (BioRad), and each sample was run in duplicate by using a Mx3005P qPCR device (Stratagene) and repeated at least three times. Relative mRNA levels were calculated with the $2^{\Delta\Delta Ct}$ method (33). Values were normalized against *Gapdh*, and the control values were expressed as 1 to indicate the fold change in mRNA expression.

Atomic force microscopy

Force-distance curve measurements were collected using an MFP-3D Molecular Force Probe AFM (Asylum Research, Santa Barbara) and a borosilicate glass particle (5 µm in diameter) on silicon nitride cantilevers (Novascan Tech Inc., Ames). The cantilevers had a nominal spring constant of 0.02 N/m and were calibrated before each experiment with the thermal noise method (34). All measurements were collected in 18.2 MΩ cm Milli-Q water. Each AFM probe was used to measure one control and one knockout sample, and the order of sample measurement was randomized for each probe. The samples were indented at a loading rate of 500 nm/s with a maximum force of 1 nN. 300 force extension curves were collected over three randomly chosen 20 µm × 20 µm areas of each sample. The results show the contributions of four $Itga11^{+/+}$ and three $Itga11^{-/-}$ samples. The determination of the Young's elastic modulus of the samples from force-distance curves was performed using the Hertz model (35, 36).

$$F = \frac{4\sqrt{R}}{3(1-\nu^2)} E\delta^{3/2}$$

where F is the loading force (N), E is the Young's modulus (Pa), ν is the Poisson ratio, R is the radius of curvature of the tip (m), and δ is the indentation depth (m). Samples were assumed to be incompressible, and a Poisson's ratio of 0.5 was used in the calculation of the Young's elastic modulus.

Statistical analysis

Statistical significance was computed with a two-tailed unpaired *t*-test or ANOVA using Prism software. The differences were considered significant at $p< 0.05$ and expressed in figures as *, $p< 0.05$; **, $p< 0.01$; *** and $p< 0.001$. Figure data are presented as means ±SEM or ±SD, as indicated in the respective figure legends. For human IHC, statistical analyses were performed by using IBM SPSS Statistics software, Version 28.0.0.0 (IBM Corporation, Armonk, NY, USA). The significance of associations was defined by using the Mann-Whitney *U* test and Kruskal-Wallis test.

Results

Integrin α11 is upregulated in the stroma of human and mouse cSCC

Integrin α11 expression and localization were examined in a collection of pre-malignant and malignant human skin lesions using IHC and a previously validated monoclonal anti-human integrin α11 antibody (26). In the benign seborrheic keratosis

and premalignant actinic keratosis specimens, as well as squamous carcinoma *in situ*, weak or moderate membranous α11 signals were regularly detected in spindle-shaped cells at the dermal-epidermal junction (Figure 1A). In the malignant keratoacanthoma and cSCCs, α11 expression showed upregulation but also considerable variation. Often, the α11-positive cells were located diffusely throughout the tumor stroma, the intensity of staining ranging from weak to strong, as well as being absent in some cases. Intense α11 staining was frequently seen as a fibrillar, tangle-like pattern at the tumor-stroma interphase. The number of α11-positive cells varied substantially, even within a given tumor sample (Figure 1A; Supplementary Figure 1). The samples with the strongest staining were classified as grade-3 cSCCs (Figure 1A). The quantification of α11 expression in skin lesions using an SI score (*i.e.*, the number of α11-positive spindle-like cells and staining intensity) showed high variability within the diagnostic groups of malignant cases (Figure 1B). Nevertheless, SI scores differed significantly between the groups of benign to premalignant keratoses and the groups of malignant carcinomas ($p<0.001$), demonstrating that the stromal upregulation of α11 integrin is associated with malignancy in human cSCC. No membranous α11 staining was observed in tumor cells, but the nuclear positivity of keratinocytes was frequently observed. Because we have not observed α11 RNA in keratinocytes (37), this signal may be an artefact related to heat-induced antigen retrieval at a high pH (38). In tumor-adjacent tissues, prominent α11 signals were also localized to the myoepithelial cell layer of the sweat glands and around the hair follicles (Figure 1A; Supplementary Figure 1).

In addition to human tissue material, we studied α11 expression and localization in healthy murine skin and in DMBA/TPA-induced skin tumors obtained from wild type FVB/N mice (39). In normal mouse skin, α11 expression was barely detected in the dermis. A significant upregulation of α11 was observed in mouse skin tumor samples, both in papillomas and in cSCCs of different grades, in which α11 was abundantly expressed in the tumor stroma (Figures 2A-C). Often but not always, α11 signals overlapped with αSMA, a common marker of myofibroblasts and myCAFs. The chondroitin sulphate proteoglycan NG2, a marker of pericytes and subsets of CAFs, showed faint signals in α11-positive stromal areas and prominent signals in the tumor vasculature, where it was associated with αSMA (Figure 2B). α11 expression was not detected in tumor areas, which were visualized by cytokeratin (Figure 2B). As in human cSCC, variation in α11 signal intensity and localization was observed between tumor samples and even different stromal regions of the same tumor. Thus, our immunostainings show that α11 is highly upregulated in both human and mouse cSCC stroma and localized in spindle-shaped cells, which, in mouse tumors, were shown to represent specific CAF subtypes. The data suggest a role for α11 in cSCC tumorigenesis and prompted us to subject α11-knockout (*Itga11*$^{-/-}$) mice to an experimental skin carcinogenesis model.

Skin tumor growth is impaired in integrin α11-deficient mice

To evaluate the relevance of integrin α11β1 integrin signaling in skin carcinogenesis, we compared the development and progression of DMBA/TPA-induced skin tumors between α11-deficient (*Itga11*$^{-/-}$) and control mice (*Itga11*$^{+/+}$) mice. The absence of α11 expression in knockout tumors was confirmed by immunofluorescence staining (Figure 2C). We observed a significant impairment in tumor growth in the *Itga11*$^{-/-}$ mice as compared with the controls. First, a delay of approximately two weeks in terms of tumor incidence (*i.e.*, the proportion of mice bearing at least one tumor) was observed in the *Itga11*$^{-/-}$ mice, with the difference being most evident at week 11, when approximately 75% of the control mice but only 25% of the *Itga11*$^{-/-}$ mice had developed measurable papillomas (Figure 3A). Impaired tumorigenesis in the *Itga11*$^{-/-}$ mice was seen even more clearly when the tumor multiplicity between these and the *Itga11*$^{+/+}$ controls was compared. A marked reduction in the number of skin tumors was apparent already at week 10, and at weeks 20–28, the *Itga11*$^{-/-}$ mice had, on average, 50% fewer papillomas than the *Itga11*$^{+/+}$ mice (Figures 3B, C). In addition, a difference in tumor size was observed between the genotypes such that, in the *Itga11*$^{-/-}$ mice, the papillomas were generally smaller than those in the controls (Supplementary Figure 2A). In consequence, the total tumor burden per mouse was significantly smaller in the *Itga11*$^{-/-}$ mice from week 10 onwards (Figure 3D).

Given the marked difference in tumor growth between the *Itga11*$^{+/+}$ and *Itga11*$^{-/-}$ mice, we addressed the impact of α11 in tumor cell proliferation by determining the numbers of actively dividing cells in tumor tissue sections. Anti-Ki67 staining showed a significant, up to 50%, reduction in the number of dividing tumor cells in *Itga11*$^{-/-}$ tumors relative to *Itga11*$^{+/+}$ tumors at week 20 (Figures 3E, F). *In vivo* 5-bromo-2'-deoxyuridine (BrdU) labelling and subsequent anti-BrdU staining confirmed this finding, showing a roughly 30% reduction of BrdU-positive cells in *Itga11*$^{-/-}$ tumors at the same time point (Supplementary Figures 2B, C). As expected, the numbers of proliferating cells were trivial in the untreated skin in both genotypes and were not counted, underpinning our observation that the upregulation of α11 expression in CAFs boosts tumor cell proliferation.

Only a small portion of papillomas progressed to invasive cSCCs in our experimental setup, and these typically presented as doughnut-shaped tumors with erosion and/or ulceration. Recording the incidence of tumors with these features at weeks 15–25 showed that, compared the to the *Itga11*$^{-/-}$ mice, the *Itga11*$^{+/+}$ mice had almost double the number of tumors with a malignant appearance (Supplementary Table 4). However, because the overall

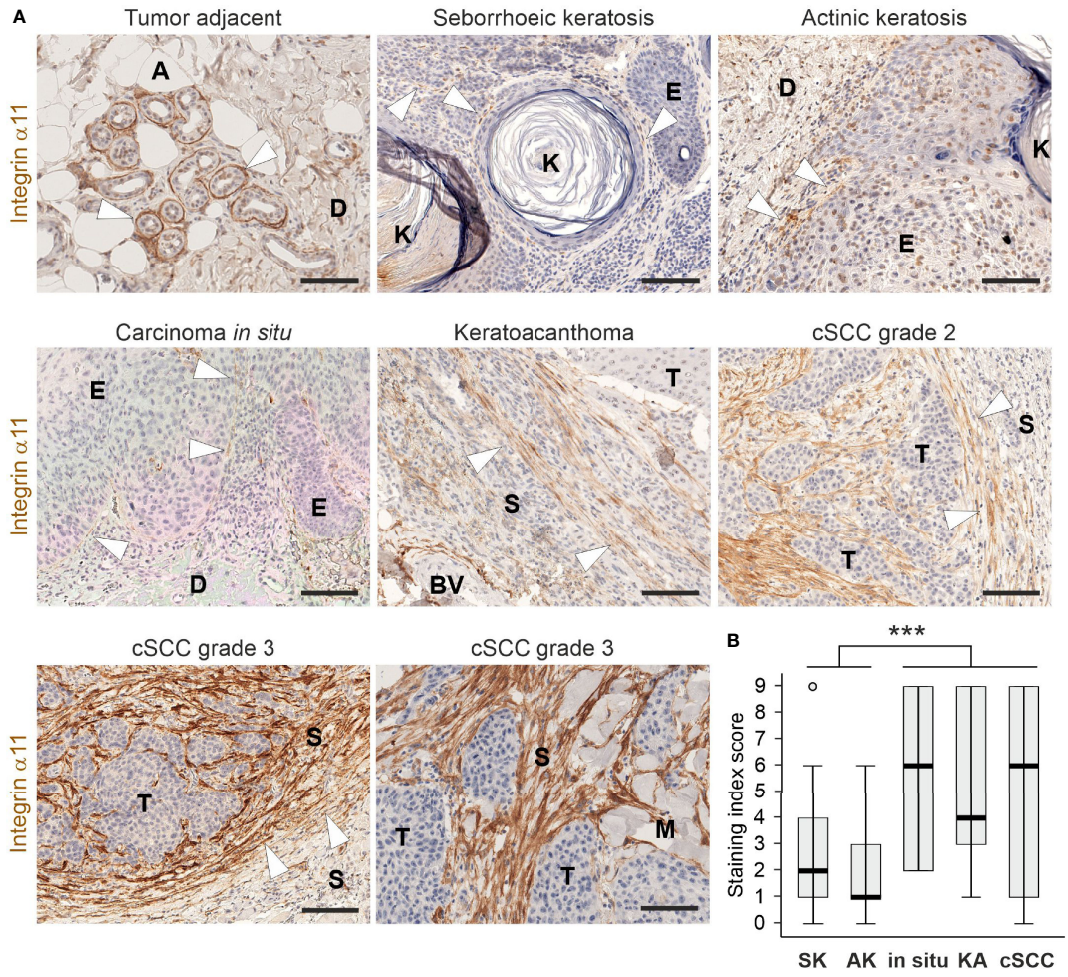

FIGURE 1
Expression and localization of integrin α11 in human cutaneous lesions. **(A)** Representative images of integrin α11 expression and localization in human skin lesions, stained with a monoclonal anti-human integrin α11 antibody (clone 210F4B6A4) (26). Integrin α11 showed strong expression around sweat glands in the tumor-adjacent normal skin, likely in the myoepithelial cells of the acini (arrowheads); scant positive signals in spindle-shaped cells at the dermal-epidermal junction (arrowheads) in benign seborrheic keratosis, premalignant actinic keratosis, and in squamous carcinoma *in situ*; generally moderate or strong signals in spindle-shaped cells distributed within the fibrillar stroma; and present in a tangle-like pattern at the tumor–stroma interphase (arrowheads) in malignant keratoacanthoma and cutaneous squamous cells carcinomas (cSCC). Stromal α11 staining is strong in grade 3 cSCCs. **(B)** A boxplot diagram representing the staining index score in seborrhoeic keratosis (SK), actinic keratosis (AK), *in situ* carcinomas (in situ), keratoacanthomas (KA), and cSCCs. Arrowheads, α11 signals. A, adipocyte, BV, blood vessel; D, dermis; E, epidermis; K, keratin; M, muscle; S, stroma; T, tumor. Scale bars, 100 µm. ***, p<0.001.

tumor number was considerably lower in the knockout mice, the calculated conversion rates were equal between the genotypes (Supplementary Figure 2D). When the dissected cSCC suspects were histologically graded, 64% (n = 9/14) of those in the *Itga1*$^{+/+}$ mice represented cSCCs of grades 1–3, and 36% (n = 5/14) represented benign or dysplastic papillomas, whereas in the *Itga11*$^{-/-}$ mice, 29% (n = 2/7) of tumors were eventually scored as cSCCs, and 71% were scored as (n = 5/7) as papillomas (Supplementary Table 4).

Alterations in the ECM and immune microenvironments in *Itga11*$^{-/-}$ skin tumors

High integrin α11 expression has been associated with the matrix-producing and -remodeling CAF subpopulations, including the cells designated as mCAFs in breast cancer (40) and myCAFs in PDAC (41). Hence, we analyzed the expression of selected ECM components in skin tumors by qRT-PCR and

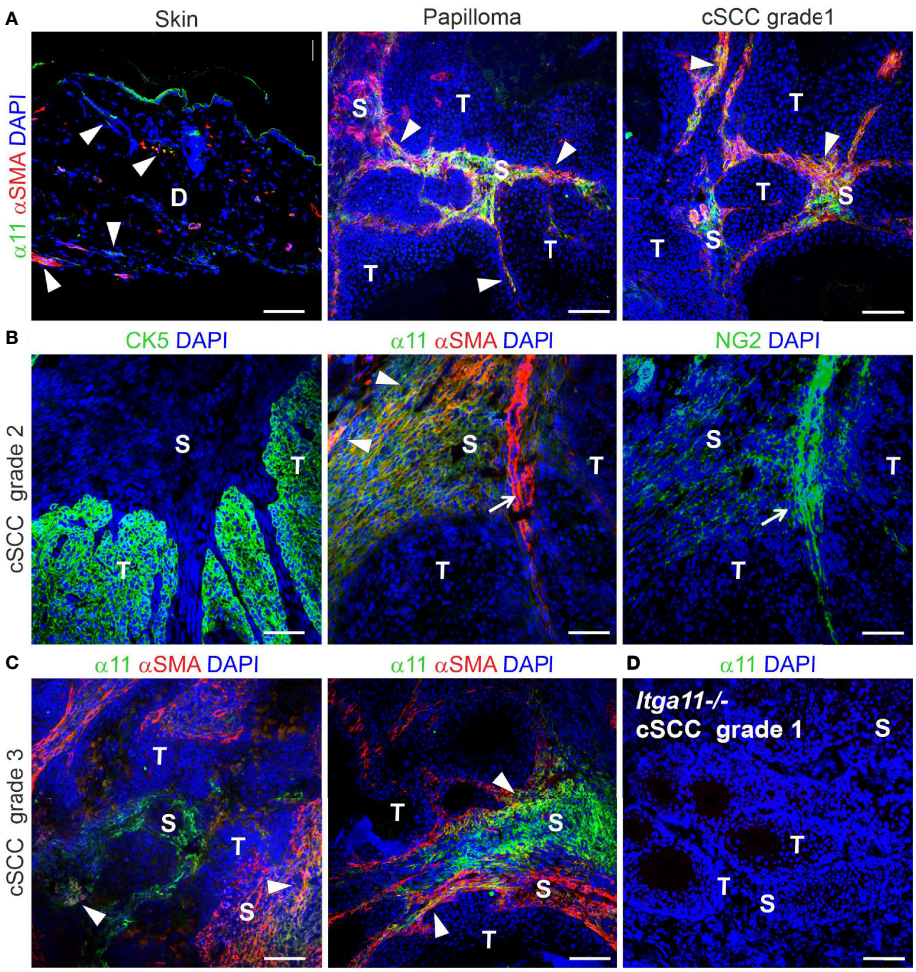

FIGURE 2
Expression and localization of integrin α11 in mouse skin and chemically induced skin tumors. Representative images of α11 immunofluorescence in normal mouse skin and skin tumors, stained with a polyclonal anti-mouse α11 antibody (28). **(A)** α11 expression is negligible in normal mouse skin; scant positive signals are found around hair follicles and in isolated dermal cells (arrowheads), sometimes overlapping with smooth muscle actin (αSMA) signals. The positive signal in the cornified epithelium represents non-specific tissue autofluorescence due to Alexa Fluor 488-conjugated secondary antibody. **(A-C)** α11 is significantly upregulated in the stroma of premalignant papillomas and malignant cSCCs of different grades and partially co-localizes with αSMA-positive cells (arrowheads). **(B)** Sequential sections of a moderately differentiated (grade 2) cSCC. Integrin α11 and αSMA are localized exclusively in the tumor stroma and show partial overlapping (arrowheads). αSMA is also detected in smooth muscle cells around some blood vessels (arrow) and is closely associated with a pericyte marker, NG2. Cytokeratin 5 (CK5) is a marker of carcinoma cells and does not co-localize with α11. **(C)** Examples of integrin α11 and αSMA staining in grade 3 cSCC; immunofluorescent signals in the stroma occasionally overlap with αSMA (arrowheads). **(D)** A well differentiated (grade 1) cSCC from a *Itga11*$^{-/-}$ mouse was used as a staining control for the α11 antibody. Scale bars: A, 100 µm, B-D, 50 µm. Markings in images: D, dermis; S, stroma; T, tumor.

found that the mRNA levels of α1 chains of collagen I (*Col1a1*) and III (*Col3a1*) and *Tnc* were significantly higher in *Itga11*$^{+/+}$ papillomas than in *Itga11*$^{-/-}$ papillomas (Figure 4A). The mRNA levels of prolyl 4-hydoxylases-1 (*Pdha1*) and -2 (*Pdha2*), the key enzymes in collagen biosynthesis, were also significantly downregulated in *Itga11*$^{-/-}$ papillomas (Figure 4B). Masson trichrome staining did not reveal obvious differences in the collagen content of tumors, although areas with hyalinized collagen, suggestive of thicker collagen fibers (42), were frequently observed in the *Itga11*$^{-/-}$ tumor stroma (Supplementary Figure 3A). Inspection of picrosirius red-stained tumor samples under polarized light showed that collagen fibers in *Itga11*$^{-/-}$ tumors often appeared orange or red, whereas they were yellow or green in *Itga11*$^{+/+}$ control

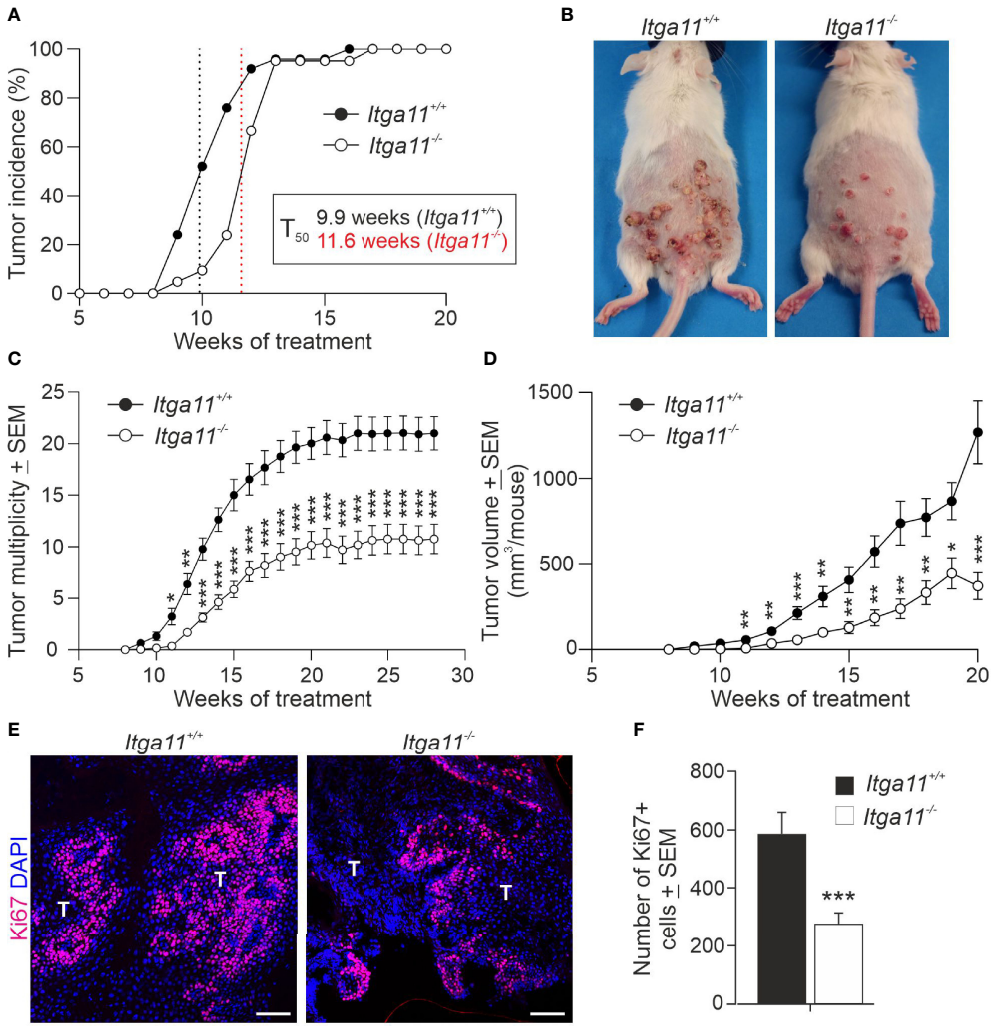

FIGURE 3
Skin tumor growth is impaired in integrin α11-deficient mice. Tumors were induced in the dorsal skin of the *Itga11*$^{+/+}$ (n = 25) and *Itga11*$^{-/-}$ (n = 21) male mice using the 7,12-dimethylbenz[a]anthracene (DMBA)/12-O-tetradecanoylphorbol-13-acetate (TPA) protocol, and tumor incidence and multiplicity were monitored for up to 28 weeks in some individuals. **(A)** Tumor incidence. At week 10, the tumor incidence in the *Itga11*$^{-/-}$ mice was approximately 50% that in the *Itga11*$^{+/+}$ mice. There was a delay of two weeks in terms of tumor incidence in the *Itga11*$^{-/-}$ mice (T_{50}); however, all mice developed skin tumors by week 13. **(B)** Representative photographs of the DMBA/TPA-treated *Itga11*$^{+/+}$ and *Itga11*$^{-/-}$ mice at week 20. **(C)** Cumulative tumor multiplicity. Compared to the *Itga11*$^{+/+}$ controls, the *Itga11*$^{-/-}$ mice developed roughly 50% fewer skin tumors upon DMBA and TPA treatments. **(D)** The total tumor burden per mouse was significantly smaller in the *Itga11*$^{-/-}$ mice from week 10 onwards. **(E, F)** Tumor cell proliferation. Representative images of Ki67 staining of the control and α11-deficient skin papillomas and quantification of proliferating Ki67-positive cells. Ten papillomas per genotype (from different mice) and four to five microscopic fields for each papilloma sample at a magnification of 200× were counted. In E, scale bars 100 μm; T, tumor. *, p<0.05, **, p<0.01, ***, p<0.001.

tumors, indicating the presence of thicker collagen fibers in the knockout samples (Figure 4C). When the red and green signals were quantified, the ratio of thick/thin collagen fibers was approximately twofold higher in the *Itga11*$^{-/-}$ papillomas as compared with that in the *Itga11*$^{+/+}$ papillomas (Figure 4D).

The ultrastructural analysis of papillomas confirmed the differences in collagen fiber organization and also revealed potential differences in the activity of fibroblasts. In the α11-deficient tumors, the collagen fibers were organized in thick, regularly aligned bundles amongst the fibroblasts, whereas in the control tumors, the fibers were dispersed into scattered scaffolds (Figure 4E). The rough endoplasmic reticulum (rER) was prominent and highly dilated in the *Itga11*$^{+/+}$ tumor fibroblasts, whereas it was clearly less dilated in the *Itga11*$^{-/-}$

10.3389/fonc.2022.981009

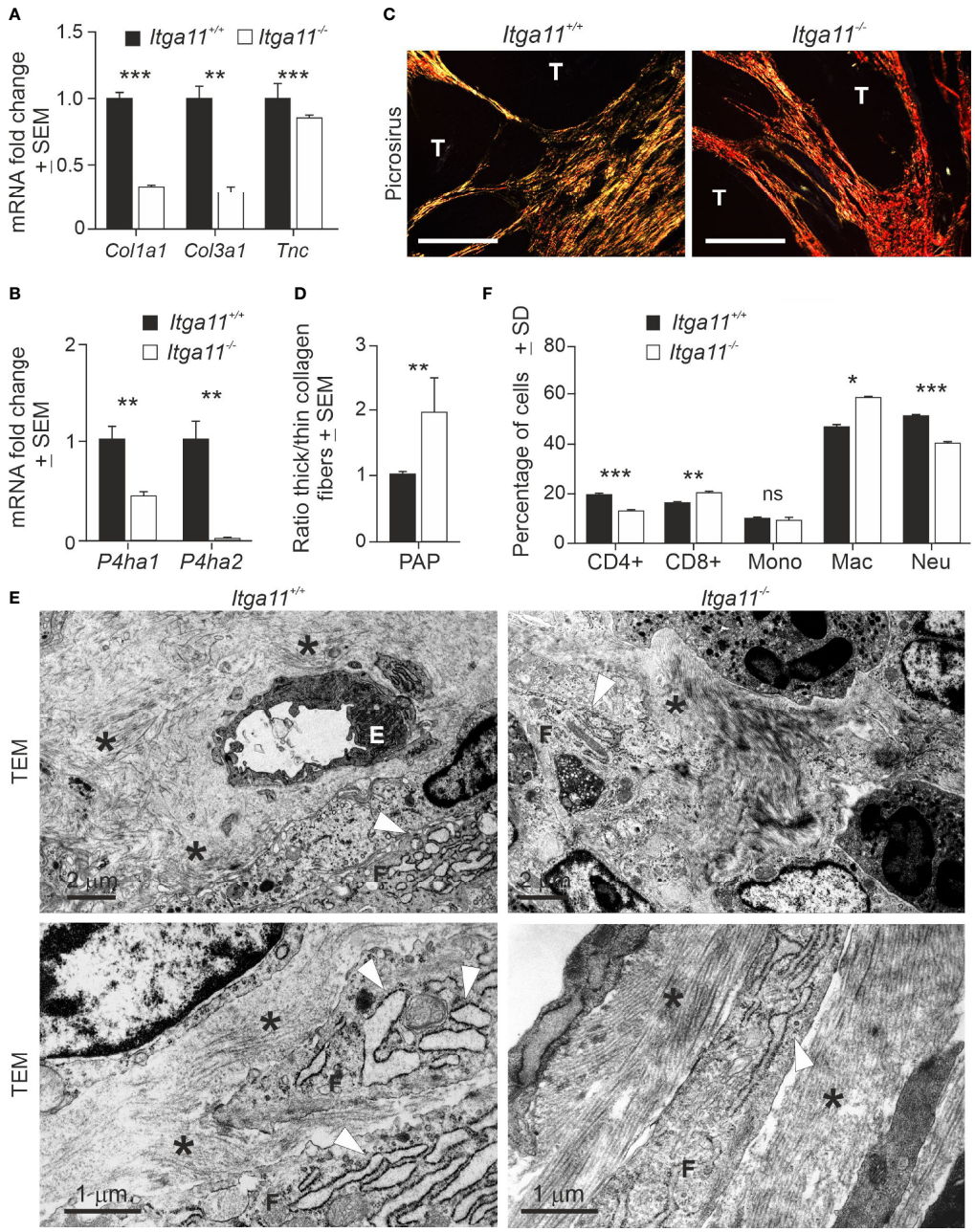

FIGURE 4
Characterization of α11-deficient of skin tumor stroma. **(A, B)** RT-qPCR analysis of collagen I (*Col1a1*) and III (*Col3a1*) α1 chain, tenascin (*Tnc*), and prolyl-4-hydoxylase 1 (*Pdha1*) and 2 (*Pdha2*) in *Itga11*$^{+/+}$ and *Itga11*$^{-/-}$ papillomas. RT-qPCR data are an average of ten samples (from different individuals) per genotype collected at weeks 19–20 and normalized with endogenous *Gapdh*. **(C)** Representative images of picrosirius red staining of *Itga11*$^{+/+}$ and *Itga11*$^{-/-}$ papillomas imaged by polarized light microscopy. Thin collagen fibers appear as yellow/green, and thick collagen bundles appear as red/orange tones. Scale bar, 200 µm. T, tumor. **(D)** The quantification of collagen birefringence shows that the ratio of thick/thin collagen fibers is significantly increased in the *Itga11*$^{-/-}$ tumors compared to the *Itga11*$^{+/+}$ tumors (n = 10 per genotype). **(E)** Transmission electron microscopy (TEM) of skin tumors (n = 3 per genotype). Representative images of two separate *Itga11*$^{+/+}$ and two *Itga11*$^{-/-}$ papillomas with different magnifications are shown. In the *Itga11*$^{+/+}$ papillomas, a prominent dilated rough endoplasmic reticulum (rER, arrowhead) of fibroblasts is evident, and collagen fibers (asterisk) are scattered in the stroma. In the *Itga11*$^{-/-}$ tumors, collagen fibers are organized parallelly in large bundles (asterisk), and the rER is less evident. E, endothelial cell; F, fibroblast; scale bars are marked in the pictures. **(F)** FACS analysis of immune cells in skin tumors. Ten papillomas per genotype, which were harvested from three individuals, were analyzed. In **(A, B, D, F)** *, p<0.05; **, p<0.01; ***, p<0.001. ns, not significant.

CAFs. An obvious, dilated rER is associated with myofibroblasts or CAFs in pathological conditions but not with resident (or less active) fibroblasts (43). Our data suggesting lower fibrillar collagen biosynthesis on the part of α11-deficient CAFs are congruent with the less active rER in these cells but stand in contrast with the observed well-organized collagen bundles in the *Itga11*$^{-/-}$ tumor stroma (Figure 4E).

We addressed the immune cell profiles in the TMEs of mouse skin tumors in order to determine whether α11-positive CAFs exerts paracrine effects on the immune environment, as well as whether these potential alterations could contribute to the observed impaired skin tumor growth in *Itga11* knockout mice. The FACS analysis showed that the *Itga11*$^{-/-}$ papillomas harbored significantly more macrophages and CD8^{+} T-cells and significantly fewer CD4^{+} T-cells and neutrophils than the *Itga11*$^{+/+}$ papillomas (Figure 4F). This result implies that the genetic depletion of α11 expression promotes the development of tumor-suppressive stroma in cSCC.

Integrin α11 regulates LOX and PDGFRβ expression in CAFs

We then deciphered the potential mechanisms that could explain the conspicuous changes observed in the collagenous matrix in α11-deficient skin tumors. Collagen assemblies are stabilized by covalent intra- and intermolecular crosslinks in collagen fibrils, which are predominantly catalyzed by lysyl oxidase (LOX) and four LOX-like enzymes (LOXL1-4) (44, 45). The RT-qPCR analysis showed a surprisingly high, on average 3,000-fold, increase in LOX transcripts in the *Itga11*$^{-/-}$ tumors in comparison with the *Itga11*$^{+/+}$ tumors (Figure 5A). Also, LOXL2 and LOXL4 mRNA levels were markedly upregulated in α11-deficient skin tumors, on average by 300-fold and 50-fold relative to the controls, respectively. In contrast, LOXL1 and LOXL3 mRNA levels were weakly downregulated in *Itga11*$^{-/-}$ tumors. The mRNA levels of TGFβ1, a key inducer of LOX family members, was also highly upregulated in *Itga11*$^{-/-}$ tumors relative to *Itga11*$^{+/+}$ tumors (Figure 5A). The immunofluorescence staining of mouse tumor tissues revealed prominent LOX signals in *Itga11*$^{-/-}$ papillomas, whereas there were clearly fewer in *Itga11*$^{+/+}$ papillomas. The LOX signals were distributed throughout the papilloma stroma and likely represented CAFs, while tumor cells were LOX-negative (Figure 5B). The quantification of stromal LOX signal intensities showed a significant difference between genotypes (Figure 5C). The large highly crosslinked collagen bundles observed in the *Itga11*$^{-/-}$ tumors are expected to lead to an increase in tissue stiffness. In agreement with this, atomic force microscopy measurements demonstrated a shift toward a higher elastic modulus in the α11-deficient skin tumors (Figure 5D).

We then addressed cell differentiation in *Itga11*$^{-/-}$ skin and skin tumors by analyzing the expression of various MSC and fibroblast markers in the knockout and control papillomas *via* qRT-PCR and by utilizing tissue immunostainings, FACS analysis, and *in vitro* cell cultures. We found that the mRNA levels of *αSMA* and *PDGFRβ*, markers of activated myofibroblasts and CAFs, were significantly lower in the *Itga11*$^{-/-}$ papillomas as compared with the *Itga11*$^{+/+}$ papillomas. In particular, *PDGFRβ* expression in knockout tumors was negligible as compared to that in control tumors. The MSC and pan-fibroblast marker *PDGFRα* showed significantly higher expression in the knockout tumors than in control tumors (Figure 5E).

Immunofluorescence demonstrated somewhat weaker PDGFRβ signals in the stroma of *Itga11*$^{-/-}$ tumors than in the *Itga11*$^{+/+}$ tumors, whereas αSMA signals were mostly alike between the two genotypes. However, the quantification of signal intensities did not reveal significant differences in PDGFRβ or αSMA expression between the *Itga11*$^{-/-}$ and *Itga11*$^{+/+}$ papillomas (Supplementary Figures 4A, B). Hyperplastic skin can be considered to represent an early step in skin tumor development (24) and was induced in *Itga11*$^{-/-}$ and *Itga11*$^{+/+}$ mice by repeated treatments of TPA. In comparison to the acetone-treated control skin, a notable increase was observed in the number of PDGFRβ–positive cells in the hyperplastic dermis of the *Itga11*$^{+/+}$ (Supplementary Figure 4C). In contrast, the number of PDGFRβ< mice cells increased only marginally in the hyperplastic skin of the *Itga11*$^{-/-}$ mice after the TPA treatments (Supplementary Figure 4C). The FACS analysis showed that the number of PDGFRα mice–lineage cells increased significantly upon TPA induction in both mouse strains but that their numbers were equal between genotypes, both in the healthy skin and in the inflamed skin (Figure 5F). These observations indicate that, in the mouse skin, α11β1 signalling affects myofibroblast activation, and especially the differentiation of the PDGFRβ–positive subpopulation, both in TPA-induced epidermal hyperplasia and chronic inflammation and during the cSCC development in the DMBA/TPA model.

Finally, to further shed light on the roles of α11β1 signaling in MSCs and address the previous findings regarding the accumulation of adipocytes in *Itga11*$^{-/-}$ skin wounds (46), we compared the differentiation potential of SVF progenitors from the knockout and control mice under *in vitro* culture conditions. This assay did not reveal differences in adipocyte differentiation between the genotypes, as assessed by cell morphology, Oil-Red-O staining of the lipid content, and mRNA expression of the adipogenic markers peroxisome-proliferator activated receptor gamma (*Pparγ*) and adipocyte protein 2 (*aP2*) (Supplementary Figure 5). Our current immunostainings of tumor tissues and FACS analysis, together with the previously published data on α11 in fibroblasts, reinforce the perception that integrin α11β1 signaling plays an active role in mediating the differentiation of skin fibroblasts into myofibroblasts and CAFs but does not play a significant role in the differentiation of SVF progenitors into subcutaneous adipocytes.

10.3389/fonc.2022.981009

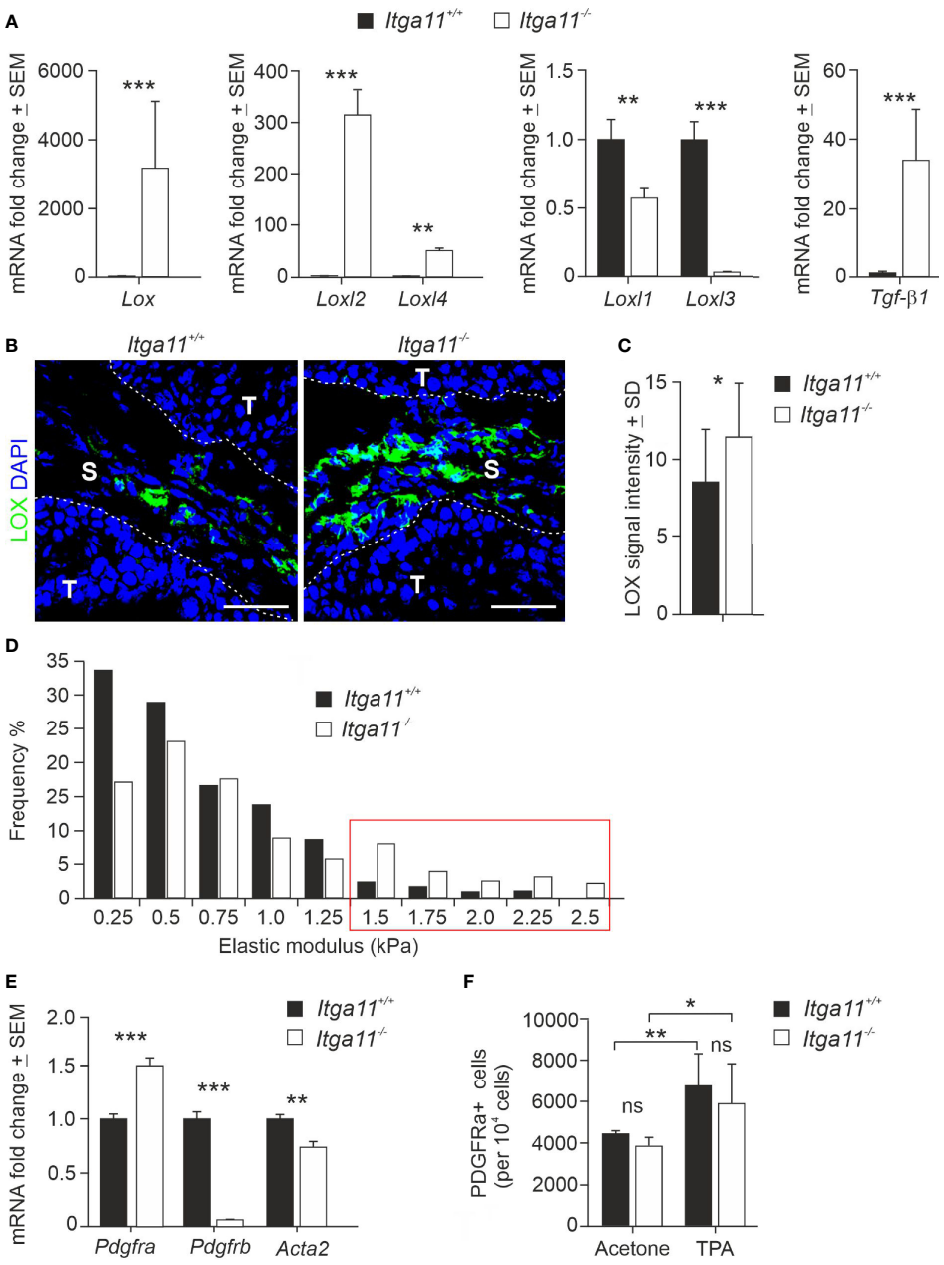

FIGURE 5
Expression of LOX family members and CAF markers in *Itga11*$^{-/-}$ skin tumors. **(A)** RT-qPCR analysis of lysyl oxidase (*Lox*), LOX-like enzymes (*Loxl1-4*), and transforming growth factor beta-1 (*Tgfβ1*) in *Itga11*$^{+/+}$ and *Itga11*$^{-/-}$ skin papillomas at week 20. The data are an average of ten samples (from different individuals) per genotype and normalized with endogenous *Gapdh*. **(B)** Representative immunofluorescence staining of LOX in *Itga11*$^{+/+}$ and *Itga11*$^{-/-}$ papillomas. LOX signals are prominent in α11-deficient skin tumors and widely distributed within the tumor stroma. Scale bars, 50 μm. S, stroma; T, tumor. **(C)** Quantification of LOX immunofluorescence in *Itga11*$^{+/+}$ and *Itga11*$^{-/-}$ papillomas. Twelve to 15 images from five tumors from five different individuals/genotype were quantified using Fiji ImageJ analysis software. **(D)** Tumor stiffness measurements by atomic force microscopy. Histograms of the Young's elastic modulus (kPa) of the *Itga11*$^{+/+}$ (n = 4) and *Itga11*$^{-/-}$ (n = 3) papillomas collected at weeks 20–25. **(E)** RT-qPCR analysis of fibroblast markers PDGFRα, PDGFRβ, and αSMA (*Acta2*) in *Itga11*$^{+/+}$ and *Itga11*$^{-/-}$ papillomas collected at week 20. Data are an average of ten samples (from different individuals) per genotype. Values were normalized with *Gapdh*. **(F)** Numbers of Lin^{-} PDGFRα^{+} cells in the acetone-treated normal and TPA-treated hyperplastic skin of the *Itga11*$^{+/+}$ and *Itga11*$^{-/-}$ mice. In **(A, C, E, F)** *, p<0.05, **, p<0.01, ***, p<0.001. ns, not significant

Discussion

Substantial evidence has been gathered to demonstrate the relevance of α11β1 signaling in CAFs in distinct solid cancer types, as well as in myofibroblasts during wound healing [reviewed in (4, 11)]. Here, we report our novel findings on the notable upregulation of integrin α11 expression in the stromal compartment of human and mouse cSCCs, as well as the significant impairment of DMBA/TPA-induced skin tumor growth in mice, accompanied by interesting alterations in the tumor stroma, in the absence of α11 integrin.

The α11 expression was most prominent in the desmoplastic stroma of malignant high-grade human cSCCs, where the intense, tangle-like α11 signals resembled the staining patterns that have previously been reported for this integrin subunit in human HNSCC (15), as well as in human breast, lung and pancreatic adenocarcinomas (12, 16, 17). The quantification of immunosignals showed that α11 expression was significantly higher in cSCC in the *in situ* stage than in benign and premalignant skin lesions, which suggests that α11 could potentially be utilized as a novel early biomarker to improve the diagnosis and prognostication of this common human cancer. However, using our current, limited cSCC material, we were unable to evaluate whether α11 can distinguish cases with a high risk of cSCC progression and metastasis from those that involve less aggressive tumors and can be treated surgically. Our ongoing work exploiting large and well-characterized cSCC cohorts with full clinical data (47) will better reveal the value of α11 as a novel biomarker in cSCC.

Recent scRNA-seq and bulk RNASeq analyses have identified integrin α11 among the upregulated genes in CAF subpopulations in several human carcinomas, including HNSCC, cutaneous melanoma, lung cancer, breast cancer, and PDAC (40, 48–50). These CAF signatures are associated with active TGFβ signaling and matrix synthesis and remodeling and, in addition to α11, include transcripts for *PDGFRB, ACTA2, FAP, LOX*, periostin, fibronectin, and various collagens, just to mention a few. Thus far, the data on CAF signatures in non-melanoma skin cancers are limited, but one study demonstrated the upregulation of a prominent number of genes involved in ECM remodeling in human basal cell carcinoma (BCC) (51). Interestingly, *ITGA11* was found among these upregulated CAF genes, together with *PDGFRB, COL1A1, COL1A3, LOXL2* and *P4HA*, which all were downregulated in our cSCC mouse model with *Itga11* depletion. The findings published by Omland and coworkers highlight the important role of the microenvironment and CAF activity in the regulation of BCC and point to a tumor-promoting signalling axis, which links integrin α11 with CAF activation and ECM remodeling in this skin cancer type. Another study showed that specific CAF phenotypes can cluster cutaneous melanomas, BCCs and cSCCs into distinct histological subgroups and that this clustering can be used to facilitate diagnosis and even predict tumor progression. In this analysis, cSCC was characterized by the high expression of CAF and epithelial-to-mesenchymal (EMT) markers PDGFRβ, αSMA, podoplanin, Zeb1, Slug, and Twist (52).

With respect to cSCC, next-generation sequencing efforts have mainly targeted transcriptional profiles and genomic alterations in carcinoma cells, but one recent study reports scRNA-seq data on various TME cell types in cSCC and also lists the top ligand-receptor pairs between tumor-specific keratinocytes and CAFs (53). *ITGB1* and *ITGA1* were found among the key CAF receptors that mediate crosstalk between tumor cells and CAFs by interacting with *COL1A1* and *TNC* and, thereby, modulating the TME. Although *ITGA11* was not found in this scRNA-seq analysis, our expression and mouse data predict similar functions on the part of α11β1 in regulating the CAF-tumor cell interplay in cSCC.

Our previous analysis of open databases showed that *ITGA11* expression was correlated positively with *PDGFRB*, *ACTA2*, *TNC*, *COL1A1*, and *COL1A3* in human breast cancer, and the immunostainings showed that α11, PDGFRβ, and TNC were colocalized to CAF subsets in human breast cancer stroma (16). By subjecting wild-type and α11-deficient CAFs from PyMT mouse mammary tumors io 3D spheroid assays, we showed that the interaction between α11 and PDGFRβ in CAFs is needed for efficient PDGFRβ signaling through JNK upon PDGF-BB stimulation. PDGFRβ activation then leads to ECM remodeling, including TNC upregulation, and promotes CAF migration and CAF-induced tumor cell invasion (16).

Our novel observation regarding reduced PDGFRβ and TNC expression in α11-deficient mouse skin tumors is in line with these previous findings on breast cancer and suggests that the α11/PDGFRβ/TNC axis may promote also skin carcinogenesis. Our attempts to establish CAF lines from *Itga11*$^{-/-}$ skin tumors using either the explant method or anti-PDGFRα antibody-based FACS were not successful, and thus, the functions and molecular mechanisms involving α11, PDGFRβ and TNC could not be studied further under *in vitro* conditions. Nevertheless, our findings on reduced PDGFRβ expression in the absence of α11, not only in *Itga11*$^{-/-}$ skin tumor stroma but also in chronically inflamed dermis, suggest the need for further studies on integrated α11β1 and PDGFRβ signaling. In fact, an early study showed that PDGFRβ is highly expressed in fibroblasts in skin biopsies of systemic sclerosis (SS) patients (54), and a recent scRNA-seq analysis identified *ITGA11* as enriched in SS skin myofibroblasts (55). Interestingly, the blocking of fibrotic activity in skin SS myofibroblasts with a YAP inhibitor, verteporfin, reduced the expression of *ITGA11, ITGB1, PDGFRB*, *COL1A1*, and many other ECM-associated genes (56), further reinforcing the view that α11 and PDGFRβ are concomitantly regulated and form a signaling hub that promotes myofibroblast activation in fibrotic tissues.

An unexpected observation in our study was the obvious alteration of the collagenous stroma in the *Itga11*$^{-/-}$ skin tumors. Despite the apparent defect in the activation of the matrix-producing CAF subtype in the knockout tumors, the collagen fibers in the α11-deficient tumor stroma were conspicuously abundant, large, and parallelly assembled, as compared to the less organized and more scattered collagen fibers in control tumors. This finding is likely due to the high expression of LOX, LOXL2, and LOXL4 in *Itga11*$^{-/-}$ tumors, driven by noticeable TGFβ1 upregulation, while LOXL1 and LOXL3 were slightly downregulated in *Itga11*$^{-/-}$. A recent study showed a strong correlation between CAF-expressed α11 and LOXL1 expressions in lung adenocarcinoma, and LOXL1 was shown play a critical role in inducing matrix remodeling and collagen fiber alignment, thereby supporting tumor growth and progression in a xenograft model (14). Similar to our observations in *Itga11*$^{-/-}$ skin tumors, LOXL1 expression was decreased in *Itga11*$^{-/-}$ mouse embryonic fibroblasts. The findings by Zeltz and coworkers in lung adenocarcinoma and by us in cSCC demonstrate a link between α11 and ECM crosslinking by LOX and LOXL enzymes but also imply that the molecular mechanisms whereby α11β1 reorganizes the ECM vary by tumor and CAF subtype.

It is well established that TGFβ signaling plays dual roles in cancer, including in cSCC (57, 58). In DBMA/TPA-treated mouse skin, TGFβ1 is upregulated in basal cells in papillomas and inhibits cell proliferation and papilloma formation, whereas carcinoma cells are devoid of TGFβ1 expression. However, the upregulation of TGFβ1 in macrophages and fibroblasts enhances malignant transformation and metastasis in the later stages of skin carcinogenesis (57). Hence, our data indicating significantly higher levels of TGFβ1 in *Itga11*$^{-/-}$ papillomas than in *Itga11*$^{+/+}$ papillomas suggest that enhanced TGFβ1 signaling could be one reason for the reduced tumor cell proliferation and impaired primary tumor growth. TGFβ1 expression in fibroblasts, in turn, promotes CAF differentiation in an autocrine manner, leading to the increased deposition of ECM proteins, desmoplasia and tissue stiffening (59). TGFβ1 induces α11 expression in skin myofibroblasts during wound healing (46), and we observed higher levels of TGFβ1 in *Itga11*$^{-/-}$ skin tumors as compared to *Itga11*$^{+/+}$ tumors. However, according to our data, the *Itga11*$^{-/-}$ skin tumor CAFs do not respond as efficiently to TGFβ1 induction as the control CAFs, as demonstrated by the downregulation of fibrillar collagen and TNC biosynthesis in the knockout tumors. The high levels of LOX, LOXL2, and LOXL4 transcripts in α11-deficient CAFs are congruent with the observed formation of extensive, linear collagen bundles and a shift toward stiffer skin tumor tissue in this mouse strain.

Elevated fibrillar collagen synthesis, crosslinking and fiber alignment are usually associated with increased cancer invasion and metastasis and poor patient outcome, as exemplified by pioneering studies on breast cancer (60, 61) and PDAC (62). However, recent data have challenged this view by showing, for example, that the deletion of either the αSMA-expressing myCAF subset or the depletion of all hepatic stellate cell-derived CAFs in PDAC mouse models decreases tumor growth and metastasis significantly (63, 64). Bhattacharjee et al. linked the tumor-promoting effects of CAFs with high expression levels for hyaluronan in myCAFs and hepatocyte growth factor in iCAFs. Moreover, tumor progression may be opposed by myCAF-synthesized fibrillar collagen I, which restrains tumor spread mechanically and, at the same time, suppresses the stiffness-induced mechanosignals from the ECM (64). In agreement with this novel experimental data, a previous work with PDAC patient samples showed that, in the absence of αSMA-positive CAFs, collagen deposition is correlated with a good prognosis (65). Considering these data regarding PDAC, our observations regarding the defects in the activation of matrix-producing CAFs, LOX upregulation, and the formation of dense and aligned collagen matrix and the impaired growth of skin tumors in *Itga11*$^{-/-}$ mice are not necessarily contradictory. In contrast, our data highlight the extreme complexity of TME, CAF, and ECM functions in tumors, as well as the central role of α11β1 signaling in CAFs, and also point to differences in their interplay in different tumor types. The dynamic interactions and crosstalk between different stromal cell types and the insoluble matrix in the TME have important immune modulatory functions in tumors, as are also evidenced by our observation regarding altered immune cell profiles in the α11-deficient skin tumors. We postulate that the effects of α11β1 signaling on the immune environment are indirect because both CAF-immune cell interactions and ECM deposition and collagen assembly are known to significantly affect immune cell recruitment and phenotypes (66–69).

In summary, we describe here, for the first time, the expression of α11 integrin in the stroma of human and mouse cSCC and show that α11β1 signaling in CAFs promotes skin carcinogenesis in a chemical mouse model. We conclude that α11β1 operates in a subset of skin tumor CAFs, likely in co-operation with PDGFRβ signaling, thereby regulating ECM synthesis and collagen assembly to encourage cSCC growth and progression. Further studies with sophisticated experimental models are needed to reveal the molecular mechanisms of α11β1 in skin tumor CAFs, as well as its role in the interplay of CAFs with other cell types in the TME in cSCC. Because α11 is not essential for skin development, it should be evaluated as a therapeutic target in skin cancer.

Data availability statement

The raw data supporting the conclusions of this article will be made available by the authors, without undue reservation.

Ethics statement

The studies involving human participants were reviewed and approved by Finnish National Supervisory Authority for Welfare and Health, The Ethical Committee of the Northern Ostrobothnia Hospital District. The patients/participants provided their written informed consent to participate in this study. The animal study was reviewed and approved by The National Animal Experiment Board of Finland, Regional State Administrative Agency.

Author contributions

Conceptualization: RH, DG, and TPi. Methodology: GM-N, H-RT, RH, GW, TPe, SM-K, JK, and JM. Investigation: GM-N, H-RT, NP, VI, RD, HL, TPe, KK and JK. Writing – Original draft: GM-N and H-RT. Writing – Review and Editing: RH, DG, VI, JM, and TPi. Visualization: GM-N, H-RT, and RH. Supervision: RH, DG, S-MK, HR, and TPi. Funding Acquisition: TPi, RH, DG, H-RT, and GW. All authors contributed to the article and approved the submitted version.

Funding

The research leading to these results has received funding from the People Programme (Marie Curie Actions) of the European Union's Seventh Framework Programme FP7/2007-2013/under REA grant agreement no. 316610 (for GM-N and HL) and from the Academy of Finland (grants 308867 and 284065 for TPi), the Cancer Foundation Finland (grants 190147 and 170138 for TPi), the Sigrid Jusélius Foundation (TPi and RH), the Jane and Aatos Erkko Foundation (TPi), the Norwegian Centre of Excellence grant from the Research Council of Norway (ID 223250) (DG), the Western Norway Regional Health Authority (ID 911899) (DG), the National Science and Engineering Research Council of Canada (GW), the Finnish Medical Society Duodecim (H-RT and NP), the Finnish Medical Foundation (H-RT and NP), and the Kerttu Saalasti Foundation (TPe).

Acknowledgments

We thank Päivi Tuomaala, Erja Tomperi, and Jaana Peters for their excellent technical assistance; Raija Sormunen and Ilkka Miinalainen for electron microscopy analyses; and Tamara Monteagudo Aboy for her contribution on human sample analysis. This work was carried out with the support of the Oulu Laboratory Animal Centre, Biocenter Oulu Research Infrastructures and Biocenter Finland.

Conflict of interest

The authors declare that the research was conducted in the absence of any commercial or financial relationships that could be construed as a potential conflict of interest.

Publisher's note

All claims expressed in this article are solely those of the authors and do not necessarily represent those of their affiliated organizations, or those of the publisher, the editors and the reviewers. Any product that may be evaluated in this article, or claim that may be made by its manufacturer, is not guaranteed or endorsed by the publisher.

Supplementary material

The Supplementary Material for this article can be found online at: https://www.frontiersin.org/articles/10.3389/fonc.2022.981009/full#supplementary-material

References

1. Pickup MW, Mouw JK, Weaver VM. The extracellular matrix modulates the hallmarks of cancer. *EMBO Rep* (2014) 15(12):1243–53. doi: 10.15252/embr.201439246

2. Chen Y, McAndrews KM, Kalluri R. 'Clinical and therapeutic relevance of cancer-associated fibroblasts'. *Nat Rev Clin Oncol* (2021) 18(12):792–804. doi: 10.1038/s41571-021-00546-5

3. Sahai E, Astsaturov I, Cukierman E, DeNardo DG, Egeblad M, Evans RM, et al. 'A framework for advancing our understanding of cancer-associated fibroblasts'. *Nat Rev Cancer* (2020) 20(3):174–86. doi: 10.1038/s41568-019-0238-1

4. Zeltz C, Navab R, Heljasvaara R, Kusche-Gullberg M, Lu N, Tsao M-S, et al. 'Integrin α11β1 in tumor fibrosis: more than just another cancer-associated fibroblast biomarker'. *J Cell Commun Signaling* (2022):1–12. doi: 10.1007/s12079-022-00673-3

5. Öhlund D, Handly-Santana A, Biffi G, Elyada E, Almeida AS, Ponz-Sarvise M, et al. Distinct populations of inflammatory fibroblasts and myofibroblasts in pancreatic cancer. *J Exp Med* (2017) 214(3):579–96. doi: 10.1084/jem.20162024

6. Elyada E, Bolisetty M, Laise P, Flynn WF, Courtois ET, Burkhart RA, et al. 'Cross-species single-cell analysis of pancreatic ductal adenocarcinoma reveals antigen-presenting cancer-associated fibroblasts'. *Cancer Discov* (2019) 9(8):1102–23. doi: 10.1158/2159-8290.CD-19-0094

7. Kalluri R. 'The biology and function of fibroblasts in cancer'. *Nat Rev Cancer* (2016) 16(9):582–98. doi: 10.1038/nrc.2016.73

8. Desgrosellier JS, Cheresh DA. Integrins in cancer: Biological implications and therapeutic opportunities. *Nat Rev Cancer* (2010) 10(1):9–22. doi: 10.1038/nrc2748

9. Hamidi H, Ivaska J. Every step of the way: Integrins in cancer progression and metastasis'. *Nat Rev Cancer* (2018) 18(9):533–48. doi: 10.1038/s41568-018-0038-z

10. Hastings JF, Skhinas JN, Fey D, Croucher DR, Cox TR. 'The extracellular matrix as a key regulator of intracellular signalling networks'. *Br J Pharmacol* (2019) 176(1):82–92. doi: 10.1111/bph.14195

11. Zeltz C, Gullberg D. The integrin-collagen connection - a glue for tissue repair? *J Cell Sci* (2016) 129(4):129(4):653–64. doi: 10.1242/jcs.180992

12. Zhu CQ, Popova SN, Brown ERS, Barsyte-Lovejoy D, Navab R, Shih W, et al. 'Integrin α11 regulates IGF2 expression in fibroblasts to enhance tumorigenicity of human non-small-cell lung cancer cells'. *Proc Natl Acad Sci USA* (2007) 104(28):11754–9. doi: 10.1073/pnas.0703040104

13. Navab R, Strumpf D, To C, Pasko E, Kim KS, Park CJ, et al. Integrin α11β1 regulates cancer stromal stiffness and promotes tumorigenicity and metastasis in non-small cell lung cancer'. *Oncogene* (2016) 35(15):1899–908. doi: 10.1038/onc.2015.254

14. Zeltz C, Pasko E, Cox TR, Navab R, Tsao MS. 'LOXL1 is regulated by integrin α11 and promotes non-small cell lung cancer tumorigenicity'. *Cancers* (2019) 11(5):705. doi: 10.3390/cancers11050705

15. Parajuli H, Teh MT, Abrahamsen S, Christoffersen I, Neppelberg E, Lybak S, et al. 'Integrin α11 is overexpressed by tumour stroma of head and neck squamous cell carcinoma and correlates positively with alpha smooth muscle actin expression'. *J Oral Pathol Med* (2017) 46(4):267–75. doi: 10.1111/jop.12493

16. Primac I, Maquoi E, Blacher S, Heljasvaara R, van Deun J, Smeland HYH, et al. 'Stromal integrin α11 regulates PDGFRβ signaling and promotes breast cancer progression'. *J Clin Invest* (2019) 129(11):4609–28. doi: 10.1172/JCI125890

17. Schnittert J, Bansal R, Mardhian DF, Van Baarlen J, Östman A, Prakash J. 'Integrin α11 in pancreatic stellate cells regulates tumor stroma interaction in pancreatic cancer'. *FASEB J* (2019) 33(5):6609–21. doi: 10.1096/fj.201802336R

18. Madan V, Lear JT, Szeimies RM. 'Non-melanoma skin cancer'. *Lancet* (2010) 375(9715):673–85. doi: 10.1016/S0140-6736(09)61196-X

19. Ratushny V, Gober MD, Hick R, Ridky TW, Seykora JT. 'From keratinocyte to cancer: The pathogenesis and modeling of cutaneous squamous cell carcinoma'. *J Clin Invest* (2012) 122(2):464–72. doi: 10.1172/JCI57415

20. Nissinen L, Farshchian M, Riihilä P, Kähäri VM. 'New perspectives on role of tumor microenvironment in progression of cutaneous squamous cell carcinoma'. *Cell Tissue Res* (2016) 365(3):691–702. doi: 10.1007/s00441-016-2457-z

21. Kavasi R-M, Neagu M, Constantin C, Munteanu A, Surcel M, Tsatsakis A, et al. Matrix effectors in the pathogenesis of keratinocyte-derived carcinomas. *Front Med* (2022) 9:879500. doi: 10.3389/fmed.2022.879500

22. Watt FM, Fujiwara H. Cell-extracellular matrix interactions in normal and diseased skin. *Cold Spring Harbor Perspect Biol* (2011) 3(4):a005124. doi: 10.1101/cshperspect.a005124

23. Zeltz C, Lu N, Heljasvaara R, Gullberg D. 'Integrins in cancer: refocusing on the tumor microenvironment'. In: Kovalzzzky I, Franchi M, Alaniz LD, editor. *The extracellular matrix and the tumor microenvironment*. Springer (2022). doi: 10.1007/978-3-030-99708-3#about-this-book

24. Abel EL, Angel JM, Kiguchi K, DiGiovanni J. Multi-stage chemical carcinogenesis in mouse skin: Fundamentals and applications. *Nat Protoc* (2009) 4(9):1350–62. doi: 10.1038/nprot.2009.120

25. Elder D, Massi D, Scolyer R, Willemze R. *'WHO classification of skin tumours. 4th ed*. Lyon': IARC (2018).

26. Smeland HYH, Askeland C, Wik E, Knutsvik G, Molven A, Edelmann RJ, et al. 'Integrin α11β1 is expressed in breast cancer stroma and associates with aggressive tumor phenotypes'. *J Pathol: Clin Res* (2020) 6(1):69–82. doi: 10.1002/cjp2.148

27. Popova SN, Barczyk M, Tiger C-F, Beertsen W, Zigrino P, Aszodi A, et al. 'α11β1 integrin-dependent regulation of periodontal ligament function in the erupting mouse incisor'. *Mol Cell Biol* (2007) 27(12):4306–16. doi: 10.1128/mcb.00041-07

28. Velling T, Kusche-Gullberg M, Sejersen T, Gullberg D, et al. 'cDNA cloning and chromosomal localization of human α11 integrin. a collagen-binding, I domain-containing, β1-associated integrin α-chain present in muscle tissues'. *J Biol Chem* (1999) 274(36):25735–42. doi: 10.1074/jbc.274.36.25735

29. Martínez-nieto G, Heljasvaara R, Heikkinen A, Kaski HK, Devarajan R, Rinne O, et al. Deletion of col15a1 modulates the tumour extracellular matrix and leads to increased tumour growth in the mmtv-pymt mouse mammary carcinoma model. *Int J Mol Sci* (2021) 22(18):9978. doi: 10.3390/ijms22189978

30. Rasi K, Piuhola J, Czabanka M, Sormunen R, Ilves M, Leskinen H, et al. Collagen XV is necessary for modeling of the extracellular matrix and its deficiency predisposes to cardiomyopathy. *Circ Res* (2010) 107(10):1241–52. doi: 10.1161/CIRCRESAHA.110.222133

31. Yang YR, Jang HJ, Choi SS, Lee YH, Lee GH, Seo YK, et al. Obesity resistance and increased energy expenditure by white adipose tissue browning in oga +/- mice. *Diabetologia* (2015) 58(12):2867-–6. doi: 10.1007/s00125-015-3736-z

32. Kilroy G, Dietrich M, Wu X, Gimble JM, Floyd ZE. 'Isolation of murine adipose-derived stromal/stem cells for adipogenic differentiation or flow cytometry-based analysis'. *Methods Mol Biol* (2018) 1773:137–46. doi: 10.1007/978-1-4939-7799-4_11

33. Livak KJ, Schmittgen TD. 'Analysis of relative gene expression data using real-time quantitative PCR and the 2-ΔΔCT method'. *Methods* (2001) 25(4):402–8. doi: 10.1006/meth.2001.1262

34. Hutter JL, Bechhoefer J. Calibration of atomic-force microscope tips. *Rev Sci Instrum* (1993) 64(7). doi: 10.1063/1.1143970

35. Hertz H. 'Uber die beruhrung fester elastischer körper'. *J Fur Die Reine Angew Math* (1881) 92:156–71. doi: 10.1515/crll.1882.92.156

36. Sneddon IN. The relation between load and penetration in the axisymmetric boussinesq problem for a punch of arbitrary profile. *Int J Eng Sci* (1965) 3(1):47–57. doi: 10.1016/0020-7225(65)90019-4

37. Zweers MC, Davidson JM, Pozzi A, Hallinger R, Janz K, Quondamatteo F, et al. 'Integrin α2β1 is required for regulation of murine wound angiogenesis but is dispensable for reepithelialization'. *J Invest Dermatol* (2007) 127(2):467–78. doi: 10.1038/sj.jid.5700546

38. Ramos-Vara JA. 'Technical aspects of immunohistochemistry'. *Vet Pathol* (2005) 42(4):405–26. doi: 10.1354/vp.42-4-405

39. Brideau G, Mäkinen MJ, Elamaa H, Tu H, Nilsson G, Alitalo K, et al. Endostatin overexpression inhibits lymphangiogenesis and lymph node metastasis in mice. *Cancer Res* (2007) 67(24):11528–35. doi: 10.1158/0008-5472.CAN-07-1458

40. Bartoschek M, Oskolkov N, Bocci M, Lövrot J, Larsson C, Sommarin M, et al. Spatially and functionally distinct subclasses of breast cancer-associated fibroblasts revealed by single cell RNA sequencing. *Nat Commun* (2018) 9(1):5150. doi: 10.1038/s41467-018-07582-3

41. Öhlund D, Elyada E, Tuveson D. 'Fibroblast heterogeneity in the cancer wound'. *J Exp Med* (2014) 211(8):1503–23. doi: 10.1084/jem.20140692

42. Kissin EY, Merkel PA, Lafyatis R. Myofibroblasts and hyalinized collagen as markers of skin disease in systemic sclerosis. *Arthritis Rheum* (2006) 54(11):3655–60. doi: 10.1002/art.22186

43. Eyden B. The myofibroblast: Phenotypic characterization as a prerequisite to understanding its functions in translational medicine: Translational medicine. *J Cell Mol Med* (2008) 12(1):22–37. doi: 10.1111/j.1582-4934.2007.00213.x

44. Maki JM. 'Lysyl oxidases in mammalian development and certain pathological conditions'. *Histol Histopathol* (2009) 24(5):651–60. doi: 10.14670/HH-24.651

45. Mayorca-Guiliani A, Erler JT. 'The potential for targeting extracellular LOX proteins in human malignancy'. *OncoTargets Ther* (2013) 6:1729–35. doi: 10.2147/OTT.S38110

46. Schulz JN, Zeltz C, Sørensen IW, Barczyk M, Carracedo S, Hallinger R, et al. 'Reduced granulation tissue and wound strength in the absence of α11β1 integrin'. *J Invest Dermatol* (2015) 135(5):1435–44. doi: 10.1038/jid.2015.24

47. Knuutila JS, Riihilä P, Kurki S, Nissinen L, Kähäri VM. Risk factors and prognosis for metastatic cutaneous squamous cell carcinoma: A cohort study. *Acta Dermato-Venereol* (2020) 100(16):adv00266. doi: 10.2340/00015555-3628

48. Dominguez CX, Müller S, Keerthivasan S, Koeppen H, Hung J, Gierke S, et al. Single-cell RNA sequencing reveals stromal evolution into LRRC15+ myofibroblasts as a determinant of patient response to cancer immunotherapy. *Cancer Discovery* (2020) 10(2):232–53. doi: 10.1158/2159-8290.CD-19-0644

49. Galbo PM, Zang X, Zheng D. Molecular features of cancer-associated fibroblast subtypes and their implication on cancer pathogenesis, prognosis, and immunotherapy resistance. *Clin Cancer Res* (2021) 27(9):2636–47. doi: 10.1158/1078-0432.CCR-20-4226

50. Zhu K, Cai L, Cui C, De Los Toyos JR, Anastassiou D. Single-cell analysis reveals the pan-cancer invasiveness-associated transition of adiposederived stromal cells into COL11A1- expressing cancer-associated fibroblasts. *PloS Comput Biol* (2021) 17(7):e1009228. doi: 10.1371/journal.pcbi.1009228

51. Omland SH, Wettergren EE, Mourier T, Hansen AJ, Asplund M, Mollerup S, et al. Cancer associated fibroblasts (CAFs) are activated in cutaneous basal cell carcinoma and in the peritumoural skin. *BMC Cancer* (2017) 17(1):675. doi: 10.1186/s12885-017-3663-0

52. Sasaki K, Sugai T, Ishida K, Osakabe M, Amano H, Kimura H, et al. Analysis of cancer-associated fibroblasts and the epithelial-mesenchymal transition in cutaneous basal cell carcinoma, squamous cell carcinoma, and malignant melanoma. *Hum Pathol* (2018) 79:1–8. doi: 10.1016/j.humpath.2018.03.006

53. Ji AL, Rubin AJ, Thrane K, Jiang S, Reynolds DL, Meyers RM, et al. 'Multimodal analysis of composition and spatial architecture in human squamous cell carcinoma'. *J Cleaner Prod* (2020) 182(2):497–514.e22. doi: 10.1016/j.cell.2020.05.039

54. Klareskog L, Gustafsson R, Scheynius A, Hällgren R. Increased expression of platelet-derived growth factor type b receptors in the skin of patients with systemic sclerosis. *Arthritis Rheum* (1990) 33(10):1534–41. doi: 10.1002/art.1780331011

55. Tabib T, Huang M, Morse N, Papazoglou A, Behera R, Jia M, et al. Myofibroblast transcriptome indicates SFRP2hi fibroblast progenitors in systemic sclerosis skin. *Nat Commun* (2021) 12(1):4384. doi: 10.1038/s41467-021-24607-6

56. Shi-wen X, Racanelli M, Ali A, Simon A, Quesnel K, Stratton RJ, et al. Verteporfin inhibits the persistent fibrotic phenotype of lesional scleroderma dermal fibroblasts. *J Cell Commun Signaling* (2021) 15(1):71–80. doi: 10.1007/s12079-020-00596-x

57. Glick AB. ' the role of TGF β signaling in squamous cell cancer: Lessons from mouse models '. *J Skin Cancer* (2012)2012:249063. doi: 10.1155/2012/249063

58. Pickup M, Novitskiy S, Moses HL. 'The roles of TGFβ in the tumour microenvironment'. *Nat Rev Cancer* (2013) 13(11):788–99. doi: 10.1038/nrc3603

59. Cox TR, Erler JT. 'Remodeling and homeostasis of the extracellular matrix: Implications for fibrotic diseases and cancer'. *DMM Dis Models Mech* (2011) 4 (2):165–78. doi: 10.1242/dmm.004077

60. Provenzano PP, Inman DR, Eliceiri KW, Knittel JG, Yan L, Rueden CT, et al. Collagen density promotes mammary tumor initiation and progression. *BMC Med* (2008) 6:11. doi: 10.1186/1741-7015-6-11

61. Levental KR, Yu H, Kass L, Yamauchi M, Gasser DL, Weaver VM, et al. Matrix crosslinking forces tumor progression by enhancing integrin signaling. *Cell* (2009) 139 (5):891–906. doi: 10.1016/j.cell.2009.10.027

62. Conklin MW, Eickhoff JC, Riching KM, Provenzano PP, Friedl A, Keely PJ, et al. Aligned collagen is a prognostic signature for survival in human breast carcinoma. *Am J Pathol* (2011) 178(3) :1221–32. doi: 10.1016/j.ajpath.2010.11.076

63. Özdemir BC, Pentcheva-Hoang T, Carstens JL, Allison JP, LeBleu VS, Kalluri R, et al. Depletion of carcinoma-associated fibroblasts and fibrosis induces immunosuppression and accelerates pancreas cancer with reduced survival. *Cancer Cell* (2014) 25(6) :719–34. doi: 10.1016/j.ccr.2014.04.005

64. Bhattacharjee S, Hamberger F, Ravichandra A, Miller M, Nair A, Affo S, et al. Tumor restriction by type I collagen opposes tumor-promoting effects of cancer-associated fibroblasts. *J Clin Invest* (2021) 131(11). doi: 10.1172/JCI146987

65. Erkan M, Michalski CW, Rieder S, Esposito I, Friess H, Kleeff J, et al. The activated stroma index is a novel and independent prognostic marker in pancreatic ductal adenocarcinoma. *Clin Gastroenterol Hepatol* (2008) 6(10):1155–61. doi: 10.1016/j.cgh.2008.05.006

66. Jiang H, Hegde S, DeNardo DG. 'Tumor-associated fibrosis as a regulator of tumor immunity and response to immunotherapy'. *Cancer Immunol Immunother* (2017) 66(8):1037–48. doi: 10.1007/s00262-017-2003-1

67. Chen Y, Kim J, Yang S, Sugimoto H, LeBleu VS, Kalluri R, et al. 'Type I collagen deletion in αSMA+ myofibroblasts augments immune suppression and accelerates progression of pancreatic cancer'. *Cancer Cell* (2021) 39(4) :548–565.e6.. doi: 10.1016/j.ccell.2021.02.007

68. Rømer AMA, Thorseth ML, Madsen DH. 'Immune modulatory properties of collagen in cancer'. *Front Immunol* (2021) 12:791453. doi: 10.3389/fimmu.2021.791453

69. Sun X, Wu B, Chiang H-C, Deng H, Zhang X, Xiong W, et al. Tumour DDR1 promotes collagen fibre alignment to instigate immune exclusion. *Nature* (2021) 599(7886) :673–78. doi: 10.1038/s41586-021-04057-2

frontiers | Frontiers in Oncology

TYPE Original Research
PUBLISHED 16 August 2022
DOI 10.3389/fonc.2022.981927

Check for updates

OPEN ACCESS

EDITED BY
M. Cecilia Caino,
University of Colorado Anschutz Medical Campus, United States

REVIEWED BY
Yao Tong,
The Scripps Research Institute, United States
Malgorzata Wygrecka,
University of Giessen, Germany

*CORRESPONDENCE
Benoit Langlois
benoit.langlois@univ-reims.fr

SPECIALTY SECTION
This article was submitted to Molecular and Cellular Oncology, a section of the journal Frontiers in Oncology

RECEIVED 29 June 2022
ACCEPTED 28 July 2022
PUBLISHED 16 August 2022

CITATION
Langlois B, Martin J, Schneider C, Hachet C, Terryn C, Rioult D, Martiny L, Théret L, Salesse S and Dedieu S (2022) LRP-1-dependent control of calpain expression and activity: A new mechanism regulating thyroid carcinoma cell adhesion. *Front. Oncol.* 12:981927. doi: 10.3389/fonc.2022.981927

COPYRIGHT
© 2022 Langlois, Martin, Schneider, Hachet, Terryn, Rioult, Martiny, Théret, Salesse and Dedieu. This is an open-access article distributed under the terms of the Creative Commons Attribution License (CC BY). The use, distribution or reproduction in other forums is permitted, provided the original author(s) and the copyright owner(s) are credited and that the original publication in this journal is cited, in accordance with accepted academic practice. No use, distribution or reproduction is permitted which does not comply with these terms.

LRP-1-dependent control of calpain expression and activity: A new mechanism regulating thyroid carcinoma cell adhesion

Benoit Langlois[1,2]*, Julie Martin[1,2], Christophe Schneider[1,2], Cathy Hachet[1,2], Christine Terryn[3], Damien Rioult[4], Laurent Martiny[1,2], Louis Théret[1,2], Stéphanie Salesse[1,2] and Stéphane Dedieu[1,2]

[1]UFR Sciences Exactes et Naturelles, Université de Reims Champagne-Ardenne, Reims, France, [2]Matrice Extracellulaire et Dynamique Cellulaire, MEDyC, UMR 7369 CNRS, Reims, France, [3]Plate-Forme Imagerie Cellulaire et Tissulaire (PICT), Université de Reims Champagne-Ardenne, UFR Médecine, Reims, France, [4]Plateau Technique Mobile de Cytométrie Environnementale MOBICYTE, Université de Reims Champagne-Ardenne/INERIS, Reims, France

The low-density lipoprotein receptor-related protein 1 (LRP1) is a multifunctional endocytic receptor mediating the clearance of various molecules from the extracellular matrix. LRP1 also regulates cell surface expression of matrix receptors by modulating both extracellular and intracellular signals, though current knowledge of the underlying mechanisms remains partial in the frame of cancer cells interaction with matricellular substrates. In this study we identified that LRP1 downregulates calpain activity and calpain 2 transcriptional expression in an invasive thyroid carcinoma cell model. LRP1-dependent alleviation of calpain activity limits cell-matrix attachment strength and contributes to FTC133 cells invasive abilities in a modified Boyden chamber assays. In addition, using enzymatic assays and co-immunoprecipitation experiments, we demonstrated that LRP1 exerts post-translational inhibition of calpain activity through PKA-dependent phosphorylation of calpain-2. This LRP-1 dual mode of control of calpain activity fine-tunes carcinoma cell spreading. We showed that LRP1-mediated calpain inhibition participates in talin-positive focal adhesions dissolution and limits β1-integrin expression at carcinoma cell surface. In conclusion, we identified an additional and innovative intracellular mechanism which demonstrates LRP-1 pro-motile action in thyroid cancer cells. LRP-1 ability to specifically control calpain-2 expression and activity highlights a novel facet of its de-adhesion receptor status.

KEYWORDS

LRP-1, cancer, adhesion receptors, cell-matrix interactions, invasive potential

Introduction

The Low-density lipoprotein (LDL) receptor-related protein-1 (LRP-1) is a large ubiquitously expressed multifunctional receptor, member of the LDL-receptor family (1). Being first identified as an endocytic receptor for α-2 macroglobulin (2, 3), LRP-1 demarks from the smaller isoforms of this ancient gene family by its ability to mediate the specific internalization and lysosomal targeting of over 30 distinct extracellular ligands. This includes proteases, protease-inhibitor complexes, matricellular proteins and growth factors (4). Initially synthesized as a 600 kDa precursor, LRP-1 is processed in the trans-Golgi by a furin-convertase to be addressed at cell surface in the mature two-chain form. It is composed of a 515 kDa extracellular α-chain, involved in the specific recognition of cell surface and soluble proteins, and a 85 kDa β-chain encompassing the transmembrane domain and a short cytoplasmic tail providing dual function to LRP-1 in the recruitment of adaptors of the endocytic machinery or signaling scaffolds (4, 5).

The diversity of cell surface interactions engaged by LRP-1 has attracted research interest in several pathological contexts including atherosclerosis, neurodegenerative and fibrotic disorders (6–8). Additionally, LRP-1 well documented function in the endocytic clearance of matrix proteases-containing complexes, including matrix metalloproteases (MMPs) (4), and plasminogen activators uPA and tPA (9–11), widely involved in invasive behavior of cancer cells, early pointed its crucial role in matrix remodeling events and designated its putative status of tumor suppressor (4, 12). Consistently, a weak expression of the receptor was observed in high grade cancer cells and tissues of various origins (11, 13, 14). However, this attractive model was counterbalanced by studies reporting LRP-1 positive contribution towards tumorigenesis and metastatic dissemination (15, 16). Moreover, the LRP-1 endocytic control of matrix proteolysis may be antagonized by its ability to control expression of matrix components (17) and proteases (18, 19) at the transcription level.

LRP-1 overall function in carcinogenesis therefore appears to be much more complex than initially assumed. Beyond endocytosis, LRP-1 was indeed reported to control activation of several intracellular signaling pathways by recruiting various scaffolding proteins on the two NPxY motifs of its intracellular domain (20, 21). In this way and in response to extracellular stimuli, LRP-1 may assemble specific signaling platforms to regulate cell proliferation, survival, differentiation and migration (22–25). Accordingly, LRP-1 dependent activation of the JAK/Stat pathway was involved in the pro-motile effect of the plasminogen activator inhibitor PAI-1 (26). In fibrosarcoma cells, LRP-1 deficiency appeared to limit invasive process by down-regulating the extracellular signal-regulated kinase (ERK) pathway (27, 28). In contrast, LRP-1 was shown to activate promigratory signals in various cell types (25, 29–31), including tumor cells (15, 19, 32–34). For instance, in breast (33) and pancreatic (34) cancer models, the secretion of HSP90α in the tumor microenvironment and its specific binding to LRP-1 at the tumor cell surface was recently linked to the induction of common, but also distinct features, of an epithelial-to-mesenchymal transition in favor of metastatic dissemination and correlated to poor prognosis of cancer patients. Noticeably, we recently described that LRP-1 contributes to thyroid carcinoma cell invasion by subtly controlling the composition and turn-over of adhesive complex (9, 28).

Accumulating evidence now shows that LRP-1 may exert a pivotal function in the dynamic of cell-matrix interactions (28, 35, 36). Consistently, the receptor was demonstrated to influence several aspects of integrin functions critically engaged during aggressive cancer cells epithelial-to-mesenchymal transition, such as activation (8), clustering (37) and endocytosis that leads to either cell surface recycling or catabolism (10, 38–40). Tumor cells migration through extracellular matrix network is a complex multistep process relying on spatially and temporally regulated assembly of adhesion sites at the leading edge, cell contraction, and focal adhesion turn-over at the rear. Although LRP-1 now emerges as a putative regulator of each process (4, 35), the intracellular events it may solicit to control both adhesion complex formation and disassembly remain partially unraveled and controversial. The intracellular cysteine proteases calpains are well known regulators of cell migration for controlling focal adhesion stability through limited proteolysis of cytoskeletal components (41). The two best characterized members of the family, calpain-1 and calpain-2, are ubiquitously expressed and can be regulated by their endogenous inhibitor calpastatin or by various post-translational modifications, including autoproteolysis, calcium or phosphoinositide binding (41–43). In this study we pursued our investigation on LRP-1-dependent intracellular signals sustaining cell-matrix interactions dynamics by testing its contribution to calpain activity control in the context of thyroid carcinoma.

Abbreviations: LRP-1, low-density lipoprotein receptor-related protein-1; PKA, protein kinase A; MMP, matrix metalloprotease; uPA, urokinase-type plasminogen activator; tPA, tissue-type plasminogen activator; JAK/Stat, janus kinase/signal transducer and activator of transcription; PAI-1, plasminogen activator inhibitor 1; ERK, extracellular signal-regulated kinase; HSP, heat shock protein; FTC, follicular thyroid carcinoma; ECM, extracellular matrix; LFA-1, lymphocyte function-associated antigen-1; FAK, focal adhesion kinase; JNK, c-Jun N-terminal kinase; MAPK, mitogen-activated protein kinase; TRPM4, transient receptor potential cation channel subfamily M; PIEZO1, piezo-type mechanosensitive ion channel component 1; MT1-MMP, membrane type 1 matrix metalloprotease; CAPN2, calpain-2; FA, focal adhesion.

Materials and methods

Antibodies and chemicals

Anti-LRP-1 α-chain (8G1), anti-LRP-1 β-chain (5A6), anti-human IgGs used as negative control for immunoprecipitation

experiments (HP6030), specific inhibitors for calpain (Calpeptin) and PKA (KT5720), and fluorigenic Calpain Substrate II were obtained from Calbiochem (distributed by VWR International, Strasbourg, France). Anti-calpain-2 (H240) used for immunoprecipitation experiments, anti-β1 (M-106), anti-calpastatin (C-20) and anti-β-actin (sc-1616) antibodies were purchased from Santa-Cruz Biotechnology (distributed by Tebu-Bio, Le Perray en Yvelines, France). Anti-phosphothreonine (9381) and HRP-conjugated anti-rabbit antibodies were from Cell Signaling (distributed by Ozyme, Saint Quentin Yvelines, France). Anti-calpain-2 (ab39165) and anti-talin (8D4) were from Abcam (Cambridge, UK). Anti-talin antibody used for immunocytochemistry (MAB1676) and anti-calpain-1 (MAB3104) were from Chemicon (distributed by Millipore, Molsheim, France). HRP-conjugated anti-mouse antibody (NA931V) was from Amersham Biosciences (Buckinghamshire, UK). Anti-pan β1 integrin (clone Mab13) and anti-active β1 integrin (9EG7) antibodies were from BD Transduction Laboratories (Mississauga, Canada). 7-amino-4-chloromethylcoumarin, t-BOC-L-leucyl-L-methionine amide (CMAC, t-BOC-Leu-Met), anti-mouse AlexaFluor 488 (A11001), AlexaFluor 568-phalloidin (A12380) and Prolong Gold antifade reagent with DAPI (P36935) were from Molecular Probes (Cergy Pontoise, France). Anti-phosphoserine (PSR-45), HRP-conjugated anti-goat secondary antibodies, leupeptin and other chemicals were purchased from Sigma-Aldrich (Steinheim, Germany).

Cell culture and transfection

The FTC133 human follicular thyroid carcinoma cell line was grown in Dulbecco's Modified Eagle Medium-Ham's F12 (Invitrogen, Cergy Pontoise, France) with 10% FBS, as previously described (44). SiRNA mediated silencing of LRP-1 was described elsewhere (9). Specific LRP-1 targeting sequences were designed by Dharmacon (distributed by Perbio Science, Brebiere, France) as follows: GACUUGCAGCCCCAAGCAGUU (sense), CUGCUU GGGGUGCAAGUCUU (antisense). Control transfection experiments were achieved by using SiGENOME Non-targeting siRNA #1 (D00121001-20) from Dharmacon. For transient transfection assays, siRNA were transfected for four hours by using Lipofectamine 2000 (Invitrogen) according to manufacturer instructions.

Reverse transcription and quantitative real-time PCR

Total RNAs isolated using the RNeasy Mini kit (Qiagen, Courtaboeuf, France) were reverse transcribed to cDNA with the ABsolute Blue verso 2-step kit and subjected to quantitative real-time PCR by using the Absolute SYBR Green mix (Thermo Fisher Scientific, Epsom, Surrey, UK) and a Chromo4 Real-Time PCR Detector system from Bio-Rad. Primers for LRP-1 were previously described (9). Primers for calpain 1, calpain 2 and β-actin were designed by Eurogentec (Seraing, Belgium) as follows: calpain 1: forward, CCTTGAGGATGATCTGGTAGA; reverse, AGCTAGTGTTCGTGCACTCTG; calpain 2: forward: CTGGAGATCTGTAACCTGACC; reverse: GGTACTGAGG GTTCATCCAGA; β-actin: forward: GTGTGACGTGGACA TCCGC; reverse: CTGCATCCTGTCGGCAATG. The relative levels of expression were quantified by using Opticon Monitor software (Bio-Rad). For each specific gene, the amount of target RNA ($2^{-\Delta\Delta Ct}$) was normalized to the internal actin reference (ΔCt) and related to the amount of target RNA in control sample, set to 1. All experiments were performed at least in triplicate with internal duplicate for each sample.

Western blot analysis

Whole-cell extracts were prepared by scrapping cells in ice-cold lysis buffer (25 mM Tris-HCl, pH 7.7, 150 mM NaCl, 0.5% glycerol, 1% Triton X-114, 5 mM EDTA, 0.5 mM EGTA, 1 mM phenylmethylsulfonyl fluoride, 1 mM orthovanadate supplemented with proteinase inhibitor cocktail). After 30 min incubation on ice, extracts were centrifugated (10,000 X *g* for 10 min at 4°C) and pellets were discarded. The protein concentration in supernatants was quantified by the Bradford method (BioRad Laboratories). Proteins were separated by electrophoresis in a 10% sodium dodecyl sulfate-polyacrylamide gel, transferred onto a nitrocellulose membrane (Whatman GmbH, Dassel, Germany), and incubated overnight at 4°C with primary antibodies. Immunoreactive bands were revealed using an ECL plus chemiluminescence kit from Amersham Biosciences by using a ChemiDoc-XRS imaging station from Bio-Rad. Immunoblots presented are representative of at least three separate experiments. The specific signal of β-actin was used to ensure equal loading.

Biotinylation of cell surface proteins and detection of cell surface integrins

Separation of cell surface proteins was conducted by immunoprecipitation of biotinylated proteins. Briefly, after culture on gelatin-coated surfaces, cells were rinsed with ice cold PBS and incubated for 30 min at 4°C under slow agitation with 0,5 mg/mL EZ-Link Sulfo-NHS-LC-Biotin (Pierce). All further steps until cell lysis were made at 4°C to avoid cell surface protein endocytosis. After 3 PBS washes, reaction was quenched by 100 mM Glycine for 30 min under gentle agitation and cells were scrapped in lysis buffer (10 mM Tris-HCl, pH 7.4, 150 mM NaCl, 0,1% Triton X-100, 5 mM EDTA, 1 mM

phenylmethylsulfonyl fluoride, 1mM orthovanadate supplemented with proteinase inhibitor cocktail). 500 µg of clarified cell extracts were then incubated for 1 hour with 40 µL of avidin beads (Pierce) under agitation. After three washes in lysis buffer, immunoprecipitated proteins were reduced and analyzed by immunoblotting. Supernatants were used to control selective fractionation of cell surface proteins. When indicated, cell surface specific integrin-containing complexes were subjected to a second immunoprecipitation step after competing biotin-avidin complexes overnight with 10 mM D-Biotin (Pierce). Procedure for immunoprecipitation is described in the following section.

Immunoprecipitation

The procedure was adapted from one previously described (9). Briefly, for the immunoprecipitation of cell surface integrin containing complexes, Biotinylated protein fraction was subjected to a second immunoprecipitation step in the same lysis buffer, as described above. Cell extracts for immunoprecipitation of calpain were prepared in a distinct lysis buffer (10 mM Tris-HCl, pH 7.4, 0.75% Brij, 75 mM NaCl, 5 mM EDTA, 1 mM phenylmethylsulfonyl fluoride, 1 mM orthovanadate supplemented with proteinase inhibitor cocktail). After centrifugation (10,000 X *g*, 10 min at 4°C) and Bradford titration, 500 µg of total proteins were incubated for 4 hours at 4°C on an orbital agitator in presence of anti-calpain antibodies. Nonspecific IgGs were used for negative controls. Immunoprecipitation was performed with 40 µL protein G-Sepharose (Amersham Biosciences) for 2 hours at 4°C under agitation. The samples were washed three times in the corresponding lysis buffer and protein complexes bound to beads were solubilized under reducing conditions and analyzed by immunoblotting as described above.

PKA activity assay

PKA activity was assessed by using ProFluor PKA assay from Promega with minor modifications to quantify specific PKA activity in raw cell extracts. Briefly, cells were detached and cultivated on gelatin-coated for 3 hours. Cells were then scrapped 48 hours post transfection on ice in PKA buffer (25 mM Tris-HCl, pH 7.4, 0,5 mM EDTA, 0,5 mM EGTA), sonicated, clarified (10,000 X *g* for 10 min at 4°C) and protein concentration was determined by Bradford method. Equal amounts of proteins were then assessed for PKA activity following standard procedure, based on phosphorylation-dependent quenching of a fluorescent PKA substrate. Results were obtained from three separate experiments with internal quadruplicate, and related to control sample, set to 1. Specificity of reaction was ensured by subtracting residual PKA activity in the presence of 10 µM of specific inhibitors H-89 and KT5720.

Calpain activity assays

Cells were scrapped on ice in lysis buffer (50 mM Hepes, pH 7.4, 150 mM NaCl, 1% Triton X-100, 0,5 mM DTT, 10 mM β-mercapto-ethanol, 20 µM leupeptin, 1 mM PMSF, 1 mM Na_3VO_4) and clarified (10,000 X *g* for 10 min at 4°C). *In vitro* calpain activity was then quantified through two different procedures. First, calpain activity was measured with Innozyme Calpain 1/2 Activity Assay Kit (Calbiochem) following manufacturer instructions. A second procedure was adapted from Goette *et al.* (45). Briefly, 100 µg of proteins were diluted in activation buffer (20 mM Tris-HCl pH 7.4, 5 mM $CaCl_2$) containing 2 µM calpain substrate II (Suc-Leu-Tyr-AMC). Background fluorescence was determined by negative control carried out for each sample in the presence of 10 mM EDTA, 10 mM EGTA and 50 µM of the specific calpain-1/2 inhibitor calpeptin. Reaction was developed in 96-wells plate at 37°C for 1 hour and fluorescence resulting from calpain-mediated release of AMC was measured at 380 nm (excitation)/430 nm (emission) wavelengths using a Perkin-Elmer LS50B spectrometer. Results were expressed as percentage of control after background subtraction. Each experiment was made at least four times with internal quadruplicate. Calpain activity was visualized in intact cells by using a previously described method (46). Cells were cultivated on gelatin-coated coverslips and incubated for 10 min in the presence of 50 µM BOC-LM-CMAC (*t* butoxycarbonyl-Leu-Met-chromomethylaminocoumarin), a cell permeant thiol-reactive substrate selective for calpains. Cells were then replaced in fresh medium for 1 hour, fixed on ice in 4% paraformaldehyde and mounted in aqueous antifading medium (Immunotech). Fluorescence resulting from Calpain-mediated CMAC release was observed under UV light with an optical microscope (BH2; Olympus). Specificity of the reaction was controlled in the presence of 50 µM calpeptin. Quantification of calpain activity was achieved by counting 300 cells from 3 distinct experiments. The number of positive cells exhibiting a clear fluorescence signal was normalized to a total cell number for each treatment and expressed as a percentage of control condition.

Boyden chamber assay

Matrigel invasion assay was performed using modified Boyden chambers in 24-well dishes with filter inserts provided with 8-µm pores (Transwell, Costar, Brumath, France), as described elsewhere (44). Matrigel-coated filters were used for invasion assays and uncoated filters were used for migration assays. Invasiveness was determined by counting cells in eight random microscopic fields per well, each seeded in triplicate.

Adhesion and trypsinization assays

Measurement of cancer cell adhesion to gelatin-coated surfaces and trypsinization assays were carried out according to a previously described method (9).

Immunofluorescence microscopy

FTC133 cells were seeded onto gelatin-coated coverslips for 2 hours at 37°C, fixed with 4% paraformaldehyde for 5 min on ice and then permeabilized in ice-cold 0,1% Triton X-100 for 10 min. After three washes with PBS, cells were incubated for 30 min with PBS containing 2% bovine serum albumin to saturate nonspecific antigens. Coverslips were then incubated for 30 min with AlexaFluor 568-phalloidin or 60 min with anti-talin antibodies followed by three washes with PBS (Phosphate Buffered Saline). Talin staining was revealed after 30 min incubation with secondary antibodies conjugated to AlexaFluor 488. Coverslips were then mounted in Prolong Gold antifade medium with DAPI to obtain nuclei counterstaining. All acquisitions were made with an Olympus BH2-RFCA epifluorescence microscope (Olympus, Japan), equipped with a 100W mercury lamp (OSRAM, GmbH), using a SPlan achromat x 40 objective (Olympus) and fluorescein, rhodamin, DAPI filters for talin, actin and nuclei staining, respectively. Antibodies used for immunostainings of integrins were incubated overnight and revealed after 1 hour incubation with Alexafluor 568-coupled secondary antibodies. Images were acquired with Zen software on a Zeiss LSM 880 Airyscan confocal microscope (Oberkochen, Germany) using a x63 Plan Apochromat objective (oil immersion, 1.40 NA). Representative images from three separate sets of cultures were treated and merged with ImageJ software. The percentage of cells positive for focal adhesions was determined as previously reported (9), by examining 300 cells from three different experiments for each condition.

Densitometric analysis and statistical evaluation

Bands from immunoblots or agarose gels were quantified by using Quantity One image-analyzer software (Bio-Rad Laboratories). All culture assays were normalized on the basis of cell viability by using the CellTiter-Glo assay from Promega. Each experiment was performed at least in triplicate and data were expressed as mean ± SEM. Comparisons between two or four samples were performed using Student's t-test or one way analysis of variance (47) with *post hoc* Tukey's test (Prism software, GraphPad Inc, San Diego, CA).

Results

LRP-1 expression contributes to repress calpain activity in invasive thyroid carcinoma cells

We previously reported that LRP-1 is involved in the regulation of cell-matrix interactions turnover by exerting an intimate control on the focal adhesion composition and dynamics (9, 28, 40). We demonstrated that LRP-1 functions as a molecular relay and provides an intracellular docking platform to regulate the incorporation and activation of MAPK into focal complexes. This work established a direct link between intracellular signaling pathways modulated by LRP-1 and dynamics of matrix attachment of migrating tumor cells. However, a complete overview of the intracellular connections of the receptor in that context is still lacking. We further investigated the still incomplete knowledge of intracellular functions of the receptor involved in the control of adhesion complexes stability. To achieve this goal, we used a validated method of invalidation of LRP-1 in FTC-133 thyroid carcinoma cells by siRNA (36) leading to a 70% decrease of its gene expression as evaluated by RT-qPCR (Figure 1A), and to a 66% decrease of its protein expression measured by western blot (Figure 1B). Calpains constitute a family of intracellular calcium-dependent cysteine-proteases which exert crucial actions on focal adhesion dynamics, and are able to cleave cytoskeleton components to mediate turnover and disassembly of focal complexes as well as the activation and clustering of extracellular matrix receptors (41, 48, 49). We tested the consequences of LRP-1 invalidation on calpain activity in FTC133 cells during the phase of attachment by performing a biochemical assay based on calpain substrate II cleavage (Figure 1C). We evidenced an increase of 34,5% of the capacity of LRP-1-silenced cells to degrade calpain substrate II *in vitro*, as compared to control tumor cells. A distinct fluorigenic assay was conducted to confirm this result using the quenching of DABCYL substrate. By using this complementary approach, we observed a 2.2 fold increase of calpain activity in LRP-1-depleted cells, as compared to control (Figure 1D). Of note, we were able to efficiently inhibit calpain activity by adding 50μM of their specific inhibitor calpeptin. A 26% inhibition was detected in control cells whereas the amplitude of this inhibition in LRP-1-silenced cells was 60%, reinforcing the idea that the baseline activity of this class of proteases is significantly higher in the absence of the receptor. Finally, we incubated thyroid carcinoma cells with the cell permeant substrate of calpains BOC-LM-CMAC in order to visualize their activities in living cells (Figure 1E) (46). We

10.3389/fonc.2022.981927

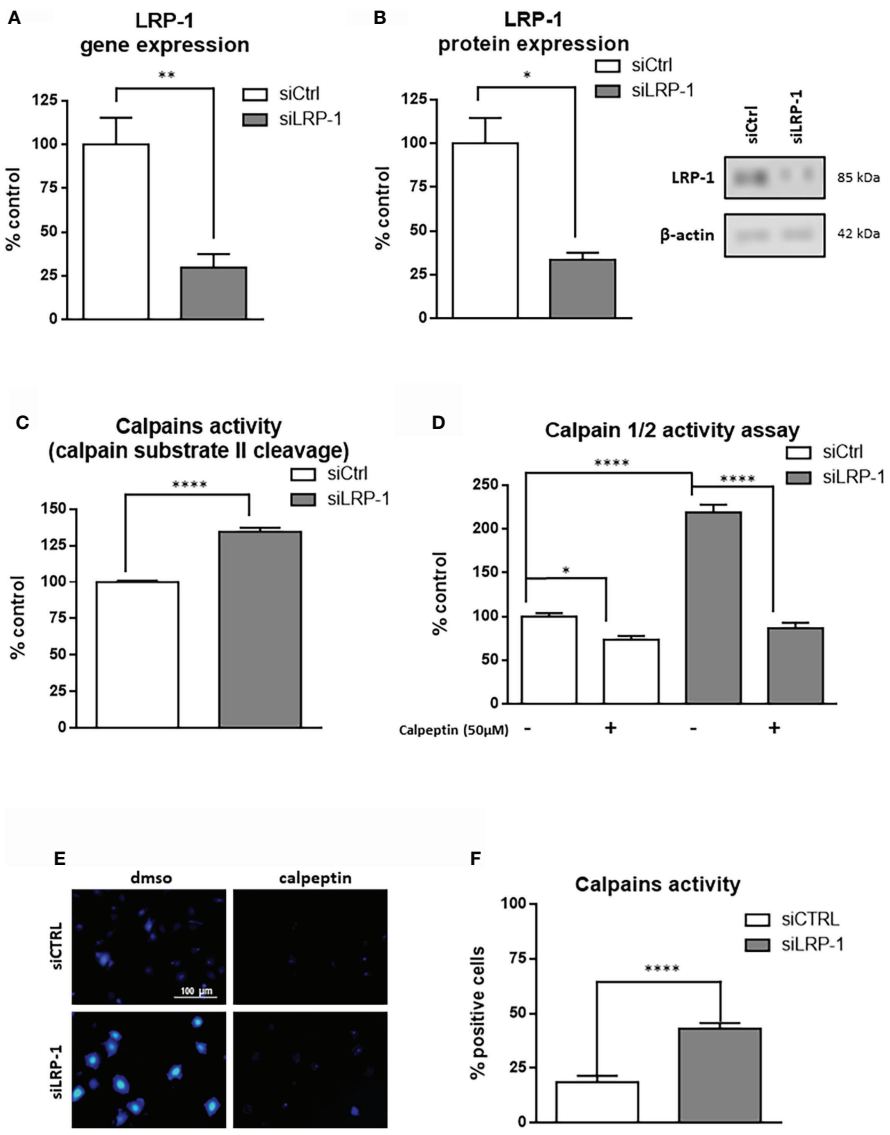

FIGURE 1
LRP-1 controls calpain activity in carcinoma cells. FTC133 cells were transfected with siRNA against LRP-1 expression (siLRP-1) or non-targeting control sequences (siCtrl) and total RNA were extracted after 48 hours. The transcriptional level of LRP-1 expression was assessed by RT-qPCR, using β-actin as a normalization control **(A)**. The LRP-1 protein expression was assessed by western blot, using β-actin as a normalization control. A representative picture of immunoblots is presented **(B)**. Whole extracts FTC133 cells transfected with siRNA sequences were used to test their ability to degrade the calpain substrate II, measured by spectrofluorimetry. Results are expressed as percentage of control after background fluorescence subtraction **(C)**. Same extracts were used to measure calpain activity by using Innozyme Calpain 1/2 Activity Assay Kit in the presence or absence of 50µM of calpeptine to ensure the specificity of the reaction **(D)**. Intracellular activity of calpains was visualized by fluorescence microscopy in intact cells treated with cell permeant calpain substrate BOC-LM-CMAC **(E)**. The percent of cells harboring strong intracellular accumulation of fluorescent CMAC, above fluorescent developed in presence of 50µM of calpeptin, was quantified **(F)**. Each value is mean ± sem for at least four independent experiments, each performed in triplicate. *, $P < 0,05$; **, $P < 0,01$; ****, $P < 0,0001$.

evaluated the proportion of cells exhibiting high calpain-dependent release of fluorescent CMAC probe (Figure 1F). In LRP-1 expressing control cells, 18,6% of the total cells were fluorescent when 43% of LRP-1 depleted cells had developed the calpain-dependent reaction. In conclusion, we showed by three independent biochemical assessments that LRP-1 silencing leads to a significant induction of intracellular calpain activity in thyroid carcinoma cells.

LRP-1-dependent attenuation of calpain activity contributes to migratory capacities of carcinoma cells by regulating cell-matrix attachment processes

We reported that LRP-1 functionalities in invasive cancer cells are not restricted to the endocytic control of extracellular matrix degrading enzymes (9). We showed that this endocytic receptor can directly feed pro-motile signals by coordinating the stability and distribution of cell surface matrix receptors through its control of downstream intracellular signaling events (28, 36, 39). In order to measure the consequences of the LRP-1-mediated control of calpain activity, we performed Boyden chamber assays with FTC133 cells LRP-1-silenced or not, in the presence or absence of the specific calpains inhibitor calpeptin (Figure 2A). As expected, we observed that LRP-1 silencing reduced carcinoma cell migration by 29% as compared to migrated control cells. Interestingly, addition of 50µM calpeptin completely restored the migration of LRP-1-silenced cells to the level of control cells. The same treatment did not exert any significant effect on LRP-1 expressing cells, suggesting that calpain activity is low. We conducted complementary modified Boyden chamber assays to analyze the invasive behavior of thyroid carcinoma cells using Matrigel as matrix barrier (Figure 2B). In that context, the consequences of LRP-1 depletion were more drastic since the proportion of invading cells was decreased by 51% in LRP-1 deficient-cells. Inhibition of calpain activity in LRP-1-depleted cells restored invasive potential that recovered 71% of the level observed in control cells. In contrast, the calpain inhibitor failed to modulate the invasive ability of LRP-1 expressing cells. We therefore demonstrated that LRP-1 maintains a low level of calpain activity that contributes to the migratory and invasive capacities of carcinoma cells. We then conducted adhesion assays to test the likely involvement of LRP-1-dependent calpain regulation in the control of carcinoma cell attachment to matrix compounds (Figure 3A) (28). We evidenced an increase of the adhesion rate of cells lacking LRP-1, as 64% more cells spread compared to control cells. Inhibition of calpain activity reduced the adhesion rate of LRP-1-silenced cells to the level of control situation. By contrast, the adhesion of LRP-1 expressing cells adhesion was not affected by calpeptin treatment. In a complementary experimental set-up, we performed detachment assays of fully spread carcinoma cells in response to the enzymatic action of trypsin, using the proportion of cells remained adherent as a readout for cell-matrix interactions strength (36). The proportion of detached cells after LRP-1 knock-down was decreased by 51% as compared to control cells (Figure 3B). Adding calpeptin during the previous phase of attachment reduced the resistance of LRP-1-silenced cells to trypsin to recover the detachment rate detected in control cells. Although a similar trend could be observed in LRP-1 expressing control tumor cells, it was not significant. Together, those data illustrated that the pro-invasive action of LRP-1 in thyroid carcinoma cells relies in part on the maintenance of a low level of calpain activity leading to a moderate cell-matrix interactions strength.

LRP-1 limits transcriptional expression of calpain-2 and inhibits calpain activity through a PKA-dependent mechanism

Having identified calpains as new intracellular targets regulated by LRP-1 in carcinoma cells, we next set up an experimental design to decipher the mechanistic nature of the process controlling their activities. First we evaluated the differential expression of members of the ubiquitous calpain family by western blot (Figures 4A, B). Although we did not observe any difference of expression neither of calpain-1 (µ-calpain) nor of calpastatin, the endogenous inhibitor of activated calpains, we evidenced a significant 5-fold increase of calpain-2 (m-calpain) protein expression in LRP-1-silenced FTC133 cells. We then analyzed the level of the transcriptional expression of the two main proteases, namely calpain 1 and calpain-2, by RT-qPCR (Figures 4C, D). Consistently, calpain-1 transcriptional level was not affected by LRP-1 modulation, whereas calpain-2 gene expression was 4,4-fold increased under LRP-1 silencing. Since the expression level of calpastatin was not altered according to the expression of LRP-1, we then focused our attention on the regulation of the calpain activity by phosphorylation. In our screen for potential LRP-1 downstream signaling events, we measured PKA activity in cellular extracts from both LRP-1-silenced and control FTC133 cells. We evidenced that LRP-1 inhibition led to a 1.6-fold decrease of PKA activity (Figure 5A). Interestingly, PKA-dependent phosphorylation of calpain-2 had already been reported to inhibit the proteolytic activity of ubiquitous calpains (46). Accordingly, the treatment of FTC133 cells with H-89, a specific inhibitor of PKA, induced a 2-fold increase of calpain activity as measured by the cleavage of calpain substrate II (Figure 5B). H-89 treatment did not significantly affect this activity when LRP-1 was silenced. To support these data, we then used two distinct inhibitors of PKA activities, H89 and KT5720, and evaluated the impact on calpain activity using the fluorogenic calpain activity assay described in Figure 1D (Figure 5C). We evidenced that H-89 or KT5720 treatment respectively resulted in about a 2-fold and 1.7-fold increase of basal calpain activity in LRP-1 expressing carcinoma cells. Inhibition of PKA by H-89 was also efficient to increase the proportion of FTC133 cells positive for calpain activity (Figure 5D). Importantly, this effect was specific for controlling cells in which PKA activity was mainly detected.

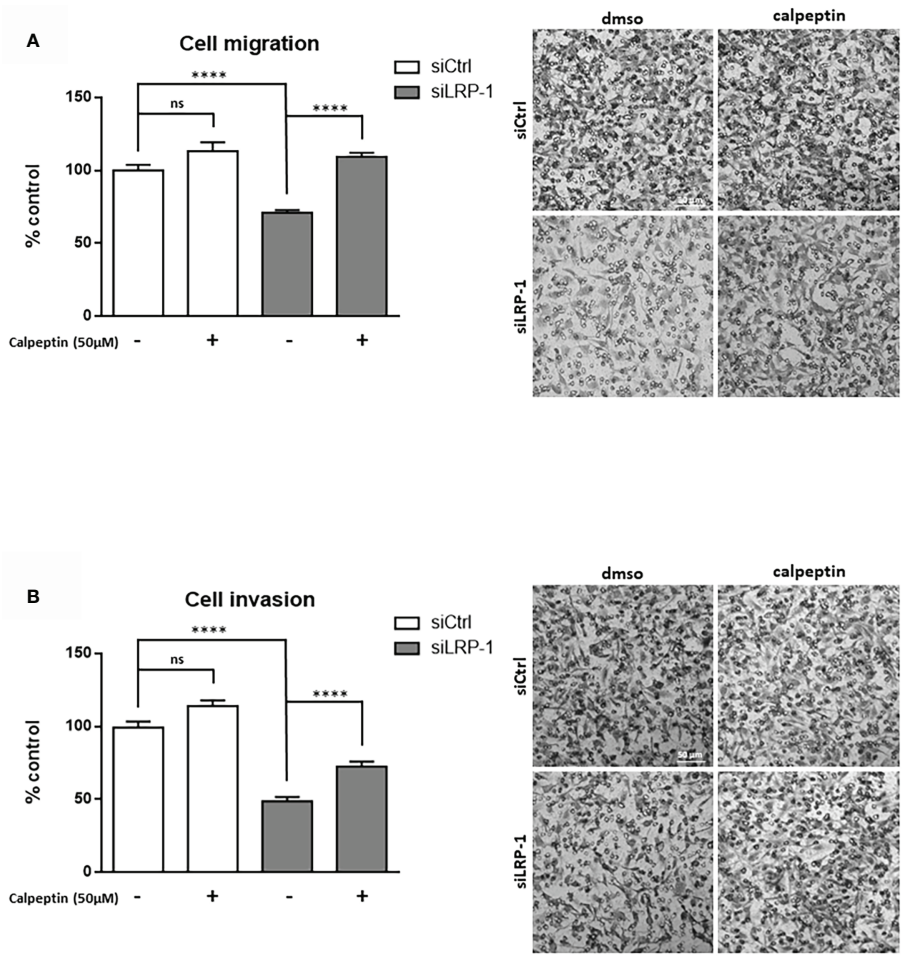

FIGURE 2
LRP-1-mediated control of calpain activity contributes to carcinoma cells migratory and invasive properties. Cell migration and invasion assays were carried out with FTC133 cells transfected with siRNA sequences, treated with 50 µM calpeptin or vehicle. Three-dimensional cell migration was assessed by using uncoated Transwell filters **(A)**. Tumor cell invasion was measured on Matrigel-coated Transwell membranes **(B)**. Representative images are shown. Migration and invasion were determined by counting cells in eight random microscopic fields per well. Results are expressed as mean ± sem after normalization by comparison with siCtrl transfected cells set to 100%, from at least four distinct experiments each performed in triplicate. ns, not significant; ****, $P < 0,0001$.

We then conducted pull-down experiments to study the phosphorylation status of calpain-2 (Figure 5E). We were able to immuno-precipitate the protein and we evidenced by western blot that its level of phosphorylation on serine residues was higher in control than in LRP-1 depleted cells. This signal was decreased in the presence of H-89, indicating that PKA-dependent mechanism was in part responsible for serine phosphorylation of calpain-2 in FTC133 cells. Adhesion assays were also conducted to demonstrate that PKA activity was functionally associated to the control of carcinoma cell attachment and spreading by LRP-1-mediated regulation of calpains (Figure 5F). Indeed, we specifically showed that inhibition of PKA by H-89 treatment in LRP-1 expressing cells enhanced their adhesion rate to gelatin to a similar level to that observed after LRP-1 inhibition. Our data indicated that PKA helped to limit calpain activity in a LRP-1-dependent manner in the frame of cell-matrix interactions established by thyroid carcinoma cells.

Regulation of calpain activity by LRP-1 plays a part in adhesion complexes lability and limits cell surface β1-integrin distribution

Considering the deep consequences of LRP-1-dependent regulation of calpain activity on the invasive potential and adhesion/deadhesion processes of tumor cells, we then analyzed

10.3389/fonc.2022.981927

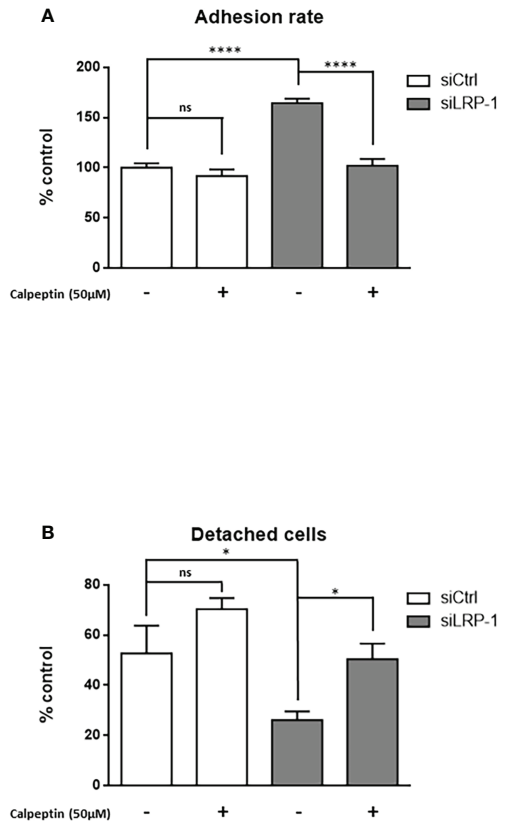

FIGURE 3
Calpain activity modulates carcinoma cells adhesion strength. FTC133 cells transfected with siCtrl or siLRP-1 RNA were seeded onto gelatin-coated plates in presence or absence of 50µM calpeptin, and the non-adherent cells were discarded after 60 minutes **(A)**. Transfected tumor cells were grown in gelatin-coated dishes for 24 hours and subjected to trypsinization assay by incubating cells with 0,025% (wt/vol) trypsin for 10 minutes **(B)**. For each cell condition, results are expressed as mean percentages of attached or detached cells ± sem, relative to control set to 1. ns, not significant; *, $P < 0,05$; ****, $P < 0,0001$.

the distribution and the morphology of cytoskeleton constituents. The fibrillar actin network of thyroid carcinoma cells after two hours of attachment was characteristic of spread and polarized cells such as mesenchymal cells (Figure 6A). Most of the fibrillar structures positively stained by phalloidin were concentrated at the cell periphery and protrusion sites. This specific pattern was not modified by calpains inhibition in control cells. In accordance with previous reports (9, 28), LRP-1 silencing induced drastic changes of carcinoma cells morphology and actin fibers distribution. Cells were overspread as compared to control cells and exhibited prominent radial and transverse fibers, widely distributed, both at tumor cell center and periphery. Under LRP-1 inhibition the calpain inhibitor induced a clear transition of cells toward the mesenchymal and elongated aspect observed in the control condition. We performed talin immuno-fluorescent staining to evaluate the consequences of calpains inhibition. In accordance with the morphological transitions described above, calpeptin did not affect the proportion of talin-positive structures in control cells, whereas LRP-1 inhibition reinforced the proportion of cells exhibiting obvious and stabilized talin-positive structures (Figure 6B). The occurrence of these complexes was specifically decreased in LRP-1-depleted cells under calpeptin treatment (Figure 6C). Our data illustrated that during the attachment of FTC133 cells to gelatin, calpains inhibition by LRP-1 sustained the polarization of thyroid carcinoma cells and constituted a limiting mechanism in focal adhesion maturation. We then measured the protein expression of talin by western blot using the 8D4 antibody, allowing the detection of the full length protein and its calpain-dependent cleavage fragment (Figure 7A). In accordance with the altered distribution of talin observed by immunocytochemistry (Figure 6B), we detected an accumulation of both native and cleaved forms of talin in LRP-1-silenced tumor cells. Interestingly, calpeptin treatment appeared to limit the accumulation of the cleaved form of talin. In order to assess the level of adhesion receptors expressed at cell surface, we performed biotin labelling of tumor cells spread on gelatin and treated with calpain inhibitor or vehicle. Precipitated protein membrane fractions were analyzed by immunoblotting (Figure 7B). Interestingly, we observed an increase of β1 integrin subunit at cell surface upon LRP-1 repression. This accumulation seemed partially decreased under calpeptin treatment. We then conducted immunostainings to qualify the distribution of β1 integrins in non-permeabilized carcinoma cells cultivated in the same conditions (Figure 7C). β1 integrins were detected in FTC133 cells and were mostly present at the periphery and at the front of spread and elongated cells. The presence of β1 integrins was accentuated in LRP-1 repressed cells and highly accumulated along the whole cell periphery. In the presence of calpeptin the polarized morphology of control cells did not show any clear critical transition, in opposition to LRP-1-silenced tumor cells which were more frequently polarized and spindle shaped and exhibited a discontinuous β1 integrin-positive margin that appeared more concentrated on distal sites of cell projections. We then conducted immunostainings by using an antibody specific for active forms of β1 integrins (Figure 7D). The localization of these forms of the receptors in non-permeabilized cells was more punctuated with some positive clusters at the leading edge of elongated control cells. These clusters were evenly observed across the ECM-attached area from overspread LRP-1-silenced cells. After inhibition of LRP-1 expression, both the number and size of theses clusters were diminished upon calpeptin treatment when LRP-1 was down-regulated. Altogether, these data showed that LRP-1-mediated control of calpain activity determined cell surface distribution of β1 integrins in thyroid carcinoma cells.

10.3389/fonc.2022.981927

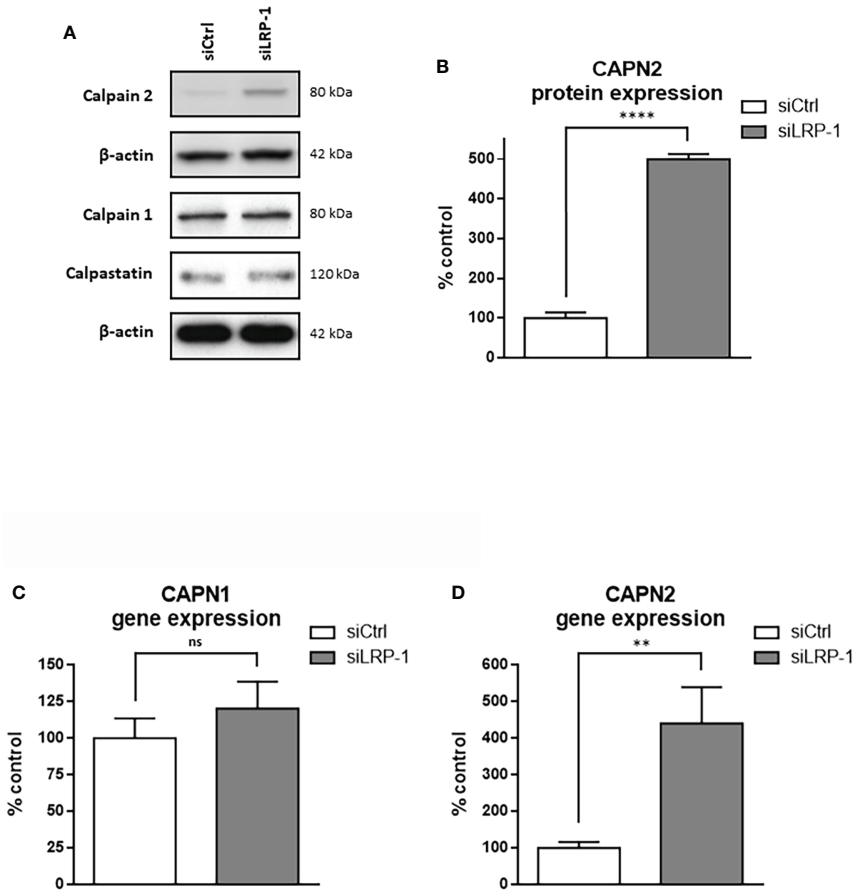

FIGURE 4
LRP-1 maintains low level of CAPN2 in carcinoma cells. Whole extracts from FTC133 cells transfected with siRNA sequences were analyzed by SDS-PAGE and western blot using specific antibodies against calpain-2, calpain-1, calpastatin and β-actin that was used as loading control. Pictures are representative of 3 independent experiments **(A)**. Densitometric analysis of calpain-2 specific bands normalized to actin signal and expressed as percentage of siCtrl transfected cells **(B)**. The transcriptional levels of calpain-1 **(C)** and calpain-2 **(D)** expressions were assessed by RT-qPCR, using β-actin as a normalization control. Results shown are expressed as mean ± sem percentage of the expression measured in control cells from 6 independent experiments. ns, not significant; **, $P < 0,01$; ****, $P < 0,0001$.

Discussion

In the present study, we identified for the first time the regulation of calpain activity as a new mechanism by which LRP-1 controls the spreading and migratory capacities of thyroid carcinoma cells. Indeed, we have shown that LRP-1 restrains calpain activity, both through a transcriptional mechanism targeting capn2 gene expression, but also *via* PKA activation and Ser-phosphorylation on calpain-2. Such a regulation contributes to the achievement of an intermediate and optimal attachment state and promigratory phenotype (Figure 8).

Our comprehension of LRP-1 contribution to cell-matrix interactions dynamics has significantly evolved in the past decade. Several studies revealed that this endocytic receptor controls cell surface stability and internalization of multiple cell surface complexes engaged during movements of migrating cells within their microenvironment, including matricellular proteins, integrins and proteoglycans (4, 28, 35, 36). This revised model of LRP-1 functionality could have been drawn earlier from studies showing that even proteolytic ligands of the receptor such as tissue plasminogen activator (tPA), bound to its inhibitor PAI-1, could trigger a full adhesion/deadhesion cascade of events when specifically complexed to LRP-1, fibronectin and LFA-1 (αLβ2) integrin (10). Proteomic and coimmunoprecipitation approaches then illustrated that LRP-1 acts as a *bona fide* adhesion receptor by itself, notably by recruiting to the intracellular tail of its β-chain focal adhesion and cytoskeleton components such as talin, paxillin or α-actinin (21, 28). These data support the idea that LRP-1 integrates extracellular and intracellular events and acts as a mechanosensing hub driving the fate, lifespan and turnover of nascent adhesion in a given cellular context. This concept was especially well documented for integrin-based adhesion to the

10.3389/fonc.2022.981927

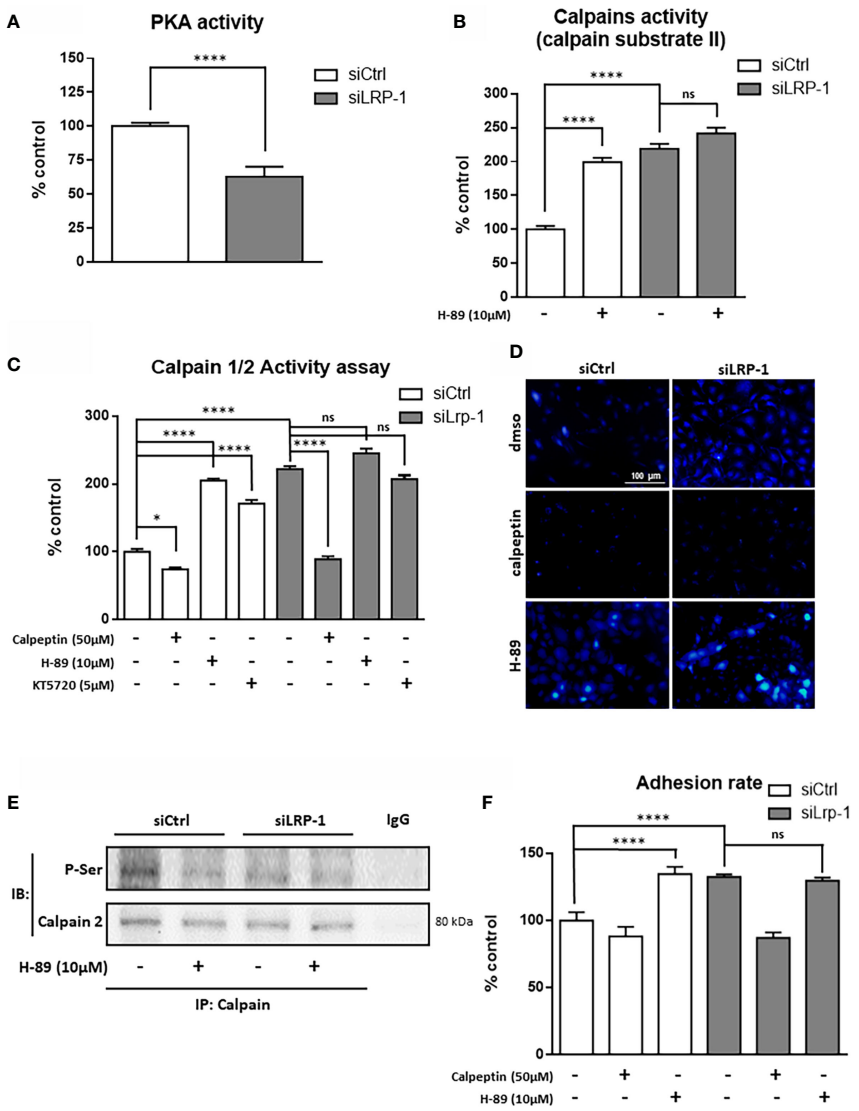

FIGURE 5
LRP-1-dependent PKA signaling limits CAPN2 activity. PKA activity was measured in whole extracts of FTC133 cells transfected with siRNA sequences and cultivated 3 hours on gelatin-coated dishes by using the fluorigenic ProFluor PKA enzymatic assay (Promega), adapted to measure specifically PKA activity in raw cellular extracts **(A)**. Extracts from FTC133 cells, treated with 10µM H-89 (PKA inhibitor) or vehicle, were used to measure the calpain specific degradation of the fluorigenic calpain substrate II **(B)**. Same extracts were used to test the impact of PKA on calpain activity measured by the Calpain ½ Activity Assay Kit in presence or absence of 50µM of calpeptin, 10µM of H-89 or 5µM of KT5720 **(C)**. Calpains-specific release of CMAC from calpains substrate BOC-LM-CMAC was analyzed in intact cells after treatment with calpeptin of H-89 **(D)**. Whole-cell extracts were isolated from FTC133 cells treated with 10µM H-89. Co-immunoprecipitation of calpain-2 were performed and phosphorylation status of the protease was analyzed by SDS-PAGE and immunoblotting using an antibody reacting with phosphorylated serine residue **(E)**. FTC133 cells transfected with siCtrl or siLRP-1 RNA were seeded onto gelatin coated plates in presence or absence of calpeptin or H-89 and the non-adherent cells were washed out after 60 minutes **(F)**. Results are representative of at least 3 independent experiments and are expressed as mean percentage from a minimum of 4 internal replicates standardized to control value. ns, not significant; *$P < 0,05$, ****, $P < 0,0001$.

extracellular matrix. After ligand binding, LRP-1 was involved in the reinforcement of cell surface expression of β1 integrins, and in their activation and signaling through integrin-linked kinase (8). LRP-1 was also identified as controlling tissue transglutaminase endocytosis, complexed with β1 integrin and fibronectin (38). We recently evidenced that the association of β1 integrin with domain II and IV of LRP-1 extracellular α-chain in thyroid carcinoma cells exerted a crucial function in routing it in a Rab11 endocytic recycling traffic (39). A parallel study showed that LRP-1 was engaged in the association with the intracellular domain of β1

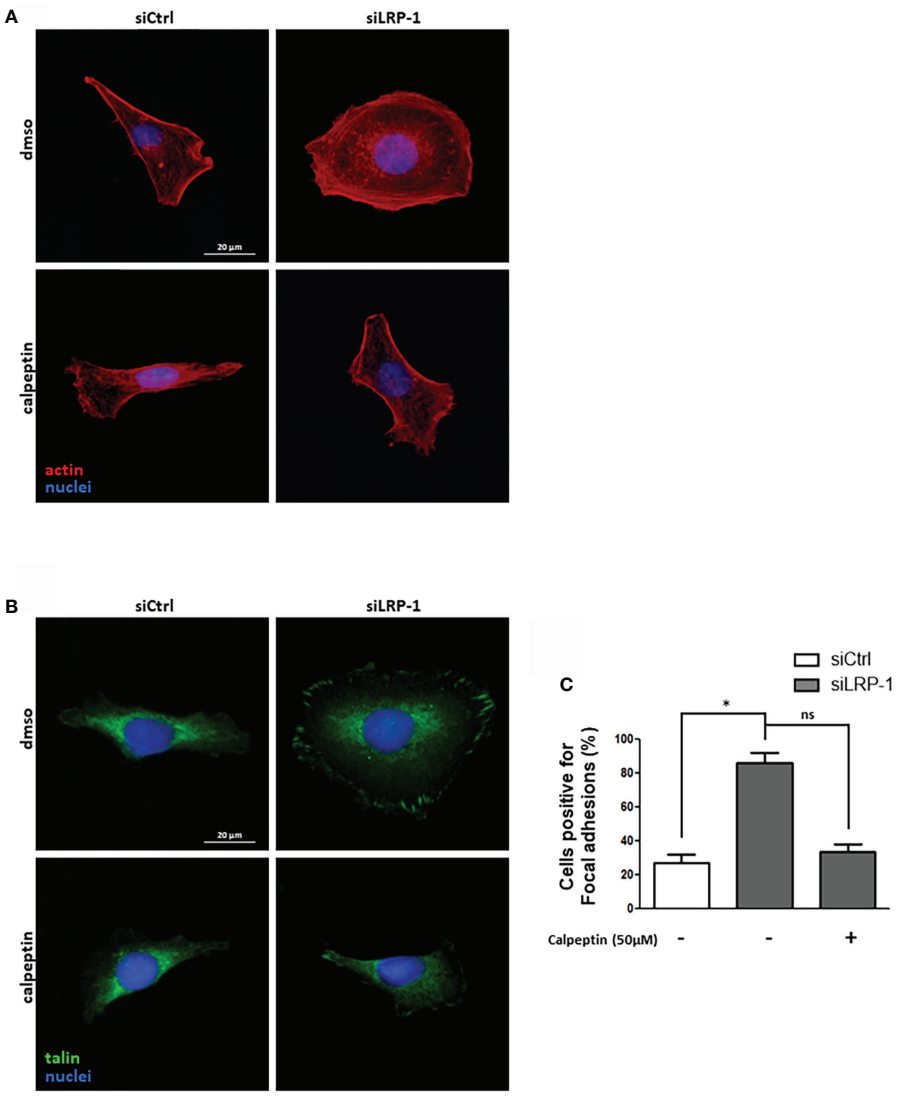

FIGURE 6
LRP-1-mediated control of calpain activity fine-tunes spreading and focal adhesion maturation in carcinoma cells. FTC133 cells transfected with siRNA sequences were cultivated two hours on gelatin-coated coverslips in the presence or absence of 50µM of calpeptin, fixed, and labelled with phalloidin to analyze their morphology and fibrillar actin network (red) by fluorescence microscopy. Nuclei were counterstained with DAPI (blue) **(A)**. Alternatively, cells were immunostained with an antibody against talin (green) to analyze the formation of focal adhesion **(B)**. The percentage of cells positive for focal adhesions was quantified following the inhibition of calpain activity by calpeptin or control treatment **(C)**. For each condition, at least one hundred of cells from three separate experiments were evaluated. ns, not significant; *, $P < 0,05$.

integrin through kindlin-2 (40), a family of adhesion scaffolds that also constitute cleavage substrates for calpains (50). Most of the published litterature illustrated the de-adhesive consequences of the complexe interactions of LRP-1 with integrins (10, 38, 39). The control of cell surface expression and activation of β1 integrin that we documented in FTC133 cells cultivated on gelatin could therefore play similar functions in other extracellular matrix environments depending on the integrin dimers specifically present at tumor cell surface. The molecular link between LRP-1, calpain activity and β1 integrin stability at cell surface of migrating thyroid carcinoma cells that we established in this study shed new light on the inner control of integrin activity by LRP-1. It also confirms that calpain activity may exert a strong influence on inside-out activation of integrins by controlling the net balance of pro and anti-adhesive signals that determines the adoption of an efficient migrating strategy for invading tumor cells.

An abundant literature described a pro-motile action of calpains linked to the release of tensions exerted at cell-matrix

10.3389/fonc.2022.981927

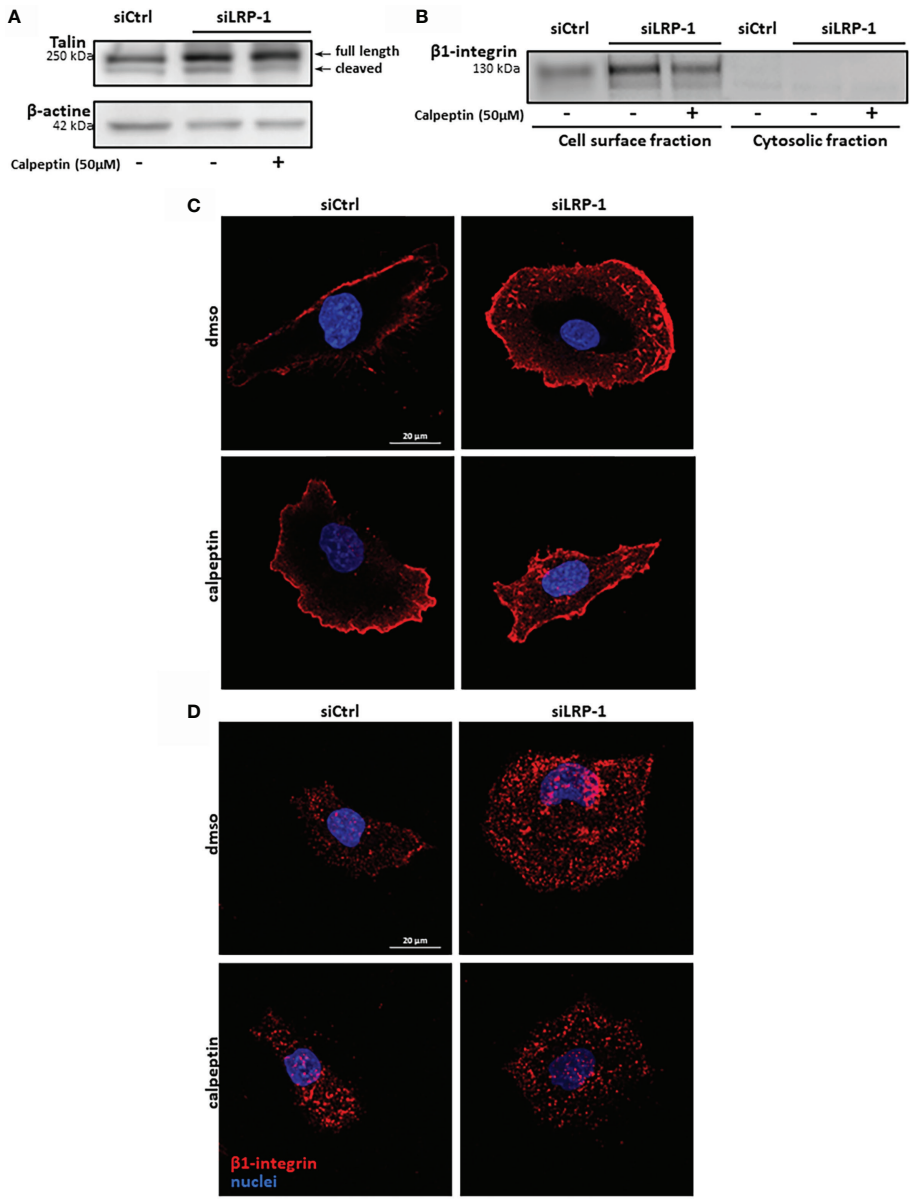

FIGURE 7
β1 integrin membrane expression is controlled by LRP-1-dependent calpains regulation. Whole extracts from FTC133 cells transfected with siRNA sequences, seeded onto gelatin and cultivated in the presence or absence of calpeptin for 3 hours were analyzed by SDS-PAGE and western blot using specific 8D4 antibodies against talin, allowing the detection of native full length and calpain-released cleaved product of talin. β-actin that was used as loading control. Picture is representative of 3 independent experiments **(A)**. FTC-133 cells were cultivated in the same conditions and biotinylated at 4°C to label cell-surface proteins. Membrane fraction was purified by precipitation of surface proteins by using avidin-sepharose beads. Surface expression of β1-integrins was analyzed by SDS-PAGE and immunoblotting. Corresponding cytosolic fractions that were not immobilized by avidin beads were loaded as a control of cell membrane purity **(B)**. Tumor cells transfected with siCtrl or siLRP-1 RNA were seeded onto gelatin coated coverslips for 2 hours in the presence of calpeptin and immune-stained with antibodies directed against either total β1-integrins pool **(C)** or active forms of the receptor **(D)**. Confocal microscope captures in Z series were acquired and projected by using maximum intensity, stacking the 10 optical slices attached to the coating. Pictures are representative of 3 separate experiments.

adhesion sites through partial proteolysis of focal contacts and cytoskeleton components (41, 48, 51). Though, a growing number of evidence conversely showed that calpains substrates cleavage can produce or unmask pro-adhesive motifs and stabilize peripheral focal adhesions. Accordingly, calpain-dependent proteolysis of paxillin negatively regulated focal adhesion dynamics and impaired cell migration (52). The binding of talin amino-terminal head domain to the intracellular tail of integrin constitutes a paradigm of inside-out activation of multiple classes of integrins that reinforces their

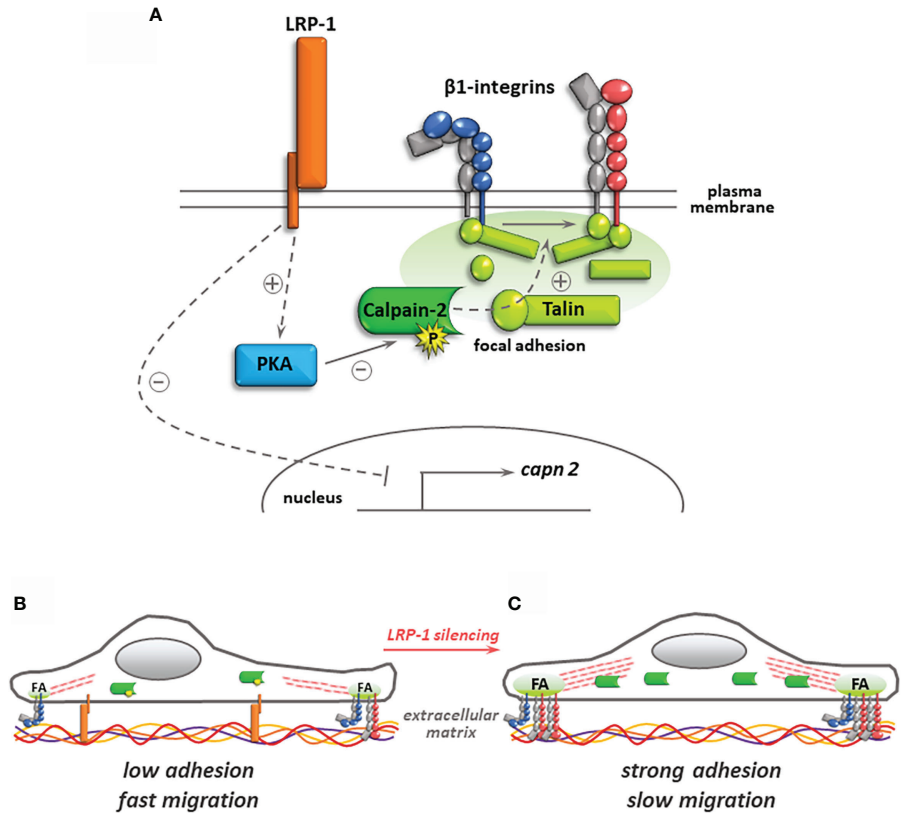

FIGURE 8
Regulation of calpain activity by LRP-1 and its consequences for thyroid carcinoma cell adhesion. In the presence of LRP-1, low transcriptional expression and PKA-mediated phosphorylation of calpain-2 controls talin-rich focal adhesion complexes dynamics and surface expression of inactive (blue) and active (red) forms of β1 integrins **(A)**. The resulting intermediate adhesive state contribute to the invasive potential of polarized tumor cells **(B)**. Under LRP-1 silencing, gene induction of calpain-2 and decrease of its PKA-dependent phosphorylation result in strong calpain activity. Subsequently, tumor cells exhibit an overspread phenotype explained by surface accumulation of β1 integrin and focal adhesion (FA) stabilization leading to impaired invasive capacities **(C)**.

affinity for extracellular ligands (53, 54). Although calpains can reduce the rate of talin stability in adhesion complexes, the local release of its head domain was associated to integrin activation and focal complexes stabilization (55, 56). Ultra-resolutive studies of talin orientation in adhesion sites revealed that its amino-terminal part was in close association with the core focal adhesion area, containing intracellular domains of integrins, whereas its rod carboxy-terminal part was more distal and oriented towards the zone of junction with actin stress fibers (57). We observed that the cell-surface accumulation of β1 integrin upon LRP-1 silencing was partially reversed by calpain inhibition and that the occurrence of the cleaved form of talin appeared to follow the presence of this integrin at the membrane of thyroid carcinoma cells. We previously showed that LRP-1 inhibition resulted in a depletion of talin-enriched complexes from FAK, which could function as a platform for calpain-2 targeting and activation (9, 58). Unlike calpain-2, which was accumulated in LRP-1-silenced cells, calpain-1 expression was surprisingly unaffected. We thus postulate that the increase in calpain activity documented here mainly involves calpain-2 isoform and that LRP-1 is controlling this dominant calpain signal to limit the adhesive strength of FTC133 cells. Capn1 and capn2 genes being located on different chromosomes, and regulated by distinct promoter regions, LRP-1-dependent signals likely mobilize a set of transcription regulators leading to the specific downregulation of calpain-2 transcriptional expression. Of note, most of the reports illustrating pro-adhesive functions of calpains were focused on calpain-2, which is in accordance with our data (41, 48, 59). Following LRP-1 repression, we showed that increased calpain activity coincided with an overspread morphology of tumor cells that accumulated more peripheral talin-positive complexes. This strongly argues for a major role of calpain-2 in favor of focal adhesion maturation and stabilization of integrin-based adhesions. In that context, the maintenance of baseline calpain activity by LRP-1 is therefore permissive to efficient tumor cell motility.

The regulation of calpain activity is complex dynamic and still lacking in mechanistic insights, especially in the field of cancer (41, 49, 60, 61). In this study, we evidenced that calpain activity are dampened by LRP-1 in thyroid carcinoma cells. An in-depth mechanical investigation revealed that this attenuation was in part linked to a specific control of calpain-2 transcription. We tested the potential contribution of two LRP-1-dependent intracellular signals, namely ERK and JNK kinases (28), but we did not evidence any variation of capn2 transcription level in the presence of specific MAPK inhibitors (data not shown). Further studies should thus address the specific LRP-1-dependent signals involved in capn2 gene expression control. In our experiments, the expression level of calpastatin was not affected by LRP-1 expression. MAPK can also influence calpains at post-translational level. Indeed, JNK kinases can phosphorylate some focal adhesion components and calpains substrates with various consequences on cell motility, but also potentially on calpains targeting to adhesion sites (62, 63). Phosphorylation by ERK1/2 MAPK had been directly involved in the activation of calpain 2 (43). We had previously shown that LRP-1 controls both the activation and the incorporation of JNK and ERK kinases to talin-rich focal adhesions (28). We therefore tested a putative cross-reaction of MAPK with calpains by measuring their activities in the presence of specific inhibitors but we could not detect any significant contribution of MAPK to LRP-1-dependent calpains regulation (data not shown). The phosphorylation of S369 residue of calpain-2 by protein kinase A (PKA) was involved in the inhibition of the protease, that subsequently became frozen in an inactive conformation (46). Ligand binding to LRP-1 had previously been involved in the activation of PKA (25). We demonstrated that PKA activity was decreased upon LRP-1 repression in thyroid carcinoma cells. Moreover, specific inhibitors of PKA significantly impaired calpain activity developed upon LRP-1 silencing and we could show by coimmunoprecipitation that the level of serine phosphorylation of calpain-2 was decreased by the PKA inhibitor H-89, specifically in LRP-1 expressing carcinoma cells. These data strongly argue that PKA activation by LRP-1 contributes to the limitation of calpain activity and establish a new functional link between LRP-1, extracellular matrix attachment and invasive properties of carcinoma cells. Among other putative mechanisms that might be at play to control the activity of calpains, are the expression, activity and distribution of calcium channels, which have not tested to date. Although, TRPM4 and PIEZO1 for instance emerge as mechanosensitive regulators of spatio-temporal confinement of calpain activity in various physio-pathological contexts (61, 64, 65). These targets provide an appealing outlook for investigating and completing our view of the multifaceted contributions of LRP-1 to extracellular stimuli and mechanical tensions integration in both nascent and mature integrin-based attachment to various extracellular matrix environments.

Considering the complexity and the multiplicity of the proteolytic targets of calpains, disentangling its control mode of tumor cell migration could be puzzling, even limiting the analysis to integrins adhesome. The level of maturation and clustering of adhesion complexes affects the spatial control of calpain activity and their targets ratio, making the net balance of their proteolytic action difficult to predict. It is interesting to note that similarly to LRP-1 (4, 9), the mobilization of calpains to adhesion sites can be coupled to membrane focalized matrix proteases, such as MT1-MMP, directed in an endocytic/recycling pathway to support persistent migration of tumor cells (47). It is tempting to propose a model where LRP-1 could organize both extracellular and intracellular proteolytic events to control tensional stress accumulating in cell-matrix adhesion sites. Moreover, common intracellular scaffolds shared between LRP-1 and some integrins could result in synergistic or competitive titrations depending on the availability and access of calpains to their substrates. Accordingly, the deregulation of some specific targets of calpains can trigger cancer cell motility and promote their aggressive behavior by displacing calpain activity from anti- to pro-metastatic substrates (66). Our work and concomitant studies from other teams demonstrated the critical role played by LRP-1 in cell polarization based on rear/front partition of focal contacts components, such as FAK or paxillin (9), or actin cytoskeleton regulators Rho and Rac small GTPases (30). Here we showed that calpain inhibition in LRP-1-silenced cells restored the mesenchymal morphology of spread FTC133 cells, suggesting that baseline calpain activity maintained through LRP-1-mediated signals contributed to polarize tumor cells. Ezrin, a cytoskeleton protein incorporated in focal complexes, was involved in the recruitment and the distribution of calpain at membrane protrusion or retraction sites (60). Moreover, the spatial restriction of active calpains can stabilize the formation of nascent filopodiae (67) as well as the maturation of dual adhesive and invasive structures such as invadopodiae (59), which could predispose cancer cells to aggressive behavior *in vivo*. A recent *in vivo* study described that calpains constitute crucial determinants of tumor cell dissemination strategies. Indeed, under hypoxic conditions, induction of calpain-2 switched the collective mode of migration of breast and head and neck cancer cells to an amoeboid metastatic behavior. This transition relied on talin cleavage and decreased strength of β1 integrin-mediated attachments, and was reverted by pharmacological challenge of calpain activity (49).

Like most drug targetable molecules that are deregulated during cancer progression, a major clinical challenge in practice could rely on the highly specific and contextual cleavage products of calpains and their associated metabolic consequences on cancer cells as well as the reactive and adaptive tumor bed. However, the novel LRP-1-mediated pathway that we identified enrich the panel of versatile functions exerted by the receptor, once again detected at the

crossroad between extracellular cues and membrane dynamics, and further illustrates its crucial role in cell-matrix adhesions adaptation to the microenvironment of cancer cells.

Data availability statement

The raw data supporting the conclusions of this article will be made available by the authors, without undue reservation.

Author contributions

BL and SD designed the study. BL, JM, CS, CH, CT, DR, LM, LT, SS and SD collected, interpreted, and analyzed the data. BL wrote the manuscript. All the authors revised the manuscript critically for important intellectual content and read and approved the final manuscript.

Funding

The project leading to this publication has received funding from Université de Reims Champagne-Ardenne, CNRS and Ligue contre le Cancer.

Acknowledgments

We thank Mrs Arlette Thomachot for her valuable editing assistance.

Conflict of interest

SD is co-founder of Apmonia-Therapeutics and acts as the chair of the Scientific and Clinical Advisory Board.

The remaining authors declare that the research was conducted in the absence of any commercial or financial relationships that could be construed as a potential conflict of interest.

Publisher's note

All claims expressed in this article are solely those of the authors and do not necessarily represent those of their affiliated organizations, or those of the publisher, the editors and the reviewers. Any product that may be evaluated in this article, or claim that may be made by its manufacturer, is not guaranteed or endorsed by the publisher.

References

1. Herz J, Strickland DK. LRP: A multifunctional scavenger and signaling receptor. *J Clin Invest* (2001) 108(6):779–84. doi: 10.1172/JCI200113992

2. Strickland DK, Ashcom JD, Williams S, Burgess WH, Migliorini M, Argraves WS. Sequence identity between the alpha 2-macroglobulin receptor and low density lipoprotein receptor-related protein suggests that this molecule is a multifunctional receptor. *J Biol Chem* (1990) 265(29):17401–4. doi: 10.1016/S0021-9258(18)38172-9

3. Lillis AP, Van Duyn LB, Murphy-Ullrich JE, Strickland DK. LDL receptor-related protein 1: unique tissue-specific functions revealed by selective gene knockout studies. *Physiol Rev* (2008) 88(3):887–918. doi: 10.1152/physrev.00033.2007

4. Van Gool B, Dedieu S, Emonard H, Roebroek AJ. The matricellular receptor lrp1 forms an interface for signaling and endocytosis in modulation of the extracellular tumor environment. *Front Pharmacol* (2015) 6:271. doi: 10.3389/fphar.2015.00271

5. van der Geer P. Phosphorylation of LRP1: regulation of transport and signal transduction. *Trends Cardiovasc Med* (2002) 12(4):160–5. doi: 10.1016/S1050-1738(02)00154-8

6. Bell RD, Deane R, Chow N, Long X, Sagare A, Singh I, et al. SRF and myocardin regulate LRP-mediated amyloid-beta clearance in brain vascular cells. *Nat Cell Biol* (2009) 11(2):143–53. doi: 10.1038/ncb1819

7. Boucher P, Gotthardt M, Li WP, Anderson RG, Herz J. LRP: role in vascular wall integrity and protection from atherosclerosis. *Science* (2003) 300(5617):329–32. doi: 10.1126/science.1082095

8. Hu K, Wu C, Mars WM, Liu Y. Tissue-type plasminogen activator promotes murine myofibroblast activation through LDL receptor-related protein 1-mediated integrin signaling. *J Clin Invest* (2007) 117(12):3821–32. doi: 10.1172/JCI32301

9. Dedieu S, Langlois B, Devy J, Sid B, Henriet P, Sartelet H, et al. LRP-1 silencing prevents malignant cell invasion despite increased pericellular proteolytic activities. *Mol Cell Biol* (2008) 28(9):2980–95. doi: 10.1128/MCB.02238-07

10. Cao C, Lawrence DA, Li Y, Von Arnim CA, Herz J, Su EJ, et al. Endocytic receptor LRP together with tPA and PAI-1 coordinates mac-1-dependent macrophage migration. *EMBO J* (2006) 25(9):1860–70. doi: 10.1038/sj.emboj.7601082

11. Sid B, Dedieu S, Delorme N, Sartelet H, Rath GM, Bellon G, et al. Human thyroid carcinoma cell invasion is controlled by the low density lipoprotein receptor-related protein-mediated clearance of urokinase plasminogen activator. *Int J Biochem Cell Biol* (2006) 38(10):1729–40. doi: 10.1016/j.biocel.2006.04.005

12. Etique N, Verzeaux L, Dedieu S, Emonard H. LRP-1: A checkpoint for the extracellular matrix proteolysis. *BioMed Res Int* (2013) 2013:152163. doi: 10.1155/2013/152163

13. Amos S, Mut M, diPierro CG, Carpenter JE, Xiao A, Kohutek ZA, et al. Protein kinase c-alpha-mediated regulation of low-density lipoprotein receptor related protein and urokinase increases astrocytoma invasion. *Cancer Res* (2007) 67(21):10241–51. doi: 10.1158/0008-5472.CAN-07-0030

14. Kancha RK, Stearns ME, Hussain MM. Decreased expression of the low density lipoprotein receptor-related protein/alpha 2-macroglobulin receptor in invasive cell clones derived from human prostate and breast tumor cells. *Oncol Res* (1994) 6(8):365–72.

15. Fayard B, Bianchi F, Dey J, Moreno E, Djaffer S, Hynes NE, et al. The serine protease inhibitor protease nexin-1 controls mammary cancer metastasis through LRP-1-mediated MMP-9 expression. *Cancer Res* (2009) 69(14):5690–8. doi: 10.1158/0008-5472.CAN-08-4573

16. Montel V, Gaultier A, Lester RD, Campana WM, Gonias SL. The low-density lipoprotein receptor-related protein regulates cancer cell survival and

metastasis development. *Cancer Res* (2007) 67(20):9817–24. doi: 10.1158/0008-5472.CAN-07-0683

17. Gaultier A, Salicioni AM, Arandjelovic S, Gonias SL. Regulation of the composition of the extracellular matrix by low density lipoprotein receptor-related protein-1: Activities based on regulation of mRNA expression. *J Biol Chem* (2006) 281(11):7332–40. doi: 10.1074/jbc.M511857200

18. Hu K, Yang J, Tanaka S, Gonias SL, Mars WM, Liu Y. Tissue-type plasminogen activator acts as a cytokine that triggers intracellular signal transduction and induces matrix metalloproteinase-9 gene expression. *J Biol Chem* (2006) 281(4):2120–7. doi: 10.1074/jbc.M504988200

19. Song H, Li Y, Lee J, Schwartz AL, Bu G. Low-density lipoprotein receptor-related protein 1 promotes cancer cell migration and invasion by inducing the expression of matrix metalloproteinases 2 and 9. *Cancer Res* (2009) 69(3):879–86. doi: 10.1158/0008-5472.CAN-08-3379

20. Gotthardt M, Trommsdorff M, Nevitt MF, Shelton J, Richardson JA, Stockinger W, et al. Interactions of the low density lipoprotein receptor gene family with cytosolic adaptor and scaffold proteins suggest diverse biological functions in cellular communication and signal transduction. *J Biol Chem* (2000) 275(33):25616–24. doi: 10.1074/jbc.M000955200

21. Guttman M, Betts GN, Barnes H, Ghassemian M, van der Geer P, Komives EA. Interactions of the NPXY microdomains of the low density lipoprotein receptor-related protein 1. *Proteomics* (2009) 9(22):5016–28. doi: 10.1002/pmic.200900457

22. Hu K, Lin L, Tan X, Yang J, Bu G, Mars WM, et al. tPA protects renal interstitial fibroblasts and myofibroblasts from apoptosis. *J Am Soc Nephrol* (2008) 19(3):503–14. doi: 10.1681/ASN.2007030300

23. Yang M, Huang H, Li J, Li D, Wang H. Tyrosine phosphorylation of the LDL receptor-related protein (LRP) and activation of the ERK pathway are required for connective tissue growth factor to potentiate myofibroblast differentiation. *FASEB J* (2004) 18(15):1920–1. doi: 10.1096/fj.04-2357fje

24. Zhang H, Lee JM, Wang Y, Dong L, Ko KW, Pelletier L, et al. Mutational analysis of the FXNPXY motif within LDL receptor-related protein 1 (LRP1) reveals the functional importance of the tyrosine residues in cell growth regulation and signal transduction. *Biochem J* (2008) 409(1):53–64. doi: 10.1042/BJ20071127

25. Zhu Y, Hui DY. Apolipoprotein e binding to low density lipoprotein receptor-related protein-1 inhibits cell migration *via* activation of cAMP-dependent protein kinase a. *J Biol Chem* (2003) 278(38):36257–63. doi: 10.1074/jbc.M303171200

26. Degryse B, Neels JG, Czekay RP, Aertgeerts K, Kamikubo Y, Loskutoff DJ. The low density lipoprotein receptor-related protein is a motogenic receptor for plasminogen activator inhibitor-1. *J Biol Chem* (2004) 279(21):22595–604. doi: 10.1074/jbc.M313004200

27. Webb DJ, Nguyen DH, Gonias SL. Extracellular signal-regulated kinase functions in the urokinase receptor-dependent pathway by which neutralization of low density lipoprotein receptor-related protein promotes fibrosarcoma cell migration and matrigel invasion. *J Cell Sci* (2000) 113(Pt 1):123–34. doi: 10.1242/jcs.113.1.123

28. Langlois B, Perrot G, Schneider C, Henriet P, Emonard H, Martiny L, et al. LRP-1 promotes cancer cell invasion by supporting ERK and inhibiting JNK signaling pathways. *PloS One* (2010) 5(7):e11584. doi: 10.1371/journal.pone.0011584

29. Cheng CF, Fan J, Fedesco M, Guan S, Li Y, Bandyopadhyay B, et al. Transforming growth factor alpha (TGFalpha)-stimulated secretion of HSP90alpha: using the receptor LRP-1/CD91 to promote human skin cell migration against a TGFbeta-rich environment during wound healing. *Mol Cell Biol* (2008) 28(10):3344–58. doi: 10.1128/MCB.01287-07

30. Mantuano E, Inoue G, Li X, Takahashi K, Gaultier A, Gonias SL, et al. The hemopexin domain of matrix metalloproteinase-9 activates cell signaling and promotes migration of schwann cells by binding to low-density lipoprotein receptor-related protein. *J Neurosci* (2008) 28(45):11571–82. doi: 10.1523/JNEUROSCI.3053-08.2008

31. Orr AW, Pallero MA, Murphy-Ullrich JE. Thrombospondin stimulates focal adhesion disassembly through gi- and phosphoinositide 3-kinase-dependent ERK activation. *J Biol Chem* (2002) 277(23):20453–60. doi: 10.1074/jbc.M112091200

32. Song H, Bu G. MicroRNA-205 inhibits tumor cell migration through down-regulating the expression of the LDL receptor-related protein 1. *Biochem Biophys Res Commun* (2009) 388(2):400–5. doi: 10.1016/j.bbrc.2009.08.020

33. Tian Y, Wang C, Chen S, Liu J, Fu Y, Luo Y. Extracellular Hsp90alpha and clusterin synergistically promote breast cancer epithelial-to-mesenchymal transition and metastasis *via* LRP1. *J Cell Sci* (2019) 132(15). doi: 10.1242/jcs.228213

34. Xue N, Du T, Lai F, Jin J, Ji M, Chen X. Secreted HSP90alpha-LRP1 signaling promotes tumor metastasis and chemoresistance in pancreatic cancer. *Int J Mol Sci* (2022) 23(10). doi: 10.3390/ijms23105532

35. Dedieu S, Langlois B. LRP-1: A new modulator of cytoskeleton dynamics and adhesive complex turnover in cancer cells. *Cell Adh Migr* (2008) 2(2):77–80. doi: 10.4161/cam.2.2.6374

36. Perrot G, Langlois B, Devy J, Jeanne A, Verzeaux L, Almagro S, et al. LRP-1–CD44, a new cell surface complex regulating tumor cell adhesion. *Mol Cell Biol* (2012) 32(16):3293–307. doi: 10.1128/MCB.00228-12

37. Spijkers PP, da Costa Martins P, Westein E, Gahmberg CG, Zwaginga JJ, Lenting PJ. LDL-receptor-related protein regulates beta2-integrin-mediated leukocyte adhesion. *Blood* (2005) 105(1):170–7. doi: 10.1182/blood-2004-02-0498

38. Zemskov EA, Mikhailenko I, Strickland DK, Belkin AM. Cell-surface transglutaminase undergoes internalization and lysosomal degradation: An essential role for LRP1. *J Cell Sci* (2007) 120(Pt 18):3188–99. doi: 10.1242/jcs.010397

39. Theret L, Jeanne A, Langlois B, Hachet C, David M, Khrestchatisky M, et al. Identification of LRP-1 as an endocytosis and recycling receptor for beta1-integrin in thyroid cancer cells. *Oncotarget* (2017) 8(45):78614–32. doi: 10.18632/oncotarget.20201

40. Wujak L, Bottcher RT, Pak O, Frey H, El Agha E, Chen Y, et al. Low density lipoprotein receptor-related protein 1 couples beta1 integrin activation to degradation. *Cell Mol Life Sci* (2018) 75(9):1671–85. doi: 10.1007/s00018-017-2707-6

41. Franco SJ, Huttenlocher A. Regulating cell migration: calpains make the cut. *J Cell Sci* (2005) 118(Pt 17):3829–38. doi: 10.1242/jcs.02562

42. Su LT, Agapito MA, Li M, Simonson WT, Huttenlocher A, Habas R, et al. TRPM7 regulates cell adhesion by controlling the calcium-dependent protease calpain. *J Biol Chem* (2006) 281(16):11260–70. doi: 10.1074/jbc.M512885200

43. Glading A, Bodnar RJ, Reynolds IJ, Shiraha H, Satish L, Potter DA, et al. Epidermal growth factor activates m-calpain (calpain II), at least in part, by extracellular signal-regulated kinase-mediated phosphorylation. *Mol Cell Biol* (2004) 24(6):2499–512. doi: 10.1128/MCB.24.6.2499-2512.2004

44. Sid B, Langlois B, Sartelet H, Bellon G, Dedieu S, Martiny L. Thrombospondin-1 enhances human thyroid carcinoma cell invasion through urokinase activity. *Int J Biochem Cell Biol* (2008) 40(9):1890–900. doi: 10.1016/j.biocel.2008.01.023

45. Goette A, Arndt M, Rocken C, Staack T, Bechtloff R, Reinhold D, et al. Calpains and cytokines in fibrillating human atria. *Am J Physiol Heart Circ Physiol* (2002) 283(1):H264–72. doi: 10.1152/ajpheart.00505.2001

46. Shiraha H, Glading A, Chou J, Jia Z, Wells A. Activation of m-calpain (calpain II) by epidermal growth factor is limited by protein kinase a phosphorylation of m-calpain. *Mol Cell Biol* (2002) 22(8):2716–27. doi: 10.1128/MCB.22.8.2716-2727.2002

47. Bravo-Cordero JJ, Cordani M, Soriano SF, Diez B, Munoz-Agudo C, Casanova-Acebes M, et al. A novel high-content analysis tool reveals Rab8-driven cytoskeletal reorganization through rho GTPases, calpain and MT1-MMP. *J Cell Sci* (2016) 129(8):1734–49. doi: 10.1242/jcs.174920

48. Bate N, Gingras AR, Bachir A, Horwitz R, Ye F, Patel B, et al. Talin contains a c-terminal calpain2 cleavage site important in focal adhesion dynamics. *PloS One* (2012) 7(4):e34461. doi: 10.1371/journal.pone.0034461

49. Te Boekhorst V, Jiang L, Mahlen M, Meerlo M, Dunkel G, Durst FC, et al. Calpain-2 regulates hypoxia/HIF-induced plasticity toward amoeboid cancer cell migration and metastasis. *Curr Biol* (2022) 32(2):412–27 e8. doi: 10.1016/j.cub.2021.11.040

50. Zhao Y, Malinin NL, Meller J, Ma Y, West XZ, Bledzka K, et al. Regulation of cell adhesion and migration by kindlin-3 cleavage by calpain. *J Biol Chem* (2012) 287(47):40012–20. doi: 10.1074/jbc.M112.380469

51. Calle Y, Carragher NO, Thrasher AJ, Jones GE. Inhibition of calpain stabilises podosomes and impairs dendritic cell motility. *J Cell Sci* (2006) 119(Pt 11):2375–85. doi: 10.1242/jcs.02939

52. Cortesio CL, Boateng LR, Piazza TM, Bennin DA, Huttenlocher A. Calpain-mediated proteolysis of paxillin negatively regulates focal adhesion dynamics and cell migration. *J Biol Chem* (2011) 286(12):9998–10006. doi: 10.1074/jbc.M110.187294

53. Tadokoro S, Shattil SJ, Eto K, Tai V, Liddington RC, de Pereda JM, et al. Talin binding to integrin beta tails: A final common step in integrin activation. *Science* (2003) 302(5642):103–6. doi: 10.1126/science.1086652

54. Wegener KL, Partridge AW, Han J, Pickford AR, Liddington RC, Ginsberg MH, et al. Structural basis of integrin activation by talin. *Cell* (2007) 128(1):171–82. doi: 10.1016/j.cell.2006.10.048

55. Yan B, Calderwood DA, Yaspan B, Ginsberg MH. Calpain cleavage promotes talin binding to the beta 3 integrin cytoplasmic domain. *J Biol Chem* (2001) 276(30):28164–70. doi: 10.1074/jbc.M104161200

56. Huang C, Rajfur Z, Yousefi N, Chen Z, Jacobson K, Ginsberg MH. Talin phosphorylation by Cdk5 regulates Smurf1-mediated talin head ubiquitylation and cell migration. *Nat Cell Biol* (2009) 11(5):624–30. doi: 10.1038/ncb1868

57. Liu J, Wang Y, Goh WI, Goh H, Baird MA, Ruehland S, et al. Talin determines the nanoscale architecture of focal adhesions. *Proc Natl Acad Sci U S A*. (2015) 112(35):E4864–73. doi: 10.1073/pnas.1512025112

58. Carragher NO, Westhoff MA, Fincham VJ, Schaller MD, Frame MC. A novel role for FAK as a protease-targeting adaptor protein: regulation by p42 ERK and src. *Curr Biol* (2003) 13(16):1442–50. doi: 10.1016/S0960-9822(03)00544-X

59. Cortesio CL, Chan KT, Perrin BJ, Burton NO, Zhang S, Zhang ZY, et al. Calpain 2 and PTP1B function in a novel pathway with src to regulate invadopodia dynamics and breast cancer cell invasion. *J Cell Biol* (2008) 180(5):957–71. doi: 10.1083/jcb.200708048

60. Hoskin V, Szeto A, Ghaffari A, Greer PA, Cote GP, Elliott BE. Ezrin regulates focal adhesion and invadopodia dynamics by altering calpain activity to promote breast cancer cell invasion. *Mol Biol Cell* (2015) 26(19):3464–79. doi: 10.1091/mbc.E14-12-1584

61. McHugh BJ, Murdoch A, Haslett C, Sethi T. Loss of the integrin-activating transmembrane protein Fam38A (Piezo1) promotes a switch to a reduced integrin-dependent mode of cell migration. *PloS One* (2012) 7(7):e40346. doi: 10.1371/journal.pone.0040346

62. Huang C, Rajfur Z, Borchers C, Schaller MD, Jacobson K. JNK phosphorylates paxillin and regulates cell migration. *Nature* (2003) 424(6945):219–23. doi: 10.1038/nature01745

63. Smadja-Lamere N, Boulanger MC, Champagne C, Branton PE, Lavoie JN. JNK-mediated phosphorylation of paxillin in adhesion assembly and tension-induced cell death by the adenovirus death factor E4orf4. *J Biol Chem* (2008) 283(49):34352–64. doi: 10.1074/jbc.M803364200

64. Saxena M, Changede R, Hone J, Wolfenson H, Sheetz MP. Force-induced calpain cleavage of talin is critical for growth, adhesion development, and rigidity sensing. *Nano Lett* (2017) 17(12):7242–51. doi: 10.1021/acs.nanolett.7b02476

65. Aglialoro F, Hofsink N, Hofman M, Brandhorst N, van den Akker E. Inside out integrin activation mediated by piezo1 signaling in erythroblasts. *Front Physiol* (2020) 11:958. doi: 10.3389/fphys.2020.00958

66. Xu Y, Bismar TA, Su J, Xu B, Kristiansen G, Varga Z, et al. Filamin a regulates focal adhesion disassembly and suppresses breast cancer cell migration and invasion. *J Exp Med* (2010) 207(11):2421–37. doi: 10.1084/jem.20100433

67. Jacquemet G, Baghirov H, Georgiadou M, Sihto H, Peuhu E, Cettour-Janet P, et al. L-type calcium channels regulate filopodia stability and cancer cell invasion downstream of integrin signalling. *Nat Commun* (2016) 7:13297. doi: 10.1038/ncomms13297

frontiers | Frontiers in Oncology

TYPE Original Research
PUBLISHED 16 August 2022
DOI 10.3389/fonc.2022.811508

Check for updates

OPEN ACCESS

EDITED BY
Alberto Passi,
University of Insubria, Italy

REVIEWED BY
Pranshu Sahgal,
Dana–Farber Cancer Institute, United States
Ioannis Papantoniou,
Faculty of Medicine, KU Leuven, Belgium

*CORRESPONDENCE
Despoina Nektaria Metsiou
metsiou@upatras.gr;
metsiou.betty@gmail.com

SPECIALTY SECTION
This article was submitted to Molecular and Cellular Oncology, a section of the journal Frontiers in Oncology

RECEIVED 08 November 2021
ACCEPTED 19 July 2022
PUBLISHED 16 August 2022

CITATION
Metsiou DN, Deligianni D, Giannopoulou E, Kalofonos H, Koutras A and Athanassiou G (2022) Adhesion strength and anti-tumor agents regulate vinculin of breast cancer cells.
Front. Oncol. 12:811508.
doi: 10.3389/fonc.2022.811508

COPYRIGHT
© 2022 Metsiou, Deligianni, Giannopoulou, Kalofonos, Koutras and Athanassiou. This is an open-access article distributed under the terms of the Creative Commons Attribution License (CC BY). The use, distribution or reproduction in other forums is permitted, provided the original author(s) and the copyright owner(s) are credited and that the original publication in this journal is cited, in accordance with accepted academic practice. No use, distribution or reproduction is permitted which does not comply with these terms.

Adhesion strength and anti-tumor agents regulate vinculin of breast cancer cells

Despoina Nektaria Metsiou[1]*, Despina Deligianni[1], Efstathia Giannopoulou[2], Haralabos Kalofonos[2], Angelos Koutras[2] and George Athanassiou[1]

[1]Laboratory of Biomechanics and Biomedical Engineering, Department of Mechanical Engineering and Aeronautics, University of Patras, Patra, Greece, [2]Clinical Oncology Laboratory, Division of Oncology, Department of Medicine, University of Patras, Patra, Greece

The onset and progression of cancer are strongly associated with the dissipation of adhesion forces between cancer cells, thus facilitating their incessant attachment and detachment from the extracellular matrix (ECM) to move toward metastasis. During this process, cancer cells undergo mechanical stresses and respond to these stresses with membrane deformation while inducing protrusions to invade the surrounding tissues. Cellular response to mechanical forces is inherently related to the reorganization of the cytoskeleton, the dissipation of cell–cell junctions, and the adhesion to the surrounding ECM. Moreover, the role of focal adhesion proteins, and particularly the role of vinculin in cell attachment and detachment during migration, is critical, indicating the tight cell–ECM junctions, which favor or inhibit the metastatic cascade. The biomechanical analysis of these sequences of events may elucidate the tumor progression and the potential of cancer cells for migration and metastasis. In this work, we focused on the evaluation of the spreading rate and the estimation of the adhesion strength between breast cancer cells and ECM prior to and post-treatment with anti-tumor agents. Specifically, different tamoxifen concentrations were used for ER^+ breast cancer cells, while even concentrations of trastuzumab and pertuzumab were used for $HER2^+$ cells. Analysis of cell stiffness indicated an increased elastic Young's modulus post-treatment in both MCF-7 and SKBR-3 cells. The results showed that the post-treatment spreading rate was significantly decreased in both types of breast cancer, suggesting a lower metastatic potential. Additionally, treated cells required greater adhesion forces to detach from the ECM, thus preventing detachment events of cancer cells from the ECM, and therefore, the probability of cell motility, migration, and metastasis was confined. Furthermore, post-detachment and post-treatment vinculin levels were increased, indicating tighter cell–ECM junctions, hence limiting the probability of cell detachment and, therefore, cell motility and migration.

KEYWORDS

adhesion forces, elasticity, cancer cells, vinculin, anti-tumor agents

1 Introduction

Breast cancer is a heterogeneous disease where different metabolic phenotypes of cancer cells predispose the tumor to progression, while metastasis is one of the leading causes of death in patients with breast cancer. Hence, the investigation of biomechanical and biochemical processes and the interplay between breast cancer cell–ECM interactions that participate during metastasis is of paramount importance (1). The mechanisms of metastasis include a sequence of attachment, spreading, and detachment events, encouraged by the dissipation of cell–cell junctions and cell–ECM adhesion forces (2). Cell spreading is an essential step for the progression of cell motility, migration, and, therefore, metastasis (3). Cancer cells adhere and spread by exerting forces on the cell membrane and the ECM. Intracellular forces drive the membrane outward during spreading and stabilize cell shape in adherent and migrating cells, while the cytoskeleton plays a pivotal role in cell spreading and detachment (4). More specifically, actin polymerization and myosin contraction contribute to cell movement within the ECM in the direction of metastasis (5, 6). The process of cell adhesion is primarily achieved by connecting intracellular cytoskeletons between cells or connecting the cellular cytoskeleton with ECM components (7). The loss of cell–cell adhesion is important for developing cancer invasion and metastasis (8–10). Reduced cell–cell adhesion due to loss of E cadherin along with loss of cell–ECM local adhesion proteins may lead to epithelial-to-mesenchymal transition (EMT), a critical condition leading to the initiation of metastasis. A key adhesion-related protein regarding cell–ECM and cell–cell junctions is vinculin. New insights have established that vinculin has no enzymatic activity, while its function is still emerging (11). Specifically, vinculin regulates the transmission of contractile forces (12), which affect metastasis. The loss of vinculin is correlated with the development of many cancers, such as squamous carcinoma rhabdomyosarcoma and breast cancer.

Recent studies suggest that cell–cell adhesiveness is generally reduced in human cancers (13). Hence, reduced intercellular adhesiveness permits cancer cells to disobey the social order, contributing in dissociation of histological structure, which is the morphological hallmark of malignant tumors, thus facilitating invasion and metastasis (14). The question that arises is how would the progression of the tumor microenvironment, specifically the spreading rate and adhesion forces between untreated and treated with anti-tumor drugs, cancer cells be affected? How do these drugs affect focal adhesion formations in the ECM and therefore the metastatic cascade?

This work aimed to investigate and elucidate the metastatic potential of cancer cells by evaluating the cell stiffness, the spread and the adhesion strength of two breast cancer cell lines with different phenotypes, MCF-7/ER$^+$ and SKBR-3/HER2$^+$, prior to and post-treatment with the antitumor agents tamoxifen, a selective estrogen receptor modulator; and trastuzumab and pertuzumab, monoclonal antibodies against HER2. Initially, we estimated the cell stiffness *via* the micropipette aspiration technique, underlying the alterations in elastic Young's modulus upon treatment. Furthermore, the spreading rate of the cell area prior to and post-treatment was determined. Finally, a range of shear stresses were applied to cancer cells, to detach from the ECM and therefore to evaluate the adhesion strength (15–17). More specifically, the rotating disc device was employed for estimating the cell–ECM adhesion strength of both cancer cell lines prior to and post-treatment with the aforementioned agents. To identify the role of vinculin in adhesion mechanisms, cancer cells exhibited immunofluorescence assay post-detachment event and post-treatment with anti-tumor agents. The understanding of the role of adhesion strength and spreading rate and their correlation with biochemical alterations can provide innovative insights into the process of cancer and may establish the basis for new therapeutic approaches (18–20).

2 Materials and methods

2.1 Cell culture

As previously, MCF-7 and SKBR3 (ATCC, USA) cancer cell lines were used (21). Briefly, MCF-7 was cultured in EMEM supplemented with 1 mM sodium pyruvate, 1.5 g/l sodium bicarbonate, 2 mM L-glutamine, 0.1 mM nonessential amino acids, and 0.01 mg/ml insulin (Sigma-Aldrich, Inc., USA). SKBR-3 cancer cells were cultured in DMEM supplemented with 2 mM L-glutamine. Both cell lines were supplemented with 100 μg/ml penicillin G/streptomycin, 50 μg/ml gentamycin, and 10% Fetal Bovine Serum (FBS). Phosphate Buffered Saline (PBS) was used for rinsing cells. All the above media and supplements were purchased from Biochrom (Berlin, Germany). Cells were cultured at 37°C, 5% CO_2, and 100% humidity. Tamoxifen was purchased from Sigma-Aldrich (Sigma-Aldrich, Inc., USA) and trastuzumab (Herceptin) and pertuzumab (Perjeta) were purchased from Roche (Roche). MCF-7 cells were treated with different concentrations of tamoxifen (10, 20, and 50 nM) while SKBR-3 cells were treated with 10 μg/ml of trastuzumab or/and pertuzumab, respectively (22–24). Dexamethasone was used as a positive control at a concentration of 10^{-8} M.

2.2 Preparation of 2D surfaces coated with collagen I

Volume of 1 ml of collagen I (cat. no. L 7220, Biochrom) was added to a 6-well polystyrene plate with an equal volume of 1× PBS and adjusted to a pH of 3.0–3.5. The PBS solution was also

adjusted to a pH of 3.0–3.5 as follows: 1 ml 1 N HCl to 100 ml PBS solution. Volume of 2 ml of the diluted collagen I solution per 10 cm^2 area of the culture flask and incubated for 2–3 h. The solution was then removed and washed with 1× PBS (pH approx. 7.3). The 6-well plate was then immediately filled with media and cancer cells were seeded.

2.3 Cell elasticity

Cancer cells exhibited a micropipette aspiration technique (MA) as previously described (21). In brief, MA was used to partially aspirate the cell membrane firmly, thus avoiding nucleus aspiration, to obtain measurements for the applied negative pressure at each time point of the resulting aspirated cell elongation. A range of suction pressure DP from 0.05 to 340 Pa was applied very slowly, to achieve a linear expression of cell deformation vs. aspiration pressure to determine the elastic Young's modulus. When the micropipette radius was exceedingly small compared to the local radius of the cell surface, the projection of cell length, L, into the micropipette was predicted to be proportional to the aspiration pressure ΔP (25). Therefore, cancer cell elasticity was determined through the slope of the curve $\Delta P = f(\frac{L}{D_p})$ *via* the interpreted equation: $E = \frac{R_p \Delta P}{2\pi L} \varphi_p$ (1) where E is the elastic Young's modulus, R_P the inner pipette radius, and φ_p represents a function of the ratio of the pipette wall thickness to the pipette radius (φ_p = 2.0–2.1 when the ratio of the pipette wall thickness to radius was equal to 0.2–1.0). Four repeated sample tests with MA were performed for each cell type condition (treated and untreated), measuring approximately 20 cells per sample.

2.4 Assessment of spreading rate

To address the cell spreading procedure, including untreated and treated with anti-tumor drugs tamoxifen, trastuzumab, and pertuzumab, cancer cells were seeded on a collagen I-coated 12-well plate and incubated for 12 h. The cell spread area was evaluated during incubation time of 0–12 h, and the attached cell membrane to the substrate contact area was determined by tracing the outline of the cell every hour using Sigma Scan Pro 5 software. The time-dependent normalized area was quantified by dividing the difference between the cell area at time t, A_t, and the initial spread area A_{intial} (the very first spread area after cell rolling upon surface) by the difference in area between the initial ($A_{initial}$) and final time points (A_{final}), where the cell was fully spread. Therefore, the cell spread area was estimated *via* the equation $A_{normalized} = \frac{A_t - A_{initial}}{A_{final} - A_{initial}}$ (2). The curves yielded the spreading rate of % $A_{normalized}$ cell area vs time for each case of control and treatment (26).

2.4.1 Evaluation of isotropic and anisotropic spreading

The evaluation of isotropic or anisotropic spreading was estimated when $HER2^+$ (SKBR-3) and ER+ (MCF-7) breast cancer cells were spread in the maximal area of contact with the ECM. Control SKBR-3 and MCF-7 cells were seeded on a collagen I-coated 12-well plate and incubated until the cell membrane reached its maximal spread potential. The cells were then fixed with 4% paraformaldehyde and permeabilized with 0.1% Triton X-100. Cells were rinsed with wash buffer and then blocked with bovine serum albumin in phosphate-buffered saline for 1 h at RT. After blocking, cells were labeled with conjugated Phalloidin TRITC (1:200, Merck/Millipore) for 1 h at RT and then rinsed with wash buffer. Then, Hoechst 33258 (1:4,000, Sigma-Aldrich) was used for nuclear counterstaining and then the cells were mounted. Fluorescent imaging was conducted on a Leica SP5 TCS equipped with a ×40/1.25NA oil immersion lens. Three different experiments were performed, and 100 cells were measured using Image J. Specifically, the associated aspect ratio was calculated as the minimal and maximal cell radius from the center of the nucleus in cartesian coordinates (R_x,R_y). An isotropic distribution of cell fibers was achieved when the aspect ratio is ˜1.

2.5 Assessment of cell detachment

Cells were grown in collagen coated circular glass coverslips, 0.7 cm in radius, immersed in 12-well plates filled with media and 10% FBS (40 × 10^3 cells/well). After 24 and 48 h of incubation of MCF-7 and SKBR-3 with the relevant drugs and inhibitors, respectively. Cell adhesion forces were evaluated using a rotating disc device for each case of untreated and treated cells. This technique utilizes shear stress generated from the rotating disc upon attached to ECM cancer cells. Specifically, a rotating disc device was employed to apply shear stress to cells. The adhesion strength of the cells was determined by estimating the essential shear stress to detach the cells from their substrate (27). The rotating disc device comprises a disc clutched to the motor and a chamber made of plexiglass® (27). The chamber was filled with PBS 1× solution at a constant 37 °C temperature. The aforementioned glass coverslips with the adherent cancer cells were glued to the disc and inserted into the rotation chamber, and hence, the cancer cells underwent shear stress (Figure 1). When the value of shear stress reaches a critical level, then 50% of the attached cancer cells are detached from the surface. The adherent fractions of cells were quantified using microscopy in combination with image processing software (Sigma Scan Pro 5). The shear stress at the surface of

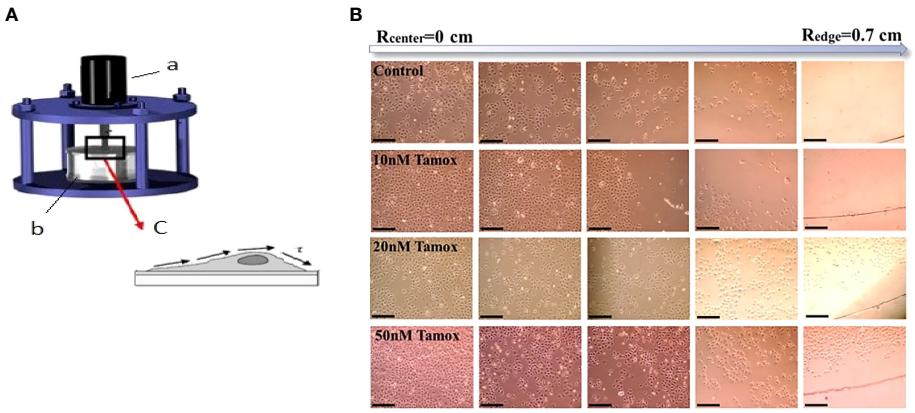

FIGURE 1
Estimation of adhesion forces by rotating disc assay. **(A)** The device consists of (a) rotor (b) tank filled with PBS at 37 °C, and (c) attached cancer cells on coverslips exhibiting shear stress (τ) (16, 17). **(B)** MCF-7 cell detachment event in different distances from the center of the disc (Rcenter = 0) to the edge (Redge = 0.7 cm) and in different tamoxifen concentrations, black scale bar 100 μm, ×10 microscope lens. Cell detachment was less favored at the highest tamoxifen concentrations.

the rotating disc was calculated from the equation: τ=0.7996 r ρ $v^{1/2}$ $\omega^{3/2}$ (3) where τ is the applied shear stress, r the distance to the center of the disc, ρ the density of the rotation buffer, v the kinematic buffer viscosity and ω the angular velocity with a range of 100–300 rpm (28). After this process, the curves of the percentage number of detached cells (referred to the distance of each cell from the center of the disc) vs required shear stress for detachment were educed and the critical shear stress for detachment was assessed. Post detachment event cells were fixed for immunofluorescence assay.

2.5.1 Immunofluorescence assay after detachment

After detachment, cells were gently rinsed with PBS and fixed with 4% paraformaldehyde and permeabilized with 0.1% Triton X-100. Cells were then rinsed with wash buffer (1× PBS containing 0.05% Tween-20). Blocking was performed with 3% bovine serum albumin in phosphate-buffered saline containing 10% FBS for 1 h at RT. After blocking, cells were labeled with anti-Vinculin for 1 h. Cells were labeled with conjugated Phalloidin TRITC (1:200, Merck/Millipore) and FITC (1:200, Jackson ImmunoResearch Laboratories, Inc.) for 1 h at RT and then rinsed with wash buffer. Then Hoechst 33258 (1:4,000, Sigma-Aldrich) was used for nuclear counterstaining and then the cells were mounted. Z-stack imaging was conducted on a Leica SP5 TCS equipped with a ×40/1.25NA oil immersion lens. Overall, more than 200 cells for each case of control and treatment were studied after multiple repeated experiments (>3), and the mean fluorescence intensity of the sum projection of vinculin was evaluated after background subtraction with the use of the software ImageJ.

2.6 Statistical analysis

The results from cell spreading and detachment were statistically analyzed and fitted using Origin Pro9 (OriginLab Corporation, Northampton, USA) and Sigma Scan Pro 5 software for evaluating normalized cell area ($A_{normalized}$). The results of the Elastic Young's modulus of cancer cells were statistically analyzed using Matlab R2021a. For each case of control and treated with anti-tumor agents, 40 cancer cells were probed using a micropipette technique over three repeated experiments. Differences between the groups and controls were assessed by one-way analysis of variance (ANOVA). Each experiment included a minimum of three repeated measurements. The results were considered to be statistically significant when $p < 0.05$.

3 Results

3.1 Elastic Young's modulus of breast cancer cells (overview)

Breast cancer elasticity post-treatment with 10 nM tamoxifen and 10 μg/ml trastuzumab was investigated in our previous work (21). Here, we aimed to further investigate whether different concentrations of Tamoxifen or different anti-tumor agents affect cell elasticity and relate these results to the potential of breast cancer cells to spread and detach. Indeed, in Table 1, the Elastic Young's modulus of both previous and current work is included. Specifically, in MCF-7 cells, we found that the Elastic Young's modulus was markedly increased as tamoxifen concentration levels were increased. Regarding

TABLE 1 Elastic Young's modulus of ER^+ cancer cells in different tamoxifen concentrations and $HER2^+$ cancer cells post-treatment with trastuzumab, pertuzumab, and their synergistic effect in even concentrations.

Breast cancer cells	ER^+	$HER2^+$	Drug	Concentration	Elastic modulus (Pa)		
					Control	24 h of treatment	48 h of treatment
MCF-7	+	–			196.3 ± 21.68 (21)		
			Tamoxifen	10 nM	–		224.64 ± 15.34*(21)
				20 nM		465.80 ± 30.15*	536.25 ± 43.42**
				50 nM		585.00 ± 24.80**	634.38 ± 35.40**
			Dexamethasone	10^{-8} M		375.42 ± 35.12**	417.03 ± 16.36**
SKBR-3	–	+			277.86 ± 12.57 (21)		
			Trastuzumab	10 μg/ml		–	343.62 ± 28.45**(21)
			Pertuzumab	10 μg/ml		360.89 ± 31.41**	559.00 ± 13.90**
			Trastuzumab + Pertuzumab	10 μg/ml		261.79 ± 11.80***	395.89 ± 45.90***
			Dexamethasone	10^{-8} M		186.42 ± 88.50**	466.45 ± 14.20*

Dexamethasone was used as positive control. Data express mean values ± SD of at least three repeated experiments, *p <0.05, **p <0.01, and ***p <0.001.

SKBR-3 cells using another anti-tumor agent, pertuzumab, the cell elasticity increased radically while the synergistic effect of trastuzumab and pertuzumab affected cell elasticity modestly regarding the isolated effect of pertuzumab.

3.2 Anti-tumor agents regulate spreading rate of breast cancer cells

For estimating spreading kinetics, the experimental data of normalized cell area versus time were fitted with a sigmoidal fit, which reflects the dose–response curve. Two distinct phases of expanded cell area were observed with a different spreading rate $A_{normalized}$/dt.

The spreading kinetics of MCF-7 cancer cells is depicted in Figure 2. Results showed that 50% of the $A_{normalized}$ of untreated (Control) cells was achieved in the very first 1.5 h, while the maximum spread area was integrated within 4 h ($p < 0.001$). Regarding 10 nM of tamoxifen-treated cells, 50% of $A_{normalized}$ was achieved within 2.17 h after 24 h of treatment, and within 2.98 after 48 h of treatment, respectively. Moreover, the maximum spread area was integrated within 4 h ($p < 0.001$) (Figure 2A). Post treatment with 20 nM tamoxifen, MCF-7 cells reached the 50% of $A_{normalized}$ within 2.80 h in both 24 h and 48 h post-treatment (Figure 2B). Furthermore, 24 h and 48 h post-treatment with 50 nM tamoxifen, 50% of $A_{normalized}$ was achieved within 2.84 h and 3.24 h, respectively (Figure 2C). Positive control cells treated with dexamethasone for 24 h and 48 h reached 50% of $A_{normalized}$ within 2.5 and 2.65 h, respectively (Figure 2D). Overall, regarding MCF-7 cells, different concentrations of tamoxifen postponed the spreading event and the maximum spread cell area of treated cells was confined compared to untreated cells. MCF-7 cells were reluctantly spread post-treatment with 50 nM tamoxifen after 48 h of treatment.

In the case of SKBR-3 cancer cells, untreated (Control) cells exhibited a rapid spreading rate, where the increase of 50% of $A_{normalized}$ was achieved within 2.7 h following the plateau and the maximum spread area was completed within 7 h. In contrast, trastuzumab treated SKBR-3 cancer cells exhibited initially a slow spreading rate followed by a rising period of spreading rate where the increase of 50% of $A_{normalized}$ was integrated within 1.8 h and 4.7 h post 24 h and 48 h of treatment with trastuzumab and the maximum spread area, within 5 h ($p < 0.001$) (Figure 3A). Regarding post-treatment with 24 h and 48 h of pertuzumab, SKBR-3 cells reached 50% of $A_{normalized}$ within 3.2 and 4.9 h, respectively (Figure 3B). The synergistic effect of trastuzumab and pertuzumab post 24 h and 48 h of treatment increased the time where 50% of $A_{normalized}$ was integrated at 4.3 and 4.8 h correspondingly (Figure 3C). Regarding positive control cells, 50% of $A_{normalized}$ achieved within 3.9 h (Figure 3D).

Overall, SKBR-3 cancer cells exhibit a slower spreading rate when treated with trastuzumab and pertuzumab, corroborating that in the presence of monoclonal antibodies, the attachment and the spreading rate are less favored.

3.3 Isotropic and anisotropic spreading

To address the isotropic and anisotropic spreading, we measured the morphology of F-actin stress fibers once control MCF-7 and SKBR-3 cells were completely stressed. MCF-7 adopted a spherical like spreading with an even distribution of F-actin fibers along the cell periphery (Figures 4A, B). MCF-7 Rx = 21.94 ± 5.20 μm and Ry = 20.54 ± 5.12 μm with the associated aspect ratio of 1.068 (˜1). However, SKBR-3 cells

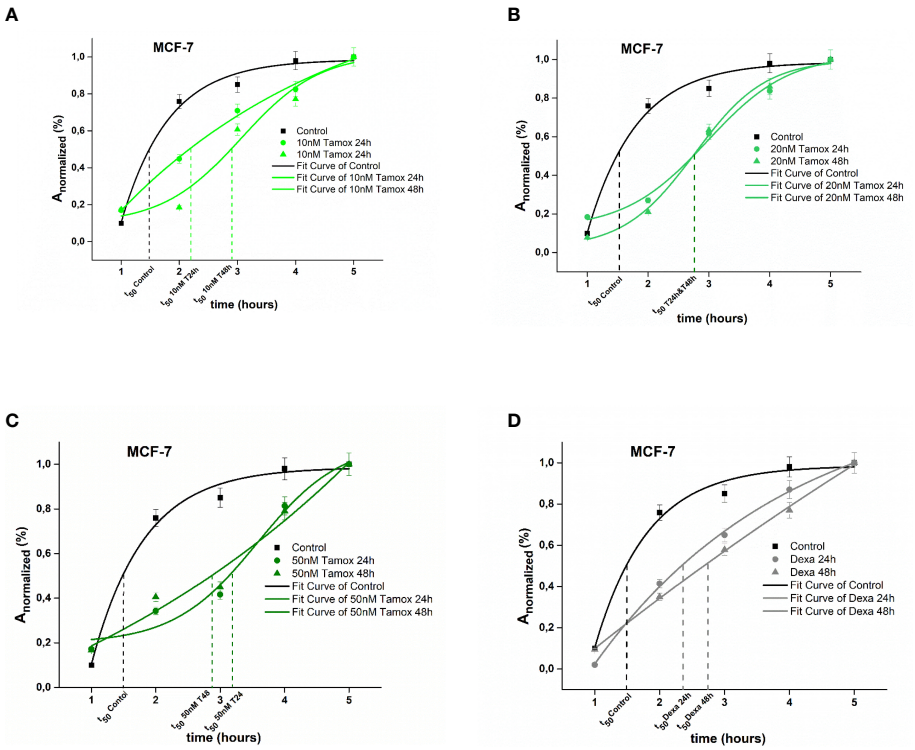

FIGURE 2
Plotted normalized cell area interprets spreading kinetics. Merged experimental curves of three repeated tests of the spreading rate ($dA_{normalized}/dt$) of Control vs 10 nM tamoxifen **(A)**, Control vs 20 nM tamoxifen **(B)**, Control vs 50 nM tamoxifen MCF-7 **(C)** and Control vs dexamethasone **(D)** are depicted.

presented highly elongated morphologies on dense F-actin networks (Figures 4C, D). The aspect ratio of SKBR-3 cells was estimated with continuous growth, implying anisotropic shape (29). Specifically, the estimated maximal and minimal radii were estimated to be Rx = 51.62 ± 11.79 μm and Ry = 6.87 ± 2.01 μm, correspondingly with the associated aspect ratio of 7.5 (>1).

3.4 The role of anti-tumor agents on adhesion forces of breast cancer cells

For the estimation of detachment forces, which is equal to the adhesion strength, a crucial detachment force was defined as the critical shear stress τ_{50}, namely, the value of the needed force where 50% of the cells were detached from the surface of the rotating disc. Figures 5, 6 show the plotted curves of the number of remaining cells after the detachment event vs the essential shear stress for cells to detach from the ECM.

In the case of MCF-7 cells, untreated cancer cells revealed a critical shear stress τ_{50} of 21.0 dyn/cm^2. Considering post-treatment with 10 nM tamoxifen dyn/cm^2 (Figure 5A) the τ_{50} was at 23.5 and 25.7 dyn/cm^2 24 h and 48 h of post-treatment. After increasing tamoxifen to 20 nM, the relevant critical shear stress $\tau_{50}$was also increased to 29.8 and 33.4 dyn/cm^2 respectively (Figure 5B). A further increase in tamoxifen concentration of 50 nM indicated 50% cell detachment at 34.7 and 38.5 dyn/cm^2 (Figure 5C). In dexamethasone-treated cells, the critical shear stress τ_{50} was 27.3 and 29.2 dyn/cm^2 after 24 h and 48 h of treatment, respectively (Figure 5D).

Overall, post-treatment with increased tamoxifen levels, the potential of MCF-7 to detach was decreased and the required shear stress for detachment compared to control cells was 14.2 % higher at 10 nM tamoxifen and dramatically increased at 48.5% and 54.2% at tamoxifen concentrations of 20 nM and 50 nM, 48 h post-treatment, respectively. These results imply that the increased tamoxifen concentration inhibits the detachment of treated cells and hence implies strong adhesion forces between the cell and ECM (Figure 5E).

In the case of SKBR-3 cancer cells, the critical shear stress τ_{50} for untreated cells was estimated at 32.7 dyn/cm^2 (Figure 5), while in the case of trastuzumab-treated cells it was at 37.2 and 42.5 dyn/cm^2 after 24 h and 48 h of treatment, correspondingly (Figure 6A). Regarding pertuzumab-treated cells, the critical shear stress τ_{50} reached 54.9 dyn/cm^2 and 55.87 dyn/cm^2 post 24 h and 48 h of treatment, respectively (Figure 6B). The

10.3389/fonc.2022.811508

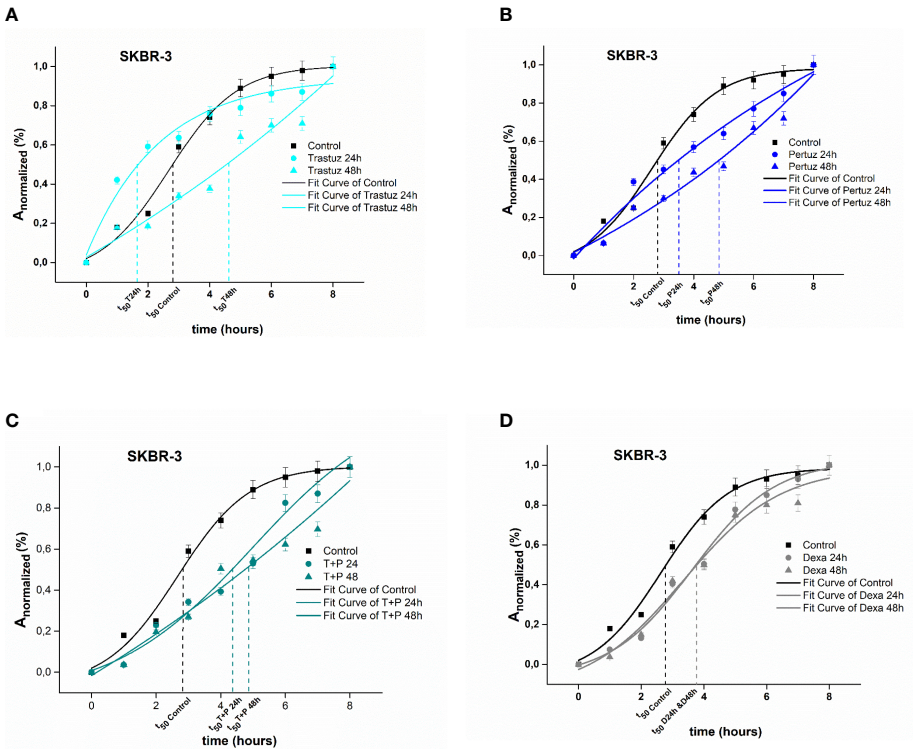

FIGURE 3
Plotted normalized cell area interprets spreading kinetics. Merged experimental curves of three repeated tests of the spreading rate ($dA_{normalized}/dt$) of Control vs trastuzumab **(A)**, Control vs pertuzumab **(B)**, Control vs trastuzumab + pertuzumab SKBR-3 **(C),** and Control vs dexamethasone **(D)** are depicted.

synergistic effect of trastuzumab + pertuzumab revealed a prerequisite critical shear stress τ_{50} of 49.5 dyn/cm^2 and 51.2 dyn/cm^2 at 24 h and 48 h of treatment, respectively (Figure 6C). Finally, critical shear stress τ_{50} for dexamethasone-treated cells was estimated at 44.5 dyn/cm^2 and 48.2 dyn/cm^2 at 24 h and 48 h post-treatment (Figure 6D).

Overall, increased shear stress was essential to detach post-treated SKBR-3 cells from the ECM. Specifically, 48 h post-treatment with trastuzumab, the essential shear stress for 50% of cell detachment was 43.1% higher than control cells, while in the case of pertuzumab it was 88% higher. Moreover, in the case of both trastuzumab and pertuzumab-treated cells, the relevant shear stress τ_{50} was 82.5% higher. The results from the detachment study suggest that in the presence of pertuzumab, cancer cells detached reluctantly from the ECM (Figure 6E).

3.5 Detachment forces and anti-tumor agents regulate vinculin and F-actin of breast cancer cells

In the case of MCF-7 cells, vinculin expression levels were markedly increased post-treatment with tamoxifen. Initially, vinculin levels of control, positive control (Dexa 24 h, 48 h), and post-treated with 10 nM tamoxifen for 24 h were at approximately even fluorescence intensities as depicted in Figures 7A, B. However, as the concentration of the drug increases, the vinculin mean intensity also increases. Notably, after 48 h of treatment with 10 nM, 20 nM, and 50 nM tamoxifen, vinculin showed a redistribution and increased signal levels (Figures 7A, B), indicating a post-treatment vinculin upregulation. Moreover, the morphology of F-actin cytoskeleton protein was not altered post-treatment. However, high levels of F-actin were detected in control cells following a reduced expression in treated cells. These results corroborate the findings from the Elastic Young's modulus evaluation, as increased post-treatment cell stiffness indicates confined migration potential (21).

Regarding SKBR-3 cells, vinculin mean fluorescence intensity was significantly increased 48 h post-treatment with trastuzumab, pertuzumab, and trastuzumab + pertuzumab, as depicted in Figures 8A, B. Furthermore, the distribution of F-actin stress fibers was altered post-treatment. Fully polymerized F-actin in control SKBR-3 cells with extended lamellipodia and filopodia indicates a high density of F-actin cross-linking, which, according to previous studies, is related to soft and therefore

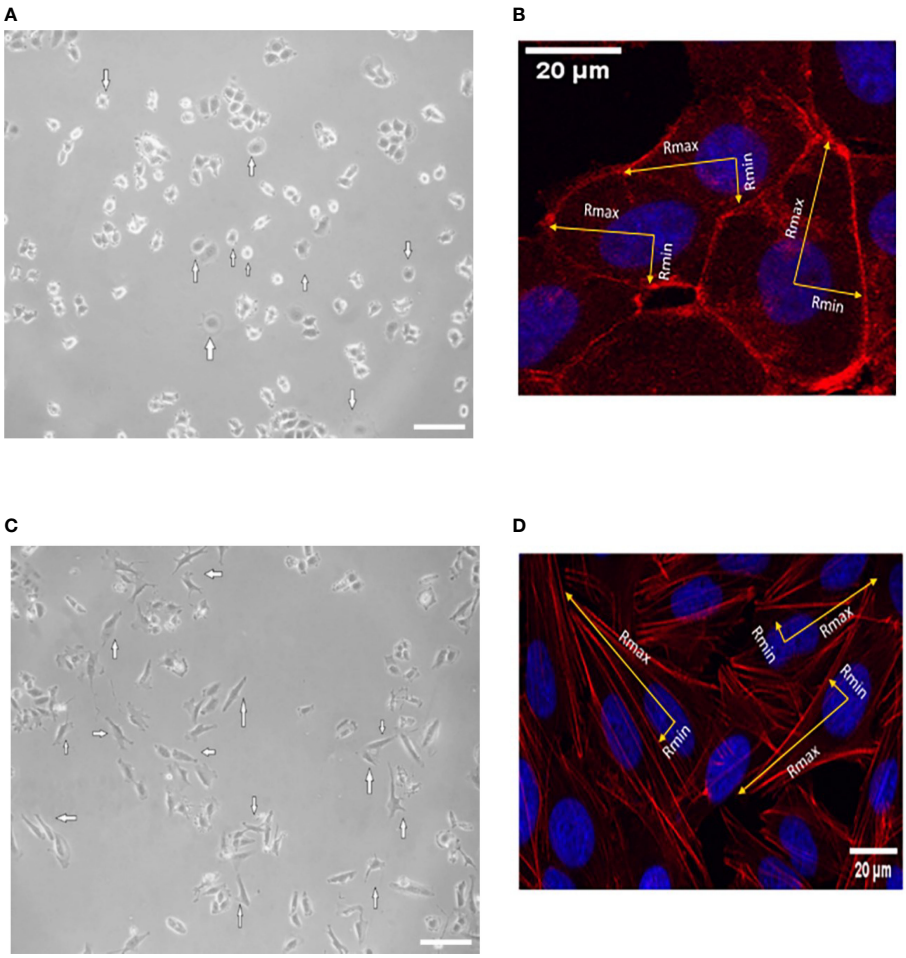

FIGURE 4
Represented images of spreading events of MCF-7 **(A, B)** and SKBR-3 **(C, D)** cancer cell lines after 20 h of incubation. White arrows indicate isotropic-like spreading in the case of MCF-7 cancer cells where the cell membrane extends and flattens evenly in all directions and a similar distance from the center of the nucleus. Anisotropic spreading occurs in the case of SKBR-3 cancer cells where the cell membrane extends unevenly from the center of the nucleus to the protrusions' leading edge. The minimum and maximum cell radii are indicated with yellow arrows. The isotropic spread occurs when the aspect ratio of Rmax and Rmin is approximately 1. White color scale bar 40 μm, ×10 microscope lens **(A, C)** and 20 μm ×40 confocal lens (**B, D**).

more elastic cells with greater potential for migration. However, in the case of post-treated SKBR-3 cells, F-actin stress fibers were depolymerized and perinuclear accumulated, revealing a roundish cell with confined protrusions. The results of increased vinculin levels with limited cell protrusions conform to the increased cell stiffness post-treatment with anti-tumor agents, indicating confined cell motility.

4 Discussion

In the series of steps that comprise the metastatic potential of cancer cells, the spreading rate upon ECM and the adhesion forces between cell and ECM are inextricably linked with the progression of the disease (4, 30, 31). Biological and biochemical mechanisms of cancer cells alter and remodel the structure of the cytoskeleton to invade the ECM. Altered cytoskeleton proteins result in changes in the ability of cancer cells to contract, spread, and move upon ECM, thus influencing their biomechanics (32). As pathological tumor progression leads to aberrant biomechanical behavior in cells and tissues, thereby affecting the tumor microenvironment and therefore participating in the malfunction of cell–ECM homeostatic equilibrium (33). Nevertheless, the influence of adhesion forces between treated with anti-tumor agent cancer cell–ECM junctions and the spreading rate of treated cancer cell membranes has not been thoroughly elucidated. In this work, we compared two breast cancer cell lines with different profiles regarding their

10.3389/fonc.2022.811508

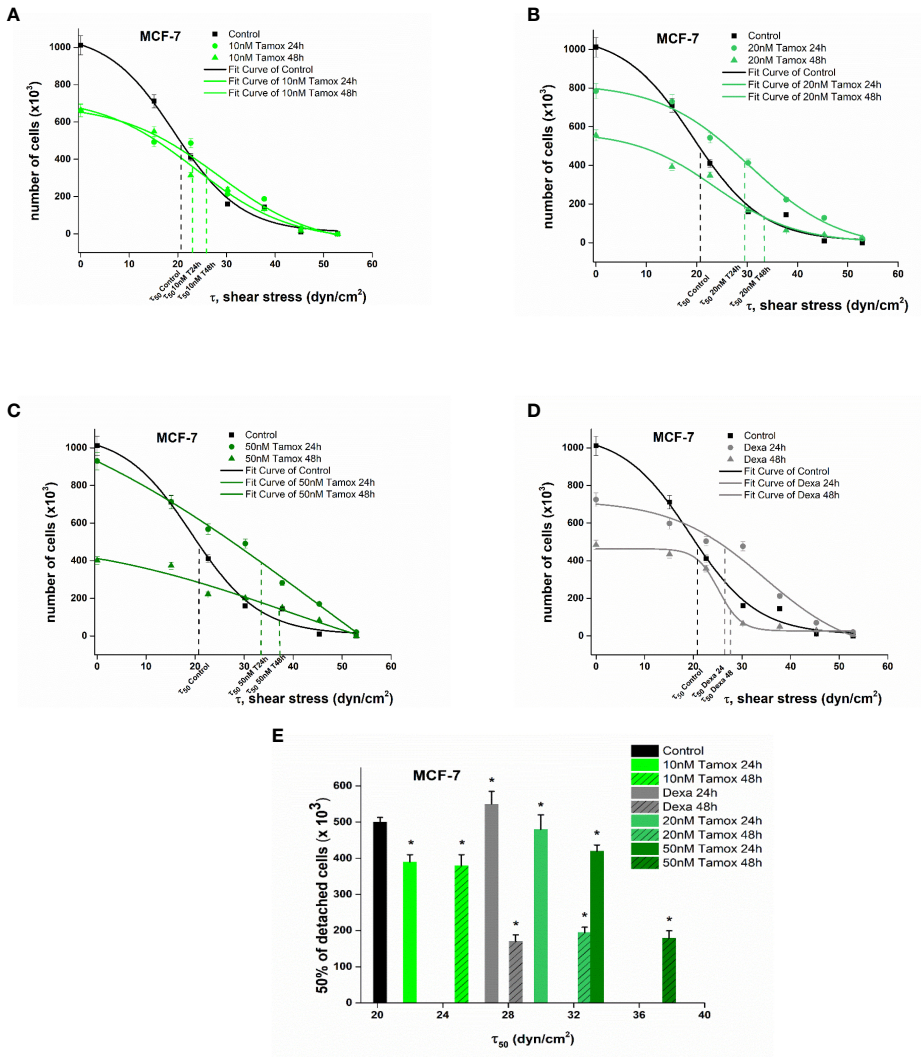

FIGURE 5
Plotted curves of the number of remaining MCF-7 cells post-detachment event vs the essential shear stress for detachment **(A–D)**. The applied shear stress is zero to attached cancer cell upon the center of the disc (r = 0) where the remained cells after detachment are 100%, no detachment was occurred and maximum when r = R_{disc} = 1 cm where all cancer cells where detached. Percentage number of remaining cells of control and treated MCF-7 breast cancer cells upon the collagen coated surface after applying a range of 0–200 dyn/cm^2 shear stresses **(E)**. Data express mean values ± SD of at least three repeated experiments, *p <0.05.

aggressiveness, to investigate the treatment mechanisms in Elastic Young's modulus, spreading rate, adhesion forces, and focal adhesion protein vinculin levels. These parameters reflect the biological and biochemical interactions between cells and the ECM, by expressing macroscopically cell biomechanics and hence indicating the mechanical behavior of malignant cells (34). Consequently, the biomechanical properties of cancer cells could be used as indicators of their biological state or metastatic potential.

Several studies have established that the high stiffness of the ECM in the tumor microenvironment contributes to cancer progression and triggers malignant transformation (35–37). Clinical studies suggest that the collagenous matrix stiffens the tumor stroma, which directly increases tumor cell proliferation and enhances metastatic colonization, and growth (38, 39). Here, we were intrigued to extend our previous work and test the hypothesis of whether different drug concentrations affect the Elastic Young's modulus in the case of MCF-7 cells and whether different anti-tumor agents and their synergistic effects could regulate the cancer cell elasticity of SKBR-3 cancer cells. Indeed, we estimated that in the case of MCF-7 cells, the Elastic Young's modulus increased as tamoxifen levels were increased from 10 to 50 nM and significantly after 48 h of treatment. Regarding SKBR-3 cancer cells, we conclude that the cell stiffness

10.3389/fonc.2022.811508

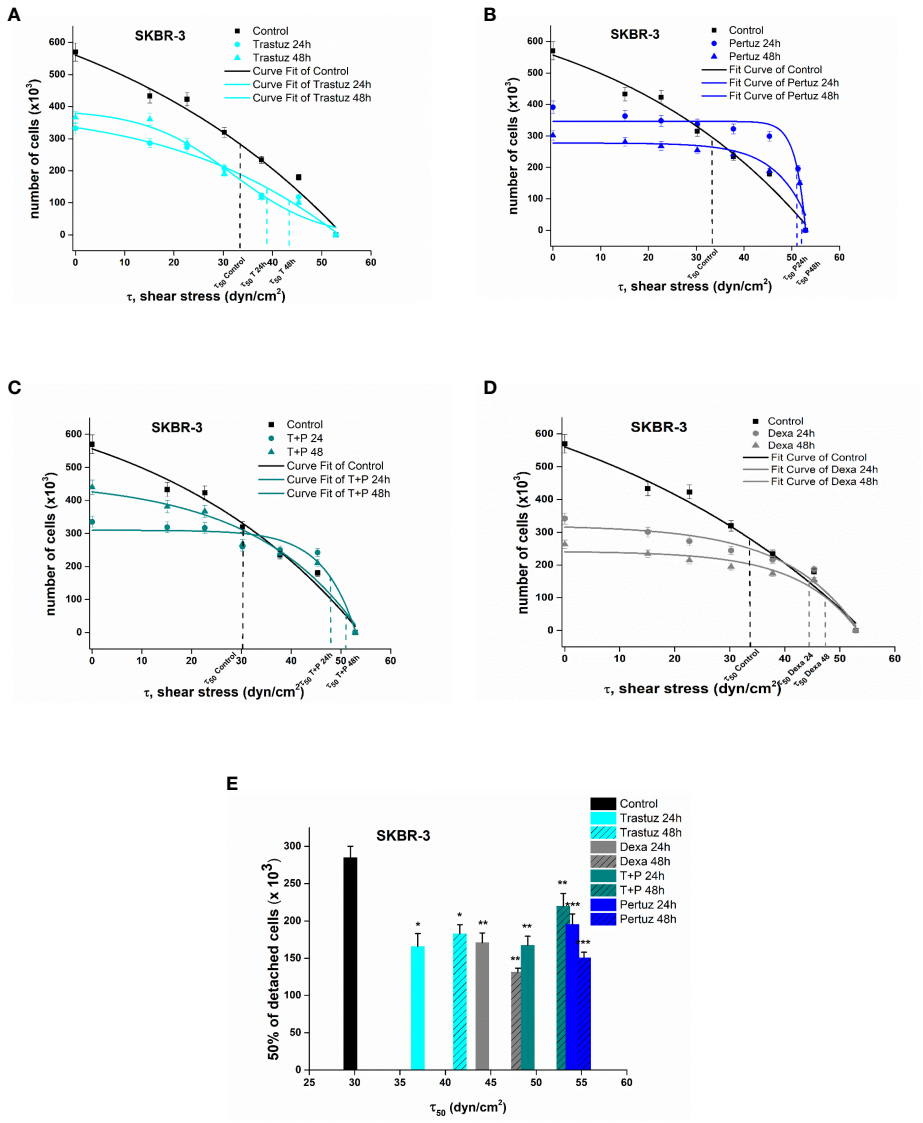

FIGURE 6
Plotted curves of the number of remaining SKBR-3 cells post detachment event vs the essential shear stress for detachment **(A–D)**. The applied shear stress is zero to attached cancer cell upon the center of the disc (r = 0) where the remained cells after detachment are 100%, no detachment was occurred and maximum when r = R_{disc} = 1 cm where all cancer cells where detached. Percentage number of remaining cells of control and treated SKBR-3 breast cancer cells upon the collagen coated surface after applying a range of 0–200 dyn/cm^2 shear stresses **(E)**. Data express mean values ± SD of at least three repeated experiments, *p <0.05, **p <0.01, and ***p <0.001.

increased markedly in post-treated cells with monoclonal antibodies. Interestingly, in the presence of pertuzumab, the Elastic Young's modulus increased in a greater rate compared with trastuzumab or their synergistic effect. Overall, the increased post-treatment cell stiffness in both ER$^+$ and HER2$^+$ cancer cells indicates a less deformable cytoskeleton, resulting in a confined potential for cell movement (Table 1) (21, 40).

Regarding spreading rate, our results suggest that in both cancer cell lines, after treatment, there was no enhancement of the spreading rate, which reflects a confined extension of the cell membrane in both MCF-7 and SKBR-3 cancer cells. Hypothesizing that spreading rate reflects the metastatic potential, the finding of the same post treatment spreading rate in both breast cancer cell lines, implies an equal metastatic potential indicating the endogenous feature of aggressive phenotype of cancer cells (Figures 2, 3). Comparing the two different cancer cell lines of this study, SKBR-3 and MCF-7, we showed that untreated SKBR-3 cells, as HER2$^+$ belongs to highly metastatic breast cancer cells with an aggressive metastatic phenotype, and therefore the slope of the

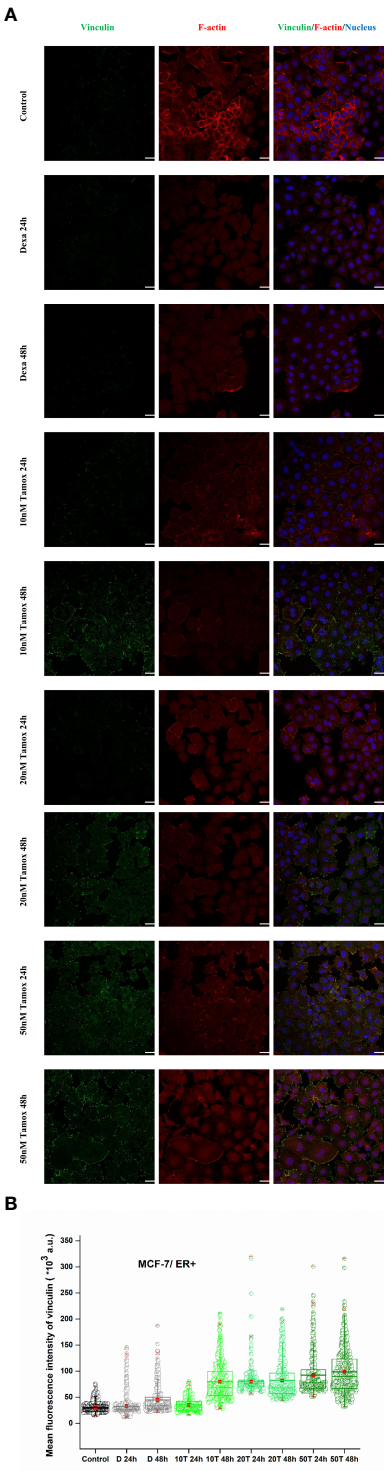

FIGURE 7
Effect of tamoxifen on vinculin expression levels. Post-detachment MCF-7 cancer cells were incubated with different concentrations of tamoxifen for 24 h and 48 h. Tamoxifen treated cells and merge plot of vinculin, F-actin and nucleus, white color scale bar 40 μm, ×40 microscope confocal lens **(A)**. Quantitative confocal microscopy analysis *via* ImageJ displays mean fluorescence intensity. Mean values ± SD of mean immunofluorescence intensity of 400 cells per treatment with three independent experiments are represented reflecting Control, decamethastone as postitive control (D 24 h, D 48 h), 10 nM tamoxifen (10 T 24 h, 10 T 48 h), 20 nM tamoxifen (20 T 24 h, 20 T 48 h) and 50 nM tamoxifen (50 T 24 h, 50 T 48 h). Box-plot whiskers represent the 5th and 95th percentile, the median value is represented by the line within the box, and the red square box depicts the mean **(B)**.

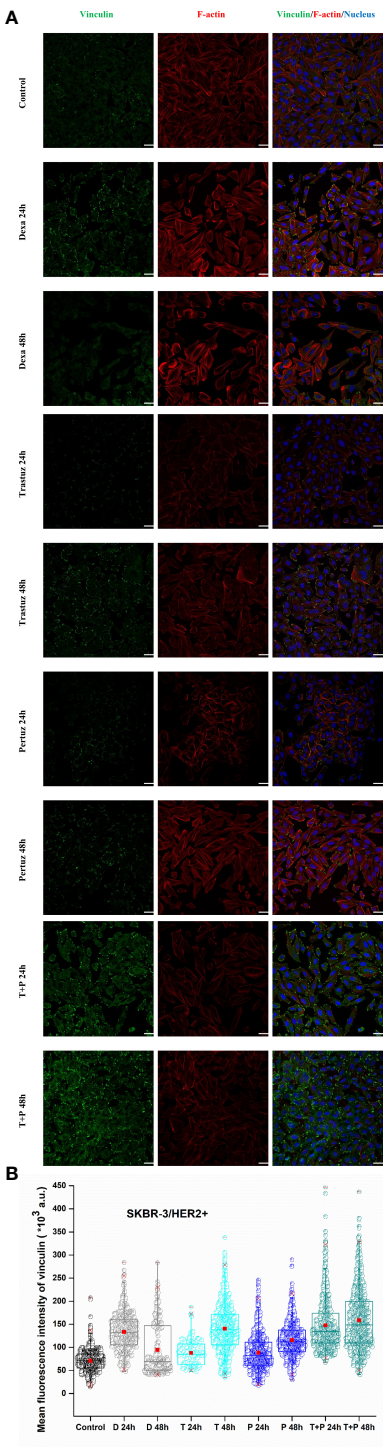

FIGURE 8
Effect of trastuzumab, pertuzumab, and their synergistic effect for double inhibition of HER2$^+$ cancer cells on vinculin expression levels and merge plot of vinculin, F-actin, and nucleus, white color scale bar 40 μm, ×40 microscope confocal lens **(A)**. After detachment, SKBR-3 cancer cells were incubated with monoclonal antibodies, trastuzumab and/or pertuzumab for 24 h and 48 h. Quantitative confocal microscopy analysis *via* ImageJ displays the mean fluorescence intensity of vinculin. Mean values ± SD of mean immunofluorescence intensity of 400 cells per treatment with three independent experiments are represented reflecting Control, dexamethasone as positive control (D 24 h, D 48 h), trastuzumab (T 24 h, T 48 h), pertuzumab (P 24 h, P 48 h), and their synergistic effect (T + P 24 h, T + P 48 h). Box-plot whiskers represent the 5th and 95th percentile, the median value is represented by the line within the box, and the red square box depicts the mean **(B)**.

curve of the spreading experiment increased more rapidly than MCF-7 cells. In contrast, the results of untreated MCF-7 cancer cells are in line with recent studies which showed that MCF-7 cells are weak metastatic cells with less invasive potential, and therefore the spreading rate procrastinates a lot compared to SKBR-3 cancer cells (41). Interestingly, regarding post-treatment results, the spreading rate of treated SKBR-3 cancer cells indicates an expeditious progress of the phenomenon, compared to tamoxifen-treated MCF-7 cancer cells. This is in line with clinical evidence that ER^+ breast tumors are less aggressive than $HER\text{-}2^+$ tumors (42). Previous studies established that spreading could occur either isotropically or anisotropically (43, 44). Isotropic spreading occurs when the cell membrane flattens equally in all directions. On the contrary, anisotropic spreading occurs when cells produce increased membrane extensions or pseudopod protrusions. In this work, MCF-7 cancer cells followed an isotropic spread (Figures 4A, B) while SKBR-3 showed an anisotropic spread (Figures 4C, D), indicating that SKBR-3 cancer cells present a more aggressive profile with increased protrusions compared to MCF-7. Furthermore, this might imply that SKBR-3 cells might be polarized, and membrane receptors related to movement are not allocated all over the membrane of cells (45).

Cellular forces are primarily generated in the cytoskeleton, which is responsible for maintaining the cell shape and organization, imparting specific mechanical properties to cells (46). In malignant transformation, the reorganization of the cytoskeleton occurs with a simultaneous loss of strong intracellular forces, contributing to a softer cancer cell with the ability to migrate easily upon ECM (47). Additionally, according to several studies, the cell–cell adhesiveness of malignant cells is generally reduced (48, 49). Hence, cancer cells readily degrade the ECM and surrounding tissues and converge to a highly aggressive and metastatic phenotype. Regarding the results of the detachment experiment with the rotating disc and correlating treated and untreated cells, we established that the adhesion strength in case of treated cancer cells was found to be 50% higher in MCF-7 and 25% higher in SKBR-3 cells (Figures 5, 6) (Table 2). These findings suggest that the external mechanical stimuli *via* shear stress induced biological pathways in post-treated cells which triggered the overexpression of focal adhesion vinculin in both intercellularly and cell–ECM junctions, thus impeding cancer cells from detaching from the ECM and hence confining the motility, migration, and metastatic potential (50, 51).

In the existing literature, the loss of vinculin is linked to the development of many cancers (10, 52, 53). Our study conforms to other studies, which showed that overexpression of vinculin causes reduced cell migration, whereas knockdown of vinculin-enhanced cell motility (54, 55). Moreover, the study by Toma-Jonik et al. showed an association between the downregulation of vinculin, the reduced adhesion and the enhanced motility of cells over-expressing active heat shock transcription factor 1 (HSF1), the major regulator of stress response, which is frequently activated in cancer (56). Coll et al. inactivated the vinculin gene in mouse embryonal carcinoma cell lines and embryonic stem cells, and their results showed that the loss of vinculin resulted in increased cell motility (57). Sadano et al. showed that highly metastatic melanoma cells lacked vinculin or expressed only scant amounts (58). Other studies have estimated that vinculin overexpression leads to stronger adhesion and less motility (12, 54). Therefore, our data are in line with these studies, as we showed that high post-treatment vinculin expression, in both ER^+ and $HER2^+$ cancer cells (Figures 7A, B, 8A, B), correlates with decreased potential for detachment and, therefore, migration upon ECM from the yielded evidence of detachment, spreading and cell stiffness. However, *in vivo* studies must elucidate and decipher the focal adhesion

TABLE 2 Cumulative results of MCF-7 and detachment of SKBR-3 breast cancer cells upon treatment.

Breast cancer cells	ER	HER2	Drug	Concentration	Control		24 h		48 h	
					$\tau_{50}(\frac{dyn}{cm^2})$	N_{50} $(\times 10^2)$	$\tau_{50}(\frac{dyn}{cm^2})$	N_{50} $(\times 10^2)$	$\tau_{50}(\frac{dyn}{cm^2})$	N_{50} $(\times 10^2)$
MCF-7	+	−			21.00	505				
			Tamoxifen	10 nM			23.50	330.00	25.70	332.00
				20 nM			29.80	392.00	33.40	278.00
				50 nM			34.70	465.00	38.50	201.00
			Dexamethasone	10^{-8} M			27.30	362.00	29.20	242.00
SKBR-3	−	+			32.70	285				
			Trastuzumab	10 μg/ml			37.20	166.00	42.50	183.00
			Pertuzumab	10 μg/ml			54.90	195.00	55.87	151.00
			Trastuzumab + Pertuzumab	10 μg/ml			49.50	167.00	51.20	220.00
			Dexamethasone	10^{-8} M			44.50	171.00	48.20	131.00

τ_{50} in $(\frac{dyn}{cm^2})$ is the essential shear stress to detach 50% of the cell population and N_{50} is the relevant number of detached cells.

distribution and localization regarding post-treatment with anti-tumor agents in cancer cells to establish the correlation between knockout of vinculin and restricted cell motility.

This study aimed to understand the regulation of cell adhesion dynamics and the role of cell adhesion protein vinculin of breast cancer cells prior to and post-treatment with anti-tumor agents and their correlation to cell motility by identifying the cell stiffness and the potential for cell spread. Moreover, cell detachment was markedly confined post-treatment with various levels of tamoxifen concentration in the case of MCF-7 cells and post-treatment with trastuzumab, pertuzumab, and their synergistic effect, in SKBR-3 cells. Our results suggest a limited potential for cell movement post-treatment with the aforementioned anti-tumor agents in both breast cancer cells, and this hypothesis was enhanced by elevated mean fluorescence intensity and, therefore, overexpression of vinculin in post-treated cells. This study of MCF-7 and SKBR-3 breast cancer, which reflects the patients with ER^+ and $HER2^+$ breast cancer, respectively, and may contribute and provide new insights into new therapeutics that are about to influence both the biochemical and biomechanical responses of cancer cells.

Data availability statement

The raw data supporting the conclusions of this article will be made available by the authors, without undue reservation.

Author contributions

DM: Study, conception, design, performed the experiments, and data analysis. DD: Supervising and review. EG: Supervising and review. HK: Supervising and review. AK: Supervising, review, study, and conception. GA: Supervision, Review, Study, and Conception. All authors contributed to the article and approved the submitted version.

Funding

This research was supported by funding from the source: "Constantin Carathéodory, E.044, 2013".

Acknowledgments

The authors want to thank the members of the Laboratory of General Biology, School of Medicine, University of Patras, for providing the Leica confocal microscopy.

Conflict of interest

The authors declare that the research was conducted in the absence of any commercial or financial relationships that could be construed as a potential conflict of interest.

Publisher's note

All claims expressed in this article are solely those of the authors and do not necessarily represent those of their affiliated organizations, or those of the publisher, the editors and the reviewers. Any product that may be evaluated in this article, or claim that may be made by its manufacturer, is not guaranteed or endorsed by the publisher.

References

1. Suresh S. Biomechanics and biophysics of cancer cells. *Acta Biomater* (2007) 3(4):413–38. doi: 10.1016/j.actbio.2007.04.002

2. Behrens J. The role of cell adhesion molecules in cancer invasion and metastasis. *Breast Cancer Res Treat* (1993) 24(3):175–84. doi: 10.1007/bf01833258

3. Hüsemann Y, Geigl JB, Schubert F, Musiani P, Meyer M, Burghart E, et al. Systemic spread is an early step in breast cancer. *Cancer Cell* (2008) 13(1):58–68. doi: 10.1016/j.ccr.2007.12.003

4. Carey SP, Charest JM, Reinhart-King CA. Forces during cell adhesion and spreading: Implications for cellular homeostasis. In: A Gefen, editor. *Cellular and biomolecular mechanics and mechanobiology*. Berlin, Heidelberg: Springer Berlin Heidelberg (2011). p. 29–69.

5. Cuvelier D, Théry M, Chu YS, Dufour S, Thiéry JP, Bornens M, et al. The universal dynamics of cell spreading. *Curr Biol* (2007) 17(8):694–9. doi: 10.1016/j.cub.2007.02.058

6. Li YR, Yang WX. Myosins as fundamental components during tumorigenesis: Diverse and indispensable. *Oncotarget* (2016) 7(29):46785–812. doi: 10.18632/oncotarget.8800

7. Guan X. Cancer metastases: Challenges and opportunities. *Acta Pharm Sin B* (2015) 5(5):402–18. doi: 10.1016/j.apsb.2015.07.005

8. Kawahara E, Tokuda R, Nakanishi I. Migratory phenotypes of hsc-3 squamous carcinoma cell line induced by egf and pma: Relevance to migration of loosening of adhesion and vinculin-associated focal contacts with prominent filopodia. *Cell Biol Int* (1999) 23(3):163–74. doi: 10.1006/cbir.1998.0331

9. Peng X, Cuff LE, Lawton CD, DeMali KA. Vinculin regulates cell-surface e-cadherin expression by binding to beta-catenin. *J Cell Sci* (2010) 123(Pt 4):567–77. doi: 10.1242/jcs.056432

10. Li T, Guo H, Song Y, Zhao X, Shi Y, Lu Y, et al. Loss of vinculin and membrane-bound B-catenin promotes metastasis and predicts poor prognosis in colorectal cancer. *Mol Cancer* (2014) 13(1):263. doi: 10.1186/1476-4598-13-263

11. Peng X, Nelson ES, Maiers JL, DeMali KA. New insights into vinculin function and regulation. *Int Rev Cell Mol Biol* (2011) 287:191–231. doi: 10.1016/b978-0-12-386043-9.00005-0

12. Mierke CT. The role of vinculin in the regulation of the mechanical properties of cells. *Cell Biochem Biophys* (2009) 53(3):115–26. doi: 10.1007/s12013-009-9047-6

13. Hirohashi S, Kanai Y. Cell adhesion system and human cancer morphogenesis. *Cancer Sci* (2003) 94(7):575–81. doi: 10.1111/j.1349-7006.2003.tb01485.x

14. Martin TA, Mason MD, Jiang WG. Tight junctions in cancer metastasis. *Front Biosci-Landm* (2011) 16(3):898–936. doi: 10.2741/3726

15. Khalili AA, Ahmad MR. A review of cell adhesion studies for biomedical and biological applications. *Int J Mol Sci* (2015) 16(8):18149–84. doi: 10.3390/ijms160818149

16. Kokkinos PA, Koutsoukos PG, Deligianni DD. Detachment strength of human osteoblasts cultured on hydroxyapatite with various surface roughness. contribution of integrin subunits. *J Mater Sci: Mater Med* (2012) 23(6):1489–98. doi: 10.1007/s10856-012-4628-0

17. Christ KV, Turner KT. Methods to measure the strength of cell adhesion to substrates. *J Adhes Sci Technol* (2010) 24(13-14):2027–58. doi: 10.1163/016942410X507911

18. Bosch-Fortea M, Martín-Belmonte F. Mechanosensitive adhesion complexes in epithelial architecture and cancer onset. *Curr Opin Cell Biol* (2018) 50:42–9. doi: 10.1016/j.ceb.2018.01.013

19. Wirtz D, Konstantopoulos K, Searson PC. The physics of cancer: The role of physical interactions and mechanical forces in metastasis. *Nat Rev Cancer* (2011) 11(7):512–22. doi: 10.1038/nrc3080

20. Xi W, Schmidt CK, Sanchez S, Gracias DH, Carazo-Salas RE, Butler R, et al. Molecular insights into division of single human cancer cells in on-chip transparent microtubes. *ACS Nano* (2016) 10(6):5835–46. doi: 10.1021/acsnano.6b00461

21. Metsiou DN, Siatis KE, Giannopoulou E, Papachristou DJ, Kalofonos HP, Koutras A, et al. The impact of anti-tumor agents on er-positive mcf-7 and Her2-positive skbr-3 breast cancer cells biomechanics. *Ann Biomed Eng* (2019) 47 (8):1711–24. doi: 10.1007/s10439-019-02284-3

22. Boekhout AH, Beijnen JH, Schellens JH. Trastuzumab. *Oncologist* (2011) 16 (6):800–10. doi: 10.1634/theoncologist.2010-0035

23. Clemons M, Danson S, Howell A. Tamoxifen ("Nolvadex"): A review. *Cancer Treat Rev* (2002) 28(4):165–80. doi: 10.1016/s0305-7372(02)00036-1

24. Yao E, Zhou W, Lee-Hoeflich ST, Truong T, Haverty PM, Eastham-Anderson J, et al. Suppression of Her2/Her3-mediated growth of breast cancer cells with combinations of gdc-0941 Pi3k inhibitor, trastuzumab, and pertuzumab. *Clin Cancer Res An Off J Am Assoc Cancer Res* (2009) 15(12):4147–56. doi: 10.1158/1078-0432.ccr-08-2814

25. Metsiou DN, Kozaniti FK, Deligianni DD. Engineering breast cancer cells and humscs microenvironment in 2d and 3d scaffolds: A mechanical study approach of stem cells in anticancer therapy. *Bioengin (Basel)* (2021) 8(11):189. doi: 10.3390/bioengineering8110189

26. Moutzouri AG, Athanassiou GM. Insights into the alteration of osteoblast mechanical properties upon adhesion on chitosan. *BioMed Res Int* (2014) 2014:740726. doi: 10.1155/2014/740726

27. Deligianni DD, Katsala ND, Koutsoukos PG, Missirlis YF. Effect of surface roughness of hydroxyapatite on human bone marrow cell adhesion, proliferation, differentiation and detachment strength. *Biomaterials* (2001) 22(1):87–96. doi: 10.1016/s0142-9612(00)00174-5

28. Reutelingsperger CPM, Van Gool RGJ, Heijnen V, Frederik P, Lindhout T. The rotating disc as a device to study the adhesive properties of endothelial cells under differential shear stresses. *J Mater Sci: Mater Med* (1994) 5(6):361–7. doi: 10.1007/BF00058964

29. Jana A, Nookaew I, Singh J, Behkam B, Franco AT, Nain AS. Crosshatch nanofiber networks of tunable interfiber spacing induce plasticity in cell migration and cytoskeletal response. *FASEB J Off Publ Fed Am Soc Exp Biol* (2019) 33 (10):10618–32. doi: 10.1096/fj.201900131R

30. Cavallaro U, Christofori G. Cell adhesion in tumor invasion and metastasis: Loss of the glue is not enough. *Biochim Biophys Acta* (2001) 1552(1):39–45. doi: 10.1016/s0304-419x(01)00038-5

31. Paszek MJ, Weaver VM. The tension mounts: Mechanics meets morphogenesis and malignancy. *J Mamm Gland Biol Neoplas* (2004) 9(4):325–42. doi: 10.1007/s10911-004-1404-x

32. Meier SR, Korwin ML, Merzbacher CI. Carbon aerogel: A new nonreflective material for the infrared. *Appl Optic* (2000) 39(22):3940–4. doi: 10.1364/ao.39.003940

33. Broders-Bondon F, Nguyen Ho-Bouldoires TH, Fernandez-Sanchez M-E, Farge E. Mechanotransduction in tumor progression: The dark side of the force. *J Cell Biol* (2018) 217(5):1571–87. doi: 10.1083/jcb.201701039

34. Hanahan D, Weinberg RA. Hallmarks of cancer: The next generation. *Cell* (2011) 144(5):646–74. doi: 10.1016/j.cell.2011.02.013

35. Massalha S, Weihs D. Metastatic breast cancer cells adhere strongly on varying stiffness substrates, initially without adjusting their morphology. *Biomechanic Model Mechanobiol* (2017) 16(3):961–70. doi: 10.1007/s10237-016-0864-4

36. Barcus CE, Keely PJ, Eliceiri KW, Schuler LA. Stiff collagen matrices increase tumorigenic prolactin signaling in breast cancer cells. *J Biol Chem* (2013) 288(18):12722–32. doi: 10.1074/jbc.M112.447631

37. Guzman A, Ziperstein MJ, Kaufman LJ. The effect of fibrillar matrix architecture on tumor cell invasion of physically challenging environments. *Biomaterials* (2014) 35(25):6954–63. doi: 10.1016/j.biomaterials.2014.04.086

38. Daniele A, Zito AF, Giannelli G, Divella R, Asselti M, Mazzocca A, et al. Expression of metalloproteinases mmp-2 and mmp-9 in sentinel lymph node and serum of patients with metastatic and non-metastatic breast cancer. *Anticancer Res* (2010) 30(9):3521–7.

39. Cox TR, Bird D, Baker AM, Barker HE, Ho MW, Lang G, et al. Lox-mediated collagen crosslinking is responsible for fibrosis-enhanced metastasis. *Cancer Res* (2013) 73(6):1721–32. doi: 10.1158/0008-5472.can-12-2233

40. Turner MS, Sens P. Inclusions on fluid membranes anchored to elastic media. *Biophys J* (1999) 76(1):564–72. doi: 10.1016/S0006-3495(99)77224-3

41. Han W, Chen S, Yuan W, Fan Q, Tian J, Wang X, et al. Oriented collagen fibers direct tumor cell intravasation. *Proc Natl Acad Sci* (2016) 113(40):11208. doi: 10.1073/pnas.1610347113

42. Vu T, Claret FX. Trastuzumab: Updated mechanisms of action and resistance in breast cancer. *Front Oncol* (2012) 2:62. doi: 10.3389/fonc.2012.00062

43. Reinhart-King CA, Dembo M, Hammer DA. Cell-cell mechanical communication through compliant substrates. *Biophys J* (2008) 95(12):6044–51. doi: 10.1529/biophysj.107.127662

44. Döbereiner HG, Dubin-Thaler BJ, Giannone G, Sheetz MP. Force sensing and generation in cell phases: Analyses of complex functions. *J Appl Physiol* (2005) 98(4):1542–6. doi: 10.1152/japplphysiol.01181.2004

45. Weigelt B, Lo AT, Park CC, Gray JW, Bissell MJ. Her2 signaling pathway activation and response of breast cancer cells to Her2-targeting agents is dependent strongly on the 3d microenvironment. *Breast Cancer Res Treat* (2010) 122(1):35–43. doi: 10.1007/s10549-009-0502-2

46. Coughlin MF, Bielenberg DR, Lenormand G, Marinkovic M, Waghorne CG, Zetter BR, et al. Cytoskeletal stiffness, friction, and fluidity of cancer cell lines with different metastatic potential. *Clin Exp Metast* (2013) 30(3):237–50. doi: 10.1007/s10585-012-9531-z

47. Swaminathan V, Mythreye K, O'Brien ET, Berchuck A, Blobe GC, Superfine R. Mechanical stiffness grades metastatic potential in patient tumor cells and in cancer cell lines. *Cancer Res* (2011) 71(15):5075–80. doi: 10.1158/0008-5472.can-11-0247

48. Levental KR, Yu H, Kass L, Lakins JN, Egeblad M, Erler JT, et al. Matrix crosslinking forces tumor progression by enhancing integrin signaling. *Cell* (2009) 139(5):891–906. doi: 10.1016/j.cell.2009.10.027

49. Friedl P, Wolf K. Tumour-cell invasion and migration: Diversity and escape mechanisms. *Nat Rev Cancer* (2003) 3(5):362–74. doi: 10.1038/nrc1075

50. Onitilo AA, Engel JM, Greenlee RT, Mukesh BN. Breast cancer subtypes based on Er/Pr and Her2 expression: Comparison of clinicopathologic features and survival. *Clin Med Res* (2009) 7(1-2):4–13. doi: 10.3121/cmr.2009.825

51. Arpino G, Milano M, De Placido S. Features of aggressive breast cancer. *Breast* (2015) 24(5):594–600. doi: 10.1016/j.breast.2015.06.001

52. Meyer T, Brinck U. Immunohistochemical detection of vinculin in human rhabdomyosarcomas. *Gen Diagn Pathol* (1997) 142(3-4):191–8.

53. Somiari RI, Sullivan A, Russell S, Somiari S, Hu H, Jordan R, et al. High-throughput proteomic analysis of human infiltrating ductal carcinoma of the breast. *Proteomics* (2003) 3(10):1863–73. doi: 10.1002/pmic.200300560

54. Rodríguez Fernández JL, Geiger B, Salomon D, Sabanay I, Zöller M, Ben-Ze'ev A. Suppression of tumorigenicity in transformed cells after transfection with vinculin cdna. *J Cell Biol* (1992) 119(2):427–38. doi: 10.1083/jcb.119.2.427

55. Gu S, Papadopoulou N, Nasir O, Föller M, Alevizopoulos K, Lang F, et al. Activation of membrane androgen receptors in colon cancer inhibits the prosurvival signals Akt/Bad *in vitro* and *in vivo* and blocks migration *Via* Vinculin/Actin signaling. *Mol Med* (2011) 17(1-2):48–58. doi: 10.2119/molmed.2010.00120

56. Toma-Jonik A, Widlak W, Korfanty J, Cichon T, Smolarczyk R, Gogler-Piglowska A, et al. Active heat shock transcription factor 1 supports migration of the melanoma cells *Via* vinculin down-regulation. *Cell Signal* (2015) 27(2):394–401. doi: 10.1016/j.cellsig.2014.11.029

57. Coll JL, Ben-Ze'ev A, Ezzell RM, Rodríguez Fernández JL, Baribault H, Oshima RG, et al. Targeted disruption of vinculin genes in F9 and embryonic stem cells changes cell morphology, adhesion, and locomotion. *Proc Natl Acad Sci Unit States America* (1995) 92(20):9161–5. doi: 10.1073/pnas.92.20.9161

58. Sadano H, Inoue M, Taniguchi S. Differential expression of vinculin between weakly and highly metastatic B16-melanoma cell lines. *Japan J Cancer Res Gann* (1992) 83(6):625–30. doi: 10.1111/j.1349-7006.1992.tb00135.x

frontiers | Frontiers in Oncology

TYPE Original Research
PUBLISHED 18 August 2022
DOI 10.3389/fonc.2022.956940

Check for updates

OPEN ACCESS

EDITED BY
Alberto Passi,
University of Insubria, Italy

REVIEWED BY
Julia Fernandez-Perez,
Maastricht University, Netherlands
Qunyi Li,
Fudan University, China

*CORRESPONDENCE
Ander Abarrategi
aabarrategi@cicbiomagune.es

†These authors have contributed equally to this work

SPECIALTY SECTION
This article was submitted to Molecular and Cellular Oncology, a section of the journal Frontiers in Oncology

RECEIVED 30 May 2022
ACCEPTED 25 July 2022
PUBLISHED 18 August 2022

CITATION
Iazzolino G, Mendibil U, Arnaiz B, Ruiz-de-Angulo A, Azkargorta M, Uribe KB, Khatami N, Elortza F, Olalde B, Gomez-Vallejo V, Llop J and Abarrategi A (2022) Decellularization of xenografted tumors provides cell-specific *in vitro* 3D environment. *Front. Oncol.* 12:956940. doi: 10.3389/fonc.2022.956940

COPYRIGHT
© 2022 Iazzolino, Mendibil, Arnaiz, Ruiz-de-Angulo, Azkargorta, Uribe, Khatami, Elortza, Olalde, Gomez-Vallejo, Llop and Abarrategi. This is an open-access article distributed under the terms of the Creative Commons Attribution License (CC BY). The use, distribution or reproduction in other forums is permitted, provided the original author(s) and the copyright owner(s) are credited and that the original publication in this journal is cited, in accordance with accepted academic practice. No use, distribution or reproduction is permitted which does not comply with these terms.

Decellularization of xenografted tumors provides cell-specific *in vitro* 3D environment

Gaia Iazzolino[1†], Unai Mendibil[1,2†], Blanca Arnaiz[1†], Ane Ruiz-de-Angulo[1], Mikel Azkargorta[3], Kepa B. Uribe[1], Neda Khatami[1], Felix Elortza[3], Beatriz Olalde[2], Vanessa Gomez-Vallejo[1], Jordi Llop[1] and Ander Abarrategi[1,4*]

[1]Center for Cooperative Research in Biomaterials (CIC biomaGUNE), Basque Research and Technology Alliance (BRTA), Donostia-San Sebastian, Spain, [2]TECNALIA, Basque Research and Technology Alliance (BRTA), Donostia-San Sebastian, Spain, [3]Center for Cooperative Research in Biosciences (CIC bioGUNE), Basque Research and Technology Alliance (BRTA), Derio, Spain, [4]Ikerbasque, Basque Foundation for Science, Bilbao, Spain

In vitro cell culture studies are common in the cancer research field, and reliable biomimetic 3D models are needed to ensure physiological relevance. In this manuscript, we hypothesized that decellularized xenograft tumors can serve as an optimal 3D substrate to generate a top-down approach for *in vitro* tumor modeling. Multiple tumor cell lines were xenografted and the formed solid tumors were recovered for their decellularization by several techniques and further characterization by histology and proteomics techniques. Selected decellularized tumor xenograft samples were seeded with the HCC1806 human triple-negative breast cancer (TNBC) basal-like subtype cell line, and cell behavior was compared among them and with other control 2D and 3D cell culture methods. A soft treatment using Freeze-EDTA-DNAse allows proper decellularization of xenografted tumor samples. Interestingly, proteomic data show that samples decellularized from TNBC basal-like subtype xenograft models had different extracellular matrix (ECM) compositions compared to the rest of the xenograft tumors tested. The *in vitro* recellularization of decellularized ECM (dECM) yields tumor-type–specific cell behavior in the TNBC context. Data show that dECM derived from xenograft tumors is a feasible substrate for reseeding purposes, thereby promoting tumor-type–specific cell behavior. These data serve as a proof-of-concept for further potential generation of patient-specific *in vitro* research models.

KEYWORDS

tumor xenograft, decellularization, *in vitro*, 3D model, breast cancer

Introduction

Understanding the biology of tumor initiation and progression processes has a huge impact on the successful development of novel and effective cancer treatments (1). Despite its high cost and ethical concerns, *in vivo* human tumor cell xenografting in mouse orthotopic and ectopic locations remains the most reliable experimental model to mimic tumor microenvironment and to study, among others, tumor formation and progression processes (2). Moreover, *in vitro* monolayer culture of cancer cells in a two-dimensional (2D) environment is a highly popular and straightforward method to perform cancer-related preclinical research (3). However, 2D cell cultures are considered too simplistic to accurately test solid tumor-derived cell behavior, as they do not resemble the tumor's three-dimensional (3D) architecture and the lack of mechanical/biochemical signals coming from 3D cell–cell and cell–matrix interactions (4, 5).

In comparison to 2D cell cultures, 3D cell culture models are more accurate tumor-mimicking approaches (6) because they present enhanced cell–matrix and cell–cell interactions while modulating differently those signaling pathways related to cell migration, morphology, proliferation, and viability (7–10). Among *in vitro* cancer 3D models, those promoting extracellular matrix (ECM) and cell interaction are considered the most relevant. For example, hydrogels formed with the ECM extracted for cell-cultured tumor cells (e.g., Matrigel) are widely exploited in cancer research as matrices for tumor cell seeding and study (3, 11). These hydrogels provide chemical and physical characteristics potentially beneficial to mimicking tumor 3D environment, as they have ECM structural proteins (e.g., collagens) to which cells can attach, along with growth factors, hormones, and other essential molecules (12). Despite having noteworthy properties, commercially available cell culture extracted ECM and their hydrogels possess various significant drawbacks. Most notably, by using this commercial ECM as a 3D culture environment, the target cells are exposed to an ECM composition different from the one of the specific tumor to be studied. Moreover, the cells at hydrogels grow as spheroids, and therefore, they lose their original morphology, mobility, and cell–cell and cell–matrix interactions. Furthermore, from a technical point of view, the postprocessing steps required after decellularization may induce a loss in the processed material and that is not assumable when handling small decellularized samples.

Aiming to define more reliable and tumor-specific 3D cancer models, bioengineered approaches have recently been explored. For example, hydrogels have been structured using 3D bioprinting technology to generate matrices or microfluidic cancer-on-a-chip models. On the other hand, spontaneous spheroids formed by target cells have been considered a potential valid *in vitro* tumor-mimicking model, while tumor organoids formed by the multiple cell types present in the targeted tumor are the ultimate promise to mimic tumor complexity in *in vitro* structures (13–21).

Decellularization is a propitious approach in which cells are removed from tissues or organs, thereby isolating the ECM structure to be recovered (22). This technique provides an advantageous approach to producing more effective tissue models in which ECM and tissue architecture are preserved (23). The advantage of using biologically derived matrices for *in vitro* 3D studies is that some part of the major proteins and factors already exist in the decellularized scaffold, which makes them useful in a wide range of applications, from physiological regenerative medicine to pathological (cancer) research studies (24–30).

Decellularized ECM (dECM) can be obtained from both normal and tumor tissues following several types of decellularization protocols, including physical, chemical, or enzymatic methods reported in the literature. The different decellularization methods alter the ECM components differently, and therefore, it is important to define the tissue-specific decellularization method in each context (31). dECM can then be used as a 3D scaffold or it can be processed for hydrogel formation (32, 33). Matrices from normal tissue can be used to recognize novel genes inducing cancer or the interactions between cancer cells and healthy ECM. On the other hand, decellularized tumor tissue is more appropriate for studying the influence of pathological ECM on controlling cancer cell function at primary or metastatic sites and the role of ECM as a modulator of cell behavior (34–37).

In this manuscript, we hypothesized that decellularized xenograft tumors can serve as an optimal 3D substrate to generate a top-down approach for *in vitro* tumor modeling. Aiming to prove that, we xenografted multiple tumor cell lines and the formed solid tumors were recovered for their decellularization by several techniques. Data indicate a soft decellularization protocol based on tumor freezing followed by EDTA treatment allows the recovery of dECM with tumor-type–specific protein components. When used as a substrate for human triple-negative breast cancer cell seeding, and compared to other 3D cell culture models, a characteristic cell behavior was observed in terms of cell morphology, proliferation, and mobility.

Materials and methods

Cell cultures

Cell lines were numbered from 1 to 13 for easy trackability of samples during the study (see Table 1). MDA-MB-231 (RRID : CVCL_0062), MIA PaCa-2 (RRID : CVCL_0428), PANC-1 (RRID : CVCL_0480), U87 (RRID : CVCL_0022), HepG2 (RRID : CVCL_0027), and Du145 (RRID : CVCL_0105) cell lines were cultured in DMEM (11995065; Gibco, UK); 4T1 (RRID : CVCL_JG34), HCC1806 (RRID : CVCL_1258), and

TABLE 1 Tumor cell lines, origin, and provided number.

Cell line number	Cell line name	Tumor tissue	Organism	Number (*n*) of implants	Time for engraftment (days)	Volume at harvest (mm^3)
1	MDA-MB-231	Breast	Human	6	45	89 ± 37
2	4T1	Breast	Mouse	6	7	463 ± 205
3	HCC 1806	Breast	Human	6	15 ± 6	321 ± 82
4	AR42J	Pancreas	Rat	7	28 ± 1	1,065 ± 390
5	Capan 1	Pancreas	Human	6	60 ± 7	223 ± 122
6	MIA PaCa-2	Pancreas	Human	6	43 ± 15	310 ± 258
7	PANC-1	Pancreas	Human	7	45	138 ± 42
8	Du145	Prostate	Human	7	33 ± 1	133 ± 25
9	PC-3	Prostate	Human	7	45	240 ± 66
10	U-87	Brain	Human	7	42 ± 3	1,140 ± 379
11	HepG2	Liver	Human	7	45	302 ± 196
12	PC-12	Adrenal gland	Rat	6	35 ± 5	504 ± 210
13	GH4	Pituitary	Rat	6	21 ± 5	262 ± 39

AR42J (RRID : CVCL_0143) cell lines were cultured in RPMI-1640 (11875101; Gibco, UK); Capan1 (RRID : CVCL_0237) and Pc3 (RRID : CVCL_0035) cell lines were cultured in F12K (21127022, Gibco, UK); and GH4 (RRID : CVCL_WX20) cell line was cultured in Ham's F10 (11550043, Thermo Fisher). All media were supplemented before being used with 10% fetal bovine serum (10500-064, Gibco, UK), 2 mM L-glutamine (25030024, Gibco, UK), and 50 U/ml penicillin and 50 µg/ml streptomycin (15070063, Gibco, UK). As an exception, AR42J cells required 20% fetal bovine serum as a supplement.

Xenografted tumor generation

Animals were cared for and handled following internal guidelines and in compliance with the European Guidelines for Accommodation and Care of Animals. The study was conducted in accordance with the Declaration of Helsinki and approved by the Ethics Committee of CICbiomaGUNE and local authorities (protocol code PRO-AE-SS-166 and date of approval 01/06/2019).

Cells were resuspended in Matrigel HC (354248, Corning, USA) diluted 1:4 in cold Dulbecco's phosphate-buffered saline (DPBS, 14040-091, Gibco, UK) and injected in the back (100 µl/animal) of 6–8-week-old athymic nude mice (Crl : NU(NCr)-Foxn1nu, Charles River). Animals were monitored for tumor growth using an electronic digital caliper 779A series (Starrett) (see Table 1). At the endpoint, animals were processed for perfusion with heparinized physiological serum. The tumors were extracted, deposited in a sterile container, and stored at −80C.

Decellularization protocol

The tumors were thawed and sectioned into 30 mg pieces for further decellularization. Six custom protocols were used in the initial studies (see Table 2).

Protocol "a" corresponds to 15 freezing cycles. Protocol "b" corresponds to three washes of DNase (Sigma-Aldrich) at 37°C in agitation. Protocol "c" uses Trypsin-EDTA (25050-014, Sigma-Aldrich, USA) over 30 min at 37°C in agitation, followed by the DNase (7469, StemCell, CA) treatment mentioned in protocol b. Protocol "d" uses EDTA (E9884, Sigma-Aldrich, USA) for 30 min at room temperature (RT) in agitation, followed by the DNase treatment mentioned in

TABLE 2 Treatment type and concentrations used in each one of the decellularization protocols.

Protocol	DNase (U/ml)	Freezing (cycles)	Trypsin (% w/v)	Triton X-100 (% w/v)	EDTA (% w/v)
a	–	15 cycle	–	–	–
b	50 U/ml	–	–	–	–
c	50 U/ml	–	0.25%	–	0.25%
d	50 U/ml	–	–	–	2%
e	50 U/ml	15 cycle	–	–	2%
f	50 U/ml	–	–	1%	–

protocol b. Protocol "e" uses the freezing cycles of protocol a, followed by treatment mentioned in protocol d. Protocol "f" uses Triton X-100 (T9284, Sigma-Aldrich, USA) for 30 min at RT in agitation, followed by the DNase treatment mentioned in protocol b. In all protocols, each step was followed by three DPBS washes in agitation for 20 min at RT.

DNA extraction and quantification

To verify the decellularization efficiency, the DNA was extracted and quantified. The extraction was performed using the EchoLUTION Tissue DNA Micro Kit (010-002-010, BioEcholife), and for the DNA quantification, a NanoDrop (Jasco V-730) spectrophotometer was used. Data were obtained as nanograms of DNA per milligram of the wet original tissue. According to the ASTM International standards, 50 ng of DNA/mg of tissue was established as the acceptable DNA threshold to consider the tumor as decellularized (38).

Histology of the decellularized tissues

Samples were embedded in Tissue Tek OCT (4583, Sakura Finetek, Japan), stored at −20°C, and sliced in the cryostat (CM1860, Leica). To check the nuclei distribution changes and the overall ECM structure, the slides were fixed for 1 h with neutral buffered 10% formalin solution (HT501128, Sigma-Aldrich, USA) and stained with hematoxylin (5 min) and eosin (2 min) (05-M06015 and 05-M10003, Bio-Optica, It).

Collagens and noncollagenous proteins of dECM were visualized by staining the samples with the Sirius Red/Fast Green Staining kit (9046, Chondrex, USA). This is a differential staining with two dyes, as Sirius Red binds to all types of collagen, whereas Fast Green stains noncollagenous proteins. All histology samples were visualized on a routine optical microscope equipped with a camera.

Scanning electron microscopy

The decellularized samples were frozen at −20°C for 24 h and subsequently lyophilized for 24 h. A sputter coater (Alto 1000, Galan) was used to coat the sample's surface with gold/palladium before their visualization in JSM-6490LV (JEOL) scanning electron microscope (SEM) equipment.

Proteomics and mass spectrometry

Proteins were extracted from decellularized samples using a mixture of 7 M urea, 2 M thiourea, 4% CHAPS, and 5 mM DTT and then digested following the filter-aided FASP protocol described by Wisniewski et al. (39) with minor modifications. Briefly, trypsin was added to a trypsin:protein ratio of 1:20, and the mixture was incubated overnight at 37°C, dried out in a RVC2 25 speedvac concentrator (Christ), and resuspended in 0.1% FA. Peptides were desalted and resuspended in 0.1% FA using C18 stage tips (Millipore).

Samples were analyzed on a timsTOF Pro with PASEF (Bruker Daltonics) coupled online to an Evosep ONE liquid chromatograph (Evosep). A total of 200 ng was directly loaded onto the Evosep ONE and resolved using the 30 sample-per-day protocol.

Protein identification and quantification were carried out using MaxQuant software (40) using default settings except for the match between runs (match time window of 5 min, alignment tie window of 20 min) and an LFQ min. ratio count of 1. Searches were carried out against a database consisting of human and mouse protein entries (Uniprot/Swissprot), with precursor and fragment tolerances of 20 ppm and 0.05 Da. Only proteins identified with at least two peptides at FDR<1% were considered for further analysis. LFQ intensities were used for further analyses and loaded onto the Perseus platform (41).

Data were loaded onto the ClustVis web tool for the visualization and clustering of multivariate data using principal component analysis (PCA) (42). Data were loaded to MetaboAnalyst to be normalized and statistically analyzed. Partial least squares discriminant analysis (PLS-DA) was used to get the variable importance in projection (VIP) and differentiate the groups. For the Gene Ontology (GO) analysis ShinyGO web tool was used. All the results were represented using Graphpad Prism software.

The original contributions presented in the study are publicly available. The mass spectrometry proteomics data have been deposited to the ProteomeXchange Consortium. Data can be found here: [PXD034597].

In vitro cell culture

HCC1806 (RRID : CVCL_1258) cell line cultured in RPMI-1640 was used for materials seeding studies. Control collagen scaffolds (20483, collagen wound dressing Suprasorb® C, Lohmann&Rauscher, Austria) and tumor-derived dECMs were firstly cut into smaller pieces of approximately 3–10 mm and sterilized. Briefly, frozen tumor small pieces were thawed and two washes of ethanol (diluted to 70%, Et 00020005P, Sharlau, Spain) for 15 min were performed, followed by cleaning and rehydration by three washes at sterile DPBS for 5 min. Furthermore, UV light irradiation was applied for 18 h inside a cabinet (Bio II Advance Plus, Telstar, Japan). The cells were deposited similarly to what was previously described for other similar materials (43–45). Each material piece was transferred to a 48-well plate well (3548, Costar, USA) and injected with 30 µl

of a cell dilution, trying to seed evenly all around the sample, resulting in 70,000 HCC1806 cells seeded per sample. In parallel, cells in sterile DPBS were mixed in a ratio of 1:4 with Matrigel® to achieve a final concentration of Matrigel of 4 mg/ml for hydrogel formation into a 96-well plate (92096, TPP, Switzerland). Cell-seeded samples were incubated at 37°C and 5% CO_2 for 1 h in a Forma Steri-cycle CO_2 incubator (Model 381 Thermo Scientific, USA), then covered with complete warm complete RPMI-1640 media and finally cultured at 37°C and 5% CO_2 for 3 days.

Cell morphology and immunostaining

Actin fibers and nuclei were stained as follows. Samples were washed with DPBS and fixed in 10% formalin solution, neutral buffered (HT501128, Sigma-Aldrich, USA) for 30 min, washed with DPBS, and incubated with DPBS containing ActinRed555 ReadyProbes reagent (1/10 dilution, R37112, Invitrogen, USA) for 30 min at 37°C. Following two washes with DPBS, the scaffolds and cells were imaged in DPBS containing 5 ng/ml 2-[4-(aminoiminomethyl)phenyl]-1H-Indole-6-carboximidamide hydrochloride (DAPI) (D9542, Sigma-Aldrich, USA).

For immunolabeling of the Ki67 nuclear marker, samples were permeabilized by 5 min incubation in DPBS supplemented with 0.1% Triton X-100 (T9284, Sigma-Aldrich, USA) and washed for 5 min in DPBS. Blocking of unspecific binding sites was achieved by 30 min incubation with 1% bovine serum albumin (BSA, A7906, Sigma-Aldrich, USA) in DPBS containing 0.1% Tween 20 (DPBST, P9416, Sigma-Aldrich, USA). The Ki67 nuclear marker was then labeled by incubation with 1% BSA in DPBST containing rabbit anti-human Ki67 primary recombinant monoclonal antibody (1:200 dilution, MA5-14520 Invitrogen, USA) at 4°C overnight in a humidified chamber. Samples were washed three times with DPBS and incubated for 1 h in the dark with a donkey anti-rabbit antibody polyclonal highly cross-absorbed with Alexa Fluor Plus 488 (dilution 1:500, A32790, Invitrogen, USA) in 1% BSA DPBST. Samples were then washed with DPBS, stained with DAPI-containing (5 ng/ml) DPBS, and imaged. All the incubation times described above were doubled in the assays, including the Matrigel® matrix.

For cell imaging, the scaffolds with fluorescently labeled cells were kept covered with DPBS in a 35-mm-diameter ≠1.5 optical glass bottom dish (D35-20-1.5-N, Cellvis, CA). Single plane images were taken in a Laser Scanning Confocal Microscope (Zeiss LSM 880, Carl Zeiss AG, Germany) with the Plan-Apochromat ×10/0.45 employing the excitation/emission wavelengths of 561 nm/610–715 nm for Actin Red 555, 405 nm/420–475 nm for DAPI, and 488 nm/500–600 nm for Ki67 labeled with Alexa Fluor 488 (AF488). For imaging the tumor-derived dECM scaffolds, 458 nm/441–471 nm or 633 nm/620–650 nm were used in reflection mode, while transmitted light was used in the case of collagen-based scaffolds or Matrigel® matrix samples. In total, 20 to 40 μm Z-stacks were imaged, and maximum intensity z-tack projections were obtained. For quantification purposes, ×10 images were used, and data were normalized to the nuclei number in each image.

For the quantification of $Ki64^+$ nuclei and the mean cell area, the FIJI image analysis software was employed. FIJI is a distribution of the popular open-source software ImageJ (National Institutes of Health, USA) focused on biological-image analysis (46).

To calculate the $Ki64^+$ nuclei, immunostaining for Ki67 in green (AF488) and counterstaining of nuclei in blue (DAPI) were employed for proliferative nuclei stain and general nuclei stain, respectively (green and blue channels). Regions of interest (ROI, objects) were automatically drawn for the nuclei, and a mask is generated. The mask was overlaid on the image with the $Ki67^+$ image. The percentage of proliferating cells was calculated as a ratio of $Ki67^+$ objects to nuclei counts (total object number).

To calculate the mean cell area, ActinRed555 and DAPI stains were employed for cell and nucleus delimitation, respectively. Once the cells were delimited (objects), the area of the objects was measured. Finally, the mean cell area was calculated by dividing the total area of the objects by the total amount of nuclei in each picture.

Live imaging

Complete RPMI-1640 media of samples in a 35-mm-diameter ≠1.5 optical glass bottom dish was replaced by warm complete RPMI-1640 media containing 1.5 to 2.5 μg/ml Calcein-AM (56496, Sigma-Aldrich, USA) and incubated for 30 min at 37°C and 5% CO_2. Samples were transferred to a Laser Scanning Confocal Microscope (Zeiss LSM 880, Carl Zeiss AG, Germany) equipped with a ×20/0.8 objective lens and a chamber to keep conditions of 95% humidity, 37°C, and 5% CO_2 during Z-stacks image acquisition period using 488 nm/500–600 nm excitation/emission wavelengths. Z-stacks are presented as maximum intensity Z-projection images employing the Zen Blue software v2.3 (Carl Zeiss AG, Germany).

For live time-lapse imaging, images were acquired for 5 h every 15 min employing the Axio Observer Z1 microscope (Carl Zeiss AG, Germany) with the EC Plan-NEOFLUAR 5×/0.16 Ph1 M27, the LED illumination module at 470 nm, and the 38 HE eGFP shift free filter set. In addition, during the acquisition, samples were kept at 37°C and 5% CO_2 inside the equipment in an Incubator XL S1 (Carl Zeiss AG, Germany). Live cell single plane images were also acquired in the LSM 880 confocal microscope with a heating insert P S1 (130-800 005, PeCon, Germany) for temperature and atmosphere control. For video processing, the Zen Blue software v2.3 (Carl Zeiss AG, Germany) was employed. The screen recorder software OBS Studio v37.2.4 (© 2022 GitHub, Inc. CA) was used for additional

video editing. To measure cell displacement, the videos were analyzed with the FIJI plugin TrackMate v2.1.0 (47) that semiautomatically segments fluorescent cells present in the first frame and generate tracks that follow each cell through the rest of the video frames giving a score equal to the number of frames in which a particular cell was found. The resulted list, including the tracking number, frame number, and the position (x/y) of each cell in the image, is next analyzed by the Chemotaxis and Migration Tool 2.0 software (ibidi GmbH, Germany) to plot a Cell Tracking graph for the displacement of cells in a centered coordinate grid and to calculate the accumulated distance of each cell after the 5 h that lasted for the recording (image scaling, 3.87 µm per pixel).

Statistics

All data were plotted and statistically analyzed using the Graphpad Prism software (La Jolla, CA, USA). In all cases, data normality was verified using the Shapiro–Wilk test and a normal QQ plot was assessed. Data that passed the normality test (alpha = 0.05) were statistically analyzed using parametric tests (ordinary one-way ANOVA) and Tukey's multiple comparisons tests. Data that did not pass the normality test (alpha = 0.05) (data in Figure 6G) were analyzed using the Kruskal–Wallis nonparametric test and Dunn's multiple comparisons tests. Data are presented as mean ± SD, and each individual point is provided in the plots. Additionally, the n number of each assay is provided in the figure legends. P values of less than 0.05 were considered statistically significant (ns $p > 0.05$; $^{*}p < 0.05$; $^{**}p < 0.01$; $^{***}p < 0.001$).

Results

A soft treatment based on Freeze-EDTA-DNAse allows tumor decellularization

Tumor xenografts (Figure 1A) obtained from the MDA-MB-231 cell line, numbered as 1 in Table 1, were tested for decellularization with multiple custom-designed decellularization protocols (see Table 2). The DNA quantification results in Figure 1B (and Supplementary Table S1) show that protocols e and f successfully reduced the DNA content below the 50-ng DNA/mg tissue threshold. The histology examination in Figure 1C, H&E staining for nucleic acids and ECM, confirms the absence of hematoxylin-related purple nucleic acid staining in e and f protocol-treated decellularized samples but the presence of eosin-related ECM pink staining in all samples. In Figure 1C, Sirius Red/Fast Green dye combination staining is shown. It is used to distinguish collagen from its surrounding materials, as Sirius Red stains collagens in red, while Fast Green stains noncollagenous proteins in green. Samples treated with the protocol e (freezing cycles followed by EDTA) stain red and green similar to the control untreated samples. However, trypsin enzyme-treated and Triton X-100 detergent-treated samples showed an absence of the green color, which is typical of the ECM noncollagenous protein staining. Altogether, data in Figure 1 indicate that the treatment of MDA-

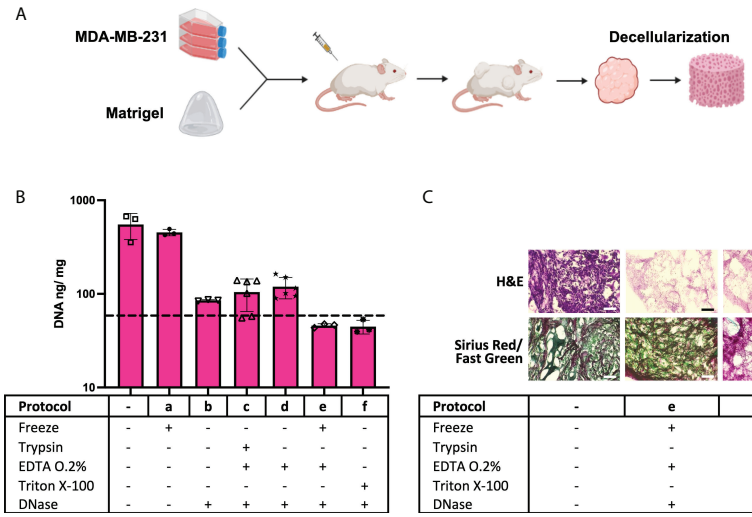

Protocol	-	a	b	c	d	e	f
Freeze	-	+	-	-	-	+	-
Trypsin	-	-	-	+	-	-	-
EDTA O.2%	-	-	-	+	+	+	-
Triton X-100	-	-	-	-	-	-	+
DNase	-	-	+	+	+	+	+

Protocol	-	e	c	f
Freeze	-	+	-	-
Trypsin	-	-	+	-
EDTA O.2%	-	+	+	-
Triton X-100	-	-	-	+
DNase	-	+	+	+

FIGURE 1
Enzyme and detergent-based protocols yield different decellularization outcomes. **(A)** Schematic of cell xenografting in mice: tumor formation, sample harvesting, and decellularization. **(B)** DNA quantification data on control samples and "a" to "f" protocol-treated samples (n = 3 to 6). The dotted line indicates the 50-ng DNA/mg tissue threshold used to define successful decellularization. **(C)** Histology assessment of samples. (Black and white scales represent 100 µm).

MB-231 cell line tumor xenografts with a protocol based on freezing cycles-EDTA-DNAse allowed for sample decellularization and proper preservation of tumor ECM in terms of collagens and proteins. Following these data, multiple types of tumor xenografts were processed using the decellularization protocol e. As it is shown in Figure 2 (and Supplementary Table S2), in all cases, the treatment yields a successful xenograft tumor sample decellularization.

Triple-negative breast cancer basal-like subtype xenograft tumors show a distinctive ECM protein composition after decellularization

A proteomic study was performed to define the composition of the decellularized ECM. Matrigel was included in the study as a control ECM. Figure 3 (and Supplementary Figure S1) shows the number of total proteins detected in each kind of sample. A GO analysis revealed an enrichment of proteins related to "extracellular space" in all tested samples and also the existence of proteins from mitochondria and endoplasmic reticulum (ER), possibly related to cellular debris (Figure 3B).

A more detailed study of extracellular space proteins (Figures 3C, D) revealed a group of roughly 200 proteins commonly present in all samples, including control Matrigel. There was another group of proteins commonly present only in xenografted tumor samples, while all samples presented a high number of sample-specific extracellular space proteins. Further GO analysis (Figure 3D) revealed a specific enrichment on proteins related to secretory vesicles and extracellular matrix. The group of extracellular space proteins present in control Matrigel was compared to all other target tumor xenograft samples, aiming to identify ECM proteins down- or upregulated in xenografted tumors compared to the control Matrigel condition. In this sense, Matrigel showed a higher amount of Fibulin-1 and LAMA5 laminin subunit, two components previously related to the inhibition of tumor progression processes because they mediate different cell attachment, migration, and organization processes into tissues.

The principal component analysis revealed again that all decellularized xenografted tumors had a protein composition different from the control Matrigel (Figure 4A). Moreover, this principal component analysis revealed that two triple-negative breast cancer xenograft-decellularized samples were different from all other samples. These samples correspond to triple-negative breast cancer (TNBC) basal-like subtype. A detailed study of discriminant differences between samples revealed the 50 more significant differentially present proteins in these two TNBC samples. The heat map representation of these proteins shows that most of them were overrepresented in these two TNBC samples, compared to all other decellularized xenografted tumor samples (Figure 4B). GO analysis of the 50 proteins indicates they were mainly proteins with catalytic activity and related to lipidic and cholesterol metabolism (Figure 4C). These differences may be related to the observed incomplete removal of cell mitochondrial and/or ER components, which would show up the differences in cell metabolism along the different tumor xenografts tested, a feature specifically relevant for TNBC basal-like subtype samples.

HCC1806 TNBC cells show substrate-specific behavior when seeded on their tumor xenograft-derived dECM

One of the potential applications of tumor dECM is as a substrate in cell culture studies to generate *in vitro* cancer models. As shown in Figure 4C, dECM from HCC1806 and 4T1-xenografted tumors show a differential composition in the proteomic PC analysis. At this point, we hypothesized that this specific protein composition may modulate cell behavior in *in vitro* studies. Therefore, we considered them a promising

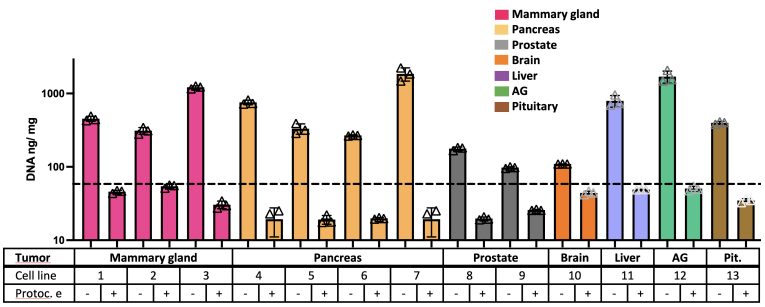

FIGURE 2
Freeze-EDTA-DNAse protocol decellularizes multiple tumor xenografts. DNA quantification data on control samples and "e" protocol-treated samples from multiple types of tumor xenografts (n = 3). The dotted line indicates the 50-ng DNA/mg tissue threshold used to define successful decellularization. Note: cell line number codes are provided in Table 1.

10.3389/fonc.2022.956940

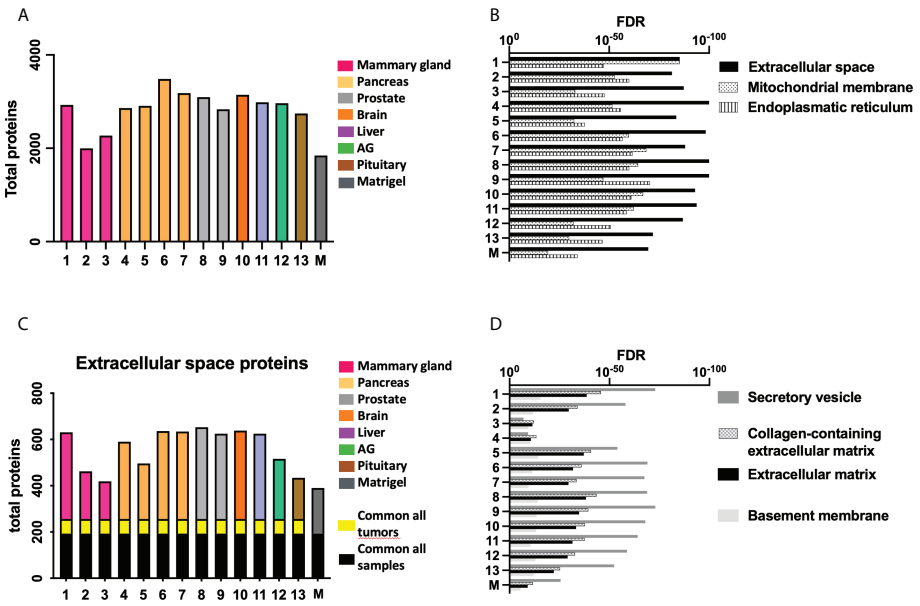

FIGURE 3
Proteomic study shows differences in ECM composition among samples. **(A)** Total amount of proteins detected in the proteomic study. **(B)** The most relevant Gene Ontology (GO) terms related to retrieved proteins in each sample. **(C)** The number of proteins from the GO term "Extracellular space" present in each sample, and the **(D)** GO terms related to these shortlisted proteins. Note: cell line number codes are provided in Table 1. The same tumor color codes are used in all panels of the figure.

substrate with specific features to be tested in a cell culture context. Specifically, we wondered whether the cells that generated these tumors would behave differently on their specific tumor-derived dECM compared to other substrates. As 4T1 is a mouse cell line, we selected the HCC1806 human cell line to follow with *in vitro* cell culture studies and characterized the potential of the generated tumor dECM as *in vitro* model for cell culture studies. First, three different tumor xenograft dECM were selected to be cell-seeded. The selected samples correspond to tumor-derived dECM from the PC-3 human prostate model, PANC-1 human pancreas model, and HCC1806 human TNBC basal-like subtype model. Moreover, a commercially available collagen-based foam was included as a control (Figure 5).

Initial SEM imaging revealed that all dECM and control collagen foam present an open porous scaffold structure (Figure 5A; Supplementary Figure S2). Three days after cell seeding, substrate-attached live cells were detected on all samples (Figure 5B, green cells correspond to calcein live dye positive cells). After sample fixation, cell morphology was analyzed by detecting the area of the cells (Figure 5C, actin cytoskeleton staining in orange, cell nuclei in blue). Images indicate morphological differences related to seeding substrate, with more spread cell morphology and bigger cells on HCC1806 xenograft dECM substrate. Additional immunostaining studies were performed to visualize proliferative cells (Figure 5D, cell nuclei in blue and Ki67 proliferation marker observed as green dots at cell nuclei area). Quantitative data were obtained for cell morphology (Figure 5E), and cell proliferation (Figure 5F) and data show statistically significant differences related to cell size and proliferation rate of the cells seeded on the HCC1806 dECM substrate.

Similar cell staining and measurement tools were used to define any potential cell-behavior difference between HC1806 xenograft dECM and other common 2D and 3D substrates, such as plastic cell culture substrate or Matrigel 3D cell culture methods. Live cells were observed in all cell-seeding models (Figure 6A, green cells correspond to calcein live dye positive cells). After fixation, actin cytoskeleton staining (Figure 6B, actin cytoskeleton staining in orange and cell nuclei in blue) and Ki67 proliferative maker staining (Figure 6C, cell nuclei in blue and Ki67 observed as green dots at cell nuclei area) were performed. Images indicate differences in cell morphology with more pronounced morphology in 2D cultures and dECM matrix compared to spheroid formation in Matrigel cell cultures. Quantitative data for cell morphology (Figure 6E) and cell proliferation (Figure 6F) show statistically significant differences in the measured parameters. Additionally, displacement of calcein-positive live cells was recorded and plotted (Figure 6D; Supplementary Figure S3), suggesting cells at Matrigel barely move. Quantification in Figure 6G indicates statistically significant differences related to cell movement.

10.3389/fonc.2022.956940

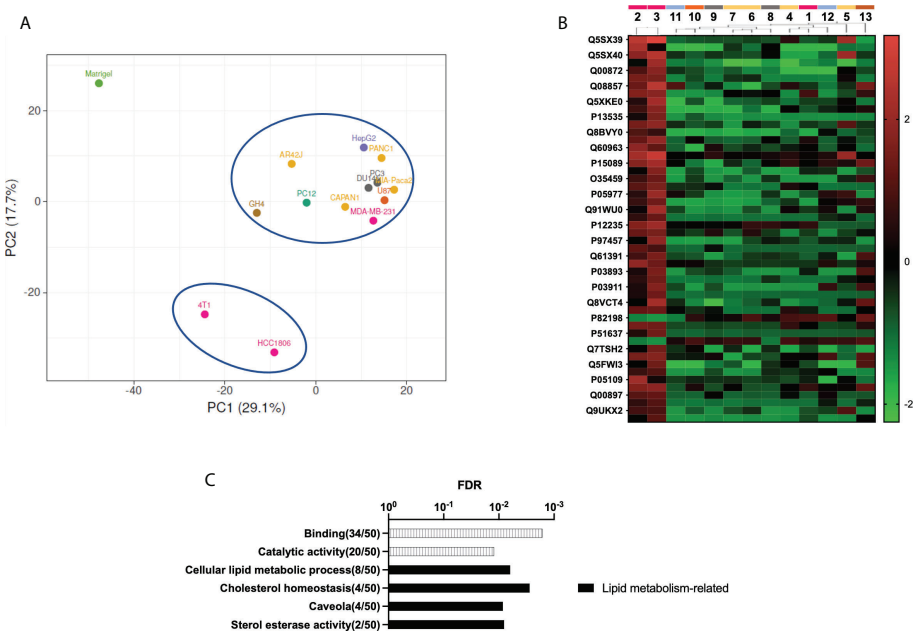

FIGURE 4
Proteomic study shows distinctive ECM on decellularized TNBC xenograft samples. **(A)** Principal component analysis (PCA). Matrigel control samples are plotted separately from all tumor xenograft samples. Tumor xenograft samples come out splinted into two groups, with the two TNBC xenograft-derived samples separated from the rest of the samples. **(B)** Heat map representation of the 50 more discriminant proteins obtained by partial least squares discriminant analysis (PLS-DA). **(C)** GO analysis of the 50 more discriminant proteins. Note: cell line number codes are provided in Table 1. The same tumor color codes are used in all panels of the figure.

Discussion

Cancer solid mass decellularization has been tested before in different research contexts and for multiple research purposes (35). In this manuscript, we aimed to prove that xenografted tumor-derived dECM may be achieved and used as a substrate on which the same cell line can be seeded again, thereby yielding a biomimetic, tumor-cell context-simulating, *in vitro* 3D cell culture system. For this purpose, we generated a multidisciplinary research approach compiling; animal research for xenotransplantation and generation of the raw tumors; material research for decellularization of samples; proteomics for sample characterization; and *in vitro* cell culture studies to prove the feasibility and outcome of the approach.

The previous bibliography in the tumor decellularization field tends to show studies decellularizing one specific type of tumor, with scarce research on optimization of the decellularization protocol and usually reporting sequential enzymatic- (trypsin) and detergent-based (Triton X-100) decellularization (48, 49). On the contrary, in the physiological tissue decellularization context, the development of tissue-specific decellularization protocols has gained relevance, and multiple decellularization protocol comparative research studies are common (50–52). Therefore, in our research approach, we defined the initial objective of the study and defined a decellularization protocol broadly useful in multiple solid tumor contexts.

In this sense, we generated a cohort of 13 different xenografted tumor cell lines, corresponding to seven different tissues of origin (Table 1). We then chose one of them to test some of the most common decellularization procedures, e.g., trypsin-EDTA and Triton X-100, in xenografted tumors (Figure 1). As controls, we included protocols with only the complementary reagents or treatments, such as multiple freezing of the raw tissue to easy cell detachment from the ECM; DNAse treatment to eliminate cell waste; and EDTA treatment as ion chelator to break integrin-ECM interaction. Note that EDTA is considered a gentler cell detaching agent when used in a cell culture context, and it is generally used in combination with trypsin, a protease effective for cell detachment purposes. Interestingly, the combination of multiple freezing with EDTA and DNAse treatments resulted in enough to induce decellularization without the need for trypsin, which is potentially deleterious for the ECM proteins, or Triton X-100, a detergent potentially harmful for the ECM, too. The histology study revealed not only decellularization with preservation of collagen matrix but also the preservation of noncollagenous proteins stained by Fast Green, an ECM component absent when samples were treated with trypsin or Triton X-100 (Figure 1C). Freezing-EDTA-DNAse treatment

10.3389/fonc.2022.956940

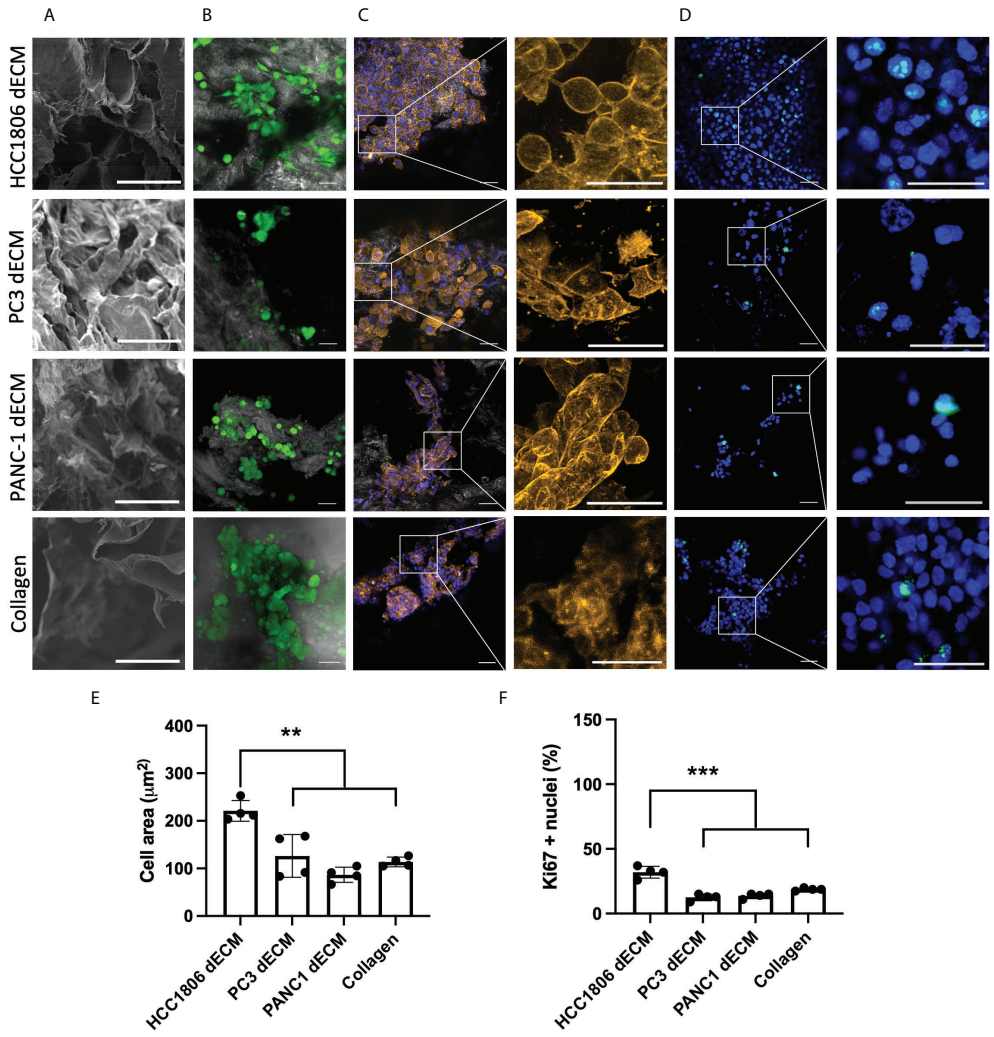

FIGURE 5
HC1806 cells show different cell behavior on HC1806 dECM compared to dECM from other tumor xenografts. **(A)** Detail of SEM imaging of samples showing surface structure (scale, 50 µm). **(B-D)** Images of cell-seeded samples. **(B)** Calcein-AM–positive cells are shown in green, while scaffold material is shown in grey (×20 (scale, 20 µm)). **(C)** Actin cytoskeleton immunostaining in orange; DAPI nuclear staining in blue (×10 (scale, 50 µm) and detailed images (scale, 20 µm)). **(D)** Ki67 immunostaining in green; DAPI nuclear staining in blue (×10 (scale, 20 µm) and detailed images (scale, 50 µm)). **(E)** Quantification of cell size (area) using actin cytoskeleton membrane distribution images. **(F)** Quantification of proliferative cells (Ki67-positive cells vs. total cells observed in each material). *N* = 3 in all cases and 2 areas measured per sample.

was further tested in all xenografted tumor types, and this approach yielded the successful decellularization of all tested samples (Figure 2).

In order to characterize the obtained tumor-derived dECM and define possible differences between xenografted tumors, a proteomic analysis was performed (Figure 3). Proteomics is a powerful tool to define the composition of a sample, in this case, dECM, but to our knowledge, it has not been applied to the study of that kind of sample before. We were able to detect thousands of individual proteins in each sample, most of them related to the extracellular matrix, extracellular vesicles, and extracellular location (Figures 3A, B). Interestingly, proteomic data from all tumor-derived samples were notably different from Matrigel, the 3D environment used to generate the implants, indicating the ECM composition develops during tumor formation and changes compared to this tumor cell-line-derived ECM (Figure 4A). While DNA and nuclear proteins were removed with the decellularization, it is worth noticing that proteomic study reveals the existence of cellular organelle waste material from mitochondria and endoplasmic reticulum in tumor-derived samples (Figure 3B).

Proteomics data analysis also revealed a different dECM composition in two of the breast cancer samples, HCC1806 and 4T1, compared to all other dECM tumor xenograft samples

10.3389/fonc.2022.956940

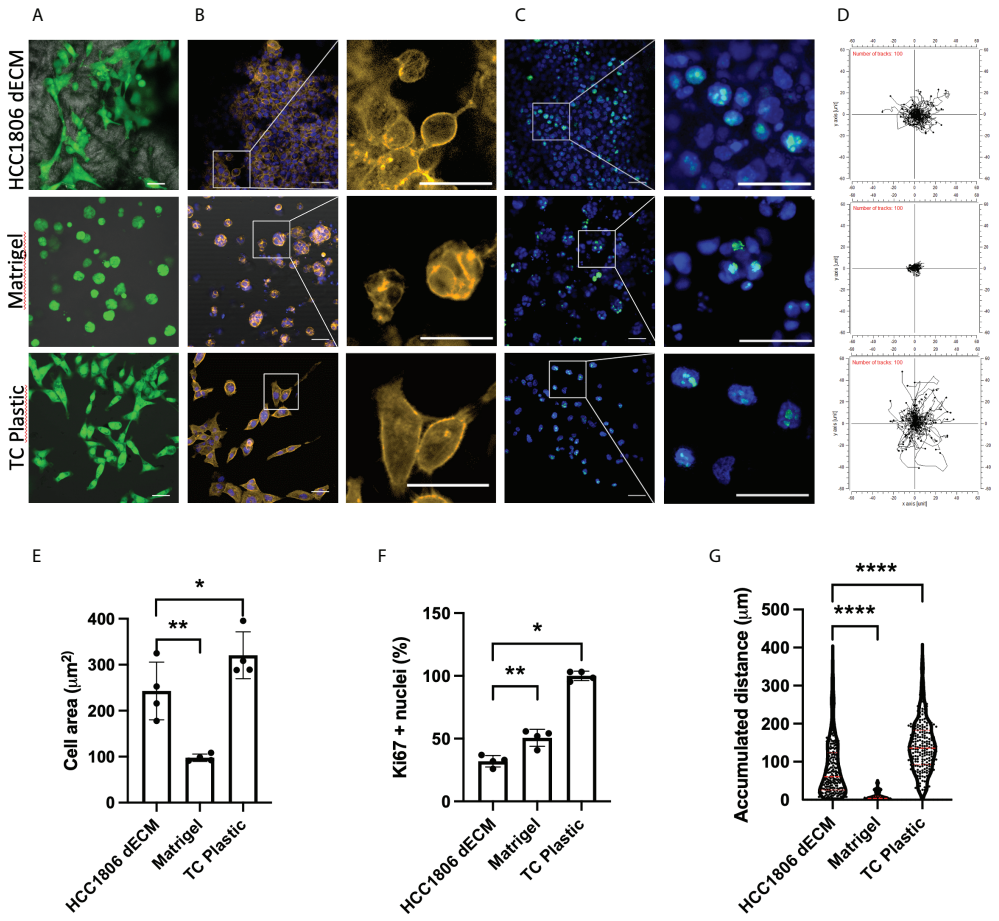

FIGURE 6
HC1806 cells show different cell behaviors on HC1806 dECM compared to other 2D and 3D culture methods. **(A–C)** Images of cell-seeded samples. **(A)** Calcein-AM–positive cells are shown in green, while scaffold material is shown in grey (×20 (scale, 20 µm)). **(B)** Actin cytoskeleton immunostaining in orange; DAPI nuclear staining in blue (×10 (scale, 20 µm) and detailed images (scale, 50 µm)). **(C)** Ki67 immunostaining in green; DAPI nuclear staining in blue (×10 (scale, 50 µm) and detailed images (scale, 20 µm)). **(D)** Plotting of the cell displacement during 5 h. Each line represents one cell; 100 cells are provided per plot. The starting point of each cell is provided centered for easy visualization. **(E)** Quantification of cell size (area) using actin cytoskeleton membrane distribution images. **(F)** Quantification of proliferative cells (Ki67-positive cells vs. total cells observed in each material). **(G)** Quantification of cell displacement measured by accumulative distance traveled. *N* = 3 in all cases and 2 areas measured per sample.

(Figure 4). The breast cancer samples included in this study correspond to the triple-negative subtype, and among them, MDA-MB-231 cells have been previously classified as mesenchymal stem-like subtype, while HCC1806 cells represent the basal-like subtype (53). A recent study based on the multiomics characterization of the mouse 4T1 TNBC cell line found significant overlap with top pathways and GO terms reported for the basal-like TNBC subtype (54). Therefore, the proteomic data here presented revealed the tumors with basal-like TNBC subtype were similar between them and different from the other dECM obtained from other xenografted tumors. A detailed study shows some specific features related to lipidic metabolism and cholesterol metabolism (Figure 4C). These processes are mainly related to mitochondria and endoplasmic reticulum, suggesting organelle waste contained in the decellularized sample may have an influence on dECM tumor-specific composition. This relationship would go unnoticed without the proteomic study here performed. It is well-known that fatty acid synthesis is upregulated in TNBC, while specifically basal-like TNBC subtypes overexpress genes involved in the utilization of exogenous fatty acids (55). The dependency of this type of tumor on cholesterol has been assessed before, by proving that the downregulation of the cholesterol metabolism suppresses its growth. Moreover, the esterification of cholesterol has been associated with the metastasis of this specific breast cancer subtype (56–58). Therefore, these data indicate that, after decellularization, some tumor-specific characteristics can be retained and observed by

proteomics, such as the upregulated lipidic metabolism at the basal-like TNBC subtypes.

We next wondered whether this specific composition of dECM in basal-like TNBC subtype samples, with some debris of mitochondria and endoplasmic reticulum related to specific lipidic and cholesterol metabolism, would have any influence on *in vitro* cell behavior when used as a substrate. Tumor-derived dECM has previously been used as a substrate for *in vitro* cell culture studies and cancer modeling. In some reports, it has been processed as hydrogels and further as inks for the printing and development of 3D bioengineered structures (34, 59). In other reports, tumor-derived dECM has been used as a 3D scaffold for cell-seeding purposes (48, 49, 60–63). Therefore, we considered using dECM directly as a substrate for seeding basal-like TNBC cells, aiming to test any substrate specificity. To our knowledge, this is the first time that a xenografted tumor dECM with no postprocessing treatment has been further tested *in vitro* with the same cell line, aiming to define any substrate vs. cell-specific behavior.

Aiming to generate data with more potentially translational meaning, we chose the HCC1806 human cell line as a testing model in further *in vitro* cell culture studies rather than the 4T1 mouse cell line. We used as substrate not only dECM from hCC1806 xenograft tumors but also dECM from other xenografted tumors types, such as the PC-3 human prostate model and PANC-1 human pancreas model, which showed a different proteomic composition compared to the basal-like TNBC subtype samples, but similar between them and also to MDA-MB-231 mesenchymal stem-like TNBC subtype (Figure 3). As a control, we included a collagen matrix, which should not provide any tumor-specific signal to the seeded cells. Interestingly, data indicate that HCC1806 cells spread and proliferate more in their own xenograft-derived dECM compared to dECM from other tumor xenografts or to the collagen scaffolds (Figure 5). This data suggest that cells recognize their own dECM, and behave specifically on it. As a complementary *in vitro* testing, we compared cells' behavior at their own xenograft tumor-derived dECM, or embedded in Matrigel which provides multiple growth signaling, or in the conventional 2D plastic surface which does not provide any 3D environment. Again, cells show different size, proliferation, and mobility features in the tested cell culture models (Figure 6).

The most notable limitations of the study are related to the availability of the raw sample. The experimental approach is time consuming, as it requires medium- to long-term mouse xenotransplantation in an ectopic location to obtain the raw tumor material. It may raise ethical concerns related to experimentation in animals and samples may differ from human primary tumor tissue samples. Moreover, relatively small-sized xenograft tumors are obtained, limiting sample availability for further multiple studies. Decellularized tumor pieces are directly used for the intended application, and it avoids the potential loss of material related to postprocessing steps required to form hydrogels. However, samples are more prone to being contaminated, and the setting up of specific, more complex sterilization protocols is required.

Altogether, we believe this approach is a valid proof-of-concept to show the relevance of optimizing the tumor decellularization protocol to generate an optimal tumor dECM material useful to study tumor-specific cell–matrix interactions. This research opens the way to further use of well-characterized xenografted tumor dECM materials as a 3D cell culture platform for basic tumor biology and tumor progression studies, as well as global gene expression studies, drug testing studies, and other *in vitro* 3D cell culture functional studies relevant in the cancer field. Moreover, it may pave the way to further patient-specific physiologically relevant *in vitro* 3D research models, in which optimized decellularization may lead to primary tumor cell testing on their own dECM, thereby providing a potentially useful tool for personalized medicine research and diagnosis purposes (37, 49, 60–62, 64).

Conclusions

A soft treatment using Freeze-EDTA/DNAse allows decellularization of the solid tumor mass of multiple types of xenografted cell lines. Interestingly, samples decellularized from basal-like triple-negative breast cancer subtype models show different proteomic ECM composition compared to the rest of the xenograft tumors tested. The *in vitro* recellularization of HCC1806 xenograft-derived dECM with HCC1806 cells yields different proliferation and cell spreading, compared to the cell behavior on dECM from other tumor origins, collagen matrices, Matrigel, or plastic cell culture surfaces. Altogether, data indicate that decellularized xenograft tumors are a feasible substrate for re-seeding purposes, thereby promoting specific cell behavior in the TNBC context. These data serve as a proof-of-concept for further potential generation of patient-specific *in vitro* research models.

Data availability statement

The datasets presented in this study can be found in online repositories. The names of the repository/repositories and accession number(s) can be found below: ProteomeXchange Consortium, [PXD034597].

Ethics statement

The animal study was reviewed and approved by Ethics Committee of CICbiomaGUNE.

Author contributions

Conceptualization and methodology: AA Formal analysis: GI, UM, BA, and MA Investigation: GI, UM, BA, AR-D-A, and KB Validation and data curation: AA Writing and original draft preparation: UM, BA, NK, and AA. Visualization: FE, BO, VG-V, JL, and AA Writing, review, and editing: AA Supervision, funding acquisition, resources, and administration: BO, VG-V, JL, and AA. All authors have read and agreed to the published version of the manuscript.

Funding

Grant RTI2018-101708-A-I00 funded by MCIN/AEI/10.13039/501100011033 and by ERDF A way of making Europe. Grants RYC2018-025502-I and PRE2018-084542 are funded by MCIN/AEI/10.13039/501100011033 and by ESF Investing in your future. Grant MDM-2017-0720 Maria de Maeztu Units of Excellence Program funded by the Spanish State Research Agency. Grant KK-2019/00093 Elkartek program funded by Basque Government. Grant CICBMG_PhD_03_2021 funded by CICbiomaGUNE and Polymat. Grant CICBMG_PhD_05_2019 funded by CICbiomaGUNE and Polymat. 2019 Leonardo Grant for Researchers and Cultural Creators, BBVA Foundation, grant number IN[19]_CMA_BIO_0119. The BBVA Foundation accepts no responsibility for the opinions, statements, and contents included, which are entirely the responsibility of the authors.

Conflict of interest

The authors declare that the research was conducted in the absence of any commercial or financial relationships that could be construed as a potential conflict of interest.

Publisher's note

All claims expressed in this article are solely those of the authors and do not necessarily represent those of their affiliated organizations, or those of the publisher, the editors and the reviewers. Any product that may be evaluated in this article, or claim that may be made by its manufacturer, is not guaranteed or endorsed by the publisher.

Supplementary material

The Supplementary Material for this article can be found online at: https://www.frontiersin.org/articles/10.3389/fonc.2022.956940/full#supplementary-material

References

1. Alemany-Ribes M, Semino CE. Bioengineering 3D environments for cancer models. *Adv Drug Deliv Rev* (2014) 79–80:40–9. doi: 10.1016/J.ADDR.2014.06.004

2. Jung J. Human tumor xenograft models for preclinical assessment of anticancer drug development. *Toxicol Res* (2014) 30(1):1–5. doi: 10.5487/TR.2014.30.1.001

3. Martinez-Pacheco S, O'driscoll L, Gaspar V, Mano JF. Pre-clinical *In vitro* models used in cancer research: Results of a worldwide survey. *Cancers* (2021) 13:6033. doi: 10.3390/CANCERS13236033

4. Nyga A, Cheema U, Loizidou M. 3D tumour models: Novel *in vitro* approaches to cancer studies. *J Cell Commun Signaling* (2011) 5:239–48. doi: 10.1007/S12079-011-0132-4/FIGURES/2

5. Papalazarou V, Salmeron-Sanchez M, Machesky LM. Tissue engineering the cancer microenvironment–challenges and opportunities. *Biophys Rev* (2018) 10:1695–711. doi: 10.1007/S12551-018-0466-8

6. Baker BM, Chen CS. Deconstructing the third dimension-how 3D culture microenvironments alter cellular cues. *J Cell Sci* (2012) 125:3015–24. doi: 10.1242/JCS.079509/258092/AM/DECONSTRUCTING-THE-THIRD-DIMENSION-HOW-3D-CULTURE

7. Thoma CR, Zimmermann M, Agarkova I, Kelm JM, Krek W. 3D cell culture systems modeling tumor growth determinants in cancer target discovery. *Adv Drug Deliv Rev* (2014) 69–70:29–41. doi: 10.1016/J.ADDR.2014.03.001

8. Bredholt G, Mannelqvist M, Stefansson IM, Birkeland E, Bø TH, Øyan AM, et al. Tumor necrosis is an important hallmark of aggressive endometrial cancer and associates with hypoxia, angiogenesis and inflammation responses. *Oncotarget* (2015) 6:39676. doi: 10.18632/ONCOTARGET.5344

9. Northcutt LA, Suarez-Arnedo A, Rafat M. Emerging biomimetic materials for studying tumor and immune cell behavior. *Ann Biomed Eng* (2019) 48:2064–77. doi: 10.1007/S10439-019-02384-0

10. Unnikrishnan K, Thomas LV, Ram Kumar RM. Advancement of scaffold-based 3D cellular models in cancer tissue engineering: An update. *Front Oncol* (2021) 11:733652/BIBTEX. doi: 10.3389/FONC.2021.733652/BIBTEX

11. Kratochvil MJ, Seymour AJ, Li TL, Paşca SP, Kuo CJ, Heilshorn SC. Engineered materials for organoid systems. *Nat Rev Mater* (2019) 4:606–22. doi: 10.1038/s41578-019-0129-9

12. Birgersdotter A, Sandberg R, Ernberg I. Gene expression perturbation *in vitro*–a growing case for three-dimensional (3D) culture systems. *Semin Cancer Biol* (2005) 15:405–12. doi: 10.1016/J.SEMCANCER.2005.06.009

13. Rodrigues J, Heinrich MA, Teixeira LM, Prakash J. 3D *In vitro* model (R) evolution: Unveiling tumor–stroma interactions. *Trends Cancer* (2021) 7:249–64. doi: 10.1016/J.TRECAN.2020.10.009

14. Wang C, Tang Z, Zhao Y, Yao R, Li L, Sun W. Three-dimensional *in vitro* cancer models: a short review. *Biofabrication* (2014) 6:22001. doi: 10.1088/1758-5082/6/2/022001

15. Fontana F, Marzagalli M, Sommariva M, Gagliano N, Limonta P. *In vitro* 3D cultures to model the tumor microenvironment. *Cancers* (2021) 13:2970. doi: 10.3390/CANCERS13122970

16. Vitale C, Marzagalli M, Scaglione S, Dondero A, Bottino C, Castriconi R. Tumor microenvironment and hydrogel-based 3D cancer models for *In vitro* testing immunotherapies. *Cancers* (2022) 14:1013. doi: 10.3390/CANCERS14041013

17. Nii T, Makino K, Tabata Y. Three-dimensional culture system of cancer cells combined with biomaterials for drug screening. *Cancers* (2020) 12:2754. doi: 10.3390/CANCERS12102754

18. Kim SK, Kim YH, Park S, Cho SW. Organoid engineering with microfluidics and biomaterials for liver, lung disease, and cancer modeling. *Acta Biomater* (2021) 132:37–51. doi: 10.1016/J.ACTBIO.2021.03.002

19. Ferreira LP, Gaspar VM, Mendes L, Duarte IF, Mano JF. Organotypic 3D decellularized matrix tumor spheroids for high-throughput drug screening. *Biomaterials* (2021) 275:120983. doi: 10.1016/J.BIOMATERIALS.2021.120983

20. Pednekar KP, Heinrich MA, van Baarlen J, Prakash J, ednekar PKP, Heinrich MA, et al. Novel 3D μtissues mimicking the fibrotic stroma in pancreatic cancer to study cellular interactions and stroma-modulating therapeutics. *Cancers* (2021) 13:5006. doi: 10.3390/CANCERS13195006

21. Bray LJ, Hutmacher DW, Bock N. Addressing patient specificity in the engineering of tumor models. *Front Bioeng Biotechnol* (2019) 7:217/BIBTEX. doi: 10.3389/FBIOE.2019.00217/BIBTEX

22. Ott HC, Clippinger B, Conrad C, Schuetz C, Pomerantseva I, Ikonomou L, et al. Regeneration and orthotopic transplantation of a bioartificial lung. *Nat Med* (2010) 16:927–33. doi: 10.1038/nm.2193

23. Ghajar CM, Kachgal S, Kniazeva E, Mori H, Costes SV, George SC, et al. Mesenchymal cells stimulate capillary morphogenesis *via* distinct proteolytic mechanisms. *Exp Cell Res* (2010) 316:813–25. doi: 10.1016/J.YEXCR.2010.01.013

24. Pinto ML, Rios E, Silva AC, Neves SC, Caires HR, Pinto AT, et al. Decellularized human colorectal cancer matrices polarize macrophages towards an anti-inflammatory phenotype promoting cancer cell invasion *via* CCL18. *Biomaterials* (2017) 124:211–24. doi: 10.1016/J.BIOMATERIALS.2017.02.004

25. Ohata K, Ott HC. Human-scale lung regeneration based on decellularized matrix scaffolds as a biologic platform. *Surg Today* (2020) 50:633–43. doi: 10.1007/S00595-020-02000-Y/FIGURES/5

26. Tong C, Li C, Xie B, Li M, Li X, Qi Z, et al. Generation of bioartificial hearts using decellularized scaffolds and mixed cells. *Biomed Eng Online* (2019) 18:1–13. doi: 10.1186/S12938-019-0691-9/FIGURES/7

27. Mazza G, Rombouts K, Rennie Hall A, Urbani L, Vinh Luong T, Al-Akkad W, et al. Decellularized human liver as a natural 3D-scaffold for liver bioengineering and transplantation. *Sci Rep* (2015) 5:1–15. doi: 10.1038/srep13079

28. Chen P, Zheng L, Wang Y, Tao M, Xie Z, Xia C, et al. Desktop-stereolithography 3D printing of a radially oriented extracellular matrix/mesenchymal stem cell exosome bioink for osteochondral defect regeneration. *Theranostics* (2019) 9:2439. doi: 10.7150/THNO.31017

29. Dequach JA, Yuan SH, Goldstein LSB, Christman KL. Decellularized porcine brain matrix for cell culture and tissue engineering scaffolds. *Tissue Engineering Part A* (2011) 17:2583–92. doi: 10.1089/TEN.TEA.2010.0724

30. Yao Q, Zheng YW, Lan QH, Kou L, Xu HL, Zhao YZ. Recent development and biomedical applications of decellularized extracellular matrix biomaterials. *Mater Sci Eng: C* (2019) 104:109942. doi: 10.1016/J.MSEC.2019.109942

31. Mendibil U, Ruiz-Hernandez R, Retegi-Carrion S, Garcia-Urquia N, Olalde-Graells B, Abarrategi A. Tissue-specific decellularization methods: Rationale and strategies to achieve regenerative compounds. *Int J Mol Sci* (2020) 21:5447. doi: 10.3390/IJMS21155447

32. Ferreira LP, Monteiro MV, Gaspar VM, Mano JF. Chapter 25:Decellularized matrix hydrogels for *In vitro* disease modeling. *RSC Soft Matter* (2021), 25:626–59. doi: 10.1039/9781839161124-00626

33. Ferreira LP, Gaspar VM, Mano JF. Decellularized extracellular matrix for bioengineering physiomimetic 3D in vitro tumor models. *Trends Biotechnol* (2020) 38:1397–414. doi: 10.1016/J.TIBTECH.2020.04.006

34. Tamayo-Angorrilla M, López de Andrés J, Jiménez G, Marchal JA. The biomimetic extracellular matrix: a therapeutic tool for breast cancer research. *Trans Res* (2021) 247:117–136. doi: 10.1016/J.TRSL.2021.11.008

35. Marques-Magalhães Â, Cruz T, Costa ÂM, Estêvão D, Rios E, Canão PA, et al. Decellularized colorectal cancer matrices as bioactive scaffolds for studying tumor-stroma interactions. *Cancers* (2022) 14:359. doi: 10.3390/CANCERS14020359

36. Hoshiba T. Decellularized extracellular matrix for cancer research. *Materials* (2019) 12:1311. doi: 10.3390/MA12081311

37. García-Gareta E, Pérez MÁ, García-Aznar JM. Decellularization of tumours: A new frontier in tissue engineering. *J Tissue Eng* (2022) 13:204173142210916. doi: 10.1177/20417314221091682

38. ASTM International. ASTM F3354-19, standard guide for evaluating extracellular matrix decellularization processes. (2019). doi: 10.1520/F3354-19

39. Wiśniewski JR, Zougman A, Nagaraj N, Mann M. Universal sample preparation method for proteome analysis. *Nat Methods* (2009) 6:359–62. doi: 10.1038/nmeth.1322

40. Cox J, Mann M. MaxQuant enables high peptide identification rates, individualized p.p.b.-range mass accuracies and proteome-wide protein quantification. *Nat Biotechnol* (2008) 26:1367–72. doi: 10.1038/NBT.1511

41. Tyanova S, Temu T, Sinitcyn P, Carlson A, Hein MY, Geiger T, et al. The Perseus computational platform for comprehensive analysis of (prote)omics data. *Nat Methods* (2016) 13:731–40. doi: 10.1038/NMETH.3901

42. Metsalu T, Vilo J. ClustVis: a web tool for visualizing clustering of multivariate data using principal component analysis and heatmap. *Nucleic Acids Res* (2015) 43:W566–70. doi: 10.1093/NAR/GKV468

43. Abarrategi A, Foster K, Hamilton A, Mian SA, Passaro D, Gribben J, et al. Versatile humanized niche model enables study of normal and malignant human hematopoiesis. *J Clin Invest* (2017) 127:543–8. doi: 10.1172/JCI89364

44. Mian SA, Abarrategi A, Kong KL, Rouault-Pierre K, Wood H, Oedekoven CA, et al. Ectopic humanized mesenchymal niche in mice enables robust engraftment of myelodysplastic stem cells. *Cancer Discovery* (2021) 2:135–45. doi: 10.1158/2643-3230.BCD-20-0161/49975/AM/ECTOPIC-HUMANIZED-MESENCHYMAL-NICHE-IN-MICE

45. Kurelac I, Abarrategi A, Ragazzi M, Iommarini L, Ganesh NU, Snoeks T, et al. A humanized bone niche model reveals bone tissue preservation upon targeting mitochondrial complex I in pseudo-orthotopic osteosarcoma. *J Clin Med* (2019) 8:2184. doi: 10.3390/JCM8122184

46. Lima RT, Sousa D, Paiva AM, Palmeira A, Barbosa J, Pedro M, et al. Modulation of autophagy by a thioxanthone decreases the viability of melanoma cells. *Molecules* (2016) 21:1343. doi: 10.3390/MOLECULES21101343

47. Ershov D, Phan M-S, Pylvänäinen JW, Rigaud SU, Blanc L, Charles-Orszag A, et al. Bringing TrackMate into the era of machine-learning and deep-learning. *bioRxiv* (2021). doi: 10.1101/2021.09.03.458852

48. Lv Y, Wang H, Li G, Zhao B. Three-dimensional decellularized tumor extracellular matrices with different stiffness as bioengineered tumor scaffolds. *Bioactive Mater* (2021) 6:2767–82. doi: 10.1016/J.BIOACTMAT.2021.02.004

49. Koh I, Cha J, Park J, Choi J, Kang SG, Kim P. The mode and dynamics of glioblastoma cell invasion into a decellularized tissue-derived extracellular matrix-based three-dimensional tumor model. *Sci Rep* (2018) 8:1–12. doi: 10.1038/s41598-018-22681-3

50. Isidan A, Liu S, Chen AM, Zhang W, Li P, Smith LJ, et al. Comparison of porcine corneal decellularization methods and importance of preserving corneal limbus through decellularization. *PLoS One* (2021) 16:e0243682. doi: 10.1371/JOURNAL.PONE.0243682

51. Kang HV, Im JH, Chung YG, Shin EY, Lee Mk, Lee JY. Comparison of two different decellularization methods for processed nerve allograft. *Cell Tissue Banking* (2021) 22:575–85. doi: 10.1007/S10561-021-09965-1/FIGURES/8

52. Gharenaz NM, Movahedin M, Mazaheri Z. Comparison of two methods for prolong storage of decellularized mouse whole testis for tissue engineering application: An experimental study. *Int J Reprod Biomed* (2021) 19:321. doi: 10.18502/IJRM.V19I4.9058

53. Lehmann BD, Bauer JA, Chen X, Sanders ME, Chakravarthy AB, Shyr Y, et al. Identification of human triple-negative breast cancer subtypes and preclinical models for selection of targeted therapies. *J Clin Invest* (2011) 121:2750–67. doi: 10.1172/JCI45014

54. Schrörs B, Boegel S, Albrecht C, Bukur T, Bukur V, Holtsträter C, et al. Multi-omics characterization of the 4T1 murine mammary gland tumor model. *Front Oncol* (2020) 10:1195/FULL. doi: 10.3389/FONC.2020.01195/FULL

55. Monaco ME. Fatty acid metabolism in breast cancer subtypes. *Oncotarget* (2017) 8:29487. doi: 10.18632/ONCOTARGET.15494

56. Han B, Alonso-Valenteen F, Wang Z, Deng N, Lee TY, Gao B, et al. A chemokine regulatory loop induces cholesterol synthesis in lung-colonizing triple-negative breast cancer cells to fuel metastatic growth. *Mol Ther* (2022) 30:672–87. doi: 10.1016/J.YMTHE.2021.07.003/ATTACHMENT/4D0C962E-A3A5-4D3D-B742-34F930779D26/MMC1.PDF

57. Shim SH, Sur S, Steele R, Albert CJ, Huang C, Ford DA, et al. Disrupting cholesterol esterification by bitter melon suppresses triple-negative breast cancer cell growth. *Mol Carcinogenesis* (2018) 57:1599–607. doi: 10.1002/MC.22882

58. Sun X, Wang M, Wang M, Yu X, Guo J, Sun T, et al. Metabolic reprogramming in triple-negative breast cancer. *Front Oncol* (2020) 10:428/BIBTEX. doi: 10.3389/FONC.2020.00428/BIBTEX

59. Keller CR, Hu Y, Ruud KF, Vandeen AE, Martinez SR, Kahn BT, et al. Human breast extracellular matrix microstructures and protein hydrogel 3D cultures of mammary epithelial cells. *Cancers* (2021) 13:5857. doi: 10.3390/CANCERS13225857

60. Liu G, Wang B, Li S, Jin Q, Dai Y. Human breast cancer decellularized scaffolds promote epithelial-to-mesenchymal transitions and stemness of breast cancer cells in vitro. *J Cell Physiol* (2019) 234:9447–56. doi: 10.1002/JCP.27630

61. Leiva MC, Garre E, Gustafsson A, Svanström A, Bogestål Y, Håkansson J, et al. Breast cancer patient-derived scaffolds as a tool to monitor chemotherapy responses in human tumor microenvironments. *J Cell Physiol* (2021) 236:4709–24. doi: 10.1002/JCP.30191

62. Gustafsson A, Garre E, Leiva MC, Salerno S, Ståhlberg A, Landberg G. Patient-derived scaffolds as a drug-testing platform for endocrine therapies in breast cancer. *Sci Rep* (2021) 11:1–12. doi: 10.1038/s41598-021-92724-9

63. Lü WD, Zhang L, Wu CL, Liu ZG, Lei GY, Liu J, et al. Development of an acellular tumor extracellular matrix as a three-dimensional scaffold for tumor engineering. *PLoS One* (2014) 9:e103672. doi: 10.1371/JOURNAL.PONE.0103672

64. Garre E, Gustafsson A, Leiva MC, Håkansson J, Ståhlberg A, Kovács A, et al. Breast cancer patient-derived scaffolds can expose unique individual cancer progressing properties of the cancer microenvironment associated with clinical characteristics. *Cancers (Basel)* (2022) 14:2172. doi: 10.3390/CANCERS14092172/S1

frontiers | Frontiers in Oncology

TYPE Review
PUBLISHED 05 September 2022
DOI 10.3389/fonc.2022.935231

Check for updates

OPEN ACCESS

EDITED BY
Alberto Passi,
University of Insubria, Italy

REVIEWED BY
Pirjo Spuul,
Tallinn University of Technology, Estonia
George N. Tzanakakis,
University of Crete, Greece

*CORRESPONDENCE
Yoshifumi Itoh
yoshi.itoh@kennedy.ox.ac.uk

SPECIALTY SECTION
This article was submitted to Molecular and Cellular Oncology, a section of the journal Frontiers in Oncology

RECEIVED 03 May 2022
ACCEPTED 10 August 2022
PUBLISHED 05 September 2022

CITATION
Itoh Y (2022) Proteolytic modulation of tumor microenvironment signals during cancer progression. *Front. Oncol.* 12:935231. doi: 10.3389/fonc.2022.935231

COPYRIGHT
© 2022 Itoh. This is an open-access article distributed under the terms of the Creative Commons Attribution License (CC BY). The use, distribution or reproduction in other forums is permitted, provided the original author(s) and the copyright owner(s) are credited and that the original publication in this journal is cited, in accordance with accepted academic practice. No use, distribution or reproduction is permitted which does not comply with these terms.

Proteolytic modulation of tumor microenvironment signals during cancer progression

Yoshifumi Itoh*

Kennedy Institute of Rheumatology, University of Oxford, Oxford, United Kingdom

Under normal conditions, the cellular microenvironment is optimized for the proper functioning of the tissues and organs. Cells recognize and communicate with the surrounding cells and extracellular matrix to maintain homeostasis. When cancer arises, the cellular microenvironment is modified to optimize its malignant growth, evading the host immune system and finding ways to invade and metastasize to other organs. One means is a proteolytic modification of the microenvironment and the signaling molecules. It is now well accepted that cancer progression relies on not only the performance of cancer cells but also the surrounding microenvironment. This mini-review discusses the current understanding of the proteolytic modification of the microenvironment signals during cancer progression.

KEYWORDS

TME, proteinases, ECM, invasion, matrikine, Soluble factors, membrane protein shedding

1 Introduction

It is now well accepted that surrounding microenvironment is a determinant of the cancer cell progression (1). Cancer cells modify a normal tissue microenvironment and turn into a tumor microenvironment (TME) that helps cancer cells to grow, invade, and metastasize (1). A major component of the TME is the extracellular matrix (ECM) (2, 3). Cancer cells recognize ECM components through ECM receptors and modify them by depositing or degrading the ECM (3). Cells within the TME, such as cancer-associated fibroblasts (CAFs) and tumor-associated macrophages (TAMs), also contribute to this process. In addition to being a glue function to connect the cells and a bordering function to separate tissues and organs, the ECM also acts as signaling molecules, a pool for cytokines and growth factors, and a scaffolding for migrating cells (3). Thus, the modification of the pericellular ECM would impact cancer progression significantly.

Invasion and metastasis are the most life-threatening feature of malignant cancers. Transformed epithelial cells gain the ability to proliferate, downregulate cell–cell adhesion, and degrade the basement membrane (BM) and stromal tissue under it. This invasion process

disturbs tissue architecture and causes the loss of tissue function. Once cancer cells reach either blood vessels or lymphatic vessels, they intravasate and traverse to distant organs. During this process, many cancer cells are attacked by immune cells. Still, some cancer cells evade this immune surveillance and reach the organ where they can extravasate and create metastatic colonies. Once they extravasate, they grow, invade tissue, and cause tissue malfunction (Figure 1).

One of the means for cancer cells to modify their microenvironment signals is by using proteolytic enzymes. These proteinases degrade the ECM for growth, invasion, metastasis, and causing tissue damage (4). Proteinases can also generate bioactive fragments from the ECM by limited processing. It also degrades or processes soluble factors and modifies the signaling events in cancer cells and other cells within the TME. Proteinases also shed transmembrane (TM) cell surface receptors for cytokines and growth factors and adhesion molecules for cell–cell and cell–ECM attachments and adhesion. Proteolytic events are non-reversible reactions and are thus effective in modulating the function of the molecules. This mini-review discusses the current understanding of proteolytic modification of microenvironment interaction in cancer.

2 Proteolytic enzymes involved in microenvironment modulation

2.1 Matrix metalloproteinase

Matrix metalloproteinases (MMPs) belong to the metzincin clan of metalloendopeptidase, and the major substrates of MMPs are ECM components (5). They harbor zinc in their catalytic site

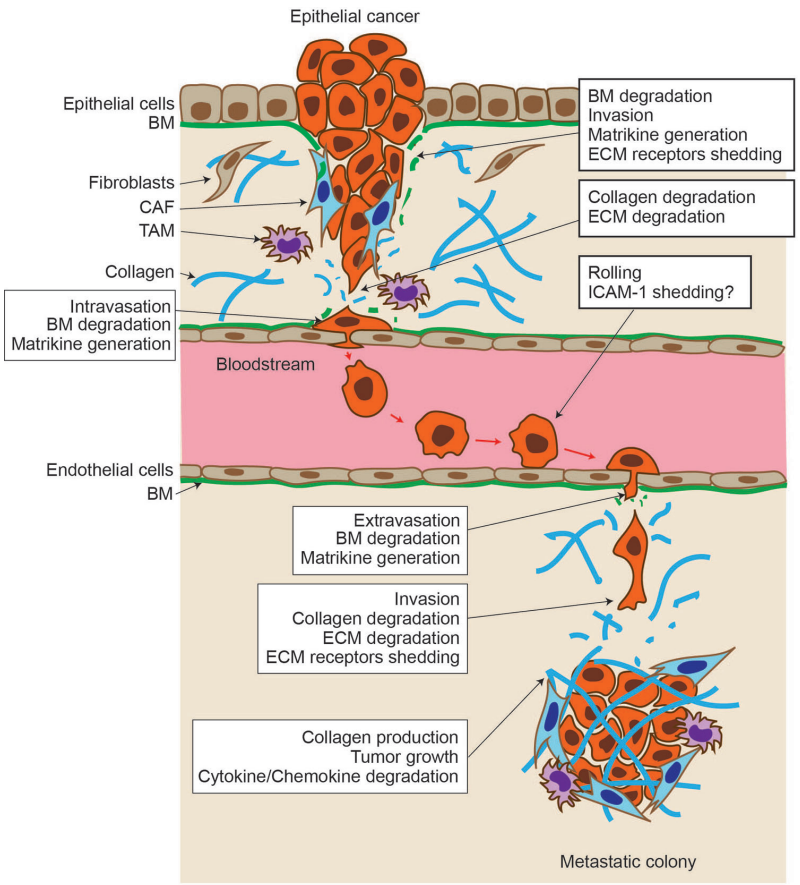

FIGURE 1
Proteolytic events during cancer progression. Epithelial cancer arises within the epithelial layer. They break through the basement membrane (BM) and invade stromal tissue. Upon BM degradation, matrikines are generated by proteolytic action, and cell surface extracellular matrix (ECM) receptor shedding promotes cancer cell motility. Stromal fibroblasts are activated and become cancer-associated fibroblasts and help cancer cells further invade. Tumor-associated macrophages (TAMs) help to evade the immune system. Cells degrade stromal the ECM further, including type I collagen, and intravasate into the vessel. Cancer cells traverse other organs through the bloodstream, interacting and rolling on the endothelial cell layer. Intercellular adhesion molecule–1 may be expressed in cancer cells, and its shedding allows cancer cells to migrate through the endothelial cell layer and extravasate. Cancer cells invade stromal tissue, form a metastatic colony, create a tumore microenvironment, and cause tissue malfunction.

for the hydrolysis of peptide bonds. There are 23 MMPs in humans, and they can be divided into two groups according to their membrane-bound nature: soluble MMPs and membrane-type MMPs (Figure 2) (6). Within soluble MMPs, they can be further classified according to domain structure. Classical MMPs contain a pre-/propeptide, a catalytic domain, a hinge, and a hemopexin domain. This group contains interstitial collagenase (MMP-1), stromelysin 1 (MMP-3), neutrophil collagenase/collagenase 2 (MMP-8), stromelysin 2 (MMP-10), macrophage elastase (MMP-12), collagenase 3 (MMP-13), MMP-19, enamelysin (MMP-20), and MMP-27. Gelatinase MMPs have three repeats of the type II fibronectin domain in the catalytic domain, allowing them to bind collagen and gelatin. This group has two gelatinases, MMP-2 (gelatinase A) and MMP-9 (gelatinase B). The third group is minimal as its domain structure consists only of a pre-/propeptide and a catalytic domain. Matrilysin 1 (MMP-7) and matrilysin 2 (MMP-26) belong to this group. The fourth group has classical MMPs' domain structure, but it has a basic amino acid motif of R-X-K/R-R that is recognized and cleaved by proprotein convertases (PCs) such as furin at the C-terminus of the propeptide, allowing them to be activated during the secretory process by PCs. This group includes stromelysin 3 (MMP-11), MMP-21, and epilysin (MMP-28). MMP-23 is a unique member of MMP that is a type II TM enzyme. The TM domain is located at the N-terminus of the propeptide, and the basic motif of R-R-R-R for activation by furin is inserted at the C-terminus of the propeptide. Thus, MMP-23 becomes a soluble enzyme upon activation. Membrane-type MMPs (MT-MMPs) have two subgroups. One is type I TM-types, including MT1-, MT2-, MT3-, and MT5-MMPs, and the other glycosylphosphatidylinositol (GPI)-anchored types, including MT4- and MT6-MMPs. As they have a membrane-anchored part at the C-terminus of the enzyme molecule, MT1-MMPs are expressed on the cell surface. All MT-MMPs have the basic motif of R-X-K/R-R motif at the C-terminus of propeptide for activation by PCs. TM-type MT-MMPs have a characteristic eight amino acid insertion in the catalytic domain called MT-Loop or IS-2. GPI-type MT-MMPs do not have this insertion.

2.2 A disintegrin and a metalloproteinase

ADAM belongs to the metzincin clan of metalloendopeptidase-like MMPs. There are 12 ADAMs that are catalytically active and eight ADAMs that are catalytically inactive (Figure 2) (7). ADAMs are type-I TM proteinases and share conserved domain structures within the family. They consist of a signal peptide, pro-domain, catalytic domain, disintegrin domain, cysteine-rich module, EGF-like domain, TM domain, and cytoplasmic domain. ADAMs also have a basic R-X-K/R-R motif at the C-terminus of propeptide for activation by PCs at trans-Golgi. Thus, ADAMs are displayed on the cell surface as an active form. ADAMs are generally considered membrane protein sheddases, cleaving a range of cell surface proteins, including cytokines, growth factors, receptors for cytokines and growth factors, and cell adhesion molecules (8). Among 12 catalytically active ADAMs, ADAM10 and ADAM17 are the most characterized dominant membrane sheddases.

2.3 A disintegrin and metalloprotease with thrombospondin type 1 motif

ADAMTS enzymes have conserved domain structures, consisting of a signal peptide, pro-domain, catalytic domain, disintegrin domain, cysteine-rich module, spacer domain, and additional repeats of thrombospondin regions for some enzymes (Figure 2) (9). ADAMTS enzymes also have a basic motif of R-X-K/R-R motif at the C-terminus of the pro-domain and are activated by PCs during secretion. Unlike ADAMs, ADAMTSs are soluble enzymes whose primary function is ECM degradation (9).

2.4 Plasmin system

The serine proteinase plasmin is the major proteinase in our body fluid (10). It is mainly produced in the liver and exists in the plasma as its precursor form, plasminogen (or Glu plasminogen with the glutamic acid at the N-terminus), at approximately 0.2 mg/ml. Its major function is fibrin degradation, but it also degrades ECM components, including fibrinogen, laminin, vitronectin, and osteocalcin. It also activates several proMMPs, including proMMP-1, proMMP-3, proMMP-9, and proMMP-13. It cleaves complement components 3 and 5 (C3 and C5), factors V, VIII, and X, and protease-activated receptors (PARs). Thus, plasmin possesses a broad substrate specificity. Plasminogen is activated by two types of plasminogen activators (PA), urokinase PA (uPA) and tissue-PA (tPA), by the cleavage in the activation loop between Arg_{561} and Val_{562}. Activated plasmin activates pro-uPA and pro-tPA, providing positive proteolytic feedback (Figure 3).

2.5 Neutrophil-derived serine proteinases

Neutrophil in the TME produces serine proteinases, including neutrophil elastase (NE), proteinase 3 (Pro3), and cathepsin G (CG) (11, 12). NE, Pro3, and CatG cleave elastin, the telopeptide region of fibrillar collagen types I, II, III; collagen types IV, VI, VIII, IX, X, and XI; and fibronectin, laminin, and aggrecan (11, 12). They can also activate proMMPs and inactivate endogenous proteinase inhibitors such as α2 antiplasmin, α1 antichymotrypsin, and the tissue inhibitors of metalloproteinases (TIMPs) (11, 12). It has also been shown that NE and CatG activate PARs (11, 12).

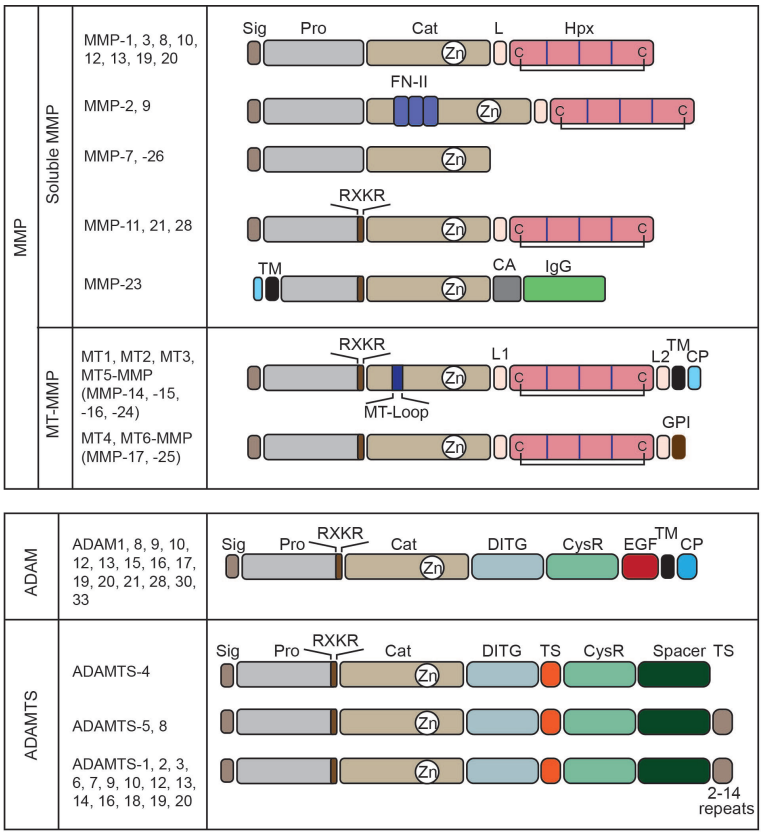

FIGURE 2
Domain structure of metalloproteinases. Matrix metalloproteinases (MMPs) can be divided into two major groups: soluble MMPs and membrane-type MMPs. According to their structures, they can be classified into six soluble MMPs and two subgroups in membrane-type MMPs. MMP-11, 21, 28, 23, and MT-MMPs have a basic motif of RXKR that is recognized and cleaved by proprotein convertases to activate the enzymes by removing their pro-domain. Sig, signal peptide; Pro, pro-domain; Cat, catalytic domain; L, linker or hinge region; Hpx, hemopexin domain; C, cysteine; FN-II, fibronectin type-II repeats; TM, transmembrane domain; CA, cysteine array; IgG, IgG-like domain; L1, linker1 or hinge region; L2, linker 2 or stalk region; MT-Loop, eight amino acids insertion unique to TM-type MT-MMPs; and CP, cytoplasmic domain. ADAM enzymes have a conserved domain structure. DITG, a disintegrin-like domain; CysR, a cysteine-rich domain; EGF, an EGF-like domain. ADAMTS enzymes also have a conserved domain structure and differ in the number of thrombospondin motifs (TS) at their C-terminus. ADAMTS-4 is the smallest, without a C-terminal TS, and ADAMTS-5 and 8 have two. Other members have 2–14 repeats. Spacer, spacer domain. Both ADAM and ADAMTS enzymes have an RXKR motif at the C-terminus of their propeptide for activation by proprotein convertases.

3 Microenvironment modification by proteolytic enzymes

3.1 Extracellular matrix degradation for cancer invasion

The ECM holds cancer and other cells together to create a TME. The ECM provides signals to cells through ECM receptors and migration cues. On the other hand, the ECM also acts as a physical barrier to invading cancer cells as it is a solid matrix. For a cancer cell to migrate through the ECM, its pore size needs to be big enough for cells to squeeze the nuclei to migrate through: 7 μm^2 for cancer cells (13). If the ECM gaps are not sufficiently large, cells will use proteolytic enzymes to enlarge the opening to migrate through. It has been well accepted that one of the major proteinases to degrade the ECM during invasion under the condition is MT1-MMP (4, 13–15). MT1-MMP degrades many ECM components, including fibrillar collagens I, II, III, fibronectin, vitronectin, laminins-1, -2, -4, and -5, fibrin/fibrinogen, perlecan, and aggrecan (4, 14). It activates other MMPs on the cell surface, namely, proMMP-2 and proMMP-13, expanding the proteolytic repertoire (14). ProMMP-2 activation is critical when cancer cells need to degrade the BM since a major component of the BM can be degraded by activated MMP-2 but not by MT1-MMP itself. It was shown that epithelial cancer cells could not invade or grow without stromal-derived proMMP-2 due to the inability to degrade type IV collagen (14, 16). MT1-MMP is also a major

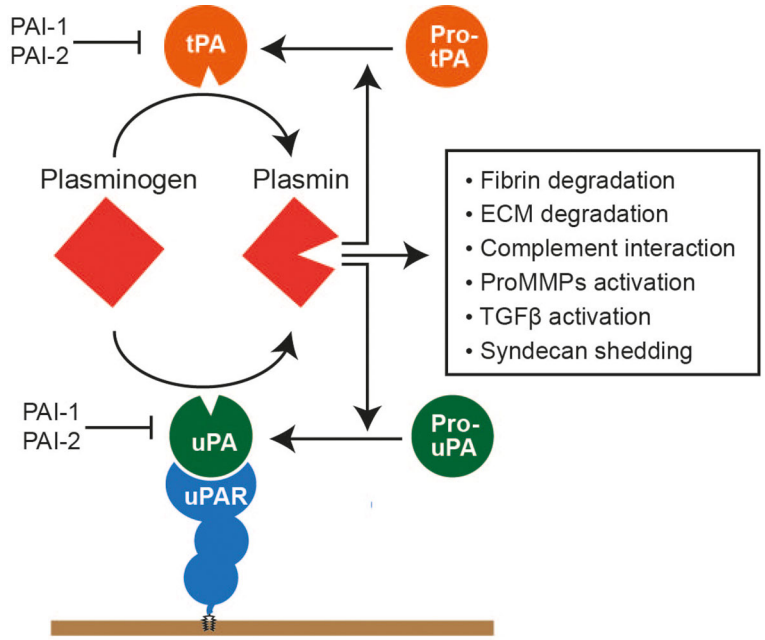

FIGURE 3
Plasmin system. Plasminogen is a precursor form of plasmin, mainly produced in the liver and present in the plasma at approximately 150–200 μg/ml. Plasminogen is activated by either a tissue plasminogen activator (tPA) or urokinase plasminogen activator (uPA). uPA is bound to the glycosylphosphatidylinositol-anchored uPA receptor and activates plasminogen on the cell surface. tPA and uPA are also produced as precursor forms, and activated plasmin can activate these activators. Activated plasmin can degrade cross-linked fibrin and various ECM components, interact with the complement system to facilitate complement cascade, activate proMMPs, activate the precursor form of TGFβ, and cause syndecan shedding.

collagenase that promotes cancer invasion in stromal tissue. There are five collagenolytic MMPs, including MMP-1, MMP-2, MMP-8, MMP-13, and MT1-MMP. However, MT1-MMP is the only collagenase that promotes cellular invasion within the type I collagen matrix (17).

MT1-MMP is regulated by different post-translational mechanisms to promote cellular invasion effectively. One is homodimer formation on the cell surface through the hemopexin (Hpx) domain and TM domain (18, 19). The homodimer state is considered an active state of the enzyme, as both the proMMP-2 activation and fibrillar collagen degradation activities of MT1-MMP on the cell surface require the enzyme to be in the dimer state (18, 20). In invading cells, the dimerization of MT1-MMP constitutively occurs at the leading edge (21). The dimerization was regulated by the coordination of the actin cytoskeleton, and Rac1 and Cdc42 activation was shown to enhance MT1-MMP dimerization (21).

The second regulation is localization at the "leading edge" membrane structures, such as lamellipodia and invadopodia. Preventing MT1-MMP localization to the leading edge would disable MT1-MMP-dependent cancer invasion as the coordination of MT1-MMP activity and migrating machinery would be lost (15). It was shown that MT1-MMP localization at the lamellipodia is mediated by interacting with a hyaluronan receptor CD44 through the Hpx domain (22). Since CD44 is associated with the actin cytoskeleton through ERM proteins at the cytoplasmic domain, MT1-MMP is also associated with F-actin indirectly.

Invadopodia is another leading-edge membrane structure, and it was initially characterized as "a vertical membrane protrusion extends towards ECM that contains proteinases to degrade ECM" (23). The key components of the invadopodium include a scaffold protein, tyrosine kinase substrate with 5 SH3 domains (Tks5), the actin-regulating molecule cortactin, neural Woskott–Aldrich syndrome protein N-WASP, and cofilin (23). Aside from these molecules, MT1-MMP is another component that provides invasive function to the membrane structure (23). It has been extensively documented that breast cancer cells extend the invadopodia structure and degrade the matrix creating punch hole degradation spots (24–29). However, as the invasion process progress, a single protrusion seems to expand to a larger cell cortex along the matrix to degrade further and push the ECM to expand the gaps of the meshwork (27). Thus, invadopodia can no longer be defined as a protruding membrane structure but as a membrane with a molecular composition of Tks5, cortactin, F-actin, and MT1-

MMP. It was shown that MT1-MMP localization at the invadopodia requires the cytoplasmic tail (CT) of the MT1-MMP (27, 30), suggesting that the CT-binding molecules play a role in MT1-MMPp localization at invadopodia. However, the crucial adaptor molecule enabling MT1-MMP localization at the invadopodia has not been identified yet.

On the other hand, two kinesin motor proteins, Kinesin-1 (KIF5B) and Kinesin-2 (KIF3A), were shown to be involved in MT1-MMP trafficking to the invadopodia (31). Recently, the picture of the MT1-MMP vesicle trafficking to invadopodia was further clarified by a study reporting that the ER (endoplasmic reticulum) protein, protrudin, is crucially involved in MT1-MMP vesicle transport to the invadopodia (Figure 4A) (32). Protrudin makes contact sites with RAB7 and phosphatidylinositol 3-phosphate (PI3P)–positive late endosomes (LEs) containing MT1-MMP. Protrudin hands over RAB7-binding KIF5 adaptor protein FYCO1, enabling the transport of MT1-MMP-containing vesicles along microtubules toward invadopodia at the plasma membrane (Figure 4A) (32).

Aside from invadopodia, MT1-MMP has been shown to localize at the focal adhesion (FA) (34–36). FA is where the distance of the plasma membrane and ECM is the closest since integrins directly interact with ECM components at FA. However, unlike invadopodia localization, MT1-MMP localization at the FA is independent of the CT of the MT1-MMP (34). It was shown that an eight-amino-acid loop structure called MT-Loop or IS-2 (^{163}PYAYIREG^{170}) within the catalytic domain is necessary to localize at the FA (34). Since MT-Loop is positioned on the opposite side of the catalytic site in the catalytic domain, it does not influence the catalytic function. Still, it acts as a molecular interface, allowing MT1-MMP to localize at the FA (34). It was recently discovered that the FA localization of MT1-MMP is carried out by direct intracellular trafficking of MT1-MMP-containing vesicles to the FA by kinesin superfamily motor proteins, KIF13A and KIF3A (33). KIF3A and KIF13A coordinately transport MT1-MMP-containing vesicles from the *trans-Golgi* to endosomes. KIF13A alone then takes over the vesicles and transports them from the endosomes to the plasma membrane (33) (Figure 4B). This is a distinct vesicle trafficking pathway from invadopodia as KIF5B is not involved (33). It is possible that KIF3A- and KIF13A-mediated trafficking can be therapeutic targets to prevent invasion in specific cancers that utilize FA-dependent invasion mechanisms.

In contrast to ECM degradation, the stiffening of the tumor ECM, called desmoplasia, is also known to correlate with tumor aggressiveness. In this case, stiffened ECM-driven signals promote the progression of cancer. This aspect is reviewed by Gkretsi and Stylianopoulos (37). It is seemingly contradictory, but cancer invasion only requires local ECM degradation; thus, it makes sense.

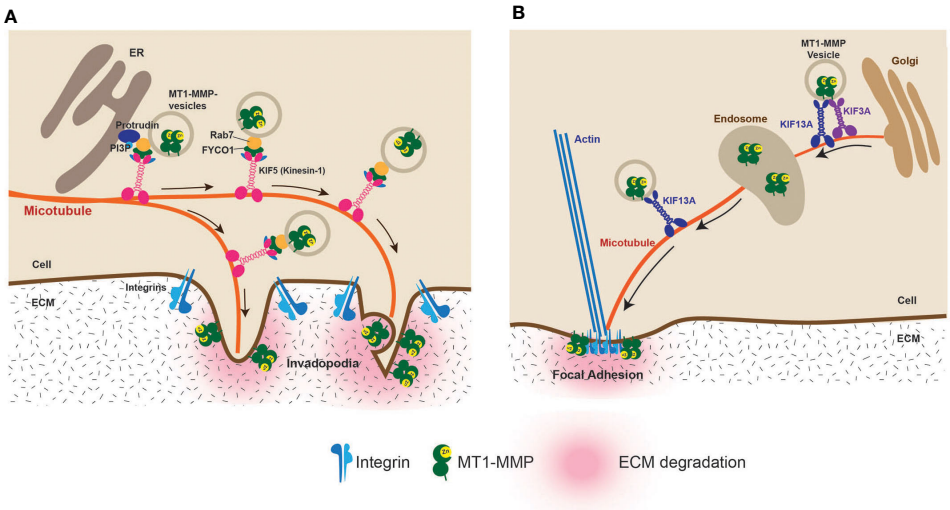

FIGURE 4
Vesicle transport of MT1-MMP to the invadopodia and the focal adhesion (FA). **(A)** Vesicle transport of MT1-MMP to the invadopodia has been extensively studied. It was shown that the endoplasmic reticulum protein protrudin plays a crucial role. Protrudin makes contact sites with RAB7 and phosphatidylinositol 3-phosphate (PI3P)–positive MT1-MMP-containing vesicles. Protrudin hands over RAB7-binding KIF5 adaptor protein FYCO1, enabling the transport of MT1-MMP-containing vesicles along microtubules toward invadopodia (32). **(B)** It was found that localization at FA is due to the direct transport of MT1-MMP-containing vesicles along the microtubules. KIF3A and KIF13A transport the vesicles between the *trans-Golgi* and the endosome. From the endosome, KIF13A solely transports the vesicles to the plasma membrane. The FA localization of MT1-MMP is essential for the HT1080 cell invasiveness (33).

3.2 Generation of matrikines: Bioactive fragments from extracellular matrix

ECM components are generally large multidomain glycoproteins that interact with each other to create a unique solid structure to support the function of the cells, tissues, and organs (2). These ECM molecules contain hidden sequences or modules that can send signals to the cells through the receptors upon exposure. These epitopes can be revealed either due to partial unfolding of the protein structures or proteolytic processing (38). These ECM fragments are termed "matrikines" (39). This section discusses collagen-derived fragments, elastin-derived fragments, and laminin-derived fragments.

3.2.1 Collagen-derived fragments

Non-fibrillar collagens consist of triple helical regions and non-triple helical regions, and some of these collagens were shown to contain antiangiogenic fragments. The first example is type XVIII collagen. It is a component of the BM and plays a significant role in providing the integrity of the structure of the BM for both endothelial and epithelial cells. It is well known that type XVIII collagen proteolysis generates angiogenesis inhibitor endostatin (38). It is a C-terminal non-collagenous domain 1 (NC1) fragment of collagen XVIII. Endostatin can be generated by many different proteinases, including the lysosome cysteine proteinases of Cathepsin L, Cathepsin B, and Cathepsin K; MMPs including MMP-3, MMP-9, MMP-12, MMP-13, MMP-20; and, to a less extent, by MMP-2 and MT1-MMP (38). An increase in the proteolytic activities of these proteinases in tumor tissue would generate endostatin and delay tumor angiogenesis and thereby tumor growth and metastasis.

The following example is type IV collagen. It is a major BM component and forms a thin sheet-like structure with laminin 5. Type IV collagen is composed of six different α chains (α1–α6) that are encoded by six different genes (COL4A1–COL4A6) (40). The three primary antiangiogenic fragments released from the α1, α2, and α3 chains of type IV collagen are arresten, canstatin, and tumstatin, respectively (40). It was shown that arresten was generated upon p53 activation in cancer cells, and it was due to p53-induced MMP activity (41). It was reported that MMP-2, MMP-3, and MMP-13 could generate tumstatin, but MMP-9 was the most efficient in liberating it from type IV collagen, and MMP-9 null mice showed significantly decreased circulating blood levels of tumstatin (42). While endostatin inhibits both physiological and tumor angiogenesis, tumstatin inhibits only tumor angiogenesis. It is because the tumstatin's receptor αvβ3 only plays a role in tumor angiogenesis (42). It was also shown that MT2-MMP could cleave the NC1 domain of type IV collagen in the submandibular gland, which promotes branching morphogenesis (43). Since MT2-MMP cleaves off all three chains, it effectively generates arresten, canstatin, and tumstatin (43).

The final example of antiangiogenic fragment generation is type XV collagen. It is classified as a chondroitin sulfate proteoglycan and a member of the multiplexin and non-fibrillar collagen subgroups (44). It is also a member of the FACIT collagen family (fibril-associated collagens with interrupted helices). Upon the cleavage of the C-terminal NC1 domain of type XV collagen on its α1 chain, restin, a 22-kDa antiangiogenic factor similar to endostatin, is produced (45). Restin exhibits antiangiogenic properties *in vivo* in xenograft carcinoma mouse models (45). However, responsible enzymes to generate restin have not been described. Similar other antiangiogenic fragments of ECM molecules include vastatin (type VIII collagen), anastellin (fibronectin), and endopellin (perlecan), but responsible proteinases are not known.

3.2.2 Elastin-derived fragments

Elastin provides elasticity and resilience to tissues, including the lungs, arteries, and skin. It shows a unique protein containing a large amount of four hydrophobic amino acids of Gly, Val, Ala, and Pro. It is heavily cross-linked at Lys residues. Due to its hydrophobicity and extensive cross-linking, elastin is insoluble, highly resistant to proteolytic degradation, and does not undergo substantial turnover in healthy tissue (46–48). However, it was found that elastin can be extensively degraded by proteinases related to inflammation and cancer.

It has been reported that MMP-7, MMP-9, and MMP-12 degraded elastin extensively and also generated fragments possessing pro-inflammatory activities (49). It has also been reported that neutrophil-derived serine proteinases, NE, CatG, and RR3, degrade elastin, and these elastin-derived peptides possess pro-inflammatory activities (50). VG-6 (VGVAPG) and AG-9 (AGVPGLGVG) peptides are especially considered to be active fragments showing various pro-inflammatory and protumorigenic activities (38).

3.2.3 Laminin-derived fragments

Laminin has also been extensively studied for biological fragments. Laminin 5 (Laminin 332) is a major component of the epithelial and endothelial BM aside from type IV collagen, and it is composed of the three laminin chains of α3, β3, and γ2. After secretion and deposition in the ECM, laminin 332 undergoes physiological maturation processes consisting of the proteolytic processing of domains located within the α3 and the γ2 chains by plasmin (51), mammalian tolloid (mTLD) (52), and bone morphogenic protein 1 (BMP-1) (53). These maturation events are essential for laminin 332 integration into the BM, where it plays a vital function in the nucleation and maintenance of anchoring structures. C-terminal globular domains 4 and 5 (LG45) of the α3 chain are proteolytically removed during

maturation, but soluble LG45 has biological functions. It was shown that soluble LG45 induced keratinocyte migration and the expression of MMP-1 and MMP-9 (54).

It was shown that a 30-kDa γ2 chain fragment containing an epidermal growth factor (EGF)–like motif (DIII, domain III) was released by the two cleavages by MT1-MMP and MMP-2 (55–57). The released DIII fragment of the γ2 chain then promotes the migration and invasion of cancer cells by engaging to the EGF receptor (56–58). It is considered that this event promotes the growth and initial breach of the BM at primary tumor sites.

3.3 Releasing extracellular matrix–bound soluble factors

One of the important biological roles of the ECM is pooling growth factors and cytokines (59, 60). There are growth factors associated with heparan sulfate (HS) and those that interact with matrix proteins (59, 60). They are secreted from the cells and retained in the ECM. Binding to the ECM prevents these soluble factors from binding to their receptors, but upon liberating from the ECM, they become bioavailable to cells to transmit the signals (59, 60). Proteolytic enzymes are responsible for this release.

One of the examples is the vascular endothelial growth factor (VEGF). The VEGF is a potent inducer of angiogenesis, implicated in cancer angiogenesis (61). It binds to HS through the heparin-binding domain with basic motifs encoded by exons 6 and 7 (61). VEGF has several alternative splicing variants, including $VGFA_{121}$, $VGFA_{165}$, $VEGF_{189}$, and $VEGF_{206}$. $VEGF_{189}$ and $VEGF_{206}$ have two heparin-binding sites, and $VEGF_{165}$ has a single heparin-binding domain encoded by exon 7, while $VGFA_{121}$ does not have the heparin-binding domain (61). $VEGF_{165}$ is the most physiologically relevant VEGF isoform, and the heparin-binding domain locates at the C-terminus. While $VEGF_{189}$ and $VEGF_{206}$ exclusively localize on the cell surface or ECM and cannot be detected in the culture medium due to two heparin-binding domains, 50%–70% of $VEGF_{165}$ can be secreted to the medium due to weaker affinity to HS (62). Serine proteinase plasmin was shown to proteolytically release the ECM-bound VEGF species of both $VEGF_{165}$ and $VEGF_{189}$ into a soluble biologically active VEGF (63), suggesting that the proteolytic cascade of plasminogen activation, a critical step during angiogenesis, can result in an angiogenic switch. It was also found that MMP-9 can cause an angiogenic switch in tumor tissue by releasing VEGF from the matrix (64).

Another example is TGF-β, which exerts both tumor-suppressive and -promoting effects (65). The suppressive effect is due to its ability to upregulate the cyclin kinase inhibitors, causing the inhibition of cell proliferation. However, as the cancer progresses, cyclin kinase inhibitors become refractory to growth inhibition and begin to produce large amounts of TGF-β (65). TGF-β is produced as an inactive pro-form and requires proteolytic conversion by furin or other proteinases, such as MMP-9, to become an active form. MMP-9 can localize at the cell surface by binding to the CD44, a hyaluronan receptor, and then activate TGFβ (66). It was also shown that MT1-MMP and MMP-2 could activate TGF-β1 (67). On the other hand, MMP-2 and MMP-9, and MT1-MMP indirectly modulate TGF-β by cleaving the latent TGFβ-binding protein 1 (LTBP-1), releasing ECM-bound TGF-β (68, 69). Since tumor cells often acquire non-responsiveness to TGF-β, the proteolytic activation of TGF-β by MMPs may exhibit cancer-promoting effects by selectively driving stroma-mediated cancer invasion and metastasis (65). It has also been shown that plasmin can release active TGFβ from the ECM (70).

Although it is not a proteolytic action, the degradation of HS chains in HS proteoglycans (HSPGs), such as syndecans and perlecan, by the hepanase glycolytic enzyme can also release growth factors and is also considered to be an essential modulator of growth factor signaling within the TME.

3.4 Processing soluble factors: cytokines and chemokines

Proteinases are known to process cytokines and modify their signals (71). Interleukin 1β (IL-1β) is degraded by MMP-1, MMP-2, MMP-3, and MMP-9, while IL-1α is resistant to these proteolytic enzymes (72). Although both IL-1α and IL-1β bind to the same IL-1 receptor (IL1R) and activate through the same pathway, they are separately encoded proteins with low sequence homology and divergent biological processes, cellular localization, and the mechanisms of activation (73). However, IL-1β was shown to be involved in cancer more than IL-1α. IL1β has two opposite roles in cancer: promoting cancer and suppressing cancer. The tumor-promoting effects of IL-1β are to promote inflammation-driven carcinogenesis and cause tissue damage by upregulating various MMPs. On the other hand, the tumor-suppressing effect is the activation of anticancer immunity (73). Cancer may take advantage of IL-1β degradation to evade immunity.

Another example of proteolytic processing is chemokines. It has been shown that MMP-dependent chemokine proteolysis can affect the biological functions of chemokines in different ways (71). First, the proteolysis inactivates the chemokine. Second, the processing generates antagonistic derivatives, which can still bind to the chemokine receptor but cannot exert chemotaxis. Third, the truncation of chemokine results in a higher chemotactic effect. It has been shown that MMP-1, MMP-2, MMP-3, MMP-9, MMP-13, and MT1-MMP inactivate CXCL12 (stromal cell-derived factor-1) (74). MMP-2 also sheds the plasma membrane-associated chemokine, CX3CL1 (fractalkine), generating a soluble chemokine. However, an additional cleavage at the N terminus of the protein by MMP-2 inactivates the chemokine, converting it into a potent antagonist (75).

MMP-9 also inactivates CXCL chemokines, including CXCL4 and CXCL1 (76). MMP-9 inactivates CXCL5 and CXCL7 as well (76). It was also shown that MMP-8 and MMP-9 inactivate CXCL9 and CXCL10 by processing their C-terminus (77).

Several inactivated chemokines can still bind to their receptors, acting as functional antagonists. MMP-1, MMP-2, MMP-3, MMP-13, and MMP-14 process CCL7 (MCP-3) into an antagonistic form (78, 79). The closely related chemokines CCL2 (MCP-1) and CCL13(MCP-4) can also be cleaved by MMP-1 and MMP-3 and CCL8 (MCP-2) by MMP-3 (79). Thus, MMPs can exhibit anti-inflammatory effects by dampening the action of chemokines.

MMP-9 was shown to process CXCL8 (IL-8), significantly increasing chemotactic activity (76). MMP-8, MMP-13, and MT1-MMP also generate truncated IL-8 species with increased activity (80, 81). MMP-8 also activates CXCL5 (81).

3.5 Membrane protein shedding and processing

ECM–cell communication is mediated by cell surface receptors and other cell surface molecules, and the proteolytic cleavage of these membrane proteins termed shedding modifies microenvironment signaling. The major shedding enzymes are MT1-MMP, ADAM17, and ADAM10 in the TME. They are type-I TM proteinases, and, together, these enzymes modify diverse signaling pathways. This section discusses six shedding examples that influence cancer progression, namely, CD44, ICAM-1, DDRs, syndecans, EphA2, and HB-EGF.

3.5.1 CD44

CD44 is a type I TM cell adhesion molecule whose ligand is hyaluronic acid (HA), a glycosaminoglycan (82–84). It has been shown that CD44 can also bind to osteopontin (85), fibronectin, type I collagen (86), type IV collagen (87), and matrix metalloproteinases (MMPs) (88). CD44 is expressed in most cell types in our body, and a shed form of soluble CD44 has been detected in the circulation and other body fluids (83). A single gene encodes CD44, but alternative splicing generates multiple isoforms. CD44 gene contains 20 exons, and the most common form of CD44, referred to as standard or hematopoietic CD44, contains 10 exons (82, 83, 89). This form is the shortest isoform, and other forms have the insertion of alternative exons (V2–V10) at a single site within the membrane-proximal region of the ectodomain (82, 83, 89). Interestingly CD44 with V3 insertion made CD44 to be modified with HS, which may provide additional functionality to the receptor: HB-EGF presentation (90). CD44 consists of N-terminal HA-binding globular domain, followed by a stem with glycosylation and GAG binding sites, a TM domain, and the cytoplasmic tail. The cytoplasmic domain binds to band 3.1 proteins (ERM proteins), linking CD44 to the actin cytoskeleton (83) (Figure 2A). It has been reported that CD44 can transition to a high-affinity state upon the stimulation of the cells by soluble factors (91–93). However, the molecular event on CD44 during the activation process is not understood.

CD44 was shed by three TM metalloproteinases, namely, MT1-MMP (94), ADAM10, and ADAM17 (95, 96). The CD44 shedding by each metalloproteinase was shown to promote cell migration (94, 95). MT1-MMP shedding occurs constitutively at the lamellipodia when CD44 and MT1-MMP are coexpressed in the cells (94). It was found that CD44 shedding by MT1-MMP promoted cancer cell migration on the HA-based substratum (94). CD44 interacts with MT1-MMP through its stem region and the hemopexin (Hpx) domain of MT1-MMP, which mediates MT1-MMP localization at the lamellipodia (22). ADAM10- or ADAM17-dependent CD44 shedding was induced by calcium influx or protein kinase C activation, respectively (97, 98). However, when cell migration on the HA-based matrix was measured, the knockdown of ADAM10 or 17 in human lung adenocarcinoma inhibited the migration by 75% in both (98), suggesting that ADAM-dependent CD44 shedding also supports cell migration on the HA matrix. Since CD44 is localized at the lamellipodia, and the suppression of Rac1 by overexpressing Rac1 dominant-negative mutant inhibited the shedding (97), CD44 shedding by these proteinases also occurs at the lamellipodia. It has been reported that adding HA to the cells initiated CD44 shedding (99), suggesting that CD44 shedding may occur at the leading edge where CD44 binds to the HA-containing substratum (Figure 2). It was shown that after shedding the ectodomain by a metalloproteinase, the soluble intracellular domain of CD44 was released by presenilin-dependent gamma-secretase (100, 101), and this fragment has a transformation activity (101). Thus, CD44 ectodomain shedding triggers transformation as well. Taking together, the membrane proteinase-dependent shedding is likely the core of CD44-mediated cell migration. As described above, CD44 is cleaved by three membrane-bound metalloproteinases, and all of this shedding promotes cell migration. However, it is unclear which shedding events play a role in different types of cell migration. In human melanoma cells, the constitutive shedding of CD44 was reported to be mediated by ADAM10 but not by MT1-MMP or ADAM17, although all these enzymes are expressed in the cells (102). Further clarifications are required in the future.

3.6 Intercellular adhesion molecule–1

Intercellular adhesion molecule (ICAM)–1 is a TM glycoprotein of the immunoglobulin (Ig)–like superfamily. It consists of five extracellular Ig–like domains (D1-D5), a TM domain, and a short cytoplasmic tail. ICAM-1 interacts with the $\alpha_L\beta_2$ integrin (lymphocyte function-associated antigen 1 or LFA-1), mediating cell–cell interaction. ICAM-1 is expressed

in endothelial cells, and $\alpha_L\beta_2$ integrin in lymphocytes and myeloid cells, and ICAM-1–$\alpha_L\beta_2$ interaction is crucial for the transendothelial migration of the lymphocytes and myeloid cells (103). Soluble proteolytically shed ICAM-1 (sICAM-1) has been detected in human serum, and it contains all five IgG domains of the D1-D5 (104). Thus, the cleavage for this shedding occurs between D5 and the TM domain. It has been shown that NE cleaves ICAM-1 (105). However, it was revealed that an antibody against D1 inhibited NE-mediated cleavage, indicating that NE is unlikely to cleave between D5 and the TM region. Therefore, NE is unlikely to be responsible for generating sICAM-1. Later, it was found that phorbol 12-myristate 13-acetate-induced ICAM-1 shedding was due to ADAM17 (106). In addition, it was found that MT1-MMP-mediated ICAM-1 shedding plays a crucial role during the transendothelial migration of monocytes (107). It was also reported that oxidative stress–induced ICAM-1 shedding was MT1-MMP dependent (108). Most recently, it has been found that ADAM10-mediated ICAM-1 shedding plays a role in the transendothelial migration of neutrophils (109). Thus, it is possible that ICAM-1 shedding may be involved in the infiltration of lymphocytes and myeloid cells within the TME. ICAM-1–$\alpha_L\beta_2$ interaction was also shown to play a role in the transendothelial migration of the melanoma (110). It was demonstrated that the coculture of melanoma cells with endothelial cells induced the expression of $\alpha_L\beta_2$ in melanoma cells, allowing them to interact with ICAM-1 in endothelial cells. Given the role of ICAM-1 shedding during the transendothelial migration of lymphocytes and myeloid cells, it is expected that the shedding also plays a role in the transendothelial migration of melanoma.

3.6.1 Syndecans

Syndecans are type 1 TM HSPGs. The HS chains at the extracellular domains interact with different ligands, including ECM glycoproteins, cytokines, chemokines, and growth factors. There are four syndecans. Syndecan-1 is highly expressed in epithelia, syndecan-2 in endothelia and fibroblasts, syndecan-3 is mainly expressed in neuronal and some musculoskeletal tissue, while syndecan-4 can be found in most tissues. A single cell can express multiple syndecans. Each syndecan is attached by three HS chains, and syndecan-1 and syndecan-3 are attached by additional two chondroitin sulfate chains. The TM domain of all syndecans contains a GXXXG motif that promotes the formation of SDS-resistant dimers (111, 112). This TM domain–mediated dimer was reported to be crucial for the function of syndecan-2 and syndecan-4 (112). Syndecans are known to be shed by many different proteinases (113). Syndecan-1 was shown to be shed by MMP-7 (114), MMP-9 (115), MT1-MMP, MT3-MMP (116), and ADAM17 (117). Syndecan-2 was shown to be shed by MMP-2, MMP-9 (118), MMP-7 (119), and MT1-MMP (120). Syndecan-3 sheddase was shown to be metalloproteinase, but it has not been identified yet (121). Serine proteinase, thrombin, was also shown to cleave syndecan-3 (122). Syndecan-4 is shed by MMP-9 (115), ADAM17 (117), ADAMTS1 (123), plasmin (124), and thrombin (122, 124). Syndecan shedding has two biological effects. First, it decreases syndecan levels on the cell surface. Several growth factors are known to interact with the HS chain of the syndecans, including fibroblasts growth factor (FGF), vascular endothelial growth factor (VEGF), EGF, hepatocyte growth factor (HGF), platelet-derived growth factor (PDGF), and transforming growth factor β1 (TGFβ1). This interaction is essential for growth factor signaling. It has been shown that HS-bound FGF-2 increased the affinity for FGFR by over one magnitude (125). Thus, loss of syndecan by shedding would greatly influence the presentation of growth factors to the receptors. The second effect is that the shed ectodomain of syndecans can act as a soluble factor that exerts biological function. For instance, shed soluble syndecan-1 from fibroblasts can mediate mitogenic responses in human breast cancer cells. This paracrine event is mediated by the HS chain, basic FGF, and stromal-derived factor 1 (126). Another example can be that shed syndecan-2 deposited to the ECM can be a ligand for the protein tyrosine phosphatase receptor CD148 to promote β1 integrin-mediated cell adhesion (127).

3.6.2 Discoidin domain receptors

Discoidin domain receptors (DDRs) are collagen receptor tyrosine kinases, and there are two types, DDR1 and DDR2. Both DDRs have a collagen-binding discoidin domain at the N-terminus of the ectodomain and tyrosine kinase domain at their cytoplasmic domain. DDRs are the only receptor tyrosine kinase whose ligands are collagens. Both DDRs bind to fibrillar collagens, but DDR1 additionally binds to type IV collagen. Under physiological conditions, DDR1 is expressed in epithelial cells, while DDR2 is expressed in mesenchymal cells.

DDR1 and DDR2 bind to the GVMGFO motif (128, 129) found in collagen types I, II, and III, distinct from the β1 integrin-binding site GFOGER (130). Thus, the binding of DDRs and integrins are independent. For DDRs to bind collagens, they must form a homodimer (131). The DDR1 dimer is likely mediated through the leucine zipper in the TM domain (132), while the DDR2 ectodomain spontaneously forms a dimer (131). Thus, ligand binding–induced dimerization, which is found in many receptor tyrosine kinases, does not apply to DDRs. It has been shown that further clustering of dimer DDRs occurs upon collagen binding. Interestingly, inter-DDR dimer phosphorylation was shown to occur between DDR1s and between DDR1 and DDR2 (133).

It was shown that the DDR1 ectodomain is proteolytically shed upon the collagen stimulation of the cells, which can be inhibited by a broad-spectrum metalloproteinase inhibitor (134). Later, the responsible enzyme was identified as ADAM10 (135). Interestingly ADAM10 and DDR1 exist as a

stable complex on the cell surface, but the shedding does not occur unless collagen binds to DDR1. Since the interaction of DDRs with collagen cannot be controlled by inside-out signaling like integrins, ectodomain shedding is the only means to dissociate cells from DDR1-mediated collagen adhesion. It was shown that shedding-deficient DDR1 had a much longer half-life of collagen-induced tyrosine phosphorylation (135), suggesting that DDR1 shedding controls the duration of collagen signaling. The DDR1-mediated collagen signal has been shown to increase cell motility (136). When cells migrate on the collagen matrix, adhesion to the matrix is essential, but dissociation from the collagen is equally important, and ADAM10-dependent DDR1 shedding plays a key role. The inhibition of DDR1 shedding by ADAM10 significantly inhibited epithelial cell migration on the collagen matrix (135). Aside from ADAM10, MT1-MMP was also reported to shed a DDR1 ectodomain. It was shown that the coexpression of MT1-MMP with DDR1 in COS7 cells caused a constitutive shedding of DDR1 ectodomain (137). However, this event was not shown in endogenous MT1-MMP and DDR1 (137). Thus, further investigation is necessary to examine the role of MT1-MMP in DDR1 shedding.

DDR2 must also be dissociated from collagen upon transmitting collagen signals, but DDR2 shedding has not been described, and an alternative mechanism has not been identified.

3.6.3 EphA2

Erythropoietin-producing hepatocellular receptor-2 (EphA2) is a member of the Eph receptor kinase family, which is overexpressed frequently in diverse cancer types (138, 139). EphA2 is also overexpressed in various cancer cell lines, such as fibrosarcoma, breast cancer, and ovarian cancer, and high EphA2 levels are correlated with increased malignancy and poor clinical prognosis (140). Furthermore, ectopic expression of EphA2 in a normal mammary epithelial cell line, MCF10A, was enough to confer tumorigenicity in mice (141). However, activation of EphA2 is known to exhibit tumor-suppressive activities (140, 142); thus, the exact mechanism of tumor-promoting activity of EphA2 was unclear. It turns out that the shedding of EphA2 by MT1-MMP was one of the mechanisms promoting cancer. It was shown that both EphA2 and MT1-MMP are upregulated in different invasive breast cancer cells, and silencing the EphA2 or MT1-MMP gene inhibited collagen invasion of the cells. It was found that the proteolytic cleavage of EphA2 by MT1-MMP initiated increased cleaved EphA2 translocation to the intracellular compartment and increased activity of RhoA small GTPase, which, in turn, caused a repulsive effect between cells, and promoted single cancer cell invasion (143). The shedding of EphA2 by MT1-MMP was also found to play other important roles in cancer progression. Without EphA2 cleavage by MT1-MMP, the ligation of ephrin A1 to EphA2 causes a significant inhibition of EGF-ErbB induced phosphor-Erk, phosphor-Akt, anchorage-independent growth, and cell migration (144). Upon EphA2 cleavage by MT1-MMP, this effect was significantly hampered; thus, EphA2 shedding by MT1-MMP converts a tumor-suppressive RTK to an oncoprotein (144).

3.6.4 Heparin-binding epidermal growth factor

Heparin-binding EGF (HB-EGF), a member of the EGF family, transduces extracellular signals *via* ErbB receptors and plays a pivotal role in many physiologic and pathologic processes (145, 146). HB-EGF is also expressed in various human carcinomas such as pancreatic, esophageal, colon, gastric, ovarian, and bladder cancers (147). HB-EGF is synthesized as a type-I TM pro-HB-EGF, and its propeptide is removed by proprotein convertases such as furin during secretion to the cell surface. The ectodomain of HB-EGF comprises a heparin-binding domain containing a core stretch of basic amino acids at its N-terminus, followed by an EGF-like domain and a juxtamembrane domain (145). Membrane-bound HB-EGF can bind to its cognate ErbB receptors expressed in other cells *in trans*, or its ectodomain can be proteolytically cleaved at the juxtamembrane region to become a soluble HB-EGF and ligate ErbB receptors in neighboring cells, transmitting a signal. It has been reported that ADAM10, ADAM12, and ADAM17 shed HB-EGF to generate a soluble HB-EGF. In addition, MMP-2 or -9 (148), MMP-7 (149), and MMP-10 (150) were also reported to shed HB-EGF as well. This shedding event makes HB-EGF bioavailable to cells within the TME.

The heparin-binding domain (HBD) of HB-EGF prevents the EGF-like domain from binding to its cognate ErbB receptors. However, heparin-binding to the HBD renders the EGF-like domain available to ligate ErbB. Thus, the binding to the HSPG is thought necessary for HB-EGF to transmit a signal to the cells. However, it was found that MT1-MMP removes the N-terminal 20 amino acids of HBD by cleaving at A_{81}-L_{82}, making an HB-EGF heparin-independent growth factor (151). It was shown that this MT1-MMP cleavage plays a significant role in cancer cell growth in a three-dimensional matrix (151).

4 Conclusion and future prospective

Within the TME, there are many signaling events in cancer cells and neighboring cells. They can be signals from the ECM, soluble factors, and cell–cell communications. As discussed above, many of these signaling events involve the proteolytic modulation of signaling molecules. Therefore, proteolytic enzymes are considered part of these signaling events, and cancer cells utilize them for their malignant progression. It becomes apparent that several enzymes promote cancer progression by modulating multiple signaling events. Especially, membrane-bound

metalloproteinase, MT1-MMP, ADAM10, and ADAM17, are significant players. For instance, MT1-MMP plays a role in ECM degradation for invasion and metastasis, laminin-5 γ2 chain processing to stimulate cell motility and growth, cleaving chemokines to modulate host immunity, shedding CD44 to promote cell migration, shedding ICAM-1 to mediate trans-endothelial migration, shedding EphA2 to enhance EGF signaling in cancer, and cleaving the N-terminus of HB-EGF to convert it to heparin-independent growth factor, promoting cancer cell growth and motility. ADAM10 and ADAM17 play a role in CD44 shedding to promote cell migration, ICAM-1 shedding to mediate the trans-endothelial migration of cells, syndecans' shedding to modulate heparan-sulfate-mediated signaling events, ADAM10-mediated DDR1 shedding to modulate DDR1-mediated cell adhesion and to control prolonged collagen signaling, and HB-EGF shedding to generate soluble HB-EGF. Thus, the inhibition of each enzyme or all these enzymes would inhibit multiple events in the TME, which significantly impact cancer progression. Therefore, these metalloproteinases can be potentially effective target molecules for cancer therapy. However, the past failures of the clinical trial of metalloproteinase inhibitors have hampered metalloproteinase inhibitor drug development. Further understanding of the regulation of these enzymes during cancer progression may reveal novel means to control the activity of these enzymes without directly inhibiting the enzyme activities so that novel treatments that target cancer invasion, growth, and metastasis can be developed in the future.

Author contributions

The author confirms being the sole contributor of this work and has approved it for publication.

Funding

This work was funded by Special fund by the Kennedy Institute of Rheumatology.

Conflict of interest

The author declares that the research was conducted in the absence of any commercial or financial relationships that could be construed as a potential conflict of interest.

Publisher's note

All claims expressed in this article are solely those of the authors and do not necessarily represent those of their affiliated organizations, or those of the publisher, the editors and the reviewers. Any product that may be evaluated in this article, or claim that may be made by its manufacturer, is not guaranteed or endorsed by the publisher.

References

1. Hanahan D, Coussens LM. Accessories to the crime: functions of cells recruited to the tumor microenvironment. *Cancer Cell* (2012) 21(3):309–22. doi: 10.1016/j.ccr.2012.02.022

2. Karamanos NK. Extracellular matrix: key structural and functional meshwork in health and disease. *FEBS J* (2019) 286(15):2826–9. doi: 10.1111/febs.14992

3. Karamanos NK, Theocharis AD, Neill T, Iozzo RV. Matrix modeling and remodeling: A biological interplay regulating tissue homeostasis and diseases. *Matrix Biol* (2019) 75-76:1–11. doi: 10.1016/j.matbio.2018.08.007

4. Piperigkou Z, Kyriakopoulou K, Koutsakis C, Mastronikolis S, Karamanos NK. Key matrix remodeling enzymes: Functions and targeting in cancer. *Cancers (Basel)* (2021) 13(6):1441. doi: 10.3390/cancers13061441

5. Nagase H, Visse R, Murphy G. Structure and function of matrix metalloproteinases and TIMPs. *Cardiovasc Res* (2006) 69(3):562–73. doi: 10.1016/j.cardiores.2005.12.002

6. Itoh Y, Nagase H. Matrix metalloproteinases in cancer. *Essays Biochem* (2002) 38:21–36. doi: 10.1042/bse0380021

7. Murphy G. The ADAMs: signalling scissors in the tumour microenvironment. *Nat Rev Cancer* (2008) 8(12):929–41. doi: 10.1038/nrc2459

8. Murphy G, Nagase H. Reappraising metalloproteinases in rheumatoid arthritis and osteoarthritis: destruction or repair? *Nat Clin Pract Rheumatol* (2008) 4(3):128–35. doi: 10.1038/ncprheum0727

9. Apte SS. ADAMTS proteins: Concepts, challenges, and prospects. *Methods Mol Biol* (2020) 2043:1–12. doi: 10.1007/978-1-4939-9698-8_1

10. Baker SK, Strickland S. A critical role for plasminogen in inflammation. *J Exp Med* (2020) 217(4):e20191865. doi: 10.1084/jem.20191865

11. Burster T, Mustafa Z, Myrzakhmetova D, Zhanapiya A, Zimecki M. Hindrance of the proteolytic activity of neutrophil-derived serine proteases by serine protease inhibitors as a management of cardiovascular diseases and chronic inflammation. *Front Chem* (2021) 9:784003. doi: 10.3389/fchem.2021.784003

12. Korkmaz B, Moreau T, Gauthier F. Neutrophil elastase, proteinase 3 and cathepsin G: physicochemical properties, activity and physiopathological functions. *Biochimie* (2008) 90(2):227–42. doi: 10.1016/j.biochi.2007.10.009

13. Wolf K, Te Lindert M, Krause M, Alexander S, Te Riet J, Willis AL, et al. Physical limits of cell migration: control by ECM space and nuclear deformation and tuning by proteolysis and traction force. *J Cell Biol* (2013) 201(7):1069–84. doi: 10.1083/jcb.201210152

14. Itoh Y. Membrane-type matrix metalloproteinases: Their functions and regulations. *Matrix Biol* (2015) 44-46:207–23. doi: 10.1016/j.matbio.2015.03.004

15. Gifford V, Itoh Y. MT1-MMP-dependent cell migration: proteolytic and non-proteolytic mechanisms. *Biochem Soc Trans* (2019) 47(3):811–26. doi: 10.1042/BST20180363

16. Taniwaki K, Fukamachi H, Komori K, Ohtake Y, Nonaka T, Sakamoto T, et al. Stroma-derived matrix metalloproteinase (MMP)-2 promotes membrane type 1-MMP-dependent tumor growth in mice. *Cancer Res* (2007) 67(9):4311–9. doi: 10.1158/0008-5472.CAN-06-4761

17. Sabeh F, Ota I, Holmbeck K, Birkedal-Hansen H, Soloway P, Balbin M, et al. Tumor cell traffic through the extracellular matrix is controlled by the membrane-anchored collagenase MT1-MMP. *J Cell Biol* (2004) 167(4):769–81. doi: 10.1083/jcb.200408028

18. Itoh Y, Ito N, Nagase H, Evans RD, Bird SA, Seiki M. Cell surface collagenolysis requires homodimerization of the membrane-bound collagenase MT1-MMP. *Mol Biol Cell* (2006) 17(12):5390–9. doi: 10.1091/mbc.e06-08-0740

19. Itoh Y, Ito N, Nagase H, Seiki M. The second dimer interface of MT1-MMP, the transmembrane domain, is essential for ProMMP-2 activation on the cell surface. *J Biol Chem* (2008) 283(19):13053–62. doi: 10.1074/jbc.M709327200

20. Itoh Y, Takamura A, Ito N, Maru Y, Sato H, Suenaga N, et al. Homophilic complex formation of MT1-MMP facilitates proMMP-2 activation on the cell surface and promotes tumor cell invasion. *EMBO J* (2001) 20(17):4782–93. doi: 10.1093/emboj/20.17.4782

21. Itoh Y, Palmisano R, Anilkumar N, Nagase H, Miyawaki A, Seiki M. Dimerization of MT1-MMP during cellular invasion detected by fluorescence resonance energy transfer. *Biochem J* (2011) 440(3):319–26. doi: 10.1042/BJ20110424

22. Mori H, Tomari T, Koshikawa N, Kajita M, Itoh Y, Sato H, et al. CD44 directs membrane-type 1 matrix metalloproteinase to lamellipodia by associating with its hemopexin-like domain. *EMBO J* (2002) 21(15):3949–59. doi: 10.1093/emboj/cdf411

23. Paterson EK, Courtneidge SA. Invadosomes are coming: new insights into function and disease relevance. *FEBS J* (2018) 285(1):8–27. doi: 10.1111/febs.14123

24. Sharma P, Parveen S, Shah LV, Mukherjee M, Kalaidzidis Y, Kozielski AJ, et al. SNX27-retromer assembly recycles MT1-MMP to invadopodia and promotes breast cancer metastasis. *J Cell Biol* (2020) 219(1):e201812098. doi: 10.1083/jcb.201812098

25. Artym VV, Zhang Y, Seillier-Moiseiwitsch F, Yamada KM, Mueller SC. Dynamic interactions of cortactin and membrane type 1 matrix metalloproteinase at invadopodia: defining the stages of invadopodia formation and function. *Cancer Res* (2006) 66(6):3034–43. doi: 10.1158/0008-5472.CAN-05-2177

26. Zagryazhskaya-Masson A, Monteiro P, Mace AS, Castagnino A, Ferrari R, Infante E, et al. Intersection of TKS5 and FGD1/CDC42 signaling cascades directs the formation of invadopodia. *J Cell Biol* (2020) 219(9):e201910132. doi: 10.1083/jcb.201910132

27. Ferrari R, Martin G, Tagit O, Guichard A, Cambi A, Voituriez R, et al. MT1-MMP directs force-producing proteolytic contacts that drive tumor cell invasion. *Nat Commun* (2019) 10(1):4886. doi: 10.1038/s41467-019-12930-y

28. Castro-Castro A, Marchesin V, Monteiro P, Lodillinsky C, Rosse C, Chavrier P. Cellular and molecular mechanisms of MT1-MMP-Dependent cancer cell invasion. *Annu Rev Cell Dev Biol* (2016) 32:555–76. doi: 10.1146/annurev-cellbio-111315-125227

29. Poincloux R, Lizárraga F, Chavrier P. Matrix invasion by tumour cells: a focus on MT1-MMP trafficking to invadopodia. *J Cell Sci 122(Pt* (2009) 17):3015–24. doi: 10.1242/jcs.034561

30. Nakahara H, Howard L, Thompson EW, Sato H, Seiki M, Yeh Y, et al. Transmembrane/cytoplasmic domain-mediated membrane type 1-matrix metalloprotease docking to invadopodia is required for cell invasion. *Proc Natl Acad Sci U.S.A.* (1997) 94(15):7959–64. doi: 10.1073/pnas.94.15.7959

31. Marchesin V, Castro-Castro A, Lodillinsky C, Castagnino A, Cyrta J, Bonsang-Kitzis H, et al. ARF6-JIP3/4 regulate endosomal tubules for MT1-MMP exocytosis in cancer invasion. *J Cell Biol* (2015) 211(2):339–58. doi: 10.1083/jcb.201506002

32. Pedersen NM, Wenzel EM, Wang L, Antoine S, Chavrier P, Stenmark H, et al. Protrudin-mediated ER-endosome contact sites promote MT1-MMP exocytosis and cell invasion. *J Cell Biol* (2020) 219(8):e202003063. doi: 10.1083/jcb.202003063

33. Gifford V, Woskowicz A, Ito N, Balint S, Lagerholm BC, Dustin ML, et al. Coordination of two kinesin superfamily motor proteins, KIF3A and KIF13A, is essential for pericellular matrix degradation by membrane-type 1 matrix metalloproteinase (MT1-MMP) in cancer cells. *Matrix Biol* (2022) 107:1–23. doi: 10.1016/j.matbio.2022.01.004

34. Woskowicz AM, Weaver SA, Shitomi Y, Ito N, Itoh Y. MT-LOOP-dependent localization of membrane type I matrix metalloproteinase (MT1-MMP) to the cell adhesion complexes promotes cancer cell invasion. *J Biol Chem* (2013) 288(49):35126–37. doi: 10.1074/jbc.M113.496067

35. Takino T, Watanabe Y, Matsui M, Miyamori H, Kudo T, Seiki M, et al. Membrane-type 1 matrix metalloproteinase modulates focal adhesion stability and cell migration. *Exp Cell Res* (2006) 312(8):1381–9. doi: 10.1016/j.yexcr.2006.01.008

36. Wang Y, McNiven MA. Invasive matrix degradation at focal adhesions occurs *via* protease recruitment by a FAK-p130Cas complex. *J Cell Biol* (2012) 196 (3):375–85. doi: 10.1083/jcb.201105153

37. Gkretsi V, Stylianopoulos T. Cell adhesion and matrix stiffness: Coordinating cancer cell invasion and metastasis. *Front Oncol* (2018) 8:145. doi: 10.3389/fonc.2018.00145

38. Brassart-Pasco S, Brezillon S, Brassart B, Ramont L, Oudart JB, Monboisse JC. Tumor microenvironment: Extracellular matrix alterations influence tumor progression. *Front Oncol* (2020) 10:397. doi: 10.3389/fonc.2020.00397

39. Maquart FX, Pasco S, Ramont L, Hornebeck W, Monboisse JC. An introduction to matrikines: extracellular matrix-derived peptides which regulate cell activity. implication in tumor invasion. *Crit Rev Oncol Hematol* (2004) 49 (3):199–202. doi: 10.1016/j.critrevonc.2003.06.007

40. Monboisse JC, Oudart JB, Ramont L, Brassart-Pasco S, Maquart FX. Matrikines from basement membrane collagens: a new anti-cancer strategy. *Biochim Biophys Acta* (2014) 1840(8):2589–98. doi: 10.1016/j.bbagen.2013.12.029

41. Assadian S, El-Assaad W, Wang XQ, Gannon PO, Barres V, Latour M, et al. p53 inhibits angiogenesis by inducing the production of arresten. *Cancer Res* (2012) 72(5):1270–9. doi: 10.1158/0008-5472.CAN-11-2348

42. Hamano Y, Zeisberg M, Sugimoto H, Lively JC, Maeshima Y, Yang C, et al. Physiological levels of tumstatin, a fragment of collagen IV alpha3 chain, are generated by MMP-9 proteolysis and suppress angiogenesis *via* alphaV beta3 integrin. *Cancer Cell* (2003) 3(6):589–601. doi: 10.1016/s1535-6108(03)00133-8

43. Rebustini IT, Myers C, Lassiter KS, Surmak A, Szabova L, Holmbeck K, et al. MT2-MMP-dependent release of collagen IV NC1 domains regulates submandibular gland branching morphogenesis. *Dev Cell* (2009) 17(4):482–93. doi: 10.1016/j.devcel.2009.07.016

44. Li D, Clark CC, Myers JC. Basement membrane zone type XV collagen is a disulfide-bonded chondroitin sulfate proteoglycan in human tissues and cultured cells. *J Biol Chem* (2000) 275(29):22339–47. doi: 10.1074/jbc.M000519200

45. Ramchandran R, Dhanabal M, Volk R, Waterman MJ, Segal M, Lu H, et al. Antiangiogenic activity of restin, NC10 domain of human collagen XV: comparison to endostatin. *Biochem Biophys Res Commun* (1999) 255(3):735–9. doi: 10.1006/bbrc.1999.0248

46. Debelle L, Tamburro AM. Elastin: molecular description and function. *Int J Biochem Cell Biol* (1999) 31(2):261–72. doi: 10.1016/s1357-2725(98)00098-3

47. Li B, Daggett V. Molecular basis for the extensibility of elastin. *J Muscle Res Cell Motil* (2002) 23(5-6):561–73. doi: 10.1023/a:1023474909980

48. Mithieux SM, Weiss AS. Elastin. *Adv Protein Chem* (2005) 70:437–61. doi: 10.1016/S0065-3233(05)70013-9

49. Heinz A, Jung MC, Duca L, Sippl W, Taddese S, Ihling C, et al. Degradation of tropoelastin by matrix metalloproteinases–cleavage site specificities and release of matrikines. *FEBS J* (2010) 277(8):1939–56. doi: 10.1111/j.1742-4658.2010.07616.x

50. Heinz A, Jung MC, Jahreis G, Rusciani A, Duca L, Debelle L, et al. The action of neutrophil serine proteases on elastin and its precursor. *Biochimie* (2012) 94(1):192–202. doi: 10.1016/j.biochi.2011.10.006

51. Goldfinger LE, Stack MS, Jones JC. Processing of laminin-5 and its functional consequences: role of plasmin and tissue-type plasminogen activator. *J Cell Biol* (1998) 141(1):255–65. doi: 10.1083/jcb.141.1.255

52. Veitch DP, Nokelainen P, McGowan KA, Nguyen TT, Nguyen NE, Stephenson R, et al. Mammalian tolloid metalloproteinase, and not matrix metalloprotease 2 or membrane type 1 metalloprotease, processes laminin-5 in keratinocytes and skin. *J Biol Chem* (2003) 278(18):15661–8. doi: 10.1074/jbc.M210588200

53. Amano S, Scott IC, Takahara K, Koch M, Champliaud MF, Gerecke DR, et al. Bone morphogenetic protein 1 is an extracellular processing enzyme of the laminin 5 gamma 2 chain. *J Biol Chem* (2000) 275(30):22728–35. doi: 10.1074/jbc.M002345200

54. Rousselle P, Beck K. Laminin 332 processing impacts cellular behavior. *Cell Adh Migr* (2013) 7(1):122–34. doi: 10.4161/cam.23132

55. Giannelli G, Falk-Marzillier J, Schiraldi O, Stetler-Stevenson WG, Quaranta V. Induction of cell migration by matrix metalloprotease-2 cleavage of laminin-5. *Science* (1997) 277(5323):225–8. doi: 10.1126/science.277.5323.225

56. Koshikawa N, Giannelli G, Cirulli V, Miyazaki K, Quaranta V. Role of cell surface metalloprotease MT1-MMP in epithelial cell migration over laminin-5. *J Cell Biol* (2000) 148(3):615–24. doi: 10.1083/jcb.148.3.615

57. Koshikawa N, Minegishi T, Sharabi A, Quaranta V, Seiki M. Membrane-type matrix metalloproteinase-1 (MT1-MMP) is a processing enzyme for human laminin gamma 2 chain. *J Biol Chem* (2005) 280(1):88–93. doi: 10.1074/jbc.M411824200

58. Schenk S, Hintermann E, Bilban M, Koshikawa N, Hojilla C, Khokha R, et al. Binding to EGF receptor of a laminin-5 EGF-like fragment liberated during MMP-dependent mammary gland involution. *J Cell Biol* (2003) 161(1):197–209. doi: 10.1083/jcb.200208145

59. Taipale J, Keski-Oja J. Growth factors in the extracellular matrix. *FASEB J* (1997) 11(1):51–9. doi: 10.1096/fasebj.11.1.9034166

60. Winkler J, Abisoye-Ogunniyan A, Metcalf KJ, Werb Z. Concepts of extracellular matrix remodelling in tumour progression and metastasis. *Nat Commun* (2020) 11(1):5120. doi: 10.1038/s41467-020-18794-x

61. Apte RS, Chen DS, Ferrara N. VEGF in signaling and disease: Beyond discovery and development. *Cell* (2019) 176(6):1248–64. doi: 10.1016/j.cell.2019.01.021

62. Ferrara N. Binding to the extracellular matrix and proteolytic processing: two key mechanisms regulating vascular endothelial growth factor action. *Mol Biol Cell* (2010) 21(5):687–90. doi: 10.1091/mbc.E09-07-0590

63. Houck KA, Leung DW, Rowland AM, Winer J, Ferrara N. Dual regulation of vascular endothelial growth factor bioavailability by genetic and proteolytic mechanisms. *J Biol Chem* (1992) 267(36):26031–7. doi: 10.1016/S0021-9258(18)35712-0

64. Bergers G, Brekken R, McMahon G, Vu TH, Itoh T, Tamaki K, et al. Matrix metalloproteinase-9 triggers the angiogenic switch during carcinogenesis. *Nat Cell Biol* (2000) 2(10):737–44. doi: 10.1038/35036374

65. Leivonen SK, Kahari VM. Transforming growth factor-beta signaling in cancer invasion and metastasis. *Int J Cancer* (2007) 121(10):2119–24. doi: 10.1002/ijc.23113

66. Yu Q, Stamenkovic I. Cell surface-localized matrix metalloproteinase-9 proteolytically activates TGF-beta and promotes tumor invasion and angiogenesis. *Genes Dev* (2000) 14(2):163–76. doi: 10.1101/gad.14.2.163

67. Mu D, Cambier S, Fjellbirkeland L, Baron JL, Munger JS, Kawakatsu H, et al. The integrin alpha(v)beta8 mediates epithelial homeostasis through MT1-MMP-dependent activation of TGF-beta1. *J Cell Biol* (2002) 157(3):493–507. doi: 10.1083/jcb.200109100

68. Dallas SL, Rosser JL, Mundy GR, Bonewald LF. Proteolysis of latent transforming growth factor-beta (TGF-beta)-binding protein-1 by osteoclasts. a cellular mechanism for release of TGF-beta from bone matrix. *J Biol Chem* (2002) 277(24):21352–60. doi: 10.1074/jbc.M111663200

69. Tatti O, Vehvilainen P, Lehti K, Keski-Oja J. MT1-MMP releases latent TGF-beta1 from endothelial cell extracellular matrix *via* proteolytic processing of LTBP-1. *Exp Cell Res* (2008) 314(13):2501–14. doi: 10.1016/j.yexcr.2008.05.018

70. Pedrozo HA, Schwartz Z, Robinson M, Gomes R, Dean DD, Bonewald LF, et al. Potential mechanisms for the plasmin-mediated release and activation of latent transforming growth factor-beta1 from the extracellular matrix of growth plate chondrocytes. *Endocrinology* (1999) 140(12):5806–16. doi: 10.1210/endo.140.12.7224

71. Van Lint P, Libert C. Chemokine and cytokine processing by matrix metalloproteinases and its effect on leukocyte migration and inflammation. *J Leukoc Biol* (2007) 82(6):1375–81. doi: 10.1189/jlb.0607338

72. Ito A, Mukaiyama A, Itoh Y, Nagase H, Thogersen IB, Enghild JJ, et al. Degradation of interleukin 1beta by matrix metalloproteinases. *J Biol Chem* (1996) 271(25):14657–60. doi: 10.1074/jbc.271.25.14657

73. Baker KJ, Houston A, Brint E. IL-1 family members in cancer; two sides to every story. *Front Immunol* (2019) 10:1197. doi: 10.3389/fimmu.2019.01197

74. McQuibban GA, Butler GS, Gong JH, Bendall L, Power C, Clark-Lewis I, et al. Matrix metalloproteinase activity inactivates the CXC chemokine stromal cell-derived factor-1. *J Biol Chem* (2001) 276(47):43503–8. doi: 10.1074/jbc.M107736200

75. Dean RA, Overall CM. Proteomics discovery of metalloproteinase substrates in the cellular context by iTRAQ labeling reveals a diverse MMP-2 substrate degradome. *Mol Cell Proteomics* (2007) 6(4):611–23. doi: 10.1074/mcp.M600341-MCP200

76. Van den Steen PE, Proost P, Wuyts A, Van Damme J, Opdenakker G. Neutrophil gelatinase b potentiates interleukin-8 tenfold by aminoterminal processing, whereas it degrades CTAP-III, PF-4, and GRO-alpha and leaves RANTES and MCP-2 intact. *Blood* (2000) 96(8):2673–81. doi: 10.1182/blood.V96.8.2673

77. Van den Steen PE, Husson SJ, Proost P, Van Damme J, Opdenakker G. Carboxyterminal cleavage of the chemokines MIG and IP-10 by gelatinase b and neutrophil collagenase. *Biochem Biophys Res Commun* (2003) 310(3):889–96. doi: 10.1016/j.bbrc.2003.09.098

78. McQuibban GA, Gong JH, Tam EM, McCulloch CA, Clark-Lewis I, Overall CM. Inflammation dampened by gelatinase a cleavage of monocyte chemoattractant protein-3. *Science* (2000) 289(5482):1202–6. doi: 10.1126/science.289.5482.1202

79. McQuibban GA, Gong JH, Wong JP, Wallace JL, Clark-Lewis I, Overall CM. Matrix metalloproteinase processing of monocyte chemoattractant proteins generates CC chemokine receptor antagonists with anti-inflammatory properties. *vivo. Blood* (2002) 100(4):1160–7. doi: 10.1182/blood.V100.4.1160.h81602001160_1160_1167

80. Tam EM, Morrison CJ, Wu YI, Stack MS, Overall CM. Membrane protease proteomics: Isotope-coded affinity tag MS identification of undescribed MT1-matrix metalloproteinase substrates. *Proc Natl Acad Sci U.S.A.* (2004) 101(18):6917–22. doi: 10.1073/pnas.0305862101

81. Tester AM, Cox JH, Connor AR, Starr AE, Dean RA, Puente XS, et al. LPS responsiveness and neutrophil chemotaxis *in vivo* require PMN MMP-8 activity. *PloS One* (2007) 2(3):e312. doi: 10.1371/journal.pone.0000312

82. Naor D, Sionov RV, Ish-Shalom D. CD44: structure, function, and association with the malignant process. *Adv Cancer Res* (1997) 71:241–319. doi: 10.1016/S0065-230X(08)60101-3

83. Ponta H, Sherman L, Herrlich PA. CD44: from adhesion molecules to signalling regulators. *Nat Rev Mol Cell Biol* (2003) 4(1):33–45. doi: 10.1038/nrm1004

84. Cichy J, Pure E. The liberation of CD44. *J Cell Biol* (2003) 161(5):839–43. doi: 10.1083/jcb.200302098

85. Weber GF, Ashkar S, Glimcher MJ, Cantor H. Receptor-ligand interaction between CD44 and osteopontin (Eta-1). *Science* (1996) 271(5248):509–12. doi: 10.1126/science.271.5248.509

86. Jalkanen S, Jalkanen M. Lymphocyte CD44 binds the COOH-terminal heparin-binding domain of fibronectin. *J Cell Biol* (1992) 116(3):817–25. doi: 10.1083/jcb.116.3.817

87. Knutson JR, Iida J, Fields GB, McCarthy JB. CD44/chondroitin sulfate proteoglycan and alpha 2 beta 1 integrin mediate human melanoma cell migration on type IV collagen and invasion of basement membranes. *Mol Biol Cell* (1996) 7(3):383–96. doi: 10.1091/mbc.7.3.383

88. Yu Q, Stamenkovic I. Localization of matrix metalloproteinase 9 to the cell surface provides a mechanism for CD44-mediated tumor invasion. *Genes Dev* (1999) 13(1):35–48. doi: 10.1101/gad.13.1.35

89. Chen C, Zhao S, Karnad A, Freeman JW. The biology and role of CD44 in cancer progression: therapeutic implications. *J Hematol Oncol* (2018) 11(1):64. doi: 10.1186/s13045-018-0605-5

90. Bennett KL, Jackson DG, Simon JC, Tanczos E, Peach R, Modrell B, et al. CD44 isoforms containing exon V3 are responsible for the presentation of heparin-binding growth factor. *J Cell Biol* (1995) 128(4):687–98. doi: 10.1083/jcb.128.4.687

91. Levesque MC, Haynes BF. Cytokine induction of the ability of human monocyte CD44 to bind hyaluronan is mediated primarily by TNF-alpha and is inhibited by IL-4 and IL-13. *J Immunol* (1997) 159(12):6184–94.

92. Cichy J, Pure E. Oncostatin m and transforming growth factor-beta 1 induce post-translational modification and hyaluronan binding to CD44 in lung-derived epithelial tumor cells. *J Biol Chem* (2000) 275(24):18061–9. doi: 10.1074/jbc.M907962199

93. Brown KL, Maiti A, Johnson P. Role of sulfation in CD44-mediated hyaluronan binding induced by inflammatory mediators in human CD14(+) peripheral blood monocytes. *J Immunol* (2001) 167(9):5367–74. doi: 10.4049/jimmunol.167.9.5367

94. Kajita M, Itoh Y, Chiba T, Mori H, Okada A, Kinoh H, et al. Membrane-type 1 matrix metalloproteinase cleaves CD44 and promotes cell migration. *J Cell Biol* (2001) 153(5):893–904. doi: 10.1083/jcb.153.5.893

95. Okamoto I, Kawano Y, Murakami D, Sasayama T, Araki N, Miki T, et al. Proteolytic release of CD44 intracellular domain and its role in the CD44 signaling pathway. *J Cell Biol* (2001) 155(5):755–62. doi: 10.1083/jcb.200108159

96. Itoh Y. Modulation of microenvironment signals by proteolytic shedding of cell surface extracellular matrix receptors. *Front Cell Dev Biol* (2021) 9:736735. doi: 10.3389/fcell.2021.736735

97. Okamoto I, Kawano Y, Tsuiki H, Sasaki J, Nakao M, Matsumoto M, et al. CD44 cleavage induced by a membrane-associated metalloprotease plays a critical role in tumor cell migration [In process citation]. *Oncogene* (1999) 18(7):1435–46. doi: 10.1038/sj.onc.1202447

98. Nagano O, Murakami D, Hartmann D, De Strooper B, Saftig P, Iwatsubo T, et al. Cell-matrix interaction *via* CD44 is independently regulated by different metalloproteinases activated in response to extracellular Ca(2+) influx and PKC activation. *J Cell Biol* (2004) 165(6):893–902. doi: 10.1083/jcb.200310024

99. Sugahara KN, Murai T, Nishinakamura H, Kawashima H, Saya H, Miyasaka M. Hyaluronan oligosaccharides induce CD44 cleavage and promote cell migration in CD44-expressing tumor cells. *J Biol Chem* (2003) 278(34):32259–65. doi: 10.1074/jbc.M300347200

100. Murakami D, Okamoto I, Nagano O, Kawano Y, Tomita T, Iwatsubo T, et al. Presenilin-dependent gamma-secretase activity mediates the intramembranous cleavage of CD44. *Oncogene* (2003) 22(10):1511–6. doi: 10.1038/sj.onc.1206298

101. Pelletier L, Guillaumot P, Freche B, Luquain C, Christiansen D, Brugiere S, et al. Gamma-secretase-dependent proteolysis of CD44 promotes neoplastic transformation of rat fibroblastic cells. *Cancer Res* (2006) 66(7):3681–7. doi: 10.1158/0008-5472.CAN-05-3870

102. Anderegg U, Eichenberg T, Parthaune T, Haiduk C, Saalbach A, Milkova L, et al. ADAM10 is the constitutive functional sheddase of CD44 in human melanoma cells. *J Invest Dermatol* (2009) 129(6):1471–82. doi: 10.1038/jid.2008.323

103. Makgoba MW, Sanders ME, Ginther Luce GE, Dustin ML, Springer TA, Clark EA, et al. ICAM-1 a ligand for LFA-1-dependent adhesion of b, T and myeloid cells. *Nature* (1988) 331(6151):86–8. doi: 10.1038/331086a0

104. Rothlein R, Mainolfi EA, Czajkowski M, Marlin SD. A form of circulating ICAM-1 in human serum. *J Immunol* (1991) 147(11):3788–93.

105. Champagne B, Tremblay P, Cantin A, St Pierre Y. Proteolytic cleavage of ICAM-1 by human neutrophil elastase. *J Immunol* (1998) 161(11):6398–405.

106. Tsakadze NL, Sithu SD, Sen U, English WR, Murphy G, D'Souza SE. Tumor necrosis factor-alpha-converting enzyme (TACE/ADAM-17) mediates the ectodomain cleavage of intercellular adhesion molecule-1 (ICAM-1). *J Biol Chem* (2006) 281(6):3157–64. doi: 10.1074/jbc.M510797200

107. Sithu SD, English WR, Olson P, Krubasik D, Baker AH, Murphy G, et al. Membrane-type 1-matrix metalloproteinase regulates intracellular adhesion molecule-1 (ICAM-1)-mediated monocyte transmigration. *J Biol Chem* (2007) 282(34):25010–9. doi: 10.1074/jbc.M611273200

108. Essick E, Sithu S, Dean W, D'Souza S. Pervanadate-induced shedding of the intercellular adhesion molecule (ICAM)-1 ectodomain is mediated by membrane type-1 matrix metalloproteinase (MT1-MMP). *Mol Cell Biochem* (2008) 314(1-2):151–9. doi: 10.1007/s11010-008-9776-7

109. Morsing SKH, Rademakers T, Brouns SLN, Stalborch ADV, Donners M, van Buul JD. ADAM10-mediated cleavage of ICAM-1 is involved in neutrophil transendothelial migration. *Cells* (2021) 10(2):232. doi: 10.3390/cells10020232

110. Ghislin S, Obino D, Middendorp S, Boggetto N, Alcaide-Loridan C, Deshayes F. LFA-1 and ICAM-1 expression induced during melanoma-endothelial cell co-culture favors the transendothelial migration of melanoma cell lines *in vitro*. *BMC Cancer* (2012) 12:455. doi: 10.1186/1471-2407-12-455

111. Dews IC, Mackenzie KR. Transmembrane domains of the syndecan family of growth factor coreceptors display a hierarchy of homotypic and heterotypic interactions. *Proc Natl Acad Sci U.S.A.* (2007) 104(52):20782–7. doi: 10.1073/pnas.0708909105

112. Choi S, Lee E, Kwon S, Park H, Yi JY, Kim S, et al. Transmembrane domain-induced oligomerization is crucial for the functions of syndecan-2 and syndecan-4. *J Biol Chem* (2005) 280(52):42573–9. doi: 10.1074/jbc.M509238200

113. Manon-Jensen T, Itoh Y, Couchman JR. Proteoglycans in health and disease: the multiple roles of syndecan shedding. *FEBS J* (2010) 277(19):3876–89. doi: 10.1111/j.1742-4658.2010.07798.x

114. Chen P, Abacherli LE, Nadler ST, Wang Y, Li Q, Parks WC. MMP7 shedding of syndecan-1 facilitates re-epithelialization by affecting alpha(2)beta(1) integrin activation. *PloS One* (2009) 4(8):e6565. doi: 10.1371/journal.pone.0006565

115. Brule S, Charnaux N, Sutton A, Ledoux D, Chaigneau T, Saffar L, et al. The shedding of syndecan-4 and syndecan-1 from HeLa cells and human primary macrophages is accelerated by SDF-1/CXCL12 and mediated by the matrix metalloproteinase-9. *Glycobiology* (2006) 16(6):488–501. doi: 10.1093/glycob/cwj098

116. Endo K, Takino T, Miyamori H, Kinsen H, Yoshizaki T, Furukawa M, et al. Cleavage of syndecan-1 by membrane type matrix metalloproteinase-1 stimulates cell migration. *J Biol Chem* (2003) 278(42):40764–70. doi: 10.1074/jbc.M306736200

117. Pruessmeyer J, Martin C, Hess FM, Schwarz N, Schmidt S, Kogel T, et al. A disintegrin and metalloproteinase 17 (ADAM17) mediates inflammation-induced shedding of syndecan-1 and -4 by lung epithelial cells. *J Biol Chem* (2010) 285 (1):555–64. doi: 10.1074/jbc.M109.059394

118. Fears CY, Gladson CL, Woods A. Syndecan-2 is expressed in the microvasculature of gliomas and regulates angiogenic processes in microvascular endothelial cells. *J Biol Chem* (2006) 281(21):14533–6. doi: 10.1074/jbc.C600075200

119. Choi S, Kim JY, Park JH, Lee ST, Han IO, Oh ES. The matrix metalloproteinase-7 regulates the extracellular shedding of syndecan-2 from colon cancer cells. *Biochem Biophys Res Commun* (2012) 417(4):1260–4. doi: 10.1016/j.bbrc.2011.12.120

120. Lee YH, Park JH, Cheon DH, Kim T, Park YE, Oh ES, et al. Processing of syndecan-2 by matrix metalloproteinase-14 and effect of its cleavage on VEGF-induced tube formation of HUVECs. *Biochem J* (2017) 474(22):3719–32. doi: 10.1042/BCJ20170340

121. Asundi VK, Erdman R, Stahl RC, Carey DJ. Matrix metalloproteinase-dependent shedding of syndecan-3, a transmembrane heparan sulfate proteoglycan, in schwann cells. *J Neurosci Res* (2003) 73(5):593–602. doi: 10.1002/jnr.10699

122. Jannaway M, Yang X, Meegan JE, Coleman DC, Yuan SY. Thrombin-cleaved syndecan-3/-4 ectodomain fragments mediate endothelial barrier dysfunction. *PloS One* (2019) 14(5):e0214737. doi: 10.1371/journal.pone.0214737

123. Rodriguez-Manzaneque JC, Carpizo D, Plaza-Calonge Mdel C, Torres-Collado AX, Thai SN, Simons M, et al. Cleavage of syndecan-4 by ADAMTS1 provokes defects in adhesion. *Int J Biochem Cell Biol* (2009) 41(4):800–10. doi: 10.1016/j.biocel.2008.08.014

124. Schmidt A, Echtermeyer F, Alozie A, Brands K, Buddecke E. Plasmin- and thrombin-accelerated shedding of syndecan-4 ectodomain generates cleavage sites at Lys(114)-Arg(115) and Lys(129)-Val(130) bonds. *J Biol Chem* (2005) 280 (41):34441–6. doi: 10.1074/jbc.M501903200

125. Pantoliano MW, Horlick RA, Springer BA, Van Dyk DE, Tobery T, Wetmore DR, et al. Multivalent ligand-receptor binding interactions in the fibroblast growth factor system produce a cooperative growth factor and heparin mechanism for receptor dimerization. *Biochemistry* (1994) 33(34):10229–48. doi: 10.1021/bi00200a003

126. Su G, Blaine SA, Qiao D, Friedl A. Shedding of syndecan-1 by stromal fibroblasts stimulates human breast cancer cell proliferation *via* FGF2 activation. *J Biol Chem* (2007) 282(20):14906–15. doi: 10.1074/jbc.M611739200

127. Whiteford JR, Xian X, Chaussade C, Vanhaesebroeck B, Nourshargh S, Couchman JR. Syndecan-2 is a novel ligand for the protein tyrosine phosphatase receptor CD148. *Mol Biol Cell* (2011) 22(19):3609–24. doi: 10.1091/mbc.E11-02-0099

128. Konitsiotis AD, Raynal N, Bihan D, Hohenester E, Farndale RW, Leitinger B. Characterization of high affinity binding motifs for the discoidin domain receptor DDR2 in collagen. *J Biol Chem* (2008) 283(11):6861–8. doi: 10.1074/jbc.M709290200

129. Xu H, Raynal N, Stathopoulos S, Myllyharju J, Farndale RW, Leitinger B. Collagen binding specificity of the discoidin domain receptors: binding sites on collagens II and III and molecular determinants for collagen IV recognition by DDR1. *Matrix Biol* (2011) 30(1):16–26. doi: 10.1016/j.matbio.2010.10.004

130. Emsley J, Knight CG, Farndale RW, Barnes MJ, Liddington RC. Structural basis of collagen recognition by integrin alpha2beta1. *Cell* (2000) 101(1):47–56. doi: 10.1016/S0092-8674(00)80622-4

131. Leitinger B. Molecular analysis of collagen binding by the human discoidin domain receptors, DDR1 and DDR2. identification of collagen binding sites in DDR2. *J Biol Chem* (2003) 278(19):16761–9. doi: 10.1074/jbc.M301370200

132. Noordeen NA, Carafoli F, Hohenester E, Horton MA, Leitinger B. A transmembrane leucine zipper is required for activation of the dimeric receptor tyrosine kinase DDR1. *J Biol Chem* (2006) 281(32):22744–51. doi: 10.1074/jbc.M603233200

133. Juskaite V, Corcoran DS, Leitinger B. Collagen induces activation of DDR1 through lateral dimer association and phosphorylation between dimers. *eLife* (2017) 6:e25716. doi: 10.7554/eLife.25716

134. Vogel WF. Ligand-induced shedding of discoidin domain receptor 1. *FEBS Lett* (2002) 514(2-3):175–80. doi: 10.1016/S0014-5793(02)02360-8

135. Shitomi Y, Thogersen IB, Ito N, Leitinger B, Enghild JJ, Itoh Y. ADAM10 controls collagen signaling and cell migration on collagen by shedding the ectodomain of discoidin domain receptor 1 (DDR1). *Mol Biol Cell* (2015) 26 (4):659–73. doi: 10.1091/mbc.E14-10-1463

136. Lu KK, Trcka D, Bendeck MP. Collagen stimulates discoidin domain receptor 1-mediated migration of smooth muscle cells through src. *Cardiovasc Pathol* (2011) 20(2):71–6. doi: 10.1016/J.Carpath.2009.12.006

137. Fu HL, Sohail A, Valiathan RR, Wasinski BD, Kumarasiri M, Mahasenan KV, et al. Shedding of discoidin domain receptor 1 by membrane-type matrix metalloproteinases. *J Biol Chem* (2013) 288(17):12114–29. doi: 10.1074/Jbc.M112.409599

138. Biao-xue R, Xi-guang C, Shuan-ying Y, Wei L, Zong-juan M. EphA2-dependent molecular targeting therapy for malignant tumors. *Curr Cancer Drug Targets* (2011) 11(9):1082–97. doi: 10.2174/156800911798073050

139. Ireton RC, Chen J. EphA2 receptor tyrosine kinase as a promising target for cancer therapeutics. *Curr Cancer Drug Targets* (2005) 5(3):149–57. doi: 10.2174/1568009053765780

140. Guo H, Miao H, Gerber L, Singh J, Denning MF, Gilliam AC, et al. Disruption of EphA2 receptor tyrosine kinase leads to increased susceptibility to carcinogenesis in mouse skin. *Cancer Res* (2006) 66(14):7050–8. doi: 10.1158/0008-5472.CAN-06-0004

141. Zhuang G, Brantley-Sieders DM, Vaught D, Yu J, Xie L, Wells S, et al. Elevation of receptor tyrosine kinase EphA2 mediates resistance to trastuzumab therapy. *Cancer Res* (2010) 70(1):299–308. doi: 10.1158/0008-5472.CAN-09-1845

142. Dohn M, Jiang J, Chen X. Receptor tyrosine kinase EphA2 is regulated by p53-family proteins and induces apoptosis. *Oncogene* (2001) 20(45):6503–15. doi: 10.1038/sj.onc.1204816

143. Sugiyama N, Gucciardo E, Tatti O, Varjosalo M, Hyytiainen M, Gstaiger M, et al. EphA2 cleavage by MT1-MMP triggers single cancer cell invasion *via* homotypic cell repulsion. *J Cell Biol* (2013) 201(3):467–84. doi: 10.1083/jcb.201205176

144. Koshikawa N, Hoshino D, Taniguchi H, Minegishi T, Tomari T, Nam SO, et al. Proteolysis of EphA2 converts it from a tumor suppressor to an oncoprotein. *Cancer Res* (2015) 75(16):3327–39. doi: 10.1158/0008-5472.CAN-14-2798

145. Raab G, Klagsbrun M. Heparin-binding EGF-like growth factor. *Biochim Biophys Acta* (1997) 1333(3):F179–99. doi: 10.1016/s0304-419x(97)00024-3

146. Higashiyama S, Nanba D. ADAM-mediated ectodomain shedding of HB-EGF in receptor cross-talk. *Biochim Biophys Acta* (2005) 1751(1):110–7. doi: 10.1016/j.bbapap.2004.11.009

147. Miyamoto S, Yagi H, Yotsumoto F, Kawarabayashi T, Mekada E. Heparin-binding epidermal growth factor-like growth factor as a novel targeting molecule for cancer therapy. *Cancer Sci* (2006) 97(5):341–7. doi: 10.1111/j.1349-7006.2006.00188.x

148. Lucchesi PA, Sabri A, Belmadani S, Matrougui K. Involvement of metalloproteinases 2/9 in epidermal growth factor receptor transactivation in pressure-induced myogenic tone in mouse mesenteric resistance arteries. *Circulation* (2004) 110(23):3587–93. doi: 10.1161/01.CIR.0000148780.36121.47

149. Kivisaari AK, Kallajoki M, Ala-aho R, McGrath JA, Bauer JW, Konigova R, et al. Matrix metalloproteinase-7 activates heparin-binding epidermal growth factor-like growth factor in cutaneous squamous cell carcinoma. *Br J Dermatol* (2010) 163(4):726–35. doi: 10.1111/j.1365-2133.2010.09924.x

150. Hu C, Zuo Y, Ren Q, Sun X, Zhou S, Liao J, et al. Matrix metalloproteinase-10 protects against acute kidney injury by augmenting epidermal growth factor receptor signaling. *Cell Death Dis* (2021) 12(1):70. doi: 10.1038/s41419-020-03301-3

151. Koshikawa N, Mizushima H, Minegishi T, Iwamoto R, Mekada E, Seiki M. Membrane type 1-matrix metalloproteinase cleaves off the NH2-terminal portion of heparin-binding epidermal growth factor and converts it into a heparin-independent growth factor. *Cancer Res* (2010) 70(14):6093–103. doi: 10.1158/0008-5472.CAN-10-0346

frontiers | Frontiers in Oncology

TYPE Original Research
PUBLISHED 18 October 2022
DOI 10.3389/fonc.2022.906260

Check for updates

OPEN ACCESS

EDITED BY
Yin-Yuan Mo,
University of Mississippi Medical Center, United States

REVIEWED BY
Chun Peng,
York University, Canada
Fiete Haack,
University of Rostock, Germany

*CORRESPONDENCE
Suniti Misra
suniti.misra@tridenttech.edu;
sunitimisra1972@gmail.com

†These authors share first authorship

SPECIALTY SECTION
This article was submitted to Molecular and Cellular Oncology, a section of the journal Frontiers in Oncology

RECEIVED 28 March 2022
ACCEPTED 15 August 2022
PUBLISHED 18 October 2022

CITATION
Ghatak S, Hascall VC, Karamanos N, Markwald RR and Misra S (2022) Chemotherapy induces feedback up-regulation of CD44v6 in colorectal cancer initiating cells through β-catenin/MDR1 signaling to sustain chemoresistance.
Front. Oncol. 12:906260.
doi: 10.3389/fonc.2022.906260

COPYRIGHT
© 2022 Ghatak, Hascall, Karamanos, Markwald and Misra. This is an open-access article distributed under the terms of the Creative Commons Attribution License (CC BY). The use, distribution or reproduction in other forums is permitted, provided the original author(s) and the copyright owner(s) are credited and that the original publication in this journal is cited, in accordance with accepted academic practice. No use, distribution or reproduction is permitted which does not comply with these terms.

Chemotherapy induces feedback up-regulation of CD44v6 in colorectal cancer initiating cells through β-catenin/MDR1 signaling to sustain chemoresistance

Shibnath Ghatak[1,2†], Vincent C. Hascall[3†], Nikos Karamanos[4], Roger R. Markwald[1] and Suniti Misra[1,2*]

[1]Department of Regenerative Medicine and Cell Biology, Medical University of South Carolina, Charleston, SC, United States, [2]Department Natural Sciences, Trident Technical College, North Charleston, SC, United States, [3]Department of Biomedical Engineering/ND20, Cleveland Clinic, Cleveland, OH, United States, [4]University of Patras, Matrix Pathobiology Res. Group, Department of Chemistry, Patras, Greece

Chemoresistance in colorectal cancer initiating cells (CICs) involves the sustained activation of multiple drug resistance (MDR) and WNT/β-catenin signaling pathways, as well as of alternatively spliced-isoforms of CD44 containing variable exon-6 (CD44v6). In spite of its importance, mechanisms underlying the sustained activity of WNT/β-catenin signaling have remained elusive. The presence of binding elements of the β-catenin-interacting transcription factor TCF4 in the *MDR1* and CD44 promoters suggests that crosstalk between WNT/β-catenin/TCF4-activation and the expression of the CD44v6 isoform mediated by FOLFOX, a first-line chemotherapeutic agent for colorectal cancer, could be a fundamental mechanism of FOLFOX resistance. Our results identify that FOLFOX treatment induced WNT3A secretion, which stimulated a positive feedback loop coupling β-catenin signaling and CD44v6 splicing. In conjunction with FOLFOX induced WNT3A signal, specific CD44v6 variants produced by alternative splicing subsequently enhance the late wave of WNT/β-catenin activation to facilitate cell cycle progression. Moreover, we revealed that FOLFOX-mediated sustained WNT signal requires the formation of a CD44v6-LRP6-signalosome in caveolin microdomains, which leads to increased FOLFOX efflux. FOLFOX-resistance in colorectal CICs occurs in the absence of tumor-suppressor disabled-2 (DAB2), an inhibitor of WNT/β-catenin signaling. Conversely, in sensitive cells, DAB2 inhibition of WNT-signaling requires interaction with a clathrin containing CD44v6-LRP6-signalosome. Furthermore, full-length CD44v6, once internalized through the caveolin-signalosome, is translocated to the nucleus where in complex with TCF4, it binds to β-catenin/TCF4-regulated *MDR1*, or to *CD44* promoters, which leads to FOLFOX-resistance and CD44v6 transcription through transcriptional-reprogramming. These findings provide evidence that

10.3389/fonc.2022.906260

targeting CD44v6-mediated LRP6/β-catenin-signaling and drug efflux may represent a novel approach to overcome FOLFOX resistance and inhibit tumor progression in colorectal CICs. Thus, sustained drug resistance in colorectal CICs is mediated by overexpression of CD44v6, which is both a functional biomarker and a therapeutic target in colorectal cancer.

KEYWORDS

colon rectal cancer (CRC), cancer initiating cells (CICs), CD44v6, WNT3A, MDR1

1 Introduction

Colorectal cancer (CRC) is the second leading cause of cancer-related deaths in Western countries, including the USA, with incidences increasing by 2% annually (1, 2). Despite improved survival attributed to early detection and chemotherapy with FOLFOX (1 x FOLFOX: 50 μM 5-fluorouracil [5-FU] + 10μM oxaliplatin [OXA] + 1 μM leucovorin), the first-line treatment for CRC, the emergence of multidrug resistance (MDR) that accounts for the poor tumor response to FOLFOX has limited the efficacy of this chemotherapeutic drug and finally results in therapy failure in CRC patients (3–7).

In recent years, a growing body of evidence suggests that tumor tissue is composed of a heterogeneous hierarchy of cells that differ in morphology, gene expression, proliferative capacity, and invasiveness (8). This heterogeneity originates from a small subset of cancer cells, called cancer stem cells or cancer initiating cells (CICs), that are the unique source of all tumor cells and responsible for tumor propagation and relapse (9–12). Since the first identification of CICs in breast cancer where a CD44/CD24 marker (13) was used to isolate the CICs, CICs have been now identified in a variety of solid tumors (5, 14–19) including colon carcinomas. Unlike naturally occurring somatic stem cells, CICs initiate tumorigenic activity when transplanted into animals (20, 21). Moreover, variation in the genetics and epigenetic damages of CRC patients is so different that markers to detect CICs from more differentiated progeny have not been completely informative across all patient tumors (22–25). In addition, most CIC enhancement markers mediate interactions between a tumor cell and its stromal environment, indicating that the tumorigenic characteristics associated with that marker may be lost after depletion of CICs from their microenvironment. However, the cell-surface markers that recognize CICs and have a functional role in the antiapoptotic signaling to drive tumorigenesis have remained poorly defined.

CD44 is a multi-structural and multi-functional transmembrane glycoprotein that acts as a receptor for hyaluronan (also called hyaluronic acid). *CD44* is encoded by a single gene containing 20 exons, ten of which are alternatively spliced to generate the numerous CD44 splice variants (CD44v) (15, 26). The standard isoform of *CD44* (*CD44s*) has no variant exons, is small, and is nearly ubiquitous in vertebrate cells (27). Experiments using knock-in mice that express either CD44v4-10 or CD44s isoforms have demonstrated that CD44v isoforms, promote adenoma formation in Apc (Min/+) mice but not the CD44s (28). Variant 6 of CD44 (CD44v6) participates in tumor development and progression in many ways that are restricted to stem cell subpopulations and promotes generation of gut adenomas in mouse models of familial adenomatous polyposis (28). Its role in CRC progression derives from its ability to bind ligands associated with both tyrosine kinase receptors and non-tyrosine receptors including c-Met, VEGF, TGFβ1 and ERB2 (29–39), leading to changes in biological activities such as activation of anti-apoptotic signaling and survival (40, 41). Studies have reported that CRC cells expressing CD166 (42), CD44 (43), CD44v6 (19), CD66c (42) and aldehyde dehydrogenase (ALDH1) (44) describe CRC/CIC characteristics. CD44v6 (+)/CICs have been associated with increased metastatic behavior in both pancreatic cancer (15, 45–47) and CRC (19). Further, in this study we showed that tumorigenic potentiality of the Non-CICs (CD44v6 (-) cells) was entirely lost in secondary xenograft tumors whereas tumorigenic potential of CD44v6 (+)/CICs in primary, secondary and tertiary recipients in xenograft models are confined to the small CD44v6 (+) population. Thus, the CD44v6 (+)/CICs cell population residing in the colon tumor mass is able to generate serial xenografts showing a virtually unlimited growth potential.

Abbreviations: CD44s, Standard isoform of CD44 having no variant exons; CD44v, CD44 splice variant; CD44v6, variant 6 of CD44; CIC, cancer initiating cell; CRC, colorectal cancer; 5-FU,5-fluorouracil; OXA, oxaliplatin; FOLFOX, 5-FU plus OXA plus leucovorin; ALDH1, aldehyde dehydrogenase; LRP6, low-density lipoprotein receptor-related protein; TCF, T-cell factor; LEF, lymphoid enhancer factor; Dkk1, Dickkopf 1; DAB2, endocytic adaptor disabled-2; DVL, Disheveled family *of* proteins in mammals; Tf, transferrin; Nano (Tf-PEG-PEI nanoparticles); MDR1, multidrug resistance protein 1; IP, immunoprecipitation; WB, Western Blotting; DN, dominant negative; sh, shRNA; SQ, sub cutaneous; R, lipid-raft fraction; NR, non lipid-raft fraction.

Recent studies indicate that several regulatory serine/arginine rich 2 splicing factors (SRSFs), such as SRSF1 (48, 49), SRSF3 (50), SRSF6 (48, 51), HNRNPA2/B1 (52), or HNRNPH (53), have oncogenic properties, whereas other factors, including RNA binding protein QKI (54), RBM5, RBM6, and RBM10 (55), act as tumor suppressors. Some of these splicing factors (SRF1/Sam68 (56) and SRSF3 (SRp20) (57) depend upon exon splicing enhancers in the case of CD44 variable exons. Their activity in promoting the inclusion of CD44 variable exons is controlled by several oncogenic signaling pathways such as, Ras/MAPK signaling (58) and β-catenin signaling (57), at least in part through modification of splicing factors at the level of activation (phosphorylation) (59–62). However, the signaling pathway between FOLFOX induced WNT3A activation and stimulation of alternative splicing in the nucleus is not well defined. In an unpublished study (manuscript under preparation), we found that transcription of the alternative splicing regulator SRSF3 responsible for production of CD44 variants (v6-v8) and SRF3 expression is regulated by WNT3A/β-catenin signaling (a FOLFOX-WNT3A-β catenin-TCF4-CD44v6 pathway). This might be the way FOLFOX regulates alternate splicing of CD44 in the nucleus by splicing factor 3 which is stimulated by β-catenin/signaling. Thus, the CD44v6 isoform is likely to be a better CIC marker than the CD44s isoform in CRCs. The WNT/β-catenin signaling pathway remains important throughout life as it has crucial roles in self-renewal for adult stem and progenitor cells (63–65). WNTs are lipid-modified glycoprotein ligands that bind to both Frizzled and low-density lipoprotein receptor-related protein 6 (LRP6) (65). In physiological conditions, in the absence of a WNT signal, β-catenin is phosphorylated and degraded by a complex composed of glycogen synthase kinase 3β (GSK3β), Axin, adenomatous polyposis coli (APC), and casein kinase 1 (CK1). Upon binding of WNT to Frizzled and LRP5/6 (65, 66), the WNT-Frizzled-LRP5/6 complex is phosphorylated and activates disheveled protein (DVL) (67). DVL activation inhibits GSK3β, which subsequently decreases β-catenin degradation and allows for its stabilization and translocation to the nucleus, where it binds to the T-cell factor (TCF)/lymphoid enhancer factor (LEF) transcription factor and activates gene transcription (68). Endocytic adaptor DAB2 is a tumor suppressor protein (69, 70) involved in several receptor-mediated pathways (71–74). In most carcinomas, the expression of DAB2 is only expressed in low levels.

Many receptors and their protein partners, including CD44, concentrate at caveolin-1 (CAV1)-enriched lipid-rafts within the plasma membrane to mediate signaling cascades (33, 75, 76). A previous study has shown that CD44 also regulates WNT signaling in the developing brain of Xenopus Leavis embryos by association with LRP6 in the membrane (77). Many of the oncogenic activities that have been previously attributed to CD44, in particular those relevant to ligand induced translocation of receptors into discrete caveolin-microdomain in the plasma membrane that strengthen signaling pathways, could be ascribed in part to CD44-mediated caveolin-dependent endocytic signaling interactions in CRC (78).

CICs develop several mechanisms that protect them from long-term side effects caused by chemotherapeutic-drugs and make them resistant to chemotherapeutic drugs (79). In the clonal evolution model, tumor cells develop drug resistance by sequential alteration of DNA by genetic modifications. This model predicts that after chemotherapy only the drug-resistant cells within the tumor survive, proliferate, and regenerate the tumor mass that is made up of the drug-resistant cells. In the CIC model, although successful cancer therapy abolishes the bulk of proliferating tumor cells, a subset of remaining CICs can survive and promote cancer relapse due to their ability to establish higher invasiveness and chemoresistance. Generally, resistance to a clinically relevant chemotherapy combination such as FOLFOX involves the participation of a variety of cellular mechanisms, including: drug target mutations; oncogene/onco-suppressor deregulations; activation of pathways blocking the drug action; increased DNA damage repair; and overexpression of a drug extrusion pump MDR-1 (multidrug resistance-1 [P-GP, ABCB1]). The decreased influx of drugs leading to the generation of reactive oxygen species (ROS) can directly induce WNT-β-catenin signaling through DVl protein-mediated drug resistance that originates due to the crosstalk between tumor and stromal cells (6, 80–82). Among the WNT targets involved in drug resistance, the drug extrusion pump MDR-1 and the cell adhesion molecules from the CD44v family are highlighted (83–87). Additionally, we showed that CD44 regulates β-catenin-COX2 signaling in colon tumor cells (30, 88). Oncogenic CD44v expression is a downstream target gene of the WNT3A/β-catenin signaling pathway (89). CICs exhibit high expression levels of the two main *MDR* genes, *ABCB1* (*MDR1*) and *ABCG2* (ATP-binding cassette G2) (79). Additionally, since the basal promoter of MDR1 has several β-catenin/TCF4/LEF binding sites (90, 91), this protein is a target gene of the β-catenin/TCF4 transcriptional regulators. Thus, activation of β-catenin augments MDR1 expression, which confirms the direct connection between the WNT/β-catenin pathway and chemoresistance (90–92). Additionally, we showed that CD44 regulates β-catenin-COX2 signaling in colon tumor cells (30, 88). CD44v expression is downstream of the WNT signaling and induced by the β-catenin/Tcf-4 signaling pathway (89). A WNT3A canonical pathway (WNT3A/Frizzled/LRP6-GSK3β-catenin/TCF4) induces drug resistance (93, 94). However, the requirement of CD44v6 for the FOLFOX induced β-catenin-TCF4/MDR1 activation remains to be addressed since induction of this pathway with a chemotherapy induced WNT ligand was not tested.

Given that CICs are defined by their capacity for the development of drug-resistance, treatment failure, and tumor relapse in cancer (5, 6, 95), we investigated the mechanisms by which CICs contribute to the cell autonomous resistance against

FOLFOX-chemotherapy with distinct modulation of WNT-CD44v6 signaling by regulating the endocytic fate of the CD44v6-LRP6 receptor interaction in membrane microdomain. We base this investigation on the following observations.

1) Our results identify that FOLFOX treatment induced WNT3a secretion, which stimulated a positive feedback loop coupling β-catenin activation signals and CD44v6 splicing for sustained drug resistance. In addition, CD44v6 could sustained cell cycle S phase responses through a positive feedback loop, where this isoform is speculated to be important for a secreted factor WNT3A signaling. 2) β-catenin interacts with TCF4 binding elements in the *MDR1* and *CD44* gene promoters. This suggests that crosstalk between WNT/β-catenin/TCF4-activation and the expression of the CD44v6 isoform mediated by FOLFOX could be a fundamental mechanism of FOLFOX resistance in colorectal CICs. 3) FOLFOX-mediated sustained WNT/β-catenin signaling requires the formation of a CD44v6-LRP6-signalosome in caveolin-microdomains, leading to increased FOLFOX efflux. Conversely, in the absence of FOLFOX, DAB2 links CD44v6 and LRP6 in clathrin containing vesicles that attenuate WNT/β-catenin signaling to maintain drug sensitivity in sensitive cells. 4) In FOLFOX resistant cells, CD44v6 is internalized through the caveolin containing signalosome, and this signalosome is recruited to the endosome for sorting of CD44v6-β-catenin/TCF4-complex vesicles, which are then destined to the nucleus. In the nucleus, CD44v6 binds to various promoters, including β-catenin/TCF4-regulated promoters, leading to FOLFOX resistance through transcriptional reprogramming. TCF4 maintains distinctive transcriptional programs *via* interactions with MDR1 and *CD44* promoters and sustains CD44v6-mediated autonomous-resistance in CICs.

2 Materials and methods

2.1 Materials

Dulbecco's Modified Eagle's Medium (DMEM), Eagle's Minimum Essential Medium (EMEM), McCoy's 5A Medium, F-12K Medium, Leibovitz's L-15 Medium, L-Glutamine, Sodium pyruvate, Penicillin (100 µg/ml) and Streptomycin (100 µg/ml), sodium pyruvate, 0.05% EDTA solution (Versene), Phosphate buffered saline (PBS, Calcium and Magnesium free), and 0.05% Trypsin were from Corning Inc. Fetal Bovine Serum (FBS) was from Atlanta Biologicals. Amphotericin B was from Hyclone, Thermo Fisher Scientific. Waltham, MA, USA. Nonidet P-40, EGTA, sodium orthovanadate, glycerol, phenylmethylsulphonyl fluoride, leupeptin, pepstatin A, aprotinin and HEPES were from Sigma-Aldrich, Inc. St. Louis, MO, USA. Recombinant human WNT3A protein (5036-WN) was from R&D Systems, Inc. Minneapolis, MN, USA). Blocking antibody for protein WNT3A (703666, Rabbit monoclonal IgG clone 1H12L14) was from Thermo Fisher Scientific, Waltham, MA, USA. The anti-Active-β-catenin antibody (05-665, anti-ABC antibody clone 8E7) was from Millipore Sigma, Burlington, MA, USA, and the anti- β-catenin antibody (610153, mouse IgG1, BD, Tempe, Arizona, USA) was used for total β-catenin detection in western blotting analysis. The antibodies p-LRP6 (Serine 1490) (#2568, Rabbit IgG), LRP6 (#2560, Rabbit mAb clone C5C7), TCF4 antibody (#2569, Rabbit mAb clone C48H11) were from Cell Signaling Technology, Inc. Danvers, MA, USA. P-Glycoprotein (MDR1) western blotting antibody (PA5-28801, Rabbit Polyclonal against Human) was from Invitrogen Thermo Fisher Scientific, Waltham, MA, USA. β-tubulin Antibody (D-10) (sc-5274, Mouse monoclonal IgG_{2b} κ, SCBT), Mouse anti-rabbit IgG-HRP (sc-2357, IgG, SCBT), Rabbit anti mouse IgG-HRP (sc-358914, IgG, SCBT), and Western blotting Luminol reagent (sc-2048, SCBT) were purchased from Santa Cruz Biotechnology, Inc. Dallas, Texas, USA. Blocking antibodies for CD44v6 (BBA13, Monoclonal Mouse IgG_1 Clone # 2F10, R&D), and isotype control (MAB002, IgG1, R&D) and the mouse IgG1 antibodies were from R&D Systems, Inc. Minneapolis, MN, USA. Radiocarbon-labeled oxaliplatin ([^{14}C] oxaliplatin) was purchased from Amersham Biosciences, Piscataway, NJ, USA.

2.2 Cell lines

Human colorectal adenocarcinoma cell lines: 1) WIDR (CCL-218) was maintained in Eagle's Minimum Essential Medium (EMEM) +10% FBS; 2) LOVO (CCL-229) was maintained in F-12K Medium 2 mM L-glutamine and 1500 mg/L sodium bicarbonate; 3) HT29 (HTB-38) was maintained in McCoy's 5A medium; 4) SW480 (CCL-228) was maintained in Leibovitz's L-15 Medium; and 6) SW948 (CCL-237) was maintained in Leibovitz's L-15 Medium that was purchased from ATCC, Manassas, Virginia. The cell lines were maintained in medium mentioned next to the cell line in humidified atmosphere in the presence of 10% FBS, Penicillin (100 µg/ml) and Streptomycin (100 µg/ml), 5% CO_2 at 37°C. HCA-7 colony 29 was purchased from European Collection of Authenticated Cell Cultures and maintained in DMEM + 10% FBS + 2 mM L-Glutamine + 110 mg/L sodium pyruvate.

2.3 Generation of drug resistant cells

To determine the mechanisms of drug (FOLFOX) resistance, we selected three cell lines (HT29, SW480, WIDR and LOVO cells [CRC cells used in Figure 1B]) out of 7 cell lines (Figure 1A), which have low basal levels of CD44v6 mRNA expression. To generate these drug resistant cells, we first determined IC_{50} values of the parent CRC cells for 5-

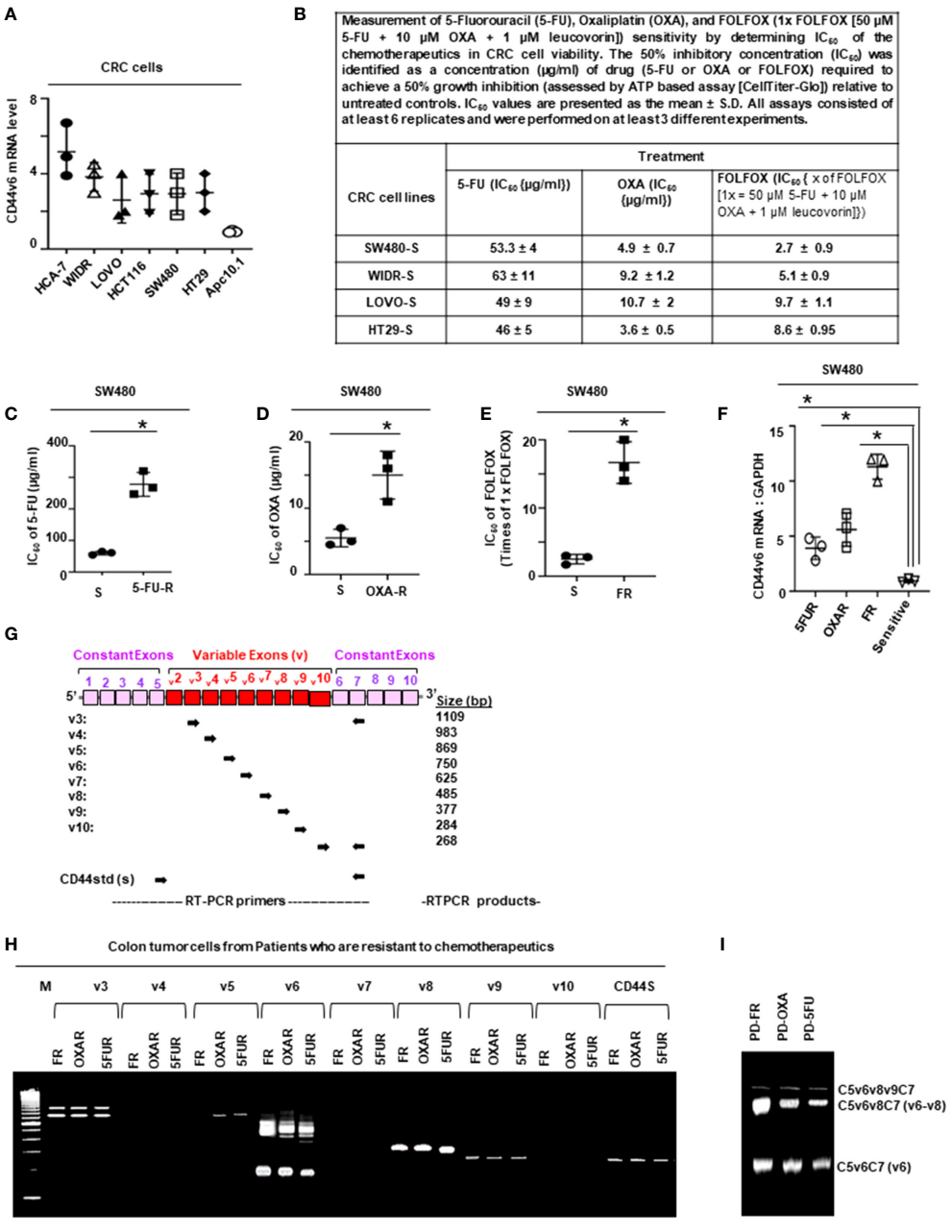

B

Measurement of 5-Fluorouracil (5-FU), Oxaliplatin (OXA), and FOLFOX (1x FOLFOX [50 µM 5-FU + 10 µM OXA + 1 µM leucovorin]) sensitivity by determining IC_{50} of the chemotherapeutics in CRC cell viability. The 50% inhibitory concentration (IC_{50}) was identified as a concentration (µg/ml) of drug (5-FU or OXA or FOLFOX) required to achieve a 50% growth inhibition (assessed by ATP based assay [CellTiter-Glo]) relative to untreated controls. IC_{50} values are presented as the mean ± S.D. All assays consisted of at least 6 replicates and were performed on at least 3 different experiments.

CRC cell lines	Treatment		
	5-FU (IC_{50} (µg/ml))	OXA (IC_{50} (µg/ml))	FOLFOX (IC_{50} { x of FOLFOX [1x = 50 µM 5-FU + 10 µM OXA + 1 µM leucovorin]})
SW480-S	53.3 ± 4	4.9 ± 0.7	2.7 ± 0.9
WIDR-S	63 ± 11	9.2 ± 1.2	5.1 ± 0.9
LOVO-S	49 ± 9	10.7 ± 2	9.7 ± 1.1
HT29-S	46 ± 5	3.6 ± 0.5	8.6 ± 0.95

FIGURE 1
FOLFOX induces CD44v6 expression. **(A)**, QPCR data for CD44v6 expression in 6 CRC cell lines are shown as fold change relative to pre-neoplastic Apc 10.1 cells as controls. **(B–E)**, The concentrations (IC_{50}) (µg/ml) of (5-FU) and (OXA) required to achieve a 50% growth inhibition relative to untreated controls using the ATP Glo-growth assay are shown **(B)**. The IC_{50} values of 5-FU **(C)**, OXA **(D)**, and FR **(E)** for sensitive (S) and corresponding FOLFOX resistant (FR) cells are shown. **(F)**, Real-time PCR data for the CD44v6 expression are presented for SW480 tumor cells resistant to either 5-Fluorouracil (5FUR), oxaliplatin (OXAR), or FOLFOX (FR) compared to sensitive (S) pairs of cells. Gene expression was normalized to the reference gene GAPDH. **(G)**, Constant and variable exons are shown for the PCR primers used to amplify CD44 variable (v) and standard (s) isoforms in the human CD44v6 gene. The primers for both the v6 and standard isoforms (CD44s) predominantly generate one PCR product c5v6c7 (v6) for CD44v6 and C5C7 for CD44s, whereas the primers for the v8 variants amplify two splice variants C5v6v7v8C7 (v6-v8) and C5v8C7 (v8). These PCR products are depicted in panel H and panel I experiments. **(H)**, RT-PCR results are shown for the CD44v isoforms using the different primers in the tumor cells derived from colorectal patients (PD) who were resistant to 5FU, OXA and FOLFOX (PD-5-FU, PD-OXA and PD-FR). **(I)**, RT-PCR results are shown for the CD44v isoforms using the different primers (C5v6v8v9C7, C5v6v8C7 and C5v6C7) in the PD-FR, PD-OXA and PD-5-FU cells. Data are presented as Mean ± SD from n = 3-6 independent replicates in three independent experiments. All semi quantitative RT-PCR data are representative of three experiments **(C–E)**, *P < 0.05 was considered significant, 50% inhibitory concentration (IC_{50}) for 5-FU in SW480-5FUR cells was compared with SW480-S cells **(C)**, for OXA in SW480-5FUR cells was compared with SW480-S cells **(D)**, and for FOLFOX n SW480-5FUR was compared with SW480-S cells **(E, F)**, *$P < 0.05$ considered significant, fold expressions of CD44v6mRNA in SW480-5FUR, SW480-OXAR, and SW480-FR cell were compared to control (SW480-S) cells.

Flourouracil (5-FU) and oxaliplatin (OXA) (see Figure 1B), because these molecules are the components of FOLFOX. The 50% inhibitory concentration (IC_{50}) was identified as a concentration of drug required to achieve a 50% growth inhibition relative to untreated controls. Next, we determined IC_{50} values of the parent sensitive SW480-S, HT29-S, WIDR-S, and LOVO-S cells for FOLFOX (1x FOLFOX = 50 μM 5-FU + 10 μM OXA + 1 μM leucovorin). The average IC_{50} values for tested CRC cells are in Figure 1B. The 5-FU resistance (5-FUR), and oxaliplatin resistance (OXAR) cells were generated by incubating the parental sensitive SW480-S, or HT29-S, or WIDR-S, and LOVO-S cells with repeated exposure to increasing concentrations of the drug (100 μM 5-FU) for generating 5-FUR cells; and 20 μM OXA for generating OXAR cells for 3 days. For generating FR cells from SW480-S and HT29-S, we incubated each of the two cells to 5 x FOLFOX for 3 days. To generate FR cells from WIDR-S and LOVO-S, we incubated each of the two cells to 10 x FOLFOX for 3 days. This exposure and withdrawal cycle was repeated five times for the above mentioned doses of each of the drug. The surviving 5-FUR, OXAR and FR clones were cultured in normal medium for 5 days and maintained with selection pressure of half the average IC_{50} dose of CRC cells for 5-FU, OXA and FOLFOX (Figure 1B). The resistances of these resistant clones were compared to sensitive pairs by determining the numbers of colonies in soft agar growth with 1x FOLFOX - 5x FOLFOX treatments

2.4 Tissue collection, isolation of CICs

All human tissues were acquired from primary human colorectal tumor patient specimens undergoing colorectal resection, in agreement with human experimental guidelines and the ethical standards of the institutional review board (IRB). Human protocols were approved by the IRB of the Medical University of South Carolina. The IRB has determined that this research project meets the criteria for 'Non Human Subjects' research. Patient-derived (PD) biopsies collected from 5-FU resistant (PD-5FUR), Oxaliplatin resistant (PD-OXAR), and FOLFOX resistant (PD-FR) tumor specimens and our FOLFOX resistant (FR), Oxaliplatin resistant (OXA-R), 5-flurouracil resistant (5-FUR) cell clones, and parental SW480 cells (sensitive [s]) cells were maintained through subcutaneous (SQ) xenografts in the flanks of immunocompromised (NOD-SCID/IL2Rγnull [NSG]) mice and in SCID mice, respectively. *Ex vivo* cultures from the fresh normal colonic tissue and colorectal PD-FR, PD-OXAR, PD-5FUR, SW480-FR, SW480-OXAR, SW480-5FUR, and SW480-S SQ tumors were rinsed in DMEM (Life Technologies) supplemented with 200 units/mL of penicillin, 200 μg/mL of streptomycin, and 4 units/mL of amphotericin B. After mincing, they were incubated with 300 units/mL of collagenase (Worthington Biochemical) at 37°C for 3 hours. A single cell suspension was obtained by filtration through a 40 μm filter. After discarding lymphocytes by gradient centrifugation, *Ex vivo* cultures were cultured in DMEM (Life Technologies) supplemented with 200 units/mL of penicillin, 200 μg/mL of streptomycin, and 4 units/mL of amphotericin B, serum-free media with basic fibroblast growth factor (bFGF, 10 ng/ml; R&D Systems) and epidermal growth factor (EGF, 10 ng/ml; R&D Systems). The cells were processed for sphere formation. Sphere-propagated cells were subjected to fluorescence-activated cell sorting (FACS) buffer [Phosphate-buffered saline (PBS) + 2% BSA + 1 mM EDTA + 0.1% sodium azide]. They were then incubated with FC blocking reagent (Millenyi Biotech) and stained with directly conjugated antibodies by incubating on ice for 20 minutes. They were then sorted in a Mo Flo cell sorter for CD44v6 CICs (CD44v6 high (+) by CD44v6-PE) and tested for tumor sphere formation at 37°C in 5% CO_2.

2.5 Cell viability and apoptosis assays

Five thousand cells were plated in triplicate into 96-well plates containing appropriate growth media and incubated overnight. After 16 hours growth, cultures were incubated in media containing no serum for 16 hours at 37°C in 5% CO_2, 95% air. Vehicle or chemotherapy drug was added to the plate. In each experiment, a total of five plates (6 wells/treatment) were used. Experiments were repeated 3 times. The growth of the cells was determined by measuring increases in readings of ATP levels for viability (CellTiter-Glo, Promega). Cell apoptosis was determined by the Caspase-Glo® 3/7 assay (Promega) using DEVD-amino luciferin substrate. The luminescent signal is proportional to caspase 3/7 activity and measured using a luminometer (Perkin Elmer).

2.6 Flow cytometric analysis of CIC cells

Flow cytometry was done using a FACS Cell Sorter. To enrich cells for CICs, single cells were labeled with a phycoerythrin (PE)-conjugated monoclonal antibody against CD44v6 (Miltenyi Biotec), and then analyzed for the expression of Fluorescein-5-isothiocyanate (FITC) with conjugated monoclonal antibody against EpCAM (R&D Systems). Purified CD44v6 (+)/EpCAM (+), and CD44v6 (–)/EpCAM (+) cells from various tumors were cultured separately and grown in fresh CIC growth medium (see below) for 2 weeks. Then, the cultured CD44v6 (+)/EpCAM (+) and CD44v6 (-)/EpCAM (+) cells were subjected to flow cytometric analysis for isolation of CD44v6 (+)/EpCAM (+)/ALDH1 (+), and CD44v6 (–)/EpCAM (+)/ALDH1 (+) cells using a FITC-conjugated monoclonal antibody against ALDH1 and grown in fresh medium for 2 weeks. Cultured

CD44v6 (+)/EpCAM (+)/ALDH1 (+) cells and CD44v6 (-) EpCAM (+)/ALDH1 (+) cells were subjected to flow cytometric analysis for isolation of CD44v6 (+)/EpCAM (+)/ALDH1 (+)/CD133 (+) (designated as CICs), and for CD44v6 (-)/EpCAM (+)/ALDH1 (+)/CD133(+) cells (designated as Non-CICs) using a FITC-conjugated monoclonal antibody against CD133.

CICs were cultured in serum-free media with basic fibroblast growth factor (bFGF, 10 ng/ml; R&D Systems) and epidermal growth factor (EGF, 10 ng/ml; R&D Systems). For isolation of CAFs, surgical tissues were similarly dissociated into single-cell suspensions, and PDGFRα-expressing cells were sorted using flow cytometry (FACS Aria II). Cells were then cultured in DMEM with 10% BSA. For cell counting before each experiment, a single-cell suspension was achieved using TrypLE (Invitrogen) dissociation.

2.7 Tumor sphere formation

An optimized serum substitute (1 x B27 supplement) (Creative Bio array, Shirley, NY, USA) was freshly added to tumor formation medium (500 ml Dulbecco's Modified Eagle Medium/F12) containing 20 ng/ml epidermal growth factor, 10 ng/ml basic fibroblast growth factor, 5 mg/ml insulin, and 0.4% bovine serum albumin. After harvesting the cells, 200 live cells/200 µl of tumor sphere medium were suspended in ice. We followed the tumor sphere formation assay protocol from the Creative Bio-array (Shirley, NY, USA). After stipulated times of incubation, tumor sphere numbers were counted under a phase-contrast microscope using the 40X magnification lens. Data are presented as a percentage of wells containing tumor spheres compared to the total number of wells.

2.8 Cell lysis, immunoprecipitation and immunoblot analysis

Cells were cultured until they were 75% confluent. They were then washed twice at 4°C with phosphate-buffered saline (PBS), and harvested with 0.05% Versene. The cells were pelleted by centrifugation at 5,000 x g for 2 minutes at 4°C. The pellets were treated with the lysis buffer (containing 1% Nonidet P-40, 0.3 M NaCl, 1.5 mM MgCl2, 0.2 mM EDTA, 5 mM sodium orthovanadate, 10% (v/v) glycerol, 100 µg/ml phenylmethylsulphonyl fluoride (PMSF), 1 µg/ml leupeptin, 1 µg/ml pepstatin A, 1 µg/ml aprotinin, and 50 mM HEPES, pH 7.5) for 30 minutes. For immunoprecipitation, the cell extracts (1 mg total proteins) were precleaned by rotation for 1 hour with 20 µl of protein G-Sepharose beads (Santa Cruz, CA). The precleaned supernatants were incubated with antibodies needed for each specific experiment overnight. After incubation with 20 µl of protein G-Sepharose beads for 1 hour, the suspension was centrifuged, and pellets washed and collected as immunoprecipitation complexes. Western blotting was done as previously described (38, 39, 96–98). Each protein was analyzed in samples from at least three independent experiments from each set of tumor cells, CICs and CAFs. Images were recorded using a luminescent image analyzer, and the intensities of the bands were quantitated by densitometry (NIH Image J software). Each protein was analyzed in samples from at least three independent experiments from each set of tumor cells, CICs and CAFs.

2.9 Cell cycle synchronization and analysis of cell cycle profile

For synchronization into the G2/M phase of the cell cycle, SW480 cells were treated with 100 ng/mL of nocodazole (Sigma-Aldrich, Inc. St. Louis, MO, USA) for 16 hours. To study the enrichment of the cells into the different cell cycle phases, cells were released by drug removal by washing twice with E8 media (E8 medium consisted just of insulin, selenium, transferrin, L-ascorbic acid, FGF2, and TGFβ in DMEM/F12 with pH adjusted with $NaHCO_3$). Sixteen hours after release from G2/M phase, when 97% of the cells were in G1 phase (cell cycle analyzed by flow cytometry) the cells were transfected with either non-targeted (Control) or CD44v6 shRNA. Twenty four hours after transfection, the cells were incubated in low serum medium (0.5% serum) with 20 ng/ml WNT3A or with 1 x FOLFOX and stimulated for 30 minutes, 1, 2, 8, 12, and 24 hours. Cell cycle profiles were analyzed using the Click-iT™ EdU Cell Proliferation Kit (Invitrogen Thermo Fisher Scientific, Waltham, MA, USA) following the manufacturer's instructions. Briefly, SW480 cells cultured cells were incubated at 37°C with 10 mM EdU (5-ethynyl-20-deoxyuridine) for 1 hour and harvested using cell dissociation buffer (Gibco Thermo Fisher Scientific, Waltham, MA, USA). After three washes with PBS/1% BSA, cells were fixed with 4% paraformaldehyde for 15 min at room temperature and released from paraformaldehyde by washing three times with PBS/1% BSA. Cells were then permeabilized for 15 minutes with saponin-based permeabilization/wash buffer and incubated with the Click-iT EDU Alexa Fluor reaction cocktail for 30 min in dark. Click-iT Assay Kits for Flow Cytometry provide the measurement by tracking new DNA content in fixed cells that were washed once with permeabilization/wash buffer and stained for DNA,content in fixed cells when combined with RNAse using the FxCycle™ Far Red stain (F10348, Invitrogen Thermo Fisher Scientific, Waltham, MA, USA) Cells were analyzed on the flow cytometer with FlowJo software.

2.10 Lipid-raft isolation

All procedures were done at 4°C. Cells were scraped into buffer containing 1% cold Triton X-100 buffer (20 mM Tris-HCl, pH 7.4, 150 mM NaCl, 1% Triton X-100, 1% deoxycholate, 0.1%

sodium dodecyl sulfate [SDS], 1 mM EGTA, 1 mM sodium orthovanadate with a cocktail of protease inhibitors at final concentrations of 0.2 mM aminoethyl-benzene sulfonyl fluoride, 1 μg/ml aprotinin, 10 μM pepstatin, 3 μM E-64, 10 μg/ml leupeptin, 2 μM pepstatin, and 50 μg/ml calpain inhibitor I) and lysed on ice for 30 minutes. After centrifugation at 800 x g to remove nuclei and cell debris, lysates were subjected to sucrose gradient fractionation as described previously (99). An equal volume of each fraction was boiled for 3 minutes in SDS-Lammeli sample buffer and subjected to western blotting analyses as described previously (38, 39, 96–98, 100, 101). On the other hand, the Triton-insoluble rafts and Triton-soluble fractions were diluted with an equal volume of extraction buffer (25 mM HEPES, pH 7.6, 0.3 M NaCl, 1.5 mM MgCl2, 0.2 mM EDTA, 1% Nonidet P-40, and 0.5 mM dithiothreitol) and subjected to immunoprecipitation as described previously.

2.11 Endosome isolation

Endosomes from SW480-FR-NON-CICs/CD44v6 cell clones expressing actin binding NLS mutant (nuclear localization signal mutant) and Δ67 mutant cells (Figures 9 and 10) were isolated by sucrose density gradient (102). All operations were done at 4°C. The cells were grown in plates and washed with PBS three times to remove growth medium. The cells in 0.5 ml of homogenization buffer (250 mM sucrose, 1 mM EDTA, 1 mM phenylmethylsulphonyl fluoride (PMSF)) were lysed by passing through a 22G needle and syringe. After centrifugation at 1000xg for 10 minutes, the supernatant was adjusted to 25% sucrose/1 mM EDTA. Step gradients in four layers were set up in SW41Ti tubes and centrifuged at 100,000×g for one hour. Fractions (2 ml) were collected from top to bottom. The densities of the fractions were measured by refractometry. The fractions were analyzed by western blotting.

2.12 Plasmids and reporter assays

2.12.1 Expression vectors

pcDNA-Wnt3A-V5 was a gift from Marian Waterman (Addgene plasmid # 35927; http://n2t.net/addgene:35927; RRID : Addgene #3 5927), human pcDNA3-β-catenin was a gift from Eric Fearon (Addgene plasmid # 16828; http://n2t.net/addgene:16828; RRID : Addgene # 16828). CD44v6 specific PCR amplification products were isolated with polyadenylated RNA from the HT29 cell line. The PCR product was cloned in the pcDNA3.1 vector and used as previously described. Myc-tagged human full length TCF4E pcDNA3 was a gift from Frank McCormick (Addgene plasmid # 32738; http://n2t.net/addgene:32738; RRID: Addgene # 32738). pDONR223_DKK1_WT was a gift from Jesse Boehm & William Hahn & Root (Addgene plasmid # 82250; http://n2t.net/addgene).

2.12.2 Reporter vectors

The MDR1 and CD44v6 reporter constructs were synthesized by Bio basic (US) and cloned into the firefly pGL3-basic vector (Promega) upstream of the Luciferase reporter gene. The constructs named: 1) mdr1 (a) contains the basal promoter and multiple (four) TCF binding sites (−1301/+1); 2) mdr1 (b) contains the basal promoter and one TCF binding site (−1067/+1); and 3) mdr1 (c) contains just the basal promoter. The constructs named: 1) CD44v6 (a) contains one TCF binding site (-1700/500); and 2) CD44v6 (b) contains basal promoter and two TCF binding sites (-2100/500). The M50 Super 8x TOPFlash vector (plasmid 12456) with a luciferase gene under the control of seven TCF/LEF-binding sites and the corresponding M51 Super 8x FOPFlash vector (plasmid 12457) with mutated TCF/LEF-binding sites were obtained from Addgene (Cambridge, MA, USA). The normalization vector pRL-TK renilla with a HSV-TK promotor driving Renilla luciferase was purchased from Promega.

2.12.3 Transient transfection and luciferase reporter assay

For the transient assays, 1.0 x 10^5 cells from both cell lines were transfected using Lipofectamine LTX 2000 (Invitrogen) with 1 μg of each Luciferase construct and 100 ng of pRL-SV40 vector (Promega), according to the manufacturer's instructions. Firefly and Renilla Luciferase activities were measured in cell lysates 48 hours after transfection using the DualGlo Luciferase Assay System (Promega) on a Veritas TM Microplate Luminometer (Perkin Elmer) following the manufacturer's protocol. All experiments were done in triplicate. Ratios of Renilla luciferase readings to firefly luciferase readings were taken for each experiment, and triplicates were averaged. The average values of the tested constructs were normalized to the activity of the empty pGL3-basic vector, which was arbitrarily set at value 1.

2.12.4 β-catenin/TCF Reporter assays

All reporter gene assays were done in 96-well plates. PD-FR/CICs or CD44v6 overexpressing SW480-FR/SQ/Non-CICs (Non-CICs/CD44v6) (1.0 × 10^4/well) were transfected with Super TOPFlash reporter (25 ng) and TK-Renilla (5 ng), and with the respective plasmid DNA as indicated using Lipofectamine™ 3000 transfection reagent according to the manufacturer's protocol. Each transfection was adjusted to 150 ng DNA/transfection with pcDNA3.1 empty vector. Where indicated, cells were transfected at 50–70% confluency with shRNA constructs using Lipofectamine™ 3000 transfection Reagent in 6 cm petri dishes according to the manufacturer's protocol 24 hours before seeding the cells for the reporter assays. 50 ng/ml of WNT3A was added 24 hours after DNA transfection. Cells were lysed 72 hours after DNA transfection with 1 × Passive Lysis Buffer (Promega), and the luciferase

TABLE 1 CD44 exon specific PCR examined using 5′ primers complementary to individual variable exons and a primer to the 3′ constitutive exon 7.

Genes	Accession number	Primers	
		Forward sequence (5'–3')	Reverse sequence (5'–3')
C_5		AAGACATCTACCCCAGCAAC	
C_7			TTTGCTCCACCTTCTTGACTCC
h-CD44V2	NM_001001389.2	GAT GAG CAC TAG TGC TAC AG	TTTGCTCCACCTTCTTGACTCC
h-CD44V3	NM_001001390.2	ACG TCT TCA AAT ACC ATC TC	TTTGCTCCACCTTCTTGACTCC
h-CD44V4	NM_001001391.2	TCA ACC ACA CCA CGG GCT TT	TTTGCTCCACCTTCTTGACTCC
h-CD44V5	NM_001001392.2	GTA GAC AGA AAT GGC ACC AC	TTTGCTCCACCTTCTTGACTCC
h-CD44V6	NM_001202555.2	CAG GCA ACT CCT AGT AGT AC	TTTGCTCCACCTTCTTGACTCC
h-CD44V7	NM_001202556.2	CAG CCT CAG CTC ATA CCA G	TTTGCTCCACCTTCTTGACTCC
h-CD44V8	NM_001202557.2	TCC AGT CAT AGT ACA ACG CT	TTTGCTCCACCTTCTTGACTCC
h-CD44V9	XM_011520485.2	CAG AGC TTC TCT ACA TCA CA	TTTGCTCCACCTTCTTGACTCC
h-CD44V10	XM_005253238.3	GGT GGA AGA AGA GAC CCA AA	TTTGCTCCACCTTCTTGACTCC
h-CD44C5V6		ATCCCTGCTACCATCCAGGCAAC	TTTGCTCCACCTTCTTGACTCC
h-CD44s	X155150 (EMBL/Genebank)	AAGACATCTACCCCAGCAAC	TTTGCTCCACCTTCTTGACTCC
h-GAPDH	NM_002046.7	ACC ACA GTC CAT GCC ATC A	TCC ACC ACC CTG TTG CTG TA

activity was measured using the Luminescence counter (PerkinElmer). TOPFlash experiments were normalized to co-transfected Renilla gene expression. In parallel to the reporter assay, transfected CICs and Non-CICs/CD44v6 cells (CD44v6 overexpressed Non-CICs) were subjected to western blotting analysis to detect MDR1, CD44v6 and β-catenin for CD44v6-β-catenin-MDR1 signaling.

2.13 Primer design and PCR

2.13.1 RNA extraction and cDNA synthesis were done following published work

Total RNA was isolated from cells using the RNeasy mini kit (Qiagen) according to the standard protocol provided by the manufacturer, with on-column DNA digestion. Five hundred ng of RNA was used for cDNA synthesis. One ml primer, 1 ml buffer (5x), 0.5 µl RNase inhibitor, 1 ml dNTP (10 mM) and 0.5 ml Reverse Transcriptase (Thermo Fisher Scientific) were mixed in a microtube (0.2 ml) (103). The synthesis was done at 50°C for 60 minutes in a thermal cycler (Bio Rad).

2.13.2 Primer design and semiquantitative RT-PCR

Primers were designed by online Primer Quest Tool (https://www.idtdna.com/PrimerQuest/Home/Index). The quality of designed primers was analyzed by Oligoaniline Tool software. The semi-quantitative PCR primer sequences used for *CD44* exon specific PCRs are given in Tables 1 and 2. Semi-quantitative PCR was done using different amounts of cDNA of RNA samples. One ml of forward (F) and of reverse (R) primers were used. For each sample, PCR was repeated three times. The reaction contained 1 ml of each cDNA sample, 0.5 ml of each primer, 5 ml Taq DNA Polymerase 2× Master Mix Red (Amplicon Co.) and 3 µl dd water in a final volume of 10 µl. Before the main reactions, the PCR conditions, including thermal conditions, and the number of cycles and the cDNA concentrations, were optimized (5, 103, 104). During the main PCR cycles, temperature conditions included one initial denaturation cycle (3 minutes at 95°C) followed by 35 cycles with a denaturation step for 5 seconds at 95°C and a combined annealing and extension step for 35 seconds at 61°C (5, 103, 104). The PCR products were electrophoresed on agarose 2.5%,

TABLE 2 CD44 exon specific PCR examined using 3′ primers complementary to v6 and v8 exons and a primer to the 5′ constitutive exon 5.

Genes	Accession number	Primers	
		Forward sequence (5'–3')	Reverse sequence (5'–3')
C_5		CATCCCAGACGAAGACAGTC	
h-CD44V6	NM_001202555.2		CAG GCA ACT CCT AGT AGT AC
h-CD44V8	NM_001202557.2		GTTGTCATTGAAAGAGGTCCT
h-CD44s	X155150 (EMBL/Genebank)	CATCCCAGACGAAGACAGTC	TTTGCTCCACCTTCTTGACTCC
h-GAPDH	NM_002046.7	ACC ACA GTC CAT GCC ATC A	TCC ACC ACC CTG TTG CTG TA
C_7			TTTGCTCCACCTTCTTGACTCC

TABLE 3 Real-time PCR (QPCR) primers for various genes associated with CICs stemness function.

Genes	Accession number	Primers	
		Forward sequence (5'–3')	Reverse sequence (5'–3')
SOX-2	NM_003106	GGACTGAGAGAAAGAAGAGGAGAG	CGCCGCCGATGATTGTTATTA
ALDH1	NM_000689.5	TGGCTTATCAGCAGGAGTGT	GCAATTCACCCACACTGTTC
OCT4	NM_002701.6	GGAGGAAGCTGACAACAATGA	CTCTCACTCGGTTCTCGATACT
c-MYC	NM_002467.6	AAGCTGAGGCACACAAAGA	GCTTGGACAGGTTAGGAGTAAA
Nanog	NM_024865.4	GCCTGTAGTCCCAGCTATTTG	GGAGTGCAGTGGTGTGATATT
TWIST1	NM_000474.4	AGACTCTGGAGCTGGATAACT	GCCTGTCTCGCTTTCTCTTT
EpCAM	NM_002354.3	AGCTGGTGTTATTGCTGTTATTG	GCATCTCACCCATCTCCTTTAT
MDR1	NM_001348945	TGCTGGTTGCTGCTTACA	GCCTATCTCCTGTCGCATTATAG
CD44v6	NM_001202555.2	GACAGAATCCCTGCTACCAATAG	TCCTTCGTGTGTGGGTAATG
NFkB	NM_003998.4	GTGACAGGAGACGTGAAGATG	TGAAGGTGGATGATTGCTAAGT
E2F1	NM_005225.3	TCCCTGAGCTGTTCTTCTG	CCTCCCTCACTTTCCCAATAAA
STAT3	NM_139276.3	GAGAAGGACATCAGCGGTAAG	CAGTGGAGACACCAGGATATTG
RUNX2	NM_001024630.4	CGGAATGCCTCTGCTGTTAT	TGTGAAGACGGTTATGGTCAAG
Snail	NM_005985.4	ACTATGCCGCGCTCTTTC	GCTGGAAGGTAAACTCTGGATTA
P300	NM_001429.4	ACTTTGGAGGCACTTTACCG	CTGTCCAGTGTCTAACTTCCTC
YB-1	NM_004559.5	TCAATGTAAGGAACGGATATGGT	AACATCAAACTCCACAGTCTCT
AP-1	NM_002228.4	GGACACGCCTTCTGAACG	CGGAGTCCAGTGTGGTTTG
Notch1	NM_017617.5	ATCAACTCACACGCCGAC	TGCATATCTTTGTTAGCCCCG
GAPDH	NM_002046.7	GAAGGTGAAGGTCG	CTTCCCGTTCTCAG
β-actin	NM_001904.4	AGAAAATCTGGCACCACACC	AGAGGCGTACAGGGATAGCA
C/EBP	NM_001806.4	CGAACTGGACACGCTGC	ACCCCAAACCACTCCCT
TCF4	NM_001083962.2	GGACCTTCTCATAATGGAGCC	TGGTTTGGCAGAAGAGAATGG

stained with ethidium bromide and photographed. The analysis of band intensities was done by ImageJ software.

2.13.3 *Quantitative real-time RT–PCR (QPCR)*

Total RNA was isolated from cells after various treatments and transfections as described in the figure legends for each specified experiment using the RNeasy mini kit (Qiagen) according to the standard protocol provided by the manufacturer, with on-column DNA digestion. RNA integrity and concentration were analyzed using Bioanalyzer, and 100 ng of RNA was retrotranscribed into cDNA using the First Strand cDNA synthesis kit from Roche Applied Science (Qiagen). SYBR Green technology (Bio-Rad) was used for all real-time PCR experiments. Amplification was done with the real-time PCR analyzer (Bio-Rad). The PCR mixture (25 µl) contained 12.5 µl of 2 SYBR Green PCR Master Mix (Bio-Rad), 5 µl of diluted RT product (1:20), and 0.5 µM sense and antisense primer sets. The QPCR primers used in this study in analyses of various genes associated with CIC stemness function are presented in Table 3. The real-time PCR assays were done in three individual experiments with duplicate samples using standard conditions (5, 104) in a CFX96 real-time PCR detection machine. After incubations at 95°C for 3 minutes, the amplification protocol consisted of 50 cycles of denaturing at 95°C for 10 seconds, followed by annealing and extension at 60°C for 30 seconds. The standard curve was made from a series dilution of template cDNA. Expression levels of tested genes were calculated after normalization with the housekeeping gene *GAPDH* or β-actin (5, 104).

2.14 RNA silencing

For determining shRNA sequences used in this study: 1) coding nucleotide sequences of the genes were obtained from the NCBI, National Institutes of Health, website (www.ncbi.nlm.nih.gov); 2) hairpin shRNAs were designed to target a transcript sequence using the Broad Institute GPP Web Portal (http://portals.broadinstitute.org/gpp/public/); and 3) sequences for cloning in pSico/pSicoR vectors were designed following the MIT Jackson Lab website (http://web.mit.edu/jacks-lab/protocols). The resulting pSicoR-CD44v6 shRNA1 (CD44v6 sh1), pSicoR-CD44v6 shRNA2 (CD44v6 sh2), pSicoR-WNT3A shRNA1 (WNT3A sh1), pSicoR-WNT3A shRNA2 (WNT3A sh2), pSicoR-β-catenin shRNA1 (β-catenin sh1), pSicoR-β-catenin shRNA2 (β-catenin sh2) transfectants constitutively silence respective CD44v6, WNT 3A and β-catenin genes in

TABLE 4 shRNA sequence in pSico and pSicoR vectors (https://web.mit.edu/jacks-lab/protocolsl).

Genes	Accession number	Primers	
		Sense sequence (5'-3')	Antisense sequence (5'-3')
CD44v6 shRNA1	Nl.1_001202555.2	TCCTCCCAGTATGACACATATTTTCAAGAGAAA TATGTGTCATACTGGGAGGTTTTTTC	TCGAGAAAAAACCTCCCAGTATGACACATATT TCTCTTGAAAATATGTGTCATACTGGGAGGA
CD44v6 shRNA2	NM_001202555.2	TGGACCMTTACCATAACTATTTCAAGAGA AA TAGTTATGGTAATTGGTCCTTTTTTC	TCGAGAAAAAAGGACCAATTACCATAACTATT TCTCTTGAAMTAGTTATGGTAATTGGTCCA
WNTJA shRNA 1	NM_033131.4	TGTAGCGAGGACATCGAGTTTGTTCAAGAGAC AAACTCGATGTCCTCGCTACTTTTTTC	TCGAGAAAAAAGTAGCGAGGACATCGAGTTT GTCTCTTGAACAAACTCGATGTCCTCGCTACA
WNTJA shRNA 2	NM_033131.4	TGAACTACGTGGAGATCATGCTTCAAGAGAGC ATGATCTCCACGTAGTTCCTTTTTTC	TCGAGAAAAAAGGAACTACGTGGAGATCATG CCTCTTGAACATGATCTCCACGTAGTTCCA
lk:atenin shRNA 1	NM_001904.4	TATCTGTCTGCTCTAGTAATAATTCAAGAGATT ATTACTAGAGCAGACAGATTTTTTTC	TCGAGAAAAAAATCTGTCTGCTCTAGTAATAAT CTCTTGAATTATTACTAGAGCAGACAGATA
lk:atenin shRNA 2	NM_001904.4	TTCTMCCTCACTTGCMTAATTTCAAGAGAAT TATTGCAAGTGAGGTTAGATTTTTTC	TCGAGAAAAAATCTAACCTCACTTGCAATAATT CTCTTGAAATTATTGCAAGTGAGGTTAGAA
Caveolin-1 shRNA1	NM_001753.5	TACCTTCACTGTGACGAAATATTCAAGAGA TATTTCGTCACAGTGAAGGTGTTTTTTC	TCGAGAAAAAACACCTTCACTGTGACGAAATA TCTCTTGAATATTTCGTCACAGTGAAGGTGA
caveolin-1 shRNA2	NM_001753.5	TACCTTCACTGTGACGAAATATTCAAGA GA TATTTCGTCACAGTGAAGGTG TTTTTTC	TCGAGAAAAAAATCAACTTGCAGAAAGAAATA TCTCTTGAATATTTCTTTCTGCAAGTTGATA
Clathrin shRNA1	NIII_004859.4	TTGACTATGGAGTCTGACAAATTTCAAGAGA ATTTGTCAGACTCCATAGTCA TTTTTTC	TCGAGAAAAAATGACTATGGAGTCTGACAAAT TCTCTTGAAATTTGTCAGACTCCATAGTCAA
Clathrin shRNA2	NM_004859.4	TACTATGGAGTCTGACAAATTTTCAAGAGA AATTTGTCAGACTCCATAGTC TTTTTTC	TCGAGAAAAAAGACTATGGAGTCTGACAAATT TCTCTTGAAAATTTGTCAGACTCCATAGTCA
Firefly luciferase shRNA1	M15077.1	TGCCCTGGTTCCTGGAACMTTTTCAAGAGA MTTGTTCCAGGAACCAGGGCTTTTTTC	TCGAGAAAAAAGCCCTGGTTCCTGGAACAATT TCTCTTGAAAATTGTTCCAGGAACCAGGGCA
Firefly luciferase shRNA2	M15077.1	TTGAGTATTTCTGTCTGATTTTTCAAGAGA AATCAGACAGAAATACTCAC TTTTTTC	TCGAGAAAAAAGTGAGTATTTCTGTCTGATTTT CTCTTGAAMTCAGACAGAAATACTCACA

the cells. pSicoR-Non targeted shRNA (NT sh) transfectants were used as control to the above shRNA transfectants (see Table 4 for shRNA sequences used in this study).

2.15 Confirming the specificity of shRNA experiments

To confirm the shRNA knockdown efficiencies in specific experiments, more than one shRNA was used. The knockdown experiments were confirmed by comparing the knockdown effects of shRNAs for CDS either with those of NCDS (as proper negative controls) or with rescue of the observed shRNA-mediated knockdown phenotype by expression of a resistant form of the targeted mRNA. This was done: 1) by transfecting the cells with specific shRNAs for the CDS of the target gene, or 2) by co-transfecting the shRNA (CDS) for the target gene with or without corresponding cDNA transfection, or 3) by the indicated shRNA-mediated knockdown and corresponding KI gene transfection. Total cell lysates were examined by Western blot analysis for the indicated proteins, and for β-tubulin or β-actin (as internal standards). In some cases Total mRNAs were analyzed for the indicated mRNAs by QPCR.

2.16 Chromatin immunoprecipitation assay

The chromatin immunoprecipitation (ChIP) assay was done using the ChIP assay kit (Upstate Biotechnology) following the manufacturer's directions as described (44). A ChIP assay was done with chromatin from SW480-FR CICs using anti-CD44v6 antibody. The immunoprecipitated DNA was amplified using ChIP primers in PCR using Taq polymerase and subcloned in the TA vector (Invitrogen). The reaction mixtures containing clones were transformed in DHα competent bacteria. Plasmids were prepared from randomly selected colonies. Plasmid DNAs from 11 clones were analyzed by M13 sequencing primers. Computer-based analysis of these DNA sequences revealed the presence of various consensus-binding sites for common transcription factors (see Table 5). QPCR analyses showed the expressions of these 11 transcription factors in CICs of SW480-FR cells.

For ChIP PCR analysis in Figures 11, 12, nuclear fractions (after crosslinking with formaldehyde) from SW480-S and SW480-FR cells were immunoprecipitated with 5 μg of anti-β-catenin or TCF4 antibodies, or with CD44v6 antibody, or with 1 μg of normal mouse IgG for 3 hours. Chromosomal DNAs were

TABLE 5 Cis-sequences bourd by CD44v6.

Transcription factors	Accession number	Abundance/11 clones
P300	NM 001429.4	11/11
STATs	NM 139276.3	11/11
TCF4	NM_001083962.2	9/11
cMyc	NM 002467.6	9/11
Snai11	NM 005985.4	8/11
Twist1	NM_000474.4	8/11
Oct4	NM_002701.6	8/11
SOX2	NM 003106	8/11
Nanog	NM 024865.4	8/11
YB-1	NM_004559.5	7/11
NFkB	NM_003998.4	7/11
E2F1	NM 005225.3	7/11
RUNX2	NM 001024630.4	7/11
AP-1	NM_002228.4	7/11
Pgp (MDR1)	NM 001348945	7/11
C/EBP	NM 001806.4	7/11
Notch1	NM_017617.5	7/11

ChiP assay was performed with chromatin from SW480-FR CICs using CD44v6 antibody. The immunoprecipitated DNA-Chromatin complex was amplified by PCR and subcloned. A total of 11 clones were sequenced. Blast analysis revealed the presence of various cis- binding sites for sternness/drug resistance related transcription factors in these DNA sequences.

purified and analyzed using semi-quantitative PCR to detect the MDR1, and for CD44v6 promoter regions, and for *MDR1* and *CD44* promoters (Figures 11, 12). SW480-FR cells were transfected with or without either NT sh, or CD44v6 sh1, or β-catenin sh1 for 48 hours. Nuclear β-catenin-associated chromatins were immunoprecipitated with β-catenin or CD44v6 antibodies for 3 hours. Chromosomal DNAs were purified and analyzed using QPCR with primers for TCF4 sites of MDR1 to detect the MDR1 promoter regions. Similarly, SW480-FR cells were transfected with or without non-targeted (NT) and β-*catenin* small hairpin RNA (shRNA) sequences, or with dominant negative TCF4 (TCF4-DN) constructs for 48 hours. Nuclear TCF4-associated chromatins were immunoprecipitated with β-catenin, or CD44v6 antibodies for 3 hours. Chromosomal DNAs were purified and analyzed using QPCR with primers for TCF4 sites of CD44v6 to detect the *CD44* promoter regions. Control IgGs were used as negative controls for immunoprecipitation. Chromatin inputs were used as loading controls for PCR. The primers used for ChIP PCR experiments studies are presented in Table 6.

2.17 *In vivo* tumorigenic potential of CICs

All animal studies described were approved by the Institutional Animal Care and Use Committee (IACUC) at the Medical University of South Carolina (IACUC # -2017-00250; approval date: 2019/03/14-2021/03/29). Procedures for animal studies were conducted in accordance with the National Institutes of Health Guide for the Care and Use of Animals. For studies of subcutaneous tumors, 2×10^3 or 5×10^5 NON-CICs, or 5×10^5 unsorted bulk tumor cells from a xenograft derived from the patient tissues (PD-FR), or from SW480-FR cells, were suspended in Matrigel and then implanted in 25 mice/cell types, 5 mice per week (Wk) in 6-wk-old female NSG mice (for PD-FR cells) or in SCID mice (for SW480-FR cells) that were obtained from The Jackson Laboratory. Tumors were monitored, and after 2 weeks from the first tumor growth, every 2 weeks, 5 mice were sacrificed, and tumors were removed and weighed to evaluate the tumor development (Figures 4B, 4D-G).

2.18 Biotin labelled receptor internalization assays

For cell surface protein labelling, cells were treated in the presence or absence of FOLFOX or WNT3A conditioned media at 37^0 C for the times indicated and washed three times with ice-cold phosphate-buffered saline (PBS; pH 8.0) to remove any contaminating proteins. Cells were biotinylated using Sulfo-NHS-SS-Biotin (21331, EZ-Link™ Sulfo-NHS-SS-Biotin, ThermoFisher Scientific). Cells from 70–80% confluent cultures (2.5×10^7 cells/ml) were resuspended in PBS, and cell

TABLE 6 ChiP PCR primers for MDR1and CD44v6 promoters.

Genes	Accession number	Primers	
		Forward sequence (5'-3')	Reverse sequence (5' 3')
MDR1 (A) [-644-(-447)]	Nlil_001348945	TAGGTCTTTCCACTAAAGTC	AGAGGACTTCACACTATCCA
MDR1 (B) [-1218-(-980)]	Nl.1_001348945	TTTCTTTCATTCCATTTATC	AAGTCTTCATATCCATATAA
MDR1 (C) [-1301-(-1056)]	Nl.1_001348945	AATGTAAGAATTTAAAATGC	CTTTGAAAAGGCTAGGAGAA
CD44v6 (A) [-1618-(-1370)]	NIII_001202555.2	AGAAGTCCTGGCATGGTTCC	TCTTCAGGGGAAGCCTTTTGA
CD44v6 (B) [-1997-(-1793)]	Nlii_001202555.2	GGATGACTTACTTGTCCCTGT	ACTCACAAGCAGGCCATTACCA

surfaces were biotinylated following the manufacture's instruction. Cell lysates were prepared in lysis buffer, and biotinylated proteins were precipitated using streptavidin beads from equal amounts of cell lysates. Precipitates were washed three times with cell lysis buffer and analyzed by SDS–PAGE and immunoblotting with appropriate antibodies.

For internalization assays, cell surface proteins were biotin-labelled as described above at room temperature for 1 hour, followed by treatment with or without WNT3A for the indicated times at 37°C. Following stimulation, cells were incubated with 0.1 M glycine in PBS for 30 min at 4°C to quench the unreacted biotin. Surface-retained biotin was removed using reduced glutathione (60 mM glutathione, 0.83 M NaCl), with 0.83 M NaOH and 1% bovine serum albumin (BSA) added before use for two 30-min incubations, followed by ice-cold PBS washes four times. Cells were collected and lysed, and biotinylated proteins isolated using streptavidin beads from equal amounts of cell lysates. The amounts of receptor bound to beads were determined by SDS–PAGE and immunoblot analysis.

2.19 Drug Efflux and Retention Assays

[^{14}C] Oxaliplatin Efflux/Retention in SW480-S and SW480-FR cells by FOLFOX induced hyaluronan-CD44v6-mediated ankyrin function were analyzed. For drug retention (105), exponentially grown SW480-S and SW480-FR tumor cells (transfected with indicated constructs or with shRNAs) were harvested by trypsinization. The single cell suspensions were plated into tissue culture plates and incubated for 24 hours for attachment. The cells were then washed three times with PBS and incubated for 24 hours with 0.2 μM oxaliplatin containing 300 dpm (2.16 pmole) [^{14}C] oxaliplatin (77.6 μCi/mmole). The cells were then washed to remove free radioactive oxaliplatin and incubated in drug-free medium containing 1 x FOLFOX or WNT3A (20 mg/ml) or no FOLFOX, or no WNT3A, or CD44v6shRNA, or $CD44_{D67}$ construct transfection for 48 hours prior to treatment with or without FOLFOX or WNT3A for 2 hours. At the end of treatment, cells were harvested, washed, and cell numbers were measured with a coulter counter. Radioactivity associated with cells (indicated as intracellular drug retention) was then measured by a liquid scintillation counter. Radioactive [^{14}C] oxaliplatin in vector control cells was used as 100% (Figure 11A).

2.20 Statistics

A two-tailed Student's t-Test was used to compare mean values between sensitive and resistant cells using the following parameters: mean ΔΔCT values for QPCR; mean colony number for soft agar growth assays; mean densitometry values for QPCR and WB; mean percentage of cell viability assay (CellTiter-Glo) and FACS analysis; mean luminescence for ATP activity in cell growth; Caspase Glow assays in Apoptosis measurements; and mean tumor weight in xenograft studies. Chi-squared analysis was done to compare incidences between sensitive and resistant cells for the following assays: number of positive wells containing tumor spheres in sphere formation assays; and number of mice developing tumors in xenograft studies. For experiments involving three or more groups, statistical significance was calculated with GraphPad Prism Software (version 8) using a 1-way or 2-way ANOVA with a Bonferroni's posttest, Student's *t* test, or log-rank (Mantel-Cox) test where appropriate (Graph-Pad Software Inc.). Data are presented as the mean ± SD.

2.21 Ethics statement

The animal study was approved by the Institutional Animal Care and Use Committee (IACUC) at the Medical University of South Carolina (MUSC). Procedures for animal studies were conducted in accordance with the National Institutes of Health Guide for the Care and Use of Animals IACUC-2017-00250 (approval date: 2019/03/14-2021/03/29).

3 Results

3.1 Upregulations of CD44v6 and active β-catenin contribute to acquired chemoresistance in colon tumor cells

In order to determine the mechanism of FOLFOX resistance in CRC, a cellular model of FOLFOX resistance was developed. Seven CRC cell lines, including the pre-neoplastic APC10.1 cells derived from the APCMin/+ mouse (31, 106), were screened for CD44v6 expression, and SW480, WIDR, LOVO, and HT29 cells that exhibited lower steady-state expressions of CD44v6 were selected (Figure 1A). In order to determine the mechanism of resistance to FOLFOX in CRC cells, FOLFOX-resistant (FR) CRC cell clones were established using serially escalated doses of FOLFOX (1-5 × FOLFOX; [1 × FOLFOX = IC_{50} of 5-FU + IC_{50} OXA + 1 μM leucovorin]) in parent sensitive CRC cells (SW480-S, WIDR-S, LOVO-S, and HT29-S) (for details, see Method section). To determine the mechanism of FOLFOX resistance in CRC, ex vivo cultures were established from patient-derived (PD) biopsies collected from 5-FU resistant (PD-5FUR), Oxaliplatin (PD-OXAR), and FOLFOX (PD-FR) tumor specimens and from subcutaneous (SQ) tumor samples derived from our FOLFOX resistant (FR) cell clones. Next, the IC_{50} concentrations of drug-values of 5-FU and OXA for inhibiting SW480, WIDR, HT29 and LOVO CRC cell growth were assessed by a cell viability ATP based assay (Cell Titer-Glo) in the presence of increasing concentrations of these drugs (5-FU, OXA, and FR). Figure 1B shows the IC_{50} values of 4 sensitive cell lines (SW480-S, WIDR-S, LOVO-S, and

HT29-S) treated with 5-FU or OXA with average values ~49-63 μg/ml for 5-FU and ~5-10 μg/ml for OXA treatments. Figures 1C-E show the IC_{50} values of sensitive SW480-S cells compared with SW480-5FU resistant (SW480-5FUR) cells, SW480-OXAR resistant (SW480-OXAR) cells, or SW480-FOLFOX resistant (SW480-FR) cells. In each case the resistant cell lines have 3-5 fold higher IC_{50} values compared to sensitive cells.

While 5-FU, OXA and FOLFOX have been associated with increased CD44v6 mRNA expression in CRC cells (5, 6), their stimulating actions to attain chemoresistance in CICs have not yet been clearly identified. To examine the effects of 5-FU, OXA, and FOLFOX on the regulation of chemoresistance by CD44v6 signaling, we first investigated CD44 variants expressions in sensitive cells and compared their expressions with those of 5-FUR, OXAR, and FR cells of SW480. A specific primer pair was used to amplify the CD44v6 variant by QRT-PCR in these sensitive and drug resistant cells of SW480. Results in Figure 1C-E demonstrate that basal CD44v6 expression was very low in SW480-S cells but significantly increased with resistance to chemotherapeutics (5-FU, OXA or FOLFOX). The basal expression of CD44v6 in these cells increased in the order of SW480-S < SW480-FR < SW480-OXAR < SW480-5-FR (Figure 1F). Similar results were found in WIDR, HT29, and LOVO CRC cells (data not shown).

We evaluated the kinetics of CD44v6 induction in SW480-S cells upon exposure to 1x FOLFOX. To determine whether FOLFOX resistance is associated with CD44v6, the expression profiles of CD44 variants in PD-FR, PD-OXAR and PD-5FUR cells were monitored by quantitative RT–PCR using distinct sets of primers. See the schematic diagram of the CD44 gene in Figure 1G. Sets of CD44 variants were detected using a series of forward 5' primers that were made to base-pair with v3, v4, v5, v6, v7, v8, v9 and v10 exons independently and with one 3' primer from the constitutive constant exon 7 (c7) (reverse primer) (shown in Figure 1G). Primers are presented in Table 1 in Methods. In addition, the CD44s standard form having no alternate splicing was detected using primers that base-pair to the constitutive constant exons 5 and 7 of CD44. Exon v6 was expressed together with exons v6–v8 and as an independent isoform (Figure 1H). The v6-v8 variants were detected using a 3′ primer from c7 (reverse primer) of CD44 and two distinct 5′-primers (forward primers) complementing to v6 and v8 exons of CD44, respectively (Figure 1G). The v6 primers and CD44s primers each principally amplified a single product (Figure 1H). The C5v6v8 primer gave rise to two alternately spliced variants of CD44 containing (1): variant exons v6 and v8 (illustrated as v6–v8); and (2) variant exon v8 (shown as v8), all joined to the 3′-constitutive exon C7 (Figure 1I). Although RT-PCR results showed that PD-FR, PD-OXAR and PD-5FUR expressed similar CD44 isoforms (Figure 1H), PD-FR specimens also express low-molecular-weight isoforms detected by the RT-PCR analysis with primers v3, v5, v6 and v9 (Figure 1H). Comparative analysis of matched colorectal cancer specimens from patients after cytotoxic treatment revealed a significant increase in *de novo* CD44v6 transcript across all drug resistant specimens (Figure 1H).

We focused on CD44v6 signaling in this study. To characterize specifically the CD44v6 transcript variant, further RT-PCR analysis was done using a forward primer that base pairs with both the v6 and C5 exons, and a reverse primer that base pairs with the C7 exon. RT-PCR results showed that PD-FR, PD-OXA and PD-5-FU cells predominantly expressed the C5v6v8C7 (v6-v8) and C5v6C7 (v6) isoforms (Figure 1I). Therefore, we concluded that C5v6v8C7 and C5v6C7 isoforms are unique to chemo resistant cells derived from patients who are resistant to 5-FU, or OXA, or FOLFOX (Figure 1I). No changes in CD44s were observed (Figure 1H). Overall, our data (Figures 1F, H, I) indicate that in patient tumor derived cells, FOLFOX and its components 5-FU and OXA considerably and distinctively induced CD44v6 transcript expression, which could interact with various cellular targets and offer one of the fundamental mechanisms for the drug resistance in CRC cells.

To determine the effects of the expression profiles of CD44 variants, SW480 cells were examined after stimulation with FOLFOX by exon-specific reverse transcription-PCR (RT-PCR). The expression levels of CD44v6 transcripts were monitored by quantitative RT–PCR using distinct sets of primers. See the schematic diagram of the CD44 gene in Figure 2A. A set of variants were detected using a 5' primer from a constitutive exon C5 and two different 3' primers complementary to either the v6 or v8 exon, respectively (primers are shown in Table 2). In addition, the standard form of CD44 (CD44s) was detected using primers that base-pair to the constitutive exons C5 and C6. The v6 primer and standard primer predominantly amplified a single product C5v6 (CD44v6 [v6]) (Figure 2B). The v8 primer amplified two spliced variants containing (1) C5v6v7v8 (referred as CD44v6-v8 [v6-v8]), and (2) C5v8 (referred as CD44v8 [v8]) all joined to the c5 constitutive exon (Figure 2A). All products were confirmed by DNA sequencing. As shown in Figure 2B, following 24 hours of serum starvation, the relative expression levels of CD44 variants were low. Stimulation of these cells with 1 x FOLFOX upregulated the v6 gene transcript that peaked between 4 and 16 hours and returned to basal levels at 24–36 hours likely due to the exhaustion of FOLFOX within the media (Figure 2B).

Next, we found that FOLFOX-resistant (FR) cells express constitutively high levels of CD44v6 and hypo-phosphorylated, active β-catenin (ABC), as a read-out for WNT pathway activity, and for increased MDR1 protein expression, as a read-out for drug resistance compared to sensitive cells (Figure 2C). In contrast, sensitive cells have low basal levels of these proteins that transiently increase following FOLFOX treatment but return to basal levels following drug withdrawal (Figure 2C). However, this induction in sensitive cells fails to reach the constitutive level as observed in resistant cells (time 0,

Figure 2C). These results of high expression of CD44v6 in SW480-FR cells (Figures 1F, H, 2B, C) were consistent with high expression of the CD44v6 transcript in PD-FR cultures (Figures 1H, I). To further validate that active β-catenin and MDR1 expressions in CRC cells are correlated with CD44v6 expression, we evaluated the effects of FOLFOX on expression of these proteins in SW480-S and SW480-FR cells following FOLFOX treatment with or without CD44v6 shRNA1, and CD44v6 shRNA2 (Figures 2D, E). These two sets of shRNAs were used to confirm that the effects of FOLFOX on CD44v6 function are specific to v6. Knockdown of CD44v6 in both FOLFOX-treated SW480-S and SW480-FR cells down-regulated expressions of pLRP6, active β-catenin, and MDR1 and inhibited the FOLFOX-induction of v6-containing variants but not of standard or v8 variants (Figures 2D, E). To further test that CD44v6-regulated WNT/β-catenin signaling affects resistance in response to FOLFOX, FOLFOX resistant SW480-FR tumor cell viability was assayed using different doses of FOLFOX in the presence or absence of two different sets of shRNAs (shRNA1 and shRNA2) targeted to CD44v6 and WNT3A (CD44v6 shRNA1/2, or *WNT3A* shRNA1/2, and CD44v6 shRNA1/2 plus pCD44v6 cDNA) (Figures 2F, G). A similar experiment was done with a second set of *shRNAs* for CD44v6 and *WNT3A* to confirm that the effects of CD44v6 and *WNT3A* are specific for FOLFOX stimulated colon tumor resistance (Figures 2G). WNT3A shRNA alone inhibited tumor cell proliferation to nearly the same extent as v6 shRNA at the highest concentration of FOLFOX treatment (Figures 2F, G). However, *WNT3A* shRNA1, or *WNT3A* shRNA2 combined with v6 cDNA overexpression nearly eliminated WNT3A shRNA-mediated inhibition of FOLFOX resistance compared to v6 cDNA + NT shRNA1, or v6 cDNA + NT shRNA2 groups in SW480-FR cells (Figures 2F, G, magenta lines compared to black lines). This suggests that WNT3A-CD44v6 interaction promotes resistance to FOLFOX induced death in the presence of the chemotherapeutic drug FOLFOX in CRC cells (Figures 2F, G). Overall, these data indicate that FOLFOX transiently upregulates CD44v6, active β-catenin and MDR1 expression in sensitive cells, while these proteins are already constitutively high in FR cells (as seen in Figure 2C) and facilitate FOLFOX resistance (Figures 2F, G). Supplemental Figure1A-C show the validation of WNT3A shRNA, CD44v6 shRNA, and v6 cDNA expression vectors. Our results (Figures 2B, C, F, G) also show that two sets of shRNAs display similar results confirming that this effect on FOLFOX resistance was specific to CD44v6 and WNT3A/CD44v6 signaling and not an off-target effect of using CD44v6 shRNA and WNT3A shRNA.

Next, results in Supplemental Figure 1D showed that knock down of WNT3A in SW480-FR cells inhibited the up-regulation of CD44v6 variants. These data indicated that WNT3A signaling may be required for FOLFOX-induced alternative splicing of CD44. These results (Figures 2F, G, and Supplemental Figure 1C) provide strong support for a positive feedback loop in which specific v6 isoform-dependent activation of WNT3A signaling in response to FOLFOX results in additional synthesis of these CD44v6 isoforms. The results confirm that the positive feedback loop altering WNT3A signaling could lead to long lasting changes in cellular properties such as cell cycle progression. A previous study showed that cytoplasmic and nuclear β-catenin are dynamically regulated during the cell cycle and increased during S phase (107). To investigate the role of the positive feedback loop between CD44v6 and WNT3A signaling in cell cycle progression, we determined the time course of active β-catenin (ABC) expression, and the cell cycle progression of quiescent cells into S phase in SW480 cells treated with CD44v6 shRNA followed by treatment with WNT3A or FOLFOX treatment for various time periods (Figures 2H, I, and Supplemental Figure 1D). After 2 hours of FOLFOX or WNT3A stimulation, 35-43% of the cells entered S phase in NT shRNA transfected cells compared with 15-23% of CD44v6 shRNA transfected SW480 cells treated with FOLFOX, and WNT3A respectively (Figure 2H, and Supplemental Figure1D). Upon WNT3A, or FOLFOX stimulation, WNT3A either by itself, or through FOLFOX, induced an initial burst of nuclear β-catenin activation independent of CD44v6. This activated signal was rapidly downregulated by CD44v6 shRNA after 2 hours. As shown in Figure 2H and Supplemental Figure 1D, ~90% of the NT shRNA treated cells had entered S phase after 10-12 hours of treatment with FOLFOX and WNT3A. In contrast, only ~7-12% of the CD44v6 shRNA-treated cells had progressed into S phase at 12 hours of stimulation with FOLFOX and WNT3A, indicating an interruption of S-phase access following down-regulation of the CD44v6 isoform. However, these results initiate a positive feedback loop between WNT3A mediated β-catenin activation and CD44v6 splicing (Figures 2H, I, and Supplemental Figure 1D) by stimulating v6-specific CD44 expression, and this could establish a mechanism for persistent activated β-catenin signaling in FOLFOX resistant cells. In addition, our FOLFOX resistant cells were generated by repeated exposure of the cells to 1x – 5x FOLFOX, and the resistant clones were maintained in 0.5 x FOLFOX selection pressure. Therefore, the FOLFOX-resistant cells sustain WNT3A production, and the maintenance of WNT3A/β-catenin signaling necessary for S phase could constitute a mechanism for a positive feedback loop between β-catenin activation and CD44v6. The depletion of this circuit by the use of v6 exon-specific shRNA in our study uncovered new understandings into how regulated alternative splicing can control intracellular β-catenin signaling sufficient to drive cell cycle progression in response to FOLFOX induced WNT3A secretion.

To further understand whether resistance to chemotherapeutics has been independently associated with increased CD44v6 variant expression that may be associated with a β-catenin/MDR1 pathway, we evaluated stemness in

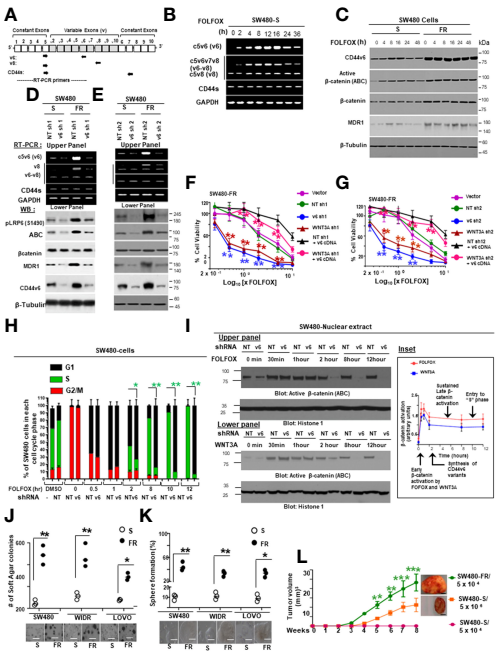

FIGURE 2
FOLFOX induced CD44v6 expression establishes FOLFOX (FR) resistant colorectal cancer cells (CRCs). **(A)**, Schematic illustration of the CD44 gene. Both constitutive (c) and variable (v) exons are represented. The PCR primers used to amplify CD44 variable and standard isoforms are shown as arrows and the PCR products are depicted in panel **(B)** experiments. **(B)**, Serum-starved SW480-S cells were stimulated with 1 x FOLFOX (50 µg/ml 5-flurouracil + 10 µM oxaliplatin + 1 µM leucovorin) at the indicated time periods. The mRNA expressions show that primers for v6 isoforms generate v6 and v6-v8 PCR products. The primers for v8 and the standard isoform of CD44 primarily generate one product. **(C)**, Western blots are shown for antibodies that recognize either CD44v6, the active hypo phosphorylated β-catenin (Active β-catenin (ABC)), β-catenin, MDR1 or β-tubulin in sensitive (S) and FR clones of SW480 cells following stimulation with 1x FOLFOX for 4-48 hours. **(D, E),** Upper panels: Semi-quantitative RT-PCR analyses are shown for CD44 variants in SW480-S and SW480-FR cells transfected with pSicoR-non targeted shRNA1 (NT sh1) or pSicoR-v6 shRNA1 (v6 sh1) **(D)**, and NT sh2 or v6 sh2 **(E)** for 72 hours followed by FOLFOX stimulation for another 12 hours. Lower Panels: Western blot analyses are shown for p-LRP6 (S1490), active ABC, β-catenin, MDR1, or β-tubulin following 1 x FOLFOX stimulation for 12 hours in cells transfected with NT sh1 or v6 sh1. **(F)**, Effects of CD44v6 shRNA1 and WNT3A shRNA1 knockdown of CD44v6 and WNT3A respectively on the viability of SW480-FR cells in presence of v6 cDNA that were treated with various concentrations of FOLFOX. An ATP based assay (CellTiter-Glo) measured cell viability compared with vector transfectant without FOLFOX treatment as 100%. Error bars represent calculated SDs (n = 3). **(G)** Same experiments as in F carried out in presence of CD44v6 shRNA2 and WNT3A shRNA2. **(H)** Sixteen hours after release from G2/M phase by nocodazole treatment, when 97% of the cells were in G1 phase (cell cycle analyzed by flow cytometry) the cells were transfected with either non-targeted (Control) or CD44v6 shRNA. Twenty four hours after transfection, the cells were incubated in low serum medium (0.5% serum) with 1 x FOLFOX for different time periods to re-enter the cell cycle. Cell cycle analysis were carried out in these cells. Samples were analyzed through a time course of 12 hours. Bar graph summarizing the flow cytometry cell cycle profile analysis of SW480 cells. Error bars represent $\pm$ SEM of five independent experiments. **(I)** Upper and lower panels: Western blot for the activated β-catenin accumulation in nuclear fraction in G2/M arrested and 1 x FOLFOX or 20 ng/ml WNT3A stimulated SW480-cells which were previously transfected with NT shRNA or v6 shRNA for 24 hours. These cells were collected at indicated times after 1 x FOLFOX or WNT3A -stimulation. Inset: A model for sustained WNT3A signaling and G1–S transition, dependent on CD44 v6 variants (details are in the text). **(J)**, Anchorage-independent growth in soft agar is shown for SW480-FR, WIDR-FR and LOVO-FR cells and compared with their sensitive (S) pairs. Scale bars, 100 µm. **(K)**, Tumor-sphere formation assays were done for the SW480-FR, WIDR-FR and LOVO-FR cells and compared with their sensitive (S) pairs. Scale bars, 100 µm. **(L)**, Tumor formation is shown in nude mice injected with either 5 x 10^4 SW480-FR cells, or 5 x 10^4 SW480-S cells, or 1 x 10^6 SW480-S cells. SW480-FR cells formed tumor nodules in all injected mice (7/7). Starting at week 3, SW480-R (5 x 10^4) cells induce tumor nodules whereas SW480-S (5 x 10^6) cells induced much smaller tumor nodules starting a week later than the SW480-FR cells (7/7 mice). SW480-S (5 x 10^4) cells were unable to induce tumors. Growth curves are shown for these xenograft tumors in immunocompromised mice. Data are presented as Mean $\pm$ SD from n = 3-6 replicates in three independent experiments. All WBs, FACS data, semi quantitative RT-PCR data are representative of three experiments **(F, G)**, *P < 0.05, **P < 0.01 were considered significant, percent cell viability in WNT3A shRNA and CD44v6 shRNA transfected cells compared with vector control and NT shRNA transfected. *P < 0.05, **P < 0.01 were considered significant, percent cell viability in WNT3A shRNA + v6 cDNA transfected cells compared with WNT3 shRNA transfected cell. Student's t-test was used to assess the significance. **(H)**, *P < 0.05, **P < 0.01 were considered significant, percent cells in S phase in CD44v6 shRNA transfected cells compared with NT shRNA transfected cell. **(J–L)** *P < 0.05, **P < 0.01, ***P < 0.001 were considered significant. Soft agar colonies, tumor sphere growth, and SQ tumor growth of SW480-FR cells were compared with SW480-S cells. Tumor growth kinetics data in (L) (n = 7) represent mean +/- SD, from at least 3 independent experiments.

sensitive and FOLFOX resistant (FR) cells of SW480, WIDR and LOVO, by determining their clonogenicity, tumor sphere formation, and their *in vivo* tumor development by implanting FR and sensitive (S) cells in immunocompromised mice. To determine the clonogenicity of these cells *in vitro*, their clonal capacity was measured in a soft agar colony formation assay. Compared to parental S cells, FR cells were able to form increased anchorage-independent growth assessed by formation of large numbers of soft agar colonies (Figure 2J). Further, compared with parental S cells, FR cells were able to form significantly greater numbers of tumor-spheres in serum free medium (Figure 2K).

Next, to evaluate whether FOLFOX resistant cells increased tumor growth *in vivo* compared to the corresponding sensitive cells, 5×10^4 SW480-FR cells, 5 x10^4 SW480-S cells and 5 x 10^6 SW480-S cells, were each implanted into 7 immunocompromised mice in 3 separate experiments. In agreement with the soft agar growth and tumor sphere formation results (Figures 2J, K), 5×10^4 FR cells generated tumors in at least 90–100% of immunocompromised mice injected with SW480-FR cells (Figure 2L, green, tumor formation = 7/7 mice), whereas 5×10^4 sensitive cells (SW480-S) were not adequate to form tumors (Figure 2L, purple, tumor formation = 0/7 mice). However, implantation of 200-fold more sensitive SW480-S cells (5×10^6) initiated tumors in three independent experiments (Figure 2L, orange, tumor formation = 6/7 mice). When tumor volumes were examined every day to evaluate the latency, tumors initiated from 5×10^4 SW480-FR cells began to increase at 2 weeks while tumors initiated from 5×10^6 SW480-S cells began to increase later at 3–4 weeks and had much smaller size at 8 weeks compared with 5×10^4 SW480-FR cell-derived sub cutaneous (SQ) tumors (averages 1175 mm^3 compared to 2400 mm^3 at 8 weeks, Figure 2L). The results from Figures 2J–L provide evidence that FOLFOX-resistant FR cells were more tumorigenic *in vitro* and *in vivo* and had greater sphere-forming activity than parental sensitive cells, which are hallmark characteristics of CRC-CICs. This provides evidence that expansion of CICs expressing CD44v6 can have an important role for the acquisition of FOLFOX resistance.

Overall, these results indicate that: 1) CD44v6 has key roles for FOLFOX-induced WNT3A/β-catenin/MDR1 activation that is clearly inhibited by CD44v6 shRNA, confirming that FOLFOX might induce WNT ligands to mediate CD44v6-dependent WNT/β-catenin signaling, 2) constitutive activation of CD44v6 and WNT3A are necessary for maintaining FOLFOX resistance in CRC cells through a WNT3A-CD44v6-β-catenin-MDR1 pathway, and 3) Our data, suggest (Figure 2H, I, and Supplemental Figure 1D) that upon FOLFOX or WNT3A stimulation, WNT/β-catenin signaling generate an early burst of β-catenin activation independent of CD44v6 variants. This activation of β-catenin is promptly down-regulated by CD44v6 shRNA and the findings suggest that a positive feedback loop between WNT/β-catenin signal activation and CD44v6 splicing occurs by stimulating v6-specific CD44 expression.

3.2 CD44v6 expression defines highly tumorigenic colorectal cancer-initiating cells

Cancer initiating cells (CICs) have two decisive features: stemness and resistance to conventional chemotherapies, and thus are a hallmark of drug resistance. CICs are considered to remain after chemotherapy to initiate metastasis (108). According to the published data, CD44v6 has important roles in the stemness of CICs (15, 19, 109). Therefore, we investigated whether expression of CD44v6 defines CRC/CIC subpopulations with drug resistance and tumorigenic properties in clinical samples (PD-FR, PD-5FUR and PD-OXAR) isolated from patients who were resistant to several chemotherapeutic drugs as well as in our FOLFOX resistant WIDR, HT29 and SW480 cells.

First, CICs were isolated from the tumor sphere-propagated cells from colorectal human specimens and colorectal xenograft (SQ) tumors by FACS sorting using several of the previously reported candidates (CD44v6, CD133, EpCAM and ALDH1) (19, 43, 110–112). The data in Figure 3A (upper panel) show that CD44v6 (+) EpCAM (+) sorted cells (10% of unsorted PD-FR tumor cells, Figure 3B) overlapped with CIC markers ALDH1 and CD133 antigen expressions in PD-FR patient tissues (lower panel of Figure 3A). The data in Figures 3C, D show the percentages of CD44v6(+) and CD44v6 (–) cells in EpCAM (+)/ALDH1 (+), and EpCAM (+)/ALDH1 (+)/CD133 (+) cells with respect to unsorted cells. Hereafter freshly isolated CD44v6 (+)/EpCAM (+)/ALDH1 (+)/CD133 (+) cells from the corresponding sphere-propagated tumor cells will be referred to as CICs, and CD44v6 (–)/EpCAM (+)/ALDH1 (+)/CD133 (+) cells as Non-CICs (Figure 3D). Results in Figure 3E showed increased CIC-stemness related gene expressions (primers are given in Table 3 in Methods) in CICs isolated from both PD-FR patient tissues and from SW480-FR/SQ tumors compared to their respective Non-CICs. Overall, the data in Figures 3A-E validate that the CICs overexpressing CD44v6 were originated from epithelial and stem cells.

Second, given that CD44v6 and β-catenin activation are CRC-CIC markers (19, 113) and that FOLFOX therapy induces CD44v6 associated β-catenin-MDR1 signaling (as seen in Figures 2C-G), we examined whether CD44v6-β-catenin signaling can classify CRC/CICs as a FOLFOX-resistant phenotype. In agreement with the results in our generated FR and S cells of SW480 (as seen in Figures 1F, 2B-E), data in clinically relevant human specimens demonstrated that basal CD44v6 expression was also significantly increased in ex vivo cultures from PD-FR tumor specimens compared to PD-OXAR and PD-5-FUR tumor specimens, and FOLFOX stimulation further increased CD44v6 mRNA expressions in each of the cultures from PD-FR, PD-OXAR and PD-5-FU specimens (Figure 3F). Next, the viable cell growth of CICs and Non-CICs derived from our PD-FR and PD-5FUR specimens were

compared to FOLFOX treatment (Figures 3G, H). The data in Figure 3G demonstrate that in a PD-FR tissue, the cell viability of CICs was little or not affected by FOLFOX treatment, whereas Non-CICs displayed an ~2.8-fold reduction in cell viability following FOLFOX therapy that correlated with increased Caspase 3 activation (Figure 3I). In PD-5FUR cells, Non-CICs displayed ~2.3 fold more sensitivity to FOLFOX (measured by Caspase 3 activity) compared with CICs from PD-5FUR SQ tumor cells (Figures 3H, J). Importantly, PD-5FUR CICs from SQ tumors displayed partial sensitivity to FOLFOX (40%) compared to no sensitivity in PD-FR CICs indicating that our PD-FR CICs are indeed resistant to FOLFOX, whereas PD-5FUR CICs are only partially resistant to FOLFOX (Figures 3G-J).

Third, we evaluated tumor sphere forming ability between CICs and Non-CICs from PD-FR and SW480-FR/SQ tumor cells. Quantification of the sphere-formation assay demonstrates that CICs have elevated tumor sphere formation efficiency (Figure 4A). To establish the effects on CICs in functional assays, we performed SQ tumor growth assays (Figures 4B, C) for CICs, Non-CICs and unsorted bulk tumor cells. Importantly, tumors derived from freshly isolated CICs from SW480-FR and PD-FR tumor samples were able to generate larger tumors compared to those induced by unsorted cells in immunocompromised mice (Figures 4B, C). When CICs were injected in immune-compromised mice, 80-100% developed tumors compared to 50-65% of mice injected with unsorted (Bulk) cells (Figure 4D). Examples of tumor growth in cultures of SW480-FR/CICs and PD-FR/CICs isolated from xenograft tumors, and the inability of Non CICs from these tumors to do so, are shown in Figures 4B-D. Moreover, the CICs increased tumor incidence and reduced the latency of tumor formation by PD-FR, HT29-FR, SW480-FR and WID-FR cells with increased tumor sizes in mice implanted with CICs compared to unsorted (Bulk) tumor cells, which required 100-fold more cells compared to CICs (Figure 4D). In concordance with results of Figures 4B, D, when implanted into immunocompromised mice, despite the higher number of unsorted bulk tumor cells (5 x 10^5) that were used, tumor formations following injection of purified CICs (2 x 10^3) were faster and more efficient than tumor formations obtained with the total unsorted bulk cancer cell population (Figures 4B-D). Importantly, as high as 5 x 10^5 Non-CICs from these specimens failed to form any tumors (Figure 4E).

Fourth, to investigate whether CICs from patient-derived PD-FR colon tumor cells, and from SW480-FR/SQ tumor cells display long-term tumorigenic potential, we evaluated their ability to generate tumors after serial transplantations. Indeed, injected CICs engrafted and generated tumors that grew rapidly and required the mouse to be sacrificed within 28 days. Similar to the results of Figures 4D-E, examples of tumor growth of freshly isolated SW480-FR/SQ/CICs and PD-FR/SQ/CICs, and the inability of Non-CICs from these tumors to do so, are shown in Figures 4F-G. Interestingly, despite the presence of CD44v6 (+) cells present in 5 x 10^5 unsorted bulk cells, tumor formation following implantation of sorted CICs was quicker and more effective than tumor generation from the 5 x 10^5 unsorted bulk tumor cell population (Figure 4F). To determine if the tumorigenic population in CRC is restricted to CD44v6 (+), CICs were evaluated by their ability to generate tumors after serial transplantations in secondary and tertiary xenograft models. To address this issue, 2 x 10^3 CICs, 5 x 10^5 Non-CICs, and 5 x 10^5 unfractionated tumor cells from primary tumor xenografts were transplanted into a secondary xenograft model. The implanted CICs increased tumor incidence, grew rapidly and reduced the latency of tumor formation by CICs with increased tumor size (Figures 4F, G). Furthermore, CICs obtained from similar CIC derived secondary xenografts were subsequently transplanted into third generation of xenografts in mice. During the *in vivo* serial transplantation, CICs did not lose their tumorigenic potential but instead increased their long-lasting faster tumor growth (as measured by the tumor volume in Figure 4G). In contrast to the data of Figures 4F, G, importantly, the tumorigenic potentiality of the Non-CICs was entirely lost in secondary recipients (Figures 4H, as well as in 4F), providing evidence that Non-CICs include mainly differentiated nontumorigenic cells whereas tumorigenic colorectal CICs are restricted to the small population of CICs expressing CD44v6 (Figures 4F-H). Thus, the CIC population in colon tumors was able to generate serial xenografts showing a nearly unlimited tumor growth potential.

The relative resistance of CICs to chemotherapy (as seen in Figure 4A-H) suggests that CICs may be enriched after chemotherapy treatment. Indeed, the CIC immunophenotype (CD44v6 (+)) was increased 1.3-8-fold after chemotherapy treatment (Figure 4I). Importantly, the CIC population in the colon tumor tissue can generate serial transplantation derived SQ tumors indicating an essentially unlimited tumorigenic potential of CICs expressing CD44v6 (Figures 4F–H). Together, these data collectively support a model in which drug resistant colorectal CICs are confined to the small CD44v6 (+)/EpCAM (+)/ALDH1 (+)/CD133 (+) cell populations isolated from sphere-propagated tumor cells (as seen in Figure 3D), which are enriched with FOLFOX therapy (Figure 4I) with high tumorigenic potential (Figures 4B-H). The tumorigenic potential of CICs was not related to a higher content of CD44v6 (+) CICs in response to FOLFOX therapy as seen in Figure 4E, but may be related to *in vivo* selection of a highly tumorigenic subpopulation of CICs (Figures 4F-H). These results favor a cell-autonomous relative chemo resistant and virtually unlimited growth potential phenotype of colorectal CICs expressing CD44v6, indicating that CD44v6 can be used as a CIC marker, and as a therapeutic target for CRC.

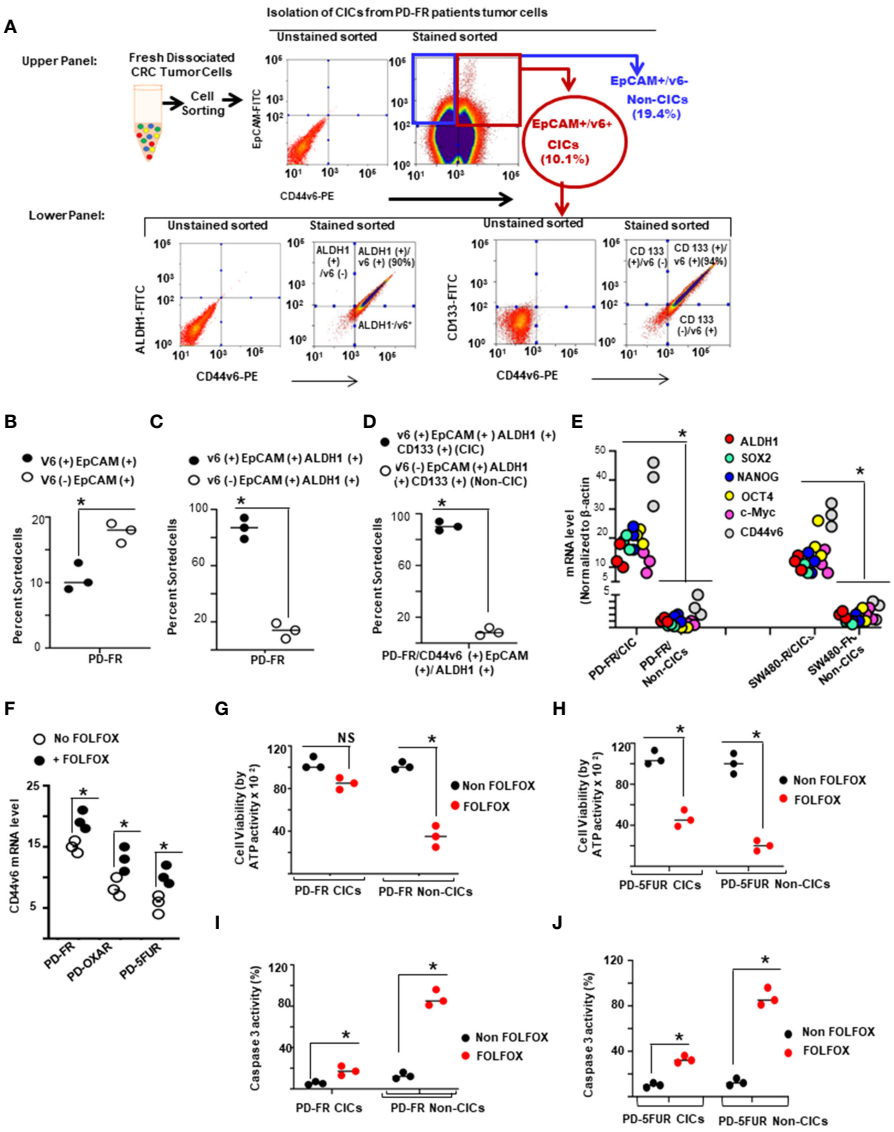

FIGURE 3
CD44v6 identifies colorectal cancer (CRC) initiating cells (CICs). **(A)**, Single-cell suspensions from patient derived (PD) specimens collected from 5-FU (PD-5FUR), Oxaliplatin (PD-OXAR) and FOLFOX (PD-FR) resistant tumor tissues, and from SW480-FR/subcutaneously (SQ) tumor cells were processed for tumor spheres. Sphere propagated cells were FACS sorted for high expressions of CD44v6-PE. CD44v6 positive (+) populations were sorted using EpCAM (−) FITC and CD44v6-PE. CD44v6 (+)/EpCAM (+) cells from various tumors were cultured separately and grown in fresh medium for 2 weeks. The cells were then subjected to flow cytometric analysis for isolation of CD44v6 (+)/EpCAM (+)/ALDH1 (+)/CD133 (+) (CICs), and for CD44v6 (−)/EpCAM (+)/ALDH1 (+)/CD133 (+) (Non-CICs) using antibodies to ALDH11-FITC, CD133-FITC or CD44v6-PE. **(B–D)**, Percentages of CD44v6 (+) and CD44v6 (−) fractions in EpCAM (+) **(B)**, in EpCAM (+)/ALDH1(+) **(C)**, and in EpCAM (+)/ALDH1 (+)/CD133 (+) **(D)** sorted cells in PD-FR tumor tissues are shown. Henceforth, the CD44v6 (+)/EpCAM (+)/ALDH1 (+)/CD133 (+) cells are identified as CICs, and the CD44v6 (−)/EpCAM (+)/ALDH1 (+)/CD133 (+) cells as Non-CICs (details in Methods). **(E)**, QPCR analyses of CIC-stemness markers (ALDH1, SOX2, OCT4, Nanog, c-Myc and CD44v6) were done on PD-FR CICs, PD-FR Non-CICs, SW480-FR CICs, and SW480-FR Non-CICs isolated from SW480-FR and SW480-S SQ tumor samples. **(F)**, CD44v6 mRNA expressions (by QPCR) are shown in PD-FR, PD-OXAR and PD-5FUR cells treated with or without 1 x FOLFOX for 12 hours. Data are presented as fold change of CD44v6 mRNA expressions relative to adjacent control cells from colon tissue. **(G, H)**, Cell viability of CICs and non-CICs from three independent PD-FR **(G)** and PD-5-FUR **(H)** cultures following treatment with or without FOLFOX were assessed by an ATP based assay (CellTiter-Glo). **(I–J)**, Apoptosis of CICs and non-CICs from three independent PD-FR **(I)** and PD-5-FUR **(J)** cultures following 1 x FOLFOX treatment were assessed by a Caspase 3 ELISA assay. Data are presented as Mean ± SD from n = 3-6 replicates in three independent experiments. All QPCR, and FACS data are representative of three independent experiments **(B–D)**, *P < 0.05, were considered significant, CD44v6 (+) cells were compared with CD44v6 (−) cells. **(E)**, *P < 0.05, were considered significant, expression of stemness associated factors of CICs were compared with Non-CICs. (FH–J), *P < 0.05, were considered significant, FOLFOX treated cells were compared with Non FOLFOX cells.

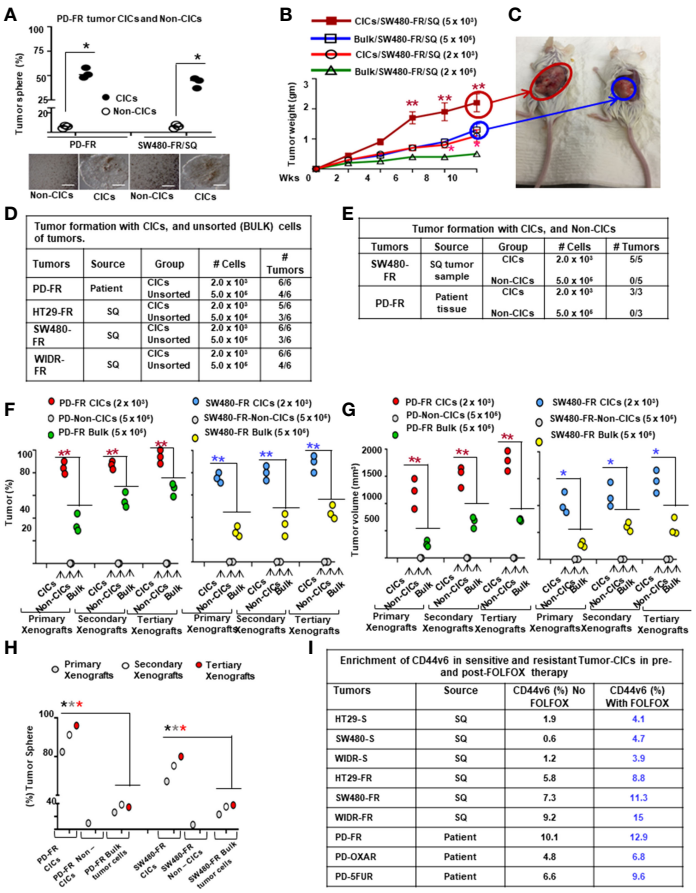

Tumors	Source	Group	# Cells	# Tumors
PD-FR	Patient	CICs	2.0 x 10³	6/6
		Unsorted	5.0 x 10⁶	4/6
HT29-FR	SQ	CICs	2.0 x 10³	5/6
		Unsorted	5.0 x 10⁶	3/6
SW480-FR	SQ	CICs	2.0 x 10³	6/6
		Unsorted	5.0 x 10⁶	3/6
WIDR-FR	SQ	CICs	2.0 x 10³	6/6
		Unsorted	5.0 x 10⁶	4/6

Tumors	Source	Group	# Cells	# Tumors
SW480-FR	SQ tumor sample	CICs	2.0 x 10³	5/5
		Non-CICs	5.0 x 10⁶	0/5
PD-FR	Patient tissue	CICs	2.0 x 10³	3/3
		Non-CICs	5.0 x 10⁶	0/3

Tumors	Source	CD44v6 (%) No FOLFOX	CD44v6 (%) With FOLFOX
HT29-S	SQ	1.9	4.1
SW480-S	SQ	0.6	4.7
WIDR-S	SQ	1.2	3.9
HT29-FR	SQ	5.8	8.8
SW480-FR	SQ	7.3	11.3
WIDR-FR	SQ	9.2	15
PD-FR	Patient	10.1	12.9
PD-OXAR	Patient	4.8	6.8
PD-5FUR	Patient	6.6	9.6

FIGURE 4
Tumor response to FOLFOX is correlated with enrichment of CD44v6 (+) CICs and resistance of CICs. **(A)**, Percentages of tumor sphere formation of PD-FR CICs and Non-CICs were measured in a sphere-formation assay. Representative pictures of tumors are shown. **(B)**, Implantation of 5 x 10^3 CICs from SW480-FR (SQ) tumors resuspended in Matrigel were tumorigenic while 100-fold more unsorted cells (Bulk) resuspended in Matrigel were required to generate tumors in four independent implantations. Five mice per group were used. SW480-FR SQ tumor weights following injection of indicated cell numbers from CICs and unsorted (Bulk) tumor cells are shown. **(C)**, A representative image of tumors initiated from **(B)** is shown. **(D)**, FACS sorted 2 x 10^3 CICs resuspended in Matrigel were tumorigenic while 250-fold more unsorted bulk cells (resuspended in Matrigel) were unable to generate the same capacity of tumorigenesis in four independent specimens. Six mice per group were used for four independent experiments. **(E)**, Numbers of SQ tumors formed by implantations of the indicated numbers of CICs and Non-CICs resuspended in Matrigel that were FACS sorted from the SW480-FR cells and PD-FR cells are shown. Five mice were used per group. **(F)**, FACS sorted CICs (2 x 10^3), Non-CICs (5 x 10^5), and the unfractionated bulk tumor cells (5 x 10^5), from indicated tumor samples were resuspended in Matrigel and implanted in immunocompromised mice. The same cells from the first generation of SQ tumors were further implanted into immunocompromised mice. The experiments were repeated to generate tumors into the third generation of xenograft tumors. Only CICs and the unfractionated bulk tumor cells were capable of inducing tumor formations. Isolation of second and third generation xenograft tumor cells displayed similar results (n = 5 mice; experiments were performed in triplicates). **(G)**, Tumor volumes from the experiment **(F)** were measured in implanted tumors from the indicated CICs, and from the unfractionated bulk tumor cells (n = 5 mice; experiments were performed in triplicates). **(H)**, Percentages of tumor sphere formation in freshly isolated dissociated primary, secondary and tertiary xenograft tumors generated with the indicated CICs, Non-CICs, and unsorted bulk tumor cells from the experiment **(F)** are shown. **(I)**, Enrichments of CICs in bulk cells from three sources – 1) patient derived specimens, 2) SQ tumor samples developed using FR-cells, and 3) the corresponding sensitive pairs, were assessed by FACS analysis for CD44v6 after FOLFOX treatment. Data are representative of four independent human specimens, and of three independent tumor samples from sensitive and FR cells. Data are presented as Mean ± SD from n = 3 replicates in three independent experiments. **(A)** *P < 0.05, were considered significant, tumor sphere growth in PD-FR CICs were compared with Non-CICs. **(B)**, *P < 0.05, **P < 0.01, were considered significant, SQ tumor growth in SW480-FR CICs were compared with bulk tumor from SW480-FR cells. Tumor growth kinetics data in **(B, C)**, n = 6 mice/each group represent mean +/- SD, from at least 3 independent experiments. **(D, E)**, n = 6 mice/each cell types (CIC or unsorted) in each cell types in three independent experiments represent mean +/- SD.**(F, G)**, n = 5 mice/each cell types (CIC, Non-CICs, or unsorted) in three independent experiments represent mean +/- SD, *P < 0.05, **P < 0.01, were considered significant, tumor growth using CICs were compared with tumors from bulk tumor cells. **(H)**, *P < 0.05, *P < 0.05, *P < 0.05, were considered significant for tumor sphere growth from cells from primary, secondary, and tertiary xenografts of CICs compared with bulk cells. Tumor growth kinetics data in L (n = 7) represent mean +/- SD, from at least 3 independent experiments.

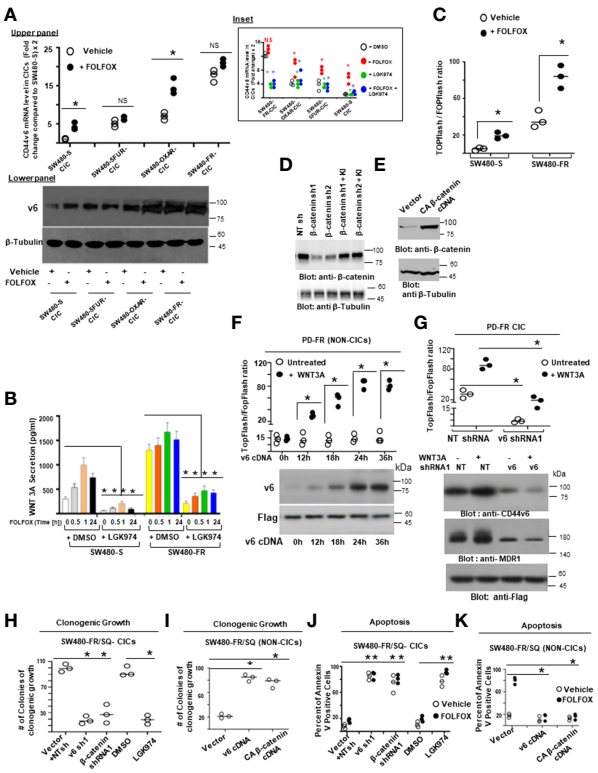

FIGURE 5
CICs isolated from resistant cells demonstrate resistance to FOLFOX treatment through WNT3A/β-catenin signaling. **(A)**, QPCR (Upper panel) and western blot (Lower Panel) data are shown for CD44v6 mRNA (Upper panel) and protein expression (Lower panel) in CICs isolated from SQ tumors of SW480-FR, SW480-OXA, SW-5-FU, and SW480-S cells that were treated with or without either 1 x FOLFOX for 12 hours, Inset: CICs isolated from SQ tumors of SW480-FR, SW480-OXA, SW-5-FU, and SW480-S cells that were treated with either 1 x FOLFOX, or 1.2 ng/ml of WNT inhibitor LGK974 (IC_{50}, for LGK974 in SW480-S and SW480-FR cells are 0.8 ng/ml and 1.15 ng/ml [data not shown]), or 1 x FOLFOX + LGK974 for 12 hours. QPCR analysis was done with total RNA extracted from these treated cells and data are shown for CD44v6 mRNA. **(B)**, Secretion of WNT3A was measured by ELISA in sensitive and FR cells of SW480 after treatment with DMSO. Or 1 x FOLFOX, or 1.2ng/ml of LGK974, or 1 x FOLFOX + LGK974 for the indicated times. **(C)**, Sensitive and FR cells of SW480 were transfected with 50 ng TOPFlash and 50 ng TK-Renilla vectors, or with 50 ng FOPFlash and 50 ng TK-Renilla vectors. The TOPFlash/FOPFlash promoter was activated by treatment with FOLFOX (1x) for 12 hours. Cells were lysed and subjected to luciferase measurements. **(D-E)**, Validations of β-catenin shRNAs (β-catenin sh1 and β-catenin sh2) **(D)** and of constitutively active β-actin **(E)** used in the following experiments **(H-K)** were examined. In "D", the indicated shRNA mediated knockdown and the corresponding knock-in **(KI)** gene transfections were dune as described in Methods. Target proteins were analyzed by WB analysis (β-tubulin, internal control). **(F)**, CD44v6 negative PD-FR/NON-CICs were transfected with either TOPFlash and control TK-Renilla vectors, or with FOPFlash and TK-Renilla vectors together with increasing time of incubation with CD44v6 cDNAs. After 48 hours, the cells were stimulated with or without 20 ng/ml WNT3A for the indicated times. Then the cells were lysed and subjected to luciferase measurements (upper panel) or, in parallel, to WB analysis for CD44v6 and Flag. **(G)**, PD-FR CICs were transfected with NT sh1, or with CD44v6 sh1. After 48 hours, cells were analyzed for WNT3A stimulated β-catenin/TCF4 promoter luciferase activity as shown in upper panel or, in parallel, to WB analysis with the indicated proteins (lower panel). **(H, J)**, SW480-FR CICs were transfected with NT sh1, or CD44v6 sh1 (v6 sh1), or β-catenin sh1, or treated with DMSO, or 1.2 ng/ml of LGK974. 48 hours after the transfections, and 12 hours after the LGK974 treatment, cell growth was assessed by counting colonies in a clonogenic growth assay **(H)**, and apoptosis was assessed by the Annexin V positive stain assay **(J)**. **(I, K)**, SW480-FR Non-CICs were transfected with vector control, v6 cDNA, or CA β-catenin cDNA. 48 hours after the transfections, cell growth was assessed by clonogenic growth assay **(I)**, and apoptosis was assessed by the Annexin V positive stain assay **(K)**. Data are presented as Mean $\pm$ SD from n = 3-4 replicates in three independent experiments. All WB data are representative of 4 independent experiments. **(A)** *$P < 0.05$ was considered significant for red asterisks, CD44v6 mRNA levels of FOLFOX treated cells were compared with the DMSO treated cells; *$P < 0.05$ considered significant for the green and blue asterisks, CD44v6 mRNA levels of 1.2 ng/ml, LGK974 and FOLFOX + LGK974 treated cells were compared with DMSO, or FOLFOX treated controls. **(B)**, *P < 0.05, was considered significant, secreted WNT3A in LGK974 treated cells of SW480-S and SW480-FR were compared with their respective DMSO treated controls. **(C)**, *P < 0.05, was considered significant, FOLFOX treated cells of SW480-S and SW480-FR were compared with their respective DMSO treated controls. **(D-E)**, *P < 0.05, was considered significant, WNT3A treated PD-FR NON-CICs **(D)** and PD-FR CICs **(E)** at various time points were compared with their respective untreated controls. **(F, H)**, *P < 0.05, was considered significant, v6 shRNA1, β-catenin shRNA1, and LGK974 treated clonogenic growth **(F)**, and Annexin V positive **(H)** CICs were compared with their appropriate vector + NTshRNA, and DMSO controls. **(G, I)**, *P < 0.05, was considered significant, v6 cDNA, CA-β-catenin CDNA overexpressed clonogenic growth **(G)**, and Annexin V positive **(I)** NON-CICs were compared with their appropriate vector controls.

3.3 FOLFOX-induced WNT3A and CD44v6 signaling establishes cell autonomous resistance to conventional FOLFOX chemotherapies in colorectal CICs

Given that human colorectal CICs can be defined based on high WNT signaling activity (113, 114), we examined if elevated CD44v6 regulated β-catenin activation, as seen in Figures (2C-E), can define the FOLFOX resistance of the CIC fraction (as seen in Figures 2F-G). To address this, first we generated drug resistant (5-FU, OXA, and FOLFOX resistant) SW480 cells. To generate these drug resistant cells, we first determined IC_{50} values of the parent SW480 cells for 5-Flourouracil (5-FU) and oxaliplatin (OXA) (see Figure 1B), because these molecules are the components of FOLFOX. FOLFOX resistance cells were generated by incubating the sensitive parental cells of SW480 (SW480-S) with repeated exposure to increasing concentrations of the drug from 1x FOLFOX (50 μM 5-FU [IC_{50} values for SW480 cells for 5-FU] + 5 μM OXA [IC_{50} values for SW480 cells for 5-FU] + 1 μM leucovorin) to 5 x FOLFOX over 5 days. This exposure and withdrawal cycle was repeated five times for each dose of the drug. The surviving 5-FU resistant (5-FUR), OXA-resistant (OXAR) and FOLFOX-resistant (FR) clones were cultured in normal medium for 5 days and maintained with selection pressure of half the IC_{50} dose of SW480 cells for 5-FU, OXA and FOLFOX. In Figure 5A, we compared expression of CD44v6 mRNA (Upper panel, Figure 5A) and protein (Lower panel, Figure 5A) in sensitive (S), 5-FUR, OXAR, and FR clones with and without 1 x FOLFOX treatment for 8 hours. Results in Figure 5A show that FR cells express significantly highest levels (~20 ± 1.67-fold mRNA [Upper panel] and ~8 fold protein [Lower panel]) of CD44v6. OXAR and 5-FUR cells express moderately higher levels (~5-6 ± 0.9 - fold mRNA [Upper panel] and ~3-3.5 fold protein [Lower panel]) compared to sensitive SW480-S cells (Figure 5A). Since these resistant cells were selected by repetitive treatment of the sensitive cells with 5 μM OXA, 50 μM 5-FU, and 5 x FOLFOX drugs and maintained under selection pressure of 25 μM of 5-FU, 2.5 μM of OXA and 0.5 x FOLFOX, the basal levels of CD44v6 mRNA and protein in these cells are already elevated, and further addition of 1 x FOLFOX to these cells has little or moderate effect on CD44v6 expression (Figure 5A), whereas addition of FOLFOX to sensitive cells increase the CD44v6 mRNA expression to ~ 5 ± 0.49-fold and CD44v6 protein by ~2 fold (Lower panel, Figure 5A). These increases in CD44v6 expression in sensitive cells were decreased (data not shown) to basal level at ~24–48 h due to the depletion of FOLFOX in the media as seen in the results of Figures 2B, C. In a further step, we analyzed the expression of CD44v6 mRNA in resistant and sensitive cells with and without treatment with WNT inhibitor LGK974 in FOLFOX treated CICs from resistant and sensitive cells (Inset, Figure 5A). The results (Inset, Figure 5A) indicate that, WNT3A inhibitor inhibited FOLFOX induced CD44v6 expression substantially in FOLFOX treated CICs from resistant and sensitive cells, suggesting that FOLFOX induced WNT3A maintains CD44v6 mRNA and protein expression in CICs. These data in Figure 5A, and in Figures 2B-C indicate that FOLFOX treated transient upregulation of WNT3A regulates CD44v6 activation in sensitive cells, and WNT3A induced constitutively active CD44v6 activation in resistant cells to maintain FOLFOX resistance in SW480-FR cells. Abrogation of the CD44v6-WNT3A signaling pathways restores sensitivity to cytotoxic drugs (Figures 2F, G).

Second, since cancer cells secrete cytokines to evade drug-induced death (115), and oxaliplatin, a component of FOLFOX, induces a WNT/β-catenin target IL-6 (116, 117), we determined whether our resistant cells and sensitive cells differentially secret WNT3A ligands in response to FOLFOX treatment. Results (Figure 5B) indicate that SW480-FR cells endogenously produce higher WNT3A levels compared to SW480-S cells, and additional FOLFOX treatment increases WNT3A secretion levels. Additionally, WNT inhibitor LGK974 inhibits the secretion of endogenous WNT3A and FOLFOX induced WNT3A protein in both the cells (Figure 5B). This higher WNT3A secretion in response to FOLFOX treatment suggests that WNT3A-induced TOPFlash transactivation may be enriched after FOLFOX treatment. To determine the reporter activity, we overexpressed a luciferase construct containing four native TCF/LEF binding sites (TOPFlash) or its negative-control counterpart (FOPFlash) containing four mutated LEF/TCF binding sites along with a Renilla construct. At 24 hours post-transfection, luciferase activity was measured using the dual-luciferase system. Indeed, the TCF/LEF responsive reporter TOPFlash transactivation increased significantly higher in SW480-FR cells compared to SW480-S cells in response to 1 x FOLFOX treatment for 12 hours (Figure 5C), indicating that FOLFOX stimulates WNT3A pathway activation.

Third to determine whether CD44v6-WNT3A signaling has a direct role in mediating FOLFOX resistance, we first investigated whether overexpression of a CD44v6 expression vector in CD44v6 negative PD-FR Non-CICs induces a time-dependent stimulation of WNT3A-mediated transactivation. Results in Figure 5F indicate that CD44v6 variant overexpression increases WNT3A-induced TOPFlash luciferase reporter activation. Conversely, we transfected PD-FR/Non-CICs expressing CD44v6 stably with the TCF/LEF responsive reporter TOPFlash and with CD44v6 shRNA. Treatment with WNT3A resulted in activation of WNT3A-induced β-catenin signaling, and this was significantly reduced by CD44v6 shRNA1 (Figure 5G). The results in Figures 5F-G provide evidence that CD44v6 clearly regulates WNT3A-induced β-catenin/TCF/LEF transactivation. Next, CD44v6 and β-catenin expressions in CICs were knocked down by

specific shRNAs, and WNT3A production was inhibited by LGK974 in CICs isolated from SW480-FR cells. In untreated and vector controls, cell viability was not reduced, and cells were resistant to apoptosis upon FOLFOX treatment in SW480-FR/CICs (Figures 5H, J). In contrast, Non-CICs show sensitivity to FOLFOX as determined by reduced colony formation in clonogenic growth assays and increased apoptosis determined by apoptosis assay (Figures 5I, K). Knockdown of either CD44v6 or β-catenin or inhibiting WNT3A production by LGK974, restored FOLFOX sensitivity in SW480-FR/CICs by reversing the resistant phenotype (Figures 5H, J), while overexpression of CD44v6 and β-catenin in SW480-FR/Non-CICs induced FOLFOX resistance (Figures 5I, K). Validations of shRNA of β-*catenin* were done by the indicated shRNA mediated knockdown and the corresponding shRNA resistant knock-in (KI) (shRNA sequences are in Table 4 in Methods) gene overexpressions and consequent analysis of indicated proteins in western blots (WB) (Figure 5D) following our previously published method (38, 39). Validation of constitutively active (pCA)-β-catenin was demonstrated by the indicated protein expressions in WB analysis (Figure 5E). The results show: 1) increased resistance of PD-FR/CICs compared to PD-FR/NON-CICs in response to FOLFOX treatment (Figures 5H versus 5I); 2) pCA-β-catenin and overexpression of v6cDNA mediated increased FOLFOX resistance in SW480-FR/NON-CICs (Figures 5I, K); and 3) knockdown of CD44v6 variant, or β-catenin, or inhibition of WNT3A by LGK974 nearly eliminated FOLFOX-resistance in SW480-FR CICs (Figures 5H, J). These data indicate that CD44v6 regulated WNT3A/β-catenin signaling has a vital role for FOLFOX resistance. Indeed, enrichment of CD44v6 expressing CICs from indicated tumor samples after FOLFOX therapy was demonstrated in Figure 4I.

Fourth, to validate that active β-catenin (ABC) and MDR1 protein expressions in CRC cells are correlated with CD44v6 expression, we evaluated the effects of FOLFOX on active β-catenin and MDR1 expressions in SW480 cells following FOLFOX treatment with or without CD44v6 shRNA transfection. Knockdown of CD44v6 variant in pCD44v6 overexpressing FOLFOX resistant cells down-regulated ABC and MDR1 expressions and inhibited the v6-containing variants but not the standard or v8 variants (as seen in Figures 2D, E). Thus, to define that CD44v6 is a positive regulator of WNT3A/β-catenin signaling, we tested whether CD44v6 transcript interacts with the nuclear complex of active β-catenin/TCF4 to transcriptionally regulate *MDR1* (118, 119). In an effort to gain a better understanding of the specific functions of the CD44v6 isoform expressed by drug resistant CRC cells, we used CD44-negative COS-7 cells (120). COS-7 cells were transfected with Flag-CD44v6 and control vector (not tagged with flag). In Figure 6A inset, we verified the CD44v6 expression and Flag expression in Flag-CD44v6 knock-in clones and in CD44v6 transfected parental COS-7 cells with either anti-CD44v6 or anti-Flag antibodies (upper panel of Figure 6A inset). This was further confirmed by immunoprecipitating cell lysates of CD44v6 × Flag knock-in and parental wild type CD44v6 transfectants of COS-7 cells with anti-Flag and subsequently western blotting with anti-CD44v6 (lower panel of Figure 6A inset). Co-IPs showed that WNT3A stimulated MDR1 and TCF4 were in a nuclear complex with CD44v6 in CD44v6 overexpressing COS-7 cell (Figure 6A, Flag tagged CD44v6 compared to Flag tagged vector transfectant cells).

Since FOLFOX stimulates WNT3A secretion and WNT3A/β-catenin transcriptional activity (Figures 5B, C), we determined whether knocking down CD44v6 expression would alter FOLFOX-mediated activation of β-catenin signaling in CICs isolated from SW480-S and SW480-FR cells. A WNT3A pathway was activated significantly with 1 x FOLFOX treatment for 12 hours in SW480-FR/CICs compared to SW480-S/CICs (as shown in Figures 6C, E compared to Figures 6B, D). This activation of β-catenin-dependent transcription in FR CICs was significantly reduced by knocking down CD44v6 in these CICs (Figures 6C, E). Together the results indicate that CD44v6 clearly regulates FOLFOX-induced β-catenin activation (hypo phosphorylated, active β-catenin [ABC] expression) in SW480-FR CICs compared to SW480-S/CICs (Figures 6C, E compared to Figures 6B, D).

Fifth, using CICs from sensitive and FR cells of SW480, we specifically tested the involvement of CD44v6 in LRP6 phosphorylation at Serine 1490, an early event in the activation of the WNT signaling (121). Importantly, FOLFOX resistant CICs predominantly express LRP6 phosphorylation at Serine 1490, whereas this phosphorylation was nearly absent in sensitive cells (Figures 6D, F compared to 6E, G). Furthermore shRNA1-mediated knockdown of CD44v6 variant in these CICs strongly inhibited WNT3A-induced phosphorylation of LRP6 (S1490) in SW480-FR CICs (Figure 6G). We also observed significant induction of ABC and MDR1 expression in SW480-FR CICs, whereas very little stimulations of endogenous expression of these two proteins by WNT3A was found in SW480-S-CICs, and these inductions are CD44v6 dependent (Figure 6G compared with Figure 6F). These results indicate that phosphoLRP6 (S1490) distributions, active β-catenin (ABC), and MDR1 expression were significantly obstructed in CICs of sensitive cells, whereas LRP6 (S1490) is a positive regulator of LRP6-mediated β-catenin (ABC) signaling in SW480-FR CICs (Figure 6G compared with Figure 6F). Moreover, WNT3A induced a mature glycosylated membrane bound form of LRP6 (upper band of LRP6) that is reduced by knocking down CD44v6 in SW480-FR CICs (Figure 6G), whereas in sensitive cells, knocking down CD44v6 represses both the immature endoplasmic reticulum bound (ER) form of LRP6 (faster migrating band) and the mature membrane bound form of LRP6 (slower moving band)

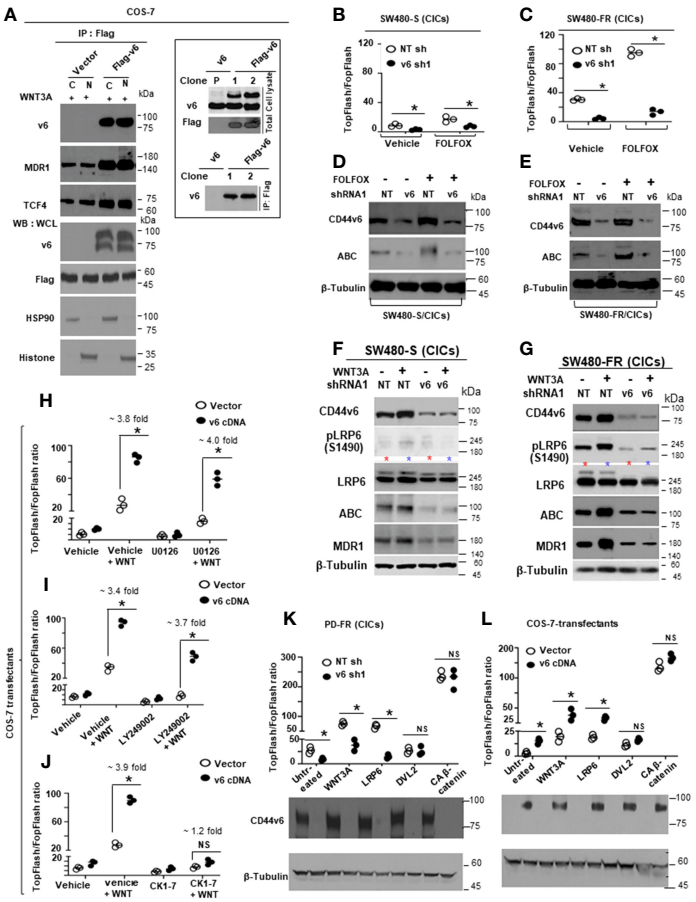

FIGURE 6
CD44v6 regulated β-catenin signaling establishes FOLFOX resistance in CRC-CICs. **(A)**, CD44 negative COS7 cells were stably transfected with vector control or with Flag-CD44v6 cDNA. Nuclear (N) and cytosolic **(C)** fractions were prepared from COS-7/Flag-tagged vector and COS-7/Flag tagged-CD44v6 stable transfectants and immunoprecipitated by the anti-Flag antibody. Flag-immunoprecipitated proteins were analyzed by Western blotting with the indicated antibodies. Upper panel of inset - Western blots of wild-type and Flag-tagged CD44v6 in Flag-CD44v6 knock-in clones and the parental clone (wild type CD44v6 transfectants of COS-7 cells) with either anti-CD44v6 or anti-Flag antibodies, Lower panel of inset - Cell lysates of CD44v6 × Flag knock-in and parental clones were immunoprecipitated with anti-Flag and western blotted with anti-CD44v6. **(B-E)**, CICs from SW480-S cells **(B, D)** and SW480-FR cells **(C, E)** were transfected with NT sh1 or v6 sh1. After 48 hours, CICs were analyzed for FOLFOX stimulated β-catenin/TCF4 promoter luciferase activity **(B, C)** as described in Figure 5C or, in parallel, to WB analysis with the indicated proteins **(D, E)**. **(F, G)**, CICs from SW480-S **(F)** and SW480-FR **(G)** cells were transfected with NT sh1 or CD44v6 sh1 vectors. After 48 hours, CICs were subjected to WB analysis for the indicated proteins. **(H–J)**, COS-7/vector and COS-7/Flag-CD44v6 stable clones were further transfected with 50 ng TOPFlash and 50 ng TK-Renilla vectors, or with 50 ng FOPFlash and 50 ng TK-Renilla vectors for 48 hours. They were then treated either with vehicle (DMSO) or with the MEK inhibitor U0126 (20 μM) **(H)**, or with the PI3K-Inhibitor Ly294002 (50 μM) **(I)**, or a casein kinase 1 inhibitor CKI-7 (hydrochloride) (CKI-7) (2 μM) **(J)** 2 hours prior to the addition of WNT3A. After 12 hours of induction with WNT3A, cells were lysed and subjected to luciferase measurements. **(K)**, PD-FR CICs were transfected with NT sh1 or v6 sh1. After 48 hours, cells were transfected with TOPFlash and TK-Renilla or with FOPFlash and TK-Renilla vectors. The TOPFlash/FOPFlash promoter was activated by stimulation with WNT3A (20 ng/ml) for 12 hours or by further transfection with LRP6, DVL2 or constitutively active (CA) β-catenin for 48 hours. Cells were lysed and subjected to luciferase measurements, and the data are presented as TOPFlash/FOPFlash promoter activity or, in parallel, to WB analysis. **(L)**, COS7-Vector and COS7-CD44v6 clones were transfected with TOPFlash and TK-Renilla vectors, or with FOPFlash and TK-Renilla vectors for 48 hours. The reporter was stimulated with 20 ng/ml WNT3A for 12 hours or by further transfection with LRP6, DVL2, or constitutively active (CA) β-catenin for 48 hours. Cells were lysed and subjected to luciferase measurements or, in parallel, to WB analysis. Data are presented as Mean ± SD from n = 3-6 replicates in three independent experiments. All WBs data are representative of 4 independent experiments. **(B, C)**, $^*P < 0.05$ was considered significant, TOPFlash/FOPFlash activity in v6shRNA1 (v6sh1) transfected SW480-S/CICs and SW480-FR/CICs were compared with their NT shRNA (NT sh) transfected cells. **(H–J)**, $^*P < 0.05$ was considered significant, TOPFlash/FOPFlash activity in WNT treated v6 cDNA overexpressed COS-7 cells were compared with untreated v6 cDNA transfectants; TOPFlash/FOPFlash activity in WNT plus inhibitors treated (U0126 [H], LY294002 [I], and CK 1-7 [J]) v6 cDNA overexpressed COS-7 cells were compared with inhibitors only treated v6 cDNA transfectants. **(K, L)**, $^*P < 0.05$ was considered significant, TOPFlash/FOPFlash activity in v6 shRNA1 (v6 sh1) transfectant of PD-FR (CICs) **(K)**, and v6 cDNA overexpressed COS-7 cells **(L)** were compared with the NT shRNA (NT sh) transfected PD-FR (CICs) **(K)**, and vector control transfected COS-7 cells **(L)**.

(Figure 6F). These results provide evidence that WNT3A stimulated CD44v6 expression drives the matured form of LRP6, and that subsequent LRP6 phosphorylation at Serine 1490 activates β-catenin signaling and its localization at the membrane in FR-CICs compared to sensitive CICs (Figure 6G compared with 6F). Moreover, knocking down CD44v6 variant in SW480-FR CICs reduced both FOLFOX and FOLFOX +WNT3A induced mature glycosylated membrane bound form of LRP6 (122) (upper band of LRP6, red and blue stars) (Figure 6G). On the other hand, in sensitive cells, knocking down CD44v6 represses both the immature endoplasmic reticulum bound (ER) form of LRP6 (faster migrating band) and the mature membrane bound form of LRP6 (slower moving band represented by red and blue stars) (Figure 6F). These results provide evidence that FOLFOX/WNT3A stimulated CD44v6 drives the matured form of LRP6, and that subsequent LRP6 phosphorylation at Serine 1490 activates β-catenin signaling and its localization at the membrane in FR-CICs compared to sensitive CICs (Figure 6G compared with 6F). In contrast, WNT3A stimulated CD44v6 drives both mature and immature forms of LRP6 and inactivates β-catenin signaling in sensitive SW480-S/CICs (Figure 6F). Together, these data demonstrate that CICs have autonomous resistance to FOLFOX therapy that is dependent on CD44v6 expression and CD44v6-dependent WNT3A signaling activation, and on MDR1 expression.

3.4 CD44v6-dependent β-catenin/ TOPFlash transactivation is mediated by the membrane WNT3A and LRP6

CD44v6 regulates multiple receptor tyrosine kinase and non-tyrosine kinase signaling pathways (29–39), and RTKs induce LRP6 phosphorylation/β-catenin signaling *via* the mitogen-activated protein kinase (MAPK)/Erk and phosphatidylinositol 3 kinase (PI3K)/Akt signal transduction pathways (123). Moreover, casein kinase 1 (CK1) family members, particularly CK1γ, are known to phosphorylate LRP6 (124). To understand the role of MEK, or PI3K or CK1 in CD44v6 regulated LRP6 phosphorylation, we used their pathway inhibitors and examined whether these pathways affect CD44v6-LRP6/WNT signaling. The results indicate that MEK or PI3K pathways did not impact CD44v6 regulated WNT3A-induced TOPFlash transactivation in a COS-7-CD44v6 stable transfectant clone (Figures 6H, I). However, inhibiting CK1 substantially blocked CD44v6 regulated LRP6 phosphorylation in response to WNT3A (Figure 6J), indicating that CD44v6 regulated WNT3A/β-catenin transcriptional activation in association with CK1. To further confirm that CD44v6 regulated WNT3A-induced TOPFlash transactivation is regulated exclusively by CD44v6 function, we knocked out CD44v6 in SW480-FR CICs and then stimulated them with WNT3A, or co-transfected them with LRP6, or with cytoplasmic protein disheveled 2 (DVL-2), or with CA β-catenin overexpressing vectors (Figure 6K). Conversely, a CD44v6 gain-of function experiment was done in pCD44v6 overexpressing COS-7 cells, which were then either stimulated with WNT3A, or co-transfected with cDNAs for LRP6, or with DVL-2, or with a CA-β-catenin plasmid (Figure 6L). Figures 6K, L show that TOPFlash promoter activation is decreased by WNT3A and LRP6 treatment when CD44v6 variant has been knocked down (Figure 6K), and that they are increased when CD44v6 is increased with transfection using CD44v6 cDNA (Figure 6L). In contrast neither the pDVL2 nor the pCA-β-catenin treatments alter TOPFlash transactivation. Therefore, TOPFlash promoter activation occurs by membrane constituents WNT3A or LRP6, but not by transfection with cDNAs for cytoplasmic molecules such as DVL2 or CA-β-catenin, providing evidence that WNT3A-induced TOPFlash transactivation occurs only in the membrane associated LRP6 activated by CD44v6 presumably in association with CK1 (Figures 6J, K, L).

3.5 Caveolin-mediated endocytosis is essential for CD44v6-LRP6-β-catenin signaling

Endocytosis of transmembrane signaling receptors is an important regulatory event in signal transduction including CD44/CD44v6 (33, 76, 125) and WNT/LRP6/β-catenin signaling (126, 127). Clathrin-mediated endocytosis has a crucial role in terminating cell survival signaling by inhibiting association of cell surface receptors (128, 129). A CAV1-endocytosis pathway has been shown to function as a platform for receptor mediated signaling by accelerating the sequestering of receptors and signaling molecules within caveolae (130, 131). With evidence that CD44v6 regulates WNT signaling at the level of association with mature LRP6 (as seen in Figure 6G), and at the membrane (as seen in Figures 6K-L), we hypothesized that formation of intact lipid-rafts at the membrane microdomain may be required for CD44v6 to interact with LRP6. To address this, lighter lipid raft (expressing caveolin-1 [CAV1]) and heavier non raft (Clathrin) membrane fractions were isolated using OptiPrep gradient centrifugation of the Triton X-100-insoluble fractions of the cell lysates that were prepared from SW480-S and SW490-FR cells after 1 x FOLFOX treatment for 30 minutes. Gradient fractions were analyzed for the cholesterol content, protein concentration, and density of the gradient layers after centrifugation. As shown in Figure 7A, the low protein content of the 1-5 fractions mostly exhibited high cholesterol

and CAV1 expression. The 6-10 fractions with low cholesterol and high protein content exhibit clathrin. To avoid contamination, we used the 3-4 fraction as shown in Figure 7A, which is the caveolin-raft fraction between 15%-20% Optiprep gradient layers and depicted as "R". Similarly, the 7-8 fraction as shown in Figure 7A is clathrin-non-raft fractions > than the 30% Optiprep gradient layer and depicted as "NR". As shown in Figure 7B, increased levels of CD44v6 and LRP6 (S1490) localized in R fractions of FR cells, which were greatly reduced in NR fractions expressing clathrin. As shown in Figure 7B, transient WNT3A stimulation had little effect on the stimulation of the relatively lower density distribution of CD44v6 and LRP6 to the R fraction in sensitive SW480-S cells compared with the significantly higher density distribution of CD44v6 and LRP6 to the R fraction in SW480-FR cells. Furthermore, phospho-LRP6 (S1490), indicative of activated WNT signaling, co-sediments at higher density with LRP6 and CD44v6 in caveolin containing fractions. Since WNT-mediated phosphorylation of LRP6 at S1490, which is postulated to be required for interaction with and modulation of the β-catenin destruction complex (124), is not observed when the receptor is internalized in clathrin containing endocytic vesicles; we can conclude that the increased WNT3A mediated CD44v6-LRP6 (S1490)/β-catenin signaling in caveolin-lipid raft is required for maintaining CIC autonomous resistance in FOLFOX-resistant cells (as seen in Figures 2F-G, Figure 4, and Figures 5F, H). Methyl-β-cyclodextrin, a cholesterol depleting agent, abolished recruitment of CD44v6 and LRP6 to lipid-rafts (Figure 7C).

To confirm the role of endocytosis in FOLFOX induced WNT/β-catenin signaling in our FR cells versus sensitive SW480 cells, we transfected these cells with a dominant-negative dynamin (DN) K44A (DN Dyn) that inhibits both clathrin and caveolin-mediated receptor endocytosis (132). After 48 hours, the cells were co-transfected with the TOPFlash reporter and increasing concentrations of DN Dyn. Our FR cells of SW480 that express high levels of CD44v6 and WNT3A (Figures 5A, B) show higher TOPFlash promoter activity than sensitive (S) cells of SW480 (Figure 7D). Additionally, this increased TOPFlash promoter activity of SW480-FR cells was inhibited by DN Dyn in a dose-dependent way (Figure 7D). To further characterize the endocytic pathway mediating WNT3A-induced TOPFlash transactivation in our FR cells compared to our sensitive SW480 cells, we treated these cells with monodansyl-cadaverine (MDC), which blocks clathrin-mediated endocytosis (133), or with nystatin, which disrupts lipid rafts and caveolin dependent endocytosis (132). Results in Figure 7E show that Nystatin, but not MDC, inhibits FOLFOX-induced WNT/β-catenin TOPFlash promoter activity in FR cells, whereas TOPFlash transactivation was significantly inhibited in SW480-S cells regardless of Nystatin or MDC treatment. In agreement to TOPFlash transactivation blockage by Nystatin, but not by MDC treatment, inhibited active β-catenin expression and its target MDR1 expression (Figure 7F). However, SW480-S cells show inhibition of the WNT3A-induced active β-catenin expression and its target MDR1 expression irrespective of whether the caveolin (Nystatin) or clathrin (MDC) endocytic pathways are modulated (Figure 7G). Overall, these results provide evidence that repeated exposure to FOLFOX as it happens in chemo resistant tumors promotes coalescence of CD44v6 and LRP6 induced by LRP6 (S1490) in a SW480-FR/caveolin compartment, whereas in SW480-S cells, brief exposure to FOLFOX fails to associate LRP6 S1490 with a CD44v6-LRP6 complex in a clathrin-microdomain (as seen in Figure 7B).

3.6 Recruitment of a CD44v6-LRP6 complex toward clathrin-dependent endocytosis in sensitive cells requires DAB2 protein in the complex

A recent study links LRP6 to DAB2 in a clathrin microdomain (134). This suggests that LRP6 and CD44v6 distributions to a clathrin domain in sensitive cells (as seen in Figure 7B) may be linked to DAB2 in response to brief treatment with FOLFOX or WNT3A. Thus, with evidence that knocking down CD44v6 substantially reduced β-catenin/TCF4 promoter TOPFlash activation in sensitive cells compared to the FR counterpart of SW480 cells (as seen in Figure 6B versus Figure 6C), we hypothesized that DAB2-mediated internalization of LRP6 through the clathrin pathway may be the likely mechanism for stabilization of the destruction complex and the subsequent attenuation of the β-catenin signaling activation. To further understand the mechanism of FOLFOX resistance through CD44v6-LRP6-WNT3A/β-catenin signaling, the levels of *DVL-2* and *DAB2* gene expressions in our sensitive and FR pairs were determined. As shown in Figure 8A, *DVL-2* is highly expressed in SW480-FR cells, whereas SW480-S cells express higher levels of *DAB2*.

Moreover, inhibiting WNT3A by LGK974 substantially suppressed DVL2 with a moderate increase in DAB2 levels (Figure 8B). Further, SW480-FR cells are WNT signaling competent as shown by active β-catenin (ABC) accumulation and MDR1 induction (Figures 8B, C), whereas in SW480-FR cells that ectopically express DAB2 cDNA (SW480/FR-DAB2 clones), WNT3A/β-catenin signaling was attenuated (Figure 8C).

To further examine this redistribution of LRP6 towards clathrin by DAB2, we fractionated the lipid raft (R, caveolin containing pooled fractions 3-4) and the non-lipid raft (NR, clathrin containing pooled fractions 7-8) fractions in SW480-FR cells that ectopically express vector and DAB2, and determined the relative associations and distributions of -catenin signaling modulators. As shown in Figures 8D, E, CD44v6 and phospho-LRP6 (S1490) distributions were substantially impacted by the presence of DAB2. In the absence of DAB2, in vector transfected cells, CD44v6 and LRP6 (S1490) co-immunoprecipitated with the

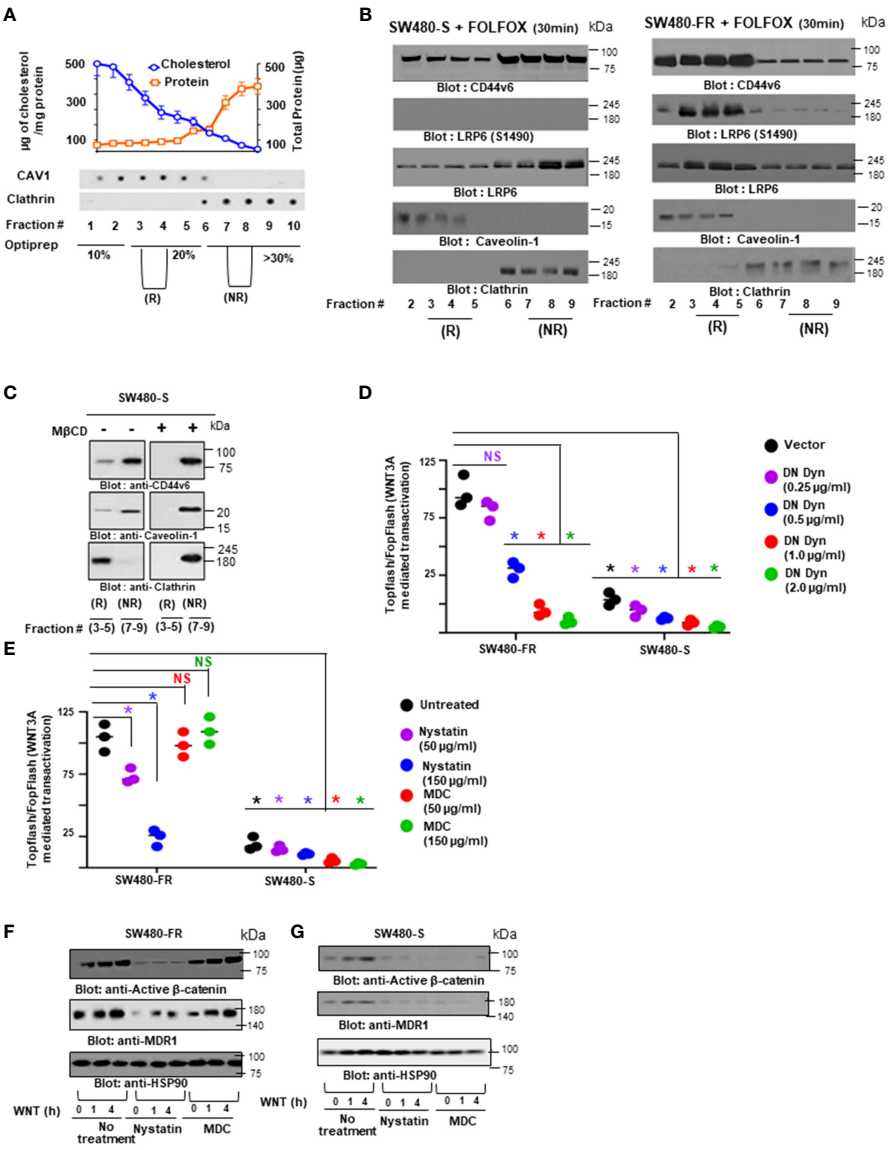

FIGURE 7
Caveolin-mediated endocytosis is essential for CD44-LRP6-β-catenin signaling to maintain FOLFOX resistance. **(A)**, Detergent-resistant membranes, Triton X-100 (1%) insoluble fractions of FR and sensitive cells, were separated in the OptiPrep linear gradients, and distributions of protein and cholesterol across the gradient are shown (details in Methods). Dot Blot analyses show the presence of caviolin1 (CAV1) and clathrin in different Optiprep fractions. **(B)**, SW480-S and SW480-FR cells were treated with 1 x FOLFOX for 30 minutes. The raft (R) < 20% OptiPrep fractions [2-5], and the non-raft (NR) > 20% OptiPrep fractions [6-9] were isolated and analyzed by western blots (WBs) for CD44v6, phosphorylated LRP6 (S1490), LRP6, caveolin-1, and clathrin. **(C)**, SW480-S cells were treated with or without 5 mM methyl-β-cyclodextrin (MβCD) for 1 hour, and the R and NR fractions were analyzed by WBs for CD44v6 and clathrin. **(D)**, SW480-FR and SW480-S cells transfected with dominant negative dynamin (DN Dyn) [DN K44A] were co-transfected with 50 ng TOPFlash and 50 ng TK-Renilla vectors, or with 50 ng FOPFlash and 50 ng TK-Renilla vectors. After stimulation with WNT3A (20 ng/ml) for 12 hours, cells were lysed and subjected to luciferase measurements. **(E)**, SW480-S and SW480-FR cells were transfected with TOPFlash and TK-Renilla vectors, or with FOPFlash and TK-Renilla vectors luciferase reporter constructs. Transfected cells were treated for 1 hour with the indicated concentrations of nystatin, known to block caveolin-1-mediated endocytosis, or with monodansylcadaverine (MDC), known to block clathrin-mediated endocytosis. After stimulation with WNT3A (20 ng/ml) for 12 hour, cells were lysed and subjected to luciferase measurements. **(F)**, SW480-FR cells and SW480-S cells **(G)** SW480-S cells were treated for 1-4 hours with Nystatin (150 µg/ml) or MDC (150 µg/ml). After stimulation with WNT3A (20 ng/ml) for 1 or 4 hour, cells were lysed and subjected to western blots. Data are presented as Mean $\pm$ SD from n = 3-6 replicates in four independent experiments. All WBs data are representative of 4 independent experiments. **(D)**, $^*P < 0.05$ was considered significant, TOPFlash/FOPFlash activity in DN Dyn transfectants of SW489-S, and SW480-FR cells were compared with their vector control transfectants. **(E)**, $^*P < 0.05$ was considered significant, Nystatin and MDC treated SW489-S, and SW480-FR cells were compared with their untreated control cells.

lighter caveolin containing R fractions, and WNT3A stimulation appears to promote this association into a caveolin-compartment. Importantly, phospho-LRP6 (S1490), indicative of activated WNT3A/β-catenin signaling, is significantly increased with caveolin containing fractions in SW480-FR-vector clones (Figure 8D) and is not present in SW480/FR-DAB2 clones following WNT3A treatment (Figure 8E).

Next, we determined the relative associations and distributions of other β-catenin modulator proteins. In agreement with the distribution of phospho-LRP6 (S1490), we also found that the presence of axin and GSK3β in caveolin-immunoprecipitates depended on WNT3A (Figures 8C, D). In contrast, in DAB2 transfected cells, clathrin co-immunoprecipitated with LRP6 and CD44v6 in a WNT3A-dependent manner, but not with axin or GSK3β. Collectively, these results provide evidence that DAB2 regulates the localization of a CD44v6-LRP6 receptor complex following WNT3A stimulation in a clathrin compartment, resulting in β-catenin destruction with attenuation of interaction with axin and GSK3β (Figures 8C, D). These results further suggest that LRP6-CD44v6 distributions to a clathrin domain in sensitive cells may be linked to DAB2 in response to brief treatment with WNT3A. In contrast, in FR cells that endogenously secrete WNT3A *via* FOLFOX (as seen in Figure 5B), WNT3A-mediated activation of LRP6 phosphorylation at S1490 through CD44v6 (as seen in Figures 6D-G, 6K, L) regulated CK1 (Figure 6J), which shunts the receptor complex to the caveolin endocytic pathway (as seen in Figure 7B).

3.7 Palmitoylation and the nuclear localization site of CD44v6 are essential for caveolin1-lipid-raft

3.7.1 Mediated endocytosis to enhance WNT3A-β-catenin mediated TCF4 promoter activation

Since β-catenin signaling modulators were associated with CD44v6 in lipid-rafts of FR cells (as seen in Figures 8C, D), we examined first the mechanism of localization of CD44v6 in lipid-rafts and then the mechanism of recruitment of LRP6 to CD44v6 in response to WNT3A that is secreted in response to FOLFOX (as seen in WNT3A stimulation by FOLFOX in Figure 5B). Previous studies identified the inhibitory effects of mutants of CD44 membrane-proximal cysteines, which are palmitoylation sites of CD44 that are essential for the association of CD44 with caveolin lipid-rafts (135, 136). In order to examine whether the CD44v6-palmitoylation sites (present at Cys354 and at Cys363), or the putative CD44v6-nuclear localization sequence (NLS) (^{360}RRRCGQKKK^{368}) are involved in association of CD44v6 with lipid rafts, we generated a series of the intracellular domain (ICD)-deletion and point mutation mutants from the pCD44v6$_{429aa}$ wild type (pCD44v6-WT) (Figure 9A). Next, we expressed these CD44v6 mutant cDNAs as well as pCD44v6-WT constructs in CD44v6 (–)/SW480-FR Non-CICs and explored whether the association of these sites of CD44v6 are involved in caveolin1-lipid raft organization through interaction with cellular β-catenin signaling modulator proteins. Data in Figure 9A, B indicate that exclusion of the palmitoylation-sites of CD44v6 by changing cysteine at C354 and C363 to alanine (C354A and C363A) did not fully prevent the re-localization of the resultant CD44v6$_{PALM}$ mutants (palmitoylation mutants) into the raft (R) fractions upon FOLFOX treatment for a brief period (30 minutes) in SW480-FR Non-CIC clones expressing these mutants.

Next, we tested whether the ICD of CD44v6 is required for lipid raft affinity through interaction with LRP6 protein. Serial deletion of most of the ICD domain of CD44v6 (CD44v6$_{\Delta 67}$ [deletion of aa 362 to 429]), and CD44v6 $_{\Delta 61C354A,\ C363A}$ (CD44v6$_{\Delta 61}$ [deletion of aa 368 to 429]) did not block fully the association of the CD44v6 mutants in control and FOLFOX treated SW480-FR/CIC-CD44v6 clones (Figure 9A, B). To verify whether CD44v6 is also associated with lipid-rafts *via* the NLS sequence [^{360}RRR^{362}CGQ^{366}KKK^{368}]) of CD44v6, a CD44v6$_{NLS}$ Mutant was generated by changing the putative NLS sequence ^{360}RRRCGQKKK^{368} to ^{360}AAACGQAAA^{368}. Because this site is required for cross-linking transmembrane receptors, including CD44v6, to actin-based cytoskeletons (137), the CD44v6-NLS-site (^{360}RRR^{362}CGQ^{366}KKK^{368}) is the site where ezrin, radixin, and moesin (ERM) bind (138). Our pCD44v6$_{\Delta 67}$Mut is devoid of NLS sites of CD44v6. As demonstrated in Figure 9B, overexpression of the pCD44v6$_{\Delta 67PALM}$ Mut and the pCD44v6$_{\Delta 61PALM+NLS}$ Mut completely block the association of CD44v6 to lipid rafts. Importantly the pCD44v6$_{NLS}$ Mut did not completely block association of this mutant to lipid rafts. Since, the engagement of the pCD44v6$_{\Delta 67PALM}$ Mut and the pCD44v6$_{\Delta 61PALM+NLS}$ Mut that were defective in PALM and NLS sites fail to induce lipid raft redistribution/reorganization of CD44v6 (Figure 9B), we can conclude that both PALM and NLS sites of CD44v6 are required for CD44v6 to be associated with lipid rafts.

To address the effects of WNT3A on endocytosis directly, first the kinetics of CD44v6 internalization were followed in SW480-FR and SW480-S cells that were incubated with biotin-conjugated anti-CD44v6 antibodies prior to WNT3A treatment for various lengths of time to allow internalization of CD44v6. Cellular intake of biotin-conjugated anti-CD44v6 antibodies increased as a function of time, and a greater intake of CD44v6 was observed with FR cells, suggesting that repeated FOLFOX exposure in SW480-FR cells increases the internalization of CD44v6 compared to that of SW480-S cells (Figure 9C). In agreement with this, increasing amounts of CD44v6, as well as of LRP6, were recovered from the early endosome fraction isolated from SW480-FR cells after WNT3A treatment for 30 minutes (Figure 9D). Pretreatment of cells with NH4+ or phenyl arsine oxide (PAO), or depletion of K+ to block

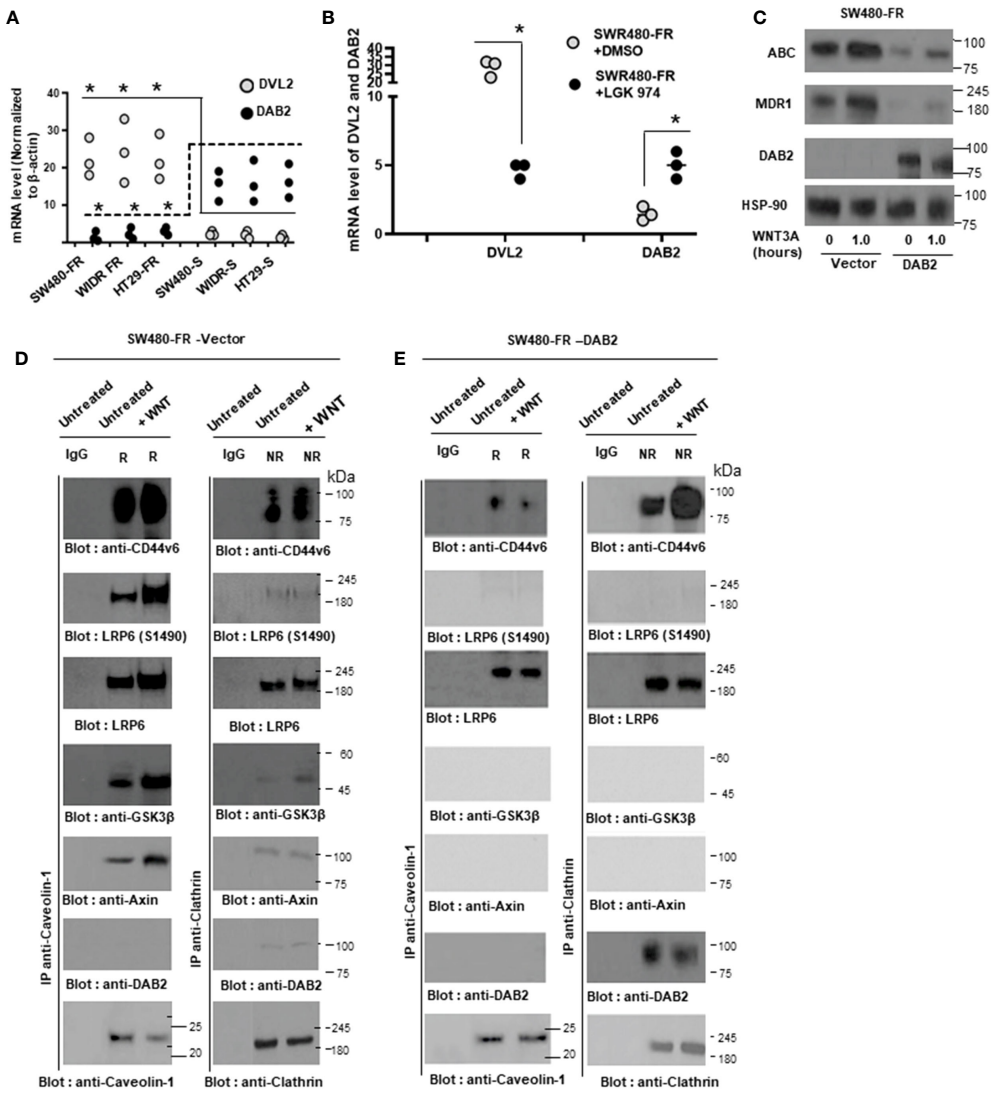

FIGURE 8
DAB2 favorably sequesters a CD44v6-LRP6 complex in the direction of clathrin-dependent endocytosis to retain FOLFOX sensitivity. **(A)**, mRNA expressions of disheveled protein 2 (DVL-2) and DAB2 protein normalized to *β*-actin in sensitive and resistant pairs of cells are shown by qPCR. **(B)**, Whole cell lysates (WCL) of Vector and DAB2 cDNA transfected SW480-FR cells at time 0 or after 12 hours treatment with or without WNT3A were analyzed by WB for the indicated proteins. Vector **(C)**, and DAB2 cDNA **(D)** transfected SW480-FR cells were treated with or without WNT3A for 12 hours, and the Triton X-100 (1%) insoluble fractions were separated into lipid raft (R) and non-raft (NR) by OptiPrep gradient centrifugation. Pooled OptiPrep gradient fractions (light fractions (3–4) and non-raft heavy fractions (7–8)) were immunoprecipitated with anti-caveolin-1 (left panels) and anti-clathrin (right panels) antibodies. Immunocomplexes were immunoblotted for CD44v6, LRP6 (S1490), LRP6, Axin, GSK3*β*, and DAB2, and for clathrin or caveolin (bottom panels). IgG antiserum was used as negative control for the various immunoprecipitations. QPCR data represent results from 3 independent experiments done in n = 3-6 replicates. All WB data are representative of 4 independent experiments. **(A)**, *$P < 0.05$ was considered significant, *DVL2* and *Dab2* mRNA expressions in FR cells were compared with S cells. **(B)**, *$P < 0.05$ was considered significant, *DVL2* and *Dab2* mRNA expressions in LGK974 treated SW480-FR cells were compared with untreated SW480-FR cells.

endocytosis, significantly inhibited the internalization and uptake of CD44v6 and LRP6 (Figure 9D). A biotin-labeled endocytosis assay showed that WNT3A stimulation indeed increased the rapid internalization of the biotin-labeled CD44v6 as well as its subsequent nuclear localization (Figure 9E). Interestingly, WNT3A stimulation only increased the rapid internalization of the biotin labeled LRP6 but not its nuclear localization (Figure 9F). Thus, following triggering by WNT3A, once internalized, endogenous LRP6 and CD44v6 then translocated to membrane-bound vesicles known as early endosomes (Figure 9F), where they are sorted, and LRP6 is recycled back to the cell surface within 4 hours of the initial

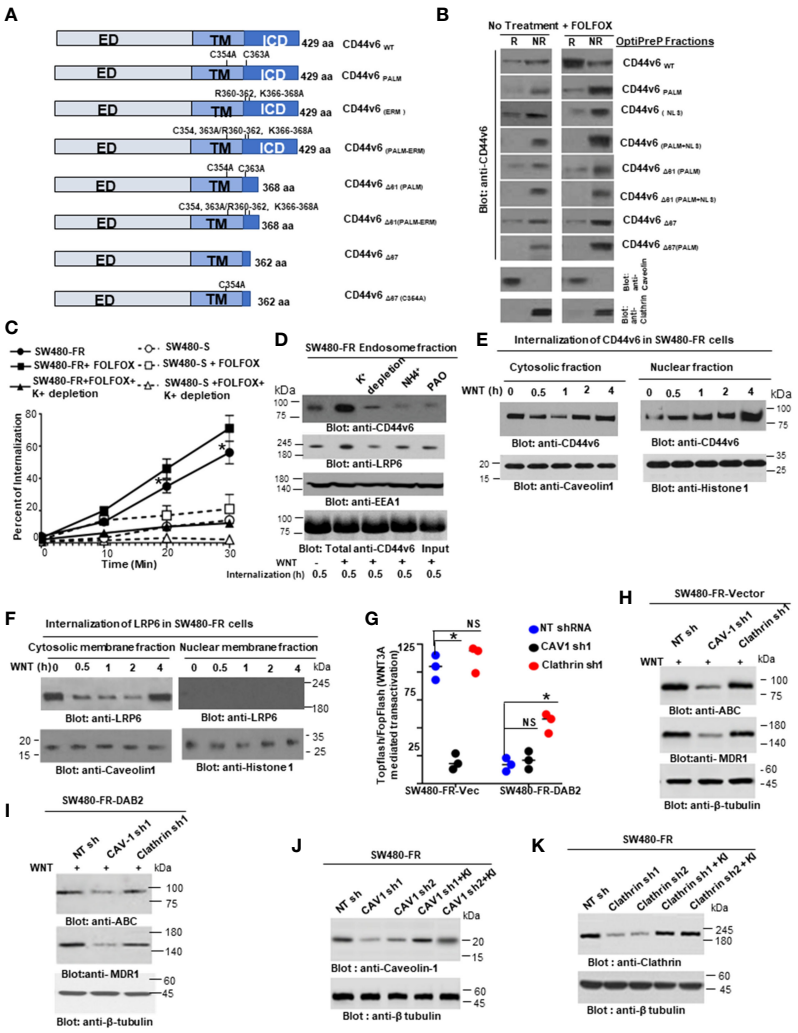

FIGURE 9
Both palmitoylation and linkage to a nuclear localization site of CD44v6 contribute to recruitment of LRP6 to caveolin1-rafts to regulate CD44v6-induced WNT3A/β-catenin signaling. **(A)**, Schematic representations of individual CD44v6 mutants are shown; ED, extracellular domain; TM, transmembrane domain; ICD, intracellular domain. **(B)**, CD44v6 negative SW480-FR/(NON-CICs) were transfected with individual CD44v6 mutants as depicted. Individual CD44v6 cell clones were either untreated (control) or challenged with 1 x FOLFOX for 30 minutes. Raft (R) and non raft (NR) fractions were prepared as described in Methods. **(C)**, SW480-S and SW480-R cells were incubated with biotin conjugated anti-CD44v6 antibody at 4°C separately followed by further incubation at 37°C for 10, 20 and 30 minutes as indicated. The percentage of internalization was measured by flow cytometry after staining with fluorescein conjugated anti-biotin antibody. Data were calculated by setting the mean fluorescence intensity of cells after biotin labeling without glutathione incubation as 100%. **(D)**, SW480-FR cells were cultured in complete media with and without K+ depletion at 37°C for 1 hour followed by further stimulation with WNT3A for 30 minutes. Total cell lysates and endosomes purified by sucrose gradient centrifugation were analyzed by western blotting. **(E-F)**, SW480-FR cells were surface labeled with biotinylating agent (non-cleavable Sulfo-NHS-LC-Biotin). Cells were stimulated with WNT3A at 37°C for the times indicated and placed at 4°C for 1 hour of labelling with the biotinylating agent. Cytosolic membrane and nuclear membrane fractions were affinity purified with avidin-conjugated beads and analyzed by western blotting. **(G-I)**, Sensitive and FR SW480 cells were stably transfected with vector or a DAB2 construct. These stable clones were co-transfected with NTshRNA1, or caveolin1 (CAV1) shRNA1, or clathrin shRNA1. After 48 hours, cells were then transfected with TOP/FOPFlash luciferase reporter constructs prior to 20 ng/ml WNT3A stimulation for 12 hours, and cell lysates were subjected to luciferase activity determination **(G)** and processed for WB analysis for the indicated proteins **(H-I)**. **(J-K)**, Validations of CAV1shRNAs (CAV1 sh1 and CAV1 sh2) and Clathrin shRNAs (Clathrin sh1 and Clathrin sh2) were done by the indicated shRNA mediated knockdown and the corresponding knock-in **(KI)** gene transfections as described in Methods. Target proteins were analyzed by WB analysis (β-tubulin, internal control). FACS data in 'C' represent are representative of 4 independent experiments. All WBs are representative of 3 independent experiments. QPCR data represent results from 3 independent experiments done in n = 3-6 replicates. **(C)**, $^*P < 0.05$ was considered significant, Internalization of SW480-FR cells was compared with SW480-S cells. Data in 'G' represent results from 3 independent experiments performed in triplicates; $^*P < 0.05$ was considered significant, TOPFlash/FOPFlash activity of CAV1 shRNA1 transfectant results were compared with NT shRNA transfectant of SW480-FR-Vector transfectant cells; TOPFlash/FOPFlash activity of clathrin shRNA1 transfectant results were compared with NT shRNA transfectant of SW480-FR-DAB2 cells.

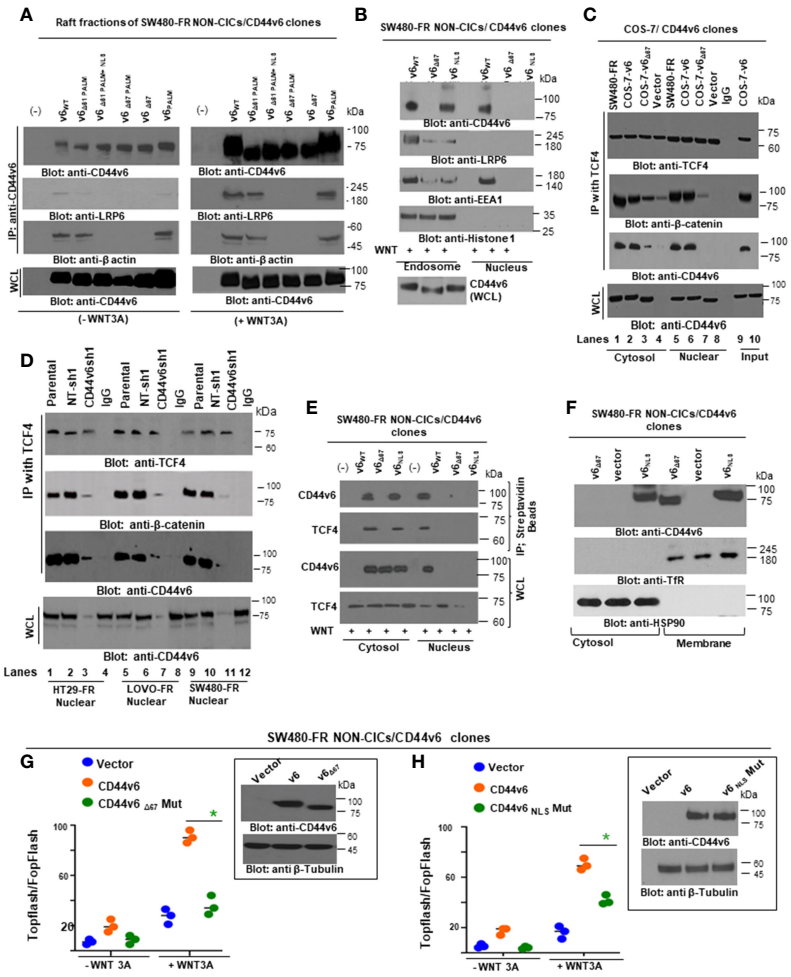

FIGURE 10
Nuclear localization site (NLS) in the ICD domain of CD44v6 is required for nuclear translocation of CD44v6 through endosomal sorting, and its subsequent association with TCF4 contributes to enrichment of TCF4/TOPFlash transcription. **(A)**, Associations of CD44v6 with LRP6 and actin were examined in pooled lipid raft fractions isolated from SW480-FR NON-CICs/CD44v6 cell clones expressing the indicated CD44v6 mutants (see the structures of CD44v6 mutants in Figure 9A). After stimulation with WNT3A for 12 hours, the cell lysates from the individual CD44v6-expressing SW480-FR NON-CIC clones were immunoprecipitated (IP) with an anti-CD44v6 antibody, followed by fractionation and western blotting. **(B)**, WB analyses are shown for endosomal and nuclear fractions in individual SW480-FR NON-CICs/CD44v6 cell clones expressing the $v6_{\Delta 67}$ mutant (devoid of ICD) and v6 $_{NLS}$ mutants (devoid of nuclear localization site; see figure 9A). **(C)**, Nuclear (N) and cytosolic **(C)** fractions were immunoprecipitated with TCF4 or IgG (Control) followed by Western blotting for the CD44v6, β-catenin, MDR1 and TCF4 proteins in the SW480-FR cells, and in the COS-7-CD44v6 clones expressing the indicated mutants and vector controls. **(D)**, Nuclear extracts were prepared from the parental HT29-FR, LOVO-FR, and SW480-FR cells, or from cell clones stably harboring lentivirus-encoded NT sh1, or v6 sh1, and they were immunoprecipitated with TCF4 antibody followed by Western blotting with the indicated antibodies. Whole cell lysates (WCL) from the same experiment were used as input and subjected to WB analysis for CD44v6. **(E)**, SW480-FR NON-CICs/CD44v6 cells were incubated with biotin-conjugated CD44v6 at 4°C for 1 hour followed by an additional hour of incubation at 37°C. Cytosolic and nuclear fractions were isolated and immunoprecipitated with streptavidin beads and analyzed by Western Blotting. **(F)**, Lysates from indicated SW480-FR-NON-CIC/CD44v6 cell clones expressing the indicated CD44v6 mutants were subjected to cytosol and membrane fractionation and then analyzed by WBs. The relative purities of the membrane and cytosolic fractions were confirmed by probing for the cytoplasmic protein HSP90 and the membrane protein transferrin receptor (Tf-R). **(G–H)**, SW480-FR-NON-CIC/CD44v6 cell clones expressing the pCD44v6/Δ67mutant **(G)**, and the pCD44v6/NLS mutant **(H)**, were transfected with TOPFlash and control TK-Renilla vectors, or with FOPFlash and TK-Renilla vectors in the presence or absence of 20 ng/ml of WNT3A. After 48 hours, cells were lysed and subjected to luciferase measurements and in parallel to WB analysis. All WBs are representative of 4 independent experiments. All luciferase data represent at least 3 independent experiments done in triplicates. **(G, H)**, *$P < 0.05$ was considered significant, TOPFlash/FOPFlash activity of WNT3A treated SW480-FR/NON-CICs/CD44v6$_{\Delta 67}$Mut cells were compared with SW480-FR/NON-CICs/CD44v6 cells, and TOPFlash/FOPFlash activity of WNT3A treated SW480-FR/NON-CICs/CD44v6$_{NLS}$Mutant was compared with SW480-FR/NON-CICs/CD44v6 cells.

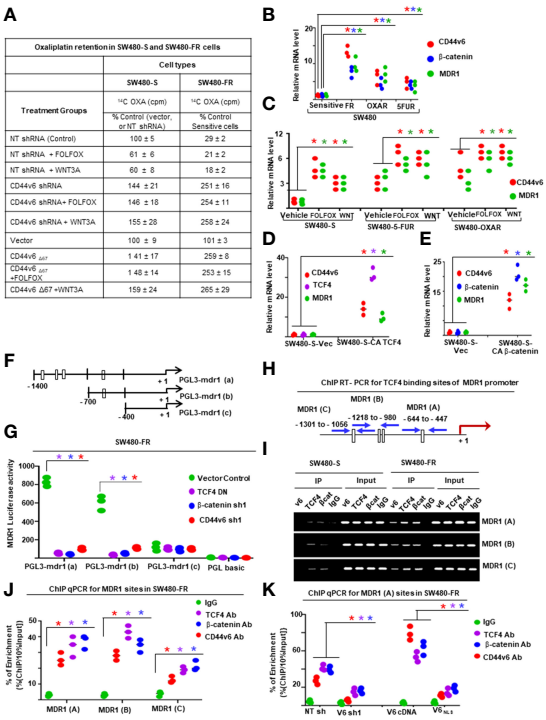

FIGURE 11
Nuclear CD44v6 associates with TCF4 and functions to modulate MDR1 transcription in FOLFOX resistant cells. **(A)**, The intracellular domain **(ICD)** of CD44v6 induces ^{14}C Oxaliplatin Efflux/Retention in SW480-S and SW480-FR cells by FOLFOX and WNT3A treatments. For analyzing drug retention, tumor cells were transfected for 48 hours with CD44v6shRNA, or with a $CD44_{\Delta 67}$ construct (devoid of the ICD region of CD44v6). They were then treated with ^{14}C-oxaliplatin for 24 hours, washed and incubated in drug-free medium alone or with 1 x FOLFOX, or with WNT3A (50 ng/ml) for 12 hours. Cells were harvested and washed, and their numbers were measured by a coulter counter. The radioactivity associated with cells (indicated as intracellular drug retention) were then measured by a liquid scintillation counter as described in Methods. **(B)**, QPCR analyses of CD44v6, *β*-catenin and *MDR1* levels in SW480-S, SW480-FR, SW480-OXAR and SW480-5FUR cells are shown. **(C)**, QPCR analyses of CD44v6 and *MDR1* mRNAs in SW480-S, SW480-5FUR and SW480-OXAR cells treated with or without 1 x FOLFOX or 20 ng/ml WNT3A for 12 hours are shown. **(D-E)**, QPCR analyses are shown for *TCF4*, CD44v6 or *MDR1* levels in SW480-S cells overexpressing constitutively active **(CA)** pTCF4 cDNA **(D)**, or for*β*-catenin, CD44v6 or MDR1 levels in SW480-S cells overexpressing pCA-*β*-catenin **(E)**. **(F-G)**, Transcription activities of the MDR1 promoter with TCF4 binding sites were measured using the indicated pGL3 reporters. **(F)**, The scheme shows the constructs with TCF binding sites in the pGL3 MDR1 promoter. **(G)**, MDR1 Luciferase activity reporter assays are shown for SW480-FR cells overexpressing shRNA for NT (Control), or *β*-catenin, or CD44v6, or a dominant negative pTCF4-DN construct. **(H-I)**, *MDR1* gene expressions regulated by TCF4 in SW480-FR cells are shown. **(H)**, The sketch map shows the predicted TCF4 binding sites (CTTTGA) within the indicated *MDR1* promoter. The transcriptional start site was at +1, and ATG is at the translation start site. The putative TCF4 binding sites (*MDR1* [A], *MDR1* [B] and *MDR*1 [C]) are shown, and their locations are labeled. **(I)**, Semiquantitative PCR products using ChIP PCR primers for *MDR1* **(A–C)** were amplified. **(J)**, ChIP assays were done using anti-CD44v6 (red), anti-TCF4 (purple), anti-*β*-catenin (blue), or irrelevant IgG antibody (green) as negative control using indicated ChIP primers in SW480-FR cells. Total genomic DNA was used as control for the PCR. Quantitative qPCR data representing the qPCR products in immunoprecipitated DNA versus 10% input DNA of ChIP primers for the designated *TCF4* binding sites on *MDR1* [A], *MDR1* [B] and *MDR*1 [C] are shown. **(K)**, ChIP assays were done using either anti-CD44v6 (red), anti-TCF4 (purple), anti *β*-catenin (blue), or irrelevant IgG antibody (green) in SW480-FR cells overexpressing CD44v6 shRNA1, or NT-shRNA1, or with pCD44v6 WT, or $pCD44v6_{NLS}$ mutant constructs. Quantitative ChIP-QPCR data representing the PCR products in immunoprecipitated DNA versus 10% input DNA of ChIP primers for the designated *TCF4* binding sites on *MDR1* **(A, H)** are shown. QPCR and ChIP PCR data represent mean +/- SD, n = 5 replicates from at least 3 independent experiments. **(B)**, *$P < 0.05$ was considered significant, CD44v6, *β*-catenin, and *MDR1* mRNA levels in 5-FUR, OXAR, and FR SW480 cells were compared with SW480 sensitive cells. **(C)**, *$P < 0.05$ was considered significant, CD44v6, and *MDR1* mRNA levels of FOLFOX and WNT treated cells were compared with vehicle controls in each cell type.**(D)**, *$P < 0.05$ was considered significant, CD44v6, TCF4 and *MDR1* mRNA levels of CA-TCF4 transfectant were compared with vector transfectant. **(E)**, *$P < 0.05$ was considered significant, CD44v6, *β*-catenin, and *MDR1* mRNA levels of CA- *β*-catenin transfectant were compared with vector transfectant. **(G)**, *$P < 0.05$ was considered significant, CD44v6, *β*-catenin, and *MDR1* mRNA levels of CA- *β*-catenin transfectant were compared with vector transfectant. **(G)**, Luciferase data in "**G"** represent results from 3 independent experiments performed in triplicates. *$P < 0.05$ was considered significant, Luciferase activity of TCF4 DN. *β*-catenin sh1, and CD44v6 sh1 transfectant of SW480-FR cells for all the PGL3-mdr1 **(A)**, PGL3-mdr1 **(B)**, and PGL3-mdr1 **(C)**, constructs were compared with that of vector control. **(J)**, *$P < 0.05$ was considered significant, ChIP PCR data for all MDR1 sites **(A–C)** of TCF4. *β*-catenin, and CD44v6 antibody data were compared with that of IgG control in SW480-FR cells.**(K)**, *$P < 0.05$ was considered significant, ChIP PCR data for MDR1 **(A)** site of TCF4. *β*-catenin, and CD44v6 antibody data were compared with that of IgG control in v6 shRNA1 (v6 sh1) and $v6_{NLS}$ Mut transfectant of SW480-FR cells were compared with respective controls such as NT shRNA, and v6 cDNA transfectant of cells.

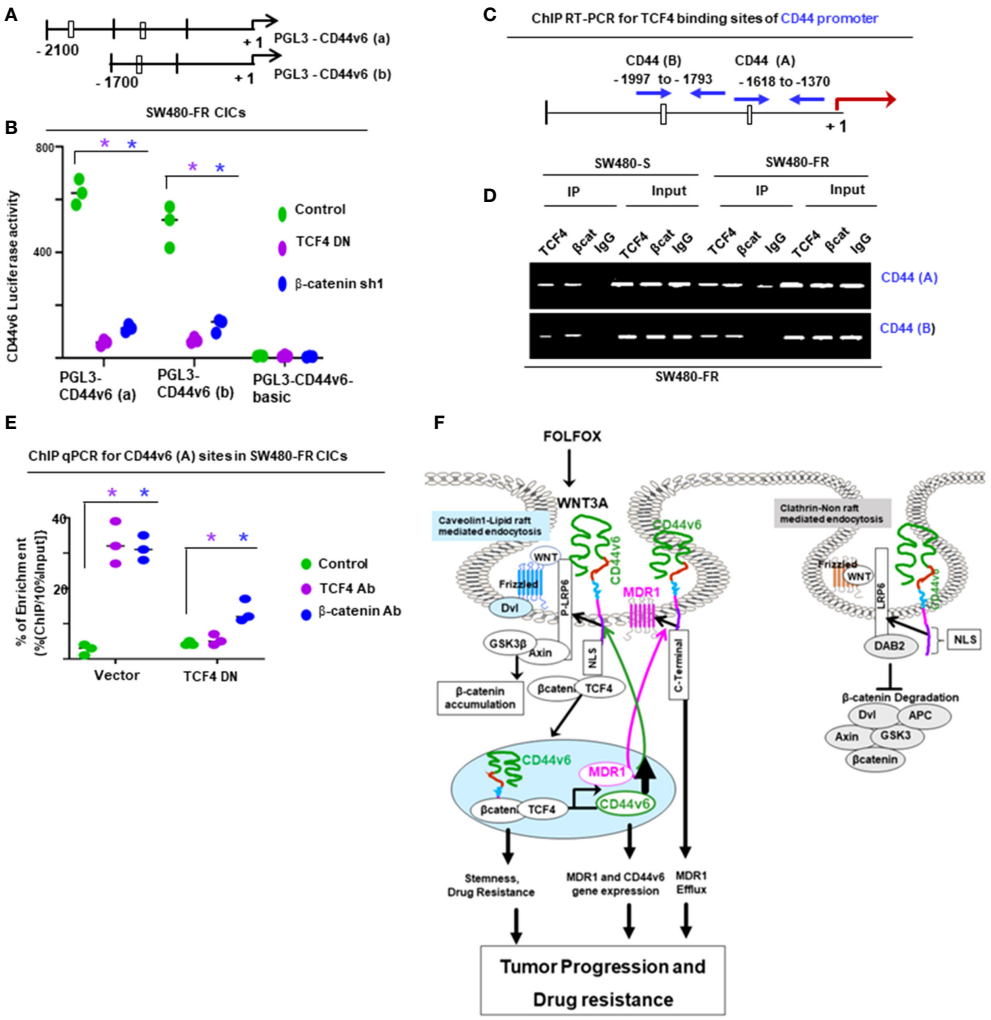

FIGURE 12
Nuclear TCF4 modulates CD44v6 transcription in resistant cells, and the ICD domain of CD44v6 is required for oxaliplatin (a component of FOLFOX) efflux. **(A-D)**, CD44v6 was transcriptionally regulated by TCF4 in SW480-FR cells. **(A)**, The sketch maps of predicted TCF4 binding sites (CTTTGA) within the CD44v6 luciferase promoter **(A)**, and CD44v6 **(B)** are shown in SW480-FR CICs. **(B)**, CD44v6 luciferase (Luc) activity reporter assays are shown for SW480-FR cells CICs overexpressing dominant negative (DN) TCF4, or *β*-catenin shRNA, or NT-shRNA (control). **(C, D)**. **(C)** The sketch map shows the predicted *TCF4* binding sites (CTTTGA) within the indicated CD44 promoter. The transcriptional start site was at +1, and ATG is at the translation start site. The putative TCF4 binding sites (CD44v6 [A], CD44v6 [B]) are shown, and their locations are labeled by blue arrows. **(D)** Semiquantitative PCR products using ChIP PCR primers for the designated TCF4 binding sites on CD44v6 **(A)** and CD44v6 **(B)**, were amplified in SW480-FR CICs. **(E)**, ChIP-qPCR using PCR primers for designated CD44v6 **(A)** sites (as shown in the schematic diagram in **(C)**) were used for amplification of the CD44v6 mRNA of untreated SW480-FR CICs cells and of CICs overexpressing the indicated vector and TCF4-DN cDNA. **(F)** Proposed model is shown for a positive feedback loop coupling *β*-catenin/TCF4 activation and CD44v6 alternate splicing that sustains cancer initiating cell proliferation and FOLFOX resistance. Left panel: In FOLFOX-resistant cells, in the absence pf DAB2, elevated WNT3A induces CD44v6 that recruits LRP6 to caveolin-micro domain through its nuclear localization site (NLS). The CD44v6-lRP6 complex is internalized through the caveolin-mediated endocytosis followed by endosomal sorting, resulting in accumulation of a TCF4-CD44v6 complex that causes transcriptional activation and the expression of its target genes including CD44v6 and *MDR1* genes. Our results are the first demonstration of a positive feedback loop linking FOLFOX mediated increased WNT3A signaling-dependent alternative splicing of CD44 which is important for cell cycle progression resulting in FOLFOX-resistance in CRC-CICs in the absence of DAB2. Right panel: In sensitive cells in the presence of DAB2, the CD44v6-LRP6 complex is internalized through the clathrin-mediated endocytosis pathway and promotes *β*-catenin destruction and fails to recruit the *β*-catenin/TCF4-CD44v6 complex into the nucleus. Data in B, E represent at least 3 independent experiments performed in triplicates. Values represent means ± SD.; n = 3–5; Semi-quantitative PCR data in "D" are representative of three experiments. **(B)**, **P* < 0.05 was considered significant, Luciferase activity of TCF4 DN. and *β*-catenin sh1 transfectant of SW480-FR cells for all the PGL3-CD44v6 **(A)**, and PGL3-CD44v6 **(B)** constructs were compared with that of vector control. **(E)**, **P* < 0.05 was considered significant, ChIP PCR data for CD44v6 **(A)** sites of TCF4. and *β*-catenin antibody data were compared with that of IgG control in SW480-FR cells.

stimulation with WNT3A (Figure 9F) presumably for reuse. In contrast, CD44v6 was delivered to the nucleus for further use (Figure 9E). Indeed, a previous study has shown that a fragment of CD44 can directly interact with the transcriptional machinery, resulting in the up-regulation of genes containing the TPA (12-*O*-tetradecanoylphorbol 13-acetate) - responsive element, including *CD44* itself (139). However, the mechanism of CD44v6 regulated LRP6 endosomal sorting and of full length-CD44v6 nuclear import/function through its engagement with WNT3A to regulate FOLFOX resistance is not known.

To further confirm whether the increased WNT3A mediated TOPFlash promoter activation can corroborate with the LRP6 (S1490)-CD44v6 complex in a caveolin compartment, we silenced both caveolin and clathrin in SW480-FR-Vec and SW480-FR-DAB2 cells by targeted shRNA for caveolin (CAV1) and clathrin. Figures 9G-I show that caveolin knockdown blocks WNT3A/β-catenin transcriptional activation, and active β-catenin (ABC) and MDR1 expressions in vector transfectant cells, whereas clathrin knockdown overturned the inhibitory effect of DAB2 on WNT3A/β-catenin mediated TOPFlash transactivation (Figure 9G) as well as on ABC and MDR1 expressions in DAB2 transfected FR cells (Figures 9H-I). Validations of CAV1 and clathrin shRNAs are shown in Figures 9J, K) following our published methods (38, 39). These results provide evidence that DAB2 segregates a LRP6-CD44v6 complex towards clathrin and away from the interaction of this complex with caveolin to inactivate WNT3A/β-catenin signaling regulated by CD44v6 (see Table 4 for shRNA sequences).

3.8 Nuclear translocation of CD44v6 with TCF4 through endosomal sorting contributes to enrichment of TCF4/TOPFlash activation

With the evidence that FOLFOX stimulates WNT3A secretion (as seen in Figure 5B) and that WNT3A enhanced the internalization of the biotin-labeled receptor LRP6 followed by nuclear localization of CD44v6 but not LRP6 (as seen in Figure 9E, F), we investigated the mechanism of recruitment of LRP6 by CD44v6 to the lipid rafts. Co-immunoprecipitation assays, as shown in Figure 10A, indicate that mutation of the PALM motif in the NLS-deleted-CD44v6$_{\Delta 67}$ (CD44v6$_{\Delta 67PALM}$ Mut), or mutation of this NLS motif in CD44v6$_{\Delta 61PALM}$ (CD44v6$_{\Delta 61PALM\text{-}NLS}$ Mut), disrupted the association of CD44v6 with LRP6 and actin protein in the lipid raft fraction predominantly in WNT3A stimulated cells. In contrast, CD44v6 proteins containing an intact NLS motif in the CD44v6$_{\Delta 61PALM}$ Mut and the CD44v6$_{PALM}$ Mut, were constantly associated with actin and LRP6, and engagement of CD44v6 strongly enhanced the formation of the CD44v6-LRP6-actin signalosome in lipid-rafts in response to WNT3A stimulation (Figure 10A). These results further corroborate that WNT3A induces a CD44v6-LRP6-actin complex in FR cells, and that CD44v6 binds LRP6 through its NLS site (Figure 10A). To substantiate that endosomal sorting as well as the NLS site of CD44v6 are essential for the nuclear localization of CD44v6 protein, we tested the subcellularly fractionated endosomal and nuclear fractions in SW480 FR-Non-CIC/CD44v6 transfected clones and found that when the wild-type (WT)-CD44v6 construct was overexpressed in the SW480 FR-Non-CICs, CD44v6 was readily detected in the endosomal and nuclear fractions, whereas LRP6 in these cells was detected only in endosomes (Figure 10B). In contrast, CD44v6$_{\Delta 67}$ failed to internalize. However, the CD44v6$_{NLS}$ mutant internalized efficiently but failed to enter the nucleus, indicating that CD44v6 is internalized through endosomal sorting and imported to the nucleus through the nuclear pore complex (Figure 10B). Thus, our data indicate that the FOLFOX induced WNT3A mediated posttranslational modifications of CD44 ((as seen in Figure 5A), were required for efficient interaction between CD44v6 clones and LRP6 in membrane and in endosome compartments in SW480-FR-Non CIC/CD44v6 transduced cells (Figures 10A, B). Our data also provide evidence that MDR1 and β-catenin participate in the formation of the CD44v6-TCF4-β-catenin-MDR1 complex in the cytosol and nucleus through its interaction with TCF4 (Figure 10C). We also observed that little β-catenin was associated with TCF4 in vector transfected COS-7 cells, whereas elevated β-catenin was found in the SW480-FR cells and in COS-7-CD44v6$_{WT}$ cells, and that removal of the CD44v6 ICD region (CD44v6$_{\Delta 67}$) prohibited its interaction with TCF4 and significantly suppressed the association of β-catenin with TCF4 (Figure 10C). To further confirm that CD44v6 facilitates the association of β-catenin with TCF4, we knocked down the expression of endogenous CD44v6 in HT29-FR, LOVO-FR, and SW480-FR cells and showed that the associations of β-catenin with TCF4 were substantially precluded (Figure 10D). When SW48-FR-Non-CIC/CD44v6 clones were incubated with biotin-labeled CD44v6 in an endocytosis assay, the internalized CD44v6 formed a complex with TCF4 in both the cytosol and in the nucleus, whereas the CD44v6$_{NLS}$ Mutant only formed a complex with TCF4 in the cytoplasm, and CD44$_{\Delta 67}$ was not internalized (Figure 10E). TCF4 translocation to the nucleus was inhibited in cells overexpressing the CD44v6$_{NLS}$ mutant (Figure 10E). These data provide evidence that internalized CD44v6 forms a complex with TCF4 in the cytosol, and CD44v6-TCF4 co-translocates to the nucleus in a CD44v6-NLS dependent manner. To test the ability of pCD44v6$_{\Delta 67}$ and pCD44v6$_{NLS}$ to amplify WNT/β-catenin signaling in SW480-FR-NON-CICs, cDNAs were overexpressed for full length pCD44v6-WT, and pCD44v6Δ67 and pCD44v6NLS mutants in SW480-FR-Non-CICs and they were tested for their ability to augment WNT/β-catenin signaling in these cells (Figures 10G, H). In contrast to full-length pCD44v6-WT, pCD44v6$_{\Delta 67}$, which is a membrane-localized protein (Figure 10F), failed to increase

WNT3A-induced TOPFlash activation (Figure 10G). Moreover, since the pCD44v6$_{NLS}$ mutant does not allow the CD44v6-TCF4 complex to migrate to the nucleus (Figure 10E), the pCD44v6$_{NLS}$ mutant failed to increase WNT/β-catenin signaling activation (Figure 10H) demonstrating that the effect of CD44v6 on WNT3A/β-catenin signaling is mediated through the CD44v6-LRP6 binding, which requires the CD44v6/NLS site (as seen in Figure 10A). CD44v6 then sorted in the endosome and translocated to the nucleus with TCF4 (as seen in Figures 10B, E) for augmentation of WNT/β-catenin signaling in FOLFOX resistant cells (as seen in Figures 7D, E).

Thus our results confirm our findings that: 1) CD44v6 regulated LRP6 activation (as seen in Figures 6F, G); 2) this activation is at the membrane level (as seen in the Figures 6K, L); 3) importantly, FOLFOX stimulated WNT3A induces lipid raft coalescence for CD44v6-LRP6 signaling (Figures 7B, D, E); 4) formation of the CD44v6-LRP6 signalosome complex in response to WNT3A stimulation (Figure 10A) requires the NLS motif in CD44v6 (Figure 10B); 5) the internalized CD44v6 formed a complex with TCF4 in both the cytosol and the nucleus, whereas the pCD44v6$_{NLS}$ mutant only formed a complex with TCF4 in the cytoplasm, and the pCD44v6$_{\Delta 67}$ mutant was not internalized (Figure 10E); and 6) TCF4 was sequestered from the nucleus in cells overexpressing the pCD44v6$_{NLS}$ mutant (Figure 10E). These data provide evidence that internalized CD44v6 formed a complex with TCF4 in the cytosol and that CD44v6-TCF4 co-migrated to the nucleus in a CD44v6-dependent manner that depends on a particular CD44v6-NLS site (Figures 10C-E) to induce TCF4/FOPFlash promoter activation (Figures 10G, H) and subsequent augmentation of drug resistance (as seen in Figures 2F, G).

3.9 Nuclear CD44v6 stimulates FOLFOX resistance through elevation of efflux of oxaliplatin

MDRl (P-gp) is known to be involved in the drug efflux and multidrug resistance of solid tumors including CRC (140–142). Recent studies have revealed that both hyaluronan and CD44/CD44v6 stimulate drug resistance by promoting transcriptional up-regulation of the *MDR1* gene and the stimulation of multidrug resistance expression in different cancer types (5, 29, 143, 144). However, the molecular mechanisms underlying the acceleration of *MDR1* gene expression and the stimulation of drug efflux by FOLFOX stimulated WNT/CD44v6 signaling are not well understood. Our data indicate that elevated MDR1 was found in the CD44v6-expressing COS7 cells, and that removal of the CD44v6 ICD (CD44v6$_{\Delta 67}$) region precluded its interaction with TCF4, and of β-catenin with MDR1, which significantly suppressed the association of TCF4 and β-catenin (as seen in Figure 10C). Moreover, knocking down the expression of endogenous CD44v6 in FR cells prohibited this association of TCF4 with β-catenin (as seen in Figure 10D) and inhibited cell viability/proliferation (as seen in Figures 2F, G). These data suggest that localization of CD44v6 in the nucleus is an important aspect of its FOLFOX resistance function. Thus, we used radioactively labeled $^{[14C]}$oxaliplatin (OXA) to measure drug effluxes after FOLFOX stimulated WNT3A/β-catenin/TCF4/MDR1 signaling in SW480-FR and SW480-S cells. Figure 11A shows that the efflux of ^{14}C-OXA (a component of FOLFOX) was elevated, leaving low levels of intracellular drug retention after the addition of 1 x FOLFOX, or of 20 ng/ml WNT3A for 2.0 hours. Elevation of efflux of ^{14}C-OXA in these cells increases in a time-dependent manner reaching a plateau level 2.0 - 2.5 hours after FOLFOX, or WNT3A treatments (data not shown). Our results clearly show that the efflux of oxaliplatin was elevated in control FR-tumor cells compared to sensitive SW480 cells (Figure 11A). This high level of FOLFOX-mediated drug efflux causes low levels of intracellular OXA retention in FR cells compared to sensitive cells (Figure 11A). The retention of OXA was further downregulated with FOLFOX or WNT3A treatments (Figure 11A). We also observed that knocking down CD44v6, or expressing pCD44v6$_{\Delta 67}$, or expressing pCD44v6$_{NLS}$ without FOLFOX or WNT3A addition reduced drug efflux, resulting in high levels of intracellular OXA retention (Figure 11A). Addition of FOLFOX, or WNT3A to the cells pre-transfected with CD44v6shRNA or with pCD44v6$_{\Delta 67}$ or with pCD44v6$_{NLS}$ could not reverse the low level of OXA efflux caused by CD44v6shRNA, or pCD44v6$_{\Delta 67}$, or pCD44v6$_{NLS}$ overexpression (Figure 11A). These results clearly indicate that the WNT3A-CD44v6-β-catenin/TCF4-CD44v6 interaction has an important role in regulating MDR1-linked drug efflux/retention and multidrug resistance.

3.10 Nuclear β-catenin/TCF4 associates with CD44v6 to modulate transcription of MDR1 and CD44v6

As noted above CD44 expression is downstream of the WNT3A/β-catenin signaling (30, 88, 89). However, a similar regulation of CD44v6 by WNT/β-catenin in response to FOLFOX stimulation has yet to be identified. Our data show that CD44v6-LRP6 is internalized in the presence of FOLFOX-stimulated WNT3A, and after internalization the CD44v6 is translocated to the nucleus by the stimulation of WNT3A. After being internalized and trafficked to the nucleus, the full-length CD44v6 form complexes with TCF4 and MDR1 because CD44v6 and *MDR1* promoters have TCF4 binding sites (see Figures 11H and 12C). To understand the mechanism of this regulation, chromatin immunoprecipitation (ChIP) was done to identify DNA sequences bound by nuclear CD44v6 and β-actin complexes. DNA fragments were pulled down by an anti-

CD44v6 antibody from a total of 11 clones. A National Center for Biotechnology Information basic local alignment search tool analysis shows that these clones contained sequences corresponding to the promoters of several genes, including *MDR1* (Table 5). Among them, 9 clones contained sequences for *TCF4*, and 11 clones contained sequences for *MDR1*. Thus, we tested whether nuclear CD44v6 exerts its transcriptional regulatory function on *MDR1* through interacting with β-catenin/TCF4 pathway.

To understand the mechanism of CD44v6-β-catenin-MDR1 regulation in CRC, we first determined the mRNA expressions of CD44v6, β-catenin and MDR1 in our sensitive and resistant SW480 cells (Figure 11B). The results show that resistant SW480-FR cells express these three molecules in significantly increased levels compared to sensitive SW480-S cells. Second, we manipulated the β-catenin signaling level through treatment of sensitive and resistant SW480 cells with 1 x FOLFOX or WNT3A and found that these treatments increased CD44v6, β-catenin and *MDR1* mRNA expressions in these cells (Figure 11C). Importantly, WNT3A had modest effects in sensitive cells compared to resistant cells (Figure 11C). Third, we overexpressed cDNAs for TCF4 and β-catenin in sensitive SW480-S cells and showed that these strategies increased CD44v6 variant and *MDR1* gene expressions (Figures 11D, E).

To further evaluate the relative contribution of TCF4 transcription factor to the regulation of MDR1 promoter activity, transient transfection assays were done using SW480-FR cells with constructs containing TCF binding sites within the *MDR1* promoter cloned into a luciferase reporter plasmid (Figure 11F). These constructs were transfected with or without manipulations of CD44v6, TCF4 and β-catenin by knocking them down and measuring their luciferase activities using a luciferase assay for the PGL3-mdr1 constructs. The results showed that luciferase activity increases in the presence of TCF binding sites in these cells (Figure 11G). Even with only one TCF binding site, pGL3-mdr1(b) construct transfection, a higher luciferase activity was observed compared with a basal promoter lacking TCF binding sites (pGL3-mdr1-c), but less activity than when more than one TCF binding site was present (pGL3-mdr1-a) (Figure 11G). The *MDR1* promoter luciferase constructs negatively responded to co-transfection with dominant-negative TCF4-DN cDNA, shRNA1 (sh1) for β-catenin and CD44v6. These inhibitory constructs reduced the responsiveness in PGL3-mdr1(a), and PGL3-mdr1(b) in SW480-FR cells (Figure 11G). These reductions provide evidence that *TCF* promoter binding and activation of *MDR1* is mediated through both CD44v6 variant and β-*catenin* in the nucleus.

We used ChIP assays to understand the interaction of CD44v6 and β-catenin proteins at TCF binding regions of the MDR1 promoter and of their bound chromatin from the protein mixture that was extracted from SW480-FR CICs. ChIP assays were done and immunoprecipitated, and the input DNAs were amplified using primers (see Table 6) covering the indicated *TCF4* binding sites as shown in Figure 11H. ChIP assays (Figure 11I) showed that β-catenin/TCF4 bound to three *MDR1* sites in both sensitive and resistant SW480 cells. CD44v6 only bound to these three sites in resistant cells and was associated with markedly increased binding of TCF4 and β-catenin when compared to sensitive cells (Figure 11I). ChIP analyses provided direct evidence for the ability of TCF4 and β-catenin to bind to the promoters of CD44v6 (Figure 11J). Knockdown of CD44v6, or blocking the NLS site of CD44v6 using the pCD44v6$_{NLS}$ mutant, showed reduced endogenous *MDR1* promoter binding in SW480-FR cells (Figure 11K). This validates our results from the luciferase reporter assay that CD44v6 and TCF4/β-catenin co-regulate *MDR1* expression in a CD44v6-regulated manner in FOLFOX resistant cells, and this CD44v6-regulated *MDR1* gene expression through *TCF4* sites requires the CD44v6 NLS site.

Several putative TCF binding sites were located 2 kilobases upstream of the transcriptional start site of the *CD44* gene (Figure 12A). A fragment of the *CD44* promoter (-2100 to 500 bp) was fused upstream of the firefly luciferase gene in pGL3-CD44v6 (a), and similarly pGL3-CD44v6 (b) was prepared (-1700 to 500 bp). Both pGL3-CD44v6 (a) and pGL3-CD44v6 (b) contain *TCF4* binding sites. Luciferase assays were used to directly examine the interaction between β-catenin/*TCF4* and the *CD44* promoter in SW480-FR CICs. The luciferase activities in SW480-FR cells transfected with dominant negative TCF4-DN and shRNA1 (sh1) for β-catenin were significantly lower than in the vector group (Figure 12B), while β-catenin and TCF4 overexpression significantly increased the luciferase activity (data not shown). This provides evidence that β-catenin/TCF4 increases CD44v6 transcription activity. To identify whether β-catenin can bind to TCF4 binding sites in the *CD44* promoter in SW480-FR cells CICs, ChIP assays were done and immunoprecipitated, and input DNAs were amplified using primers (see Table 6) covering the indicated TCF4 binding sites of the *CD44* promoter as shown in Figure 12C. To validate these results, conventional ChIP analyses were done, and they provided direct evidence for the ability of TCF4 to bind to the *CD44* promoter in SW480-FR CICs (Figures 12D, E). As noted in Figures 5B, C, FOLFOX induces secretion of WNT3A and WNT3A/β-catenin transactivation in CICs. Further, Figures 5 and 6 show that FOLFOX mediates CD44v6 expression to regulate WNT3A/β-catenin TCF4 signaling, and in this section, we showed that a β-catenin/TCF4 pathway promotes both *CD44* and *MDR1* gene expressions in FR-CICs (Figures 11 and 12).

Overall, this study indicates that FOLFOX treatment induces both WNT3A and CD44v6 through its NLS site, recruits LRP6 to CAV1-rafts, and activates LRP6 (S1490) to promote WNT3A/β-catenin/TCF4 signaling that induces CD44v6 expression (Figures 5-12). This functions through a positive feed-back loop between CD44v6 and FOLFOX induced WNT3A/β-catenin/TCF4 activation stimulates *MDR1* gene expression and CD44v6 splicing that sustains FOLFOX resistance. Furthermore, we have found that the failure to recruit MDR1 into a complex with CD44v6 using overexpression of pCD44v6Δ67 or silencing CD44v6 variants abolishes FOLFOX-induced active multidrug efflux and increases drug retention.

4 Discussion

5-FU, a component of FOLFOX, promotes CD44v6 (6), and induces stemness/self-renewal in CRC activation by WNT/β-catenin signaling (145), and CICs are more resistant to therapy. Thus, it is not difficult to understand how the induction of CD44v6 and WNT/β-catenin signaling in human colorectal CICs directly affects the treatment outcome. WNT/β-catenin signaling is one of the key cascades regulating development and stemness, and has also been tightly associated with CICs in the gut and with promoting self-renewal of CRC-CICs (19, 146–148). Our data indicate strong support that WNT signaling and CD44v6-containing variant expression might be coordinately controlled by a positive feedback loop in CICs isolated from FOLFOX resistant colorectal tumor. This is in accordance with our findings that feedback regulation is a key aspect of CD44v6 signaling in which WNT/β-catenin signaling promotes CD44v6 splicing, and CD44v6 then sustains WNT/β-catenin signaling, which is important for cell sycle progression and uncontrolled drug resistance in CRC-CICs (Figure 2). In line with this, negative feedback mechanisms are likely necessary in normal colon cells to regulate uncontrolled WNT/β-catenin/CD44v6 activation. Further, targeting WNT or CD44v6 showed increased FOLFOX sensitivity and completely blocked the WNT3A mediated transactivation of the CICs cell cycle profile and drug resistance (as seen in Figures 2F, G, H, Supplemental Figure 1D, 2I and 5G). This indicates that the CIC's FOLFOX resistance was generated by WNT/β-catenin *via* CD44v6.

In our recent study, the importance of CD44v6-YB-1-MDR1 signaling that maintains chemo resistance in CICs was described (5). However, upstream signaling mechanisms leading to drug resistance with potential crosstalk between CD44v6 signaling and WNT-receptor LRP6 involvement in FOLFOX-therapy in CRC are largely unknown. To explore the link between chronic FOLFOX-therapy stress and colorectal CIC "stemness", we initiated a comprehensive molecular and functional analysis of CD44v6 regulation of WNT/β-catenin signaling and its effects in CICs isolated from FOLFOX resistant human tumor specimens, and from SQ tumor samples. Since the expression of CIC markers may not be regulated in a coordinated fashion, we analyzed three widely used stem-cell/progenitor markers (EpCAM, ALDH1 and CD133) in CD44v6 (+) FACS sorted cells to isolate CICs and used them in several cellular/molecular functional tests. These included WNT/β-catenin/TCF4 mediated TOPFlash promoter activity, lipid raft localization assays, internalization/endosomal sorting and nuclear trafficking analysis, cell viability, Annexin V positive cells expressing cell apoptosis, tumor sphere formation, xenograft tumor growth, and MDR1 and CD44v6 transcriptions through a nuclear CD44v6-TCF4 complex.

We investigated drug resistance and consequent tumor relapse as a mechanism to mediate self-renewal functions of CICs (149) and evaluated the tumorigenic potential of freshly isolated CD44v6 (+) CICs and CD44v6 (–) populations (Non-CICs), and of unsorted bulk cells to form colon tumors by implantation of these cells into immunocompromised mice. In this xenograft model of CRC, implantation of 5 x 10^5 Non-CICs from colorectal tumor cells did not induce tumor formation (Figures 4F-G). Even though a higher number of CD44v6 (+) cells was present in 5 x 10^5 unfractionated bulk tumor cells, tumor formation capacity of as few as 2 x 10^3 CD44v6 (+) CICs was faster and more efficient than tumor formation obtained with the unfractionated bulk tumor cells (Figures 4F-4G). To evaluate whether CD44v6 (+) CICs can reproduce long-term tumorigenic potential in progressive recipients, we analyzed their ability to generate tumor sphere formation after serial transplantations in secondary and tertiary mouse recipients. During the *in vivo* passaging, CD44v6 (+) CICs did not lose their tumorigenic potential but instead increased their faster tumor size and growth (Figure 4G). Data in Figure 4H show that only CD44v6 (+) CICs form tumor spheres in primary, second and third generations of mice whereas tumorigenic potential of CD44v6-Non-CICs was completely lost in secondary and tertiary recipients of xenografts. Thus, the CD44v6 (+) CICs are confined to a small cell population resident in the colon tumor and have the ability to reproduce long-term tumorigenic potential in serial recipient xenografts with unlimited tumorigenic potential, whereas CD44v6 (–)Non-CICs include transient amplifying of differentiated cells.

Gain-in-function and loss-in-function of CD44v6 experiments (Figures 6K, L) demonstrated that CD44v6 acts at the level of WNT3A and LRP6 and upstream of DVL-2 and β-catenin. Nonetheless DVL-2 was shown to be required for LRP6 phosphorylation (150). These data are further supported by the finding that CD44v6 regulates WNT3A-dependent LRP6 phosphorylation at the level of CIC membranes (as seen in Figures 6F, G, K, L). These data and the findings show that either clathrin-mediated (Non-lipid raft) or caveolin-mediated

(lipid-raft) internalization of LRP6 is key for the WNT/β-catenin signaling. This led us to study the interaction of DAB2 with CD44v6 and LRP6 in Non-lipid raft or lipid-raft micro-domains that regulate WNT3A/β-catenin signaling. Additionally, we provide evidence that WNT3A-mediated interaction of CD44v6 with LRP6 phosphorylation (LRP6 [S1490]) by CD44v6 is required for its association with DVL-2 and caveolin in lipid rafts, whereas DAB2 attenuates the WNT signaling by shifting the CD44v6-LRP6 complex to clathrin mediated endocytosis in sensitive cells (Figures 7, 8). In the absence of DAB2, WNT induces internalization of CD44v6, which in turn interacts with LRP6 through caveolin mediated endocytosis (Figure 7B) and promotes membrane localization of matured LRP6. This results in WNT/β-catenin signaling in a CD44v6 mediated CK2-dependent manner but not through CD44v6 regulated (MAPK)/Erk and phosphatidylinositol 3 kinase (PI3K)/Akt pathways (Figure 6), whereas in its presence DAB2 binds CD44v6 and LRP6 in a WNT-dependent manner, and pushes LRP6 towards clathrin mediated endocytosis and suppresses β-catenin signaling and MDR1 expression (Figure 8). We propose, therefore, that FOLFOX regulates cellular DVL-2 and DAB2 levels that modulate CD44v6-LRP6 interaction and consequent WNT/β-catenin signaling by regulating endocytosis of LRP6 and CD44v6.

In a further step, we have presented new evidence indicating that FOLFOX induces WNT signaling through CD44v6 mediated recruitment of LRP6/LRP6 (S1490) to caveolin-dependent internalization of these receptors (Figure 7, Figures 9C-F). The internalized CD44v6 and LRP6 were sorted in endosomes, and CD44v6 formed a complex with TCF4 in both the cytosol and nucleus. Then the CD44v6 with TCF4 co-translocated to the nucleus in a CD44v6-dependent manner, and this association requires the nuclear localization signal (NLS) of CD44v6 (Figures 10B-E). The NLS motif that mediates CD44v6 nuclear translocation was mapped to the intracellular domain of CD44v6 (Figure 9A). Importantly, internalized CD44v6 forms a complex with TCF4 and β-catenin, and this complex is translocated to the nucleus through a CD44v6 dependent manner (Figure 10C). Expression of a CD44 (NLS) mutant sequesters TCF4 in the cytosol (Figure 10E). In the nucleus, the TCF4 remains associated with CD44v6 and binds to the *TCF4, MDR1* and *CD44* promoters, leading to increased *MDR1* activity and drug efflux (Figures 11, 12). Further our data provide evidence that WNT3A-mediated phosphorylation of S1490 of LRP6 mediated by CD44v6 is required for its association with DVL-2 and caveolin, whereas DAB2 attenuates the WNT signaling by shifting the CD44v6-LRP6 complex to clathrin mediated endocytosis in sensitive cells (Figures 8 and 9G-I). Consequently, all these events contribute to CD44v6-WNT3A-mediated therapeutic drug resistance in CICs of colon tumor cells. This provides evidence that targeting the CD44v6-WNT3A mediated β-catenin/TCF4-MDR1 signaling pathways and the increased MDR1 efflux function may represent a novel approach to overcome chemotherapy resistance in colon tumor CICs.

5 Conclusion

5.1 Proposed model for a positive feedback loop that couples β-catenin/TCF4 activation and CD44v6 alternate splicing that sustains CIC drug resistance

We propose that FOLFOX mediated WNT3A stimulation of CD44v6 through its NLS site recruits LRP6 in a caveolin-microdomain in the absence of DAB2. The CD44v6-LRP6 (S1490)/LRP6-signalosome is internalized through endosomal sorting resulting in nuclear accumulation of a β-catenin/TCF4-CD44v6 complex, which then transcriptionally activates stemness-associated *MDR1* and a CD44v6-containing isoform, which sustains drug-resistance in CRC-CICs. In contrast, a CD44v6-LRP6 complex is internalized through the clathrin microdomain in sensitive cells and fails to recruit the β-catenin/TCF4-CD44v6 complex in the nucleus. Our data, suggest a biphasic activation of β-catenin in response to either WNT3A or FOLFOX (Figure 2I). Furthermore, upon WNT3A stimulation either alone or through FOLFOX (Figure 5B) produces an early surge of nuclear β-catenin activation independent of CD44v6 variants. This signal is rapidly down regulated by CD44v6 shRNA when FOLFOX or WNT3A generates CD44v6 expression after 2 hour of either WNT3A, or of FOLFOX stimulation (Figure 2I). However WNT3A/β-catenin activation signal initiates a positive feedback loop by inducing CD44v6 expression through alternative splicing (Figure 12F).

Data availability statement

The datasets presented in this study can be found in online repositories. The names of the repository/repositories and accession number(s) can be found below: https://www.ncbi.nlm.nih.gov/, (http://portals.broadinstitute.org/gpp/public/).

Ethics statement

The studies involving human participants were reviewed and approved by Medical University of South Carolina. The patients/participants provided their written informed consent to participate in this study. The animal study was reviewed and approved by IACUC, all animal care and experiments were in accordance with the institutional guidelines of IACUC-2017-00250 (approval date: 2019/03/14- 2021/03/29).

Author contributions

The paper was written by SM and SG. SG and SM designed the study, physically worked together at any time and made an

equal contribution to the conception of every claim of the work involved for the study. Being an expert for his work on hyaluronic acid and CD44 research, VH analyzed the effect of CD44v6shRNA on β-catenin/TCF4 signaling. VH reviewed, edited the multiple versions of the drafts and final versions of the text, figures, figure legends, participated in designing experiments and supplied reagents. RM participated in conception of the idea in validating the CICs and CAFs that were used in this study. RM edited the drafts, provided reagents, and participated in designing experiments. NK, further discussed with SM and SG to validating the specificity of the shRNAs. NK helped in editing the drafts and participated in the experimental design. We thank Christopher Koivisto from Hollings Cancer Center for sharing his views for this manuscript. All authors contributed to the article and approved the submitted version.

Funding

This work was supported by the: 1) 1R03CA167722-01A1 (to SM and SG); 2) 1K12HL141952-02 (to VH); 3) 2P20GM10399; NIH IDeA Network for SC Biomedical Research Excellence, 40 2 P30 GM131959-01, 5) 19TPA34900016 (to RM), and 7) SCTR grant (UL1 TR001450 for SM).

Conflict of interest

The authors declare that the research was conducted in the absence of any commercial or financial relationships that could be construed as a potential conflict of interest.

Publisher's note

All claims expressed in this article are solely those of the authors and do not necessarily represent those of their affiliated organizations, or those of the publisher, the editors and the reviewers. Any product that may be evaluated in this article, or claim that may be made by its manufacturer, is not guaranteed or endorsed by the publisher.

Supplementary material

The Supplementary Material for this article can be found online at: https://www.frontiersin.org/articles/10.3389/fonc.2022.906260/full#supplementary-material

SUPPLEMENTARY FIGURE 1
(A, B), Validations of CD44v6 shRNAs (v6 sh1 and v6 sh2) and WNT3A shRNAs (WNT3A sh1 and WNT3A sh2) used in panels **(D–G)** were done by the indicated shRNA mediated knockdown and the corresponding knock-in (KI) gene transfections in SW480-FR cells as described in Methods. Target proteins were analyzed by WB analysis (β-tubulin, internal control). **(C)**, The effect of shRNA-mediated knockdown of CD44v6 in SW480-FR cells on the expression of CD44v6 mRNA was determined by real-time PCR (at 24 h; RQ, relative quantification). Validation of expression vector CD44v6 cDNA (v6 cDNA) was done by WB analysis (β-tubulin, internal control) **(D)**, Bar graph summarizing the flow cytometry cell cycle profile analysis after WNT3A stimulation in G2.M-arrested-SW480-cells which were previously transfected with NT shRNA or v6 shRNA for 24 hours. These cells were collected at indicated times after WNT3A -stimulation and cell cycle were analyzed (details in Method section). Data are presented as Mean $\pm$ SD from n = 3 replicates in three independent experiments. FACs data are representative of three experiments *P < 0.05, **P < 0.01 were considered significant, percent cells in S phase in CD44v6 shRNA transfected cells compared with NT shRNA transfected cell.

References

1. Siegel RL, Miller KD, Fedewa SA, Ahnen DJ, Meester RGS, Barzi A, et al. Colorectal cancer statistics, 2017. *CA Cancer J Clin* (2017) 67(3):177–93. doi: 10.3322/caac.21395

2. Siegel RL, Miller KD, Jemal A. Cancer statistics, 2016. *CA Cancer J Clin* (2016) 66(1):7–30. doi: 10.3322/caac.21332

3. Augestad KM, Rose J, Crawshaw B, Cooper G, Delaney C. Do the benefits outweigh the side effects of colorectal cancer surveillance? a systematic review. *World J Gastrointest Oncol* (2014) 6(5):104–11. doi: 10.4251/wjgo.v6.i5.104

4. Renouf DJ, Woods R, Speers C, Hay J, Phang PT, Fitzgerald C, et al. Improvements in 5-year outcomes of stage II/III rectal cancer relative to colon cancer. *Am J Clin Oncol* (2013) 36(6):558–64. doi: 10.1097/COC.0b013e318256f5dcs

5. Ghatak S, Hascall VC, Markwald RR, Misra S. FOLFOX therapy induces feedback upregulation of CD44v6 through YB-1 to maintain stemness in colon initiating cells. *Int J Mol Sci* (2021) 22(2):753–90. doi: 10.3390/ijms22020753

6. Lv L, Liu HG, Dong SY, Yang F, Wang QX, Guo GL, et al. Upregulation of CD44v6 contributes to acquired chemoresistance *via* the modulation of autophagy in colon cancer SW480 cells. *Tumour Biol* (2016) 37(7):8811–24. doi: 10.1007/s13277-015-4755-6

7. Hammond WA, Swaika A, Mody K. Pharmacologic resistance in colorectal cancer: a review. *Ther Adv Med Oncol* (2016) 8(1):57–84. doi: 10.1177/1758834015614530

8. Singh AK, Arya RK, Maheshwari S, Singh A, Meena S, Pandey P, et al. Tumor heterogeneity and cancer stem cell paradigm: updates in concept, controversies and clinical relevance. *Int J Cancer* (2015) 136(9):1991–2000. doi: 10.1002/ijc.28804

9. Valent P, Bonnet D, De Maria R, Lapidot T, Copland M, Melo JV, et al. Cancer stem cell definitions and terminology: the devil is in the details. *Nat Rev Cancer* (2012) 12(11):767–75. doi: 10.1038/nrc3368

10. Barker N, Ridgway RA, van Es JH, van de Wetering M, Begthel H, van den Born M, et al. O. j. sansom and h. clevers: Crypt stem cells as the cells-of-origin of intestinal cancer. *Nature* (2009) 457(7229):608–11. doi: 10.1038/nature07602

11. Blanpain C. Tracing the cellular origin of cancer. *Nat Cell Biol* (2013) 15 (2):126–34. doi: 10.1038/ncb2657

12. Ricci-Vitiani L, Fabrizi E, Palio E, De Maria R. Colon cancer stem cells. *J Mol Med (Berl)* (2009) 87(11):1097–104. doi: 10.1007/s00109-009-0518-4

13. Al-Hajj M, Wicha MS, Benito-Hernandez A, Morrison SJ, Clarke MF. Prospective identification of tumorigenic breast cancer cells. *Proc Natl Acad Sci U.S.A.* (2003) 100(7):3983–8. doi: 10.1073/pnas.0530291100

14. Walcher L, Kistenmacher AK, Suo H, Kitte R, Dluczek S, Strauss A, et al. Cancer stem cells-origins and biomarkers: Perspectives for targeted personalized therapies. *Front Immunol* (2020) 11:1280. doi: 10.3389/fimmu.2020.01280

15. Zoller M. CD44: can a cancer-initiating cell profit from an abundantly expressed molecule? *Nat Rev Cancer* (2011) 11(4):254–67. doi: 10.1038/nrc3023

16. Tirino V, Desiderio V, Paino F, De Rosa A, Papaccio F, Fazioli F, et al. Human primary bone sarcomas contain CD133+ cancer stem cells displaying high tumorigenicity in vivo. *FASEB J* (2011) 25(6):2022–30. doi: 10.1096/fj.10-179036

17. Wang Z, Zhao K, Hackert T, Zoller M. CD44/CD44v6 a reliable companion in cancer-initiating cell maintenance and tumor progression. *Front Cell Dev Biol* (2018) 6:97. doi: 10.3389/fcell.2018.00097

18. Takaishi S, Okumura T, Tu S, Wang SS, Shibata W, Vigneshwaran R, et al. Identification of gastric cancer stem cells using the cell surface marker CD44. *Stem Cells* (2009) 27(5):1006–20. doi: 10.1002/stem.30

19. Todaro M, Gaggianesi M, Catalano V, Benfante A, Iovino F, Biffoni M, et al. CD44v6 is a marker of constitutive and reprogrammed cancer stem cells driving colon cancer metastasis. *Cell Stem Cell* (2014) 14(3):342–56. doi: 10.1016/j.stem.2014.01.009

20. Prasetyanti PR, Medema JP. Intra-tumor heterogeneity from a cancer stem cell perspective. *Mol Cancer* (2017) 16(1):41. doi: 10.1186/s12943-017-0600-4

21. Natarajan TG, Ganesan N, Fitzgerald KT. Cancer stem cells and markers: new model of tumorigenesis with therapeutic implications. *Cancer biomark* (2010) 9(1-6):65–99. doi: 10.3233/CBM-2011-0173

22. Hong SN. Genetic and epigenetic alterations of colorectal cancer. *Intest Res* (2018) 16(3):327–37. doi: 10.5217/ir.2018.16.3.327

23. Sadanandam A, Lyssiotis CA, Homicsko K, Collisson EA, Gibb WJ, Wullschleger S, et al. A colorectal cancer classification system that associates cellular phenotype and responses to therapy. *Nat Med* (2013) 19(5):619–25. doi: 10.1038/nm.3175

24. Sanchez JA, Krumroy L, Plummer S, Aung P, Merkulova A, Skacel M, et al. Genetic and epigenetic classifications define clinical phenotypes and determine patient outcomes in colorectal cancer. *Br J Surg* (2009) 96(10):1196–204. doi: 10.1002/bjs.6683

25. Ogino S, Fuchs CS, Giovannucci E. How many molecular subtypes? implications of the unique tumor principle in personalized medicine. *Expert Rev Mol Diagn* (2012) 12(6):621–8. doi: 10.1586/erm.12.46

26. Screaton GR, Bell MV, Jackson DG, Cornelis FB, Gerth U, Bell JI. Genomic structure of DNA encoding the lymphocyte homing receptor CD44 reveals at least 12 alternatively spliced exons. *Proc Natl Acad Sci U.S.A.* (1992) 89(24):12160–4. doi: 10.1073/pnas.89.24.12160

27. Naor D, Wallach-Dayan SB, Zahalka MA, Sionov RV. Involvement of CD44, a molecule with a thousand faces, in cancer dissemination. *Semin Cancer Biol* (2008) 18(4):260–7. doi: 10.1016/j.semcancer.2008.03.015

28. Zeilstra J, Joosten SP, van Andel H, Tolg C, Berns A, Snoek M, et al. Pals: Stem cell CD44v isoforms promote intestinal cancer formation in apc(min) mice downstream of wnt signaling. *Oncogene* (2014) 33(5):665–70. doi: 10.1038/onc.2012.611

29. Misra S, Ghatak S, Toole BP. Regulation of MDR1 expression and drug resistance by a positive feedback loop involving hyaluronan, phosphoinositide 3-kinase, and ErbB2. *J Biol Chem* (2005) 280(21):20310–5. doi: 10.1074/jbc.M500737200

30. Misra S, Hascall VC, Berger FG, Markwald RR, Ghatak S. Hyaluronan, CD44, and cyclooxygenase-2 in colon cancer. *Connect Tissue Res* (2008) 49(3):219–24. doi: 10.1080/03008200802143356

31. Misra S, Hascall VC, De Giovanni C, Markwald RR, Ghatak S. Delivery of CD44 shRNA/nanoparticles within cancer cells: perturbation of hyaluronan/CD44v6 interactions and reduction in adenoma growth in apc min/+ MICE. *J Biol Chem* (2009) 284(18):12432–46. doi: 10.1074/jbc.M806772200

32. Misra S, Toole BP, Ghatak S. Hyaluronan constitutively regulates activation of multiple receptor tyrosine kinases in epithelial and carcinoma cells. *J Biol Chem* (2006) 281(46):34936–41. doi: 10.1074/jbc.C600138200

33. Ghatak S, Misra S, Toole BP. Hyaluronan constitutively regulates ErbB2 phosphorylation and signaling complex formation in carcinoma cells. *J Biol Chem* (2005) 280(10):8875–83. doi: 10.1074/jbc.M410882200

34. Sherman L, Wainwright D, Ponta H, Herrlich P. A splice variant of CD44 expressed in the apical ectodermal ridge presents fibroblast growth factors to limb mesenchyme and is required for limb outgrowth. *Genes Dev* (1998) 12(7):1058–71. doi: 10.1101/gad.12.7.1058

35. Bourguignon LY, Gilad E, Peyrollier K. Heregulin-mediated ErbB2-ERK signaling activates hyaluronan synthases leading to CD44-dependent ovarian tumor cell growth and migration. *J Biol Chem* (2007) 282(27):19426–41. doi: 10.1074/jbc.M610054200

36. Orian-Rousseau V, Chen L, Sleeman JP, Herrlich P, Ponta H. CD44 is required for two consecutive steps in HGF/c-met signaling. *Genes Dev* (2002) 16(23):3074–86. doi: 10.1101/gad.242602

37. Tremmel M, Matzke A, Albrecht I, Laib AM, Olaku V, Ballmer-Hofer K, et al. A CD44v6 peptide reveals a role of CD44 in VEGFR-2 signaling and angiogenesis. *Blood* (2009) 114(25):5236–44. doi: 10.1182/blood-2009-04-219204

38. Ghatak S, Hascall VC, Markwald RR, Feghali-Bostwick C, Artlett CM, Gooz M, et al. Transforming growth factor beta1 (TGFbeta1)-induced CD44V6-NOX4 signaling in pathogenesis of idiopathic pulmonary fibrosis. *J Biol Chem* (2017A) 292(25):10490–519. doi: 10.1074/jbc.M116.752469

39. Ghatak S, Markwald RR, Hascall VC, Dowling W, Lottes RG, Baatz JE, et al. Transforming growth factor beta1 (TGFbeta1) regulates CD44V6 expression and activity through extracellular signal-regulated kinase (ERK)-induced EGR1 in pulmonary fibrogenic fibroblasts. *J Biol Chem* (2017B) 292(25):10465–89. doi: 10.1074/jbc.M116.752451

40. Bourguignon LY. CD44-mediated oncogenic signaling and cytoskeleton activation during mammary tumor progression. *J Mammary Gland Biol Neoplasia* (2001) 6(3):287–97. doi: 10.1023/A:1011371523994

41. Marhaba R, Zoller M. CD44 in cancer progression: adhesion, migration and growth regulation. *J Mol Histol* (2004) 35(3):211–31. doi: 10.1023/b:hijo.0000032354.94213.69

42. Vermeulen L, Todaro M, de Sousa Mello F, Sprick MR, Kemper K, Perez Alea M, et al. Single-cell cloning of colon cancer stem cells reveals a multi-lineage differentiation capacity. *Proc Natl Acad Sci U.S.A.* (2008) 105(36):13427–32. doi: 10.1073/pnas.0805706105

43. Ohata H, Ishiguro T, Aihara Y, Sato A, Sakai H, Sekine S, et al. Induction of the stem-like cell regulator CD44 by rho kinase inhibition contributes to the maintenance of colon cancer-initiating cells. *Cancer Res* (2012) 72(19):5101–10. doi: 10.1158/0008-5472.CAN-11-3812

44. Huang EH, Hynes MJ, Zhang T, Ginestier C, Dontu G, Appelman H, et al. Aldehyde dehydrogenase 1 is a marker for normal and malignant human colonic stem cells (SC) and tracks SC overpopulation during colon tumorigenesis. *Cancer Res* (2009) 69(8):3382–9. doi: 10.1158/0008-5472.CAN-08-4418

45. Zoller M. Tetraspanins: push and pull in suppressing and promoting metastasis. *Nat Rev Cancer* (2009) 9(1):40–55. doi: 10.1038/nrc2543

46. Gherardi E, Birchmeier W, Birchmeier C, Vande Woude G. Targeting MET in cancer: rationale and progress. *Nat Rev Cancer* (2012) 12(2):89–103. doi: 10.1038/nrc3205

47. Hermann PC, Huber SL, Herrler T, Aicher A, Ellwart JW, Guba M, et al. Distinct populations of cancer stem cells determine tumor growth and metastatic activity in human pancreatic cancer. *Cell Stem Cell* (2007) 1(3):313–23. doi: 10.1016/j.stem.2007.06.002

48. Karni R, de Stanchina E, Lowe SW, Sinha R, Mu D, Krainer AR. The gene encoding the splicing factor SF2/ASF is a proto-oncogene. *Nat Struct Mol Biol* (2007) 14(3):185–93. doi: 10.1038/nsmb1209

49. Anczukow O, Rosenberg AZ, Akerman M, Das S, Zhan L, Karni R, et al. The splicing factor SRSF1 regulates apoptosis and proliferation to promote mammary epithelial cell transformation. *Nat Struct Mol Biol* (2012) 19(2):220–8. doi: 10.1038/nsmb.2207

50. Jia R, Li C, McCoy JP, Deng CX, Zheng ZM. SRp20 is a proto-oncogene critical for cell proliferation and tumor induction and maintenance. *Int J Biol Sci* (2010) 6(7):806–26. doi: 10.7150/ijbs.6.806

51. Cohen-Eliav M, Golan-Gerstl R, Siegfried Z, Andersen CL, Thorsen K, Orntoft TF, et al. The splicing factor SRSF6 is amplified and is an oncoprotein in lung and colon cancers. *J Pathol* (2013) 229(4):630–9. doi: 10.1002/path.4129

52. Golan-Gerstl R, Cohen M, Shilo A, Suh SS, Bakacs A, Coppola L, et al. Splicing factor hnRNP A2/B1 regulates tumor suppressor gene splicing and is an oncogenic driver in glioblastoma. *Cancer Res* (2011) 71(13):4464–72. doi: 10.1158/0008-5472.CAN-10-4410

53. Lefave CV, Squatrito M, Vorlova S, Rocco GL, Brennan CW, Holland EC, et al. Splicing factor hnRNPH drives an oncogenic splicing switch in gliomas. *EMBO J* (2011) 30(19):4084–97. doi: 10.1038/emboj.2011.259

54. Zong FY, Fu X, Wei WJ, Luo YG, Heiner M, Cao LJ, et al. The RNA-binding protein QKI suppresses cancer-associated aberrant splicing. *PloS Genet* (2014) 10(4):e1004289. doi: 10.1371/journal.pgen.1004289

55. Bechara EG, Sebestyen E, Bernardis I, Eyras E, Valcarcel J. RBM5, 6, and 10 differentially regulate NUMB alternative splicing to control cancer cell proliferation. *Mol Cell* (2013) 52(5):720–33. doi: 10.1016/j.molcel.2013.11.010

56. Valacca C, Bonomi S, Buratti E, Pedrotti S, Baralle FE, Sette C, et al. Sam68 regulates EMT through alternative splicing-activated nonsense-mediated mRNA decay of the SF2/ASF proto-oncogene. *J Cell Biol* (2010) 191(1):87–99. doi: 10.1083/jcb.201001073

57. Goncalves V, Matos P, Jordan P. The beta-catenin/TCF4 pathway modifies alternative splicing through modulation of SRp20 expression. *RNA* (2008) 14 (12):2538–49. doi: 10.1261/rna.1253408

58. Cheng C, Sharp PA. Regulation of CD44 alternative splicing by SRm160 and its potential role in tumor cell invasion. *Mol Cell Biol* (2006) 26(1):362–70. doi: 10.1128/MCB.26.1.362-370.2006

59. Zhou Z, Qiu J, Liu W, Zhou Y, Plocinik RM, Li H, et al. The akt-SRPK-SR axis constitutes a major pathway in transducing EGF signaling to regulate alternative splicing in the nucleus. *Mol Cell* (2012) 47(3):422–33. doi: 10.1016/j.molcel.2012.05.014

60. Zhou Z, Qiu J, Liu W, Zhou Y, Plocinik RM, Li H, et al. The akt-SRPK-SR axis constitutes a major pathway in transducing EGF signaling to regulate alternative splicing in the nucleus. *Mol Cell* (2018) 71(5):872. doi: 10.1016/j.molcel.2018.08.024

61. Goncalves V, Henriques AF, Pereira JF, Costa AN, Moyer MP, Moita LF, et al. Corrigendum: Phosphorylation of SRSF1 by SRPK1 regulates alternative splicing of tumor-related Rac1b in colorectal cells. *RNA* (2016) 22(1):166. doi: 10.1261/rna.055020.115

62. Goncalves V, Henriques AF, Pereira JF, Neves Costa A, Moyer MP, Moita LF, et al. Phosphorylation of SRSF1 by SRPK1 regulates alternative splicing of tumor-related Rac1b in colorectal cells. *RNA* (2014) 20(4):474–82. doi: 10.1261/rna.041376.113

63. Lee MA, Park JH, Rhyu SY, Oh ST, Kang WK, Kim HN. Wnt3a expression is associated with MMP-9 expression in primary tumor and metastatic site in recurrent or stage IV colorectal cancer. *BMC Cancer* (2014) 14:125. doi: 10.1186/1471-2407-14-125

64. Clevers H. Wnt/beta-catenin signaling in development and disease. *Cell* (2006) 127(3):469–80. doi: 10.1016/j.cell.2006.10.018

65. Clevers H, Nusse R. Wnt/beta-catenin signaling and disease. *Cell* (2012) 149 (6):1192–205. doi: 10.1016/j.cell.2012.05.012

66. Cadigan KM, Liu YI. Wnt signaling: complexity at the surface. *J Cell Sci* (2006) 119(Pt 3):395–402. doi: 10.1242/jcs.02826

67. Malbon CC, Wang HY. Dishevelled: a mobile scaffold catalyzing development. *Curr Top Dev Biol* (2006) 72:153–66. doi: 10.1016/S0070-2153(05)72002-0

68. Logan CY, Nusse R. The wnt signaling pathway in development and disease. *Annu Rev Cell Dev Biol* (2004) 20:781–810. doi: 10.1146/annurev.cellbio.20.010403.113126

69. Sheng Z, He J, Tuppen JA, Sun W, Fazili Z, Smith ER, et al. Structure, sequence, and promoter analysis of human disabled-2 gene (DAB2). *Genomics* (2000) 70(3):381–6. doi: 10.1006/geno.2000.6383

70. Sheng Z, Sun W, Smith E, Cohen C, Sheng Z, Xu XX. Restoration of positioning control following disabled-2 expression in ovarian and breast tumor cells. *Oncogene* (2000) 19(42):4847–54. doi: 10.1038/sj.onc.1203853

71. Xu XX, Yang W, Jackowski S, Rock CO. Cloning of a novel phosphoprotein regulated by colony-stimulating factor 1 shares a domain with the drosophila disabled gene product. *J Biol Chem* (1995) 270(23):14184–91. doi: 10.1074/jbc.270.23.14184

72. Hocevar BA, Smine A, Xu XX, Howe PH. The adaptor molecule disabled-2 links the transforming growth factor beta receptors to the smad pathway. *EMBO J* (2001) 20(11):2789–801. doi: 10.1093/emboj/20.11.2789

73. Hocevar BA, Prunier C, Howe PH. Disabled-2 (Dab2) mediates transforming growth factor beta (TGFbeta)-stimulated fibronectin synthesis through TGFbeta-activated kinase 1 and activation of the JNK pathway. *J Biol Chem* (2005) 280(27):25920–7. doi: 10.1074/jbc.M501150200

74. Prunier C, Hocevar BA, Howe PH. Wnt signaling: physiology and pathology. *Growth Factors* (2004) 22(3):141–50. doi: 10.1080/08977190410001720860

75. van Meer G, Voelker DR, Feigenson GW. Membrane lipids: where they are and how they behave. *Nat Rev Mol Cell Biol* (2008) 9(2):112–24. doi: 10.1038/nrm2330

76. Neame SJ, Uff CR, Sheikh H, Wheatley SC, Isacke CM. CD44 exhibits a cell type dependent interaction with triton X-100 insoluble, lipid rich, plasma membrane domains. *J Cell Sci* (1995) 108(Pt 9):3127–35. doi: 10.1242/jcs.108.9.3127

77. Schmitt M, Metzger M, Gradl D, Davidson G, Orian-Rousseau V. CD44 functions in wnt signaling by regulating LRP6 localization and activation. *Cell Death Differ* (2015) 22(4):677–89. doi: 10.1038/cdd.2014.156

78. Lee JL, Wang MJ, Sudhir PR, Chen JY. CD44 engagement promotes matrix-derived survival through the CD44-SRC-integrin axis in lipid rafts. *Mol Cell Biol* (2008) 28(18):5710–23. doi: 10.1128/MCB.00186-08

79. Steinbichler TB, Dudas J, Skvortsov S, Ganswindt U, Riechelmann and Skvortsova H. II: Therapy resistance mediated by cancer stem cells. *Semin Cancer Biol* (2018) 53:156–67. doi: 10.1016/j.semcancer.2018.11.006

80. De Mattia E, Cecchin E, Toffoli G. Pharmacogenomics of intrinsic and acquired pharmacoresistance in colorectal cancer: Toward targeted personalized therapy. *Drug Resist Update* (2015) 20:39–70. doi: 10.1016/j.drup.2015.05.003

81. Longley DB, Johnston PG. Molecular mechanisms of drug resistance. *J Pathol* (2005) 205(2):275–92. doi: 10.1002/path.1706

82. Funato Y, Michiue T, Asashima M, Miki H. The thioredoxin-related redox-regulating protein nucleoredoxin inhibits wnt-beta-catenin signalling through dishevelled. *Nat Cell Biol* (2006) 8(5):501–8. doi: 10.1038/ncb1405

83. Masuda H, Tanaka T, Takahama U. Cisplatin generates superoxide anion by interaction with DNA in a cell-free system. *Biochem Biophys Res Commun* (1994) 203(2):1175–80. doi: 10.1006/bbrc.1994.2306

84. Kruidering M, Van de Water B, de Heer E, Mulder GJ, Nagelkerke JF. Cisplatin-induced nephrotoxicity in porcine proximal tubular cells: mitochondrial dysfunction by inhibition of complexes I to IV of the respiratory chain. *J Pharmacol Exp Ther* (1997) 280(2):638–49.

85. Weng MS, Chang JH, Hung WY, Yang YC, Chien MH. The interplay of reactive oxygen species and the epidermal growth factor receptor in tumor progression and drug resistance. *J Exp Clin Cancer Res* (2018) 37(1):61. doi: 10.1186/s13046-018-0728-0

86. Chen MK, Du Y, Sun L, Hsu JL, Wang YH, Gao Y, et al. H2O2 induces nuclear transport of the receptor tyrosine kinase c-MET in breast cancer cells *via* a membrane-bound retrograde trafficking mechanism. *J Biol Chem* (2019) 294 (21):8516–28. doi: 10.1074/jbc.RA118.005953

87. Robinson S, Manas D, Mann D, White S, Mann J. Tumour cytokine production after FOLFOX chemotherapy is mediated by the NF-κB DNA damage response-an important contribution to chemo induced liver injury. *EJSO* (2011) 37(11):995. doi: 10.1016/j.ejso.2011.08.077

88. Misra S, Obeid LM, Hannun YA, Minamisawa S, Berger FG, Markwald RR, et al. Hyaluronan constitutively regulates activation of COX-2-mediated cell survival activity in intestinal epithelial and colon carcinoma cells. *J Biol Chem* (2008) 283(21):14335–44. doi: 10.1074/jbc.M703811200

89. Wielenga VJ, Smits R, Korinek V, Smit L, Kielman M, Fodde R, et al. Expression of CD44 in apc and tcf mutant mice implies regulation by the WNT pathway. *Am J Pathol* (1999) 154(2):515–23. doi: 10.1016/S0002-9440(10)65297-2

90. Correa S, Binato R, Du Rocher B, Castelo-Branco MT, Pizzatti L, Abdelhay E. Wnt/beta-catenin pathway regulates ABCB1 transcription in chronic myeloid leukemia. *BMC Cancer* (2012) 12:303. doi: 10.1186/1471-2407-12-303

91. Chakraborty PK, Lee WK, Molitor M, Wolff NA, Thevenod F. Cadmium induces wnt signaling to upregulate proliferation and survival genes in sub-confluent kidney proximal tubule cells. *Mol Cancer* (2010) 9:102. doi: 10.1186/1476-4598-9-102

92. Martin-Orozco E, Sanchez-Fernandez A, Ortiz-Parra I, Ayala-San Nicolas M. WNT signaling in tumors: The way to evade drugs and immunity. *Front Immunol* (2019) 10:2854. doi: 10.3389/fimmu.2019.02854

93. Katoh M, Katoh M. WNT signaling pathway and stem cell signaling network. *Clin Cancer Res* (2007) 13(14):4042–5. doi: 10.1158/1078-0432.CCR-06-2316

94. MacDonald BT, Tamai K, He X. Wnt/beta-catenin signaling: components, mechanisms, and diseases. *Dev Cell* (2009) 17(1):9–26. doi: 10.1016/j.devcel.2009.06.016

95. Nicolazzo C, Loreni F, Caponnetto S, Magri V, Vestri AR, Zamarchi R, et al. Baseline CD44v6-positive circulating tumor cells to predict first-line treatment failure in patients with metastatic colorectal cancer. *Oncotarget* (2020) 11 (45):4115–22. doi: 10.18632/oncotarget.27794

96. Ghatak S, Bogatkevich GS, Atnelishvili I, Akter T, Feghali-Bostwick C, Hoffman S, et al. Overexpression of c-met and CD44v6 receptors contributes to autocrine TGF-beta1 signaling in interstitial lung disease. *J Biol Chem* (2014) 289 (11):7856–72. doi: 10.1074/jbc.M113.505065

97. Ghatak S, Hascall VC, Markwald RR, Misra S. Stromal hyaluronan interaction with epithelial CD44 variants promotes prostate cancer invasiveness by augmenting expression and function of hepatocyte growth factor and androgen receptor. *J Biol Chem* (2010) 285(26):19821–32. doi: 10.1074/jbc.M110.104273

98. Ghatak S, Misra S, Norris RA, Moreno-Rodriguez RA, Hoffman S, Levine RA, et al. Periostin induces intracellular cross-talk between kinases and hyaluronan in atrioventricular valvulogenesis. *J Biol Chem* (2014) 289(12):8545–61. doi: 10.1074/jbc.M113.539882

99. von Haller PD, Donohoe S, Goodlett DR, Aebersold R, Watts JD. Mass spectrometric characterization of proteins extracted from jurkat T cell detergent-resistant membrane domains. *Proteomics* (2001) 1(8):1010–21. doi: 10.1002/1615-9861(200108)1:8<1010::AID-PROT1010>3.0.CO;2-L

100. Graham JM. OptiPrep density gradient solutions for mammalian organelles. *ScientificWorldJournal* (2002) 2:1440–3. doi: 10.1100/tsw.2002.840

101. Macdonald JL, Pike LJ. A simplified method for the preparation of detergent-free lipid rafts. *J Lipid Res* (2005) 46(5):1061–7. doi: 10.1194/jlr.D400041-JLR200

102. Walker LR, Hussein HA, Akula SM. Subcellular fractionation method to study endosomal trafficking of kaposi's sarcoma-associated herpesvirus. *Cell Biosci* (2016) 6:1. doi: 10.1186/s13578-015-0066-2

103. Andoorfar S, Hosseini Tafreshi SA, Rezvani Z. Assessment of the expression level of miRNA molecules using a semi-quantitative RT-PCR approach. *Mol Biol Rep* (2019) 46(5):5057–62. doi: 10.1007/s11033-019-04959-5

104. Misra S, Ghatak S, Moreno-Rodrigue R, Norris R, Hascall V, RR M. Periostin/Filamin-a: a candidate centralregulatory axis for valve fibrogenesisand matrix compaction. *Front Cell Dev Biol* (2021) 10(3389). doi: 10.3389/fcell.2021.649862

105. Hah SS, Henderson PT, Turteltaub KW. Towards biomarker-dependent individualized chemotherapy: exploring cell-specific differences in oxaliplatin-DNA adduct distribution using accelerator mass spectrometry. *Bioorg Med Chem Lett* (2010) 20(8):2448–51. doi: 10.1016/j.bmcl.2010.03.020

106. De Giovanni C, Landuzzi L, Nicoletti G, Astolfi A, Croci S, Micaroni M, et al. Apc10.1: an ApcMin/+ intestinal cell line with retention of heterozygosity. *Int J Cancer* (2004) 109(2):200–6. doi: 10.1002/ijc.11690

107. Olmeda D, Castel S, Vilaro S, Cano A. Beta-catenin regulation during the cell cycle: implications in G2/M and apoptosis. *Mol Biol Cell* (2003) 14(7):2844–60. doi: 10.1091/mbc.e03-01-0865

108. Brabletz T, Jung A, Spaderna S, Hlubek F, Kirchner T. Opinion: migrating cancer stem cells - an integrated concept of malignant tumour progression. *Nat Rev Cancer* (2005) 5(9):744–9. doi: 10.1038/nrc1694

109. Sun H, Rana S, Wang Z, Zhao K, Schnolzer M, Provaznik J, et al. The pancreatic cancer-initiating cell marker CD44v6 affects transcription, translation, and signaling: Consequences for exosome composition and delivery. *J Oncol* (2019) 2019:3516973. doi: 10.1155/2019/3516973

110. Dalerba P, Cho RW, Clarke MF. Cancer stem cells: models and concepts. *Annu Rev Med* (2007) 58:267–84. doi: 10.1146/annurev.med.58.062105.204854

111. Vermeulen L, Sprick MR, Kemper K, Stassi G, Medema JP. Cancer stem cells–old concepts, new insights. *Cell Death Differ* (2008) 15(6):947–58. doi: 10.1038/cdd.2008.20

112. Horst D, Kriegl L, Engel J, Kirchner T, Jung A. Prognostic significance of the cancer stem cell markers CD133, CD44, and CD166 in colorectal cancer. *Cancer Invest* (2009) 27(8):844–50. doi: 10.1080/07357900902744502

113. Vermeulen L, De Sousa EMF, van der Heijden M, Cameron K, de Jong JH, Borovski T, et al. Wnt activity defines colon cancer stem cells and is regulated by the microenvironment. *Nat Cell Biol* (2010) 12(5):468–76. doi: 10.1038/ncb2048

114. Prasetyanti PR, Zimberlin CD, Bots M, Vermeulen L, Melo Fde S, Medema JP. Regulation of stem cell self-renewal and differentiation by wnt and notch are conserved throughout the adenoma-carcinoma sequence in the colon. *Mol Cancer* (2013) 12(1):126. doi: 10.1186/1476-4598-12-126

115. Jones VS, Huang RY, Chen LP, Chen ZS, Fu L, Huang RP. Cytokines in cancer drug resistance: Cues to new therapeutic strategies. *Biochim Biophys Acta* (2016) 1865(2):255–65. doi: 10.1016/j.bbcan.2016.03.005

116. Tonini G, Santini D, Vincenzi B, Borzomati D, Dicuonzo G, La Cesa A, et al. Oxaliplatin may induce cytokine-release syndrome in colorectal cancer patients. *J Biol Regul Homeost Agents* (2002) 16(2):105–9.

117. Robinson KF, Narasipura SD, Wallace J, Ritz EM, Al-Harthi L. Beta-catenin and TCFs/LEF signaling discordantly regulate IL-6 expression in astrocytes. *Cell Commun Signal* (2020) 18(1):93. doi: 10.1186/s12964-020-00565-2

118. Asakuno K, Kohno K, Uchiumi T, Kubo T, Sato S, Isono M, et al. Involvement of a DNA binding protein, MDR-NF1/YB-1, in human MDR1 gene expression by actinomycin d. *Biochem Biophys Res Commun* (1994) 199(3):1428–35. doi: 10.1006/bbrc.1994.1390

119. Bargou RC, Jurchott K, Wagener C, Bergmann S, Metzner S, Bommert K, et al. Nuclear localization and increased levels of transcription factor YB-1 in primary human breast cancers are associated with intrinsic MDR1 gene expression. *Nat Med* (1997) 3(4):447–50. doi: 10.1038/nm0497-447

120. Jiang H, Peterson RS, Wang W, Bartnik E, Knudson CB, Knudson W. A requirement for the CD44 cytoplasmic domain for hyaluronan binding, pericellular matrix assembly, and receptor-mediated endocytosis in COS-7 cells. *J Biol Chem* (2002) 277(12):10531–8. doi: 10.1074/jbc.M108654200

121. Tamai K, Zeng X, Liu C, Zhang X, Harada Y, Chang Z, et al. A mechanism for wnt coreceptor activation. *Mol Cell* (2004) 13(1):149–56. doi: 10.1016/s1097-2765(03)00484-2

122. Hsieh JC, Lee L, Zhang L, Wefer S, Brown K, DeRossi C, et al. Mesd encodes an LRP5/6 chaperone essential for specification of mouse embryonic polarity. *Cell* (2003) 112(3):355–67. doi: 10.1016/s0092-8674(03)00045-x

123. Krejci P, Aklian A, Kaucka M, Sevcikova E, Prochazkova J, Masek JK, et al. Receptor tyrosine kinases activate canonical WNT/beta-catenin signaling *via* MAP kinase/LRP6 pathway and direct beta-catenin phosphorylation. *PloS One* (2012) 7(4):e35826. doi: 10.1371/journal.pone.0035826

124. Liang J, Fu Y, Cruciat CM, Jia S, Wang Y, Tong Z, et al. Transmembrane protein 198 promotes LRP6 phosphorylation and wnt signaling activation. *Mol Cell Biol* (2011) 31(13):2577–90. doi: 10.1128/MCB.05103-11

125. van Meer G. Cellular lipidomics. *EMBO J* (2005) 24(18):3159–65. doi: 10.1038/sj.emboj.7600798

126. Conner SD, Schmid SL. Regulated portals of entry into the cell. *Nature* (2003) 422(6927):37–44. doi: 10.1038/nature01451

127. Sorkin A, Von Zastrow M. Signal transduction and endocytosis: close encounters of many kinds. *Nat Rev Mol Cell Biol* (2002) 3(8):600–14. doi: 10.1038/nrm883

128. Hanover JA, Willingham MC, Pastan I. Kinetics of transit of transferrin and epidermal growth factor through clathrin-coated membranes. *Cell* (1984) 39(2 Pt 1):283–93. doi: 10.1016/0092-8674(84)90006-0

129. Beguinot L, Lyall RM, Willingham MC, Pastan I. Down-regulation of the epidermal growth factor receptor in KB cells is due to receptor internalization and subsequent degradation in lysosomes. *Proc Natl Acad Sci U.S.A.* (1984) 81(8):2384–8. doi: 10.1073/pnas.81.8.2384

130. Le Roy C, Wrana JL. Clathrin- and non-clathrin-mediated endocytic regulation of cell signalling. *Nat Rev Mol Cell Biol* (2005) 6(2):112–26. doi: 10.1038/nrm1571

131. Razani B, Woodman SE, Lisanti MP. Caveolae: from cell biology to animal physiology. *Pharmacol Rev* (2002) 54(3):431–67. doi: 10.1124/pr.54.3.431

132. Doherty GJ, McMahon HT. Mechanisms of endocytosis. *Annu Rev Biochem* (2009) 78:857–902. doi: 10.1146/annurev.biochem.78.081307.110540

133. Yamamoto H, Sakane H, Yamamoto H, Michiue T, Kikuchi A. Wnt3a and Dkk1 regulate distinct internalization pathways of LRP6 to tune the activation of beta-catenin signaling. *Dev Cell* (2008) 15(1):37–48. doi: 10.1016/j.devcel.2008.04.015

134. Jiang Y, He X, Howe PH. Disabled-2 (Dab2) inhibits wnt/beta-catenin signalling by binding LRP6 and promoting its internalization through clathrin. *EMBO J* (2012) 31(10):2336–49. doi: 10.1038/emboj.2012.83

135. Liu D, Sy MS. A cysteine residue located in the transmembrane domain of CD44 is important in binding of CD44 to hyaluronic acid. *J Exp Med* (1996) 183(5):1987–94. doi: 10.1084/jem.183.5.1987

136. Thankamony SP, Knudson W. Acylation of CD44 and its association with lipid rafts are required for receptor and hyaluronan endocytosis. *J Biol Chem* (2006) 281(45):34601–9. doi: 10.1074/jbc.M601530200

137. Tsukita S, Oishi K, Sato N, Sagara J, Kawai A, Tsukita S. ERM Family members as molecular linkers between the cell surface glycoprotein CD44 and actin-based cytoskeletons. *J Cell Biol* (1994) 126(2):391–401. doi: 10.1083/jcb.126.2.391

138. Legg JW, Isacke CM. Identification and functional analysis of the ezrin-binding site in the hyaluronan receptor, CD44. *Curr Biol* (1998) 8(12):705–8. doi: 10.1016/S0960-9822(98)70277-5

139. Kajita M, Itoh Y, Chiba T, Mori H, Okada A, Kinoh H, et al. Membrane-type 1 matrix metalloproteinase cleaves CD44 and promotes cell migration. *J Cell Biol* (2001) 153(5):893–904. doi: 10.1083/jcb.153.5.893

140. Gottesman MM, Pastan IH. The role of multidrug resistance efflux pumps in cancer: Revisiting a JNCI publication exploring expression of the MDR1 (P-glycoprotein) gene. *J Natl Cancer Inst* (2015) 107(9):1–3. doi: 10.1093/jnci/djv222

141. Gros P, Croop J, Housman D. Mammalian multidrug resistance gene: complete cDNA sequence indicates strong homology to bacterial transport proteins. *Cell* (1986) 47(3):371–80. doi: 10.1016/0092-8674(86)90594-5

142. Fojo AT, Ueda K, Slamon DJ, Poplack DG, Gottesman MM, Pastan I. Expression of a multidrug-resistance gene in human tumors and tissues. *Proc Natl Acad Sci U.S.A.* (1987) 84(1):265–9. doi: 10.1073/pnas.84.1.265

143. Misra S, Ghatak S, Zoltan-Jones A, Toole BP. Regulation of multidrug resistance in cancer cells by hyaluronan. *J Biol Chem* (2003) 278(28):25285–8. doi: 10.1074/jbc.C300173200

144. Bourguignon LY, Peyrollier K, Xia W, Gilad E. Hyaluronan-CD44 interaction activates stem cell marker nanog, stat-3-mediated MDR1 gene expression, and ankyrin-regulated multidrug efflux in breast and ovarian tumor cells. *J Biol Chem* (2008) 283(25):17635–51. doi: 10.1074/jbc.M800109200

145. Cho YH, Ro EJ, Yoon JS, Mizutani T, Kang DW, Park JC, et al. 5-FU promotes stemness of colorectal cancer *via* p53-mediated WNT/beta-catenin pathway activation. *Nat Commun* (2020) 11(1):5321. doi: 10.1038/s41467-020-19173-2

146. de Lau W, Barker N, Low TY, Koo BK, Li VS, Teunissen H, et al. Lgr5 homologues associate with wnt receptors and mediate r-spondin signalling. *Nature* (2011) 476(7360):293–7. doi: 10.1038/nature10337

147. Leedham SJ, Rodenas-Cuadrado P, Howarth K, Lewis A, Mallappa S, Segditsas S, et al. A basal gradient of wnt and stem-cell number influences regional

tumour distribution in human and mouse intestinal tracts. *Gut* (2013) 62(1):83–93. doi: 10.1136/gutjnl-2011-301601

148. Ootani A, Li X, Sangiorgi E, Ho QT, Ueno H, Toda S, et al. Sustained *in vitro* intestinal epithelial culture within a wnt-dependent stem cell niche. *Nat Med* (2009) 15(6):701–6. doi: 10.1038/nm.1951

149. Meacham CE, Morrison SJ. Tumour heterogeneity and cancer cell plasticity. *Nature* (2013) 501(7467):328–37. doi: 10.1038/nature12624

150. Bilic J, Huang YL, Davidson G, Zimmermann T, Cruciat CM, Bienz M, et al. Wnt induces LRP6 signalosomes and promotes dishevelled-dependent LRP6 phosphorylation. *Science* (2007) 316(5831):1619–22. doi: 10.1126/science.1137065

Advantages of publishing in Frontiers

OPEN ACCESS
Articles are free to read for greatest visibility and readership

FAST PUBLICATION
Around 90 days from submission to decision

HIGH QUALITY PEER-REVIEW
Rigorous, collaborative, and constructive peer-review

TRANSPARENT PEER-REVIEW
Editors and reviewers acknowledged by name on published articles

Frontiers
Avenue du Tribunal-Fédéral 34
1005 Lausanne | Switzerland

Visit us: www.frontiersin.org
Contact us: frontiersin.org/about/contact

REPRODUCIBILITY OF RESEARCH
Support open data and methods to enhance research reproducibility

DIGITAL PUBLISHING
Articles designed for optimal readership across devices

FOLLOW US
@frontiersin

IMPACT METRICS
Advanced article metrics track visibility across digital media

EXTENSIVE PROMOTION
Marketing and promotion of impactful research

LOOP RESEARCH NETWORK
Our network increases your article's readership